A **AgeAccel, Univariate**

Meta P=1.9e-11, Heterog. P=0.082

Cohort	N	(events)	HR [95% CI]
WHI White	995	309	0.993 [0.971 , 1.016]
LBC 1921	445	312	1.030 [1.013 , 1.048]
LBC 1936	919	106	1.030 [1.003 , 1.059]
NAS	647	221	0.999 [0.975 , 1.023]
FHS	2614	236	1.035 [1.011 , 1.060]
KORA	1257	42	1.033 [0.975 , 1.093]
InCHIANTI	506	91	1.034 [0.992 , 1.078]
Rotterdam	710	32	1.049 [0.993 , 1.110]
BLSA White	317	26	1.100 [1.023 , 1.183]
TwinsUK	805	30	1.072 [0.988 , 1.162]
WHI Black	675	176	1.027 [1.004 , 1.050]
ARIC Black	2768	1075	1.024 [1.012 , 1.037]
WHI Hispanic	431	78	1.038 [0.988 , 1.091]
Meta (FE)			1.024 [1.017 , 1.031]

0.900 1.100 1.300
Hazard Ratio

B **IEAA, Univariate**

Meta P=8.2e-09, Heterog. P=0.61

HR [95% CI]
0.998 [0.975 , 1.021]
1.023 [1.004 , 1.042]
1.022 [0.992 , 1.053]
1.010 [0.984 , 1.037]
1.028 [1.003 , 1.055]
1.033 [0.972 , 1.098]
1.034 [0.990 , 1.080]
1.028 [0.961 , 1.100]
1.114 [1.025 , 1.212]
1.036 [0.947 , 1.134]
1.029 [1.005 , 1.054]
1.023 [1.011 , 1.036]
1.022 [0.971 , 1.076]
Meta (FE) 1.022 [1.014 , 1.029]

0.905 1.000 1.105 1.221
Hazard Ratio

C **EEAA.static, Univariate**

Meta P=7.5e-43, Heterog. P=0.0067

HR [95% CI]
1.016 [0.998 , 1.035]
1.030 [1.017 , 1.044]
1.031 [1.004 , 1.059]
1.039 [1.015 , 1.063]
1.063 [1.043 , 1.083]
1.095 [1.053 , 1.138]
1.036 [1.004 , 1.070]
1.096 [1.034 , 1.161]
1.043 [0.980 , 1.111]
1.102 [1.036 , 1.172]
1.036 [1.014 , 1.059]
1.041 [1.031 , 1.051]
1.049 [1.011 , 1.088]
Meta (FE) 1.040 [1.034 , 1.046]

0.951 1.051 1.162
Hazard Ratio

SPECIAL COLLECTION ON STEVE HORVATH'S PUBLICATIONS IN AGING (ALBANY NY)

Univariate Cox regression meta-analysis of all-cause mortality, see Chen et al "DNA methylation-based measures of biological age: meta-analysis predicting time to death"

Steve Horvath's Publications in Aging (Albany NY)

AgING

Submission
Please submit your manuscript on-line at http://aging.msubmit.net

Editorial
For editorial inquiries, please call us or email editors@impactaging.com

Production
For questions related to preparation of your article for publication, please call us or email krasnova@impactaging.com

Indexing
If you have questions about the indexing status of your paper, please email kurenova@impactaging.com

Billing/Payments
If you have questions about billing/invoicing or would like to make a payment, please call us or email payment@impactaging.com

Media
If you have questions about post publication promotion, Altmetric, video interviews or social media, please email media@impactjournals.com

Printing
Each issue or paper can be printed on demand. To make a printing request, please call us or email printing@impactjournals.com

Publisher's Office
Aging is published by Impact Journals, LLC
To contact the Publisher's Office, please email: publisher@impactjournals.com, visit www.impactjournals.com, or call 1-800-922-0957

IMPACT JOURNALS

Table of Contents

An epigenetic biomarker of aging for lifespan and healthspan

Leukocyte telomere length, T cell composition and DNA methylation age

Accelerated epigenetic aging in Werner syndrome

An epigenetic aging clock for dogs and wolves

Longitudinal study of surrogate aging measures during human immunodeficiency virus seroconversion

Epigenetic clock analysis of diet, exercise, education, and lifestyle factors

Specific premature epigenetic aging of cartilage in osteoarthritis

DNA methylation-based measures of biological age: meta-analysis predicting time to death

Huntington's disease accelerates epigenetic aging of human brain and disrupts DNA methylation levels

Epigenetic age of the pre-frontal cortex is associated with neuritic plaques, amyloid load, and Alzheimer's disease related cognitive functioning

Decreased epigenetic age of PBMCs from Italian semi-supercentenarians and their offspring

Increased epigenetic age and granulocyte counts in the blood of Parkinson's disease patients

DNA methylation age of blood predicts future onset of lung cancer in the women's health initiative

Epigenetic age analysis of children who seem to evade aging

The cerebellum ages slowly according to the epigenetic clock

DNA-methylation-based telomere length estimator: comparisons with measurements from flow FISH and qPCR

Emily E. Pearce[1], Steve Horvath[2,3], Shilpa Katta[4,5], Casey Dagnall[4,5], Geraldine Aubert[6,7], Belynda D. Hicks[4,5], Stephen R. Spellman[8], Hormuzd Katki[9], Sharon A. Savage[1], Rotana Alsaggaf[1,*], Shahinaz M. Gadalla[1,*]

[1]Clinical Genetics Branch, Division of Cancer Epidemiology and Genetics, National Cancer Institute, National Institutes of Health, Rockville, MD 20850, USA
[2]Department of Biostatistics, Fielding School of Public Health, University of California School of Public Health, Los Angeles, CA 90095, USA
[3]Department of Human Genetics, David Geffen School of Medicine, University of California, Los Angeles, CA 90095, USA
[4]Cancer Genomics Research Laboratory, Division of Cancer Epidemiology and Genetics, National Cancer Institute, National Institutes of Health, Rockville, MD 20850, USA
[5]Leidos Biomedical Research, Inc., Frederick National Laboratory for Cancer Research, Frederick, MD 21701, USA
[6]Terry Fox Laboratory, British Columbia Cancer Agency, Vancouver, BC V5Z 1L3, Canada
[7]Repeat Diagnostics Inc, North Vancouver, BC V7M 1A5, Canada
[8]Center for International Blood and Marrow Transplant Research, Medical College of Wisconsin, Milwaukee, WI 53226, USA
[9]Biostatistics Branch, Division of Cancer Epidemiology and Genetics, National Cancer Institute, National Institutes of Health, Bethesda, MD 20892, USA
*Equal contribution

Correspondence to: Shahinaz M. Gadalla, Rotana Alsaggaf; **email:** gadallas@mail.nih.gov, rotana.alsaggaf@nih.gov

ABSTRACT

Telomere length (TL) is a marker of biological aging associated with several health outcomes. High throughput reproducible TL measurements are needed for large epidemiological studies. We compared the novel DNA methylation-based estimator (DNAmTL) with the high-throughput quantitative PCR (qPCR) and the highly accurate flow cytometry with fluorescent *in situ* hybridization (flow FISH) methods using blood samples from healthy adults. We used Pearson's correlation coefficient, Bland Altman plots and linear regression models for statistical analysis. Shorter DNAmTL was associated with older age, male sex, white race, and cytomegalovirus seropositivity (p<0.01 for all). DNAmTL was moderately correlated with qPCR TL (N=635, r=0.41, *p* < 0.0001) and flow FISH total lymphocyte TL (N=144, r=0.56, *p* < 0.0001). The agreements between flow FISH TL and DNAmTL or qPCR were acceptable but with wide limits of agreement. DNAmTL correctly classified >70% of TL categorized above or below the median, but the accuracy dropped with increasing TL categories. The ability of DNAmTL to detect associations with age and other TL-related factors in the absence of strong correlation with measured TL may indicate its capture of aspects of telomere maintenance mechanisms and not necessarily TL. The inaccuracy of DNAmTL prediction should be considered during data interpretation and across-study comparisons.

INTRODUCTION

Telomeres consist of tandem DNA nucleotide repeats (TTAGGG)n and a protein complex that cap chromosome ends to ensure chromosomal stability [1]. Telomeres shorten as cells divide, eventually leading to replicative senescence and/or apoptosis, making telomere length (TL) a useful marker of cellular and thus biological age [2, 3]. TL has been associated with a variety of age-related diseases and health outcomes including cardiovascular disease, metabolic syndrome, and cancer (reviewed in [4]). TL is used clinically to diagnose patients with inherited telomere biology disorders such as dyskeratosis congenita and has shown promise in guiding donor selection for hematopoietic cell transplant (HCT) [5–8].

Several methods have been developed for measuring TL, each with its own strengths and limitations [9, 10]. The current gold standard is the Southern blot Telomere Restriction Fragment (TRF) method; it measures average absolute TL (in kilobases, kb), and requires large quantities of high-quality DNA [11]. Another accurate method is fluorescence *in situ* hybridization (flow FISH) in which fluorescently labeled peptide nucleic acid (PNA) probes detect telomeric repeats in total leukocytes and leukocyte subsets to determine average TL as calibrated using TRF and presented in kb. This method requires viable leukocytes and special expertise [10, 12]. A widely used method is quantitative polymerase chain reaction (qPCR) that measures TL based on the ratio between telomere copy number and that of a single-copy gene (T/S) in the same DNA sample [13, 14]. qPCR is frequently used to determine TL in epidemiologic studies because of its high-throughput and small DNA requirements; however, its reliability is limited by its high sensitivity to pre-analytic factors, such as DNA extraction or storage [15]. Other methods target the shortest telomeres such as single telomere length analysis (STELA) and the Telomere Shortest Length Assay (TeSLA) [16, 17]. Large scale genomic and epigenomic data offer opportunities for new approaches to TL calculation, such as TelSeq, an open-source software that is correlated with Southern blot (r~0.6) and estimates TL in kb using whole-genome sequence data [18].

Existing methods and high throughput adaptations have extended telomere research to population-level studies; however, there remains a need for TL measurement tools that overcome the limitations of current techniques: the sample quantities and analysis time required by the most accurate methods, and the limited reliability of high-throughput methods. DNA methylation regulates gene expression and has been associated with both chronological age and telomere shortening [19–21]. A new method utilizing whole genome DNA methylation array data to predict TL in kb was recently introduced [22] and may be useful to explore TL questions using available methylation array databases. This study aims to independently evaluate the performance of DNAmTL in comparison with TL measured by flow FISH and qPCR and evaluate the relationship between DNAmTL and participant characteristics known to be associated with TL.

RESULTS

Participant characteristics

The study included 635 healthy adults (median age=34 years, range=19-61) who were HCT donors; blood samples were available at the Center for International Blood and Marrow Transplant Research (CIBMTR) biorepository and were part of the National Cancer Institute (NCI) Transplant Outcomes in Aplastic Anemia (TOAA) Study. Of the 635 individuals, 425 (67%) were male, 478 (75%) were white, and 239 (38%) were cytomegalovirus (CMV) seropositive (Table 1).

Association between DNAmTL and TL-related participant characteristics

A statistically significant strong negative association between DNAmTL and chronological age was noted; the correlation coefficient (r) = -0.65, p<0.0001 (Figure 1A). Shorter DNAmTL was associated with male sex (p=0.0001) and CMV positive serostatus (p=0.0004). African Americans had longer DNAmTL compared with other race groups; the difference between TL in African Americans and Whites was statistically significant (p=0.003), but no difference was noted between Whites and other race groups (p=0.95) (Figure 1B). In a multivariable regression model including all previously tested variables, DNAmTL decreased by 21 bp per year (p<0.0001), and was 116 bp longer in women than men (p<0.0001), 213 bp longer in African Americans than whites (p<0.0001), and 83 bp shorter in CMV seropositive individuals than those who were seronegative (p<0.0001) (Table 2).

DNAmTL reliability and comparisons with qPCR or flow FISH TL

In 48 samples with blinded duplicate of MethylationEpic array data, the mean coefficient of variation (CV) of calculated DNAmTL was 1% (range= 0.08-3.1%). These blinded duplicate samples also had high DNAmTL correlation (r=0.93, p<0.0001).

Table 1. Characteristics of study participants.

Variable	Total (n=635) N (%)
Age	
19-24	118 (19%)
25-29	124 (19%)
30-34	96 (15%)
35-39	107 (17%)
40-44	91 (14%)
45-61	99 (16%)
Sex	
Male	425 (67%)
Female	210 (33%)
Race	
White	478 (75%)
African American	40 (6%)
Other	93 (15%)
Missing	24 (4%)
CMV serostatus	
Positive	239 (38%)
Negative	370 (58%)
Missing	26 (4%)
Telomere length (TL)	**Median (Range)**
DNAmTL (kb)	7.4 (6.6-8.4)
flow FISH TL (kb)[1]	7.0 (3.7-11.2)
qPCR (z-score)	-0.17 (-2.34-4.96)

[1]flow FISH TL was available for 144 participants. Abbreviations: CMV indicates cytomegalovirus; DNAmTL (kb) indicates DNA methylation-based estimator of telomere length in kilobases; flow FISH TL (kb) indicates lymphocyte telomere length measured by fluorescent *in situ* hybridization with flow cytometry in kilobases; qPCR (z-score) indicates calculated z-score of telomere length measured by quantitative polymerase chain reaction.

Comparison of the TL estimated by DNAmTL and measured by flow FISH in the 144 individuals with both measures showed a statistically significant difference (median 7.4 *vs.* 7 kb respectively, p<0.0001), and moderate correlation (r = 0.56, *p* <0.0001; Figure 2A). In the full cohort (N=635), predicted TL by DNAmTL and qPCR measured TL were also statistically significantly different (median z-score TL =0.05 *vs.* -0.17 standard deviations from the mean, respectively, p=0.03), and showed modest correlation (r=0.41, p<0.0001; Figure 2B). No statistically significant differences in the correlations between TL

from DNAmTL and qPCR were noted by sex (p-interaction=0.31), race (p-interaction=0.10), or age (p-interaction=0.11).

Bland Altman analysis of DNAmTL compared with flow FISH TL demonstrated a mean bias of 0.35 kb (standard deviation [SD]=1.86), and a wide limit of agreement (LoA = -1.51 to 2.21 kb). DNAmTL resulted in a narrower range of TL compared with flow FISH with overestimation of the shortest TL and underestimation of the longest (Figure 3A). The mean bias was 0.023 (SD= 1.09) for DNAmTL and qPCR TL (Figure 3B).

We then used classifier matrices to assess the agreement between DNAmTL or qPCR TL with that of flow FISH when categorized as long *versus* short based on the TL median. DNAmTL correctly classified 72% of the individuals as having long (TL above median) or short (TL below the median) with 77% sensitivity and 66% specificity, relative to flow FISH. Similarly, agreement between qPCR and flow FISH showed 79% accuracy, 79% sensitivity, and 79% specificity (Figure 4A, 4B). When the analysis was repeated to evaluate the ability
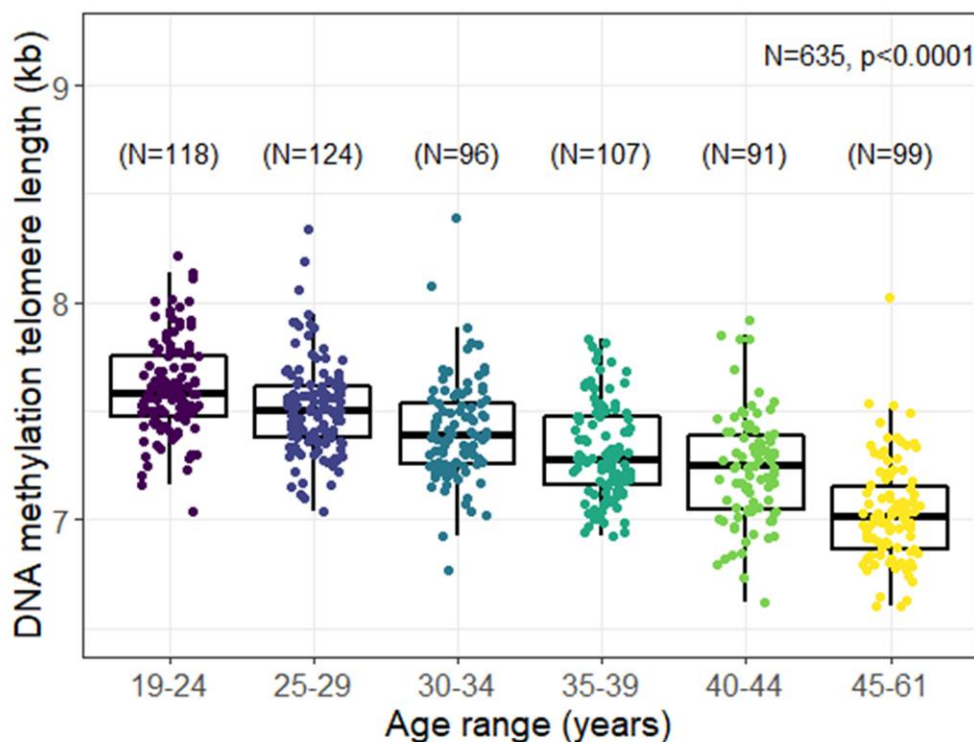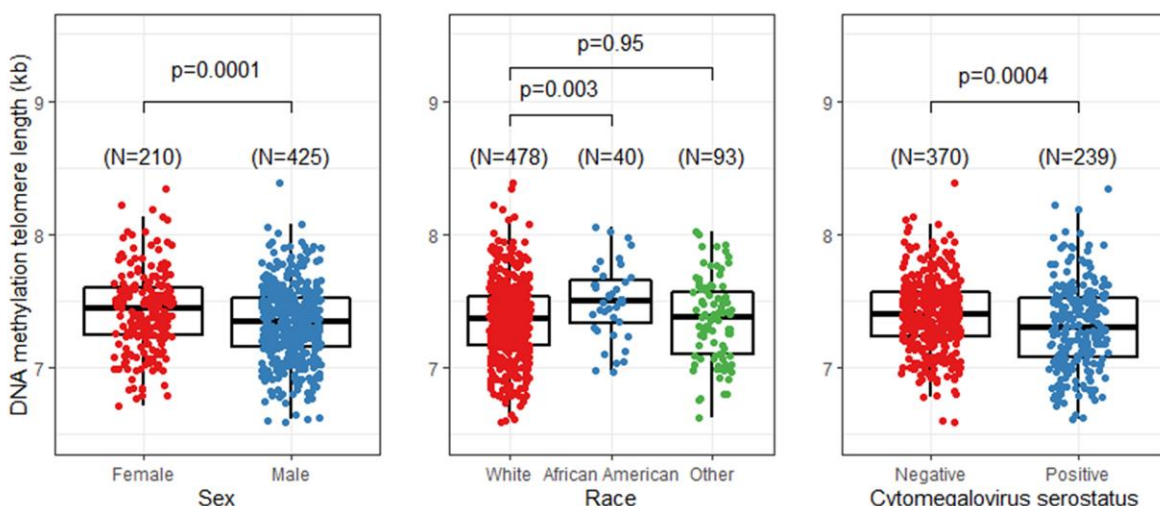
Figure 1. Unadjusted relationship between DNA methylation telomere length (DNAmTL) and selected participant characteristics. (**A**) DNAmTL by age categories. (**B**) DNAmTL by sex, race, or cytomegalovirus (CMV) serostatus.

Table 2. Adjusted associations between DNAmTL and selected participant characteristics.

Variables[1]	β	p-value
Age	-0.021	<0.0001
Sex		
Male	REF	
Female	0.116	<0.0001
Race		
White	REF	
African American	0.213	<0.0001
Other	0.010	0.68
CMV serostatus		
Negative	REF	
Positive	-0.083	<0.0001

[1]All variables in the table were included in the same model.
Abbreviation: CMV indicates cytomegalovirus.

of DNAmTL or qPCR to correctly classify TL in tertiles or quartiles, accuracy of both methods decreased. For DNAmTL, the TL accuracy for the tertile classifier=57%, and for the quartile classifier =42%. Similar results were noted with qPCR TL (tertile accuracy=67%, quartile accuracy=52%). Of note, both DNAmTL and qPCR TL showed highest agreement with flow FISH at the longest and shortest TL categories for both tertiles and quartiles.

DISCUSSION

In this study, we found that DNAmTL detected the expected variations in TL by age, sex, race, and CMV serostatus (a marker of chronic infection). However, its correlation with TL measured by flow FISH or qPCR was modest and the limits of measurement agreement were wide. On the binary scale, both DNAmTL and qPCR correctly classified approximately two-thirds of
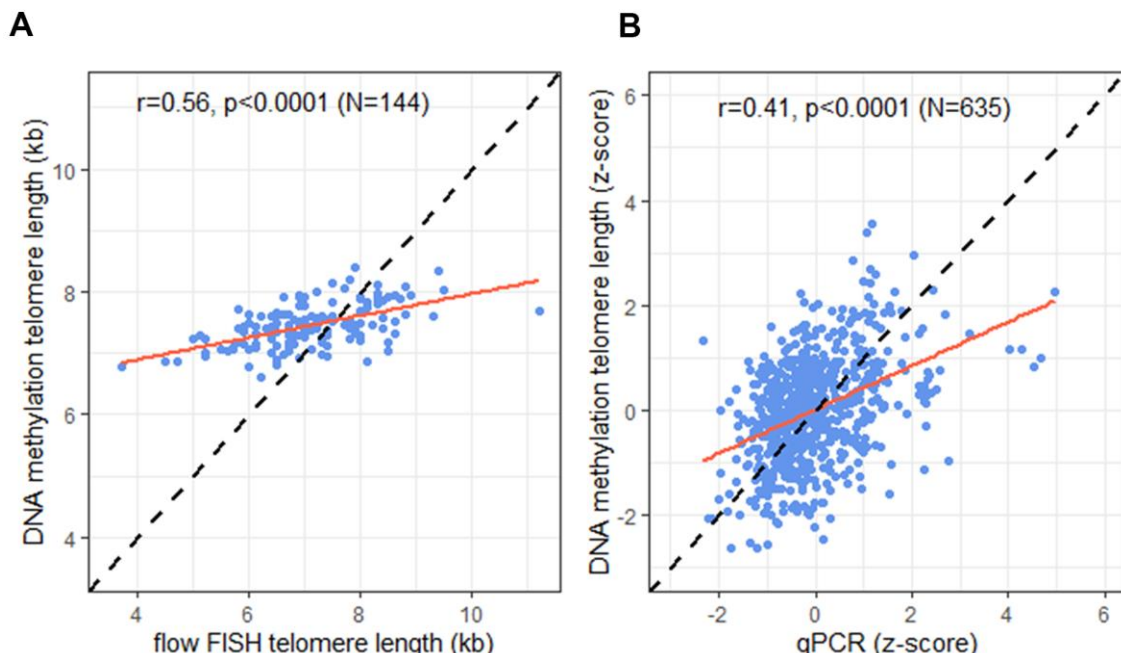
Figure 2. Correlation of telomere length (TL) measurement tools. (**A**) DNA methylation telomere length (DNAmTL) and flow FISH TL in kilobases (kb); (**B**) DNAmTL and qPCR in z-scores. Dashed line represents perfect agreement. Solid red line represents regression line.
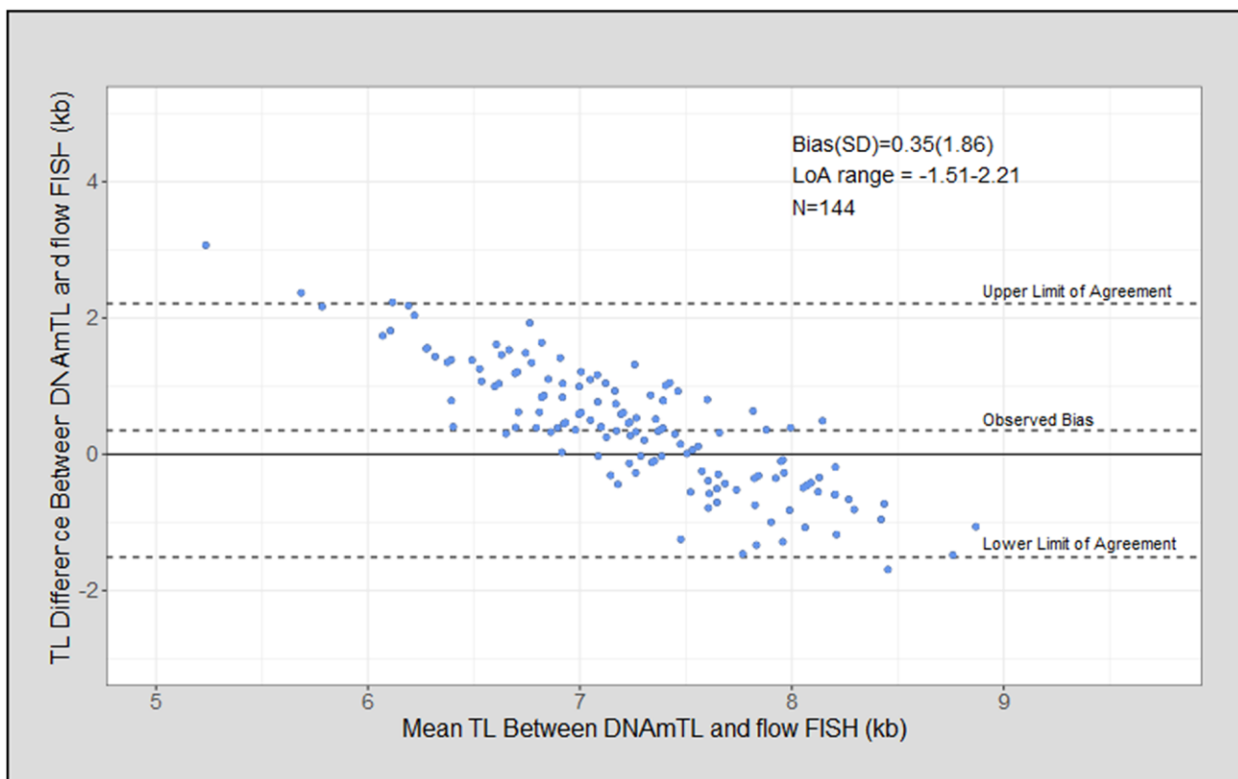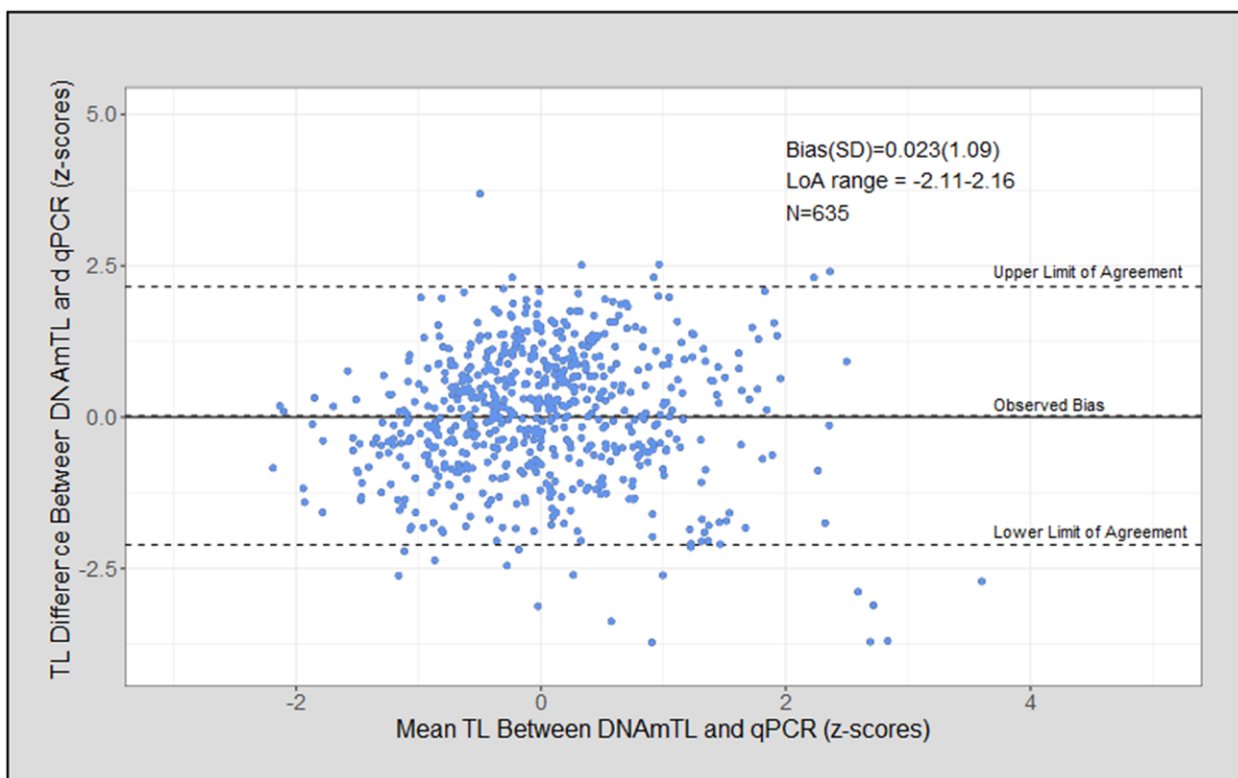
Figure 3. Telomere length (TL) measurement agreement between measurment tools. (**A**) DNA methylation telomere length (DNAmTL) and flow FISH in kilobases (kb); (**B**) DNAmTL and qPCR in z-scores.

the individuals into long or short TL (cutoff at the median) when tested against flow FISH. The accuracy of both methods declined when TL was classified into more than two categories. These results suggest there may be opportunities for using methylation array data to explore TL variability in large epidemiological studies but call for caution in directly comparing DNAmTL results with standard TL measurement methods because of its limited accuracy.

The current study showed a modest correlation between DNAmTL and flow FISH (r=0.56), or qPCR (r=0.41).
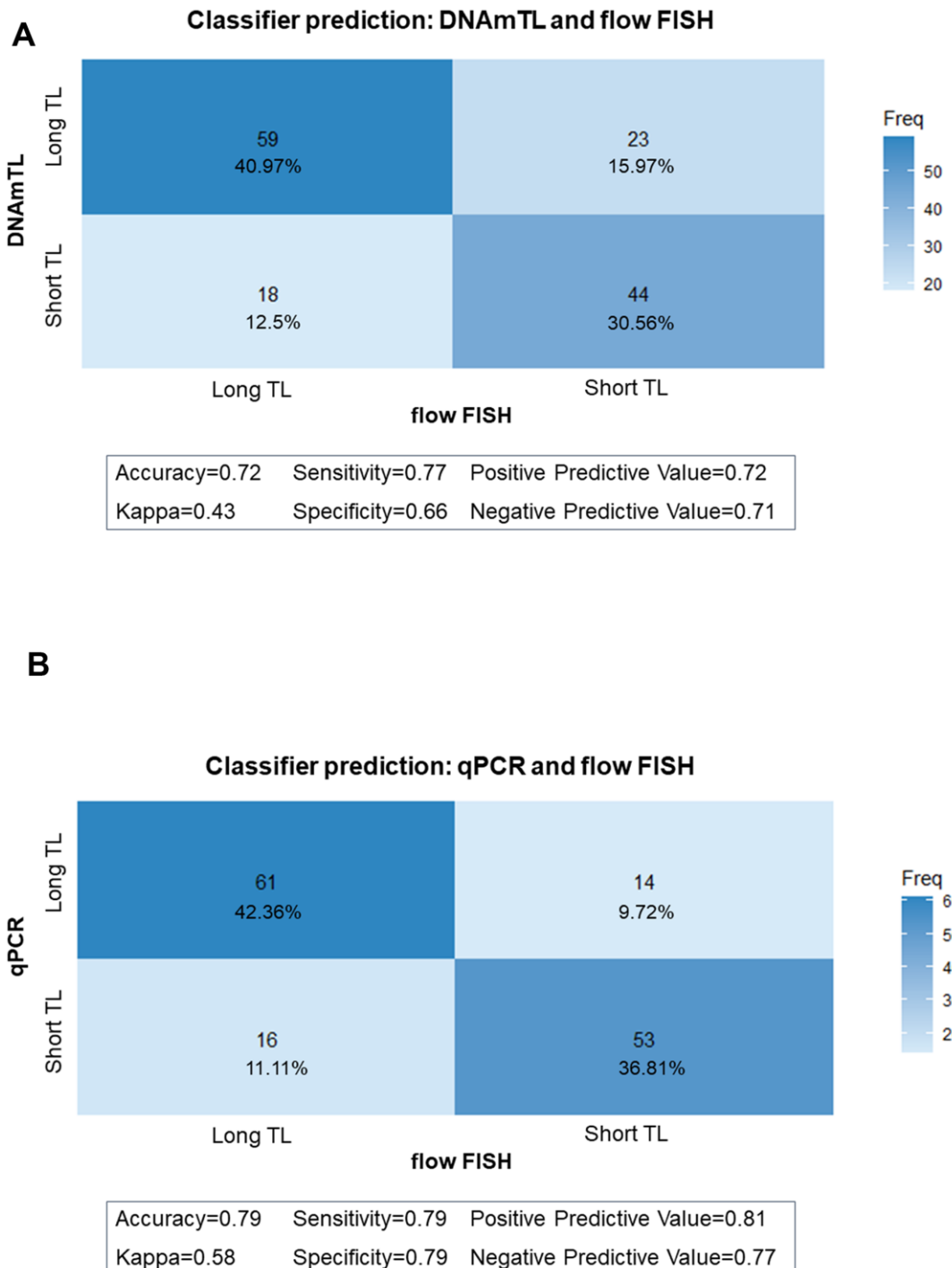
Figure 4. Classifier matrices comparing telomere length (TL) categories (above and below median). (**A**) between flow FISH and DNA methylation telomere length (DNAmTL); (**B**) between flow FISH and qPCR.

A previously published report showed a consistent correlation between DNAmTL and TRF (N of datasets=4, N of samples = 4788, range of r= 0.41- 0.5), but the correlation between DNAmTL and qPCR was variable (N of datasets=3, N of samples = 2136, range of r= -0.01-0.38) [22]. This may reflect the known lab-to-lab variation for qPCR TL assay or be affected by assay reproducibility. Here, we showed a mean CV for DNAmTL of 1% indicating a high reproducibility of TL estimates based on 48 replicates. A previous study showed a CV of 1.7% for TRF and >5% for qPCR [23].

In line with previous studies using the Bland Altman analysis comparing agreements between TL measurement methods [24–26], DNAmTL showed acceptable agreement with TL measured by qPCR (mean bias ± SD = 0.023 ± 1.09) or flow FISH assay (mean bias ± SD = 0.35 ± 1.86) with almost all observations falling within two standard deviations for the limits of agreement. However, the observed wide limits of agreement (*e.g.,* -1.51 to 2.21 kb in the flow FISH comparison) reflect a lack of accuracy that may limit the applicability of DNAmTL. When evaluating the ability of DNAmTL or qPCR to accurately categorize TL as compared with flow FISH, the study showed attenuated accuracy as the number of categories increased. This may highlight the importance of taking assay measurement error into account when calculating the minimum required sample size for new studies to be able to detect significant differences [27, 28].

Despite the modest correlation between DNAmTL and measured TL by evaluated assays, DNAmTL showed the expected negative TL-age correlation. Of note, the observed DNAmTL correlation with age was stronger (r= -0.64) than that reported with other TL measurement assays in this dataset (r = -0.30 for qPCR TL, and r= -0.33 for flow FISH TL) [25]. Additionally, in a meta-analysis of 124 cross-sectional and 5 longitudinal studies, the pooled TL-age correlation for TRF was r= -0.34 and for qPCR r= -0.29 [29]. On the other hand, comparisons of DNAmTL differences across age groups in the current cross-sectional study suggested that for every year increase in age, DNAmTL decreased by 21 bp. This is slightly lower than other methods in which a decrease of 30-60 bp per year was detected [30]. Notably, the majority of previous literature on TL dynamics also used a cross-sectional approach; longitudinal studies with serial samples are needed to address this question. DNAmTL also detected known TL relationships with sex, race [31, 32] and chronic infections [33, 34]. Of interest, DNAmTL in the current study detected greater TL differences by race and sex than those reported by TRF in a study including 1510 individuals (of whom 142 were African Americans and 888 were females) [35]. This may be influenced by sex- or race-specific methylation

differences [36]. Yet, it is also possible that the relatively small sample size of certain subgroups in our study may have resulted in imprecise estimates. DNAmTL also demonstrated the expected associations with BMI and smoking behavior in another study [22]. These observations, despite modest correlations with other methods, support that DNAmTL may be capturing a broader aspect of the biological processes underlying cellular aging than just telomere shortening. Previously reported *in vitro* examination of cultured somatic cells showed that DNAmTL captured cellular proliferation independent of telomere attrition and telomerase activity [22]. Therefore, more robust associations between DNAmTL and TL-related factors that may themselves be more strongly linked to cellular aging than to telomere shortening are biologically plausible and point to the utility of future studies of DNAmTL in capturing such variations.

The strengths of the current study included the availability of TL measurements from multiple assays allowing for a comprehensive comparison with the new DNAmTL estimator in a relatively large sample size of healthy individuals. Flow FISH data provided an accurate TL measurement comparison with DNAmTL, and qPCR data allowed us to compare DNAmTL to a method widely used in epidemiological studies. Our study was limited by the age range (19-61 years), so our estimates may not be generalizable to all ages. Additionally, our DNAmTL associations with TL-known factors were not adjusted for other possible confounders such as socioeconomic status, smoking, or BMI, due to lack of information. However, the association between these factors and TL is not firmly established [37–40]. In addition, the study population consisted of pre-screened, healthy, HCT donors, therefore these factors are unlikely to have significant effects on our results. Although we measured TL using several assays (flow FISH and qPCR), we were limited by the absence of TL measurement by TRF, the gold standard in TL research. Of note, a strong correlation between TL measured by flow FISH and TRF has been reported (R^2 = 0.73; p < 0.001) [41].

In conclusion, the results of this study suggest that DNAmTL holds promise as a method for approximating TL as long as its limitations are understood. In the current era of genomic data sharing there is an opportunity to use DNAmTL to explore different avenues of telomere and aging research using methylation data in the public domain. The sensitivity of DNAmTL in detecting known TL associations and its ability to approximate average TL suggest it may have utility in epidemiologic studies. However, because DNAmTL correlation and agreement with other methods is only modest, researchers should exercise caution when using DNAmTL in contexts where accuracy is of primary importance. Additional studies are

needed to better understand what specific aspects of cellular aging or telomere maintenance are being captured by DNAmTL.

MATERIALS AND METHODS

Study participants

The study participants were HCT donors in the TOAA project, a collaboration between NCI and CIBMTR [42]. Blood samples (frozen whole blood (N=416), or peripheral blood mononuclear cells (PBMC; N=219) collected before hematopoietic stem cell donation were available at the CIBMTR biorepository (https://www.cibmtr.org/Pages/index.aspx).

Telomere length measurement

For the flow FISH assay, total leukocytes were isolated from cryopreserved PBMCs. The fluorescence intensity in total lymphocytes and lymphocyte subsets, defined by labeled antibodies specific for CD20, CD45RA and CD57, relative to internal control cells and unstained controls were measured on a FACSCalibur instrument (Becton Dickinson) to calculate the median telomere length from duplicate measurements. For the present study, we analyzed TL measurements for total lymphocytes. More detailed description of flow FISH methods used in this study can be found elsewhere [42].

DNA for qPCR assays was extracted with the QIAamp Maxi Kit procedure (Qiagen, Inc., Valencia, CA). We used *Telo_RP* and *Telo_FP* primers (for the telomeric PCR) and *36B4_FP* and *36B4_RP* primers for the single-copy gene (36B4). Raw T/S ratio was standardized by dividing the raw ratio with the average T/S ratio of internal quality control (QC) calibrator samples. All samples were measured in triplicate and averages were used in the final calculations. More detailed description of the qPCR method used in this study can be found elsewhere [42]. qPCR analysis was completed in stages; to ensure comparability between TOAA sub-cohorts, we standardized TL based on the TL distribution within the sub-cohorts using z-scores $(Z = \frac{x-\mu}{\sigma})$ where X is the observed TL, μ is the mean TL, and σ is the TL standard deviation. Calculated z-score is interpreted as the number of standard deviations from the mean.

Prediction of telomere length using DNA methylation array data

For DNA methylation profiling, we used TOAA blood extracted DNA and the Illumina Infinium Methylation EPIC Bead™ array which covers more than 850,000 methylation sites across the genome. We excluded

samples where >4% of probes failed detection (n=2). Functional normalization was used to account for potential batch effects using the "minfi" R package. Forty-eight blinded duplicate samples included to assess within and across plate differences had a high concordance rate (Pearson's r ≥ 0.98). The Horvath DNAmTL was used for TL estimation as previously published [22]. In the original study, machine learning techniques were used to identify CpG sites (cytosine-phosphate-guanine dinucleotides) predictive of TRF-measured leukocyte TL; this resulted in the selection of 140 specific CpG sites using data from a diverse sample of 2,256 individuals. The use of linear regression models allowed for the transformation of DNA methylation levels to express TL predictions in kb.

Statistical analysis

We used Pearson's correlation coefficient to evaluate the strength of linear association between DNAmTL and other TL measurement methods (flow FISH, and qPCR). A multivariable linear regression model was used to assess the association between DNAmTL and participant characteristics (age, sex, race, and CMV serostatus). All tests were two-sided with statistical significance defined as p < 0.05.

Bland Altman analysis was used to assess agreement between TL measurement methods by studying the mean difference between the two methods and constructing limits of agreement (defined as area within two standard deviations of the mean difference). The Y-axis shows the measurement difference, and the X-axis represents the average of the two measures. Bias is estimated as the mean difference between TL measurements in each comparison, with the zero line representing perfect agreement [43]. We used a classifier matrix (also known as confusion matrix) to assess the ability of qPCR and DNAmTL to accurately classify categories of TL in comparison with flow FISH using the R package (caret). Performance metrics included accuracy, sensitivity, specificity, and negative and positive predictive values. Data analysis and visualization was performed using SAS® statistical software, version 9.4 and RStudio, version 1.3.959.

Data availability

Data from this study are available and can be shared after fulfilling data sharing requirements; all relevant data and methods are reported in the article.

AUTHOR CONTRIBUTIONS

Aubert, Casey L. Dagnall, Shilpa Katta, Steve Horvath, and Belynda Hicks. Statistical Analysis: Emily E. Pearce, Hormuzd Katki, and Rotana Alsaggaf. Data interpretation and manuscript drafting: Emily E. Pearce, Rotana Alsaggaf, Sharon A. Savage, and Shahinaz M. Gadalla. Manuscript critical review: All authors.

CONFLICTS OF INTEREST

FUNDING

REFERENCES

1. Blackburn EH. Structure and function of telomeres. Nature. 1991; 350:569–73.
   https://doi.org/10.1038/350569a0 PMID:1708110

2. Counter CM. The roles of telomeres and telomerase in cell life span. Mutat Res. 1996; 366:45–63.
   https://doi.org/10.1016/s0165-1110(96)90006-8 PMID:8921986

3. Feldser DM, Hackett JA, Greider CW. Telomere dysfunction and the initiation of genome instability. Nat Rev Cancer. 2003; 3:623–27.
   https://doi.org/10.1038/nrc1142 PMID:12894250

4. Aubert G, Lansdorp PM. Telomeres and aging. Physiol Rev. 2008; 88:557–79.
   https://doi.org/10.1152/physrev.00026.2007 PMID:18391173

5. Alter BP, Baerlocher GM, Savage SA, Chanock SJ, Weksler BB, Willner JP, Peters JA, Giri N, Lansdorp PM. Very short telomere length by flow fluorescence *in situ* hybridization identifies patients with dyskeratosis congenita. Blood. 2007; 110:1439–47.
   https://doi.org/10.1182/blood-2007-02-075598 PMID:17468339

6. Gadalla SM, Wang T, Haagenson M, Spellman SR, Lee SJ, Williams KM, Wong JY, De Vivo I, Savage SA. Association between donor leukocyte telomere length and survival after unrelated allogeneic hematopoietic cell transplantation for severe aplastic anemia. JAMA. 2015; 313:594–602.
   https://doi.org/10.1001/jama.2015.7 PMID:25668263

7. Gadalla SM, Aubert G, Wang T, Haagenson M, Spellman SR, Wang L, Katki HA, Savage SA, Lee SJ. Donor telomere length and causes of death after unrelated hematopoietic cell transplantation in patients with marrow failure. Blood. 2018; 131:2393–98.
   https://doi.org/10.1182/blood-2017-10-812735 PMID:29632022

8. Alder JK, Hanumanthu VS, Strong MA, DeZern AE, Stanley SE, Takemoto CM, Danilova L, Applegate CD, Bolton SG, Mohr DW, Brodsky RA, Casella JF, Greider CW, et al. Diagnostic utility of telomere length testing in a hospital-based setting. Proc Natl Acad Sci USA. 2018; 115:E2358–65.
   https://doi.org/10.1073/pnas.1720427115 PMID:29463756

9. Baird DM. New developments in telomere length analysis. Exp Gerontol. 2005; 40:363–68.
   https://doi.org/10.1016/j.exger.2005.02.008 PMID:15919587

10. Aubert G, Hills M, Lansdorp PM. Telomere length measurement-caveats and a critical assessment of the available technologies and tools. Mutat Res. 2012; 730:59–67.
    https://doi.org/10.1016/j.mrfmmm.2011.04.003 PMID:21663926

11. Kimura M, Stone RC, Hunt SC, Skurnick J, Lu X, Cao X, Harley CB, Aviv A. Measurement of telomere length by the Southern blot analysis of terminal restriction fragment lengths. Nat Protoc. 2010; 5:1596–607.
    https://doi.org/10.1038/nprot.2010.124 PMID:21085125

12. Baerlocher GM, Vulto I, de Jong G, Lansdorp PM. Flow cytometry and FISH to measure the average length of telomeres (flow FISH). Nat Protoc. 2006; 1:2365–76.

https://doi.org/10.1038/nprot.2006.263
PMID:17406480

13. Cawthon RM. Telomere measurement by quantitative PCR. Nucleic Acids Res. 2002; 30:e47.
https://doi.org/10.1093/nar/30.10.e47
PMID:12000852

14. Cawthon RM. Telomere length measurement by a novel monochrome multiplex quantitative PCR method. Nucleic Acids Res. 2009; 37:e21.
https://doi.org/10.1093/nar/gkn1027 PMID:19129229

15. Dagnall CL, Hicks B, Teshome K, Hutchinson AA, Gadalla SM, Khincha PP, Yeager M, Savage SA. Effect of pre-analytic variables on the reproducibility of qPCR relative telomere length measurement. PLoS One. 2017; 12:e0184098.
https://doi.org/10.1371/journal.pone.0184098
PMID:28886139

16. Baird DM, Rowson J, Wynford-Thomas D, Kipling D. Extensive allelic variation and ultrashort telomeres in senescent human cells. Nat Genet. 2003; 33:203–07.
https://doi.org/10.1038/ng1084 PMID:12539050

17. Lai TP, Zhang N, Noh J, Mender I, Tedone E, Huang E, Wright WE, Danuser G, Shay JW. A method for measuring the distribution of the shortest telomeres in cells and tissues. Nat Commun. 2017; 8:1356.
https://doi.org/10.1038/s41467-017-01291-z
PMID:29116081

18. Ding Z, Mangino M, Aviv A, Spector T, Durbin R, and UK10K Consortium. Estimating telomere length from whole genome sequence data. Nucleic Acids Res. 2014; 42:e75.
https://doi.org/10.1093/nar/gku181 PMID:24609383

19. Buxton JL, Suderman M, Pappas JJ, Borghol N, McArdle W, Blakemore AI, Hertzman C, Power C, Szyf M, Pembrey M. Human leukocyte telomere length is associated with DNA methylation levels in multiple subtelomeric and imprinted loci. Sci Rep. 2014; 4:4954.
https://doi.org/10.1038/srep04954 PMID:24828261

20. Gadalla SM, Katki HA, Shebl FM, Giri N, Alter BP, Savage SA. The relationship between DNA methylation and telomere length in dyskeratosis congenita. Aging Cell. 2012; 11:24–28.
https://doi.org/10.1111/j.1474-9726.2011.00755.x
PMID:21981348

21. Fraga MF, Agrelo R, Esteller M. Cross-talk between aging and cancer: the epigenetic language. Ann N Y Acad Sci. 2007; 1100:60–74.
https://doi.org/10.1196/annals.1395.005
PMID:17460165

22. Lu AT, Seeboth A, Tsai PC, Sun D, Quach A, Reiner AP, Kooperberg C, Ferrucci L, Hou L, Baccarelli AA, Li Y,

Harris SE, Corley J, et al. DNA methylation-based estimator of telomere length. Aging (Albany NY). 2019; 11:5895–923.
https://doi.org/10.18632/aging.102173
PMID:31422385

23. Aviv A, Hunt SC, Lin J, Cao X, Kimura M, Blackburn E. Impartial comparative analysis of measurement of leukocyte telomere length/DNA content by Southern blots and qPCR. Nucleic Acids Res. 2011; 39:e134.
https://doi.org/10.1093/nar/gkr634 PMID:21824912

24. Behrens YL, Thomay K, Hagedorn M, Ebersold J, Henrich L, Nustede R, Schlegelberger B, Göhring G. Comparison of different methods for telomere length measurement in whole blood and blood cell subsets: Recommendations for telomere length measurement in hematological diseases. Genes Chromosomes Cancer. 2017; 56:700–08.
https://doi.org/10.1002/gcc.22475 PMID:28593741

25. Wang Y, Savage SA, Alsaggaf R, Aubert G, Dagnall CL, Spellman SR, Lee SJ, Hicks B, Jones K, Katki HA, Gadalla SM. Telomere Length Calibration from qPCR Measurement: Limitations of Current Method. Cells. 2018; 7:183.
https://doi.org/10.3390/cells7110183 PMID:30352968

26. Gutierrez-Rodrigues F, Santana-Lemos BA, Scheucher PS, Alves-Paiva RM, Calado RT. Direct comparison of flow-FISH and qPCR as diagnostic tests for telomere length measurement in humans. PLoS One. 2014; 9:e113747.
https://doi.org/10.1371/journal.pone.0113747
PMID:25409313

27. Devine OJ, Smith JM. Estimating sample size for epidemiologic studies: the impact of ignoring exposure measurement uncertainty. Stat Med. 1998; 17:1375–89.
https://doi.org/10.1002/(sici)1097-0258(19980630)17:12<1375::aid-sim857>3.0.co;2-d
PMID:9682326

28. Lindrose AR, McLester-Davis LW, Tristano RI, Kataria L, Gadalla SM, Eisenberg DT, Verhulst S, Drury S. Method comparison studies of telomere length measurement using qPCR approaches: A critical appraisal of the literature. PLoS One. 2021; 16:e0245582.
https://doi.org/10.1371/journal.pone.0245582
PMID:33471860

29. Müezzinler A, Zaineddin AK, Brenner H. A systematic review of leukocyte telomere length and age in adults. Ageing Res Rev. 2013; 12:509–19.
https://doi.org/10.1016/j.arr.2013.01.003
PMID:23333817

30. Steenstrup T, Kark JD, Verhulst S, Thinggaard M, Hjelmborg JV, Dalgård C, Kyvik KO, Christiansen L,

Mangino M, Spector TD, Petersen I, Kimura M, Benetos A, et al. Telomeres and the natural lifespan limit in humans. Aging (Albany NY). 2017; 9:1130–42.
https://doi.org/10.18632/aging.101216
PMID:28394764

31. Dalgård C, Benetos A, Verhulst S, Labat C, Kark JD, Christensen K, Kimura M, Kyvik KO, Aviv A. Leukocyte telomere length dynamics in women and men: menopause vs age effects. Int J Epidemiol. 2015; 44:1688–95.
https://doi.org/10.1093/ije/dyv165 PMID:26385867

32. Brown L, Needham B, Ailshire J. Telomere Length Among Older U.S. Adults: Differences by Race/Ethnicity, Gender, and Age. J Aging Health. 2017; 29:1350–66.
https://doi.org/10.1177/0898264316661390
PMID:27469599

33. Dowd JB, Bosch JA, Steptoe A, Jayabalasingham B, Lin J, Yolken R, Aiello AE. Persistent Herpesvirus Infections and Telomere Attrition Over 3 Years in the Whitehall II Cohort. J Infect Dis. 2017; 216:565–72.
https://doi.org/10.1093/infdis/jix255 PMID:28931225

34. Asghar M, Hasselquist D, Hansson B, Zehtindjiev P, Westerdahl H, Bensch S. Chronic infection. Hidden costs of infection: chronic malaria accelerates telomere degradation and senescence in wild birds. Science. 2015; 347:436–38.
https://doi.org/10.1126/science.1261121
PMID:25613889

35. Lynch SM, Peek MK, Mitra N, Ravichandran K, Branas C, Spangler E, Zhou W, Paskett ED, Gehlert S, DeGraffinreid C, Rebbeck TR, Riethman H. Race, Ethnicity, Psychosocial Factors, and Telomere Length in a Multicenter Setting. PLoS One. 2016; 11:e0146723.
https://doi.org/10.1371/journal.pone.0146723
PMID:26752285

36. Zhang FF, Cardarelli R, Carroll J, Fulda KG, Kaur M, Gonzalez K, Vishwanatha JK, Santella RM, Morabia A. Significant differences in global genomic DNA methylation by gender and race/ethnicity in peripheral blood. Epigenetics. 2011; 6:623–29.
https://doi.org/10.4161/epi.6.5.15335 PMID:21739720

37. Robertson T, Batty GD, Der G, Fenton C, Shiels PG, Benzeval M. Is socioeconomic status associated with biological aging as measured by telomere length? Epidemiol Rev. 2013; 35:98–111.

https://doi.org/10.1093/epirev/mxs001
PMID:23258416

38. Needham BL, Adler N, Gregorich S, Rehkopf D, Lin J, Blackburn EH, Epel ES. Socioeconomic status, health behavior, and leukocyte telomere length in the National Health and Nutrition Examination Survey, 1999-2002. Soc Sci Med. 2013; 85:1–8.
https://doi.org/10.1016/j.socscimed.2013.02.023
PMID:23540359

39. Mundstock E, Sarria EE, Zatti H, Mattos Louzada F, Kich Grun L, Herbert Jones M, Guma FT, Mazzola In Memoriam J, Epifanio M, Stein RT, Barbé-Tuana FM, Mattiello R. Effect of obesity on telomere length: Systematic review and meta-analysis. Obesity (Silver Spring). 2015; 23:2165–74.
https://doi.org/10.1002/oby.21183
PMID:26407932

40. Astuti Y, Wardhana A, Watkins J, Wulaningsih W, and PILAR Research Network. Cigarette smoking and telomere length: A systematic review of 84 studies and meta-analysis. Environ Res. 2017; 158:480–89.
https://doi.org/10.1016/j.envres.2017.06.038
PMID:28704792

41. Khincha PP, Dagnall CL, Hicks B, Jones K, Aviv A, Kimura M, Katki H, Aubert G, Giri N, Alter BP, Savage SA, Gadalla SM. Correlation of Leukocyte Telomere Length Measurement Methods in Patients with Dyskeratosis Congenita and in Their Unaffected Relatives. Int J Mol Sci. 2017; 18:1765.
https://doi.org/10.3390/ijms18081765
PMID:28805708

42. Gadalla SM, Wang T, Dagnall C, Haagenson M, Spellman SR, Hicks B, Jones K, Katki HA, Lee SJ, Savage SA. Effect of Recipient Age and Stem Cell Source on the Association between Donor Telomere Length and Survival after Allogeneic Unrelated Hematopoietic Cell Transplantation for Severe Aplastic Anemia. Biol Blood Marrow Transplant. 2016; 22:2276–82.
https://doi.org/10.1016/j.bbmt.2016.09.012
PMID:27641680

43. Bland JM, Altman DG. Statistical methods for assessing agreement between two methods of clinical measurement. Lancet. 1986; 1:307–10.
PMID:2868172

Epigenetic mutation load is weakly correlated with epigenetic age acceleration

Qi Yan[1], Kimberly C. Paul[1], Ake T. Lu[2], Cynthia Kusters[1], Alexandra M. Binder[1,3], Steve Horvath[2,4], Beate Ritz[1,5]

[1]Department of Epidemiology, UCLA Fielding School of Public Health, Los Angeles, CA 90095, USA
[2]Department of Human Genetics, David Geffen School of Medicine, University of California Los Angeles, Los Angeles, CA 90095, USA
[3]Population Sciences in the Pacific Program (Cancer Epidemiology), University of Hawaii Cancer Center, University of Hawaii at Manoa, Honolulu, HI 96813, USA
[4]Department of Biostatistics, Fielding School of Public Health, University of California Los Angeles, Los Angeles, CA 90095, USA
[5]Department of Neurology, UCLA School of Medicine, Los Angeles, CA 90095, USA

ABSTRACT

DNA methylation (DNAm) age estimators are widely used to study aging-related conditions. It is not yet known whether DNAm age is associated with the accumulation of stochastic epigenetic mutations (SEMs), which reflect dysfunctions of the epigenetic maintenance system. Here, we defined epigenetic mutation load (EML) as the total number of SEMs per individual. We assessed associations between EML and DNAm age acceleration estimators using biweight midcorrelations in four population-based studies (total n = 6,388). EML was not only positively associated with chronological age (meta r = 0.171), but also with four measures of epigenetic age acceleration: the Horvath pan tissue clock, intrinsic epigenetic age acceleration, the Hannum clock, and the GrimAge clock (meta-analysis correlation ranging from r = 0.109 to 0.179). We further conducted pathway enrichment analyses for each participant's SEMs. The enrichment result demonstrated the stochasticity of epigenetic mutations, meanwhile implicated several pathways: signaling, neurogenesis, neurotransmitter, glucocorticoid, and circadian rhythm pathways may contribute to faster DNAm age acceleration. Finally, investigating genomic-region specific EML, we found that EMLs located within regions of transcriptional repression (TSS1500, TSS200, and 1stExon) were associated with faster age acceleration. Overall, our findings suggest a role for the accumulation of epigenetic mutations in the aging process.

INTRODUCTION

Epigenetic changes are an important hallmark of aging [1–3]. DNA methylation analysis provided promising molecular biomarkers of aging [4], with several epigenetic aging clocks having been introduced and used by aging researchers in recent years [5–12]. Age-adjusted epigenetic age estimates (referred to as epigenetic age acceleration) have been linked to a large number of age-related conditions [6, 7, 13–20].

Here we set out to investigate whether DNAm clocks possibly capture any dysfunction of the epigenetic maintenance system (EMS) of a cell [5, 13, 21]. Age is known to greatly increase the variability of DNA methylation levels and the epigenetic profiles of

monozygotic twins diverge considerably with age [22, 23]. Gentilini et al [24] proposed that stochastic epigenetic mutations (SEMs) increase exponentially with chronological age. The association of SEMs and aging was for the first time longitudinally assessed in the Swedish twin cohort [25] which confirmed that epigenetic mutations accumulate with age in an individual. In addition, SEMs have recently been associated with hepatocellular carcinoma staging [26], exposure to endocrine-disrupting compounds [27], socioeconomic position, and lifestyle factors [28]. Despite extensive research in this field, to our knowledge, most previous studies focused on chronological age rather than epigenetic age and epigenetic age acceleration. One study found SEM counts to be positively associated with epigenetic age acceleration based on both the Horvath and Hannum clocks [27]. Another recent study focused on Hannum, GrimAge, and intrinsic epigenetic age estimators within the Generation Scotland and the Lothian Birth Cohort, and reported positive associations between SEM counts and all three epigenetic age measurements [29]. To address the complexity of the aging process and the biological mechanisms underlying different epigenetic clocks, it may be useful to systematically study multiple clocks at the same time. In addition, biologic pathway enrichment analysis may help us gain an understanding of the pathophysiology of accelerated aging.

We pooled four population-based studies (total n = 6,388) to systematically investigate whether SEM counts are associated with epigenetic age acceleration. We included four DNAm aging clocks that represent different manifestations of the epigenetic aging processes, including: the pan-tissue chronological age estimator by Horvath (2013, Horvath clock) [5]; an intrinsic epigenetic age measure derived from the Horvath clock by additionally regressing out cell compositions (intrinsic clock) [30]; the leukocyte-based chronological age estimator by Hannum et al. (2013, Hannum clock) [11]; and the epigenetic mortality risk predictor developed recently by Lu et al. (2019, GrimAge clock) [7]. Age-adjusted versions of these biomarkers are generally being referred to as measures of epigenetic age acceleration and denoted as AgeAccelHorvath, intrinsic epigenetic age acceleration (IEAA), AgeAccelHannum, and AgeAccelGrim, respectively. We also coined the new term "epigenetic mutation load (EML)" as representing the total number of SEMs observed for each individual. In this article, we will 1) relate EML to different epigenetic age acceleration measures; 2) functionally annotate mutated CpG sites; 3) conduct biological pathway enrichment analysis; 4) relate DNA region-specific EMLs to epigenetic measures of age acceleration; and 5) compare SEMs with the Shannon entropy measure as the latter

can be interpreted as alternative measure for the decline of epigenetic maintenance.

RESULTS

Study population demographics

Our study includes 6,388 individuals from 4 studies: the Framingham Heart Study (FHS) Offspring Cohort, the Women's Health Initiative (WHI), the Jackson Heart Study (JHS), and the Parkinson's Environment and Genes (wave 1) known as the PEG1 study.

The main characteristics of the study populations are shown in Table 1. Briefly, FHS provided data for 2,326 individuals, with nearly half of them male (n = 1077; 46%) and all are white. Of the 2,091 female participants from the WHI, 989 (47%) are non-Hispanic white, 431 (21%) Hispanic, and 671 (32%) African American. JHS investigated 1,734 African American individuals with a majority of female participants (n = 1086; 63%). The 237 PEG1 control study participants were mostly non-Hispanic white (n = 207; 87%), and half were male (n = 126; 53%). The age ranges varied with the JHS having the largest range (22-93; mean = 56.2), and WHI the smallest (50-80; mean = 65.4). Mean ages of all populations ranged between 56.2 and 67.4. Additional details on cohorts and participant characteristics can be found in the Methods.

Epigenetic mutation load is the number of SEMs

All DNA methylation data was extracted from blood samples with the Illumina Infinium platform (450K array for PEG1, FHS, and WHI studies; EPIC array for WHI). Following a published and validated approach [24, 26, 31], a SEM is observed for a given person at a specific CpG site if an individual's methylation level is more than three times the interquartile range (IQR) lower than the 25th percentile ($Q1 - 3 \times IQR$), or more than three times the IQR higher than the 75th percentile ($Q3 + 3 \times IQR$). The 25th and 75th percentile, and correspondingly the IQR, for each CpG locus was estimated across all samples. Furthermore, we defined the epigenetic mutation load (EML) of each study participant according to the total number of SEMs.

EML was highly variable across people (Supplementary Table 1), with a mean value ranging from 1647 to 3401 depending on the total number of CpGs measured on different arrays (FHS: 2433; WHI: 1647; JHS: 3401; PEG1: 2137). Since EMLs were not normally distributed, natural log-transformed EML values were used in all analyses.

EML was not associated with microarray slides (ANOVA $p = 0.135$) or position on the array (ANOVA

Table 1. Distribution of demographics and DNAm aging clocks.

	FHS (n = 2326)	WHI (n= 2091)	JHS (n= 1734)	PEG 1 (n = 237)
Age				
Min	40	50	22	35
Max	92	80	93	92
Mean (SD)	66.36 (8.94)	65.34 (7.10)	56.21 (12.30)	67.42 (12.82)
Sex				
Male (%)	1,077 (46)	0 (0)	648 (37)	126 (53)
Female (%)	1,249 (54)	2,091 (100)	1,086 (63)	111 (47)
Race/Ethnicity				
White (%)	2,326 (100)	989(47)	0 (0)	207 (87)
Hispanic (%)	0 (0)	431 (21)	0 (0)	19 (8)
African American (%)	0 (0)	671 (32)	1734 (100)	0 (0)
Native American (%)	0 (0)	0 (0)	0 (0)	11 (5)
AgeAccelHorvath				
Min	-16.03	-22.56	-16.57	-13.44
Median	-0.38	-0.07	-0.07	-0.13
Max	41.62	29.35	22.81	22.98
Mean (SD)	-0.08 (4.81)	0.10 (5.18)	0.04 (4.45)	0.00 (5.31)
IEAA				
Min	-21.83	-21.46	-15.67	-12.17
Median	-0.17	-0.05	0.07	-0.13
Max	26.93	24.89	22.40	20.28
Mean (SD)	-0.03 (4.59)	0.02 (4.88)	0.05 (4.34)	0.00 (4.92)
AgeAccelHannum				
Min	-19.25	-19.50	-11.59	-12.92
Median	-0.18	0.02	-0.15	-0.27
Max	27.97	18.19	19.35	12.53
Mean (SD)	-0.02 (4.83)	0.02 (4.80)	0.03 (3.49)	0.00 (4.42)
AgeAccelGrim				
Min	-10.92	-10.03	-13.66	-8.74
Median	-0.76	-0.47	-0.81	-0.64
Max	22.51	16.35	24.94	14.62
Mean (SD)	0.02 (4.86)	0.01 (3.80)	0.01 (4.81)	0.00 (4.50)

p = 0.458). Also, EML was not correlated with the average intensity of bisulfite conversion controls (Pearson r = -0.085, p = 0.194). Thus, we concluded that the EML was independent of batches or other technical aspects.

Correlations among DNAm aging clocks

We calculated all DNAm aging estimators including the Horvath clock, the Hannum clock, the GrimAge clock, the PhenoAge clock, the SkinBlood clock, as well as an epigenetic estimate of telomere length (DNAmTL) using the online DNA Methylation Age Calculator (https://dnamage.genetics.ucla.edu/).

As expected, chronological age was strongly positively correlated with all epigenetic age estimators (Pearson r ranging from 0.79 to 0.93, Supplementary Figure 1), and these aging clocks were also strongly correlated with each other (Pearson r ranging from 0.73 to 0.90,

Supplementary Figure 1). Meanwhile, the epigenetic estimate of telomere length, DNAmTL, was negatively correlated with chronological age and the epigenetic age estimates (Pearson r ranging from -0.63 to -0.72, Supplementary Figure 1).

For each clock, we calculated DNA methylation-based age acceleration based on the residuals of the regression of DNA methylation age on each participants' chronological age. Thus, due to this approach, none of the epigenetic measures of age accelerations are correlated with chronological age (Pearson r = 0) as can be seen from Figure 1 and Supplementary Figure 2. AgeAccelHorvath is highly correlated (Pearson r = 0.93) with IEAA because both are based on the Horvath pan tissue clock. AgeAccelHannum was moderately associated with both AgeAccelHorvath and IEAA (Pearson r = 0.48 and 0.4 respectively). AgeAccelGrim showed only weak correlations with the other epigenetic measures of age acceleration which reflects the fact that

GrimAge clock is a mortality risk predictor as opposed to an age estimator. Overall, the moderate pairwise correlations between the DNAm based biomarkers reflect different properties: some are highly confounded by blood cell composition and capture immunosenescence (Hannum, GrimAge, DNAmTL) while others are not (Horvath pan tissue, IEAA) [13, 32].

Association between EML and DNAm aging clocks

We estimated the association between EML, chronological age, cell composition, and DNAm age acceleration using biweight midcorrelation (bicor) for each dataset separately and calculated pooled statistics using Stouffer's method. Bicor is a median-based measurement of correlation that is robust to outliers [33]. We adjusted for potential confounders including age, sex,

race/ethnicity, and cell compositions (naïve CD8 cells, CD8+CD28-CD45RA- T cells, Plasma Blasts, CD4 T cells, and Granulocytes) by regressing out the effects of these factors and retaining the residuals only for analysis. Results for AgeAccelHorvath, IEAA, AgeAccelHannum, and AgeAccelGrim are shown in Table 2 and Figure 2, while other clocks can be found in Supplementary Table 2. These analyses show that EML per study participant was positively correlated with chronological age (meta r = 0.171, meta P-value = 1.64E-42). Furthermore, EML was negatively correlated with CD4+ T cells (meta r = -0.121, meta P-value = 4.24E-22), plasmablasts (meta r = -0.085, meta P-value = 1.14E-11), and granulocytes (meta r = -0.064, meta P-value = 3.70E-07), but positively with exhausted CD8+ (defined as CD8+CD28-CD45RA-) T cells. These results are consistent with known age-related changes in blood cell composition [34, 35].
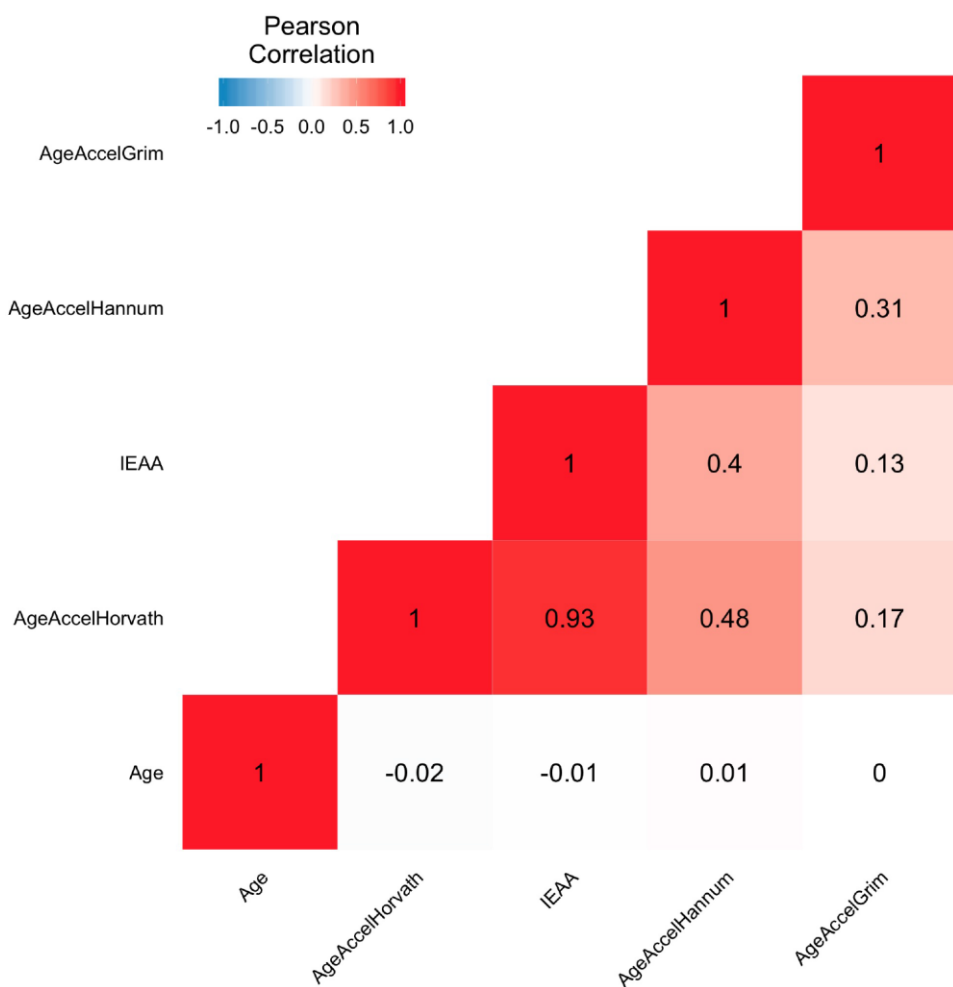
Figure 1. Heatmap of pairwise correlations of chronological age and epigenetic age accelerations. The heat map color-codes the pairwise Pearson correlations of chronological age and epigenetic age accelerations in the Framingham Heart Study (N=2326). Age represents the chronological age. AgeAccelHorvath, IEAA, AgeAccelHannum, and AgeAccelGrim represent measures of epigenetic age acceleration derived from the Horvath pan tissue clock, the intrinsic clock, the Hannum clock, and the GrimAge clock, respectively. The shades of color (blue, white, and red) visualize correlation values from -1 to 1. Each square reports a Pearson correlation coefficient.

Table 2. Biweight midcorrelation analysis of EML.

Outcome = log(EML) [**]	Meta [*]		FHS (n = 2326)		WHI (n= 2091)		JHS (n= 1734)		PEG 1 (n = 237)	
	Meta r	Meta P_value	Bicor r	P_value	Bicor r	P_value	Bicor r	P_value	Bicor r	P_value
Age	0.171	1.64E-42	0.244	7.15E-33	0.104	1.73E-06	0.145	1.50E-09	0.176	6.45E-03
DNAm Age Acceleration										
AgeAccelHorvath	0.109	3.25E-18	0.106	3.11E-07	0.140	1.34E-10	0.079	9.68E-04	0.071	2.75E-01
IEAA	0.112	4.04E-19	0.109	1.26E-07	0.144	3.85E-11	0.080	8.50E-04	0.073	2.63E-01
AgeAccelHannum	0.179	2.43E-46	0.225	4.12E-28	0.156	6.55E-13	0.148	6.33E-10	0.095	1.46E-01
AgeAccelGrim	0.162	2.25E-38	0.173	3.74E-17	0.180	9.91E-17	0.111	3.46E-06	0.224	5.23E-04
Cell types										
CD8.naive	-0.021	9.19E-02	-0.072	5.20E-04	0.020	3.66E-01	-0.011	6.58E-01	0.042	5.23E-01
CD8pCD28nCD45RAn	0.077	9.23E-10	0.085	3.90E-05	0.086	8.16E-05	0.052	2.88E-02	0.082	2.07E-01
PlasmaBlast	-0.085	1.14E-11	-0.054	8.94E-03	-0.070	1.39E-03	-0.140	4.89E-09	-0.110	9.23E-02
CD4T	-0.121	4.24E-22	-0.146	1.68E-12	-0.113	2.17E-07	-0.096	6.79E-05	-0.118	6.95E-02
Gran	-0.064	3.70E-07	-0.075	2.72E-04	-0.016	4.74E-01	-0.091	1.60E-04	-0.170	8.67E-03

[*]Meta-analysis using Stouffer's method with weights given by the square root of the number of (non-missing) samples in each data set.
[**]Adjusted for Age, Sex, Race/ethnicity, Cell types.

EML was also positively correlated with AgeAccelHorvath, IEAA, AgeAccelHannum, and AgeAccelGrim, with AgeAccelHannum exhibiting the strongest correlation (meta r = 0.179; meta P-value = 2.43E-46).

We further distinguished between epigenetic age acceleration and deceleration to determine correlations with EML. The correlation between EML and age acceleration was largely the same as what we presented originally. Interestingly, the correlation between EML and age deceleration was much smaller in size and less statistically significant (see Supplementary Table 3).

Sensitivity analyses

We evaluated associations between EML, chronological age, cell compositions, and age accelerations in males and females separately (Supplementary Table 4). For both sexes, EML remained positively correlated with chronological age, exhausted CD8+ T cells, and age acceleration suggesting that EML and age acceleration are independent of sex.

Several sensitivity analyses were conducted to ensure the reliability and reproducibility of the observed associations. To address a possibly non-linear relationship between epigenetic aging and chronological age, we additionally adjusted for a square term in age, (age^2, Supplementary Table 5). Also, to assess the potential for additional confounding, we adjusted for body mass index (Supplementary Table 6). This led to qualitatively similar results.

In order to explore whether the criteria used to define SEM will change results, we conducted another sensitivity analysis using two new SEM measures: 1)

loose SEM: defined as a specific CpG site with its methylation level exceeding two times the interquartile range (IQR) of the first quartile ($Q1 - 2 \times IQR$) or the third quartile ($Q3 + 2 \times IQR$) across all subjects; and 2) stringent SEM: defined as a specific CpG site with its methylation level exceeding four times the interquartile range (IQR) of the first quartile ($Q1 - 4 \times IQR$) or the third quartile ($Q3 + 4 \times IQR$) across all subjects. We then calculated the total number of SEMs according to the loose and stringent definition for each person (loose or stringent EML, respectively). The biweight midcorrelations between loose or stringent EMLs and measures of epigenetic age accelerations were very similar to the original results (Supplementary Table 7).

We also explored the effect of different normalization methods for the methylation data (Illumina background correction, functional normalization, Noob, and quantile normalization). We found that the association between EML and age acceleration was not influenced by the normalization method (Supplementary Table 8).

Functional annotations

To test whether individual SEMs were randomly distributed across the genome or were more likely to be found in certain genomic regions or biological pathways, we conducted enrichment analyses to assess whether SEMs were enriched in clock-CpGs (Horvath clock, PhenoAge clock, Hannum clock), genomic regions (transcription start sites (TSS1500, TSS200), untranslated regions (5'UTR, 3'UTR), 1st Exon, and gene body), or regulatory features (i.e., enhancers, DNase hypersensitive sites, open chromatin regions, transcription factor binding site, promoters). For each participant, we first annotated the probes and each mutation based on the location related to genes (i.e.,

TSS1500, TSS200, 5'UTR, 1st EXON, gene body, 3'UTR), or regulatory features using the manifest provided by Illumina. Then we conducted hypergeometric tests for each region and each subject separately using a nominal significance threshold of 0.05. Last, for each region, we summarized the number of individuals for which the test was significant (Supplementary Tables 9–11).
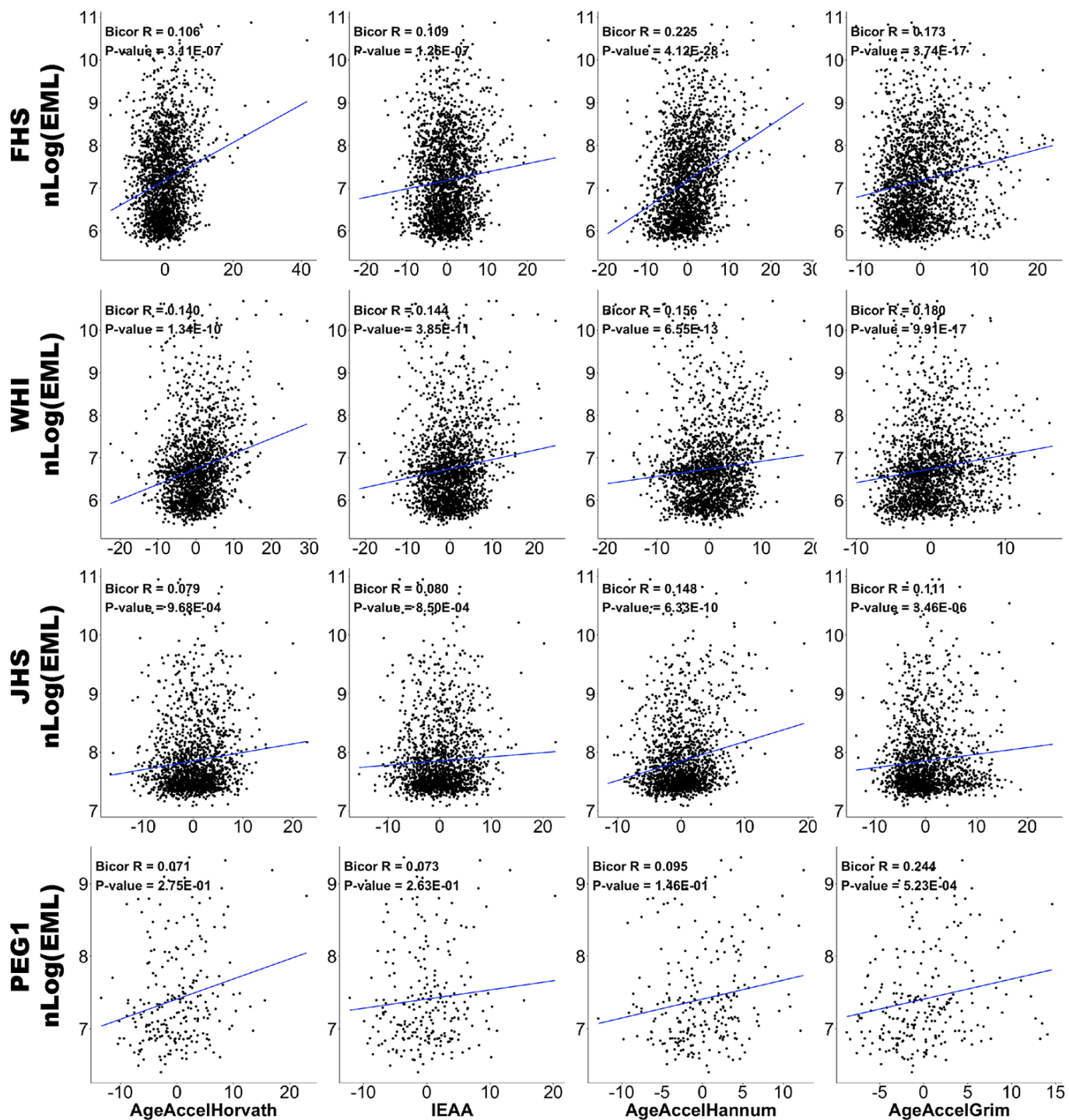
Figure 2. Correlations between EML and epigenetic age accelerations. Scatter plots of DNAm age acceleration estimators (x-axis; AgeAccelHorvath, IEAA, AgeAccelHannum, and AgeAccelGrim in each column, respectively) versus natural log-transformed EMLs (y-axis). Data from FHS, WHI, JHS, and PEG1 are plotted in four rows respectively. Each panel reports a biweight midcorrelation coefficient and correlation test p-value.

The results show that for each clock-CpG set or region, only a small proportion of participants have their SEMs enriched which illustrating both the stochastic nature and inter-personal variation of SEMs.

Pathway enrichment analysis

Next, we examined whether, among study participants who exhibit faster age accelerations, SEMs are enriched in particular biological pathways. We first conducted KEGG pathway enrichment analyses for each study participant. Then for each KEGG pathway, we calculated the number of people with enriched SEMs for this particular pathway. Finally, we investigated the association between SEMs enrichment in a particular pathway and age accelerations using linear regression. Additional details can be found in the method section.

Supplementary Tables 12–16 showed the top 10 pathways that were commonly enriched in each study, and generally we found that SEMs enriched in these pathways were also statistically significantly associated with faster age accelerations (AgeAccelHorvath, IEAA, AgeAccelHannum, and AgeAccelGrim, respectively).

Briefly, in all four study populations, we identified similar enrichment patterns, and SEMs enriched in signaling pathways, axon guidance, glutamatergic synapse, morphine addiction, glucocorticoid pathway (Cushing syndrome), or circadian rhythm pathways were associated with faster AgeAccelHorvath, AgeAccelHannum, and IEAA. Whereas the associations between pathway enrichment and AgeAccelGrim or AgeAccelPheno were less strong and not necessarily statistically significant. We only observed SEMs enriched in neuroactive ligand-receptor interaction was associated with faster AceAccelGrim and AgeAccelPheno.

Region-specific EML

To address the functionality of SEMs on biological age acceleration, we calculated the number of SEMs co-located with clock CpGs for each study participant (i.e., clock-specific SEMs) and assessed whether there were any clock-specific EMLs corresponding to age acceleration (Supplementary Table 17), but we observed no statistically significant association with the three clocks tested (Horvath clock: 353 CpGs; Hannum clock: 71 CpGs; PhenoAge clocks: 513 CpGs).

Next, we divided CpGs into different genomics region/regulatory feature groups based on the annotations, and then calculated EMLs within each region for each study participant (i.e., genomic region-specific EML; regulatory region-specific EML) (Table 3 and Supplementary Table 18). EMLs in TSS1500, TSS200, and the 1stExon regions were related to faster age accelerations. Also, EML in DNase hypersensitive regions was positively correlated with faster age accelerations. In contrast, 3'UTR specific-EML was associated with younger chronologic age and slower age acceleration.

The direction of SEM

Based on the direction of the mutation, we separated SEMs into hypomethylated SEM ($Q1 - 3 \times IQR$) and hypermethylated SEM ($Q3 + 3 \times IQR$) and calculated hypomethylated and hypermethylated EMLs respectively within FHS. We assessed the correlations between the newly calculated directional EMLs and epigenetic age acceleration. The results remained largely the same (See Supplementary Table 19). Furthermore, consistent with previous studies [29], hypermethylated SEMs were mainly located in CpG islands, while hypomethylated SEMs were enriched in the open seas (see Supplementary Tables 20, 21).

Shannon entropy, EML, and DNAm age acceleration

As an alternate measure for a well-functioning EMS that maintains genomic stability, we calculated the Shannon entropy of the whole methylome based on the 450K or EPIC array. An increase in entropy means that the methylome becomes less predictable across the population of cells, i.e. when the methylation fractions (beta values) tend towards 50%.

We found the Shannon entropy to be positively correlated with chronologic age (meta r = 0.046, meta P-value = 2.16E-04), EML (meta r = 0.234, meta P-value = 7.71E-78), and all four measures of age accelerations (meta P-value: AgeAccelHorvath = 8.79E-09, IEAA = 6.56E-04, AgeAccelHannum = 1.80E-22, AgeAccelGrim = 1.67E-22) (Table 4 and Supplementary Table 22).

DISCUSSION

It has previously been proposed that aging-related decline in epigenetic maintenance increases the occurrence of SEMs in individuals [24, 25]. Our data suggest that the EML per study participant are weakly but statistically significantly associated with several widely used measures of epigenetic age acceleration based on epigenetic clocks.

It has been hypothesized that DNA methylation clocks may capture the imperfection of the EMS resulting in epigenetic instability [5, 13, 21]. Our study provides new evidence for this hypothesis showing that the accumulation of stochastic epigenetic mutations is

Table 3. Meta-analysis[*]**: Biweight midcorrelation analysis of genomic region-specific EML.**

Outcome = log(Region-EML)[**]	TSS1500 (50999 CpGs)		TSS200 (41175 CpGs)		5'UTR (23024 CpGs)		1stExon (7669 CpGs)		Gene Body (135960 CpGs)		3'UTR (14010 CpGs)	
	Meta r	Meta P_value	Meta r	Meta P_value	Meta r	Meta P_value	Meta r	Meta P_value	Meta r	Meta P_value	Meta r	Meta P_value
Age	0.103	1.42E-16	0.074	3.39E-09	-0.046	2.44E-04	0.126	7.86E-24	-0.122	1.81E-22	-0.085	1.38E-11
DNAm Age Acceleration												
AgeAccelHorvath	0.050	7.35E-05	-0.004	7.52E-01	-0.055	9.43E-06	0.074	4.13E-09	-0.060	1.96E-06	-0.064	3.35E-07
IEAA	0.058	3.16E-06	-0.006	6.52E-01	-0.052	2.94E-05	0.067	9.83E-08	-0.063	4.04E-07	-0.064	2.66E-07
AgeAccelHannum	0.098	5.06E-15	0.076	1.62E-09	-0.044	4.93E-04	0.154	1.00E-34	-0.140	4.87E-29	-0.111	6.74E-19
AgeAccelGrim	-0.001	9.40E-01	0.054	1.45E-05	-0.012	3.57E-01	0.082	6.30E-11	-0.053	1.94E-05	-0.073	5.52E-09
Cell types												
CD8.naive	-0.048	1.23E-04	-0.035	5.18E-03	-0.023	6.55E-02	-0.044	4.66E-04	0.053	1.96E-05	0.037	3.10E-03
CD8pCD28nCD45RAn	0.043	5.51E-04	-0.032	1.07E-02	0.015	2.25E-01	-0.020	1.08E-01	0.016	2.06E-01	-0.018	1.41E-01
PlasmaBlast	0.041	1.04E-03	-0.019	1.28E-01	-0.019	1.23E-01	-0.022	7.45E-02	-0.023	6.96E-02	-0.012	3.32E-01
CD4T	0.043	5.19E-04	-0.066	1.34E-07	-0.013	2.91E-01	-0.095	2.97E-14	0.002	8.74E-01	0.024	5.09E-02
Gran	-0.008	5.43E-01	-0.082	5.17E-11	-0.039	1.85E-03	-0.113	1.82E-19	0.067	9.65E-08	0.065	1.72E-07

[*] Meta-analysis using Stouffer's method with weights given by the square root of the number of (non-missing) samples in each data set.

[**] Adjusted for Age, Sex, Race/ethnicity, Cell types, Log(total EML).

Table 4. Association between Shannon entropy and age, AgeAccel, EML.

Outcome =Entropy[**]	Meta[*]		FHS (n = 2326)		WHI (n= 2091)		JHS (n= 1734)		PEG 1 (n = 237)	
	Meta r	Meta P_value	Bicor r	P_value	Bicor r	P_value	Bicor r	P_value	Bicor r	P_value
Age	0.046	2.16E-04	0.001	9.55E-01	0.068	2.01E-03	0.071	2.92E-03	0.117	7.30E-02
DNAm Age Acceleration										
AgeAccelHorvath	0.072	8.79E-09	0.081	9.11E-05	0.160	1.76E-13	-0.039	1.02E-01	0.006	9.22E-01
IEAA	0.043	6.56E-04	0.035	9.02E-02	0.131	1.70E-09	-0.052	3.16E-02	0.018	7.83E-01
AgeAccelHannum	0.122	1.80E-22	0.155	6.23E-14	0.136	4.60E-10	0.063	9.10E-03	0.096	1.41E-01
AgeAccelGrim	0.122	1.67E-22	0.077	1.89E-04	0.228	3.86E-26	0.043	7.17E-02	0.164	1.14E-02
EML	0.234	7.71E-78	0.089	1.63E-05	0.294	6.87E-43	0.325	7.22E-44	0.281	1.10E-05

[*] Meta-analysis using Stouffer's method with weights given by the square root of the number of (non-missing) samples in each data set.

[**] Adjusted for Age, Sex, Race/ethnicity, Cell types.

associated with epigenetic age acceleration according to four clocks: the Horvath, the intrinsic, the Hannum, and the GrimAge clock. The first three clocks have been built to predict chronological age while the GrimAge clock was designed as a mortality risk predictor that explicitly uses chronological age as one of its predictors. We observed statistically significant associations between EML and age acceleration measured by all four clocks, with the AgeAccelHannum and AgeAccelGrim being most strongly associated with EML. One explanation might be that these clocks have different relationships to blood cell composition. While measures of epigenetic age acceleration based on Horvath's pan tissue clock, AgeAccelHorvath and IEAA, are at best weakly related to changes in blood cell composition, AgeAccelHannum and AgeAccelGrim correlate more strongly with blood cell counts and markers of immunosenescence. Therefore, similar to the Hannum and GrimAge clocks, EML also reflects changes in blood cell composition i.e. the immune system. Previously, studies showed that DNAm

biomarkers of aging that capture altered immune cell composition are better predictors of mortality [7, 13]. Thus, not only the intracellular accumulation of epigenetic mutations we investigated here, but also changes in cell composition contribute to EML as part of the biological aging processes that diverge from chronological age. This finding is also consistent with several previous studies [25, 27, 29].

It is worth noting that only the intracellular accumulation of epigenetic mutations suggests that an insufficient EMS may be involved in increasing the EML, thus we ascribe greater weight and importance to the correlations with the Horvath clock and IEAA. The relatively weak correlations between EML and AgeAccelHorvath or IEAA indicate that these DNAm age estimators also capture other hallmarks of the aging process apart from a dysfunctional EMS [3]. The size of the correlations for these age acceleration measures and EML are comparable to those reported for many other known risk factors of aging. For example, in the

WHI cohort, the correlation between BMI and AgeAccelGrim is 0.14; the correlation between exercise and AgeAccelGrim is -0.1; and the correlations for many other risk factors are below +/- 0.3 (See Lu et al) [7]. Correlations between risk factors and IEAA are even smaller (r between 0.08 and -0.06, see Quach et al. Figure 1) [36]. Nevertheless, the fact that associations between EML and AgeAccelHorvath or IEAA are, at best, weak reminds us that other mechanisms and factors apart from EMS also play important roles in the ageing process. Indeed, future in vivo or in vitro studies are needed to better understand the causal relationship between EML and epigenetic aging.

EML exhibited much stronger correlations with age acceleration than deceleration. This result suggests that epigenetic age acceleration and deceleration may have different biological mechanisms, and that the maintenance of epigenetic stability plays more of a role in the acceleration of epigenetic age than the deceleration.

Our finding that EML is statistically significantly albeit weakly correlated with various measures of epigenetic age acceleration is consistent with several previous studies [27, 29]. In order to understand the biological foundation for EML contributions to the epigenetic aging process, we conducted several functional and pathway enrichment analyses. Functional annotation and pathway enrichment analysis showed no predominant regions or biological pathways as being enriched with SEMs. This is in line with previous observations that a majority of SEMs are randomly distributed across the genome and that the locations necessarily differ between individuals as the name suggests [27]. Despite this inherent inter-individual variation, we found that individuals with SEMs enriched in signaling pathways, neurogenesis, neurotransmission, glucocorticoid, or circadian rhythm pathways were more likely to show age acceleration as measured by AgeAccelHorvath, IEAA, and AgeAccelHannum. These non-random patterns – if confirmed – may very well reflect the accumulation of SEMs in pathways related to biological mechanisms that are involved in aging. For example, some signaling pathways such as oxytocin signaling and MAPK/ERK signaling pathway have been associated with age-related muscle maintenance and regeneration [37], while excess glucocorticoid levels may reflect a lifelong accumulation of stressors and this pathway plays a key role in frailty [38] and the aging process [21]. Furthermore, some clock-CpGs are located in glucocorticoid response elements [39]. We also found SEMs enriched in several neurogenesis or neurotransmission-related pathways that may be

contributing to the ticking rate of clocks. This is consistent with the previous finding that DNAm age acceleration is linked to neuropathology [18, 40], especially Parkinson's disease [16] and Down syndrome [15]. Moreover, our finding of SEM enrichment in the circadian entrainment pathway supports the hypothesis that the DNAm age estimators are related to the oscillation of the circadian rhythm [13]. Interestingly, although patterns were similar, we found less evidence for pathway enrichment with SEMs and age acceleration based on the GrimAge and PhenoAge clocks. This may again underscore that different clocks indeed capture different aspects of the aging process.

EMLs within TSS1500, TSS200, and especially the 1stExon regions were found to be associated with faster age accelerations, and for these regions methylation levels have been shown to be related to gene expression [41, 42]. Therefore, our result may suggest that the accumulation of random epigenetic mutations in these regions may influence biological aging processes through gene expression regulation. Interestingly, even though we would also have expected this, we did not observe such associations for promoter regions. Further studies are needed to investigate the biologic consequences of region-specific effects of epigenetic mutations on aging.

The Shannon Entropy measure reflects higher levels of entropy such that the methylome becomes less predictable across the population of cells due to the failure of DNAm maintenance [11]. Epigenetic Shannon entropy as well as this measure's variability increase with age [10, 11, 43, 44]. In our study, EML and Shannon entropy was strongly correlated, confirming that both measure aspects of the EMS, even though EML and entropy capture different aspects of epigenetic stability. SEM represents rare methylation value extremes at a site due to the accumulation of maintenance failures whereas entropy reflects an ongoing 'smoothing' of the epigenetic landscape such that beta values tend towards 50% [45].

There are limitations of our study. First, it is possible that some unmeasured confounders biased our results. Sensitivity analyses, however, showed that the SEM measure was not affected by potential technical artifacts or poor sample quality, and the association between EML and age acceleration was independent of potential confounders including chronological age, sex, race/ethnicity, and BMI. Hence, although technical effects and confounding are hard to avoid, the observed associations between EML and age accelerations were robust to adjustments for a number of covariates. Second, from all four studies, we only had cross-sectional data available. Therefore, we were unable to

investigate the accumulation of epigenetic mutations over time within individuals. Finally, DNA methylation was measured in blood samples only. Therefore, pathway results need to be interpreted with caution as many of the identified pathways listed above have no direct relevance to the function of the blood tissue. While this seems to support the inherent randomness of SEMs, stochastic epigenetic mutations may still accumulate in a non-random pattern within certain biological pathways if repair mechanisms fail systematically due to properties related to these pathways across different tissues. Also, it has been shown that epigenetic changes in blood may indeed reflect epigenetic fingerprints of other target tissues [46, 47]. Nevertheless, tissue- and cell-specific analyses are needed to better understand the relationship between stochastic epigenetic mutations and aging processes in different tissues.

In summary, using large datasets from multiple population-based studies, we were able to show that EML per study participant is associated with different epigenetic aging markers (aging clocks) and importantly with epigenetic age acceleration. Moreover, epigenetic mutations enriched in particular biological pathways or genomic regions related to gene expression were associated with accelerated aging and these may contribute to the ticking of the epigenetic clock. Our findings from pathway enrichment analyses also suggest some interesting biological mechanisms that may influence the ticking of the epigenetic aging clocks and drive the acceleration of the biological aging process.

MATERIALS AND METHODS

Study population

Our study is based on data from four studies: the Framingham Heart Study (FHS) Offspring Cohort, the Women's Health Initiative (WHI), the Jackson Heart Study (JHS), and the Parkinson's Environment and Genes (wave 1) known as the PEG1 study.

We used 2,326 individuals from the FHS Offspring cohort [48]. The FHS cohort is a large-scale longitudinal study started in 1948, initially investigating the common factors of characteristics that contribute to cardiovascular disease (CVD) (https://www.framinghamheartstudy.org/index.php). The study at first enrolled participants living in the town of Framingham, Massachusetts, who were free of overt symptoms of CVD, heart attack, or stroke at enrollment. In 1971, the study started FHS Offspring Cohort to enroll a second generation of the original participants' adult children and their spouses (n= 5124) for conducting similar examinations. The FHS Offspring Cohort collected medical history and measurement data,

immunoassays at exam 7, and blood DNA methylation profiling at exam 8. Participants from the FHS Offspring Cohort were eligible for our study if they attended both the seventh and eighth examination cycles and consented to have their molecular data used for the study. We used the 2,326 participants from the group of Health/ Medical/Biomedical (IRB, MDS) consent and available for both Immunoassay array DNA methylation array data. The FHS data are available in dbGaP (accession number: phs000363.v16.p10 and phs000724.v2.p9).

The WHI is a national study that enrolled postmenopausal women aged 50-79 years into the clinical trials (CT) or observational study (OS) cohorts between 1993 and 1998 [49, 50]. We included 2,091 WHI participants with available phenotype and DNA methylation array data from "*Broad Agency Award 23*" (WHI BA23). WHI BA23 focuses on identifying miRNA and genomic biomarkers of coronary heart disease (CHD), integrating the biomarkers into diagnostic and prognostic predictors of CHD and other related phenotypes, and other objectives can be found in https://www.whi.org/researchers/data/WHIStudies/StudySites/BA23/Pages/home.aspx.

The JHS is a large, population-based observational study evaluating the etiology of cardiovascular, renal, and respiratory diseases among African Americans residing in the three counties (Hinds, Madison, and Rankin) that make up the Jackson, Mississippi metropolitan area [51]. The age at enrollment for the unrelated cohort was 35-84 years; the family cohort included related individuals >21 years old. Participants provided extensive medical and social history, had an array of physical and biochemical measurements and diagnostic procedures, and provided genomic DNA during a baseline examination (2000-2004) and two follow-up examinations (2005-2008 and 2009-2012). Annual follow-up interviews and cohort surveillance are ongoing. In our analysis, we used the visits at baseline from 1,734 individuals as part of project JHS ancillary study ASN0104, available with both phenotype and DNA methylation array data.

The PEG1 study was conducted during 2000-2007 to investigate the causes of Parkinson's disease (PD) in agricultural regions of the California central valley. We analyzed blood samples from 238 healthy controls enrolled from Kern, Tulare, or Fresno counties. Controls were required to be over the age of 35, having lived within one of the counties for at least 5 years prior to enrollment, and do not have a diagnosis of Parkinsonism. Demographic information, lifestyle factors, and medication use were collected in standardized interviews, including lifetime information of cigarette smoking and coffee/ tea consumption.

For PEG1, FHS, and WHI, peripheral blood samples were collected, and bisulfite conversion using the Zymo EZ DNA Methylation Kit (Zymo Research, Orange, CA, USA) as well as subsequent hybridization of the HumanMethylation450k Bead Chip (Illumina, San Diego, CA), and scanning (iScan, Illumina) were performed according to the manufacturer's protocols by applying standard settings. For JHS, DNA methylation quantification was conducted using HumanMethylation EPIC Bead Chip (Illumina, San Diego, CA).

Preprocess

For PEG1 samples, raw signal intensities were retrieved using the function *read.metharray.exp* of the R package *minfi* from the Bioconductor open-source software (http://www.bioconductor.org/), followed by linear dye bias correction, noob background correction, and functional normalization using the same R package [52–55]; β-value was used for all the analyses. One sample was identified as low quality due to low median methylated and unmethylated signal intensities across the entire array and thus removed from the study population. Detection p-values were derived using the function *detectionP* as the probability of the total signal (methylation + unmethylated) being detected above the background signal level, as estimated from negative-control probes. All in all, 845 probes with a detection p-value above 0.05 in at least 5% of samples were removed. Also, 645 probes with a bead count <3 in at least 5% of samples; 11,334 probes on the X or Y chromosome; 7,306 probes containing a SNP at the CpG interrogation site and/or at the single nucleotide extension for 5% maf; and 27,332 cross-reactive probes were also removed. In total, 438,050 probes were included for downstream analyses.

For FHS and WHI samples, 11,334 probes on the X or Y chromosome; 7,306 probes containing a SNP at the CpG interrogation; and 27,332 cross-reactive probes were also removed. In total, 439,540 probes were included for downstream analyses.

For JHS samples, 19,532 probes on the X or Y chromosome; 53,435 probes containing a SNP at the CpG interrogation and cross-reactive were also removed. In total, 793,869 probes were included for downstream analyses.

SEM calculation

The calculation of SEM was consistent with a previously published and validated approach [24, 26, 31]. CpG with methylation levels three times the interquartile range above the third quartile or below the first quartile was identified as a SEM. Toward this end, we calculated the IQR for each of the 438,050 probes in each dataset (for PEG1, FHS, and WHI) or the 793,969 probes (for JHS). Then, SEMs were identified based on extreme methylation levels. Finally, we summed across the count of all SEMs per sample and defined the total number of SEMs of each study participant as epigenetic mutation load (EML). EML was not normally distributed; therefore, we used the natural log of the number of SEMs for all regression analyses.

In FHS, we separated SEMs into hypermethylated and hypomethylated SEMs based on the direction of the mutation. We also defined consistently hypermethylated or hypomethylated SEMs as a CpG mutated in the same direction in more than 10 participants.

In order to assess whether the criteria used for SEMs will change the results, we defined loose SEM and stringent SEM as described above. We then calculated the total numbers of loose and stringent SEMs for each person.

DNA methylation age

We included eight different DNAm aging biomarkers in this study. Utilizing our online DNA Methylation Age Calculator (https://dnamage.genetics.ucla.edu/), we calculated DNA methylation-based ages and the age accelerations based on the residuals of the regression of DNA methylation age on each participants' chronological age for each clock.

Four types of DNA methylation-based biomarkers were included in the main analyses. Briefly, Horvath clock was calculated using a linear combination of 353 CpGs that have previously been shown to predict chronological age in multiple tissues [5]; and the intrinsic clock was derived from the Horvath clock by additionally regressing out cell compositions [30]; Hannum clock was calculated using a linear combination of 71 CpGs to predict chronological age in blood [11]; and GrimAge clock) was calculated from a linear combination of 7 DNAm plasma protein surrogates and a DNAm-based estimator of smoking pack-years designed to predict mortality [7].

Other DNAm aging biomarkers were included in the Supplementary analyses, including: the extrinsic clock [30], PhenoAge clock [6], SkinBlood clock [56], DNAm based estimator of telomere length [57], each of the 7 DNAm protein surrogates underlying the definition of the GrimAge clock [7], as well as DNAm based estimate of smoking pack-years.

Cell composition

White blood cell composition was imputed for each study participant using our online published DNA Methylation Age Calculator, https://dnamage.genetics.ucla.edu/. The following imputed blood cell counts were included in downstream analyses: CD4+ T, naïve CD8+ T, exhausted cytotoxic CD8+ T cells (defined as CD8 positive CD28 negative CD45R negative, CD8+CD28-CD45RA-), plasmablasts, and granulocytes. Naïve CD8+ T, exhausted cytotoxic CD8+ T cells, and plasmablasts were calculated based on the Horvath method [58]. The remaining cell types were imputed using the Houseman method [59].

Shannon entropy

The formula of Shannon entropy is:

$$Entropy = \frac{1}{N \times log_2(\frac{1}{2})}$$
$$\times \sum_{i=1}^{N}[\beta_i \times log_2(\beta_i) + (1 - \beta_i)$$
$$\times log_2(1 - \beta_i)]$$

where β_i represents the methylation beta value for the ith probe (CpG site) in the array, N represents the total number of probes included in the formula [11].

Statistical analysis

All analyses were conducted using R v3.6.1. We used Pearson correlations to assess the relations between different DNAm ages and age accelerations. We evaluated potential batch effects by assessing the difference of EMLs in microarray slides or position on the array with the ANOVA test. To eliminate the possibility that SEMs are driven by incomplete bisulfite conversion, Pearson correlations between EMLs and the average intensity of bisulfite conversion controls were also calculated. Average intensity of bisulfite conversion controls was derived using the *ENmix* R package [60].

To assess the association between EML and age/age accelerations/cell compositions, we applied biweight midcorrelation (bicor) implemented in the WGCNA R package. We adjusted for potential confounders including age, sex, race/ethnicity, and cell compositions (naïve CD8 cells, CD8+CD28-CD45RA- T cells, Plasma Blasts, CD4 T cells, and Granulocytes) by regressing out the effects of these factors and retaining the residuals of log(EML)only for analysis.

We also conducted stratified analyses to evaluate the associations between EML, chronological age, epigenetic estimates of cell composition, and epigenetic age acceleration in males and females separately for the PEG1, FHS, and JHS studies. To ensure the reliability and reproducibility of the associations, several sensitivity analyses were conducted. In addition to the potential confounders mentioned above, we adjusted for a quadratic term in age (age^2) to account for non-linear relationships and body mass index.

To evaluate the effect of data preprocessing steps, we repeated the analysis using four different normalization methods (Illumina background correction, noob, functional normalization, and quantile normalization implemented in the *minfi* package) in the PEG dataset.

We analyzed each dataset separately, therefore in order to obtain an overall p-value across all four studies, we conducted meta-analyses using Stouffer's method for meta-analysis estimates of the correlation coefficient (meta r), and the corresponding two-sided p-values (meta p-value).

Functional annotation, region-specific SEMs, and pathway enrichment analysis

For each participant, we annotated the probes and SEMs based on the location in relation to genes (TSS1500, TSS200, 5'UTR, 1st Exon, gene body, and 3'UTR), or regulatory features (enhancer region, DNase hypersensitive region, open chromatin region, transcription factor binding site, and promoter region) using the manifest provided by Illumina. To test for region specific enrichment, we conducted hypergeometric tests for each region and each subject separately. A p-value less than 0.05 was considered statistically significant. For biological pathway enrichment analysis, the *enrichKEGG* function implemented in the *ClusterProfiler* package [61] was used to assess whether study participant's SEMs were enriched in particular KEGG pathways (P-value threshold = 0.05). For each genomic region or KEGG pathway, we then summarized how many study participants had their SEMs enriched. We also investigated the association between SEMs enrichment in each KEGG pathway and age accelerations using linear regression, adjusted for the total number of SEMs per study participant:

$$For\ pathway\ j : AgeAccel_i$$
$$= \beta_0 + \beta_1\ Enrich_{ij}$$
$$+ \beta_2 \log(Total\ EML_i) + \varepsilon_i$$

where *AgeAccel* stands for age accelerations (AgeAccelHorvath, IEAA, AgeAccelHannum, AgeAccelGrim); *Enrich* stands for enrichment for pathway j (significant: 1, non-significant: 0); *Total EML* stands for log transformed total EML for participant i.

AUTHOR CONTRIBUTIONS

QY, SH and BR conceived of the study. QY carried out the statistical analyses. KP, AL, CK, and AB contributed to the data analysis plan, participated in the critical interpretation of the results, and contributed to the writing of the manuscript.

ACKNOWLEDGMENTS

CONFLICTS OF INTEREST

FUNDING

REFERENCES

1. Kennedy BK, Berger SL, Brunet A, Campisi J, Cuervo AM, Epel ES, Franceschi C, Lithgow GJ, Morimoto RI, Pessin JE, Rando TA, Richardson A, Schadt EE, et al. Geroscience: linking aging to chronic disease. Cell. 2014; 159:709–13.
https://doi.org/10.1016/j.cell.2014.10.039
PMID:25417146

2. Oberdoerffer P, Sinclair DA. The role of nuclear architecture in genomic instability and ageing. Nat Rev Mol Cell Biol. 2007; 8:692–702.
https://doi.org/10.1038/nrm2238 PMID:17700626

3. López-Otín C, Blasco MA, Partridge L, Serrano M, Kroemer G. The hallmarks of aging. Cell. 2013; 153:1194–217.
https://doi.org/10.1016/j.cell.2013.05.039
PMID:23746838

4. Jylhävä J, Pedersen NL, Hägg S. Biological age predictors. EBioMedicine. 2017; 21:29–36.
https://doi.org/10.1016/j.ebiom.2017.03.046
PMID:28396265

5. Horvath S. DNA methylation age of human tissues and cell types. Genome Biol. 2013; 14:R115.
https://doi.org/10.1186/gb-2013-14-10-r115
PMID:24138928

6. Levine ME, Lu AT, Quach A, Chen BH, Assimes TL, Bandinelli S, Hou L, Baccarelli AA, Stewart JD, Li Y, Whitsel EA, Wilson JG, Reiner AP, et al. An epigenetic biomarker of aging for lifespan and healthspan. Aging (Albany NY). 2018; 10:573–91.
https://doi.org/10.18632/aging.101414
PMID:29676998

7. Lu AT, Quach A, Wilson JG, Reiner AP, Aviv A, Raj K, Hou L, Baccarelli AA, Li Y, Stewart JD, Whitsel EA, Assimes TL, Ferrucci L, Horvath S. DNA methylation GrimAge strongly predicts lifespan and healthspan. Aging (Albany NY). 2019; 11:303–27.
https://doi.org/10.18632/aging.101684
PMID:30669119

8. Vidal-Bralo L, Lopez-Golan Y, Gonzalez A. Simplified assay for epigenetic age estimation in whole blood of

adults. Front Genet. 2016; 7:126.
https://doi.org/10.3389/fgene.2016.00126
PMID:27471517

9. Zhang Y, Wilson R, Heiss J, Breitling LP, Saum KU, Schöttker B, Holleczek B, Waldenberger M, Peters A, Brenner H. DNA methylation signatures in peripheral blood strongly predict all-cause mortality. Nat Commun. 2017; 8:14617.
https://doi.org/10.1038/ncomms14617
PMID:28303888

10. Weidner CI, Lin Q, Koch CM, Eisele L, Beier F, Ziegler P, Bauerschlag DO, Jöckel KH, Erbel R, Mühleisen TW, Zenke M, Brümmendorf TH, Wagner W. Aging of blood can be tracked by DNA methylation changes at just three CpG sites. Genome Biol. 2014; 15:R24.
https://doi.org/10.1186/gb-2014-15-2-r24
PMID:24490752

11. Hannum G, Guinney J, Zhao L, Zhang L, Hughes G, Sadda S, Klotzle B, Bibikova M, Fan JB, Gao Y, Deconde R, Chen M, Rajapakse I, et al. Genome-wide methylation profiles reveal quantitative views of human aging rates. Mol Cell. 2013; 49:359–67.
https://doi.org/10.1016/j.molcel.2012.10.016
PMID:23177740

12. Garagnani P, Bacalini MG, Pirazzini C, Gori D, Giuliani C, Mari D, Di Blasio AM, Gentilini D, Vitale G, Collino S, Rezzi S, Castellani G, Capri M, et al. Methylation of ELOVL2 gene as a new epigenetic marker of age. Aging Cell. 2012; 11:1132–34.
https://doi.org/10.1111/acel.12005
PMID:23061750

13. Horvath S, Raj K. DNA methylation-based biomarkers and the epigenetic clock theory of ageing. Nat Rev Genet. 2018; 19:371–84.
https://doi.org/10.1038/s41576-018-0004-3
PMID:29643443

14. Zheng SC, Widschwendter M, Teschendorff AE. Epigenetic drift, epigenetic clocks and cancer risk. Epigenomics. 2016; 8:705–19.
https://doi.org/10.2217/epi-2015-0017
PMID:27104983

15. Horvath S, Garagnani P, Bacalini MG, Pirazzini C, Salvioli S, Gentilini D, Di Blasio AM, Giuliani C, Tung S, Vinters HV, Franceschi C. Accelerated epigenetic aging in down syndrome. Aging Cell. 2015; 14:491–95.
https://doi.org/10.1111/acel.12325
PMID:25678027

16. Horvath S, Ritz BR. Increased epigenetic age and granulocyte counts in the blood of Parkinson's disease patients. Aging (Albany NY). 2015; 7:1130–42.
https://doi.org/10.18632/aging.100859
PMID:26655927

17. Maierhofer A, Flunkert J, Oshima J, Martin GM, Haaf T, Horvath S. Accelerated epigenetic aging in werner syndrome. Aging (Albany NY). 2017; 9:1143–52.
https://doi.org/10.18632/aging.101217
PMID:28377537

18. Levine ME, Lu AT, Bennett DA, Horvath S. Epigenetic age of the pre-frontal cortex is associated with neuritic plaques, amyloid load, and Alzheimer's disease related cognitive functioning. Aging (Albany NY). 2015; 7:1198–211.
https://doi.org/10.18632/aging.100864
PMID:26684672

19. Levine ME, Hosgood HD, Chen B, Absher D, Assimes T, Horvath S. DNA methylation age of blood predicts future onset of lung cancer in the women's health initiative. Aging (Albany NY). 2015; 7:690–700.
https://doi.org/10.18632/aging.100809
PMID:26411804

20. Ghosh J, Mainigi M, Coutifaris C, Sapienza C. Outlier DNA methylation levels as an indicator of environmental exposure and risk of undesirable birth outcome. Hum Mol Genet. 2016; 25:123–29.
https://doi.org/10.1093/hmg/ddv458 PMID:26566672

21. Epigenetics of Aging and Longevity: Translational Epigenetics, volume 4. Moskalev A, Vaiserman AM, (Editors). Academic Press, 2017.

22. Fraga MF, Ballestar E, Paz MF, Ropero S, Setien F, Ballestar ML, Heine-Suñer D, Cigudosa JC, Urioste M, Benitez J, Boix-Chornet M, Sanchez-Aguilera A, Ling C, et al. Epigenetic differences arise during the lifetime of monozygotic twins. Proc Natl Acad Sci USA. 2005; 102:10604–09.
https://doi.org/10.1073/pnas.0500398102
PMID:16009939

23. Talens RP, Christensen K, Putter H, Willemsen G, Christiansen L, Kremer D, Suchiman HE, Slagboom PE, Boomsma DI, Heijmans BT. Epigenetic variation during the adult lifespan: cross-sectional and longitudinal data on monozygotic twin pairs. Aging Cell. 2012; 11:694–703.
https://doi.org/10.1111/j.1474-9726.2012.00835.x
PMID:22621408

24. Gentilini D, Garagnani P, Pisoni S, Bacalini MG, Calzari L, Mari D, Vitale G, Franceschi C, Di Blasio AM. Stochastic epigenetic mutations (DNA methylation) increase exponentially in human aging and correlate with X chromosome inactivation skewing in females. Aging (Albany NY). 2015; 7:568–78.
https://doi.org/10.18632/aging.100792 PMID:26342808

25. Wang Y, Karlsson R, Jylhävä J, Hedman ÅK, Almqvist C, Karlsson IK, Pedersen NL, Almgren M, Hägg S. Comprehensive longitudinal study of epigenetic

mutations in aging. Clin Epigenetics. 2019; 11:187.
https://doi.org/10.1186/s13148-019-0788-9
PMID:31818313

26. Gentilini D, Scala S, Gaudenzi G, Garagnani P, Capri M, Cescon M, Grazi GL, Bacalini MG, Pisoni S, Dicitore A, Circelli L, Santagata S, Izzo F, et al. Epigenome-wide association study in hepatocellular carcinoma: identification of stochastic epigenetic mutations through an innovative statistical approach. Oncotarget. 2017; 8:41890–902.
https://doi.org/10.18632/oncotarget.17462
PMID:28514750

27. Curtis SW, Cobb DO, Kilaru V, Terrell ML, Marder ME, Barr DB, Marsit CJ, Marcus M, Conneely KN, Smith AK. Exposure to polybrominated biphenyl and stochastic epigenetic mutations: application of a novel epigenetic approach to environmental exposure in the michigan polybrominated biphenyl registry. Epigenetics. 2019; 14:1003–18.
https://doi.org/10.1080/15592294.2019.1629232
PMID:31200609

28. Fiorito G, McCrory C, Robinson O, Carmeli C, Rosales CO, Zhang Y, Colicino E, Dugué PA, Artaud F, McKay GJ, Jeong A, Mishra PP, Nøst TH, et al, and BIOS Consortium, and Lifepath consortium. Socioeconomic position, lifestyle habits and biomarkers of epigenetic aging: a multi-cohort analysis. Aging (Albany NY). 2019; 11:2045–70.
https://doi.org/10.18632/aging.101900
PMID:31009935

29. Seeboth A, McCartney DL, Wang Y, Hillary RF, Stevenson AJ, Walker RM, Campbell A, Evans KL, McIntosh AM, Hägg S, Deary IJ, Marioni RE. DNA methylation outlier burden, health, and ageing in generation Scotland and the lothian birth cohorts of 1921 and 1936. Clin Epigenetics. 2020; 12:49.
https://doi.org/10.1186/s13148-020-00838-0
PMID:32216821

30. Chen BH, Marioni RE, Colicino E, Peters MJ, Ward-Caviness CK, Tsai PC, Roetker NS, Just AC, Demerath EW, Guan W, Bressler J, Fornage M, Studenski S, et al. DNA methylation-based measures of biological age: meta-analysis predicting time to death. Aging (Albany NY). 2016; 8:1844–65.
https://doi.org/10.18632/aging.101020
PMID:27690265

31. Gentilini D, Somigliana E, Pagliardini L, Rabellotti E, Garagnani P, Bernardinelli L, Papaleo E, Candiani M, Di Blasio AM, Viganò P. Multifactorial analysis of the stochastic epigenetic variability in cord blood confirmed an impact of common behavioral and environmental factors but not of in vitro conception.

Clin Epigenetics. 2018; 10:77.
https://doi.org/10.1186/s13148-018-0510-3
PMID:29930742

32. Horvath S, Gurven M, Levine ME, Trumble BC, Kaplan H, Allayee H, Ritz BR, Chen B, Lu AT, Rickabaugh TM, Jamieson BD, Sun D, Li S, et al. An epigenetic clock analysis of race/ethnicity, sex, and coronary heart disease. Genome Biol. 2016; 17:171.
https://doi.org/10.1186/s13059-016-1030-0
PMID:27511193

33. Langfelder P, Horvath S. Fast R functions for robust correlations and hierarchical clustering. J Stat Softw. 2012; 46:i11.
PMID:23050260

34. Wang Y, Karlsson R, Lampa E, Zhang Q, Hedman ÅK, Almgren M, Almqvist C, McRae AF, Marioni RE, Ingelsson E, Visscher PM, Deary IJ, Lind L, et al. Epigenetic influences on aging: a longitudinal genome-wide methylation study in old swedish twins. Epigenetics. 2018; 13:975–87.
https://doi.org/10.1080/15592294.2018.1526028
PMID:30264654

35. Franceschi C, Bonafè M, Valensin S, Olivieri F, De Luca M, Ottaviani E, De Benedictis G. Inflamm-aging. An evolutionary perspective on immunosenescence. Ann N Y Acad Sci. 2000; 908:244–54.
https://doi.org/10.1111/j.1749-6632.2000.tb06651.x
PMID:10911963

36. Quach A, Levine ME, Tanaka T, Lu AT, Chen BH, Ferrucci L, Ritz B, Bandinelli S, Neuhouser ML, Beasley JM, Snetselaar L, Wallace RB, Tsao PS, et al. Epigenetic clock analysis of diet, exercise, education, and lifestyle factors. Aging (Albany NY). 2017; 9:419–46.
https://doi.org/10.18632/aging.101168
PMID:28198702

37. Elabd C, Cousin W, Upadhyayula P, Chen RY, Chooljian MS, Li J, Kung S, Jiang KP, Conboy IM. Oxytocin is an age-specific circulating hormone that is necessary for muscle maintenance and regeneration. Nat Commun. 2014; 5:4082.
https://doi.org/10.1038/ncomms5082 PMID:24915299

38. Clegg A, Hassan-Smith Z. Frailty and the endocrine system. Lancet Diabetes Endocrinol. 2018; 6:743–52.
https://doi.org/10.1016/S2213-8587(18)30110-4
PMID:30017798

39. Zannas AS, Arloth J, Carrillo-Roa T, Iurato S, Röh S, Ressler KJ, Nemeroff CB, Smith AK, Bradley B, Heim C, Menke A, Lange JF, Brückl T, et al. Lifetime stress accelerates epigenetic aging in an urban, African American cohort: relevance of glucocorticoid signaling. Genome Biol. 2015; 16:266.
https://doi.org/10.1186/s13059-015-0828-5

PMID:26673150

40. Marioni RE, Shah S, McRae AF, Ritchie SJ, Muniz-Terrera G, Harris SE, Gibson J, Redmond P, Cox SR, Pattie A, Corley J, Taylor A, Murphy L, et al. The epigenetic clock is correlated with physical and cognitive fitness in the lothian birth cohort 1936. Int J Epidemiol. 2015; 44:1388–96.
https://doi.org/10.1093/ije/dyu277 PMID:25617346

41. Jiao Y, Widschwendter M, Teschendorff AE. A systems-level integrative framework for genome-wide DNA methylation and gene expression data identifies differential gene expression modules under epigenetic control. Bioinformatics. 2014; 30:2360–66.
https://doi.org/10.1093/bioinformatics/btu316 PMID:24794928

42. Brenet F, Moh M, Funk P, Feierstein E, Viale AJ, Socci ND, Scandura JM. DNA methylation of the first exon is tightly linked to transcriptional silencing. PLoS One. 2011; 6:e14524.
https://doi.org/10.1371/journal.pone.0014524 PMID:21267076

43. Bell CG, Lowe R, Adams PD, Baccarelli AA, Beck S, Bell JT, Christensen BC, Gladyshev VN, Heijmans BT, Horvath S, Ideker T, Issa JJ, Kelsey KT, et al. DNA methylation aging clocks: challenges and recommendations. Genome Biol. 2019; 20:249.
https://doi.org/10.1186/s13059-019-1824-y PMID:31767039

44. Slieker RC, van Iterson M, Luijk R, Beekman M, Zhernakova DV, Moed MH, Mei H, van Galen M, Deelen P, Bonder MJ, Zhernakova A, Uitterlinden AG, Tigchelaar EF, et al, and BIOS consortium. Age-related accrual of methylomic variability is linked to fundamental ageing mechanisms. Genome Biol. 2016; 17:191.
https://doi.org/10.1186/s13059-016-1053-6 PMID:27654999

45. Field AE, Robertson NA, Wang T, Havas A, Ideker T, Adams PD. DNA methylation clocks in aging: categories, causes, and consequences. Mol Cell. 2018; 71:882–95.
https://doi.org/10.1016/j.molcel.2018.08.008 PMID:30241605

46. Lowe R, Rakyan VK. Correcting for cell-type composition bias in epigenome-wide association studies. Genome Med. 2014; 6:23.
https://doi.org/10.1186/gm540 PMID:25031617

47. Breeze CE, Paul DS, van Dongen J, Butcher LM, Ambrose JC, Barrett JE, Lowe R, Rakyan VK, Iotchkova V, Frontini M, Downes K, Ouwehand WH, Laperle J, et al. eFORGE: a tool for identifying cell type-specific signal in epigenomic data. Cell Rep. 2016; 17:2137–50.

https://doi.org/10.1016/j.celrep.2016.10.059 PMID:27851974

48. Dawber TR, Meadors GF, Moore FE Jr. Epidemiological approaches to heart disease: the framingham study. Am J Public Health Nations Health. 1951; 41:279–81.
https://doi.org/10.2105/ajph.41.3.279 PMID:14819398

49. Design of the women's health initiative clinical trial and observational study. The women's health initiative study group. Control Clin Trials. 1998; 19:61–109.
https://doi.org/10.1016/s0197-2456(97)00078-0 PMID:9492970

50. Anderson GL, Manson J, Wallace R, Lund B, Hall D, Davis S, Shumaker S, Wang CY, Stein E, Prentice RL. Implementation of the women's health initiative study design. Ann Epidemiol. 2003; 13:S5–17.
https://doi.org/10.1016/s1047-2797(03)00043-7 PMID:14575938

51. Taylor HA Jr, Wilson JG, Jones DW, Sarpong DF, Srinivasan A, Garrison RJ, Nelson C, Wyatt SB. Toward resolution of cardiovascular health disparities in African Americans: design and methods of the jackson heart study. Ethn Dis. 2005; 15:S6–4.
PMID:16320381

52. Triche TJ Jr, Weisenberger DJ, Van Den Berg D, Laird PW, Siegmund KD. Low-level processing of illumina infinium DNA methylation BeadArrays. Nucleic Acids Res. 2013; 41:e90.
https://doi.org/10.1093/nar/gkt090 PMID:23476028

53. Aryee MJ, Jaffe AE, Corrada-Bravo H, Ladd-Acosta C, Feinberg AP, Hansen KD, Irizarry RA. Minfi: a flexible and comprehensive bioconductor package for the analysis of infinium DNA methylation microarrays. Bioinformatics. 2014; 30:1363–69.
https://doi.org/10.1093/bioinformatics/btu049 PMID:24478339

54. Fortin JP, Labbe A, Lemire M, Zanke BW, Hudson TJ, Fertig EJ, Greenwood CM, Hansen KD. Functional normalization of 450k methylation array data improves replication in large cancer studies. Genome Biol. 2014; 15:503.
https://doi.org/10.1186/s13059-014-0503-2 PMID:25599564

55. Fortin JP, Triche TJ Jr, Hansen KD. Preprocessing, normalization and integration of the illumina HumanMethylationEPIC array with minfi. Bioinformatics. 2017; 33:558–60.
https://doi.org/10.1093/bioinformatics/btw691 PMID:28035024

56. Horvath S, Oshima J, Martin GM, Lu AT, Quach A, Cohen H, Felton S, Matsuyama M, Lowe D, Kabacik S, Wilson JG, Reiner AP, Maierhofer A, et al. Epigenetic

clock for skin and blood cells applied to hutchinson gilford progeria syndrome and ex vivo studies. Aging (Albany NY). 2018; 10:1758–75.
https://doi.org/10.18632/aging.101508
PMID:30048243

57. Lu AT, Seeboth A, Tsai PC, Sun D, Quach A, Reiner AP, Kooperberg C, Ferrucci L, Hou L, Baccarelli AA, Li Y, Harris SE, Corley J, et al. DNA methylation-based estimator of telomere length. Aging (Albany NY). 2019; 11:5895–923.
https://doi.org/10.18632/aging.102173
PMID:31422385

58. Horvath S, Levine AJ. HIV-1 infection accelerates age according to the epigenetic clock. J Infect Dis. 2015; 212:1563–73.
https://doi.org/10.1093/infdis/jiv277 PMID:25969563

59. Houseman EA, Accomando WP, Koestler DC, Christensen BC, Marsit CJ, Nelson HH, Wiencke JK, Kelsey KT. DNA methylation arrays as surrogate measures of cell mixture distribution. BMC Bioinformatics. 2012; 13:86.
https://doi.org/10.1186/1471-2105-13-86
PMID:22568884

60. Xu Z, Niu L, Li L, Taylor JA. ENmix: a novel background correction method for illumina HumanMethylation450 BeadChip. Nucleic Acids Res. 2016; 44:e20.
https://doi.org/10.1093/nar/gkv907
PMID:26384415

61. Yu G, Wang LG, Han Y, He QY. clusterProfiler: an R package for comparing biological themes among gene clusters. OMICS. 2012; 16:284–87.
https://doi.org/10.1089/omi.2011.0118
PMID:22455463
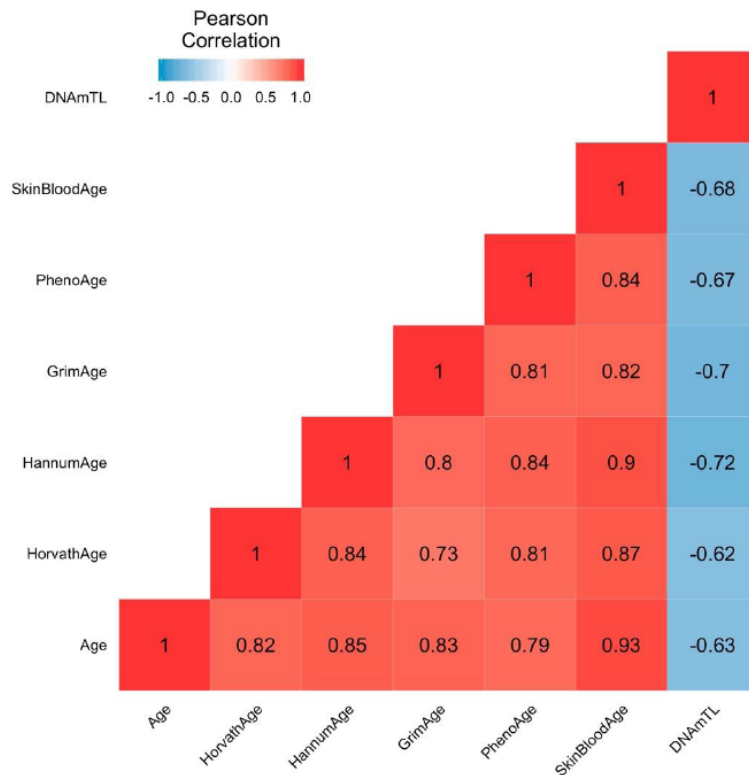
Supplementary Figure 1. Heatmap of pairwise correlations of chronological age and epigenetic ages. The heatmap color-codes the pairwise Pearson correlations of chronological age and epigenetic age in the Framingham Heart Study (N=2326). Age represents the chronological age. HorvathAge, HannumAge, GrimAge, PhenoAge, SkinBloodAge represent measures of epigenetic age derived from the Horvath pan tissue clock, the Hannum clock, the GrimAge clock, the PhenoAge clock, and the SkinBloodAge clock, respectively. DNAmTL represent DNAm-based surrogate markers of telomere length. The shades of color (blue, white, and red) visualize correlation values from -1 to 1. Each square reports a Pearson correlation coefficient.
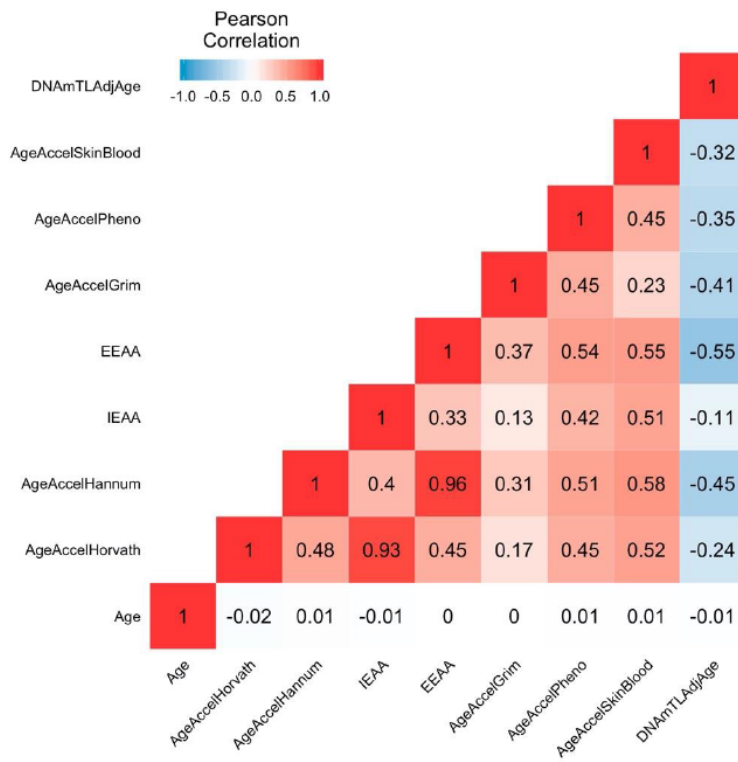
Supplementary Figure 2. Heatmap of pairwise correlations of chronological age and epigenetic age accelerations. The heatmap color-codes the pairwise Pearson correlations of chronological age and epigenetic age accelerations in the Framingham Heart Study (N=2326). Age represents the chronological age. AgeAccelHorvath, AgeAccelHannum, IEAA, EEAA, AgeAccelGrim, AgeAccelPheno, and AgeAccelSkinBlood represent measures of epigenetic age acceleration derived from the Horvath pan tissue clock, the Hannum clock, the intrinsic clock, the extrinsic clock, the GrimAge clock, the PhenoAge clock, the SkinBloodAge clock, respectively. DNAmTLAdjAge represents age adjusted DNAm-based surrogate markers of telomere length. The shades of color (blue, white, and red) visualize correlation values from -1 to 1. Each square reports a Pearson correlation coefficient.

Supplementary Tables

Supplementary Table 1. Distribution of EML for each dataset.

	FHS (450K)	WHI (450K)	JHS (EPIC)	PEG1 (450K)
min(EML)	264	213	1194	603
max(EML)	52783	43768	56691	11645
mean(EML)	2433	1647	3401	2137
sd(EML)	4183	3937	4512	1953
% of probes as SEM	86%	85%	77%	45%

Supplementary Table 2. Biweight midcorrelation analysis of EML.

Outcome = log(EML) **	Meta *		FHS (n = 2326)		WHI (n= 2091)		JHS (n= 1734)		PEG 1 (n = 237)	
	Meta r	Meta P_value	Bicor r	P_value	Bicor r	P_value	Bicor r	P_value	Bicor r	P_value
Age	0.171	1.64E-42	0.244	7.15E-33	0.104	1.73E-06	0.145	1.50E-09	0.176	6.45E-03
BMI	0.005	7.94E-01	0.017	4.23E-01	-0.009	6.91E-01				
DNAm Age Acceleration										
AgeAccelHorvath	0.109	3.25E-18	0.106	3.11E-07	0.140	1.34E-10	0.079	9.68E-04	0.071	2.75E-01
IEAA	0.112	4.04E-19	0.109	1.26E-07	0.144	3.85E-11	0.080	8.50E-04	0.073	2.63E-01
EEAA (Unadjusted for cell types)	0.236	5.82E-79	0.297	1.12E-48	0.212	1.31E-22	0.166	3.09E-12	0.211	1.05E-03
AgeAccelHannum	0.179	2.43E-46	0.225	4.12E-28	0.156	6.55E-13	0.148	6.33E-10	0.095	1.46E-01
AgeAccelGrim	0.162	2.25E-38	0.173	3.74E-17	0.180	9.91E-17	0.111	3.46E-06	0.224	5.23E-04
DNAmADMAdjAge	0.068	4.75E-08	0.121	4.58E-09	0.070	1.41E-03	-0.017	4.71E-01	0.157	1.58E-02
DNAmB2MAdjAge	0.143	3.47E-30	0.189	4.69E-20	0.129	3.44E-09	0.074	2.05E-03	0.287	7.20E-06
DNAmCystatinCAdjAge	0.153	3.02E-34	0.119	8.71E-09	0.241	6.48E-29	0.081	7.30E-04	0.183	4.64E-03
DNAmGDF15AdjAge	0.148	3.64E-32	0.167	6.09E-16	0.127	5.80E-09	0.142	3.01E-09	0.162	1.27E-02
DNAmLeptinAdjAge	-0.025	4.65E-02	-0.021	3.19E-01	-0.035	1.11E-01	-0.031	2.03E-01	0.063	3.34E-01
DNAmPACKYRSAdjAge	0.161	8.96E-38	0.166	7.99E-16	0.172	2.23E-15	0.137	1.10E-08	0.150	2.13E-02
DNAmPAI1AdjAge	0.031	1.47E-02	0.024	2.49E-01	-0.004	8.59E-01	0.061	1.07E-02	0.173	7.56E-03
DNAmTIMP1AdjAge	0.028	2.35E-02	0.070	7.04E-04	0.010	6.41E-01	-0.001	9.72E-01	-0.010	8.80E-01
AgeAccelPheno	0.123	7.28E-23	0.178	4.45E-18	0.106	1.13E-06	0.078	1.20E-03	0.042	5.22E-01
DNAmTLAdjAge	-0.065	1.91E-07	-0.080	1.17E-04	-0.033	1.36E-01	-0.082	6.05E-04	-0.082	2.11E-01
DNAmAgeSkinBloodClockAdjAge	0.047	1.93E-04	0.102	8.32E-07	0.022	3.17E-01	0.019	4.27E-01	-0.080	2.22E-01

Biweight midcorrelation analyses of EML with chronological age, BMI, AgeAccelHorvath, IEAA, extrinsic epigenetic age acceleration (EEAA) derived from the Hannum clock by up-weighting the contribution of age-related blood cell counts, AgeAccelHannum, AgeAccelGrim, age adjusted DNAm-based surrogate markers of adrenomedullin (DNAmADMAdjAge), beta-2 microglobulin (DNAmB2MAdjAge), cystatin C (DNAmCystatinCAdjAge), growth differentiation factor 15 (DNAmGDF15AdjAge), leptin (DNAmLeptinAdjAge), plasminogen activation inhibitor 1 (DNAmPAI1AdjAge), tissue inhibitor metalloproteinase 1 (DNAmTIMP1AdjAge), smoking pack-years (DNAmPACKYRSAdjAge), AgeAccelPheno, age adjusted DNAm-based surrogate markers of telomere length (DNAmTLAdjAge), and age adjusted SkinBlood clock.
* Meta-analysis using Stouffer's method with weights given by the square root of the number of (non-missing) samples in each data set.
** All analyses except EEAA were adjusted for Age, Sex, Race/ethnicity, Cell types; EEAA was not adjusted for cell types.

Supplementary Table 3. Biweight midcorrelation analysis of EML in FHS, stratified by the direction of acceleration.

Outcome = log(EML) [*]	Acceleration		Deceleration	
	Bicor r	**P_value**	**Bicor r**	**P_value**
AgeAccelHorvath	0.178	3.81E-09	-0.039	1.71E-01
IEAA	0.150	4.09E-07	-0.064	2.66E-02
EEAA (Unadjusted for cell types)	0.299	4.74E-25	0.089	2.20E-03
AgeAccelHannum	0.239	3.96E-16	0.085	3.12E-03
AgeAccelGrim	0.136	1.64E-05	0.060	2.77E-02
DNAmADMAdjAge	0.149	5.88E-07	0.029	3.14E-01
DNAmB2MAdjAge	0.130	1.90E-05	0.070	1.34E-02
DNAmCystatinCAdjAge	0.135	8.79E-06	-0.026	3.54E-01
DNAmGDF15AdjAge	0.149	1.61E-06	0.078	4.90E-03
DNAmLeptinAdjAge	0.015	6.04E-01	0.068	2.26E-02
DNAmPACKYRSAdjAge	0.077	2.43E-02	0.049	6.15E-02
DNAmPAI1AdjAge	0.075	1.33E-02	-0.035	2.25E-01
DNAmTIMP1AdjAge	0.092	2.17E-03	-0.058	4.30E-02
AgeAccelPheno	0.206	4.49E-12	0.036	2.08E-01
DNAmTLAdjAge	0.064	2.51E-02	-0.127	2.27E-05
DNAmAgeSkinBloodClockAdjAge	0.168	1.40E-08	-0.023	4.17E-01

* Adjusted for Age, Sex, Cell types.

Supplementary Table 4. Stratification analysis: biweight midcorrelation analysis of EML, stratified by sex.

	PEG 1				FHS				WHI		JHS			
Outcome = log(EML) [*]	Male (n = 126)		Female (n = 111)		Male (n = 1077)		Female (n = 1249)		Femal (n= 2091)		Male (n = 648)		Female (n = 1086)	
	Bicor r	P_value	Bicor r	P_value	Bicor r	P_value	Bicor r	P_value	Bicor r	P_value	Bicor r	P_value	Bicor r	P_value
Age	0.201	2.40E-02	0.200	3.53E-02	0.225	7.53E-14	0.259	1.54E-20	0.104	1.73E-06	0.134	5.98E-04	0.150	7.24E-07
BMI					0.026	3.90E-01	0.025	3.75E-01	-0.009	6.91E-01				
DNAm Age Acceleration														
AgeAccelHorvath	0.105	2.43E-01	0.041	6.71E-01	0.086	4.69E-03	0.126	7.67E-06	0.140	1.34E-10	0.068	8.27E-02	0.082	6.87E-03
IEAA	0.110	2.21E-01	0.033	7.32E-01	0.108	4.02E-04	0.116	4.06E-05	0.144	3.85E-11	0.076	5.19E-02	0.086	4.63E-03
EEAA (Unadjusted for cell types)	0.205	2.13E-02	0.245	9.45E-03	0.305	1.27E-24	0.315	3.35E-30	0.212	1.31E-22	0.180	4.20E-06	0.155	2.90E-07
AgeAccelHannum	0.080	3.73E-01	0.106	2.66E-01	0.215	9.77E-13	0.257	3.02E-20	0.156	6.55E-13	0.158	5.16E-05	0.144	2.05E-06
AgeAccelGrim	0.192	3.13E-02	0.299	1.43E-03	0.218	4.20E-13	0.167	2.71E-09	0.180	9.91E-17	0.082	3.79E-02	0.134	9.43E-06
DNAmADMAdjAge	0.100	2.67E-01	0.223	1.88E-02	0.207	6.85E-12	0.091	1.35E-03	0.070	1.41E-03	-0.024	5.37E-01	0.011	7.06E-01
DNAmB2MAdjAge	0.300	6.40E-04	0.230	1.50E-02	0.238	2.16E-15	0.147	1.94E-07	0.129	3.44E-09	0.063	1.08E-01	0.077	1.13E-02
DNAmCystatinCAdjAge	0.195	2.86E-02	0.187	4.89E-02	0.181	2.42E-09	0.075	7.81E-03	0.241	6.48E-29	0.039	3.25E-01	0.105	5.43E-04
DNAmGDF15AdjAge	0.129	1.49E-01	0.172	7.03E-02	0.211	2.85E-12	0.134	2.06E-06	0.127	5.80E-09	0.097	1.37E-02	0.167	2.91E-08
DNAmLeptinAdjAge	-0.073	4.19E-01	0.138	1.49E-01	0.071	1.94E-02	-0.037	1.89E-01	-0.035	1.11E-01	0.043	2.75E-01	0.046	1.27E-01
DNAmPACKYRSAdjAge	0.184	3.89E-02	0.120	2.10E-01	0.161	1.06E-07	0.179	2.09E-10	0.172	2.23E-15	0.113	4.05E-03	0.147	1.19E-06
DNAmPAI1AdjAge	0.026	7.70E-01	0.362	9.25E-05	0.028	3.66E-01	0.039	1.65E-01	-0.004	8.59E-01	0.053	1.76E-01	0.065	3.21E-02
DNAmTIMP1AdjAge	-0.038	6.72E-01	0.031	7.50E-01	0.100	1.07E-03	0.060	3.41E-02	0.010	6.41E-01	-0.031	4.27E-01	0.016	5.97E-01
AgeAccelPheno	0.123	1.68E-01	-0.080	4.02E-01	0.211	2.66E-12	0.152	6.90E-08	0.106	1.13E-06	0.079	4.47E-02	0.080	8.40E-03
DNAmTLAdjAge	-0.052	5.64E-01	-0.166	8.26E-02	-0.061	4.61E-02	-0.101	3.63E-04	-0.033	1.36E-01	-0.088	2.56E-02	-0.069	2.21E-02
DNAmAgeSkinBloodClockAdjAge	-0.029	7.45E-01	-0.141	1.40E-01	0.105	5.37E-04	0.102	2.90E-04	0.022	3.17E-01	-0.010	7.99E-01	0.032	2.88E-01
Cell types														

CD8.naive	0.043	6.32E-01	0.044	6.47E-01	-0.076	1.27E-02	-0.068	1.62E-02	0.020	3.66E-01	-0.008	8.30E-01	-0.010 7.32E-01
CD8pCD28nCD45RAn	0.018	8.44E-01	0.179	6.00E-02	0.076	1.26E-02	0.096	7.00E-04	0.086	8.16E-05	0.068	8.43E-02	0.030 3.28E-01
PlasmaBlast	-0.089	3.19E-01	-0.125	1.92E-01	-0.012	6.90E-01	-0.088	1.81E-03	-0.070	1.39E-03	-0.148	1.60E-04	-0.139 4.57E-06
CD4T	-0.134	1.35E-01	-0.133	1.65E-01	-0.150	7.97E-07	-0.143	4.03E-07	-0.113	2.17E-07	-0.049	2.17E-01	-0.120 7.55E-05
Gran	-0.182	4.18E-02	-0.128	1.80E-01	-0.065	3.37E-02	-0.084	2.81E-03	-0.016	4.74E-01	-0.065	9.80E-02	-0.111 2.57E-04

[*] All analyses except EEAA were adjusted for Age, Sex, Race/ethnicity, Cell types; EEAA was not adjusted for cell types.

Supplementary Table 5. Sensitivity analysis: biweight midcorrelation analysis of EML, additionally adjusted for age[2].

	PEG 1 (n = 237)				FHS (n = 2326)				WHI (n= 2091)				JHS (n= 1734)			
	Model 1[*]		Model 2[**]		Model 1[*]		Model 2[**]		Model 1[*]		Model 2[**]		Model 1[*]		Model 2[**]	
Outcome = log(EML)	Bicor r	P_value	Bicor r	P_value	Bicor r	P_value	Bicor r	P_value	Bicor r	P_value	Bicor r	P_value	Bicor r	P_value	Bicor r	P_value
AgeAccelHorvath	0.071	2.75E-01	0.089	1.72E-01	0.106	3.11E-07	0.106	3.08E-07	0.140	1.34E-10	0.141	9.63E-11	0.079	9.68E-04	0.100	2.84E-05
IEAA	0.073	2.63E-01	0.091	1.61E-01	0.109	1.26E-07	0.109	1.23E-07	0.144	3.85E-11	0.144	3.19E-11	0.080	8.50E-04	0.102	2.18E-05
EEAA (Unadjusted for cell types)	0.211	1.05E-03	0.225	4.80E-04	0.297	1.12E-48	0.298	7.40E-49	0.212	1.31E-22	0.210	2.35E-22	0.166	3.09E-12	0.168	2.13E-12
AgeAccelHannum	0.095	1.46E-01	0.111	8.81E-02	0.225	4.12E-28	0.225	3.79E-28	0.156	6.55E-13	0.156	8.30E-13	0.148	6.33E-10	0.158	3.69E-11
AgeAccelGrim	0.224	5.23E-04	0.219	7.01E-04	0.173	3.74E-17	0.173	3.87E-17	0.180	9.91E-17	0.180	1.09E-16	0.111	3.46E-06	0.118	8.87E-07
DNAmADMAdjAge	0.157	1.58E-02	0.156	1.63E-02	0.121	4.58E-09	0.121	4.65E-09	0.070	1.41E-03	0.069	1.56E-03	-0.017	4.71E-01	-0.019	4.34E-01
DNAmB2MAdjAge	0.287	7.20E-06	0.288	6.61E-06	0.189	4.69E-20	0.188	4.84E-20	0.129	3.44E-09	0.128	4.33E-09	0.074	2.05E-03	0.072	2.75E-03
DNAmCystatinCAdjAge	0.183	4.64E-03	0.182	4.96E-03	0.119	8.71E-09	0.119	8.84E-09	0.241	6.48E-29	0.240	8.64E-29	0.081	7.30E-04	0.075	1.69E-03
DNAmGDF15AdjAge	0.162	1.27E-02	0.162	1.26E-02	0.167	6.09E-16	0.167	6.12E-16	0.127	5.80E-09	0.126	7.40E-09	0.142	3.01E-09	0.143	2.11E-09
DNAmLeptinAdjAge	0.063	3.34E-01	0.061	3.46E-01	-0.021	3.19E-01	-0.021	3.23E-01	-0.035	1.11E-01	-0.034	1.20E-01	-0.031	2.03E-01	-0.031	2.02E-01
DNAmPACKYRSAdjAge	0.150	2.13E-02	0.144	2.64E-02	0.166	7.99E-16	0.166	8.60E-16	0.172	2.23E-15	0.173	1.67E-15	0.137	1.10E-08	0.148	6.41E-10
DNAmPAI1AdjAge	0.173	7.56E-03	0.170	8.84E-03	0.024	2.49E-01	0.024	2.48E-01	-0.004	8.59E-01	-0.001	9.57E-01	0.061	1.07E-02	0.067	5.03E-03
DNAmTIMP1AdjAge	-0.010	8.80E-01	-0.008	9.08E-01	0.070	7.04E-04	0.070	7.11E-04	0.010	6.41E-01	0.008	7.01E-01	-0.001	9.72E-01	-0.002	9.42E-01
AgeAccelPheno	0.042	5.22E-01	0.051	4.36E-01	0.178	4.45E-18	0.178	4.22E-18	0.106	1.13E-06	0.107	9.47E-07	0.078	1.20E-03	0.083	5.33E-04
DNAmTLAdjAge	-0.082	2.11E-01	-0.087	1.84E-01	-0.080	1.17E-04	-0.080	1.16E-04	-0.033	1.36E-01	-0.033	1.30E-01	-0.082	6.05E-04	-0.093	1.08E-04
DNAmAgeSkinBloodClockAdjAge	-0.080	2.22E-01	-0.045	4.91E-01	0.102	8.32E-07	0.102	7.97E-07	0.022	3.17E-01	0.024	2.79E-01	0.019	4.27E-01	0.047	5.25E-02

[*] Adjusted (Age, Sex, Race/ethnicity, Cell types)
[**] Adjusted (Age, Age2, Sex, Race/ethnicity, Cell types)

Supplementary Table 6. Sensitivity analysis: biweight midcorrelation analysis of EML, additionally adjusted for BMI.

	FHS (n = 2326)				WHI (n= 2091)			
	Model 1[*]		Model 2[**]		Model 1[*]		Model 2[**]	
Outcome = log(EML)	Bicor r	P_value	Bicor r	P_value	Bicor r	P_value	Bicor r	P_value
AgeAccelHorvath	0.106	3.11E-07	0.110	1.16E-07	0.140	1.34E-10	0.144	4.13E-11
IEAA	0.109	1.26E-07	0.113	4.37E-08	0.144	3.85E-11	0.148	1.36E-11
EEAA (Unadjusted for cell types)	0.297	1.12E-48	0.298	1.29E-48	0.212	1.31E-22	0.216	2.92E-23
AgeAccelHannum	0.225	4.12E-28	0.226	3.19E-28	0.156	6.55E-13	0.157	5.85E-13
AgeAccelGrim	0.173	3.74E-17	0.172	8.56E-17	0.180	9.91E-17	0.181	1.02E-16
DNAmADMAdjAge	0.121	4.58E-09	0.123	2.93E-09	0.070	1.41E-03	0.074	7.79E-04
DNAmB2MAdjAge	0.189	4.69E-20	0.190	2.84E-20	0.129	3.44E-09	0.130	2.44E-09
DNAmCystatinCAdjAge	0.119	8.71E-09	0.117	1.51E-08	0.241	6.48E-29	0.244	1.31E-29
DNAmGDF15AdjAge	0.167	6.09E-16	0.165	1.37E-15	0.127	5.80E-09	0.127	7.21E-09
DNAmLeptinAdjAge	-0.021	3.19E-01	-0.021	3.21E-01	-0.035	1.11E-01	-0.029	1.93E-01
DNAmPACKYRSAdjAge	0.166	7.99E-16	0.164	1.88E-15	0.172	2.23E-15	0.169	1.09E-14
DNAmPAI1AdjAge	0.024	2.49E-01	0.021	3.16E-01	-0.004	8.59E-01	0.007	7.34E-01
DNAmTIMP1AdjAge	0.070	7.04E-04	0.068	1.03E-03	0.010	6.41E-01	0.016	4.71E-01

AgeAccelPheno	0.178	4.45E-18	0.180	2.10E-18	0.106	1.13E-06	0.111	4.26E-07
DNAmTLAdjAge	-0.080	1.17E-04	-0.079	1.47E-04	-0.033	1.36E-01	-0.033	1.35E-01
DNAmAgeSkinBloodClockAdjAge	0.102	8.32E-07	0.104	5.72E-07	0.022	3.17E-01	0.024	2.71E-01

[*] Adjusted (Age, Sex, Race/ethnicity, Cell types)

[**] Adjusted (Age, Sex, Race/ethnicity, Cell types, BMI)

Supplementary Table 7. Sensitivity analysis: Biweight midcorrelation analysis of EML in FHS using different SEM cutoffs in FHS.

Outcome = log(EML) [*]	EML (3IQR)		EML (2IQR) [**]		EML (4IQR) [***]	
	Bicor r	P_value	Bicor r	P_value	Bicor r	P_value
Age	0.244	7.15E-33	0.223	1.02E-27	0.247	1.13E-33
BMI	0.017	4.23E-01	0.006	7.60E-01	0.019	3.49E-01
DNAm Age Acceleration						
AgeAccelHorvath	0.106	3.11E-07	0.073	4.38E-04	0.112	5.44E-08
IEAA	0.109	1.26E-07	0.077	2.00E-04	0.135	5.28E-11
EEAA (Unadjusted for cell types)	0.297	1.12E-48	0.281	1.89E-43	0.293	2.46E-47
AgeAccelHannum	0.225	4.12E-28	0.224	5.97E-28	0.204	1.98E-23
AgeAccelGrim	0.173	3.74E-17	0.147	1.03E-12	0.180	1.75E-18
DNAmADMAdjAge	0.121	4.58E-09	0.084	4.41E-05	0.133	1.31E-10
DNAmB2MAdjAge	0.189	4.69E-20	0.178	3.79E-18	0.180	2.28E-18
DNAmCystatinCAdjAge	0.119	8.71E-09	0.116	2.03E-08	0.111	6.85E-08
DNAmGDF15AdjAge	0.167	6.09E-16	0.157	2.52E-14	0.161	4.38E-15
DNAmLeptinAdjAge	-0.021	3.19E-01	-0.019	3.62E-01	-0.027	1.97E-01
DNAmPACKYRSAdjAge	0.166	7.99E-16	0.142	5.64E-12	0.176	1.05E-17
DNAmPAI1AdjAge	0.024	2.49E-01	0.005	8.17E-01	0.037	7.75E-02
DNAmTIMP1AdjAge	0.070	7.04E-04	0.068	9.46E-04	0.071	6.02E-04
AgeAccelPheno	0.178	4.45E-18	0.173	3.96E-17	0.164	1.37E-15
DNAmTLAdjAge	-0.080	1.17E-04	-0.068	1.04E-03	-0.073	4.37E-04
DNAmAgeSkinBloodClockAdjAge	0.102	8.32E-07	0.072	5.20E-04	0.116	1.77E-08
Cell types						
CD8.naive	-0.072	5.20E-04	-0.038	6.97E-02	-0.084	4.77E-05
CD8pCD28nCD45RAn	0.085	3.90E-05	0.112	6.64E-08	0.038	6.37E-02
PlasmaBlast	-0.054	8.94E-03	-0.096	3.13E-06	-0.021	3.10E-01
CD4T	-0.146	1.68E-12	-0.176	9.14E-18	-0.149	5.34E-13
Gran	-0.075	2.72E-04	-0.074	3.37E-04	-0.066	1.52E-03

[*] Adjusted for age, sex, cell types.

[**] SEMs (2IQR) were defined as DNA methylation mutations that were greater than 2 times the IQR above the upper quartile of a given CpG or less than 2 times the IQR below the lower quartile of a given CpG.

[***] SEMs (4IQR) were defined as DNA methylation mutations that were greater than 4 times the IQR above the upper quartile of a given CpG or less than 4 times the IQR below the lower quartile of a given CpG.

Supplementary Table 8. Sensitivity analysis: biweight midcorrelation analysis of EML derived from methylation data with various normalization methods (Illumina, Noob and Quantile normalization).

Outcome = log(EML)	PEG 1 (n = 237)							
	Illumina		Functional		Noob		Quantile	
	Bicor r	P_value	Bicor r	P_value	Bicor r	P_value	Bicor r	P_value
Adjusted (Age, Sex, Race/ethnicity, Cell types)								
AgeAccelHorvath	0.075	2.49E-01	0.070	2.82E-01	0.077	2.40E-01	0.021	7.50E-01
IEAA	0.080	2.17E-01	0.067	3.07E-01	0.074	2.59E-01	0.029	6.55E-01
AgeAccelHannum	0.109	9.29E-02	0.093	1.52E-01	0.104	1.10E-01	0.036	5.86E-01
AgeAccelGrim	0.203	1.71E-03	0.213	9.69E-04	0.241	1.82E-04	0.134	3.93E-02
Cell types								
CD8.naive	0.070	2.84E-01	0.042	5.23E-01	0.029	6.52E-01	0.066	3.10E-01
CD8pCD28nCD45RAn	0.063	3.34E-01	0.082	2.07E-01	0.097	1.36E-01	0.074	2.58E-01
PlasmaBlast	-0.104	1.11E-01	-0.110	9.23E-02	-0.111	8.91E-02	-0.068	2.98E-01
CD4T	-0.080	2.20E-01	-0.118	6.95E-02	-0.115	7.66E-02	0.018	7.85E-01
Gran	-0.152	1.90E-02	-0.170	8.67E-03	-0.163	1.21E-02	-0.013	8.48E-01

Supplementary Table 9. SEMs enriched within clock CpGs.

Clock	FHS (n = 2326)	WHI (n= 2091)	JHS (n= 1734)	PEG 1 (n = 237)
	N	N	N	N
HorvathClock (353 CpGs)				
Significant	46	34	22	4
Non-Significant	2280	2057	1712	233
PhenoClock (513 CpGs)				
Significant	151	97	121	19
Non-Significant	2175	1994	1613	218
HannumClock (71 CpGs)				
Significant	26	10	19	5
Non-Significant	2300	2081	1715	232

Supplementary Table 10. SEMs enriched within gene regions

Genomic region	FHS (n = 2326)	WHI (n= 2091)	JHS (n= 1734)	PEG 1 (n = 237)
	N	N	N	N
TSS1500				
Significant	545	110	229	23
Non-Significant	1781	1981	1505	214
TSS200				
Significant	908	385	372	142
Non-Significant	1418	1706	1362	95
5'UTR				
Significant	213	71	64	8
Non-Significant	2113	2020	1670	229
1stExon				
Significant	595	346	322	84
Non-Significant	1731	1745	1412	153
Gene Body				
Significant	296	693	357	24
Non-Significant	2030	1398	1377	213
3'UTR				
Significant	110	276	179	6
Non-Significant	2216	1815	1555	231

Supplementary Table 11. SEMs enriched within regulatory regions.

	JHS (n= 1734)
Genomic region	**N**
Enhancer from FANTOM5	
Significant	54
Non-Significant	1680
DNase hypersensitive from ENCODE	
Significant	284
Non-Significant	1450
Open chromatin from ENCODE	
Significant	436
Non-Significant	1298
Transcription factor binding site from ENCODE	
Significant	383
Non-Significant	1351
Promoter from Methylation Consortium	
Significant	165
Non-Significant	1578

Supplementary Table 12. Top SEMs enriched KEGG pathways significantly associated with faster AgeAccelHorvath.

	KEGG Pathway	Description	Number of people with SEMs enriched	AgeAccel_Coef[*]	AgeAccel_Pvalue
FHS (n = 2326)	hsa05165	Human papillomavirus infection	355	1.664	7.62E-07
	hsa04360	Axon guidance	347	1.726	8.53E-07
	hsa05032	Morphine addiction	346	2.138	1.13E-11
	hsa04713	Circadian entrainment	341	1.796	4.97E-08
	hsa05033	Nicotine addiction	339	2.239	4.33E-13
	hsa04510	Focal adhesion	332	1.684	1.25E-06
	hsa04080	Neuroactive ligand-receptor interaction	326	2.487	2.84E-15
	hsa04724	Glutamatergic synapse	300	2.412	7.38E-13
	hsa04934	Cushing syndrome	297	2.041	1.15E-08
	hsa04727	GABAergic synapse	294	2.419	7.00E-13
WHI (n= 2091)	hsa00053	Ascorbate and aldarate metabolism	312	0.800	1.88E-02
	hsa04514	Cell adhesion molecules (CAMs)	237	1.255	8.19E-04
	hsa04724	Glutamatergic synapse	231	1.220	5.95E-03
	hsa04360	Axon guidance	229	2.071	8.38E-06
	hsa04713	Circadian entrainment	208	2.083	4.77E-06
	hsa05166	Human T-cell leukemia virus 1 infection	193	-1.660	5.10E-05
	hsa05032	Morphine addiction	189	2.541	1.45E-08
	hsa04934	Cushing syndrome	171	1.504	3.23E-03
	hsa04921	Oxytocin signaling pathway	167	1.445	6.29E-03
	hsa04020	Calcium signaling pathway	165	2.235	8.79E-06
JHS (n= 1734)	hsa05032	Morphine addiction	402	1.167	9.84E-04
	hsa04713	Circadian entrainment	395	0.830	2.73E-02
	hsa04921	Oxytocin signaling pathway	372	0.798	3.33E-02
	hsa04020	Calcium signaling pathway	327	1.258	8.01E-04
	hsa04512	ECM-receptor interaction	317	1.032	1.44E-02
	hsa04727	GABAergic synapse	282	1.093	9.28E-03
	hsa04934	Cushing syndrome	249	1.370	1.00E-03
	hsa04014	Ras signaling pathway	245	0.957	3.90E-02
	hsa05412	Arrhythmogenic right ventricular cardiomyopathy (ARVC)	227	1.690	1.44E-04
	hsa04261	Adrenergic signaling in cardiomyocytes	226	1.006	2.95E-02

	KEGG Pathway	Description			
PEG 1 (n = 237)	hsa04360	Axon guidance	59	0.319	9.06E-01
	hsa04713	Circadian entrainment	52	0.226	9.06E-01
	hsa05224	Breast cancer	46	0.586	8.45E-01
	hsa05165	Human papillomavirus infection	45	2.202	3.04E-01
	hsa05032	Morphine addiction	44	0.182	9.21E-01
	hsa05226	Gastric cancer	44	0.868	7.78E-01
	hsa04934	Cushing syndrome	43	0.907	7.78E-01
	hsa04390	Hippo signaling pathway	39	0.916	7.78E-01
	hsa04724	Glutamatergic synapse	39	1.630	5.97E-01
	hsa04015	Rap1 signaling pathway	37	-0.390	8.94E-01

[*] Age acceleration residual as dependent variable, significant enrichment as independent variable, adjusted for nlog(EML)

Supplementary Table 13. Top SEMs enriched KEGG pathways significantly associated with faster AgeAccelHannum

	KEGG Pathway	Description	Number of people with SEMs enriched	AgeAccel_Coef[*]	AgeAccel_Pvalue
FHS (n = 2326)	hsa05165	Human papillomavirus infection	355	1.143	1.14E-03
	hsa04360	Axon guidance	347	0.792	3.98E-02
	hsa05032	Morphine addiction	346	2.222	1.67E-12
	hsa04713	Circadian entrainment	341	1.959	2.24E-09
	hsa05033	Nicotine addiction	339	2.083	1.69E-11
	hsa04510	Focal adhesion	332	1.074	3.35E-03
	hsa04080	Neuroactive ligand-receptor interaction	326	2.262	1.13E-12
	hsa04724	Glutamatergic synapse	300	2.029	1.84E-09
	hsa04934	Cushing syndrome	297	2.283	1.57E-10
	hsa00053	Ascorbate and aldarate metabolism	296	0.917	5.61E-03
WHI (n= 2091)	hsa04724	Glutamatergic synapse	231	1.461	5.59E-04
	hsa04360	Axon guidance	229	1.477	1.19E-03
	hsa04713	Circadian entrainment	208	1.987	7.57E-06
	hsa05166	Human T-cell leukemia virus 1 infection	193	-1.133	5.13E-03
	hsa05032	Morphine addiction	189	2.373	5.72E-08
	hsa04934	Cushing syndrome	171	2.160	9.38E-06
	hsa04921	Oxytocin signaling pathway	167	1.330	9.42E-03
	hsa04020	Calcium signaling pathway	165	1.844	1.77E-04
	hsa04510	Focal adhesion	145	-1.175	4.02E-02
	hsa04024	cAMP signaling pathway	137	2.147	3.52E-05
JHS (n= 1734)	hsa04360	Axon guidance	451	0.630	3.43E-02
	hsa05032	Morphine addiction	402	0.927	5.24E-04
	hsa04713	Circadian entrainment	395	0.582	3.85E-02
	hsa04020	Calcium signaling pathway	327	0.898	1.62E-03
	hsa04512	ECM-receptor interaction	317	0.841	6.33E-03
	hsa04727	GABAergic synapse	282	1.503	4.07E-08
	hsa05165	Human papillomavirus infection	277	0.685	3.43E-02
	hsa04934	Cushing syndrome	249	1.445	9.84E-07
	hsa04024	cAMP signaling pathway	239	0.906	7.88E-03
	hsa05412	Arrhythmogenic right ventricular cardiomyopathy (ARVC)	227	0.865	1.91E-02
PEG 1 (n = 237)	hsa04360	Axon guidance	59	0.418	8.86E-01
	hsa04713	Circadian entrainment	52	1.182	7.74E-01
	hsa05224	Breast cancer	46	-0.554	8.86E-01
	hsa05165	Human papillomavirus infection	45	0.654	8.68E-01
	hsa05032	Morphine addiction	44	0.060	9.81E-01
	hsa05226	Gastric cancer	44	0.345	8.86E-01
	hsa04934	Cushing syndrome	43	0.820	8.66E-01

	KEGG Pathway	Description	Number of people with SEMs enriched	AgeAccel_Coef*	AgeAccel_Pvalue
	hsa04390	Hippo signaling pathway	39	0.524	8.86E-01
	hsa04724	Glutamatergic synapse	39	1.877	6.22E-01
	hsa04015	Rap1 signaling pathway	37	-0.117	9.61E-01

* Age acceleration residual as dependent variable, significant enrichment as independent variable, adjusted for nlog(EML)

Supplementary Table 14. Top SEMs enriched KEGG pathways significantly associated with faster IEAA.

	KEGG Pathway	Description	Number of people with SEMs enriched	AgeAccel_Coef*	AgeAccel_Pvalue
FHS (n = 2326)	hsa05165	Human papillomavirus infection	355	0.887	2.56E-02
	hsa05032	Morphine addiction	346	1.055	3.76E-03
	hsa04713	Circadian entrainment	341	0.939	1.50E-02
	hsa05033	Nicotine addiction	339	1.560	3.24E-06
	hsa04080	Neuroactive ligand-receptor interaction	326	1.678	1.16E-06
	hsa04724	Glutamatergic synapse	300	1.392	2.08E-04
	hsa04934	Cushing syndrome	297	1.055	1.22E-02
	hsa04727	GABAergic synapse	294	1.400	2.06E-04
	hsa04020	Calcium signaling pathway	292	1.850	7.65E-07
	hsa05224	Breast cancer	291	1.021	1.53E-02
WHI (n= 2091)	hsa04724	Glutamatergic synapse	231	1.048	1.74E-02
	hsa04360	Axon guidance	229	1.439	2.09E-03
	hsa04713	Circadian entrainment	208	1.645	2.88E-04
	hsa05166	Human T-cell leukemia virus 1 infection	193	-1.187	4.08E-03
	hsa05032	Morphine addiction	189	2.108	3.21E-06
	hsa04921	Oxytocin signaling pathway	167	1.072	4.54E-02
	hsa04020	Calcium signaling pathway	165	1.789	3.44E-04
	hsa04015	Rap1 signaling pathway	163	1.306	1.63E-02
	hsa04024	cAMP signaling pathway	137	2.296	1.60E-05
	hsa05033	Nicotine addiction	135	2.201	1.11E-05
JHS (n= 1734)	hsa05032	Morphine addiction	402	0.884	3.66E-02
	hsa04934	Cushing syndrome	249	1.005	4.40E-02
	hsa05412	Arrhythmogenic right ventricular cardiomyopathy (ARVC)	227	1.322	8.85E-03
	hsa05033	Nicotine addiction	222	1.367	3.57E-03
	hsa05226	Gastric cancer	166	1.293	2.91E-02
	hsa04080	Neuroactive ligand-receptor interaction	164	2.127	2.41E-05
	hsa05414	Dilated cardiomyopathy (DCM)	155	1.893	2.23E-04
	hsa04721	Synaptic vesicle cycle	115	2.110	2.54E-04
	hsa05410	Hypertrophic cardiomyopathy (HCM)	108	2.627	1.26E-05
	hsa04950	Maturity onset diabetes of the young	81	1.958	8.00E-03
PEG 1 (n = 237)	hsa04360	Axon guidance	59	-0.324	9.32E-01
	hsa04713	Circadian entrainment	52	-0.461	9.10E-01
	hsa05224	Breast cancer	46	-0.076	9.81E-01
	hsa05165	Human papillomavirus infection	45	2.479	1.66E-01
	hsa05032	Morphine addiction	44	-0.302	9.32E-01
	hsa05226	Gastric cancer	44	0.063	9.81E-01
	hsa04934	Cushing syndrome	43	0.413	9.32E-01
	hsa04390	Hippo signaling pathway	39	0.472	9.10E-01
	hsa04724	Glutamatergic synapse	39	1.412	7.33E-01
	hsa04015	Rap1 signaling pathway	37	-1.111	8.06E-01

* Age acceleration residual as dependent variable, significant enrichment as independent variable, adjusted for nlog(EML)

Supplementary Table 15. Top SEMs enriched KEGG pathways significantly associated with faster AgeAccelGrim.

	KEGG Pathway	Description	Number of people with SEMs enriched	AgeAccel_Coef[*]	AgeAccel_Pvalue
FHS (n = 2326)	hsa04360	Axon guidance	347	-0.798	4.97E-02
	hsa04510	Focal adhesion	332	-0.855	3.24E-02
	hsa04080	Neuroactive ligand-receptor interaction	326	-0.742	4.31E-02
	hsa04390	Hippo signaling pathway	284	-1.431	5.72E-04
	hsa04151	PI3K-Akt signaling pathway	265	-0.956	2.56E-02
	hsa05205	Proteoglycans in cancer	263	-1.454	8.02E-04
	hsa05226	Gastric cancer	256	-1.399	1.04E-03
	hsa04512	ECM-receptor interaction	252	-0.865	3.81E-02
	hsa04550	Signaling pathways regulating pluripotency of stem cells	249	-1.598	1.57E-04
	hsa04010	MAPK signaling pathway	240	-1.168	9.80E-03
WHI (n= 2091)	hsa04510	Focal adhesion	145	-1.069	2.69E-02
	hsa04010	MAPK signaling pathway	135	-1.251	1.37E-02
	hsa05033	Nicotine addiction	135	0.969	2.45E-02
	hsa04080	Neuroactive ligand-receptor interaction	130	1.157	8.32E-03
	hsa04072	Phospholipase D signaling pathway	129	-1.556	1.20E-03
	hsa04310	Wnt signaling pathway	117	-1.251	1.72E-02
	hsa04152	AMPK signaling pathway	111	-1.792	4.40E-04
	hsa04911	Insulin secretion	102	1.178	1.86E-02
	hsa04014	Ras signaling pathway	95	-1.463	1.03E-02
	hsa04144	Endocytosis	91	-1.763	1.12E-03
JHS (n= 1734)	hsa04724	Glutamatergic synapse	573	-0.148	9.05E-01
	hsa04360	Axon guidance	451	0.254	8.92E-01
	hsa04725	Cholinergic synapse	437	0.164	9.05E-01
	hsa04510	Focal adhesion	413	-0.163	9.07E-01
	hsa05032	Morphine addiction	402	0.352	7.97E-01
	hsa00053	Ascorbate and aldarate metabolism	400	0.093	9.38E-01
	hsa04713	Circadian entrainment	395	0.240	8.92E-01
	hsa04015	Rap1 signaling pathway	391	0.228	8.95E-01
	hsa00040	Pentose and glucuronate interconversions	374	-0.038	9.62E-01
	hsa04080	Neuroactive ligand-receptor interaction	164	1.793	9.56E-03
PEG 1 (n = 237)	hsa04360	Axon guidance	59	-0.468	9.20E-01
	hsa04713	Circadian entrainment	52	-0.521	9.20E-01
	hsa05224	Breast cancer	46	-2.263	4.84E-01
	hsa05165	Human papillomavirus infection	45	-1.114	8.36E-01
	hsa05032	Morphine addiction	44	-0.895	9.20E-01
	hsa05226	Gastric cancer	44	-1.497	6.67E-01
	hsa04934	Cushing syndrome	43	0.378	9.20E-01
	hsa04390	Hippo signaling pathway	39	-0.786	9.20E-01
	hsa04724	Glutamatergic synapse	39	0.526	9.20E-01
	hsa04015	Rap1 signaling pathway	37	-1.882	6.67E-01

[*] Age acceleration residual as dependent variable, significant enrichment as independent variable, adjusted for nlog(EML)

Supplementary Table 16. Top SEMs enriched KEGG pathways significantly associated with faster AgeAccelPheno.

	KEGG Pathway	Description	Number of people with SEMs enriched	AgeAccel_Coef*	AgeAccel_Pvalue
FHS (n = 2326)	hsa05165	Human papillomavirus infection	355	0.003	1.00E+00
	hsa04360	Axon guidance	347	-1.074	2.14E-01
	hsa05032	Morphine addiction	346	0.409	8.14E-01
	hsa04713	Circadian entrainment	341	0.078	9.62E-01
	hsa05033	Nicotine addiction	339	0.300	8.43E-01
	hsa04510	Focal adhesion	332	0.049	9.74E-01
	hsa04080	Neuroactive ligand-receptor interaction	326	0.120	9.13E-01
	hsa04724	Glutamatergic synapse	300	-0.022	9.84E-01
	hsa04934	Cushing syndrome	297	-0.255	8.99E-01
	hsa00053	Ascorbate and aldarate metabolism	296	0.168	9.02E-01
WHI (n= 2091)	hsa04940	Type I diabetes mellitus	493	-0.525	4.15E-01
	hsa05330	Allograft rejection	337	-0.167	8.74E-01
	hsa05332	Graft-versus-host disease	313	-0.344	6.60E-01
	hsa00053	Ascorbate and aldarate metabolism	312	0.285	7.38E-01
	hsa00040	Pentose and glucuronate interconversions	305	0.127	9.19E-01
	hsa05416	Viral myocarditis	299	-0.086	9.67E-01
	hsa00860	Porphyrin and chlorophyll metabolism	272	0.048	9.81E-01
	hsa05320	Autoimmune thyroid disease	272	-0.228	8.32E-01
	hsa04612	Antigen processing and presentation	257	-0.228	8.32E-01
	hsa00980	Metabolism of xenobiotics by cytochrome P450	253	-0.017	9.88E-01
JHS (n= 1734)	hsa04724	Glutamatergic synapse	573	0.029	9.58E-01
	hsa04360	Axon guidance	451	0.290	8.08E-01
	hsa04725	Cholinergic synapse	437	0.150	8.98E-01
	hsa04510	Focal adhesion	413	-0.604	5.25E-01
	hsa05032	Morphine addiction	402	0.785	3.30E-01
	hsa00053	Ascorbate and aldarate metabolism	400	0.464	5.82E-01
	hsa04713	Circadian entrainment	395	1.052	1.57E-01
	hsa04080	Neuroactive ligand-receptor interaction	164	2.014	3.77E-02
	hsa05414	Dilated cardiomyopathy (DCM)	155	2.054	3.77E-02
	hsa05410	Hypertrophic cardiomyopathy (HCM)	108	2.306	4.22E-02
PEG 1 (n = 237)	hsa04360	Axon guidance	59	-0.606	9.29E-01
	hsa04713	Circadian entrainment	52	0.351	9.53E-01
	hsa05224	Breast cancer	46	-1.177	9.29E-01
	hsa05165	Human papillomavirus infection	45	0.292	9.62E-01
	hsa05032	Morphine addiction	44	-0.684	9.29E-01
	hsa05226	Gastric cancer	44	0.589	9.29E-01
	hsa04934	Cushing syndrome	43	0.075	9.86E-01
	hsa04390	Hippo signaling pathway	39	-2.425	7.03E-01
	hsa04724	Glutamatergic synapse	39	1.064	9.29E-01
	hsa04015	Rap1 signaling pathway	37	-0.464	9.29E-01

* Age acceleration residual as dependent variable, significant enrichment as independent variable, adjusted for nlog(SEM)

Supplementary Table 17. Association between Clock region-specific EML and corresponding DNAm AgeAccel.

Outcome = log(clock EML) Model [*]	PEG 1 (n = 237)		FHS (n = 2326)		WHI (n= 2091)		JHS (n= 1734)	
	Bicor r	P_value	Bicor r	P_value	Bicor r	P_value	Bicor r	P_value
HorvathClock (353 CpGs) v. AgeAccel	0.008	9.07E-01	0.020	8.35E-01	0.034	1.23E-01	0.180	4.16E-14
PhenoClock (513 CpGs) v. AgeAccelPheno	0.008	9.03E-01	0.013	5.29E-01	0.058	8.26E-03	0.064	7.57E-03
HannumClock (71CpGs) v. AgeAccelHannum	0.071	2.77E-01	-0.030	1.51E-01	0.017	4.28E-01	0.044	6.84E-02

[*] Adjusted for Age, Sex, Cell types, Race/ethnicity, Log(total EML)

Supplementary Table 18. Biweight midcorrelation analysis of regulatory region-specific EML in JHS.

Outcome = log(Region EML) [*]	Enhancer (CpGs = 26395)		DNAse (CpGs = 466862)		Open Chromatin (CpGs = 108758)		TFBS (CpGs = 122647)		Promoter (CpGs = 110008)	
	Bicor r	P_value	Bicor r	P_value	Bicor r	P_value	Bicor r	P_value	Bicor r	P_value
Age	-0.045	6.01E-02	0.169	1.24E-12	0.019	4.34E-01	-0.065	7.11E-03	-0.027	2.58E-01
DNAm Age Acceleration										
AgeAccelHorvath	-0.027	2.66E-01	0.129	6.75E-08	0.026	2.73E-01	-0.012	6.14E-01	-0.003	8.94E-01
IEAA	-0.027	2.64E-01	0.132	3.26E-08	0.025	3.04E-01	-0.023	3.34E-01	-0.002	9.32E-01
AgeAccelHannum	-0.059	1.36E-02	0.236	2.08E-23	0.002	9.26E-01	-0.089	1.94E-04	-0.029	2.35E-01
AgeAccelGrim	0.022	3.66E-01	0.098	4.01E-05	0.018	4.56E-01	-0.038	1.17E-01	-0.013	5.99E-01
Cell types										
CD8.naive	-0.004	8.69E-01	-0.101	2.40E-05	0.029	2.20E-01	0.027	2.67E-01	-0.029	2.23E-01
CD8pCD28nCD45RAn	0.016	5.10E-01	0.073	2.33E-03	-0.004	8.57E-01	-0.024	3.21E-01	0.038	1.12E-01
PlasmaBlast	-0.020	3.98E-01	-0.011	6.41E-01	0.038	1.11E-01	0.016	4.99E-01	-0.040	9.44E-02
CD4T	-0.012	6.05E-01	-0.090	1.79E-04	0.086	3.33E-04	0.109	5.20E-06	0.016	5.03E-01
Gran	-0.067	5.15E-03	-0.181	3.39E-14	0.106	8.95E-06	0.151	2.47E-10	-0.049	4.21E-02

[*] Adjusted for Age, Sex, Cell types, Log(total EML).

Supplementary Table 19. Biweight midcorrelation analysis of EML in FHS, stratified by the direction of SEM.

Outcome = log(EML) [*]	All EML		Hypermethylated EML		Hypomethylated EML	
	Bicor r	P_value	Bicor r	P_value	Bicor r	P_value
Age	0.244	7.15E-33	0.271	1.81E-40	0.139	1.53E-11
BMI	0.017	4.23E-01	0.016	4.49E-01	0.012	5.53E-01
DNAm Age Acceleration						
AgeAccelHorvath	0.106	3.11E-07	0.101	1.19E-06	0.092	9.46E-06
IEAA	0.109	1.26E-07	0.100	1.34E-06	0.107	2.22E-07
EEAA (Unadjusted for cell types)	0.297	1.12E-48	0.268	1.20E-39	0.286	7.07E-45
AgeAccelHannum	0.225	4.12E-28	0.225	3.85E-28	0.192	1.05E-20
AgeAccelGrim	0.173	3.74E-17	0.167	5.80E-16	0.125	1.29E-09
DNAmADMAdjAge	0.121	4.58E-09	0.121	4.26E-09	0.076	2.62E-04
DNAmB2MAdjAge	0.189	4.69E-20	0.197	7.10E-22	0.088	2.26E-05
DNAmCystatinCAdjAge	0.119	8.71E-09	0.125	1.39E-09	0.031	1.29E-01
DNAmGDF15AdjAge	0.167	6.09E-16	0.181	1.58E-18	0.093	7.75E-06
DNAmLeptinAdjAge	-0.021	3.19E-01	-0.003	8.74E-01	-0.047	2.23E-02
DNAmPACKYRSAdjAge	0.166	7.99E-16	0.142	5.10E-12	0.172	7.31E-17
DNAmPAI1AdjAge	0.024	2.49E-01	0.056	6.70E-03	-0.053	1.12E-02
DNAmTIMP1AdjAge	0.070	7.04E-04	0.083	5.69E-05	0.021	3.06E-01
AgeAccelPheno	0.178	4.45E-18	0.168	3.52E-16	0.133	1.14E-10
DNAmTLAdjAge	-0.080	1.17E-04	-0.088	1.99E-05	-0.057	5.93E-03

DNAmAgeSkinBloodClockAdjAge	0.102	8.32E-07	0.127	7.26E-10	0.044	3.36E-02
Cell types						
CD8.naive	-0.072	5.20E-04	-0.071	5.91E-04	-0.040	5.38E-02
CD8pCD28nCD45RAn	0.085	3.90E-05	0.045	2.83E-02	0.104	5.07E-07
PlasmaBlast	-0.054	8.94E-03	-0.043	3.92E-02	-0.060	3.98E-03
CD4T	-0.146	1.68E-12	-0.138	2.08E-11	-0.096	3.89E-06
Gran	-0.075	2.72E-04	-0.106	3.10E-07	-0.017	4.15E-01

[*] Adjusted for age, sex, cell types.

Supplementary Table 20. FHS: Distribution of hype- and hypomethylated SEMs in relation to CpG island.

	Constantly Hypermethylated SEM [*]	Constantly Hypomethylated SEM [**]
Open Sea	8403	41533
Island	45807	5366
N_Shelf	711	5101
N_Shore	11205	6769
S_Shelf	619	4913
S_Shore	8483	5233

[*] Constantly hypermethylated SEMs were defined as DNA methylation mutations identified in more than 10 participants that were greater than three times the IQR above the upper quartile of a given CpG.
[**] Constantly hypomethylated SEMs were defined as DNA methylation mutations identified in more than 10 participants that were less than three times the IQR above the lower quartile of a given CpG.

Supplementary Table 21. FHS: Distribution of hype- and hypomethylated SEMs in relation to genomic region.

	Constantly Hypermethylated SEM [*]	Constantly Hypomethylated SEM [**]
TSS1500	11769	5841
TSS200	13399	1639
5'UTR	4536	3350
1st Exon	2160	628
Gene body	12757	26197
3' UTR	559	3442

[*] Constantly hypermethylated SEMs were defined as DNA methylation mutations identified in more than 10 participants that were greater than three times the IQR above the upper quartile of a given CpG.
[**] Constantly hypomethylated SEMs were defined as DNA methylation mutations identified in more than 10 participants that were less than three times the IQR above the lower quartile of a given CpG.

Supplementary Table 22. Association between Shannon entropy and age, AgeAccel, EML.

Outcome =Entropy [*]	FHS (n = 2326)		WHI (n= 2091)		JHS (n= 1734)		PEG 1 (n = 237)	
	Bicor r	P_value	Bicor r	P_value	Bicor r	P_value	Bicor r	P_value
Age	0.001	9.55E-01	0.068	2.01E-03	0.071	2.92E-03	0.117	7.30E-02
DNAm Age Acceleration								
AgeAccelHorvath	0.081	9.11E-05	0.160	1.76E-13	-0.039	1.02E-01	0.006	9.22E-01
IEAA	0.035	9.02E-02	0.131	1.70E-09	-0.052	3.16E-02	0.018	7.83E-01
EEAA (Unadjusted for cell types)	0.038	6.39E-02	0.090	3.60E-05	0.017	4.73E-01	0.123	5.93E-02
AgeAccelHannum	0.155	6.23E-14	0.136	4.60E-10	0.063	9.10E-03	0.096	1.41E-01
AgeAccelGrim	0.077	1.89E-04	0.228	3.86E-26	0.043	7.17E-02	0.164	1.14E-02
DNAmADMAdjAge	0.001	9.62E-01	0.205	2.80E-21	-0.022	3.49E-01	0.075	2.53E-01
DNAmB2MAdjAge	0.033	1.12E-01	0.057	9.76E-03	-0.019	4.19E-01	0.157	1.59E-02
DNAmCystatinCAdjAge	0.110	9.87E-08	0.422	5.62E-91	0.075	1.67E-03	0.200	1.93E-03
DNAmGDF15AdjAge	0.095	4.70E-06	0.226	1.53E-25	0.230	2.54E-22	0.076	2.45E-01
DNAmLeptinAdjAge	-0.023	2.68E-01	-0.060	6.11E-03	0.031	2.01E-01	-0.034	6.05E-01
DNAmPACKYRSAdjAge	0.091	1.17E-05	0.125	9.64E-09	0.054	2.46E-02	0.112	8.44E-02
DNAmPAI1AdjAge	-0.036	8.02E-02	0.009	6.68E-01	-0.007	7.78E-01	0.099	1.30E-01
DNAmTIMP1AdjAge	0.015	4.73E-01	-0.041	5.96E-02	-0.085	4.17E-04	-0.113	8.17E-02
AgeAccelPheno	0.079	1.35E-04	0.069	1.68E-03	-0.008	7.47E-01	-0.018	7.88E-01
DNAmTLAdjAge	0.002	9.36E-01	0.042	5.41E-02	0.017	4.78E-01	0.010	8.80E-01
DNAmAgeSkinBloodClockAdjAge	-0.025	2.35E-01	-0.063	4.18E-03	-0.001	9.81E-01	-0.072	2.67E-01
SEM	0.089	1.63E-05	0.294	6.87E-43	0.325	7.22E-44	0.281	1.10E-05

[*] Adjusted for Age, Sex, Race/ethnicity, Cell types.

Research Paper

Blood DNA methylation sites predict death risk in a longitudinal study of 12,300 individuals

Elena Colicino[1,*], Riccardo Marioni[2,*], Cavin Ward-Caviness[3,33,*], Rahul Gondalia[4,*], Weihua Guan[5,*], Brian Chen[6,*], Pei-Chien Tsai[7,*], Tianxiao Huan[8,*], Gao Xu[9,*], Agha Golareh[9], Joel Schwartz[10], Pantel Vokonas[11], Allan Just[1], John M. Starr[12], Allan F. McRae[13], Naomi R. Wray[13], Peter M. Visscher[13], Jan Bressler[14], Wen Zhang[15], Toshiko Tanaka[6], Ann Zenobia Moore[6], Luke C. Pilling[16], Guosheng Zhang[17], James D. Stewart[4], Yun Li[4], Lifang Hou[18], Juan Castillo-Fernandez[7], Tim Spector[7], Douglas P. Kiel[19], Joanne M. Murabito[20], Chunyu Liu[21], Mike Mendelson[22], Tim Assimes[23], Devin Absher[24], Phil S. Tsaho[25], Ake T. Lu[25], Luigi Ferrucci[26], Rory Wilson[27,33], Melanie Waldenberger[27,33], Holger Prokisch[28], Stefania Bandinelli[29,#], Jordana T. Bell[7,#], Daniel Levy[30,#], Ian J. Deary[31,#], Steve Horvath[25,#], Jim Pankow[32,#], Annette Peters[33,#], Eric A. Whitsel[4,#], Andrea Baccarelli[9,#]

[1]Icahn School of Medicine at Mount Sinai, New York, NY 10029, USA
[2]Centre for Genomic and Experimental Medicine, Institute of Genetics and Molecular Medicine, University of Edinburgh, Edinburgh EH4 2XU, UK
[3]US Environmental Protection Agency, Chapel Hill, NC 27514, USA,
[4]Gillings School of Global Public Health, University of North Carolina, Chapel Hill, NC 27514, USA
[5]Division of Biostatistics, School of Public Health, University of Minnesota, Minneapolis, MN 55455, USA
[6]Longitudinal Study Section, Translational Gerontology Branch, National Institute of Aging, Bethesda, MD 20892, USA
[7]Department of Twin Research and Genetic Epidemiology, King's College London, London SE1 7EH, UK
[8]National Heart, Lung, and Blood Institute, Bethesda, MD 20892, USA
[9]Columbia University Mailman School of Public Health, New York, NY 10032, USA
[10]Harvard T.H. Chan School of Public Health, Boston, MA 02115, USA
[11]VA Boston Healthcare System and Boston University Schools of Public Health and Medicine, Boston, MA 02215, USA
[12]Alzheimer Scotland Dementia Research Centre, University of Edinburgh, Edinburgh EH8 9JZ, UK
[13]Institute for Molecular Bioscience, University of Queensland, Brisbane, QLD, Australia
[14]University of Texas Health Science Center at Houston, Houston, TX 77030, USA
[15]Department of Biostatistics and Data Science, School of Public Health, University of Texas Health Science Center at Houston, Houston, TX 77030, USA
[16]Epidemiology and Public Health Group, University of Exeter Medical School, Exeter, UK
[17]Department of Genetics, University of North Carolina, Chapel Hill, NC 27514, USA
[18]Feinberg School of Medicine, Northwestern University, Chicago, IL 60611, USA
[19]Hebrew SeniorLife Institute for Aging Research and Department of Medicine, Beth Israel Deaconess Medical Center and Harvard Medical School, Boston, MA 02215, USA
[20]Section General Internal Medicine, Department of Medicine, Boston University School of Medicine, Boston, MA 02215, USA
[21]Boston University School of Public Health, Boston, MA 02215, USA
[22]Boston University School of Medicine, Boston, MA 02215, USA
[23]Stanford University School of Medicine, Stanford, CA 94305, USA

[24]Hudson Alpha Institute for Biotechnology, Huntsville, AL 35806, USA

[25]Department of Human Genetics, David Geffen School of Medicine, University of California Los Angeles, Los Angeles, CA 90095, USA

[26]National Institute of Aging, Bethesda, MD 20892, USA

[27]Research Unit of Molecular Epidemiology, Helmholtz Zentrum Munich, German Research Center for Environmental Health, Neuherberg D-85764, Germany

[28]Institute of Human Genetics, Helmholtz Zentrum Munich, German Research Center for Environmental Health, Neuherberg S-85764, Germany

[29]Geriatric Unit, Azienda Sanitaria Firenze, Florence, Italy

[30]Framingham Heart Study, Framingham, MA 01702, USA

[31]Department of Psychology, University of Edinburgh, Edinburgh EH8 9JZ, UK

[32]Division of Epidemiology and Community Health, School of Public Health, University of Minnesota, Minneapolis, MN 55455, USA

[33]Institute for Epidemiology II, Helmholtz Zentrum Munich, German Research Center for Environmental Health, Neuherberg D-85764, Germany

*First authors
#Last authors

ABSTRACT

DNA methylation has fundamental roles in gene programming and aging that may help predict mortality. However, no large-scale study has investigated whether site-specific DNA methylation predicts all-cause mortality. We used the Illumina-HumanMethylation450-BeadChip to identify blood DNA methylation sites associated with all-cause mortality for 12, 300 participants in 12 Cohorts of the Heart and Aging Research in Genetic Epidemiology (CHARGE) Consortium. Over an average 10-year follow-up, there were 2,561 deaths across the cohorts. Nine sites mapping to three intergenic and six gene-specific regions were associated with mortality ($P < 9.3\text{x}10^{-7}$) independently of age and other mortality predictors. Six sites (cg14866069, cg23666362, cg20045320, cg07839457, cg07677157, cg09615688)—mapping respectively to *BMPR1B*, *MIR1973*, *IFITM3*, *NLRC5*, and two intergenic regions—were associated with reduced mortality risk. The remaining three sites (cg17086398, cg12619262, cg18424841)—mapping respectively to *SERINC2*, *CHST12*, and an intergenic region—were associated with increased mortality risk. DNA methylation at each site predicted 5%–15% of all deaths. We also assessed the causal association of those sites to age-related chronic diseases by using Mendelian randomization, identifying weak causal relationship between cg18424841 and cg09615688 with coronary heart disease. Of the nine sites, three (cg20045320, cg07839457, cg07677157) were associated with lower incidence of heart disease risk and two (cg20045320, cg07839457) with smoking and inflammation in prior CHARGE analyses. Methylation of cg20045320, cg07839457, and cg17086398 was associated with decreased expression of nearby genes (*IFITM3, IRF, NLRC5, MT1, MT2, MARCKSL1*) linked to immune responses and cardiometabolic diseases. These sites may serve as useful clinical tools for mortality risk assessment and preventative care.

INTRODUCTION

The human epigenome contains DNA methylation marks that progressively change as we age. DNA methylation can influence gene expression and manifests in response to both environmental and hereditary factors [1, 2]. Biological age estimations, constructed from DNA methylation marks and referred to as "epigenetic aging clocks", have been associated with environmental exposures, morbidities, and mortality [9–13]. As these clocks were designed to track chronological age, not to predict mortality, further study is necessary to fully elucidate indicators of all-cause mortality. To date, no large-scale analysis has been conducted to identify variations in DNA methylation at individual 5'-cytosine-phosphate-guanosine-3' (CpG) sites associated with future mortality risk. Here, we present an epigenome-wide methylation analysis of 12,300 participants and 2,561 (21%) deaths from 12 American and European cohorts to determine whether site-specific DNA methylation predicts all-cause mortality, independent of age, lifestyle factors, and clinical predictors of mortality including comorbidities. We also assessed the causal relationship of identified sites with age-related chronic diseases using Mendelian randomization approaches, and we related the sites to epigenetic aging clocks and a mortality risk score, an epigenetic indicator of mortality previously created and validated with DNA methylation arrays in two European cohorts.

RESULTS

Cohorts

Across studies in the Cohorts of the Heart and Aging Research in Genetic Epidemiology (CHARGE) Consortium, mortality rates ranged from 3%–70% of all participants, and the average time to death or censoring ranged from 4.4–16.6 years (Supplementary Table 1). Each study conducted epigenome-wide mortality analyses, adjusting for two sets of harmonized risk factors and confounders, and shared results for meta-analysis (Figure 1).

Meta-analysis

Inverse variance-weighted fixed-effects meta-analysis of 426,724 CpGs identified 51 Bonferroni-significant and
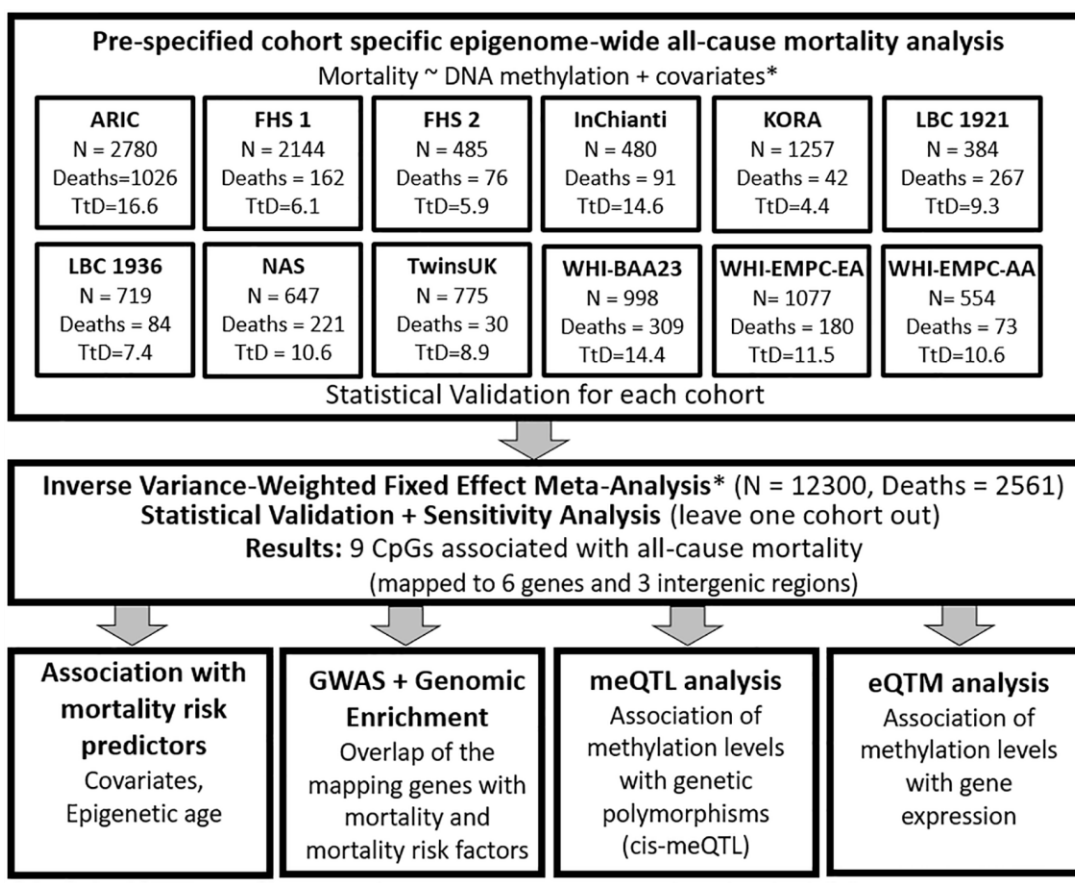
Figure 1. Workflow of the study.

257 FDR-significant ($P < 3.03 \times 10^{-5}$) CpGs in a basic model adjusting for age, sex, technical covariates, and white blood cell proportions (Figure 2A and Supplementary Table 2). We also identified three Bonferroni-significant and nine FDR-significant ($P < 9.3 \times 10^{-7}$) CpGs in a fully-adjusted model also adjusting for education, smoking status, pack-years smoked, body mass index, recreational physical activity, alcohol consumption, hypertension, diabetes, and history of cancer and coronary heart disease (Figures 2B, 3A and Supplementary Table 3). For 188 (73%) basic-adjusted FDR-significant CpGs and six (67%) fully-adjusted CpGs, higher blood DNA methylation was associated with lower all-cause mortality (Figure 2 and Supplementary Tables 2, 3).

All nine fully-adjusted FDR-significant CpGs had similar magnitude of associations with mortality in the basic model, although only five were also FDR-significant in the basic model (Figure 3B). Hazard ratios (HRs) of the nine fully-adjusted FDR-significant CpGs ranged 0.53–1.26 per 10% increase in DNA methylation

levels, where 1 represents 100% methylation (Supplementary Table 4). Six sites (cg14866069, cg23666362, cg20045320, cg07839457, cg07677157, cg09615688) were associated with reduced mortality risk, while the remaining three sites (cg17086398, cg12619262, cg18424841) were associated with increased mortality risk (Figure 3A and Supplementary Tables 3, 4). Three fully-adjusted CpGs (cg07677157, cg09615688, cg18424841) were in intergenic regions; the remaining six (cg17086398, cg14866069, cg23666362, cg12619262, cg20045320, cg07839457) were within 10,000 bp of a gene, with two CpGs (cg07839457, cg23666362) mapped respectively to nucleotide-binding oligomerization domain-like receptor caspase recruitment domain containing 5 (*NLRC5*) and microRNA 1973 (*MIR1973*) within 1,500 bp of transcription start sites, and one (cg17086398) in the serine incorporator 2 (*SERINC2*) gene body (Supplementary Table 3).

Meta-analysis results did not appear to suffer from systematic bias due to unmeasured confounding, as assessed by genomic inflation (basic model: $\lambda = 1.12$,
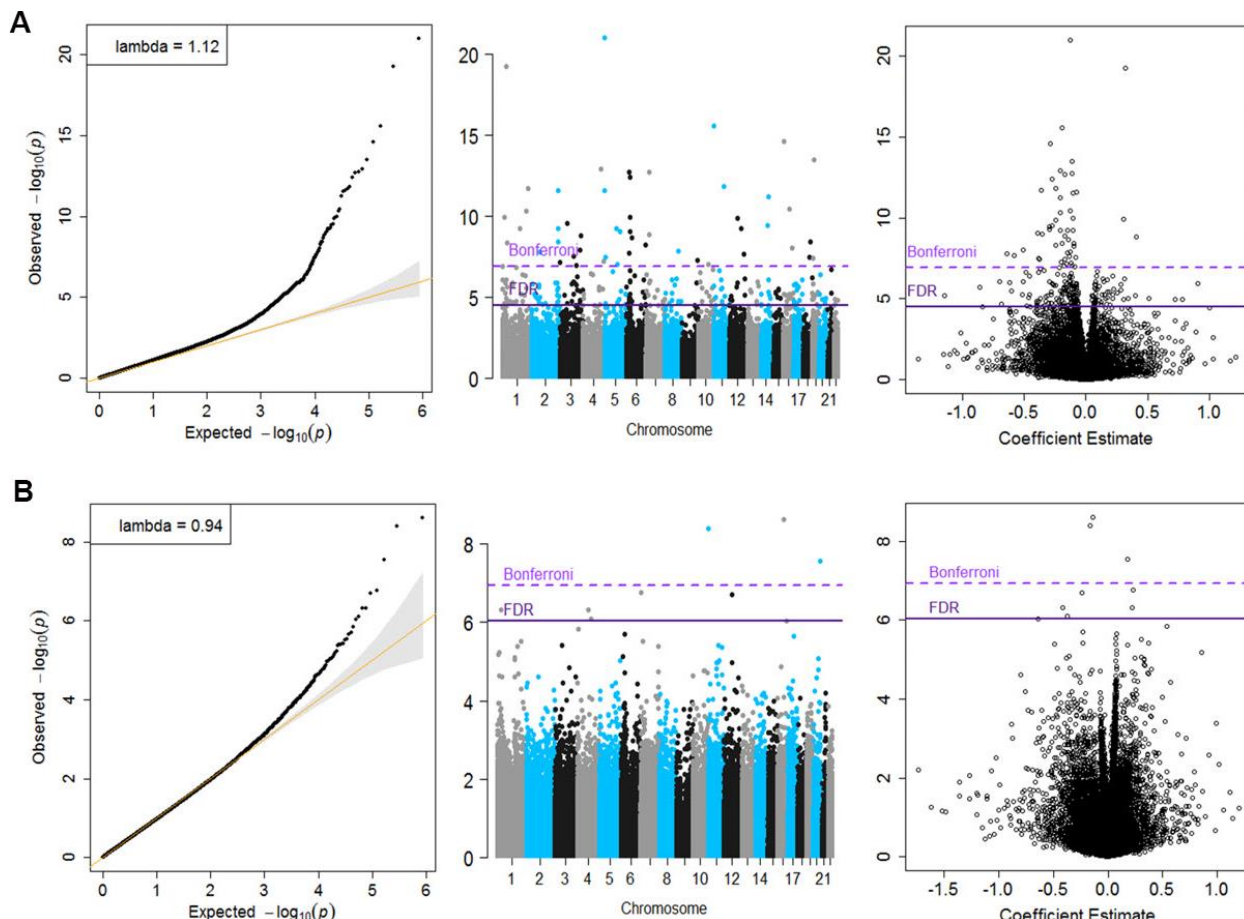
Figure 2. Quantile-Quantile plots, Manhattan and Volcano for the basic model (Panel A) and for the fully adjusted model (Panel B).

fully adjusted model λ = 0.94, Figure 2 and Supplementary Table 5). Cohort-specific inflation was also minimal, with lambdas close to one for most cohorts. Volcano plots showed symmetry in the direction of the associations with all-cause mortality (Figure 2). All nine fully-adjusted FDR-significant CpGs showed low/medium heterogeneity (Supplementary Tables 7) and consistent magnitude of the estimated HRs across studies (Figure 3A). We further validated our results by excluding cohorts with high proportion of deaths (30%) and inflation (λ > 1.5). In these sensitivity analyses, HRs for the nine FDR-significant CpGs were consistent with main results in terms of direction, magnitude, and statistical significance (Supplementary Figure 1 and Supplementary Tables 8, 9).

Three of the nine fully-adjusted FDR-significant CpGs (cg20045320, cg07677157, cg07839457) were associated with lower incidence of coronary heart disease rates (P < Bonferroni threshold of 0.005) (Figure 4 and Supplementary Table 10).

Miettinen's population attributable factor, epigenetic aging clocks, and mortality risk score

To assess the extent that methylation levels of each CpG predict all-cause mortality, we calculated Miettinen's population attributable fraction on data from the Normative Aging Study (NAS) and the Women Health Initiative-Epigenetic Mechanisms of Particulate Matter-Mediated Cardiovascular Disease (WHI-EMPC) for European and African American ancestries. DNA methylation levels above the average at each CpG predicted, individually and independently of other factors, 5%–15% of all deaths (Figure 3C and Supplementary Table 11). In the same datasets, all nine CpGs were associated with age, cumulative smoking, body mass index, and physical activity (P < 0.05). Seven out of nine CpGs (cg17086398, cg14866069, cg23666362, cg20045320, cg7677157, cg07839457, cg09615688) had negative relationships with age (Supplementary Table 12). Seven CpGs were strongly associated with epigenetic aging clocks and mortality risk scores; all significant associations had the same direction and similar magnitude across the four epigenetic aging clocks (Supplementary Table 13), even if none of those sites was included in any of the clocks. Those CpGs had consistent and independent association with all-cause mortality when adjusted for epigenetic aging clocks and mortality risk scores (Supplementary Tables 14, 15). In overall meta-analysis, we identified 57 out of 58 CpGs of the risk score, and those sites had low to moderate association with DNA methylation levels at our FDR-significant CpGs with a balance between
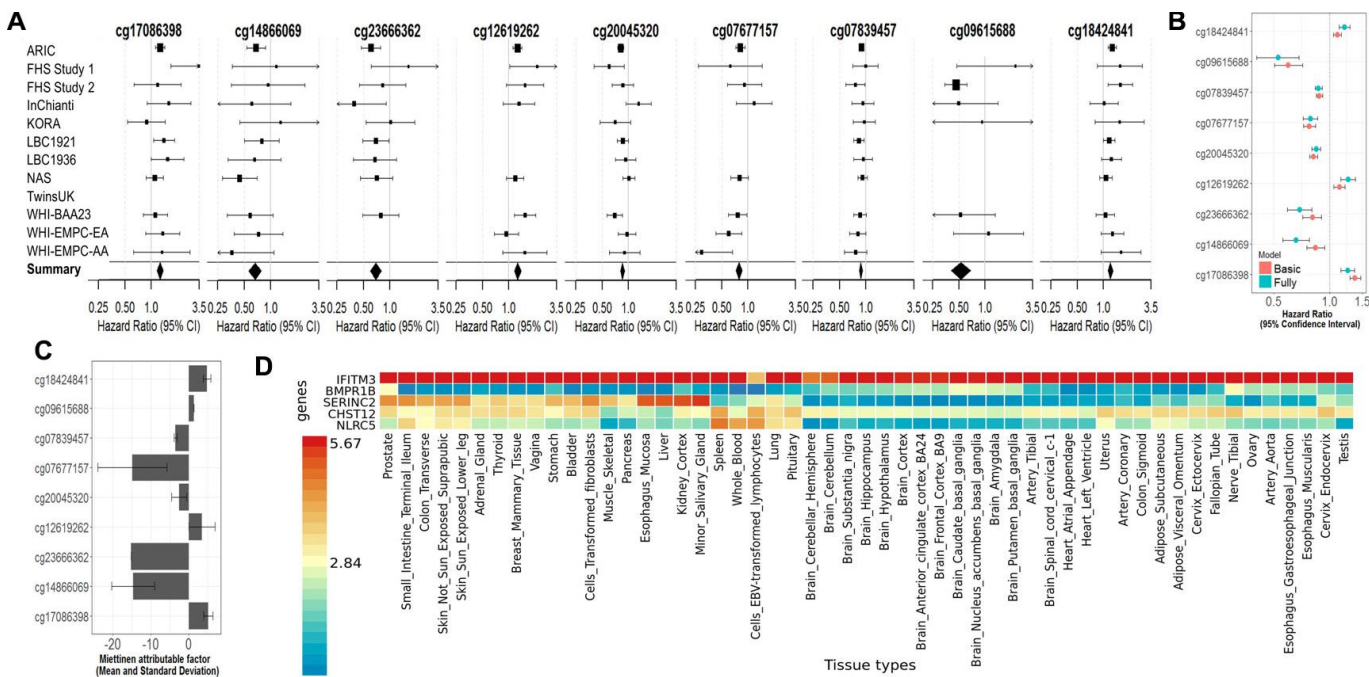
Figure 3. (**A**) Forest Plots for the association of methylation levels of the FDR-significant fully-adjusted CpGs with risk of all-cause mortality in the CHARGE consortium. (**B**) Sensitivity analysis. Comparison of the hazard ratio of the basic-adjusted and the fully-adjusted fixed effect meta-analysis. (**C**) Attributable factor. Predicted Contribution (%) of increased methylation levels (above the mean) of each CpG to the all-cause mortality associations in NAS, WHI-EMPC (EA) and WHI-EMPC (AA). (**D**) Functional Mapping and Annotation results in order to examine tissue specificity of the genes mapped to the FDR-significant fully-adjusted CpGs.

positive and negative correlations (Supplementary Figure 2A, 2B). In overall meta-analysis, the association between all-cause mortality and DNA methylation levels at the majority (34 out of 58) of mortality risk score CpGs had consistent direction with previous results. Among those CpGs, only two (cg25193885 and cg19859270) showed nominally significant association with mortality (Supplementary Figure 2A, 2B).

Pathways analyses and DNA methylation integration with quantitative trait loci analysis (meQTL) and with gene expression (eQTM)

Extended genome-wide enrichment analysis showed that two of the CpGs (cg07839457 and cg17086398) mapped to genes (*NLRC5* and *SERINC2,* respectively) previously associated with high-density lipoprotein cholesterol levels (FDR P = 0.02) and alcohol dependence (FDR P = 0.004) in genome-wide association studies (GWAS) analyses (Supplementary Table 16) [14]. We confirmed these results using Database for Annotation, Visualization and Integrated Discovery (DAVID) and KEGG, identifying and testing for enriched underlying biological processes in publicly available gene ontology databases (Supplementary Tables 17, 18).

To characterize the functional relevance of FDR-significant CpGs, we performed covariate-adjusted methylation quantitative trait locus (meQTL) analyses using available unique single-nucleotide-polymorphism (SNP)–CpG combinations from 713 participants in the Cooperative Health Research in the Region Augsburg (KORA) study [15]. We identified nine Bonferroni-significant unique cis-regulatory polymorphisms associated with two 1000 bp-distant CpGs (cg09615688, cg18424841) (Supplementary Figure 3A and Supplementary Table 19). None of the nine identified polymorphisms overlapped with previous genetic results from the National Human Genome Research Institute-EBI GWAS Catalog (Supplementary Table 16).

We also evaluated expression quantitative trait methylation (eQTM) associations using 998 KORA participants. We identified three CpGs with FDR-significant associations with decreased leukocyte expression levels of nearby genes, among the 13, 351 unique associations between gene-expression and DNA methylation levels at FDR-significant fully-adjusted CpGs. Namely, DNA methylation levels of cg07839457 (in *NLRC5*) were associated with *NLRC5* expression as well as with that of a ~300 Mb-distant set of *metallothionein* (*MT*) *1* and *2* genes, which are linked to oxidative stress and immune responses [16, 17]. DNA methylation of cg17086398 in *SERINC2* was inversely associated with myristoylated alanine-rich C-kinase substrate like 1 (*MARCKSL1*) expression, which is involved in migration of cancer cells [18]. DNA methylation at cg20045320 in *IFITM3* was associated with lower expression of *IFITM3* and *IRF*, which have a critical role in immune responses (Supplementary Figure 3B and Supplementary Table 20) [6, 19].

We finally used functional mapping and annotation to examine tissue-specific expression. Genes identified in the fully-adjusted model showed universal expression at varying levels across tissues. *IFITM3* was highly expressed in all tissues; *BMPR1B* showed low expression across all tissues, except for moderate expression in the prostate and tibial nerve. Remaining genes had moderate or low expression in a wide range of tissues, except for *SERINC2,* which showed high expression in the liver, kidney, salivary gland, and esophagus. *MIR1973* was not represented in the dataset (Figure 3D).

Mendelian randomization

To evaluate the causal relationship of FDR-significant CpGs to mortality-related risk factors and diseases, we included two sets of Mendelian randomization analysis using methQTL data from KORA and publicly available ARIES data. Only two FDR-significant CpGs
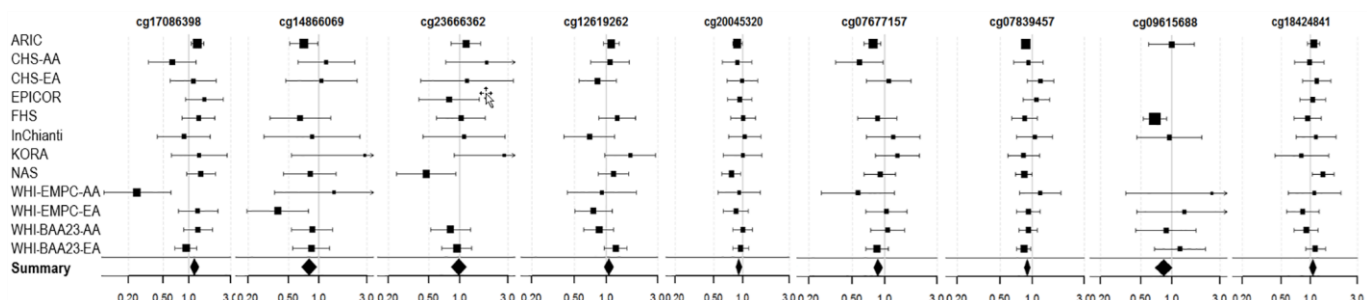
Figure 4. Forest Plots for the association of methylation levels of the FDR-significant fully-adjusted CpGs with risk of future incident coronary heart disease in the CHARGE consortium.

(cg18424841 and cg09615688) overlapped with methQTLs in either KORA or ARIES and with SNPs associated with coronary heart disease (CHD) or kidney function. A GWAS assessing longevity and age-related chronic diseases (CHD and kidney function) [34–38] showed no overlap with KORA and ARIES methQTLs even when using a moderate threshold for proxy variants (proxy $r^2 > 0.75$). In KORA, cg09615688 showed evidence of a positive causal effect on CHD (OR = 1.51; 95% CI = 1.02, 2.23; Wald ratio method), directionally consistent with the association of overall meta-analysis on mortality. However, this causal estimate at this site was not represented in ARIES methQTL data. Cg18424841 had multiple variants in KORA methQTL data and a single variant in ARIES methQTL data. We did not observe consistent evidence of a causal effect of cg18424841 on CHD. Indeed, weak evidence for a causal effect of cg18424841 on CHD was observed in ARIES using the Wald ratio method but not in KORA using pleiotropy-robust, multi-variant, or Wald ratio methods. We did not find evidence for a causal effect of cg18424841 on kidney function in either KORA or ARIES (Supplementary Table 21).

Cell-type fractions and all-cause mortality

Cell-type fractions, mostly neutrophil–lymphocyte ratio (NLR), have been often associated with comorbidities and mortality and have been recognized to influence DNA methylation levels [20–22]. We identified that NLR was significantly associated with all-cause mortality only when data were not adjusted for Houseman cell proportions using NAS data (Supplementary Table 22). Interestingly, NLR had no significant association with all-cause mortality when we adjusted for DNA methylation levels at cg07839457, mapped to immune-related gene *NLRC5*. However, the contribution of NLR on mortality at that specific site may be minimized due to adjustment of prior history of cancer and comorbidities in all models.

DISCUSSION

This study is the largest to date investigating site-specific DNA methylation and all-cause mortality. We identified new whole blood DNA methylation marks that predict all-cause mortality risk, independent from chronological age, lifestyle habits, and morbidity. These newly identified sites may be useful in developing clinical tools for risk assessment and mortality preventive intervention strategies.

All nine FDR-significant CpGs demonstrated novel association with all-cause mortality and were not part of epigenetic aging clocks or mortality risk scores [9, 11–13]. Further, the CpGs were associated with mortality

independent from epigenetic aging and mortality signatures. All-cause mortality was associated with a mortality risk score in a model including seven FDR-significant CpGs, although those associations may be driven by the inclusion of CpGs related to our FDR-significant sites. This suggests that whole blood DNA methylation levels at FDR-significant CpGs may be sentinels for epigenetic disruptions leading to aging acceleration and contributing to mortality. In addition, the association between DNA methylation levels at FDR-significant CpGs with chronological aging may suggest that those CpGs are stronger independent biomarkers of aging than other epigenetic aging signatures.

In previous CHARGE meta-analyses [3, 4], DNA methylation of two of the newly-identified CpGs, cg20045320 and cg07839457 (mapping to interferon induced transmembrane protein 3 [*IFITM3*] and *NLRC5*) were respectively associated with smoking and cardiovascular-related chronic inflammation, both factors of mortality. Cardiovascular disease, especially CHD, is a major contributor to mortality [23]. The direction of association with incident heart disease was consistent with that of all-cause mortality. Thus, DNA methylation at these CpGs may contribute to development and progression of CHD and, consequently, to risk of death. To validate this idea, we used a Mendelian randomization approach and identified one site, cg09615688, with a causal effect on CHD in KORA data and weak evidence for the causal effect of cg18424841 on CHD in ARIES data.

Expression of several genes mapped to the fully-adjusted FDR-significant CpGs has been associated with mortality predictors and mortality. Elevated and persistent gene expression levels of *NLRC5*, a master regulator of the immune response [16], has demonstrated an inverse correlation with familial longevity and mortality predictors, such as elevated blood pressure, arterial stiffness, chronic levels of inflammatory cytokines, metabolic dysfunction, and oxidative stress [5]. In addition, expression of *IFITM3* provides an essential barrier to influenza A virus infection *in vivo* and *in vitro*. Absence of *IFITM3* leads to uncontrolled viral replication and a predisposition to morbidity and subsequent mortality [6]. Further, expression of *BMPR1B* enhances cancer cell migration, and approaches targeting *BMPR1B* inhibit metastatic activity in breast cancer [7]. Finally, expression of *MIR1973*, part of a family of microRNAs, increases resistant lung adenocarcinoma cells, with subsequent low apoptosis intensity [8]. This body of evidence may suggest an active role of DNA methylation levels in regulating relevant gene expression and reducing all-cause mortality risk.

The overall meta-analyses included 12 cohorts with varying biological age and mortality. There was a balance between six studies with long (≥10 years) and six cohorts with short (<10 years) average time to follow-up or death. All cohorts showed consistency in magnitudes and directionality for the association with mortality of four CpGs (cg12619262, cg20045320, cg07839457, cg18424841). Two studies (FHS study 1 and KORA) showed non-significant opposing directionality when compared with the rest of the cohorts for several CpGs (FHS-Study 1: cg14866069, cg23666362, cg09615688; KORA: cg17086398, cg14866069, cg23666362). However, both cohorts had among the shortest average time-to-death (FHS-Study 1: 6.1 years; KORA: 4.4 years) and youngest average population age (FHS-Study 1: 65 years; KORA: 61 years). Both cohorts also had limited contribution in our meta-analysis due to reduced number of deaths (FHS-Study 1: 62; KORA: 42). Our results may indicate that DNA methylation levels at these select CpGs were relevant for mortality risk prediction of longer time-to-death in both adults and older-age adults.

Cell-type fractions, including NLR, as related to cancer and systemic inflammation have been related to mortality in different populations [20–22]. When we excluded Houseman cell proportions, NLR was strongly associated with mortality at all CpGs except cg07839457, which is mapped to the immune-related gene *NLRC5*. This may suggest that the contribution of NLR on mortality is minimized when controlled for prior history of cancer and related comorbidities.

In summary, we identified nine CpGs with a novel association with all-cause mortality, responsive to several external stimuli including alcohol consumption and smoking, and more than 10 years before death. These sites thus may be considered sentinels for epigenetic disruptions leading to age-related disease, such as cardiovascular disease, and contributing to mortality. Further studies have to confirm these associations in other tissues and in different populations.

MATERIALS AND METHODS

Participating cohort studies

Our meta-analysis included 12,300 participants from 12 population-based cohorts of the Heart and Aging Research in Genetic Epidemiology Consortium (CHARGE; Supplementary material): Atherosclerosis Risk In Communities (ARIC), two studies from the Framingham Heart Study (FHS), Invecchiare in Chianti (InChianti), Kooperative Gesundheitsforschung in der Region Augsburg (KORA), Lothian Birth Cohort 1921 (LBC1921) and 1936 (LBC1936), Normative Aging

Study (NAS), UK Adult Twin Registry (TwinsUK), and three studies from the Women's Health Initiative (WHI), including Broad Agency Announcement 23 (WHI-BAA23) and Epigenetic Mechanisms of PM-Mediated CVD Risk (WHI-EMPC), both European (WHI-EMPC-EA) and African American ancestries (WHI-EMPC-AA). For each participant, we derived years of follow-up using time between the blood draw used for DNA methylation analysis and death or last follow-up. Each cohort excluded participants with diagnosed leukemia (ICD-9: 203–208) or undergoing chemotherapy treatment, which both modify blood-derived data [24, 25]. All participating cohorts shared cohort descriptive statistics and results files from pre-specified in-house mortality analyses (Figure 1). Further information about death ascertainment, covariates measurement and harmonization, protocols, and methods of each cohort are included in the Supplemental Materials. The institutional review committees of each cohort approved this study, and all participants provided written informed consent. Data and analytical codes that support our findings are available from the corresponding author upon request.

Blood DNA methylation measurements and quality control

Each cohort independently conducted laboratory DNA methylation measurements and internal quality control. All samples underwent bisulfite conversion via the EZ-96 DNA Methylation kit (Zymo Research) and were processed with the Illumina Infinium HumanMethylation450 (450K) BeadChip (Illumina) at Illumina or in cohort-specific laboratories. Quality control of samples included exclusion on the basis of Illumina's detection *P*-value, low sample DNA concentration, sample call rate, CpG specific percentage of missing values, bisulfite conversion efficiency, gender verification with multidimensional scaling plots, and other quality control metrics specific to cohorts. Each cohort used validated statistical methods for normalizing methylation data on untransformed methylation beta values (ranging 0–1). Some cohorts also made independent probe exclusions. Further details are provided in the Supplemental Material. For meta-analysis, additional probe exclusions were made across all cohorts. In detail, we also excluded control probes, non-CpG sites, probes that mapped to allosomal chromosomes, cross-reactive CpGs, probes with underlying SNPs within 10 bp of the CpG sequence, non-varying CpGs defined by interquartile range of <0.1%, CpGs with ≥10% of missing information, and CpGs with non-converging results [26–28]. We included only CpGs that were available in more than three cohorts. A total of 426, 724 CpGs were included in the meta-analysis (Supplementary Table 5).

The official gene name of each CpG site was noted via Illumina's genome coordinate. We used the name provided by Illumina with the UCSC Genome Browser and annotation data in Bioconductor. All annotations use the human February 2009 (GRCh37/hg19) assembly.

Cohort-specific statistical analyses

Each cohort independently ran a common pre-specified statistical analysis in R.version 3.5.1. We estimated the association between locus-by-locus blood DNA methylation levels and all-cause mortality in each cohort using a Cox-regression model. Proportional hazard assumptions were confirmed for each model in all cohorts. Familial relationship was also accounted for, when appropriate, in the model; FHS analyses included cluster for family structure, and TwinsUK analyses used random intercepts for zygosity and family structure. To avoid non-convergent results, cohorts with low deaths (KORA and TwinsUK) used a two-step analysis, in which covariates were first linearly regressed on each probe, and then residuals were used to perform a Cox mortality analysis.

Each cohort adjusted for harmonized covariates in the basic model: age (categories for decades), sex, and technical covariates (plate, chip, row, and column). A second set of fully-adjusted analyses adjusted for this initial list of covariates in addition to education level, self-reported recreational physical activity, smoking status, cumulative smoking (pack-years), body mass index, alcohol intake, hypertension, diabetes, and any personal history of cancer. Cohorts independently estimated cell type proportions using the reference-based Houseman method, which was subsequently extended by Horvath. Cell type correction was applied by including estimated cell type proportions (CD4T, NK cells, monocytes, granulocytes, plasma B cells, CD8T naïve, and memory and effector T cells) as covariates in cohort-specific statistical models. Each cohort underwent statistical validation of Cox-proportional hazard assumptions before being included in the meta-analysis.

Meta-analysis

We performed inverse variance-weighted fixed-effects meta-analysis. Due to the variability of available CpG sites across cohorts after quality-control steps, we included only CpG sites that were available in three or more cohorts. We accounted for multiple testing by controlling at 5% both the Bonferroni correction and false discovery rate (FDR) using the Benjamini-Hochberg procedure.

For FDR-significant CpGs, we confirmed robustness of the models and results in additional analyses using the leave-one-out cohort validation method, by excluding one cohort at a time and then comparing model estimates for each CpG. We compared effect hazard ratio (HR) and 95% confidence interval (95% CI) for the model to estimates for our models to evaluate the consistency of our findings. For each CpG, we evaluated goodness of the meta-analysis model using the I² statistic measure of inter-study variability from random-effect meta-analyses.

Enrichment analysis

We enriched our results using a publicly available catalog of all published GWAS relating genetic variants with human diseases (National Human Genome Research Institute-EBI GWAS Catalog) to elucidate potential associations [14]. Enrichment analysis was performed in R using one-sided Fisher exact test. We controlled for false positives with the FDR procedure.

We evaluated whether CpG sites associated with mortality were enriched with genomic features provided in the Illumina annotation file (version 1.2; http://support.illumina.com/array/array_kits/infinium_humanmethylation450_beadchip_kit/downloads.html) to identify CpG location relative to the gene (i.e., body, first exon, 3'-UTR, 5'-UTR, within 200 bp of transcriptional start site [TSS200]), and within 1500 bp of transcriptional start site [TSS1500]) and relation of the CpG site to a CpG island, northern shelf, northern shore, southern shelf, and southern shore.

We also tested each gene mapped to the newly identified CpGs for tissue-specific expression using data from the Genotype Tissue Expression (GTEx) project as integrated by the Functional Mapping and Annotation (FUMA) tool [29], which allowed us to extract and interpret relevant biological information from publicly available repositories and provide interactive figures for prioritized genes. As a result, we obtained a heatmap of genes with normalized gene expression values (reads per kilo base per million). To obtain differentially expressed gene sets for each of 53 tissue types in the database, we used two-sided Student's t-tests on normalized expression per gene per tissue against all other tissues. We controlled for multiple comparison with Bonferroni correction. Finally, we distinguished between genes upregulated and downregulated in a specific tissue compared to other tissues by accounting for sign of the t-score [29].

Pathway analyses

To functionally interpret the genomic information identified from FDR-significant CpGs, we used the Kyoto Encyclopedia of Genes and Genomes (KEGG)

pathway database, which links genomic information with higher-order functional information. Genomic information stored in the GENES database is a collection of gene catalogs for all completely sequenced genomes and some partial genomes with up-to-date annotation of gene functions. Higher-order functional information stored in the PATHWAY database contains graphical representations of cellular processes, such as metabolism, membrane transport, signal transduction, and cell cycle [30]. We controlled our results for multiple comparisons with the FDR approach. We finally confirmed our results with the Database for Annotation, Visualization and Integrated Discovery (DAVID). We tested for enrichment in gene ontology biological processes and applied the Benjamini-Hochberg procedure to control for false positivity. We mapped each CpG significantly associated with mortality to genes on the basis of the 450K BeadChip annotation file. We excluded CpGs lacking annotated genes within 10 Mb (n = 3). Using topGO in R, we tested for gene enrichment over the background array (16, 119 unique annotated Entrez Gene IDs) by using Fisher's exact tests with a minimum of two genes per node.

Integrating DNA methylation with quantitative trait loci analysis (meQTL)

A subset of 713 KORA samples was genotyped on an Affymetrix Axiom array. We removed variants with a call rate of <0.98, Hardy-Weinberg equilibrium $P < 5x10^{-6}$, and minor allele frequency < 0.01. We considered only variants with an information score > 3. Imputation was performed using the 1000 Genomes Project phase I version 3 reference panel with IMPUTE 2.3.0. Phasing of data was performed using SHAPEIT v2. We retained approximately 10,000,000 variants for analyses. In each model, we used DNA methylation beta values as independent variables and SNPs as dependent variables. We adjusted each model for age, sex, body mass index, and white blood cell proportions. We used OmicABEL [31] for the analyses and genotype probabilities for each variant. Due to large size of the output, we retained only variants with $P < 1x10^{-4}$. We considered genome-wide significant results at $P < 1x10^{-14}$. We reported only associations with CpGs significant in the epigenome-wide association study.

Integrating DNA methylation with gene expression (eQTM)

In KORA, 998 individuals had both valid methylation and blood gene expression data, which we used to assess whether DNA methylation was correlated with gene expression. Gene expression data (Illumina HumanHT-12 v3 Expression BeadChip) was quality controlled with GenomeStudio, and samples with

<6,000 detected genes were excluded from analysis. All samples were log2-transformed and quantile-normalized using the Bioconductor package lumi [32]. A total of 48,803 expression probes passed quality control. We used R (version 3.3.1) to run a linear mixed effects model adjusting for covariates (age, sex, blood cell proportions, and technical variables of RNA integrity number, sample storage time, and RNA amplification batch) and a random intercept for RNA amplification batch. Models were run for each of the nine newly-identified CpGs associated with mortality. We filtered results to report only CpG-expression probe pairs located on the same chromosome. Start and end sites for each gene were determined according to the Illumina HT annotation file. A cutoff of 500,000 bp was used to differentiate cis- vs. trans-eQTMs.

Miettinen's population attributable factor and mendelian randomization analysis

To assess the contribution of methylation levels of each CpG to all-cause mortality, we calculated Miettinen's population attributable fraction on data from the in-house Normative Aging Study (NAS) and Women Health Initiative-Epigenetic Mechanisms of Particulate Matter-Mediated Cardiovascular Disease (WHI-EMPC) for European and African American ancestries. Population attributable fraction takes into account strength of association between the risk factor (DNA methylation higher than the mean in specific CpG sites) and outcome (mortality) as well as prevalence of the risk factor in the population [33]. This metric provides estimates of the public health importance of risk factors, ascertaining what proportion of the outcome is due to exposure to the risk factor, and distinguishes between etiologic fraction attributable to or related to the given risk factor depending on whether all or just some confounding by extraneous factors was under control [33]. To support information about the population attributable factor, we also included two Mendelian randomization approaches.

We identified the causal effect on all-cause mortality of FDR-significant CpGs by using two sample Mendelian randomization analyses and summary statistics from published GWAS for chronic diseases and longevity [34] and chronic diseases, including CHD [35], kidney function (serum creatinine), [36] blood pressure, [37] and type 2 diabetes [38]. We extracted GWAS information with MR-base [14]. We also extracted SNP-methylation association summary statistics from both KORA and publicly available ARIES [39] methQTL data; for ARIES, we used MR-base [40]. To account for multiple variants and pleiotropy, we used multiple Mendelian randomization methods—when only one variant was present, we used the Wald Ratio method [41]; when we

had multiple variants, we used MR Egger [42], weighted median [43], and weighted mode [44], as these three methods use different assumptions to provide consistent causal effect estimates even with invalid instruments arising from horizontal pleiotropy, a primary source of bias in multi-variant Mendelian randomization analyses.

FDR-significant CpGs, DNA methylation-related aging measures, and mortality risk score

PhenoAge, a composite measure of CpG sites representing phenotypic age, captures differences between lifespan and health span. The Horvath clock is a linear combination of sites identifying the cumulative effect of an epigenetic maintenance system [1, 45]. Among the 513 CpGs comprising PhenoAge, 41 are shared with the Horvath clock. While both aging measures correlate strongly with age in every tissue and cell type tested, and both captured risks for mortality across multiple tissues and cells, PhenoAge is highly predictive of nearly every morbidity [1, 10]. Blood PhenoAge outperformed the Horvath clock with regard to predictions for a variety of aging outcomes, including all-cause mortality. The mortality risk score instead was based on results using discovery cohort ESTHER (61 years old on average) and both ESTHER and KORA for validation [11].

To investigate whether the association of FDR-significant CpGs with mortality was independent of DNA methylation aging measures and risk score, we included acceleration of PhenoAge and Horvath clock, defined respectively as discrepancies between age with PhenoAge and Horvath clock age and the risk score. We also identified the correlation between each CpG included in the risk score and our FDR-significant CpGs, and we compared our pooled meta-analysis results with previous findings.

Cell-type fractions and all-cause mortality

Cell-type fractions, mostly NLR, influence DNA methylation levels and have been associated with comorbidities and mortality [20–22]. To elucidate which cell proportions were associated with mortality when adjusting for DNA methylation at FDR-significant CpGs, we included NLR, which has been associated with lung cancer risk and mortality [21] as well was cardiovascular disease and mortality in prospective studies [22]. NLR computation was performed using DNA methylation data via Koestler et al. [46]

CONFLICTS OF INTEREST

The authors declare that they have no conflicts of interest.

REFERENCES

1. Horvath S. DNA methylation age of human tissues and cell types. Genome Biol. 2013; 14:R115. https://doi.org/10.1186/gb-2013-14-10-r115 PMID:24138928

2. Argentieri MA, Nagarajan S, Seddighzadeh B, Baccarelli AA, Shields AE. Epigenetic pathways in human disease: the impact of DNA methylation on stress-related pathogenesis and current challenges in biomarker development. EBioMedicine. 2017; 18:327–50. https://doi.org/10.1016/j.ebiom.2017.03.044 PMID:28434943

3. Joehanes R, Just AC, Marioni RE, Pilling LC, Reynolds LM, Mandaviya PR, Guan W, Xu T, Elks CE, Aslibekyan S, Moreno-Macias H, Smith JA, Brody JA, et al. Epigenetic signatures of cigarette smoking. Circ Cardiovasc Genet. 2016; 9:436–47. https://doi.org/10.1161/CIRCGENETICS.116.001506 PMID:27651444

4. Aslibekyan S, Agha G, Colicino E, Do AN, Lahti J, Ligthart S, Marioni RE, Marzi C, Mendelson MM, Tanaka T, Wielscher M, Absher DM, Ferrucci L, et al. Association of methylation signals with incident coronary heart disease in an epigenome-wide assessment of circulating tumor necrosis factor α. JAMA Cardiol. 2018; 3:463–72. https://doi.org/10.1001/jamacardio.2018.0510 PMID:29617535

5. Furman D, Chang J, Lartigue L, Bolen CR, Haddad F, Gaudilliere B, Ganio EA, Fragiadakis GK, Spitzer MH, Douchet I, Daburon S, Moreau JF, Nolan GP, et al. Expression of specific inflammasome gene modules stratifies older individuals into two extreme clinical and immunological states. Nat Med. 2017; 23:174–84. https://doi.org/10.1038/nm.4267 PMID:28092664

6. Everitt AR, Clare S, Pertel T, John SP, Wash RS, Smith SE, Chin CR, Feeley EM, Sims JS, Adams DJ, Wise HM, Kane L, Goulding D, et al. GenISIS Investigators, and MOSAIC Investigators. IFITM3 restricts the morbidity and mortality associated with influenza. Nature. 2012; 484:519–23. https://doi.org/10.1038/nature10921 PMID:22446628

7. Allison SE, Chen Y, Petrovic N, Zimmermann S, Moosmann B, Jansch M, Cui PH, Dunstan CR, Mackenzie PI, Murray M. Activation of the pro-migratory bone morphogenetic protein receptor 1B gene in human MDA-MB-468 triple-negative breast cancer cells that over-express CYP2J2. Int J Biochem Cell Biol. 2016; 80:173–78. https://doi.org/10.1016/j.biocel.2016.10.004 PMID:27720933

8. Fomicheva KA, Knyazev EN, Mal'tseva DV. hsa-miR-1973 MicroRNA is significantly and differentially expressed in MDA-MB-231 cells of breast adenocarcinoma and xenografts derived from the tumor. Bull Exp Biol Med. 2017; 163:660–62. https://doi.org/10.1007/s10517-017-3873-0 PMID:28948560

9. Chen BH, Marioni RE, Colicino E, Peters MJ, Ward-Caviness CK, Tsai PC, Roetker NS, Just AC, Demerath EW, Guan W, Bressler J, Fornage M, Studenski S, et al.

DNA methylation-based measures of biological age: meta-analysis predicting time to death. Aging (Albany NY). 2016; 8:1844–65.
https://doi.org/10.18632/aging.101020
PMID:27690265

10. Marioni RE, Shah S, McRae AF, Chen BH, Colicino E, Harris SE, Gibson J, Henders AK, Redmond P, Cox SR, Pattie A, Corley J, Murphy L, et al. DNA methylation age of blood predicts all-cause mortality in later life. Genome Biol. 2015; 16:25.
https://doi.org/10.1186/s13059-015-0584-6
PMID:25633388

11. Zhang Y, Wilson R, Heiss J, Breitling LP, Saum KU, Schöttker B, Holleczek B, Waldenberger M, Peters A, Brenner H. DNA methylation signatures in peripheral blood strongly predict all-cause mortality. Nat Commun. 2017; 8:14617.
https://doi.org/10.1038/ncomms14617
PMID:28303888

12. Hannum G, Guinney J, Zhao L, Zhang L, Hughes G, Sadda S, Klotzle B, Bibikova M, Fan JB, Gao Y, Deconde R, Chen M, Rajapakse I, et al. Genome-wide methylation profiles reveal quantitative views of human aging rates. Mol Cell. 2013; 49:359–67.
https://doi.org/10.1016/j.molcel.2012.10.016
PMID:23177740

13. Weidner CI, Lin Q, Koch CM, Eisele L, Beier F, Ziegler P, Bauerschlag DO, Jöckel KH, Erbel R, Mühleisen TW, Zenke M, Brümmendorf TH, Wagner W. Aging of blood can be tracked by DNA methylation changes at just three CpG sites. Genome Biol. 2014; 15:R24.
https://doi.org/10.1186/gb-2014-15-2-r24
PMID:24490752

14. MacArthur J, Bowler E, Cerezo M, Gil L, Hall P, Hastings E, Junkins H, McMahon A, Milano A, Morales J, Pendlington ZM, Welter D, Burdett T, et al. The new NHGRI-EBI catalog of published genome-wide association studies (GWAS catalog). Nucleic Acids Res. 2017; 45:D896–901.
https://doi.org/10.1093/nar/gkw1133
PMID:27899670

15. Ligthart S, Marzi C, Aslibekyan S, Mendelson MM, Conneely KN, Tanaka T, Colicino E, Waite LL, Joehanes R, Guan W, Brody JA, Elks C, Marioni R, et al, and WHI-EMPC Investigators, and CHARGE epigenetics of Coronary Heart Disease. DNA methylation signatures of chronic low-grade inflammation are associated with complex diseases. Genome Biol. 2016; 17:255.
https://doi.org/10.1186/s13059-016-1119-5
PMID:27955697

16. Meissner TB, Li A, Biswas A, Lee KH, Liu YJ, Bayir E, Iliopoulos D, van den Elsen PJ, Kobayashi KS. NLR family member NLRC5 is a transcriptional regulator of MHC class I genes. Proc Natl Acad Sci USA. 2010; 107:13794–99.
https://doi.org/10.1073/pnas.1008684107
PMID:20639463

17. Ruttkay-Nedecky B, Nejdl L, Gumulec J, Zitka O, Masarik M, Eckschlager T, Stiborova M, Adam V, Kizek R. The role of metallothionein in oxidative stress. Int J Mol Sci. 2013; 14:6044–66.
https://doi.org/10.3390/ijms14036044 PMID:23502468

18. Björkblom B, Padzik A, Mohammad H, Westerlund N, Komulainen E, Hollos P, Parviainen L, Papageorgiou AC, Iljin K, Kallioniemi O, Kallajoki M, Courtney MJ, Mågård M, et al. C-jun n-terminal kinase phosphorylation of MARCKSL1 determines actin stability and migration in neurons and in cancer cells. Mol Cell Biol. 2012; 32:3513–26.
https://doi.org/10.1128/MCB.00713-12
PMID:22751924

19. Taniguchi T, Takaoka A. The interferon-Alpha/beta system in antiviral responses: a multimodal machinery of gene regulation by the IRF family of transcription factors. Curr Opin Immunol. 2002; 14:111–16.
https://doi.org/10.1016/s0952-7915(01)00305-3
PMID:11790540

20. Palmerini T, Mehran R, Dangas G, Nikolsky E, Witzenbichler B, Guagliumi G, Dudek D, Genereux P, Caixeta A, Rabbani L, Weisz G, Parise H, Fahy M, et al. Impact of leukocyte count on mortality and bleeding in patients with myocardial infarction undergoing primary percutaneous coronary interventions: analysis from the harmonizing outcome with revascularization and stent in acute myocardial infarction trial. Circulation. 2011; 123:2829–37.
https://doi.org/10.1161/CIRCULATIONAHA.110.985564
PMID:21632496

21. Grieshober L, Graw S, Barnett MJ, Thornquist MD, Goodman GE, Chen C, Koestler DC, Marsit CJ, Doherty JA. Methylation-derived neutrophil-to-lymphocyte ratio and lung cancer risk in heavy smokers. Cancer Prev Res (Phila). 2018; 11:727–34.
https://doi.org/10.1158/1940-6207.CAPR-18-0111
PMID:30254071

22. Kim S, Eliot M, Koestler DC, Wu WC, Kelsey KT. Association of neutrophil-to-lymphocyte ratio with mortality and cardiovascular disease in the jackson heart study and modification by the duffy antigen variant. JAMA Cardiol. 2018; 3:455–62.
https://doi.org/10.1001/jamacardio.2018.1042
PMID:29801037

23. He FJ, MacGregor GA. How far should salt intake be reduced? Hypertension. 2003; 42:1093–99.
https://doi.org/10.1161/01.HYP.0000102864.05174.E8
PMID:14610100

24. Flanagan JM, Wilson A, Koo C, Masrour N, Gallon J, Loomis E, Flower K, Wilhelm-Benartzi C, Hergovich A, Cunnea P, Gabra H, Braicu EI, Sehouli J, et al. Platinum-based chemotherapy induces methylation changes in blood DNA associated with overall survival in patients with ovarian cancer. Clin Cancer Res. 2017; 23:2213–22.
https://doi.org/10.1158/1078-0432.CCR-16-1754
PMID:27663594

25. Figueroa ME, Lugthart S, Li Y, Erpelinck-Verschueren C, Deng X, Christos PJ, Schifano E, Booth J, van Putten W, Skrabanek L, Campagne F, Mazumdar M, Greally JM, et al. DNA methylation signatures identify biologically distinct subtypes in acute myeloid leukemia. Cancer Cell. 2010; 17:13–27.
https://doi.org/10.1016/j.ccr.2009.11.020
PMID:20060365

26. Chen YA, Lemire M, Choufani S, Butcher DT, Grafodatskaya D, Zanke BW, Gallinger S, Hudson TJ, Weksberg R. Discovery of cross-reactive probes and polymorphic CpGs in the illumina infinium HumanMethylation450 microarray. Epigenetics. 2013; 8:203–09.
https://doi.org/10.4161/epi.23470
PMID:23314698

27. Teschendorff AE, Marabita F, Lechner M, Bartlett T, Tegner J, Gomez-Cabrero D, Beck S. A beta-mixture quantile normalization method for correcting probe design bias in illumina infinium 450 K DNA methylation data. Bioinformatics. 2013; 29:189–96.
https://doi.org/10.1093/bioinformatics/bts680
PMID:23175756

28. Logue MW, Smith AK, Wolf EJ, Maniates H, Stone A, Schichman SA, McGlinchey RE, Milberg W, Miller MW. The correlation of methylation levels measured using illumina 450K and EPIC BeadChips in blood samples. Epigenomics. 2017; 9:1363–71.
https://doi.org/10.2217/epi-2017-0078
PMID:28809127

29. Watanabe K, Taskesen E, van Bochoven A, Posthuma D. Functional mapping and annotation of genetic associations with FUMA. Nat Commun. 2017; 8:1826.
https://doi.org/10.1038/s41467-017-01261-5
PMID:29184056

30. Kanehisa M, Goto S. KEGG: kyoto encyclopedia of genes and genomes. Nucleic Acids Res. 2000; 28:27–30.
https://doi.org/10.1093/nar/28.1.27
PMID:10592173

31. Fabregat-Traver D, Sharapov SZ, Hayward C, Rudan I, Campbell H, Aulchenko Y, Bientinesi P. High-Performance Mixed Models Based Genome-Wide Association Analysis with omicABEL software. F1000Res. 2014; 3:200.
https://doi.org/10.12688/f1000research.4867.1
PMID:25717363

32. Schurmann C, Heim K, Schillert A, Blankenberg S, Carstensen M, Dörr M, Endlich K, Felix SB, Gieger C, Grallert H, Herder C, Hoffmann W, Homuth G, et al. Analyzing illumina gene expression microarray data from different tissues: methodological aspects of data analysis in the metaxpress consortium. PLoS One. 2012; 7:e50938.
https://doi.org/10.1371/journal.pone.0050938
PMID:23236413

33. Laaksonen MA, Härkänen T, Knekt P, Virtala E, Oja H. Estimation of population attributable fraction (PAF) for disease occurrence in a cohort study design. Stat Med. 2010; 29:860–74.
https://doi.org/10.1002/sim.3792
PMID:20213711

34. Pilling LC, Kuo CL, Sicinski K, Tamosauskaite J, Kuchel GA, Harries LW, Herd P, Wallace R, Ferrucci L, Melzer D. Human longevity: 25 genetic loci associated in 389,166 UK biobank participants. Aging (Albany NY). 2017; 9:2504–20.
https://doi.org/10.18632/aging.101334
PMID:29227965

35. Nikpay M, Goel A, Won HH, Hall LM, Willenborg C, Kanoni S, Saleheen D, Kyriakou T, Nelson CP, Hopewell JC, Webb TR, Zeng L, Dehghan A, et al. A comprehensive 1,000 genomes-based genome-wide association meta-analysis of coronary artery disease. Nat Genet. 2015; 47:1121–30.
https://doi.org/10.1038/ng.3396
PMID:26343387

36. Pattaro C, Teumer A, Gorski M, Chu AY, Li M, Mijatovic V, Garnaas M, Tin A, Sorice R, Li Y, Taliun D, Olden M, Foster M, et al. ICBP Consortium, AGEN Consortium, CARDIOGRAM, CHARGe-Heart Failure Group, and ECHOGen Consortium. Genetic associations at 53 loci highlight cell types and biological pathways relevant for kidney function. Nat Commun. 2016; 7:10023.
https://doi.org/10.1038/ncomms10023
PMID:26831199

37. Warren HR, Evangelou E, Cabrera CP, Gao H, Ren M, Mifsud B, Ntalla I, Surendran P, Liu C, Cook JP, Kraja AT, Drenos F, Loh M, et al, and International Consortium of Blood Pressure (ICBP) 1000G Analyses, and BIOS Consortium, and Lifelines Cohort Study, and Understanding Society Scientific group, and CHD Exome Consortium, and ExomeBP Consortium, and T2D-GENES Consortium, and GoT2DGenes Consortium, Cohorts for Heart and Ageing Research in Genome Epidemiology (CHARGE) BP Exome Consortium, and International Genomics of Blood Pressure (iGEN-BP) Consortium, and UK Biobank CardioMetabolic

Consortium BP working group. Genome-wide association analysis identifies novel blood pressure loci and offers biological insights into cardiovascular risk. Nat Genet. 2017; 49:403–15.
https://doi.org/10.1038/ng.3768
PMID:28135244

38. Gaulton KJ, Ferreira T, Lee Y, Raimondo A, Mägi R, Reschen ME, Mahajan A, Locke A, Rayner NW, Robertson N, Scott RA, Prokopenko I, Scott LJ, et al, and DIAbetes Genetics Replication And Meta-analysis (DIAGRAM) Consortium. Genetic fine mapping and genomic annotation defines causal mechanisms at type 2 diabetes susceptibility loci. Nat Genet. 2015; 47:1415–25.
https://doi.org/10.1038/ng.3437
PMID:26551672

39. Gaunt TR, Shihab HA, Hemani G, Min JL, Woodward G, Lyttleton O, Zheng J, Duggirala A, McArdle WL, Ho K, Ring SM, Evans DM, Davey Smith G, Relton CL. Systematic identification of genetic influences on methylation across the human life course. Genome Biol. 2016; 17:61.
https://doi.org/10.1186/s13059-016-0926-z
PMID:27036880

40. Hemani G, Zheng J, Elsworth B, Wade KH, Haberland V, Baird D, Laurin C, Burgess S, Bowden J, Langdon R, Tan VY, Yarmolinsky J, Shihab HA, et al. The MR-base platform supports systematic causal inference across the human phenome. Elife. 2018; 7:e34408.
https://doi.org/10.7554/eLife.34408
PMID:29846171

41. Didelez V, Sheehan N. Mendelian randomization as an instrumental variable approach to causal inference. Stat Methods Med Res. 2007; 16:309–30.
https://doi.org/10.1177/0962280206077743
PMID:17715159

42. Bowden J, Davey Smith G, Burgess S. Mendelian randomization with invalid instruments: effect estimation and bias detection through egger regression. Int J Epidemiol. 2015; 44:512–25.
https://doi.org/10.1093/ije/dyv080
PMID:26050253

43. Bowden J, Davey Smith G, Haycock PC, Burgess S. Consistent estimation in mendelian randomization with some invalid instruments using a weighted median estimator. Genet Epidemiol. 2016; 40:304–14.
https://doi.org/10.1002/gepi.21965
PMID:27061298

44. Hartwig FP, Davey Smith G, Bowden J. Robust inference in summary data mendelian randomization via the zero modal pleiotropy assumption. Int J Epidemiol. 2017; 46:1985–98.
https://doi.org/10.1093/ije/dyx102
PMID:29040600

45. Levine ME, Lu AT, Quach A, Chen BH, Assimes TL, Bandinelli S, Hou L, Baccarelli AA, Stewart JD, Li Y, Whitsel EA, Wilson JG, Reiner AP, et al. An epigenetic biomarker of aging for lifespan and healthspan. Aging (Albany NY). 2018; 10:573–91.
https://doi.org/10.18632/aging.101414
PMID:29676998

46. Koestler DC, Usset J, Christensen BC, Marsit CJ, Karagas MR, Kelsey KT, Wiencke JK. DNA methylation-derived neutrophil-to-lymphocyte ratio: an epigenetic tool to explore cancer inflammation and outcomes. Cancer Epidemiol Biomarkers Prev. 2017; 26:328–38.
https://doi.org/10.1158/1055-9965.EPI-16-0461
PMID:27965295

SUPPLEMENTARY MATERIALS

Supplementary material - cohort description

The atherosclerosis risk in communities (ARIC) study

ARIC cohort description
The ARIC Study is a population-based prospective cohort study of cardiovascular disease risk in four US communities [1]. Between 1987 and 1989, 7,082 men and 8,710 women aged 45–64 years were enrolled in Forsyth County, North Carolina; Jackson, Mississippi (African Americans only); suburban Minneapolis, Minnesota; and Washington County, Maryland. The ARIC Study protocol was approved by the institutional review board of each participating university, and participants provided written informed consent. Participants underwent a baseline clinical examination (Visit 1) and four subsequent follow-up clinical exams (Visits 2–5). The present analysis is restricted to African Americans from Jackson and Forsyth County centers. Baseline for mortality follow-up is either Visit 2 (1990–1992) or Visit 3 (1993–1995), when the DNA used for methylation quantification was collected. Covariates were measured at the time of blood draw, unless otherwise specified. Data on education, smoking status, smoking pack-years, alcohol intake, and physical activity were obtained by self-report at Visit 1. Trained technicians took fasting blood samples and measured height and weight using standard protocols. Diabetes was defined as a fasting blood glucose level of ≥126 mg/dL, non-fasting blood glucose level of ≥200 mg/dL, self-reported physician diagnosis of diabetes, or use of antidiabetic medication in the past 2 weeks. Hypertension was defined as systolic blood pressure ≥140 mm Hg, diastolic blood pressure ≥90 mm Hg, or self-reported use of antihypertensive medication in the past 2 weeks. History of cancer was defined by self-report or incident cancer cases found between Visit 1 and time of blood draw found through cancer registry and hospital linkage. History of coronary heart disease (CHD) was defined as self-reported history at baseline or an adjudicated event (Myocardial infarction (MI), silent MI, coronary artery bypass surgery, or angioplasty) found between Visit 1 and time of blood draw.

ARIC death ascertainment
Deaths among cohort participants were identified through December 2012 via annual telephone calls and by surveillance of local death certificates and obituaries. If a participant was lost to telephone follow-up, a National Death Index search was conducted.

ARIC DNA methylation quantification
Genomic DNA was extracted from peripheral blood leukocyte samples using the Gentra Puregene Blood Kit (Qiagen; Valencia, CA, USA) according to the manufacturer's instructions (https://www.qiagen.com). Bisulfite conversion of 1 μg genomic DNA was performed using the EZ-96 DNA Methylation Kit (Deep Well Format) (Zymo Research; Irvine, CA, USA) according to the manufacturer's instructions (https://www.zymoresearch.com). Bisulfite conversion efficiency was determined by PCR amplification of converted DNA before proceeding with methylation analyses on the Illumina platform using Zymo Research's Universal Methylated Human DNA Standard and Control Primers. The Illumina Infinium HumanMethylation450K Beadchip array (HM450K) was used to measure DNA methylation (Illumina, Inc.; San Diego, CA, USA). Background subtraction was conducted with the GenomeStudio software using built-in negative control bead types on the array. Positive and negative controls and sample replicates were included on each 96-well plate assayed. After exclusion of controls, replicates, and samples with integrity issues or failed bisulfite conversion, a total of 2,841 study participants had HM450K data available for further quality control (QC) analyses. We removed poor-quality samples with pass rate of <99% (i.e., if the sample had at least 1% of CpG sites with detection P-value > 0.01 or missing), indicative of lower DNA quality or incomplete bisulfite conversion, and samples with a possible gender mismatch based on evaluation of selected CpG sites on the Y chromosome. Additional details have been published elsewhere [2 , 3].

Framingham heart study offspring cohort (FHS)

FHS study participants
The FHS Offspring Cohort began enrollment in 1971 and included 5,124 offspring of the FHS original cohort as well as spouses of the offspring. Participants were eligible for the current study if they attended the eighth examination cycle (2005–2008) and consented to have their DNA used for genetic research. All participants provided written informed consent at the time of each examination visit. The study protocol was approved by the Institutional Review Board at Boston University Medical Center (Boston, MA). FHS data are available in dbGaP (accession number: phs000724.v2.p9).

FHS death ascertainment
Deaths among FHS participants that occurred before January 1, 2013 were ascertained using multiple strategies, including routine contact with participants for health history updates, surveillance at the local

hospital, obituaries in the local newspaper, and queries to the National Death Index. Death certificates, hospital and nursing home records before death, and autopsy reports were requested. When cause of death was undeterminable, the next of kin were interviewed. The date and cause of death were reviewed by an endpoint panel of three investigators.

FHS DNA methylation quantification

Peripheral blood samples were collected at the 8th examination. Genomic DNA was extracted from buffy coats using the Gentra Puregene DNA extraction kit (Qiagen) and bisulfite converted using the EZ DNA Methylation kit (Zymo Research). DNA methylation quantification was conducted in two laboratory batches using the Illumina Infinium HumanMethylation450 array. Methylation beta values were generated using the Bioconductor *minfi* package with background correction. Sample exclusion criteria included poor SNP matching of control positions, missing rate >1%, outliers from multi-dimensional scaling, and sex mismatch. In addition, we excluded individuals with leukemia and those who received chemotherapy. Additional sample exclusions included those with mismatches in their reported sex and methylation-predicted sex as well as methylation-predicted tissues that were not blood. Lastly, samples with correlation with our reference population of r < 0.80 were excluded. Predicted sex, tissues, correlation with reference population, and DNA methylation-predicted ages were computed using our online age calculator (http://labs.genetics.ucla.edu/horvath/dnamage). Background subtraction was applied using the *preprocessIllumina* command in the *minfi* Bioconductor package [4]. In total, 2,635 samples and 443,304 CpG probes remained for analysis.

Invecchiare in chianti (InCHIANTI) study

InChianti study participants

The InCHIANTI Study is a population-based prospective cohort study of residents ≥20 years old from two areas in the Chianti region of Tuscany, Italy. Sampling and data collection procedures have been described elsewhere [5]. Briefly, 1,326 participants donated a blood sample at baseline (1998–2000), of which 784 also donated a blood sample at 9-year follow-up (2007–2009). DNA methylation was assayed using the Illumina Infinium HumanMethylation450 platform in DNA samples corresponding to participants with sufficient DNA at both baseline and Year 9 visits (n = 499). All participants provided written informed consent to participate in this study. The study complied with the Declaration of Helsinki. The Italian National Institute of Research and Care on

Aging Institutional Review Board approved the study protocol.

InChianti death ascertainment

Vital status was ascertained using data from the Tuscany Regional Mortality General Registry. Deaths were assessed until December 1, 2014.

InChianti DNA methylation quantification

Genomic DNA was extracted from buffy coat samples using an AutoGen Flex and quantified on a Nanodrop1000 spectrophotometer before bisulfite conversion. Genomic DNA was bisulfite converted using the Zymo EZ-96 DNA Methylation Kit (Zymo Research) per the manufacturer's protocol. CpG methylation status of 485, 577 CpG sites was determined using the Illumina Infinium HumanMethylation450 BeadChip per the manufacturer's protocol, as previously described [6]. Initial data analysis was performed using GenomeStudio 2011.1 (Model M Version 1.9.0, Illumina Inc.). Threshold call rate for inclusion of samples was 95%. Quality control of sample handling included comparison of clinically reported sex versus sex of the same samples determined by analysis of methylation levels of CpG sites on the X chromosome [6]. Background subtraction was applied using the *preprocessIllumina* command in the *minfi* Bioconductor package [4].

Cooperative health research in the region of augsburg (KORA) F4 cohort

KORA cohort description

The KORA study is an independent population-based cohort from Augsburg, Southern Germany. Whole blood samples of the KORA F4 survey (examination 2006–2008), a seven-year follow-up study of the KORA S4 cohort, were used. Out of 4,621 participants for the KORA S4 baseline study, 3,080 participants participated in the KORA F4 follow-up study [7]. Participants provided written informed consent, and the study was approved by the local ethics committee (Bayerische Landesärztekammer). For 1,799 subjects, methylation data as well as information about death ascertainment was available. Before analyses, all individuals with a detection P-value > 0.05 for >1% of probes were removed (375 individuals). Sex checks performed during calculation of DNAmAge resulted in the removal of another 167 individuals, 137 of whom had an "unsure" gender. This left 1,257 individuals for analysis. At the KORA F4 follow-up examination, all individuals completed questionnaires and physical examinations conducted by trained staff covering demographics, lifestyle, and medical history since the KORA S4 examination. Collected information included age, sex, years of education, smoking status (current regular, current irregular, former, never), pack-years, alcohol consumption

(g/day), physical activity (active, inactive), diabetes status, hypertension status, self-reported cancer diagnosis, and body mass index (BMI), among other clinical variables [7].

KORA mortality ascertainment

The vital status of all F4 participants was ascertained through the population registries inside and outside the study area in 2011 (cut-off date: December 31, 2011). Record linkage was based on name, sex, date of birth, and address. If the person died, the time and location of death was assessed via population registries, and a copy of the death certificate was obtained from the Regional Health Department. If the person moved out of the study area, time of the move and information on the new address was typically available. Vital status could not be assessed for those who had moved to a foreign country or to an unknown location in the country. Causes of death were ICD-9 revision coded. There were a total of 42 deaths, including 16 from cardiovascular disease and 17 from cancer.

KORA DNA methylation measures

Whole blood was drawn into serum gel tubes. We bisulfite-converted 1 µg of genomic DNA using the EZ-96 DNA Methylation Kit (Zymo Research) according to the manufacturer's procedure, with the alternative incubation conditions recommended when using the Illumina Infinium Methylation Assay. Genome-wide DNA methylation was analyzed in 1,799 subjects using the Illumina Infinium HumanMethylation450 BeadChip Array. Raw methylation data were extracted using the Illumina Genome Studio (version 2011.1) with the methylation module (version 1.9.0). Preprocessing was performed with R (version 3.0.1). Probes with signals from less than three functional beads and probes with a detection P-value > 0.01 were defined as low-confidence probes. Probes that covered SNPs (MAF in Europeans > 5%) were excluded from the data set. A color bias adjustment was performed with the R package lumi (version 2.12.0) by smooth quantile normalization and background correction based on negative control probes present on the Infinium HumanMethylation BeadChip. This was performed separately for the two-color channels and chips. β-values corresponding to low-confidence probes were set to missing. A 95% call rate threshold was applied on samples and CpG sites. Beta-mixture quantile normalization (BMIQ) was applied by using the R package wateRmelon, version 1.0.3. Plate and batch effects were investigated by principle component analysis and eigenR2 analysis, because KORA F4 samples were processed on 20 96-well plates across nine different batches.

Probes with a detection P > 0.05 for > 1% of samples were removed as well as all "ch" and "rs" probes, leaving a total of 431, 217 probes for analysis. Although raw beta values were used in Dr. Horvath's online calculator to determine cell counts, normalized data was used for the final analyses.

To reduce non-biological variability between observations, data were normalized using quantile normalization on raw signal intensities. Precisely, quantile normalization was stratified to six probe categories based on probe type and color channel (i.e., Infinium I signals from beads targeting methylated CpG sites obtained through red and green color channels, Infinium I signals from beads targeting unmethylated CpG sites obtained through red and green color channels, and Infinium II signals obtained through red and green color channels [8]) using the R package *limma*, version 3.16.5 [9]. Further, to correct the shift in the distribution of methylation values observed for the two different assay designs (Infinium I and Infinium II) on the BeadChip, BMIQ was applied [10] using the R package wateRmelon, version 1.0.3 [11].

Lothian birth cohorts of 1921 and 1936 (LBC1921 and LBC1936)

LBC cohort description

LBC1921 and LBC1936 are two longitudinal studies of aging [12, 13] that derive from the Scottish Mental Surveys of 1932 and 1947, respectively, when nearly all 11-year-old children in Scotland completed a test of general cognitive ability [14]. Survivors living in the Lothian area of Scotland were recruited in late-life at a mean age of 79 years for LBC1921 (n = 550) and mean age of 70 years for LBC1936 (n = 1,091). Follow-up took place at ages 70, 73, and 76 years in LBC1936 and ages 79, 83, 87, and 90 years in LBC1921. Collected data include genetic information, longitudinal epigenetic information, longitudinal brain imaging (LBC1936), numerous blood biomarkers, and anthropomorphic and lifestyle measures. Post-QC, DNA methylation data were available for 920 LBC1936 participants at age 70 years and for 446 LBC1921 participants at age 79 years. At each in-person visit, participants completed questionnaires regarding demography, lifestyle, and medical history. They reported chronological age, years of education, smoking status (never, former, current), pack-years consumption (continuous), alcohol consumption (light, moderate, and heavy drinkers), self-reported type 2 diabetes, cancer, and hypertension. BMI was computed from anthropometric measures. Participants were asked to remove their shoes before a SECA stadiometer was used to assess height in centimeters. Weight (after removing shoes and outer clothing) was measured in

kilograms using a digital readout from electronic SECA scales.

LBC mortality ascertainment

For both LBC1921 and LBC1936, mortality status was obtained via data linkage from the National Health Service Central Register, provided by the General Register Office for Scotland (now National Records of Scotland). Participant deaths and cause of death are routinely flagged to the research team about every 12 weeks. The last update available for the current project was 26th November 2014.

LBC DNA methylation measures

Detailed information about collection and QC steps on LBC methylation data have been reported previously [12, 15]. Briefly, the Illumina Infinium HumanMethylation450 BeadChip was used to measure DNA methylation in whole blood of consenting participants. Background correction was performed, and QC was used to remove probes with a low detection rate, low quality (manual inspection), and low call rate as well as samples with a poor match between genotypes and SNP control probes or incorrect predicted sex. Additional QC was performed to remove samples and probes in which >1% of probes or samples, respectively, had a detection $P > 0.05$. The working set included 442,227 CpG probes.

Normative aging study (NAS)

NAS cohort description

The ongoing longitudinal US Department of Veterans Affairs NAS was established in 1963 and included men 21–80 years old and free of known chronic medical conditions at entry [16]. Participants were invited to medical examinations every three to five years. At each visit, men provided information on medical history, lifestyle, and demographic factors and underwent physical examinations and laboratory tests. DNA samples were collected from 675 active participants between 1999–2007 [16]. We excluded participants who were non-white or who reported leukemia at the time of DNA extraction, leaving a total of 646 individuals with a single observation each. Participants provided written informed consent at each visit. The NAS study was approved by the institutional review boards of participating institutions. At each in-person visit, participants completed questionnaires regarding demography, lifestyle, and medical history. They reported chronological age, years of education, smoking status (never, former, current), pack-years consumption (continuous), alcohol consumption (<2, ≥2 drinks/day), physical activity (<12, 12–30, ≥30 metabolic equivalent hours [MET-h] per week), type 2 diabetes (self-reported diagnosis and/or use of diabetes medications), diagnosis of CHD (validated on medical records, ECG, and physician exams), diagnosis of malignant cancer in the five years prior the visit (diagnosed with ICD-9 code). High blood pressure was defined as antihypertensive medication use, systolic blood pressure ≥140 mmHg, or diastolic blood pressure ≥90 mmHg at study visit. BMI was computed from anthropometric measures, performed with participants in undershorts and socks [17].

NAS mortality ascertainment

Official death certificates were obtained for decedents from the appropriate state health departments and were reviewed by a physician. An experienced research nurse coded the cause of death using ICD-9. Both participant deaths and causes of death were routinely updated by the research team, and the last update available was December 31, 2013 [12].

NAS DNA methylation measures

DNA was extracted from buffy coats using the QIAamp DNA Blood Kit (Qiagen). We used 500 ng of DNA for bisulfite conversion using the EZ-96 DNA Methylation Kit (Zymo Research). To reduce chip and plate effects, we used a two-stage age-stratified algorithm to randomize samples and ensure similar age distributions across chips and plates; 12 samples that were sampled across all age quartiles were randomized to each chip, and then chips were randomized to plates (8 chips/plate).

QC analysis was performed to remove samples and probes, where >1% of probes or samples, respectively, had a detection $P > 0.05$. Remaining samples were preprocessed using the Illumina-type background correction [18] and normalized with dye-bias [19] and BMIQ [20] adjustments, which were used to generate beta methylation values. The working set included 477, 928 CpG probes. DNA methylation age was computed using the Horvath calculator from background-corrected methylation data, and QC analysis was performed only on samples, leaving 485, 512 CpG and CpH probes in the working set.

TwinsUK

TwinsUK study participants

The TwinsUK cohort was established in 1992 and recruited both monozygotic and dizygotic same-sex twins in the United Kingdom. The majority of participants are female, Caucasian, and mostly disease-free at time of ascertainment. There are >13, 000 twin participants in the cohort, of which 805 were included in the current study. Whole blood samples were collected during participants' clinical visits, along with questionnaire data on phenotype and lifestyle factors. All subjects provided written informed consent [21].

Information on physical activity, smoking pack-years, plate number, and chip position number were not available for subjects in the TwinsUK dataset and therefore were not adjusted as covariates in all analyses.

TwinsUK death ascertainment

Mortality data were collected using two approaches: 1) during routine contact for standard clinical visits in TwinsUK, and 2) using queries to the National Death Register. Date and cause of death were recorded.

TwinsUK DNA methylation quantification

DNA samples were extracted from whole blood using the DNeasy kit (Qiagen). DNA was bisulfite converted using the EZ DNA methylation kit (Zymo Research). Methylation levels were profiled using the Illumina Infinium HumanMethylation450 array, and methylation betas were generated using the R package *minfi* with background correction. Raw beta levels were subjected to BMIQ dilation to correct for technical effects. Probe exclusion criteria included probes that mapped to multiple locations in the reference sequence and probes in which >1% of subjects had detection $P > 0.05$. Individuals with >5% missing probes, with mismatched sex, and with mismatched genotypes were also excluded. Methylation-predicted sex, methylation-predicted blood cell types, correlations with the reference population, and DNA methylation-predicted age were computed using the online epigenetic age calculator (http://labs.genetics.ucla.edu/horvath/dnamage).

Women's health initiative–broad agency announcement 23 (WHI-BAA23)

WHI-BAA23 cohort description

Subjects included a subsample of participants of the WHI study, a national study that began in 1993 and enrolled postmenopausal women 50–79 years of age into one of three randomized clinical trials. Women were selected from one of two WHI large sub-cohorts that had previously undergone genome-wide genotyping as well as profiling for 7 cardiovascular disease-related biomarkers, including total cholesterol, high-density lipoprotein, low-density lipoprotein, triglycerides, C-reactive protein (CRP), creatinine, insulin, and glucose through two core WHI ancillary studies [22]. The first cohort is the WHI SNP Health Association Resource (SHARe) cohort of minorities that includes >8,000 African American (AA) women and >3,500 Hispanic women. Women were genotyped through the WHI core study M5-SHARe (www.whi.org/researchers/data/WHIStudies/StudySites/M5) and underwent biomarker profiling through WHI Core study W54-SHARe (...data/WHIStudies/StudySites/W54). The second cohort consists of a combination of European Americans (EA) from two hormonal therapy trials selected

for GWAS and biomarkers in core studies W58 (.../data/WHIStudies/StudySites/W58) and W63 (.../data/WHIStudies/StudySites/W63). From these two cohorts, two sample sets were formed. Sample Set 1 is a sample set of 637 CHD cases and 631 non-CHD cases as of Sept 30, 2010. Sample Set 2 is a non-overlapping sample of 432 cases of CHD and 472 non-CHD cases as of September 17, 2012. The ethnic groups differed in terms of age distribution, as Caucasian women tended to be older. We acknowledge a potential for selection bias using the above-described sampling scheme in WHI but suspect that if such bias is present, it is minimal. First, selection bias is introduced by restricting our methylation profiling at baseline to women with GWAS and biomarker data from baseline as well, given the requirement that these subjects must have signed the WHI supplemental consent for broad sharing of genetic data in 2005. However, we believe that selection bias at this stage is minimized by inclusion of subjects who died between time of start of the WHI study and time of supplemental consent in 2005, which excluded only ~6%–8% of all WHI participants. Subjects unable or unwilling to sign consent in 2005 may not represent a random subset of all participants who survived to 2005. Second, some selection bias may also occur if similar gross differences exist in the characteristics of participants who consented to be followed in the two WHI extension studies beginning in 2005 and 2010 compared to non-participants at each stage. We believe these selection biases, if present, have minimal effects on our effect estimates. Data are available from this page: https://www.whi.org/researchers/Stories/June%202015%20WHI%20Investigators'%20Datasets%20Released.aspx, as well as https://www.whi.org/researchers/data/Documents/WHI%20Data%20Preparation%20and%20Use.pdf

WHI-BAA23 death ascertainment

We used the variable "DEATHALL" from form 124/120 that incorporated any report of death (as of August 2015).

WHI-BAA23 DNA methylation quantification

In brief, bisulfite conversion using the Zymo EZ DNA Methylation Kit (Zymo Research) as well as subsequent hybridization of the Illumina HumanMethylation450k Bead Chip and scanning (iScan, Illumina) were performed according to the manufacturer's protocols by applying standard settings. DNA methylation levels (β values) were determined by calculating the ratio of intensities between methylated (signal A) and un-methylated (signal B) sites. Specifically, β value was calculated from the intensity of methylated (M corresponding to signal A) and un-methylated (U corresponding to signal B) sites, as the ratio of fluorescent signals $\beta = \text{Max}(M,0)/[\text{Max}(M,0)+\text{Max}$

(U,0)+100]. Thus, β values range from 0 (completely un-methylated) to 1 (completely methylated).

Women's health initiative—epigenetic mechanisms of PM-Mediated CVD risk (WHI-EMPC)

WHI-EMPC cohort description
WHI-EMPC is an ancillary study of epigenetic mechanisms underlying associations between ambient particulate matter (PM) air pollution and cardiovascular disease in the WHI clinical trials (CT) cohort. It is funded by the National Institute of Environmental Health Sciences (R01-ES020836).

The WHI-EMPC study population is a stratified, random sample of 2,200 WHI CT participants who were examined in 1993–2001; had available buffy coats, core analytes, electrocardiograms, and ambient concentrations of PM; and were not taking anti-arrhythmic medications at the time.

As such, WHI-EMPC is representative of the larger, multiethnic WHI CT population from which it was sampled: 68,132 participants aged 50–79 years who were randomized to hormone therapy, calcium/vitamin D supplementation, and/or dietary modification in 40 U.S. clinical centers at baseline exam (1993–1998) and re-examined in the fasting state one, three, six, and nine years later [23, 24]. During participant visits, data on age, race/ethnicity, education, smoking status (current, former, never), pack-years of smoking, alcohol consumption (drinks per week), recreational physical activity (MET-hours/week), weight/height/BMI, systolic and diastolic blood pressure, medication use, CHD, type 2 diabetes, and cancer diagnosis were obtained.

Hypertension status was based on systolic blood pressure ≥140 mmHg or diastolic blood pressure ≥90 mmHg or antihypertensive medication use (angiotensin converting enzyme inhibitors, angiotensin II receptor antagonists, beta blockers, calcium channel blockers, thiazides). CHD was defined by a history of myocardial infarction (acute, hospitalized, definite or probable events supported by cardiac pain, electrocardiogram, and biomarker data) or revascularization procedure (coronary artery bypass graft, percutaneous coronary angioplasty, stent) and was self-reported at baseline and confirmed by physician-review, classification, and local/central adjudication of medical records during follow-up. Type 2 diabetes was defined by a self-reported history of physician-treated diabetes, fasting glucose ≥126 mg/dL, non-fasting glucose ≥200 mg/dL, or anti-diabetic medication use. Cancer was defined by a diagnosis of any cancer, excluding leukemia and other hematologic malignancies (Hodgkin's lymphoma, non-Hodgkin's lymphoma, multiple myeloma).

Current analyses involve information collected at the first available visit with available DNA methylation data and stratification by race/ethnicity [European (WHI-EMPC-EA) and African American (WHI-EMPC-AA) ancestries].

WHI-EMPC mortality ascertainment
All-cause mortality and sub-classification of the underlying cause of death to cardiovascular or cancer mortality were based on WHI physician review of death certificates, medical records, and autopsy reports. Cardiovascular disease mortality was defined as death due to definite or possible CHD, cerebrovascular disease, or other or unknown cardiovascular disease. Cancer mortality was defined as death due to any cancer. Participants affected by leukemia or other hematologic malignancies (i.e., Hodgkin's lymphoma, non-Hodgkin's lymphoma, multiple myeloma) were excluded due to known effects on red cell, white cell, and platelet counts.

WHI-EMPC DNA methylation quantification
Genome-wide DNA methylation at CpG sites was measured using the Illumina 450K Infinium Methylation BeadChip, quantitatively represented by beta (percentage of methylated cytosines over the sum of methylated and unmethylated cytosines) and quality-controlled using the following filters: detection $P > 0.01$ in >10% of samples, detection $P > 0.01$ or missing in >1% of probes, and probes with a coefficient of variation <5%, yielding values of beta at 293,171 sites. DNA methylation data were normalized using BMIQ [25] and stage-adjusted using ComBat [10]. Modeled epigenome-wide associations also adjusted for cell subtype proportions (CD8-T, CD4-T, B cell, natural killer, monocyte, and granulocyte) [26] and for technical covariates, including plate, chip, row, and column.

REFERENCES

1. The atherosclerosis risk in communities (ARIC) study: design and objectives. The ARIC investigators. Am J Epidemiol. 1989; 129:687–702.
PMID:2646917

2. Demerath EW, Guan W, Grove ML, Aslibekyan S, Mendelson M, Zhou YH, Hedman ÅK, Sandling JK, Li LA, Irvin MR, Zhi D, Deloukas P, Liang L, et al. Epigenome-wide association study (EWAS) of BMI, BMI change and waist circumference in african american adults identifies multiple replicated loci. Hum Mol Genet. 2015; 24:4464–79.
https://doi.org/10.1093/hmg/ddv161
PMID:25935004

3. Bose M, Wu C, Pankow JS, Demerath EW, Bressler J, Fornage M, Grove ML, Mosley TH, Hicks C, North K, Kao WH, Zhang Y, Boerwinkle E, Guan W. Evaluation of microarray-based DNA methylation measurement using technical replicates: the atherosclerosis risk in communities (ARIC) study. BMC Bioinformatics. 2014; 15:312.
https://doi.org/10.1186/1471-2105-15-312
PMID:25239148

4. Aryee MJ, Jaffe AE, Corrada-Bravo H, Ladd-Acosta C, Feinberg AP, Hansen KD, Irizarry RA. Minfi: a flexible and comprehensive bioconductor package for the analysis of infinium DNA methylation microarrays. Bioinformatics. 2014; 30:1363–69.
https://doi.org/10.1093/bioinformatics/btu049
PMID:24478339

5. Ferrucci L, Bandinelli S, Benvenuti E, Di Iorio A, Macchi C, Harris TB, Guralnik JM. Subsystems contributing to the decline in ability to walk: bridging the gap between epidemiology and geriatric practice in the InCHIANTI study. J Am Geriatr Soc. 2000; 48:1618–25.
https://doi.org/10.1111/j.1532-5415.2000.tb03873.x
PMID:11129752

6. Moore AZ, Hernandez DG, Tanaka T, Pilling LC, Nalls MA, Bandinelli S, Singleton AB, Ferrucci L. Change in epigenome-wide DNA methylation over 9 years and subsequent mortality: results from the InCHIANTI study. J Gerontol A Biol Sci Med Sci. 2016; 71:1029–35.
https://doi.org/10.1093/gerona/glv118
PMID:26355017

7. Rückert IM, Heier M, Rathmann W, Baumeister SE, Döring A, Meisinger C. Association between markers of fatty liver disease and impaired glucose regulation in men and women from the general population: the KORA-F4-study. PLoS One. 2011; 6:e22932.
https://doi.org/10.1371/journal.pone.0022932
PMID:21850244

8. Bibikova M, Barnes B, Tsan C, Ho V, Klotzle B, Le JM, Delano D, Zhang L, Schroth GP, Gunderson KL, Fan JB, Shen R. High density DNA methylation array with single CpG site resolution. Genomics. 2011; 98:288–95.
https://doi.org/10.1016/j.ygeno.2011.07.007
PMID:21839163

9. Smyth GK. Limma: linear models for microarray data. Bioinformatics and computational biology solutions using R and Bioconductor: Springer. 2005; 397–420.
https://doi.org/10.1007/0-387-29362-0_23

10. Teschendorff AE, Marabita F, Lechner M, Bartlett T, Tegner J, Gomez-Cabrero D, Beck S. A beta-mixture quantile normalization method for correcting probe design bias in illumina infinium 450 K DNA methylation data. Bioinformatics. 2013; 29:189–96.
https://doi.org/10.1093/bioinformatics/bts680
PMID:23175756

11. Pidsley R, Y Wong CC, Volta M, Lunnon K, Mill J, Schalkwyk LC. A data-driven approach to preprocessing illumina 450K methylation array data. BMC Genomics. 2013; 14:293.
https://doi.org/10.1186/1471-2164-14-293
PMID:23631413

12. Marioni RE, Shah S, McRae AF, Chen BH, Colicino E, Harris SE, Gibson J, Henders AK, Redmond P, Cox SR, Pattie A, Corley J, Murphy L, et al. DNA methylation age of blood predicts all-cause mortality in later life. Genome Biol. 2015; 16:25.
https://doi.org/10.1186/s13059-015-0584-6
PMID:25633388

13. Taylor AM, Pattie A, Deary IJ. Cohort profile update: the lothian birth cohorts of 1921 and 1936. Int J Epidemiol. 2018; 47:1042–42r.
https://doi.org/10.1093/ije/dyy022
PMID:29546429

14. Marioni RE, McRae AF, Bressler J, Colicino E, Hannon E, Li S, Prada D, Smith JA, Trevisi L, Tsai PC, Vojinovic D, Simino J, Levy D, et al. Meta-analysis of epigenome-wide association studies of cognitive abilities. Mol Psychiatry. 2018; 23:2133–44.
https://doi.org/10.1038/s41380-017-0008-y
PMID:29311653

15. Shah S, McRae AF, Marioni RE, Harris SE, Gibson J, Henders AK, Redmond P, Cox SR, Pattie A, Corley J, Murphy L, Martin NG, Montgomery GW, et al. Genetic and environmental exposures constrain epigenetic drift over the human life course. Genome Res. 2014; 24:1725–33.
https://doi.org/10.1101/gr.176933.114
PMID:25249537

16. Bell B, Rose CL, Damon A. The veterans administration longitudinal study of healthy aging. Gerontologist. 1966; 6:179–84.
https://doi.org/10.1093/geront/6.4.179
PMID:5342911

17. Troisi RJ, Heinold JW, Vokonas PS, Weiss ST. Cigarette smoking, dietary intake, and physical activity: effects on body fat distribution—the normative aging study. Am J Clin Nutr. 1991; 53:1104–11.
https://doi.org/10.1093/ajcn/53.5.1104
PMID:1850574

18. Triche TJ Jr, Weisenberger DJ, Van Den Berg D, Laird PW, Siegmund KD. Low-level processing of illumina infinium DNA methylation BeadArrays. Nucleic Acids Res. 2013; 41:e90.
https://doi.org/10.1093/nar/gkt090 PMID:23476028

19. Davis S, Du P, Bilke S, Triche T, Jr and Bootwalla M.

methylumi: Handle Illumina methylation R package version 2140 2015.

20. Teschendorff AE, Jones A, Fiegl H, Sargent A, Zhuang JJ, Kitchener HC, Widschwendter M. Epigenetic variability in cells of normal cytology is associated with the risk of future morphological transformation. Genome Med. 2012; 4:24.
https://doi.org/10.1186/gm323
PMID:22453031

21. Nica AC, Parts L, Glass D, Nisbet J, Barrett A, Sekowska M, Travers M, Potter S, Grundberg E, Small K, Hedman AK, Bataille V, Tzenova Bell J, et al, and MuTHER Consortium. The architecture of gene regulatory variation across multiple human tissues: the MuTHER study. PLoS Genet. 2011; 7:e1002003.
https://doi.org/10.1371/journal.pgen.1002003
PMID:21304890

22. Curb JD, McTiernan A, Heckbert SR, Kooperberg C, Stanford J, Nevitt M, Johnson KC, Proulx-Burns L, Pastore L, Criqui M, Daugherty S, and WHI Morbidity and Mortality Committee. Outcomes ascertainment and adjudication methods in the women's health initiative. Ann Epidemiol. 2003; 13:S122–28.
https://doi.org/10.1016/s1047-2797(03)00048-6
PMID:14575944

23. Design of the women's health initiative clinical trial and observational study. The women's health initiative study group. Control Clin Trials. 1998; 19:61–109.
https://doi.org/10.1016/s0197-2456(97)00078-0
PMID:9492970

24. Anderson GL, Manson J, Wallace R, Lund B, Hall D, Davis S, Shumaker S, Wang CY, Stein E, Prentice RL. Implementation of the women's health initiative study design. Ann Epidemiol. 2003; 13:S5–17.
https://doi.org/10.1016/s1047-2797(03)00043-7
PMID:14575938

25. Leek JT, Johnson WE, Parker HS, Jaffe AE, Storey JD. The sva package for removing batch effects and other unwanted variation in high-throughput experiments. Bioinformatics. 2012; 28:882–83.
https://doi.org/10.1093/bioinformatics/bts034
PMID:22257669

26. Houseman EA, Accomando WP, Koestler DC, Christensen BC, Marsit CJ, Nelson HH, Wiencke JK, Kelsey KT. DNA methylation arrays as surrogate measures of cell mixture distribution. BMC Bioinformatics. 2012; 13:86.
https://doi.org/10.1186/1471-2105-13-86
PMID:22568884
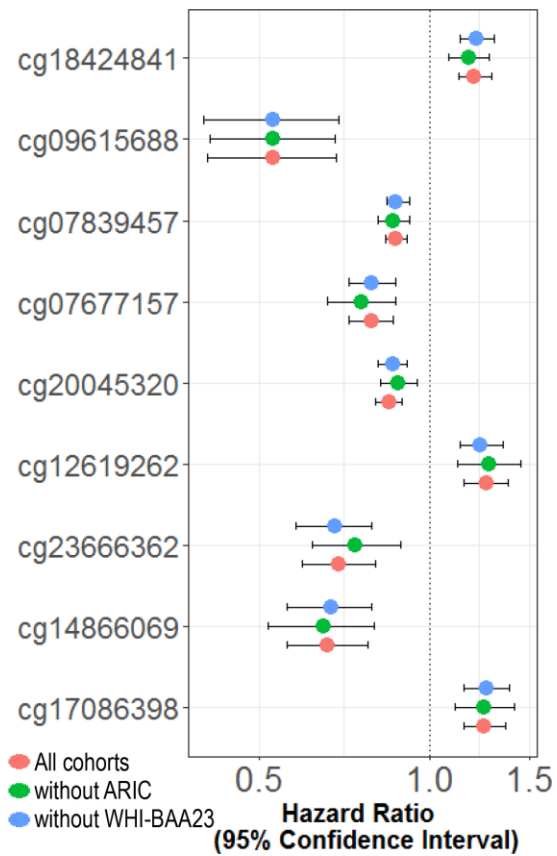
Supplementary Figure 1. Sensitivity analysis comparing hazard ratios of the fully-adjusted meta-analysis, including all cohorts, all excluding ARIC, or all excluding WHI-BAA23.
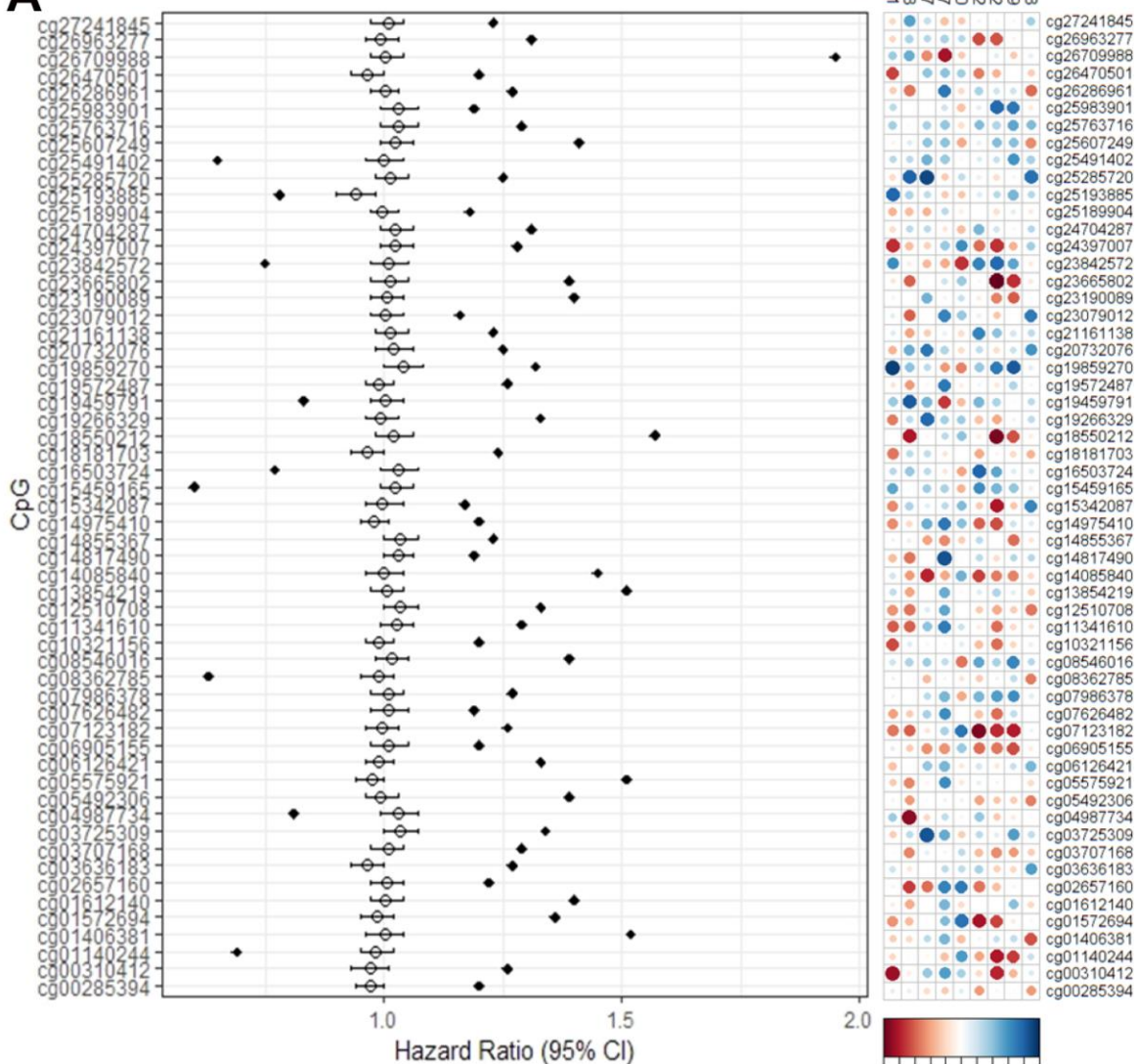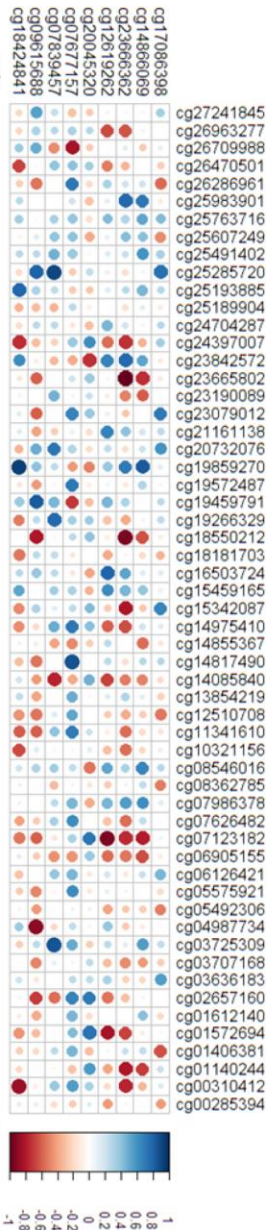
Supplementary Figure 2. (**A**) All-cause mortality association of 57 out of 58 CpGs identified with mortality in Zhang et al. (black dots) and all-cause mortality association of the same CpGs in the pooled meta-analysis (white dots with 95% confidence intervals). (**B**) Association of methylation levels of 57 out of 58 CpGs identified with mortality in Zhang et al. and our FDR-significant CpGs in all cohorts.
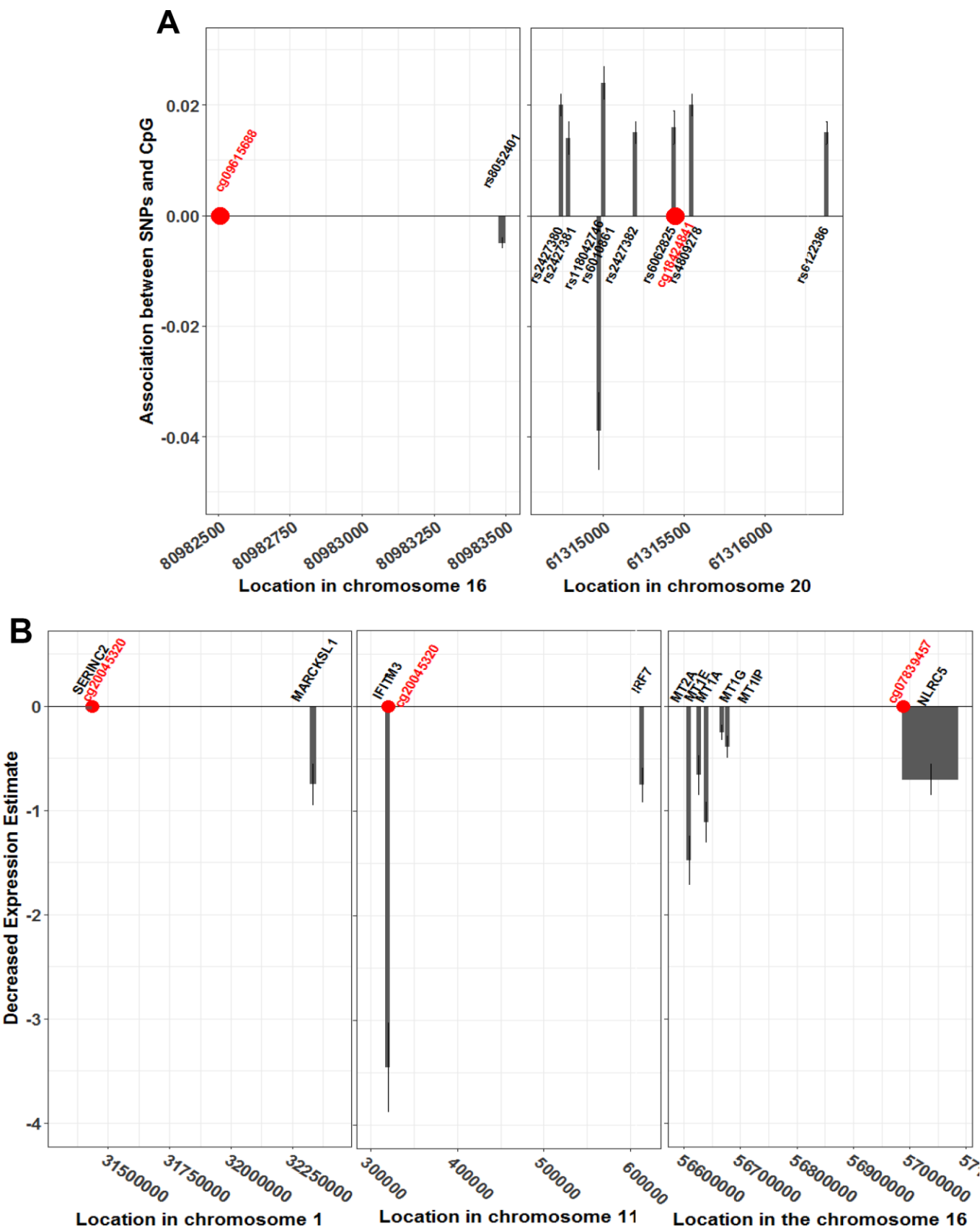
Supplementary Figure 3. (**A**) Methylation quantitative trait loci (meQTL) analysis and (**B**) expression quantitative quantitative trait methylation (eQTM) analysis in KORA.

Supplementary Tables

Please browse Full Text version to see the data of Supplementary Tables 1, 2, 6, 10, 12, 17.

Supplementary Table 1. Covariates included in the analysis of each cohort (*variables that differ across cohorts due to type of cutoff used in data collection) SD = standard deviation; CHD = coronary heart disease.

Supplementary Table 2. CpG loci where blood DNA methylation was associated (FDR<0.05) with all-cause mortality in fixed-effect meta-analysis from the basic model (i.e., age, gender, technical covariates, and white cell subtypes).

Supplementary Table 3. CpG loci where blood DNA methylation was associated (FDR<0.05) with all-cause mortality in the fixed-effect meta-analysis from the fully adjusted model.

Probe name	CHR	Distance to nearest gene (bp)	Nearest gene (10 Mp)[a]	Gene group	Relation to CpG Island	HR[b]	95% CI	p	Mean methylation level	Bonferroni significance	FDR-significant in basic model	Methylation level (Mean±SD)
cg17086398	1	0	SERINC2	Body		1.25	(1.15;1.36)	4.86E-07	0.29		1	0.29 ± 0.06
cg14866069	4	579	BMPR1B			0.66	(0.56;0.78)	4.85E-07	0.85			0.85 ± 0.05
cg23666362	4	516	MIR1973	TSS1500		0.69	(0.59;0.8)	8.00E-07	0.82			0.81 ± 0.04
cg12619262	7	6276	CHST12			1.26	(1.16;1.37)	1.76E-07	0.75			0.75 ± 0.07
cg20045320	11	116	IFITM3		S_Shore	0.85	(0.8;0.9)	4.06E-09	0.54	1	1	0.54 ± 0.09
cg07677157	12		NA[a]			0.79	(0.72;0.86)	2.00E-07	0.16		1	0.18 ± 0.06
cg07839457	16	435	NLRC5	TSS1500	N_Shore	0.87	(0.84;0.91)	2.40E-09	0.46	1	1	0.45 ± 0.11
cg09615688	16		NA[a]			0.53	(0.41;0.68)	9.32E-07	0.91		1	0.90 ± 0.03
cg18424841	20		NA[a]		Island	1.2	(1.13;1.28)	2.80E-08	0.7	1		0.69 ± 0.09

[a]Nearest gene was far more than 10 Mp.
[b]Effect estimates represent hazard ratio per 10% increase in DNA methylation. CHR = chromosome; HR = hazard ratio; 95% CI = 95% confidence interval; p = p-value; SD = standard deviation.

Supplementary Table 4. Hazard ratios for FDR-significant fully-adjusted CpGs in basic and fully adjusted models CHR = chromosome; HR = hazard ratio; 95% CI = 95% confidence interval; p = p-value; SD = standard deviation.

Probe name	CHR	Fully adjusted model			Basic model		
		HR	95% CI	p	HR	95% CI	p
cg17086398	1	1.25	(1.15; 1.36)	4.86E-07	1.37	(1.28; 1.47)	5.32E-20
cg14866069	4	0.66	(0.56; 0.78)	4.85E-07	0.84	(0.75; 0.94)	2.21E-03
cg23666362	4	0.69	(0.59; 0.8)	8.04E-07	0.81	(0.72; 0.9)	2.02E-04
cg12619262	7	1.26	(1.15; 1.38)	1.76E-07	1.13	(1.05; 1.21)	6.77E-04
cg20045320	11	0.85	(0.80; 0.90)	4.06E-09	0.82	(0.78; 0.86)	2.61E-16
cg07677157	12	0.79	(0.72; 0.86)	2.00E-07	0.78	(0.72; 0.84)	1.31E-10
cg07839457	16	0.87	(0.84; 0.91)	2.40E-09	0.88	(0.85; 0.92)	3.40E-11
cg09615688	16	0.53	(0.41; 0.68)	9.32E-07	0.60	(0.51; 0.72)	8.96E-09
cg18424841	20	1.20	(1.13; 1.28)	2.80E-08	1.10	(1.05; 1.15)	2.00E-04

Supplementary Table 5. Summary of models.

Cohorts	Model used	Maximum # probes considered	Basic model		Fully adjusted model	
			Lambda	FDR-significant CpGs	Lambda	FDR-significant CpGs
ARIC	Cox Regression	406712	2.46	226	1.63	5
FHS Study 1	Cox Regression[b]	417934	0.94	3	1.04	0
FHS Study 2	Cox Regression[b]	407580	1.32	17	1.16	1
InChianti	Cox Regression	407179	1.41	0	1.44	0
KORA	Cox Regression[a]	330133	0.96	4	0.94	0
LBC 1921	Cox Regression	393529	1.15	0	1.22	0
LBC 1936	Cox Regression	385450	1.04	0	1	0
NAS	Cox Regression	395005	0.86	0	0.9	0
TwinsUK	Cox Regression [a,c]	426,120	1.02	0	0.98	0
WHI-BAA23	Cox Regression	419176	1.7	14	2.02	1
WHI-EMPC-EA	Cox Regression[d]	250537	1.23	9	0.93	0
WHI-EMPC-AA	Cox Regression[d]	218018	0.92	0	1.09	0
All cohorts	Fixed effect meta-analysis[e]	426724	1.12	257	0.94	9

[a]Cohort used as predictor of residuals from linear regression analysis between each probe and sets of covariates.
[b]Cohort included cluster for family structure.
[c]Cohort included random intercepts for zygosity and family structure.
[d]Cohort considered only CpGs with coefficient of variation >5%.
[e]Analysis of each CpG site included results of at least three cohorts.
Basic model: adjusted for age (categories), gender, technical variables, white blood cell count.
Fully adjusted model: adjusted for age (categories), gender, technical variables, white blood cell count, education level, physical activity, smoking status, smoking consumption (packyears), body mass index (categories), alcohol consumption, prior coronary heart disease (y/n), diabetes (y/n), hypertension (y/n), cancer (y/n).

Supplementary Table 6. I² measure of heterogeneity from random-effect meta-analysis in each FDR-significant basic-adjusted CpG.

Supplementary Table 7. I² measure of heterogeneity from random-effect meta-analysis in each FDR-significant fully-adjusted CpG.

Probe name	CHR	Distance to nearest gene (bp)	Nearest gene (10 Mp)[a]	Gene group	Relation to CpG island	I²
cg17086398	1	0	*SERINC2*	Body		0.02
cg14866069	4	579	*BMPR1B*			0
cg23666362	4	516	*MIR1973*	TSS1500		0.01
cg12619262	7	6276	*CHST12*			0.01
cg20045320	11	116	*IFITM3*		S_Shore	53.53
cg07677157	12		NA[a]			0
cg07839457	16	435	*NLRC5*	TSS1500	N_Shore	0
cg09615688	16		NA[a]			29.9
cg18424841	20		NA[a]		Island	2.65

[a]Nearest gene was far more than 10 Mp.
[b]Effect estimates represent hazard ratio per 10% increase in DNA methylation.
CHR = chromosome; HR = hazard ratio; 95% CI = 95% confidence interval; p = p-value; SD = standard deviation.

Supplementary Table 8. FDR-significant fully-adjusted CpGs in fixed effect meta-analysis with exclusion of ARIC.

Probe name	CHR	Distance to nearest gene (bp)	Nearest gene (10 Mp)[a]	Gene group	Relation to CpG island	HR	95% CI	p	Mean DNA methylation level
cg17086398	1	0	*SERINC2*	Body		1.25	(1.11; 1.41)	3.80E-04	0.29
cg14866069	4	579	*BMPR1B*			0.65	(0.52; 0.8)	6.86E-05	0.84
cg23666362	4	516	*MIR1973*	TSS1500		0.74	(0.62; 0.89)	1.35E-03	0.8
cg12619262	7	6276	*CHST12*			1.27	(1.12; 1.45)	3.31E-04	0.74
cg20045320	11	116	*IFITM3*		S_Shore	0.88	(0.82; 0.95)	8.76E-04	0.54
cg07677157	12		NA[a]			0.76	(0.66; 0.87)	4.78E-05	0.19
cg07839457	16	435	*NLRC5*	TSS1500	N_Shore	0.86	(0.81; 0.92)	3.70E-06	0.45
cg09615688	16		NA[a]			0.53	(0.41; 0.68)	9.32E-07	0.89
cg18424841	20		NA[a]		Island	1.17	(1.08; 1.27)	1.90E-04	0.68

[a]Nearest gene was far more than 10 Mp.
[b]Effect estimates represent hazard ratio per 10% increase in DNA methylation.
CHR = chromosome; HR = hazard ratio; 95% CI = 95% confidence interval; p = p-value; SD = standard deviation.

Supplementary Table 9. FDR-significant fully-adjusted CpGs in fixed effect meta-analysis with exclusion of WHI-Study 1.

Probe name	CHR	Distance to nearest gene (bp)	Nearest gene (10 Mp)[a]	Gene group	Relation to CpG island	HR	95% CI	p	Mean DNA methylation level
cg17086398	1	0	*SERINC2*	Body		1.26	(1.15; 1.38)	4.30E-07	0.29
cg14866069	4	579	*BMPR1B*			0.67	(0.56; 0.79)	2.23E-06	0.85
cg23666362	4	516	*MIR1973*	TSS1500		0.68	(0.58; 0.79)	1.16E-06	0.81
cg12619262	7	6276	*CHST12*			1.23	(1.13; 1.35)	5.93E-06	0.74
cg20045320	11	116	*IFITM3*		S_Shore	0.86	(0.81; 0.91)	2.94E-07	0.54
cg07677157	12		NA[a]			0.79	(0.72; 0.87)	2.57E-06	0.17
cg07839457	16	435	*NLRC5*	TSS1500	N_Shore	0.87	(0.84; 0.92)	1.30E-08	0.45
cg09615688	16		NA[a]			0.53	(0.4; 0.69)	2.57E-06	0.9
cg18424841	20		NA[a]		Island	1.21	(1.13; 1.3)	1.53E-08	0.69

[a]Nearest gene was far more than 10 Mp.
[b]Effect estimates represent hazard ratio per 10% increase in DNA methylation.
CHR = chromosome; HR = hazard ratio; 95% CI = 95% confidence interval; p = p-value; SD = standard deviation.

Supplementary Table 10. Fixed effects meta-analysis results on incident coronary heart disease from the CHARGE Consortium.

Supplementary Table 11. Miettinen's population attributable factor for NAS, WHI-EMPC-EA, and WHI-EMPC-AA as well as weighted combination (average).

CpG	NAS	WHI-EMPC-EA	WHI-EMPC-AA	Mean	SD
cg17086398	6.47	5.55	3.57	5.20	1.21
cg14866069	-17.20	-6.77	-20.09	-14.69	5.72
cg23666362	-15.19	.	.	-15.19	0.00
cg12619262	7.33	-1.18	4.27	3.48	3.52
cg20045320	-5.34	-0.67	-1.42	-2.48	2.05
cg07677157	-7.29	-9.43	-27.86	-14.86	9.23
cg07839457	-4.08	-3.07	-3.43	-3.53	0.42
cg09615688	.	1.43	.	1.43	0.00
cg18424841	5.97	3.51	4.91	4.80	1.01

Supplementary Table 12. Standardized betas identifying the linear relationship between FDR-significant fully-adjusted CpGs and conventional risk factors.

Supplementary Table 13. Standardized betas identifying the linear relationship between FDR-significant fully-adjusted CpGs and epigenetic aging clock in NAS, after adjusting all conventional risk factors.

Epigenetic age	cg17086398	cg14866069	cg23666362	cg12619262	cg20045320	cg07677157	cg07839457	cg18424841
	Est (p)	Est (p)	Est (p)	Est (p)	Est (p)	Est (p)	Est (p)	Est (p)
Horvath epigenetic aging clock (years)	-0.09(0.1)	0.03(0.51)	0.01(0.78)	0.23(0)	-0.27(0)	-0.13(0.02)	-0.19(0)	0.11(0.03)
Hannum epigenetic aging clock (years)	-0.07(0.24)	-0.17(0)	-0.14(0.01)	0.36(0)	-0.08(0.23)	-0.06(0.34)	-0.28(0)	0.18(0)
Weidener epigenetic aging clock (years)	0.02(0.69)	-0.03(0.39)	-0.01(0.72)	0.08(0.1)	-0.07(0.11)	-0.04(0.46)	-0.04(0.41)	0.06(0.16)
PhenoAge (years)	-0.04 (0.5)	-0.11 (0.01)	-0.11 (0.02)	0.02 (0.76)	-0.27 (0)	0 (0.93)	-0.19 (0)	0.13 (0.01)
Mortality risk score	0.04 (0.44)	-0.22 (0)	-0.19 (0)	0.34 (0)	-0.19 (0)	-0.49 (0)	-0.03 (0.57)	-0.07 (0.22)

Est = estimate; p = p-value.

Supplementary Table 14. Association with all-cause mortality and DNA methylation levels at FDR-significant CpGs, adjusting for epigenetic acceleration ages in the Normative Aging Study (NAS).

Association with mortality	CpG alone	CpG + DNAmAge acceleration		CpG + PhenoAge acceleration	
		CpG	DNAmAge acceleration	CpG	PhenoAge acceleration
	HR (95% CI)	HR (95% CI)	HR (95% CI)	HR (95% CI)	HR (95% CI)
cg17086398	1.03 (0.83-1.27)	1.02 (0.82-1.27)	0.99 (0.97-1.03)	1.02 (0.82-1.26)	1.01 (0.98-1.03)
cg14866069	0.44 (0.30-0.70)	0.44 (0.30-0.69)	0.99 (0.97-1.02)	0.44 (0.28-0.70)	1.00 (0.98-1.03)
cg23666362	0.80 (0.52-1.23)	0.80 (0.52-1.23)	1.00 (0.97-1.03)	0.78 (0.50-1.20)	1.01 (0.99-1.03)
cg12619262	1.08 (0.88-1.33)	1.09 (0.89-1.34)	0.99 (0.97-1.02)	1.09 (0.88-1.33)	1.01 (0.98-1.03)
cg20045320	0.94 (0.81-1.09)	0.93 (0.81-1.08)	0.99 (0.97-1.02)	0.94 (0.82-1.09)	1.01 (0.98-1.03)
cg07677157	0.70 (0.52-0.94)	0.70 (0.52-0.94)	0.99 (0.97-1.02)	0.70 (0.52-0.94)	1.00 (0.98-1.03)
cg07839457	0.87 (0.78-0.97)	0.86 (0.77-0.96)	0.99 (0.97-1.02)	0.87 (0.78-0.97)	1.01 (0.98-1.03)
cg18424841	1.09 (0.94-1.26)	1.07 (0.92-1.25)	1.00 (0.97-1.02)	1.09 (0.94-1.26)	1.01 (0.98-1.03)

Supplementary Table 15. Association with all-cause mortality and DNA methylation levels at FDR-significant CpGs adjusting for mortality risk score in the Normative Aging Study (NAS).

Association with mortality	CpG alone	CpG + mortality risk score	
		CpG	Mortality risk score
	HR (95% CI)	HR (95% CI)	HR (95% CI)
cg17086398	1.03 (0.83-1.27)	1.12 (0.89-1.41)	1.68 (1.15-2.47)
cg14866069	0.44 (0.30-0.70)	0.45 (0.28-0.74)	1.39 (0.95-2.04)
cg23666362	0.80 (0.52-1.23)	0.87 (0.55-1.36)	1.55 (1.06-2.27)
cg12619262	1.08 (0.88-1.33)	1.01 (0.81 – 1.26)	1.60 (1.08-2.35)
cg20045320	0.94 (0.81-1.09)	0.96 (0.82-1.12)	1.57 (1.08-2.28)
cg07677157	0.70 (0.52-0.94)	0.74 (0.55-1.01)	1.46 (1.00-2.14)
cg07839457	0.87 (0.78-0.97)	0.88 (0.79-0.99)	1.51 (1.05-2.18)
cg18424841	1.09 (0.94-1.26)	1.07 (0.92-1.24)	1.59 (1.10-2.30)

Supplementary Table 16. Enrichment analysis for genes identified in GWAS of death-related factors.

Disease	Gene	Enrichment p-value	Enrichment_FDR
Alcohol dependence	SERINC2	0.002	0.004
HDL cholesterol	NLRC5	0.022	0.022

p = p-value; FDR = false discovery rate.

Supplementary Table 17. KEGG pathways for FDR-significant CpGs in the basic model.

Supplementary Table 18. Pathways analysis with DAVID.

Gene	Official gene name	Diseases	Disease class	p
NLRC5	NLR family CARD domain containing 5	Chronic renal failure, kidney failure, chronic coronary disease, erythrocyte count, type 2 diabetes	CARDIOVASCULAR, HEMATOLOGICAL, METABOLIC, RENAL	>0.05
BMPR1B	Bone morphogenetic protein receptor type 1B	Alcoholism, attention deficit disorder with hyperactivity, bone mineral density, cleft lip, cleft palate, hypertension, increased ovulation rate, juvenile polyposis, obesity, premature ovarian failure, polycystic ovarian syndrome, primary ovarian insufficiency, puberty (delayed), puberty (precocious), thrombophilia, tobacco use disorder	CARDIOVASCULAR, CHEMDEPENDENCY, DEVELOPMENTAL, METABOLIC, OTHER, PSYCH, REPRODUCTION	>0.05
CHST12	Carbohydrate sulfotransferase 12	Malaria, placenta diseases, pregnancy complications, parasitic	INFECTION	>0.05
IFITM3	Interferon induced transmembrane protein 3	Ulcerative colitis	IMMUNE	>0.05

Supplementary Table 19. Association between fully-adjusted FDR-significant CpGs and SNPs (meQTL analysis) in KORA.

Fully-adjusted FDR-significant CpGs			SNP			Est.	SE	*p*
Name	CHR	Position	Name	CHR	Position			
cg09615688	16	80982506	rs8052401	16	80983487	-0.005	0.001	3.81E-08
cg18424841	20	61315444	rs2427380	20	61314740	0.020	0.002	2.27E-16
cg18424841	20	61315444	rs2427381	20	61314785	0.014	0.003	2.50E-08
cg18424841	20	61315444	rs118042746	20	61314972	-0.039	0.007	2.47E-09
cg18424841	20	61315444	rs6010861	20	61315002	0.024	0.003	9.67E-17
cg18424841	20	61315444	rs2427382	20	61315199	0.015	0.002	6.91E-10
cg18424841	20	61315444	rs6062825	20	61315436	0.016	0.003	2.37E-06
cg18424841	20	61315444	rs4809278	20	61315545	0.020	0.002	6.81E-16
cg18424841	20	61315444	rs6122386	20	61316386	0.015	0.002	6.20E-10

CHR = chromosome; Est = estimate; SE = standard error; p = p-value.

Supplementary Table 20. Association between fully-adjusted FDR-significant CpGs and gene expression (eQTM analysis) in KORA.

Probe name	CHR	Distance to nearest gene (bp)	Nearest gene	Influenced gene name	Est	SE	*p*	FDR
cg17086398	1	0	*SERINC2*	*MARCKSL1*	-0.75	0.20	1.77E-04	5.92E-03
cg20045320	11	116	*IFITM3*	*IFITM3*	-3.45	0.43	3.19E-15	7.48E-13
cg20045320	11	116	*IFITM3*	*IRF7*	-0.76	0.17	8.78E-06	4.11E-04
cg07839457	16	435	*NLRC5*	*MT2A*	-1.48	0.24	7.92E-10	9.27E-08
cg07839457	16	435	*NLRC5*	*MT1E*	-0.66	0.19	5.17E-04	1.34E-02
cg07839457	16	435	*NLRC5*	*MT1A*	-1.11	0.20	1.98E-08	1.54E-06
cg07839457	16	435	*NLRC5*	*MT1G*	-0.25	0.07	6.70E-04	1.57E-02
cg07839457	16	435	*NLRC5*	*MT1IP*	-0.39	0.10	1.64E-04	5.92E-03
cg07839457	16	435	*NLRC5*	*NLRC5*	-0.70	0.15	3.67E-06	2.15E-04

CHR = chromosome; Est = estimate; SE = standard error; p = p-value; FDR = false discovery rate.

Supplementary Table 21. Causal association between coronary heart disease, kidney function (serum creatinine), and methylation at FDR-significant CpGs in KORA and ARIES.

Disease	Methylation locus	OR	95% LCI	95% UCI	P	methQTL cohort	N SNPs	MR method
	cg09615688	1.508	1.0199	2.2297	0.0395	KORA	1	Wald ratio
	cg18424841	1.0058	0.9994	1.0122	0.0743	ARIES	1	Wald ratio
	cg18424841	0.8506	0.7292	0.9922	0.0944	KORA	7	MR Egger
	cg18424841	1.01	0.9218	1.1068	0.8375	KORA	7	Weighted mode
	cg18424841	1.0007	0.9399	1.0656	0.9814	KORA	7	Weighted median
	cg09615688	0.8816	0.7449	1.0435	0.1429	KORA	1	Wald ratio
	cg18424841	1.0014	0.9989	1.0039	0.2771	ARIES	1	Wald ratio
	cg18424841	0.9279	0.8297	1.0377	0.4148	KORA	3	MR Egger
	cg18424841	0.9903	0.957	1.0246	0.6305	KORA	3	Weighted mode
	cg18424841	0.9939	0.9637	1.025	0.6969	KORA	3	Weighted median

Odds ratio (OR), lower 95% confidence interval (LCI), and upper 95% confidence interval (UCI) given per 10% higher methylation. Associations for coronary heart disease taken from (PMC4589895) and association for serum creatinine taken from (PMC4735748). Associations for ARIES methQTLs extracted from MR-base (PMC5976434) using middle age estimates for methQTLs from ARIES cohort (PMC4818469). MR = mendelian randomization; N SNPs = number of SNPs (instruments) used for the MR analyses; P = p-value.

Supplementary Table 22. Association of neutrophil–lymphocyte ratio (NLR) with all-cause mortality, with and without adjustment for cell type proportion in Normative Aging Study.

NLR association with mortality	Without adjusting for cell proportions		Adjusting for cell proportions	
	HR (95% CI)	*p*	HR (95% CI)	*p*
without any CpG inclusion	1.08 (1.00 – 1.17)	0.04	1.06 (0.92 – 1.21)	0.43
cg17086398	1.08 (1.00 – 1.17)	0.045	1.06 (0.93 – 1.21)	0.41
cg14866069	1.13 (1.05 – 1.22)	0.002	1.03 (0.90 – 1.18)	0.68
cg23666362	1.10 (1.02 – 1.19)	0.017	1.04 (0.90 – 1.20)	0.61
cg12619262	1.08 (1.00 – 1.17)	0.042	1.05 (0.92 – 1.21)	0.45
cg20045320	1.08 (1.00 – 1.17)	0.042	1.05 (0.92 – 1.20)	0.46
cg07677157	1.09 (1.01 – 1.18)	0.034	1.06 (0.93 – 1.21)	0.39
cg07839457	1.07 (0.99 – 1.15)	0.06	1.00 (0.88 – 1.15)	0.97
cg18424841	1.10 (1.02 – 1.19)	0.02	1.06 (0.93 – 1.21)	0.38

Epigenome-wide association study of leukocyte telomere length

Yunsung Lee[1,#], Dianjianyi Sun[2,3,#], Anil P.S. Ori[4], Ake T. Lu[5], Anne Seeboth[6], Sarah E. Harris[7,8], Ian J. Deary[7,8], Riccardo E. Marioni[6,7], Mette Soerensen[9,10,11], Jonas Mengel-From[9,10], Jacob Hjelmborg[9], Kaare Christensen[9,10], James G. Wilson[12,13], Daniel Levy[14,15], Alex P. Reiner[16], Wei Chen[3], Shengxu Li[17], Jennifer R. Harris[1,18], Per Magnus[18], Abraham Aviv[19,*], Astanand Jugessur[1,18,20,*], Steve Horvath[5,21,*]

[1]Department of Genetics and Bioinformatics, Norwegian Institute of Public Health, Oslo, Norway
[2]Department of Epidemiology and Biostatistics, School of Public Health, Peking University Health Science Center, Beijing, China
[3]Department of Epidemiology, Tulane University, New Orleans, LA 70118, USA
[4]Center for Neurobehavioral Genetics, Semel Institute for Neuroscience and Human Behavior, University of California Los Angeles, Los Angeles, CA 90095, USA
[5]Department of Human Genetics, David Geffen School of Medicine, University of California Los Angeles, Los Angeles, CA 90095, USA
[6]Centre for Genomic and Experimental Medicine, Institute of Genetics and Molecular Medicine, University of Edinburgh, Edinburgh, UK
[7]Centre for Cognitive Ageing and Cognitive Epidemiology, University of Edinburgh, Edinburgh, UK
[8]Department of Psychology, University of Edinburgh, Edinburgh, UK
[9]Epidemiology, Biostatistics and Biodemography, Department of Public Health, University of Southern Denmark, Odense C, Denmark
[10]Department of Clinical Genetics, Odense University Hospital, Odense C, Denmark
[11]Center for Individualized Medicine in Arterial Diseases, Department of Clinical Biochemistry and Pharmacology, Odense University Hospital, Odense C, Denmark
[12]Department of Physiology and Biophysics, University of Mississippi Medical Center, Jackson, MS 39216, USA
[13]Department of Cardiology, Beth Israel Deaconess Medical Center, Boston, MA 02215, USA
[14]The Framingham Heart Study, Framingham, MA 01702, USA
[15]Population Sciences Branch, Division of Intramural Research, National Heart, Lung, and Blood Institute, National Institutes of Health, Bethesda, MD 20892, USA
[16]Public Health Sciences Division, Fred Hutchinson Cancer Research Center, Seattle, WA 98109, USA
[17]Children's Minnesota Research Institute, Children's Hospitals and Clinics of Minnesota, Minneapolis, MN 55404, USA
[18]Centre for Fertility and Health, Norwegian Institute of Public Health, Oslo, Norway
[19]Center of Development and Aging, New Jersey Medical School, Rutgers State University of New Jersey, Newark, NJ 07103, USA
[20]Department of Global Public Health and Primary Care, University of Bergen, Bergen, Norway
[21]Department of Biostatistics, Fielding School of Public Health, University of California Los Angeles, Los Angeles, CA 90095, USA
[#]Co-first authors
[*]Co-last authors

Correspondence to: Steve Horvath; **email:** shorvath@mednet.ucla.edu

ABSTRACT

Telomere length is associated with age-related diseases and is highly heritable. It is unclear, however, to what extent epigenetic modifications are associated with leukocyte telomere length (LTL). In this study, we conducted a large-scale epigenome-wide association study (EWAS) of LTL using seven large cohorts (n=5,713) – the Framingham Heart Study, the Jackson Heart Study, the Women's Health Initiative, the Bogalusa Heart Study, the Lothian Birth Cohorts of 1921 and 1936, and the Longitudinal Study of Aging Danish Twins. Our stratified analysis suggests that EWAS findings for women of African ancestry may be distinct from those of three other groups: males of African ancestry, and males and females of European ancestry. Using a meta-analysis framework, we identified DNA methylation (DNAm) levels at 823 CpG sites to be significantly associated (P<1E-7) with LTL after adjusting for age, sex, ethnicity, and imputed white blood cell counts. Functional enrichment analyses revealed that these CpG sites are near genes that play a role in circadian rhythm, blood coagulation, and wound healing. Weighted correlation network analysis identified four co-methylation modules associated with LTL, age, and blood cell counts. Overall, this study reveals highly significant relationships between two hallmarks of aging: telomere biology and epigenetic changes.

INTRODUCTION

Telomeres are the $(TTAGGG)_n$ repeats located at the ends of each chromosome. Their broad function is to prevent genomic instability [1]. Telomeres in adult germ cells [2], bone marrow [3, 4] and embryonic stem cells [5] are largely maintained by telomerase. After birth, however, telomeres in somatic cells gradually shorten because of the repressed activities of telomerase [3–6]. In cultured cells, when telomeres become critically short, the cell reaches replicative senescence [1, 7]. Telomere length (TL) is reported to be shorter in leukocytes of men than women, but this sex difference may depend on the measurement method [8]. In their meta-analysis of data from 36 cohorts with a total of 36,230 participants, Gardner and colleagues found longer telomeres in women only for the terminal restriction fragments (TRF) Southern blot method [8]. By contrast, no sex effect was detected for the other TL measurement methods including the widely used quantitative real-time polymerase chain reaction (qPCR) protocol originally described by Cawthon [9]. TL is also shorter in leukocytes of individuals of European ancestry than individuals of African ancestry [10, 11]. Further, leukocyte telomere length (LTL) is associated with the two disease categories that largely define longevity in contemporary humans—cancer and cardiovascular disease [12–14].

High heritability estimates for LTL have been reported irrespective of the methods used for measuring LTL; reported heritability estimates are between 36% and 82% based on Southern blot [15–18], and between 51% and 76% based on qPCR [19, 20]. Genome-wide association studies (GWAS) conducted in large observational cohorts have identified 11 loci associated with LTL [21–24]. A subset of these loci harbor telomere maintenance genes. These loci, however, explain only a small proportion of the genetic variance in LTL. Similarly, relatively little is known about epigenetic changes and LTL. Here, we focus on the relationship between LTL and DNA methylation levels in leukocytes. Epigenome-wide association studies (EWAS) have emerged as a powerful tool for evaluating genome-wide changes in DNAm for a given phenotype of interest [25]. Previous studies have explored the association between DNAm and LTL [26–28], but these studies were somewhat limited due to moderate sample sizes or the focus on specific regions in the genome. Here, we conduct the largest EWAS of LTL to date in different groups defined by sex and ethnicity.

RESULTS

Epigenome-wide association study of leukocyte telomere length

We considered two sets of adjustments for LTL confounders: 1) partially adjusted LTL for age, sex, and ethnicity and 2) fully adjusted LTL for age, sex, ethnicity, and imputed white blood cell counts (CD4+ naïve, CD8+ naïve and exhausted cytotoxic T cell). We conducted a large-scale multi-ancestry EWAS of the partially and fully adjusted LTL using seven cohorts – the Framingham Heart Study (FHS, n=874), the Jackson Heart Study (JHS, n=1,637), the Women's Health Initiative (WHI, n=818), the Bogalusa Heart Study (BHS, n=831), the Lothian Birth Cohorts (LBC1921 and LBC1936, n=403 and n=906, respectively), and the Longitudinal Study of Aging Danish Twins (LSADT, n=244). The analysis flow is depicted in Figure 1. We note that adjustment in this script indicates a mixture of data stratification and regression adjustment.

Overall, 8,716 CpG sites were significantly (P<1E-07) associated with the partially adjusted LTL in the global meta-analysis. The top four genes with the largest number of significant CpGs were *VARS* (16 CpGs), *PRDM16* (15 CpGs), *MAGI2* (14 CpGs) and *MSI2* (13 CpGs). In the group-specific meta-analyses, we found 87 significant CpGs in men of European ancestry, 14 significant CpGs in men of African ancestry, 298 significant CpGs in women of European ancestry, and 20 significant CpGs in women of African ancestry (Supplementary File 1).

We identified 823 significant (P<1E-07) CpG sites associated with the fully adjusted LTL through the global meta-analysis. Our statistical significance threshold (1E-07) corresponds to a 5% family-wise error for 450K array studies [29]. Table 1 presents the top 30 CpGs among the 823 significant CpGs and groups them by

Figure 1. Analysis flow chart.

Table 1. The top 30 most significant CpG sites associated with the fully adjusted LTL.
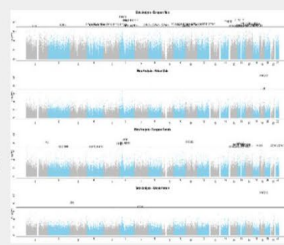
CpG	Gene	Chr	Relation to UCSC CpG island	UCSC RefGene group	Meta-Analysis				
					Global meta Z (P) n=5,713	European male Z (P) n=1,389	African male Z (P) n=697	European female Z (P) n=2,095	African female Z (P) n=1,532
cg08899667	*VARS*	6	N_Shelf	Body	-10.1 (4E-24)	-5.2 (3E-07)	-6.0 (2E-09)	-5.1 (4E-07)	-4.2 (3E-05)
cg02980249	*VARS*	6	N_Shelf	Body	-8.7 (2E-18)	-5.8 (5E-09)	-4.0 (6E-05)	-4.8 (2E-06)	-3.4 (7E-04)
cg02597894	*VARS*	6	N_Shelf	Body	-8.1 (4E-16)	-4.8 (2E-06)	-4.2 (3E-05)	-5.2 (2E-07)	-2.7 (6E-03)
cg04368724	*VARS*	6	N_Shelf	Body	-8.0 (9E-16)	-3.0 (2E-03)	-5.0 (5E-07)	-4.2 (3E-05)	-4.0 (8E-05)
cg04018738	*VARS*	6	N_Shelf	Body	-8.0 (2E-15)	-3.6 (3E-04)	-4.6 (4E-06)	-4.4 (1E-05)	-3.5 (4E-04)
cg24771152	*VARS*	6	N_Shelf	Body	-7.8 (6E-15)	-3.8 (2E-04)	-4.3 (2E-05)	-4.0 (6E-05)	-3.7 (2E-04)
cg20507228	*MAN2A2*	15	-	Body	-9.2 (5E-20)	-5.4 (8E-08)	-5.7 (2E-08)	-3.6 (3E-04)	-3.5 (4E-04)
cg08972170	*C7orf41*	7	-	Body	-9.0 (2E-19)	-3.7 (2E-04)	-4.9 (8E-07)	-4.1 (5E-05)	-5.4 (7E-08)
cg27343900*	*ERGIC1*	5	-	Body	-8.8 (1E-18)	-6.1 (8E-10)*	-5.1 (3E-07)	-4.2 (2E-05)	-2.4 (2E-02)
cg10549018	*TLL2*	10	-	Body	-8.6 (1E-17)	-5.3 (1E-07)	-3.9 (1E-04)	-4.5 (8E-06)	-4.0 (7E-05)
cg26709300*	*YPEL3*	16	N_Shore	1stExon;Body	-8.6 (1E-17)	-3.9 (8E-05)	-5.4 (6E-08)*	-2.4 (2E-02)	-4.8 (1E-06)
cg27106909*	*YPEL3*	16	N_Shore	1stExon;5′UTR;5′UTR	-8.5 (2E-17)	-5.6 (2E-08)*	-5.1 (3E-07)	-2.5 (1E-02)	-3.4 (6E-04)
cg12798040*	*XRCC3*	14	-	Body	-8.5 (2E-17)	-5.4 (8E-08)*	-5.4 (8E-08)*	-4.1 (4E-05)	-2.2 (2E-02)
cg02194129	*XRCC3*	14	-	Body	-8.3 (1E-16)	-4.9 (1E-06)	-5.0 (5E-07)	-4.3 (2E-05)	-2.6 (9E-03)
cg19841423*	*ZGPAT;LIME1*	20	S_Shore	Body;TSS1500	-8.4 (3E-17)	-5.0 (6E-07)	-5.5 (5E-08)*	-3.7 (2E-04)	-2.7 (8E-03)
cg02810967	*NCAPG;DCAF16*	4	S_Shore	Body;TSS1500	8.3 (9E-17)	4.4 (1E-05)	5.4 (9E-08)	4.1 (4E-05)	2.8 (5E-03)
cg19935065	*DNTT*	10	-	TSS1500	-8.1 (4E-16)	-3.5 (4E-04)	-4.9 (1E-06)	-5.0 (5E-07)	-3.2 (1E-03)
cg11093760	*CILP*	15	-	5′UTR;1stExon	-8.1 (5E-16)	-5.9 (4E-09)	-4.1 (5E-05)	-3.3 (1E-03)	-3.1 (2E-03)
cg19097500	*NFIA*	1	N_Shore	TSS1500	-8.1 (6E-16)	-5.4 (7E-08)	-3.7 (2E-04)	-3.7 (2E-04)	-3.6 (3E-04)
cg09626867	*EXOSC7*	3	-	Body	-8.1 (7E-16)	-5.2 (2E-07)	-4.1 (3E-05)	-4.5 (6E-06)	-2.8 (5E-03)
cg04509882	*EIF4G1*	3	-	Body;1stExon;5′UTR	-8.1 (8E-16)	-5.5 (4E-08)	-4.3 (2E-05)	-3.3 (1E-03)	-3.1 (2E-03)
cg23661483	*ILVBL*	19	S_Shelf	Body	-8.0 (9E-16)	-3.7 (2E-04)	-4.3 (2E-05)	-5.4 (7E-08)	-3.3 (1E-03)
cg01012082	*NCOA2*	8	-	3′UTR	-8.0 (1E-15)	-4.7 (3E-06)	-4.0 (7E-05)	-4.4 (1E-05)	-3.4 (8E-04)
cg21461082	*PRMT2*	21	Island	Body	8.0 (2E-15)	2.9 (4E-03)	4.4 (9E-06)	4.5 (6E-06)	4.4 (1E-05)
cg25921609	*MYH10*	17	N_Shore	Body	-7.9 (3E-15)	-5.2 (3E-07)	-3.6 (3E-04)	-4.5 (6E-06)	-3.1 (2E-03)
cg24420089*	*PTDSS2*	11	N_Shore	Body	-7.8 (8E-15)	-3.4 (7E-04)	-5.8 (7E-09)*	-2.3 (2E-02)	-3.5 (5E-04)
cg07414525	*CHL1*	3	-	Body	-7.8 (9E-15)	-3.5 (4E-04)	-3.0 (3E-03)	-3.5 (5E-04)	-5.8 (6E-09)
cg14817906	*CNNM4*	2	-	Body	-7.7 (1E-14)	-4.4 (1E-05)	-4.1 (4E-05)	-3.9 (8E-05)	-3.2 (1E-03)
cg04860432*	*PTGER2*	14	S_Shore	Body	-7.7 (2E-14)	-5.8 (7E-09)*	-4.3 (1E-05)	-2.3 (2E-02)	-2.7 (7E-03)
cg23570810	*IFITM1*	11	N_Shore	Body	7.7 (2E-14)	4.2 (3E-05)	4.2 (2E-05)	4.2 (2E-05)	3.0 (2E-03)

* The CpGs were more strongly associated with LTL in one or two sex and ethnicity specific groups than in the rest of the groups.

their annotated gene names. Among the top 30 CpGs, six were in *VARS*, two were in *YPEL2* and two were in *XRCC3*. The CpGs highlighted by an asterisk in Table 1 were more strongly associated with LTL in one or two sex and ethnicity-specific groups than in the rest of the groups. Specifically, the LTL-DNAm correlations at cg27343900 (in *ERGIC1*) and cg12798040 (in *XRCC3*) were stronger in men of European ancestry than in women of African ancestry. The LTL-DNAm correlation at cg27106909 near *YPEL3* was stronger in men of European ancestry than in women of European ancestry.

Figure 2 displays regional test statistics of LTL-associated CpGs on top of the local DNAm correlation structure for the top four genes listed in Table 1. *VARS* showed a cluster of CpGs above and right below the threshold of significance, while *MAN2A2*, *C7orf41* (current name, *MTURN*) and *ERGIC1* had one or two significant CpGs.

The clusters detected in *VARS* might be because of the high probe density on the array and the strong inter-CpG correlations.

The group-specific meta-analyses also detected several significant (P<1E-07) CpGs associated with the fully adjusted LTL. Figure 3 shows that 25 CpGs were significant in men of European ancestry, three CpGs in men of African ancestry, 19 CpGs in women of European ancestry, and four CpGs in women of African ancestry.

Figure 4 displays scatter plots across the four group-specific meta-analyses. The correlation coefficient of each scatter plot was lowest between African American females and European males (r=-0.02) and highest between European females and European males (r=0.40). Population and sample size differences between strata may influence the correlations. The black dots in the panels refer to the top 30 CpG sites detected through the global meta-analysis. Across the 30 CpGs, we did observe high correlations (r≈0.92).

Figure 2. Regional Manhattan plots and inter-CpG correlations for the top four genes identified in the global meta-analysis. (**A**) *VARS*; (**B**) *MAN2A2*; (**C**) *C7orf41 (MTURN)*; (**D**) *ERGIC1*.

Functional enrichment analysis of LTL-associated CpG sites

To infer the biological meaning underlying LTL-associated CpG sites, the Genomic Regions Enrichment of Annotations Tool (GREAT) was used to associate differentially methylated probes (DMPs) with nearby genes of known pathway annotations. We performed both a gene-based and a region-based enrichment analysis for (1) all DMPs (n=850), (2) hypermethylated probes (n=95), and (3) hypomethylated probes (n=755).

Analyzing all DMPs, we found 11 biological annotations to be significantly enriched with both the gene-based as well as the region-based test (Supplementary File 2, Figure S1, Table S1). Of these, five annotations showed a region-fold enrichment > 1.5; the circadian clock (3.9x), blood coagulation (1.9x), hemostasis (1.9x), wound healing (1.8x), and response to wounding (1.7x). Other annotations also related to circadian rhythm, blood coagulation and wound healing,

further strengthening the main observations (Supplementary File 2, Tables S1, S2).

Next, analyzing hypomethylated probes only, we found that CpGs negatively correlated with LTL mainly explain the above-mentioned functional enrichment. In contrast, hypermethylated probes led to less significant enrichment p values, a finding likely due to the lower number of CpGs (Supplementary File 3). We observed an enrichment of genes involved in mitogen-activated protein kinase phosphatase activity and immune regulation (Supplementary File 2, Figure S1). As part of a robustness/sensitivity analysis, we repeated the enrichment study after excluding CpGs with single-nucleotide polymorphisms (SNPs) in the extension base (global minor allele frequency > 1%) or probes prone to mapping to multiple regions in the genome. Across overlapping annotations (n=1,590), we found high concordance with our initial findings (r=0.97, P<2.2E-16), indicating that our results are highly robust against potentially faulty probes. Details can be found in Supplementary File 3.
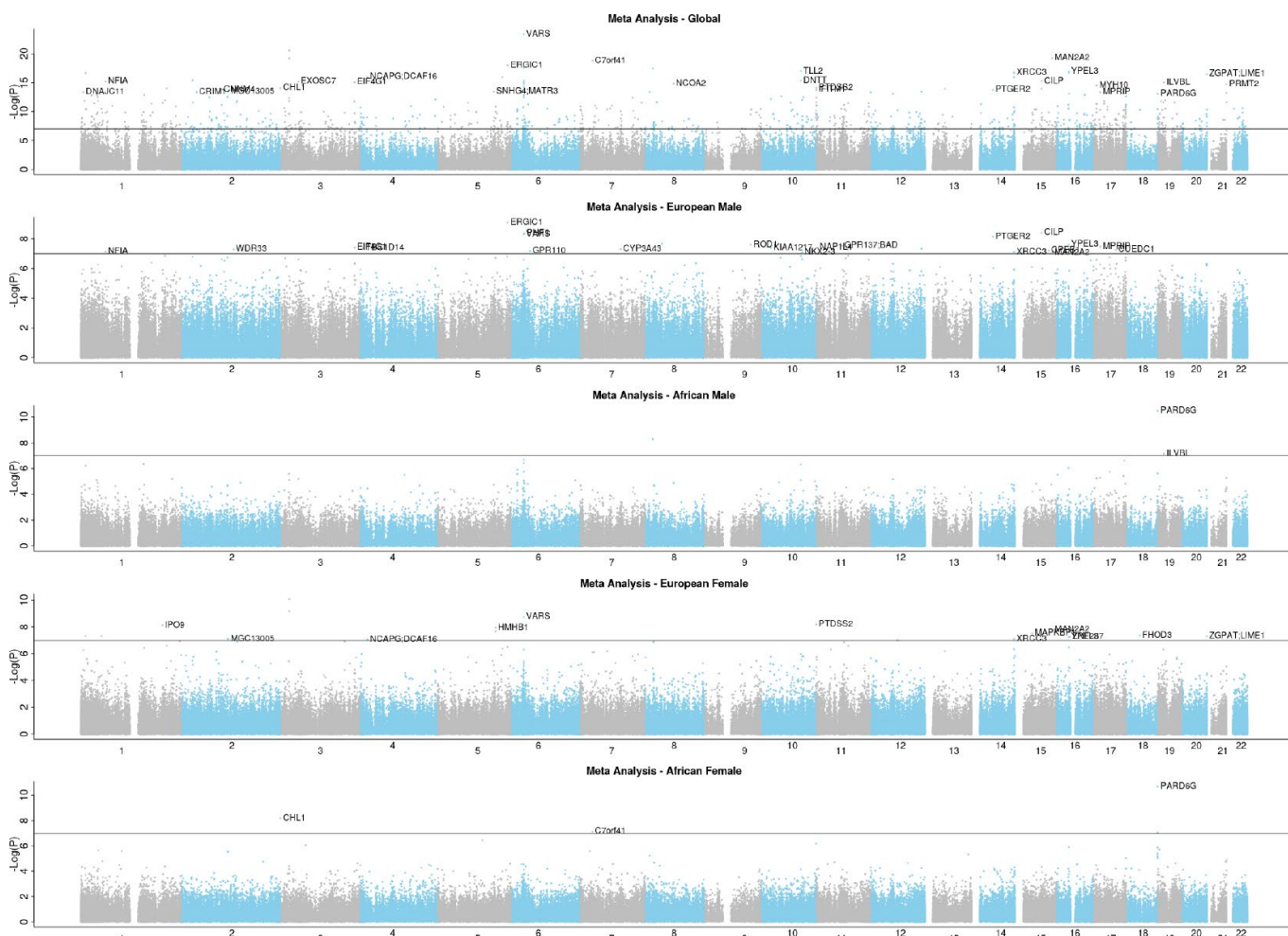
Figure 3. EWAS Manhattan plots of the fully adjusted LTL.

DNA methylation in subtelomeric regions

We observed a higher proportion of the positive LTL-DNAm correlations in subtelomeric regions than in non-subtelomeric regions when we focused on the 823 significant CpGs that were associated with the fully adjusted LTL. The proportion of the positive LTL-DNAm correlations was 17.1% in the subtelomeric regions and 9.9% in the non-subtelomeric bodies (Chi-squared test, P=0.01; Supplementary File 2, Table S3). The subtelomeric regions were defined as each chromosome's head and tail, each of which was 5% of each chromosome's length. However, this approach may not be optimal for the following reasons: 1) the inter-CpG correlations may differ between the non-subtelomeric and subtelomeric regions; 2) one cannot clearly dichotomize genomic loci into non-subtelomeric and subtelomeric regions; and 3) the LTL measurements were not chromosome-specific but averaged across all chromosomes.

Summary-data-based Mendelian randomization

We calculated the causal effects of the 823 CpGs (significantly associated with the fully adjusted LTL) on LTL using summary-data-based Mendelian randomization (SMR) [30] and found that 16 CpGs had a significant (P<0.05) causal effect on LTL (Supplementary File 2, Table S5). The causal effect of cg00622799 near *RTEL1* led to the lowest p-value (P= 6E-4) among the 823 CpGs when SNP rs909334 was used as an instrumental variable. A non-significant p-value (P=0.21) for the test for heterogeneity in independence instruments (HEIDI) is desirable because it indicates that rs909334 (instrumental variable) is the only SNP that influences LTL through the DNAm level at cg00622799. A GWAS of LTL [21] and cis methylation quantitative trait locus (cis-mQTL, a reduced GWAS of DNAm) [31] were used to obtain the SMR causal effects (betas), p-values and HEIDI p-values. The SMR p-value identifies possible methylation sites via which genetic
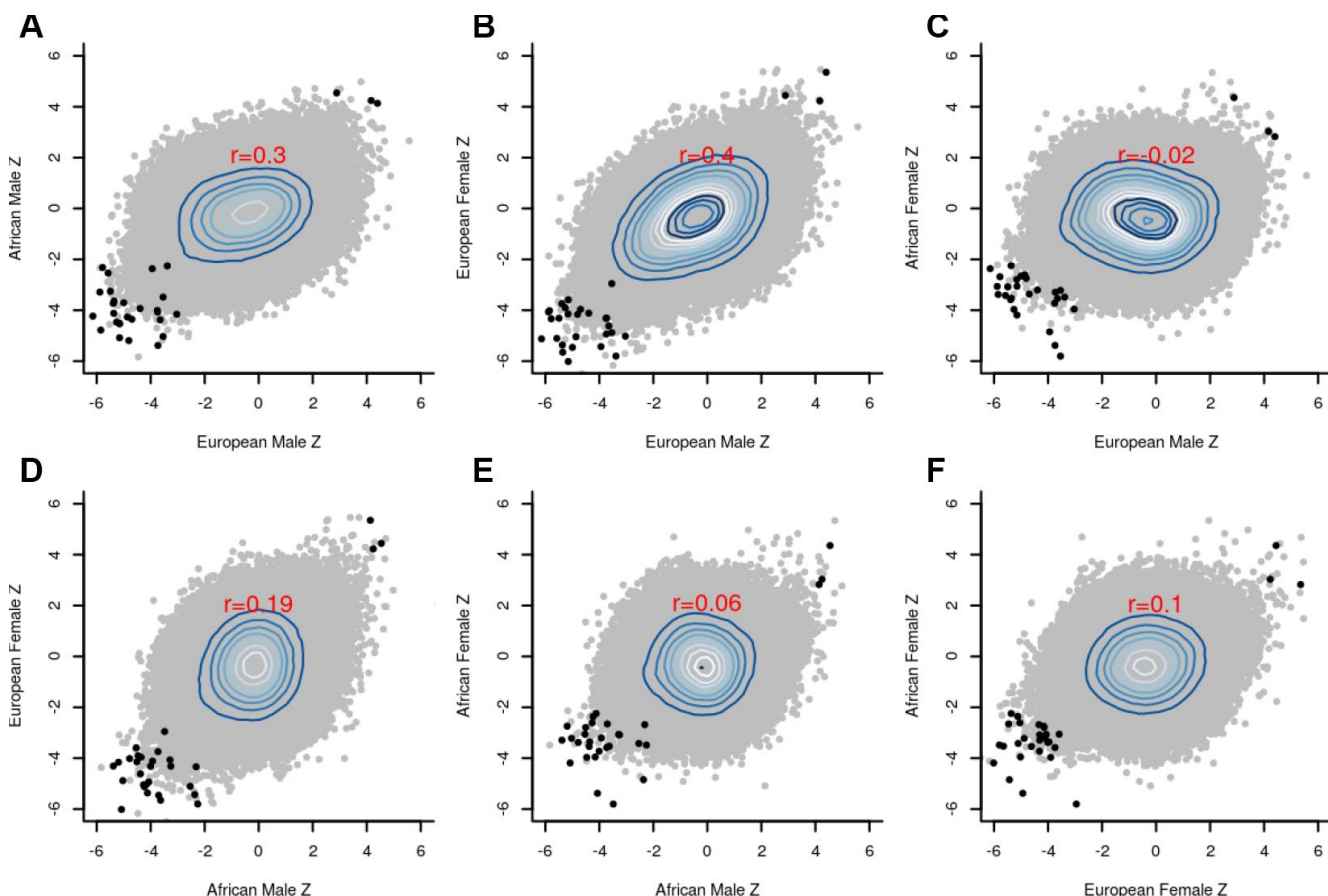
Figure 4. Scatter plots between the group-specific meta-Z scores. (**A**) European male *vs* African male; (**B**) European male *vs* European female; (**C**) European male *vs* African female; (**D**) African male *vs* European female; (**E**) African male *vs* African female; (**F**) African female *vs* European female; The black dots in the panels refer to the top 30 CpG sites detected by the global meta-analysis, whereas the grey dots indicate the remaining CpG sites. Pearson correlation coefficients (red font) reveal strong agreement (r=0.4) between males and females of European ancestry.

variants (SNPs) might be influencing LTL. The HEIDI p-value then indicates the evidence that there is (1) a single causal SNP whose effect on LTL is mediated through the methylation CpG site (HEIDI P>0.05) or (2) different SNPs linked to the methylation level and LTL (HEIDI P<0.05).

Additionally, we examined whether the 823 CpGs overlapped significantly with 54,942 known cis-methylation QTLs. Strikingly, a highly significant number of CpGs (188 CpGs out of 823 CpGs) were known cis-mQTLs (hypergeometric test P= 1.02E-16). To carry out this overlap analysis, we retrieved 188 SNPs each of which corresponded to the 188 CpGs from the cis-mQTL summary statistics. Next, we looked up each of the 188 SNPs in the most recent GWAS catalogue database (v1.02, https://www.ebi.ac.uk/gwas/docs/file-downloads). 22 SNPs were associated with complex traits (Supplementary File 2, Table S6). Among these 22 SNPs, rs2540949 in *CEP68* was associated with atrial fibrillation, and rs17708984 in *TPM4* (GWAS P=6E-16) was associated with platelet count (Supplementary File 2, Table S6). Platelet count is related to blood coagulation and wound healing, which were identified through the functional gene enrichment analysis of the LTL-associated CpGs described above.

Weighted correlation network analysis (WGCNA)

Weighted correlation network analysis (WGCNA) identified four important co-methylated modules (labeled black, red, ivory and yellow in Figure 5) using FHS, JHS and WHI (n=3,329). Hypermethylation in the black module was associated with increased age, shortened LTL, decreased CD8+ naïve T cell counts, and increased exhausted cytotoxic T cell counts, whereas hypermethylation in the red module showed opposite correlations. Elevated methylation levels in the yellow module were correlated with longer LTL and higher CD8+ naïve T cell counts. The ivory module had a pattern similar to the one in the black module. None of the modules revealed any strong correlation with the fully adjusted LTL, which is not surprising as this measure of LTL is adjusted for age and white blood cell type composition. The relationships between co-methylated module representatives and traits of interest (LTL, the partially adjusted LTL, fully adjusted LTL, age, and white blood cell counts) are displayed in Figure 6.

DISCUSSION

This multi-ethnic EWAS of LTL is the largest to date and revealed strong associations between LTL and DNAm levels in all groups defined by sex and ancestry. Our stratified analysis showed that the EWAS findings for women of African ancestry are distinct from those of three other groups: males of African ancestry, males and females of European ancestry. A detailed analysis reveals that this difference does not reflect differences in sample size, age distribution, or LTL. We analyzed 1,532 blood samples from women of African ancestry, 697 from men of African ancestry, 1,389 from men of European ancestry, and 2,095 from women of European ancestry. Although men of African ancestry had the smallest sample size, their EWAS results were consistent with those from the two European groups.

Our unadjusted meta-analysis across the groups revealed profound relationships between TL and global DNA methylation levels, which largely reflect confounding by blood cell composition. However, one can observe genome-wide significant relationships between methylation levels and LTL even after adjusting for differences in blood cell composition. In particular, we report 823 CpGs (close to or within 557 genes) that are significantly correlated with the fully adjusted LTL. More than 88 percent (730 CpGs) of these 823 significant CpG sites exhibit a negative correlation with LTL, meaning that higher methylation levels are associated with shorter LTL at these CpG sites.

Among the 823 CpGs, the top 10 CpGs were linked to seven genes/loci (*VARS, MAN2A2, C7orf41, ERGIC1, TLL2, YPEL3 and XRCC3*). *VARS* encodes the enzyme Valyl-tRNA synthetase that is critical in eukaryotic translation [32]. Mutations in *VARS* cause neurodevelopmental disorders, such as microcephaly, cortical dysgenesis, seizures, and progressive cerebral atrophy [32, 33]. *MAN2A2* encodes alpha-mannosidase 2x that is active in N-glycan biosynthesis [34]. *MAN2A2* null males were largely infertile in mouse studies [35]. *C7orf41* (current official name, *MTURN*), encodes Maturin, a protein that controls neurogenesis in the early nervous systems [36]. *ERGIC1* encodes a cycling membrane protein that contributes to membrane trafficking and selective cargo transport between intermediate compartments [37, 38]. *TLL2* encodes Tolloid-like protein 2 [39] and is associated with attention-deficit/hyperactivity disorder [40]. *YPEL3* codes for Yippee-like 3, a protein that suppresses tumor growth, proliferation and metastasis in several types of cancer [41, 42]. *XRCC3* encodes a RecA/Rad51-related protein that maintains chromosome stability and repairs DNA damage [43, 44].

Functional enrichment studies demonstrate that the significant CpG sites were located near genes that play a role in circadian clock, blood coagulation, and wound healing, respectively. A rich literature links TL to circadian rhythm. For example, cellular senescence impairs circadian rhythmicity both in vitro and in vivo [45]. Sleep disorders and shorter sleep duration are
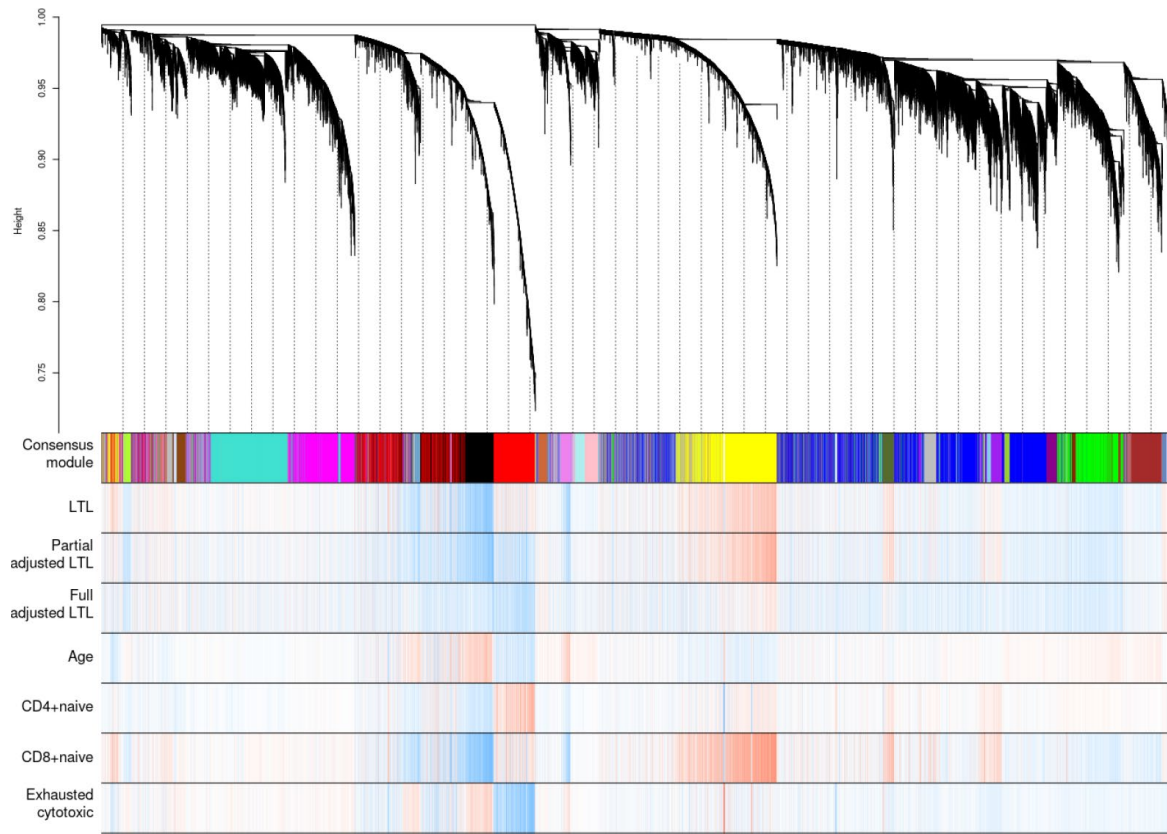
Figure 5. Hierarchical clustering of CpG sites by weighted gene co-expression network analysis (WGCNA). Each data point on the x-axis of the dendrogram refers to an individual CpG site. The color band 'Consensus module' displays co-methylated modules (clusters) in different colors. The other color bands highlight the degree of correlations between DNA methylation of CpG sites and traits of interest. Red represents a positive correlation, whereas blue represents a negative correlation.

	LTL	Partial adjusted LTL[1]	Full adjusted LTL[2]	Age	CD4+naive	CD8+naive	Exhausted cytotoxic
steelblue	2.7 (0.007)	1.6 (0.1)	0.96 (0.3)	-2.2 (0.03)	0.96 (0.3)	2.7 (0.006)	-3.6 (3e-04)
sienna3	0.69 (0.5)	1.2 (0.2)	1.2 (0.2)	2.3 (0.02)	3.8 (1e-04)	-1.2 (0.2)	1.7 (0.1)
yellowgreen	-1.9 (0.06)	-1.1 (0.3)	-0.93 (0.4)	2.7 (0.007)	-0.19 (0.8)	-3.2 (0.002)	-2.8 (0.0005)
brown	-1.6 (0.1)	-0.97 (0.3)	-0.66 (0.5)	2.2 (0.03)	0.37 (0.7)	-3.9 (1e-04)	-2.8 (0.0006)
plum1	2.6 (0.009)	1.3 (0.2)	0.63 (0.5)	-2.9 (0.004)	3.3 (0.001)	2.8 (0.004)	-5.9 (4e-09)
ivory	-4.8 (2e-06)	-0.59 (0.6)	1.3 (0.2)	12 (1e-31)	-29 (1e-189)	-14 (2e-45)	25 (2e-140)
yellow	5.8 (6e-09)	3.4 (6e-04)	0.51 (0.6)	-7.1 (1e-12)	3.8 (2e-04)	18 (3e-72)	-0.57 (0.6)
darkolivegreen	4.7 (2e-06)	2.8 (0.006)	0.067 (0.9)	-5.2 (2e-07)	5.4 (1e-10)	14 (2e-47)	-3.3 (9e-04)
green	-3.5 (5e-04)	-2.7 (0.008)	-2.1 (0.04)	2.3 (0.02)	1.7 (0.09)	-4.9 (9e-07)	-3 (0.003)
orangered4	-2.5 (0.01)	-2 (0.05)	-1.5 (0.1)	1.6 (0.1)	1.9 (0.05)	-3.7 (2e-04)	-2.7 (0.0006)
purple	0.8 (0.4)	0.36 (0.7)	-1.1 (0.3)	-1.5 (0.1)	4.7 (2e-06)	7 (3e-12)	-3.6 (3e-04)
darkmagenta	-2.8 (0.006)	-2.2 (0.03)	-1.7 (0.09)	1.8 (0.08)	0.17 (0.9)	-4.1 (4e-05)	-2.2 (0.03)
blue	-2.1 (0.04)	-1.8 (0.06)	-1.4 (0.2)	1.1 (0.3)	-0.95 (0.3)	-3.6 (3e-04)	-2.3 (0.02)
skyblue	2.7 (0.006)	0.87 (0.4)	-0.8 (0.4)	-5.1 (3e-07)	3.6 (3e-04)	9.6 (5e-22)	-3.8 (2e-04)
turquoise	-0.58 (0.6)	-0.72 (0.5)	-0.65 (0.5)	-0.87 (0.4)	3.4 (6e-04)	0.15 (0.9)	2.2 (0.03)
saddlebrown	1.4 (0.2)	0.62 (0.5)	0.24 (0.8)	-2.2 (0.03)	4.8 (2e-06)	2.9 (0.004)	2.5 (0.01)
lightsteelblue1	-0.88 (0.4)	-0.98 (0.3)	-0.39 (0.7)	-0.13 (0.9)	-6.5 (7e-11)	-2.2 (0.03)	2.8 (0.006)
magenta	-0.93 (0.4)	-0.68 (0.5)	-0.49 (0.6)	0.15 (0.9)	-0.97 (0.3)	-0.071 (0.9)	2.8 (0.005)
mediumpurple3	-1.4 (0.2)	-1 (0.3)	-0.95 (0.3)	0.86 (0.4)	0.12 (0.9)	-0.51 (0.6)	1.1 (0.3)
black	-9.1 (8e-20)	-4.3 (2e-05)	-1.4 (0.1)	13 (5e-41)	-11 (3e-27)	-20 (3e-89)	5.6 (2e-08)
skyblue3	-8.2 (2e-16)	-3.3 (8e-04)	-1 (0.3)	13 (2e-39)	-8.8 (9e-19)	-16 (4e-60)	7.1 (1e-12)
red	0.66 (0.5)	-2.4 (0.02)	-2.4 (0.02)	-8.4 (6e-17)	12 (7e-31)	2.8 (0.005)	-17 (2e-66)
lightcyan1	-0.5 (0.6)	-2 (0.04)	-2 (0.05)	-4 (6e-05)	10 (5e-24)	-0.068 (0.9)	-13 (2e-40)
greenyellow	-5.4 (9e-08)	-4 (7e-05)	-2.3 (0.02)	4.1 (5e-05)	7.2 (7e-13)	9.5 (2e-21)	3.3 (9e-04)
violet	-8.6 (6e-18)	-3.3 (0.001)	-1.1 (0.3)	15 (8e-52)	-8.5 (2e-17)	-17 (9e-68)	4.5 (9e-06)
pink	-2.3 (0.02)	-0.54 (0.6)	-0.78 (0.4)	4.8 (1e-06)	-1.2 (0.2)	-1.2 (0.2)	0.29 (0.8)
paleturquoise	-1.6 (0.1)	-0.45 (0.6)	-0.49 (0.6)	3.4 (6e-04)	-3 (0.002)	-1.8 (0.07)	1.2 (0.2)
grey	-0.52 (0.6)	-1.3 (0.2)	-0.76 (0.4)	-2.5 (0.01)	-2.5 (0.01)	-0.12 (0.9)	0.65 (0.5)

Figure 6. Heat map of correlations between the co-methylated module representatives and LTL, the partially adjusted LTL, the fully adjusted LTL, age, and blood cell counts. The numbers in the cells refer to meta-Z scores and their corresponding p-values. Meta-Z scores were calculated based on biweight midcorrelations between DNAm and a trait of interest in the six strata. [1]Partially adjusted LTL for age, sex and ethnicity. [2]Fully adjusted LTL for age, sex, ethnicity, CD4+ naïve, CD8+ naïve and exhausted cytotoxic T cell.

associated with shorter telomeres [46, 47]. Telomerase and TERT mRNA expression are furthermore under the control of CLOCK-BMAL1 regulation (a core component of the circadian clock) and exhibit endogenous circadian rhythms [48]. CLOCK-deficient mice display shortened TL and abnormal oscillations of telomerase activity [48]. Our results are in line with these findings and support a relationship between LTL and circadian rhythm.

TL has also been associated with wound healing and blood coagulation. For example, mice with longer telomeres show higher wound healing rates of the skin [49]. Furthermore, exogenous delivery of the human TERT gene significantly improved wound healing in an aged rabbit model [50]. In humans, poor wound healing has been reported in individuals with dyskeratosis congenita, a rare congenital disorder caused by a defect in telomere maintenance [51]. While assigning causality remains a challenge, our findings do provide evidence that telomere functioning is associated with the circadian clock, wound healing and blood coagulation through the DNA methylome in a population-based sample. Future work is needed to further understand the mechanisms by which this is regulated and how it impacts human health and diseases.

Our findings were based on a considerably larger sample size (n=5,713) than previous studies. Buxton et al. (2014) used 24 blood and 36 Epstein-Barr virus cell-line samples of 44 to 45 years old males and identified 65 and 36 TL-associated gene promoters, respectively [27]. Gadalla et al. (2012) was based on a sample of 40 cases with dyskeratosis congenita and 51 controls [28], and the authors reported a positive correlation between LTL and methylation at LINE-1 and subtelomeric sites only among the cases. Bell and colleagues performed an EWAS of age, TL and other age-related phenotypes using 172 samples of female twins [26]. Due to the small sample size, the authors could not find genome-wide significant associations between DNAm levels and TL.

We adjusted LTL for imputed blood cell composition in addition to age, sex, and ethnicity, because blood cell composition confounds the relationship between DNAm [52, 53] and LTL [54]. Consistent with previous findings, our WGCNA analyses in Figure 5 also showed that the black, red, and yellow modules were highly related to both blood cell counts and LTL. One concern was that blood cell counts might be causally influenced by DNAm and LTL (i.e., blood cell counts might be a collider between DNAm and LTL), which may introduce bias in LTL-DNAm correlations. Thus, we ran another EWAS without considering blood cell counts and compared LTL-DNAm correlations before and after adjustment for blood cell counts (Supplementary File 1). The correlations listed

in Table 1 became slightly weaker after adjustment for blood cell counts but remained significant nonetheless. However, the number of associated CpG sites was greatly reduced after adjustment for blood cell counts. Cell type heterogeneity is thus an important variable to consider in studies of telomere length. Future work should be extended to cell type-specific analysis as well as to tissues beyond whole blood.

We did not adjust LTL for cigarette smoking in our main analyses because smoking had a non-significant effect on LTL (FHS: P=0.83 for never *vs* former smoker and P=0.76 for never *vs* current smoker; WHI: P=0.20 for never *vs* former smoker and P=0.24 for never *vs* current smoker), though suggestive associations could be found in JHS (P=0.08 for never *vs* former smoker and P=0.02 for never *vs* current smoker). These results pointing to a very weak effect of smoking are consistent with those from Astuti and colleagues [55] who reported that 50 of 84 studies found no association between smoking and TL, although their meta-analysis concluded that smokers may have shorter TL. Our sensitivity analyses also revealed that all the 823 CpGs remained significant regardless of smoking variables. Our EWAS summary statistics includes this sensitivity analysis with additional adjustment for smoking (see the names of columns starting with "aaa" in Supplementary File 1).

One limitation of our study is that it does not elucidate the biological pathways or mechanisms linking DNAm and LTL. In other words, our findings do not explain whether DNAm shortens or lengthens LTL, or whether LTL regulates DNAm. Second, we did not include genotypic information in our analyses. Other studies have suggested that genomic variants might regulate DNAm [31] and LTL [21–24, 56]. Third, LTL measurement is sensitive to the methods used for DNA extraction and LTL estimation [57]. Fourth, we only used EWAS and WGCNA to analyze the data. A supervised machine-learning approach for predicting TL based on DNAm levels will be described in a separate article [58].

This study represents the largest EWAS analysis of DNA methylation and LTL to date. We identified over 800 genome-wide significant CpG sites that are located in or near genes with links to circadian rhythm, blood coagulation and wound healing. These findings link two hallmarks of aging: epigenetic changes and telomere biology.

MATERIALS AND METHODS

Study population

The FHS Offspring Cohort started in 1971 to inaugurate epidemiological studies of young adults in Framingham,

Massachusetts, USA. The FHS recruited 5,124 individuals and invited them to examinations at the FHS facilities [59]. The JHS recruited 5,306 African Americans from 2000 to 2004 in the Jackson metropolitan area, Mississippi, USA, to investigate risk factors for cardiovascular disease [60]. Participants provided medical history, social records and whole-blood samples. The WHI started in 1992 and enrolled 64,500 postmenopausal women aged between 50 and 79 years into either clinical trials or observational studies [61]. Among many sub-studies, WHI "Broad Agency Award 23" has provided both blood-based LTL and DNAm array data. The BHS started in 1972 and has recruited multiple waves of participants from childhood, adolescence and adulthood in Louisiana, USA [62]. The LBC1921 and LBC1936 are longitudinal studies of 550 individuals born in Scotland in 1921 and of 1091 individuals born in Scotland in 1936. The studies were set up in 1999 and 2004, respectively, with the aim of studying cognitive aging [63, 64]. The LSADT was initiated in 1995 and is a cohort-sequential study of Danish twins aged 70 years or more [65, 66]. Surviving twins were surveyed every second year until 2005. In 1997, whole blood samples were collected from 689 same-sex twins and the present study included all twin pairs who participated in the 1997 wave and for whom LTL measurements were available.

The sample size of each cohort used in this study as follows: FHS (n=874), JHS (n=1,637), WHI (n=818), BHS (n=831), LBC1921 (n=403), LBC1936 (n=906), and LSADT (n=244).

Measurement of LTL

LTL was measured by either of two methods: Southern blot [67] or qPCR [9]. All cohorts used Southern blot, except for LBC1921 and LBC1936 that used qPCR. LTL measurement by Southern blot provides the mean of TRFs, whereas qPCR provides the ratio of telomeric template to glyceraldehyde 3-phosphate dehydrogenase. The average inter-assay coefficients of variation were 2.4% in FHS, 2.0% in JHS, 2.0% in WHI, 1.4% in BHS, 5.1% in LBC (LBC1921 and LBC1936 combined), and 2.5% in LSADT. Further details on the measurement of LTL in each cohort are provided in Supplementary File 2.

Measurement of DNA methylation

DNAm data were generated on either of two different Illumina array platforms: the Illumina Infinium HumanMehtylation450 Bead-Chip (Illumina, San Diego, CA, USA) or the Illumina Infinium MethylationEPIC Bead-Chip (Illumina, San Diego, CA, USA). Beta values were computed, which quantify methylation levels between 0 and 1, with 0 being unmethylated and 1 being fully methylated. Further details on normalization and quality control of the data can be found in Supplementary File 2.

Statistical analysis

We stratified the seven cohorts (FHS, JHS, WHI, BHS, LBC1921, LBC1936 and LSADT) by sex, ethnicity and batch, which resulted in 16 strata (Table 2).

In each of the 16 strata, we applied two sets of adjustments on LTL using a regression: 1) partially adjusted for age alone, and 2) fully adjusted for age and DNAm-based estimated cell type proportions (CD4+ naïve, CD8+ naïve T cell and exhausted cytotoxic T cell). In FHS and LSADT, we used a linear mixed model to regress LTL on the adjusting variable(s) (fixed effect) and family structure (random effect). In JHS, WHI, BHS, LBC1921 and LBC1936, an ordinary linear regression was used. The blood cell type proportions were estimated using Horvath's DNAm age calculator (https://dnamage.genetics.ucla.edu/home), with the exception of LSADT where the blood cell counts were estimated using Houseman et al. (2012)'s method [68].

The **R** package for weighted gene co-expression network analysis (WGCNA; [69]) was used to compute epigenome-wide biweight midcorrelations between DNAm levels and adjusted LTL in each of the 16 strata. The biweight midcorrelation is an attractive method for computing correlation coefficients because 1) it is more robust than Pearson correlation and 2) unlike the Spearman correlation, it preserves the biological signal as shown in large empirical studies [70]. We focused on 441,870 autosomal probes that were shared between the 450K and the EPIC array. We combined the 16 sets of EWAS summary statistics into four group-specific or one global meta summary statistics as described in Figure 1. Meta Z values and the corresponding p−values were computed as $\sum Z_i w_i / \sqrt{\sum w_i^2}$ and $2(1 - \Phi(|Z_{meta}|))$, where w_i is the square root of the sample size in the ith stratum, respectively.

Genomic Regions Enrichment of Annotations Tools (GREAT, v3.0) was used to predict the biological function of DMPs by associating both proximal and distal genomic CpG sites with their putative target genes [71]. GREAT implements both a gene-based test and a region-based test using the hypergeometric and binomial test, respectively, to assess enrichment of genomic regions in biological annotations. DMPs were uploaded to the GREAT web portal (http://great.stanford.edu/public/html/) and analyses were run using the hg19 reference annotation and the whole genome as background. Genomic regions were assigned to genes if they are between 5 Kb upstream and 1 Kb downstream of the TSS, plus up to 1 Mb distal.

Table 2. Sample size of the 16 strata used in the meta-analyses.

Cohort	Stratum	Sample size	Mean age (range)	Mean LTL[2] (range)	Age-LTL correlation[3]
FHS	European female	442	57 (33-81)	7.07 (5.51-8.7)	-0.29
	European male	432	58 (36-82)	6.92 (5.59-8.52)	-0.34
JHS	African female	1034	56 (23-92)	7.22 (4.93-10.03)	-0.39
	African male	603	55 (22-93)	7.06 (5.12-9.24)	-0.45
WHI	African female	342	63 (50-80)	7.12 (5.57-9.06)	-0.24
	European female	476	68 (51-80)	6.77 (5.24-8.49)	-0.27
BHS	African female	156	44 (30-54)	7.34 (5.35-9.22)	-0.08
	African male	94	44 (33-49)	7.21 (5.60-9.47)	-0.17
	European female	315	43 (29-55)	6.82 (5.02-9.17)	-0.08
	European male	266	43 (28-52)	6.75 (5.27-8.54)	-0.18
LBC1921[1]	European female	242	79 (78-80)	3.99 (3.00-4.72)	-0.29
	European male	161	79 (78-81)	4.26 (3.46-5.31)	-0.29
LBC1936[1]	European female	448	70 (68-71)	4.05 (2.69-6.00)	0.01
	European male	458	70 (68-71)	4.33 (2.99-7.12)	0.17
LSADT	European female	172	79 (73-90)	5.79 (3.94-7.38)	-0.25
	European male	72	79 (74-87)	5.60 (4.53-6.78)	-0.17

[1] LBC recruited adults living in and around Edinburgh and who were born in 1921 and 1936.
[2] In kilobases; LTL measurement in TRF (Southern blot): FHS, JHS, WHI, BHS and LSADT; LTL measurement in T/S (qPCR): LBC1921 and LBC1936.
[3] Pearson correlation coefficients.

Pathway annotations from GO Biological Processes, GO Cellular Component, GO Molecular Function, MSigDB, and PANTHER were used to infer the biological meanings behind the DMPs that were associated with LTL. GREAT outputs statistics of the gene-based and region-based tests, which were subsequently adjusted for multiple testing using the Bonferroni correction.

The SMR executable software (https://cnsgenomics.com/software/smr/#Download) was used to calculate the causal effects of the selected CpGs on LTL [30]. The SMR obtains a causal effect estimate $(\hat{b}_{CpG,LTL} = \hat{b}_{SNP,LTL}/\hat{\beta}_{SNP,CpG})$ by dividing the effect of a SNP on LTL $(\hat{b}_{SNP,LTL})$ by the effect of a SNP on CpG $(\hat{\beta}_{SNP,CpG})$. GWAS of LTL summary data by Codd and colleagues [21] was downloaded from the European Network for Genetic and Genomic Epidemiology consortium (https://downloads.lcbru.le.ac.uk/engage). The mQTL data by McRae and colleagues [31] were downloaded from the SMR website (http://cnsgenomics.com/data/SMR/LBC_BSGS_meta.tar.gz).

WGCNA performed a consensus network analysis using FHS, JHS and WHI. 30,000 randomly selected CpG sites were used to improve readability (resulting in a single cluster tree) and offset computational limitations. WGCNA hierarchically clustered the 30,000 CpGs based on their similarities. The merging threshold of clusters (modules) was 0.15. All the statistical analyses were performed using **R** version 3.5.1.

Abbreviations

LTL: leukocyte telomere length; TL: telomere length, DNAm: DNA methylation; TRF: terminal restriction fragment; qPCR: quantitative real-time polymerase chain reaction; GWAS: Genome-wide association study; EWAS: epigenome-wide association study; FHS: the Framingham Heart Study; JHS: the Jackson Heart Study; WHI: the Women's Health Initiative; BHS: the Bogalusa Heart Study; LBC: the Lothian Birth Cohorts; LSADT: the Longitudinal Study of Aging Danish Twins; DMP: differentially methylated probe; SNP: single-nucleotide polymorphism; SMR: summary-data-based Mendelian randomization; HEIDI: heterogeneity in independence instruments; mQTL: methylation quantitative trait locus; WGCNA: Weighted correlation network analysis; DC: dyskeratosis congenital; qPCR: quantitative real-time polymerase chain reaction; GREAT: Genomic Regions Enrichment of Annotations Tools.

AUTHOR CONTRIBUTIONS

YL and SH conducted EWAS of LTL using FHS, JHS and WHI and wrote the manuscript. DS, AS and MS conducted EWAS of LTL using BHS, LBC and LSADT, respectively. AO conducted gene enrichment analyses and wrote the biological interpretations. The remaining authors contributed data, helped with manuscript preparation, and interpreted the results.

CONFLICTS OF INTEREST

The authors have no conflicts of interest.

REFERENCES

1. Blackburn EH. Telomeres and telomerase: their mechanisms of action and the effects of altering their functions. FEBS Lett. 2005; 579:859–62.
https://doi.org/10.1016/j.febslet.2004.11.036
PMID:15680963

2. Wright WE, Piatyszek MA, Rainey WE, Byrd W, Shay JW. Telomerase activity in human germline and embryonic tissues and cells. Dev Genet. 1996; 18:173–79.

https://doi.org/10.1002/(SICI)1520-6408(1996)18:2<173::AID-DVG10>3.0.CO;2-3
PMID:8934879

3. Chiu CP, Dragowska W, Kim NW, Vaziri H, Yui J, Thomas TE, Harley CB, Lansdorp PM. Differential expression of telomerase activity in hematopoietic progenitors from adult human bone marrow. Stem Cells. 1996; 14:239–48.
https://doi.org/10.1002/stem.140239 PMID:8991544

4. Yui J, Chiu CP, Lansdorp PM. Telomerase activity in candidate stem cells from fetal liver and adult bone marrow. Blood. 1998; 91:3255–62.
PMID:9558381

5. Shay JW, Wright WE. The reactivation of telomerase activity in cancer progression. Trends Genet. 1996; 12:129–31.
https://doi.org/10.1016/0168-9525(96)30018-8
PMID:8901415

6. Gomes NM, Ryder OA, Houck ML, Charter SJ, Walker W, Forsyth NR, Austad SN, Venditti C, Pagel M, Shay JW, Wright WE. Comparative biology of mammalian telomeres: hypotheses on ancestral states and the roles of telomeres in longevity determination. Aging Cell. 2011; 10:761–68.
https://doi.org/10.1111/j.1474-9726.2011.00718.x
PMID:21518243

7. Allsopp RC, Vaziri H, Patterson C, Goldstein S, Younglai EV, Futcher AB, Greider CW, Harley CB. Telomere length predicts replicative capacity of human fibroblasts. Proc Natl Acad Sci USA. 1992; 89:10114–18.
https://doi.org/10.1073/pnas.89.21.10114
PMID:1438199

8. Gardner M, Bann D, Wiley L, Cooper R, Hardy R, Nitsch D, Martin-Ruiz C, Shiels P, Sayer AA, Barbieri M, Bekaert S, Bischoff C, Brooks-Wilson A, et al, and Halcyon study team. Gender and telomere length: systematic review and meta-analysis. Exp Gerontol. 2014; 51:15–27.
https://doi.org/10.1016/j.exger.2013.12.004
PMID:24365661

9. Cawthon RM. Telomere measurement by quantitative PCR. Nucleic Acids Res. 2002; 30:e47.
https://doi.org/10.1093/nar/30.10.e47
PMID:12000852

10. Hunt SC, Chen W, Gardner JP, Kimura M, Srinivasan SR, Eckfeldt JH, Berenson GS, Aviv A. Leukocyte telomeres are longer in African Americans than in whites: the National Heart, Lung, and Blood Institute Family Heart Study and the Bogalusa Heart Study. Aging Cell. 2008; 7:451–58.
https://doi.org/10.1111/j.1474-9726.2008.00397.x
PMID:18462274

11. Elbers CC, Garcia ME, Kimura M, Cummings SR, Nalls MA, Newman AB, Park V, Sanders JL, Tranah GJ, Tishkoff SA, Harris TB, Aviv A. Comparison between southern blots and qPCR analysis of leukocyte telomere length in the health ABC study. J Gerontol A Biol Sci Med Sci. 2014; 69:527–31.
https://doi.org/10.1093/gerona/glt121
PMID:23946336

12. Aviv A, Shay JW. Reflections on telomere dynamics and ageing-related diseases in humans. Philos Trans R Soc Lond B Biol Sci. 2018; 373:373.
https://doi.org/10.1098/rstb.2016.0436
PMID:29335375

13. Stone RC, Horvath K, Kark JD, Susser E, Tishkoff SA, Aviv A. Telomere Length and the Cancer-Atherosclerosis Trade-Off. PLoS Genet. 2016; 12:e1006144.
https://doi.org/10.1371/journal.pgen.1006144
PMID:27386863

14. Samavat H, Xun X, Jin A, Wang R, Koh WP, Yuan JM. Association between prediagnostic leukocyte telomere length and breast cancer risk: the Singapore Chinese Health Study. Breast Cancer Res. 2019; 21:50.
https://doi.org/10.1186/s13058-019-1133-0
PMID:30995937

15. Andrew T, Aviv A, Falchi M, Surdulescu GL, Gardner JP, Lu X, Kimura M, Kato BS, Valdes AM, Spector TD. Mapping genetic loci that determine leukocyte telomere length in a large sample of unselected female sibling pairs. Am J Hum Genet. 2006; 78:480–86.
https://doi.org/10.1086/500052
PMID:16400618

16. Hjelmborg JB, Dalgård C, Möller S, Steenstrup T, Kimura M, Christensen K, Kyvik KO, Aviv A. The heritability of leucocyte telomere length dynamics. J Med Genet. 2015; 52:297–302.
https://doi.org/10.1136/jmedgenet-2014-102736
PMID:25770094

17. Slagboom PE, Droog S, Boomsma DI. Genetic determination of telomere size in humans: a twin study of three age groups. Am J Hum Genet. 1994; 55:876–82.
PMID:7977349

18. Vasa-Nicotera M, Brouilette S, Mangino M, Thompson JR, Braund P, Clemitson JR, Mason A, Bodycote CL, Raleigh SM, Louis E, Samani NJ. Mapping of a major locus that determines telomere length in humans. Am J Hum Genet. 2005; 76:147–51.
https://doi.org/10.1086/426734 PMID:15520935

19. Broer L, Codd V, Nyholt DR, Deelen J, Mangino M, Willemsen G, Albrecht E, Amin N, Beekman M, de Geus EJ, Henders A, Nelson CP, Steves CJ, et al. Meta-analysis of telomere length in 19,713 subjects reveals high

heritability, stronger maternal inheritance and a paternal age effect. Eur J Hum Genet. 2013; 21:1163–68.
https://doi.org/10.1038/ejhg.2012.303
PMID:23321625

20. Zhu Y, Voruganti VS, Lin J, Matsuguchi T, Blackburn E, Best LG, Lee ET, MacCluer JW, Cole SA, Zhao J. QTL mapping of leukocyte telomere length in American Indians: the Strong Heart Family Study. Aging (Albany NY). 2013; 5:704–16.
https://doi.org/10.18632/aging.100600
PMID:24036517

21. Codd V, Nelson CP, Albrecht E, Mangino M, Deelen J, Buxton JL, Hottenga JJ, Fischer K, Esko T, Surakka I, Broer L, Nyholt DR, Mateo Leach I, et al, and CARDIoGRAM consortium. Identification of seven loci affecting mean telomere length and their association with disease. Nat Genet. 2013; 45:422–7, 427e1–2.
https://doi.org/10.1038/ng.2528
PMID:23535734

22. Levy D, Neuhausen SL, Hunt SC, Kimura M, Hwang SJ, Chen W, Bis JC, Fitzpatrick AL, Smith E, Johnson AD, Gardner JP, Srinivasan SR, Schork N, et al. Genome-wide association identifies OBFC1 as a locus involved in human leukocyte telomere biology. Proc Natl Acad Sci USA. 2010; 107:9293–98.
https://doi.org/10.1073/pnas.0911494107
PMID:20421499

23. Mangino M, Christiansen L, Stone R, Hunt SC, Horvath K, Eisenberg DT, Kimura M, Petersen I, Kark JD, Herbig U, Reiner AP, Benetos A, Codd V, et al. DCAF4, a novel gene associated with leucocyte telomere length. J Med Genet. 2015; 52:157–62.
https://doi.org/10.1136/jmedgenet-2014-102681
PMID:25624462

24. Mangino M, Hwang SJ, Spector TD, Hunt SC, Kimura M, Fitzpatrick AL, Christiansen L, Petersen I, Elbers CC, Harris T, Chen W, Srinivasan SR, Kark JD, et al. Genome-wide meta-analysis points to CTC1 and ZNF676 as genes regulating telomere homeostasis in humans. Hum Mol Genet. 2012; 21:5385–94.
https://doi.org/10.1093/hmg/dds382
PMID:23001564

25. Rakyan VK, Down TA, Balding DJ, Beck S. Epigenome-wide association studies for common human diseases. Nat Rev Genet. 2011; 12:529–41.
https://doi.org/10.1038/nrg3000
PMID:21747404

26. Bell JT, Tsai PC, Yang TP, Pidsley R, Nisbet J, Glass D, Mangino M, Zhai G, Zhang F, Valdes A, Shin SY, Dempster EL, Murray RM, et al, and MuTHER Consortium. Epigenome-wide scans identify differentially methylated regions for age and age-related phenotypes in a healthy ageing population.

PLoS Genet. 2012; 8:e1002629.
https://doi.org/10.1371/journal.pgen.1002629
PMID:22532803

27. Buxton JL, Suderman M, Pappas JJ, Borghol N, McArdle W, Blakemore AI, Hertzman C, Power C, Szyf M, Pembrey M. Human leukocyte telomere length is associated with DNA methylation levels in multiple subtelomeric and imprinted loci. Sci Rep. 2014; 4:4954.
https://doi.org/10.1038/srep04954
PMID:24828261

28. Gadalla SM, Katki HA, Shebl FM, Giri N, Alter BP, Savage SA. The relationship between DNA methylation and telomere length in dyskeratosis congenita. Aging Cell. 2012; 11:24–28.
https://doi.org/10.1111/j.1474-9726.2011.00755.x
PMID:21981348

29. Mansell G, Gorrie-Stone TJ, Bao Y, Kumari M, Schalkwyk LS, Mill J, Hannon E. Guidance for DNA methylation studies: statistical insights from the Illumina EPIC array. BMC Genomics. 2019; 20:366.
https://doi.org/10.1186/s12864-019-5761-7
PMID:31088362

30. Zhu Z, Zhang F, Hu H, Bakshi A, Robinson MR, Powell JE, Montgomery GW, Goddard ME, Wray NR, Visscher PM, Yang J. Integration of summary data from GWAS and eQTL studies predicts complex trait gene targets. Nat Genet. 2016; 48:481–87.
https://doi.org/10.1038/ng.3538 PMID:27019110

31. McRae AF, Marioni RE, Shah S, Yang J, Powell JE, Harris SE, Gibson J, Henders AK, Bowdler L, Painter JN, Murphy L, Martin NG, Starr JM, et al. Identification of 55,000 Replicated DNA Methylation QTL. Sci Rep. 2018; 8:17605.
https://doi.org/10.1038/s41598-018-35871-w
PMID:30514905

32. Stephen J, Nampoothiri S, Banerjee A, Tolman NJ, Penninger JM, Elling U, Agu CA, Burke JD, Devadathan K, Kannan R, Huang Y, Steinbach PJ, Martinis SA, et al. Loss of function mutations in VARS encoding cytoplasmic valyl-tRNA synthetase cause microcephaly, seizures, and progressive cerebral atrophy. Hum Genet. 2018; 137:293–303.
https://doi.org/10.1007/s00439-018-1882-3
PMID:29691655

33. Karaca E, Harel T, Pehlivan D, Jhangiani SN, Gambin T, Coban Akdemir Z, Gonzaga-Jauregui C, Erdin S, Bayram Y, Campbell IM, Hunter JV, Atik MM, Van Esch H, et al. Genes that Affect Brain Structure and Function Identified by Rare Variant Analyses of Mendelian Neurologic Disease. Neuron. 2015; 88:499–513.
https://doi.org/10.1016/j.neuron.2015.09.048
PMID:26539891

34. Misago M, Liao YF, Kudo S, Eto S, Mattei MG, Moremen KW, Fukuda MN. Molecular cloning and expression of cDNAs encoding human alpha-mannosidase II and a previously unrecognized alpha-mannosidase IIx isozyme. Proc Natl Acad Sci USA. 1995; 92:11766–70.
https://doi.org/10.1073/pnas.92.25.11766
PMID:8524845

35. Akama TO, Nakagawa H, Sugihara K, Narisawa S, Ohyama C, Nishimura S, O'Brien DA, Moremen KW, Millan JL, Fukuda MN. Germ cell survival through carbohydrate-mediated interaction with Sertoli cells. Science. 2002; 295:124–27.
https://doi.org/10.1126/science.1065570
PMID:11778047

36. Martinez-De Luna RI, Ku RY, Lyou Y, Zuber ME. Maturin is a novel protein required for differentiation during primary neurogenesis. Dev Biol. 2013; 384:26–40.
https://doi.org/10.1016/j.ydbio.2013.09.028
PMID:24095902

37. Breuza L, Halbeisen R, Jenö P, Otte S, Barlowe C, Hong W, Hauri HP. Proteomics of endoplasmic reticulum-Golgi intermediate compartment (ERGIC) membranes from brefeldin A-treated HepG2 cells identifies ERGIC-32, a new cycling protein that interacts with human Erv46. J Biol Chem. 2004; 279:47242–53.
https://doi.org/10.1074/jbc.M406644200
PMID:15308636

38. Vainio P, Mpindi JP, Kohonen P, Fey V, Mirtti T, Alanen KA, Perälä M, Kallioniemi O, Iljin K. High-throughput transcriptomic and RNAi analysis identifies AIM1, ERGIC1, TMED3 and TPX2 as potential drug targets in prostate cancer. PLoS One. 2012; 7:e39801.
https://doi.org/10.1371/journal.pone.0039801
PMID:22761906

39. Scott IC, Clark TG, Takahara K, Hoffman GG, Eddy RL, Haley LL, Shows TB, Greenspan DS. Assignment of TLL1 and TLL2, which encode human BMP-1/Tolloid-related metalloproteases, to chromosomes 4q32—>q33 and 10q23—>q24 and assignment of murine Tll2 to chromosome 19. Cytogenet Cell Genet. 1999; 86:64–65.
https://doi.org/10.1159/000015412
PMID:10516436

40. Lesch KP, Timmesfeld N, Renner TJ, Halperin R, Röser C, Nguyen TT, Craig DW, Romanos J, Heine M, Meyer J, Freitag C, Warnke A, Romanos M, et al. Molecular genetics of adult ADHD: converging evidence from genome-wide association and extended pedigree linkage studies. J Neural Transm (Vienna). 2008; 115:1573–85.
https://doi.org/10.1007/s00702-008-0119-3
PMID:18839057

41. Tuttle R, Miller KR, Maiorano JN, Termuhlen PM, Gao Y, Berberich SJ. Novel senescence associated gene, YPEL3, is repressed by estrogen in ER+ mammary tumor cells and required for tamoxifen-induced cellular senescence. Int J Cancer. 2012; 130:2291–99.
https://doi.org/10.1002/ijc.26239
PMID:21671470

42. Tuttle R, Simon M, Hitch DC, Maiorano JN, Hellan M, Ouellette J, Termuhlen P, Berberich SJ. Senescence-associated gene YPEL3 is downregulated in human colon tumors. Ann Surg Oncol. 2011; 18:1791–96.
https://doi.org/10.1245/s10434-011-1558-x
PMID:21267786

43. Pierce AJ, Johnson RD, Thompson LH, Jasin M. XRCC3 promotes homology-directed repair of DNA damage in mammalian cells. Genes Dev. 1999; 13:2633–38.
https://doi.org/10.1101/gad.13.20.2633
PMID:10541549

44. Tebbs RS, Zhao Y, Tucker JD, Scheerer JB, Siciliano MJ, Hwang M, Liu N, Legerski RJ, Thompson LH. Correction of chromosomal instability and sensitivity to diverse mutagens by a cloned cDNA of the XRCC3 DNA repair gene. Proc Natl Acad Sci USA. 1995; 92:6354–58.
https://doi.org/10.1073/pnas.92.14.6354
PMID:7603995

45. Kunieda T, Minamino T, Katsuno T, Tateno K, Nishi J, Miyauchi H, Orimo M, Okada S, Komuro I. Cellular senescence impairs circadian expression of clock genes in vitro and in vivo. Circ Res. 2006; 98:532–39.
https://doi.org/10.1161/01.RES.0000204504.25798.a8
PMID:16424366

46. Gaspar LS, Álvaro AR, Moita J, Cavadas C. Obstructive Sleep Apnea and Hallmarks of Aging. Trends Mol Med. 2017; 23:675–92.
https://doi.org/10.1016/j.molmed.2017.06.006
PMID:28739207

47. James S, McLanahan S, Brooks-Gunn J, Mitchell C, Schneper L, Wagner B, Notterman DA. Sleep Duration and Telomere Length in Children. J Pediatr. 2017; 187:247–52.e1.
https://doi.org/10.1016/j.jpeds.2017.05.014
PMID:28602380

48. Chen WD, Wen MS, Shie SS, Lo YL, Wo HT, Wang CC, Hsieh IC, Lee TH, Wang CY. The circadian rhythm controls telomeres and telomerase activity. Biochem Biophys Res Commun. 2014; 451:408–14.
https://doi.org/10.1016/j.bbrc.2014.07.138
PMID:25109806

49. Varela E, Muñoz-Lorente MA, Tejera AM, Ortega S, Blasco MA. Generation of mice with longer and better preserved telomeres in the absence of genetic manipulations. Nat Commun. 2016; 7:11739.

https://doi.org/10.1038/ncomms11739
PMID:27252083

50. Mogford JE, Liu WR, Reid R, Chiu CP, Said H, Chen SJ, Harley CB, Mustoe TA. Adenoviral human telomerase reverse transcriptase dramatically improves ischemic wound healing without detrimental immune response in an aged rabbit model. Hum Gene Ther. 2006; 17:651–60.
https://doi.org/10.1089/hum.2006.17.651
PMID:16776573

51. Marciniak RA, Johnson FB, Guarente L. Dyskeratosis congenita, telomeres and human ageing. Trends Genet. 2000; 16:193–95.
https://doi.org/10.1016/S0168-9525(00)01984-3
PMID:10782108

52. Horvath S. DNA methylation age of human tissues and cell types. Genome Biol. 2013; 14:R115.
https://doi.org/10.1186/gb-2013-14-10-r115
PMID:24138928

53. Horvath S. Erratum to: DNA methylation age of human tissues and cell types. Genome Biol. 2015; 16:96.
https://doi.org/10.1186/s13059-015-0649-6
PMID:25968125

54. Weng NP, Levine BL, June CH, Hodes RJ. Human naive and memory T lymphocytes differ in telomeric length and replicative potential. Proc Natl Acad Sci USA. 1995; 92:11091–94.
https://doi.org/10.1073/pnas.92.24.11091
PMID:7479943

55. Astuti Y, Wardhana A, Watkins J, Wulaningsih W, Network PR, and PILAR Research Network. Cigarette smoking and telomere length: A systematic review of 84 studies and meta-analysis. Environ Res. 2017; 158:480–89.
https://doi.org/10.1016/j.envres.2017.06.038
PMID:28704792

56. Lu AT, Xue L, Salfati EL, Chen BH, Ferrucci L, Levy D, Joehanes R, Murabito JM, Kiel DP, Tsai PC, Yet I, Bell JT, Mangino M, et al. GWAS of epigenetic aging rates in blood reveals a critical role for TERT. Nat Commun. 2018; 9:387.
https://doi.org/10.1038/s41467-017-02697-5
PMID:29374233

57. Barrett JH, Iles MM, Dunning AM, Pooley KA. Telomere length and common disease: study design and analytical challenges. Hum Genet. 2015; 134:679–89.
https://doi.org/10.1007/s00439-015-1563-4
PMID:25986438

58. Lu AT, Seeboth A, Tsai PC, Sun D, Quach A, Reiner AP, Kooperberg C, Ferrucci L, Hou L, Baccarelli A, Li Y, Harris SE, Corley J, et al. DNA methylation-based estimator of telomere length. Aging (Albany NY). 2019. [Epub ahead of print].
https://doi.org/10.18632/aging.102173
PMID:31422385

59. Kannel WB, Feinleib M, McNamara PM, Garrison RJ, Castelli WP. An investigation of coronary heart disease in families. The Framingham offspring study. Am J Epidemiol. 1979; 110:281–90.
https://doi.org/10.1093/oxfordjournals.aje.a112813
PMID:474565

60. Taylor HA Jr, Wilson JG, Jones DW, Sarpong DF, Srinivasan A, Garrison RJ, Nelson C, Wyatt SB. Toward resolution of cardiovascular health disparities in African Americans: design and methods of the Jackson Heart Study. Ethn Dis. 2005; 15:S6-4-17. PMID:16320381

61. Anderson G, Cummings S, Freedman LS, Furberg C, Henderson M, Johnson SR, Kuller L, Manson J, Oberman A, Prentice RL, Rossouw JE. Design of the Women's Health Initiative clinical trial and observational study. The Women's Health Initiative Study Group. Control Clin Trials. 1998; 19:61–109.
https://doi.org/10.1016/S0197-2456(97)00078-0
PMID:9492970

62. Berenson GS. Bogalusa Heart Study: a long-term community study of a rural biracial (black/white) population. Am J Med Sci. 2001; 322:267–74.
https://doi.org/10.1097/00000441-200111000-00007
PMID:11721800

63. Deary IJ, Gow AJ, Pattie A, Starr JM. Cohort profile: the Lothian Birth Cohorts of 1921 and 1936. Int J Epidemiol. 2012; 41:1576–84.
https://doi.org/10.1093/ije/dyr197 PMID:22253310

64. Taylor AM, Pattie A, Deary IJ. Cohort Profile Update: The Lothian Birth Cohorts of 1921 and 1936. Int J Epidemiol. 2018; 47:1042–1042-r.
https://doi.org/10.1093/ije/dyy022
PMID:29546429

65. Christensen K, Holm NV, McGue M, Corder L, Vaupel JW. A Danish population-based twin study on general health in the elderly. J Aging Health. 1999; 11:49–64.
https://doi.org/10.1177/089826439901100103
PMID:10848141

66. McGue M, Christensen K. Social activity and healthy aging: a study of aging Danish twins. Twin Res Hum Genet. 2007; 10:255–65.
https://doi.org/10.1375/twin.10.2.255
PMID:17564515

67. Kimura M, Stone RC, Hunt SC, Skurnick J, Lu X, Cao X, Harley CB, Aviv A. Measurement of telomere length by the Southern blot analysis of terminal restriction fragment lengths. Nat Protoc. 2010; 5:1596–607.
https://doi.org/10.1038/nprot.2010.124

PMID:21085125

68. Houseman EA, Accomando WP, Koestler DC, Christensen BC, Marsit CJ, Nelson HH, Wiencke JK, Kelsey KT. DNA methylation arrays as surrogate measures of cell mixture distribution. BMC Bioinformatics. 2012; 13:86.
https://doi.org/10.1186/1471-2105-13-86
PMID:22568884

69. Langfelder P, Horvath S. WGCNA: an R package for weighted correlation network analysis. BMC Bioinformatics. 2008; 9:559.
https://doi.org/10.1186/1471-2105-9-559
PMID:19114008

70. Song L, Langfelder P, Horvath S. Comparison of co-expression measures: mutual information, correlation, and model based indices. BMC Bioinformatics. 2012; 13:328.
https://doi.org/10.1186/1471-2105-13-328
PMID:23217028

71. McLean CY, Bristor D, Hiller M, Clarke SL, Schaar BT, Lowe CB, Wenger AM, Bejerano G. GREAT improves functional interpretation of cis-regulatory regions. Nat Biotechnol. 2010; 28:495–501.
https://doi.org/10.1038/nbt.1630
PMID:20436461

SUPPLEMENTARY MATERIALS

Please browse Full Text version to see the data of Supplementary Files 1, 2, 3.

Supplementary File 1. Part of summary statistics of EWAS of adjusted LTL (global meta P<1E-05 with full adjustment). Each row corresponds to a single CpG site. The annotations are based on the Human genome 19 (NCBI 37). The remaining columns indicate the biweight midcorrelations and their corresponding Z-scores, p-values and sample size. The suffix "a_" means that LTL was adjusted for age, sex and ethnicity. The suffix "aa_" means that LTL was adjusted for age, sex, ethnicity and blood cell counts.

The suffix "aaa_" means that LTL was adjusted for age, sex, ethnicity, blood cell counts and smoking.

Supplementary File 2.Additional analyses for 1) functional enrichment analysis, 2) the LTL-DNAm correlation in subtelomeric regions, 3) summary-data-based Mendelian randomization, 4) sensitivity analyses, and 5) detailed descriptions of each study cohort.

Supplementary File 3. GREAT gene enrichment analyses.

DNA methylation-based estimator of telomere length

Ake T. Lu[1], Anne Seeboth[2], Pei-Chien Tsai[3,4,5], Dianjianyi Sun[6,7], Austin Quach[1], Alex P. Reiner[8], Charles Kooperberg[8], Luigi Ferrucci[9], Lifang Hou[10], Andrea A. Baccarelli[11], Yun Li[12], Sarah E. Harris[13,14], Janie Corley[13,14], Adele Taylor[13,14], Ian J. Deary[13,14], James D. Stewart[15], Eric A. Whitsel[15,16], Themistocles L. Assimes[17,18], Wei Chen[7], Shengxu Li[19], Massimo Mangino[3], Jordana T. Bell[3], James G. Wilson[20], Abraham Aviv[21], Riccardo E. Marioni [2,13], Kenneth Raj[22*], Steve Horvath[1,23*]

[1]Department of Human Genetics, David Geffen School of Medicine, University of California Los Angeles, Los Angeles, CA 90095, USA
[2]Centre for Genomic and Experimental Medicine, Institute of Genetics and Molecular Medicine, University of Edinburgh, Edinburgh EH4 2XU, UK
[3]Department of Twin Research and Genetic Epidemiology, Kings College London, London SE1 7EH, UK
[4]Department of Biomedical Sciences, Chang Gung University, Taoyuan, Taiwan
[5]Genomic Medicine Research Core Laboratory, Chang Gung Memorial Hospital, Linkou, Taiwan
[6]Department of Epidemiology and Biostatistics, School of Public Health, Peking University Health Science Center, Beijing, China
[7]Department of Epidemiology, Tulane University School of Public Health and Tropical Medicine, New Orleans, LA 70112, USA
[8]Public Health Sciences Division, Fred Hutchinson Cancer Research Center, Seattle, WA 98109, USA
[9]Longitudinal Studies Section, Translational Gerontology Branch, National Institute on Aging, National Institutes of Health, Baltimore, MD 21224, USA
[10]Center for Population Epigenetics, Robert H. Lurie Comprehensive Cancer Center and Department of Preventive Medicine, Northwestern University Feinberg School of Medicine, Chicago, IL 60611, USA
[11]Laboratory of Environmental Epigenetics, Departments of Environmental Health Sciences Epidemiology, Columbia University Mailman School of Public Health, New York, NY 10032, USA
[12]Departments of Genetics, Biostatistics, Computer Science, University of North Carolina, Chapel Hill, NC 27599, USA
[13]Centre for Cognitive Ageing and Cognitive Epidemiology, Department of Psychology, University of Edinburgh, Edinburgh EH8 9JZ, UK
[14]Department of Psychology, University of Edinburgh, Edinburgh EH8 9JZ, UK
[15]Department of Epidemiology, Gillings School of Global Public Health, University of North Carolina, Chapel Hill, NC 27599, USA
[16]Department of Medicine, School of Medicine, University of North Carolina, Chapel Hill, NC 27599, USA
[17]VA Palo Alto Health Care System, Palo Alto CA 94304, USA
[18]Department of Medicine, Stanford University School of Medicine, Stanford, CA 94305, USA
[19]Children's Minnesota Research Institute, Children's Hospitals and Clinics of Minnesota, Minneapolis, MN 55404, USA
[20]Department of Physiology and Biophysics, University of Mississippi Medical Center, Jackson, MS 39216, USA
[21]Center of Development and Aging, New Jersey Medical School, Rutgers State University of New Jersey, Newark, NJ 07103, USA
[22]Radiation Effects Department, Centre for Radiation, Chemical and Environmental Hazards, Public Health England, Chilton, Didcot, Oxfordshire OX11 0RQ, UK
[23]Department of Biostatistics, Fielding School of Public Health, University of California Los Angeles, Los Angeles, CA 90095, USA
*Joint last authors

ABSTRACT

Telomere length (TL) is associated with several aging-related diseases. Here, we present a DNA methylation estimator of TL (DNAmTL) based on 140 CpGs. Leukocyte DNAmTL is applicable across the entire age spectrum and is more strongly associated with age than measured leukocyte TL (LTL) (*r* ~-0.75 for DNAmTL versus *r* ~ -0.35 for LTL). Leukocyte DNAmTL outperforms LTL in predicting: i) time-to-death (p=2.5E-20), ii) time-to-coronary heart disease (p=6.6E-5), iii) time-to-congestive heart failure (p=3.5E-6), and iv) association with smoking history (p=1.21E-17). These associations are further validated in large scale methylation data (n=10k samples) from the Framingham Heart Study, Women's Health Initiative, Jackson Heart Study, InChianti, Lothian Birth Cohorts, Twins UK, and Bogalusa Heart Study. Leukocyte DNAmTL is also associated with measures of physical fitness/functioning (p=0.029), age-at-menopause (p=0.039), dietary variables (omega 3, fish, vegetable intake), educational attainment (p=3.3E-8) and income (p=3.1E-5). Experiments in cultured somatic cells show that DNAmTL dynamics reflect in part cell replication rather than TL *per se*. DNAmTL is not only an epigenetic biomarker of replicative history of cells, but a useful marker of age-related pathologies that are associated with it.

INTRODUCTION

Telomeres are repetitive nucleotide sequences at the end of chromosomes that shorten with replication of somatic cells. Since the number of cell replication *in vivo* increases with age, telomere length (TL) is negatively correlated with age of proliferating somatic cells. Meta-analysis of 124 cross-sectional studies and 5 longitudinal studies showed that the correlation between leukocyte telomere length (LTL) and age ranges between r=-0.295 and r=-0.338 across adults [1].

TL variation within somatic tissues of the individual is much smaller than that between individuals. Within the individual, TL variation across somatic tissues such as blood, skin, muscle and fat largely reflects their replicative history prior to adulthood, given that the rates of TL shortening in these tissues are similar during adulthood [2]. Shorter LTL is associated with cardio-vascular disease, psychological stress, and lifespan [3-10].

Another DNA-based biomarker that changes with age is methylation of cytosine residues of cytosine-phosphate-guanine dinucleotides (CpGs). Machine learning-based analyses of these changes generated algorithms, known as epigenetic clocks that use specific CpG methylation levels to estimate age (i.e., DNAm age) [11-14] and/or physiological age [15-17]. Although both DNAm age

and LTL are associated with chronological age, they exhibit only weak correlations with each other after adjusting for age [18-20], suggesting the distinct nature of their underlying mechanisms.

DNA methylation assays are already highly robust and ready for biomarker development [21]. By contrast, despite two decades of population-based telomere research, the measurement of TL remains challenging and can be subject to technical confounding factors including but not limited to different methods of DNA extraction [22-24]. Furthermore, the terminal restriction fragments (TRFs), measured by Southern blotting, the accepted 'gold standard' of TL measurements, include not only the canonical region of telomeres but also the potentially variable sub-telomeric region [22, 25]. It would be ideal if the robustness inherent in DNA methylation analyses can be extended to TL measurement. Although there are reports of TL-related DNA methylation changes [26], it was unknown whether these reflect actual TL or associated biological features, including health outcomes.

We present here a novel DNAm TL estimator (DNAmTL) based on methylation profiles of 140 CpGs. This epigenetic biomarker was developed by regressing measured LTL on blood methylation data from n=2,256 individuals (training set). We show that DNAmTL correlates negatively with age in different tissues and

cell types and outperforms TRF-based LTL in predicting mortality and time-to-heart disease, as well as being associated with smoking history and other age-related conditions.

We also validated the applicability of DNAmTL on a large-scale data set (N=9,345) and uncovered associations between age-adjusted DNAmTL with diet and clinical biomarkers.

Monitoring cultured cells with or without telomerase revealed that DNAmTL records cell replication independently of telomere attrition.

RESULTS

Training and validation data from 3 cohorts

In stage 1 of our project, we evaluated data from n=3,334 individuals for whom both LTL and Illumina methylation array data were available. These were from three different studies: Framingham Heart Study offspring cohort (FHS, N=878), Women's Health Initiative (WHI, N=818) and Jackson Heart Study cohort (JHS, N=1638, Table 1 and Supplementary Note 1). The same laboratory measured LTL by Southern blotting of the terminal restriction fragments [25]. DNA methylation levels were measured in different labs using the Illumina Infinium methylation array platform.

An overview of the data sets is found in Table 1. These US cohorts were comprised of two ethnic groups: 41% of European ancestry and 59% of African Ancestry. The age of the individuals ranged from 22 to 93 years. The training set used for constructing DNAmTL was comprised of N=2,256 individuals from the WHI and JHS cohorts for whom LTL and DNAm data were assessed from the same blood sample (collected at the same time). Although fewer than 20% of individuals in the training set were of European ancestry, our test data demonstrated that the resulting DNAmTL estimator applied equally well to individuals of European ancestry. We used two test data sets. The first test data set involved N=1,078 individuals comprised of N=100 from the WHI, N=100 from JHS, and N=878 from the FHS cohorts. The second test data set was collected in stage 2 of our analysis: it involved N=9,815 DNA methylation samples from additional cohorts (Bogalusa, Twins UK, Lothian Birth cohorts, InCHIANTI) to evaluate correlations between LTL and numerous age-related conditions and lifestyle factors. We also evaluated DNAmTL in publicly-available data from adipose tissue (N=648 from the Twins UK study [27, 28]), liver (N=85) [28, 29], and

monocytes (n=1264 from the Multi-Ethnic Study of Atherosclerosis) [30]. Finally, we tested DNAmTL in *in vitro* studies to ascertain its applicability to cultured cells and to probe the nature of DNAmTL's association with TL. Additional details of these studies can be found in Supplementary Notes 1 and 2.

DNAmTL versus measured TL in blood and adipose tissue

We restricted the analysis to CpGs that are present on both the Illumina Infinium 450K array and the Illumina EPIC methylation array (Methods). Using the training data (n=2,256), we regressed measured LTL (mean TRFs) on blood CpG methylations using an elastic net regression model [31]. This resulted in the automatic selection of 140 CpGs whose methylation levels best-predicted LTL (Supplementary Data 1). The linear regression model allows a direct prediction of TL based on DNA methylation levels. The predicted TL value, also referred to as DNAmTL, possesses the same units (kilobase) as that of mean TRF. The correlation coefficient between DNAmTL and LTL in the training data was r=0.63, which was overly optimistic, as subsequent independent validation with test data sets produced lower correlations of r>0.40 (Figure 1). Further, using 12 large validation data sets, we found that the correlation between DNAmTL and LTL ranged from r=0.38 to r=0.5 (last column of Table 1) with the exception of the Lothian Birth cohorts (where it was close to zero). The correlations between DNAmTL and LTL were not confounded by age, as was evident from the high correlations between age-adjusted DNAmTL and age-adjusted LTL (e.g. r=0.34 in FHS and r=0.43 in Bogalusa Herat Study, Supplementary Figures 1A and 2A). A stratified analysis showed that the correlation between DNAmTL and LTL were neither confounded by sex (Supplementary Figures 1-2B and C) nor ethnicity (Supplementary Figure 2D and E). The DNAmTL biomarker was robust against potential effects of pre-processing steps in the DNAm data analysis as can be seen from the diverse normalization methods used by the different cohorts (Table 1). The DNAmTL measurement was also robust across time as can be seen with the FHS cohort where the blood samples for the LTL measurement (FHS exam 6) were collected 9.3 years earlier than those used for the DNAm measurement (FHS exam 8). This time lag biased the correlation toward the null hypothesis, i.e. generated a correlation (r=0.44, Figure 1B) that was overly conservative. A separate analysis of non-blood tissue revealed a higher correlation of r=0.65 between DNAmTL and TRF-based in adipose tissue samples from the Twins UK study (Supplementary Figure 3B).

Table 1. Overview of training and test data.

Data	N	Female	Race	Age	Array Normalization	Telomere length statistics LTL	DNAmTL	Corr
Train								
WHI BA23	718	100%	EUR (59%) AFR (41%)	66.5 (50.2,80.2)	GenomeStudio	6.9 (5.2,9.1)	6.9 (6.0, 7.8)	0.62
JHS	1538	64%	AFR	56.6 (22.2,93.1)	Noob [68]	7.1 (4.9,10)	7.2 (5.9, 8.1)	0.62
Test								
FHS	878	51%	EUR	57.0 (33.0,82.0)	Noob [68]	7 (5.5,8.7)	6.8 (5.4, 8.1)	0.44
WHI BA23	100	100%	EUR (49%) AFR (51%)	65.3 (51.9,79.8)	GenomeStudio	6.9 (5.6,9)	6.9 (6.2, 7.5)	0.41
JHS	100	55%	AFR	53.5 (22.9,80)	Noob [68]	7.2 (5.6,9)	7.1 (6.6, 7.8)	0.50
Validation analysis								
FHS[a,b]	2356	54%	EUR	66.4 (40, 92)		7.0 (5.5,8.7)	6.8 (5.4, 8.1)	0.44
WHI BA23[a]	1389	100%	EUR (41%) AFR (28%) HISP (31%)	65.4 (50.1, 80.2)	Noob [68]	6.9 (5.6,9)	6.9 (6.2, 7.5)	0.41
WHI EMPC	1972	100%	EUR (56%) AFR (28%) HISP(16%)	62.9 (49.5, 82.0)	BMIQ [57]	--	--	--
JHS[a]	209	56%	AFR	59.8 (22.9, 84.6)	Noob [68]	7.2 (5.6,9)	7.1 (6.6, 7.8)	0.50
InChianti[c]	924 (484)	54%	EUR	72 (21, 100)	Noob [68]	--	--	--
Twins UK[d]	794	100%	EUR	57.2 (24.0,81.1)	BMIQ [57]	3.5 (1.7, 6.4)	7.0 (5.6, 7.9)	0.38
LBC 1921[e]	436	60%	EUR	79.1 (77.7, 80.6)	Noob [68]	4.1 (1.9, 5.3)	6.6 (5.7, 7.4)	-0.01
LBC 1936[e]	906	50%	EUR	69.6 (67.6, 71.3)	Noob [68]	4.1 (2.7, 7.1)	6.7 (6.1, 7.5)	0.08
BHS	831	57%	EUR (70%) AFR (30%)	43.8 (28.4, 54.6)	watermelon [69]	6.9 (5.2, 9.5)	7.0 (6.4, 7.6)	0.43

AfricanA=African American; EUR=European; HISP=Hispanics; LTL=leukocyte telomere length.

The distributions of Age, LTL, and DNAmTL are presented in median (range) format.

[a]The validation set consists of two groups of individuals: (1) those individuals with TL measures that were included in test process, (2) those individuals without TL measures.

[b]The age distribution was based on exam 8.

[c]The statistics are based on the number of 924 observations across 484 individuals.

[d]Of the 794 individuals, 779 were available with LTL measures.

[e]All subjects of the Lothian *Birth* Cohorts were born at roughly the same time (within 1.9 to 3.7 years).

We display characteristics of (1) 3334 study participants in the training and test data sets that were used to develop and validate DNAmTL, and (2) 9345 participants (9875 blood samples) from 9 cohorts across 7 studies. The participated studies include Framingham Heart Study (FHS) offspring cohort, Women's Health Initiative (WHI), Jackson Heart Study (JHS), InChianti, Twins UK, Lothian Birth Cohorts (LBC), and Bogalusa Heart Study (BHS). Leukocyte TL measures were based on terminal restriction fraction measurement by Southern blotting Southern blotting in FHS, WHI, JHS, and BHS and were based on quantitative real-time polymerase chain reaction (qPCR) in Twins UK and LBC. The column "Array Normalization" refers to different methods of pre-processing DNA methylation array data.
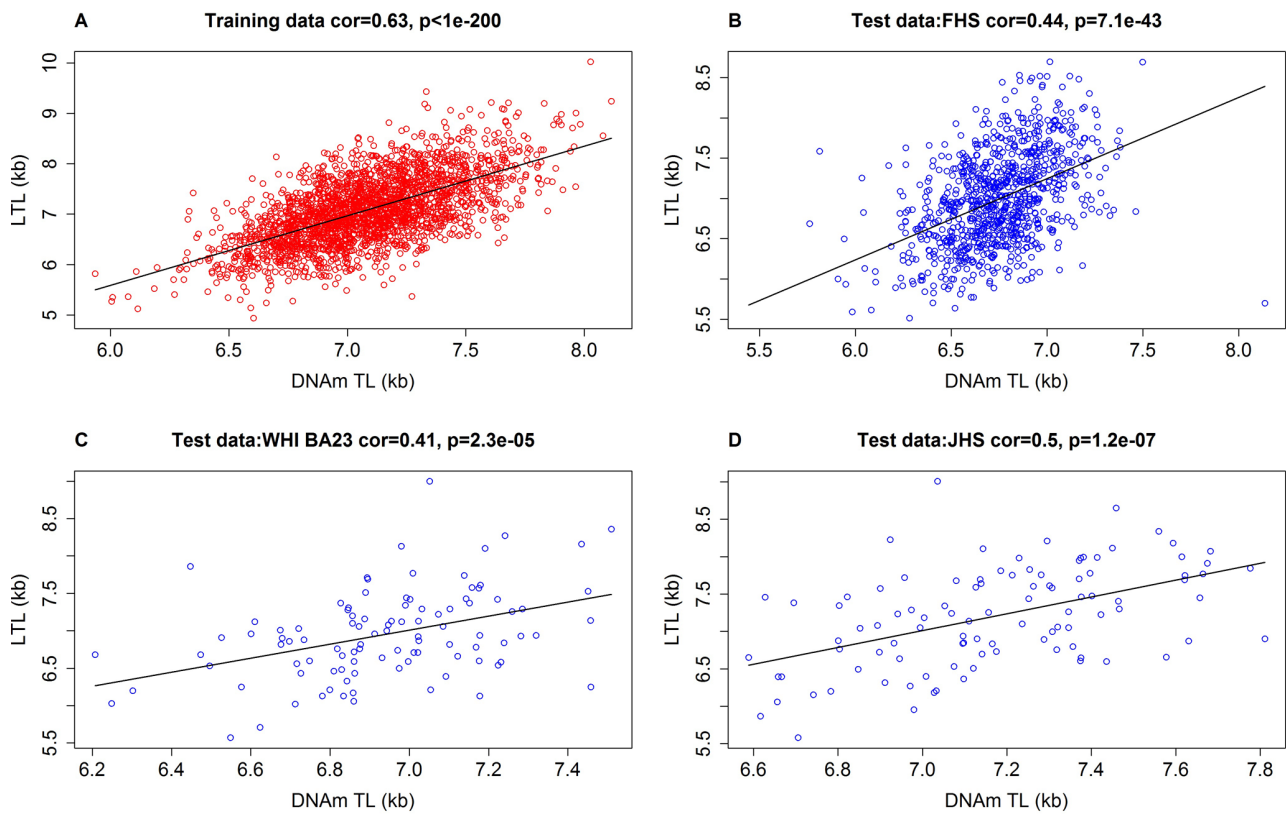
Figure 1. Measured LTL versus DNAmTL in training and test datasets. Scatter plots of DNA methylation-based telomere length (DNAmTL, x-axis) versus observed LTL measured by terminal restriction fragmentation (y-axis). DNAmTL and LTL are in units of kilobase (kb). (**A**) Training data. (**B**) Test data from the Framingham Heart Study. (**C**) Test data from the Women's Health Initiative (BA23 sub-study). (**D**) Test data from the Jackson Heart Study. Each panel reports a Pearson correlation coefficient and correlation test p-value. Table 1 reports analogous results for additional cohorts (Bogalusa, Twins UK, etc).

DNAmTL across different blood cell types

To test whether DNAmTL differs across blood types, we used sorted blood cells and peripheral blood mononuclear cells (PBMCs) from 6 men (aged between 27 and 32 years old, Methods). We observed a statistically significant difference in median DNAmTL values (p=0.0033, Supplementary Figure 4) even though they were roughly comparable: CD8+ T cells (median=8.25), CD4+ T cells (median=7.64), B cells (median DNAmTL=7.43), PBMCs (median DNAmTL=7.55).

DNAmTL versus qPCR TL in the Twins UK study

We obtained leukocyte DNAm data from 792 participants (all women) from the Twins UK study whose LTL was measured by Southern blotting (N=346) and/or quantitative polymerase chain reaction (qPCR, N=779) (Supplementary Note 1). The correlation between DNAmTL and qPCR- based LTL (r=0.39, Supplementary Figure 5A) was similar to that

of LTL measured by Southern blotting (r=0.40, Supplementary Figure 5B).

DNAmTL correlates more strongly with age than TL

Although DNAmTL was developed based on LTL, it displayed substantially stronger negative correlations with age at the time of blood draw ($r \sim -0.80$ to -0.62) than did measured LTL, based on our test datasets ($r \sim -0.40$ to -0.30, Figure 2). Multivariate regression models in the test data show that LTL shortened by 0.022 kilobases per year (p=2.3E-27) after adjusting for sex, race/ethnicity and other confounders (Table 2). Analogous multivariate regression models showed that DNAmTL reduced by 0.018 kilobases per year, but this was associated with a far more significant p value (p=6.0E-125) than that of measured LTL (p=2.3E-27). Although the DNAm-based biomarkers were derived from profiles of adults (22-93 years old), the resulting DNAmTL algorithm was equally applicable to profiles

from children; even to those who were younger than 13 years of age, where a strong negative correlation of r=-0.81 was observed between DNAmTL of blood and age (Supplementary Figure 6A). Such expected negative correlations with age were also seen with DNAmTL in adipose tissue (r=-0.41. Supplementary Figure 3A), liver (r=-0.71, Supplementary Figure 7A), and in (sorted) monocytes (r=-0.60, Supplementary Figure 8A).
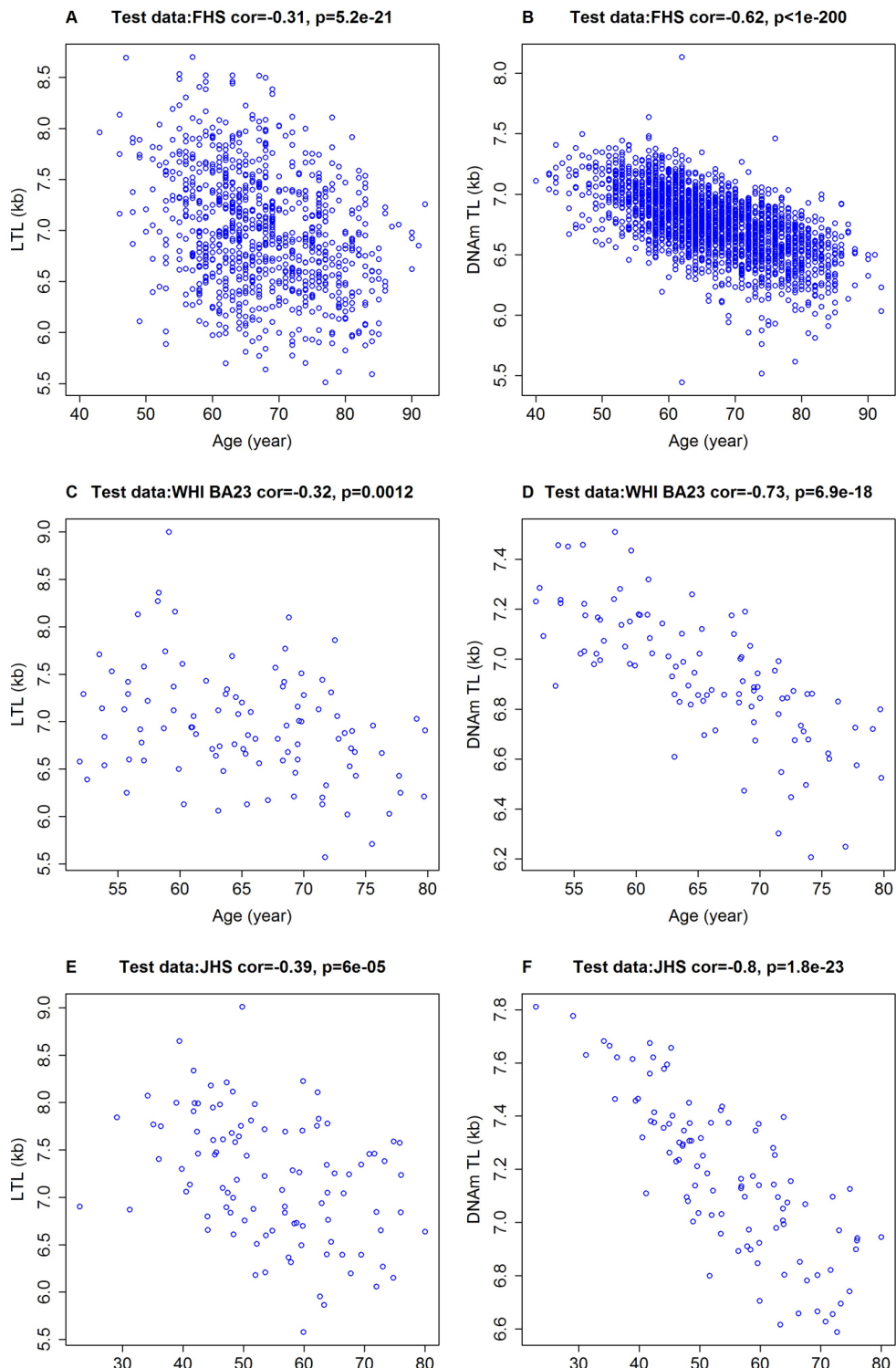
Figure 2. Chronological age versus measured LTL and DNAmTL. Chronological age versus measured LTL (panels **A**, **C**, **E**, in units of kilobase [kb]) and DNAmTL (panels **B**, **D**, **F**, in units of kb). (**A**, **B**) Test data from the FHS. (**C**, **D**) Test data from the WHI (N=100), (**E**, **F**) Test data from the JHS (N=100). Each panel reports a Pearson correlation coefficient and correlation test p-value.

Table 2. Multivariate regression analysis of leukocyte telomere length.

Variable	Coefficient (SE)	t-statistic	P
Outcome: actual LTL (mean TRF)			
Intercept	8.43 (0.201)	41.88	2.43E-227
Age	-0.022 (0.002)	-11.14	2.33E-27
Female	0.132 (0.036)	3.71	2.15E-4
Race: European	0.029 (0.112)	0.26	7.97E-1
smoke: Former	0.132 (0.063)	2.11	3.50E-2
smoke: Never	0.113 (0.062)	1.82	6.95E-2
BMI	-0.007 (0.003)	-2.15	3.16E-2
JHS	0.005 (0.126)	0.04	9.66E-1
WHI BA23	-0.093 (0.084)	-1.10	2.73E-1
Outcome: DNAmTL			
Intercept	8.046 (0.069)	116.16	<1.0E-300
Age	-0.018 (0.001)	-27.32	5.97E-125
Female	0.099 (0.012)	8.14	1.14E-15
Race: European	-0.136 (0.039)	-3.52	4.57E-4
smoke: Former	0.08 (0.022)	3.72	2.09E-4
smoke: Never	0.096 (0.021)	4.51	7.11E-6
BMI	-0.002 (0.001)	-2.19	2.91E-2
JHS	0.069 (0.044)	1.59	1.11E-1
WHI BA23	0.049 (0.029)	1.69	9.15E-2

BMI=body mass index; SE=standard error.

In the upper panel, we present results from a multivariate linear regression model analysis of actual LTL (mean TRF, dependent variable) on different covariates (rows) in the test data set (comprised of 1078 individuals). The model was regressed on age, sex, race/ethnicity, smoking status, and study cohort. Race/ethnicity is a dichotomized variable (European versus African Ancestry). Smoking status is a three-category variable: never, former and current smokers (as a reference). Study cohort is a trivariate variable (FHS, WHI BA23 and JHS cohort).

Effect of sex and ethnicity

Because age would confound any potential relationship between DNAmTL and age-related traits such as health, it would be useful to derive an age-adjusted estimate of DNAmTL (referred to as DNAmTL*adjAge*). We therefore regressed DNAmTL on age and the resulting raw residual was defined as DNAmTLadjAge. A negative value of DNAmTLadjAge would indicate DNAmTL that is shorter than expected based on age, while a positive value would indicate the opposite. We noted that DNAmTLadjAge is heritable (heritability

h^2=0.46, p=4.5E-11) according to a pedigree-based polygenic model analysis in the FHS cohort (N>2000, Methods).

Women tend to exhibit longer LTL than men of the same age [32]. Similarly, our multivariate regression models revealed that age-adjusted LTL and age-adjusted DNAmTL were indeed longer in females than in males. The p-values for age-adjusted LTL measured in this study (p=2.15E-4, N=1078) and that of a previous study [32] (p=5E-3, N ~ 730) were far less significant than those for age-adjusted DNAmTL

(p=1.14E-15, Table 2). Roughly, women showed longer telomere length than men by 0.1 kilobase, given by DNAm or TRF measures (Table 2). We also found longer age-adjusted DNAmTL in female compared to male liver samples (P=0.017, Supplementary Figure 7C). With regards to ethnicity, age-adjusted DNAmTL of PBMCs (Table 2) and monocytes (Supplementary Figure 8B) revealed that US population of African ancestry have a longer LTL than those of European ancestry, consistent with previous observations made with TRF-based measured TL. Once again, the association of age-adjusted DNAmTL (p=1.6E-33, N ~ 1200) with ethnicity was stronger than those seen with age-adjusted LTL measured by TRF (p=1E-4) or quantitative polymerase chain reaction (p=1E-3, N ~ 2450) [33]. Overall, these results demonstrate that DNAmTL exhibits substantially more significant associations with age, sex and ethnicity than measured LTL.

DNAmTL is often superior to measured LTL in predicting mortality and health outcomes

Next, we compared the performance of DNAmTLadjAge with age-adjusted LTL in predicting time-to-death or time-to-heart disease in the training and test datasets (N=3,334) for which both measures were available (Figure 3). We found that longer DNAmTLadjAge was significantly associated with a lower hazard ratio (HR) for time-to-death, all-cause mortality (HR=0.31 and P=6.7E-9), time-to-coronary heart disease (CHD, HR=0.55and, p=9.5E-3), and time-to-congestive heart failure (CHF, HR=0.32and, p=9.7E-4, Figure 3). In women, later age at menopause was associated with significantly higher values of DNAmTLadjAge (p=0.025). Furthermore, physical activity was also positively associated with DNAmTLadjAge (p=0.013).

By comparison, the results from age-adjusted LTLs (LTLadjAge) were far less significant in predicting lifespan (HR=0.81 and p=4.7E-3 compared to HR=0.31 and p=6.7E-9 for DNAmTL, Figure 3A, B) and were *not* significantly associated with time-to-CHD, time-to-CHF, age at menopause and physical activity (p>0.3, Figure 3).

We want to emphasize that our comparison between DNAmTLadjAge and LTLadjAge involved the same set of individuals for whom both measures were available, i.e. each association test used the same sample size and distribution in age, sex, and ethnicity. These results show that DNAmTLadjAge outperforms LTLadjAge when it comes to predicting important health-related conditions. However, our comparative analysis was subject to a limitation: the measures of LTLadjAge and

DNAmTLadjAge in the FHS cohort corresponded to two different blood samples collected at different time points. We addressed this limitation in two ways. First, we repeated the analysis by omitting the FHS data. In the resulting test data (n=100 samples from the WHI and n=100 samples from the JHS), DNAmTLadjAge continued to outperform LTLadjAge (Supplementary Table 1). Second, we compared DNAmTLadjAge with LTL in a host of additional cohorts (Bogalusa Heart Study, Twins UK, Lothian Birth Cohorts) as detailed below.

Evaluating DNAmTL in large scale validation data

In the second phase of validation, we sought to test these associations with even larger, independent data sets. In total, we analyzed N=9,875 Illumina methylation arrays from blood samples of N=9,345 individuals from 9 cohorts across 7 studies: FHS, WHI BA23, WHI EMPC, JHS, InChianti, Lothian Birth Cohorts of 1921 and 1936 (LBC), UK Twins, and Bogalusa Heart Study (BHS, Table 1, Methods, and Supplementary Note 1). Of the samples, 4,039 individuals were available with measured LTL measurements based on Southern blot or quantitative polymerase chain reaction (qPCR). The data set was comprised of three different ethnic groups: European (77%), African (15%), and Hispanic (8%) ancestries. All but one cohort (BHS) were available for mortality analysis (N=9,044 methylation arrays on 8,514 individuals) with sufficient follow-up period. The mean chronological age at the time of the blood draw was 65.6 years and the mean follow-up time (for all-cause mortality) was 11.8 years (Supplementary Table 2). Once again, DNAmTL was negatively correlated with chronological age in all cohorts with sufficient variation in chronological age ($-0.83 \leq r \leq -0.42$), in which we excluded the Lothian Birth Cohort studies comprising individuals with similar ages (Supplementary Figure 9).

Further analyses of these data confirmed that higher values of DNAmTLadjAge were indeed associated with longer lifespan (Figure 4). Each kilobase increase of DNAmTLadjAge was associated with a hazard ratio of 0.37 for mortality (p=2.5E-20, Figure 4A), similar to what we observed in the training and test dataset (HR=0.31, Figure 3A). Higher values of DNAmTLadjAge were also associated with longer time-to-CHD (HR=0.51 and p=6.6E-5) and longer time-to-CHF (HR=0.27 and p=3.6E-6, Figure 4 D and G), mirroring yet again the results obtained from the training and test data sets.

Two types of multivariate Cox regression models demonstrated that these associations remained significant
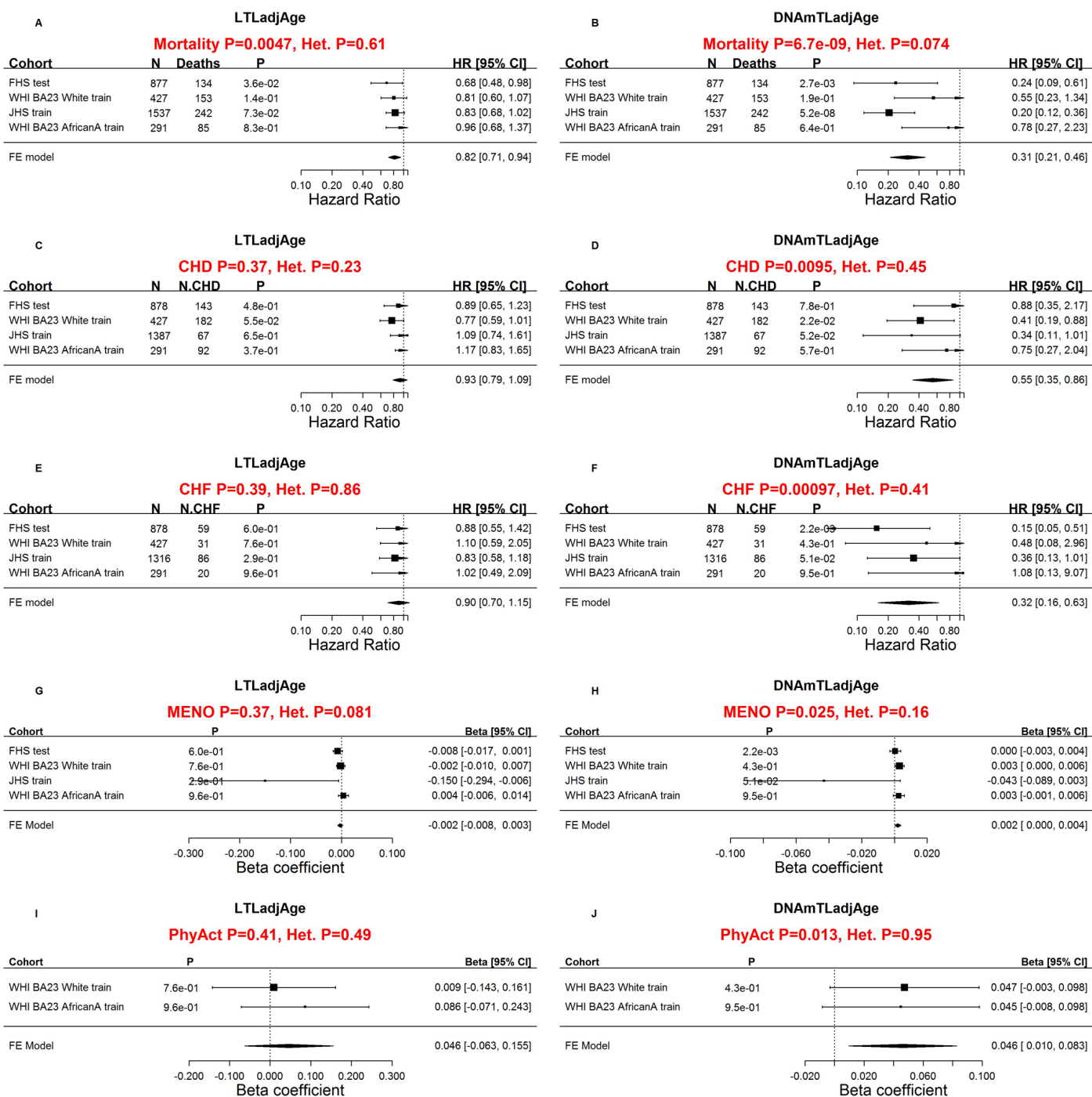
Figure 3. Comparing measured LTL with DNAmTL with respect to age-related conditions. Meta-analysis forest plots for relating age-related conditions (rows) to age-adjusted LTL (left panels) and age-adjusted DNAmTL (right panels). Panels in the first row (**A**, **B**) presents meta-analysis forest plots for Cox regression models of time-to-death. Meta-analysis of Cox regression models for (**C**, **D**) time-to-coronary heart disease (CHD) and (**E**, **F**) time-to-congestive heart failure (CHF). Rows in the forest plot correspond to training and test datasets (used for developing DNAmTL) stratified by race/ethnicity Each row presents the summary statistic at a (stratified) study dataset and reports sample size (N), number of events, P value, hazard ratio and a 95% confidence interval resulting from a Cox regression model. (**G**, **H**) Meta-analysis for the association with age at menopause. (**I**, **J**) Meta-analysis for the association with self-reported physical activity status (yes/no). (**G**-**J**) Each row (study data set) presents the summary statistic, P value, beta coefficient and a 95% confidence interval resulting from a linear (mixed) regression model. In general, an insignificant Cochran Q test p-value (denoted by Het. P) is desirable because it suggests that results do not differ significantly across the strata. However, an insignificant Q test p-value could also reflect lack of statistical power.

even after adjusting for (1) blood cell counts (Figure 4 B, E, H), and (2) classical risk factors (Figure 4 C, F, I) including body mass index, educational level, alcohol intake, smoking pack-years, prior history of diabetes, prior history of cancer, and hypertension status.

We went further and evaluated DNAmTLadjAge in different strata including age (younger/older than 65 years), prevalent clinical conditions at baseline and found that DNAmTLadjAge remained a significant predictor of time-to-death in each of these strata (Supplementary Table 3), e.g. HR=0.26 for individuals aged < 65 years and HR=0.41 for older individuals aged

years. DNAmTLadjAge also remained a significant predictor of time-to-CHF in most strata (Supplementary Table 4) and of time-to-CHD in specific strata such older age, normal BMI, or higher education attainment (Supplementary Table 5).

Our analyses revealed that higher DNAmTLadjAge values were associated with measures of physical fitness/functioning (P=7.6E-3), and disease-free status (p=0.019), while prior history of cancer was associated with lower DNAmTLadjAge values (p=0.053, Supplementary Figure 10). Interestingly, we also found a nominally significant association (p=0.026) between
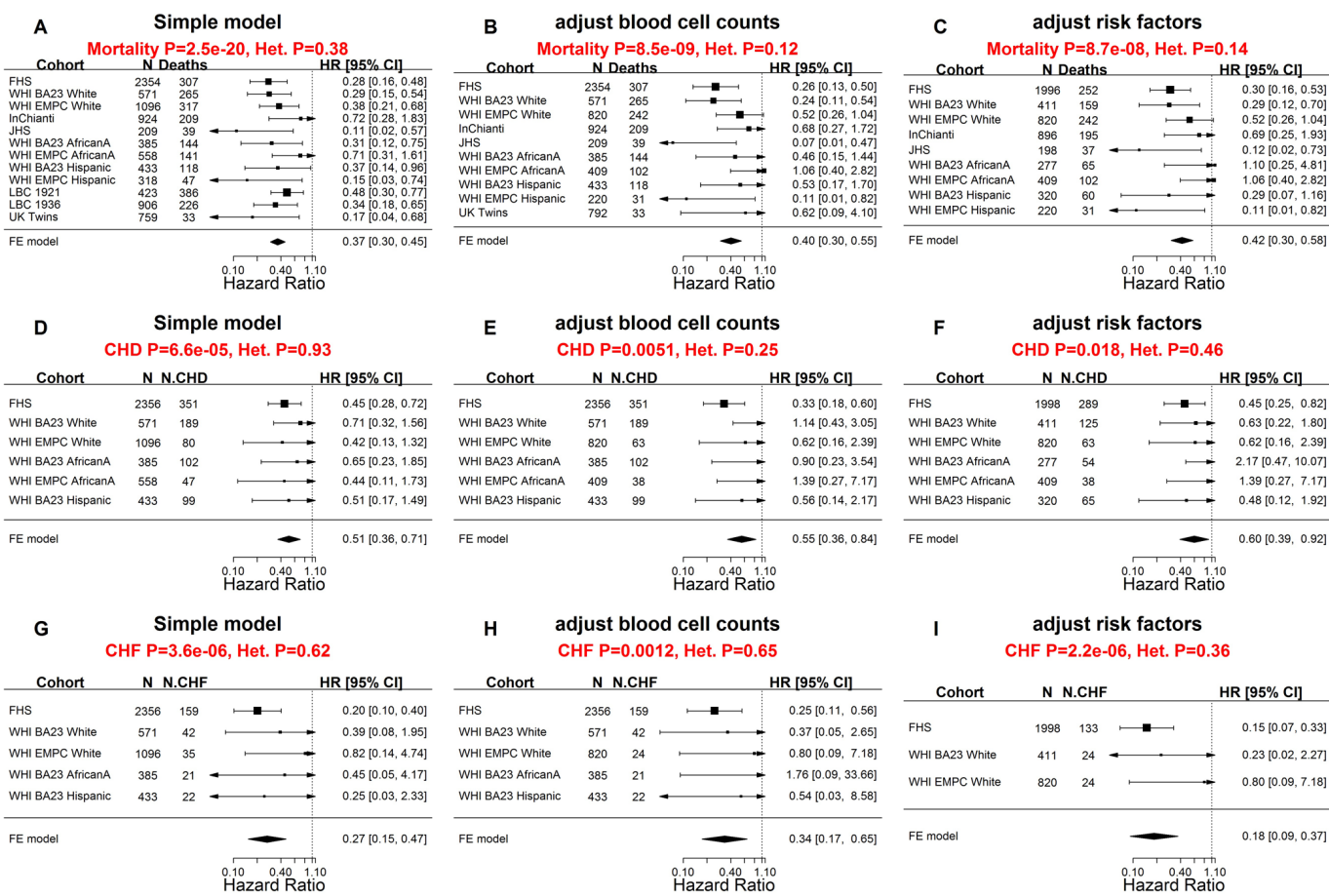
Figure 4. Meta-analysis forest plots for predicting time-to-death due to all-cause mortality and time-to-cardiovascular disease in independent validation data. Meta-analysis forest plot for combining Cox regression hazard ratios for time-to-death, time-to-coronary heart disease (CHD), and time-to-congestive heart failure (CHF), based on age-adjusted DNAmTL (DNAmTLadjAge). The sample sizes for the analysis were up to 9,044 methylation arrays (8,541 individuals) across 8 cohorts. Left panels, middle panels, and right panels report meta-analysis results for (1) simple Cox regression models, (2) multivariate Cox models adjusted for blood cell counts, and (3) multivariate Cox model adjusted for traditional risk factors, respectively. Each row reports the hazard ratio associated with DNAmTLadjAge. (1) The simple Cox models (left panels) were adjusted for chronological age, sex and adjusted for intra-pedigree correlation and batch effects as needed. (2) The models in the middle panels involved additional covariates: imputed blood cell counts based on DNA methylation data. (3) The models in the right panels different from those of (1) by additional demographic characteristics, psychosocial behavior, and clinical covariates (Methods). Each panel reports a meta-analysis forest plot for combining hazard ratios associated with time to event. Each row presents the summary statistic at a (stratified) study dataset and reports sample size (N), number of events, hazard ratio and a 95% confidence interval resulting from a Cox regression model. In general, an insignificant Cochran Q test p-value (denoted by Het. P) is desirable.

age-at-menopause and DNAmTLadjAge. We found that one year later age-at-menopause was associated 0.001 kilobase longer LTL (Supplementary Figure 10A). Our cross-sectional analyses, however, do not allow determination of cause-and-effect relationships, but we note that age-at-menopause is also associated with epigenetic aging [34].

Life-style factors and clinical biomarkers

To assess the effect of life-style factors and diet on DNAmTLadjAge in blood, we meta-analyzed large data sets from the FHS and WHI cohort (N up to 6,977, Methods) including their associations with clinical measurements. Age-adjusted DNAmTL was positively

	Variable	N data	N	Meta Bicor	Meta P	FHS Bicor	FHS P	WHI Bicor	WHI P	LBC 1921 Z	LBC 1921 P	LBC 1936 Z	LBC 1936 P
Diet	log2(Total energy)	2	3555	--	2.6E-01	--	--	0.00	9.5E-01	--	--	2.3	2.0E-02
	Carbohydrate	1	2789	0.04	2.1E-02	--	--	0.04	2.1E-02	--	--	--	--
	Protein	2	3555	--	2.1E-01	--	--	0.01	6.9E-01	--	--	1.9	5.2E-02
	Fat	2	3555	--	2.0E-01	--	--	-0.04	3.7E-02	--	--	1.2	2.3E-01
	log2(1+Red meat)	3	5678	--	1.2E-01	0.01	7.7E-01	-0.03	6.8E-02	--	--	-1.3	1.9E-01
	log2(1+Poultry)	3	5687	--	3.4E-01	-0.02	4.4E-01	-0.02	3.5E-01	--	--	0.5	6.3E-01
	log2(1+Fish)	3	5662	--	1.8E-02	0.01	7.7E-01	0.05	4.7E-03	--	--	0.6	5.5E-01
	log2(1+Dairy)	3	5656	--	7.1E-03	0.06	4.3E-03	0.01	5.0E-01	--	--	1.3	2.1E-01
	log2(1+Whole grains)	2	4952	--	2.9E-01	0.02	4.7E-01	0.01	4.5E-01	--	--	--	--
	log2(1+Nuts)	2	3509	--	1.3E-01	--	--	0.03	1.0E-01	--	--	0.1	9.1E-01
	log2(Fruits)	3	5649	--	3.1E-05	0.02	2.8E-01	0.07	3.3E-04	--	--	2.8	6.0E-03
	log2(Vegetables)	3	5655	--	1.2E-03	0.03	1.4E-01	0.03	9.7E-02	--	--	3.3	1.0E-03
	log2(Carotene)	1	766	--	4.5E-03	--	--	--	--	--	--	2.8	5.0E-03
	log(OMEGA3)	1	2151	0.06	4.0E-03	0.06	4.0E-03	--	--	--	--	--	--
	log(VitaminE)	2	2908	--	3.9E-01	-0.02	4.4E-01	--	--	--	--	3.0	3.0E-03
DietaryBiomarkers	Retinol	2	2798		4.6E-01	--	--	-0.02	4.2E-01	--	--	-0.1	9.3E-01
	Mean carotenoids	1	2019	0.10	1.5E-05	--	--	0.10	1.5E-05	--	--	--	--
	Lycopene	1	2020	0.04	9.5E-02	--	--	0.04	9.5E-02	--	--	--	--
	log2(alpha-Carotene)	1	2020	0.08	3.9E-04	--	--	0.08	3.9E-04	--	--	--	--
	log2(beta-Carotene)	1	2019	0.07	9.5E-04	--	--	0.07	9.5E-04	--	--	--	--
	log2(Lutein+Zeaxanthin)	1	2020	0.06	3.5E-03	--	--	0.06	3.5E-03	--	--	--	--
	log2(beta-Cryptoxanthin)	1	2020	0.10	3.8E-06	--	--	0.10	3.8E-06	--	--	--	--
	log2(alpha-Tocopherol)	1	2020	0.05	3.2E-02	--	--	0.05	3.2E-02	--	--	--	--
	log2(gamma-Tocopherol)	1	2020	-0.06	1.1E-02	--	--	-0.06	1.1E-02	--	--	--	--
Measurements	A1C	2	1282	--	8.0E-02	--	--	--	--	0.8	4.0E-01	-2.6	8.0E-03
	log2(C-reactive protein)	3	5279	--	4.3E-09	-0.11	3.1E-07	-0.06	4.4E-03	--	--	-1.7	9.9E-02
	log2(Insulin)	1	3175	-0.06	3.5E-04	--	--	-0.06	3.5E-04	--	--	--	--
	log2(Glucose)	2	5613	--	1.0E-01	-0.04	7.3E-02	-0.01	5.3E-01	--	--	--	--
	log2(Triglyceride)	3	6437	--	3.2E-04	-0.06	5.3E-03	-0.04	2.4E-02	--	--	-0.9	3.8E-01
	Total cholesterol	4	6938	--	5.5E-03	0.04	3.4E-02	0.00	7.8E-01	4.0	6.3E-05	1.0	3.0E-01
	LDL cholesterol	1	3215	0.00	8.6E-01	--	--	0.00	8.6E-01	--	--	--	--
	HDL cholesterol	3	6436	--	8.2E-03	0.03	2.0E-01	0.06	1.6E-03	--	--	-1.0	3.0E-01
	log2(Creatinine)	4	5654	--	9.7E-01	0.02	2.4E-01	-0.03	2.1E-01	-1.0	3.4E-01	0.7	4.7E-01
	log2(Urine Creatinine)	1	2319	-0.03	1.6E-01	-0.03	1.6E-01	--	--	--	--	--	--
	Systolic blood pressure	4	6977	--	8.5E-01	-0.02	4.6E-01	0.00	8.6E-01	3.0	3.0E-03	-1.1	2.8E-01
	Diastolic blood pressure	4	6977	--	3.7E-02	0.06	4.9E-03	0.01	4.2E-01	2.5	1.3E-02	-2.0	4.3E-02
	log2(Waist / hip ratio)	2	5466	--	2.4E-03	-0.04	3.3E-02	-0.04	3.0E-02	--	--	--	--
	BMI	4	6942	--	3.6E-03	-0.03	1.6E-01	-0.03	1.0E-01	-1.1	2.7E-01	-1.9	5.2E-02
Life style	Education	4	6624	--	3.3E-08	0.04	5.1E-02	0.08	1.6E-05	1.0	3.0E-01	3.1	2.0E-03
	Income	1	3186	0.07	3.1E-05	--	--	0.07	3.1E-05	--	--	--	--
	log2(1+Exercise)	1	3061	0.04	2.4E-02	--	--	0.04	2.4E-02	--	--	--	--
	Current smoker	4	6932	--	2.2E-16	-0.12	6.7E-09	-0.09	3.7E-07	-0.3	8.6E-01	-3.6	3.5E-04
	log2(1+Alcohol)	4	6484		6.6E-01	-0.03	2.1E-01	0.02	3.0E-01	0.8	3.9E-01	-1.6	1.1E-01

Figure 5. Cross sectional associations between age-adjusted DNAmTL versus lifestyle/dietary variables. Association analysis between age-adjusted DNAmTL (DNAmTLadjAge) and 43 variables including 15 self-reported diet, 9 dietary biomarkers, 14 variables related to metabolic traits and central adiposity, and 5 life style factors, based on the meta-analysis across the FHS WHI, LBC 1921 and LBC 1936 cohort. Robust correlation coefficients (biweight midcorrelation) analysis were performed on the FHS and WHI cohort while generalized linear regression analysis adjusted for sex was performed on the LBC 1921 and 1936 cohort, respectively. For each variable, we display number of datasets, number of total subjects, the robust correlation results from the meta-analysis, FHS, and the WHI cohort and the Z statistics for the LBC respectively. The meta-analysis was based on Stouffer's method for the majority of the variables or fixed effect models. The 2-color scale (blue to red) color-codes bicor correlation coefficients in the range [-1, 1] or Z statistics. The green color scale (light to dark) applied to unadjusted P values. Cell entry "--" denotes not available. The correlation analysis results stratified by sex using the FHS cohort are listed in Supplementary Figure 11 and stratified by ethnic group using the WHI cohort are listed in Supplementary Figure 12, respectively.

correlated with plasma-based estimates of mean carotenoid levels (robust correlation r=0.10, unadjusted p=1.5E-5), beta-Cryptoxanthin (r=0.10 and p=3.8E-6) and high-density lipoprotein (HDL, r=0.04 and p=1.3E-3) (Figure 5, Supplementary Figures 11 and 12). The positive correlation between DNAmTLadjAge and self-reported measures of carotene intake (p=4.0E-3, N=766 from the Lothian Birth Cohort from the year 1936) was consistent with these findings. Positive associations with DNAmTLadjAge were also observed for self-reported measures of fruit (p=3.1E-5), vegetable (p=1.2E-3), dairy (p=7.1E-3), fish (P=0.018), and carbohydrate consumption (p=0.02). Positive correlations were also evident between DNAmTLadjAge and socio-economic factors such as level of educational attainment (p=3.3E-8) and income (p=3.1E-5). These associations held for each sex separately in the FHS cohort (Supplementary Figure 11).

There were also features that correlated negatively with DNAmTL. Smoking was strongly associated with lower DNAmTL values in leukocytes (p=2.3E-16) and in adipose tissue (P=0.036, Supplementary Figure 3D). C-reactive protein (p=4.3E-9), triglyceride levels (p=3.2E-4) and insulin levels (p=3.5E-4) were negatively cor-

related with DNAmTLadjAge in both FHS and WHI cohorts. There were also negative correlations of DNAmTLadjAge (in leukocytes) with waist-to-hip ratio (p=2.4E-3), body-mass index (BMI, p=3.6E-3) and physical exercise (p=0.02).

We caution the reader that our p-values are not adjusted for multiple comparisons.

DNAmTL of leukocytes exhibits stronger association with smoking than does measured LTL

Next, we used 4,039 subjects from our seven validation cohorts to interrogate the impact of smoking on telomere shortening in leukocytes (Methods). A detailed smoking history (smoking pack-years) was known for roughly half of these individuals (N=2216). The smoking variable was based on pack-years when available otherwise based on never versus ever smoking. We adjusted the smoking variable for potential confounders (age, sex and ethnicity) of the relationship with LTL. Our large-scale meta-analysis showed that DNAmTL greatly outperformed measured LTL (Stouffer's meta p=1.2E-17 versus meta p=0.029) with regards to association with smoking (Table 3).

Table 3. Smoking impacting on DNA methylation-based telomere length.

Cohort	N	Variable	DNAmTL		LTL	
			T	P	T	P
FHS[1]	878	Pack years	-2.08	3.81E-2	0.54	0.59
WHI BA23[1]	97	Pack years	0.45	6.53E-1	1.30	0.2
JHS[1]	100	Smoker	-3.00	3.38E-3	-1.87	6.40E-2
LBC 1921[2]	404	Pack years	-3.53	4.59E-4	-0.92	0.36
LBC 1936[2]	796	Pack years	-3.55	4.04E-4	0.55	0.58
UK Twin[2]	792	Smoker	-2.79	5.23E-3	-3.23	1.23E-3
BHS[1]	831	Smoker	-6.83	1.70E-11	-1.83	6.77E-2
ALL	**4039**	**Smoking impact**	**-8.55**	**1.21E-17**	**-2.19**	**0.029**

The Smoker variable was coded as a binary variable for never versus ever smokers, where estimate was referred to ever smokers.
[1]Telomere length was based on terminal restriction fraction measurement by Southern blotting.
[2]Telomere length was measured using quantitative real-time polymerase chain reaction (qPCR).

The table summarized the meta-analysis for the smoking impact on plasma DNA methylation based telomere length (DNAm TL) versus the impact on qPCR or southern blot-based leukocyte TL. The association tests were performed at each study cohort respectively then combined by the Stouffer's method weighted by square root of sample size. The smoking variable was based on a binary variable for former/current smokers versus never or pack years provided the variable was available.

According to fixed effect models analysis (Methods), we found DNAmTL was shortened by 0.022±0.0002 kilobases per smoking pack-year (P=5.9E-07) while TL was not significantly lengthened by 1.3E-04±5.0E-04 kilobases per smoking pack-year (P=0.79). In an analogous analysis, we found that smokers had significantly shorter DNAmTL by 0.063±0.009 kilobases associated with a very robust P value (3.2E-13). The smokers also exhibited shorter TL (0.01±0.003 kilobases) but with far less significant P value (7.5E-04). Focusing on individual cohorts corroborated these findings, e.g. the association of smoking with DNAmTL (p=1.70E-11) was significantly greater than the association of smoking with LTL (p=6.77E-2, Table 3) in the BHS cohort. We also carried out a sensitivity analysis that compared age-adjusted LTL between current smokers and former/never smokers in the BHS and subgroups defined by sex and ethnicity. Our sensitivity analysis confirmed that smoking was indeed significantly associated with shorter age-adjusted DNAmTL in each subgroup (1.95E-8 ≤ p ≤ 4.39E-3, Supplementary Figure 13). Conversely, no significant associations were observed between LTL and smoking in these subgroups (0.12 ≤ p ≤ 0.87, Supplementary Figure 14).

Omega 3 intake is associated with longer DNAmTL

We were interested in investigating the relationship between DNAmTL and omega-3 polyunsaturated fatty acid (PUFA) supplementation in a large observational cohort study. We found omega-3 supplement intake to correlate positively with age-adjusted DNAmTL (bicor r=0.088 and p=4.4E-5), and this correlation was far more significant than that exhibited by age-adjusted LTL (bicor r=0.085 and p=0.016, Supplementary Figure 15). For DNAmTLadjAge, the effect of omega 3 supplementation was more pronounced in males (r=0.08, p=0.012) than in females (r=0.047, p=0.11). A multivariate linear mixed effects model analysis resulted in suggestive evidence (p=0.09) that omega-3 intake is associated with longer DNAmTLadjAge even after adjusting for sex, BMI, educational levels, and smoking pack year.

DNAmTL relates to imputed blood cell composition

LTL is known to correlate with the abundance of naïve CD8+ T cells and other cell types [8]. Similarly, we found DNAmTL to be significantly correlated with several quantitative measures of leukocytes that were imputed using DNAm data (Methods) such as naïve CD8+ T cells ($r = 0.42$, p=2.2E-151) and exhausted CD8+ T cells ($r = -0.36$, p=3.0E-102; Supplementary Figure 16 and Supplementary Data 2). A multivariate regression model revealed that 25% of the variation of

age-adjusted DNAmTL and 4.6 % of the variation in age-adjusted LTL could be attributed to imputed leukocyte cell composition in the FHS test data. Overall, DNAmTL exhibited substantially stronger correlations with imputed leukocyte cell composition than did LTL (Supplementary Figure 16 and Supplementary Data 2).

DNAmTL CpGs tend to be located near telomeres and enriched with cis-mQTL

To test if the 140 CpGs of DNAmTL model were enriched at regions near telomeres, we performed hypergeometric tests based on the regions threshold up to 3 Mb (Methods). Our analysis showed that the 140 CpGs had moderate enrichment (hypergeometric p=8.1E-3, Supplementary Table 6) within sub-telomeric regions. Sensitivity analysis based on different thresholds validated the result (p=5.9E-3 ≤ P ≤ 0.039, Supplementary Table 6). Furthermore, we tested whether the 140 CpG sites overlapped with 52,916 *cis* methylation quantitative trait loci (*cis*-mQTL [35], Methods). Strikingly, 51 out of the 140 CpGs markers were known *cis*-mQTL (hypergeometric p=2.6E-15, Supplementary Data 1) which is consistent with the high heritability observed for DNAmTL (additive h^2=0.46). Several of the 51 SNPs (from *cis*-mQTL) were implicated in complex traits according to GWAS data bases (Methods), e.g. rs2147904 in 1p34.2 (P ≥ 1.0E-14), rs305082 in 16q24.1 (P ≥8.0E-131) and rs945631 in 1p22.1 (P=2.0E-8) are known to be associated with granulocyte composition in blood. Further, rs945631 is also implicated in circulating phospholipid trans fatty acids at a suggestive P value=3.0E-06 (Supplementary Data 3). Bipolar disorder (P ≥ 2.0E-09) was identified when we inspected the SNPs in linkage disequilibrium with the 51 markers (Methods and Supplementary Data 3).

DNAmTL and LTL exhibits different patterns of SNP associations

Alternatively, we briefly examined SNP association of DNAmTL across 10 loci implicated in measured LTL with genome-wide significance [36-38] (Methods). We previously found that SNPs in the *TERT* locus to be associated with epigenetic aging rates [19]. Inspecting the overlap regions between the 10 loci and the 140 CpGs (in DNAmTL, Supplementary Data 1), cg00580497 is located nearby the right arm of the *TERT* locus (within 500kb) and cg02282640 is located nearby the right arm of another highlighted gene *MPHOSPH6* [38]. However, using the FHS cohort, we did not find these SNPs or those at other loci to exhibit any significant associations (P<0.05) with DNAmLTLadjAge (Supplementary Table 7).

Functional annotation of CpGs implicated in DNAmTL

We analyzed the genomic locations of the 140 CpGs underlying the DNAmTL using the GREAT software tool which assigns potential biological meaning to a set of genomic locations (here CpGs) by analyzing the annotations of nearby genes. Ten gene sets were identified as significant at a stringent Bonferroni corrected significance level (p<0.05) including "Cadherin, N-terminal" that mediate cell adhesion, polarization and migration (nominal p=1.0E-7) and SODD/TNFR1 signaling pathway (nominal p=5.2E-5, Supplementary Data 4). When focusing only on the subset of 72 CpGs that have negative coefficients in the DNAmTL model (increasingly de-methylated with telomere shortening), we found 10 statistically significant gene sets at a Bonferroni corrected p<0.05 including calcium-dependent adhesion and "Cadherin, N-terminal" (p=2.8E-10). When focusing only on the 68 CpGs with positive coefficients in the DNAmTL model we identified 4 gene sets at a Bonferroni corrected p<0.05 including the vascular endothelial growth factor (VEGF) signaling pathway (p=7.4E-5). The expression of these gene sets remains to be validated, and for moment their identities do not immediately proffer obvious clues as to how they may be linked with telomere attrition, making their involvement all the more intriguing.

DNAmTL is often inferior to epigenetic clocks

Numerous lines of evidence suggest that telomere attrition and epigenetic aging are distinct cellular features that are well-associated with the aging process. As such both TL and epigenetic clocks are potential estimators of biological age [9]. To ascertain how related they are to each other, we calculated, pairwise correlations between DNAmTLadjAge and four "age-independent" measures of epigenetic age acceleration derived from (1) the pan-tissue epigenetic clock by Horvath (2013) [12] (2) the blood-based clock by Hannum et al. (2013) [11], (3) the DNAm PhenoAge estimator by Levine et al. (2018) [15], and (4) the DNAm GrimAge estimator by Lu et al. (2019) [17]. Using N=2356 samples from the FHS, we found that DNAmTLadjAge exhibited moderate negative correlations with the four epigenetic age acceleration measures ($-0.44 \leq r \leq -0.20$, Supplementary Figure 17). We then compared the performance between DNAmTL and epigenetic clocks in predicting health outcomes. Using the validation data (N=6,850), we found that DNAmTLadjAge rivals measures of age acceleration based on Hannum's [11] or Horvath's clock [12], but was clearly inferior to age-adjusted DNAm PhenoAge [15] or DNAm GrimAge [17]. In particular, we demonstrated that AgeAccelGrim (based

on DNAm GrimAge) greatly outperformed DNAmTLadjAge with regards to predicting time-to-death (Cox P=5.8E-71 for AgeAccelGrim versus p=4.1E-15 for DNAmTLadjAge), time-to-CHD (p=2.5E-23 for AgeAccelGrim versus p=6.6E-5), and time-to-CHF (p=1.8E-35 versus p=3.6E-6, Supplementary Figure 18).

DNAmTL applied to *in vitro* cultured cells

All the above analyses have shown that associations of several human traits and health outcomes with DNAmTL were much stronger than with LTL. What then might be the biological meaning of DNAmTL? We examined this question by monitoring DNAmTL in cultured somatic cells without and with expressed telomerase activity. Primary keratinocytes isolated from healthy human skin were grown with serial passaging upon confluence, where cell numbers were obtained, and their population doublings determined. DNA methylation profiles of cells after different population doublings were measured using Illumina EPIC array. DNAmTL was correlated with population doubling in both telomerase- negative and telomerase-positive cells, which displayed no telomere shortening (Figure 6 and Figure 7). Collectively, these findings suggest that DNAmTL records cell replication rather than TL. In the following, we provide more details. Primary keratinocytes isolated from healthy human skin were grown with serial passaging upon confluence, where cell numbers were obtained, and their population doublings determined. DNA methylation profiles of cells after different population doublings were measured using Illumina EPIC array. As would be expected, DNAmTL of keratinocytes from five heathy donors reduced in function of cumulative population doubling (Figure 6A). Accordingly, while the DNAmTL values of neonatal donors 1 to 4 were mutually comparable, that of donor 5, which are keratinocytes from a 65 years-old donor was markedly smaller, which is in keeping with established telomere biology. However, when neonatal fibroblasts and adult coronary endothelial cells (EC) were compared, the DNAmTL values of adult EC were greater than those of neonatal fibroblasts **(**Figure 6B**)**. Possible tissue-specific influence on telomere length was ruled out by TRF southern blot analyses which revealed that telomeres of neonatal fibroblasts were indeed longer than those of adult endothelial cells **(**Figure 6C**)**. This challenges the notion that DNAmTL is a surrogate for telomere length in non-blood tissue. If it were, then DNAmTL of primary cells that are transduced with hTERT should be augmented since this enzyme replicates and stabilizes telomeres. The results in Figure 7A show that this was not the case, as DNAmTL values of primary human fibroblasts continued to decrease even though they became immor-
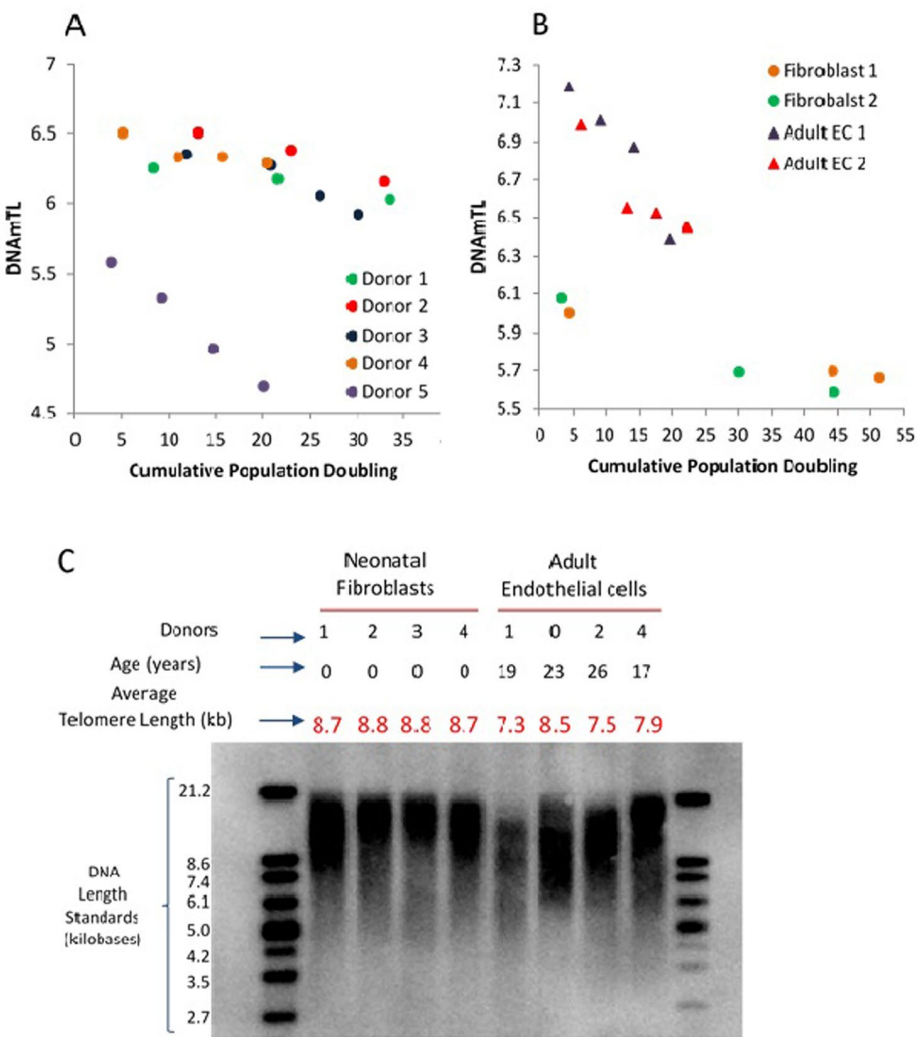
Figure 6. Application of DNAmTL on *in vitro* keratinocytes, neonatal fibroblasts and adult coronary artery endothelial cells. Panel (**A**) depicts decreasing DNAmTL values of keratinocytes from five heathy donors as a function of cumulative population doubling (y-axis, in units in kilobase). Panel (**B**) show that DNAmTL values of neonatal fibroblasts are smaller than those of adult coronary artery endothelial cells (EC). Both cell types exhibit decreasing DNAmTL in function of cumulative population doubling (x-axis). Panel (**C**) is the average telomere length measurement of neonatal fibroblasts and adult endothelial cells, which revealed that the telomeres of the former are longer than those of the latter.

talized, and TRF Southern blotting (Figure 7B) confirmed that their telomeres were indeed significantly increased and stabilized after the introduction of hTERT. Collectively, these studies show that DNAmTL is not the same as telomere length (especially when it comes to in vitro studies), hence indicating that it is instead, a DNA methylation-based surrogate for biological outcomes that are linked to telomere length in blood samples from adults.

DISCUSSION

Considerable technical challenges are inherent in the process of measuring telomere length [39-41]. Our stu-

dy was motivated by the recent insight that machine-learning methods (such as elastic net) can be used to develop remarkably robust DNAm based estimators of chronological age and mortality risk [12, 14, 15, 17]. This robustness is due as much to the mathematical prowess of machine learning, as to the nature of the biomolecule that is measured, namely methylated DNA. Previously reported telomere-associated changes of methylation at sub-telomeric regions [26] raised the possibility that these changes may be predictive of telomere length.

Our overall goals were a) to test whether an optimal pattern of DNAm associated with TL, i.e., DNAmTL,
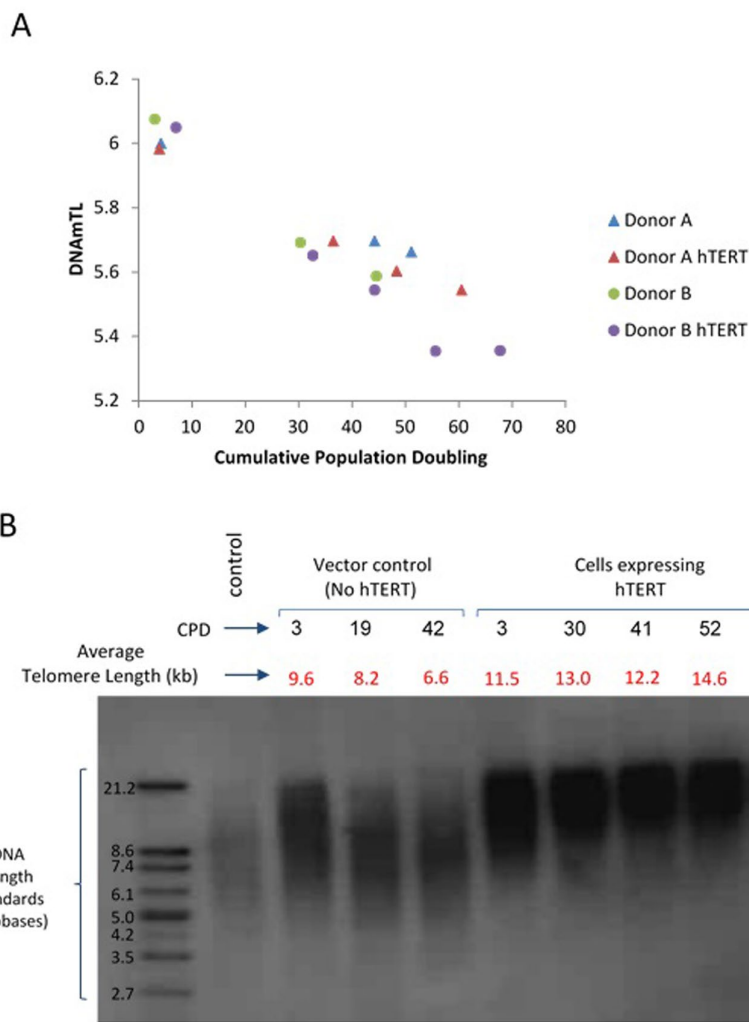
Figure 7. Application of DNAmTL on hTERT-transduced primary human fibroblasts. Panel (**A**) DNAmTL of primary neonatal fibroblasts without (Donor A and B) or with hTERT (Donor A hTERT and Donor B hTERT) transduction demonstrated linear and continued decrease in value regardless of hTERT status. This contrasts with average telomere length measurement by TRF southern blotting (Panel **B**), which revealed substantial increase in telomere length of primary neonatal fibroblasts that were transduced with hTERT-expression vector.

captures associations with features of human aging-related traits and behaviors, and b) to gain a better understanding of the biological meaning of such associations. Using independent test data, we show that DNAmTL exhibits moderately strong correlations with measured TL (based on Southern blotting or qPCR) in blood and adipose tissue of individuals of different racial groups.

Since leukocyte DNAmTL is based on accurate measurements of methylated CpG, it is possible that its associations with LTL-related traits might actually be more robust than mean LTL. Indeed, we found that DNAmTL outperformed LTL (based on Southern blotting or qPCR) in detecting association with age, sex,

ethnicity, lifestyle factors (diet, smoking, education, body mass index), and several clinical biomarkers (lipid levels, insulin). In addition, DNAmTL had a better predictive power than LTL for time-to-death and time-to coronary heart disease or heart failure. DNAmTL was also associated with physical functioning, age-at-menopause and diet (vegetable consumption, omega 3 intake) in the following direction: longer DNAmTL was associated with good health behavior and practices.

In addition to accurate measurement of methylated CpG, there might be another explanation for these associations and their biological meaning. Our studies in cultured cells with or without telomerase indicate that DNAmTL changes in function of cell replication

independently of telomere attrition. Hence DNAmTL might be a read-out of cellular proliferation. This would be consistent with the better ability of leukocyte DNAmTL than LTL to capture associations with human traits and exposures that likely increase the turnover of hematopoietic stem/progenitor cells (HSPCs), which is the main determinant of LTL shortening [42-44]. Given the wide inter-individual LTL variation at birth [45], at any age, LTL reflects not only the accruing number of HSPC replication but also LTL at birth. Moreover, HSPC do have some telomerase activity [46], which is likely variable across individuals; therefore, HSPC TL shortening per replication might differ across individuals. The joint effect of inter-individual variations in LTL at birth and the amount of LTL shortening per HSPC replication thereafter might confound the ability of LTL to serve as an index of HSPC replication. This, however, does not apply to DNAmTL, as it is independent of telomerase activity.

Our results demonstrate that DNAmTL provides an attractive alternative to measured average TL when it comes to predicting health outcomes. The superiority of DNAmTL over measured LTL when it comes to determining the effects of modifiable behavior (e.g., smoking, BMI), is clearly an important feature that make DNAmTL a useful tool in seeking behavioral interventions that support healthy aging. The view that DNAmTL captures biologically relevant variation is also supported by our study of blood cell counts where DNAmTLadjAge is more strongly related to widely used biomarkers of immune-senescence (naive and exhausted cytotoxic T cells) than is measured LTL.

Although the training data were based on leukocyte DNA methylation profiles, we show that DNAmTL is applicable to other tissues as well (e.g. liver, adipose, and sorted monocytes). The general applicability of DNAmTL is important, if it were to be a powerful and robust tool. Similar extrapolation of DNAmTL is seen with its applicability to the entire age-span, despite the fact that the training data were based on adults (22-94 years old).

Having outlined the strengths of the analyses, we wish to acknowledge several limitations and how they were mitigated. First, the training and validation data used in the development of DNAmTL differed in terms of the underlying ethnic composition. However, subsequent analyses demonstrated that DNAmTL applies to all groups – indicating yet again that DNAmTL has successfully captured the underlying biological principle associated with LTL. Second, the DNA methylation data and LTL measurements in the Framingham test data were collected at different time points as described above. Nevertheless, the conclusions

derived from those particular assessments were confirmed with analyses of a subset where both LTL measurements and DNAmTL were carried out with the same DNA samples. Importantly, we validated the significant correlation between DNAmTL and LTL in additional cohorts (Table 1). Third, our training data focused only on blood samples. We have demonstrated, however, that DNAmTL also applies to adipose and liver tissue, and we have also *in vitro* evidence that it also applies to keratinocytes and fibroblasts. It is to be noted that the unit of DNAmTL is retained as kilobases even though our in vitro studies demonstrate that its impressive correlation with TL notwithstanding, DNAmTL does not estimate actual telomere length. The preservation of the kilobase unit is purely on the basis that DNAmTL was trained using telomeres that are measured in these units.

While one of the 140 CpGs underlying DNAmTL is located near the TERT locus, it remains to be seen how these CpGs relate to telomere biology. The moderate enrichment of the DNAmTL CpGs within regions proximal to telomeres is consistent with previous reports of TL-associated changes in sub-telomeric methylation levels [26]. Our *cis*-mQTL study revealed 51 neighboring SNPs. Several of these SNPs are related to blood cell composition (e.g. granulocytes) and one SNP was found to be associated with bipolar disorder, which might be linked to LTL [47, 48].

We initiated this investigation, leveraging experience gained from our work with epigenetic clocks, [12, 14, 15, 17], which we have used in past research to demonstrate the difference between telomere attrition and epigenetic aging [49]. Our present findings support this conclusion. The epigenetic clocks and DNAmTL do not share CpGs and the respective genes proximal to their CpGs also do not seem to overlap in function. For example, the 140 CpGs underlying DNAmTL tend to be located near cadherin and cell signaling genes while other functional categories were implicated by epigenetic clocks. We find that DNAmTL is associated with the four epigenetic clocks in the expected way, which is that low values of DNAmTLadjAge correspond to high epigenetic age acceleration. Comparative analysis of 3 large cohorts revealed that DNAmTL is in general inferior to epigenetic clocks (especially DNAm GrimAge [17]) in predicting lifespan and other age-related traits. This is unsurprising as DNAm GrimAge was trained using lifespan data. The DNAmTL is nonetheless, an important epigenetic biomarker because it might provide a mechanistic link between cell replication and aging-related diseases and environmental exposures. Notwithstanding the clear difference between telomere-associated aging and epigenetic aging, there is a moderate level of

association between DNAmTL and epigenetic clocks, which is to be expected as they (directly or indirectly) relate to age-related DNAm changes, distinctiveness aside [50].

The successful transition of telomere-associated aging into a methylation-based assay allows one to use a single platform (e.g. the Illumina methylation array) to measure two distinct mechanisms of aging - epigenetic aging and telomere-associated aging.

Like epigenetic clocks, we expect that DNAmTL will become a useful biomarker in human interventional studies. A proof-of-concept study is provided by our preliminary analysis of omega-3 polyunsaturated fatty acid (PUFAs) supplementation. Several large-scale studies failed to detect convincing association between omega-3 PUFA supplementation and risk of cardiac death, sudden death, myocardial infarction, stroke, or all-cause mortality [51-53]. However, we find omega-3 intake to be positively correlated with DNAmTLadjAge (robust r=0.088 and P=4.4E-5) and with age-adjusted TRF-based LTL (robust r=0.085 and P=0.016, Supplementary Figure 15). Future randomized control-led trials should aim to validate these associations. Overall, we expect that DNAmTL will become an attractive molecular biomarker of aging due to its greater sensitivity to age related conditions than measured TL, its ease of use and robustness.

MATERIALS AND METHODS

Epidemiological cohorts

To establish DNAm-based telomere length in leukocytes we used N=2256 individuals from the WHI BA23 and JHS cohort in the training process and N=1078 individuals from the FHS cohort, WHI [54, 55], JHS [56] cohort in the test process, as listed in Table 1. More details of the study cohorts are described in Supplementary Note 1.

Our validation analyses involved N=9,785 Illumina Infinium 450k or EPIC 850k arrays measuring blood methylation levels in N=9,345 individuals from seven independent cohorts across nine studies: the FHS dataset (N=2,356), WHI BA23 (N=1,389), WHI EMPC (N=1972), JHS (N=209), InChianti (N=924 from 1 to 2 longitudinal measures on 484 individuals), Lothian Birth Cohort of 1921 (N=404) and 1946 (N=906), Twins UK (N=794) and Bogalusa Heart Study (N=831, Table 1, Supplementary Table 1, and Supple-mentary Note 1). All statistical analyses were adjusted for the correlation structure due to pedigree effects or repeated measurements as described below.

LTL measurements in training and test datasets

The same lab generated the LTL data across the 3 cohorts [25]. LTL was measured using Southern blots of the terminal restriction fragment length. After extraction, DNA was inspected for integrity, digested, resolved by gel electrophoresis, transferred to a membrane, hybridized with labeled probes and exposed to X-ray film using chemiluminescence, as previously described in [25]. The inter-assay coefficient of variation for blinded pair sets was 2.0% for the WHI, 1.4% for the JHS and 2.4% for the FHS [25].

Average telomere length measurement of *in vitro* cultured cells

DNA from primary human fibroblasts were extracted according to the protocol provided by Zymo Research (USA) using the mini-prep kit (Cat No: D4004). 1.5 micrograms of DNA were digested with Hinf I and RsaI prior to being resolved through a 0.8 % agarose gel. DNA was transferred to Hybond N+ nylon membrane by Southern transfer, after which it was baked for 20 minutes 120°C. The subsequent steps of this process are as described in the protocol provided by TeloTAGGG (Cat No:12209136001, Sigma Aldrich, USA). Chemiluminescence signal was captured using a Kodak Gel Documentation apparatus and quantified using Kodak quantification software. Average telomere length was ascertained using the formula described within the protocol provided.

Transduction of primary human fibroblasts with hTERT

Primary human fibroblasts were isolated from neonatal foreskin and transduced with hTERT using recombinant retroviruses according to methods previously described [49].

Estimation of surrogate DNAm based telomere length in leukocytes

We developed an estimate of LTL based only on DNA methylation levels. The estimate was established using the elastic net regression model implemented in the R package *glmnet* [51]. The elastic net regression model corresponds to a choice of 0.5 for the alpha parameter in the *glmnet* function. Ten-fold cross validation was performed in the (WHI and JHS) training data to specify the underlying tuning parameter λ. The final model was based on *lambda.1se*, i.e., the λ value that led to the minimum cross validated error within one standard error.

DNAmTL applied to different blood cell types

To evaluate how DNAmTL (and epigenetic clocks such as DNAmAge [12], and DNAmAgeSkinBlood [14]) differ across different blood cell types, we analyzed DNA methylation data from sorted blood cells from 6 men aged from 27 and 32 years old. DNA methylation profiles were generated from peripheral blood mononuclear cells (PBMC) and single cell types: CD4+T, CD8+T, and B cells were measured using the Illumina Infinium 450k platform.

DNA methylation data

The DNA methylation profiling was based on the Illumina Infinium HumanMethylation450K BeadChip in the FHS and WHI cohort and was based on the Illumina Infinium EPIC 850K BeadChip in the JHS cohort. To ensure future use with EPIC arrays, we focused on the subset of 450,161 CpGs that were present on both platforms. We kept the original normalization methods to ensure consistency with previous publications. The WHI BA23 were normalized using the background correction method implemented in the software *GenomeStudio*. WHI EMPC were normalized based on BMIQ [57] for beta-mixture quantile normalization. The JHS data were normalized using the "noob" normalization method implemented in the *minfi* R package [58, 59].

Statistical models used in validation analysis

Our validation analysis involved several regression models. Cox regression for various censored outcomes such as time to death (all-cause mortality), time-to-CHD, time-to-CHF, and time to any cancer. Multivariate linear regression for our DNAm based measures (independent variable) associated with and number of age-related conditions (dependent variable) and physical function score, respectively. Linear regression was used to relate age at menopause (independent variable) with DNAmTL. Logistic regression analysis for binary outcomes allowing us to estimate odds ratios for the binary variables such as cancer status, hypertension, type 2 diabetes, and disease-free status. The multimorbidity index was defined as the number of age-related conditions including arthritis, cataract, cancer, CHD, CHF, emphysema, glaucoma, lipid condition, osteoporosis, type 2 diabetes (see Supplementary Note 1). In our validation analysis, we used the age-adjusted variable, DNAmTLadjAge, which is not correlated with chronological age. All regression models included the following covariates: chronological age, sex, and batch effect as needed. To avoid bias due to familial correlations from pedigrees in the FHS cohort or intra-

subject correlations resulting from repeated measurements, we used the following techniques. For censored time variables, we used robust standard errors, the Huber sandwich estimator, implemented in the R function "*coxph*". We used linear mixed models with a random intercept term, implemented in the R function "*lme*". We used generalized estimation equation models (GEE), implemented in the *gee* function, for our logistic regression models. Additional covariates related to demographic characteristics, psychosocial behaviors and clinical covariates were adjusted in multivariate Cox models analysis. Those additional covariates include BMI, educational attainment (category), alcohol consumption (gram/day), self-reported smoking pack-years, three medical covariates: status of (any) cancer, hypertension and type 2 diabetes at baseline. BMI was categorized into 3 groups: 18.5 -24.9 (normal), b) 25 to 29.9 (overweight), and c) >=30 (obese). The categories associated with educational attainment were a) less than high school, b) high school degree, c) some college, and d) college degree and above. Smoking pack-years and educational variables were not available in the JHS cohort. Smoking status (never, former and current) was used in the analysis of the JHS cohort. Our stratified analysis was conducted in strata defined by age (<65 versus ≥ 65 years), BMI, education, prior history of hypertension, type 2 diabetes or cancer. All models used in the stratified analysis adjusted for age, sex, and (possibly) batch effect.

Meta-analysis

We mainly used fixed effects meta-analysis models weighted by inverse variance to combine the results across validation study sets into a single estimate. Toward this end, we used the *metafor* R function. Alternatively, we used Stouffer's meta-analysis method (weighted by the square root of sample size) to combine results for variables whose scale/definition differed across study sets, e.g. multimorbidity (number of age-related conditions), disease-free status and physical function scores.

Cox models that include blood cell counts

We also fit multivariate Cox regression models that adjusted for imputed blood cell counts in addition to chronological age, batch, and pedigree structure, for predicting time-to-death and time-to-CHD. The blood cell counts were imputed based on DNA methylation levels as described elsewhere [60, 61]. To avoid multi-collinearities between blood cell counts, we only included the following seven blood cell counts into the multivariate model: naïve CD8+T, exhausted cytotoxic CD8+ T cells, plasma blasts, CD4+T, natural killer cells, monocytes and granulocytes.

Heritability analysis

In general, DNAm based biomarkers are highly heritable [19, 62, 63]. To evaluate whether DNAmTLadjAge is heritable as well, we estimated the narrow sense heritability h^2 using the polygenic models defined in SOLAR and its R interface solarius [64]. Heritability is defined as the total proportion of phenotypic variance attributable to genetic variation in the polygenic model. The quantitative trait DNAmTL was adjusted for both age and sex. The robust polygenic model (with the option of a t-distribution) was used to estimate heritability. The heritability estimate corresponds to the variance component associated with the kinship coefficient. We used all individuals from the FHS cohort for whom DNA methylation data were available (irrespective of the availability of the observed LTL measure).

SNP associations of DNAmTL

We performed 14 SNP associations across 10 distinct susceptibility loci associated with LTL reported from three large-scale studies: (I) meta-analysis association of LTL in chromosome 5 *TERT* only (N=53,724) [36], (II) a genome-wide meta-analysis of LTL (N=37,684) [37], or (III) a genome-wide meta-analysis of LTL (N=26,089) [38]. SNP associations were performed for DNAmTLadjAge and LTLadjAge respectively, using the individuals of the FHS cohort available for both measures (N=811). The association analysis was based on linear mixed models whose random covariance matrix was determined by kinship coefficients of the pedigree structure, adjusted for sex and three principal components as fixed effects. We conducted the association tests using the function "relmatLmer" from the R library "lme4qt".

LTL measures versus blood cell composition

The imputed blood cell abundance measures were related to TRF based and DNAm based LTL measures, using the training datasets from the WHI BA23 and the JHS cohort and the test dataset from the FHS cohort, involving n=3,134 individuals. The following imputed blood cell counts were analyzed: B cell, naïve CD4+ T, CD4+ T, naïve CD8+ T, CD8+ T, exhausted cytotoxic CD8+ T cells (defined as CD8 positive CD28 negative CD45R negative), plasma blasts, natural killer cells, monocytes, and granulocytes. The blood cell composition imputation of the naive T cells, exhausted T cells, and plasma blasts was based on the Horvath method [65]. The remaining cell types were imputed using the Houseman method [61]. More details are described in Supplementary Methods. To avoid confounded by age, we used the age-adjusted DNAmTL

(DNAmTLadjAge) variable for analysis. The correlation results were combined across studies via the same fixed effects meta-analysis model.

GREAT analysis

We applied the GREAT analysis software tool to three sets of CpGs: (1) all the 140 CpGs underlying DNAmTL model, (2) the 72 CpGs with negative coefficients in the model, and (3) the other 68 CpGs with positive coefficients in the model. CpGs in non-coding regions typically lack annotation with respect to biological functions. GREAT assigns biological meaning to a set of non-coding genomic regions (implicated by the CpGs) by analyzing the annotations of the nearby genes. Toward this end, the GREAT software performs both a binomial test (over genomic regions) and a hypergeometric test over genes when using a whole genome background. We performed the enrichment based on default settings (Proximal: 5.0 kb upstream, 1.0 kb downstream, plus Distal: up to 1,000 kb) for gene sets associated with GO terms, MSigDB, PANTHER, KEGG and InterPro pathway. To avoid large numbers of multiple comparisons, we restricted the analysis to the gene sets with between 5 and 3,000 genes. We report nominal P values and two adjustments for multiple comparisons: Bonferroni correction and the Benjamini-Hochberg false discovery rate.

Diet and lifestyle factors

We performed a robust correlation analysis (biweight midcorrelation, bicor) or generalized linear regression analysis between DNAmTLadjAge and 43 variables including 15 self-reported dietary variables, 9 dietary biomarkers, 14 variables related to metabolic related traits and central adiposity, and 5 life style factors, using the FHS, WHI, LBC 1921 and/or LBC 1936 cohort (N up to 6977), as listed in the first two columns in Figure 5. In the FHS cohort, we conducted the robust correlation analysis in males and females, respectively. Next we combined the results via fixed effect models weighted by inverse variance. In the FHS cohort, we used linear mixed effects models to account for pedigree structure. In the WHI cohort, we conducted the robust correlation analysis in each ethnic group separately. Next we combined the results via fixed effects meta-analysis models. In the LBC cohorts, we performed generalized linear regression analysis adjusted for sex for the 1921 and 1936 follow-up, respectively. Most of the final results were combined based on the Stouffer's method weighted by the square root of sample size across the study cohorts. A few variables that were only available in both FHS and WHI cohort and presented in the same scaling of effect sizes were combined based on the fixed effect models

weighted by inverse variance. In the FHS cohort, the diet and the clinical variables were based on the datasets archived in dbGAP pht002350.v4.p10 and pht000742.v5.p10, respectively. Both datasets were collected at exam 8, aligned with the blood drawn for DNA methylation profiles. In the WHI cohort, blood biomarkers were measured from fasting plasma collected at baseline. Food groups and nutrients are inclusive, including all types and all preparation methods, e.g. folic acid includes synthetic and natural, and dairy includes cheese and all types of milk. The individual variables are explained in [66].

Interrogating smoking impact on telomere length in blood

We used the 4,039 subjects across seven studies from our validation cohorts to compare the smoking association with (1) DNAm TL and with (2) measured LTL. Multivariate linear regression analysis of telomere length on smoking was performed on each study, adjusted for chronological age and adjusted sex, ethnicity and pedigree effects as needed. Smoking information was based on pack years when available (N=2216) otherwise based on a binary variable (never smokers versus ever smokers). The Stouffer's method weighted by square root of sample size was performed to combine the results across all studies. Fixed effect models weighted by inverse variance were applied to the studies with pack years information and the other studies only with the binary smoking variable, respectively.

Enrichment analysis of CpGs in DNAmTL near telomeres

We performed hypergeometric analysis for evaluating the overlap between the 140 CpGs comprising our DNAm TL model and the CpGs nearby telomere regions from 3 mega base (Mb) at each chromosome tail. In the hypergeometric test, the margin for the total number of CpGs across whole genome was based on 453093 CpGs present in both 450k and Epic arrays. We also performed sensitivity analysis based on a variety of regions thresholded at 2, 4, 6 and 8 Mb respectively.

Enrichment analysis of CpGs in DNAmTL annotated with DNA methylation quantitative trait locus (mQTL), conducted in McRae et al. [35]. The hypergeometric test was used to evaluate the overlap of the 140 CpGs with 52915 cis-mQTL. The mQTL CpGs were identified using a stringent criterion described in the original reference: a cis-mQTL was identified either in the

Brisbane Systems Genetics Study or in the Lothian Birth Cohorts at P < 1.0E-11 and was replicated in the other cohort at P < 1.0E-6.

The resulting 51 SNPs underlying cis-mQTL loci were cross referenced to GWAS Catalog tool (version v1.02 database, see URL). We not only report SNPs that met genome-wide (P < 5.0E-8) significance levels but also suggestive significance (P< 5.0E-6). Similarly, we characterized the 51 SNP using the HaploReg (version 4.1) tool [67] (see URL) which allows one to visualize SNPs in linkage disequilibrium (LD $r^2 \geq 0.8$ based on European ancestry).

In vitro cultured cell procedure

Isolation and culture of primary cells
Primary human neonatal fibroblasts were isolated from circumcised foreskins. Informed consent was obtained prior to collection of human skin samples with approval from the Oxford Research Ethics Committee; reference 10/H0605/1. The tissue was cut into small pieces and digested overnight at 4 °C with 0.5 mg/ml Liberase DH in CnT-07 keratinocyte medium (CellnTech) supplemented with penicillin/streptomycin (Sigma) and gentamycin/amphotericin (Life Tech). Following digestion, the epidermis was peeled off from the tissue pieces. The de-epidermized tissue pieces were placed faced down on plastic cell culture plates and allowed to partially dry before addition of DMEM supplemented with 10% FBS and antibiotics. After several days incubation in a 37 °C, 5% CO_2 humidified environment, fibroblasts can be seen to migrate out from the tissue pieces and when their growth reached confluence, they were trypsinized, counted and seeded into fresh plates for experiments. Adult human coronary artery endothelial cells (HCAEC) were purchased from Cell Applications (USA) and cultured in MesoEndo Cell Growth Medium (Sigma) at 37 °C humidified incubator with 5% CO_2.

Neonatal foreskin fibroblasts
100,000 cells were seeded into a 10cm plate and cultured as described above. Upon confluence the cells were harvested with trypsin digestion followed by neutralization with soybean trypsin inhibitor. The number of cells was ascertained and 100,000 was taken and seeded into a fresh plate. The remaining cells were used for DNA extraction. Population doubling was calculated with the following formula: [log(number of cells harvested) − log(number of cells seeded)] x 3.32. Cumulative population doubling was obtained by addition of population doubling of each passage.

Adult human coronary artery endothelial cells

500,000 cells were seeded into a fibronectin-coated 75cm^2 flask and cultured as described. The procedure of passing the cells, counting and ascertaining population doubling is similar to those described for neonatal foreskin fibroblasts above.

Retroviral-mediated transduction of cells with hTERT vectors

Retroviral vectors bearing wildtype hTERT (Addgene, cat. 1774), was transfected into Phoenix A cells using the calcium chloride method according to the manufacturer's instructions (Profection Cat No: E1200 Promega). The next day, media were removed from the transfectants and replaced with DMEM supplemented with 10% foetal calf serum. The following day, the media containing recombinant retroviruses were collected, filtered through 0.45micron filter and mixed with polybrene (Sigma) up to 9ug/ml and used to feed the cells intended for infection. The next day, fresh media containing puromycin (1ug/ml) was given to the cells. After 3-4 days when all the control cells in the uninfected plates were dead, the surviving infectants were grown and used for experiments as described above.

DNA extraction in the in vitro experiments

DNA was extracted from cells using the Zymo Quick DNA mini-prep plus kit (D4069) according to the manufacturer's instructions and DNA methylation levels were measured on Illumina 850 EPIC arrays according to the manufacturer's instructions.

URLs

GWASCatalog,
https://www.ebi.ac.uk/gwas/search?query=28346442
HaploReg,
http://www.broadinstitute.org/mammals/haploreg/haploreg.php

AUTHOR CONTRIBUTIONS

ATL and SH developed the DNAm based LTL and conceived of the study. ATL carried out most of the statistical analyses. AS, PCT, DS, and AQ carried out study-specific statistical analyses. KR carried out the in vitro cell culture experiments. The remaining authors contributed data and statistical analyses, helped with the write up, and participated in the interpretation of the results.

CONFLICTS OF INTEREST

The authors declare no conflicts of interest.

REFERENCES

1. Nordfjäll K, Svenson U, Norrback KF, Adolfsson R, Roos G. Large-scale parent-child comparison confirms a strong paternal influence on telomere length. Eur J Hum Genet. 2010; 18:385–89.
https://doi.org/10.1038/ejhg.2009.178
PMID:19826452

2. Daniali L, Benetos A, Susser E, Kark JD, Labat C, Kimura M, Desai K, Granick M, Aviv A. Telomeres shorten at equivalent rates in somatic tissues of adults. Nat Commun. 2013; 4:1597.
https://doi.org/10.1038/ncomms2602
PMID:23511462

3. Epel ES, Blackburn EH, Lin J, Dhabhar FS, Adler NE, Morrow JD, Cawthon RM. Accelerated telomere shortening in response to life stress. Proc Natl Acad Sci USA. 2004; 101:17312–15.
https://doi.org/10.1073/pnas.0407162101
PMID:15574496

4. Fitzpatrick AL, Kronmal RA, Gardner JP, Psaty BM, Jenny NS, Tracy RP, Walston J, Kimura M, Aviv A. Leukocyte telomere length and cardiovascular disease in the cardiovascular health study. Am J Epidemiol. 2007; 165:14–21.
https://doi.org/10.1093/aje/kwj346 PMID:17043079

5. Willeit P, Willeit J, Brandstätter A, Ehrlenbach S, Mayr A, Gasperi A, Weger S, Oberhollenzer F, Reindl M, Kronenberg F, Kiechl S. Cellular aging reflected by leukocyte telomere length predicts advanced atherosclerosis and cardiovascular disease risk. Arterioscler Thromb Vasc Biol. 2010; 30:1649–56.
https://doi.org/10.1161/ATVBAHA.110.205492
PMID:20508208

6. Mather KA, Jorm AF, Parslow RA, Christensen H. Is telomere length a biomarker of aging? A review. J Gerontol A Biol Sci Med Sci. 2011; 66:202–13.
https://doi.org/10.1093/gerona/glq180
PMID:21030466

7. Needham BL, Rehkopf D, Adler N, Gregorich S, Lin J, Blackburn EH, Epel ES. Leukocyte telomere length and mortality in the National Health and Nutrition Examination Survey, 1999-2002. Epidemiology. 2015; 26:528–35.
https://doi.org/10.1097/EDE.0000000000000299
PMID:26039272

8. Chen BH, Carty CL, Kimura M, Kark JD, Chen W, Li S, Zhang T, Kooperberg C, Levy D, Assimes T, Absher D, Horvath S, Reiner AP, Aviv A. Leukocyte telomere length, T cell composition and DNA methylation age. Aging (Albany NY). 2017; 9:1983–95.
https://doi.org/10.18632/aging.101293
PMID:28930701

9. Jylhävä J, Pedersen NL, Hägg S. Biological Age Predictors. EBioMedicine. 2017; 21:29–36.
https://doi.org/10.1016/j.ebiom.2017.03.046
PMID:28396265

10. Aviv A, Shay JW. Reflections on telomere dynamics and ageing-related diseases in humans. Philos Trans R Soc Lond B Biol Sci. 2018; 373:20160436.
https://doi.org/10.1098/rstb.2016.0436
PMID:29335375

11. Hannum G, Guinney J, Zhao L, Zhang L, Hughes G, Sadda S, Klotzle B, Bibikova M, Fan JB, Gao Y, Deconde R, Chen M, Rajapakse I, et al. Genome-wide methylation profiles reveal quantitative views of human aging rates. Mol Cell. 2013; 49:359–67.
https://doi.org/10.1016/j.molcel.2012.10.016
PMID:23177740

12. Horvath S. DNA methylation age of human tissues and cell types. Genome Biol. 2013; 14:R115.
https://doi.org/10.1186/gb-2013-14-10-r115
PMID:24138928

13. Lin Q, Weidner CI, Costa IG, Marioni RE, Ferreira MR,

Deary IJ, Wagner W. DNA methylation levels at individual age-associated CpG sites can be indicative for life expectancy. Aging (Albany NY). 2016; 8:394–401. https://doi.org/10.18632/aging.100908 PMID:26928272

14. Horvath S, Oshima J, Martin GM, Lu AT, Quach A, Cohen H, Felton S, Matsuyama M, Lowe D, Kabacik S, Wilson JG, Reiner AP, Maierhofer A, et al. Epigenetic clock for skin and blood cells applied to Hutchinson Gilford Progeria Syndrome and *ex vivo* studies. Aging (Albany NY). 2018; 10:1758–75. https://doi.org/10.18632/aging.101508 PMID:30048243

15. Levine ME, Lu AT, Quach A, Chen BH, Assimes TL, Bandinelli S, Hou L, Baccarelli AA, Stewart JD, Li Y, Whitsel EA, Wilson JG, Reiner AP, et al. An epigenetic biomarker of aging for lifespan and healthspan. Aging (Albany NY). 2018; 10:573–91. https://doi.org/10.18632/aging.101414 PMID:29676998

16. Horvath S, Raj K. DNA methylation-based biomarkers and the epigenetic clock theory of ageing. Nat Rev Genet. 2018; 19:371–84. https://doi.org/10.1038/s41576-018-0004-3 PMID:29643443

17. Lu AT, Quach A, Wilson JG, Reiner AP, Aviv A, Raj K, Hou L, Baccarelli AA, Li Y, Stewart JD, Whitsel EA, Assimes TL, Ferrucci L, Horvath S. DNA methylation GrimAge strongly predicts lifespan and healthspan. Aging (Albany NY). 2019; 11:303–27. https://doi.org/10.18632/aging.101684 PMID:30669119

18. Breitling LP, Saum K-U, Perna L, Schöttker B, Holleczek B, Brenner H. Frailty is associated with the epigenetic clock but not with telomere length in a German cohort. Clin Epigenetics. 2016; 8: 21. https://doi.org/10.1186/s13148-016-0186-5 PMID: 26925173

19. Lu AT, Xue L, Salfati EL, Chen BH, Ferrucci L, Levy D, Joehanes R, Murabito JM, Kiel DP, Tsai PC, Yet I, Bell JT, Mangino M, et al. GWAS of epigenetic aging rates in blood reveals a critical role for TERT. Nat Commun. 2018; 9:387. https://doi.org/10.1038/s41467-017-02697-5 PMID:29374233

20. Marioni RE, Harris SE, Shah S, McRae AF, von Zglinicki T, Martin-Ruiz C, Wray NR, Visscher PM, Deary IJ. The epigenetic clock and telomere length are independently associated with chronological age and mortality. Int J Epidemiol. 2016; 45:424–32. https://doi.org/10.1093/ije/dyw041 PMID:27075770

21. BLUEPRINT consortium. Quantitative comparison of DNA methylation assays for biomarker development

and clinical applications. Nat Biotechnol. 2016; 34:726–37. https://doi.org/10.1038/nbt.3605 PMID:27347756

22. Denham J, Marques FZ, Charchar FJ. Leukocyte telomere length variation due to DNA extraction method. BMC Res Notes. 2014; 7:877. https://doi.org/10.1186/1756-0500-7-877 PMID:25475541

23. Verhulst S, Susser E, Factor-Litvak PR, Simons MJ, Benetos A, Steenstrup T, Kark JD, Aviv A. Commentary: the reliability of telomere length measurements. Int J Epidemiol. 2015; 44:1683–86. https://doi.org/10.1093/ije/dyv166 PMID:26403812

24. Tolios A, Teupser D, Holdt LM. Preanalytical Conditions and DNA Isolation Methods Affect Telomere Length Quantification in Whole Blood. PLoS One. 2015; 10:e0143889. https://doi.org/10.1371/journal.pone.0143889 PMID:26636575

25. Kimura M, Stone RC, Hunt SC, Skurnick J, Lu X, Cao X, Harley CB, Aviv A. Measurement of telomere length by the Southern blot analysis of terminal restriction fragment lengths. Nat Protoc. 2010; 5:1596–607. https://doi.org/10.1038/nprot.2010.124 PMID:21085125

26. Hu H, Li B, Duan S. The Alteration of Subtelomeric DNA Methylation in Aging-Related Diseases. Front Genet. 2019; 9:697. https://doi.org/10.3389/fgene.2018.00697 PMID:30687384

27. Grundberg E, Meduri E, Sandling JK, Hedman AK, Keildson S, Buil A, Busche S, Yuan W, Nisbet J, Sekowska M, Wilk A, Barrett A, Small KS, et al, and Multiple Tissue Human Expression Resource Consortium. Global analysis of DNA methylation variation in adipose tissue from twins reveals links to disease-associated variants in distal regulatory elements. Am J Hum Genet. 2013; 93:876–90. https://doi.org/10.1016/j.ajhg.2013.10.004 PMID:24183450

28. Horvath S, Erhart W, Brosch M, Ammerpohl O, von Schönfels W, Ahrens M, Heits N, Bell JT, Tsai PC, Spector TD, Deloukas P, Siebert R, Sipos B, et al. Obesity accelerates epigenetic aging of human liver. Proc Natl Acad Sci USA. 2014; 111:15538–43. https://doi.org/10.1073/pnas.1412759111 PMID:25313081

29. Ahrens M, Ammerpohl O, von Schönfels W, Kolarova J, Bens S, Itzel T, Teufel A, Herrmann A, Brosch M, Hinrichsen H, Erhart W, Egberts J, Sipos B, et al. DNA methylation analysis in nonalcoholic fatty liver disease suggests distinct disease-specific and

remodeling signatures after bariatric surgery. Cell Metab. 2013; 18:296–302. https://doi.org/10.1016/j.cmet.2013.07.004 PMID:23931760

30. Reynolds LM, Taylor JR, Ding J, Lohman K, Johnson C, Siscovick D, Burke G, Post W, Shea S, Jacobs DR Jr, Stunnenberg H, Kritchevsky SB, Hoeschele I, et al. Age-related variations in the methylome associated with gene expression in human monocytes and T cells. Nat Commun. 2014; 5:5366. https://doi.org/10.1038/ncomms6366 PMID:25404168

31. Zou H, Hastie T. Regularization and variable selection via the elastic net. J R Stat Soc Series B Stat Methodol. 2005; 67:301–20. https://doi.org/10.1111/j.1467-9868.2005.00503.x

32. Dalgård C, Benetos A, Verhulst S, Labat C, Kark JD, Christensen K, Kimura M, Kyvik KO, Aviv A. Leukocyte telomere length dynamics in women and men: menopause vs age effects. Int J Epidemiol. 2015; 44:1688–95. https://doi.org/10.1093/ije/dyv165 PMID:26385867

33. Hunt SC, Chen W, Gardner JP, Kimura M, Srinivasan SR, Eckfeldt JH, Berenson GS, Aviv A. Leukocyte telomeres are longer in African Americans than in whites: the National Heart, Lung, and Blood Institute Family Heart Study and the Bogalusa Heart Study. Aging Cell. 2008; 7:451–58. https://doi.org/10.1111/j.1474-9726.2008.00397.x PMID:18462274

34. Levine ME, Lu AT, Chen BH, Hernandez DG, Singleton AB, Ferrucci L, Bandinelli S, Salfati E, Manson JE, Quach A, Kusters CD, Kuh D, Wong A, et al. Menopause accelerates biological aging. Proc Natl Acad Sci USA. 2016; 113:9327–32. https://doi.org/10.1073/pnas.1604558113 PMID:27457926

35. McRae AF, Marioni RE, Shah S, Yang J, Powell JE, Harris SE, Gibson J, Henders AK, Bowdler L, Painter JN, Murphy L, Martin NG, Starr JM, et al. Identification of 55,000 Replicated DNA Methylation QTL. Sci Rep. 2018; 8:17605. https://doi.org/10.1038/s41598-018-35871-w PMID:30514905

36. Bojesen SE, Pooley KA, Johnatty SE, Beesley J, Michailidou K, Tyrer JP, Edwards SL, Pickett HA, Shen HC, Smart CE, Hillman KM, Mai PL, Lawrenson K, et al, and Australian Cancer Study, and Australian Ovarian Cancer Study, and Kathleen Cuningham Foundation Consortium for Research into Familial Breast Cancer (kConFab), and Gene Environment Interaction and Breast Cancer (GENICA), and Swedish Breast Cancer Study (SWE-BRCA), and Hereditary Breast and Ovarian Cancer Research Group Netherlands (HEBON), and Epidemiological study of BRCA1 & BRCA2 Mutation Carriers (EMBRACE), and Genetic Modifiers of Cancer Risk in BRCA1/2 Mutation Carriers (GEMO). Multiple independent variants at the TERT locus are associated with telomere length and risks of breast and ovarian cancer. Nat Genet. 2013; 45:371–84, e1–2. https://doi.org/10.1038/ng.2566 PMID:23535731

37. Codd V, Nelson CP, Albrecht E, Mangino M, Deelen J, Buxton JL, Hottenga JJ, Fischer K, Esko T, Surakka I, Broer L, Nyholt DR, Mateo Leach I, et al, and CARDIoGRAM consortium. Identification of seven loci affecting mean telomere length and their association with disease. Nat Genet. 2013; 45:422–27, e1–2. https://doi.org/10.1038/ng.2528 PMID:23535734

38. Pooley KA, Bojesen SE, Weischer M, Nielsen SF, Thompson D, Amin Al Olama A, Michailidou K, Tyrer JP, Benlloch S, Brown J, Audley T, Luben R, Khaw KT, et al. A genome-wide association scan (GWAS) for mean telomere length within the COGS project: identified loci show little association with hormone-related cancer risk. Hum Mol Genet. 2013; 22:5056–64. https://doi.org/10.1093/hmg/ddt355 PMID:23900074

39. Steenstrup T, Hjelmborg JVB, Mortensen LH, Kimura M, Christensen K, Aviv A. Leukocyte telomere dynamics in the elderly. Eur J Epidemiol. 2013; 28: 181-87. https://doi.org/10.1007/s10654-013-9780-4 PMID: 23430034

40. Chen W, Kimura M, Kim S, Cao X, Srinivasan SR, Berenson GS, Kark JD, Aviv A. Longitudinal versus cross-sectional evaluations of leukocyte telomere length dynamics: age-dependent telomere shortening is the rule. J Gerontol A Biol Sci Med Sci. 2011; 66:312–19. https://doi.org/10.1093/gerona/glq223 PMID:21310811

41. Steenstrup T, Hjelmborg JV, Kark JD, Christensen K, Aviv A. The telomere lengthening conundrum--artifact or biology? Nucleic Acids Res. 2013; 41:e131. https://doi.org/10.1093/nar/gkt370 PMID:23671336

42. Sidorov I, Kimura M, Yashin A, Aviv A. Leukocyte telomere dynamics and human hematopoietic stem cell kinetics during somatic growth. Exp Hematol. 2009; 37:514–24. https://doi.org/10.1016/j.exphem.2008.11.009 PMID:19216021

43. Shepherd BE, Guttorp P, Lansdorp PM, Abkowitz JL. Estimating human hematopoietic stem cell kinetics using granulocyte telomere lengths. Exp Hematol. 2004; 32:1040–50.

https://doi.org/10.1016/j.exphem.2004.07.023
PMID:15539081

44. Kimura M, Gazitt Y, Cao X, Zhao X, Lansdorp PM, Aviv A. Synchrony of telomere length among hemato-poietic cells. Exp Hematol. 2010; 38:854–59. https://doi.org/10.1016/j.exphem.2010.06.010 PMID:20600576

45. Factor-Litvak P, Susser E, Kezios K, McKeague I, Kark JD, Hoffman M, Kimura M, Wapner R, Aviv A. Leukocyte Telomere Length in Newborns: Implications for the Role of Telomeres in Human Disease. Pediatrics. 2016; 137:e20153927. https://doi.org/10.1542/peds.2015-3927 PMID:26969272

46. Lansdorp PM. Role of telomerase in hematopoietic stem cells. Ann N Y Acad Sci. 2005; 1044:220–27. https://doi.org/10.1196/annals.1349.027 PMID:15958715

47. Huang YC, Wang LJ, Tseng PT, Hung CF, Lin PY. Leukocyte telomere length in patients with bipolar disorder: an updated meta-analysis and subgroup analysis by mood status. Psychiatry Res. 2018; 270:41–49. https://doi.org/10.1016/j.psychres.2018.09.035 PMID:30243131

48. Powell TR, Dima D, Frangou S, Breen G. Telomere Length and Bipolar Disorder. Neuropsychopharmacology. 2018; 43:445–53. https://doi.org/10.1038/npp.2017.125 PMID:28621334

49. Kabacik S, Horvath S, Cohen H, Raj K. Epigenetic ageing is distinct from senescence-mediated ageing and is not prevented by telomerase expression. Aging (Albany NY). 2018; 10:2800–15. https://doi.org/10.18632/aging.101588 PMID:30332397

50. Vetter VM, Meyer A, Karbasiyan M, Steinhagen-Thiessen E, Hopfenmüller W, Demuth I. Epigenetic Clock and Relative Telomere Length Represent Largely Different Aspects of Aging in the Berlin Aging Study II (BASE-II). J Gerontol A Biol Sci Med Sci. 2019; 74:27–32. https://doi.org/10.1093/gerona/gly184 PMID:30137208

51. Rizos EC, Ntzani EE, Bika E, Kostapanos MS, Elisaf MS. Association between omega-3 fatty acid supplementation and risk of major cardiovascular disease events: a systematic review and meta-analysis. JAMA. 2012; 308:1024–33. https://doi.org/10.1001/2012.jama.11374 PMID:22968891

52. Aung T, Halsey J, Kromhout D, Gerstein HC, Marchioli R, Tavazzi L, Geleijnse JM, Rauch B, Ness A, Galan P, Chew EY, Bosch J, Collins R, et al, and Omega-3 Treatment Trialists' Collaboration. Associations of Omega-3 Fatty Acid Supplement Use With Cardiovascular Disease Risks: Meta-analysis of 10 Trials Involving 77 917 Individuals. JAMA Cardiol. 2018; 3:225–34. https://doi.org/10.1001/jamacardio.2017.5205 PMID:29387889

53. Rizos EC, Elisaf MS. Does Supplementation with Omega-3 PUFAs Add to the Prevention of Cardiovascular Disease? Curr Cardiol Rep. 2017; 19:47. https://doi.org/10.1007/s11886-017-0856-8 PMID:28432658

54. Anonymous A, and The Women's Health Initiative Study Group. Design of the Women's Health Initiative clinical trial and observational study. Control Clin Trials. 1998; 19:61–109. https://doi.org/10.1016/S0197-2456(97)00078-0 PMID:9492970

55. Anderson GL, Manson J, Wallace R, Lund B, Hall D, Davis S, Shumaker S, Wang CY, Stein E, Prentice RL. Implementation of the women's health initiative study design. Ann Epidemiol. 2003 (Suppl 9); 13:S5–17. https://doi.org/10.1016/S1047-2797(03)00043-7 PMID:14575938

56. Taylor HA Jr, Wilson JG, Jones DW, Sarpong DF, Srinivasan A, Garrison RJ, Nelson C, Wyatt SB. Toward resolution of cardiovascular health disparities in African Americans: design and methods of the Jackson Heart Study. Ethn Dis. 2005 (Suppl 6); 15:S6–4, 17. PMID:16320381

57. Teschendorff AE, Marabita F, Lechner M, Bartlett T, Tegner J, Gomez-Cabrero D, Beck S. A beta-mixture quantile normalization method for correcting probe design bias in Illumina Infinium 450 k DNA methylation data. Bioinformatics. 2013; 29:189–96. https://doi.org/10.1093/bioinformatics/bts680 PMID:23175756

58. Triche TJ Jr, Weisenberger DJ, Van Den Berg D, Laird PW, Siegmund KD. Low-level processing of Illumina Infinium DNA Methylation BeadArrays. Nucleic Acids Res. 2013; 41:e90–90. https://doi.org/10.1093/nar/gkt090 PMID:23476028

59. Fortin JP, Triche TJ Jr, Hansen KD. Preprocessing, normalization and integration of the Illumina HumanMethylationEPIC array with minfi. Bioinformatics. 2017; 33:558–60. https://doi.org/10.1093/bioinformatics/btw691 PMID:28035024

60. Horvath S, Gurven M, Levine ME, Trumble BC, Kaplan H, Allayee H, Ritz BR, Chen B, Lu AT, Rickabaugh TM, Jamieson BD, Sun D, Li S, et al. An epigenetic clock

analysis of race/ethnicity, sex, and coronary heart disease. Genome Biol. 2016; 17:171. https://doi.org/10.1186/s13059-016-1030-0 PMID:27511193

61. Houseman EA, Accomando WP, Koestler DC, Christensen BC, Marsit CJ, Nelson HH, Wiencke JK, Kelsey KT. DNA methylation arrays as surrogate measures of cell mixture distribution. BMC Bioinformatics. 2012; 13:86. https://doi.org/10.1186/1471-2105-13-86 PMID:22568884

62. Lu AT, Hannon E, Levine ME, Crimmins EM, Lunnon K, Mill J, Geschwind DH, Horvath S. Genetic architecture of epigenetic and neuronal ageing rates in human brain regions. Nat Commun. 2017; 8:15353. https://doi.org/10.1038/ncomms15353 PMID:28516910

63. Lu AT, Hannon E, Levine ME, Hao K, Crimmins EM, Lunnon K, Kozlenkov A, Mill J, Dracheva S, Horvath S. Genetic variants near MLST8 and DHX57 affect the epigenetic age of the cerebellum. Nat Commun. 2016; 7:10561. https://doi.org/10.1038/ncomms10561 PMID:26830004

64. Ziyatdinov A, Brunel H, Martinez-Perez A, Buil A, Perera A, Soria JM. solarius: an R interface to SOLAR for variance component analysis in pedigrees. Bioinformatics. 2016; 32:1901–02. https://doi.org/10.1093/bioinformatics/btw080 PMID:27153684

65. Horvath S, Levine AJ. HIV-1 infection accelerates age according to the epigenetic clock. J Infect Dis. 2015; 212:1563–73. https://doi.org/10.1093/infdis/jiv277 PMID:25969563

66. Quach A, Levine ME, Tanaka T, Lu AT, Chen BH, Ferrucci L, Ritz B, Bandinelli S, Neuhouser ML, Beasley JM, Snetselaar L, Wallace RB, Tsao PS, et al. Epigenetic clock analysis of diet, exercise, education, and lifestyle factors. Aging (Albany NY). 2017; 9:419–46. https://doi.org/10.18632/aging.101168 PMID:28198702

67. Ward LD, Kellis M. HaploReg: a resource for exploring chromatin states, conservation, and regulatory motif alterations within sets of genetically linked variants. Nucleic Acids Res. 2012; 40:D930–34. https://doi.org/10.1093/nar/gkr917 PMID:22064851

68. Aryee MJ, Jaffe AE, Corrada-Bravo H, Ladd-Acosta C, Feinberg AP, Hansen KD, Irizarry RA. Minfi: a flexible and comprehensive Bioconductor package for the analysis of Infinium DNA methylation microarrays. Bioinformatics. 2014; 30:1363–69. https://doi.org/10.1093/bioinformatics/btu049 PMID:24478339

69. Pidsley R, Y Wong CC, Volta M, Lunnon K, Mill J, Schalkwyk LC. A data-driven approach to pre-processing Illumina 450K methylation array data. BMC Genomics. 2013; 14:293. https://doi.org/10.1186/1471-2164-14-293 PMID:23631413

SUPPLEMENTARY MATERIAL

Table of Contents

Supplementary Note 1. Description of datasets in training, test and validation analysis

Supplementary Note 2. Other datasets

Supplementary Methods. Estimation of blood cell counts based on DNAm levels

Supplementary Figures

Supplementary Tables

Supplementary References

Supplementary Data

Supplementary Data 1. Annotation of DNAmTL model

Supplementary Data 2. Correlation analysis between age-adjusted (DNAm) LTL and imputed blood cell composition

Supplementary Data 3. GWAS catalog of DNAmLTL-mQTL associated SNPs

Supplementary Data 4. GREAT analysis for functional annotation of CpGs implicated in DNAmTL

Optimism is not associated with two indicators of DNA methylation aging

Eric S. Kim[1,2,3], Kelvin Fong[4], Lewina Lee[5,6], Avron Spiro[7,8], Joel Schwartz[9,10], Eric Whitsel[11,12], Steve Horvath[13,14], Cuicui Wang[9], Lifang Hou[15], Andrea A. Baccarelli[16], Yun Li[17,18,19], James Stewart[20], JoAnn E. Manson[10,21], Francine Grodstein[10,22], Dawn L. DeMeo[21,22,*], Laura D. Kubzansky[1,2,*]

[1]Department of Social and Behavioral Sciences, Harvard T.H. Chan School of Public Health, Boston, MA 02115, USA
[2]Lee Kum Sheung Center for Health and Happiness, Harvard T.H. Chan School of Public Health, Boston, MA 02115, USA
[3]Program on Integrative Knowledge and Human Flourishing, Institute for Quantitative Social Science, Harvard University, Cambridge, MA 02138, USA
[4]School of Forestry and Environmental Studies, Yale University, New Haven, CT 06511, USA
[5]VA Boston Healthcare System, Boston, MA 02130, USA
[6]Department Psychiatry, Boston University School of Public Health, Boston, MA 02118, USA
[7]Massachusetts Veterans Epidemiology Research and Information Center (MAVERIC), VA Boston Healthcare System, Boston, MA 02130, USA
[8]Department of Epidemiology, Boston University Schools of Public Health and Medicine, Boston, MA 02118, USA
[9]Department of Environmental Health, Harvard T.H. Chan School of Public Health, Boston, MA 02115, USA
[10]Department of Epidemiology, Harvard T.H. Chan School of Public Health, Boston, MA 02115, USA
[11]Department of Epidemiology, Gillings School of Global Public Health, Chapel Hill, NC 27599, USA
[12]Department of Medicine, School of Medicine, University of North Carolina, Chapel Hill, NC 27599, USA
[13]Department of Human Genetics, University of California, Los Angeles, CA 90095, USA
[14]Department of Biostatistics, David Geffen School of Medicine, University of California, Los Angeles, CA 90095, USA
[15]Department of Preventive Medicine, Northwestern Feinberg School of Medicine, Northwestern University, Chicago, IL, 60611, USA
[16]Department of Environmental Health Sciences, Columbia Mailman School of Public Health, New York, NY 10032, USA
[17]Department of Genetics, University of North Carolina, Chapel Hill, NC 27599, USA
[18]Department of Biostatistics, University of North Carolina, Chapel Hill, NC 27599, USA
[19]Department of Computer Science, University of North Carolina, Chapel Hill, NC, 27599 USA
[20]Cardiovascular Program, Department of Epidemiology, University of North Carolina Gillings School of Global Public Health, Chapel Hill, NC, 27599, USA
[21]Department of Medicine, Brigham and Women's Hospital, Harvard Medical School, Boston, MA 02115, USA
[22]Channing Division of Network Medicine, Brigham and Women's Hospital, Boston, MA 02115, USA
* Co-senior authors

ABSTRACT

Evidence indicates associations between higher optimism and reduced risk of age-related conditions and premature mortality. This suggests optimism is a positive health asset, but research identifying potential biological mechanisms underlying these associations remains limited. One potential pathway is slower cellular aging, which may delay age-related deterioration in health. Data were from the Women's Health Initiative (WHI) (N=3,298) and the Veterans Affairs Normative Aging Study (NAS) (N=514), and included dispositional and explanatory style optimism measures. We evaluated whether higher optimism was associated with metrics suggestive of less cellular aging, as indicated by two DNA methylation algorithms, intrinsic (IEAA) and extrinsic epigenetic age acceleration (EEAA); these algorithms represent accelerated biologic aging that exceeds chronological age. We used linear regression models to test our hypothesis while considering several covariates (sociodemographics, depressive symptoms, health behaviors). In both cohorts, we found consistently null associations of all measures of optimism with both measures of DNA methylation aging, regardless of covariates considered. For example, in fully-adjusted models, dispositional optimism was not associated with either IEAA (WHI:β=0.02; 95% Confidence Interval [CI]:-0.15-0.20; NAS:β=-0.06; 95% CI:-0.56-0.44) or EEAA (WHI:β=-0.04; 95% CI: -0.26-0.17; NAS:β=-0.17; 95% CI: -0.80-0.46). Higher optimism was not associated with reduced cellular aging as measured in this study.

INTRODUCTION

Aging and age-related health conditions have become critical public health issues. According to recent projections, the percentage of people aged >65 years in the United States is expected to increase by more than 60% over the next 15 years [1]. Growing evidence suggests that higher levels of optimism are associated with reduced risk of a wide range of age-related conditions such as cardiovascular events, lung function decline, cognitive impairment, and premature mortality (including both overall mortality and deaths due to heart disease, stroke, or cancer) [2–11]. For example, in a prospective study of 70,021 older women followed over 8 years, women in the highest (versus lowest quartile of optimism had a 38% reduced risk (95% confidence interval [CI]: 0.50, 0.76) of heart disease mortality and a 39% reduced risk (95% CI: 0.43, 0.85) of stroke mortality after adjusting for sociodemographic factors [2]. Prospective studies in other cohorts have reported similar findings [5,12–14].

Optimism, which has been defined either as the generalized expectation that good things will happen or according to the ways in which people explain the causes of good and bad events, may therefore be a powerful, positive health asset. Biologic mechanisms underlying the optimism-health associations are not yet well-established, but understanding biologic pathways could point to novel means of improving health in aging. Given the broad associations between optimism and health across disease endpoints, it is possible that optimism is related to systemic processes that affect multiple outcomes. Given consistent findings with age-related diseases, one candidate process is slower cellular

aging, whereby optimism could reduce or delay age-related deterioration in health.

Recent work has identified DNA methylation (DNAm) as a strong component of biologic aging, and developed "epigenetic clocks" designed to capture methylation-based markers of aging. Horvath et al. proposed an "epigenetic clock" derived from age-associated methylation changes in 353 Cytosine-phosphate-Guanosine sites (CpGs) across the genome that are involved in important biological processes (e.g., DNA replication and repair, lipid metabolism, oxidative stress, and other chronic disease related processes) [15,16]. This clock score is well-validated across multiple cell types and tissues, and in epidemiologic studies it predicts cognitive function, lung function, grip strength, and premature mortality, among other outcomes [16–18]. Hannum et al. also derived an epigenetic clock score in a slightly different way, leveraging DNA methylation in blood at 71 CpG sites [15]. A measure of methylation age acceleration can be derived using either of these scores to capture a positive difference between DNA methylation and chronologic age.

Prior work has suggested epigenetic aging might explain observed relationships between negative psychological factors and health. For example, stress-related epigenetic aging has been proposed as a possible explanatory factor linking psychological stress and higher risk of developing age-related diseases, with several studies demonstrating higher levels of lifetime stress are associated with accelerated DNA methylation age (DNAm) [19,20]. While less work has examined positive psychological factors in relation to epigenetic

aging, to assess potential protective effects on aging processes, given prior findings of protective effects in relation to chronic disease outcomes, such relations are plausible. Optimism may be associated with a slower rate of epigenetic aging if it either reduces stress exposure, or buffers its effects – although it is important to note that optimism does not simply reflect the absence of stress and in fact may have independent effects on biological processes [6]. Optimism has been characterized as an asset or resource that people can utilize throughout life and across multiple domains [11,21,22]. Generally, psychological health assets like optimism, tend to be stable across time, although they can be responsive to life changes such as unemployment or divorce [23], or to interventions, such as activities that promote psychological well-being [24–26].

In the current study, we sought to test the hypothesis that higher optimism would be associated with metrics suggestive of less cellular aging, as indicated by two DNA methylation age algorithms, intrinsic (IEAA) and extrinsic epigenetic age acceleration (EEAA); these algorithms represent accelerated biologic aging that exceeds chronological age. Intrinsic epigenetic age acceleration captures properties of aging that are independent of cell type and organ whereas extrinsic epigenetic acceleration likely reflects both epigenetic variation and age-related changes in cell distributions in blood [27]. We used data from two ongoing epidemio-logic cohorts that include women or men, the Women's Health Initiative (WHI) and the VA Normative Aging Study (NAS). Based on prior work we identified relevant covariates for consideration including socio-demographic factors, health status, and health behaviors, which might confound or lie on the pathway between optimism and DNA methylation, as well as depression, which is correlated with both optimism and DNA methylation profiles [28].

RESULTS

Sample description

The WHI sample consisted of 3,298 women including 1,665 Whites, 961 Blacks, and 561 Hispanics, and 111 in the "Other" race/ethnicity category. Chronological age in the WHI sample ranged from 50-79 years (mean=64). Most women were married (or in marriage-like relationships: 56%), and most had education after high school (some college or an associate degree: 26%, or a college or graduate degree: 30%). The NAS sample consisted of 514 men (99% White) ranging in chronological age from 56-91 years (mean=73). Most men were married (76%), and had either a high school degree (20%) or college or graduate degrees (35%). Table 1, Tables S1, and S2 [see Appendix A 1 for Tables S1 and S2] provide additional details about participants.

Table 1. Characteristics of study participants at baseline – Women's Health Initiative and Normative Aging Study.

Characteristics	Women's Health Initiative (WHI) (n=3,298)		Normative Aging Study (NAS) (n=514)	
	Optimism Levels		Optimism Levels	
	Quartile 1 (n = 1,004)	Quartile 4 (n = 753)	1st Quartile (n=129)	4th Quartile (n=129)
Demographic Factors				
Mean Age (SD)	63.4 (7.2)	63.2 (7.2)	72.9 (6.6)	73.2 (6.4)
Race/Ethnicity (%)				
White	43.7	51.9	99.2	99.2
Black / African-American	28.1	33.2	0.8	0.8
Hispanic / Latino	23.7	12.4	0	0
Other	4.5	2.5	0	0
Missing	0	0	0	0
Marital Status (%)				
Marriage or marriage-like relationship	50.6	57.2	73.6	74.4

Divorced or single	25.0	23.5	16.3	15.5
Widowed	23.4	19.0	9.3	10.1
Missing	1.0	0.3	0.8	0
Education (%)				
Less than high school	32.4	14.6	5.4	2.3
High school graduate	22.2	13.9	20.9	20.9
Some college or associate degree	24.0	28.7	24.8	16.3
College or more	20.5	41.8	27.9	39.5
Missing	0.9	0.9	20.9	20.9
Income (%)				
WHI				
Less than $20,000	35.2	17.4		
$20,000 to $49,999	41.7	44.5		
$50,000 to $74,999	9.1	16.2		
$75,000 or more	6.6	15.7		
Missing	7.5	6.2		
NAS				
Less than $60,000			29.5	26.4
$60,000 to $69,999			19.4	19.4
$70,000 to $89,999			21.7	25.6
$90,000 or more			25.6	27.9
Don't know			0	0
Missing			3.9	0.8
Health Factors				
Depressed (%)*				
Not depressed	73.5	93.4	68.2	96.1
Depressed	20.3	4.0	28.7	0.8
Missing	6.2	2.7	3.1	3.1
Chronic Condition (%)**				
No chronic condition	36.7	39.8	48.1	64.3
Chronic condition	52.1	49.4	51.9	35.7
Missing	11.3	10.8	0.0	0.0
Health Behaviors				
Smoking (%)				

Never smoker	52.5	52.6	28.7	33.3
Past smoker	34.7	37.3	69.0	62.8
Current smoker	12.1	8.6	2.3	3.9
Missing	0.8	1.5	0	0
Physical activity level (METS/week; %)				
<3.0	41.6	32.3	38.0	19.4
3.0-8.99	23.5	22.7	27.1	29.5
9.0-17.99	14.4	19.5	20.2	19.4
18.0-26.99	7.1	9.4	4.7	10.1
≥27	6.4	9.7	10.1	21.7
Missing	7.0	6.4	0	0
Diet				
WHI				
Mean Healthy Eating Index (SD)	63.6 (11.5)	65.7 (11.2)		
NAS				
Mean Fruit Intake (SD)			2.6 (1.8)	2.5 (1.6)
Mean Vegetable Intake (SD)			3.1 (1.9)	3.5 (2)
Current drinker (%)				
Non drinker	42.2	36.3	29.5	19.4
Current drinker	57.1	63.4	69.8	79.8
Missing	0.7	0.4	0.8	0.8
Body Mass Index (%)				
Normal (<24.9)	19.6	24.0	16.3	21.7
Overweight (25.0-29.9)	35.6	32.3	50.4	56.6
Obese (≥30.0)	44.3	42.6	33.3	21.7
Missing	0.5	1.1	0	0

Notes - *Depressive symptoms in WHI were measured using the Burnam Screening Algorithm, a questionnaire that includes 6 items from the Center for Epidemiologic Studies Depression Scale (CES-D) and two from the Diagnostic Interview Scale (DIS), with a cutoff of ≥0.06 indicating depression. Depressive symptoms in NAS were measured using the Brief Symptom Inventory (BSI), with a cutoff of ≥0.638 indicating depression
**Chronic conditions in WHI included: 1) hypertension, 2) high cholesterol, 3) cardiovascular disease, 4) diabetes, 5) stroke, 6) cancer. Chronic conditions in NAS included: 1) cardiovascular disease, 2) diabetes, 3) stroke, 4) cancer

Optimism and DNA methylation age

In WHI, when considering both dispositional optimism and DNAm age as continuous variables, we observed no association of optimism with IEAA (mean difference, β=0.07; 95% CI: -0.10,0.24; Table 2); however, we did observe an association with EEAA (mean difference, β=-0.35; 95% CI: -0.55,-0.13) in unadjusted models such that higher optimism was associated with lower DNAm age. In models that adjusted for basic confounders, we observed no relation of optimism to IEAA (β=0.02; 95% CI: -0.16,0.19; Table 2) and associations with EEAA were attenuated and no longer statistically significant (β=-0.06; 95% CI: -0.28,0.16). After further adjusting for the full set of covariates, associations were not meaningfully different (Table 2).

When evaluating the association between dispositional optimism and DNAm age in NAS, we observed a pattern of null findings in unadjusted as well in all the other models. For example, in our basic adjusted models, optimism was not associated with IEAA (β=-0.06; 95% CI: -0.55,0.42; Table 3) or EEAA (β=-0.23; 95% CI: -0.83,0.38).

We also evaluated quartiles of optimism in relation to both EEAA and IEAA, in the WHI and NAS. Findings were null in both cohorts for IEAA. In the WHI women, in the unadjusted model, individuals in the lowest (versus highest) quartile of optimism had a lower mean EEAA score (β=-0.73; 95% CI: -1.32,-0.15; Table 3). However, this association was no longer statistically significant after adjusting for additional covariates, and all findings with EEAA were null in the NAS.

Table 2. Mean differences (Regression Coefficients) for association between optimism (LOT-R) and DNA methylation age in WHI (n=3,298)*.

	Optimism				
Outcome	Continuous Optimism Score**	Quartile 1 (n = 1,004)	Quartile 2 (n = 809)	Quartile 3 (n = 732)	Quartile 4 (n = 753)
Intrinsic Epigenetic Age Acceleration	Mean Difference ß (95% CI)		Mean Difference ß (95% CI)	Mean Difference ß (95% CI)	Mean Difference ß (95% CI)
Unadjusted Model	0.07 (-0.10, 0.24)	Ref.	0.01 (-0.44, 0.46)	-0.01 (-0.48, 0.45)	0.13 (-0.33, 0.58)
Basic Confounders Model***	0.02 (-0.16, 0.19)	Ref.	-0.11 (-0.56, 0.35)	-0.16 (-0.64, 0.31)	-0.03 (-0.50, 0.45)
All Covariates Model****	0.02 (-0.15, 0.20)	Ref.	-0.06 (-0.52, 0.40)	-0.14 (-0.61, 0.34)	-0.01 (-0.49, 0.47)
Extrinsic Epigenetic Age Acceleration					
Unadjusted Model	-0.35 (-0.55, -0.13)	Ref.	-0.52 (-1.09, 0.06)	-0.93 (-1.52, -0.34)	-0.73 (-1.32, -0.15)
Basic Confounders Model***	-0.06 (-0.28, 0.16)	Ref.	-0.19 (-0.76, 0.38)	-0.53 (-1.13, 0.06)	-0.05 (-0.65, 0.54)
All Covariates Model****	-0.04 (-0.26, 0.17)	Ref.	-0.10 (-0.67, 0.47)	-0.43 (-1.02, 0.16)	-0.02 (-0.62, 0.58)

Notes - *All models adjusted for WHI substudy (EMPC or BAA23)
**Per 1 SD increase in LOT-R score
***Confounders model adjusts for: race, education, income, marital status, chronic conditions, depression,
****All covariates model additionally adjusts for: physical activity, smoking, BMI, diet, alcohol consumption, which may be intermediates or confounders

Table 3. Mean differences (Regression Coefficients) for association between optimism (LOT) and DNA methylation age in NAS (n=514).

	Optimism				
	Continuous	Quartile 1	Quartile 2	Quartile 3	Quartile 4
Outcome	Optimism Score*	(n = 129)	(n = 128)	(n = 128)	(n = 129)
Intrinsic Epigenetic Age	Mean Difference		Mean Difference	Mean Difference	Mean Difference
Acceleration	ß (95% CI)		ß (95% CI)	ß (95% CI)	ß (95% CI)
Unadjusted Model,	-0.02 (-0.47, 0.43)	Ref.	0.10 (-1.13, 1.33)	0.14 (-1.05, 1.33)	0.41 (-0.87, 1.69)
Confounders Model**	-0.02 (-0.51, 0.48)	Ref.	0.12 (-1.16, 1.40)	0.12 (-1.13, 1.36)	0.45 (-0.98, 1.89)
All Covariates Model***	-0.06 (-0.56, 0.44)	Ref.	0.09 (-1.22, 1.39)	0.12 (-1.15, 1.38)	0.54 (-0.92, 2.00)
Extrinsic Epigenetic Age					
Acceleration					
Unadjusted Model	-0.27 (-0.81, 0.28)	Ref.	0.73 (-0.75, 2.22)	0.56 (-0.88, 2.01)	0.98 (-0.57, 2.53)
Confounders Model**	-0.21 (-0.82, 0.41)	Ref.	0.60 (-0.99, 2.19)	0.53 (-1.02, 2.08)	0.58 (-1.21, 2.37)
All Covariates Model***	-0.17 (-0.80, 0.46)	Ref.	0.65 (-0.98, 2.29)	0.45 (-1.13, 2.03)	0.48 (-1.35, 2.31)

Notes - *Per 1 SD increase in LOT-R score
**Confounders model adjusts for: race, education, income, marital status, chronic conditions, depression,
***All covariates model additionally adjusts for: physical activity, smoking, BMI, diet, alcohol consumption, which could be potential confounders or intermediates

Table 4. Mean differences (Regression Coefficients) for association between optimism (PSM-R) and DNA methylation age in NAS (n=514).

	Optimism				
	Continuous	Quartile 1	Quartile 2	Quartile 3	Quartile 4
Outcome	Optimism Score*	(n = 129)	(n = 128)	(n = 128)	(n = 129)
Intrinsic Epigenetic Age	Mean Difference		Mean Difference	Mean Difference	Mean Difference
Acceleration	ß (95% CI)		ß (95% CI)	ß (95% CI)	ß (95% CI)
Unadjusted Model	0.31 (-0.14, 0.76)	Ref.	0.46 (-0.80, 1.71)	0.13 (-1.12, 1.38)	1.16 (-0.11, 2.42)
Confounders Model**	0.32 (-0.18, 0.81)	Ref.	0.42 (-0.93, 1.78)	0.03 (-1.33, 1.38)	1.14 (-0.24, 2.52)
All Covariates Model***	0.29 (-0.21, 0.79)	Ref.	0.17 (-1.23, 1.57)	-0.04 (-1.42, 1.33)	1.06 (-0.36, 2.48)
Extrinsic Epigenetic Age					
Acceleration					
Unadjusted Model	-0.06 (-0.60, 0.49)	Ref.	-0.16 (-1.69, 1.37)	-1.04 (-2.56, 0.48)	-0.25 (-1.79, 1.28)
Confounders Model**	-0.11 (-0.72, 0.51)	Ref.	-0.20 (-1.89, 1.48)	-1.22 (-2.91, 0.47)	-0.47 (-2.19, 1.25)
All Covariates***	-0.04 (-0.67, 0.59)	Ref.	0.12 (-1.64, 1.87)	-0.92 (-2.64, 0.81)	-0.17 (-1.95, 1.60)

Notes - *Per 1 SD increase in Malinchoc optimism score (a higher score on this assessment indicates higher levels of pessimism, while a lower score indicates higher levels of optimism)
**Confounders model adjusts for: race, education, income, marital status, chronic conditions, depression,
***All covariates model additionally adjusts for: physical activity, smoking, BMI, diet, alcohol consumption, which could be potential confounders or intermediate

Additional analyses

In both the WHI and NAS, after excluding individuals with depression, associations for optimism with either IEAA and EEAA remained consistently null (Appendix A 1, Table S3 and Table S4). Further, no statistically significant associations with IEAA and EEAA were evident for either the pessimism or the optimism subscales. Associations between the explanatory style optimism and both IEAA and EEAA were also uniformly null in all models (Table 4). In analyses stratified by race in WHI (Black and White women), associations remained consistently null across strata (data not shown). Findings from analyses that included the 736 WHI women who did not have the full set of covariates, were similarly null (data not shown). Finally, in WHI, after additionally adjusting for case-control status, WHI observational study membership, as well as clinical trial membership findings were uniformly null across all models (data not shown).

DISCUSSION

We examined the association between optimism and epigenetic age acceleration measured by DNA methyltion in two well characterized cohorts. We were able to examine two forms of optimism, dispositional and explanatory style. Regardless of which measure we considered and across cohorts, we found consistently null associations between optimism and both measures of DNA methylation aging, the intrinsic and extrinsic epigenetic age acceleration measure. While we did find one statistically significant association between the highest versus lowest quartile of dispositional optimism and lower EEAA score in an unadjusted model, it was evident only among the women. Thus, we remain cautious about interpreting this finding as occurring for reasons other than chance. Findings were unchanged in secondary analyses where we excluded those with depression, separately examined the optimism and pessimism subscales of the LOT, or considered another validated measure of optimism (PSM-R) available in the men.

There may be several explanations for these null associations. Our specific measures of epigenetic age acceleration may not be as relevant for optimism as other formulations might be. The DNA methylation age measures considered here reflect underlying aging processes that are at least partially under genetic control, and are more weakly associated with several lifestyle factors [27]. Pathway analysis suggests the components of the DNA methylation age [16,18] are enriched for immune cell trafficking and development, and these processes may not be strongly influenced by optimism. Further work is needed to evaluate other

potential biologic mechanisms of optimism, both epigenetic and others, that may underlie the association of optimism with health. For example, one recently developed metric, DNA methylation PhenoAge, has a stronger association with lifestyle and wellness factors than the IEAA or EEAA measures [29], and as a result, may be more strongly linked to optimism. It is possible that other age acceleration scores that capture processes more tightly linked to optimism will also be developed. Further, although we did not observe evidence of a direct effect between optimism and DNAm age, future research should evaluate if optimism might moderate (or "dampen") the effects of various stressors on DNAm age.

With increasing availability of epigenetic information, we will have additional opportunities to assess if the biologic correlates of optimism will be better captured by additional epigenetic metrics of aging [29,30], or if specific scores are less effective than broader agnostic analyses of the epigenome. Future studies that have repeated measures of DNA methylation aging could also provide a stronger test of the hypothesis that optimism influences epigenetic aging by evaluating if optimism is associated with changes in the rate of DNA methylation aging over time. However, another plausible explanation for our null findings could be that the biological pathways by which optimism works to reduce risk of age-related chronic diseases simply do not include changes in DNAm aging. Assessing these possibilities and alternative biological pathways for the observed association between optimism and chronic diseases of aging will be important next steps for this research.

The current study has some limitations. Both optimism and DNA methylation were assessed at a single point in time. Measurement error can be particularly problematic in studies such as ours, that rely on a single biomarker measurement [31], which likely has some random variability. Associations were cross-sectional and given the composition of each sample, findings may not be broadly generalizable, particularly to younger individuals. Nonetheless, this study has important strengths. We used two large and richly characterized cohorts and were able to assess associations in both men and women as well as adjust for potential confounders. Further, two forms of optimism, dispositional and explanatory style were assessed, with a commonly used validated measure dispositional optimism in both cohorts and a validated measure of explanatory style optimism in the NAS. Findings were remarkably similar across measures and cohorts. In conclusion, we examined associations between optimism and epigenetic aging in older men and women from two long-running cohorts with large sample sizes and found

no statistically significant associations between optimism and intrinsic or extrinsic epigenetic age acceleration. Our findings may indicate that optimism is not specifically associated with biological mechanisms underlying these metrics of epigenetic age and age acceleration. It may also be that the combination of genes included in these epigenetic aging scores do not well-reflect the biological effects of optimism, and analyses of other clock scores, or broader agnostic or pathway analyses of DNA methylation could yield greater insight into biological processes underlying optimism.

Given robust and consistent findings that optimism is associated with reduced risk of developing a range of age-related diseases as well as overall mortality, and that the relationships are not fully explained by health behaviors [32], identifying novel pathways to improving health in aging remains an important goal. Our findings assess only one metric of epigenetic aging, but new methods and measures for assessing these processes are in active development (or recently available), suggesting continued effort to understand the range of epigenetic and other underlying biological mechanisms is warranted.

MATERIALS AND METHODS

Study Population

Women's Health Initiative
The Women's Health Initiative (WHI) is a long-term study focused on identifying strategies for preventing major chronic diseases in postmenopausal women. Starting in 1993, racially and ethnically diverse women aged 50-79 years were recruited throughout the U.S. and entered either clinical trial(s) (WHI-CT; N=68,132) or the observational study (WHI-OS; N=93,676). Data were collected at 40 clinical centers throughout the country. At baseline, women completed self-administered questionnaires including information about sociodemographic factors, psychosocial characteristics, health behaviors, and chronic conditions. Further, after fasting overnight, they visited study clinics where certified clinical center staff collected blood specimens and performed anthropometric measurements.

The present study draws on data from two WHI substudies. The first substudy (Epigenetic Mechanisms of PM-Mediated Cardiovascular Disease Risk (EMPC; AS315; n=2,200) included a stratified random sample representative of the larger WHI CT population [27]. The second substudy (Integrative Genomics and Risk of Coronary Heart Disease and Related Phenotypes in the Women's Health Initiative; BAA23; n=2,107) examined genomic determinants of coronary heart disease (CHD),

using a nested case-control design (with oversampling of African Americans and Hispanics) in the WHI observational study and CT study populations. When data from both substudies were combined, there were 118 women who were in both substudies; thus, only data from EMPC was used when overlap existed (results were very similar when data from BAA23 were used instead). Further, 148 women were excluded because they had missing data on optimism and a further 7 were excluded due to missing data on the DNA methylation measures. Finally, some covariates were assessed only at baseline, and because some women had their blood drawn after baseline (n=736) they were excluded from primary analyses, resulting in a final analytic sample of 3,298 WHI women. In secondary analyses, we evaluated the main association of interest after including the 736 women, without fully control for covariates.

VA Normative Aging Study
The VA Normative Aging Study (NAS) is a longitudinal investigation of normal aging processes in community-dwelling men, initiated in 1963. The study enrolled healthy men aged 21 to 81 years who were free of known chronic medical conditions. Men provided information on demographic factors, medical history, psychosocial factors, and lifestyle factors on a regular basis. They were interviewed at the VA Boston hospital every 3-5 years, and also participated in a physical exam and laboratory tests. Blood was drawn at each physical exam. Eligibility for this study required continued participation as of the time when DNA samples were first collected. Dropout has been < 1% per year in this cohort. Among the active 1,749 NAS participants at the time, DNA samples were collected from 1999-2009 for 774 participants. Among these, we excluded from analysis 260 men who did not have an optimism measurement before a DNA sample was taken. The final analytic sample included 514 NAS men with both DNA and measures of optimism.

Because restrictions apply to the public availability of these data, they are available from the WHI and NAS study coordinators upon reasonable request.

Measures

Optimism assessment
WHI: In WHI, dispositional optimism was assessed at baseline using the Life Orientation Test-Revised (LOT-R). The measure has demonstrated good discriminant and convergent validity, as well as good reliability [33]. Negatively worded items were reverse coded, and then all items were summed to create a composite score that ranged from 6 to 30, with higher scores indicating higher optimism. Following standard WHI protocol, the

score was set to missing if study respondents were missing any of the LOT-R items. To facilitate comparisons of effect sizes across studies, we standardized optimism scores *(Mean(M)=0, Standard Deviation(SD)=1)*. Internal consistency reliability was high in the analytic sample at baseline (Cronbach α=0.75). To assess the possibility of discontinuous or threshold effects, we also created quartiles of optimism based on the score distribution in the sample. Mean optimism scores by quartile were: 19, 23, 24, and 27. Following prior work on dispositional optimism [34], in secondary analyses, we also evaluated the optimistic (Cronbach α=0.77) and pessimistic (Cronbach α=0.74) subscales of LOT-R, each composed of three items from the overall scale.

NAS: In NAS, dispositional optimism was assessed using both the Revised Optimism-Pessimism Scale (PSM-R) and the original Life Orientation Test (LOT). The LOT is the parent scale from which the LOT-R was largely derived and includes 8 items that contribute to the scale score. Items were reverse coded as necessary and summed to create a composite score that ranged from 7 to 32 in this sample, with higher scores indicating higher optimism. Again, we standardized optimism scores *(M=0, SD=1)*. Internal consistency reliability was high in the analytic sample at baseline (Cronbach α=0.78). We created quartiles of optimism based on the score distribution in the sample and mean optimism scores by quartile were: 16, 20, 22, and 26. In secondary analyses, we evaluated the optimistic (Cronbach α=0.75) and pessimistic (Cronbach α=0.80) subscales of LOT, each composed of four items from the overall scale.

Another measure of optimism based on explanatory style was assessed using the PSM–R, developed and validated by Malinchoc, Offord, and Colligan [35,36]. This bipolar scale measures the way individuals explain the causes of both good and bad events, and characterized explanatory style on a continuum from optimistic to pessimistic, by using 263 items selected from the revised Minnesota Multiphasic Personality Inventory (MMPI–2). Following the scoring algorithm, items were combined into a composite bipolar score reflecting a more optimistic explanatory style at the low end of the continuum and a more pessimistic one at the high end. This measure has predicted reduced risk of heart disease and slower lung function decline in the NAS cohort [3,37]. Internal consistency reliability was high in the analytic sample at baseline (Cronbach α=0.78), and prior research demonstrates this scale has high test-retest reliability of 0.90 [36]. To assess the possibility of discontinuous or threshold effects, we also created quartiles of optimism based on the score

distribution in the sample. Mean scores by quartile were: 58, 47, 41, and 32.

Assessment of DNA methylation and DNA methylation age acceleration

WHI. Methylation analysis for both substudies was performed using the Illumina Infinium Human-Methylation450 Beadchip, which measures single-CpG resolution DNA methylation levels at 485,577 unique CpG sites in the human genome. The BAA23 WHI substudy samples were processed at the HudsonAlpha Institute of Biotechnology. The EMPC WHI substudy samples were processed at the Northwestern University Genomics Core. All measurements were quality-controlled and batch adjusted as described elsewhere [27].

NAS. Methylation data were generated at the Northwestern University Genomics Core Facility. All measurements underwent quality-control. The Bioconductor minfi package Illumina-type background correction without normalization was used to preprocess the samples and generate methylation beta values to compute DNAm-age [38].

Epigenetic age acceleration scores. In all of the analyses, we considered both the intrinsic epigenetic age acceleration score (IEAA) [16] and the extrinsic epigenetic age acceleration score (EEAA) [15]. The two scores were calculated identically in WHI and NAS based on scripts developed by Horvath the IEAA variable is denoted as *AAHOAdjCellCounts* and the EEAA variable is denoted as *BioAge4HAStaticAdjAge*). Both the EEAA and IEAA measures represent accelerated biological aging that exceeds chronological age, with positive values indicating that epigenetic age is higher than chronological age. Both measures are calculated by obtaining the residual when regressing DNAm age on chronological age. Intrinsic epigenetic age acceleration captures properties of aging that are independent of cell type and organ whereas extrinsic epigenetic acceleration likely reflects both epigenetic variation and age-related changes in cell distributions in blood [27]. In WHI, the correlation between IEAA and EEAA was 0.36 and in NAS the correlation was 0.32.

Assessment of potential confounders and other covariates

WHI. Potential confounders included sociodemographic factors and depression. Sociodemographic variables were obtained from the baseline questionnaire and included age (continuous), race (White, Black/African-American, Hispanic/Latino, Other), marital status

(married/marriage like-relationship, divorced/single, widowed), education (less than high school, high school graduate, some college or associate degree, college or more), income (<$20,000, $20,000-$49,999, $50,000-$74,999, $75,000+, don't know). Depression status (yes/no) was defined according to Burnam Screening Algorithm questionnaire that includes 6 items from the Center for Epidemiologic Studies Depression Scale (CES-D) and two from the Diagnostic Interview Scale (DIS) [39,40], with a cutoff of ≥0.06 indicating depression [39]. Health conditions were self-reported (yes/no) and included: hypertension, high cholesterol, cardiovascular disease, diabetes, stroke, cancer. Height and weight were measured by trained staff and used to calculate Body Mass Index (BMI) in kg/m^2. and then, three BMI categories were created (<24.9, 25.0 to 29.9,≥30.0). Potential confounding or intermediate variables included the following health behaviors, all self-reported on the baseline questionnaire: cigarette smoking (never, former, current smoker), physical activity (weekly expenditure of metabolic equivalent tasks (METs; <3 METs/week, 3-<9 METs/week, 9-<19 METs/week, 18-<27 METs/week, 27+ METs/week), alcohol intake (non-drinker, current drinker), diet (122-item food frequency questionnaire (FFQ) [41]; overall diet quality was quantified using the Alternative Healthy Eating Index (scale 0-110; the AHEI includes 11 different diet components).

NAS. Potential confounders included sociodemographic factors, depression, and chronic conditions. Socio-demographic variables were obtained from the baseline questionnaire and included age (continuous), educational attainment (years), race/ethnicity (white/non-white), marital status (married/not married). Depressive symptoms were assessed with a subscale from the Brief Symptom Inventory [42], with a cutoff of ≥0.638 indicating depression. Information about health conditions was self-reported (yes/no), updated every 3-5 years, and included: coronary heart disease, stroke, diabetes, and cancer. BMI in kg/m^2 was calculated from weight and height measured by study staff (<24.9, 25.0-29.9, ≥30.0). Further variables included the following health behaviors (updated every 3-5 years), which could be confounders or intermediates: cigarette smoking status (current, former, never), physical activity (created based on questions asking about energy expenditure (e.g., frequency of sports activities, flights of stairs climbed/day, distance walked, etc., to calculate the following metabolic equivalent of tasks (METs) categories; <3 METs/week, 3-<9 METs/week, 9-<19 METs/week, 18-<27 METs/week, 27+ METs/week), alcohol intake, (<2 drinks versus 2+ drinks), and diet (frequency of fruit and vegetable consumption).

Statistical analysis

In primary analyses, we considered optimism as a continuous standardized variable, where associations represent the change in DNAm age as a function of a 1 standard deviation increase in optimism, and also evaluated optimism categorized into quartiles (based on the sample-specific distribution of scores). All models were run separately within each cohort. Several sets of models were tested using ordinary least square regression. The first model did not adjust for any covariates. The second model added basic potential confounders including race, education, income, marital status, chronic conditions, and depression. A third model further added variables that could be potential confounders or intermediates including physical activity, smoking, BMI, diet, and alcohol consumption. We conducted several secondary analyses. First, to test potential residual confounding due to depression, we excluded those with high levels of depressive symptoms. Second, to evaluate whether associations differed by the optimism or pessimism subscale, we separately evaluated these two subscales. Third, to evaluate the consistency of results across different measures of optimism, we conducted analyses in NAS using the PSM-R instead of the LOT. Fourth, In WHI we conducted stratified analyses in Black and White women. Fifth, we evaluated findings after adding to our sample 736 WHI women who had blood draws after the baseline assessment, and who did not have full covariate data. Finally, to evaluate potential confounding caused by case-control status (CHD-no CHD over follow-up), WHI observational study membership, or clinical trial membership (hormone therapy (HT), dietary modification (DM), or calcium and Vitamin D supplementation (CaD)), we adjusted for all of these factors in the WHI cohort.

All analyses were completed using Stata (StataCorp. 2017. Stata Statistical Software: Release 15.0. College Station, TX: StataCorp LP) or R 3.4.1 (R Core Team (2017). R Foundation for Statistical Computing, Vienna, Austria).

Ethics Approval

For WHI, institutional review board approval was obtained at each clinical center and all participants provided written informed consent. For NAS, participants provided written informed consent to the VA Institutional Review Board.

Availability of Data and Materials

The data that support the findings of this study are available upon reasonable request to Ron Spiro

(aspiro3@bu.edu) for NAS data. Details regarding access to all WHI data are available at: https://www.whi.org/researchers/data/Pages/Home.aspx.

Abbreviations

WHI: Women's Health Initiative; NAS: Veterans Affairs Normative Aging Study; DNAm: DNA methylation age; IEAA: Intrinsic epigenetic age acceleration; EEAA: Extrinsic epigenetic age acceleration; LOT: Life Orientation Test; LOT-R: Life Orientation Test-Revised; CHD: Coronary heart disease CT: Clinical trial; OS: Observational trial.

AUTHOR CONTRIBUTIONS

ESK, LDK, FG, DLD contributed to the study concept and design; ESK, KF, LDK, FG, DLD contributed to acquisition, analysis, or interpretation of data; the manuscript was written by ESK, LDK, FG, DLD, with input from all-co-authors and critical revision of the manuscript for important intellectual content. All authors read and approved the final manuscript.

ACKNOWLEDGEMENTS

CONFLICTS OF INTEREST

Eric S. Kim has worked as a consultant with AARP and UnitedHealth Group. The other authors report no financial interests or potential conflicts of interest.

FUNDING

REFERENCES

1. Colby LS, and Ortman JM. Projections of the size and composition of the U.S. population: 2014 to 2060, Current Population Reports. U.S. Census Bureau, Washington, DC. 2015; P25-1143. https://www.census.gov/library/publications/2015/d emo/p25-1143.html

2. Kim ES, Hagan KA, Grodstein F, DeMeo DL, De Vivo I, Kubzansky LD. Optimism and cause-specific mortality: a prospective cohort study. Am J Epidemiol. 2017; 185:21–29. https://doi.org/10.1093/aje/kww182 PMID:27927621

3. Kubzansky LD, Wright RJ, Cohen S, Weiss S, Rosner B, Sparrow D. Breathing easy: a prospective study of

optimism and pulmonary function in the normative aging study. Ann Behav Med. 2002; 24:345–53. https://doi.org/10.1207/S15324796ABM2404_11 PMID:12434946

4. Gawronski KA, Kim ES, Langa KM, Kubzansky LD. Dispositional optimism and incidence of cognitive impairment in older adults. Psychosom Med. 2016; 78:819–28. https://doi.org/10.1097/PSY.0000000000000345 PMID:27284699

5. Tindle HA, Chang YF, Kuller LH, Manson JE, Robinson JG, Rosal MC, Siegle GJ, Matthews KA. Optimism, cynical hostility, and incident coronary heart disease and mortality in the Women's Health Initiative. Circulation. 2009; 120:656–62. https://doi.org/10.1161/CIRCULATIONAHA.108.82764 2 PMID:19667234

6. Kubzansky LD, Huffman JC, Boehm JK, Hernandez R, Kim ES, Koga HK, Feig EH, Lloyd-Jones DM, Seligman ME, Labarthe DR. Positive psychological well-being and cardiovascular disease: JACC health promotion series. J Am Coll Cardiol. 2018; 72:1382–96. https://doi.org/10.1016/j.jacc.2018.07.042 PMID:30213332

7. James P, Kim ES, Kubzansky LD, Zevon ES, Trudel-Fitzgerald C, Grodstein F. Optimism and healthy aging in women. Am J Prev Med. 2019; 56:116–24. https://doi.org/10.1016/j.amepre.2018.07.037 PMID:30573140

8. Kim ES, James P, Zevon ES, Trudel-Fitzgerald C, Kubzansky LD, Grodstein F. Optimism and Healthy Aging in Women and Men. Am J Epidemiol. 2019; 188:1084–91. https://doi.org/10.1093/aje/kwz056 PMID:30834429

9. Carver CS, Scheier MF. Dispositional optimism. Trends Cogn Sci. 2014; 18:293–99. https://doi.org/10.1016/j.tics.2014.02.003 PMID:24630971

10. Chopik WJ, Kim ES, Smith J. Changes in optimism are associated with changes in health over time among older adults. Soc Psychol Personal Sci. 2015; 6:814–22. https://doi.org/10.1177/1948550615590199 PMID:27114753

11. Scheier MF, Carver CS. Dispositional optimism and physical health: A long look back, a quick look forward. Am Psychol. 2018; 73:1082–94. https://doi.org/10.1037/amp0000384 PMID:30525784

12. Giltay EJ, Kamphuis MH, Kalmijn S, Zitman FG, Kromhout D. Dispositional optimism and the risk of cardiovascular death: the Zutphen Elderly Study. Arch Intern Med. 2006; 166:431–36. https://doi.org/10.1001/archinte.166.4.431. http://dx.doi.org/ PMID:16505263

13. Kim ES, Smith J, Kubzansky LD. Prospective study of the association between dispositional optimism and incident heart failure. Circ Heart Fail. 2014; 7:394–400. https://doi.org/10.1161/CIRCHEARTFAILURE.113.000 644 PMID:24647117

14. Giltay EJ, Geleijnse JM, Zitman FG, Hoekstra T, Schouten EG. Dispositional optimism and all-cause and cardiovascular mortality in a prospective cohort of elderly dutch men and women. Arch Gen Psychiatry. 2004; 61:1126–35. https://doi.org/10.1001/archpsyc.61.11.1126 PMID:15520360

15. Hannum G, Guinney J, Zhao L, Zhang L, Hughes G, Sadda S, Klotzle B, Bibikova M, Fan JB, Gao Y, Deconde R, Chen M, Rajapakse I, et al. Genome-wide methylation profiles reveal quantitative views of human aging rates. Mol Cell. 2013; 49:359–67. https://doi.org/10.1016/j.molcel.2012.10.016 PMID:23177740

16. Horvath S. DNA methylation age of human tissues and cell types. Genome Biol. 2013; 14:R115. https://doi.org/10.1186/gb-2013-14-10-r115 PMID:24138928

17. Chen BH, Marioni RE, Colicino E, Peters MJ, Ward-Caviness CK, Tsai PC, Roetker NS, Just AC, Demerath EW, Guan W, Bressler J, Fornage M, Studenski S, et al. DNA methylation-based measures of biological age: meta-analysis predicting time to death. Aging (Albany NY). 2016; 8:1844–65. https://doi.org/10.18632/aging.101020 PMID:27690265

18. Horvath S, Raj K. DNA methylation-based biomarkers and the epigenetic clock theory of ageing. Nat Rev Genet. 2018; 19:371–84. https://doi.org/10.1038/s41576-018-0004-3 PMID:29643443

19. Gassen NC, Chrousos GP, Binder EB, Zannas AS. Life stress, glucocorticoid signaling, and the aging epigenome: implications for aging-related diseases. Neurosci Biobehav Rev. 2017; 74:356–65. https://doi.org/10.1016/j.neubiorev.2016.06.003 PMID:27343999

20. Wolf EJ, Morrison FG. Traumatic stress and accelerated cellular aging: from epigenetics to cardiometabolic disease. Curr Psychiatry Rep. 2017; 19:75. https://doi.org/10.1007/s11920-017-0823-5 PMID:28852965

21. Fredrickson BL. The role of positive emotions in positive psychology. The broaden-and-build theory of

positive emotions. Am Psychol. 2001; 56:218–26.
https://doi.org/10.1037/0003-066X.56.3.218
PMID:11315248

22. Rozanski A, Kubzansky LD. Psychologic functioning and physical health: a paradigm of flexibility. Psychosom Med. 2005 (Suppl 1); 67:S47–53. https://doi.org/10.1097/01.psy.0000164253.69550.49 PMID:15953801

23. Fujita F, Diener E. Life satisfaction set point: stability and change. J Pers Soc Psychol. 2005; 88:158–64. https://doi.org/10.1037/0022-3514.88.1.158 PMID:15631581

24. Malouff JM, Schutte NS. Can psychological interventions increase optimism? A meta-analysis. J Posit Psychol. 2017; 12:594–604. https://doi.org/10.1080/17439760.2016.1221122

25. Celano CM, Albanese AM, Millstein RA, Mastromauro CA, Chung WJ, Campbell KA, Legler SR, Park ER, Healy BC, Collins LM, Januzzi JL, Huffman JC. Optimizing a positive psychology intervention to promote health behaviors following an acute coronary syndrome: the Positive Emotions after Acute Coronary Events-III (PEACE-III) randomized factorial trial. Psychosom Med. 2018; 80:526–34. https://doi.org/10.1097/PSY.0000000000000584 PMID:29624523

26. Mohammadi N, Aghayousefi A, Nikrahan GR, Adams CN, Alipour A, Sadeghi M, Roohafza H, Celano CM, Huffman JC. A randomized trial of an optimism training intervention in patients with heart disease. Gen Hosp Psychiatry. 2018; 51:46–53. https://doi.org/10.1016/j.genhosppsych.2017.12.004 PMID:29316450

27. Quach A, Levine ME, Tanaka T, Lu AT, Chen BH, Ferrucci L, Ritz B, Bandinelli S, Neuhouser ML, Beasley JM, Snetselaar L, Wallace RB, Tsao PS, et al. Epigenetic clock analysis of diet, exercise, education, and lifestyle factors. Aging (Albany NY). 2017; 9:419–46. https://doi.org/10.18632/aging.101168 PMID:28198702

28. Uddin M, Koenen KC, Aiello AE, Wildman DE, de los Santos R, Galea S. Epigenetic and inflammatory marker profiles associated with depression in a community-based epidemiologic sample. Psychol Med. 2011; 41:997–1007. https://doi.org/10.1017/S0033291710001674 PMID:20836906

29. Levine ME, Lu AT, Quach A, Chen BH, Assimes TL, Bandinelli S, Hou L, Baccarelli AA, Stewart JD, Li Y, Whitsel EA, Wilson JG, Reiner AP, et al. An epigenetic biomarker of aging for lifespan and healthspan. Aging (Albany NY). 2018; 10:573–91.

https://doi.org/10.18632/aging.101414
PMID:29676998

30. Jylhävä J, Pedersen NL, Hägg S. Biological age predictors. EBioMedicine. 2017; 21:29–36. https://doi.org/10.1016/j.ebiom.2017.03.046 PMID:28396265

31. Kubzansky LD, Seeman TE, Glymour MM. Biological pathways linking social conditions and health: plausible mechanisms and emerging puzzles, in: Berkman, L.F., Kawachi, I., Glymour, M.M. (Eds.), Social Epidemiology. Oxford University Press, New York. 2014; pp. 512–561.

32. Boehm JK, Kim ES, Kubzansky LD. Positive Psychological Wellbeing, in: Kivimaki, M., Batty, D.G., Kawachi, I., Steptoe, A. (Eds.), The Routledge International Handbook of Psychosocial Epidemiology. Routledge., New York. 2017; pp. 156–170.

33. Scheier MF, Carver CS, Bridges MW. Distinguishing optimism from neuroticism (and trait anxiety, self-mastery, and self-esteem): a reevaluation of the Life Orientation Test. J Pers Soc Psychol. 1994; 67:1063–78. https://doi.org/10.1037/0022-3514.67.6.1063 PMID:7815302

34. Segerstrom SC, Evans DR, Eisenlohr-Moul TA. Optimism and pessimism dimensions in the Life Orientation Test-Revised: method and meaning. J Res Pers. 2011; 45:126–29. https://doi.org/10.1016/j.jrp.2010.11.007

35. Malinchoc M, Offord KP, Colligan RC. PSM-R: revised optimism-pessimism scale for the MMPI-2 and MMPI. J Clin Psychol. 1995; 51:205–14. https://doi.org/10.1002/1097-4679(199503)51:2<205::AID-JCLP2270510210>3.0.CO;2-2 PMID:7797644

36. Colligan RC, Offord KP, Malinchoc M, Schulman P, Seligman ME. CAVEing the MMPI for an Optimism-Pessimism Scale: seligman's attributional model and the assessment of explanatory style. J Clin Psychol. 1994; 50:71–95. https://doi.org/10.1002/1097-4679(199401)50:1<71::AID-JCLP2270500107>3.0.CO;2-8 PMID:8150997

37. Kubzansky LD, Sparrow D, Vokonas P, Kawachi I. Is the glass half empty or half full? A prospective study of optimism and coronary heart disease in the normative aging study. Psychosom Med. 2001; 63:910–16. https://doi.org/10.1097/00006842-200111000-00009 PMID:11719629

38. Aryee MJ, Jaffe AE, Corrada-Bravo H, Ladd-Acosta C, Feinberg AP, Hansen KD, Irizarry RA. Minfi: a flexible and comprehensive Bioconductor package for the analysis of Infinium DNA methylation microarrays. Bioinformatics. 2014; 30:1363–69.

https://doi.org/10.1093/bioinformatics/btu049
PMID:24478339

39. Burnam MA, Wells KB, Leake B, Landsverk J. Development of a brief screening instrument for detecting depressive disorders. Med Care. 1988; 26:775–89. https://doi.org/10.1097/00005650-198808000-00004 PMID:3398606

40. Radloff LS. The CES-D Scale: a self-report depression scale for research in the general population. Appl Psychol Meas. 1977; 1:385–401. https://doi.org/10.1177/014662167700100306

41. Patterson RE, Kristal AR, Tinker LF, Carter RA, Bolton MP, Agurs-Collins T. Measurement characteristics of the Women's Health Initiative food frequency questionnaire. Ann Epidemiol. 1999; 9:178–87. https://doi.org/10.1016/S1047-2797(98)00055-6 PMID:10192650

42. Derogatis LR, Melisaratos N. The Brief Symptom Inventory: an introductory report. Psychol Med. 1983; 13:595–605. https://doi.org/10.1017/S0033291700048017 PMID:6622612

SUPPLEMENTARY MATERIAL

Table S1. Characteristics of Women's Health Initiative participants at baseline (n=3,298).

	Optimism Score			
	Quartile 1	Quartile 2	Quartile 3	Quartile 4
Characteristic	(n = 1,004)	(n = 809)	(n = 732)	(n = 753)
Demographic Factors				
Mean Age (SD)	63.4 (7.2)	63.8 (7.0)	64.0 (7.0)	63.2 (7.2)
Race/Ethnicity (%)				
White	43.7	51.6	57.1	51.9
Black / African-American	28.1	28.4	27.2	33.2
Hispanic / Latino	23.7	16.7	13.0	12.4
Other	4.5	3.3	2.7	2.5
Missing	0	0	0	0
Marital Status (%)				
Marriage or marriage-like relationship	50.6	59.8	56.8	57.2
Divorced or single	25.0	20.0	20.9	23.5
Widowed	23.4	19.7	21.7	19.0
Missing	1.0	0.5	0.6	0.3
Education (%)				
Less than high school	32.4	24.2	23.4	14.6
High school graduate	22.2	20.0	17.5	13.9
Some college or associate degree	24.0	24.7	26.1	28.7
College or more	20.5	30.2	32.5	41.8
Missing	0.9	0.9	0.6	0.9
Income (%)				
Less than $20,000	35.2	25.0	22.1	17.4
$20,000 to $49,999	41.7	45.2	43.7	44.5
$50,000 to $74,999	9.1	14.8	20.2	16.2
$75,000 or more	6.6	9.2	10.5	15.7
Missing	7.5	5.8	3.4	6.2
Health Factors				
Depressed (%)*				
Not depressed	73.5	90.2	90.6	93.4
Depressed	20.3	7.2	7.0	4.0
Missing	6.2	2.6	2.5	2.7
Chronic Condition (%**)				
No chronic condition	36.7	36.7	37.2	39.8

Chronic condition	52.1	52.0	49.5	49.4
Missing	11.3	11.3	13.4	10.8
Health Behaviors				
Smoking (%)				
Never smoker	52.5	53.2	49.5	52.6
Past smoker	34.7	36.6	41.4	37.3
Current smoker	12.1	8.2	7.9	8.6
Missing	0.8	2.1	1.2	1.5
Physical activity level (METS/week; %)				
<3.0	41.6	32.6	32.8	32.3
3.0-8.99	23.5	24.0	21.5	22.7
9.0-17.99	14.4	19.0	18.9	19.5
18.0-26.99	7.1	7.5	8.9	9.4
≥27	6.4	9.9	8.7	9.7
Missing	7.0	6.9	9.3	6.4
Mean Diet (Healthy Eating Index; SD)	63.6 (11.5)	65.7 (11.3)	64.7 (11.7)	65.7 (11.2)
Current drinker (%)				
Non drinker	42.2	36.2	35.0	36.3
Current drinker	57.1	62.8	64.1	63.4
Missing	0.7	1.0	1.0	0.4
Body Mass Index (%)				
Normal (<24.9)	19.6	22.3	25.7	24.0
Overweight (25.0-29.9)	35.6	35.5	33.5	32.3
Obese (≥30.0)	44.3	41.5	40.6	42.6
Missing	0.5	0.7	0.3	1.1

Notes- *Depressive symptoms were measured using the Burnam Screening Algorithm, a questionnaire that includes 6 items from the Center for Epidemiologic Studies Depression Scale (CES-D) and two from the Diagnostic Interview Scale (DIS), with a cutoff of ≥0.06 indicating depression

**Chronic conditions include: 1) hypertension, 2) high cholesterol, 3) cardiovascular disease, 4) diabetes, 5) stroke, 6) cancer

Table S2. Characteristics of Normative Age Study (NAS) participants at baseline (n=514).

Characteristic	Optimism Score			
	Quartile 1 (n = 129)	Quartile 2 (n = 128)	Quartile 3 (n = 128)	Quartile 4 (n = 129)
Demographic Factors				
Mean Age (SD)	72.9 (6.6)	72.3 (6.7)	72.8 (6.7)	73.2 (6.4)
Race/Ethnicity (%)				
White	99.2	100	99.2	99.2
Black / African-American	0.8	0	0	0.8
Hispanic / Latino	0	0	0.8	0
Other	0	0	0	0
Missing	0	0	0	0
Marital Status (%)				
Marriage or marriage-like relationship	73.6	75.8	78.9	74.4
Divorced or single	16.3	12.5	11.7	15.5
Widowed	9.3	10.2	8.6	10.1
Missing	0.8	1.6	0.8	0
Education (%)				
Less than high school	5.4	6.2	1.6	2.3
High school graduate	20.9	19.5	20.3	20.9
Some college or associate degree	24.8	13.3	16.4	16.3
College or more	27.9	34.4	37.5	39.5
Missing	20.9	26.6	24.2	20.9
Income (%)				
Less than $60,000	29.5	30.5	23.4	26.4
$60,000 to $69,999	19.4	20.3	19.5	19.4
$70,000 to $89,999	21.7	21.9	14.1	25.6
$90,000 or more	25.6	26.6	43.0	27.9
Don't know	0	0	0	0
Missing	3.9	0.8	0	0.8
Health Factors				
Depressed (%)*				
Not depressed	68.2	89.8	84.4	96.1
Depressed	28.7	7.0	10.9	0.8
Missing	3.1	3.1	4.7	3.1
Chronic Condition (%**)				
No chronic condition	48.1	59.4	59.4	64.3
Chronic condition	51.9	40.6	40.6	35.7

Missing	0.0	0.0	0.0	0.0

Health Behaviors

Smoking (%)

Never smoker	28.7	35.9	25.0	33.3
Past smoker	69.0	58.6	72.7	62.8
Current smoker	2.3	5.5	2.3	3.9
Missing	0	0	0	0

Physical activity level (METS/week; %)

<3.0	38	19.5	30.5	19.4
3.0-8.99	27.1	36.7	32.0	29.5
9.0-17.99	20.2	12.5	14.1	19.4
18.0-26.99	4.7	10.9	10.2	10.1
≥27	10.1	19.5	13.3	21.7
Missing	0	0.8	0	0
Mean Fruit Intake (SD)	2.6 (1.8)	2.4 (1.5)	2.8 (1.7)	2.5 (1.6)
Mean Vegetable Intake (SD)	3.1 (1.9)	3.3 (2.2)	3.6 (2.4)	3.5 (2)

Current drinker (%)

Non drinker	29.5	27.3	22.7	19.4
Current drinker	69.8	68.8	75.0	79.8
Missing	0.8	3.9	2.3	0.8

Body Mass Index (%)

Normal (<24.9)	16.3	20.3	20.3	21.7
Overweight (25.0-29.9)	50.4	55.5	50.0	56.6
Obese (≥30.0)	33.3	24.2	29.7	21.7
Missing	0	0	0	0

Notes- *Depressive symptoms were measured using the Brief Symptom Inventory (BSI), with a cutoff of ≥0.638 indicating depression

**Chronic conditions include: 1) cardiovascular disease, 2) diabetes, 3) stroke, 4) cancer

Table S3. Mean differences (Regression Coefficients) for association between optimism and DNA methylation age in Women's Health Inititative, after excluding women with depression (n=2,834)*

	Optimism				
	Continuous	Quartile 1	Quartile 2	Quartile 3	Quartile 4
Outcome	Optimism Score[b]	(n = 738)	(n = 730)	(n = 663)	(n = 703)
Horvath Clock Score (IEAA)					
Confounders Model[c]	-0.02 (-0.21, 0.18)	Ref.	-0.24 (-0.75, 0.27)	-0.21 (-0.73, 0.32)	-0.05 (-0.57, 0.48)
Hannum Clock Score (EEAA)					
Confounders Model[c]	0.00 (-0.25, 0.24)	Ref.	0-.10 (-0.73, 0.53)	-0.43 (-1.09, 0.22)	-0.06 (-0.71, 0.59)

Notes- *All models adjusted for WHI substudy (EMPC or BAA23)
**Per 1 SD increase in LOT-R score

Table S4. Mean differences (Regression Coefficients) for association between optimism and DNA methylation age in Normative Age Study (NAS), after excluding men with depression (n=435).

	Optimism				
	Continuous	Quartile 1	Quartile 2	Quartile 3	Quartile 4
Outcome	Optimism Score[a]	(n = 88)	(n = 115)	(n = 108)	(n = 124)
Horvath Clock Score (IEAA)					
Confounders Model[b]	-0.06 (-0.61, 0.48)	Ref.	0.18 (-1.18, 1.55)	0.31 (-1.03, 1.66)	0.37 (-1.26, 2.00)
Hannum Clock Score (EEAA)					
Confounders Model[b]	-0.26 (-0.94, 0.43)	Ref.	0.28 (-1.64, 2.20)	-1.12 (-2.98, 0.74)	0.52 (-1.32, 2.36)

Notes- *Per 1 SD increase in LOT score
**Confounders model adjusts for: race, education, income, marital status, chronic conditions, depression

Research Paper

Placental epigenetic clocks: estimating gestational age using placental DNA methylation levels

Yunsung Lee[1], Sanaa Choufani[2], Rosanna Weksberg[3], Samantha L. Wilson[4,5], Victor Yuan[4,5], Amber Burt[6], Carmen Marsit[6], Ake T. Lu[7], Beate Ritz[8], Jon Bohlin[9], Håkon K. Gjessing[9,10], Jennifer R. Harris[1,9], Per Magnus[9], Alexandra M. Binder[8,1,*], Wendy P. Robinson[4,5,*], Astanand Jugessur[1,9,10,*], Steve Horvath[7,11,*]

[1]Department of Genetics and Bioinformatics, Norwegian Institute of Public Health, Oslo, Norway
[2]Genetics and Genome Biology Program, Research Institute, The Hospital for Sick Children, Toronto, Ontario, Canada
[3]Genetics and Genome Biology Program, Research Institute, The Hospital for Sick Children and Institute of Medical Science, University of Toronto, Toronto, Ontario, Canada
[4]Department of Medical Genetics, University of British Columbia, Vancouver, British Columbia, Canada
[5]B.C. Children's Hospital Research Institute, Vancouver, British Columbia, Canada
[6]Department of Environmental Health, Rollins School of Public Health, Emory University, Atlanta, GA 30322, USA
[7]Department of Human Genetics, David Geffen School of Medicine, University of California Los Angeles, Los Angeles, CA 90095, USA
[8]Department of Epidemiology, University of California Los Angeles, Los Angeles, CA 90095, USA
[9]Centre for Fertility and Health, Norwegian Institute of Public Health, Oslo, Norway
[10]Department of Global Public Health and Primary Care, University of Bergen, Bergen, Norway
[11]Department of Biostatistics, Fielding School of Public Health, University of California Los Angeles, Los Angeles, CA 90095, USA
*Co-senior authors

ABSTRACT

The human pan-tissue epigenetic clock is widely used for estimating age across the entire lifespan, but it does not lend itself well to estimating gestational age (GA) based on placental DNAm methylation (DNAm) data. We replicate previous findings demonstrating a strong correlation between GA and genome-wide DNAm changes. Using substantially more DNAm arrays (n=1,102 in the training set) than a previous study, we present three new placental epigenetic clocks: 1) a robust placental clock (RPC) which is unaffected by common pregnancy complications (e.g., gestational diabetes, preeclampsia), 2) a control placental clock (CPC) constructed using placental samples from pregnancies without known placental pathology, and 3) a refined RPC for uncomplicated term pregnancies. These placental clocks are highly accurate estimators of GA based on placental tissue; e.g., predicted GA based on RPC is highly correlated with actual GA (r>0.95 in test data, median error less than one week). We show that epigenetic clocks derived from cord blood or other tissues do not accurately estimate GA in placental samples. While fundamentally different from Horvath's pan-tissue epigenetic clock, placental clocks closely track fetal age during development and may have interesting applications.

INTRODUCTION

Gestational age (GA) of the fetus is used to forecast the date of delivery, optimize prenatal care, and monitor the growth and development of the fetus relative to other pregnancies. Short GA at delivery impacts neonatal morbidity and mortality [1-3], as well as brain development [4-6]. Thus, accurate classification of the fetus may help predict neonatal risk. In this regard, the World Health Organization defined extremely preterm (<28 weeks of gestation), very preterm (28-32 weeks of gestation) and moderate or late preterm (32-37 weeks of gestation) birth to reflect the newborn's developmental stage [7].

Traditional methods for estimating GA include early obstetric ultrasound measures or calculations based on the last menstrual period (LMP) [8]. The early ultrasound method estimates GA based on the visible fetal size (e.g., crown-rump length during the first trimester [9-11] or biparietal diameter after the second trimester [12-15]). The LMP method calculates GA based on the time elapsed since the known first day of the LMP. The early ultrasound method is widely accepted as the gold standard due to its higher accuracy [16] but is not routinely available in low and middle-income countries. More accurate classification of GA at birth may help predict neonatal risk for adverse outcomes and measure GA more accurately than through the assessment of physical and neurological features of the newborn, especially when early ultrasound measures are lacking, or the infant is growth-restricted but not preterm.

Here, we aim to develop a new molecular estimator of GA based on placental tissue samples that is more accurate than the previous clock [17]. Earlier studies have revealed profound molecular changes in placental chorionic villi, the placental structures that project into maternal decidua and are bathed in maternal blood, during gestation [18-22]. We focus on placental DNA methylation (DNAm) data, because prior work demonstrated that accurate estimators of chronological age (epigenetic clocks) can be developed based on DNAm levels from a variety of tissues [23], that one can estimate GA based on DNAm data derived from umbilical cord blood samples [24, 25], and most pertinently that one can estimate GA based on placental methylation data (Mayne et al. 2017) [17]. Our study provides more accurate placenta-based GA estimators (i.e., placental epigenetic clocks) than those developed previously, because we use a substantially larger sample for our training set (more than six times larger than that of Mayne et al. 2017). We aim to develop three different placental epigenetic clocks: 1) a "robust placental clock" (RPC) that is largely unaffected by pregnancy conditions (e.g., preeclampsia, gestational diabetes, and trisomy), 2) a "control placental clock" (CPC), tailor-made for measuring GA in normal pregnancies, and 3) a "refined RPC", trained for uncomplicated term (GA>36) pregnancies. For the RPC, we purposely included placental samples from a variety of pregnancy complications in the training data (e.g., hypertension or diabetes) as well as congenital abnormalities (e.g., trisomy 13, 18 and 21).

RESULTS

Placental DNA methylation data

We downloaded publicly available DNAm data from Gene Expression Omnibus (GEO, https://www.ncbi.nlm.nih.gov/geo/; Table 1) that assessed DNAm levels in placental tissues. Eighteen datasets used the Illumina HumanMethylation 450K BeadChip (450K) platform and one used the more recent Illumina Methylation EPIC BeadChip (EPIC) array. Our analyses focused on the 441,870 autosomal CpG probes that are shared between the two Illumina platforms such that the resulting GA estimators (RPC and CPC) would be applicable to data from both platforms.

Robust placental clock (RPC)

An overview of our analysis is presented in Figure 1. We developed the RPC using several placental DNAm datasets (training n=1,102, Table 1, Figure 1). We regressed GA (dependent variable) on DNAm levels of CpG sites using a penalized regression model (elastic net regression [26]). The elastic net regression model automatically selected 558 CpG sites for the RPC model (Supplementary File 1). Predicted GA is a weighted average of DNAm levels at these 558 CpGs, where the weights are the regression coefficients.

Figure 2 shows the results of a comparison between the RPC and the placental clock from Mayne et al. (2017) in independent test data (test n=187, Table 1). The predictive accuracy of the placental clocks was quantified using the median absolute error (MAE, defined as the median absolute deviation between predicted GA and observed GA), and the degree of the linear association between predicted GA and observed GA was measured using the Pearson correlation coefficient (r). According to both measures, the RPC (MAE=0.96 weeks; 95% confidence interval (CI) [0.88, 1.19], r=0.99; 95% CI [0.98, 0.99]) outperformed Mayne's placental clock (MAE=2.63 weeks; 95% CI [2.17, 3.01], r=0.94; 95% CI [0.92, 0.96]). Note that Mayne's placental clock underestimated GA in two data sets: GSE73375 (green dots) and GSE75196 (blue dots), and overestimated GA in two other data sets: GSE66210 (black) and GSE70453 (red).

Table 1. Description of the publicly available placental DNAm data.

GEO Number	Placental tissue type	GEO submitter	N	Platform	Normalization method	Probe exclusion criteria[11]	GA range (weeks)
Training data							
GSE71678	Fetal side, near the cord insertion	Marsit et al.	343	450K[2]	funNorm[4]	SC, CH, SNP, DP	30-42
GSE75248	Fetal side	Marsit et al.	334	450K[2]	funNorm[4]	SC, CH, SNP, DP	37-42
GSE71719	Fetal side, near the cord insertion	Marsit et al.	44	450K[2]	noob[5]	SC, CH, SNP, DP	37-41
RL[1]	Fetal side, chorionic villi	-	121	450K[2]	funNorm[4]	SC	14-42
GSE100197	Fetal side, chorionic villi	Robinson et al.	16	450K[2]	SWAN[6]	SC, SNP, DP, MB	26-39
GSE108567	Fetal side, chorionic villi	Robinson et al.	7	450K[2]	SWAN[6]	SC, CH, SNP, DP, BR	29-38
GSE69502	Fetal side, chorionic villi	Robinson et al.	7	450K[2]	SWAN[6]	SC, CH, SNP, DP, BR	16-24
GSE74738	Fetal side, chorionic villi	Robinson et al.	8	450K[2]	SWAN[6]	SC, CH, SNP, DP, BR	6-13
GSE115508	Fetal side, chorionic villi	Robinson et al.	44	EPIC[3]	funNorm[4]	SC, CH, SNP, DP, BR	28-37
GSE44667	Fetal side, chorionic villi	Robinson et al.	27	450K[2]	SWAN[6]	SC, SNP, DP, MB	25-37
GSE49343	Fetal side, chorionic villi	Robinson et al.	13	450K[2]	SWAN[6]	SC, SNP, DP	5-39
GSE42409	Fetal side, chorionic villi	Robinson et al.	4	450K[2]	SWAN[6]	SC, SNP, DP	26-33
GSE120250	Fetal side, near the cord insertion	Weksberg et al.	86	450K[2]	GenomeStudioNorm[7]	SC, SNP, DP	35-41
GSE98224	Fetal side	Cox et al.	48	450K[2]	SWAN[6]	SC, SNP, DP, MB	27-41
Test data							
GSE70453	Maternal side, decidua near the cord	Binder et al.	82	450K[2]	BMIQ[8]	SC, CR, SNP	35-42
GSE73375	Fetal side	Fry et al.	36	450K[2]	quanNorm[9]	DP	22-41
GSE75196	Fetal side	Chiu et al.	24	450K[2]	dasen[10]	SC, SNP, DP, BR	32-40
GSE76641	Fetal side, chorionic villi	Slieker et al.	4	450K[2]	funNorm[4]	SC, SNP, DP, BR	9-22
GSE66210	Fetal side, chorionic villi	Bojesen et al.	41	450K[2]	GenomeStudioNorm[7]	-	11-15

[1] Placental DNAm data generated from the Robinson laboratory at the University of British Columbia (Vancouver, BC, Canada); The data for which is publicly available as part of the GEO data sets listed below.

[2] 450K: Illumina Infinium HumanMethylation450 BeadChip

[3] EPIC: Infinium MethylationEPIC BeadChip

[4] funNorm: Functional normalization [27]

[5] noob: Normal-exponential out-of-band [29]

[6] SWAN: Subset-quantile within array normalization [28]

[7] GenomeStudioNorm: Genome Studio normalization

(details available in the GenomeStudio Methylation Module v1.8 User Guide, https://www.illumina.com/content/dam/illumina-support/documents/documentation/software_documentation/genomestudio/genomestudio-2011-1/genomestudio-methylation-v1-8-user-guide-11319130-b.pdf)

[8] BMIQ: Beta-mixture quantile dilation [30]

[9] quanNorm: Quantile normalization [31, 32]

[10] dasen: Data-driven separate normalization [33]

[11] Probe exclusion criteria

SC: Sex chromosome, CH: Cross-hybridizing, SNP: Single nucleotide polymorphism, DP: Detection P-value < 0.01, MB: Missing beta > 5%, and BR: Bead replicates < 3.

1. Data acquisition (GEO)
Collected DNAm datasets
(450K & EPIC) with gestational age (GA).
Split them into training and test data

Training data (n=1,102)

GSE71678, GSE75248, GSE71719, RL,
GSE100197, GSE108567, GSE69502, GSE74738,
GSE115508, GSE44667, GSE49343, GSE42409,
GSE120250, GSE98224

Test data (n=187)
GSE70453, GSE73375, GSE75196,
GSE76641, GSE62210

2. Placenta clock development

2-1. Data cleaning
    a. Recalculated GA in weeks.
    b. Removed re-used samples and replicates
    c. Removed DNAm outliers.
    d. Imputed missing data with median values.
    e. Standardized GA.

2-3. Elastic net regression
    a. Ridge-Lasso ratio (alpha) = 0.5
    b. 10-fold cross validation for a scale parameter.
    c. Calculated weights of selected CpG sites.

3. Performance check on test data
Predicted GA using the derived placental clock.
Compared the performance with Mayne et al.(2017)'s clock.

Figure 1. Flow chart of the RPC development.

The advantage of the RPC is particularly pronounced in later gestation, e.g., when restricting the analysis to placental samples with GA > 25 weeks, the RPC (MAE=0.89 [0.73, 1.02], r=0.82 [0.76, 0.87]) greatly outperforms Mayne's clock (MAE=2.25 [1.9, 2.63], r=0.61 [0.05,0.71], Figure 2C and 2D).

As expected by its construction, the RPC predicted GA accurately even in placental samples with adverse pregnancy conditions such as preeclampsia, gestational diabetes, and trisomy 13, 18 or 21 (Supplementary Figure S1). However, Mayne's placental clock underestimated GA in placental samples from pre-eclampsia cases and overestimated GA in cases of gestational diabetes and trisomy (Supplementary Figure S1). In case of trisomy, the RPC (MAE=2.26 [1.63, 2.88], r=0.12 [-0.25, 0.46]) was more accurate than Mayne's clock (MAE=3.99 [3.35, 5.4], r=0.02 [-0.34, 0.39]) but still showed a slight overestimation. The RPC's GA estimate was not associated with fetal sex (Supplementary Figure S2). We could not evaluate the effect of ethnicity because our test data did not include ethnic information except for GSE73375 (n=36, Supplementary Figure S3).

The training data used in the construction of the RPC employed several different normalization methods:

functional normalization (funNorm, [27]), subset-quantiles within arrays (SWAN, [28]) and the normal-exponential out-of-band (noob, [29]) approach. This lack of uniformity in normalization methods in the training data has a statistical advantage: it makes it more likely that the RPC will be robust with respect to different normalization methods. In support of this, we found that the RPC validated in test data that were normalized using various methods: beta-mixture quantile dilation (BMIQ, [30]), quantile normalization (quanNorm, [31, 32]), data-driven separate normalization (dasen, [33]) as detailed in Table 1.

Control placental clock (CPC)

We trained the CPC on placental samples (training n=963, Table 1) that had been designated as "control" samples. Hence, placental samples with higher GA were probably from relatively normal pregnancies. However, placental samples with lower GA might contain samples that would be considered abnormal (i.e., premature rupture of membranes, spontaneous premature labor) but minimal placental pathology relative to pre-eclampsia cases. The analysis flow was identical as for the RPC, except for the composition of the training and test sets (Supplementary Figure S4). The elastic net regression model used for the CPC automatically selected 546 CpG sites (Supplementary File 1).
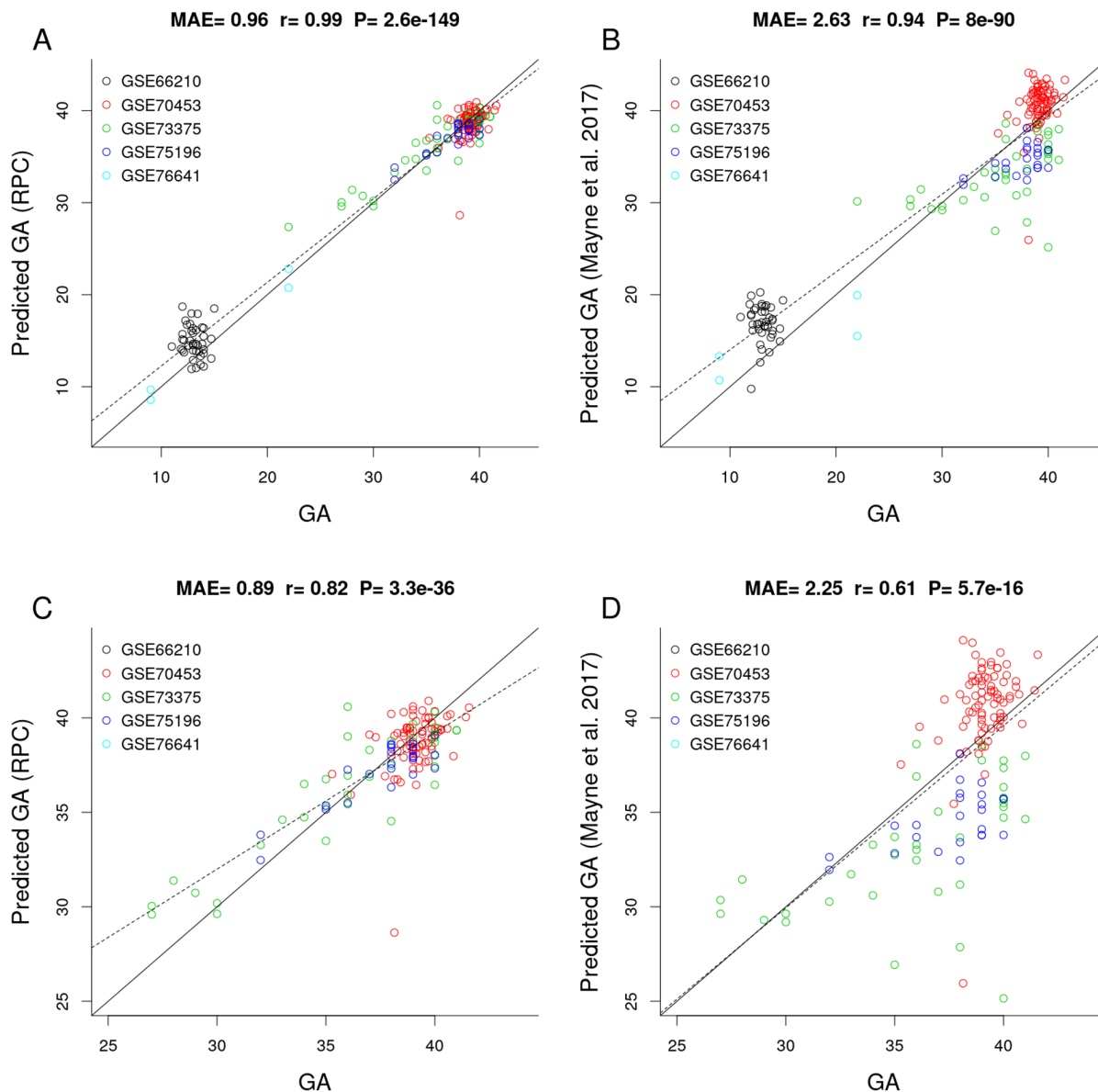
Figure 2. Gestational age estimation of the RPC and Mayne et al. (2017)'s placental clock. (**A**) Scatter plot between observed GA and DNAm-predicted GA (RPC) across all trimesters. (**B**) Scatter plot between observed GA and DNAm-predicted GA (Mayne et al. 2017) across all trimesters. (**C**) Zoom-in on panel **A** restricting GA > 25 weeks. (**D**) Zoom-in on panel **B** restricting GA > 25 weeks.

To assess whether adverse pregnancy conditions influence the epigenetic GA estimate, we applied the CPC to placental samples associated with chromosomal abnormalities (confined placental mosaicism, diandric triploidy, trisomy 13, 16, 18 and 21), neural tube defects (anencephaly and spinal bifida), intrauterine growth restriction, maternal complications (gestational diabetes and preeclampsia), and chorioamnionitis (test, n=326). Interestingly, the CPC accurately predicted the GA of fetuses with the above-mentioned conditions (MAE=1.02, r=0.98, Figure 3A) even though the CPC was constructed using unaffected control samples only.

To test whether pregnancy conditions are associated with faster/slower epigenetic aging, we used epigenetic measures of GA acceleration that were formally defined as raw residuals resulting from regressing the DNAm GA estimate on observed GA. By definition, this residual-based measure of GA acceleration is not correlated with true GA (r=0). GA acceleration did not significantly deviate from zero for any pregnancy conditions mentioned above (Figure 3B), but we acknowledge the small sample sizes for diandric triploidy (n=3) and trisomy 16 (n=3). When restricting the analysis to placental samples from the first

trimester (weeks 1 to 12), we found the CPC's GA estimates to be slightly inaccurate, which was due to the small training set (only n=7 fetuses with GA < 12 weeks).

Refined robust placental clock for uncomplicated term pregnancies

For researchers who are particularly interested in uncomplicated term pregnancies, we also developed a second version of the RPC using placental samples from "uncomplicated term" pregnancies (defined as GA > 36 weeks) without any known pregnancy condition.

Toward this end, we selected "uncomplicated" term placental samples (n=733) from the training set used for the original RPC. Further, we restricted the penalized regression model analysis to the 558 CpGs that make up the original RPC. The penalized regression model automatically selected 395 CpG sites out of the 558 sites (Supplementary File 1). We find that the "refined" RPC for uncomplicated term pregnancies leads to highly accurate GA estimates (MAE=1.49, r=0.98, Figure 4A) in the RPC's test set (n=187).
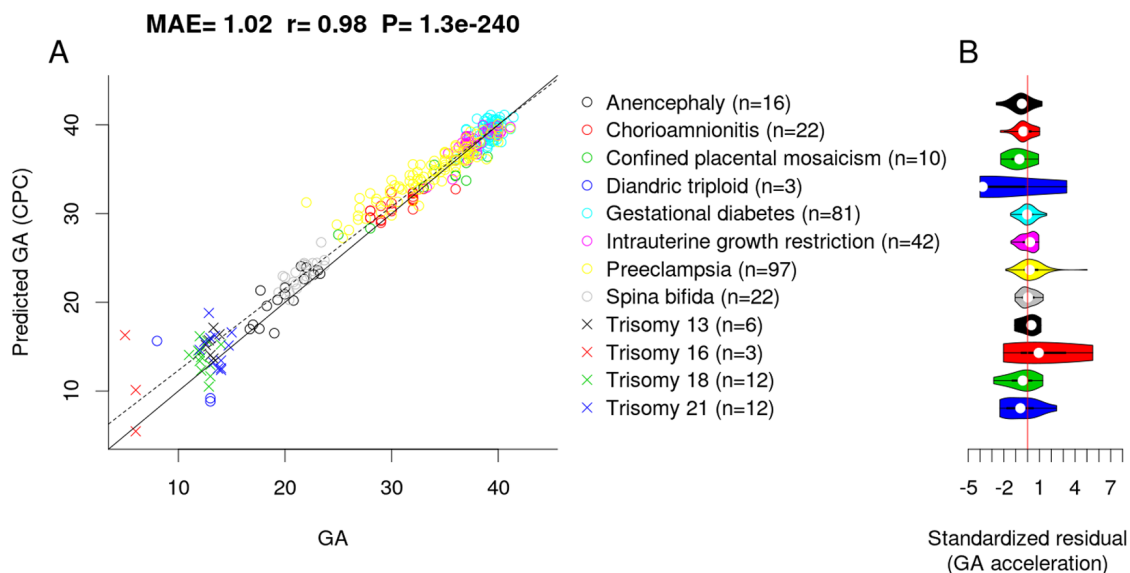
Figure 3. Effect of pregnancy condition on the GA estimate by CPC. (**A**) Scatter plot between GA and DNAm-predicted GA (CPC) across all trimesters. (**B**) Violin plot of GA acceleration (standardized residual) for each pregnancy condition.
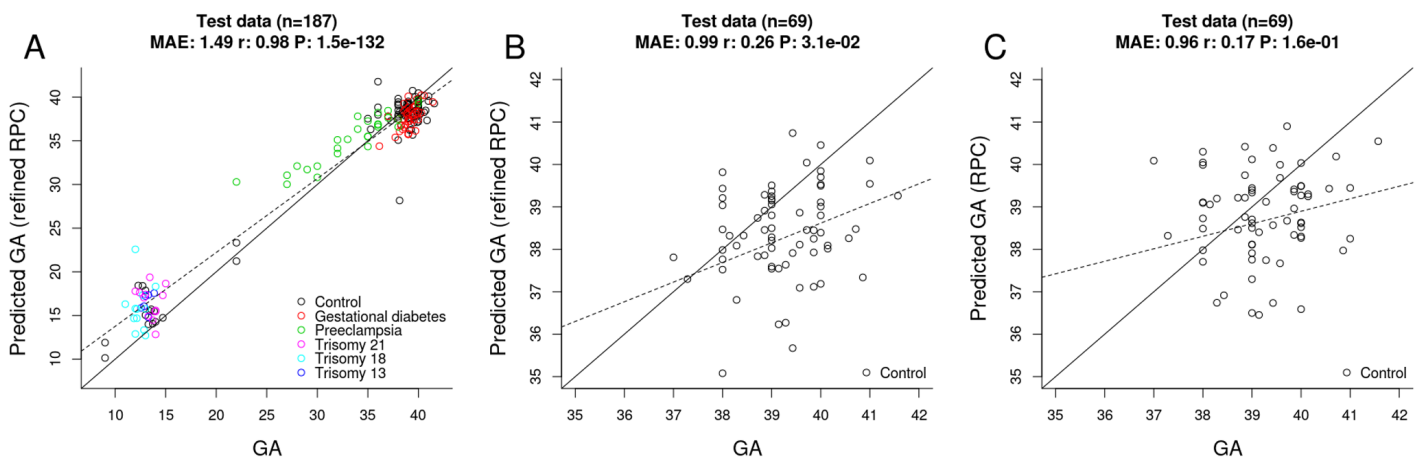
Figure 4. Gestational age estimation by the refined RPC and the RPC. (**A**) Scatter plot between observed GA and DNAm-predicted GA (by the refined RPC) – all samples from the RPC's test data (n=187). (**B**) Scatter plot between observed GA and DNAm-predicted GA (by the refined RPC) - uncomplicated term samples from the RPC's test data (n=69). (**C**) Scatter plot between observed GA and DNAm-predicted GA (by the RPC) - uncomplicated term samples from the RPC's test data (n=69).

Evaluating other epigenetic clocks

Using RPC's test data (n=187), we found that previously published epigenetic clocks derived from cord blood samples or other tissues do not apply to the estimation of GA based on placental samples.

No significant correlation between GA and predicted DNAm age could be observed for clocks by Hannum (2013) [34], Horvath (2013) [23], Levine (2018) [35], and Horvath (2018) [36] (Supplementary Figure S5). However, the DNAm age estimate is close to zero for Horvath's pan-tissue clock and the more recently developed Skin & Blood clock. Similarly, GA estimators for cord blood (Bohlin's cord blood clock [24], Knight's cord blood clock [25]) failed to accurately predict GA in placental samples (Supplementary Figure S6). Overall, these studies demonstrate that the placenta is quite distinct from other tissues regarding the development and application of DNAm based age estimators.

Fetal sex-classifier based on DNAm

Several GEO datasets did not report fetal sex (e.g., GSE70453, GSE73375 and GSE76641) and CpGs present on sex chromosomes. Therefore, we developed a fetal sex-classifier based RPC's training data (n=1,102) using CpGs that are present on autosomes. Toward this end, we regressed fetal sex (binary outcome) on 441,870 autosomal CpG sites using an elastic net implemented in the glmnet R package [37]. The elastic net automatically selected 220 autosomal CpG sites. The classification accuracy was 100% for the placental test data from GSE75196 (n=24). Interestingly, the placental sex classifier turns out to be highly accurate, when applied to blood-based DNAm data from adults (e.g., an accuracy of 96% in the data
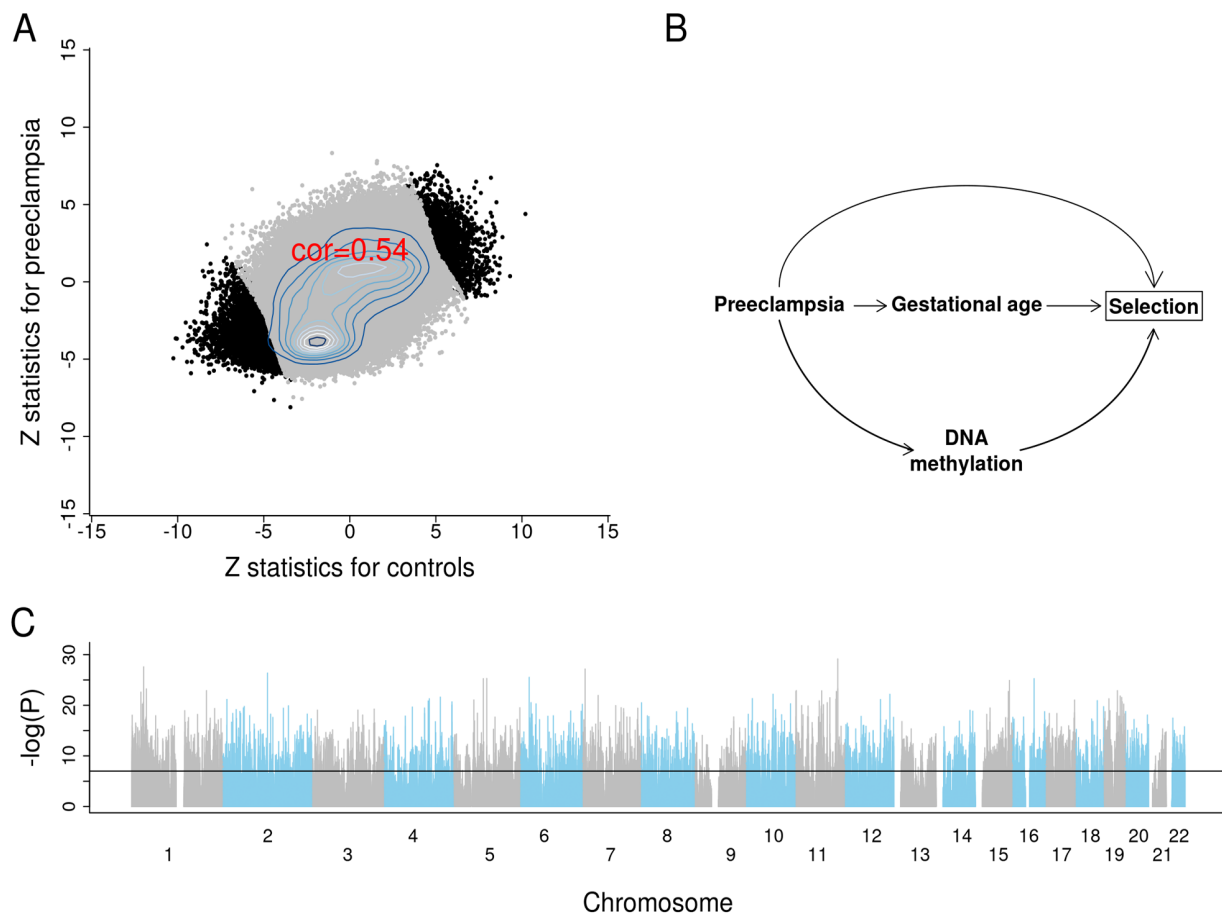
Figure 5. Results of EWAS and potential confounding between DNA methylation and gestational age due to selection bias. (**A**) Scatter plots between Z scores from controls and Z scores from preeclampsia. (**B**) The depicted minimal causal diagram under the null hypothesis of no effect of GA on DNAm. Here, the pregnancy condition (preeclampsia) would induce a spurious association between DNAm and GA, because preeclampsia could prompt earlier delivery (shorter GA) and influence DNAm. Note that the association between GA and DNAm is not due to a direct causal relationship between DNAm and GA. Rather, the association is confounded by preeclampsia. If the selection criteria differ substantially across studies, the placental clock models may not perform well. (**C**) EWAS Manhattan plot of GA.

from the Framingham Heart Study, n=2,356). As the sex of the fetus is typically identical to the sex of its placenta (except for rare cases of chimerism or sex-chromosome mosaicism), the sex-classifier was used to impute fetal sex in GSE66210, GSE70453, GSE73375 and GSE76641.

Epigenome-wide association studies of gestational age

We briefly report the results from an epigenome-wide association study (EWAS) of GA to demonstrate the profound effect of GA on placental DNAm levels. To protect against confounding by preeclampsia, we conducted EWAS in two separate strata: first, for placental samples from control pregnancies (n=831); second, for placental samples from pregnancies with preeclampsia (n=70). We combined the summary statistics from the two EWAS using Stouffer's method for meta-analysis [38]. The two EWAS summary statistics presented consistent DNAm-GA correlations across 441,870 autosomal CpGs (Figure 5A).

Strikingly, 10,827 CpG sites exhibit a genome-wide significant correlation with GA (P<1E-07; Figure 5C, Supplementary File 2).

Among these sites, 5,940 were in CpGs islands, 262 were in the north shelf, 1,165 in the north shore, 241 in the south shelf, and 902 in the south shore. The top four genes with the largest number of significant CpG sites were *MAD1L1* (17 CpGs), *BRD2* (13 CpGs), *INPP5A* (12 CpGs) and *RPTOR* (9 CpGs). The top 25 CpG sites and their nearest gene(s) are reported in Table 2.

The RPC had 36 epigenome-wide significant (P<1E-07) CpG sites, the CPC had 39, and the refined RPC had 32.

DISCUSSION

Using the largest placental training set to date (n=1,102), we developed highly robust molecular estimators of GA. The robust placental epigenetic clock (RPC) is expected to perform well, even when applied to cases with adverse fetal outcomes or pregnancy complications. We developed this clock using a placenta-based training set that included several adverse conditions, including chromosomal abnormalities (trisomy and triploidy), neural tube defects (anencephaly and spinal bifida), intrauterine growth restriction, maternal complications (gestational diabetes and preeclampsia), and chorioamnionitis.

Table 2. The top 25 CpG sites associated with GA.

CpG	Gene	Chr	Relation to UCSC CpG Island	UCSC RefGene Group	Meta Z (P) (n=901)	Z (P) of Control (n=831)	Z (P) of Preeclampsia (n=70)
cg23034799	*CADM1*	11	Island	TSS200	-11.4 (7E-30)	-10.3 (6E-23)	-4.9 (2E-06)
cg03418552	*CADM1*	11	Island	TSS200	-10.1 (6E-24)	-9.4 (8E-20)	-3.9 (2E-04)
cg21155609	*FAM167B*	1	N_Shore	1stExon	11. (3E-28)	10.2 (1E-22)	4.4 (2E-05)
cg27339550	*ZNF853*	7	Island	TSS1500	-10.9 (7E-28)	-9.2 (4E-19)	-5.9 (1E-08)
cg20025003	*TFCP2L1*	2	Island	TSS200	-10.8 (4E-27)	-9.5 (6E-20)	-5.2 (6E-07)
cg02215898		6	Island		-10.6 (3E-26)	-10.1 (2E-22)	-3.7 (3E-04)
cg11544721	*CETN3*	5	Island	Body	-10.5 (5E-26)	-10. (4E-22)	-3.7 (3E-04)
cg01152986	*SETD6;SETD6*	16	Island	TSS200	-10.5 (5E-26)	-9.7 (7E-21)	-4.2 (4E-05)
cg08757742	*RASGRF2*	5	Island	TSS200	-10.5 (6E-26)	-9.2 (6E-19)	-5.2 (6E-07)
cg26662656		15	N_Shelf		10.5 (1E-25)	8.2 (1E-15)	6.7 (2E-10)
cg13458335	*BMP8B*	1	Island	TSS1500	-10.1 (6E-24)	-9. (2E-18)	-4.6 (8E-06)
cg20630277	*MRPL23*	11	Island	Body	-10. (1E-23)	-9. (2E-18)	-4.4 (2E-05)
cg21908248	*PPP1R15B*	1	Island	1stExon	-10. (1E-23)	-9. (4E-18)	-4.5 (1E-05)
cg26940573	*ZNF566*	19	Island	1stExon;5'UTR;TSS200	-10. (1E-23)	-8.8 (9E-18)	-4.7 (5E-06)
cg13242525	*FAM86C*	11	Island	TSS1500	-10. (1E-23)	-8.2 (2E-15)	-5.9 (2E-08)
cg13512138	*CHID1*	11	Island	5'UTR	-10. (2E-23)	-8.8 (1E-17)	-4.7 (4E-06)
cg05569874	*SEMA4B*	15	Island	5'UTR;1stExon	-10. (2E-23)	-9.3 (2E-19)	-3.8 (2E-04)
cg21060796	*LAYN*	11	Island	Body	-10. (2E-23)	-8.5 (1E-16)	-5.2 (6E-07)
cg01103597	*RUNX3*	1		Body	9.9 (3E-23)	8.5 (1E-16)	5.1 (7E-07)
cg12799981	*ASCC1;C10orf104*	10	N_Shore	1stExon;5'UTR;TSS1500	-9.9 (7E-23)	-9.4 (1E-19)	-3.4 (7E-04)
cg12888127	*KNTC1;RSRC2*	12	Island	TSS1500;TSS200	-9.9 (7E-23)	-9.2 (4E-19)	-3.7 (3E-04)
cg03366925	*GLI3*	7	Island	TSS1500	-9.8 (1E-22)	-8.5 (1E-16)	-4.9 (2E-06)
cg19599862	*ZNF226*	19		1stExon;5'UTR	-9.8 (1E-22)	-8.2 (1E-15)	-5.4 (2E-07)
cg16449659	*TIGD4;ARFIP1*	4	S_Shore	TSS1500;5'UTR	-9.7 (2E-22)	-9.1 (1E-18)	-3.7 (3E-04)
cg27006129	*ZNF114*	19	N_Shore	TSS1500	-9.7 (3E-22)	-7.9 (1E-14)	-5.7 (3E-08)

In contrast, the only other published placental clock by Mayne and colleagues was trained on a small training set (n=170). In our independent test set (n=187), Mayne's clock under/overestimated GA according to pregnancy conditions. (Supplementary Figure S1). These systematic deviations from Mayne's clock might reflect interesting biological effects or technical artifacts (batch effects, normalization methods). Another potential limitation of Mayne's clock is that the authors limited the eligible CpG sites to the approxi-mately 18,437 autosomal sites on the 27K and 450K bead chips. This might explain why the Mayne's clock uses only 62 CpG sites, whereas our RPC uses 558.

To infer biological processes under the 558 and 546 CpG sites, we conducted functional gene enrichment analyses using the Genomic Regions Enrichment of Annotation Tool (GREAT, v.3.0, [39]). However, we did not find any significant biological annotations associated with fetal aging. Elastic net regressions automatically select predictive CpG sites of gestational age (GA), but these CpG sites are not always bio-logically meaningful.

Our study had several limitations. First, the "observed" GA used for building these epigenetic clocks were estimated either by early pregnancy ultrasound or the LMP method. Although early pregnancy ultrasound based on fetal growth is the gold standard in a clinical setting, it is susceptible to variations in fetal size and leads to a systematic underestimation of GA in smaller fetuses [40-42].

There is also a concern that some of the training sets might be subject to systematic confounding due to adverse pregnancy conditions, as is the case for preeclampsia (Figure 5B). GA tends to be overestimated for placentas linked to preeclampsia, which is consistent with the associated pathology of advanced villous maturation, as well as previous reports of molecular signs of advanced aging [17, 43]. In this hypothetical example, preeclampsia confounds the association between placental DNAm and GA (Figure 5B, [44-46]). However, this type of confounding probably does not affect our placental clocks for the following reasons. First, the CPC for control samples and the refined RPC for uncomplicated term samples also accurately predicted GA even in pregnancies with known complications. Second, our EWAS of GA reveals pro-found associations between GA and DNA methylation levels even after stratifying the analysis by pre-eclampsia.

Moreover, it is possible that the RPC and the CPC might not perform well in case of non-live births, because the proportion of non-live births was extremely small amongst the third trimester samples in the training datasets, while unavoidably all first and second trimester samples are non-live births. In addition, it has been suggested that gravidity or parity may change placental physiology (e.g., higher placental weight associated with higher parity [47]) and therefore might modify the relationship between the placental epi-genome and GA.

The clinical application of the RPC might be limited, because obtaining placental samples during pregnancy is highly invasive (e.g., chorionic villus sampling [48, 49]). However, the existence of a predictive placental clock – the RPC – opens the possibility to develop another epigenetic clock based on cell-free fetal DNA (cffDNA). cffDNA is fragmented from placenta trophoblasts [50, 51], and circulates in maternal blood during pregnancy [52]. If the development of a cffDNA clock is successful, clinicians readily estimate GA simply by collecting and analyzing maternal blood anytime during pregnancy.

METHODS

Study population

We collected publicly available data from Gene Expression Omnibus (GEO) using the GEOparse Python package (Python 3.6.5: Anaconda, Inc.). Table 1 details each dataset. GSE71678 examined the correlation between placental DNAm and arsenic exposures in the New Hampshire Birth Cohort Study [53]. GSE75248 examined placental DNAm in relation to newborns' neurobehavioral outcomes [54]. GSE71719 studied the association between DNA hydroxymethylation and gene expression using placental samples [55]. The Robinson laboratory (RL) at the University of British Columbia (Vancouver, BC, Canada) transferred placental DNAm data that are publicly available in the GEO database. GSE100197 and GSE98224 were studies that aimed to find placental DNAm profiles for preeclampsia and intrauterine growth restriction in women recruited at the University of British Columbia Women's and Children's Hospital (Vancouver, Canada) and at Mount Sinai Hospital (Toronto, Canada), respectively [56]. GSE108567 investigated batch effects in DNAm micro array data [57]. GSE69502 explored DNAm patterns in multi-tissue samples (placental chorionic villi, kidney, spinal cord, brain, and muscle) from fetuses that were aborted due to neural tube defects [58]. GSE74738 aimed to identify differentially-methylated imprinted regions using a genome-wide approach [59]. GSE115508 compared DNAm patterns in cases of placental inflammation (acute chorioamnionitis) with those in unaffected controls [60]. GSE44667 studied the

association between placental DNAm in gene enhancer regions and early-onset preeclampsia [61]. GSE49343 investigated placental DNAm with trisomy and preeclampsia [62]. GSE42409 enhanced probe annotation of Illumina HumanMethylation 450K BeadChip to facilitate biologically meaningful data interpretation [63]. GSE120250 examined the impact of assisted reproductive technology on the placental DNA methylome [64]. GSE70453 conducted epigenome-wide and transcriptome-wide analyses of gestational diabetes [65]. GSE73375 examined DNAm in the preeclamptic placenta in relation to the transforming growth factor beta pathway [66]. GSE75196 studied different DNAm patterns in patients with preeclampsia and unaffected controls [67]. GSE76641 studied the transcriptional and DNAm trajectory of 21 organs during fetal development [68].

Measurement of DNA methylation

Either the Illumina Infinium HumanMethylation450 BeadChip or the Infinium MethylationEPIC BeadChip was used to measure DNAm level at each CpG site. The DNAm level (β-value) was the ratio of two fluorescence signals (methylated and unmethylated). The minfi R package [31] was used to preprocess all the DNAm datasets except for GS2E115508 and GSE120250 (preprocessed by Illumina's proprietary software, Genome Studio). The preprocessing methods and probe exclusion criteria differed across studies. For example, Marsit and colleagues, the largest GEO submitter, used the funNorm, whereas Robinson and colleagues mostly used the funNorm or the SWAN (Table 1). Other GEO submitters used the BMIQ, funNorm, quanNorm, dasen, or noob. Most GEO submitters excluded probes on sex-chromosomes, near single nucleotide polymorphisms, with cross-hybridization or with a detection p-value > 0.01.

Pre-processing of DNA methylation data

We ensured that all samples were included only one time in our training data. Some GEO datasets re-used the same samples or included technical replicates. For example, 154 samples were re-used in GSE100197, GSE108567, GSE69502, GSE74738, GSE44667, GSE49343 and RL data; and 15 technical replicates were found in GSE100197 and RL data. The sample size (N) in Table 1 refers to the counts after excluding the re-used samples and replicates.

We detected and removed outliers using the following steps: 1) we defined a gold standard DNAm profile as the inter-sample median value. For each CpG, we computed the median beta value across all placental samples. 2) The gold standard was correlated with each placental sample to calculate the Pearson correlation coefficient. 3) Placental samples were excluded if their correlation with the gold standard profile was lower than 0.9. Overall, only four putative outliers were removed from the analysis.

Missing DNAm levels were imputed with the gold standard DNAm levels. Thus, if the beta value of a CpG was missing, the missing value was imputed with the interpersonal median value across all samples. These imputations were only implemented in the training data.

Elastic net regression of gestational age

We fit a penalized regression model using the "glmnet" R package [37]. GA was regressed on 441,870 CpG sites that are shared between the 450K and the EPIC array. The glmnet mixing parameter alpha was set to 0.5 (specifying elastic net regression), and the shrinkage parameter, lambda resulting in the minimum mean square error, was chosen using 10-fold cross-validation in the training data. The RPC automatically selected 558 CpG sites (lambda=0.0936), the CPC did 546 CpG sites (lambda=0.0892), the refined RPC did 395 CpG sites (lambda=0.0116), and the fetal sex-classifier did 220 CpGs (lambda=0.0073). The number of overlapping CpGs between the RPC and CPC was 199. Supplementary File 1 includes CpG sites and their corresponding coefficients for the RPC, CPC, refined RPC and fetal sex-classifier.

Epigenome-wide association study of gestational age

We used the R function "standardScreeningNumericTrait" from the weighted gene co-expression network analysis R package (WGCNA; [69]) to carry out a robust correlation test (based on the biweight midcorrelation) between each CpG and GA. We conducted two separate EWAS of GA: one in control placental samples (n=831) and the other in placental samples from preeclampsia cases (n=70). We computed biweight midcorrelations between DNAm levels and GA, and the corresponding Z statistics and p-values in each stratum. The Z statistics of the two sets of EWAS were combined using the weighted Stouffer's method [38] as: $\sum Z_i w_i / \sqrt{\sum w_i^2}$, where w_i is the square root of the sample size in the ith stratum. The corresponding p-values were computed as $2(1 - \Phi(|Z_{\text{meta}}|))$. The EWAS was limited on the 411,870 autosomal probes available on both the 450K and the EPIC array platform.

Software availability

The coefficient values of the placental clocks and the fetal sex classifier can be found in Supplementary File 1.

Abbreviations

GA: gestational age; DNAm: DNA methylation; LMP: last menstrual period; RPC: robust placental clock; CPC: control placental clock; GEO: Gene Expression Omnibus; 450K: Illumina HumanMethylation 450K BeadChip; EPIC: Illumina MethylationEPIC BeadChip; MAE: median absolute error; funNorm: functional normalization; SWAN: subset-quantiles within arrays; noob: normal-exponential out-of-band; BMIQ: beta-mixture quantile dilation; quanNorm: quantile normalization; dasen: data-driven separate normalization; WGCNA: weighted gene co-expression network analysis; EWAS: epigenome-wide association study; cffDNA: cell-free fetal DNA.

AUTHOR CONTRIBUTIONS

YL and SH developed the placental clocks and wrote the manuscript. The remaining authors contributed data, edited the manuscript, and interpreted the results.

ACKNOWLEDGEMENTS

We appreciate all the placenta donors and GEO submitters for making their placental DNAm data publicly available.

CONFLICTS OF INTEREST

The authors declare no conflicts of interest.

FUNDING

REFERENCES

1. Engle WA. Morbidity and mortality in late preterm and early term newborns: a continuum. Clin Perinatol. 2011; 38:493–516.
   https://doi.org/10.1016/j.clp.2011.06.009
   PMID:21890021

2. Hansen AK, Wisborg K, Uldbjerg N, Henriksen TB. Risk of respiratory morbidity in term infants delivered by elective caesarean section: cohort study. BMJ. 2008; 336:85–87.
   https://doi.org/10.1136/bmj.39405.539282.BE
   PMID:18077440

3. Young PC, Glasgow TS, Li X, Guest-Warnick G, Stoddard G. Mortality of late-preterm (near-term) newborns in Utah. Pediatrics. 2007; 119:e659–65.
   https://doi.org/10.1542/peds.2006-2486
   PMID:17332185

4. Davis EP, Buss C, Muftuler LT, Head K, Hasso A, Wing DA, Hobel C, Sandman CA. Children's Brain Development Benefits from Longer Gestation. Front Psychol. 2011; 2:1.
   https://doi.org/10.3389/fpsyg.2011.00001
   PMID:21713130

5. Parikh LI, Reddy UM, Männistö T, Mendola P, Sjaarda L, Hinkle S, Chen Z, Lu Z, Laughon SK. Neonatal outcomes in early term birth. Am J Obstet Gynecol. 2014; 211:265.e1–11.
   https://doi.org/10.1016/j.ajog.2014.03.021
   PMID:24631438

6. Yang S, Platt RW, Kramer MS. Variation in child cognitive ability by week of gestation among healthy term births. Am J Epidemiol. 2010; 171:399–406.
   https://doi.org/10.1093/aje/kwp413 PMID:20080810

7. Organization WH. Born too soon: the global action report on preterm birth. 2012.

8. Lynch CD, Zhang J. The research implications of the selection of a gestational age estimation method. Paediatr Perinat Epidemiol. 2007 (Suppl 2); 21:86–96.
   https://doi.org/10.1111/j.1365-3016.2007.00865.x
   PMID:17803622

9. Robinson HP, Fleming JE. A critical evaluation of sonar "crown-rump length" measurements. Br J Obstet Gynaecol. 1975; 82:702–10.
   https://doi.org/10.1111/j.1471-0528.1975.tb00710.x
   PMID:1182090

10. Papageorghiou AT, Kemp B, Stones W, Ohuma EO, Kennedy SH, Purwar M, Salomon LJ, Altman DG,

Noble JA, Bertino E, Gravett MG, Pang R, Cheikh Ismail L, et al, and International Fetal and Newborn Growth Consortium for the 21st Century (INTERGROWTH-21st). Ultrasound-based gestational-age estimation in late pregnancy. Ultrasound Obstet Gynecol. 2016; 48:719–26. https://doi.org/10.1002/uog.15894 PMID:26924421

11. Papageorghiou AT, Kennedy SH, Salomon LJ, Ohuma EO, Cheikh Ismail L, Barros FC, Lambert A, Carvalho M, Jaffer YA, Bertino E, Gravett MG, Altman DG, Purwar M, et al, and International Fetal and Newborn Growth Consortium for the 21st Century (INTERGROWTH-21st). International standards for early fetal size and pregnancy dating based on ultrasound measurement of crown-rump length in the first trimester of pregnancy. Ultrasound Obstet Gynecol. 2014; 44:641–48. https://doi.org/10.1002/uog.13448 PMID:25044000

12. Campbell S, Newman GB. Growth of the fetal biparietal diameter during normal pregnancy. J Obstet Gynaecol Br Commonw. 1971; 78:513–19. https://doi.org/10.1111/j.1471-0528.1971.tb00309.x PMID:5559266

13. Hadlock FP, Deter RL, Harrist RB, Park SK. Fetal biparietal diameter: a critical re-evaluation of the relation to menstrual age by means of real-time ultrasound. J Ultrasound Med. 1982; 1:97–104. https://doi.org/10.7863/jum.1982.1.3.97 PMID:6152941

14. Kurtz AB, Wapner RJ, Kurtz RJ, Dershaw DD, Rubin CS, Cole-Beuglet C, Goldberg BB. Analysis of biparietal diameter as an accurate indicator of gestational age. J Clin Ultrasound. 1980; 8:319–26. https://doi.org/10.1002/jcu.1870080406 PMID:6772680

15. Campbell S, Thoms A. Ultrasound measurement of the fetal head to abdomen circumference ratio in the assessment of growth retardation. Br J Obstet Gynaecol. 1977; 84:165–74. https://doi.org/10.1111/j.1471-0528.1977.tb12550.x PMID:843490

16. Mongelli M, Wilcox M, Gardosi J. Estimating the date of confinement: ultrasonographic biometry versus certain menstrual dates. Am J Obstet Gynecol. 1996; 174:278–81. https://doi.org/10.1016/S0002-9378(96)70408-8 PMID:8572021

17. Mayne BT, Leemaqz SY, Smith AK, Breen J, Roberts CT, Bianco-Miotto T. Accelerated placental aging in early onset preeclampsia pregnancies identified by DNA methylation. Epigenomics. 2017; 9:279–89. https://doi.org/10.2217/epi-2016-0103 PMID:27894195

18. Mikheev AM, Nabekura T, Kaddoumi A, Bammler TK, Govindarajan R, Hebert MF, Unadkat JD. Profiling gene expression in human placentae of different gestational ages: an OPRU Network and UW SCOR Study. Reprod Sci. 2008; 15:866–77. https://doi.org/10.1177/1933719108322425 PMID:19050320

19. Sitras V, Fenton C, Paulssen R, Vårtun Å, Acharya G. Differences in gene expression between first and third trimester human placenta: a microarray study. PLoS One. 2012; 7:e33294. https://doi.org/10.1371/journal.pone.0033294 PMID:22442682

20. Uusküla L, Männik J, Rull K, Minajeva A, Kõks S, Vaas P, Teesalu P, Reimand J, Laan M. Mid-gestational gene expression profile in placenta and link to pregnancy complications. PLoS One. 2012; 7:e49248. https://doi.org/10.1371/journal.pone.0049248 PMID:23145134

21. Winn VD, Haimov-Kochman R, Paquet AC, Yang YJ, Madhusudhan MS, Gormley M, Feng KT, Bernlohr DA, McDonagh S, Pereira L, Sali A, Fisher SJ. Gene expression profiling of the human maternal-fetal interface reveals dramatic changes between midgestation and term. Endocrinology. 2007; 148:1059–79. https://doi.org/10.1210/en.2006-0683 PMID:17170095

22. Novakovic B, Yuen RK, Gordon L, Penaherrera MS, Sharkey A, Moffett A, Craig JM, Robinson WP, Saffery R. Evidence for widespread changes in promoter methylation profile in human placenta in response to increasing gestational age and environmental/stochastic factors. BMC Genomics. 2011; 12:529. https://doi.org/10.1186/1471-2164-12-529 PMID:22032438

23. Horvath S. DNA methylation age of human tissues and cell types. Genome Biol. 2013; 14:R115. https://doi.org/10.1186/gb-2013-14-10-r115 PMID:24138928

24. Bohlin J, Håberg SE, Magnus P, Reese SE, Gjessing HK, Magnus MC, Parr CL, Page CM, London SJ, Nystad W. Prediction of gestational age based on genome-wide differentially methylated regions. Genome Biol. 2016; 17:207. https://doi.org/10.1186/s13059-016-1063-4 PMID:27717397

25. Knight AK, Craig JM, Theda C, Bækvad-Hansen M, Bybjerg-Grauholm J, Hansen CS, Hollegaard MV, Hougaard DM, Mortensen PB, Weinsheimer SM, Werge TM, Brennan PA, Cubells JF, et al. An epigenetic clock for gestational age at birth based on blood methylation data. Genome Biol. 2016; 17:206. https://doi.org/10.1186/s13059-016-1068-z PMID:27717399

26. Zou H, Hastie T. Regularization and variable selection via the elastic net. J R Stat Soc Series B Stat Methodol. 2005; 67:301–20.
https://doi.org/10.1111/j.1467-9868.2005.00503.x

27. Fortin JP, Labbe A, Lemire M, Zanke BW, Hudson TJ, Fertig EJ, Greenwood CM, Hansen KD. Functional normalization of 450k methylation array data improves replication in large cancer studies. Genome Biol. 2014; 15:503. https://doi.org/10.1186/s13059-014-0503-2 PMID:25599564

28. Maksimovic J, Gordon L, Oshlack A. SWAN: subset-quantile within array normalization for illumina infinium HumanMethylation450 BeadChips. Genome Biol. 2012; 13:R44. https://doi.org/10.1186/gb-2012-13-6-r44 PMID:22703947

29. Triche TJ Jr, Weisenberger DJ, Van Den Berg D, Laird PW, Siegmund KD. Low-level processing of Illumina Infinium DNA Methylation BeadArrays. Nucleic Acids Res. 2013; 41:e90.
https://doi.org/10.1093/nar/gkt090 PMID:23476028

30. Teschendorff AE, Marabita F, Lechner M, Bartlett T, Tegner J, Gomez-Cabrero D, Beck S. A beta-mixture quantile normalization method for correcting probe design bias in Illumina Infinium 450 k DNA methylation data. Bioinformatics. 2013; 29:189–96. https://doi.org/10.1093/bioinformatics/bts680 PMID:23175756

31. Aryee MJ, Jaffe AE, Corrada-Bravo H, Ladd-Acosta C, Feinberg AP, Hansen KD, Irizarry RA. Minfi: a flexible and comprehensive Bioconductor package for the analysis of Infinium DNA methylation microarrays. Bioinformatics. 2014; 30:1363–69. https://doi.org/10.1093/bioinformatics/btu049 PMID:24478339

32. Touleimat N, Tost J. Complete pipeline for Infinium(®) Human Methylation 450K BeadChip data processing using subset quantile normalization for accurate DNA methylation estimation. Epigenomics. 2012; 4:325–41. https://doi.org/10.2217/epi.12.21 PMID:22690668

33. Pidsley R, Y Wong CC, Volta M, Lunnon K, Mill J, Schalkwyk LC. A data-driven approach to pre-processing Illumina 450K methylation array data. BMC Genomics. 2013; 14:293. https://doi.org/10.1186/1471-2164-14-293 PMID:23631413

34. Hannum G, Guinney J, Zhao L, Zhang L, Hughes G, Sadda S, Klotzle B, Bibikova M, Fan JB, Gao Y, Deconde R, Chen M, Rajapakse I, et al. Genome-wide methylation profiles reveal quantitative views of human aging rates. Mol Cell. 2013; 49:359–67. https://doi.org/10.1016/j.molcel.2012.10.016 PMID:23177740

35. Levine ME, Lu AT, Quach A, Chen BH, Assimes TL, Bandinelli S, Hou L, Baccarelli AA, Stewart JD, Li Y, Whitsel EA, Wilson JG, Reiner AP, et al. An epigenetic biomarker of aging for lifespan and healthspan. Aging (Albany NY). 2018; 10:573–91. https://doi.org/10.18632/aging.101414 PMID:29676998

36. Horvath S, Oshima J, Martin GM, Lu AT, Quach A, Cohen H, Felton S, Matsuyama M, Lowe D, Kabacik S, Wilson JG, Reiner AP, Maierhofer A, et al. Epigenetic clock for skin and blood cells applied to Hutchinson Gilford Progeria Syndrome and *ex vivo* studies. Aging (Albany NY). 2018; 10:1758–75. https://doi.org/10.18632/aging.101508 PMID:30048243

37. Friedman J, Hastie T, Tibshirani R. Regularization Paths for Generalized Linear Models via Coordinate Descent. J Stat Softw. 2010; 33:1–22. https://doi.org/10.18637/jss.v033.i01 PMID:20808728

38. Stouffer SA, Suchman EA, DeVinney LC, Star SA, Williams RM Jr. (1949). The American soldier: Adjustment during army life. (Studies in social psychology in World War II), Vol. 1.

39. McLean CY, Bristor D, Hiller M, Clarke SL, Schaar BT, Lowe CB, Wenger AM, Bejerano G. GREAT improves functional interpretation of cis-regulatory regions. Nat Biotechnol. 2010; 28:495–501. https://doi.org/10.1038/nbt.1630 PMID:20436461

40. Dietz PM, England LJ, Callaghan WM, Pearl M, Wier ML, Kharrazi M. A comparison of LMP-based and ultrasound-based estimates of gestational age using linked California livebirth and prenatal screening records. Paediatr Perinat Epidemiol. 2007 (Suppl 2); 21:62–71. https://doi.org/10.1111/j.1365-3016.2007.00862.x PMID:17803619

41. Henriksen TB, Wilcox AJ, Hedegaard M, Secher NJ. Bias in studies of preterm and postterm delivery due to ultrasound assessment of gestational age. Epidemiology. 1995; 6:533–37. https://doi.org/10.1097/00001648-199509000-00012 PMID:8562631

42. Morin I, Morin L, Zhang X, Platt RW, Blondel B, Bréart G, Usher R, Kramer MS. Determinants and consequences of discrepancies in menstrual and ultrasonographic gestational age estimates. BJOG. 2005; 112:145–52. https://doi.org/10.1111/j.1471-0528.2004.00311.x PMID:15663577

43. Leavey K, Benton SJ, Grynspan D, Bainbridge SA, Morgen EK, Cox BJ. Gene markers of normal villous maturation and their expression in placentas with maturational pathology. Placenta. 2017; 58:52–59.

https://doi.org/10.1016/j.placenta.2017.08.005
PMID:28962696

44. Jia RZ, Zhang X, Hu P, Liu XM, Hua XD, Wang X, Ding HJ. Screening for differential methylation status in human placenta in preeclampsia using a CpG island plus promoter microarray. Int J Mol Med. 2012; 30:133–41.
https://doi.org/10.3892/ijmm.2012.983
PMID:22552323

45. Kulkarni A, Chavan-Gautam P, Mehendale S, Yadav H, Joshi S. Global DNA methylation patterns in placenta and its association with maternal hypertension in pre-eclampsia. DNA Cell Biol. 2011; 30:79–84.
https://doi.org/10.1089/dna.2010.1084
PMID:21043832

46. Yuen RK, Peñaherrera MS, von Dadelszen P, McFadden DE, Robinson WP. DNA methylation profiling of human placentas reveals promoter hypomethylation of multiple genes in early-onset preeclampsia. Eur J Hum Genet. 2010; 18:1006–12.
https://doi.org/10.1038/ejhg.2010.63
PMID:20442742

47. Wallace JM, Bhattacharya S, Horgan GW. Gestational age, gender and parity specific centile charts for placental weight for singleton deliveries in Aberdeen, UK. Placenta. 2013; 34:269–74.
https://doi.org/10.1016/j.placenta.2012.12.007
PMID:23332414

48. Kazy Z, Rozovsky IS, Bakharev VA. Chorion biopsy in early pregnancy: A method of early prenatal diagnosis for inherited disorders. Prenat Diagn. 1982; 2:39–45.
https://doi.org/10.1002/pd.1970020107

49. Ward RH, Modell B, Petrou M, Karagözlu F, Douratsos E. Method of sampling chorionic villi in first trimester of pregnancy under guidance of real time ultrasound. Br Med J (Clin Res Ed). 1983; 286:1542–44.
https://doi.org/10.1136/bmj.286.6377.1542
PMID:6405878

50. Alberry M, Maddocks D, Jones M, Abdel Hadi M, Abdel-Fattah S, Avent N, Soothill PW. Free fetal DNA in maternal plasma in anembryonic pregnancies: confirmation that the origin is the trophoblast. Prenat Diagn. 2007; 27:415–18.
https://doi.org/10.1002/pd.1700 PMID:17286310

51. Gupta AK, Holzgreve W, Huppertz B, Malek A, Schneider H, Hahn S. Detection of fetal DNA and RNA in placenta-derived syncytiotrophoblast microparticles generated in vitro. Clin Chem. 2004; 50:2187–90.
https://doi.org/10.1373/clinchem.2004.040196
PMID:15502097

52. Lo YM, Tein MS, Lau TK, Haines CJ, Leung TN, Poon PM, Wainscoat JS, Johnson PJ, Chang AM, Hjelm NM. Quantitative analysis of fetal DNA in maternal plasma and serum: implications for noninvasive prenatal diagnosis. Am J Hum Genet. 1998; 62:768–75.
https://doi.org/10.1086/301800 PMID:9529358

53. Green BB, Karagas MR, Punshon T, Jackson BP, Robbins DJ, Houseman EA, Marsit CJ. Epigenome-Wide Assessment of DNA Methylation in the Placenta and Arsenic Exposure in the New Hampshire Birth Cohort Study (USA). Environ Health Perspect. 2016; 124:1253–60. https://doi.org/10.1289/ehp.1510437
PMID:26771251

54. Paquette AG, Houseman EA, Green BB, Lesseur C, Armstrong DA, Lester B, Marsit CJ. Regions of variable DNA methylation in human placenta associated with newborn neurobehavior. Epigenetics. 2016; 11:603–13. https://doi.org/10.1080/15592294.2016.1195534
PMID:27366929

55. Green BB, Houseman EA, Johnson KC, Guerin DJ, Armstrong DA, Christensen BC, Marsit CJ. Hydroxymethylation is uniquely distributed within term placenta, and is associated with gene expression. FASEB J. 2016; 30:2874–84.
https://doi.org/10.1096/fj.201600310R
PMID:27118675

56. Wilson SL, Leavey K, Cox BJ, Robinson WP. Mining DNA methylation alterations towards a classification of placental pathologies. Hum Mol Genet. 2018; 27:135–46. https://doi.org/10.1093/hmg/ddx391
PMID:29092053

57. Price EM, Robinson WP. Adjusting for Batch Effects in DNA Methylation Microarray Data, a Lesson Learned. Front Genet. 2018; 9:83.
https://doi.org/10.3389/fgene.2018.00083
PMID:29616078

58. Price EM, Peñaherrera MS, Portales-Casamar E, Pavlidis P, Van Allen MI, McFadden DE, Robinson WP. Profiling placental and fetal DNA methylation in human neural tube defects. Epigenetics Chromatin. 2016; 9:6. https://doi.org/10.1186/s13072-016-0054-8
PMID:26889207

59. Hanna CW, Peñaherrera MS, Saadeh H, Andrews S, McFadden DE, Kelsey G, Robinson WP. Pervasive polymorphic imprinted methylation in the human placenta. Genome Res. 2016; 26:756–67.
https://doi.org/10.1101/gr.196139.115
PMID:26769960

60. Konwar C, Price EM, Wang LQ, Wilson SL, Terry J, Robinson WP. DNA methylation profiling of acute chorioamnionitis-associated placentas and fetal membranes: insights into epigenetic variation in spontaneous preterm births. Epigenetics Chromatin.

2018; 11:63. https://doi.org/10.1186/s13072-018-0234-9 PMID:30373633

61. Blair JD, Yuen RK, Lim BK, McFadden DE, von Dadelszen P, Robinson WP. Widespread DNA hypomethylation at gene enhancer regions in placentas associated with early-onset pre-eclampsia. Mol Hum Reprod. 2013; 19:697–708. https://doi.org/10.1093/molehr/gat044 PMID:23770704

62. Blair JD, Langlois S, McFadden DE, Robinson WP. Overlapping DNA methylation profile between placentas with trisomy 16 and early-onset preeclampsia. Placenta. 2014; 35:216–22. https://doi.org/10.1016/j.placenta.2014.01.001 PMID:24462402

63. Price ME, Cotton AM, Lam LL, Farré P, Emberly E, Brown CJ, Robinson WP, Kobor MS. Additional annotation enhances potential for biologically-relevant analysis of the Illumina Infinium HumanMethylation450 BeadChip array. Epigenetics Chromatin. 2013; 6:4. https://doi.org/10.1186/1756-8935-6-4 PMID:23452981

64. Choufani S, Turinsky AL, Melamed N, Greenblatt E, Brudno M, Bérard A, Fraser WD, Weksberg R, Trasler J, Monnier P, Fraser WD, Audibert F, Dubois L, et al, and 3D cohort study group. Impact of assisted reproduction, infertility, sex and paternal factors on the placental DNA methylome. Hum Mol Genet. 2019; 28:372–85. https://doi.org/10.1093/hmg/ddy321 PMID:30239726

65. Binder AM, LaRocca J, Lesseur C, Marsit CJ, Michels KB. Epigenome-wide and transcriptome-wide analyses reveal gestational diabetes is associated with alterations in the human leukocyte antigen complex. Clin Epigenetics. 2015; 7:79. https://doi.org/10.1186/s13148-015-0116-y PMID:26244062

66. Martin E, Ray PD, Smeester L, Grace MR, Boggess K, Fry RC. Epigenetics and Preeclampsia: Defining Functional Epimutations in the Preeclamptic Placenta Related to the TGF-β Pathway. PLoS One. 2015; 10:e0141294. https://doi.org/10.1371/journal.pone.0141294 PMID:26510177

67. Yeung KR, Chiu CL, Pidsley R, Makris A, Hennessy A, Lind JM. DNA methylation profiles in preeclampsia and healthy control placentas. Am J Physiol Heart Circ Physiol. 2016; 310:H1295–303. https://doi.org/10.1152/ajpheart.00958.2015 PMID:26968548

68. Roost MS, Slieker RC, Bialecka M, van Iperen L, Gomes Fernandes MM, He N, Suchiman HE, Szuhai K, Carlotti F, de Koning EJ, Mummery CL, Heijmans BT, Chuva de Sousa Lopes SM. DNA methylation and transcriptional trajectories during human development and reprogramming of isogenic pluripotent stem cells. Nat Commun. 2017; 8:908. https://doi.org/10.1038/s41467-017-01077-3 PMID:29030611

69. Langfelder P, Horvath S. WGCNA: an R package for weighted correlation network analysis. BMC Bioinformatics. 2008; 9:559. https://doi.org/10.1186/1471-2105-9-559 PMID:19114008

SUPPLEMENTARY MATERIAL

Supplementary File 1

This file includes CpG sites and their corresponding coefficients used for the RPC, CPC, refined RPC and fetal sex-classifier.

Supplementary File 2

This file includes part of summary statistics of EWAS of GA (the 10,827 CpG sites with meta P<1E-07).

Rapamycin retards epigenetic ageing of keratinocytes independently of its effects on replicative senescence, proliferation and differentiation

Steve Horvath[1,2], Ake T. Lu[1] Howard Cohen[3], Ken Raj[4]

[1]Human Genetics, David Geffen School of Medicine, University of California, Los Angeles, Los Angeles, CA 90095, USA
[2]Biostatistics, Fielding School of Public Health, University of California, Los Angeles, Los Angeles, CA 90095, USA
[3]Elizabeth House Medical Practice, Warlingham, Surrey CR6 9LF, United Kingdom
[4]Radiation Effects Department, Centre for Radiation, Chemical and Environmental Hazards, Public Health England, Chilton, Didcot, Oxfordshire OX11 0RQ, United Kingdom

ABSTRACT

The advent of epigenetic clocks has prompted questions about the place of epigenetic ageing within the current understanding of ageing biology. It was hitherto unclear whether epigenetic ageing represents a distinct mode of ageing or a manifestation of a known characteristic of ageing. We report here that epigenetic ageing is not affected by replicative senescence, telomere length, somatic cell differentiation, cellular proliferation rate or frequency. It is instead retarded by rapamycin, the potent inhibitor of the mTOR complex which governs many pathways relating to cellular metabolism. Rapamycin however, is also an effective inhibitor of cellular senescence. Hence cellular metabolism underlies two independent arms of ageing – cellular senescence and epigenetic ageing. The demonstration that a compound that targets metabolism can slow epigenetic ageing provides a long-awaited point-of-entry into elucidating the molecular pathways that underpin the latter. Lastly, we report here an *in vitro* assay, validated in humans, that recapitulates human epigenetic ageing that can be used to investigate and identify potential interventions that can inhibit or retard it.

INTRODUCTION

One of the biggest challenges in ageing research is the means of measuring age independently of time. This need becomes particularly clear when we wish to evaluate the effects of drugs or compounds on ageing, where the use of time as a measure of age is clearly inappropriate. In recent years, several age-estimators known as epigenetic clocks have been developed, which are based on methylation states of specific CpGs, some of which become increasingly methylated, while others decreasingly so with age [1]. Age estimated by these clocks is referred to as epigenetic age or more precisely, DNA methylation age (DNAm age). The "ticking" of these clocks is constituted by methylation changes that

occur at specific CpGs of the genome. Significantly, the increased rate by which these specific methylation changes occur is associated with many age-related health conditions [1-9], indicating that epigenetic clocks, capture biological ageing (epigenetic ageing) at least to some extent. The numerous epigenetic clocks that have been independently developed [10-16] differ in accuracy, biological interpretation and applicability, whereby some epigenetic clocks are compatible only to some tissues such as blood. In this regard, the pan-tissue epigenetic clock [2] stands out because it is applicable to virtually all tissues of the body, with the exception of sperm. It estimates the same epigenetic age for different post-mortem tissues (except the cerebellum and female breast) from the same individual [2, 8]. Although the

pan-tissue epigenetic clock performs extremely well with *in vivo* cell samples, its accuracy was not as good with fibroblasts and other *in vitro* cell samples. We addressed this recently by developing an even more accurate multi-tissue age estimator, which we refer to as skin & blood clock [3], which is applicable for *in vivo* as well as *in vitro* samples of human fibroblasts, keratinocytes, buccal cells, blood cells, saliva and endothelial cells. *In vitro* human cell culture systems offer many advantages including tight control of growth conditions, nutrients, cell proliferation rates, detailed morphological analyses and genetic manipulation, all of which are impractical or inappropriate in human cohort studies. Hence the availability of an *in vivo* epigenetic clock, such as the skin & blood clock that can also be used for *in vitro* experiments is an important and significant step towards uncovering the molecular mechanisms that underpin epigenetic ageing.

Although the molecular mechanisms of epigenetic ageing remain largely uncharacterised, the cellular aspects however, have been explored to a greater albeit limited degree. The similar epigenetic ages detected amongst different tissue of the same body [2, 8] suggests that epigenetic age is not a measure of cellular proliferation since the rate and frequency of proliferation differ greatly between different tissues such as blood, which is highly proliferative and heart cells, which are post-mitotic. It is intuitive to make a connection between epigenetic ageing and senescent cells, which increases in number with age and which mediates phenotypic ageing [8, 17]. This attractive link however, was discounted by previous reports which clearly excluded DNA damage, telomere attrition and cellular senescence as drivers of epigenetic aging [18].

A way to further characterise epigenetic ageing is through the evaluation of validated anti-aging interventions on it. Such an intervention is the nutrient response pathway regulated by the mammalian target of rapamycin (mTOR) [19-21]. Although originally developed as an immunosuppressant, rapamycin has emerged as one of the most impressive life-extending compounds [22]. It has been repeatedly shown to extend the lives of different animal species including those of yeast [23], flies [24] and mice [25, 26]. The structure of rapamycin presents two major sites for potential interactions. The binding of one site to FKBP12 protein, allows its other site to bind and inhibit the mTOR kinase [27]. This kinase is part of a complex that promotes cell growth, proliferation and cell survival [28, 29]. This may be why mTOR activity is often elevated in cancer cells; the rationale behind its use as an anti-cancer drug [30]. By inhibiting mTOR activity, rapamycin also recapitulates to some extent, the effect of calorie-restriction, which has also been repeatedly

shown to prolong the lives of many different animal species [31]. As such, rapamycin is widely considered to be a promising anti-ageing intervention. Here we characterise epigenetic aging in primary human keratinocytes from multiple donors by testing their sensitivities to rapamycin and we observed that it can indeed mitigate epigenetic ageing independently of cellular senescence, proliferation, differentiation and telomere elongation.

RESULTS

Opposing effects of Rapamycin and ROCK inhibitor on keratinocyte proliferation

The availability of an epigenetic clock, such as the skin & blood clock, which is applicable to cultured cells, allows epigenetic ageing to be studied beyond the purely descriptive nature afforded by epidemiological analyses alone. Towards this end, we have established *in vitro* epigenetic ageing systems using primary human cells. One of this is based on primary keratinocytes that are derived from healthy human skins. As previously reported by others, we observed that the proliferation rate of these cells, which is defined as the number of population doublings per unit of time, can be significantly altered by different compounds. Rapamycin, which is the primary focus of this investigation reduces cellular proliferation rate, while Y-27632, which inhibits Rho kinase (ROCK inhibitor) increases it, and a mixture of both modestly alleviates the repressive effect of rapamycin (Figure 1 and Table 1). The opposing effects of these compounds on keratinocyte proliferation present us with the opportunity to test whether cellular proliferation rate impacts epigenetic ageing while carrying out our primary aim of interrogating the effects of rapamycin on epigenetic ageing.

Effects of Rapamycin and Y-27632 on epigenetic ageing

Primary keratinocytes were isolated from human neonatal foreskins from three donors (Donor A, B and C) and were put in culture with standard media or media supplemented with rapamycin, Y-27632 or a cocktail of both of these compounds (methods). The cells were passaged continually and population doublings at each passage recorded. In time all cells, regardless of donor or treatment underwent replicative senescence, where they ceased to increase their numbers after at least 2 weeks in culture with regular replenishment of media. Interestingly, two of the three donor cells treated with rapamycin underwent further proliferation before replicative senescence, indicating that their proliferative capacity was increased (Figure 1 and Table 2). This was also observed with Y-27632-treated cells. DNA

methylation profiles from a selection of passages of these cells were obtained and analysed with the skin & blood clock. It is clear from Figure 2 that while Y-27632 did not impose any appreciable effect, rapamycin retarded epigenetic ageing of these cells. This is evident even when Y-27632 was present with rapamycin. These empirical observations demonstrate three fundamental features of epigenetic ageing. First, increased cellular proliferation rate, as instigated by Y-27632 (Figure 1 and Table 1) does not affect epigenetic ageing. This
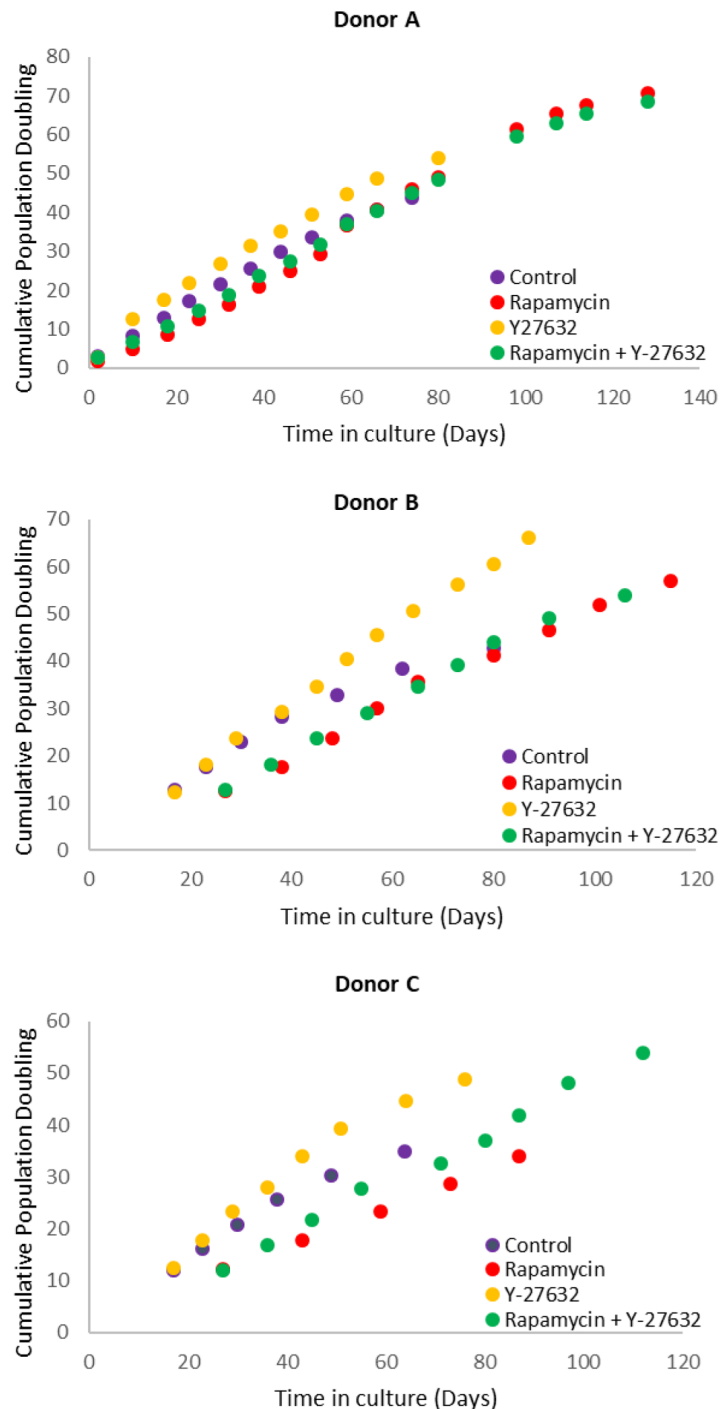
Figure 1. Effects of rapamycin and Y-27632 on the proliferation of keratinocytes from Donors A, B and C that were used in the subsequent experiments. Cells from Donors A, B and C were cultured in the continued presence of the indicated compounds. Population doubling at every cell passage was ascertained until replicative senescence, and plotted against time.

echoes the conclusion derived from analyses of *in vivo* tissues, using the pan-tissue age estimator [2] and confirmed by Yang et al. [32] who specifically derived a DNA methylation-based mitotic clock to be able to measure cellular proliferation, as epigenetic ageing clocks were not able to do so. Second, increased proliferative capacity (the number of times cells proliferate before replicative senescence) is not inextricably linked with retardation of epigenetic ageing since rapamycin and Y-27632 can both instigate the former, but only rapamycin-treated cells exhibited retardation of epi-genetic ageing. Third, epigenetic ageing is not a measure of replicative senescence since all rapamycin-treated cells eventually underwent replicative senescence and yet remained younger than the un-treated control cells; an observation that would not be made were epigenetic age a measure of senescent cells.

Somatic cell differentiation does not drive epigenetic ageing

Having ruled out cellular proliferation rate and proliferation capacity, as well as replicative senescence as drivers of epigenetic ageing, we considered the possible role of somatic cell differentiation in this regard. We observed that healthy primary keratinocytes in culture are heterogeneous in size and shape, but those that were growing in the presence of rapamycin were much more regular in shape and have considerably fewer enlarged cells (Figure 3A). Staining with antibodies against p16; a marker of senescent cells [33],

and involucrin; a marker of early keratinocyte differentiation [34], showed that the enlarged cells were a mixture of senescent cells and differentiating cells, with some cells exhibiting both markers (Figure 3B). As our previous investigations [18] and observations above have uncoupled cellular senescence from epigenetic ageing, we questioned whether cellular differentiation could instead be the driver and the ability of rapamycin to reduce spontaneous differentiation may be the way by which it retards epigenetic ageing.

In the experiments described thus far, primary keratinocytes were grown in a culture condition where the medium used (CnT-07) was designed with the expressed purpose of encouraging the proliferation of progenitor keratinocytes, while restricting their spontaneous differentiation; evidently not eliminating it altogether. To test the hypothesis that cellular differentiation drives epigenetic ageing, we opted to encourage spontaneous keratinocyte differentiation to see if this would cause a rise in their epigenetic age. To this end, we cultured human primary keratinocytes in a different medium, as reported by Rheinwald and Green [35], and with mouse 3T3 cells, which serve as feeder cells. Crucially, this culture condition which we term RG not only supports the proliferation of keratinocytes, it also permitted spontaneous differentiation to a much greater extent than does CnT media. Figure 4A shows a typical keratinocyte colony grown in RG condition. The colony is constituted by small proliferating cells as well as considerable number of large cells in different stages of differentiation.

Table 1. Population doubling times (in hours) of primary neonatal foreskin keratinocytes from three donors (A, B and C) cultured in various conditions.

Culture condition	Donor A	Donor B	Donor C
Control	38.1	38.2	41.6
Rapamycin	42.8	46.5	66.0
Y-27632	30.1	31.6	30.3
Rapamycin + Y-27632	39.6	44.5	49.1

Table 2. Cumulative population doubling of keratinocyte cultures from three donors (A, B and C) at the point of replicative senescence.

Culture condition	Donor A	Donor B	Donor C
Control	44	43	35
Rapamycin	71	57	34
Y-27632	54	66	49
Rapamycin + Y-27632	69	54	54
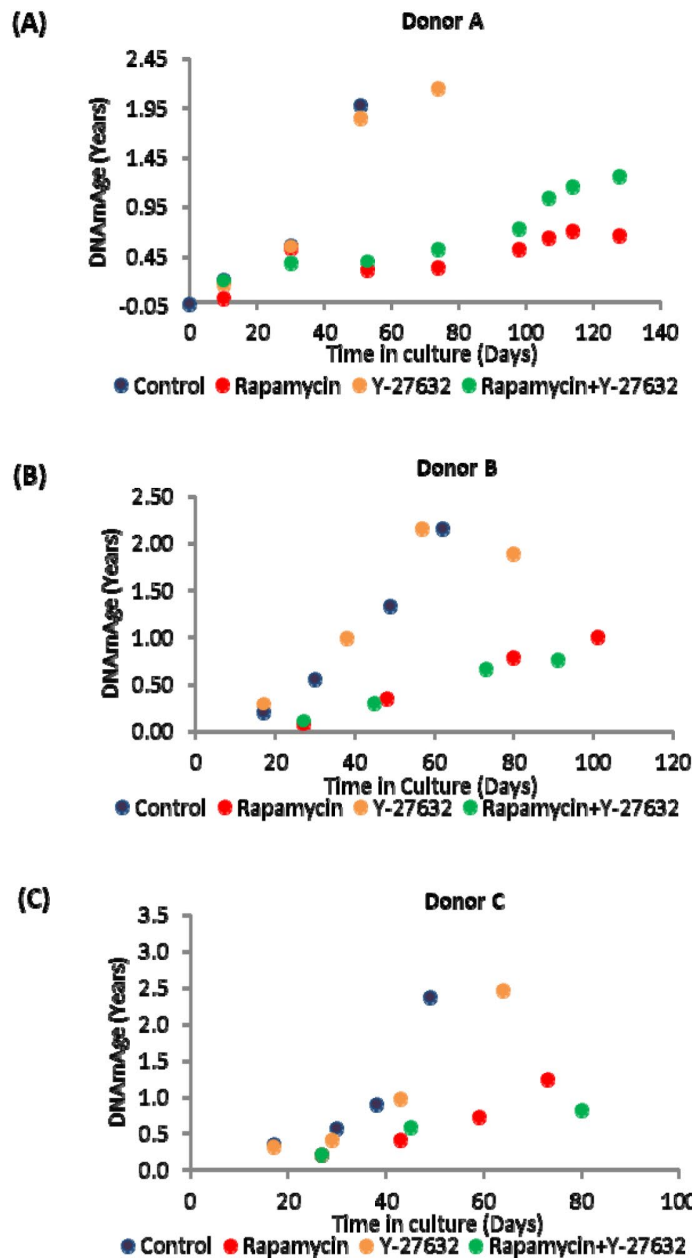
Figure 2. Ageing dynamics of keratinocytes of (A) Donor A, (B) Donor B and (C) Donor C in the presence or absence of rapamycin and Y-27632. Methylation profiles of DNA from selected passages of each cell population were analysed and their ages estimated with the skin and blood clock. The colour allocated to each culture condition is preserved throughout for ease of comparison.

Primary keratinocytes from the same human donor (Donor D) were cultured in these two different conditions described above (CnT and RG). DNA methylation profiles from four passages of cells, with known number of population doubling were obtained and their ages were estimated by the skin & blood clock. Figure 4B shows that encouraging greater keratinocyte differentiation by culturing them in RG condition did not increase epigenetic ageing, demonstrating that contrary to the hypothesis, epigenetic ageing is not increased by greater keratinocyte differentiation and therefore the retardation of epigenetic ageing by rapamycin is not mediated through its suppression of spontaneous somatic cell differentiation. Collectively, these experiments have demonstrated that rapamycin is an effective retardant of epigenetic ageing, and that this activity is mediated independently of its effects on replicative senescence and somatic cell differentiation.
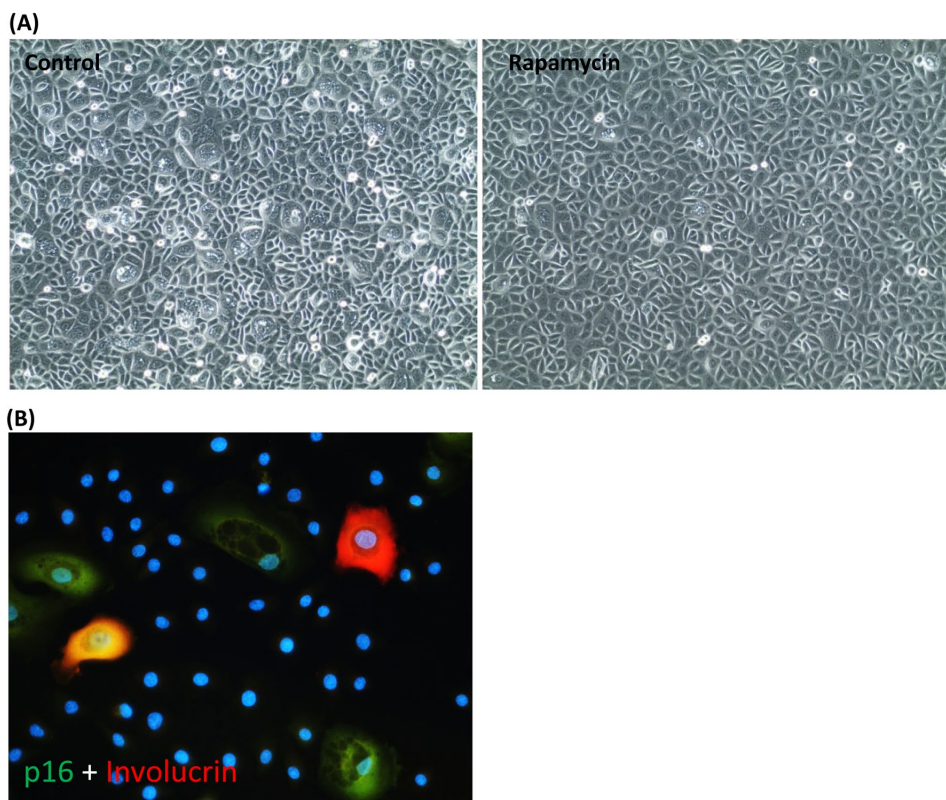
Figure 3. Rapamycin suppresses the emergence of senescent cells and spontaneous keratinocyte differentiation. (**A**) Phase contrast picture of primary keratinocytes cultured in CnT-07 medium in the absence (left panel) or presence (right panel) of rapamycin. (**B**) The large keratinocytes seen in (**A**) were stained positive with antibodies against p16 (in green), involucrin (red) or both, p16 and involucrin (yellow). Nuclei were stained with DAPI.

DISCUSSION

It is widely assumed that extension of lifespan is a result of retardation of ageing. While there is no counter-evidence to challenge this highly intuitive association, supporting empirical evidence to confirm it is not easy to acquire. As a case in point, improvement in public health in the past century has extended life-span, but there is no directly measurable evidence that this was accompanied by a reduction in the rate of ageing. The same question could be asked of any intervention that purports to extend life. The scarcity of empirical evidence is due in part to the lack of a good measure of age that is not based on time. In this regard, the relatively recent development of epigenetic clocks is of great interest [1]. Despite their impressive performance, almost nothing is known about the molecular com-ponents and pathways that underpin them. At the cellular level however, more is known, but from the perspective of what epigenetic ageing is not, rather than what it is. The bringing together of rapamycin and the skin & blood clock in the experiments above have shed

light on both of them. This has been significantly enhanced by comparison with the effects, or not, of the Rho kinase inhibitor, Y-27632. As a case in point, the retardation of epigenetic ageing by rapamycin could have been erroneously ascribed to the retardation of the rate of keratinocyte proliferation, were it not for the fact that Y-27632 augments proliferation rate but does not increase epigenetic ageing. This precludes a simplistic and incorrect correlation between the rate of cellular proliferation and epigenetic ageing. Recently Yang et al demonstrated that epigenetic ageing clock tracks cellular proliferation very poorly compared to the purpose-built DNA methylation-based mitotic clock [32].

The impulse to turn our attention and ascribe retardation of epigenetic ageing to reduced senescent cells is understandable since rapamycin does indeed reduce the emergence of these cells in cultures, as consistent with previous characterisation and description [36-41]. This notion however is inconsistent with our previous finding that the epigenetic age of a cellular population is

not dependent on the presence of senescent cells [18], and this conclusion is further confirmed here, where all the rapamycin-treated cells eventually senesced, without any rise in their epigenetic age. Therefore, while rapamycin's inhibition of senescence is not in doubt, this is not the means by which it retards the progression of epigenetic age of keratinocytes.

To test whether somatic cell differentiation drives epigenetic ageing, we refrained from using chemical means to induce terminal differentiation of keratinocytes as this could introduce DNA methylation changes that might confound interpretation of the results. Instead, we exploited the propensity of keratinocytes to spontaneously differentiate, which they do significantly better in RG medium than in CnT-07 medium [42]. The hypothesis that differentiation drives epigenetic ageing was clearly refuted by these observations. While we still do not know what cellular feature is associated with epigenetic ageing, we can now remove somatic cell differentiation from the list of possibilities and place it with cellular senescence, proliferation and telomere length maintenance, which represent cellular features that are all not linked to epigenetic ageing.
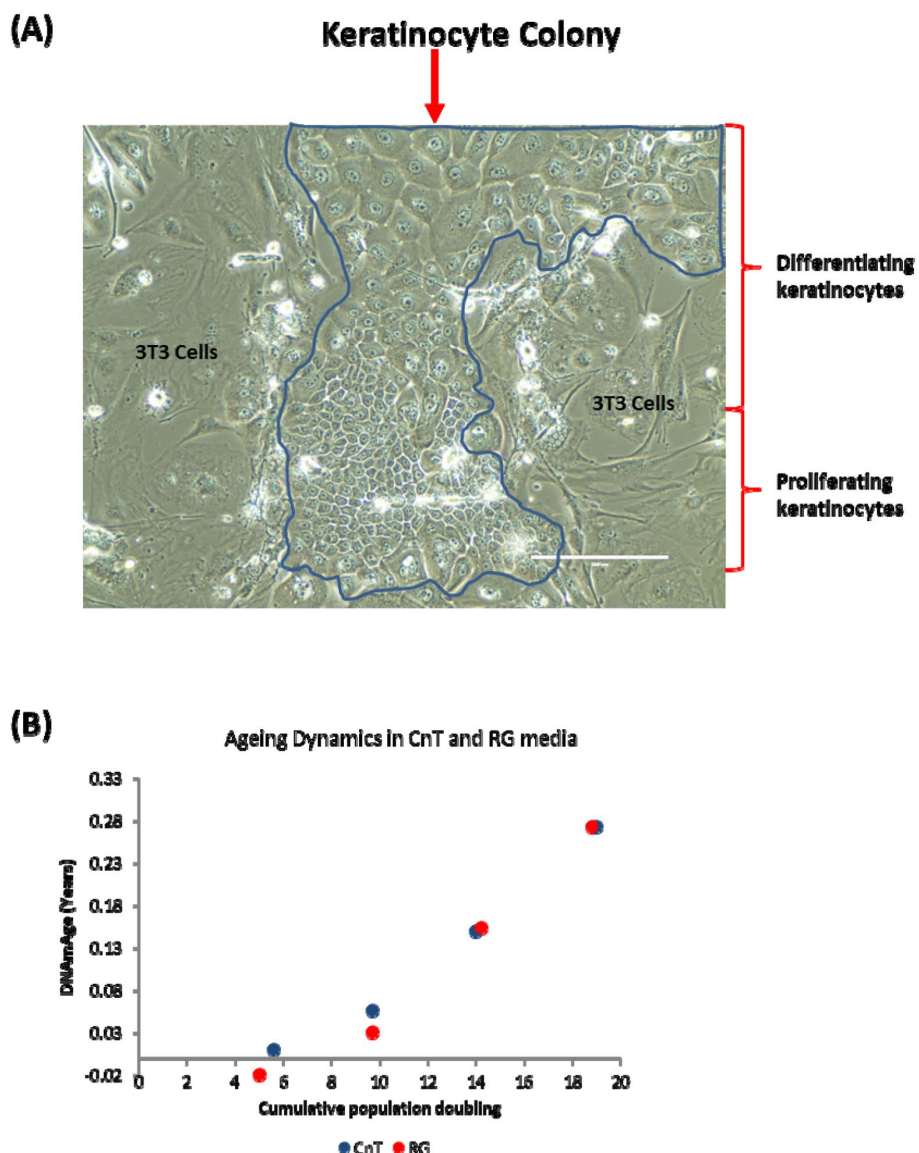
Figure 4. Keratinocyte differentiation does not drive epigenetic ageing. (**A**) Phase contrast image of a primary keratinocyte colony grown in the presence of irradiated J2-3T3 feeder cells in RG medium. The keratinocyte colony is demarcated within the blue boarder and proliferating or differentiating keratinocytes are indicated. Cells external of the boarder are irradiated 3T3-J2 feeder cells. (**B**) Comparison of epigenetic aging between primary keratinocytes grown in CnT-07 media (CnT) and RG media (RG).

The ability of rapamycin to suppress the progression of epigenetic ageing is very encouraging for many reasons not least because it provides a valuable point-of-entry into molecular pathways that are potentially associated with it. Evidently, the target of rapamycin, the mTOR complex is of particular interest. It acts to promote many processes including, but not limited to protein synthesis, autophagy, lipid synthesis and glycolysis [29, 43, 44]. The experiments above were not designed to identify the specific mTOR activity or activities that underpin epigenetic ageing, but they point to further experiments involving gene manipulation and drugs that could be brought to address this question. It is of great significance that we have previously identified through genome-wide association studies (GWAS), genetic variants near MLST8 coding region whose expression levels are positively correlated with epigenetic aging rates in human cerebellum [45]. MLST8 is a subunit of the mTORC1 and mTORC2 complexes, and its gene expression levels increase with chronological age in multiple brain regions [45]. It is pivotal for mTOR function as its deletion prevents the formation of mTORC1 and mTORC2 complexes [46]. The convergence of the GWAS observation with the experimental system described here is a testament of the strength of the skin & blood clock in uncovering biological features that are consistent between the human level and cellular level. It lends weight to the emerging view that the mTOR pathway may be the underlying mechanism that supports epigenetic ageing.

It is of interest to note that the experimental set-up above constitutes an *in vitro* ageing assay that is applicable not only to pure research but to screening and discovering other compounds and treatments that may mitigate or suppress epigenetic ageing. Most biological models of human diseases or conditions are derived from molecular, cellular or animal systems that rightly require rigorous validation in humans. In this regard, the epigenetic clock is distinct in being derived from, and validated at the human level. Hence *in vitro* experimental observations made with it carry a significant level of relevance and can be readily compared with an already available collection of human data generated by the epigenetic clock – the MSLT8 described above is an example in point. An added advantage of such a validated *in vitro* ageing system for human cells is the ability to test the efficacy of potential mitigators of ageing in a well-controlled manner, within a relatively short time, at a significantly low cost and with the ability to ascertain whether the effects are on life-span, ageing or both; all of which are not readily achieved with human cohort studies.

We wish to acknowledge some limitations inherent in this investigation. First, we have not tested this activity of rapamycin on all cell types and we caution the reader that interventions against epigenetic aging can be cell-type specific: for example, menopausal hormone therapy appears to slow epigenetic ageing of buccal cells (which are predominantly keratinocytes) but not that of blood [47]. Second, while we have used primary keratinocytes derived from numerous donors, they were all from neonatal tissues. This is a necessary constrain at this early stage of the investigation in order to avoid confounding effects of age. It would be necessary to test the efficacy of rapamycin on adult donors across the entire age spectrum (0-100 years). Finally, it is important to note that it is inadvisable (actively discouraged) to directly extrapolate the studies here, especially in terms of the magnitude of age suppression, to potential effects of rapamycin on humans.

In summary, the observations above represent the first biological connection between epigenetic ageing and rapamycin. These results for human cells add to the evidence that extension of life, at least by rapamycin, is indeed accompanied by retardation of ageing. These observations also suggest that the life-extending property of rapamycin may be a resultant of its multiple actions which include, but not necessarily limited to suppression of cellular senescence [36-38, 48] and epigenetic aging, with the possibility of augmentation of cellular proliferative potential.

MATERIALS AND METHODS

In vitro cultured cell procedure

Isolation and culture of primary keratinocytes
Primary human neonatal fibroblasts were isolated from circumcised foreskins. Informed consent was obtained prior to collection of human skin samples with approval from the Oxford Research Ethics Committee; reference 10/H0605/1. The tissue was cut into small pieces and digested overnight at 4 °C with 0.5 mg/ml Liberase DH in CnT-07 keratinocyte medium (CellnTech) supplemented with penicillin/streptomycin (Sigma) and gentamycin/amphotericin (Life Tech). Following digestion, the epidermis was peeled off from the tissue pieces and placed in 1 millilitre (ml) of trypsin-versene. After approximately 5 minutes of physical desegregation with forceps, 4 ml of soybean trypsin inhibitor was added to the cell suspension and transferred into a tube for centrifugation at 1,200 revolutions per minute for 5 minutes. The cell pellet was resuspended in CnT-07 media and seeded into fibronectin/collagen-coated plates. Cells were grown at 37 °C, with 5% CO_2 in a humidified incubator. Growth medium was changed every other day. Upon confluence, cells were trypsinised, counted and 100,000 were seeded into fresh fibronectin/collagen-coated plates. Population doubling

was calculate using the following formula: [Log(number of harvested cells)- log(number of seeded cells)] X 3.32. Rapamycin was used at 25nM and Y-27632 at 1μM concentrations and were present in the media of treated cells for the entire duration of the experiments. RG medium was prepared by mixing three parts of F12 medium with one part DMEM, supplemented with 5% foetal calf serum, 0.4ug/ml hydrocortisone, 8.4ng/ml cholera toxin, 5ug/ml insulin, 24ug/ml adenine and 10ng/ml epidermal growth factor. 3T3-J2 cells were cultured in DMEM supplemented with 10% foetal calf serum. To prepare feeder cells, 3T3-J2 cells were irradiated at 60Gy and seeded onto fibronectin/collagen-coated plates in RG medium at least 6 hours but no more than 24 hours prior to seeding of keratinocytes. To harvest keratinocytes grown in RG media, feeder cells were first removed with squirting of the monolayer with trypsin-versene for approximately 3 minutes, after which the monolayer was rinsed with 7ml of Phosphate Buffered Saline (PBS) followed by incubation of the monolayer with 0.5ml of trypsin-versene. When all the keratinocytes have lifted off the plate, 1ml of soybean trypsin inhibitor was added to the cell suspension. Cells were counted and 100,000 were seeded into fresh plates as described above.

Immunofluorescence

Cells were grown on glass coverslips that were pre-coated with fibronectin-collagen. When ready, the cells were fixed with formalin for 10 minutes, followed by three rinses with Phosphate Buffered Saline (PBS). Cell membranes were permeabilised with 0.5% TritonX-100 for 15 minutes followed by three 5 minute rinses with PBS. Primary antibodies diluted in 2% foetal calf serum in PBS were added to the cells. After 1 hour the antibodies were removed followed by three 5 minute rinsing, after which secondary antibodies (diluted in 2% foetal calf serum in PBS) was added. After 30minutes, the antibodies were removed and the cells were rinsed five times with 1ml PBS each time for five minutes followed by a final rinse in 1 ml distilled water before mounting on glass slide with Vectastain. Cells were imaged using a fluorescence microscope. Antibodies used were as follows: Anti-Involucrin (Abcam ab53112) diluted at 1:1000 and Anti-p16 (Bethyl laboratories A303-930A-T) diluted at 1:500.

DNA methylation studies and epigenetic clock

DNA was extracted from cells using the Zymo Quick DNA mini-prep plus kit (D4069) according to the manufacturer's instructions and DNA methylation levels were measured on Illumina 850 EPIC arrays according to the manufacturer's instructions. The Illumina BeadChips (EPIC or 450K) measures bisulfite-conversion-based, single-CpG resolution DNAm levels at different CpG sites in the human genome. These data were generated by following the standard protocol of Illumina methylation assays, which quantifies methylation levels by the β value using the ratio of intensities between methylated and un-methylated alleles. Specifically, the β value is calculated from the intensity of the methylated (M corresponding to signal A) and un-methylated (U corresponding to signal B) alleles, as the ratio of fluorescent signals $\beta = Max(M,0)/[Max(M,0)+ Max(U,0)+100]$. Thus, β values range from 0 (completely un-methylated) to 1 (completely methylated). We used the "noob" normalization method, which is implemented in the "minfi" R package [49, 50]. The mathematical algorithm and available software underlying the skin & blood clock (based on 391 CpGs) is presented in Horvath et al., 2018 [3].

AUTHOR CONTRIBUTIONS

ACKNOWLEDGEMENTS

CONFLICTS OF INTEREST

FUNDING

REFERENCES

1. Horvath S, Raj K. DNA methylation-based biomarkers and the epigenetic clock theory of ageing. Nat Rev Genet. 2018; 19:371–84.
https://doi.org/10.1038/s41576-018-0004-3
PMID:29643443

2. Horvath S. DNA methylation age of human tissues and cell types. Genome Biol. 2013; 14:R115.

https://doi.org/10.1186/gb-2013-14-10-r115
PMID:24138928

3. Horvath S, Oshima J, Martin GM, Lu AT, Quach A, Cohen H, Felton S, Matsuyama M, Lowe D, Kabacik S, Wilson JG, Reiner AP, Maierhofer A, et al. Epigenetic clock for skin and blood cells applied to Hutchinson Gilford Progeria Syndrome and *ex vivo* studies. Aging (Albany NY). 2018; 10:1758–75.
https://doi.org/10.18632/aging.101508
PMID:30048243

4. Horvath S, Erhart W, Brosch M, Ammerpohl O, von Schönfels W, Ahrens M, Heits N, Bell JT, Tsai PC, Spector TD, Deloukas P, Siebert R, Sipos B, et al. Obesity accelerates epigenetic aging of human liver. Proc Natl Acad Sci USA. 2014; 111:15538–43.
https://doi.org/10.1073/pnas.1412759111
PMID:25313081

5. Horvath S, Garagnani P, Bacalini MG, Pirazzini C, Salvioli S, Gentilini D, Di Blasio AM, Giuliani C, Tung S, Vinters HV, Franceschi C. Accelerated epigenetic aging in Down syndrome. Aging Cell. 2015; 14:491–95.
https://doi.org/10.1111/acel.12325 PMID:25678027

6. Horvath S, Gurven M, Levine ME, Trumble BC, Kaplan H, Allayee H, Ritz BR, Chen B, Lu AT, Rickabaugh TM, Jamieson BD, Sun D, Li S, et al. An epigenetic clock analysis of race/ethnicity, sex, and coronary heart disease. Genome Biol. 2016; 17:171.
https://doi.org/10.1186/s13059-016-1030-0
PMID:27511193

7. Horvath S, Langfelder P, Kwak S, Aaronson J, Rosinski J, Vogt TF, Eszes M, Faull RL, Curtis MA, Waldvogel HJ, Choi OW, Tung S, Vinters HV, et al. Huntington's disease accelerates epigenetic aging of human brain and disrupts DNA methylation levels. Aging (Albany NY). 2016; 8:1485–512.
https://doi.org/10.18632/aging.101005
PMID:27479945

8. Horvath S, Mah V, Lu AT, Woo JS, Choi OW, Jasinska AJ, Riancho JA, Tung S, Coles NS, Braun J, Vinters HV, Coles LS. The cerebellum ages slowly according to the epigenetic clock. Aging (Albany NY). 2015; 7:294–306.
https://doi.org/10.18632/aging.100742
PMID:26000617

9. Horvath S, Ritz BR. Increased epigenetic age and granulocyte counts in the blood of Parkinson's disease patients. Aging (Albany NY). 2015; 7:1130–42.
https://doi.org/10.18632/aging.100859
PMID:26655927

10. Hannum G, Guinney J, Zhao L, Zhang L, Hughes G, Sadda S, Klotzle B, Bibikova M, Fan JB, Gao Y, Deconde R, Chen M, Rajapakse I, et al. Genome-wide methylation profiles reveal quantitative views of human aging rates. Mol Cell. 2013; 49:359–67.
https://doi.org/10.1016/j.molcel.2012.10.016
PMID:23177740

11. Weidner CI, Lin Q, Koch CM, Eisele L, Beier F, Ziegler P, Bauerschlag DO, Jöckel KH, Erbel R, Mühleisen TW, Zenke M, Brümmendorf TH, Wagner W. Aging of blood can be tracked by DNA methylation changes at just three CpG sites. Genome Biol. 2014; 15:R24.
https://doi.org/10.1186/gb-2014-15-2-r24
PMID:24490752

12. Eipel M, Mayer F, Arent T, Ferreira MR, Birkhofer C, Gerstenmaier U, Costa IG, Ritz-Timme S, Wagner W. Epigenetic age predictions based on buccal swabs are more precise in combination with cell type-specific DNA methylation signatures. Aging (Albany NY). 2016; 8:1034–48. https://doi.org/10.18632/aging.100972
PMID:27249102

13. Koch CM, Wagner W. Epigenetic-aging-signature to determine age in different tissues. Aging (Albany NY). 2011; 3:1018–27.
https://doi.org/10.18632/aging.100395
PMID:22067257

14. Bocklandt S, Lin W, Sehl ME, Sánchez FJ, Sinsheimer JS, Horvath S, Vilain E. Epigenetic predictor of age. PLoS One. 2011; 6:e14821.
https://doi.org/10.1371/journal.pone.0014821
PMID:21731603

15. Hernandez DG, Nalls MA, Gibbs JR, Arepalli S, van der Brug M, Chong S, Moore M, Longo DL, Cookson MR, Traynor BJ, Singleton AB. Distinct DNA methylation changes highly correlated with chronological age in the human brain. Hum Mol Genet. 2011; 20:1164–72.
https://doi.org/10.1093/hmg/ddq561
PMID:21216877

16. Florath I, Butterbach K, Müller H, Bewerunge-Hudler M, Brenner H. Cross-sectional and longitudinal changes in DNA methylation with age: an epigenome-wide analysis revealing over 60 novel age-associated CpG sites. Hum Mol Genet. 2014; 23:1186–201.
https://doi.org/10.1093/hmg/ddt531
PMID:24163245

17. Muñoz-Espín D, Serrano M. Cellular senescence: from physiology to pathology. Nat Rev Mol Cell Biol. 2014; 15:482–96. https://doi.org/10.1038/nrm3823
PMID:24954210

18. Kabacik S, Horvath S, Cohen H, Raj K. Epigenetic ageing is distinct from senescence-mediated ageing and is not prevented by telomerase expression. Aging (Albany NY). 2018; 10:2800–15.
https://doi.org/10.18632/aging.101588
PMID:30332397

19. Sharp ZD, Curiel TJ, Livi CB. Chronic mechanistic

target of rapamycin inhibition: preventing cancer to delay aging, or vice versa? Interdiscip Top Gerontol. 2013; 38:1–16. https://doi.org/10.1159/000343625 PMID:23503511

20. Betz C, Hall MN. Where is mTOR and what is it doing there? J Cell Biol. 2013; 203:563–74. https://doi.org/10.1083/jcb.201306041 PMID:24385483

21. Cornu M, Albert V, Hall MN. mTOR in aging, metabolism, and cancer. Curr Opin Genet Dev. 2013; 23:53–62. https://doi.org/10.1016/j.gde.2012.12.005 PMID:23317514

22. Ehninger D, Neff F, Xie K. Longevity, aging and rapamycin. Cell Mol Life Sci. 2014; 71:4325–46. https://doi.org/10.1007/s00018-014-1677-1 PMID:25015322

23. Powers RW 3rd, Kaeberlein M, Caldwell SD, Kennedy BK, Fields S. Extension of chronological life span in yeast by decreased TOR pathway signaling. Genes Dev. 2006; 20:174–84. https://doi.org/10.1101/gad.1381406 PMID:16418483

24. Bjedov I, Toivonen JM, Kerr F, Slack C, Jacobson J, Foley A, Partridge L. Mechanisms of life span extension by rapamycin in the fruit fly Drosophila melanogaster. Cell Metab. 2010; 11:35–46. https://doi.org/10.1016/j.cmet.2009.11.010 PMID:20074526

25. Harrison DE, Strong R, Sharp ZD, Nelson JF, Astle CM, Flurkey K, Nadon NL, Wilkinson JE, Frenkel K, Carter CS, Pahor M, Javors MA, Fernandez E, Miller RA. Rapamycin fed late in life extends lifespan in genetically heterogeneous mice. Nature. 2009; 460:392–95. https://doi.org/10.1038/nature08221 PMID:19587680

26. Zhang Y, Bokov A, Gelfond J, Soto V, Ikeno Y, Hubbard G, Diaz V, Sloane L, Maslin K, Treaster S, Réndon S, van Remmen H, Ward W, et al. Rapamycin extends life and health in C57BL/6 mice. J Gerontol A Biol Sci Med Sci. 2014; 69:119–30. https://doi.org/10.1093/gerona/glt056 PMID:23682161

27. Choi J, Chen J, Schreiber SL, Clardy J. Structure of the FKBP12-rapamycin complex interacting with the binding domain of human FRAP. Science. 1996; 273:239–42. https://doi.org/10.1126/science.273.5272.239 PMID:8662507

28. Stanfel MN, Shamieh LS, Kaeberlein M, Kennedy BK. The TOR pathway comes of age. Biochim Biophys Acta. 2009; 1790:1067–74. https://doi.org/10.1016/j.bbagen.2009.06.007 PMID:19539012

29. Johnson SC, Rabinovitch PS, Kaeberlein M. mTOR is a key modulator of ageing and age-related disease. Nature. 2013; 493:338–45. https://doi.org/10.1038/nature11861 PMID:23325216

30. Ilagan E, Manning BD. Emerging role of mTOR in the response to cancer therapeutics. Trends Cancer. 2016; 2:241–51. https://doi.org/10.1016/j.trecan.2016.03.008 PMID:27668290

31. Heilbronn LK, Ravussin E. Calorie restriction and aging: review of the literature and implications for studies in humans. Am J Clin Nutr. 2003; 78:361–69. https://doi.org/10.1093/ajcn/78.3.361 PMID:12936916

32. Yang Z, Wong A, Kuh D, Paul DS, Rakyan VK, Leslie RD, Zheng SC, Widschwendter M, Beck S, Teschendorff AE. Correlation of an epigenetic mitotic clock with cancer risk. Genome Biol. 2016; 17:205. https://doi.org/10.1186/s13059-016-1064-3 PMID:27716309

33. Rayess H, Wang MB, Srivatsan ES. Cellular senescence and tumor suppressor gene p16. Int J Cancer. 2012; 130:1715–25. https://doi.org/10.1002/ijc.27316 PMID:22025288

34. Rice RH, Qin Q, Pilato A, Rubin AL. Keratinocyte differentiation markers: involucrin, transglutaminase, and toxicity. J Natl Cancer Inst Monogr. 1992; 87–91. PMID:1356394

35. Rheinwald JG, Green H. Serial cultivation of strains of human epidermal keratinocytes: the formation of keratinizing colonies from single cells. Cell. 1975; 6:331–43. https://doi.org/10.1016/S0092-8674(75)80001-8 PMID:1052771

36. Leontieva OV, Demidenko ZN, Blagosklonny MV. Dual mTORC1/C2 inhibitors suppress cellular geroconversion (a senescence program). Oncotarget. 2015; 6:23238–48. https://doi.org/10.18632/oncotarget.4836 PMID:26177051

37. Leontieva OV, Blagosklonny MV. Gerosuppression by pan-mTOR inhibitors. Aging (Albany NY). 2016; 8:3535–51. https://doi.org/10.18632/aging.101155 PMID:28077803

38. Leontieva OV, Blagosklonny MV. While reinforcing cell cycle arrest, rapamycin and Torins suppress senescence in UVA-irradiated fibroblasts. Oncotarget. 2017; 8:109848–56. https://doi.org/10.18632/oncotarget.17827 PMID:29312653

39. Blagosklonny MV. Rapamycin, proliferation and geroconversion to senescence. Cell Cycle. 2018; 17:2655–65.
https://doi.org/10.1080/15384101.2018.1554781
PMID:30541374

40. Wang R, Sunchu B, Perez VI. Rapamycin and the inhibition of the secretory phenotype. Exp Gerontol. 2017; 94:89–92.
https://doi.org/10.1016/j.exger.2017.01.026
PMID:28167236

41. Herranz N, Gallage S, Mellone M, Wuestefeld T, Klotz S, Hanley CJ, Raguz S, Acosta JC, Innes AJ, Banito A, Georgilis A, Montoya A, Wolter K, et al. mTOR regulates MAPKAPK2 translation to control the senescence-associated secretory phenotype. Nat Cell Biol. 2015; 17:1205–17.
https://doi.org/10.1038/ncb3225 PMID:26280535

42. Green H, Rheinwald JG, Sun TT. Properties of an epithelial cell type in culture: the epidermal keratinocyte and its dependence on products of the fibroblast. Prog Clin Biol Res. 1977; 17:493–500.
PMID:928463

43. Weichhart T. mTOR as Regulator of Lifespan, Aging, and Cellular Senescence: A Mini-Review. Gerontology. 2018; 64:127–34.
https://doi.org/10.1159/000484629 PMID:29190625

44. Kim J, Guan KL. mTOR as a central hub of nutrient signalling and cell growth. Nat Cell Biol. 2019; 21:63–71. https://doi.org/10.1038/s41556-018-0205-1
PMID:30602761

45. Lu AT, Hannon E, Levine ME, Hao K, Crimmins EM, Lunnon K, Kozlenkov A, Mill J, Dracheva S, Horvath S. Genetic variants near MLST8 and DHX57 affect the epigenetic age of the cerebellum. Nat Commun. 2016; 7:10561.
https://doi.org/10.1038/ncomms10561
PMID:26830004

46. Kakumoto K, Ikeda J, Okada M, Morii E, Oneyama C. mLST8 Promotes mTOR-Mediated Tumor Progression. PLoS One. 2015; 10:e0119015.
https://doi.org/10.1371/journal.pone.0119015
PMID:25906254

47. Levine ME, Lu AT, Chen BH, Hernandez DG, Singleton AB, Ferrucci L, Bandinelli S, Salfati E, Manson JE, Quach A, Kusters CD, Kuh D, Wong A, et al. Menopause accelerates biological aging. Proc Natl Acad Sci USA. 2016; 113:9327–32.
https://doi.org/10.1073/pnas.1604558113
PMID:27457926

48. Leontieva OV, Demidenko ZN, Blagosklonny MV. Contact inhibition and high cell density deactivate the mammalian target of rapamycin pathway, thus suppressing the senescence program. Proc Natl Acad Sci USA. 2014; 111:8832–37.
https://doi.org/10.1073/pnas.1405723111
PMID:24889617

49. Triche TJ Jr, Weisenberger DJ, Van Den Berg D, Laird PW, Siegmund KD. Low-level processing of Illumina Infinium DNA Methylation BeadArrays. Nucleic Acids Res. 2013; 41:e90.
https://doi.org/10.1093/nar/gkt090 PMID:23476028

50. Fortin JP, Triche TJ Jr, Hansen KD. Preprocessing, normalization and integration of the Illumina HumanMethylationEPIC array with minfi. Bioinformatics. 2017; 33:558–60.
https://doi.org/10.1093/bioinformatics/btw691
PMID:28035024

Epigenetic clock analysis of human fibroblasts *in vitro*: effects of hypoxia, donor age, and expression of hTERT and SV40 largeT

Mieko Matsuyama[1], David J. WuWong[1], Steve Horvath[2], Shigemi Matsuyama[1,3]

[1]Division of Hematology and Oncology, Department of Medicine, School of Medicine, Case Western Reserve University, Cleveland, OH 44106, USA
[2]Department of Human Genetics and Biostatistics, David Geffen School of Medicine, University of California Los Angeles, Los Angeles, CA 90095, USA
[3]Case Comprehensive Cancer Center, Cleveland, OH 44106, USA

Correspondence to: Shigemi Matsuyama, **email:** shigemi.matsuyama@case.edu

ABSTRACT

Aging is associated with a genome-wide change of DNA methylation (DNAm). "DNAm age" is defined as the predicted chronological age by the age estimator based on DNAm. The estimator is called the epigenetic clock. The molecular mechanism underlining the epigenetic clock is still unknown. Here, we evaluated the effects of hypoxia and two immortalization factors, hTERT and SV40-LargeT (LT), on the DNAm age of human fibroblasts *in vitro*. We detected the cell division-associated progression of DNAm age after >10 population doublings. Moreover, the progression of DNAm age was slower under hypoxia (1% oxygen) compared to normoxia (21% oxygen), suggesting that oxygen levels determine the speed of the epigenetic aging. We show that the speed of cell division-associated DNAm age progression depends on the chronological age of the cell donor. hTERT expression did not arrest cell division-associated progression of DNAm age in most cells. SV40LT expression produced inconsistent effects, including rejuvenation of DNAm age. Our results show that a) oxygen and the targets of SV40LT (e.g. p53) modulate epigenetic aging rates and b) the chronological age of donor cells determines the speed of mitosis-associated DNAm age progression in daughter cells.

INTRODUCTION

There are two fundamental questions regarding the mechanism of aging. The first question is what kind of time-dependent changes (chemical and/or biological changes) drive aging. It is expected that there are factors other than time controlling the speed of aging since there is a variation of the lifespan and the timing of the onset of age-associated diseases. Therefore, the second question is what are these factors regulating the speed of aging. The present study investigates these two questions by focusing on the epigenetic aging of primary cultured human cells.

It is now widely accepted that there is an age associated change in DNAm in human as well as other species

[1–5]. Most of the previously reported age-dependent DNAm changes were tissue- or cell type-specific (Reviewed in [1]). Recently, the pan-tissue age estimator was developed based on the DNAm levels of 353 CpG sites [3]. In 2018, another age estimator was developed that predicts the chronological age of skin and blood cells more accurately than the pan-tissue age estimator [6]. This new age estimator uses the DNAm levels of 391 CpG sites (60 CpG sites are overlapped with the pan-tissue age estimator) [6]. The DNAm-based age estimator are called the epigenetic clock, and the predicted age by the clock is called DNAm age [1]. The DNAm age functions as a biomarker to predict the risk of age-associated diseases as accelerated DNAm age has been observed in a variety of conditions,

including obesity [7], HIV infection [8], Down syndrome [9], Parkinson's disease [10], Werner syndrome [11], and menopause [12].

The DNAm age of blood is predictive of lifespan, even after adjusting for chronological age and other risk factors [13, 14]. Lifestyle factors have only a weak effect on the DNAm age of blood [15], suggesting that DNAm age largely reflects cell-intrinsic properties. In a recent study, we tested this postulated cellular autonomy by measuring DNAm age in blood cells of leukemia patients after hematopoietic stem cell transfer (HSCT) from allogeneic donors [16]. We found that the DNAm age of the donor's blood cells was not influenced by the recipient's body, whether younger or older, and that the DNAm age progressed as if the donor cells were still in the donor's body, even 17 years after HSCT [16]. This finding further supports that the epigenetic clock is a cell-intrinsic phenomenon at least in hematopoietic cells.

Overall, there is strong indirect evidence that the epigenetic clock relates to one or more innate aging processes. However, it has been challenging to dissect the molecular mechanisms underlying the epigenetic clock. To address this challenge, *in vitro* models may be used. Here, we used primary cultured human fibroblasts to carry out an epigenetic clock analysis of three conditions that relate to the replicative lifespan: hypoxia, donor age,

and immortalization. The present results provide clues to identify molecular machineries controlling the epigenetic aging. Based on our findings in this study, we will discuss the hypothetical molecular mechanisms regulating the progression of the DNAm age.

RESULTS

Effects of hypoxia on cell proliferation

Human dermal fibroblasts from neonates were cultured under normoxic conditions in a CO_2 incubator [5% CO_2 and 21% O_2 (atmospheric)] as well as under hypoxic conditions (5% CO_2 and 1% O_2). The cells were collected and passaged every 4-6 days. Excess cells that were not used for the passage were frozen at -80C for protein and DNA analysis. As previously established [17], in normoxia, the cell division speed declined after PD30 (Figure 1, black symbols), and the cell size increased (Figure 2A and BB). In contrast, under hypoxia, the cells maintained a constant division speed after PD30 (Figure 1, red symbols), and the cells did not become as large as the cells under normoxia (Figure 2C), though a small proportion of cells did show size enlargement (arrows in Figure 2C). The stabilization of HIF1α (hypoxia-induced factor 1α) was confirmed in all four cell lines incubated under hypoxia (Figure 2D and Supplementary Figure 1).
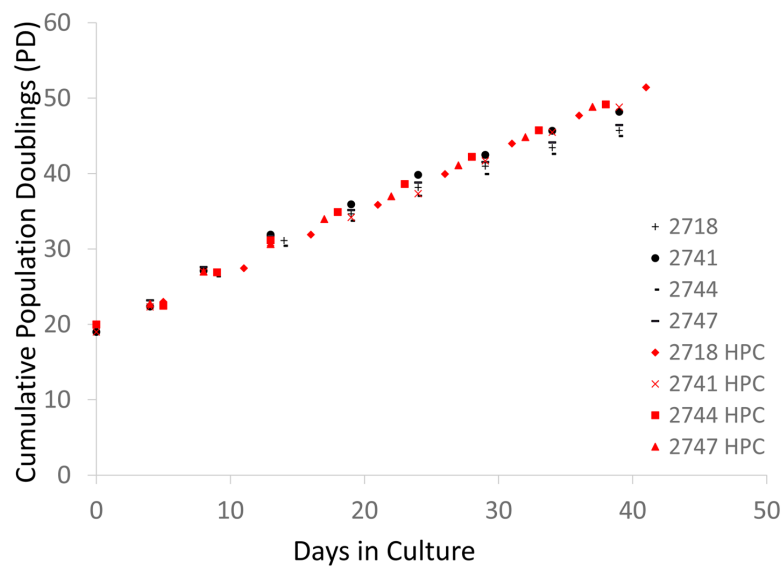
Figure 1. Cell division records of neonate fibroblast cell lines cultured in normoxia and hypoxia. Each 4-digit number in the graph (#2718, #2741, #2744, and # 2747) indicates the batch of the cell line from the vendor (Cell Applications, San Diego, CA). The graph shows the cumulative population doublings (PD) of each cell line in normoxia and hypoxia. Black and red symbols indicate the data from normoxia and hypoxia, respectively.

Effects of hypoxia on the progression of DNAm age

DNAm age was estimated by two methods that apply to *in vitro* studies: Horvath's pan tissue clock based on 353 CpGs [3] and the more recent skin & blood clock based on 391 CpG sites [6]. The corresponding DNAm age estimates will be referred to as DNAmAge[353CpG] and DNAmAge[391CpG], respectively. Previously, we reported that DNAmAge[391CpG] predicts the chronological age of cultured fibroblasts more accurately than the original DNAmAge[353CpG] [6]. The present study used both DNAmAge[353CpG] and DNAmAge[391CpG] so that the present results can be compared with previous studies.

As shown in Figure 3, the progression of DNAmAge[391CpG] (Figure 3A, 3C) and DNAmAge[353CpG] (Figure 3B, 3D) was observed after eight passages, which is equal to an additional 22.3-31.5 population doublings (PD) (Figure 3A, 3B). These increases of DNAm age (both DNAmAge[391CpG] and DNAmAge[353CpG]) were statistically significant in normoxia (*p<0.05, **p<0.005, Figure 3C and 3D), indicating that 6 weeks of cell culture is sufficient to detect progression of the DNAm age. As previously reported, DNAmAge[391CpG] accurately predicted the donor's age (0 years old for neonate cells) whereas DNAmAge[353CpG] overestimated the donor's age (4-12 years old for neonate cells) of the cultured fibroblasts (Figure 3B, 3D). Importantly, hypoxia slowed the progression of both DNAmAge[391CpG] and DNAmAge[353CpG] in all 4 cell lines examined (Figure

4A, 4B). The average values of DNAm age progression per PD are shown in Figure 4C and 4D. The effect of hypoxia on slowing DNAm age progression was statistically significant when contrasting the ratio of speeds (Figure 4E, 4F). Hypoxia allows fibroblasts to continue cell division by extending the replicative lifespan [17]. Similarly, we found that fibroblasts were able to divide more under hypoxia than under normoxia (Figure 1). Nevertheless, the progression of DNAm age per cell division or PD diminished in the hypoxia group.

Comparison of cell division-associated DNAm age progression between neonate and adult fibroblasts

In addition to fibroblasts from neonates, we also examined fibroblasts from adult donors. We used a total of 11 different fibroblast lines; 5 from neonates and 6 from adult donors (Figure 5). DNAmAge[391CpG] and DNAmAge[353CpG] progressed by cell division in the majority of adult cells (4 cell lines among 6 cell lines for DNAmAge[391CpG] (Figure 5A) and 5 cell lines among 6 cell lines for DNAmAge[353CpG] (Figure 5B)). However, the speed of DNAm age progression varied depending on the age of the cells. The cell division-associated progression of DNAmAge[353CpG] became slower as the starting age became older (Figure 5B, 5D). In contrast, DNAmAge[391CpG] showed a different trend. The progression of DNAmAge[391CpG] became relatively more significant the older the starting age (Figure 5A, 5C). Interestingly, 2 cases among 6 cases, DNAmAge[391CpG] showed rejuvenation (light blue and green symbols in
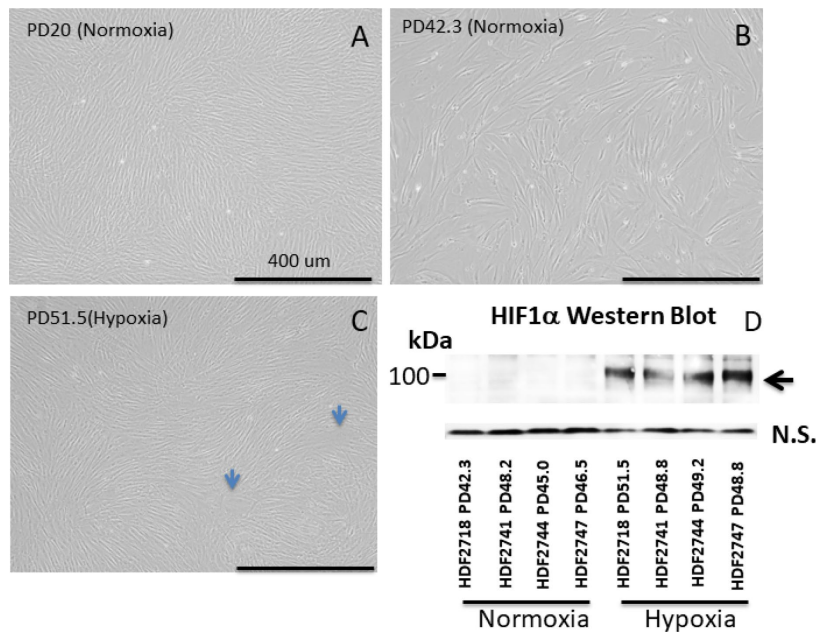
Figure 2. Cell division records of neonate fibroblast cell lines cultured in normoxia and hypoxia. Each 4-digit number in the graph (#2718, #2741, #2744, and # 2747) indicates the batch of the cell line from the vendor (Cell Applications, San Diego, CA). The graph shows the cumulative population doublings (PD) of each cell line in normoxia and hypoxia. Black and red symbols indicate the data from normoxia and hypoxia, respectively.
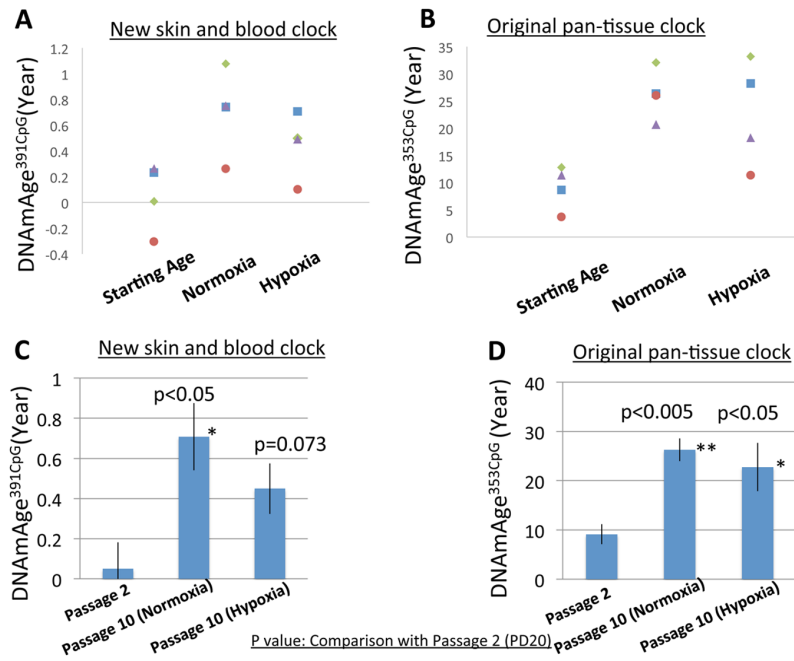
Figure 3. DNAm age progression in normoxia and hypoxia. (**A** and **B**) The DNAm age of each cell line at early PD (19-20) (passage 2) and accumulated PD (42.3-51.5) (passage 10) is shown. The DNAm age of the same cell line is shown by the same color. Results for DNAmAge[391CpG] (**A**) and DNAmAge[353CpG] (**B**) are shown. Each dot is the average of a duplicate DNAm analysis for each condition. (**C** and **D**) The average DNAm ages of 4 cell lines at passage 2, passage 10 (Normoxia), and passage 10 (Hypoxia) are shown (n=4). Results for DNAmAge[391CpG] (**C**) and DNAmAge[353CpG] (**D**) are shown. The P values on the figure show the statistical comparison with the data at passage 20. *p<0.05, **p<0.005 (t-test).
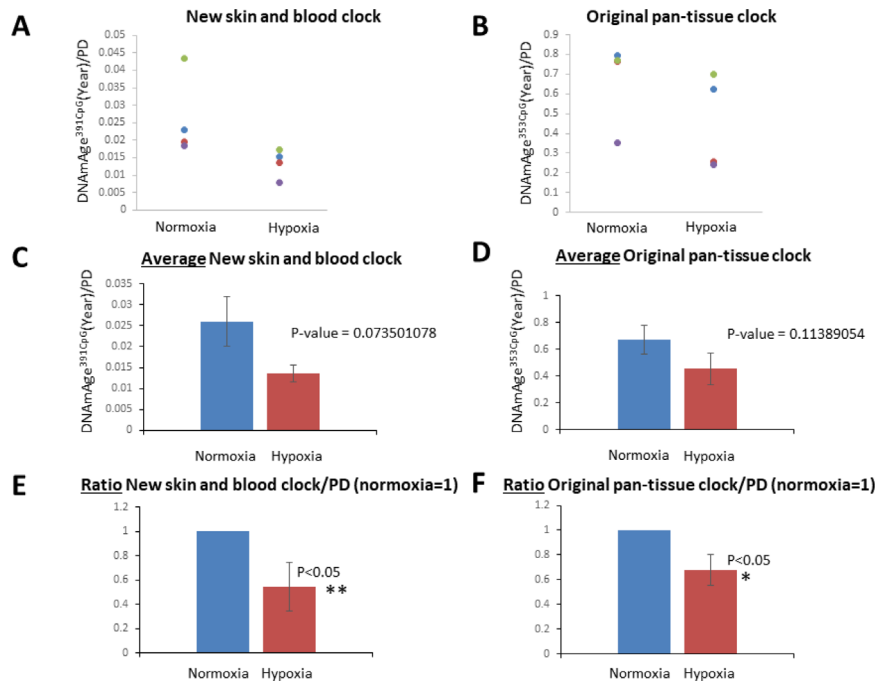
Figure 4. Hypoxia slowed the speed of the cell division-associated DNAm age progression. (**A** and **B**) DNAmAge[391CpG]/PD (**A**) and DNAmAge[353CpG]/PD (**B**) of each cell line in normoxia and hypoxia are shown. The result from the same cell line is marked with the same color. In all cell lines examined, hypoxia slowed the speed of DNAm age progression. (**C** and **D**) Average and S.E. of DNAmAge[391CpG]/PD and DNAmAge[353CpG]/PD are shown. (**E** and **F**) In these graphs, DNAm age/PD in normoxia is designated as 1 in all cell lines, and the ratio of DNAm age in normoxia and hypoxia was calculated. In both DNAmAge[391CpG] and DNAmAge[353CpG], hypoxia slowed the speed of the progression of DNAm age and the effects were statistically significant (t-test).

Figure 5C)]. At present, it is not certain whether this rejuvenation phenomenon is always reproducible at this rate (2 out of 6, i.e. 33%) even if we increase the sample number. Larger scale experiments are needed to validate this phenomenon.

Effects of the expression of hTERT or SV40LT on the DNAm age

Next, we examined the effects of two commonly used immortalization methods: hTERT and SV40LT expression (reviewed in [18]). Retrovirus vectors were used to introduce the hTERT or SV40LT gene into the primary cultured fibroblasts as previously described [19, 20]. Retrovirus infection was performed at passage 2 (PD10-15), and the cells were cultured for more than 6 additional passages. We examined 5 different primary cultured fibroblast cell lines obtained from 5 different adult donors. As shown in Figure 6A and 6C, hTERT expression resulted in continuous progression of DNAmAge^{391CpG} in all cell lines examined. In the case of DNAmAge^{353CpG} analysis, hTERT expression maintained the progression of DNAmAge in 4 of 5 cell lines (Figure 6E, 6G), as previously reported [6, 21]. On the other hand, the effects of SV40LT were inconsistent:

DNAmAge^{391CpG} and DNAmAge^{353CpG} progression was maintained or reversed depending on the cell line (Figure 6B, 6C (DNAmAge^{391CpG}) and Figure 6F, 6G (DNAmAge^{353CpG})). For example, SV40LT expression resulted in the rejuvenation (decrease) of DNAmAge^{353CpG} in 2 cell lines after several passages (Figure 6G, dots below the line of 0 year/PD). In Figure 6D and 6H, the mean and S.E. of the speed of DNAm age progression per PD is shown. There were no significant differences (control, hTERT or SV40LT expression). The extremely large S.E. of the SV40LT group in Figure 6H reflects the inconsistent (acceleration or rejuvenation) effects on DNAmAge^{353CpG}, as mentioned previously.

DISCUSSION

The present study demonstrated that (1) hypoxia slows down the progression of DNAm age, (2) cell division-associated DNAm age progression depends on the chronological age of the cell donor, (3) SV40LT immortalization induces abnormal progression of DNAm age, and (4) hTERT expression does not arrest progression of DNAmAge.
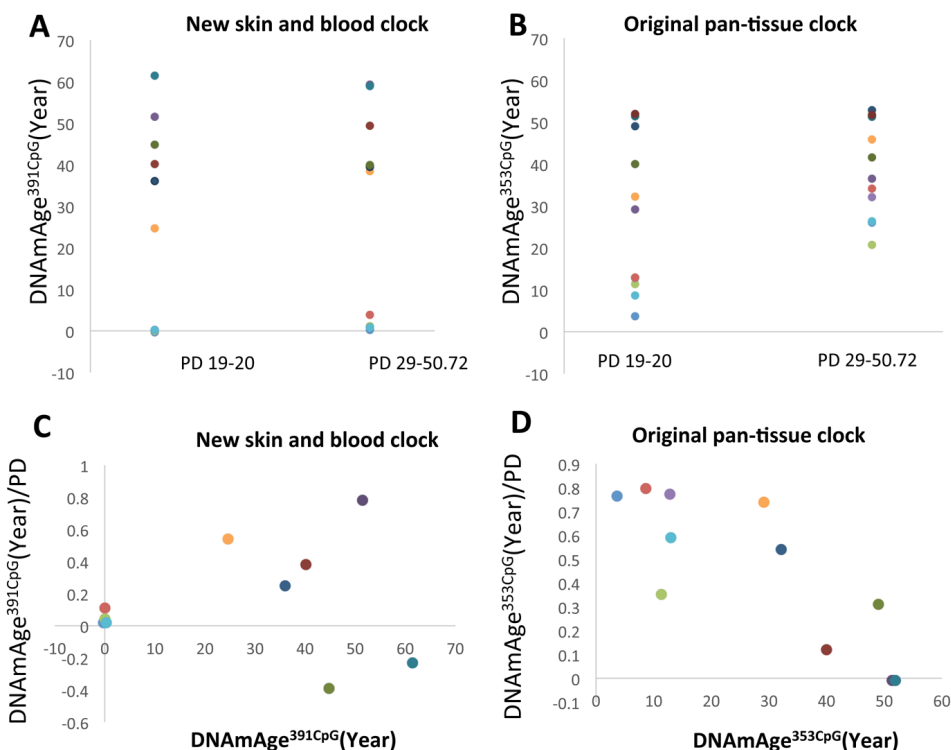
Figure 5. The progression of DNAm age after more than 10 PD of fibroblasts from donors of different ages. (**A** and **B**) The progression of DNAmAge^{391CpG} (**A**) and DNAmAge^{353CpG} (**B**) after more than 10 PD of cell culture is shown. Each panel shows the following information: (**A** and **B**) Changes of DNAm age after more than 10 PD. (**C** and **D**) The Y axis indicates the values of DNAmAge^{391CpG}/PD (**C**) and DNAmAge^{353CpG}/PD (**D**). The X-axis indicates the DNAm age at the beginning of this experiment. The impact of PD on the speed of DNAm age progression becomes greater when the starting DNAmAge^{391CpG} is older, but becomes lesser when the starting DNAmAge^{353CpG} is older. The dots with the same color are the results from the same cell line.

The present study showed that DNAm age of fibroblasts progressed after multiple cell divisions *in vitro*. In this study, neonate fibroblasts were cultured approximately 6 weeks with 8 passages (4-6 days per passage). This means that 6 weeks is long enough to detect the progression of DNAm age in cell culture experiments. However, the speed of DNAm age progression in cell culture was much faster than the chronological time. For example, approximately 0.65 years [Figure 3C; from 0.05 ± 0.131 (passage 2) to 0.708 ± 0.168 (passage 8)] of DNAmAge[391CpG] progressed over 6 weeks (equivalent to 0.12 years) under normoxia (Figure 3C); that is, the speed of DNAmAge[391CpG] progression was 5 times faster than the chronological time. Interestingly, this speed became slower under hypoxia; 0.4 years [Figure 3C; from 0.05 ± 0.131 (passage 2) to 0.450 ± 0.126 (passage 8)] of DNAmAge[391CpG] progression for 6 weeks (0.12 years) (Figure 3C). The oxygen concentration in the human body is much lower than that of the air (21%

oxygen). For example, the oxygen concentration of the brain, liver and kidney is reported to be approximately 2-3% and that of the hematopoietic stem cell niche is approximately 1-2% [22, 23]. One of the reasons for the fast progression of the DNAm age in the conventional cell culture may be the high oxygen concentration (normoxia) in the medium. The present study suggests that oxygen increases epigenetic aging, a finding which could elucidate the molecular mechanism of the epigenetic clock. It is well established that Hypoxia-Inducible Factor 1α (HIF1α, a transcriptional factor), mediates various cellular responses to hypoxia [24]. HIF1α is reported to decrease expression levels of DNA methyl-transferases (DNMTs: DNMT1, 3A and 3B), whereas it increases expression of DNA de-methylatiing enzymes (Ten-eleven Translocation (TET) 2 and 3) [24]. Thus, HIF1α -induced modulations of the balance of DNMTs and TETs is a plausible mechanism of how hypoxia slows down the epigenetic clock.
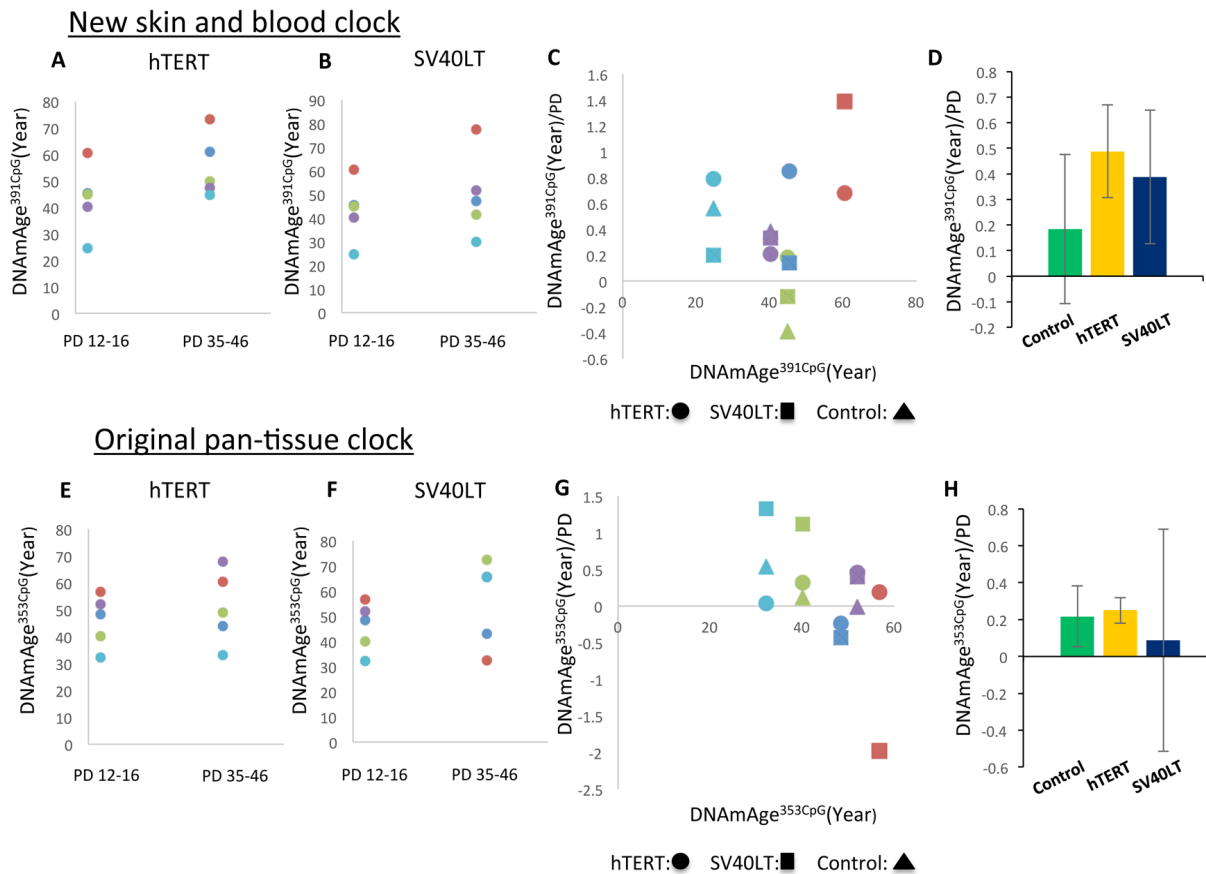
Figure 6. Effects of hTERT and SV40LT transfection on the DNAm age of fibroblasts. These panels show DNAmAge[391CpG] (**A**–**D**) and DNAmAge[353CpG] (**E**–**H**) of fibroblasts transfected with the hTERT and SV40LT genes, respectively. The changes of DNAm age more than 20 PD after hTERT (**A** and **E**) or SV40LT (**B** and **F**) gene transfection are shown. The dots with the same color are the results from the same cell line. Panels (**C** and **D**) show DNAmAge[391CpG]/PD (**C**) and DNAmAge[353CpG]/PD (**G**) of each cell line transfected with the hTERT or SV40LT gene. As references, the DNAm age/PD values of non-transfected cells are shown for 3 cell lines. The starting DNAm age values are shown on the X axis. Panels (**D** and **H**) show the average and S.E. of DNAmAge[391CpG]/PD (**D**) and DNAmAge[353CpG]/PD (**H**) of non-transfected control cells (n=3), hTERT (n=5), and SV40LT (n=5). The effects of SV40LT were not consistent, and the S.E. of the average is very large.

In addition to oxygen, there are other factors in conventional cell culture systems that could potentially impact the epigenetic aging. For example, the fibroblast culture medium (FGM) used in this study contains fetal calf serum (FCS) and 8 mM glucose, which could be the reasons of the accelerated epigenetic aging of cells in the conventional cell culture system. Further investigation of the effects of these and other constituents of cell culture systems is warranted to identify the factors accelerating the progression of DNAm age.

In this study, we examined fibroblasts from donors of various ages. Neonate cells progressed their $DNAmAge^{353CpG}$ at a higher rate than adult cells did. As shown in Figure 5C, 5D, the progression per each cell division became less when the starting age was older. This result suggests that mitosis is accounted as a factor progressing $DNAmAge^{353CpG}$ when the human body is growing (e.g. neonate), but it becomes less critical after the human body has reached maturity. In the case of $DNAmAge^{391CpG}$, 67% (4 cell lines among 6 cell lines) of adult cell lines (>25 years old) showed faster progression than neonate cells. This means that older cells are more sensitive to cell division in terms of progression of $DNAmAge^{391CpG}$ (Figure 5B). Since $DNAmAge^{391CpG}$ predicts the chronological age of cfibroblasts more accurately than $DNAmge^{353CpG}$, we speculate that the observation based on $DNAmAge^{391CpG}$ represent the significance of cell division in the epigenetic aging process of fibroblasts. Although the two epigenetic age estimators showed different behaviors, the common point is that the speed of the cell division-associated progression of DNAm age was found to be different between neonate and adult cells. The present result suggests that the age of mother cells is a factor controlling the speed of mitosis-associated progression of the DNAm age in daughter cells.

The age-dependent increases of the methylation of CpGs in KLF14 gene locus (KLF14-CpGs) has been reported in human [25, 26] as well as mouse and monkey [27]. KLF14-CpGs are included in the two age estimator programs used in this study [3, 6]. Recently, it was found that hypermethylation of KLF14-CpGs is associated with the decrease of DNMT1 gene expression in human fibroblasts [28]. There is another study reporting the age-dependent decrease of the gene expression of DNMT1 and DNMT3B in human peripheral mononuclear cells [29]. The present study showed that mitosis-associated progression of DNAm age was influenced by the age of the cell. This observation may be explained by the change of the expression levels of DNMTs that is linked with the age-dependent hypermethylation of KLF14-CpGs.

We examined the effects of two immortalization treatments on the epigenetic age of cultured cells: expression of hTERT and SV40LT. In the case of hTERT expression, $DNAmAge^{391CpG}$ increased in all 5 cell lines examined (Figure 6A, 6C) and $DNAmAge^{353CpG}$ increased in 4 of the 5 cell lines (Figure 6E, 6G). This is consistent with previous reports using keratinocytes, fibroblasts and endothelial cells [6, 21]. In the case of $DNAmAge^{353CpG}$, one of the 5 cell lines showed a slight decrease (Figure 6E dark blue dots). At present, we do not have a clear explanation of this unexpected result. However, one of the technical pitfalls of retrovirus-mediated transfection is the uncontrolled integration of the transfected gene into the host chromosomes. Thus, chromosomal position effects and copy number variations related to the integrated hTERT gene might lead to differences in DNAm age among transfected cell lines.

For certain cancer types, p53 mutations have been associated with *slower* epigenetic age acceleration in malignant tissue samples [3, 30]. Horvath (2013) hypothesized that p53 might be part of an epigenomic maintenance system that underlies epigenetic aging. Our *in vitro* studies of SV40LT (which is a well-known p53 inhibitor) support such a role for p53 in maintaining the normal progression of the epigenetic clock. Specifically, we found that SV40LT had inconsistent effects on both $DNAmAge^{391CpG}$ and $DNAmAge^{353CpG}$. These data support the hypothesis that p53 inactivation induces malfunction of the cellular system governing the process of epigenetic aging. As a caveat, SV40LT also perturbs other genes besides p53. It is known to perturb the retinoblastoma family of tumor suppressors and pp2A phosphatase [31, 32]. To further determine the role of p53 in the regulation of the epigenetic aging, the specific inhibition of p53 by siRNA or targeted mutation of p53 by CRISPR/Cas9, for examples, will be necessary.

The present study suggests that mitosis-associated progression of the epigenetic clock is under the influence of oxygen level, the age of the cell, and tumor suppressors. Although cell division progresses the DNAm age, its speed is expected to be very different depending on the differentiation status and other environmental conditions. It is because the multiple cell types with different proliferation history show a similar DNAm age which is very close to the chronological age of the whole body. Our finding indicates that oxygen, the age, and tumor suppressors are the candidates of these factors controlling the speed of the epigenetic clock in different tissues. Further studies are necessary to investigate how multiple cell types in a human body can progress the DNAm age at the similar speed as the chronological age progresses.

METHODS

Epigenetic clocks

Several DNAm-based biomarkers have been proposed in the literature which differ in terms of their applicability (some are developed for specific tissues such as blood) and in terms of their biological interpretation. In this study, we focused on two epigenetic clocks that apply to fibroblasts. The pan-tissue epigenetic clock (Horvath 2013) is based on 353 CpGs. It applies to all sources of DNA (with the exception of sperm). The resulting age estimate (in units of years) is referred to as DNAmAge^{353CpG}. Different postmortem tissues collected from the same individual have roughly the same epigenetic age [3, 6]. Hence, the pan tissue clock does not measure proliferative history (or mitotic age) in most cell types and tissues. We recently developed a new epigenetic age estimator (referred to as the skin and blood clock or DNAmAge^{391CpG}) that leads to substantially more accurate age estimates in fibroblasts, keratinocytes, buccal cells, blood cells, saliva, and endothelial cells [3].

DNA extraction and methylation analysis

DNA was extracted and purified from 2-3 million cells/sample by using a QIAGEN DNA extraction kit (Cat #51304) according to the manufacturer's protocol. To remove RNA, RNAase (ThermoFisher Cat# EN0531, final 100 μg/ml) was added to the cell suspension buffer during the DNA extraction procedure. DNA methylation levels were measured on Illumina 450K arrays according to the manufacturer's instructtions. The Illumina BeadChip (450K) measures bisulfite-conversion-based, single-CpG resolution DNAm levels at different CpG sites in the human genome. These data were generated by following the standard protocol for Illumina methylation assays, which quantifies methylation levels by the β value using the ratio of intensities between methylated and un-methylated alleles. Specifically, the β value is calculated from the intensity of the methylated (M corresponding to signal A) and un-methylated (U corresponding to signal B) alleles, as the ratio of fluorescent signals $\beta = Max(M,0)/[Max(M,0)+Max(U,0)+100]$. Thus, β values range from 0 (completely un-methylated) to 1 (completely methylated). We used the "noob" normalization method, which is implemented in the "minfi" R package [33, 34].

Cell culture

Human dermal fibroblasts were obtained from two different sources, Cell Applications (San Diego, CA) and the Progeria Research Foundation (PRF). The cells from PRF are from healthy donors who did not have Progeria-related mutations. Fibroblasts were obtained as a frozen stock, and these cells had already reached 9-10 population doublings. Fibroblasts were cultured using Human Fibroblast Growth (HGF) Medium (Cell Applications) that contains 8 mM glucose and 2% FCS as a supplement. The cell density was 0.2 million cells/15 ml/dish at the beginning of each passage culture. When cells reached the confluent condition after 4-6 days, they were collected and the total cell number was determined. At each passage stage, unused cells were frozen for DNAm analysis and HIF1α protein expression. To examine the effects of hypoxia, cells were cultured in an hypoxia chamber (1% O2) as explained in the Results section.

hTERT and SV40Large T expression

hTERT or SV40LT (Large T) was expressed using retrovirus-mediated gene transfection according to previously established methods [19, 20]. The plasmids necessary for retrovirus synthesis were the kind gifts from Dr. Mark Jackson (Pathology, Case Western Reserve University).

Western blot

Cell pellets were lysed in RIPA buffer (20 times pipetting and 20 min rotation at 4°C), and the soluble fraction was collected after centrifugation at 14,000 rpm for 30 min. Samples with 20 μg total protein was loaded in each lane. HIF1α antibody and the secondary antibody (anti-rabbit goat IgG-HRP) were purchased from NOVUS Biologicals (Cat # NB100-479) and DAKO (Cat # P0448), respectively. Chemiluminescence substrate was purchased from Kindle Biosciences (Cat #R1004) (www.kindlebio.com). Western blot image was obtained by using a digital camera (KwicQuant Imager, Kindle Biosciences).

CONFLICTS OF INTEREST

The authors declare no conflicts of interest.

FUNDING

REFERENCES

1. Horvath S, Raj K. DNA methylation-based biomarkers and the epigenetic clock theory of ageing. Nat Rev Genet. 2018; 19:371–84.
https://doi.org/10.1038/s41576-018-0004-3

PMID:29643443

2. Hannum G, Guinney J, Zhao L, Zhang L, Hughes G, Sadda S, Klotzle B, Bibikova M, Fan JB, Gao Y, Deconde R, Chen M, Rajapakse I, et al. Genome-wide methylation profiles reveal quantitative views of human aging rates. Mol Cell. 2013; 49:359–67.
https://doi.org/10.1016/j.molcel.2012.10.016
PMID:23177740

3. Horvath S. DNA methylation age of human tissues and cell types. Genome Biol. 2013; 14:R115.
https://doi.org/10.1186/gb-2013-14-10-r115
PMID:24138928

4. Spólnicka M, Piekarska RZ, Jaskuła E, Basak GW, Jacewicz R, Pięta A, Makowska Ż, Jedrzejczyk M, Wierzbowska A, Pluta A, Robak T, Berent J, Branicki W, et al. Donor age and C1orf132/MIR29B2C determine age-related methylation signature of blood after allogeneic hematopoietic stem cell transplantation. Clin Epigenetics. 2016; 8:93.
https://doi.org/10.1186/s13148-016-0257-7
PMID:27602173

5. Weidner CI, Wagner W. The epigenetic tracks of aging. Biol Chem. 2014; 395:1307–14.
https://doi.org/10.1515/hsz-2014-0180
PMID:25205717

6. Horvath S, Oshima J, Martin GM, Lu AT, Quach A, Cohen H, Felton S, Matsuyama M, Lowe D, Kabacik S, Wilson JG, Reiner AP, Maierhofer A, et al. Epigenetic clock for skin and blood cells applied to Hutchinson Gilford Progeria Syndrome and ex vivo studies. Aging (Albany NY). 2018; 10:1758–75.
https://doi.org/10.18632/aging.101508
PMID:30048243

7. Horvath S, Erhart W, Brosch M, Ammerpohl O, von Schönfels W, Ahrens M, Heits N, Bell JT, Tsai PC, Spector TD, Deloukas P, Siebert R, Sipos B, et al. Obesity accelerates epigenetic aging of human liver. Proc Natl Acad Sci USA. 2014; 111:15538–43.
https://doi.org/10.1073/pnas.1412759111
PMID:25313081

8. Horvath S, Levine AJ. HIV-1 Infection Accelerates Age According to the Epigenetic Clock. J Infect Dis. 2015; 212:1563–73.
https://doi.org/10.1093/infdis/jiv277
PMID:25969563

9. Horvath S, Garagnani P, Bacalini MG, Pirazzini C, Salvioli S, Gentilini D, Di Blasio AM, Giuliani C, Tung S, Vinters HV, Franceschi C. Accelerated epigenetic aging in Down syndrome. Aging Cell. 2015; 14:491–95.
https://doi.org/10.1111/acel.12325 PMID:25678027

10. Horvath S, Ritz BR. Increased epigenetic age and granulocyte counts in the blood of Parkinson's disease patients. Aging (Albany NY). 2015; 7:1130–42.
https://doi.org/10.18632/aging.100859
PMID:26655927

11. Maierhofer A, Flunkert J, Oshima J, Martin GM, Haaf T, Horvath S. Accelerated epigenetic aging in Werner syndrome. Aging (Albany NY). 2017; 9:1143–52.
https://doi.org/10.18632/aging.101217
PMID:28377537

12. Carroll JE, Irwin MR, Levine M, Seeman TE, Absher D, Assimes T, Horvath S. Epigenetic Aging and Immune Senescence in Women With Insomnia Symptoms: Findings From the Women's Health Initiative Study. Biol Psychiatry. 2017; 81:136–44.
https://doi.org/10.1016/j.biopsych.2016.07.008
PMID:27702440

13. Chen BH, Marioni RE, Colicino E, Peters MJ, Ward-Caviness CK, Tsai PC, Roetker NS, Just AC, Demerath EW, Guan W, Bressler J, Fornage M, Studenski S, et al. DNA methylation-based measures of biological age: meta-analysis predicting time to death. Aging (Albany NY). 2016; 8:1844–65.
https://doi.org/10.18632/aging.101020
PMID:27690265

14. Marioni RE, Shah S, McRae AF, Chen BH, Colicino E, Harris SE, Gibson J, Henders AK, Redmond P, Cox SR, Pattie A, Corley J, Murphy L, et al. DNA methylation age of blood predicts all-cause mortality in later life. Genome Biol. 2015; 16:25.
https://doi.org/10.1186/s13059-015-0584-6
PMID:25633388

15. Quach A, Levine ME, Tanaka T, Lu AT, Chen BH, Ferrucci L, Ritz B, Bandinelli S, Neuhouser ML, Beasley JM, Snetselaar L, Wallace RB, Tsao PS, et al. Epigenetic clock analysis of diet, exercise, education, and lifestyle factors. Aging (Albany NY). 2017; 9:419–46.
https://doi.org/10.18632/aging.101168
PMID:28198702

16. Sorras AM, Dahl A, Horvath S, Matsuyama S. Epigenetic Age is a Cell-Intrinsic Property in Transplanted Human Hematopoietic Cells. Aging Cell. 2019; 18:e12897.
https://doi.org/10.1111/acel.12897 PMID:30712319

17. Welford SM, Bedogni B, Gradin K, Poellinger L, Broome Powell M, Giaccia AJ. HIF1alpha delays premature senescence through the activation of MIF. Genes Dev. 2006; 20:3366–71.
https://doi.org/10.1101/gad.1471106
PMID:17142669

18. Campisi J, d'Adda di Fagagna F. Cellular senescence: when bad things happen to good cells. Nat Rev Mol Cell Biol. 2007; 8:729–40.
https://doi.org/10.1038/nrm2233

PMID:17667954

19. Hahn WC, Counter CM, Lundberg AS, Beijersbergen RL, Brooks MW, Weinberg RA. Creation of human tumour cells with defined genetic elements. Nature. 1999; 400:464–68.
https://doi.org/10.1038/22780 PMID:10440377

20. Zhao JJ, Gjoerup OV, Subramanian RR, Cheng Y, Chen W, Roberts TM, Hahn WC. Human mammary epithelial cell transformation through the activation of phosphatidylinositol 3-kinase. Cancer Cell. 2003; 3:483–95.
https://doi.org/10.1016/S1535-6108(03)00088-6 PMID:12781366

21. Kabacik S, Horvath S, Cohen H, Raj K. Epigenetic ageing is distinct from senescence-mediated ageing and is not prevented by telomerase expression. Aging (Albany NY). 2018; 10:2800–15.
https://doi.org/10.18632/aging.101588 PMID:30332397

22. Carreau A, El Hafny-Rahbi B, Matejuk A, Grillon C, Kieda C. Why is the partial oxygen pressure of human tissues a crucial parameter? Small molecules and hypoxia. J Cell Mol Med. 2011; 15:1239–53.
https://doi.org/10.1111/j.1582-4934.2011.01258.x PMID:21251211

23. McKeown SR. Defining normoxia, physoxia and hypoxia in tumours-implications for treatment response. Br J Radiol. 2014; 87:20130676.
https://doi.org/10.1259/bjr.20130676 PMID:24588669

24. McCarty G, Loeb DM. Hypoxia-sensitive epigenetic regulation of an antisense-oriented lncRNA controls WT1 expression in myeloid leukemia cells. PLoS One. 2015; 10:e0119837.
https://doi.org/10.1371/journal.pone.0119837 PMID:25794157

25. Zhu T, Zheng SC, Paul DS, Horvath S, Teschendorff AE. Cell and tissue type independent age-associated DNA methylation changes are not rare but common. Aging (Albany NY). 2018; 10:3541–57.
https://doi.org/10.18632/aging.101666 PMID:30482885

26. Naue J, Hoefsloot HC, Mook OR, Rijlaarsdam-Hoekstra L, van der Zwalm MC, Henneman P, Kloosterman AD, Verschure PJ. Chronological age prediction based on DNA methylation: massive parallel sequencing and random forest regression. Forensic Sci Int Genet. 2017; 31:19–28.
https://doi.org/10.1016/j.fsigen.2017.07.015 PMID:28841467

27. Maegawa S, Lu Y, Tahara T, Lee JT, Madzo J, Liang S, Jelinek J, Colman RJ, Issa JJ. Caloric restriction delays age-related methylation drift. Nat Commun. 2017; 8:539.
https://doi.org/10.1038/s41467-017-00607-3 PMID:28912502

28. Wezyk M, Spólnicka M, Pośpiech E, Pepłońska B, Zbieć-Piekarska R, Ilkowski J, Styczyńska M, Barczak A, Zboch M, Filipek-Gliszczynska A, Skrzypczak M, Ginalski K, Kabza M, et al. Hypermethylation of TRIM59 and KLF14 Influences Cell Death Signaling in Familial Alzheimer's Disease. Oxid Med Cell Longev. 2018; 2018:6918797.
https://doi.org/10.1155/2018/6918797 PMID:29849909

29. Ciccarone F, Malavolta M, Calabrese R, Guastafierro T, Bacalini MG, Reale A, Franceschi C, Capri M, Hervonen A, Hurme M, Grubeck-Loebenstein B, Koller B, Bernhardt J, et al. Age-dependent expression of DNMT1 and DNMT3B in PBMCs from a large European population enrolled in the MARK-AGE study. Aging Cell. 2016; 15:755–65.
https://doi.org/10.1111/acel.12485 PMID:27169697

30. Horvath S. Erratum to: DNA methylation age of human tissues and cell types. Genome Biol. 2015; 16:96.
https://doi.org/10.1186/s13059-015-0649-6 PMID:25968125

31. DeCaprio JA, Ludlow JW, Figge J, Shew JY, Huang CM, Lee WH, Marsilio E, Paucha E, Livingston DM. SV40 large tumor antigen forms a specific complex with the product of the retinoblastoma susceptibility gene. Cell. 1988; 54:275–83.
https://doi.org/10.1016/0092-8674(88)90559-4 PMID:2839300

32. Ahuja D, Sáenz-Robles MT, Pipas JM. SV40 large T antigen targets multiple cellular pathways to elicit cellular transformation. Oncogene. 2005; 24:7729–45.
https://doi.org/10.1038/sj.onc.1209046 PMID:16299533

33. Triche TJ Jr, Weisenberger DJ, Van Den Berg D, Laird PW, Siegmund KD. Low-level processing of Illumina Infinium DNA Methylation BeadArrays. Nucleic Acids Res. 2013; 41:e90.
https://doi.org/10.1093/nar/gkt090 PMID:23476028

34. Aryee MJ, Jaffe AE, Corrada-Bravo H, Ladd-Acosta C, Feinberg AP, Hansen KD, Irizarry RA. Minfi: a flexible and comprehensive Bioconductor package for the analysis of Infinium DNA methylation microarrays. Bioinformatics. 2014; 30:1363–69.
https://doi.org/10.1093/bioinformatics/btu049 PMID:24478339

Original Raw data of HIF1α Western blot
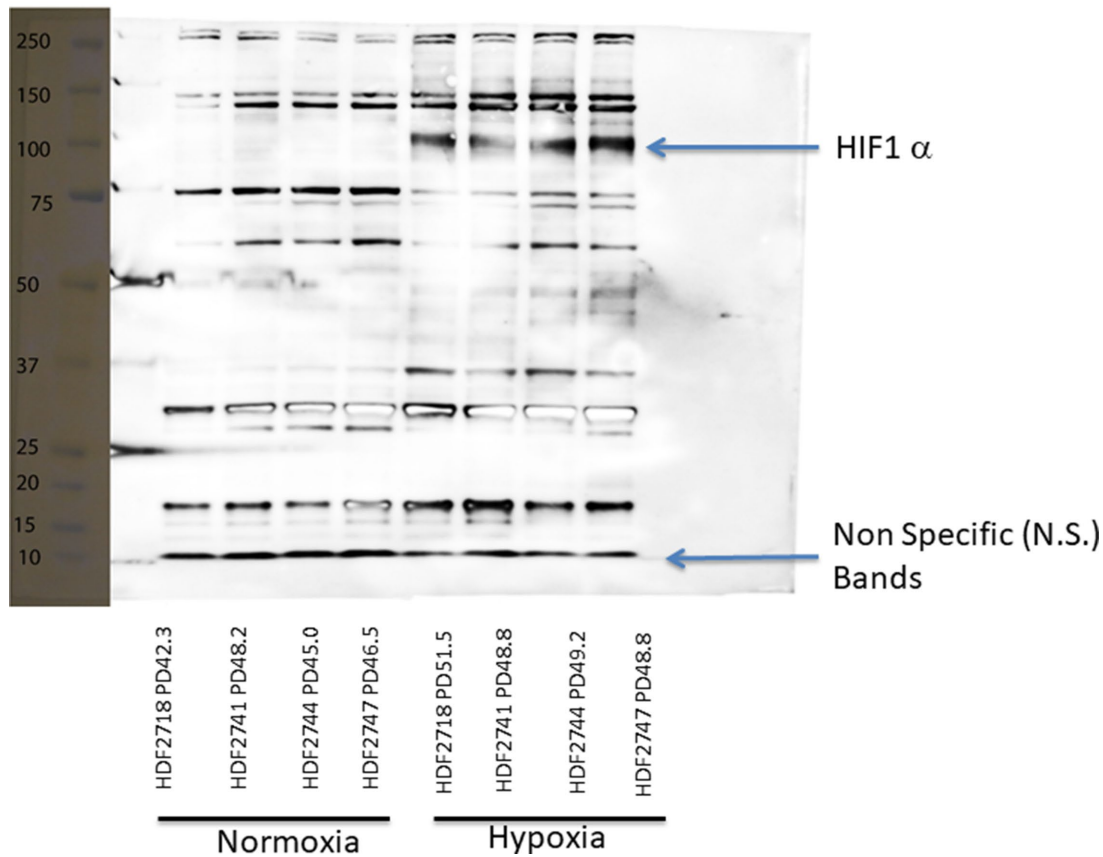
Supplementary Figure 1.

Research Paper

DNA methylation GrimAge strongly predicts lifespan and healthspan

Ake T. Lu[1], Austin Quach[1], James G. Wilson[2], Alex P. Reiner[3], Abraham Aviv[4], Kenneth Raj[5], Lifang Hou[6], Andrea A. Baccarelli[7], Yun Li[8], James D. Stewart[9], Eric A. Whitsel[9,10], Themistocles L. Assimes[11,12], Luigi Ferrucci[13], Steve Horvath[1,14]

[1]Department of Human Genetics, David Geffen School of Medicine, University of California Los Angeles, Los Angeles, CA 90095, USA
[2]Department of Physiology and Biophysics, University of Mississippi Medical Center, Jackson, MS 39216, USA
[3]Public Health Sciences Division, Fred Hutchinson Cancer Research Center, Seattle, WA 98109, USA
[4]Center of Development and Aging, New Jersey Medical School, Rutgers State University of New Jersey, Newark, NJ 07103, USA
[5]Radiation Effects Department, Centre for Radiation, Chemical and Environmental Hazards, Public Health England, Chilton, Didcot, Oxfordshire, OX11 0RQ, United Kingdom
[6]Center for Population Epigenetics, Robert H. Lurie Comprehensive Cancer Center and Department of Preventive Medicine, Northwestern University Feinberg School of Medicine, Chicago, IL 60611, USA
[7]Laboratory of Environmental Epigenetics, Departments of Environmental Health Sciences Epidemiology, Columbia University Mailman School of Public Health, New York, NY 10032, USA
[8]Departments of Genetics, Biostatistics, Computer Science, University of North Carolina, Chapel Hill, NC 27599, USA
[9]Department of Epidemiology, Gillings School of Global Public Health, University of North Carolina, Chapel Hill, NC 27599, USA
[10]Department of Medicine, School of Medicine, University of North Carolina, Chapel Hill, NC 27516, USA
[11]Department of Medicine (Division of Cardiovascular Medicine), Stanford University School of Medicine, Stanford, CA 94305, USA
[12]VA Palo Alto Health Care System, Palo Alto, CA 94304, USA
[13]Longitudinal Studies Section, Translational Gerontology Branch, National Institute on Aging, National Institutes of Health, USA, Baltimore, MD 21224, USA
[14]Department of Biostatistics, Fielding School of Public Health, University of California Los Angeles, Los Angeles, CA 90095, USA

Correspondence to: Steve Horvath; **email:** shorvath@mednet.ucla.edu
Keywords: epigenetics, DNA methylation, proteomics, mortality
Received: August 24, 2018 **Accepted:** November 22, 2018 **Published:** January 21, 2019

ABSTRACT

It was unknown whether plasma protein levels can be estimated based on DNA methylation (DNAm) levels, and if so, how the resulting surrogates can be consolidated into a powerful predictor of lifespan. We present here, seven DNAm-based estimators of plasma proteins including those of plasminogen activator inhibitor 1 (PAI-1) and growth differentiation factor 15. The resulting predictor of lifespan, DNAm GrimAge (in units of years), is a composite biomarker based on the seven DNAm surrogates and a DNAm-based estimator of smoking pack-years. Adjusting DNAm GrimAge for chronological age generated novel measure of epigenetic age acceleration, *AgeAccelGrim*.

Using large scale validation data from thousands of individuals, we demonstrate that DNAm GrimAge stands out among existing epigenetic clocks in terms of its predictive ability for time-to-death (Cox regression P=2.0E-75), time-to-coronary heart disease (P=6.2E-24), time-to-cancer (P= 1.3E-12), its strong relationship with computed tomography data for fatty liver/excess visceral fat, and age-at-menopause (P=1.6E-12). AgeAccelGrim is strongly associated with a host of age-related conditions including comorbidity count (P=3.45E-17). Similarly, age-adjusted DNAm PAI-1 levels are associated with lifespan (P=5.4E-28), comorbidity count (P= 7.3E-56) and type 2 diabetes (P=2.0E-26). These DNAm-based biomarkers show the expected relationship with lifestyle factors including healthy diet and educational attainment.

Overall, these epigenetic biomarkers are expected to find many applications including human anti-aging studies.

INTRODUCTION

DNAm levels have been used to build accurate composite biomarkers of chronological age [1-4]. DNAm-based age (epigenetic age) estimators, include the pan tissue epigenetic clock by Horvath 2013 [1], based on 353 CpGs, and an estimator developed by Hannum 2013 [2], based on 71 CpGs in leukocytes. These estimators predict lifespan after adjusting for chronological age and other risk factors [5-9]. Moreover, they are also associated with a large host of age-related conditions [10-20]. Recently, DNAm-based biomarkers for lifespan (time-to-death due to all-cause mortality) have been developed [21, 22]. For example, Zhang et al (2017) combined mortality associated CpGs [21] into an overall mortality risk score, while Levine et al (2018) developed a lifespan predictor, DNAm PhenoAge, by regressing a phenotypic measure of mortality risk on CpGs [22].

Many analytical strategies are available for developing lifespan predictors from DNAm data. The reported single stage approach involves the direct regression of time-to-death (due to all-cause mortality) on DNAm levels. By contrast, the current study employed a novel two-stage procedure: In stage 1, we defined DNAm-based surrogate biomarkers of smoking pack-years and a selection of plasma proteins that have previously been associated with mortality or morbidity. In stage 2, we regressed time-to-death on these DNAm-based surrogate biomarkers. The resulting mortality risk estimate of the regression model is then linearly transformed into an age estimate (in units of years). We coin this DNAm-based biomarker of mortality "DNAm GrimAge" because high values are grim news, with regards to mortality/morbidity risk. Our comprehensive studies demonstrate that DNAm GrimAge stands out when it comes to associations with age-related conditions, clinical biomarkers, and computed tomography data.

RESULTS

Overview of the two-stage approach for defining DNAm GrimAge

We constructed the DNAm GrimAge in two-stages. First, we defined surrogate DNAm biomarkers of physiological risk factors and stress factors. These include the following plasma proteins: adrenomedullin, C-reactive protein, plasminogen activation inhibitor 1 (PAI-1), and growth differentiation factor 15 (GDF15) [23, 24]. In addition, given that smoking is a significant risk factor of mortality and morbidity, we also used DNAm-based estimator of smoking pack-years. Second, we combined these biomarkers into a single composite biomarker of lifespan, DNAm GrimAge, which is expressed in units of years. We then performed a large-scale meta-analysis (involving more than 7000 Illumina array measurements), showing that DNAm GrimAge is a better predictor of lifespan than currently available DNAm-based predictors.

Our studies reveal a surprising finding; which is that in some instances, the DNAm-based surrogate biomarkers (e.g. for smoking pack-years) is a better predictors of mortality than the actual observed (self-reported) biomarker. We also correlated DNAm GrimAge with lifestyle factors and a host of age-related conditions, e.g. we demonstrate that these DNAm-based biomarkers predict time to cardiovascular disease. Finally, we show that DNAm GrimAge is also associated with age-related changes in blood cell composition and leukocyte telomere length.

Training and test data from the Framingham Heart Study

We began by correlating the levels of 88 plasma protein variables (measured using immunoassays) with DNAm array data generated from the same blood samples of n=2,356 individuals from the Framingham heart study

(FHS) Offspring Cohort [25] (Supplementary Note 1). We divided the FHS data randomly into a training set (70% of the FHS pedigrees, N= 1731 individuals from 622 pedigrees) and a test data set (30% pedigrees, N=625 individuals from 266 pedigrees, Supplementary Table 1). The mean age of individuals donating DNA for the training set was 66 years, while that of individuals in the test dataset was 67. These participants had similar demographic profiles, smoking history, and number of years' follow-up as those in the training set (Supplementary Table 1).

Stage 1: DNAm-based surrogate biomarkers of plasma proteins and smoking pack-years

We used the training data to define DNAm-based surrogate markers of 88 plasma protein variables and smoking pack-years. We restricted the analysis to CpGs that are present on both the Illumina Infinium 450K array and the new Illumina EPIC methylation array in order to ensure future compatibility. Each of the 88 plasma protein variables (dependent variable) was regressed on chronological age, sex, and the CpGs levels in the training data using an elastic net regression model [26], which automatically selected a subset of CpGs (typically fewer than 200 CpGs) whose linear combination best predicted the corresponding plasma level in the training data (Methods). For example, the DNAm levels of 137 CpGs and 211 CpGs allowed us to estimate the plasma levels of GDF15 and PAI-1, respectively. The predicted DNAm values of GDF15 and PAI-1 can then be used as surrogate markers for the measured plasma levels. In general, we denote DNAm-based surrogate markers of plasma proteins and smoking pack-years by adding the prefix "DNAm" to the respective variable name, e.g. DNAm pack-years (Fig. 1 and Supplementary Table 2).

Not all of the available 88 plasma protein levels were successfully imputed based on DNAm data.
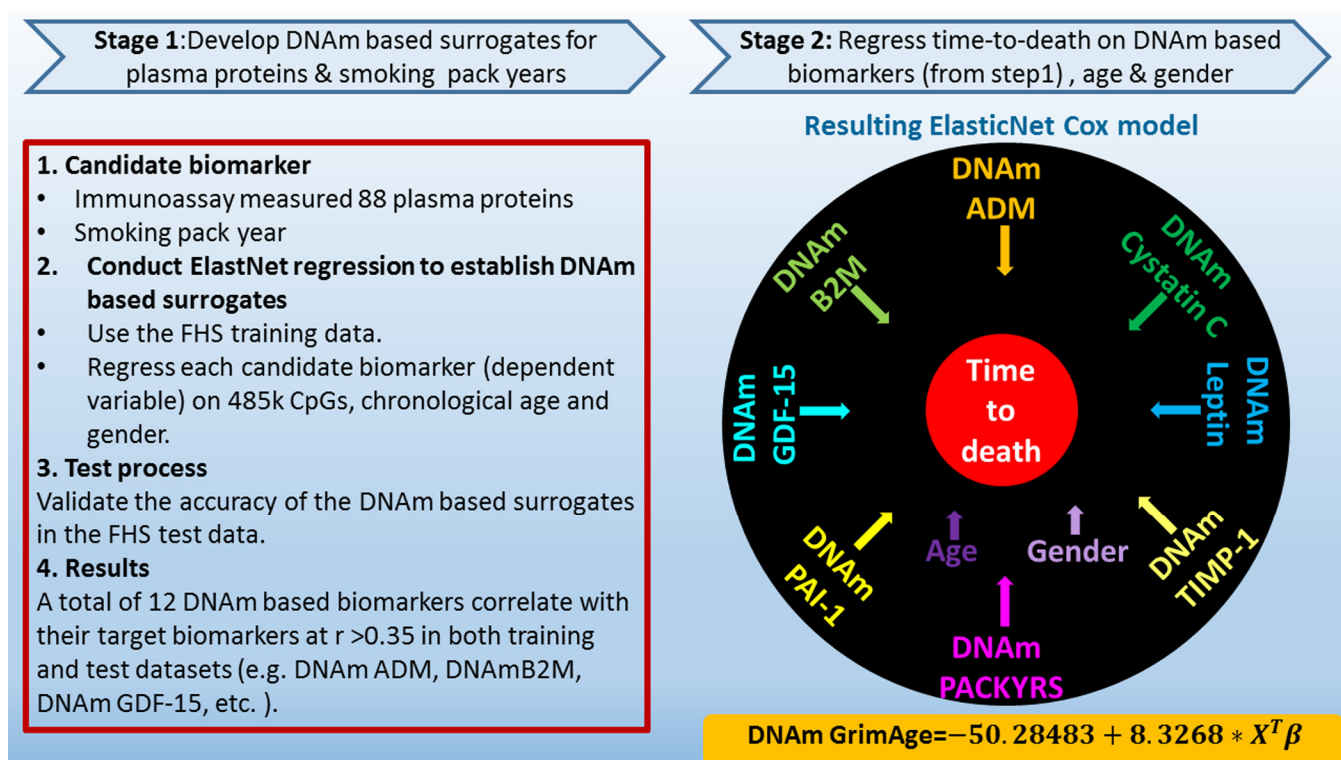
Figure 1. Flowchart for developing DNAm GrimAge. Surrogate DNAm-based biomarkers for smoking pack-years and plasma protein levels were defined and validated using training and test data from the Framingham Heart study (stage 1). Only 12 out of 88 plasma proteins exhibited a correlation r >0.35 with their respective DNAm-based surrogate marker in the test data. In stage 2, time-to-death (due to all-cause mortality) was regressed on chronological age, sex, and DNAm-based biomarkers of smoking pack-years and the 12 above mentioned plasma protein levels. The elastic net regression model automatically selected the following covariates: chronological age (Age), sex (Female), and DNAm based surrogates for smoking pack-years (DNAm PACKYRS), adrenomedullin levels (DNAm ADM), beta-2 microglobulin (DNAm B2M), cystatin C (DNAm Cystatin C), growth differentiation factor 15 (DNAm GDF-15), leptin (DNAm Leptin), plasminogen activation inhibitor 1 (DNAm PAI-1), tissue inhibitor metalloproteinase 1 (DNAm TIMP-1). The linear combination of the covariate values $X^T\beta$ was linearly transformed to be in units of years. Technically speaking, DNAm GrimAge is a mortality risk estimator. Metaphorically speaking, it estimates biological age.

Table 1. Reproducibility and age correlations of DNAm based surrogate biomarkers.

Correlation (r)	Training (N=1731)		Test (N=625)	
	Observed biomarker	Age	Observed biomarker	Age
DNAm based surrogate				
adrenomedullin	0.65	0.63	0.38	0.64
beta-2-microglobulin	0.62	0.83	0.43	0.85
CD56	0.86	0.17	0.36	0.17
ceruloplasmin	0.56	0.04	0.49	-0.02
cystatin-C	0.58	0.81	0.39	0.83
EGF fibulin-like ECM protein1	0.59	0.72	0.41	0.87
growth differentiation factor 15	0.74	0.71	0.53	0.81
leptin	0.68	0.06	0.35	0.05
myoglobin	0.50	-0.04	0.38	0.03
plasminogen activator inhibitor 1	0.69	0.19	0.36	0.16
serum paraoxonase/arylesterase 1	0.57	-0.22	0.51	-0.22
tissue Inhibitor Metalloproteinases 1	0.43	0.92	0.35	0.90
smoking pack-years	0.79	0.17	0.66	0.13

The table reports the correlation coefficients between the observed marker (i.e. observed plasma protein level or self-reported smoking pack-years) and its respective DNAm-based surrogate marker in 1) the FHS training data and 2) the FHS test data. Each of the DNA-based surrogate biomarkers (rows) leads to a correlation $r > 0.35$ in both training and test datasets (columns 2 and 4). DNAm-based pack-years is highly correlated with the self-report pack-years in both training and test datasets ($r \geq 0.66$). The table also reports the correlation coefficients between the DNAm-based surrogate biomarkers (rows) and chronological age in the FHS training and test data (columns 3 and 5).

Instead, only 12 of the 88 plasma proteins exhibited a moderately high correlation coefficient (r>0.35) between their measured levels and their respective DNAm-based surrogate marker in the test data set (Table 1). We focused on these 12 DNAm surrogate biomarkers in stage 2. Additionally, we constructed a DNAm-based surrogate of self-reported smoking pack-years, DNAm pack-years, based on a linear combination of 172 CpGs.

Stage 2: Constructing a composite biomarker of lifespan based on surrogate biomarkers

In stage 2, we developed a predictor of mortality by regressing time-to-death due to all-cause mortality (dependent variable) on the following covariates: the DNAm-based estimator of smoking pack-years, chronological age at the time of the blood draw, sex, and the 12 DNAm-based surrogate biomarkers of plasma protein levels. The elastic net Cox regression model automatically selected the following covariates: DNAm pack-years, age, sex, and the following 7 DNAm-based surrogate markers of plasma proteins:

adrenomedullin (ADM), beta-2-microglobulim (B2M), cystatin C (Cystatin C), GDF-15, leptin (Leptin), PAI-1, and tissue inhibitor metalloproteinases 1 (TIMP-1), (Supplementary Table 2). DNAm-based biomarkers for smoking pack-years and the 7 plasma proteins are based on fewer than 200 CpGs each, totaling 1,030 unique CpGs (Supplementary Table 2). Details on the plasma proteins can be found in Supplementary Note 2.

The linear combination of covariates resulting from the elastic net Cox regression model can be interpreted as an estimate of the logarithm of the hazard ratio of mortality. We linearly transformed this parameter into an age estimate, i.e., DNAm GrimAge, by performing a linear transformation whose slope and intercept terms were chosen by forcing the mean and variance of DNAm GrimAge to match that of chronological age in the training data (Methods, Fig. 1). In independent test data, DNAm GrimAge is calculated without estimating any parameter because the numeric values of all parameters were chosen in the training data. Following the terminology from previous articles on DNAm-based biomarkers of aging, we defined a novel measure of

epigenetic age acceleration, AgeAccelGrim, which, by definition, is *not* correlated (r=0) with chronological age. Toward this end, we regressed DNAm GrimAge on chronological age using a linear regression model and defined AgeAccelGrim as the corresponding raw residual (i.e. the difference between the observed value of DNAm GrimAge minus its expected value). Thus, a positive (or negative) value of AgeAccelGrim indicates that the DNAm GrimAge is higher (or lower) than expected based on chronological age.

Unless indicated otherwise, we used AgeAccelGrim (rather than DNAm GrimAge) in association tests of age-related conditions because age was a confounder in

these analyses. For the same reason, we also used age-adjusted versions of our DNA-based surrogate markers (for smoking pack-years and the seven plasma protein levels). In general, all association tests were adjusted for chronological age and, when required, other confounders as well (such as sex, Methods).

Pairwise correlations between DNAm GrimAge and surrogate biomarkers

Using the test data from the FHS, we calculated pairwise correlations between DNAm GrimAge and its underlying variables (Fig. 2 and Supplementary Table 2). DNAm GrimAge is highly correlated with DNAm
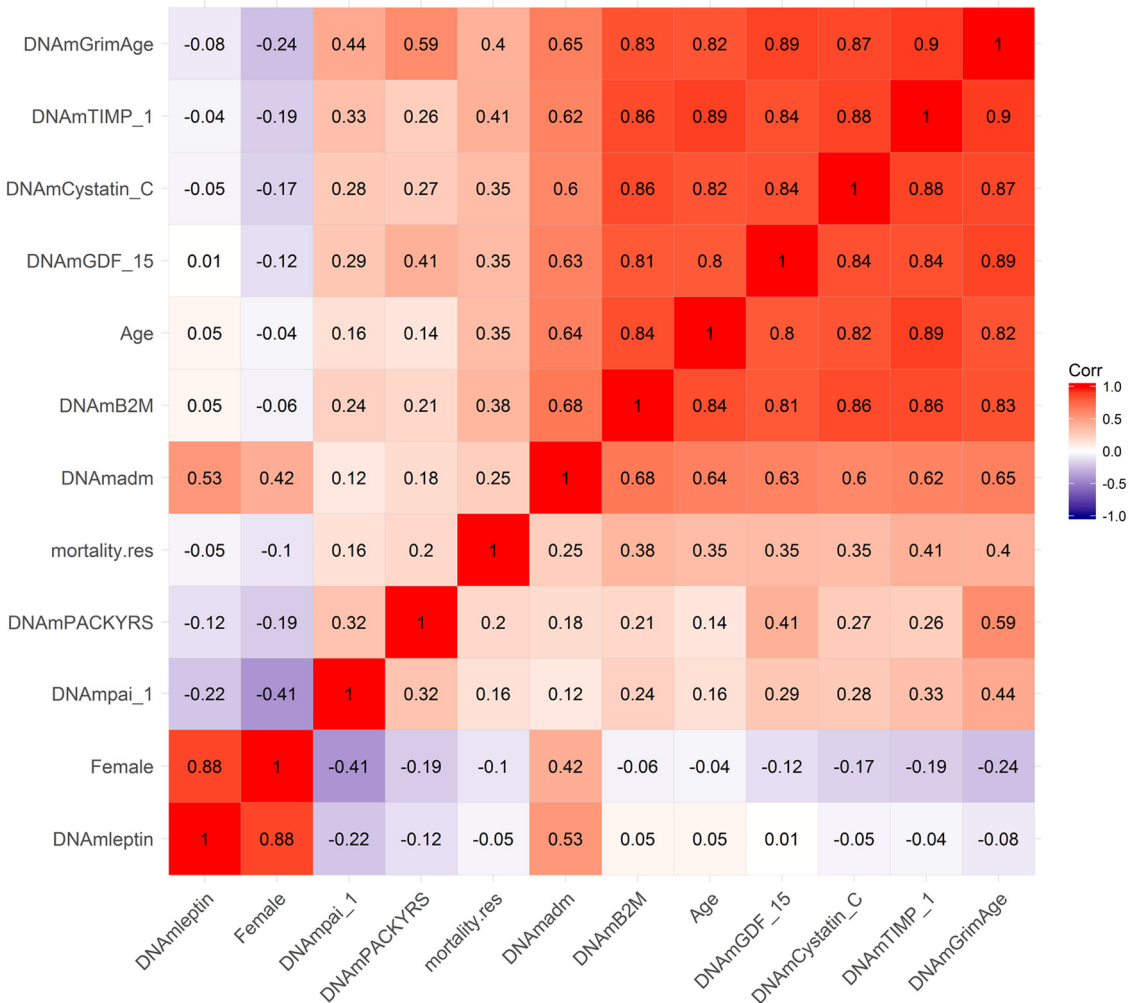
Figure 2. Heat map of pairwise correlations of DNAm based biomarkers. The heat map color-codes the pairwise Pearson correlations of select variables (surrounding the definition of DNAm GrimAge) in the test data from the Framingham Heart Study (N=625). DNAm GrimAge is defined as a linear combination of chronological age (Age), sex (Female takes on the value 1 for females and 0 otherwise), and eight DNAm-based surrogate markers for smoking pack-years (DNAm PACKYRS), adrenomedullin levels (DNAm ADM), beta-2 microglobulin (DNAm B2M), cystatin C (DNAm Cystatin C), growth differentiation factor 15 (DNAm GDF-15), leptin (DNAm Leptin), plasminogen activation inhibitor 1 (DNAm PAI-1), issue inhibitor metalloproteinase 1 (DNAm TIMP-1). The figure also includes an estimator of mortality risk, *mortality.res*, which can be interpreted as a measure of "excess" mortality risk compared to the baseline risk in the test data. Formally, mortality.res is defined as the deviance residual from a Cox regression model for time-to-death due to all-cause mortality. The rows and columns of the Figure are sorted according to a hierarchical clustering tree. The shades of color (blue, white, and red) visualize correlation values from -1 to 1. Each square reports a Pearson correlation coefficient.

TIMP-1 (r=0.90) and chronological age (r=0.82). An estimate of excess mortality risk (called mortality residual *mortality.res*) exhibits higher positive correlations with both DNAm GrimAge and DNAm TIMP-1 ($r \sim 0.40$) than with chronological age ($r \sim 0.35$, Fig. 2), in keeping with our later finding that these DNAm biomarkers are better predictors of lifespan than chronological age. With the exception of DNAm Leptin, all of the DNAm-based biomarkers exhibited positive correlations with the measure of excess mortality risk ($0.41 \geq r \geq 0.16$, Fig. 2). With the exception of DNAm Leptin, all DNAm based surrogate biomarkers exhibited moderate to strong pairwise correlations with each other. DNAm Leptin is elevated in females (Supplementary Fig. 1A, B) consistent with what has been reported in the literature [27, 28]. After stratifying by sex, we find that plasma leptin levels increase weakly with age (r=0.18 and P=2.1E-3 in males; r=0.19, P=4.8E-4 in females, Supplementary Fig. 1E, F).

Predicting time-to-death in validation data

To evaluate whether our novel DNAm-based biomarkers are better predictors of lifespan than chronological age, we analyzed N=7,375 Illumina methylation arrays generated from blood samples of 6,935 individuals comprising 3 ethnic/racial groups: 50% European ancestry (Caucasians), 40% African Americans, and 10% Hispanic ancestry (Table 2, Methods, and Supplementary Note 1). The data came from different cohort studies: test data from the FHS, BA23 and EMPC study from the Women's Health Initiative (WHI), the InCHIANTI cohort study, and African Americans from the Jackson Heart Study (JHS). We stratified each cohort by race/ethnicity (resulting in 9 strata) to avoid confounding and to ascertain whether the mortality predictors apply to each group separately.

The mean chronological age at the time of the blood draw was 63.0 years. The mean follow-up time (used for assessing time-to-death due to all-cause mortality) was 13.7 years. Since chronological age is one of the component variables underlying DNAmGrimAge, it is not surprising that the latter is highly correlated with age in each of the study cohorts ($r \geq 0.79$, Supplementary Fig. 2).

While each (age-adjusted) component variable underlying DNAm GrimAge is a significant predictor of lifespan (Fig. 3), DNAm pack-years (meta-analysis P=1.7E-47) and DNAm PAI-1(P=5.4E-28) exhibit the most significant meta-analysis P-values. The fixed effects meta-analysis P-values reveal that AgeAccelGrim stands out when it comes to lifespan prediction (meta-analysis P=2.0E-75, Fig. 3A). The same applies when the analysis is restricted to never-

smokers (Supplementary Fig. 3) or to former/current smokers (Supplementary Fig. 4). AgeAccelGrim remains a highly significant predictor of lifespan after restricting the analysis to never-smokers (N=3,988, meta analysis P=1.1E-16, Supplementary Fig. 3A) or to former/current smokers (P=3.5E-33, Supplementary Fig. 4A).

Instances in which DNAm-based surrogates outperform observed biomarkers

The DNAm-based surrogate biomarker for smoking pack-years has two surprising properties. First, it predicts lifespan in never-smokers (P=1.6E-6, Supplementary Fig. 3I). Second, the surrogate marker is a more significant predictor of lifespan than self-reported pack-years: P=8.5E-5 for DNAm marker versus P=2.1E-3 for observed pack-years in in the FHS test data; similarly, P=5.3E-4 versus 0.18 in the InChianti Study (Supplementary Table 3). The superior predictive performance of DNAm based surrogate biomarkers vis-à-vis their observed/ counter parts also applies to PAI-1 plasma levels (P=8.7E-4 for the DNAm marker versus P=0.074 for the observed levels), TIMP-1 (P=3.8E-4 for the DNAm marker versus P=0.017), and to a lesser extent to cystatin C (P=0.019 for the DNAm estimator versus P=0.054 for the observed level, Supplementary Table 4).

Mortality prediction based on observed plasma protein levels

The AgeAccelGrim is a composite biomarker derived from DNAm-based surrogate biomarkers of plasma protein levels and smoking pack-years. This begs the question whether a predictor of lifespan based directly on observed plasma protein levels and self-reported smoking pack-years, would outperform its DNAm-based analog? Analogous to our construction of DNAm GrimAge, we used a Cox regression model to regress time to-death on the observed plasma protein levels and self-reported pack-year in the training data (Methods). The resulting mortality risk estimator (defined as weighted average of the observed biomarkers) was linearly transformed into units of years. The resulting predictor, i.e., *observed* GrimAge, and its age-adjusted version. i.e., *DNAm* based AgeAccelGrim, were compared in the FHS, showing similar HRs (*observed* AgeAccelGrim HR=1.10, P=3.2E-7; DNAm based AgeAccelGrim HR= 1.12, P=8.6E-5, Supplementary Table 5). Overall, this comparison shows that DNAm levels in general and our DNAm-based surrogate biomarkers in particular capture a substantial proportion of the information that is captured by the 7 selected plasma proteins and self-reported smoking pack-years. Since our study focuses on DNAm-based biomarkers, we will only consider DNAm-based biomarkers in the following.
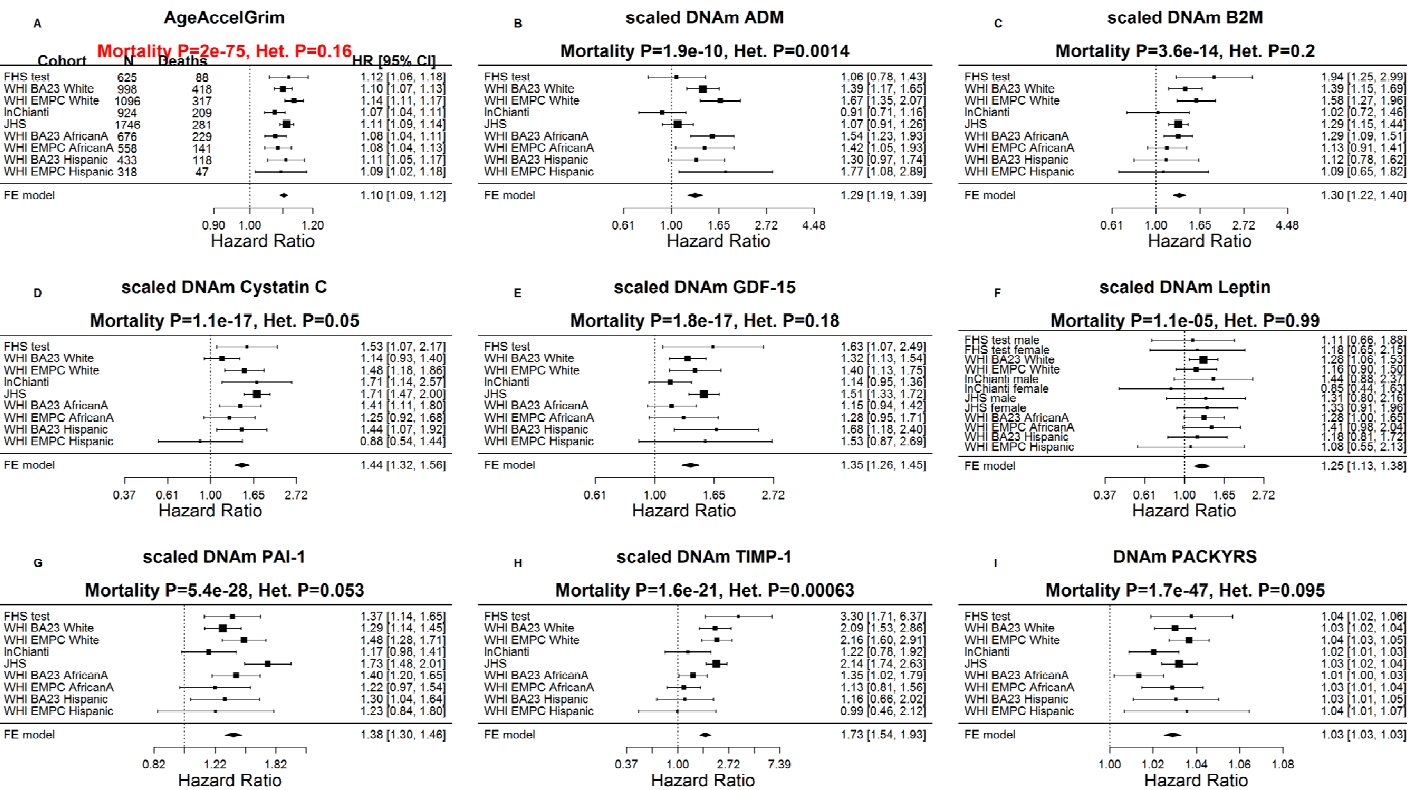
Figure 3. Meta analysis forest plots for predicting time-to-death due to all-cause mortality. Each panel reports a meta-analysis forest plot for combining hazard ratios predicting time-to-death based on a DNAm-based biomarker (reported in the figure heading) across different strata formed by racial group within cohort. (**A**) Results for AgeAccelGrim. Each row reports a hazard ratio (for time-to-death) and a 95% confidence interval resulting from a Cox regression model in each of 9 strata (defined by cohort and racial groups). Results for (age-adjusted) DNAm-based surrogate markers of (**B**) adrenomedullin (ADM), (**C**) beta-2 microglobulin (B2M), (**D**) cystatin C (Cystatin C), (**E**) growth differentiation factor 15 (GDF-15), (**F**) leptin, (**G**) plasminogen activation inhibitor 1 (PAI-1), (H) tissue inhibitor metalloproteinase 1 (TIMP-1) and (**I**) smoking pack-years (PACKYRS). The sub-title of each panel reports the meta-analysis p-value and a p-value for a test of heterogeneity Cochran Q test (Het.). (**A**) Each hazard ratio (HR) corresponds to a one-year increase in AgeAccelGrim. (**B**-**H**) Each hazard ratio corresponds to an increase in one-standard deviation. (**I**) Hazard ratios correspond to a 1 year increase in pack-years. The most significant meta-analysis P value (here AgeAccelGrim) is marked in red. A *non*-significant Cochran Q test p-value is desirable because it indicates that the hazard ratios do not differ significantly across the strata. For example, the hazard ratios associated with AgeAccelGrim exhibit insignificant heterogeneity across the strata (**Cochran Q test P_{I^2}**=0.16).

Age-related conditions

Our Cox regression analysis of time-to-coronary heart disease (CHD), reveals that AgeAccelGrim is highly predictive of incident CHD (HR=1.07, P=6.2E-24 and P_{I^2}=0.4, Fig. 4A). As expected, several underlying DNAm-based surrogate biomarkers also individually predict incident CHD; notably the age-adjusted versions of DNAm smoking pack-years (HR=1.02, P=6.4E-14) and DNAm PAI-1 (HR=1.31 per SD, P=3.6E-12).

Similarly, time-to-congestive heart failure (CHF) is also associated with AgeAccelGrim (HR=1.10 and P=4.9E-9), age-adjusted DNAm cystatin C (HR=2.02 and

Cross sectional studies reveal that AgeAccelGrim is associated with hypertension (odds ratio [OR]=1.04 and P= 5.1E-13, Supplementary Fig. 6), type 2 diabetes (OR=1.02 and P=0.01, Supplementary Fig. 7), and physical functioning (Stouffer P=1.7E-8, Supplementary Fig. 8). All of the reported associations are in the expected directions, e.g. higher values of AgeAccelGrim are associated with lower physical functioning levels. In women, early age at menopause is associated with significantly higher values of AgeAccelGrim (P=1.6E-12, Supplementary Fig. 9A) and to a lesser extent with all of the age-adjusted versions of the DNAm based surrogate markers, notably DNA cystatin C (P=2.2E-6) and DNAm GDF-15 (P=1.3E-5, Supplementary Fig. 9).
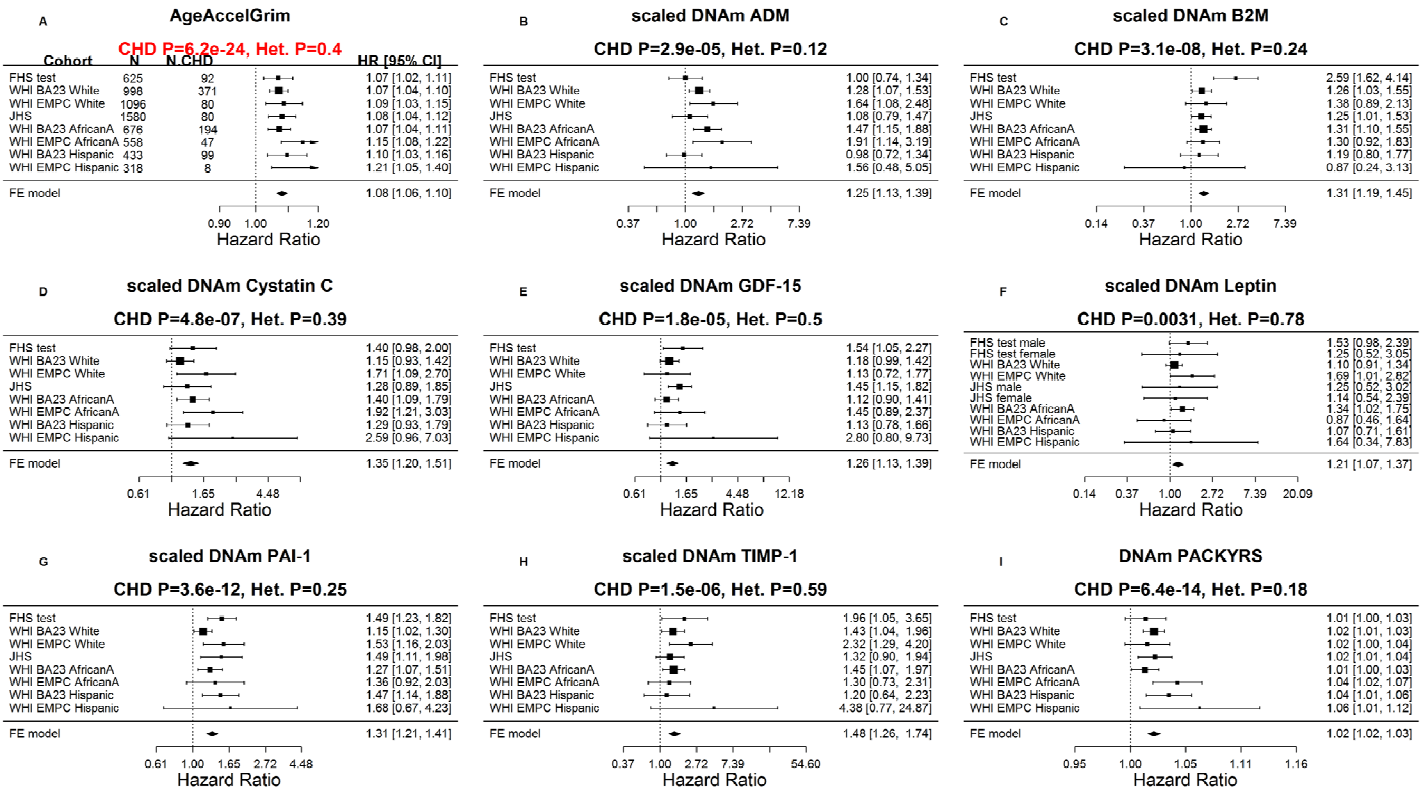
Figure 4. Meta analysis forest plots for predicting time-to-coronary heart disease. Each panel reports a meta-analysis forest plot for combining hazard ratios predicting time to CHD and the DNAm-based biomarker (reported in the figure heading) across different strata formed by racial groups within cohorts. (**A**) Results for AgeAccelGrim. Each row reports a hazard ratio (for time-to-CHD) and a 95% confidence interval resulting from a Cox regression model in each of 9 strata (defined by cohort and racial groups). Results for (age adjusted) DNAm-based surrogate markers of (**B**) adrenomedullin (ADM), (**C**) beta-2 microglobulin (B2M), (**D**) cystatin C (Cystatin C), (**E**) growth differentiation factor 15 (GDF-15), (**F**) leptin, (**G**) plasminogen activation inhibitor 1 (PAI-1), (**H**) tissue inhibitor metalloproteinase 1 (TIMP-1) and (**I**) smoking pack-years (PACKYRS). The sub-title of each panel reports the meta-analysis p-value and a p-value for a test of heterogeneity Cochran Q test (Het.). (**A**) Each hazard ratio (HR) corresponds to a one-year increase in AgeAccelGrim. (**B**-**H**) Each hazard ratio corresponds to an increase in one-standard deviation. (**I**) Hazard ratios correspond to a one unit increased in DNAm pack-years. The most significant meta-analysis P value (here AgeAccelGrim) is marked in red.

DNAm plasminogen activation inhibitor 1

AgeAccelGrimAge outperforms (age-adjusted versions of) DNAm smoking pack-years and the 7 DNAm-based surrogate markers of plasma protein levels individually with regards to prediction of time-to-death or time-to-coronary heart disease (Figs. 3 and 4). However, age-adjusted DNAm PAI-1 outperforms AgeAccelGrim for several age-related traits (Supplementary Fig. 5-9), notably the comorbidity index (defined as the total number of age-related conditions) where Stouffer's meta-analysis P value for DNAm PAI-1 (P=7.3E-56) is more significant than that for AgeAccelGrim (P=2.0E-16, Fig. 5). As with AgeAccelGrim, higher levels of age-adjusted DNAm PAI-1 are associated with hypertension status, type 2 diabetes status, time-to-CHD (Fig. 4), time-to-CHF, and early age at menopause (Supple-

mentary Figs. 5-7 and 9), while lower levels are associated with disease free status (Stouffer P=2.9E-11, Supplementary Fig. 10) and better physical functioning (Stouffer P=1.4E-8, Supplementary Fig. 8).

Heritability analysis

We used pedigree based polygenic models (Methods) to measure heritability estimates of AgeAccelGrim and the individual biomarkers. There is significant heritability for AgeAccelGrim (h^2 =0.30, P=0.022) and observed AgeAccelGrim (h^2 =0.37, P=0.006, Supplementary Table 6). Similarly, several of our DNAm-based surrogate biomarkers (PAI1, B2M, ADM, and GDF15) and their observed counterparts are also highly heritable (Supplementary Table 6), e.g. DNAm PAI-1 (h^2 =0.34 and P=7.1E-3), observed PAI-1 levels (h^2 =0.51 and

P=6.2E-4), DNAm Beta 2 microglobulin levels (h^2 =0.45 and P=2.4E-3), and observed B2M (h^2 =0.34 and P=3.3E-3). Overall, these results suggest that many observed and DNAm-based biomarkers are heritable.

AgeAccelGrim versus other epigenetic measures of age acceleration

Using the same validation datasets (N=7,375 arrays), we compared DNAm GrimAge with three widely-used DNA-based biomarkers of aging: DNAm age estimator based on different somatic tissues by Horvath (2013) [1],the DNAm age estimator based on leukocytes by Hannum (2013) [2] and the DNAm PhenoAge estimator by Levine (2018) [22]. The respective age-adjusted measures of epigenetic age acceleration will be denoted as AgeAccel (or AgeAccelerationResidual), AgeAccel Hannum, and AgeAccelPheno following the notation of previous publications. The four epigenetic measures of age acceleration (including AgeAccelGrim) are in units

of year. AgeAccelGrim exhibits moderate positive correlations with each of the three alternative measures of epigenetic age acceleration ($0.17 \leq r \leq 0.45$, Supplementary Fig. 11) with the strongest correlation with AgeAccelPheno. The relatively weak correlation with Horvath's pan-tissue clock (r=0.17) probably reflects the fact that DNAm GrimAge was developed exclusively with blood methylation data. It is evident that AgeAccelGrim is superior with respect to meta-analysis P-values for prediction of time-to-death: AgeAccelGrim (P=2.0E-75, HR=1.10), AgeAccel (Meta P=8.9E-5, HR=1.02, Supplementary Fig. 12), AgeAccelHannum (Meta P=6.8E-16, HR=1.04), AgeAccelPheno (Meta P=3.5E-36, HR=1.05). The results remain qualitatively the same after restricting the analysis to never-smokers or former/current smokers (Supplementary Figs. 13 and 14).

Similarly, AgeAccelGrim stands out when comparing individuals in the top 20% percentile of epigenetic age
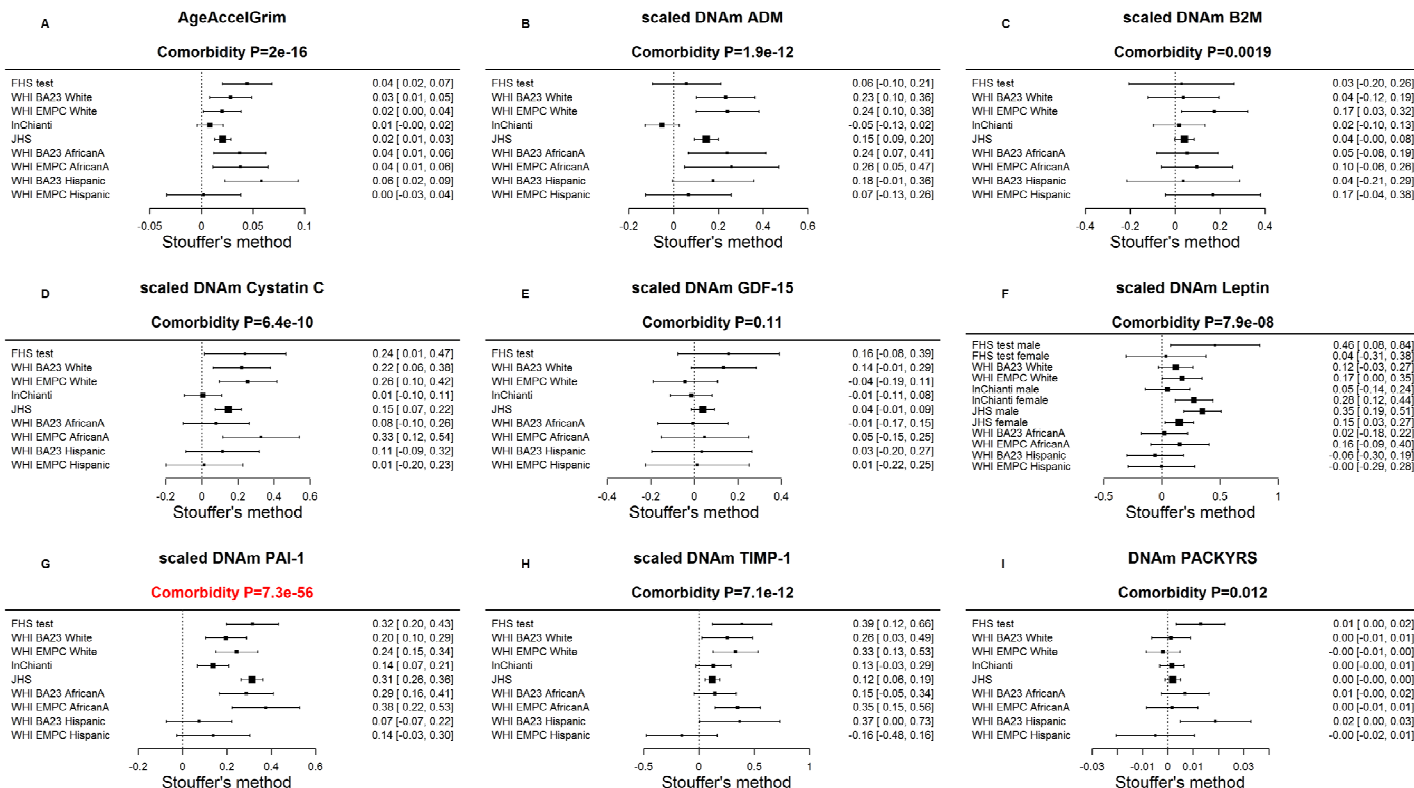
Figure 5. Meta-analysis of associations with total number of age-related conditions. Each panel reports a meta-analysis forest plot for combining regression coefficients between the comorbidity index and the DNAm-based biomarker (reported in the figure heading) across different strata, which are formed by racial group within cohort. (**A**) Meta analysis of the regression slope between AgeAccelGrim and the comorbidity index. Analogous results for (age-adjusted) DNAm based surrogate markers of (**B**) adrenomedullin (ADM), (**C**) beta-2 microglobulin (B2M), (**D**) cystatin C (Cystatin C), (**E**) growth differentiation factor 15 (GDF-15), (**F**) leptin, (**G**) plasminogen activation inhibitor 1 (PAI-1), (**H**) tissue inhibitor metalloproteinase 1 (TIMP-1) and (**I**) smoking pack-years (PACKYRS). The individual study results were combined using fixed effect meta-analysis (reported in the panel heading). Cochran Q test for heterogeneity across studies (Het.). The effect sizes correspond to one year of age acceleration in panel **A**, one pack-year in panel I and one standard deviation in other panels for DNAm proteins. The estimate with the most significant meta P value is marked in red.

acceleration to those in the bottom 20% percentile (Stouffer meta-analysis P= 6.4E-38, Supplementary Fig. 15), AgeAccelPheno (P=5.7E-21), AgeAccelHannum (P=1.3E-5), and AgeAccel (P=0.17).

When it comes to significant associations with comorbidity index, age-adjusted DNAm PAI-1($P_{DNAm\,PAI-1}$=7.3E-56, Fig.5) outperforms all other DNAm-based biomarkers including AgeAccelGrim ($P_{AgeAccelGrim}$ =2.0E-16) and AgeAccelPheno ($P_{AgeAccelPheno}$=7.8E-21, Supplementary Fig. 16).

AgeAccelGrim is more informative than AgeAccelPheno in predicting time-to-CHD ($P_{AgeAccelGrim}$ =6.2E-24 and $HR_{AgeAccelGrim}$=1.07 versus $P_{AgeAccelPheno}$= 1.7E-8 and $HR_{AgeAccelPheno}$ =1.03, Supplementary Fig. 17) even after stratifying the analysis by smoking status (Supplementary Figs. 18 and 19).

AgeAccelGrim greatly outperforms the other 3 measures of epigenetic age acceleration including predicting time to (any) cancer (AgeAccelGrim P= 1.3E-12 versus AgeAccelPheno P=2.7E-3, Supplementary Fig. 20) and as related to an inverse association with early age at menopause in women (AgeAccelGrim P=1.6E-12 versus AgeAccel P=2.2E-3, Supplementary Fig. 21). A sensitivity analysis reveals that the latter finding remains qualitatively the same even after removing the InChianti cohort, which exhibited the strongest negative association between epigenetic age acceleration and age at menopause (Supplementary Fig. 22).

Multivariate Cox models adjusting for traditional risk factors

The above-mentioned Cox regression models were adjusted for age at blood draw (baseline), batch, pedigree, and intra-subject correlation as needed. We also fit multivariate Cox regression models that included additional covariates assessed at baseline: body mass index, educational level, alcohol intake, smoking pack-years, prior history of diabetes, prior history of cancer, and hypertension status (Methods). Even after adjusting for these known risk factors for morbidity, AgeAccelGrim remained a highly significant predictor of lifespan (P=5.7E-29, Supplementary Fig. 23) and time-to-CHD (P=3.7E-11, Supplementary Fig. 24) and outperformed previously published measures of epigenetic age acceleration.

Stratified analyses

We evaluated AgeAccelGrim and underlying DNAm biomarkers in different strata characterized by age (younger/older than 65 years), body mass index (obese versus non-obese), educational attainment, prevalent condition at baseline such as prior history of cancer, type 2 diabetes, or hypertension. In all of these strata, AgeAccelGrim remains a significant predictor of time-to-death (Supplementary Table 7) and time-to-CHD (Supplementary Table 8). Furthermore, AgeAccelGrim outperforms existing DNAm-based biomarkers of aging in all strata except for one (comprised of n=281 individuals with a prior history of cancer).

These subgroup analysis results also confirm that epigenetic age acceleration is an independent predictor of earlier mortality even after adjusting for possible confounders and within major subgroups of the population. Additional results applied to age-adjusted DNAm proteins and DNAm pack-years are listed in Supplementary Data 1. With few exceptions, we found that DNAm-based PAI-1, TIMP-1 and pack-years remained highly significant in each stratum.

Exceptionally fast/slow agers

The DNAm GrimAge estimate allows an intuitive interpretation as physiological age since it is in units of years. However, if someone is 8 years older than expected, this does not mean that this person has on average a 8 year shorter life expectancy. Rather, one should use the hazard ratio when it comes to assessing mortality risks. It is a statistical co-incidence that the hazard ratio associated with one-year increase in AgeAccelGrim is the same in strata comprised of never-smokers (HR=1.10, Supplementary Fig. 3A), former/current smokers (HR=1.10, Supplementary Fig. 4A), and among all individuals combined (HR=1.10, Fig. 3A). This allows us to evaluate the mortality risks in exceptionally fast and slow agers (according to AgeAccelGrim) irrespective of their smoking status. The top 5th percentile and the 95% percentile of AgeAccelGrim corresponds to -7.5 years and + 8.3 years respectively (Supplementary Table 9). A person in the top 95th percentile of AgeAccelGrim (=8.3 years) faces a hazard of death that is twice that of the average person in their stratum (whose AgeAccelGrim equals 0). Specifically, fast aging status is associated with a hazard ratio of $HR=2.2=1.10^{8.3}$. Conversely, a slow ager in the bottom 5th percentile (-7.5 years) faces a hazard of death that is half that of the average person in their stratum, $HR=0.49=1.10^{-7.5}$.

DNAm GrimAge versus single stage estimators of mortality risk

DNAm GrimAge was built using a novel two-stage approach that critically depended on the development of DNAm-based surrogate biomarkers. To justify the

utility of this indirect approach, we compared DNAm GrimAge with several DNAm-based mortality risk predictors that were developed by directly regressing lifespan on DNAm data (referred to as single stage mortality predictors). To this end, we developed a new mortality predictor, DNAm Mortality (in year units) by directly regressing time-to-death (due to all-cause mortality) on CpGs in the FHS training data. DNAm Mortality was calculated as linear combination of 59 CpGs. The direct approach entailed the constructions of DNAm Mortality, an elastic net Cox regression model, and linear transformation of the mortality risk to ensure that the values of DNAm Mortality are in units of years (Methods). In addition, we also evaluated the published mortality predictor by Zhang [21] which, remarkably, is based on only 10 CpGs (Methods). The latter two (single-stage) lifespan predictors were found to correlate highly with each other ($r=0.77$ in the FHS test data).

The novel age-adjusted DNAm Mortality estimator ($HR=1.07$, $P=3.0E-44$) and both versions of Zhang's mortality risk estimator ($P=4.2E-39$, Supplementary Fig. 25) lead to a less significant meta-analysis P-value for lifespan prediction than AgeAccelGrim ($P=2.0E-75$). It is not meaningful to compare HR estimates (here $HR=1.02$ and $HR=1.10$, respectively) because these HR estimates critically depend on the scale/distribution of the respective mortality predictors. To provide a meaningful and scale-independent comparison, we focused on the meta-analysis P-values.

AgeAccelGrim also stands out in terms of its meta-analysis P-value for predicting time-to-CHD (AgeAccelGrim $P=6.2E-24$, AgeAccelMortality $P=4.6E-11$, AgeAccelZhang $P=9.5E-12$, Supplementary Fig. 26).

It is useful to characterize the different lifespan predictors in terms of their correlation with DNAm pack-years because smoking is a major risk factor. Age-adjusted DNAm pack-years exhibits positive correlations with both DNAm Mortality and Zhang's mortality predictor ($r \geq 0.55$). The connection of single stage mortality predictors to smoking can also be observed at the CpG level. DNAm Mortality, Zhang's mortality predictor, and DNAm pack-years explicitly use CpG cg05575921 (in the *AHRR* gene on chromosome 5p15.33), which has previously been identified by epigenome-wide association studies of cumulative smoking exposure [21, 29]. Overall, these results suggest that the two single-stage lifespan predictors relate more strongly to cumulative smoking exposure than does AgeAccelGrim.

Association with blood cell composition

DNAm data allow one to estimate several quantitative measures of blood cell types as described in Methods [30, 31]. We previously showed that DNAm biomarkers of aging, which capture age-related changes in blood cell composition, are better predictors of lifespan than those that are independent of blood cell counts [7]. Therefore, we hypothesized that several of our novel DNAm biomarkers would exhibit significant correlations with these imputed measures of blood cell composition. This is indeed the case as can be seen from our large scale meta-analysis across the validation data (Supplementary Fig. 27, Supplementary Data 2). AgeAccelGrim is significantly associated with a decrease in naive CD8 naïve cells ($r=-0.22$, $P=9.2E-62$, Supplementary Fig. 27A and Supplementary Data 2), CD4+T cells ($r=-0.21$, $P=1.8E-57$), and B cells ($r=-0.18$, $P=9.7E-43$) and with an increase in granulocytes/neutrophils ($r=0.24$, $P=1.5E-74$) and plasma blasts ($r=0.22$, $P=7.3E-63$). While these results demonstrate that AgeAccelGrim is associated with an age-related decline in immune system functioning, our cross sectional analysis does not allow us to dissect cause-and-effect relationships.

Age-adjusted DNAm TIMP-1 exhibits the most significant correlations with the measures of blood cell composition (e.g. proportion of granulocytes $r=0.36$, $P=2.7E-172$, Supplementary Fig. 27H and Supplementary Data 2) followed by age-adjusted DNAm Cystatin C (proportion of CD4+ T cells counts $r=-0.33$, $P=3.4E-142$). Although many of our DNAm biomarkers are correlated with blood cell counts, this does not mean that these measures *only* capture changes in blood cell composition as can be seen from the following. First, measures of blood cell composition correlate weakly with our age-adjusted DNAm surrogate markers of smoking pack-years (strongest correlation $r=-0.14$, Supplementary Fig. 27I) and PAI-1 levels (strongest correlation $r=0.17$, Supplementary Fig. 27G) even though both biomarkers are strongly associated with mortality risk and age-related conditions as shown above. Second, the DNAm surrogate markers remain significant predictors of mortality in multivariate Cox regression models that include blood cell counts as additional covariates as detailed in the following.

Cox models that include blood cell counts

Our multivariate Cox regression models demonstrate that AgeAccelGrim remains highly predictive of lifespan ($P=2.6E-53$) even after adjusting for seven co-variates that assess imputed blood cell counts (Supplementary Fig. 28A). Note that this p-value is only slightly lower than that obtained without adjustment for

blood cell counts (P=2.0E-75 in Fig. 3A). Further, AgeAccelGrim remains highly predictive for time-to-CHD (OR=1.07, P=1.1E-17 Supplementary Fig. 29A) even after adjusting for blood cell counts.

Similarly, our other DNAm biomarkers (such as DNAm PAI-1, DNAm PACKYRS) remain predictive of lifespan and time-to-CHD after adjusting for blood cell counts (Supplementary Figs. 28 B-I and 29 B-I). While this adjustment typically lowers statistical significance levels, there is one notable exception: DNAm leptin levels exhibits *more* significant P values after adjusting for blood cell counts (Supplementary Fig. 28 F versus Fig. 3F; Supplementary Fig. 29F versus Fig. 4F).

Association with leucocyte telomere length

Leukocyte telomere length (LTL) has been found to be weakly predictive of mortality and cardiovascular disease. Our meta-analysis reveals a statistically significant but weak negative correlation between LTL and AgeAccelGrim (r= -0.12 and meta P= 3.3E-10, Supplementary Table 10) across data from the FHS, WHI (BA23 sub-study) and JHS (total N =2,702, 27% White and 73% African American). Similarly, LTL exhibits (weak) negative correlations with DNAm based surrogate biomarkers for GDF-15 (r= -0.10, meta P= 3.4E-7), DNAm PAI-1 (r= -0.10, meta P= 5.1E-8) and DNAm smoking pack-years (r= -0.09 and meta P= 2.9E-6).

Functional annotation of sets of CpGs

The genomic locations of the 1030 CpGs underlying the DNAm GrimAge estimator were analyzed using the GREAT software tool [32] which assigns biological meaning to a set of genomic locations (here CpGs) by analyzing the annotations of nearby genes. At a false discovery rate of FDR < 0.05 we found 361 gene sets from GO, KEGG, PANTHER. Among those, 28 surpassed the more stringent Bonferroni correction including MHC class II receptor activity (nominal P=1.2E-6), cytokine-mediated signaling pathway (P=6.9E-5), response to interferon-gamma (P=1.5e-4), regulation of protein sumoylation (P=4.4E-5), endoderm formation (P=5.9E-5), epigenetic regulation of gene expression (P=6.7E-5), and fatty acid transmembrane transport (P=9.5E-5).

Similarly, we evaluated sets of CpGs underlying DNAm-based surrogate biomarkers. At FDR < 0.05, we found n=388, 307, and 153 significant gene sets for DNAm B2M, PAI-1, and Cystatin-C, respectively. Of those, the top gene sets are involved in immune function (nominal P=1.1E-9 for DNAm B2M CpGs), adipo-

cytokine signaling pathway (P =3.6E-7 for DNAm PAI-1 CpGs) or lipid function (P =3.8E-7 for DNAm PAI-1 CpGs). The significant gene sets for all DNAm surrogate biomarkers can be found in Supplementary Data 3.

Diet, education, and life style factors

Several previous measures of epigenetic age acceleration in blood have been shown to exhibit statistically significant but weak correlations with lifestyle factors and biomarkers of metabolic syndrome [22, 33]. Here we revisited these cross-sectional studies in the WHI (comprising approximately 4000 post-menopausal women, Methods) with our novel measures of AgeAccelGrim and its underlying DNAm-based surrogate biomarkers (Fig. 6).

All (age-adjusted) DNAm-based biomarkers correlate with plasma biomarkers measuring vegetable consumption, but AgeAccelGrim (robust correlation coefficient r=-0.26, P=9E-39, Fig. 6) and DNAm PAI-1 (r=-0.25, P=7E-36) stand out in terms of their strong relationship with mean carotenoid levels (Fig. 6, Supplementary Fig. 30). Far less significant associations could be observed for self-reported measures of fruit, vegetable, and dairy intake, which highlights the limitations of self-reported measures of dietary intake.

The following novel results could not be observed with previous DNAm-based biomarkers of aging: (self-reported) proportion of carbohydrate consumption was associated with lower AgeAccelGrim (robust correlation r=-0.12, P=4E-13) and DNAm PAI-1 (r=-0.15, P=3E-20). Conversely, an increased proportion of fat intake (but not protein intake) was associated with increased AgeAccelGrim (r=0.09, P=2E-8) and DNAm PAI-1 (r=0.13, P=1E-14). Measures of lipid metabolism, triglyceride levels and HDL cholesterol levels, were significantly correlated with AgeAccelGrim (r=0.11 and r=-0.10, respectively) and even more so with (age adjusted) DNAm PAI-1 levels (r=0.34 and r=-0.11). Similarly, measures of glucose metabolism, insulin- and glucose levels, exhibited positive correlations with AgeAccelGrim (r=0.16 and r=0.12, respectively) and with (age adjusted) DNAm PAI-1 levels (r=0.30 and r=0.22).

Similar to what we observed with previous DNAm based biomarkers of aging, plasma C-reactive protein levels exhibited comparatively strong positive correlations with DNAm-based biomarkers, particularly AgeAccelGrim (r=0.28, P=2E-52), DNAm TIMP-1 (r=0.27, P=2E-49), and DNAm PAI-1 (r=0.26, P=1E-46).

Category	Variable	n	AgeAccelGrim bicor	AgeAccelGrim p	adj.DNAm GDF-15 bicor	p	adj.DNAm B2M bicor	p	adj.DNAm Cystatin C bicor	p	adj.DNAm TIMP-1 bicor	p	adj.DNAm ADM bicor	p	adj.DNAm PAI-1 bicor	p	adj.DNAm Leptin bicor	p	adj.DNAm PACKYRS bicor	p
Diet	log2(Total energy)	3700	-0.02	0.15	-0.02	0.27	-0.03	0.06	-0.04	0.02	-0.02	0.35	0.01	0.69	0.03	0.05	0.01	0.55	-0.05	3E-3
Diet	Carbohydrate	3700	-0.12	4E-13	-0.03	0.07	-0.01	0.38	0.02	0.26	-0.03	0.12	-0.06	5E-4	-0.15	3E-20	-0.09	3E-8	-0.08	2E-6
Diet	Protein	3700	-0.01	0.39	0.00	0.96	0.00	0.91	0.00	0.85	0.01	0.63	0.02	0.22	0.02	0.34	0.02	0.30	-0.02	0.21
Diet	Fat	3700	0.09	2E-8	0.02	0.18	0.03	0.05	-0.02	0.16	0.03	0.08	0.03	0.08	0.13	1E-14	0.10	2E-9	0.05	0.01
Diet	log2(1+Red meat)	3700	0.06	3E-4	0.01	0.46	0.02	0.28	-0.02	0.20	0.03	0.07	0.05	4E-3	0.12	6E-13	0.07	1E-5	0.00	0.92
Diet	log2(1+Poultry)	3700	0.03	0.08	0.04	0.02	-0.03	0.09	-0.01	0.79	0.01	0.48	-0.01	0.41	-0.01	0.54	0.00	0.89	0.05	3E-3
Diet	log2(1+Fish)	3700	0.00	0.87	-0.02	0.13	-0.03	0.05	-0.05	4E-3	0.01	0.64	-0.03	0.11	0.01	0.47	0.01	0.69	0.01	0.42
Diet	log2(1+Dairy)	3700	-0.09	1E-7	-0.06	2E-4	-0.04	0.02	-0.06	5E-4	-0.05	2E-3	0.02	0.34	-0.01	0.46	0.00	0.86	-0.11	6E-11
Diet	log2(1+Whole grains)	3700	-0.07	2E-5	-0.03	0.12	-0.03	0.07	-0.03	0.05	-0.05	0.10	-0.03	0.05	-0.04	0.03	-0.01	0.54	-0.06	5E-4
Diet	log2(1+Nuts)	3700	-0.02	0.15	-0.05	3E-3	-0.03	0.07	-0.09	7E-8	-0.03	0.19	-0.01	0.38	-0.01	0.75	0.02	0.29	-0.02	0.13
Diet	log2(Fruits)	3700	-0.10	1E-10	-0.03	0.05	-0.04	0.02	-0.01	0.51	-0.03	0.04	-0.03	0.06	-0.04	0.01	-0.04	0.01	-0.09	5E-9
Diet	log2(Vegetables)	3700	-0.08	7E-7	-0.06	1E-4	-0.03	0.04	-0.07	4E-5	-0.04	0.03	-0.02	0.14	-0.03	0.10	0.00	0.84	-0.06	3E-4
Dietary biomarkers	Retinol	2267	-0.01	0.49	-0.02	0.37	0.00	0.95	-0.05	0.01	-0.03	0.17	0.04	0.04	0.17	9E-17	0.00	0.94	-0.02	0.27
Dietary biomarkers	Mean carotenoids	2266	-0.26	9E-39	-0.13	1E-10	-0.18	3E-19	-0.16	9E-15	-0.22	4E-28	-0.19	3E-21	-0.25	7E-36	-0.15	3E-14	-0.13	7E-11
Dietary biomarkers	Lycopene	2267	-0.07	6E-4	-0.06	0.01	-0.11	8E-8	-0.04	0.07	-0.13	1E-10	-0.06	2E-3	-0.08	2E-4	-0.04	0.03	-0.03	0.21
Dietary biomarkers	log2(alpha-Carotene)	2267	-0.28	4E-44	-0.13	3E-10	-0.15	8E-14	-0.16	1E-14	-0.21	2E-26	-0.15	4E-13	-0.25	3E-34	-0.15	1E-13	-0.18	2E-18
Dietary biomarkers	log2(beta-Carotene)	2266	-0.22	5E-28	-0.10	3E-6	-0.12	6E-9	-0.14	3E-12	-0.17	8E-18	-0.18	1E-18	-0.24	4E-33	-0.13	4E-10	-0.09	4E-6
Dietary biomarkers	log2(Lutein+Zeaxanthin)	2267	-0.14	9E-12	-0.10	6E-7	-0.15	4E-14	-0.13	6E-10	-0.17	3E-16	-0.16	2E-15	-0.16	8E-16	-0.11	2E-7	-0.02	0.30
Dietary biomarkers	log2(beta-Cryptoxanthin)	2267	-0.22	2E-26	-0.08	3E-5	-0.12	2E-8	-0.08	7E-5	-0.11	2E-7	-0.14	1E-11	-0.18	3E-18	-0.13	3E-10	-0.11	3E-8
Dietary biomarkers	log2(alpha-Tocopherol)	2267	-0.06	3E-3	-0.01	0.65	0.01	0.53	-0.07	1E-3	0.01	0.76	0.03	0.21	0.10	9E-7	-0.02	0.30	-0.03	0.11
Dietary biomarkers	log2(gamma-Tocopherol)	2267	0.14	2E-11	0.02	0.25	0.00	0.98	0.08	4E-5	0.02	0.25	0.04	0.03	0.14	4E-12	0.09	2E-5	0.05	0.02
Measurements	log2(C-reactive protein)	2809	0.28	2E-52	0.11	2E-9	0.14	1E-13	0.17	6E-20	0.27	2E-49	0.17	7E-20	0.26	1E-46	0.12	2E-10	0.14	6E-14
Measurements	log2(Insulin)	4042	0.16	2E-26	0.07	2E-5	0.12	6E-15	0.17	7E-10	0.17	8E-30	0.13	4E-16	0.30	1E-87	0.15	7E-22	0.04	0.01
Measurements	log2(Glucose)	4144	0.12	2E-14	0.02	0.12	0.03	0.02	0.07	9E-6	0.06	2E-5	0.07	3E-6	0.22	1E-46	0.09	1E-9	0.06	6E-5
Measurements	log2(Triglyceride)	4148	0.11	5E-13	0.02	0.10	0.07	6E-6	0.02	0.10	0.06	1E-4	0.17	4E-30	0.34	1E-116	0.11	8E-13	-0.03	0.07
Measurements	Total cholesterol	4148	0.01	0.65	0.01	0.69	-0.10	7E-12	0.06	1E-4	-0.10	2E-11	-0.02	0.15	-0.01	0.56	-0.05	2E-3	0.07	2E-6
Measurements	LDL cholesterol	4084	0.00	0.83	0.03	0.03	-0.12	4E-14	0.13	1E-16	-0.13	4E-16	-0.06	7E-5	-0.10	1E-11	-0.08	6E-8	0.12	1E-14
Measurements	HDL cholesterol	4145	-0.10	1E-10	-0.08	3E-7	-0.05	3E-3	-0.21	1E-42	-0.01	0.43	-0.08	1E-7	-0.11	6E-13	-0.03	0.07	-0.08	8E-8
Measurements	log2(Creatinine)	2748	0.03	0.07	0.04	0.04	0.03	0.10	0.03	0.15	0.04	0.02	-0.01	0.64	-0.06	3E-3	0.02	0.32	0.04	0.02
Measurements	Systolic blood pressure	4177	0.07	9E-7	0.01	0.51	0.03	0.03	0.09	1E-8	0.06	2E-4	0.05	1E-3	0.07	1E-6	0.02	0.17	0.05	1E-3
Measurements	Diastolic blood pressure	4178	-0.01	0.36	-0.04	0.01	-0.02	0.14	0.07	2E-5	-0.03	0.10	-0.03	0.03	-0.01	0.55	-0.04	0.02	0.00	0.88
Measurements	BMI	4145	0.14	1E-20	0.05	7E-4	0.08	5E-8	0.11	9E-14	0.17	1E-28	0.12	1E-14	0.22	5E-50	0.13	1E-18	0.04	0.01
Measurements	log2(Waist / hip ratio)	4037	0.19	4E-34	0.10	3E-11	0.09	2E-9	0.11	4E-12	0.12	8E-16	0.12	3E-15	0.23	1E-50	0.12	6E-14	0.12	4E-14
Life style	Education	4143	-0.09	2E-9	-0.09	7E-10	-0.05	8E-4	-0.11	4E-13	-0.03	0.02	-0.05	1E-3	-0.03	0.10	-0.01	0.42	-0.07	1E-6
Life style	Income	4054	-0.07	2E-6	-0.08	1E-7	-0.03	0.07	-0.14	3E-19	-0.04	0.02	-0.04	0.01	-0.02	0.31	-0.02	0.22	-0.07	1E-5
Life style	log2(1+Exercise)	3914	-0.10	3E-10	-0.05	6E-4	0.06		-0.06	5E-5	-0.06	6E-5	-0.05	7E-4	-0.08	1E-7	-0.06	4E-4	-0.05	3E-3
Life style	Current smoker	2321	0.44	5E-113	0.19	1E-21	-0.01	0.67	0.12	2E-9	0.01	0.50	0.05	0.05	0.01	0.59	0.00	0.87	0.52	1E-164
Life style	log2(1+Alcohol)	3700	-0.04	0.02	-0.04	0.02	-0.06	6E-4	-0.04	0.01	-0.03	0.06	-0.02	0.35	-0.01	0.49	-0.01	0.44	-0.02	0.26

Figure 6. Cross sectional correlations between DNAm biomarkers and lifestyle factors. Robust correlation coefficients (biweight midcorrelation [62]) between 1) AgeAccelGrim and its eight age-adjusted underlying DNAm-based surrogate biomarkers and 2) 38 variables including self-reported diet, 9 dietary biomarkers, 12 variables related to metabolic traits and central adiposity, and 5 life style factors. The 2-color scale (blue to red) color-codes bicor correlation coefficients in the range [-1, 1]. The green color scale (light to dark) applied to unadjusted P values. The analysis was performed on the WHI cohort in up to 4200 postmenopausal women. An analogous analysis stratified by race/ethnicity can be found in Supplementary Fig 30.

Measures of adiposity, BMI and waist-to-hip ratio, are associated with increased AgeAccelGrim, age-adjusted DNAm PAI-1, and other DNAm-based surrogate biomarkers. Higher education and income are associated with lower AgeAccelGrim (P=2E-9 and P=2E-6). AgeAccelGrim stands out when it comes to detecting a beneficial effect of physical exercise (r=-0.10, P=3E-10).

Several of our results in the WHI could be replicated in a smaller dataset (N< 625 individuals from the FHS test data) that included lipid and metabolic biomarker data (Supplementary Fig. 31). In the FHS, hemoglobin A1C and albumin levels (in urine) exhibited significant positive correlations with AgeAccelGrim, age-adjusted DNAm PAI-1 ($0.10 \leq r \leq 0.12$ and $1.4E-7 \leq P \leq 2.3E-3$),

and to a lesser extent with our other DNAm based surrogate biomarkers (Supplementary Fig. 31).

Omega-3 polyunsaturated fatty acid supplementation

Omega-3 polyunsaturated fatty acid (PUFAs) supplementation is increasingly used for protection against cardiovascular disease. However, omega-3 PUFA supplementation was not found to be associated with a lower risk of cardiac death, sudden death, myocardial infarction, stroke, or all-cause mortality, [34-36]. We studied the association between self-reported omega-3 intake and AgeAccelGrim in n=2,174 participants of the FHS and found that omega-3 acids intake was negatively correlated with AgeAccelGrim (robust correlation r=-0.10, P=4.6E-7, linear mixed effects P=1.3E-5, Supplementary Table 11). The effect of omega 3 supplementation is more pronounced in males (r=-0.08, P=0.012) than in females (r=-0.05, P=0.07).

A multivariate linear mixed model analysis revealed an association between AgeAgelGrim and omega-3 acid levels (linear mixed effects P=0.017) after adjusting for gender, educational levels, data status (an indicator of training data), and smoking pack-year.

Computed tomography measures of fatty organs

Computed tomography (CT) imaging techniques provide "shadow images of fat" that can be used for the indirect quantification of organ quality (e.g. liver). Radiographic pixels measure the density of an organ (referred to as attenuation) in Hounsfield units (HU). CT scans are used for diagnosing fatty liver disease: a low density/attenuation value (low HU) is associated with *high* fat content in the liver.

We analyzed CT scan data from liver, spleen, paraspinal muscle, visceral adipose tissue (VAT), and sub-cutaneous adipose tissue (SAT) from the Framingham Heart Study cohort [37, 38] (Methods).

As expected, BMI exhibited strong positive correlations with volumetric measures of SAT (r=0.82, Fig. 7) and VAT (r=0.69). Further, we observed strong negative correlations between body mass index and density (attenuation) values in liver (r=-0.55, p=1E-101, Fig. 7), spleen (r=-0.62,P=3E-157), paraspinal muscle (r=-0.34, P=7E-42), subcutaneous adipose tissue (SAT, r=-0.42, P=2E-49), and visceral adipose tissue (VAT, r=-0.60, P=1E-126). With the exception of muscle, CT values exhibit only weak correlations with chronological age in this cohort comprised of older individuals (Supplementary Fig. 32). We previously found that body

mass index is strongly correlated (r=0.42) with epigenetic age acceleration in human liver but exhibits only weak correlations with epigenetic age acceleration in blood (r around 0.10) [39].

Compared to previous epigenetic biomarkers of aging (Supplementary Fig. 33), AgeAccelGrim and DNAm PAI-1 stand out in terms of their strong correlations with CT-derived measures of adiposity (Fig. 7): AgeAccelGrim is negatively correlated with liver density (bicor= -0.24, P=1.79E-10) and positively correlated with VAT volume (bicor=0.23, P=1.77E-12) in both sexes.

Most of our DNAm-based surrogate biomarkers of proteins are significantly associated with CT measures of adiposity (Fig. 7) except for our DNAm-based surrogate biomarkers of B2M and smoking pack-years (which exhibit non-significant correlations after adjusting for multiple comparisons).

The strong marginal correlations between AgeAccelGrim and CT measures beg the question whether they reflect confounding by BMI or sex. This is not the case as can be seen from a multivariate regression model that regressed AgeAccelGrim (dependent variable) on BMI, sex, and several CT derived measures of organ density and fat volume. Even after adjusting for potential confounders, AgeAccelGrim exhibits a significant association with liver density (P=6.86E-4) (Model I in Supplementary Table 12 and Methods). Interestingly, BMI is no longer associated with AgeAccelGrim after adjusting the analysis for liver density or VAT volume (Supplementary Table 12) which suggests that liver density mediates the relationship between BMI and AgeAccelGrim.

A multivariate model analysis reveals that AgeAccelGrim is more strongly associated with VAT volume (P= 5.54E-4) than with SAT volume (Model II in Supplementary Table 12) which supports the widely held view that VAT is more dangerous than SAT.

A comprehensive multivariate model that includes both organ density measures and volumetric measures of SAT/VAT reveals that liver density (P=7.32E-3) exhibits the most significant association with AgeAccelGrim (Model III in Supplementary Table 12).

Age-adjusted DNAm-based surrogate markers of PAI-1, ADM, TIMP-1, and leptin also exhibit significant correlation with the CT measures (Fig. 7). The finding associated with age-adjusted DNAm leptin echoes the earlier significant association between immunoassay based leptin with SAT and VAT variables [37].

		N	BMI bicor	P	AgeAccelGrim bicor	P	adj.DNAm ADM bicor	P	adj.DNAm B2M bicor	P	adj.DNAm Cystatin C bicor	P	adj.DNAm GDF-15 bicor	P	adj.DNAm Leptin bicor	P	adj.DNAm PAI-1 bicor	P	adj.DNAm TIMP-1 bicor	P
All	LIVER	1177	-0.55	1.0E-101	-0.24	1.8E-10	-0.21	1.2E-10	-0.06	3.3E-01	-0.11	9.6E-04	-0.12	2.2E-02	-0.28	1.1E-14	-0.41	2.9E-37	-0.17	1.7E-06
	SPLEEN	1055	-0.62	3.1E-157	-0.19	2.4E-09	-0.17	1.4E-09	-0.03	2.0E-01	-0.09	1.1E-03	-0.09	6.5E-03	-0.18	1.2E-04	-0.23	1.9E-15	-0.08	5.9E-04
	MUSCLE	1172	-0.34	7.3E-42	-0.18	6.6E-07	-0.14	1.6E-08	-0.07	2.2E-02	-0.11	3.2E-04	-0.10	1.0E-05	-0.13	1.4E-04	-0.19	4.4E-09	-0.13	1.5E-04
	SAT (CM^3)	1160	0.82	<1.0E-280	0.18	8.2E-10	0.21	5.9E-17	0.06	1.6E-03	0.11	7.1E-09	0.07	3.2E-02	0.29	1.0E-21	0.28	6.1E-25	0.17	3.2E-08
	SAT	1160	-0.42	2.1E-49	-0.09	8.4E-03	-0.10	3.9E-02	-0.02	2.7E-01	-0.07	3.5E-02	-0.04	7.0E-01	-0.14	3.9E-04	-0.15	6.5E-08	-0.10	2.0E-02
	VAT (CM^3)	1171	0.69	3.0E-195	0.23	1.8E-12	0.21	7.5E-17	0.04	1.4E-01	0.13	5.2E-06	0.09	1.1E-03	0.30	1.8E-11	0.42	1.5E-41	0.18	1.4E-08
	VAT	1171	-0.60	1.0E-126	-0.17	4.9E-08	-0.16	5.0E-08	-0.02	3.8E-01	-0.05	2.0E-05	-0.05	1.8E-01	-0.26	4.9E-09	-0.37	2.4E-34	-0.16	8.1E-06
Male	LIVER	519	-0.50	9.8E-28	-0.22	1.5E-03	-0.14	8.1E-03	-0.02	6.3E-01	-0.06	3.3E-01	-0.11	1.4E-01	-0.26	1.7E-07	-0.39	2.1E-10	-0.13	1.7E-02
	SPLEEN	446	-0.50	4.9E-29	-0.17	6.2E-04	-0.11	9.2E-03	-0.03	3.3E-01	-0.07	2.4E-01	-0.05	2.0E-01	-0.06	2.0E-01	-0.10	6.7E-02	-0.08	2.9E-02
	MUSCLE	516	-0.27	3.5E-14	-0.16	4.6E-03	-0.09	6.9E-03	-0.04	4.7E-01	-0.05	4.8E-01	-0.08	1.1E-03	-0.05	1.0E-01	-0.09	4.2E-01	-0.15	1.6E-02
	SAT (CM^3)	508	0.75	3.5E-59	0.14	8.7E-04	0.15	1.1E-04	0.02	1.1E-01	0.08	5.4E-04	0.05	2.7E-01	0.24	4.3E-08	0.20	2.9E-06	0.17	2.2E-04
	SAT	508	-0.43	2.8E-18	-0.08	1.0E-01	-0.10	2.5E-01	-0.02	3.4E-01	-0.10	2.2E-02	-0.06	9.1E-01	-0.11	3.0E-02	-0.10	1.9E-04	-0.13	4.7E-02
	VAT (CM^3)	515	0.65	3.0E-42	0.21	5.7E-05	0.16	6.4E-04	0.03	5.7E-01	0.10	3.6E-02	0.09	1.0E-01	0.25	1.5E-05	0.35	1.3E-10	0.19	1.5E-04
	VAT	515	-0.55	8.6E-30	-0.15	2.9E-03	-0.11	5.0E-02	-0.03	4.7E-01	-0.13	8.5E-03	-0.04	8.2E-01	-0.21	2.0E-03	-0.31	5.4E-10	-0.17	3.4E-03
Female	LIVER	658	-0.59	1.6E-44	-0.26	6.3E-08	-0.27	3.2E-09	-0.09	3.7E-01	-0.16	5.0E-04	-0.14	7.3E-02	-0.29	1.1E-08	-0.42	9.2E-23	-0.20	2.5E-05
	SPLEEN	609	-0.69	2.4E-61	-0.20	2.3E-06	-0.22	3.6E-08	-0.02	4.1E-01	-0.10	9.1E-04	-0.12	1.5E-02	-0.26	5.1E-07	-0.33	1.1E-14	-0.09	8.9E-03
	MUSCLE	656	-0.39	3.7E-23	-0.20	6.1E-05	-0.18	7.1E-07	-0.09	1.2E-02	-0.16	4.3E-05	-0.11	4.0E-03	-0.19	5.0E-06	-0.27	2.2E-10	-0.13	4.0E-03
	SAT (CM^3)	652	0.86	2.9E-115	0.21	5.8E-07	0.25	2.2E-12	0.09	6.8E-03	0.14	6.3E-06	0.07	5.9E-02	0.34	2.4E-14	0.35	2.8E-17	0.16	5.7E-05
	SAT	652	-0.40	7.7E-24	-0.10	4.1E-02	-0.09	8.4E-02	-0.03	5.6E-01	-0.04	6.4E-02	-0.03	6.2E-01	-0.17	1.4E-03	-0.19	1.2E-04	-0.08	2.0E-01
	VAT (CM^3)	656	0.72	2.0E-70	0.24	1.2E-08	0.25	5.8E-11	0.05	8.4E-02	0.15	9.9E-06	0.10	3.5E-04	0.33	7.9E-10	0.47	1.4E-26	0.18	3.0E-05
	VAT	656	-0.64	4.0E-53	-0.19	8.2E-06	-0.21	1.5E-07	-0.01	6.1E-01	-0.12	1.0E-03	-0.06	7.0E-02	-0.29	1.1E-08	-0.42	5.4E-21	-0.15	9.9E-04

Figure 7. Computed tomography variables versus with body mass index and age-adjusted DNAm biomarkers in the FHS. The columns correspond to BMI, AgeAccelGrim and age-adjusted DNAm surrogates of plasma proteins. The rows correspond to computed tomography-derived organ density measures (Hounsfield units) or volumetric measures for subcutaneous adipose tissue (SAT CM3) or visceral adipose tissue (VAT CM3). The columns report the available sample size (n) in the FHS, the robust correlation coefficient (bicor, based on the biweight midcorrelation coefficient [62]). To avoid confounding by pedigree structure, we computed the p-value using a linear mixed effect model (pedigree as random effect). The bicor correlation coefficients are color-coded (blue to red) across its range of [-1, 1]. P-values are color-coded in green (light to dark green scale). We applied the correlation analysis to males and females, respectively, and then combined the results via fixed effect models weighted by inverse variance (listed in the top rows, denoted as "ALL").

Age adjusted DNAm PAI-1 exhibits the strongest associations with CT-based measures of adiposity: it is strongly and positively correlated with VAT volume (r=0.42, P=1.5E-41, Figu 7), SAT volume (r=0.28) and negatively correlated with liver density (r=-0.41, P=2.9E-37), VAT density (r=-0.37), and spleen density (r=-0.23). A multivariate regression analysis of age-adjusted PAI-1 (dependent variable) reveals highly significant associations with liver density (P=3.17E-14 in Model I) and VAT volume (P=4.22E-13, Model II in Supplementary Table 13) even after adjusting for BMI and other confounders. Including all CT variables as covariates in a multivariate model reveals significant associations with both liver density (P=3.16E-8) and VAT volume (P=1.38E-7, Model III in Supplementary Table 13).

Overall, these results suggest that fatty liver and excess VAT are the most significant CT-based measures of (age-adjusted) DNAm PAI-1 and DNAm Grim.

DISCUSSION

Several articles have previously described DNAm-based biomarkers for measuring tissue age and for predicting lifespan [10, 40]. This work shows that DNAm GrimAge, which is as a linear combination of chronological age, sex, and DNAm-based surrogate biomarkers for seven plasma proteins and smoking pack-years, outperforms all other DNAm-based biomarkers, on a variety of health-related metrics. An age-adjusted version of DNAm GrimAge, which can be regarded as a new measure of epigenetic age acceleration (AgeAccelGrim), is associated with a host of age-related conditions, lifestyle factors, and clinical biomarkers. Using large scale validation data from three ethnic groups, we demonstrate that AgeAccelGrim stands out among pre-existing epigenetic clocks in terms of its predictive ability for time-to-death, time-to-coronary heart disease, time-to-cancer, its association with computed tomography data for fatty liver/excess fat, and early age at menopause.

Our DNAm-based surrogate biomarker of smoking might complement self-reported assessments of pack-years. The surprising finding that DNAm pack-years outperforms self-reported pack-years in predicting lifespan could reflect a) erroneous self-reporting or b) the fact that DNAm pack-years captures intrinsic variation across individuals with lasting biological damage that results from smoking, i.e., inter-individual sensitivities to smoking.

Markers of inflammation and metabolic conditions are associated with several epigenetic biomarkers including AgeAccelGrim, age-adjusted DNAm TIMP-1, and DNAm PAI-1. However, DNAm PAI-1 stands out when it comes to associations with type 2 diabetes status, glucose-, insulin-, triglyceride levels, anthropometric measures of adiposity (body mass index and waist-to-hip ratio), and computed tomography data on fatty liver and excess adipose tissue.

Our DNAm-based surrogate biomarkers of plasma protein levels may be leveraged by researchers who rely on bio-banked DNA samples without the availability of plasma samples. Strong evidence supports links between plasma proteins used in the construction of GrimAge and various age-related conditions: ADM levels are increased in individuals with hypertension and heart failure [41]. Plasma B2M is a clinical biomarker associated with cardiovascular disease, kidney function, and inflammation [42]. Plasma cystatin-C is used to assess kidney function [43]. ADM, B2M, cystatin C, and leptin relate to many age-related traits including cognitive functioning [44-46]. GDF-15 is involved in age-related mitochondrial dysfunction [46]. PAI-1 plays a central role in a number of age-related subclinical and clinical conditions[47], and recent genetic studies link PAI-1 to lifespan [48]. The tissue inhibitor of metalloproteinases, TIMP-1, plays an anti-apoptotic function [49]. We acknowledge the following limitations. The levels of relatively few plasma proteins (12 out of 88) were accurately imputed based on DNAm levels in blood. In the FHS data, the measurement of the plasma proteins (exam 7) preceded the measurement of blood DNAm data (exam 8) by 6.6 years, suggesting that the DNAm profiles may not represent a highly accurate snapshot of the status of these proteins at the time of blood collection. That said, the elucidation of cause-and-effect relationships between plasma proteins and DNAm will require future longitudinal cohort studies and mechanistic evaluations. Despite their obvious strengths, DNAm-based bio-markers are unlikely to replace existing clinical bio-markers such as blood glucose or blood pressure measurements in medical practice. Rather, these epigenetic biomarkers are expected to complement existing clinical biomarkers when evaluating the

individual's 'aging' status. Since DNAm captures important properties of the DNA molecule, these DNAm biomarkers are proximal to innate aging processes [10].

Beyond lifespan prediction, AgeAccelGrim (and several of its underlying surrogate biomarkers including DNAm PAI-1) relate to many age-related conditions (multi-morbidity, metabolic syndrome, markers of inflammation) in the expected way, i.e. high values are associated with a bad risk profile.

In general, epigenetic aging is distinct from senescence-mediated aging and is not prevented by telomerase expression [50-52]. In spite of this, we do find that higher values of AgeAccelGrim (and several DNAm-based surrogate markers) are associated with shorter telomere length and an imputed blood cell composition that is indicative of immunosenescence.

Overall, we expect that these DNAm-based biomarkers will find useful applications in numerous human studies, especially those of anti-aging interventions.

METHODS

Study cohort

To establish DNAm based estimators and DNAm GrimAge, we used 2,356 individuals composed of 888 pedigrees from the FHS cohort [25], a large-scale longitudinal study started in 1948, initially investigating risk factors for cardiovascular disease (CVD). The FHS cohort contains medical history and measurements, immunoassays at exam 7, and blood DNA methylation profiling at exam 8. The technology of immunoassay was based on Luminex xMAP assay, an extension of the enzyme-linked immunosorbent assay (ELISA) performed with multiple analyte-specific capture antibodies bound to a set of fluorescent beads. The DNA methylation profiling was based on the Illumina Infinium HumanMethylation450K BeadChip.

We assigned 70% pedigrees (1731 individuals/622 pedigrees) to the training process and the remaining 30% of pedigrees (625 individuals/266 pedigrees) to the FHS test data (Supplementary Table 1). The training dataset was used to build the DNAm based surrogate markers for plasma proteins, smoking pack-years, and the composite biomarker DNAm GrimAge.

Validation data from 5 cohorts

Our validation analyses involved 7,375 Illumina arrays measuring blood methylation levels in N=6,935 individuals from five independent cohorts: the FHS test

dataset (N=625), WHI BA23 (N=2107), WHI EMPC study (N=1972), JHS (N=1747), and InChianti (N=924 from 1 to 2 longitudinal measures on 484 individuals, Table 2 and Supplementary Note 1). All the statistical analyses were adjusted for the correlation structure due to pedigree effects or repeated measurements as described below.

Estimation of surrogate DNAm based biomarkers

We developed estimators for plasma proteins based on blood methylation data. We leveraged immunoassay measurements in the FHS which profiled 88 plasma protein biomarkers (in units of pg/mL), including cardiovascular disease related plasma proteins such as C-reactive protein [53] and growth differentiation factor 15 (GDF-15) [54]. For each protein marker, missing values were imputed by the respective median value. The median missing rate was < 0.3%. Next the resulting observed plasma levels were regressed on DNAm data in the FHS training data.

Each plasma protein was regressed on the CpGs using the elastic net regression model implemented in the R package *glmnet*. Ten-fold cross validation was performed in the FHS training data to specify the underlying tuning parameter λ. The selection of CpGs by the penalized regression model is not robust. Similar estimator could be built using different sets of CpGs.

We required the predicted variable associated with the target variable with >0.35 correlation in both training and test datasets. Only 12 out of 88 proteins exhibited a correlation greater than 0.35 between observed plasma levels and their respective DNAm based estimators in the FHS test data (Table 1). The missing rates of the 12 ImmunoAssay proteins were less than 0.7%. The correlation estimates have a distribution of 0.64±0.12 [0.43, 0.86] (mean±SD [range]) in the training dataset and a distribution of 0.43±0.09 [0.35, 0.66] in the test dataset.

DNA methylation data

Our study involved DNA methylation data generated on two different Illumina array platforms: Illumina Inf 450K array and the Illumina EPIC array. Our analysis focused on the subset of 450,161 CpGs that were present on both platforms. We used meta analysis techniques to combine the results from the difference cohorts since the respective methylation data were normalized using different methods, e.g. the WHI BA23 were normalized using the background correction method implemented in GenomeStudio. By contrast, the JHS data were normalized using the "noob" normalization method implemented in the *minfi* R package

[55, 56]. We kept the original normalization methods to ensure consistency with previous publications.

Smoking Pack-Years

The variable "smoking pack-years" attempts to measure the cumulative amount of cigarettes consumed by the smoker. It is calculated by the number of packs of cigarettes smoked per day multiplied by the number of years the person smoked. We computed smoking pack-years using the information up to exam 8 in the FHS cohort.

Definition of DNAm GrimAge

We again used an elastic net Cox regression model[26] to regress time-to-death (due to all-cause mortality) since exam 7 on the 12 DNAm based surrogate markers for plasma proteins and on DNAm PACKYR, chronological age, and sex. As part of stage 2, we validated the accuracy of the DNAm based surrogate markers for their observed counterparts in the FHS test dataset. However, mortality predictor (DNAmGrimAge) was only fit in the FHS training dataset (N=1731). In the training dataset, we performed 10-fold cross validation to specify the value of the tuning parameter λ. A completely unbiased evaluation of DNAm GrimAge is achieved in the validation data sets (WHI, JHS, and InChianti).

Calibration of DNAm GrimAge into units of years

The final elastic net Cox model listed in Supplementary Table 2 results in an uncalibrated DNAm GrimAge estimate, which can be interpreted as the linear combination of the covariates, $X^T \beta$, or alternatively as the logarithm of the hazard ratio,

$$\log[h(t)/h_0(t)] = X^T \beta,$$

where $h_0(t)$ is the baseline hazard at time. The linear combination, $X^T \beta$, can be interpreted as an un-calibrated version of DNAm GrimAge. To facilitate an intuitive interpretation as a physiological age estimator, we linearly transformed it so that the resulting estimate would be in units of years. Toward this end, we imposed the following requirement:

the mean and variance of the resulting value, DNAm GrimAge, should be the same as the mean and variance of the age variable in the FHS training data (exam 7).

This resulted in the following transformation

DNAm GrimAge $= -50.28483 + 8.3268 * X^T \beta$.

Observed GrimAge

While our DNAm GrimAge was defined with respect to DNAm based surrogate biomarkers, our *observed* Grim

Age estimators is *not* based on DNA methylation levels. Rather, it is based on observed plasma protein levels, self-report pack-years, age, and gender. Observed GrimAge was built by fitted a Cox regression model using the observed variables in the same FHS training data that were used for building the DNAm GrimAge estimator. We computed a corresponding measure of age acceleration, called *observed* AgeAccelGrim, by adjusting observed GrimAge for chronological age (defined as raw residual resulting from regressing observed GrimAge on chronological age).

Statistical models used in validation analysis

Validation analysis was performed on 7,735 observations across 6,395 individuals (Table 2 and Supplementary Note 1) coming from five datasets: the FHS test dataset (N=625), WHI BA23 (N=2107), WHI EMPC (N=1972), Jackson Heart Study (JHS, N=1747), and InChianti study (N=924 from 1 to 2 longitudinal measures on 484 individuals, Table 2 and Supplementary Note 1). Our validation analysis involved i) Cox regression for time to death, for time-to-CHD, and for time to coronary heart failure, ii) linear regression for our DNAm based measures (independent variable) associated with and number of age-related conditions (dependent variable) and physical function score, respectively, iii) linear regression for age at menopause (independent variable) associated with our DNAm measure, iv) logistic regression analysis for estimating the odds ratios of our DNAm based measure associated with any cancer, hypertension, type 2 diabetes, emphy-

sema, and disease free status. The variable of "number of age-related conditions" includes arthritis, cataract, cancer, CHD, CHF, emphysema, glaucoma, lipid condition, osteoporosis, type 2 diabetes, etc. (see Supplementary Note 1). In our validation analysis, we used AgeAccelGrim (the age-adjusted measure of DNAm GrimAge), and used the scaled measures of seven DNAm surrogates for plasma proteins based on the mean and standard deviation (SD) of the FHS training dataset such that the effect size was approximately corresponding to one SD. All the models were adjusted for age, and adjusted for batch effect as needed. To avoid the bias due to familial correlations from pedigrees in the FHS cohort or the intra subject correlations from the repeated measures, we accounted for the correlations accordingly in all the analyses in the following. In Cox regression analysis, we used robust standard errors, the Huber sandwich estimator, implemented in R *coxph* function. We used linear mixed models with a random intercept term, implemented in *lme* R function. We used generalized estimation equation models (GEE), implemented in R *gee* function, for our logistic regression models. Additional covariates related to demographic characteristics, psychosocial behaviors and clinical covariates were adjusted in multivariate Cox models analysis. The additional covariates includes BMI (category), education attainment (category), alcohol consumption (gram/day), self report smoking pack-years, three medical covariates: status of cancer, hypertension and type 2 diabetes at baseline. The categories associated with BMI ranges are a) 18.5 -25 (normal), b) 25 to 30

Table 2. Overview of the cohorts used in the validation analysis.

| Study | N | Female | Age | Smoking status | | | Pack-years | Years of Follow-up |
				Never	Former	Current		
FHS* test	625	53%	66.9±8.64 [61,73]	37%	52%	10%	14.7±19.91 [0,23]	7.7±1.78 [7.3,8.8]
WHI BA23	2107	100%	65.3±7.1 [60,70.9]	52%	36%	10%	9.5±18.55 [0,12.5]	16.9±4.63 [15.8,19.9]
WHI EMPC	1972	100%	63.3±7.03 [57.9,68.7]	52%	38%	9%	9±17.27 [0,12.5]	18±4.02 [17.9,20.1]
JHS	1747	63%	56.2±12.31 [46.5,65.4]	65%	21%	14%	NA	11.7±2.55 [11.2,13.1]
InChianti**	924 (484)	54%	67±16.64 [60,78]	57%	29%	14%	10.3±17.33 [0,16.8]	5.4±4.84 [0.1,9.3]

NA=not available.

Quantitative variables are presented in the format of mean ±SD [25th, 75th].

*The distribution of age is based on exam 8.

**The statistics are based on the number of 924 observations across 484 individuals.

The table summarizes the characteristics of 6,935 individuals (corresponding to 7,375 Illumina arrays) from five independent cohorts that were used in our validation analysis. For example, up to two longitudinal measurements were available for each of 484 individuals in the InChianti cohort.

(over), and c) >30 (obese). The categories associated with education attainment are a) less than high school, b) high school degree, c) some college, and d) college degree and above. Both smoking pack-years and education variables were not available in the JHS cohort. Smoking category (never, former and current) was used in the analysis using the JHS cohort.

Meta analysis

We used fixed effect models weighted by inverse variance to combine the results across validation study sets into a single estimate by using the *metafor* R function in most situations. We also used Stouffer's meta analysis method (weighted by the square root of the sample size) in specific situations where the harmonization of covariates across cohorts was challenging, e.g. when evaluating the number of age-related conditions, disease free status and physical function scores (Fig. 5).

Heritability analysis

In general, epigenetic measures of age acceleration are highly heritable [52, 57, 58]. To evaluate whether AgeAccelGrim is heritable as well, we estimated the narrow sense heritability h^2 using the polygenic models defined in SOLAR [59] and its R interface solarius [60]. Heritability is defined as the total proportion of phenotypic variance attributable to genetic variation in the polygenic model. All traits were adjusted for age and gender. The robust polygenic model (with the option of a t-distribution) was used to estimate heritability of AgeAccelGrim and DNAm based proteins. The heritability estimate correspondents to the variance component associated with the kinship coefficient. If the corresponding P value is significant (P<0.05), the underlying trait is deemed to be heritable.

Two stage estimate of mortality versus a single stage estimate of mortality

To develop our *single stage* mortality estimator, DNAm Mortality, we used elastic net Cox regression to regress time-to-death on the CpG markers, chronological age and sex in the FHS training data. We used the same options in the training process (i.e., 10-fold cross validation for choosing the lambda tuning parameter). The resulting mortality risk estimator, (uncalibrated) DNA Mortality, is a linear combination of 59 CpGs and chronological age. Next we used the same age calibration method that we previously used for DNAm GrimAge to arrive at a mortality risk estimator in units of years, DNAm Mortality. We also evaluated the two mortality risk estimators by Zhang (on the basis of 10 CpGs) [21]. The first risk estimator from Zhang is a

composite score based on 10 CpGs with weights determined by a Cox regression with lasso penalty. Of the 10 CpGs, cg06126421 and cg23665802 were absent in the JHS cohort and had to be imputed (by the respective median values in the FHS training data).

To provide an unbiased comparison with our mortality predictors, we applied our age calibration method to the Zhang estimator as well, resulting in the mortality predictor "DNAmZhang". The second Zhang estimator, referred as DNAmZhangScore, was defined as the total sum of scores of the 10 CpGs with aberrant methylation [21]. The resulting risk score ranges from 0 to 10.

AgeAccelGrim versus blood cell composition

The imputed blood cell abundance measures were related to DNAm Grim Age models using the validation study sets: FHS test, WHI BA23, JHS, and InChianti, involving n=6,003 individuals. The following imputed blood cell counts were analyzed: B cell, naïve CD4+ T, CD4+ T, naïve CD8+ T, CD8+ T, exhausted cytotoxic CD8+ T cells (defined as CD8 positive CD28 negative CD45R negative), plasma blasts, natural killer cells, monocytes, and granulocytes. The abundance of naive T cells, exhausted T cells, and plasma blasts were based on the Horvath method [61]. The remaining cell types were imputed using the Houseman method [31]. More details were described in Supplementary Methods. To avoid confounding by age, we used AgeAccelGrim and adjusted all DNAm based surrogate biomarkers by chronological age (by forming residuals). The correlation results were combined across studies via the same fixed effect models.

Cox models that include blood cell counts

We also fit multivariate Cox regression models that adjusted for imputed blood cell counts in addition to chronological age, batch, and pedigree structure, for predicting time-to-death and time-to-CHD. The blood cell counts were imputed based on DNA methylation levels (as detailed above). To avoid multi-collinearities between blood cell counts, we only included the following 7 blood cell counts into the multivariate model: naïve CD8+T, exhausted cytotoxic CD8+ T cells, plasma blasts, CD4+T, natural killer cells, monocytes and granulocytes.

GREAT analysis

We applied the GREAT analysis software tool [32] to sets of CpGs (e.g. 1030 CpGs underlying DNAm GrimAge).CpGs in non-coding regions typically lack annotation with respect to biological functions. GREAT assigns biological meaning to a set of non-coding geno-

mic regions (implicated by the CpGs) by analyzing the annotations of the nearby genes. Toward this end, the GREAT software performs both a binomial test (over genomic regions) and a hypergeometric test over genes when using a whole genome background. We performed the enrichment based on default settings (Proximal: 5.0 kb upstream, 1.0 kb downstream, plus Distal: up to 1,000 kb) for gene sets associated with GO terms, MSigDB, PANTHER and KEGG pathway. To avoid large numbers of multiple comparisons, we restricted the analysis to the gene sets with between 10 and 3,000 genes. We report nominal P values and two adjustments for multiple comparisons: Bonferroni correction and the Benjamini-Hochberg false discovery rate.

Lifestyle factors including diet and education

We performed a robust correlation analysis (biweight midcorrelation, bicor [62]) between our novel biomarkers (AgeAccelGrim and its eight age-adjusted components) and 38 variables from the WHI including 12 self-reported dietary variables, behavioral variables, 9 dietary biomarkers, 12 variables related to metabolic related traits and central adiposity, and 5 life style factors. We combined the postmenopausal women from the WHI BA23 and WHI EMPC (roughly n= 4000 women). This cross sectional, robust correlation analysis was conducted in all groups combined and in three separate ethnic groups (Hispanic ancestry, European ancestry, African Ancestry). Ancestry information was verified using ancestry informative SNP markers. Blood biomarkers were measured from fasting plasma collected at baseline. Food groups and nutrients are inclusive, including all types and all preparation methods, e.g. folic acid includes synthetic and natural, dairy includes cheese and all types of milk. The individual variables are explained in [33].

Computed tomography data from the Framingham Heart Study

The computed tomography (CT) in liver, spleen, paraspinal muscle, subcutaneous adipose tissue (SAT), and visceral adipose tissue (VAT) were performed in n=2,803 individuals from the FHS Offspring, Third Generation and Omni 2 Cohort participants between September 2008 and December 2011 [37, 38]. Of those, 1,177 Offspring Cohort participants were included in our FHS study. The age at CT scan was in general slightly older than the age at blood draw for the DNA methylation profile (mean age difference= 3.7 years, ranging from 1.2 to 6.1 years).

Organ density measures, more precisely CT attenuation coefficients, reflect how easily a target can be penetrated by an X-ray. The Hounsfield unit (HU) scale is a

linear transformation of the original linear attenuation coefficient measurement into one in which the radiodensity of distilled water is defined as zero Hounsfield units (HU). Radiation attenuation in liver, spleen, or muscle is inversely related to respective measures of fat content.

The CT measures from three areas of the liver, two areas of the spleen and two areas of the paraspinal muscle were averaged to determine the average Hounsfield units in liver, spleen and muscle, respectively. The CT-scan measures of visceral and sub-cutaneous adipose tissue are described in [38].

In our analysis, we first performed marginal robust correlation analysis (biweight midcorrelation, bicor coefficient) [62] to study the association between the CT-scan derived measures and DNAm based biomarkers. As gender affects adipose associated parameters, we performed the analysis in males and females, separately. Next we combined the results across the two genders using fixed effects meta analysis. To adjust for potential confounders, we also performed three types of multivariate linear mixed effects models that included gender, BMI as fixed effects and pedigree structure as random effect. In Model I, we regressed a DNAm based biomarker (e.g. AgeAccelGrim) on CT derived covariates: liver density, spleen density, and paraspinal muscle density. In Model II, we regressed the DNAm based biomarker (dependent variable) on volumetric measures of adipose tissue (both SAT and VAT volume). We omitted measures of adipose tissue density from the analysis since a) they were not significant after adjusting for SAT/VAT volumes, and b) we wanted to protect the model fit from issues of multi-collinearity.

In Model III, we used all CT measures as covariates (i.e. liver, spleen and muscle density, SAT volume, and VAT volume). We used the BMI measure assessed at exam 9 in the FHS, i.e. the closest exam following the CT-scan exam.

AUTHOR CONTRIBUTIONS

ATL and SH developed the DNAm based biomarkers (including DNAm GrimAge) and conceived of the study. ATL carried out most of the statistical analyses. AQ carried out the analysis of lifestyle factors. The remaining authors contributed data, helped with the write up, and participated in the interpretation of the results.

CONFLICTS OF INTEREST

The Regents of the University of California is the sole owner of a provisional patent application directed at

this invention for which ATL and SH are named inventor.

REFERENCES

1. Horvath S. DNA methylation age of human tissues and cell types. Genome Biol. 2013; 14:R115. https://doi.org/10.1186/gb-2013-14-10-r115

2. Hannum G, Guinney J, Zhao L, Zhang L, Hughes G, Sadda S, Klotzle B, Bibikova M, Fan JB, Gao Y, Deconde R, Chen M, Rajapakse I, et al. Genome-wide methylation profiles reveal quantitative views of human aging rates. Mol Cell. 2013; 49:359–67. https://doi.org/10.1016/j.molcel.2012.10.016

3. Lin Q, Weidner CI, Costa IG, Marioni RE, Ferreira MR, Deary IJ, Wagner W. DNA methylation levels at individual age-associated CpG sites can be indicative for life expectancy. Aging (Albany NY). 2016; 8:394–401. https://doi.org/10.18632/aging.100908

4. Horvath S, Oshima J, Martin GM, Lu AT, Quach A, Cohen H, Felton S, Matsuyama M, Lowe D, Kabacik S, Wilson JG, Reiner AP, Maierhofer A, et al. Epigenetic clock for skin and blood cells applied to Hutchinson Gilford Progeria Syndrome and *ex vivo* studies. Aging (Albany NY). 2018; 10:1758–75. https://doi.org/10.18632/aging.101508

5. Marioni RE, Shah S, McRae AF, Chen BH, Colicino E, Harris SE, Gibson J, Henders AK, Redmond P, Cox SR, Pattie A, Corley J, Murphy L, et al. DNA methylation age of blood predicts all-cause mortality in later life. Genome Biol. 2015; 16:25. https://doi.org/10.1186/s13059-015-0584-6

6. Perna L, Zhang Y, Mons U, Holleczek B, Saum KU, Brenner H. Epigenetic age acceleration predicts cancer, cardiovascular, and all-cause mortality in a German case cohort. Clin Epigenetics. 2016; 8:64. https://doi.org/10.1186/s13148-016-0228-z

7. Chen BH, Marioni RE, Colicino E, Peters MJ, Ward-Caviness CK, Tsai PC, Roetker NS, Just AC, Demerath EW, Guan W, Bressler J, Fornage M, Studenski S, et al. DNA methylation-based measures of biological age: meta-analysis predicting time to death. Aging (Albany NY). 2016; 8:1844–65. https://doi.org/10.18632/aging.101020

8. Horvath S, Ritz BR. Increased epigenetic age and granulocyte counts in the blood of Parkinson's disease patients. Aging (Albany NY). 2015; 7:1130–42. https://doi.org/10.18632/aging.100859

9. Horvath S, Langfelder P, Kwak S, Aaronson J, Rosinski J, Vogt TF, Eszes M, Faull RL, Curtis MA, Waldvogel HJ, Choi OW, Tung S, Vinters HV, et al. Huntington's disease accelerates epigenetic aging of human brain and disrupts DNA methylation levels. Aging (Albany NY). 2016; 8:1485–512. https://doi.org/10.18632/aging.101005

10. Horvath S, Raj K. DNA methylation-based biomarkers and the epigenetic clock theory of ageing. Nat Rev Genet. 2018; 19:371–84. https://doi.org/10.1038/s41576-018-0004-3

11. Zheng SC, Widschwendter M, Teschendorff AE. Epigenetic drift, epigenetic clocks and cancer risk.

Epigenomics. 2016; 8:705–19.
https://doi.org/10.2217/epi-2015-0017

12. Jung M, Pfeifer GP. Aging and DNA methylation. BMC Biol. 2015; 13:7. https://doi.org/10.1186/s12915-015-0118-4

13. Nwanaji-Enwerem JC, Weisskopf MG, Baccarelli AA. Multi-tissue DNA methylation age: molecular relationships and perspectives for advancing bio-marker utility. Ageing Res Rev. 2018; 45:15–23. https://doi.org/10.1016/j.arr.2018.04.005

14. Levine ME, Lu AT, Chen BH, Hernandez DG, Singleton AB, Ferrucci L, Bandinelli S, Salfati E, Manson JE, Quach A, Kusters CD, Kuh D, Wong A, et al. Menopause accelerates biological aging. Proc Natl Acad Sci USA. 2016; 113:9327–32. https://doi.org/10.1073/pnas.1604558113

15. Levine ME, Hosgood HD, Chen B, Absher D, Assimes T, Horvath S. DNA methylation age of blood predicts future onset of lung cancer in the women's health initiative. Aging (Albany NY). 2015; 7:690–700. https://doi.org/10.18632/aging.100809

16. Horvath S, Garagnani P, Bacalini MG, Pirazzini C, Salvioli S, Gentilini D, Di Blasio AM, Giuliani C, Tung S, Vinters HV, Franceschi C. Accelerated epigenetic aging in Down syndrome. Aging Cell. 2015; 14:491–95. https://doi.org/10.1111/acel.12325

17. Horvath S, Pirazzini C, Bacalini MG, Gentilini D, Di Blasio AM, Delledonne M, Mari D, Arosio B, Monti D, Passarino G, De Rango F, D'Aquila P, Giuliani C, et al. Decreased epigenetic age of PBMCs from Italian semi-supercentenarians and their offspring. Aging (Albany NY). 2015; 7:1159–70. https://doi.org/10.18632/aging.100861

18. Maierhofer A, Flunkert J, Oshima J, Martin GM, Haaf T, Horvath S. Accelerated epigenetic aging in Werner syndrome. Aging (Albany NY). 2017; 9:1143–52. https://doi.org/10.18632/aging.101217

19. Levine ME, Lu AT, Bennett DA, Horvath S. Epigenetic age of the pre-frontal cortex is associated with neuritic plaques, amyloid load, and Alzheimer's disease related cognitive functioning. Aging (Albany NY). 2015; 7:1198–211. https://doi.org/10.18632/aging.100864

20. Marioni RE, Shah S, McRae AF, Ritchie SJ, Muniz-Terrera G, Harris SE, Gibson J, Redmond P, Cox SR, Pattie A, Corley J, Taylor A, Murphy L, et al. The epigenetic clock is correlated with physical and cognitive fitness in the Lothian Birth Cohort 1936. Int J Epidemiol. 2015; 44:1388–96. https://doi.org/10.1093/ije/dyu277

21. Zhang Y, Wilson R, Heiss J, Breitling LP, Saum KU, Schöttker B, Holleczek B, Waldenberger M, Peters A, Brenner H. DNA methylation signatures in peripheral blood strongly predict all-cause mortality. Nat Commun. 2017; 8:14617. https://doi.org/10.1038/ncomms14617

22. Levine ME, Lu AT, Quach A, Chen BH, Assimes TL, Bandinelli S, Hou L, Baccarelli AA, Stewart JD, Li Y, Whitsel EA, Wilson JG, Reiner AP, et al. An epigenetic biomarker of aging for lifespan and healthspan. Aging (Albany NY). 2018; 10:573–91. https://doi.org/10.18632/aging.101414

23. Ignjatovic V, Lai C, Summerhayes R, Mathesius U, Tawfilis S, Perugini MA, Monagle P. Age-related differences in plasma proteins: how plasma proteins change from neonates to adults. PLoS One. 2011; 6:e17213. https://doi.org/10.1371/journal.pone.0017213

24. Ridker PM, Buring JE, Cook NR, Rifai N. C-reactive protein, the metabolic syndrome, and risk of incident cardiovascular events: an 8-year follow-up of 14 719 initially healthy American women. Circulation. 2003; 107:391–97. https://doi.org/10.1161/01.CIR.0000055014.62083.05

25. Dawber TR, Meadors GF, Moore FE Jr. Epidemiological approaches to heart disease: the Framingham Study. Am J Public Health Nations Health. 1951; 41:279–81. https://doi.org/10.2105/AJPH.41.3.279

26. Zou H, Hastie T. Regularization and variable selection via the elastic net. J R Stat Soc Series B Stat Methodol. 2005; 67:301–20. https://doi.org/10.1111/j.1467-9868.2005.00503.x

27. Considine RV, Sinha MK, Heiman ML, Kriauciunas A, Stephens TW, Nyce MR, Ohannesian JP, Marco CC, McKee LJ, Bauer TL, Caro JF. Serum immunoreactive-leptin concentrations in normal-weight and obese humans. N Engl J Med. 1996; 334:292–95. https://doi.org/10.1056/NEJM199602013340503

28. Rosenbaum M, Nicolson M, Hirsch J, Heymsfield SB, Gallagher D, Chu F, Leibel RL. Effects of gender, body composition, and menopause on plasma concentrations of leptin. J Clin Endocrinol Metab. 1996; 81:3424–27. https://doi.org/10.1210/jcem.81.9.8784109

29. Gao X, Jia M, Zhang Y, Breitling LP, Brenner H. DNA methylation changes of whole blood cells in response to active smoking exposure in adults: a systematic review of DNA methylation studies. Clin Epigenetics. 2015; 7:113. https://doi.org/10.1186/s13148-015-0148-3

30. Horvath S, Gurven M, Levine ME, Trumble BC, Kaplan H, Allayee H, Ritz BR, Chen B, Lu AT, Rickabaugh TM,

Jamieson BD, Sun D, Li S, et al. An epigenetic clock analysis of race/ethnicity, sex, and coronary heart disease. Genome Biol. 2016; 17:171. https://doi.org/10.1186/s13059-016-1030-0

31. Houseman EA, Accomando WP, Koestler DC, Christensen BC, Marsit CJ, Nelson HH, Wiencke JK, Kelsey KT. DNA methylation arrays as surrogate measures of cell mixture distribution. BMC Bioinformatics. 2012; 13:86. https://doi.org/10.1186/1471-2105-13-86

32. McLean CY, Bristor D, Hiller M, Clarke SL, Schaar BT, Lowe CB, Wenger AM, Bejerano G. GREAT improves functional interpretation of cis-regulatory regions. Nat Biotechnol. 2010; 28:495–501. https://doi.org/10.1038/nbt.1630

33. Quach A, Levine ME, Tanaka T, Lu AT, Chen BH, Ferrucci L, Ritz B, Bandinelli S, Neuhouser ML, Beasley JM, Snetselaar L, Wallace RB, Tsao PS, et al. Epigenetic clock analysis of diet, exercise, education, and lifestyle factors. Aging (Albany NY). 2017; 9:419–46. https://doi.org/10.18632/aging.101168

34. Rizos EC, Ntzani EE, Bika E, Kostapanos MS, Elisaf MS. Association between omega-3 fatty acid supplementation and risk of major cardiovascular disease events: a systematic review and meta-analysis. JAMA. 2012; 308:1024–33. https://doi.org/10.1001/2012.jama.11374

35. Aung T, Halsey J, Kromhout D, Gerstein HC, Marchioli R, Tavazzi L, Geleijnse JM, Rauch B, Ness A, Galan P, Chew EY, Bosch J, Collins R, et al, and Omega-3 Treatment Trialists' Collaboration. Associations of Omega-3 Fatty Acid Supplement Use With Cardiovascular Disease Risks: Meta-analysis of 10 Trials Involving 77 917 Individuals. JAMA Cardiol. 2018; 3:225–34. https://doi.org/10.1001/jamacardio.2017.5205

36. Rizos EC, Elisaf MS. Does Supplementation with Omega-3 PUFAs Add to the Prevention of Cardiovascular Disease? Curr Cardiol Rep. 2017; 19:47. https://doi.org/10.1007/s11886-017-0856-8

37. Long MT, Pedley A, Massaro JM, Hoffmann U, Fox CS. The Association between Non-Invasive Hepatic Fibrosis Markers and Cardiometabolic Risk Factors in the Framingham Heart Study. PLoS One. 2016; 11:e0157517. https://doi.org/10.1371/journal.pone.0157517

38. Lee JJ, Pedley A, Hoffmann U, Massaro JM, Keaney JF Jr, Vasan RS, Fox CS. Cross-Sectional Associations of Computed Tomography (CT)-Derived Adipose Tissue Density and Adipokines: The Framingham Heart Study. J Am Heart Assoc. 2016; 5:e002545. https://doi.org/10.1161/JAHA.115.002545

39. Horvath S, Erhart W, Brosch M, Ammerpohl O, von Schönfels W, Ahrens M, Heits N, Bell JT, Tsai PC, Spector TD, Deloukas P, Siebert R, Sipos B, et al. Obesity accelerates epigenetic aging of human liver. Proc Natl Acad Sci USA. 2014; 111:15538–43. https://doi.org/10.1073/pnas.1412759111

40. Jylhävä J, Pedersen NL, Hägg S. Biological Age Predictors. EBioMedicine. 2017; 21:29–36. https://doi.org/10.1016/j.ebiom.2017.03.046

41. Wong HK, Cheung TT, Cheung BM. Adrenomedullin and cardiovascular diseases. JRSM Cardiovasc Dis. 2012; 1:1–7. https://doi.org/10.1258/cvd.2012.012003

42. Liabeuf S, Lenglet A, Desjardins L, Neirynck N, Glorieux G, Lemke HD, Vanholder R, Diouf M, Choukroun G, Massy ZA, and European Uremic Toxin Work Group (EUTox). Plasma beta-2 microglobulin is associated with cardiovascular disease in uremic patients. Kidney Int. 2012; 82:1297–303. https://doi.org/10.1038/ki.2012.301

43. Ferguson TW, Komenda P, Tangri N. Cystatin C as a biomarker for estimating glomerular filtration rate. Curr Opin Nephrol Hypertens. 2015; 24:295–300. https://doi.org/10.1097/MNH.0000000000000115

44. Larrayoz IM, Ferrero H, Martisova E, Gil-Bea FJ, Ramírez MJ, Martínez A. Adrenomedullin Contributes to Age-Related Memory Loss in Mice and Is Elevated in Aging Human Brains. Front Mol Neurosci. 2017; 10:384. https://doi.org/10.3389/fnmol.2017.00384

45. Smith LK, He Y, Park JS, Bieri G, Snethlage CE, Lin K, Gontier G, Wabl R, Plambeck KE, Udeochu J, Wheatley EG, Bouchard J, Eggel A, et al. β2-microglobulin is a systemic pro-aging factor that impairs cognitive function and neurogenesis. Nat Med. 2015; 21:932–37. https://doi.org/10.1038/nm.3898

46. Fujita Y, Taniguchi Y, Shinkai S, Tanaka M, Ito M. Secreted growth differentiation factor 15 as a potential biomarker for mitochondrial dysfunctions in aging and age-related disorders. Geriatr Gerontol Int. 2016 (Suppl 1); 16:17–29. https://doi.org/10.1111/ggi.12724

47. Cesari M, Pahor M, Incalzi RA. Plasminogen activator inhibitor-1 (PAI-1): a key factor linking fibrinolysis and age-related subclinical and clinical conditions. Cardiovasc Ther. 2010; 28:e72–91. https://doi.org/10.1111/j.1755-5922.2010.00171.x

48. Khan SS, Shah SJ, Klyachko E, Baldridge AS, Eren M, Place AT, Aviv A, Puterman E, Lloyd-Jones DM, Heiman M, Miyata T, Gupta S, Shapiro AD, et al. A null mutation in SERPINE1 protects against biological

aging in humans. Sci Adv. 2017; 3:eaao1617. https://doi.org/10.1126/sciadv.aao1617

49. Ashutosh CC, Chao C, Borgmann K, Brew K, Ghorpade A. Tissue inhibitor of metalloproteinases-1 protects human neurons from staurosporine and HIV-1-induced apoptosis: mechanisms and relevance to HIV-1-associated dementia. Cell Death Dis. 2012; 3:e332. https://doi.org/10.1038/cddis.2012.54

50. Kabacik S, Horvath S, Cohen H, Raj K. Epigenetic ageing is distinct from senescence-mediated ageing and is not prevented by telomerase expression. Aging (Albany NY). 2018; 10:2800–15. https://doi.org/10.18632/aging.101588

51. Lowe D, Horvath S, Raj K. Epigenetic clock analyses of cellular senescence and ageing. Oncotarget. 2016; 7:8524–31. https://doi.org/10.18632/oncotarget.7383

52. Lu AT, Xue L, Salfati EL, Chen BH, Ferrucci L, Levy D, Joehanes R, Murabito JM, Kiel DP, Tsai PC, Yet I, Bell JT, Mangino M, et al. GWAS of epigenetic aging rates in blood reveals a critical role for TERT. Nat Commun. 2018; 9:387. https://doi.org/10.1038/s41467-017-02697-5

53. Ridker PM. High-sensitivity C-reactive protein: potential adjunct for global risk assessment in the primary prevention of cardiovascular disease. Circulation. 2001; 103:1813–18. https://doi.org/10.1161/01.CIR.103.13.1813

54. Andersson C, Enserro D, Sullivan L, Wang TJ, Januzzi JL Jr, Benjamin EJ, Vita JA, Hamburg NM, Larson MG, Mitchell GF, Vasan RS. Relations of circulating GDF-15, soluble ST2, and troponin-I concentrations with vascular function in the community: The Framingham Heart Study. Atherosclerosis. 2016; 248:245–51. https://doi.org/10.1016/j.atherosclerosis.2016.02.013

55. Triche TJ Jr, Weisenberger DJ, Van Den Berg D, Laird PW, Siegmund KD. Low-level processing of Illumina Infinium DNA Methylation BeadArrays. Nucleic Acids Res. 2013; 41:e90. https://doi.org/10.1093/nar/gkt090

56. Fortin JP, Triche TJ Jr, Hansen KD. Preprocessing, normalization and integration of the Illumina HumanMethylationEPIC array with minfi. Bioinformatics. 2017; 33:558–60. https://doi.org/10.1093/bioinformatics/btw691

57. Lu AT, Hannon E, Levine ME, Crimmins EM, Lunnon K, Mill J, Geschwind DH, Horvath S. Genetic architecture of epigenetic and neuronal ageing rates in human brain regions. Nat Commun. 2017; 8:15353. https://doi.org/10.1038/ncomms15353

58. Lu AT, Hannon E, Levine ME, Hao K, Crimmins EM, Lunnon K, Kozlenkov A, Mill J, Dracheva S, Horvath S. Genetic variants near MLST8 and DHX57 affect the epigenetic age of the cerebellum. Nat Commun. 2016; 7:10561. https://doi.org/10.1038/ncomms10561

59. Almasy L, Blangero J. Multipoint quantitative-trait linkage analysis in general pedigrees. Am J Hum Genet. 1998; 62:1198–211. https://doi.org/10.1086/301844

60. Ziyatdinov A, Brunel H, Martinez-Perez A, Buil A, Perera A, Soria JM. solarius: an R interface to SOLAR for variance component analysis in pedigrees. Bioinformatics. 2016; 32:1901–02. https://doi.org/10.1093/bioinformatics/btw080

61. Horvath S, Levine AJ. HIV-1 infection accelerates age according to the epigenetic clock. J Infect Dis. 2015; 212:1563–73. https://doi.org/10.1093/infdis/jiv277

62. Langfelder P, Horvath S. WGCNA: an R package for weighted correlation network analysis. BMC Bioinformatics. 2008; 9:559. https://doi.org/10.1186/1471-2105-9-559

SUPPLEMENTARY MATERIAL

Please browse the Full Text version to see the data related to this manuscript:

Supplementary Note 1. Description of datasets

Supplementary Note 2. DNAm based surrogates for plasma proteins

Supplementary Methods. Estimation of blood cell counts based on DNAm levels

Supplementary Figures 1-33

Supplementary Tables 1-13

Supplementary References

Supplementary Data 1

Supplementary Data 2

Supplementary Data 3

Cell and tissue type independent age-associated DNA methylation changes are not rare but common

Tianyu Zhu[1], Shijie C Zheng[1], Dirk S. Paul[2], Steve Horvath[3,4], Andrew E. Teschendorff [1,5]

[1]CAS Key Laboratory of Computational Biology, CAS-MPG Partner Institute for Computational Biology, Shanghai Institute of Nutrition and Health, Shanghai Institute for Biological Sciences, University of Chinese Academy of Sciences, Chinese Academy of Sciences, Shanghai 200031, China
[2]Cardiovascular Epidemiology Unit, Department of Public Health and Primary Care, University of Cambridge, Strangeways Research Laboratory, Cambridge, CB1 8RN, UK
[3]Department of Human Genetics, David Geffen School of Medicine, University of California Los Angeles, CA 90095, USA
[4]Department of Biostatistics, Fielding School of Public Healthy, University of California Los Angeles, Los Angeles, CA 90095, USA
[5]UCL Cancer Institute, Paul O'Gorman Building, University College London, London WC1E 6BT, UK

Correspondence to: Andrew E. Teschendorff; **email:** a.teschendorff@ucl.ac.uk
Keywords: DNA methylation, epigenetic drift, epigenetic clock
Received: September 21, 2018   **Accepted:** November 15, 2018   **Published:** November 27, 2018

ABSTRACT

Age-associated DNA methylation changes have been widely reported across many different tissue and cell types. Epigenetic 'clocks' that can predict chronological age with a surprisingly high degree of accuracy appear to do so independently of tissue and cell-type, suggesting that a component of epigenetic drift is cell-type independent. However, the relative amount of age-associated DNAm changes that are specific to a cell or tissue type versus the amount that occurs independently of cell or tissue type is unclear and a matter of debate, with a recent study concluding that most epigenetic drift is tissue-specific. Here, we perform a novel comprehensive statistical analysis, including matched multi cell-type and multi-tissue DNA methylation profiles from the same individuals and adjusting for cell-type heterogeneity, demonstrating that a substantial amount of epigenetic drift, possibly over 70%, is shared between significant numbers of different tissue/cell types. We further show that ELOVL2 is not unique and that many other CpG sites, some mapping to genes in the Wnt and glutamate receptor signaling pathways, are altered with age across at least 10 different cell/tissue types. We propose that while most age-associated DNAm changes are shared between cell-types that the putative functional effect is likely to be tissue-specific.

INTRODUCTION

Age-associated DNA methylation (DNAm) changes have been reported for a long time [1-3]. One of the first studies to indicate that age-associated DNAm changes, termed epigenetic drift, could be largely tissue specific was a study by Christensen et al. [4]. This first study

however only sampled a small percentage of the DNA methylome, was largely underpowered and did not adjust for potentially confounding cell-type hetero-geneity [5, 6]. Building on an observation that DNAm over specific Polycomb Repressor Complex-2 (PRC2) promoter loci correlates with age across many different tissue-types [7] , it was demonstrated that age-associat-

ed DNAm changes can be used to build remarkably accurate predictors of chronological age, termed epigenetic clocks [8-11], which also appear to work independently of tissue or cell-type [9].

Interestingly, a recent study has suggested however that most age-associated DNAm changes are tissue-specific [12]. Indeed, the study concluded that, with the exception of the *ELOVL2* promoter, epigenetic drift is not shared between tissues. This is a surprising conclusion given that several pan-tissue epigenetic clocks have been constructed [9, 13, 14]. It led us to investigate the tissue and cell-type specific nature of epigenetic drift in more detail. In doing so, we have identified a number of critical issues with the statistical analyses performed in [12], which may have led to premature conclusions. First, the study performs the primary analyses using very stringent Bonferroni-corrected thresholds. While this controls for the Family-Wise-Error-Rate (FWER), the use of a Bonferroni threshold is known to suffer from a very large False Negative Rate (FNR), i.e. to a substantial reduction in power. This is particularly pertinent because their analyses generally compare age-associated differentially methylated positions (aDMPs) between studies and tissues, which according to our estimates were not adequately powered. Second, the authors do not report P-values of overlap, only overlapping fractions, which does not allow the statistical significance of the overlaps to be assessed. Assessing statistical significance is important because if aDMPs are not preferentially shared between tissue-types, then the reported overlaps should not deviate significantly from random. Third, the authors perform additional analyses using an arbitrary threshold on the effect size, as an alternative to statistics and P-values to select aDMPs, to argue that the "lack of overlap of aDMPs derived from different tissues" is not due to a lack of power. As we shall show here, using only a threshold on the effect size to select aDMPs is a highly problematic procedure, because of issues like heteroscedasticity, selection bias and study-specific confounding factors. Indeed, a fourth key concern is that the analysis performed in[12] does not always fully adjust for cell-type heterogeneity, especially in complex tissues such as buccal, kidney, brain or liver. As shown recently by us, tissues like buccal, kidney or liver are highly heterogeneous, containing a substantial amount of immune-cell infiltrates [15], which means that adjustment for variations in the amount of infiltrating leukocytes and other stromal cells is critically important [5, 15, 16].

To address these issues, we here provide a complementary analysis to the one presented in [12], adjusting for cell-type heterogeneity, and using, wherever possible, matched multi cell-type or multi-tissue EWAS data from the same individuals, since such data allows for a more objective comparison between tissues and cell-types. This new analysis demonstrates that the conclusions drawn in [12] are too premature, and that the evidence so far points to at least 70% of epigenetic drift being shared by at least two different cell or tissue types.

RESULTS

Most age-associated DMPs are shared between blood cell subtypes

First, we aimed to demonstrate that age-associated DMPs (aDMPs) derived from different cell or tissue types do exhibit a highly statistically significant overlap. We note that a highly significant overlap would be a strong cue that aDMPs shared between relevant cell or tissue-types is the norm and not the exception. In order to avoid the confounding effect of cell-type heterogeneity we first focused on three DNAm datasets profiling purified blood cell subtypes. Specifically, we analysed Illumina 450k DNAm data of 1199 purified CD14+ monocyte and 214 purified CD4+ T-cell samples from Reynolds et al. [17], and of 100 purified CD8+ T-cells from Tserel et al. [18]. For each dataset, we derived age-associated DMPs (aDMPs), adjusting for potential technical confounders (Methods). We used two different significance thresholds: a false discovery rate (FDR) < 0.05, and a Bonferroni-adjusted P_{bonf} < 0.05 thresholds. The former admits 5% of false positives but ensures that the FNR is not abnormally high, whereas the Bonferroni threshold ensures in principle no false positive but at the expense of a much larger FNR. Using an FDR < 0.05 threshold, we observed a very strong and highly statistically sig-nificant overlap of aDMPs between all 3 cell-types (Fig. 1A). For instance, almost 4000 aDMPs were found to be shared between all 3 cell-types using an FDR < 0.05 threshold (Fig. 1A). The high statistical significance of the overlaps remained if Bonferroni thresholds were used (Fig. 1B). Thus, even though "only" 198 aDMPs were in common between all 3 cell-types when using Bonferroni thresholds, this number was highly sig-nificant, i.e. much higher than what would be expected if aDMPs were cell-type specific.

An alternative to estimating significance of overlaps, is to evaluate the consistency of the t-statistics between aDMPs, which therefore also takes into account the directionality of DNAm change. This can be done by generating scatterplots of the t-statistics of selected aDMPs in one dataset against the corresponding t-statistics in another dataset, the rationale being that if an aDMP declared in one dataset is not an aDMP in another, then its t-statistic in this other set will be

distributed with a mean value of 0. Thus, if aDMPs are cell-type specific and only valid in one dataset, their t-statistics in the other set profiling a different cell-type should form a data cloud centered around 0. Applying this strategy to the three purified blood cell type data-sets above, revealed in each case that t-statistics were strongly skewed away from 0 and very strongly positively correlated (Fisher-test P-values <1e-100, Fig. 1C).
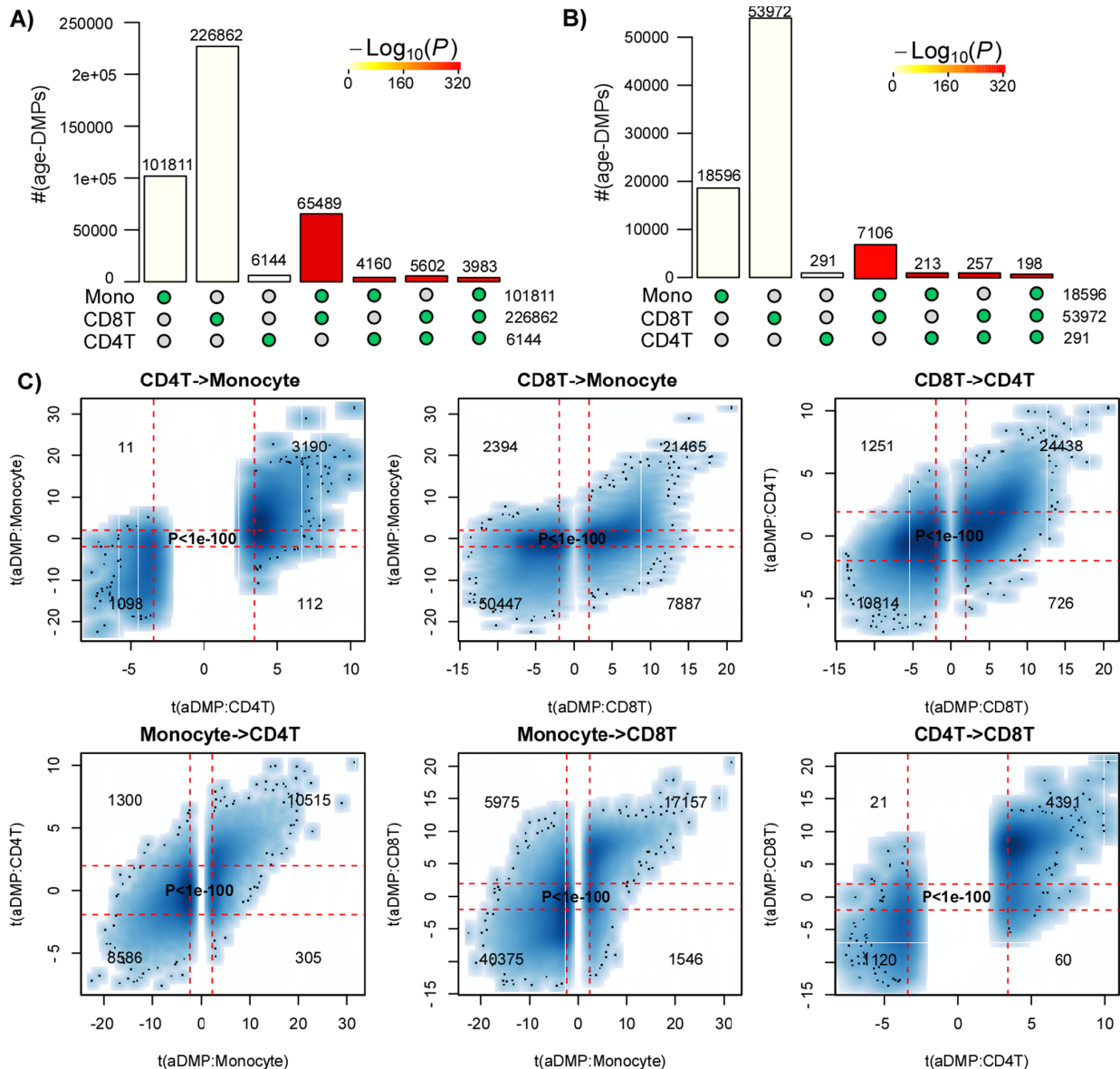
In order to validate these findings, we analyzed independent data from a multi cell-type EWAS from the BLUEPRINT consortium [19], encompassing Illumina 450k data from CD4+ T-cells, CD14+ monocytes and CD16+ neutrophils for a total of 139 individuals. We note that the matched nature of this dataset naturally adjusts for age-range and sample size, since all 3 cell-types are available for each of the 139 individuals. We performed exactly the same analysis as before, which

Figure 1. Most age-DMPs are shared between blood cell subtypes. (**A**) Landscape overlap diagram for age-DMPs defined using FDR<0.05 threshold in three separate purified blood cell subtype datasets (1199 Monocytes from Reynolds et al, 214 CD4+ T-cells from Reynolds et al and 100 CD8+ T-cells from Tserel et al). Barplots indicate the number of aDMPs found in each purified cell-type, or the corresponding aDMP overlap between cell-types. For the overlapping categories, the P-value of the overlap is indicated by the color of the bar, as shown. (**B**) As A), but now using a Bonferroni corrected P<0.05 threshold. (**C**) Smoothed scatterplots of t-statistics of age-DMPs called in a given blood cell subtype vs. the corresponding t-statistics in another cell subtype, as indicated for the 3 pairwise comparisons. In each panel, we only depict the 100 most outlier data points, provide the number of probes in each significant quadrant and the P-value assessing agreement is from a one-tailed Fisher-test. The vertical red lines indicate the line of FDR<0.05, whilst the horizontal lines depict the "validation threshold" of P<0.05.

confirmed that overlaps were highly statistically significant, using either a FDR or Bonferroni-based threshold (Fig. 2A-B), and importantly, that there was also a very strong correlation between the t-statistics of corresponding aDMPs (Fisher test P-values < 1e-100, Fig. 2C), further supporting the view that a large fraction of aDMPs in one blood cell-type constitute aDMPs in another.
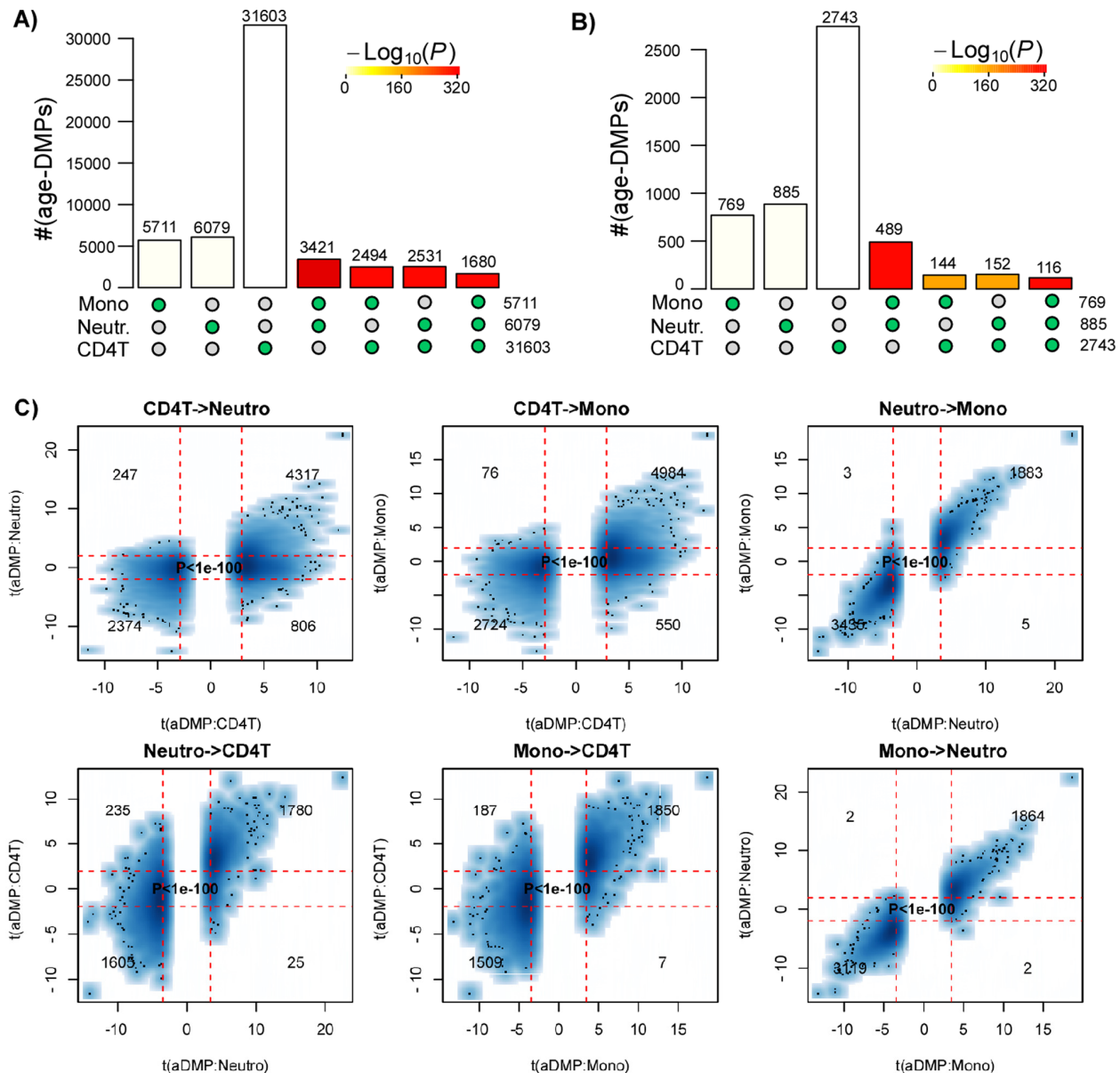
Many age-associated DMPs are shared between tissue types

Next, we decided to compare aDMPs across different tissues. These comparisons are particularly problematic if tissues derive from different datasets that profiled variable numbers of samples, with different age-ranges and subject to potentially different confounding factors,

Figure 2. Most age-DMPs are shared between blood cell subtypes: validation in BLUEPRINT. (**A**) Landscape overlap diagram for age-DMPs defined using FDR<0.05 threshold in the matched multi cell-types DNAm dataset from BLUEPRINT (139 monocyte samples, 139 matched CD4+ T-cell samples and 139 matched neutrophil samples. Barplots indicate the number of aDMPs found in each purified cell-type, or the corresponding aDMP overlap between cell-types. For the overlapping categories, the P-value of the overlap is indicated by the color of the bar, as shown. (**B**) As (**A**), but now using a Bonferroni corrected P<0.05 threshold. (**C**) Smoothed scatterplots of t-statistics of age-DMPs called in a given blood cell subtype vs. the corresponding t-statistics in another cell subtype, as indicated for the 3 pairwise comparisons. In each panel, we only depict the 100 most outlier data points, provide the number of probes in each significant quadrant and the P-value assessing agreement is from a one-tailed Fisher-test. The vertical red lines indicate the line of FDR<0.05, whilst the horizontal lines depict the "validation threshold" of P<0.05.

all of which could greatly impact on statistical significance estimates [20]. Thus, ideally, a cross-tissue comparison should include multiple tissue samples from the same set of individuals, all profiled as part of the same study. Therefore, we analyzed Illumina 850k data from an EWAS profiling blood, buccal and cervical samples from a common set of 263 women (Methods). Because blood is a complex mixture of many immune-cell (IC) subtypes, and buccal and cervical samples are highly contaminated by immune cells [15], we identified aDMPs in each tissue after adjustment for batch effects and cell-type heterogeneity using EpiDISH [21] (in the case of blood) and HEpiDISH [15] (in the case of buccal and cervix). Although aDMPs identified with or without cell-type correction were highly correlated (Fig. 3A), we

observed that adjusting or not for cell-type heterogeneity did have a marked impact on the number of aDMPs, and that the number of aDMPs also varied substantially between tissue-types (Fig. 3B). Of note, using either an FDR < 0.05 or Bonferroni adjusted P-value < 0.05 thresholds, the overlap of aDMPs between the 3 tissues was highly significant (Fig. 3C, P<1e-100), mimicking the result obtained on blood cell subtypes. For instance, we observed a total of 2200 aDMPs in common between blood, buccal and cervix, an overlap which cannot be explained by random chance (Fig. 3C, P<1e-100). Scatterplots of t-statistics of aDMPs between tissues further supported an extremely strong correlation, suggesting that shared aDMPs between blood, buccal and cervix is the norm and not the exception (Fig. 3D-F).
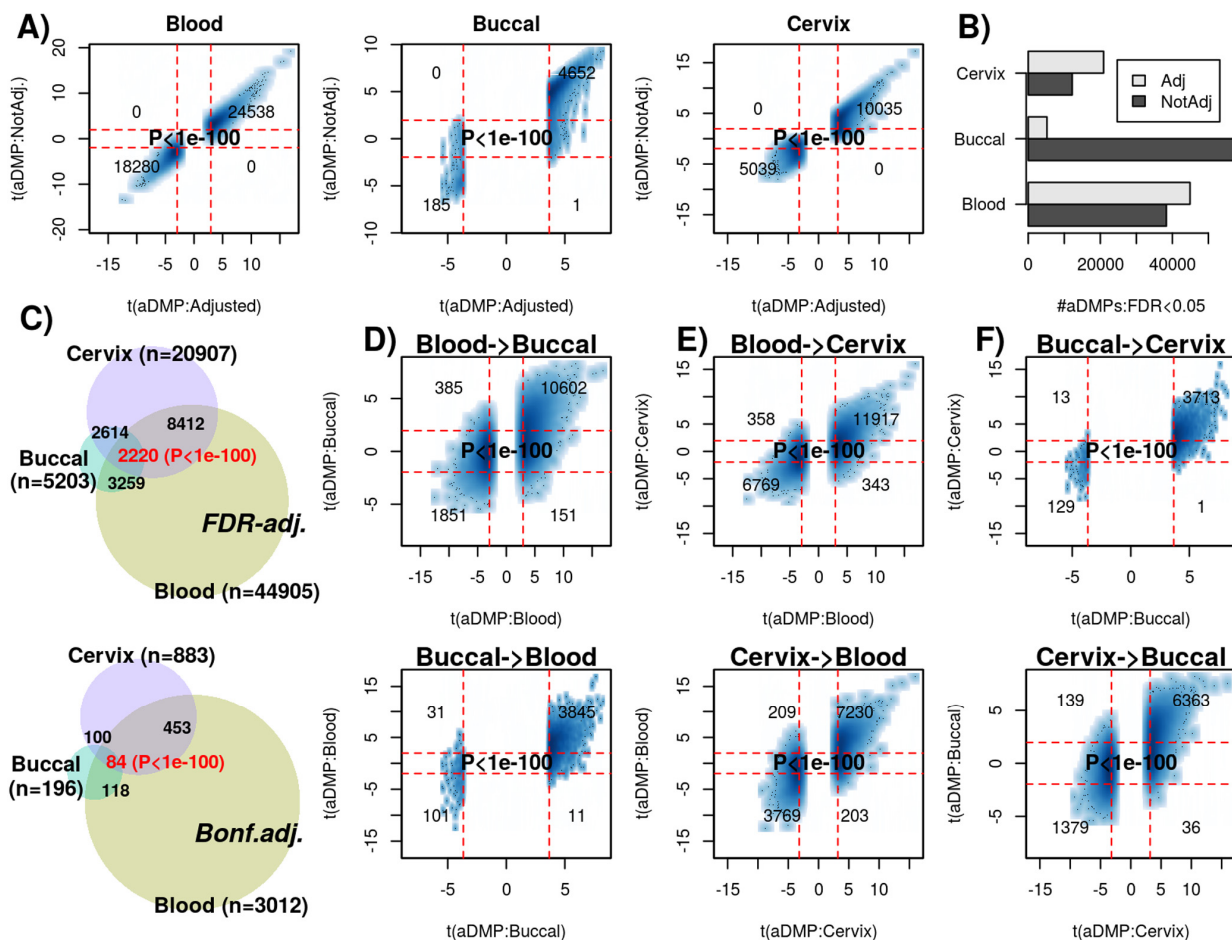
Figure 3. Most age-DMPs are shared between tissue-types. (**A**) Smoothed scatterplots of age-DMP (aDMP) t-statistics obtained after adjustment for cell-type heterogeneity (x-axis) against the corresponding t-statistics without adjustment (y-axis), for 3 different tissue-types (Blood, Buccal and Cervix) separately. In each scatterplot, we only depict the 100 most outlier data points, provide the number of probes in each significant quadrant and the P-value is from a one-tailed Fisher-test. The vertical red lines indicate the line of FDR<0.05, whilst the horizontal lines depict the "validation threshold" of P<0.05. (**B**) Barplot of the number of aDMPs (FDR<0.05) in each tissue-type before and after adjustment for cell-type heterogeneity. (**C**) Venn-diagrams representing the number of overlapping aDMPs between the 3 tissue-types using an FDR<0.05 threshold for calling aDMPs (top panel) and using a Bonferroni threshold (lower panel). P-value as estimated using a nested Hypergeometric test. (**D**) Smoothed scatterplots of aDMP t-statistics (adjusted for cell-type heterogeneity) in blood (x-axis) against their corresponding t-statistics in buccal (y-axis) for top panel, with lower panel depicting the reverse analysis, as indicated. (**E-F**) As (**D**), but for the combinations blood-cervix and buccal-cervix, respectively.
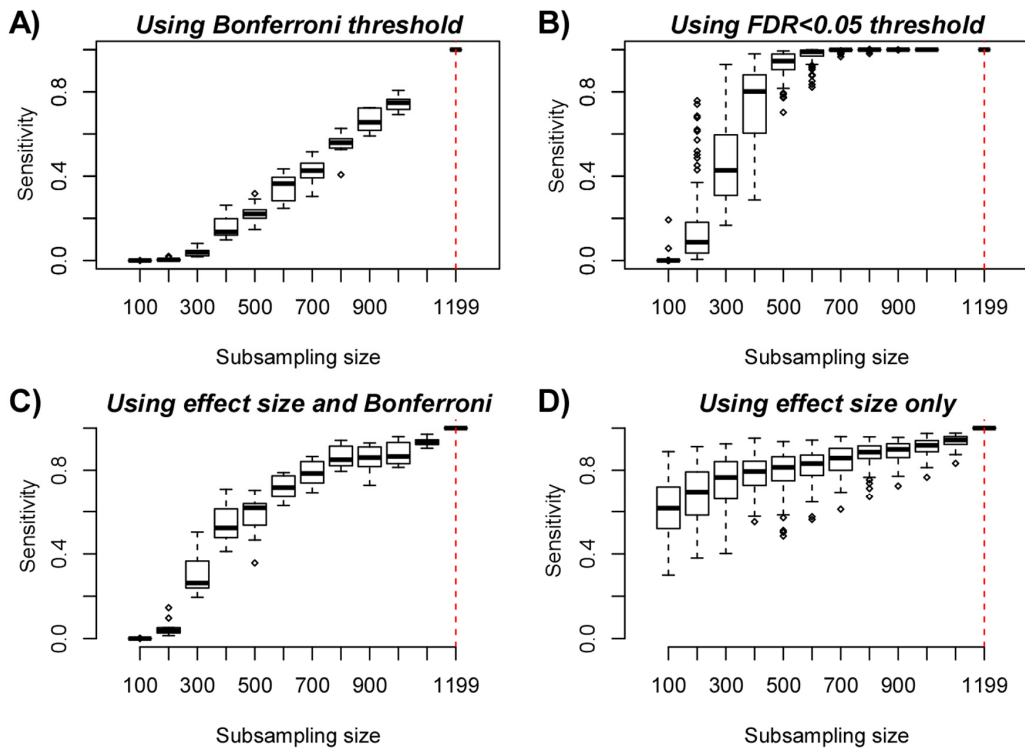
Figure 4. Empirical Power Analysis. (**A**) Boxplot of the sensitivity (y-axis) to detect gold-standard aDMPs, defined at the full purified monocyte sample size n=1199, at random subsampling sizes (x-axis), as indicated. Each boxplot displays the sensitivity over 10 separate runs, in each run aDMPs were defined at the Bonferroni 0.05 level. (**B**) As A), but now defining aDMPs in each run as those with an FDR<0.05. Because the FDR estimates are more unstable, we performed 100 runs at each subsampling size. (**C**) As A), but now defining the gold-standard set of aDMPs by imposing a threshold on the effect size (2% DNAm change over 10 years), in addition to a Bonferroni adjusted P-value < 0.05. At each subsampling run, aDMPs were also defined using the same criterion and 10 runs were performed at each subsampling size. (**D**) As A), but now only using the threshold on the effect size to define gold-standard aDMPs and to define aDMPs each subsampling size. A total of 100 runs at each subsampling size were performed.

Studies profiling only a few hundred samples are underpowered to detect most age-DMPs

The previous analyses clearly support the view that at least thousands of aDMPs are shared between two and three tissue/cell-types. However, is this lower bound a significant underestimate on the true number of aDMPs that are shared between any two given cell or tissue types? To address this question requires careful consideration of the expected power of the studies. To estimate empirically the expected power as a function of sample size, we devised a subsampling strategy using the Reynolds monocyte dataset (Methods). We reasoned that this set, due to its large size (n=1199) and purified nature of the cell population, would allow us to object-tively define a gold-standard set of aDMPs in mono-cytes. Using a stringent Bonferroni-adjusted P<0.05 threshold and using all 1199 monocyte samples, we thus defined a gold-standard set of 18596 monocyte aDMPs. We note that although this is certainly only a small subset of all true monocyte aDMPs, that it would never-

theless allow us to assess the impact of sample size on power. We next subsampled 100 samples from the 1199, and re-derived a new set of aDMPs at the same Bonferroni threshold. This subsampling strategy was performed for increasing subsampling size (from 100 to 1000, in units of 100), and a total of 10 times for each subsampling size. Sensitivity to detect the 18596 gold-standard aDMPs was computed and plotted against sub-sampling size, revealing that for sample sizes on the order of 100 or 200, the sensitivity was very low (Fig. 4A). Indeed, for a subsample of 100, we estimated a mean sensitivity of only 0.00001, for a subsample of size 200 the mean sensitivity was 0.005, for 300 the value was 0.04, and at a value of 600 (i.e. about half of the full set) the sensitivity was still only 0.35. Thus, in light of this, if we were to now compare aDMPs across different tissue-types with some of the corresponding datasets in the order of 100-200 samples, as done in [12], then even if all aDMPs were shared between tissue-types, we would never be able to detect much overlap and we would wrongly conclude that most

aDMPs are "dataset-specific", i.e. tissue-specific in the context of the analysis presented in [12]. For instance, using a Bonferroni threshold we observed an overlap of "only" 213 aDMPs between the 18596 gold-standard monocyte aDMPs and the 291 aDMPs derived from the 214 CD4+ T-cell samples (Fig. 1B), and so we would be inclined to conclude that most aDMPs are cell-type specific. However, assuming that all aDMPs are shared between monocytes and CD4+ T-cells, our subsampling analysis (Fig. 4A) would suggest that the expected sensitivity to detect the 18596 gold-standard monocyte aDMPs using the 214 T-cell samples would be a value between 0.005 (n=200) and 0.04 (n=300) (Fig. 4A), with the value closer to 0.005. Indeed, under this shared aDMP scenario, the detected overlap of 213 aDMPs represents a sensitivity fraction estimate of 213/18596 ≈ 0.01, in line with our subsampling estimate. Thus, the observed overlap of aDMPs at the given sample sizes of the two studies is not inconsistent with the great majority of aDMPs being shared between monocytes and T-cells. We note that this result is also highly congruent with the statistical significance estimates obtained previously via the Fisher-test (Fig. 1B-C).

We further note that using a more relaxed FDR < 0.05 threshold, sensitivity would be substantially higher: at about n=600, sensitivity is already close to 1, and for 300 samples, sensitivity is over 0.4 (Fig. 4B). Thus, when comparing aDMPs between multiple cell or tissue-types it is even more critical to use FDR-based thresholds, since otherwise using Bonferroni-based adjustment, the expected overlap of aDMPs derived from say 4 separate studies will be zero, even if all aDMPs are common to all 4 cell/tissue-types. Our analysis suggests that many hundreds if not thousands of samples would be needed to ensure that overlaps over 3 or more studies would have the appropriate sensitivity to detect the majority of shared aDMPs (Fig. 4A-B). We verified that all these results are independent of whether an additional threshold on the effect size is used to select aDMPs (Fig. 4C). Indeed, using an additional and identical threshold on the effect size to define aDMPs as used in [12], i.e demanding at least a 2% change in DNAm over 10 years in addition to Bonferroni significance, yielded higher sensitivities, but at sample sizes of 100 and 200, the expected sensitivity was still only 0.0002 and 0.05, respectively (Fig. 4C).

Using only a threshold on effect size for feature selection suffers from strong selection bias

If we were to ignore statistical significance estimates (which depend on sample size) altogether, and instead rank features by effect size using the above mentioned threshold (a 2% DNAm change over 10 years) to declare aDMPs, we can see that sensitivities increase

substantially, exhibiting a much lower dependency on sample size (Fig. 4D). For instance, at n=100, the sensitivity would be as high as 0.6 (Fig. 4D). At first, this seems to support the argument by Slieker et al. that an observed lack of overlapping aDMPs defined via an effect size threshold would imply that aDMPs are largely tissue-specific. However, this argument is problematic, primarily for two reasons. First, selecting aDMPs based on effect size still suffers from selection bias, i.e. the fact that in the dataset where aDMPs are selected effect sizes will naturally be higher than in independent studies. This selection bias arises in real data because of numerous study-specific confounders which can significantly inflate or deflate effect sizes. Indeed, our subsampling analysis shows that the sensitivity to detect aDMPs at a sample size of 100 to be approximately 40% lower than at the full sample size (n=1199) (Fig. 4D), which is a substantial reduction given that the subsample derives from the same dataset. While this also demonstrates that using an effect size to rank and select aDMPs does not guarantee that the ranking and selection is independent of sample size, as claimed in [12], we stress that the selection bias will be even more pronounced when comparing across independent studies. Thus, the observation made by Slieker et al. [12] that the effect sizes of aDMPs selected from one dataset appear reduced in another set profiling a different tissue could easily be the result of selection bias, and nothing to do with the nature of the different tissue being profiled.

A second major problem associated with using an effect size threshold to select and validate aDMPs is related to confounding factors such as cell-type heterogeneity, which may artificially deflate effect sizes in spite of associations with age remaining highly significant. To demonstrate this, we posited that the fraction of aDMPs derived in the monocyte set that would validate in a large whole blood set [10] (which contains monocytes) would be much reduced if an effect size criterion is used throughout, as compared to using a statistic and P-value. Confirming this, out of the 844 aDMPs with an effect size larger than 2% over 10 years in the Reynolds monocyte set, only about 40% passed this same threshold across the 656 whole blood samples from Hannum et al. [10] (Fig. 5A-B). While the fraction validating in whole blood was similar if a Bonferroni threshold is used (fraction was 41%), the fraction doubled to 84% if an FDR<0.05 threshold was used instead (Fig. 5B). Thus, using only an effect size threshold to select and evaluate overlap of aDMPs between studies could lower sensitivities by as much as another 40% in relation to using an FDR-based threshold. Of note, using effect size thresholds in the original beta-value basis, which is highly heteroscedastic, may also strongly bias aDMPs towards those

with intermediate DNAm values. Indeed, we verified that selecting aDMPs using the 2% change over 10-year threshold resulted in very few or no aDMPs with mean DNAm values close to 0 or 1 (Fig. 5C). Since the mean DNAm level of a CpG site in a complex tissue may be strongly influenced by cell-type heterogeneity, using an effect size threshold to select or validate aDMPs could therefore easily miss a large fraction of true aDMPs.

In summary, the implicit assumption made by Slieker et al. [12] that the effect size of an aDMP should not depend on sample size and on other factors such as cell-type heterogeneity of the tissue or other confounders, appears to not hold and would lead to the false conclusion that a lack of overlapping aDMPs, all selected using effect size thresholds, is due to a lack of shared aDMPs. In fact, our analysis above clearly indicates that using only effect sizes to select aDMPs could result in a severe overall selection bias, with sensitivities reduced by as much as 80% if not more.

FDR analysis suggests that most of the DNA methylome is altered with age

A clue as to how many aDMPs are cell/tissue specific can also be inferred from the FDR characteristics in the largest datasets. For the 1199 monocyte sample set from Reynolds et al. we used the estimated FDR values (q-values) to further estimate that on average only 52419 of the 482,091 probes (i.e. 10%) are not associated with age, suggesting therefore that approximately 90% of the

DNA methylome is altered with age. Because FDR estimates are notoriously sensitive to confounding factors, it is important to check the consistency of the FDR estimates in Reynolds et al. against those obtained in smaller studies, ideally profiling identical or related cell-types. For the 201 monocyte samples profiled with Illumina 450k as part of BLUEPRINT, we estimated 41% of the probes to be aDMPs, whereas the fraction of aDMPs was similar, around 45%, for the 104 monocyte samples (52 twin pairs) from Paul et al. [22]. In the case of whole blood, in Hannum et al. which encompassed 656 samples and therefore approximately half of the numbers in the Reynolds monocyte set, FDR values yielded an estimate of approximately 66% aDMPs. This value is very close to the one we estimated for the 689 whole blood samples profiled in Liu et al. [5]: the fraction of probes estimated there to be aDMPs was 68%. For a smaller set such as the 263 whole blood samples from FORECEE, FDR values yielded a correspondingly lower estimate of only 12% aDMPs.

Thus, assuming that the fraction of aDMPs (~90%) in the Reynolds monocyte set is inflated due to some confounder, it is unlikely to be inflated by more than 25%, since the fraction of predicted aDMPs in two large whole blood studies was consistently over 65%. This supports the view that a very high fraction (likely to be well over 65%) of the DNA methylome of blood cell subtypes is altered with age, and therefore this also means that there would be a large overlap of aDMPs between any two blood cell subtypes, consistent with
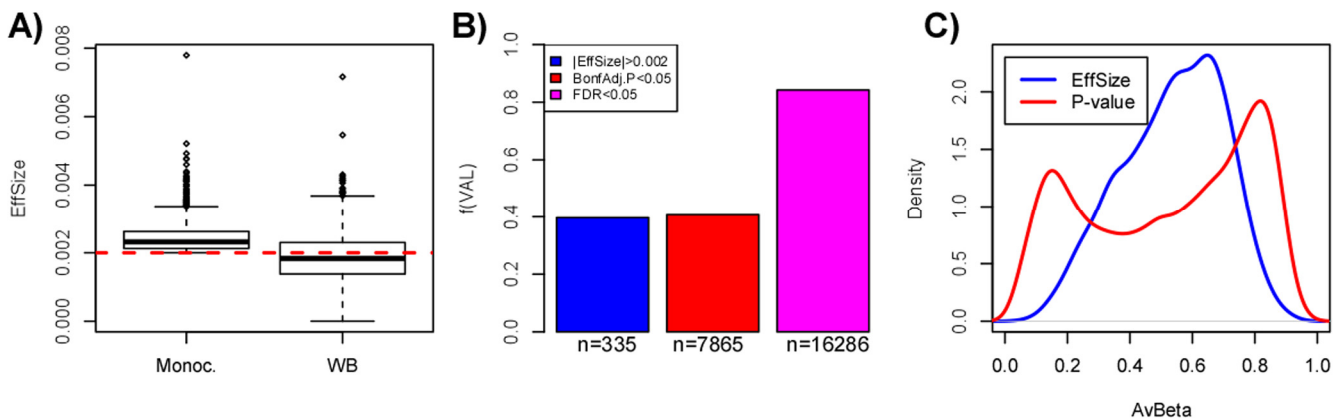
Figure 5. Pitfalls of using a threshold on effect-size only to select aDMPs. (**A**) Boxplots comparing the effect size distribution for the 844 aDMPs defined in the Reynolds monocyte set against their effect sizes in the whole blood dataset from Hannum et al. (**B**) Barplots comparing the fraction of aDMPs, defined either by the effect size threshold (blue) or P-value threshold (red & magenta, Bonferroni-adjusted), that validate in the whole blood set from Hannum et al. In Hannum et al, validated aDMPs were defined either as those passing the same effect size threshold (blue), or the same Bonferroni-threshold (red), or a more relaxed FDR<0.05 threshold (magenta). The numbers below the bars indicate the absolute number of aDMPs validating in Hannum et al. This panel demonstrates that using the same effect size threshold to define aDMPs in a dataset of complex tissue samples could miss up to 40% of true aDMPs. (**C**) Comparison of the density profiles of the average DNAm for the 844 aDMPs defined by having an effect size larger (in absolute magnitude) than 0.002 (equivalent to a 2% DNAm change over 10 years) (blue line) across the 1199 monocyte samples of Reynolds et al., versus the corresponding density profile of the 18596 gold-standard aDMPs with Bonferroni adjusted P-values < 0.05.

our observations. Moreover, the fact that we observe equally strong overlaps of aDMPs between tissues like blood and cervix, further suggests that relatively high fractions of the DNA methylome of other cell-types (e.g. epithelial and fibroblasts) are also altered with age.

Most of Horvath's clock CpGs are pan-tissue aDMPs

Finally, to demonstrate that there are indeed many examples of aDMPs that are shared between tissues, we analyzed in detail the 353 CpGs that make up Horvath's clock [9]. Specifically, we computed their t-statistics and P-values using linear models against age, including potential covariates as confounding factors, across a total of 10 different cell/tissue types, which included Monocytes, CD4+ and CD8+ T-cells, B-cells, Neutrophils, Buccal, Cervix, Liver, Brain and Fibroblasts (Methods). In the case of buccal, cervix and liver we adjusted for variations in the epithelial, fibroblast and immune cell fractions, whereas in the case of brain we adjusted for variations in neuronal and non-neuronal fractions (Methods, Table S1). Although only 3% (i.e 10 CpGs) of the 353 clock CpGs were aDMPs in all 10

tissues, approximately 78% were aDMPs across at least 3 different cell/tissue types, with only 7% appearing to be "tissue or cell-type specific" (Fig. 6, Table S2). The 10 CpGs defining aDMPs in all 10 tissue/cell types mapped to genes that included *VGF, GRIA2, FZD9, KLF14, RHBDD1, KCNC2, NHLRC1, P2RX6* and *CECR6*. Of note, *FZD9* is a transmembrane receptor for Wnt signaling proteins, whilst *GRIA2* is a glutamate neurotransmitter receptor, both of which have previously been demonstrated to be part of interactome "hotspots" of age-associated DNAm which occur independently of cell or tissue-type [23]. Thus, this confirms that *ELOVL2* is not unique and that many of Horvath's clock CpGs constitute aDMPs across several cell/tissue types.

DISCUSSION

Here we have tried to address what appears to be an apparent paradox between a number of studies reporting pan-tissue epigenetic clocks that yield DNAm-based correlates of age independently of cell or tissue-type [9, 13, 14], and a recent study suggesting that only sites mapping to the *ELOVL2* promoter constitute cell and
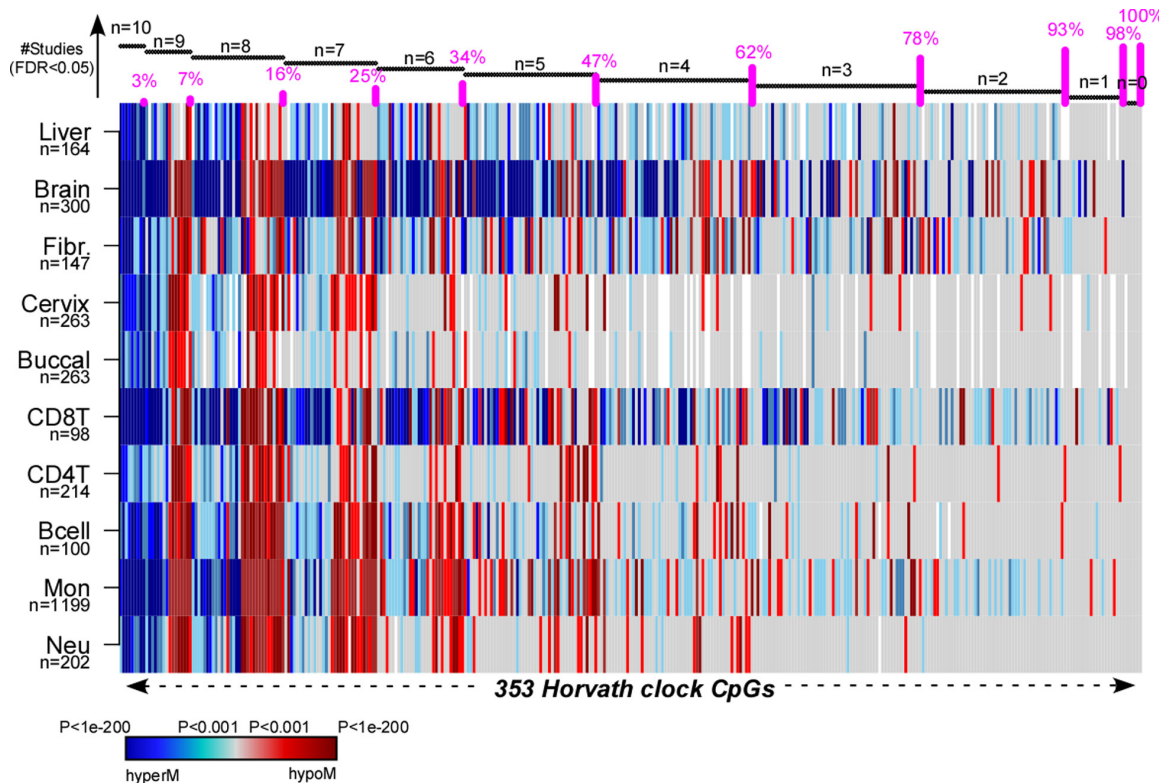
Figure 6. Pan-tissue analysis of Horvath's clock CpGs. Heatmap displays the signed P-values of the 353 Horvath Clock CpGs across 10 independent cell or tissue-types, where the P-values derive from a linear model of DNAm against age plus additional confounders as covariates. Blue denotes highly significantly age-associated hypermethylation (hyperM), red denotes highly significant hypomethylation (hypoM). The 353 clock CpGs have been ranked according to the number of cell/tissue types where they are age-DMPs (using FDR<0.05), indicated by horizontal black bars at top. The cumulative proportion of the 353 CpGs that are age-DMPs in 10, 9, 8, 7, 6, 5, 4, 3, 2 or 1 studies are shown as vertical bars.

tissue-type independent aDMPs [12]. While we agree with Slieker et al. [12] that specific sites mapping to *ELOVL2* are special aDMPs in the sense that their effect sizes are particularly large across a number of different tissue-types, our analysis suggests that most aDMPs are valid across multiple different tissue types, suggesting that shared aDMPs are common.

In a nutshell, their argument was based on a lack of "substantial overlap" of aDMPs derived from different tissues, either when using a very stringent Bonferroni-adjusted threshold, or when using a threshold on the effect size, which in principle is sample-size independent. In our view, this analysis is problematic. First of all, to state that overlaps of aDMPs were not substantial without assessing the statistical significance of the overlaps themselves is a common pitfall not unique to their study. The expected number of over-lapping aDMPs will naturally be small if a very stringent Bonferroni correction is used to define aDMPs. Even so, and as demonstrated here using several multi-tissue and multi-cell type EWAS, the overlaps using Bonferroni thresholds were highly statistically significant, a strong cue that the number of overlapping aDMPs between tissues and cell-types is not random. Indeed, using a more relaxed FDR<0.05 threshold, we have seen that there are at least thousands of aDMPs that are shared between blood cell-subtypes and also between unrelated tissues such as blood, cervix and buccal.

Second, the use of a very stringent Bonferroni threshold is specially misleading since most of the studies analysed in [12] were not adequately powered. Indeed, we devised an empirical subsampling analysis, which clearly demonstrated that datasets profiling only a few hundred samples or less are inadequate for assessing overlaps of aDMPs. If using Bonferroni thresholds, our power analysis suggests that many hundreds if not a thousand samples in individual studies are needed to achieve the desired high sensitivities across independent studies. We stress that these power estimates are true even for studies profiling the same cell or tissue-type, and therefore to reject the null hypothesis that most aDMPs are cell-type independent would require studies at least as large as these. That many hundreds if not thousands of samples are needed to detect large numbers of overlapping aDMPs should not be surprising: indeed, it has long been known that the ranking of features derived from large omic datasets is extremely unstable, requiring sample sizes in the order of thousands to ensure robustness of rankings under even small sample perturbations [24]. This applies particularly to data and phenotypes characterized by small effect sizes, and would therefore apply to the case of DNAm and age. Indeed, Principal Component

Analysis (PCA) on whole blood sets has consistently revealed that age-associated components of DNAm variation are generally only ranked 5th or 6th [7, 25], which typically account only for a relatively small proportion (usually around 1%) of the total DNAm data variance. Thus, overlap analysis of aDMPs between pairs, or several groups, of datasets is potentially very misleading if effect sizes are small and if specific datasets are not adequately powered.

The third key problem is the use a threshold on the effect size as the sole criterion to select aDMPs, and to subsequently argue that the lack of overlap of aDMPs is not due to lack of power. While we agree that the effect size is in principle not dependent on sample-size, the lack of overlap of aDMPs defined in this way could be due to other factors. Indeed, our subsampling analysis indicated that even when using only an effect size threshold to select aDMPs, that this could still lead to reductions in sensitivity of at least 40% in studies containing only a hundred or a few hundred samples. This "selection bias", which naturally inflates the effect sizes of the features in the studies they were derived from in comparison to other independent studies, can be further aggravated by confounders such as cell-type heterogeneity. For instance, we have demonstrated how the sensitivity to detect aDMPs defined in a pure cell-type is reduced by as much as another 40% if assessed in a cell-type mixture such as blood. Thus, overall, using only effect size thresholds to define aDMPs across tissues or cell-types could result in sensitivities to detect shared aDMPs being reduced by as much as 80% if not more. Moreover, we have shown that selected aDMPs whose effect sizes marginally miss what is an arbitrary threshold of 2% DNAm change over 10-years in independent datasets, could still be highly significantly associated with age in these same sets.

We further note that using only an effect size to select interesting features represents a "step-back" to the very old days when microarray data was first analysed, and when using thresholds on "fold-changes" in gene-expression was a common procedure. In those days, fold-changes were used because no, or very few, replicate samples were available. It was soon realized however that improved statistical inference is achieved by ranking features by a statistic. It is therefore surprising and also extremely unlikely, that an analysis based only on effect sizes can lead to critical insight not obtainable via statistics. Of note, imposing a threshold on the effect size after selecting features by statistics is a perfectly acceptable procedure.

Another related problem of using only a threshold on effect sizes to select features and which applies specifically to DNAm data, is the heteroscedasticity of

beta-values [26]. Indeed, as shown here, performing such feature selection directly on beta-values could aggravate the selection bias even further by tuning the selection of aDMPs to those exhibiting intermediate average DNAm values. This is particularly relevant in the context of assessing tissue-specificity of aDMPs, since many of the enhancer regions that are known to be highly cell-type specific would naturally exhibit such intermediate levels of DNAm. Thus, the average DNAm of such regions may be particularly variable across studies profiling different tissues, which could lead to a high FNR and reduced power.

Irrespective of all the above statistical issues, there are other strong arguments supporting the view that shared aDMPs between cell and tissue-types is the norm and not the exception. First, is the observation that in the largest studies, FDR estimates consistently indicate that most of the DNA methylome is altered with age. Using the 1199 monocyte samples from Reynolds we estimated that over 90% of the Illumina 450k probes are aDMPs. Somewhat smaller but still relatively high fractions of approximately 65% were obtained in two separate large (n>650) whole blood studies. We further note that overlaps between aDMPs from different tissues like cervix, buccal and blood were as strong as those seen between different blood cell subtypes, a strong indication that for other cell-types, say epithelial and fibroblasts, most of the DNA methylome is altered with age (as otherwise it is unlikely that we would observe such strong overlaps). Second, that most of the DNA methylome is altered with age is also highly consistent with the report of large (>1Mb) age hypomethylated blocks where sites that are normally methylated lose DNAm, and with CpG islands contained within these blocks (where sites are normally unmethylated) gaining DNAm [27, 28]. Thus, if these large-scale age-associated DNAm alterations apply to cell-types generally, and we see no good reason why they should not, shared aDMPs must be the norm, not the exception. Third, we and others [7, 13, 29, 30] have observed how specific PRC2 marked sites in the genome, which are constitutively unmethylated across many fetal tissue types, consistently acquire DNAm during aging, independently of tissue or cell-type. It could well be that these specific cell-type independent aDMPs were missed in the analysis of Slieker et al. due to lack of power and the use of an effect-size threshold which would bias selection against these particular sites, since these exhibit low average DNAm. Fourth, the existence of pan-tissue epigenetic clocks which can reliably predict chronological age independently of tissue or cell-type is unlikely to happen if not for a substantial number of shared aDMPs. Indeed, we estimated that at most only 7% of the 353 CpGs making up Horvath's clock may be tissue or cell-type specific.

For other aDMPs, we estimate that at the very most only 30% to 35% are cell or tissue-type specific since this is the estimated fraction of non age-DMPs in blood cell-types, and only these could be called cell-type specific aDMPs in other non-blood cell-types. Fifth, the special status of *ELOVL2* as defining the only tissue-independent aDMPs is questionable, since according to our analysis, at least another 10 CpGs mapping to unrelated genes (e.g. *FZD9, GRIA2*) constitute aDMPs across at least 10 different cell/tissue types, with almost 80% of the 353 Horvath clock CpGs defining aDMPs across at least 3 cell/tissue types.

There are of course several caveats to our analysis, which however also apply to the study of Slieker et al. [12]. First is the lack of studies profiling thousands of purified cell-types. As our empirical power analysis strongly indicates, thousands of samples would be needed to reliably determine which loci are age and not age-associated, and sample purity is important to remove cell-type composition as a potential confounder. It should be noted that even for FACS sorted cell populations, these are still only a composite and that age-associated variations in the underlying subpopulations may account for aDMPs that survive cell-type adjustment at a coarser resolution level. Another caveat is that not all tissue and cell-types analysed here derived from the same individuals, meaning that comparisons between tissues can be problematic due to differences in age-range, age distribution, gender and other study-specific factors, all of which can affect genome-wide statistical significance estimates and confound analyses. On the other hand, our analysis did include one matched multi cell-type and one matched multi tissue-type DNAm dataset, in each case encompassing 3 different cell/tissue types from the same individuals, for which age-distribution and sex were perfectly matched. Results derived from these matched DNAm sets were in line with those obtained using unmatched sets, suggesting that the unmatched nature of some of the datasets is not a major limitation. In future however, it will be important to profile thousands of highly purified samples from a significant number of different cell-types, all from the same individuals to rigorously establish the fraction of aDMPs that are shared between cell-types.

Finally, we discuss the potential implications of our findings. First, it is important to point out that even if age-associated DNAm changes are widespread across the genome that downstream functional effects may be rare. There are several reasons why this would be the case. First, we have previously observed that age-associated promoter hypermethylation in blood occurred mostly at genes that are not expressed at birth (cord blood), while age-associated hypomethylation was

seen mostly at genes that were expressed [28]. Thus, it would appear that a substantial proportion of aDMPs at regulatory elements may only act to stabilize pre-existing gene expression levels, and therefore will be non-functional. Second, most aDMPs are characterized by relatively small changes in DNAm (typically only about 1-5% over a decade), which means that the changes are occurring only in a relatively small fraction (1-5%) of the cells present in the tissue. Thus, while age-associated DNAm changes may affect gene expression in these 1-5% of cells, when averaged across the whole tissue, the associated mRNA changes are likely to be insignificant, without affecting tissue/organ function. As far as the tissue-specificity of aDMPs is concerned, we remark that although our analysis points towards shared aDMPs between cell-types being the norm and not the exception, that functional effects of epigenetic drift may nevertheless be tissue-specific. A concrete example is that of CpG sites mapping to the promoter of the *HAND2* gene, a target gene of the progesterone receptor. It has been indicated that gradual age-associated epigenetic silencing of *HAND2* in the endometrial stroma could inactivate the progesterone tumor suppressor pathway, sensitizing endometrial epithelial cells to oncogenic oestrogen, thus pre-disposing them to carcinogenic transformation [31]. Interestingly, *HAND2* promoter sites have also been observed to undergo hypermethylation with age in blood [28], yet the potential functional and biological significance of this hypermethylation in blood is unclear. Thus, while specific aDMPs may be shared between tissue-types, it is only in specific tissues or cell-types that any associated functional deregulation may be of biological and clinical significance. It will be interesting for future studies to investigate whether the example of *HAND2* could serve as a more general paradigm for how shared aDMPs may exhibit functional effects in a tissue-specific manner.

In summary, our novel analysis of existing datasets suggests that aDMPs shared between different cell and tissue-types is common, and not exceptional. We estimate at most 30% of aDMPs to be cell-or-tissue-type specific.

METHODS

DNAm datasets

DNAm data from purified blood cell types
We used Illumina 450k DNAm data from Reynolds et al. [17], encompassing DNAm profiles for 1202 purified monocyte and 214 CD4+ T-cell samples. Data was downloaded from GEO (GEO accession numbers: GSE56581, GSE56046) and further processed and normalized as described by us previously [13]. Because

of confounding by gender and race, we removed 3 monocyte samples which had unique gender/race combination, leaving a total of 1199 monocyte samples. Age range for monocytes was 44 to 83. Age range for CD4+ T-cells was 45 to 79. The CD8+ T cell data was derived from Tserel et al. [18] (GEO accession number: GSE59065), containing 100 CD8+ T cell samples, with age ranging between 22 and 84. The raw data was normalized with BMIQ [32]. Blueprint data was derived from the European Genome-phenome Archive (EGA accession number: EGAS00001001456, BLUEPRINT study) [19], containing 139 CD4+ naive T-cells, 202 Neutrophil and 201 Monocyte samples with age range between 22 and 77. For the matched multi cell-type aDMP analysis we used the 139 individuals with all 3 cell-types measured. Data was normalized as described previously [19].

Multi-tissue (blood, buccal and cervix) DNAm dataset
DNA methylation data encompassing whole blood, buccal swabs and cervical smears from 272 women were obtained as part of the ethically approved FORECEE study [33]. Briefly, samples from five different European centres were sent to UCL for storage at -80C until DNA extraction. DNA extraction was performed using a Zymo spin column system. Genome-wide DNA methylation was profiled using the Infinium MethylationEPIC BeadChips (Illumina). In the case of blood and cervical samples, 500ng of genomic DNA were bisulfite convert-ed, whereas in the case of buccal swabs, where yields were lower, 200ng were used. Pilot data had confirmed the use of 200ng to be sufficient for reliable assay-perfor-mance. BeadChips were processed by UCL Genomics using the standard recommended protocol. DNA was hybridized to BeadChips and single nucleotide extension followed by immunohisto-chemistry were performed using a Freedom EVO robot (Tecan). BeadChips were subsequently imaged using the iScan Microarray Scanner (Illumina). All idat files were then processed with minfi (v.1.22) using the Illumina definition of beta-value. Using the detection P-values estimated by minfi, we first computed coverage per probe (fraction of samples with detection P-value < 0.05), removing low quality probes (coverage < 0.99) and subsequently computing coverage per sample over the good-quality probes, removing low quality samples (coverage < 0.95). The small remaining number of missing values were imputed using impute.knn (with k=5) from the impute R-package [34]. Raw data and all idat files are available from GEO under accession number GSE117370.

Liver DNAm dataset
We constructed a merged Illumina 450k set by combining BMIQ normalized data from two separate studies (GSE61258 & GSE48325). The merged set was defined over 417,123 probes and 164 samples.

Fibroblast DNAm dataset

We used the Illumina DNAm 450k dataset from [35], consisting of a merged set of 147 fibroblast samples.

Brain DNAm dataset

We downloaded the Illumina DNAm 450k set GSE74193 [36] from GEO. Only control non-fetal samples were used (n=300). Probes were removed if the fraction of failed samples (p>0.01) was more than 0.25, otherwise values were imputed using impute.knn function. The resulting matrix had 473536 probes left. Subsequently type-2 probe bias was normalized with BMIQ.

Construction of brain DNAm reference

We used the Illumina DNAm 450k Brain reference dataset [37] in RGSet object format from Bioconductor package FlowSorted.DLPFC.450k. It was then processed with minfi (v.1.22) using the Illumina definition of beta-value. Using the detection P-values estimated by minfi, we first computed coverage per probe (fraction of samples with detection P-value < 0.05), removing low quality probes (coverage < 0.99). The small remaining number of missing values were imputed using impute.knn (with k=5) from the impute R-package [34]. The resulting beta value matrix had 471209 probes left and 58 samples with half of them being neurons and the other being non-neurons. We compared neuron samples to non-neuron samples to derive DMCs requiring Bonferroni adjusted P value threshold 0.05 from moderated t test. DMCs were filtered further by demanding at least a 70% DNAm difference between neurons and non-neurons.

.
Identification of age-DMPs

In each dataset we used linear models with the DNAm value as the response variable and with age of the sample as the predictor. Depending on the dataset, linear models were run with additional covariates to account for potential confounding factors. In the case of purified cell samples, covariates included those provided by the publications which included batch or ethnicity information. In the case of Reynolds et al., age-DMPs were derived by linear regression on 482127 (CD4T) and 482091 (Monocytes) probes, with gender and race as covariates (which dominated variation as determined by a PCA). In the case of the CD8+ T-cells, age-DMPs were derived by linear regression on 472484 probes, with gender and array number as covariates (which dominated variation as determined by a PCA). In the case of Blueprint data, age-DMPs were derived by linear regression on 473719 probes, with gender and batch number as covariates (which dominated variation as determined by a PCA).

In the case of complex tissues, besides adjusting for batch effects (if these were present), we also corrected for cell-type heterogeneity. Briefly, in the case of whole blood, we used our previously validated DNAm reference matrix for blood with our EpiDISH algorithm [21] to obtain cell-type fraction estimates for the 7 main immune cell subtypes: neutrophils, basophils, monocytes, B-cells, NK-cells, CD4+ and CD8+ T-cells. In the case of other tissues, like buccal and cervix, we used the corresponding DNAm reference matrix from our HEpiDISH algorithm [15] to obtain cell-type fractions for the total epithelial, total fibroblast and the 7 main immune cell subtypes. In the case of liver, we derived aDMPs using sex, body-mass index, cohort and cell-type fractions as covariates. In each case, the estimated cell-type fractions were used as covariates in the linear models. In the case of brain, we derived aDMPs using sex, plate, position and brain cell fraction (neuron and non-neuron) as covariates.

Age-DMPs (aDMPs) were generally defined at two distinct thresholds: at a false discovery rate (FDR) threshold less than 0.05, where FDR values were estimated using the *q-value* procedure [38], and using a much more conservative Bonferroni threshold (P < $0.05/n$ with n the number of probes for which the linear model was run).

Subsampling power analysis in Reynolds Monocyte set

We used the large (n=1199) purified monocyte sample set from Reynolds et al. to define a gold-standard list of 18596 monocyte aDMPs using a Bonferroni threshold. We then subsampled 100, 200, 300, 400, 500, 600, 700, 800, 900, 1000 samples from the original 1199 and redefined aDMPs at each subsampling size using the same Bonferroni threshold. At each subsample size we estimated the sensitivity to detect the 18596 aDMPs from the full set. A total of 10 different runs were performed at each subsample size. We also derived aDMPs and sensitivities at each subsample size but now using an FDR<0.05 threshold. Because the FDR estimation is more unstable, we performed 100 different Monte-Carlo runs at each subsampling size.

The whole analysis above was repeated by defining aDMP by the additional requirement, that the effect size (i.e. slope) is larger than 2% over 10 years, i.e. a slope value of absolute magnitude larger than 0.002, which is the effect size threshold used in [12]. In a final analysis, we repeated the procedure but now defining aDMPs using only the threshold on the effect size, discarding statistics and P-values.

Data availability

All data analyzed in this manuscript are publicly available from EGA https://ega-archive.org/ accession number EGAS00001001456 and GEO (http:www.ncbi.nlm.nih.gov/geo/) under accession numbers GSE117370, GSE56581, GSE56046 and GSE59065.

CONFLICTS OF INTEREST

The authors declare that they have no competing interests.

FUNDING

REFERENCES

1. Ahuja N, Li Q, Mohan AL, Baylin SB, Issa JP. Aging and DNA methylation in colorectal mucosa and cancer. Cancer Res. 1998; 58:5489–94.

2. Ahuja N, Issa JP. Aging, methylation and cancer. Histol Histopathol. 2000; 15:835–42.
https://doi.org/10.14670/HH-15.835

3. Fraga MF, Ballestar E, Paz MF, Ropero S, Setien F, Ballestar ML, Heine-Suñer D, Cigudosa JC, Urioste M, Benitez J, Boix-Chornet M, Sanchez-Aguilera A, Ling C, et al. Epigenetic differences arise during the lifetime of monozygotic twins. Proc Natl Acad Sci USA. 2005; 102:10604–09.
https://doi.org/10.1073/pnas.0500398102

4. Christensen BC, Houseman EA, Marsit CJ, Zheng S, Wrensch MR, Wiemels JL, Nelson HH, Karagas MR, Padbury JF, Bueno R, Sugarbaker DJ, Yeh RF, Wiencke JK, Kelsey KT. Aging and environmental exposures alter tissue-specific DNA methylation dependent upon CpG island context. PLoS Genet. 2009; 5:e1000602.
https://doi.org/10.1371/journal.pgen.1000602

5. Liu Y, Aryee MJ, Padyukov L, Fallin MD, Hesselberg E, Runarsson A, Reinius L, Acevedo N, Taub M, Ronninger M, Shchetynsky K, Scheynius A, Kere J, et al. Epigenome-wide association data implicate DNA methylation as an intermediary of genetic risk in rheumatoid arthritis. Nat Biotechnol. 2013; 31:142–47. https://doi.org/10.1038/nbt.2487

6. Houseman EA, Accomando WP, Koestler DC, Christensen BC, Marsit CJ, Nelson HH, Wiencke JK, Kelsey KT. DNA methylation arrays as surrogate measures of cell mixture distribution. BMC Bioinformatics. 2012; 13:86.
https://doi.org/10.1186/1471-2105-13-86

7. Teschendorff AE, Menon U, Gentry-Maharaj A, Ramus SJ, Weisenberger DJ, Shen H, Campan M, Noushmehr H, Bell CG, Maxwell AP, Savage DA, Mueller-Holzner E, Marth C, et al. Age-dependent DNA methylation of genes that are suppressed in stem cells is a hallmark of cancer. Genome Res. 2010; 20:440–46.
https://doi.org/10.1101/gr.103606.109

8. Weidner CI, Lin Q, Koch CM, Eisele L, Beier F, Ziegler P, Bauerschlag DO, Jöckel KH, Erbel R, Mühleisen TW, Zenke M, Brümmendorf TH, Wagner W. Aging of blood can be tracked by DNA methylation changes at just three CpG sites. Genome Biol. 2014; 15:R24.
https://doi.org/10.1186/gb-2014-15-2-r24

9. Horvath S. DNA methylation age of human tissues and cell types. Genome Biol. 2013; 14:R115.
https://doi.org/10.1186/gb-2013-14-10-r115

10. Hannum G, Guinney J, Zhao L, Zhang L, Hughes G, Sadda S, Klotzle B, Bibikova M, Fan JB, Gao Y, Deconde R, Chen M, Rajapakse I, et al. Genome-wide methylation profiles reveal quantitative views of human aging rates. Mol Cell. 2013; 49:359–67.
https://doi.org/10.1016/j.molcel.2012.10.016

11. Bocklandt S, Lin W, Sehl ME, Sánchez FJ, Sinsheimer JS, Horvath S, Vilain E. Epigenetic predictor of age. PLoS One. 2011; 6:e14821.
https://doi.org/10.1371/journal.pone.0014821

12. Slieker RC, Relton CL, Gaunt TR, Slagboom PE, Heijmans BT. Age-related DNA methylation changes are tissue-specific with ELOVL2 promoter methylation as exception. Epigenetics Chromatin. 2018; 11:25.
https://doi.org/10.1186/s13072-018-0191-3

13. Yang Z, Wong A, Kuh D, Paul DS, Rakyan VK, Leslie RD, Zheng SC, Widschwendter M, Beck S, Teschendorff AE. Correlation of an epigenetic mitotic clock with cancer risk. Genome Biol. 2016; 17:205.
https://doi.org/10.1186/s13059-016-1064-3

14. Levine ME, Lu AT, Quach A, Chen BH, Assimes TL, Bandinelli S, Hou L, Baccarelli AA, Stewart JD, Li Y, Whitsel EA, Wilson JG, Reiner AP, et al. An epigenetic biomarker of aging for lifespan and healthspan. Aging (Albany NY). 2018; 10:573–91.
https://doi.org/10.18632/aging.101414

15. Zheng SC, Webster AP, Dong D, Feber A, Graham DG, Sullivan R, Jevons S, Lovat LB, Beck S, Widschwendter M, Teschendorff AE. A novel cell-type deconvolution algorithm reveals substantial contamination by

immune cells in saliva, buccal and cervix. Epigenomics. 2018; 10:925–40. https://doi.org/10.2217/epi-2018-0037

16. Jaffe AE, Irizarry RA. Accounting for cellular heterogeneity is critical in epigenome-wide association studies. Genome Biol. 2014; 15:R31. https://doi.org/10.1186/gb-2014-15-2-r31

17. Reynolds LM, Taylor JR, Ding J, Lohman K, Johnson C, Siscovick D, Burke G, Post W, Shea S, Jacobs DR Jr, Stunnenberg H, Kritchevsky SB, Hoeschele I, et al. Age-related variations in the methylome associated with gene expression in human monocytes and T cells. Nat Commun. 2014; 5:5366. https://doi.org/10.1038/ncomms6366

18. Tserel L, Kolde R, Limbach M, Tretyakov K, Kasela S, Kisand K, Saare M, Vilo J, Metspalu A, Milani L, Peterson P. Age-related profiling of DNA methylation in CD8+ T cells reveals changes in immune response and transcriptional regulator genes. Sci Rep. 2015; 5:13107. https://doi.org/10.1038/srep13107

19. Chen L, Ge B, Casale FP, Vasquez L, Kwan T, Garrido-Martín D, Watt S, Yan Y, Kundu K, Ecker S, Datta A, Richardson D, Burden F, et al. Genetic Drivers of Epigenetic and Transcriptional Variation in Human Immune Cells. Cell. 2016; 167:1398–1414.e24. https://doi.org/10.1016/j.cell.2016.10.026

20. Leek JT, Scharpf RB, Bravo HC, Simcha D, Langmead B, Johnson WE, Geman D, Baggerly K, Irizarry RA. Tackling the widespread and critical impact of batch effects in high-throughput data. Nat Rev Genet. 2010; 11:733–39. https://doi.org/10.1038/nrg2825

21. Teschendorff AE, Breeze CE, Zheng SC, Beck S. A comparison of reference-based algorithms for correcting cell-type heterogeneity in Epigenome-Wide Association Studies. BMC Bioinformatics. 2017; 18:105. https://doi.org/10.1186/s12859-017-1511-5

22. Paul DS, Teschendorff AE, Dang MA, Lowe R, Hawa MI, Ecker S, Beyan H, Cunningham S, Fouts AR, Ramelius A, Burden F, Farrow S, Rowlston S, et al. Increased DNA methylation variability in type 1 diabetes across three immune effector cell types. Nat Commun. 2016; 7:13555. https://doi.org/10.1038/ncomms13555

23. West J, Beck S, Wang X, Teschendorff AE. An integrative network algorithm identifies age-associated differential methylation interactome hotspots targeting stem-cell differentiation pathways. Sci Rep. 2013; 3:1630. https://doi.org/10.1038/srep01630

24. Ein-Dor L, Kela I, Getz G, Givol D, Domany E. Outcome signature genes in breast cancer: is there a unique set? Bioinformatics. 2005; 21:171–78.

https://doi.org/10.1093/bioinformatics/bth469

25. Teschendorff AE, Menon U, Gentry-Maharaj A, Ramus SJ, Gayther SA, Apostolidou S, Jones A, Lechner M, Beck S, Jacobs IJ, Widschwendter M. An epigenetic signature in peripheral blood predicts active ovarian cancer. PLoS One. 2009; 4:e8274. https://doi.org/10.1371/journal.pone.0008274

26. Du P, Zhang X, Huang CC, Jafari N, Kibbe WA, Hou L, Lin SM. Comparison of Beta-value and M-value methods for quantifying methylation levels by microarray analysis. BMC Bioinformatics. 2010; 11:587. https://doi.org/10.1186/1471-2105-11-587

27. Vandiver AR, Irizarry RA, Hansen KD, Garza LA, Runarsson A, Li X, Chien AL, Wang TS, Leung SG, Kang S, Feinberg AP. Age and sun exposure-related widespread genomic blocks of hypomethylation in nonmalignant skin. Genome Biol. 2015; 16:80. https://doi.org/10.1186/s13059-015-0644-y

28. Yuan T, Jiao Y, de Jong S, Ophoff RA, Beck S, Teschendorff AE. An integrative multi-scale analysis of the dynamic DNA methylation landscape in aging. PLoS Genet. 2015; 11:e1004996. https://doi.org/10.1371/journal.pgen.1004996

29. Nejman D, Straussman R, Steinfeld I, Ruvolo M, Roberts D, Yakhini Z, Cedar H. Molecular rules governing de novo methylation in cancer. Cancer Res. 2014; 74:1475–83. https://doi.org/10.1158/0008-5472.CAN-13-3042

30. Chen Y, Breeze CE, Zhen S, Beck S, Teschendorff AE. Tissue-independent and tissue-specific patterns of DNA methylation alteration in cancer. Epigenetics Chromatin. 2016; 9:10. https://doi.org/10.1186/s13072-016-0058-4

31. Jones A, Teschendorff AE, Li Q, Hayward JD, Kannan A, Mould T, West J, Zikan M, Cibula D, Fiegl H, Lee SH, Wik E, Hadwin R, et al. Role of DNA methylation and epigenetic silencing of HAND2 in endometrial cancer development. PLoS Med. 2013; 10:e1001551. https://doi.org/10.1371/journal.pmed.1001551

32. Teschendorff AE, Marabita F, Lechner M, Bartlett T, Tegner J, Gomez-Cabrero D, Beck S. A beta-mixture quantile normalization method for correcting probe design bias in Illumina Infinium 450 k DNA methylation data. Bioinformatics. 2013; 29:189–96. https://doi.org/10.1093/bioinformatics/bts680

33. Widschwendter M, Jones A, Evans I, Reisel D, Dillner J, Sundström K, Steyerberg EW, Vergouwe Y, Wegwarth O, Rebitschek FG, Siebert U, Sroczynski G, de Beaufort ID, et al, and FORECEE (4C) Consortium. Epigenome-based cancer risk prediction: rationale, opportunities and challenges. Nat Rev Clin Oncol. 2018; 15:292–309.

https://doi.org/10.1038/nrclinonc.2018.30

34. Troyanskaya O, Cantor M, Sherlock G, Brown P, Hastie T, Tibshirani R, Botstein D, Altman RB. Missing value estimation methods for DNA microarrays. Bioinformatics. 2001; 17:520–25.
https://doi.org/10.1093/bioinformatics/17.6.520

35. Horvath S, Oshima J, Martin GM, Lu AT, Quach A, Cohen H, Felton S, Matsuyama M, Lowe D, Kabacik S, Wilson JG, Reiner AP, Maierhofer A, et al. Epigenetic clock for skin and blood cells applied to Hutchinson Gilford Progeria Syndrome and *ex vivo* studies. Aging (Albany NY). 2018; 10:1758–75.
https://doi.org/10.18632/aging.101508

36. Jaffe AE, Gao Y, Deep-Soboslay A, Tao R, Hyde TM, Weinberger DR, Kleinman JE. Mapping DNA methylation across development, genotype and schizophrenia in the human frontal cortex. Nat Neurosci. 2016; 19:40–47.
https://doi.org/10.1038/nn.4181

37. Guintivano J, Aryee MJ, Kaminsky ZA. A cell epigenotype specific model for the correction of brain cellular heterogeneity bias and its application to age, brain region and major depression. Epigenetics. 2013; 8:290–302. https://doi.org/10.4161/epi.23924

38. Storey JD, Tibshirani R. Statistical significance for genomewide studies. Proc Natl Acad Sci USA. 2003; 100:9440–45.
https://doi.org/10.1073/pnas.1530509100

SUPPLEMENTARY MATERIAL

Please browse the Full Text version to see the data of Supplementary Tables.

Table S1. Contains the DNAm reference matrix for estimating neuronal and non-neuronal fractions in a brain sample.

Table S2. Contains the t-statistics and P-values of age-association for all 353 Horvath clock CpGs across 10 tissue/cell types with CpGs ranked according to number of tissue/cell types in which they are significant.

A multi-tissue full lifespan epigenetic clock for mice

Michael J. Thompson[1],[*], Karolina Chwiałkowska[2], Liudmilla Rubbi[1], Aldons J. Lusis[3], Richard C. Davis[3], Anuj Srivastava[4], Ron Korstanje[5], Gary A. Churchill[5], Steve Horvath[6],[*], Matteo Pellegrini[1],[*]

[1]Molecular, Cell and Developmental Biology, University of California Los Angeles, Los Angeles, CA 90095, USA
[2]Centre for Bioinformatics and Data Analysis, Medical University of Bialystok, Bialystok, Poland
[3]Department of Microbiology, Immunology and Molecular Genetics, Department of Medicine, and Department of Human Genetics, University of California Los Angeles, Los Angeles CA 90095, USA
[4]The Jackson Laboratory, Farmington, CT 06032, USA
[5]The Jackson Laboratory, Bar Harbor, Maine 04609, USA
[6]Department of Human Genetics and Biostatistics, University of California Los Angeles, Los Angeles CA 90095, USA
[*] Equal contribution

Correspondence to: Steve Horvath; **email:** shorvath@mednet.ucla.edu

ABSTRACT

Human DNA-methylation data have been used to develop highly accurate biomarkers of aging ("epigenetic clocks"). Recent studies demonstrate that similar epigenetic clocks for mice (*Mus Musculus*) can be slowed by gold standard anti-aging interventions such as calorie restriction and growth hormone receptor knock-outs. Using DNA methylation data from previous publications with data collected in house for a total 1189 samples spanning 193,651 CpG sites, we developed 4 novel epigenetic clocks by choosing different regression models (elastic net- versus ridge regression) and by considering different sets of CpGs (all CpGs vs highly conserved CpGs). We demonstrate that accurate age estimators can be built on the basis of highly conserved CpGs. However, the most accurate clock results from applying elastic net regression to all CpGs. While the anti-aging effect of calorie restriction could be detected with all types of epigenetic clocks, only ridge regression based clocks replicated the finding of slow epigenetic aging effects in dwarf mice. Overall, this study demonstrates that there are trade-offs when it comes to epigenetic clocks in mice. Highly accurate clocks might not be optimal for detecting the beneficial effects of anti-aging interventions.

INTRODUCTION

Our understanding of age-related epigenetic changes in DNA-methylation in humans has progressed rapidly with the technical advancement of genomic platforms [1-14]. For mammalian genomes, DNA methylation is a modification that regulates gene expression via its presence or absence at gene promoters and enhancers. During development, germline DNA methylation is erased, but re-established in tissue-specific patterns as tissue development programs unfold after implantation [15]. Age-based methylation changes accompany the functional decline of adult stem cells [16-18], and even small changes can lead to loss of regulatory control of gene transcription, either directly or via additive effects [19].

The correlation between chronological age and DNA methylation over the course of an entire lifespan is strong [20-23]. Recent studies have taken advantage of this relationship to accurately estimate chronological age based on the methylation levels of multiple CpG

dinucleotides [10, 13, 24]. For example, the human multi-tissue epigenetic age estimation method combines the weighted average of DNA methylation levels of 353 CpGs into an age estimate that is referred to as DNAm age or epigenetic age [13]. Most importantly, we and others have shown that human epigenetic age relates to biological age, not just chronological age. This is demonstrated by the finding that the discrepancy between DNAm age and chronological age (what we term "epigenetic age acceleration") is predictive of all-cause mortality even after adjusting for a variety of known risk factors [25-29]. Epigenetic age acceleration is associated with lung cancer risk [30], cognitive and physical functioning [31], Alzheimer's disease [32], centenarian status [29, 33], Down syndrome [34], Werner Syndrome [35], HIV infection [36], Huntington's disease [37], obesity [38], menopause [39], osteoarthritis [40], and Parkinson's disease [41]. Moreover, we have demonstrated that the human epigenetic clock applies without change to chimpanzees [13] but it loses utility for other animals as a results of evolutionary genome sequence divergence. Moving beyond primates into the broader mammalian arena, we recently constructed an epigenetic clock for canids using DNA-methylation data from *Canis familiaris* (domesticated dog) and *Canis lupus* (wolf) [42].

Recently, other groups constructed epigenetic clocks for mice and used these to evaluate gold standard longevity interventions [43]. Petkovich, et al., derived a clock from blood samples of approximately 250 mice in order to examine changes induced by diet treatments and changes associated with genetic backgrounds that produce dwarfism (and long-lived) phenotypes [44]. Similarly, Cole, et al. examined the effects of genetic background (dwarf genotypes) and diet interventions on longevity, and their data was utilized by Wang, et al. to construct a DNA-methylation clock [45, 46]. Stubbs, et al, developed a clock for multiple tissue types. Application of their clock to samples from experimental interventions yielded biologically meaningful differences in epigenetic age [47]. Overall, these independent publications led to the important insight that epigenetic clocks for mice detect anti-epigenetic aging effects of gold standard interventions such as calorie restriction and growth hormone receptor knockouts.

Our current study addressed the following aims. First, to develop a multi-tissue DNA-methylation based estimator of chronological age across the entire lifespan based on new and existing reduced representation bisulfite sequencing (RRBS) data. Second, to evaluate the robustness of reported findings surrounding gold standard anti-aging interventions using the novel epigenetic clocks. Third, to assess whether one can

develop an epigenetic clock based on roughly 1k CpGs in evolutionarily conserved genomic regions.

To address these aims, we combined hundreds of new DNA-methylation samples collected from several mouse tissues with publicly available data from previous studies of mouse DNA-methylation. These data include samples obtained with RRBS and whole-genome bisulfite sequencing (WGBS). We compared clocks built with different regression methods using hundreds of thousands of CpGs as input as well as a clock constructed from a limited set of mammalian-conserved CpGs. We evaluated the performance of these clocks across samples and tissues. We applied the most accurate clock to samples from previous longevity studies of mice to measure the effects of these interventions on epigenetic aging. And, finally, we performed a GWAS analysis using epigenetic age as a trait in a subset of age-matched mouse samples covering 88 strains.

RESULTS

Data set

Based on calculations and criteria described in the Methods section, we constructed a matrix of high confidence methylation levels for 1189 mouse samples at 193,651 CpG sites. Of these 1189 mice, 893 were used as the training set for regression models described below. This was the largest matrix we could construct while minimizing missing values to 2% of total. The remaining 296 samples were held out entirely from the training so they could be used to investigate the effects of the experimental treatments (e.g. calorie restriction) and growth hormone receptor knockouts.

Four different epigenetic clocks

We considered 4 types of epigenetic clocks. The first two clocks are constructed on the basis of all 193,651 CpG sites (covariates). In particular, the "elastic net clock" used an elastic net model to regress chronological age (dependent variable) on all methylation levels. The second clock ("ridge regression clock") used a ridge regression model instead of an elastic net regression model. The two "conserved" clocks were constructed using elastic net regression and ridge regression, respectively, using 952 highly conserved CpGs, i.e. located in highly conserved stretches of DNA (Methods).

Accuracy with respect to chronological age

We compared the four different epigenetic clocks with respect to estimating chronological age at the time of

DNA sample collection (Table 1). The training set estimates of accuracy are overly optimistic and should be ignored. To arrive at unbiased estimates of the age correlation R (defined as Pearson correlation between DNAm age and chronological age) and the median absolute error (mae), the table reports three types of cross-validation estimates: i) leave-one-batch-out estimate (row "batch" in Table 1), ii) leave-one-sample-out estimate (row "sample" in Table 1), and iii) a 10 fold cross validation estimate. The three different cross validation estimates lead to the same conclusion: elastic net regression outperforms the other clocks when it comes to CV estimates of age correlations and median error. For example, the elastic net clock leads to a (leave-one-batch-out) age correlation of R=0.82 and a median error of 2.5 months. Although the conserved clocks are clearly inferior to those based on all CpGs, their accuracy remains impressive. For example, the elastic net conserved clock leads to a (leave-one-batch-out) age correlation of R=0.68 and a median error of 3.8 months.

We find that these epigenetic clocks are multi-tissue clocks, i.e. they lead to accurate age estimates in all considered tissues: results for the ridge regression clock based on all CpGs can be found Fig. 1. Analogous results for elastic net clocks based on all CpGs or based on only conserved CpG clock can be found in Suppl. Fig. 1 and Suppl. Fig. 2, respectively. We also find that accurate age estimates are made for samples taken from time points from post-natal mice to mice of advanced age, as can be seen in these figures.

Statistically speaking, the construction of epigenetic clocks is highly degenerate. That is, there are many clocks that select different sites, use slightly different weights, and achieve similar performance. For this reason, we have not emphasized the specific sites used in our clocks, as we do not believe that they are unique, but rather one set among many that could be used to construct clocks. However, we have included two Supplementary Tables of information for two of the

Table 1. Summary performance statistics of epigenetic aging models ("clocks").

CpGs	Estimate	Regression	Age cor.	mae	mean model size	model size std dev
All CpGs Clock	Training set	Ridge	1.00	0.1	193651	0
		Elastic net	0.99	0.7	582	0
	LO-Batch-Out	Ridge	0.79	3.1	193641	0
		Elastic	0.82	2.5	529	81
	LO-Sample-Out	Ridge	0.85	2.1	193651	0
		Elastic	0.89	1.8	444	81
	10-fold CV	Ridge	0.88	0.3	193641	0
		Elastic	0.89	1.2	463	134
Conserved CpGs Clock	Training	Ridge	0.85	2.7	952	0
		Elastic	0.91	1.9	274	0
	LO-Batch-Out	Ridge	0.64	4.0	952	0
		Elastic	0.68	3.8	214	39
	LO-Sample-Out	Ridge	0.75	3.3	952	0
		Elastic	0.78	2.4	236	6
	10-fold CV	Ridge	0.77	3.5	952	0
		Elastic	0.80	2.5	247	23

Accuracy of estimating chronological age for 4 different epigenetic clocks. The 4 clocks differ in terms of the CpGs that were used in their construction (first column) and in terms of the underlying regression model (third column). The second column describes the method for estimating the predictive accuracy. The training set estimates are overly optimistic and should be ignored. Leave-one-batch out estimates and leave-one-sample-out estimates provide accuracy estimates that are far less biased than those obtained in the training set. The mean model size refers to the number of CpGs selected by the penalized regression model. Since the ridge regression is based on all CpGs, the standard deviation is zero.

clocks. Supp. Table 1 provides the CpGs used in the elastic net model derived from all available methylation data, along with the regression model coefficients, and the distance of each CpG to the transcription start site of the nearest gene(s). Supp. Table 2 provides the same information but for the elastic net model derived from the subset of RRBS data corresponding to CpGs that are evolutionarily well-conserved in mammals. For the ridge regression clock based on all CpGs, this information is provided as a text file on the Gene Expression Omnibus (https://www.ncbi.nlm.nih.gov/geo/) under super-series accession number: GSE120137.
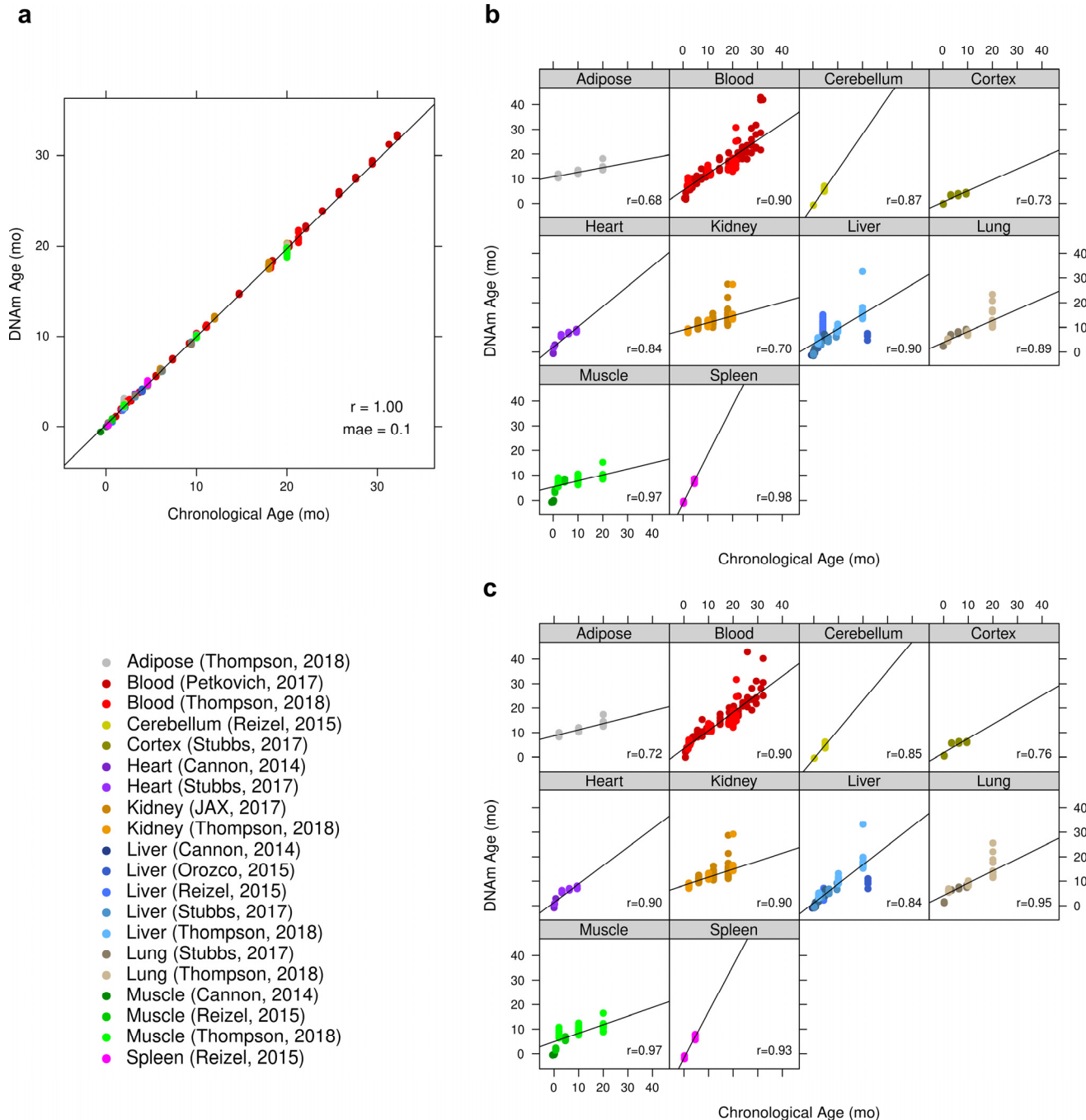
Figure 1. Accuracy of ridge regression epigenetic age predictions. DNA methylation age (y-axis) versus chronological age (x-axis) for all mouse samples. (**a**) Performance of ridge regression clock based on all 192K CpGs in all training samples. The training set estimates of the accuracy are overly optimistic and should be ignored. (**b**) Results by tissue type of cross-validated predictions obtained by iteratively withholding one "batch" (tissue x publication). For the batch cross-validation of this clock, the global Pearson correlation between predicted and chronological age was 0.79 (p < 2E-195) with a mae of 3.1 months. All models in these iterative cross-validations had the same size of 193,651 CpGs. (**c**) Scatter plots by tissue type based on DNAm age estimates made with an iterative leave-one-sample-out cross-validation. The correlation between predicted and chronologic age was 0.85 (p < 6E-258) with a mae of 2.1 months.

Table 2. Datasets.

Reference	Tissue	Strain	Age Dist.
Novel. Current study	Adipose (56) Blood (72) Kidney (56) Liver (60) Lung (60) Muscle (60)	C57BL/6J (200) BALB/cByJ (164)	N=364 mean = 10.9 median = 10 std dev = 7.4 min = 1.7 max=21.3
Stubbs (2017)	Cortex (16) Heart (15) Liver (15) Lung (15)	C57BL/6	N=61 mean = 5.1 median = 6.21 std dev = 3.4 min = 0.2 max = 9.4
Cole (2017) [45]	Liver (32)	Ames Prop1 Dwarf (16) UM-HET3 (16)	N = 32 mean = 13.5 median = 22 std dev = 9.8 min = 2 max = 22
Petkovich (2017) [44]	Blood (231)	C57BL/6 (161) B6D2F1 (22) GHRKO (26) Snell ([DW/J x C3H/HEJ]/F2) (22)	N = 231 mean = 14.7 median = 9.5 min = 0.6 max = 32.2
Novel. Current study. JAX lab	Kidney (190)	Diversity Outbred (190)	N = 190 mean = 12.1 median = 12 std dev = 4.9 min = 6 max = 18
Reizel (2015) [76]	Cerebellum (8) Liver (49) Muscle (25) Spleen (10)	C57BL/6	N = 92 mean = 2.8 median = 4.6 std dev =1.9 min = 0.23 max = 4.6
Cannon (2016) [67]	Heart (5) Liver (22) Muscle (5)	C57BL/6	N=32 mean = 0.8 median = 0.6 std dev = 0.9 min = -0.6 max = 2.1
Cannon (2014) [52]	Liver (40)	C57BL/6	N = 40 mean = 2.07 std dev = 0 min = 2.07 max = 2.07
Orozco (2014) [66]	Liver (105)	91 different strains	N = 105 mean = 4 median = 4 std dev = 0 min = 4 max = 4
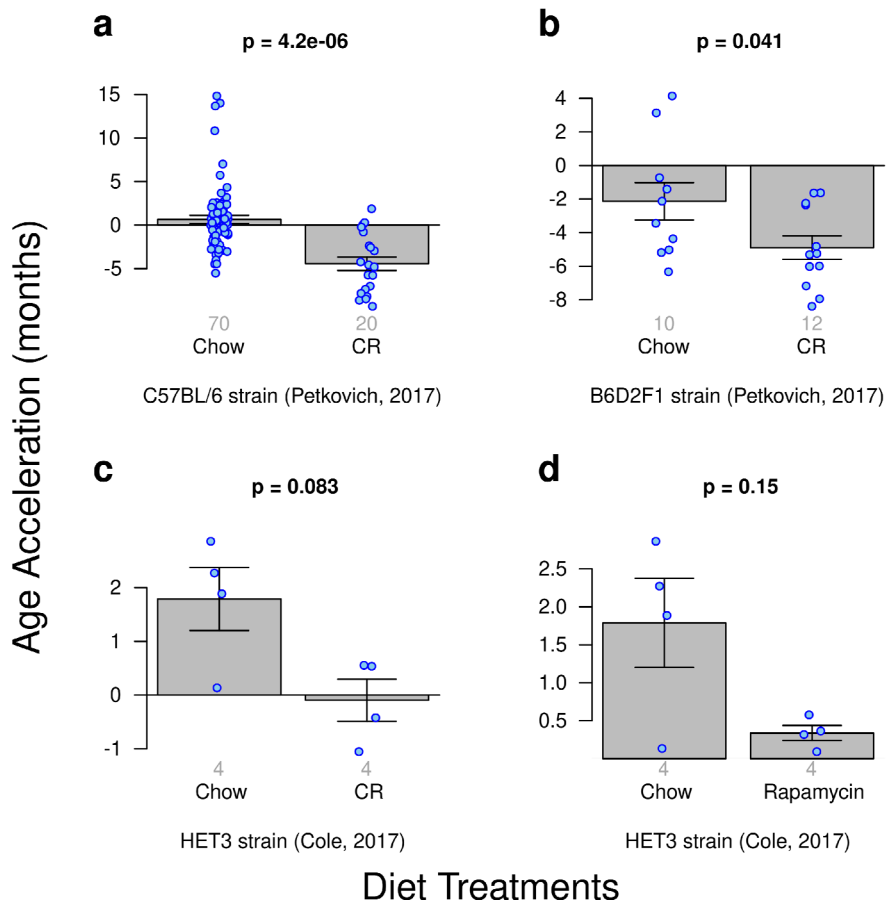
Figure 2. Age acceleration due to diet treatments. Results obtained from ridge regression clock. A meta-analysis p-value for the 3 calorie-restriction (CR) experiments is included. (**a**) Calorie restriction versus standard diet in the C57BL/J strain. (**b**) Calorie restriction versus standard chow diet in the B6D2F1 strain. (**c**) Calorie restriction versus standard diet for the HET3 strain. **d**) Rapamycin enriched diet versus standard diet for the HET3 strain.

Diet effects on epigenetic aging

We analyzed data from 3 calorie restriction experiments and 1 rapamycin diet treatment experiment. These "test data" had been left out of the training set used in the construction of our epigenetic clocks. The most significant results could be observed for the ridge regression clock based on all CpGs (Fig. 2): significantly delayed epigenetic aging effects can be observed in calorie restricted C57BL/6 mice (p=4.2E-6, Fig. 2a) and in B6D2F1 mice (p=0.041, Fig. 2b). A similar pattern could be observed for calorie restricted HET3 mice (Fig. 2c) but the results did not quite reach statistical significance (p=0.083), which might reflect the low sample size (4 CR vs 4 chow fed HET3 mice) or the fact that the latter data had been generated using a dif-

ferent platform (WGBS). However, the age estimates of the WGBS samples (HET3 strain) were consistent with those obtained for RRBS samples despite the absence of WGBS samples from the training set.

CR induced anti-epigenetic aging effects could also be observed with the 2 elastic net clocks (based on all CpGs and on highly conserved CpGs, respectively) but the results were less significant than the above mentioned effects observed for the ridge regression clock (Suppl. Fig. 3).

No significant effect for rapamycin

The single comparison of mice fed with a rapamycin-enriched diet to those fed a standard diet did not yield a

significant difference in age acceleration irrespective of the underlying clock (e.g. p=0.15, Fig. 2d) which might reflect the low sample size (4 Chow vs 4 Rapamycin fed mice) or the fact that the latter data had been generated using a different platform (WGBS).

Delayed epigenetic aging in dwarf mice

A few transgenic strains of mice have maximum life spans substantially greater than that of most other strains. In particular, the Ames and Snell mice, which have mutations in pituitary transcription factors (and hence are deficient in growth hormones, luteinizing hormone, thyroid-stimulating hormone, and IGF1) have extensions in maximal lifespan of up to 65% [48-50].

Using publicly available data, we aimed to replicate the findings from previous publications on delayed epigenetic aging effects in dwarf mice. Three different experiments within our composite dataset were design-ed to examine DNA methylation and dwarfism: i) growth hormone receptor knock out mice (GHR-KO) versus wild type mice ([C57BL/6J x BALB/cByJ]/F2), ii) Snell dwarf (SD) mice versus wildtype mice WT ([DW/J x C3H/HEJ]/F2), and iii) Ames dwarf mice versus WT where these were generated by mating either homozygous (df/df) or heterozygous (df/+) dwarf males with heterozygous females (df/+), respectively. The Ames dwarf mouse line carries a recessive mutation in the Prop1 gene and homozygous animals [Prop1(df)/Prop1(df)] show dwarfness and exhibit extended lifespan [51]. Heterozygous littermates [Prop1+/Prop1(df)] were generated by breeding heterozygous females with homozygous males are of normal size.

The ridge regression clock based on all CpGs managed to detect a delayed-epigenetic aging effect in all three types of dwarf mice (Fig. 3). Despite low sample sizes, the trend for homozygous dwarf strains to slow the epigenetic clock is clear and statistically significant
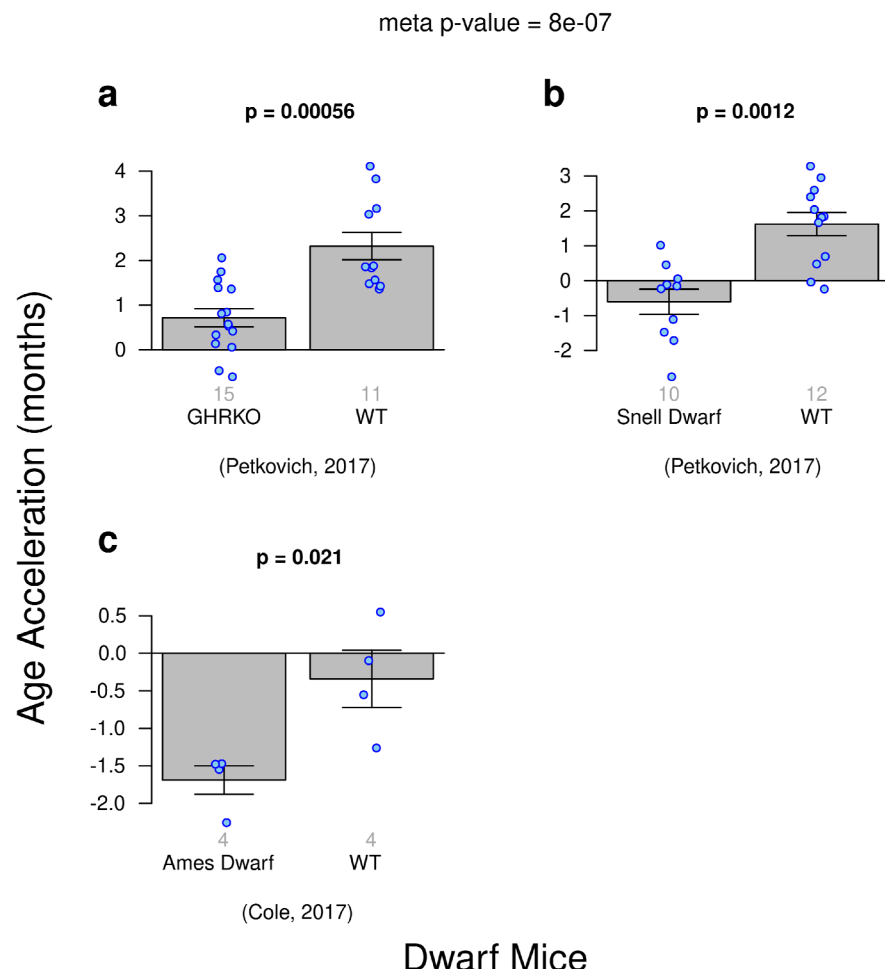
Figure 3. Age acceleration and Dwarfism in mice. Results obtained from ridge regression clock. A meta-analysis p-value for the 3 experiments is included. (**a**) Genetic knockout dwarf mice versus wild type. (**b**) Snell dwarf mice versus wild type. **c**) Ames Dwarf mice versus wild type.

with a meta-analysis p-value of 8E-7. However, these results are not statistically robust with respect to different epigenetic clocks: the association of dwarfism and slow epigenetic aging could *not* be detected with the same significance with the two elastic net regression clocks (Suppl. Fig. 4).

Maternal diet effects on epigenetic aging

Cannon, et al. investigated the potential influence of maternal diet on gene expression and DNA methylation in their offspring [52]. Our ridge regression clock reveals that the slowest epigenetic aging effects can be observed in low fat diet-fed offspring of low fat diet-fed mothers (Fig. 4).

Although, this finding is biologically plausible it is not statistically robust with respect to other epigenetic clocks. In particular, it cannot be observed for the two elastic net regression clocks (Suppl. Fig. 5)

GWAS of epigenetic age in mice

We used epigenetic age as trait in our Genome Wide Association Study (GWAS) in the Hybrid Mouse Diversity Panel (HMDP). We calculated epigenetic age via a cross validation approach in order to avoid overfitting. Specifically, epigenetic age was computed for 88 strains using the ridge regression based clock and leaving out from the training set the sample whose age was estimated. The mean calculated epigenetic age was

Figure 4. Age acceleration and maternal diet. Results obtained from ridge regression clock. (**a**) Offspring of mothers fed a high fat diet (HFD) who were fed either a high fat or low fat diet (LFD). (**b**) Offspring of mothers fed a low fat diet who were fed either a high fat or low fat diet.

Table 3. Top ten SNPs from GWAS analysis of DNAm age predictions corresponding to peaks connected to LD blocks in HDMP (~2 Mbp). P-values were computed with a linear mixed-model (LMM).

SNP ID	Chr	Position	LMM p-value	Nearest gene(s)
JAX00189882	6	77104479	1.08E-04	Ctnna2, Lrrtm1
JAX00141186	6	55124351	1.59E-04	Plekha8, Mturn, Znrf2, Nod1, Ggct, Gars, Crhr2, Inmt, Mindy4, Aqp1, Ghrhr, Adcyap1r1
JAX00613802	6	73641278	1.67E-04	Dnah6, Suclg1, 4931417E11Rik
JAX00651898	7	115070069	3.06E-04	Calca, Calcb, Insc, Sox6
JAX00373522	14	14657081	4.48E-04	Olfr720, Olfr31, Il3ra, Slc4a7, Nek10
JAX00049927	14	9498134	4.83E-04	Fhit
JAX00140799	6	49976398	5.06E-04	Npy, Mpp6, Gsdme, Osbp13
JAX00189488	4	95990791	5.48E-04	Fggy, Hook1, Cyp2j13, Cyp2j12, Cyp2j11, Cyp2j8
JAX00087970	19	25717022	5.66E-04	Kank1, Dmrt1, Dmrt3, Dmrt2
JAX00374020	14	17587871	7.02E-04	Thrb

4.18 months (±0.95) in the range of 2.3-7.1 months with a median of 4.1 months. A set of 196,148 SNPs (MAF>5%) was used for association studies. We used linear mixed models to correct for population structure using the pyLMM software. As our cohort size was limited, we were not able to identify peaks whose significance was beyond the Bonferroni threshold in this analysis (Fig. 5a). Therefore the results presented in Table 3 with the top 10 SNPS are only suggestive of an association and will need to be confirmed in the future with a larger cohort.

We analysed the genes that were found proximal (500 kbp up- and downstream) to the identified peak SNP site. This list contains several genes that have previously been implicated in aging: *Aqp1* (*Aquaporin 1*) [53], *Npy* (*Neuropeptide Y*)[54], *Adcyap1r1* (*Adenylate cyclase-activating polypeptide type I receptor 1*) as a receptor for PACAP (Pituitary Adenylate Cyclase-Activating Peptide) [55, 56]. The most notable is *Npy*, which encodes a hormone responsible for appetite control [57], regulation of fat metabolism [58], and plays a critical role in caloric restriction (CR) mediat-
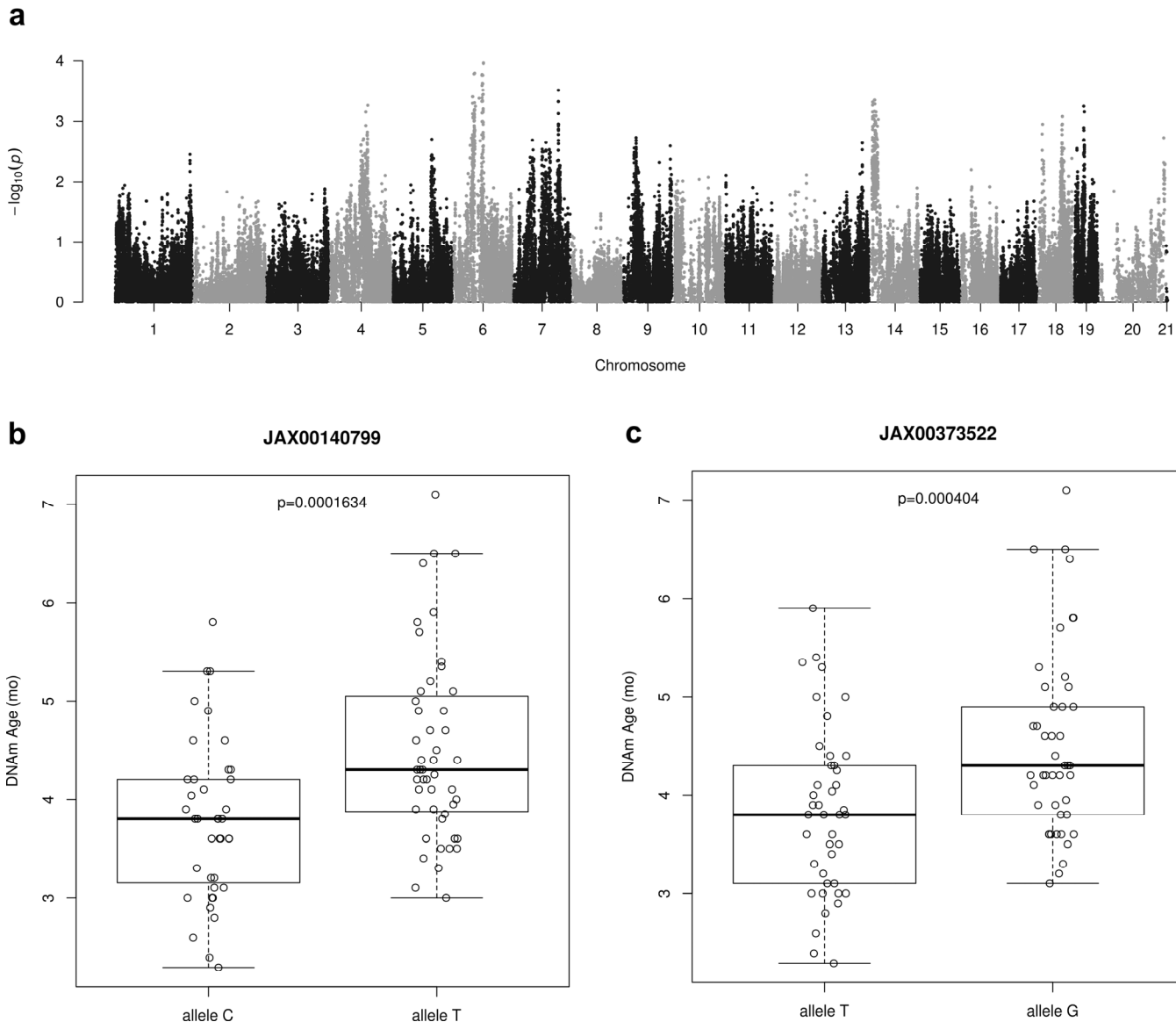
Figure 5. Genome-wide association results for DNAm Age. (**a**) Manhattan plot presenting genome-wide association results for DNAm Age. Epigenetic age predictions were calculated using all CpGs clock with ridge regression and leave-one-sample-out estimates. GWAS analysis was based on linear mixed model and a set of 196,148 SNPs (MAF > 0.05) from HMDP mice strains. (**b**) This SNP as identified using GWAS analysis of epigenetic age predictions. It is located in an LD block on chromosome 6 and contains the genes *Npy*, *Mpp6*, *Gsdme* and *Osbp13*. A one-sided t-test of DNAm ages between the two allelic groups shown is statistically significant. (**c**) It is located in an LD block on chromosome 6 and contains the genes *Npy*, *Mpp6*, *Gsdme* and *Osbp13*. A one-sided t-test of DNAm ages between the two allelic groups shown is statistically significant.

ed lifespan extension [59]. As examples, we found statistically significant differences (p < 0.001) in average DNAm ages of mice strains having allele C or T within SNP JAX00140799 (Fig. 5b) and between mice strains having allele T or C within SNP JAX00373522 (Fig. 5c).

DISCUSSION

Based on multiple tissue samples taken from previous studies and our own in-house collection we compiled a dataset of 1189 mouse DNA methylation measurements across hundreds of thousands of CpGs. These samples represent the most comprehensive dataset thus far of matched single base resolution methylomes in mice across multiple tissues and ages.

We demonstrate that these data enable construction of highly accurate multi-tissue age estimation methods (epigenetic clocks) for mice that apply to the entire life course (from birth to old age). We demonstrate that these clocks perform well on new tissues not included in the training of the clock by performing tissue exclusion cross-validation. This gives us confidence that these clocks will work on new samples from other tissue types as well. However, we cannot rule out that these clocks fail in specific cell types. Epigenetic age estimators that focus on specific tissues or cell types can have greater accuracy than pan tissue age estimators [60].

Our study leads to several novel insights. First, our first prototype of an age estimator based on fewer than 1000 highly conserved CpGs demonstrates that it will be feasible to build highly accurate DNAm age estimator on the basis of highly conserved CpGs.

Second, we find that epigenetic clocks that are optimal for estimating age (namely those based on elastic net regression) may be inferior to less accurate clocks (based on ridge regression) when it comes to gold standard anti-aging interventions. Only our ridge regression clock manages to corroborate most of the previously reported findings, *e.g.* only the ridge clock showed that dwarf strains show slower epigenetic aging relative to wild-type strains. The anti-epigenetic aging effects of calorie restriction are highly robust and could be observed with all clocks. Moreover, by utilizing epigenetic ages as phenotypic traits in a GWAS study of 88 strains of mice we found suggestive associations with several genes, including neuropeptide Y whose role in appetite control and calorie restriction mediated lifespan extension is well documented. However, none of our clocks managed to detect an anti-aging effect of rapamycin in a small data set which might reflect the low sample sizes or technical reasons including low

coverage afforded by the measurement platform (WGBS).

All clocks were able to detect a slowing of the epigenetic clock in mice fed a calorie restricted diet, though with differing sensitivity, suggesting that the effects of calorie restriction are pervasive across the methylomes. In contrast, the slowing of epigenetic aging in mice fed a low fat diet for two generations were not detected by the clocks with fewer CpGs (elastic net), suggesting these effects are either more subtle or more localized in the methylome.

These results suggest that the multi-tissue ridge regression DNA-methylation clock is most useful in assessing "biological age" for a variety of treatments, experimental interventions, and genetic backgrounds. However, the elastic net clocks are better for assessing chronological age. We evaluated both ridge and lasso regression in previous studies with human data and found that lasso outperformed ridge not just in terms of accuracy but also in terms of interpretability (unreported findings). Therefore, it is a curious finding that ridge regression has some merits when it comes to mice.

We speculate that one reason that ridge regression works best in our context is that our dataset is more heterogeneous than those used in previous studies. Our dataset includes mice of different ages, strains and diverse tissues, all collected in different labs and resulting in a whole that is larger than any previous dataset. Because genetic diversity in mice is high, it is possible that lasso models that only use a limited number of sites are more prone to be influenced by genetic variation (as DNA methylation is often associated with genetic variation). Thus, on the whole, it is possible that the ridge approach minimizes these effects by using all sites, and thus leads to the most robust overall performance.

The DNAm age estimates from our mouse clocks exhibit a correlation coefficient with chronological age that ranges from R=0.79 to 0.89 (Table 1). These correlations are only slightly weaker than those observed for human studies (R=0.96 for the pan tissue estimator from Horvath). We have no doubt that more accurate mouse clocks can be built by reducing technical variation and by employing even larger data sets.

We acknowledge several limitations. Our genetic study of epigenetic aging rates was under-powered. Large scale *human* studies have implicated genome-wide significant loci including the *TERT* gene [61-63]. We did not assess the intra-assay variation of replicate

samples in the current article but refer the interested reader to relevant articles [59, 60].

Rigorous quantitative comparisons to previously published mouse clocks (*e.g.* comparing age correlation values) could not be made due to technical differences in the processing of sequence data, in the estimation and correction of methylation calls, in the limited tissue sampling of previous clocks, and, most importantly, in the simple absence of particular CpGs in the various datasets and clock models. The subset of CpGs with high coverage in one RRBS data set tends to exhibit poor overlap with a subset of CpGs from another RRBS data set. This poor overlap of CpGs makes it difficult to validate epigenetic clocks based on RRBS data. We are currently working on a custom methylation array platform that avoids these pitfalls.

METHODS

Data sets

We generated reduced representation bisulfite sequencing **(**RRBS) methylation data for mouse adipose, blood, liver, and kidney, muscle, and lung tissue samples using the protocol below.

DNA methylation assay

Genomic DNA was isolated by standard phenol-chloroform extraction method and used as input to prepare Reduced Representation Bisulfite Sequencing (RRBS) libraries as described previously [64] with minor modifications. For each sample 50-100 ng of purified genomic DNA was digested with 20 U of MspI (NEB, cat # R0106L) at 37°C o/n in the presence of RNase Cocktail Mix (Ambion, cat # AM2286). End-repair and dA-tailing was performed by the addition of Klenow Fragment 3'->5' exo- (NEB, cat # M0212L) in the presence of dATP, dGTP and d5mCTP (Fermentas). Adapter Ligation was performed by the addition of 0.3 µl of Illumina TruSeq methylated Adapters (Illumina, TruSeq Nano cat# FC-121-4001) and 2 µl of Illumina Ligation Mix 2 (Illumina, TruSeq Nano cat# FC-121-4001). Samples were pooled and purified using an equal volume of SPRI beads (Beckman Coulter, cat # B23318). Size-selection was performed using SPRI beads to enrich for fragments from 200 to 300 bp. Bisulfite treatment was performed using Epitect Bisulfite kit (QIAGEN, cat # 59104) according to manufacturer's protocol, except that two consecutive rounds of conversion are performed, for a total of 10 hr of incubation. Purified converted DNA was PCR amplified using MyTaq HS Mix (Bioline, cat# BIO-25045) and TruSeq PCR Primer Cocktail (Illumina, TruSeq Nano cat# FC-121-4001) according to the

following protocol: initial denaturation at 98°C for 30s; 12 cycles of 98°C for 15s, 60°C for 30s, 72°C for 30s; final extension at 72°C for 5 min. Amplified libraries were purified twice with an equal amount of SPRI beads to remove primer and adapter dimers. Libraries were sequenced 100 bp single-end on an Illumina HiSeq4000. For the kidney data from JAX laboratories, the sequencing protocol was as follows. RRBS libraries were prepared using 100 ng DNA, the Ovation RRBS Methyl-Seq System 1–16 (NuGEN Technologies, San Carlo, CA) part number 0353, and the EpiTect Fast 96 Bisulfite Conversion kit (Qiagen, Hilden, Germany) part number 59720. The manufacturer's protocols were followed except for the number of PCR cycles in the library amplification step, which was increased, from 12 to 13. Libraries were quantified using the Library Quantification Kit (Kapa Biosystems, Wilmington, MA) part number KK4835, normalized to 10nM, and pooled in groups of 12. Each pool was sequenced 1 x 100 bp on one lane of the HiSeq2500 (Illumina, San Diego, CA) at The New York Genome Center (New York, NY).

These datasets were integrated with RRBS data made available to the public via the GEO repository [65]. We included datasets from previous RRBS-based "epigenetic clock" studies [44, 47] along with RRBS data from an EWAS study of metabolic traits [66], from a study of maternal diet effects on gene expression and DNA methylation [52], from a study of post-natal hepatocyte development [67], from a multi-tissue study of sex hormone effects on DNA methylation [68].

Kidney data from the Jackson Laboratory

Kidneys were collected from male and female Diversity Outbred mice at ages 6, 12 and 18 months. Mice were group housed in SPF condition and fed a standard lab chow diet (5K0G) with 6% calories from fat. Tissues were flash frozen in LN2, pulverized and mixed prior to DNA extraction. RRBS sequencing was carried out at the New York Genome Center. Although whole-genome bisulfite-sequencing data (WGBS) has a variety of characteristic differences from RRBS, we obtained the set of this data collected previously to examine longevity interventions in mice and build an epigenetic clock [45, 46].

Data processing

Where possible, we downloaded the raw sequencing files from previous studies via (GEO) and performed alignments and methylation calling identically as for our in-house data using BS_Seeker2 with default parameters [69]. All mouse methylation data in this study utilized mouse genome mm10 coordinates. When

technical replicates were available for a given sample, they were merged by summing the sequencing counts. For the kidney data from JAX laboratories, a Bismark-based pipeline was initially used as follows [70]. All the samples were subjected to QC using the trim galore module then trimming of the diversity adapters was performed by trimRRBSdiversityAdaptCustomers.py script from NuGen. High quality trimmed reads were aligned to all eight diversity outbred founder strains (A/J, C57BL/6J, 129S1/SvImJ, NOD/ShiLtJ, NZO/HlLtJ, CAST/EiJ, PWK/PhJ, and WSB/EiJ,) separately using Bismark at default parameters. The alignment to founder genomes except C57BL/6J were converted to reference genome coordinates (mm10) using g2gtools v1. Then, we selected the reads which were mapped to the same locus in multiple founders strains (assigned to founder strains with minimum edit distance) or mapped uniquely to one founder strains by custom in-house script. The bed file of estimated methylation proportion of each founder (except C57BL/6J) was converted to reference genome coordinate by g2gtools v1 and, finally, combined to provide the methylation proportion in each diversity outbred animals.

For each CpG site in each sample we estimated the methylation frequency as the number of methylated mapped read counts over the total mapped read counts. Where available, the counts for the forward and reverse Cytosines of the CpG were pooled and treated as a single measurement. We then computed a 95% confidence interval with a Bayesian approach using a Beta distribution (0.5,0.5) ("Jeffrey's Prior") for all methylation values [71,72]. For inclusion in our analysis, we required that each CpG site had confident methylation frequencies in at least 95% of samples. Confidence was defined as having a confidence interval smaller than 0.50. True missing values or measurements failing that confidence interval filter were imputed using k-nearest-neighbor approach with k=5. This select strategy resulted in CpGs whose mean methylation levels ranged from zero to 1 (Suppl. Fig. 6).

Sample exclusion

In order to maximize the number of samples and coverage of the methylomes, it was necessary to exclude a number of samples both from our new data and from previously published datasets. First, we removed samples with fewer than 500,000 measured CpGs. Next, after an initial matrix was constructed, we iteratively removed samples with the most missing values until we arrived at a matrix with ~2% total missing values.

Penalized regression models

Penalized regression models were created with glmnet [73]. We investigated models produced by both elastic net regression (alpha=0.5) and ridge regression (alpha=0). The optimal penalty parameters in all cases were determined automatically by using a 10 fold internal cross-validation (cv.glmnet) on the training set. By definition, the alpha value for the elastic net regression was set to 0.5 (midpoint between ridge and lasso type regression) and was not optimized for model performance. We omitted the results from lasso regression models (alpha=1) because the age estimates tended to be less accurate than those from elastic net regression.

The covariates in our data (methylation of CpGs) are known to have a high degree of multicollinearity. While lasso and elastic net regression allow regression coefficients to go to zero and thus yield a sort of "feature selection" which is desirable for interpretability, the correlations among methylation sites may contain subtle information that might be useful to retain (which supports the use of ridge regression).

Cross-validation estimates of accuracy

We performed three types of cross-validation schemes for arriving at unbiased (or at least less biased) estimates of the accuracy of the different DNAm based age estimators. One type consisted of leaving out a single sample (LOOCV) from the regression, predicting an age for that sample, and iterating over all samples. The second type (10-fold) was similar to the first except that 10% of samples were withheld per iteration. The third type consisted of iteratively leaving out all samples of a particular "batch" where batched was defined as combination of tissue type and publication of origin. For example, three batches resulted from a single publication if the underlying RRBS data were obtained from 3 distinct tissues. Samples from longevity intervention studies (CR, Rapamycin, dwarf mice) along with their respective control samples were excluded from all instances of training-set construction.

Conserved-CpG clock

Our team is currently developing a mammalian DNA-methylation array for measuring methylation levels in mammals. The primary selection criteria for CpGs for the probe-design of this bead-chip array was conservation of the local sequence context of the CpG across 60 sequenced mammalian genomes. We obtained the list of candidate CpGs in this effort and intersected it with CpGs in our high-quality RRBS data.

Epigenetic age acceleration

To investigate effects of biological interventions and genetic background on epigenetic aging, we employ a quantity termed "age acceleration". In the simplest form, it is just the difference between the epigenetic age estimated by the clock and the chronological age. However, this measure can be age-dependent itself, causing difficulty in interpretation. Instead, age acceleration is computed as the residual, per sample, after fitting predicted ages to chronological ages. This fitting is done on a per-batch basis. P-values for age acceleration comparisons found in Figs 2, 3, 4, and Suppl. Figs 3, 4 and 5 were obtained using the non-parametric Kruskal-Wallis test.

Genome-wide association study

GWAS was performed using 88 strains from the Hybrid Mouse Diversity Panel (HMDP, listed in Suppl. Table 1), that have been extensively used as a resource for systems genetics analyses [66, 74, 75]. Of the total of 459 895 SNPs, we selected a set of 196 148 SNPs that exhibited minor allele frequency greater than 5%. DNAm ages, computed using all CpGs clock with ridge regression and leave-one-sample-out estimates, were treated as phenotypes in the association studies. All of the mice were at chronological age of 4 months. GWAS was conducted using the linear mixed model python package pyLMM to account for population structure and relatedness among the mouse strains. We selected the top SNPs in each of the peaks from the pyLMM analysis that were located a minimum of 2 Mbp apart, which is the average of LD block size for SNPs in the HMDP.

Data availability

Raw sequencing data and processed data for samples collected at UCLA and JAX, as well as re-processed data from previous studies have been made available at the Gene Expression Omnibus (https://www.ncbi.nlm.nih.gov/geo/) under super-series accession number: GSE120137

CONFLICTS OF INTEREST

The authors declare there are no potential conflicts of interest.

FUNDING

REFERENCES

1. Christensen BC, Houseman EA, Marsit CJ, Zheng S, Wrensch MR, Wiemels JL, Nelson HH, Karagas MR, Padbury JF, Bueno R, Sugarbaker DJ, Yeh RF, Wiencke JK, Kelsey KT. Aging and environmental exposures alter tissue-specific DNA methylation dependent upon CpG island context. PLoS Genet. 2009; 5:e1000602.
https://doi.org/10.1371/journal.pgen.1000602

2. Bollati V, Schwartz J, Wright R, Litonjua A, Tarantini L, Suh H, Sparrow D, Vokonas P, Baccarelli A. Decline in genomic DNA methylation through aging in a cohort of elderly subjects. Mech Ageing Dev. 2009; 130:234–39. https://doi.org/10.1016/j.mad.2008.12.003

3. Rakyan VK, Down TA, Maslau S, Andrew T, Yang TP, Beyan H, Whittaker P, McCann OT, Finer S, Valdes AM, Leslie RD, Deloukas P, Spector TD. Human aging-associated DNA hypermethylation occurs preferentially at bivalent chromatin domains. Genome Res. 2010; 20:434–39.
https://doi.org/10.1101/gr.103101.109

4. Teschendorff AE, Menon U, Gentry-Maharaj A, Ramus SJ, Weisenberger DJ, Shen H, Campan M, Noushmehr H, Bell CG, Maxwell AP, Savage DA, Mueller-Holzner E, Marth C, et al. Age-dependent DNA methylation of genes that are suppressed in stem cells is a hallmark of cancer. Genome Res. 2010; 20:440–46.
https://doi.org/10.1101/gr.103606.109

5. Horvath S, Zhang Y, Langfelder P, Kahn RS, Boks MP, van Eijk K, van den Berg LH, Ophoff RA. Aging effects on DNA methylation modules in human brain and blood tissue. Genome Biol. 2012; 13:R97.
https://doi.org/10.1186/gb-2012-13-10-r97

6. Numata S, Ye T, Hyde TM, Guitart-Navarro X, Tao R, Wininger M, Colantuoni C, Weinberger DR, Kleinman JE, Lipska BK. DNA methylation signatures in development and aging of the human prefrontal cortex. Am J Hum Genet. 2012; 90:260–72.
https://doi.org/10.1016/j.ajhg.2011.12.020

7. Alisch RS, Barwick BG, Chopra P, Myrick LK, Satten GA, Conneely KN, Warren ST. Age-associated DNA methylation in pediatric populations. Genome Res. 2012; 22:623–32.
https://doi.org/10.1101/gr.125187.111

8. Johansson A, Enroth S, Gyllensten U. Continuous Aging of the Human DNA Methylome Throughout the

Human Lifespan. PLoS One. 2013; 8:e67378. https://doi.org/10.1371/journal.pone.0067378

9. Day K, Waite LL, Thalacker-Mercer A, West A, Bamman MM, Brooks JD, Myers RM, Absher D. Differential DNA methylation with age displays both common and dynamic features across human tissues that are influenced by CpG landscape. Genome Biol. 2013; 14:R102. https://doi.org/10.1186/gb-2013-14-9-r102

10. Bocklandt S, Lin W, Sehl ME, Sánchez FJ, Sinsheimer JS, Horvath S, Vilain E. Epigenetic predictor of age. PLoS One. 2011; 6:e14821. https://doi.org/10.1371/journal.pone.0014821

11. Garagnani P, Bacalini MG, Pirazzini C, Gori D, Giuliani C, Mari D, Di Blasio AM, Gentilini D, Vitale G, Collino S, Rezzi S, Castellani G, Capri M, et al. Methylation of ELOVL2 gene as a new epigenetic marker of age. Aging Cell. 2012; 11:1132–34. https://doi.org/10.1111/acel.12005

12. Hannum G, Guinney J, Zhao L, Zhang L, Hughes G, Sadda S, Klotzle B, Bibikova M, Fan JB, Gao Y, Deconde R, Chen M, Rajapakse I, et al. Genome-wide methylation profiles reveal quantitative views of human aging rates. Mol Cell. 2013; 49:359–67. https://doi.org/10.1016/j.molcel.2012.10.016

13. Horvath S. DNA methylation age of human tissues and cell types. Genome Biol. 2013; 14:R115. https://doi.org/10.1186/gb-2013-14-10-r115

14. Lin Q, Weidner CI, Costa IG, Marioni RE, Ferreira MR, Deary IJ, Wagner W. DNA methylation levels at individual age-associated CpG sites can be indicative for life expectancy. Aging (Albany NY). 2016; 8:394–401. https://doi.org/10.18632/aging.100908

15. Cedar H, Bergman Y. Programming of DNA methylation patterns. Annu Rev Biochem. 2012; 81:97–117. https://doi.org/10.1146/annurev-biochem-052610-091920

16. Przybilla J, Galle J, Rohlf T. Is adult stem cell aging driven by conflicting modes of chromatin remodeling? BioEssays. 2012; 34:841–48. https://doi.org/10.1002/bies.201100190

17. Przybilla J, Rohlf T, Loeffler M, Galle J. Understanding epigenetic changes in aging stem cells--a computational model approach. Aging Cell. 2014; 13:320–28. https://doi.org/10.1111/acel.12177

18. Beerman I, Bock C, Garrison BS, Smith ZD, Gu H, Meissner A, Rossi DJ. Proliferation-dependent alterations of the DNA methylation landscape underlie hematopoietic stem cell aging. Cell Stem Cell. 2013; 12:413–25. https://doi.org/10.1016/j.stem.2013.01.017

19. Beerman I, Rossi DJ. Epigenetic regulation of hematopoietic stem cell aging. Exp Cell Res. 2014; 329:192–99. https://doi.org/10.1016/j.yexcr.2014.09.013

20. Gibbs WW. Biomarkers and ageing: the clock-watcher. Nature. 2014; 508:168–70. https://doi.org/10.1038/508168a

21. Jung M, Pfeifer GP. Aging and DNA methylation. BMC Biol. 2015; 13:7. https://doi.org/10.1186/s12915-015-0118-4

22. Benayoun BA, Pollina EA, Brunet A. Epigenetic regulation of ageing: linking environmental inputs to genomic stability. Nat Rev Mol Cell Biol. 2015; 16:593–610. https://doi.org/10.1038/nrm4048

23. Horvath S, Raj K. DNA methylation-based biomarkers and the epigenetic clock theory of ageing. Nat Rev Genet. 2018; 19:371–84. https://doi.org/10.1038/s41576-018-0004-3

24. Hannum G, Guinney J, Zhao L, Zhang L, Hughes G, Sadda S, Klotzle B, Bibikova M, Fan JB, Gao Y, Deconde R, Chen M, Rajapakse I, et al. Genome-wide methylation profiles reveal quantitative views of human aging rates. Mol Cell. 2013; 49:359–67. https://doi.org/10.1016/j.molcel.2012.10.016

25. Marioni RE, Shah S, McRae AF, Chen BH, Colicino E, Harris SE, Gibson J, Henders AK, Redmond P, Cox SR, Pattie A, Corley J, Murphy L, et al. DNA methylation age of blood predicts all-cause mortality in later life. Genome Biol. 2015; 16:25. https://doi.org/10.1186/s13059-015-0584-6

26. Christiansen L, Lenart A, Tan Q, Vaupel JW, Aviv A, McGue M, Christensen K. DNA methylation age is associated with mortality in a longitudinal Danish twin study. Aging Cell. 2016; 15:149-54. https://doi.org/10.1111/acel.12421

27. Perna L, Zhang Y, Mons U, Holleczek B, Saum KU, Brenner H. Epigenetic age acceleration predicts cancer, cardiovascular, and all-cause mortality in a German case cohort. Clin Epigenetics. 2016; 8:64. https://doi.org/10.1186/s13148-016-0228-z

28. Chen BH, Marioni RE, Colicino E, Peters MJ, Ward-Caviness CK, Tsai PC, Roetker NS, Just AC, Demerath EW, Guan W, Bressler J, Fornage M, Studenski S, et al. DNA methylation-based measures of biological age: meta-analysis predicting time to death. Aging (Albany NY). 2016; 8:1844–65. https://doi.org/10.18632/aging.101020

29. Horvath S, Pirazzini C, Bacalini MG, Gentilini D, Di Blasio AM, Delledonne M, Mari D, Arosio B, Monti D, Passarino G, De Rango F, D'Aquila P, Giuliani C, et al. Decreased epigenetic age of PBMCs from Italian semi-

supercentenarians and their offspring. Aging (Albany NY). 2015; 7:1159–70.
https://doi.org/10.18632/aging.100861

30. Levine ME, Hosgood HD, Chen B, Absher D, Assimes T, Horvath S. DNA methylation age of blood predicts future onset of lung cancer in the women's health initiative. Aging (Albany NY). 2015; 7:690–700.
https://doi.org/10.18632/aging.100809

31. Marioni RE, Shah S, McRae AF, Ritchie SJ, Muniz-Terrera G, Harris SE, Gibson J, Redmond P, Cox SR, Pattie A, Corley J, Taylor A, Murphy L, et al. The epigenetic clock is correlated with physical and cognitive fitness in the Lothian Birth Cohort 1936. Int J Epidemiol. 2015; 44:1388–96.
https://doi.org/10.1093/ije/dyu277

32. Levine ME, Lu AT, Bennett DA, Horvath S. Epigenetic age of the pre-frontal cortex is associated with neuritic plaques, amyloid load, and Alzheimer's disease related cognitive functioning. Aging (Albany NY). 2015; 7:1198–211.
https://doi.org/10.18632/aging.100864

33. Horvath S, Mah V, Lu AT, Woo JS, Choi OW, Jasinska AJ, Riancho JA, Tung S, Coles NS, Braun J, Vinters HV, Coles LS. The cerebellum ages slowly according to the epigenetic clock. Aging (Albany NY). 2015; 7:294–306.
https://doi.org/10.18632/aging.100742

34. Horvath S, Garagnani P, Bacalini MG, Pirazzini C, Salvioli S, Gentilini D, Di Blasio AM, Giuliani C, Tung S, Vinters HV, Franceschi C. Accelerated epigenetic aging in Down syndrome. Aging Cell. 2015; 14:491–95. https://doi.org/10.1111/acel.12325

35. Maierhofer A, Flunkert J, Oshima J, Martin GM, Haaf T, Horvath S. Accelerated epigenetic aging in Werner syndrome. Aging (Albany NY). 2017; 9:1143–52.
https://doi.org/10.18632/aging.101217

36. Horvath S, Levine AJ. HIV-1 infection accelerates age according to the epigenetic clock. J Infect Dis. 2015; 212:1563–73. https://doi.org/10.1093/infdis/jiv277

37. Horvath S, Langfelder P, Kwak S, Aaronson J, Rosinski J, Vogt TF, Eszes M, Faull RL, Curtis MA, Waldvogel HJ, Choi OW, Tung S, Vinters HV, et al. Huntington's disease accelerates epigenetic aging of human brain and disrupts DNA methylation levels. Aging (Albany NY). 2016; 8:1485–512.
https://doi.org/10.18632/aging.101005

38. Horvath S, Erhart W, Brosch M, Ammerpohl O, von Schönfels W, Ahrens M, Heits N, Bell JT, Tsai PC, Spector TD, Deloukas P, Siebert R, Sipos B, et al. Obesity accelerates epigenetic aging of human liver. Proc Natl Acad Sci USA. 2014; 111:15538–43.
https://doi.org/10.1073/pnas.1412759111

39. Levine ME, Lu AT, Chen BH, Hernandez DG, Singleton AB, Ferrucci L, Bandinelli S, Salfati E, Manson JE, Quach A, Kusters CD, Kuh D, Wong A, et al. Menopause accelerates biological aging. Proc Natl Acad Sci USA. 2016; 113:9327–32.
https://doi.org/10.1073/pnas.1604558113

40. Vidal L, Lopez-Golan Y, Rego-Perez I, Horvath S, Blanco FJ, Riancho JA, Gomez-Reino JJ, Gonzalez A. Specific increase of methylation age in osteoarthritis cartilage. Osteoarthritis Cartilage. 2016; 24:S63.
https://doi.org/10.1016/j.joca.2016.01.140

41. Horvath S, Ritz BR. Increased epigenetic age and granulocyte counts in the blood of Parkinson's disease patients. Aging (Albany NY). 2015; 7:1130–42.
https://doi.org/10.18632/aging.100859

42. Thompson MJ, vonHoldt B, Horvath S, Pellegrini M. An epigenetic aging clock for dogs and wolves. Aging (Albany NY). 2017; 9:1055–68.
https://doi.org/10.18632/aging.101211

43. Wagner W. Epigenetic aging clocks in mice and men. Genome Biol. 2017; 18:107.
https://doi.org/10.1186/s13059-017-1245-8

44. Petkovich DA, Podolskiy DI, Lobanov AV, Lee SG, Miller RA, Gladyshev VN. Using DNA Methylation Profiling to Evaluate Biological Age and Longevity Interventions. Cell Metab. 2017; 25:954–960.e6.
https://doi.org/10.1016/j.cmet.2017.03.016

45. Cole JJ, Robertson NA, Rather MI, Thomson JP, McBryan T, Sproul D, Wang T, Brock C, Clark W, Ideker T, Meehan RR, Miller RA, Brown-Borg HM, Adams PD. Diverse interventions that extend mouse lifespan suppress shared age-associated epigenetic changes at critical gene regulatory regions. Genome Biol. 2017; 18:58. https://doi.org/10.1186/s13059-017-1185-3

46. Wang T, Tsui B, Kreisberg JF, Robertson NA, Gross AM, Yu MK, Carter H, Brown-Borg HM, Adams PD, Ideker T. Epigenetic aging signatures in mice livers are slowed by dwarfism, calorie restriction and rapamycin treatment. Genome Biol. 2017; 18:57.
https://doi.org/10.1186/s13059-017-1186-2

47. Stubbs TM, Bonder MJ, Stark AK, Krueger F, von Meyenn F, Stegle O, Reik W, Reik W, and BI Ageing Clock Team. Multi-tissue DNA methylation age predictor in mouse. Genome Biol. 2017; 18:68.
https://doi.org/10.1186/s13059-017-1203-5

48. Brown-Borg HM. The somatotropic axis and longevity in mice. Am J Physiol Endocrinol Metab. 2015; 309:E503–10.
https://doi.org/10.1152/ajpendo.00262.2015

49. Coschigano KT, Holland AN, Riders ME, List EO, Flyvb-

jerg A, Kopchick JJ. Deletion, but not antagonism, of the mouse growth hormone receptor results in severely decreased body weights, insulin, and insulin-like growth factor I levels and increased life span. Endocrinology. 2003; 144:3799–810. https://doi.org/10.1210/en.2003-0374

50. Flurkey K, Papaconstantinou J, Miller RA, Harrison DE. Lifespan extension and delayed immune and collagen aging in mutant mice with defects in growth hormone production. Proc Natl Acad Sci USA. 2001; 98:6736–41. https://doi.org/10.1073/pnas.111158898

51. Brown-Borg HM, Borg KE, Meliska CJ, Bartke A. Dwarf mice and the ageing process. Nature. 1996; 384:33. https://doi.org/10.1038/384033a0

52. Cannon MV, Buchner DA, Hester J, Miller H, Sehayek E, Nadeau JH, Serre D. Maternal nutrition induces pervasive gene expression changes but no detectable DNA methylation differences in the liver of adult offspring. PLoS One. 2014; 9:e90335. https://doi.org/10.1371/journal.pone.0090335

53. Dempsey KM, Ali HH. Identifying aging-related genes in mouse hippocampus using gateway nodes. BMC Syst Biol. 2014; 8:62. https://doi.org/10.1186/1752-0509-8-62

54. Botelho M, Cavadas C, Neuropeptide Y. Neuropeptide Y: An Anti-Aging Player? Trends Neurosci. 2015; 38:701–11. https://doi.org/10.1016/j.tins.2015.08.012

55. Banki E, Sosnowska D, Tucsek Z, Gautam T, Toth P, Tarantini S, Tamas A, Helyes Z, Reglodi D, Sonntag WE, Csiszar A, Ungvari Z. Age-related decline of autocrine pituitary adenylate cyclase-activating polypeptide impairs angiogenic capacity of rat cerebromicrovascular endothelial cells. J Gerontol A Biol Sci Med Sci. 2015; 70:665–74. https://doi.org/10.1093/gerona/glu116

56. Reglodi D, Jungling A, Longuespée R, Kriegsmann J, Casadonte R, Kriegsmann M, Juhasz T, Bardosi S, Tamas A, Fulop BD, Kovacs K, Nagy Z, Sparks J, et al. Accelerated pre-senile systemic amyloidosis in PACAP knockout mice - a protective role of PACAP in age-related degenerative processes. J Pathol. 2018; 245:478–90. https://doi.org/10.1002/path.5100

57. Beck B. [Feeding regulatory peptides: hopes and limits for the treatment of obesities]. J Soc Biol. 2006; 200:7–16. https://doi.org/10.1051/jbio:2006002

58. Park S, Komatsu T, Kim SE, Tanaka K, Hayashi H, Mori R, Shimokawa I. Neuropeptide Y resists excess loss of fat by lipolysis in calorie-restricted mice: a trait potential for the life-extending effect of calorie restriction. Aging Cell. 2017; 16:339–48. https://doi.org/10.1111/acel.12558

59. Chiba T, Tamashiro Y, Park D, Kusudo T, Fujie R, Komatsu T, Kim SE, Park S, Hayashi H, Mori R, Yamashita H, Chung HY, Shimokawa I. A key role for neuropeptide Y in lifespan extension and cancer suppression via dietary restriction. Sci Rep. 2014; 4:4517. https://doi.org/10.1038/srep04517

60. Horvath S, Oshima J, Martin G, Raj K, Matsuyama S. Epigenetic age estimator for skin and blood applied to Hutchinson Gilford Progeria. 2018. Aging (Albany NY). 2018; 10:1758–75.

61. Lu AT, Xue L, Salfati EL, Chen BH, Ferrucci L, Levy D, Joehanes R, Murabito JM, Kiel DP, Tsai PC, Yet I, Bell JT, Mangino M, et al. GWAS of epigenetic aging rates in blood reveals a critical role for TERT. Nat Commun. 2018; 9:387. https://doi.org/10.1038/s41467-017-02697-5

62. Lu AT, Hannon E, Levine ME, Crimmins EM, Lunnon K, Mill J, Geschwind DH, Horvath S. Genetic architecture of epigenetic and neuronal ageing rates in human brain regions. Nat Commun. 2017; 8:15353. https://doi.org/10.1038/ncomms15353

63. Lu AT, Hannon E, Levine ME, Hao K, Crimmins EM, Lunnon K, Kozlenkov A, Mill J, Dracheva S, Horvath S. Genetic variants near MLST8 and DHX57 affect the epigenetic age of the cerebellum. Nat Commun. 2016; 7:10561. https://doi.org/10.1038/ncomms10561

64. Orozco LD, Farrell C, Hale C, Rubbi L, Rinaldi A, Civelek M, Pan C, Lam L, Montoya D, Edillor C, Seldin M, Boehnke M, Mohlke KL, et al. Epigenome-wide association in adipose tissue from the METSIM cohort. Hum Mol Genet. 2018; 27:2586–2586. https://doi.org/10.1093/hmg/ddy205

65. Barrett T, Wilhite SE, Ledoux P, Evangelista C, Kim IF, Tomashevsky M, Marshall KA, Phillippy KH, Sherman PM, Holko M, Yefanov A, Lee H, Zhang N, et al. NCBI GEO: archive for functional genomics data sets--update. Nucleic Acids Res. 2013; 41:D991–95. https://doi.org/10.1093/nar/gks1193

66. Orozco LD, Morselli M, Rubbi L, Guo W, Go J, Shi H, Lopez D, Furlotte NA, Bennett BJ, Farber CR, Ghazalpour A, Zhang MQ, Bahous R, et al. Epigenome-wide association of liver methylation patterns and complex metabolic traits in mice. Cell Metab. 2015; 21:905–17. https://doi.org/10.1016/j.cmet.2015.04.025

67. Cannon MV, Pilarowski G, Liu X, Serre D. Extensive Epigenetic Changes Accompany Terminal Differentiation of Mouse Hepatocytes After Birth. G3 (Bethesda). 2016; 6:3701–09. https://doi.org/10.1534/g3.116.034785

68. Reizel Y, Spiro A, Sabag O, Skversky Y, Hecht M, Keshet

I, Berman BP, Cedar H. Gender-specific postnatal demethylation and establishment of epigenetic memory. Genes Dev. 2015; 29:923–33. https://doi.org/10.1101/gad.259309.115

69. Guo W, Fiziev P, Yan W, Cokus S, Sun X, Zhang MQ, Chen PY, Pellegrini M. BS-Seeker2: a versatile aligning pipeline for bisulfite sequencing data. BMC Genomics. 2013; 14:774. https://doi.org/10.1186/1471-2164-14-774

70. Krueger F, Andrews SR. Bismark: a flexible aligner and methylation caller for Bisulfite-Seq applications. Bioinformatics. 2011; 27:1571–72. https://doi.org/10.1093/bioinformatics/btr167

71. Clopper CP, Pearson ES. E.S. The use of confidence or fiducial limits illustrated in the case of the binomial. Biometrika. 1934; 26:404–13. https://doi.org/10.1093/biomet/26.4.404

72. Jeffreys H. An invariant form for the prior probability in estimation problems. Proc R Soc Lond A Math Phys Sci. 1946; 186:453–61. https://doi.org/10.1098/rspa.1946.0056

73. Friedman J, Hastie T, Tibshirani R. Regularization Paths for Generalized Linear Models via Coordinate Descent. J Stat Softw. 2010; 33:1–22. https://doi.org/10.18637/jss.v033.i01

74. Bennett BJ, Farber CR, Orozco L, Kang HM, Ghazalpour A, Siemers N, Neubauer M, Neuhaus I, Yordanova R, Guan B, Truong A, Yang WP, He A, et al. A high-resolution association mapping panel for the dissection of complex traits in mice. Genome Res. 2010; 20:281–90. https://doi.org/10.1101/gr.099234.109

75. Lusis AJ, Seldin MM, Allayee H, Bennett BJ, Civelek M, Davis RC, Eskin E, Farber CR, Hui S, Mehrabian M, Norheim F, Pan C, Parks B, et al. The Hybrid Mouse Diversity Panel: a resource for systems genetics analyses of metabolic and cardiovascular traits. J Lipid Res. 2016; 57:925–42. https://doi.org/10.1194/jlr.R066944

76. Reizel Y, Spiro A, Sabag O, Skversky Y, Hecht M, Keshet I, Berman BP, Cedar H. Gender-specific postnatal demethylation and establishment of epigenetic memory. Genes Dev. 2015; 29:923–33. https://doi.org/10.1101/gad.259309.115

This information is provided as supporting information and results to the main ones presented in the manuscript.

SUPPLEMENTARY FIGURES
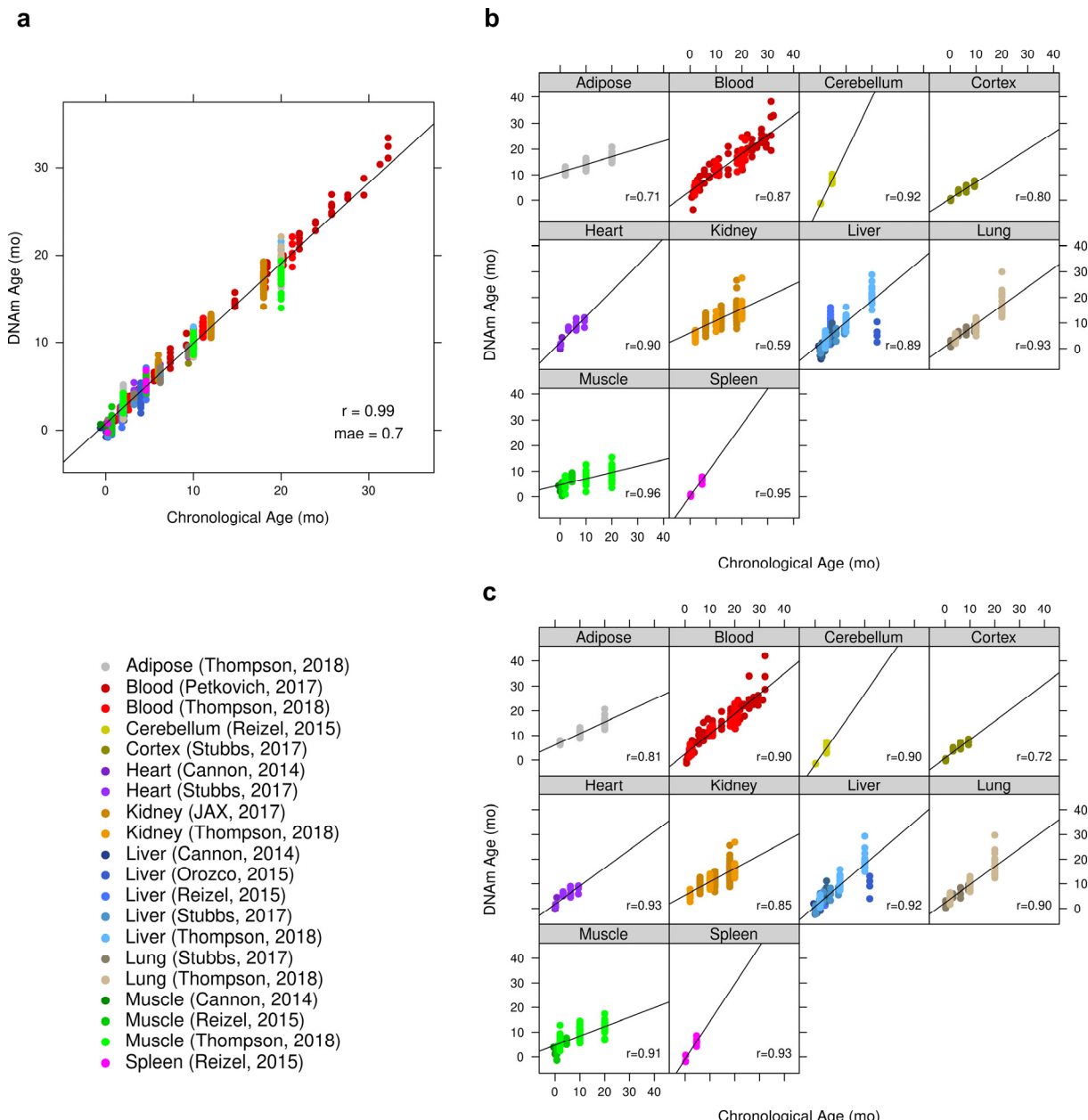
Supplementary Figure 1. Accuracy of the elastic net clock based on all CpGs. DNA methylation age (y-axis) versus chronological age (x-axis) for all mouse samples. (**a**) Performance of elastic regression clock on all training samples. (**b**) Results by tissue type of cross-validated predictions obtained by iteratively withholding one "batch" (tissue x publication). (**c**) Results by tissue type of predictions from leave-one-out-cross-validation.
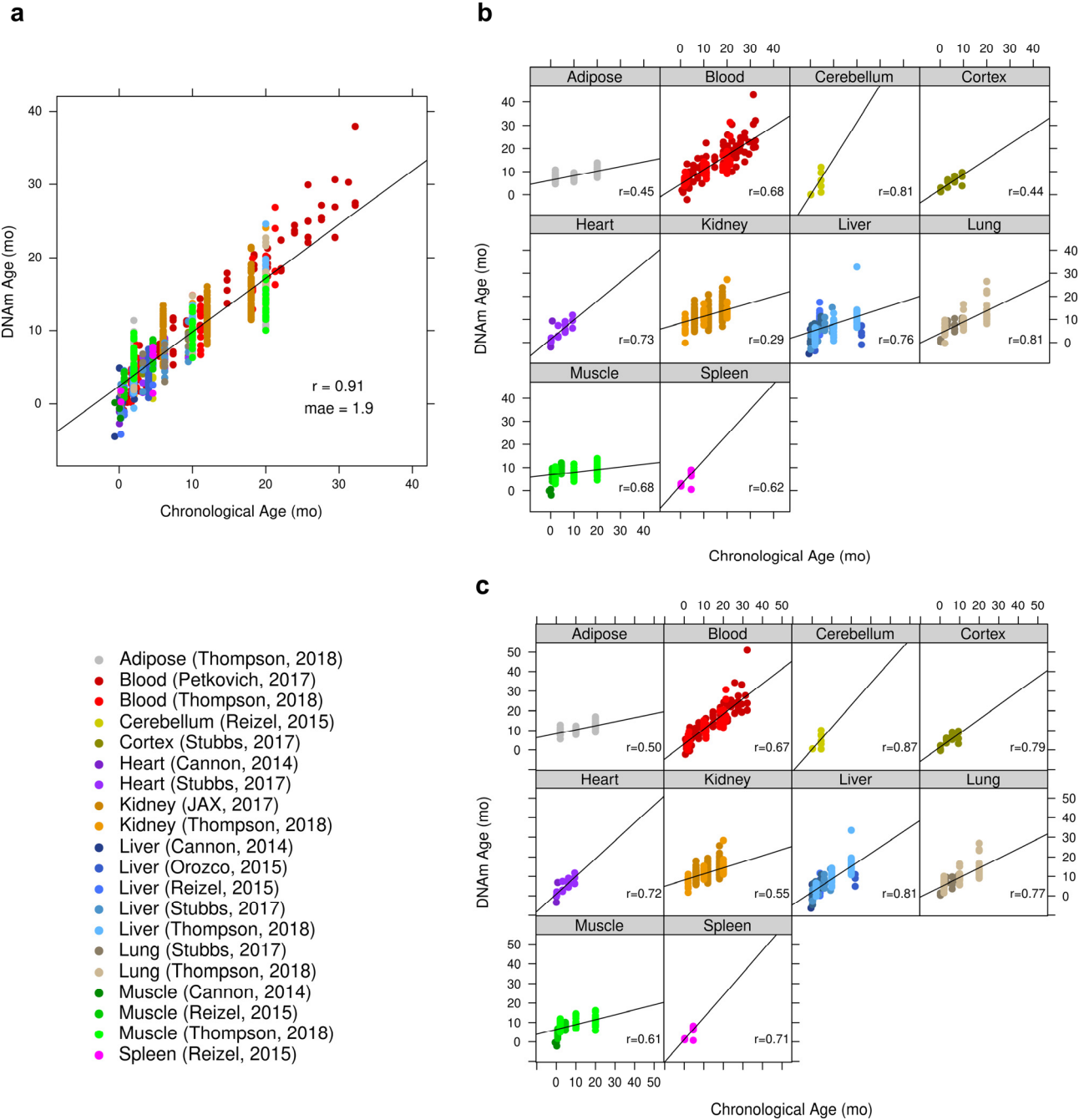
Supplementary Figure 2. Accuracy of the conserved clock based on elastic net regression. DNA methylation age (y-axis) versus chronological age (x-axis) for all mouse samples. (**a**) Performance of elastic net regression clock on all training samples. (**b**) Results by tissue type of cross-validated predictions obtained by iteratively withholding one "batch" (tissue x publication). (**c**) Results by tissue type of predictions from leave-one-out-cross-validation.
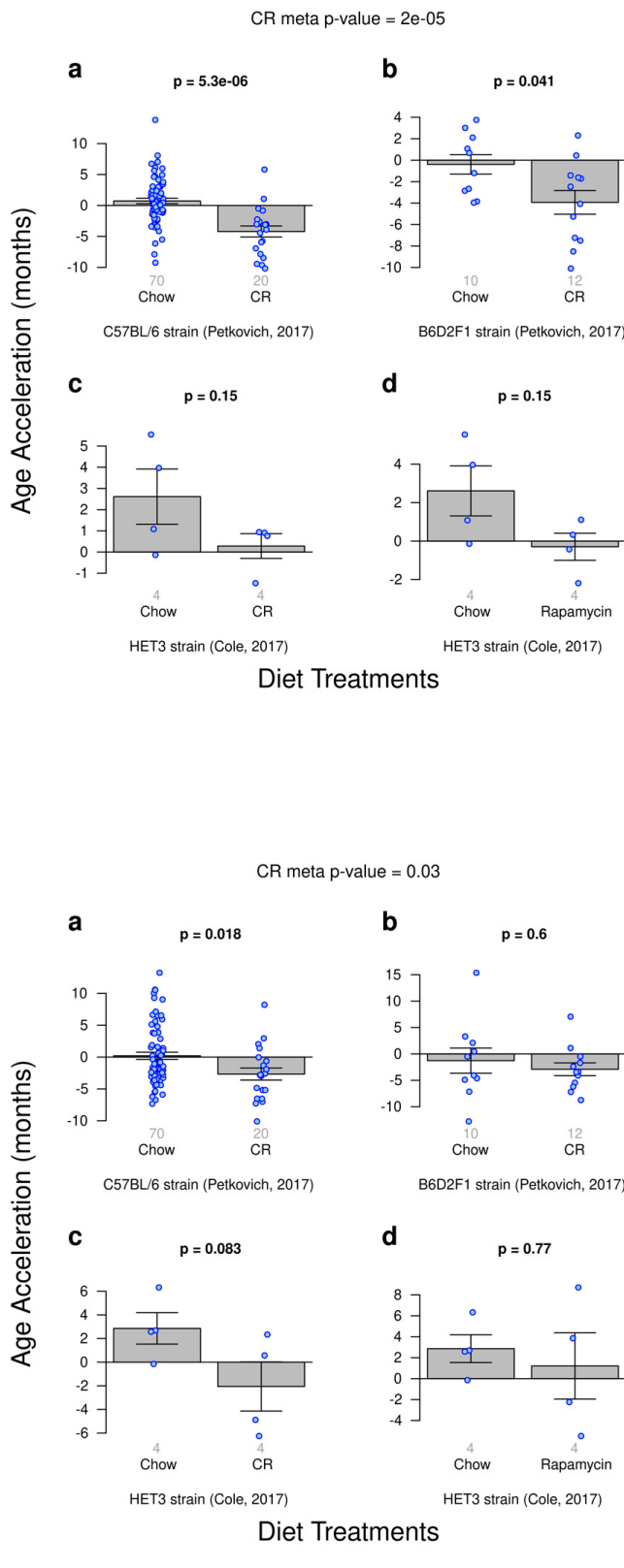
Supplementary Figure 3. This figure corresponds to Fig. 2 in the main text for diet treatments and longevity. The upper panel shows the same results for an elastic net clock using all CpGs as input. The lower panel shows the same results for an elastic net clock using only conserved CpGs as input. Overall, the results for these two clocks are less significant than those observed for the ridge regression clock. But both of these clocks detect anti-epigenetic aging effects CR in the C57BL/6 strain (panel a).
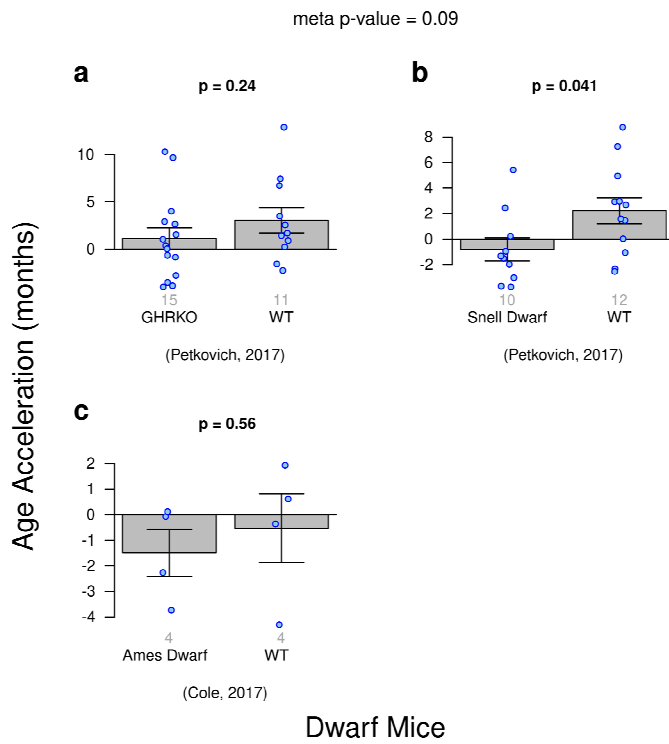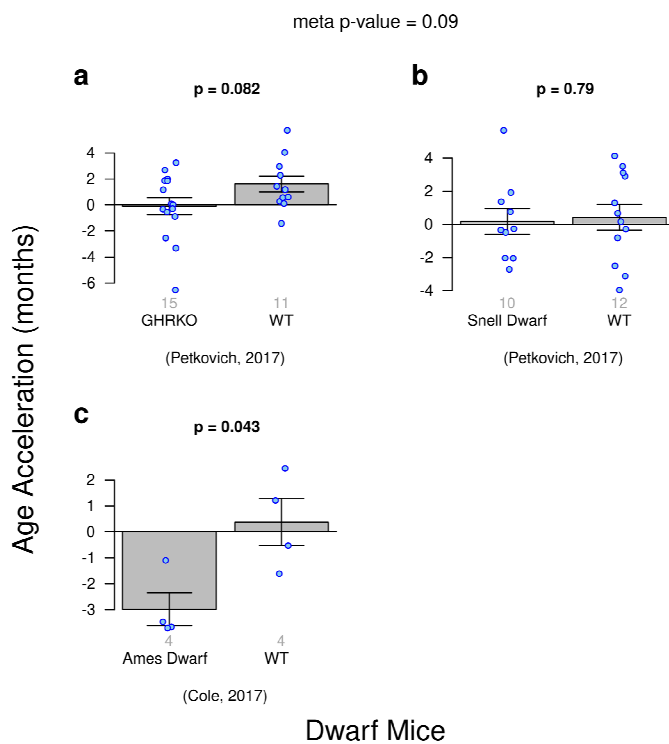
Supplementary Figure 4. This figure corresponds to Fig. 3 in the main text for dwarfism and longevity. The upper panel shows the same results for an elastic net clock using all CpGs as input. The lower panel shows the same results for an elastic net clock using only conserved CpGs as input.

a p = 0.35

b p = 0.16

Maternal HFD   Maternal LFD

Maternal Diet (Cannon, 2014)

a p = 0.62

b p = 0.73

Maternal HFD   Maternal LFD

Maternal Diet (Cannon, 2014)
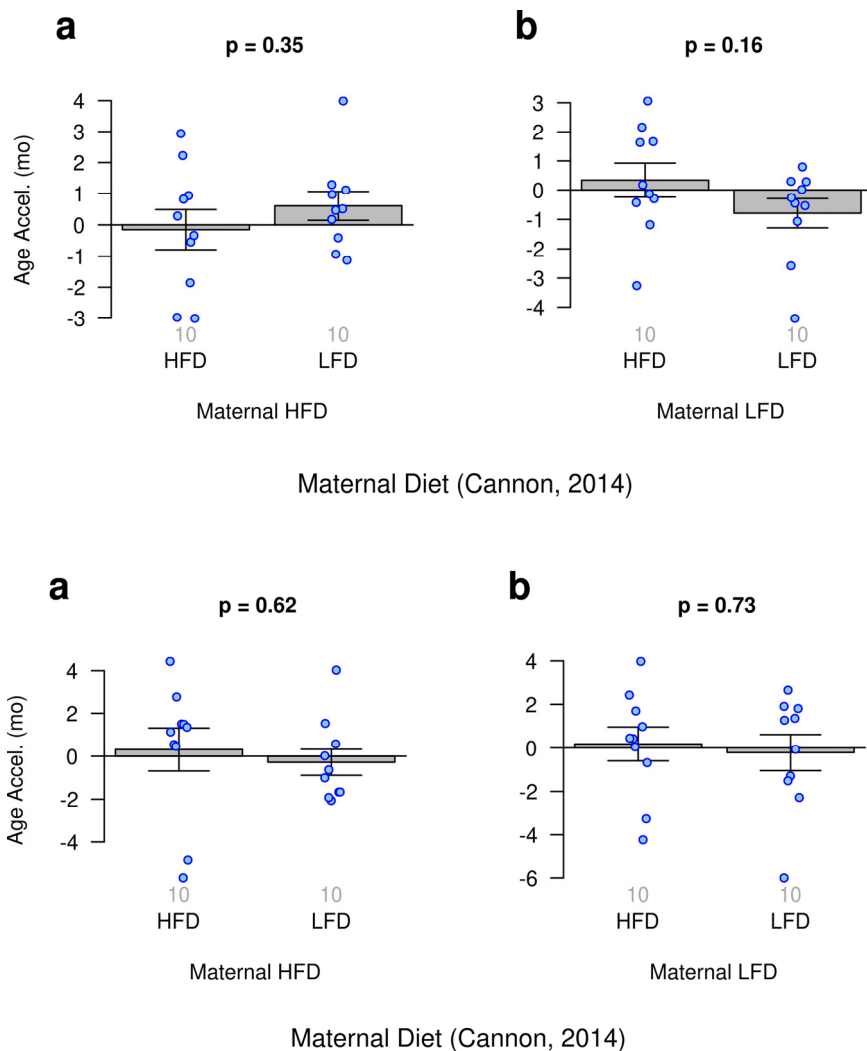
Supplementary Figure 5. This figure corresponds to Fig. 4 in the main text for the effects of maternal diet on DNA methylation in offspring. The upper panel shows the same results for an elastic net clock using all CpGs as input. The lower panel shows the same results for an elastic net clock using only conserved CpGs as input.
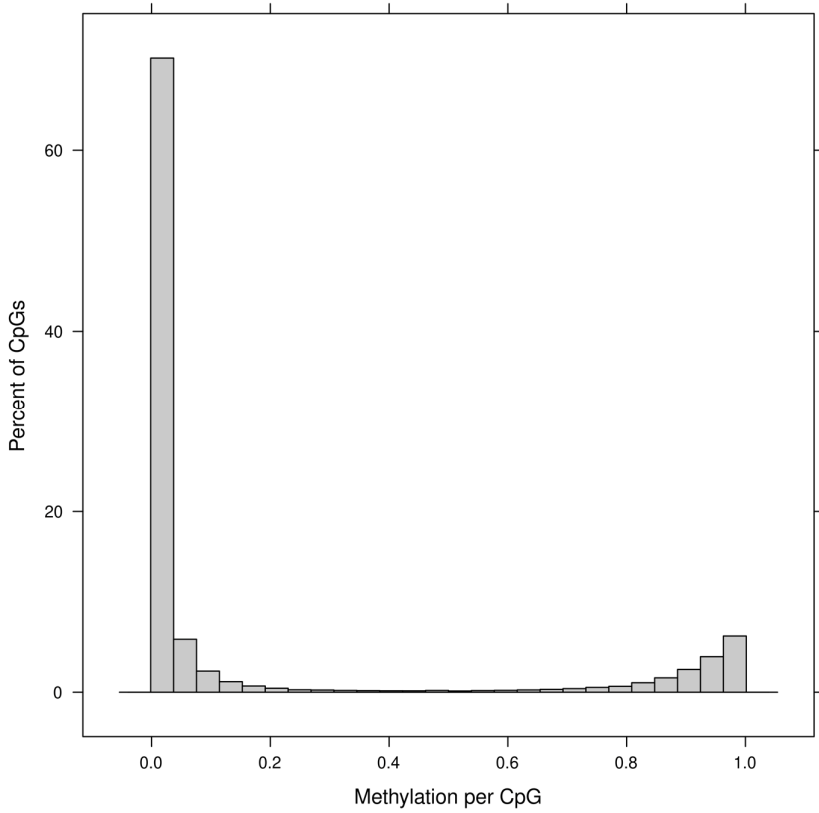
Supplementary Figure 6. Histogram of methylation levels of all CpGs in the training set of samples.

SUPPLEMENTARY TABLES

Please browse Full Text version to see the data of Supplementary Tables:

Supplementary Table 1. CpGs utilized in the elastic net age clock derived from all CpGs measured. Listed are the genomic coordinates, the linear coefficients of the model, and the distances to the transcription site (TSS) of the nearest genes.

Supplementary Table 2. CpGs utilized in the elastic net age clock derived from evolutionarily conserved CpGs for which methylation data was available. Listed are the genomic coordinates, the linear coefficients of the model, and the distances to the transcription site (TSS) of the nearest genes.

Supplementary Table 3. List of strains from the Hybrid Mouse Diversity Panel (HMDP) used in the Genome-Wide Association Study.

Research Paper

Epigenetic ageing is distinct from senescence-mediated ageing and is not prevented by telomerase expression

Sylwia Kabacik[1], Steve Horvath[2], Howard Cohen[3], Kenneth Raj[1]

[1]Cellular Biology Group, Radiation Effects Department, Centre for Radiation, Chemicals and Environmental Hazards (CRCE) Public Health England (PHE) Dicot, Chilton OX11 0RQ, Oxfordshire, United Kingdom
[2]Departments of Human Genetics and Biostatistics, David Geffen School of Medicine, University of California Los Angeles, Los Angeles, CA 90095, USA
[3]Elizabeth House Medical Practice, Warlingham, Surrey CR6 9LF, United Kingdom

ABSTRACT

The paramount role of senescent cells in ageing has prompted suggestions that re-expression of telomerase may prevent ageing; a proposition that is predicated on the assumption that senescent cells are the sole cause of ageing. Recently, several DNA methylation-based age estimators (epigenetic clocks) have been developed and they revealed that increased epigenetic age is associated with a host of age-related conditions, and is predictive of lifespan. Employing these clocks to measure epigenetic age *in vitro*, we interrogated the relationship between epigenetic ageing and telomerase activity. Although hTERT did not induce any perceptible change to the rate of epigenetic ageing, hTERT-expressing cells, which bypassed senescence, continued to age epigenetically. Employment of hTERT mutants revealed that neither telomere synthesis nor immortalisation is necessary for the continued increase in epigenetic age by these cells. Instead, the extension of their lifespan is sufficient to support continued epigenetic ageing of the cell. These characteristics, observed in cells from numerous donors and cell types, reveal epigenetic ageing to be distinct from replicative senescence. Hence, while re-activation of hTERT may stave off physical manifestation of ageing through avoidance of replicative senescence, it would have little impact on epigenetic ageing which continues in spite of telomerase activity.

INTRODUCTION

Although ageing is readily observed at the level of the organism, our understanding of why and how this process occurs has remained speculative until normal human cells were successfully cultured outside the body, where they were found to have a finite capacity to proliferate. Hayflick estimated that a population of human cells grown *ex vivo* can double approximately sixty times after which they adopt a permanent state of dormancy termed replicative senescence [1, 2]. The cause of this natural limitation to proliferation was

eventually found to lie in the "end-replication problem", which if not addressed by the cell, would lead to telomere attrition at every round of DNA replication [3, 4]. It was eventually demonstrated that this does indeed occur and when telomeres shorten to a critical length they trigger cells to adopt the senescent state [5, 6]. The identification of telomerase, which replicates telomeres [7, 8], and the fact that most adult somatic cells do not produce this enzyme, provided the last major piece of the puzzle that describes the ageing process from events beginning with molecules, proceeding to cells and culminating in the organism. Significantly, this chain of

events can be prevented by ectopic expression of hTERT, the catalytic sub-unit of telomerase, which can preserve telomere length and avert senescence of some cells [9, 10]. Impressively, these profound insights into the process of human ageing were acquired from careful study of *ex vivo* cell behaviour.

It was initially thought that the functional and physical deterioration that characterise organismal ageing are a result of insufficient replenishment of cells due to telomere-mediated restriction of cellular proliferation. Senescent cells, which accumulate increasingly in tissues in function of age, were assumed to be passive and merely a consequence of the above-described processes. This notion was short-lived when senescent cells were found to secrete molecules that are detrimental to cells and tissues; a cellular characteristic described as senescence-associated secretory phenotype (SASP) [11-13]. The role of senescent cells in actively causing age-related physical deterioration was elegantly revealed when reversal of ageing phenotype in organs and tissues was observed following the removal of senescent cells in mice [14]. As such, it would follow that if cells were prevented from becoming senescent in the first place, ageing could be avoided. Although there are external instigators such as stress and DNA damage that can also cause cells to become senescent [15], replicative senescence is particular in that it is an intrinsic feature that is part of cellular proliferation and occurs even in an ideal environment. As expression of hTERT has been repeatedly demonstrated to prevent replicative senescence of many different cell types, it is reasonable to consider ectopic expression or re-activation of endogenous hTERT expression as potential means to prevent replicative senescence, delay ageing and improve health [16].

The above proposition would be valid if senescent cells were indeed the only cause of ageing. Relatively recently, an apparently distinct form of ageing, called epigenetic ageing was described (reviewed in [17]). This discovery stems from observations that the methylation states of some specific cytosines that precede guanines (CpGs) in the human genome changed rather reliably and strictly with age [18-22]. This allowed supervised machine learning methods to be applied to DNA methylation data to generate DNA methylation-based age estimators (epigenetic clocks) of epigenetic age, which in the majority of the human population is similar with chronological age [23-27]. The difference between epigenetic age and chronological age, which reflects the rate of epigenetic aging, carries biological significance: increased epigenetic aging is associated with numerous age-related pathologies and conditions [17, 28-41]. Conversely, healthy lifestyle and diet is associated with

younger epigenetic age [17, 42]. Furthermore, epigenetic age can be reversed or reset, as expression of Yamanaka factors in somatic adult cells reset their epigenetic ages to zero [26, 43]. Hence, epigenetic age is not merely an alternative means of determining chronological age but is to some degree a measure of biological age or health; a proposition that is further supported by the impressive demonstration that acceleration of epigenetic ageing is associated with increased risk of all-cause mortality [34, 39]. Collectively, the descriptions above highlight the fact that epigenetic ageing, in spite of the mathematical origins of its discovery, is not a mathematical contrivance but a genuine ageing process innate in cells.

Several DNAm-based biomarkers have been reported in the literature that differ in terms of their applicability (some were developed for specific tissues such as blood) and their biological interpretation. The pan-tissue epigenetic clock developed by Horvath [26] is applicable to almost all sources of DNA with the exception of sperm. The resulting age estimate by this clock is referred to as epigenetic age or more precisely DNAm age. Although the pan-tissue epigenetic clock is highly accurate and applicable to the vast majority of tissues in the body, it performs sub-optimally when estimating the age of fibroblasts. In response to this, we recently developed a new epigenetic age estimator, referred to as skin & blood clock that is more accurate in estimating age of different cell types including fibroblasts, keratinocytes, buccal cells, blood cells, saliva and endothelial cells [44]. Studies employing skin & blood clock and the pan-tissue epigenetic age clock revealed a startling consistency of epigenetic age across diverse tissues from the same individual, even though cellular proliferation rates and frequencies of these tissues are not the same [26, 44]. This suggests that the ticking of the epigenetic clock is not a reflection of proliferation frequency, which is in stark contrast to telomere length, which enumerates cellular division. It would therefore appear that the process of epigenetic ageing is distinct from that which is driven by telomere-mediated senescence. To understand their relationship or interaction, if one indeed exists, we set out to test the impact of hTERT on epigenetic ageing. To this end we employed wild type hTERT that can prevent telomere attrition and its mutants that cannot [45], with some still able to nevertheless prolong cellular lifespan [46]. Expressing these hTERT constructs in primary cells from numerous donors, ages and cell types, we observe that while hTERT expression can indeed prevent cellular senescence, it does not prevent cells from undergoing epigenetic ageing and that extension of cellular lifespan is sufficient to support continued epigenetic ageing of the cell. These simple observations provide a very important piece to the puzzle of the
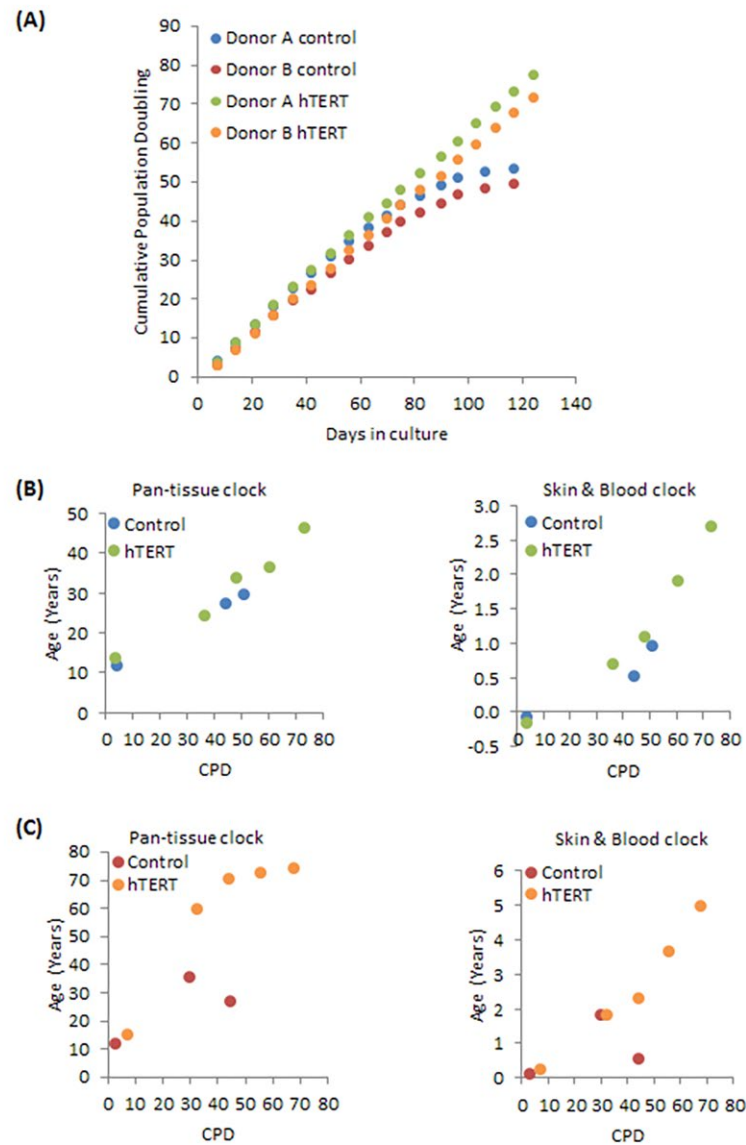
Figure 1. Effects of hTERT on growth and epigenetic ageing of human primary neonatal fibroblasts. (**A**) Growth dynamics of primary cells from two different donors (A and B) transduced with either empty vector (control) or hTERT expressing vector (hTERT). The ages of a selection of cell passages of donor A (**B**) and donor B (**C**) were imputed by the pan-tissue clock (left panel) or the skin & blood clock (right panel). The ages are plotted against cumulative population doubling (CPD) that corresponded to the passage of cells that were analysed.

ageing process because it reveals the distinctiveness of epigenetic ageing from replicative senescence-mediated ageing. They provide further empirical support to the epidemiological observation that hTERT variant that is associated with longer telomeres are also associated with greater epigenetic ageing [47].

RESULTS

To test the effect of hTERT on epigenetic ageing, we first transduced primary neonatal foreskin fibroblasts with hTERT vectors and subjected them and the control isogenic cells, which harbour empty vectors, to continuous culture with passaging. The growth curve in Figure 1A shows that control fibroblasts from neonatal donors A and B (blue and red dots) senesced after about a hundred days in culture and having doubled approximately 50 times (supplementary Figures 1 and 2A). Unsurprisingly, cells bearing hTERT expression vector bypassed replicative senescence. They proliferated unabated beyond 130 days and 75 cumulative population doubling. The last green and
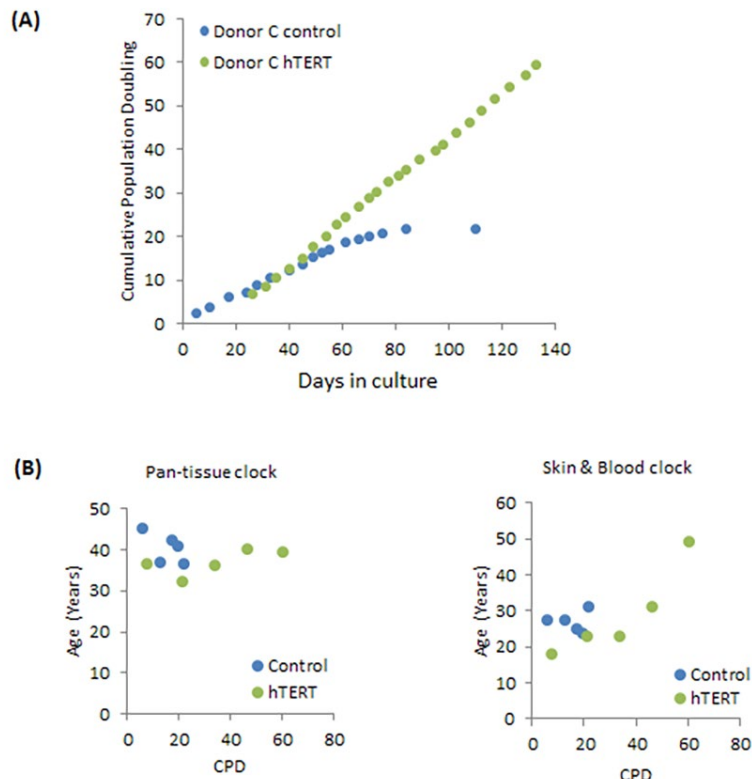
Figure 2. Effects of hTERT on growth and epigenetic ageing of adult primary human coronary artery endothelial cells. (**A**) Growth dynamics of primary cells from one donor (C) transduced with either empty vector (control) or hTERT expression vector (hTERT). (**B**) The ages of a selection of cell passages of donor C were imputed by the pan-tissue clock (left panel) or the skin & blood clock (right panel). The ages are plotted against cumulative population doubling (CPD) that corresponded to the passage of cells that were analysed.

orange dots represent the time-point at which the experiments were terminated, and not the end of cellular viability. These cells have effectively become immortalised. Cellular DNA from a selection of cell passages were subjected to methylation analyses with Illumina EPIC array. The resulting data were processed using the pan-tissue clock and the new skin & blood clock. The results in Figure 1B (for Donor A) and Figure 1C (for Donor B) show control cells to age in culture and this was not perturbed by hTERT expression. Importantly, cells transduced with hTERT not only evaded replicative senescence, their epigenetic ages continued to steadily increase past the point of replicative senescence encountered by their respective isogenic control counterparts (last blue and red dots). While this behaviour is observed with results derived from both epigenetic ageing clocks, the pan-tissue clock clearly displays an off-set from the chronological age of the neonatal cells, which is zero years, as correctly indicated by the skin & blood clock. Incidentally, this systematic offset/error in accurately estimating the epigenetic age of young fibroblasts was one of the reasons for developing the skin & blood clock.

To ascertain whether the effect of hTERT seen in neonatal foreskin fibroblasts was observable in cells from another tissue and age, we utilised human coronary artery endothelial cells (HCAEC) from adult donor (Donor C; 19 years old). The growth dynamics of these cells as shown in Figure 2A are similar in principle with those of the neonatal fibroblasts, with the difference being the earlier time-point at which the control cells senesce (Supplementary Figure 2B). This is consistent with them being adult cells and as such would have lower replicative potential. As with neonatal fibroblasts, the adult HCAEC expressing hTERT were also immortalised. A startling difference however, is apparent when the ages of these cells were estimated by the two clocks (Figure 2B). While once again the skin & blood clock showed hTERT-expressing cells, which bypassed replicative senescence, to continue ageing steadily, the epigenetic age estimates from the pan tissue clock were much higher and with no significant change in age (Figure 2B). We have observed similar pattern with HCAEC isolated from another donor (26 years old) [44].

Table 1. Mutants of hTERT used in the experiments.

	Catalytic activity	Extension of Life-span	Telomere Synthesis	Immortalisation
hTERT wt	YES	YES	YES	YES
hTERT IA	YES	YES	NO	NO
hTERT N-DAT116	YES	YES	NO	NO
hTERT N-DAT92	YES	NO	NO	NO

The characteristics of the hTERT mutants in the left column are indicated by yes or no in regards to whether they are capable of lifespan extension, telomere synthesis or cellular immortalisation.
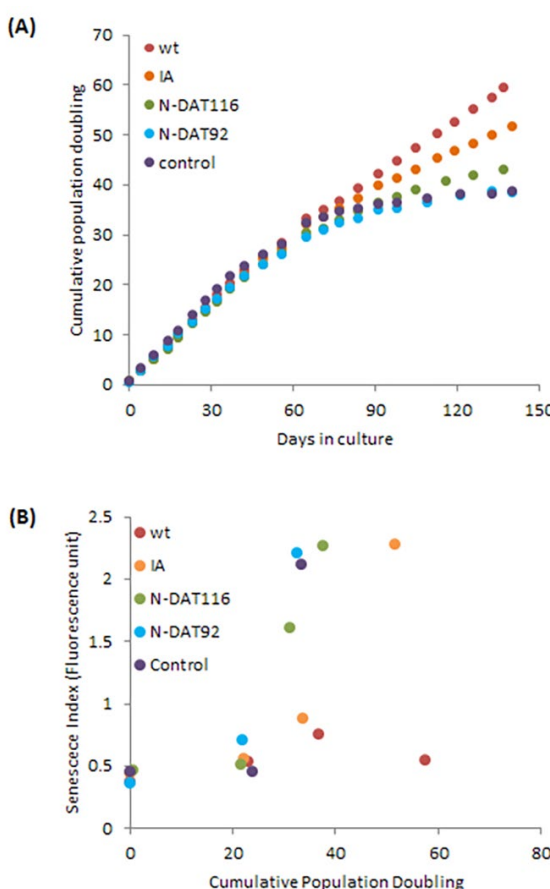
Figure 3. Effects of hTERT and its mutants on growth and senescence of human primary neonatal fibroblasts. (**A**) Growth dynamics of primary cells transduced with either empty vector (control), vector expressing wildtype hTERT (WT), IA mutant (IA), N-DAT116 mutant (N116) or N-DAT92 mutant (N92). (**B**) Cells from a selection of passages were subjected to senescence assay and the senescence index is plotted against cumulative population doubling that corresponded to the passage of cells that were analysed.

To further investigate the relationship between hTERT and epigenetic ageing, we employed a previously validated and published panel of hTERT mutants which all possess catalytic activity but are compromised in one or several hTERT properties, namely, extension of replicative lifespan, telomere synthesis or immortalisation (Table 1 and Supplementary Figure 3) [48]. The growth characteristics of the neonatal foreskin fibroblasts transduced with these vectors confirmed that cells expressing wildtype hTERT bypassed replicative senescence (Figure 3) and aged steadily pass the point of replicative senescence encountered by the control cells (Figure 4A). Notably the hTERT IA mutant [46], which can significantly extend replicative lifespan (Figure 3) but can neither replicate telomeres nor immortalise cells, is also able to elicit steady epigenetic ageing pass the point of replicative senescence of the control cells (Figure 4B). This feature is particularly important because it shows that neither telomere synthesis nor immortalisation contribute to the steady rise in epigenetic ageing seen with hTERT-expressing cells. Instead extension of cellular lifespan appears to be the critical property associated with increased epigenetic ageing. Accordingly, the N-DAT116 mutant [46], which was reportedly also able to extend cellular lifespan of human mammary epithelial cells [46, 48], but did so only very marginally with neonatal fibroblasts, did not cause a substantial rise in epigenetic ageing (Figure 4C). Likewise the N-DAT92 [46] hTERT mutant that does not increase lifespan also did not increase epigenetic ageing (Figure 4D). The patterns described above largely hold true between the two epigenetic age clocks. It is evident that age scatter plots derived from the pan-tissue clock appear more linear, as is seen in the composite plot in Figure 4E. This is not surprising as the spread of ages estimated by it is much greater than those by the skin & blood clock. Notwithstanding the age off-set that is apparent with the
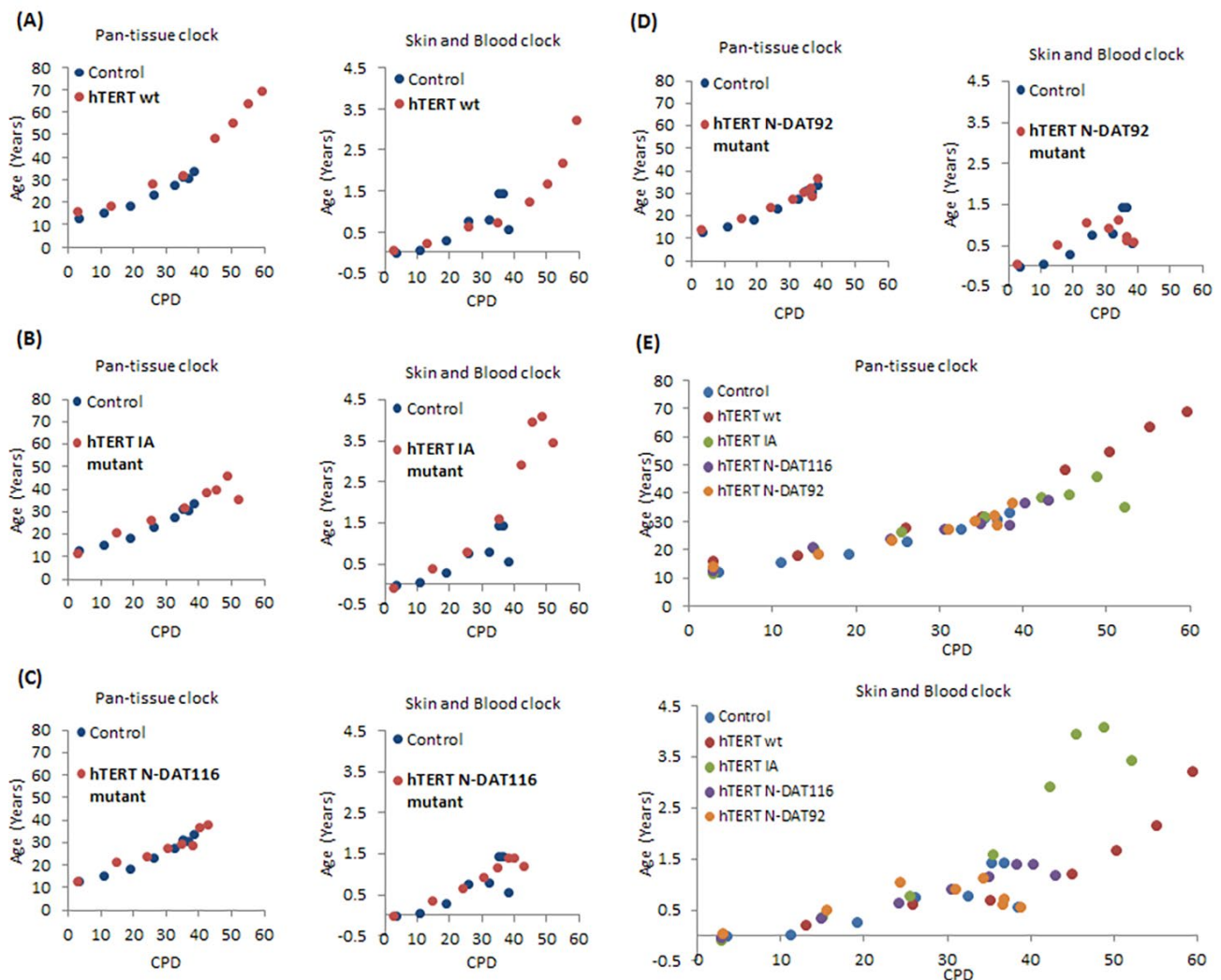
Figure 4. Effects of hTERT and its mutants on epigenetic ageing of human primary neonatal fibroblasts. Ages of primary human neonatal fibroblasts bearing empty vector (blue dots), wildtype hTERT (**A**), IA mutant (**B**), N-DAT116 mutant (**C**) or N-DAT92 mutant (**D**) were determined using the pan-tissue clock (left panel) and the skin & blood clock (right panel). (**E**) Composite plot of all the hTERT mutants. The ages of cells from a selection of passages are plotted against cumulative population doubling (CPD) that corresponded to the passages of cells that were analysed.

pan-tissue clock, and the greater noise of the skin & blood clock, their results are consistent in showing that while hTERT can prevent replicative senescence, it is ineffective in stopping epigenetic ageing.

DISCUSSION

We carried out these simple but very long-drawn out experiments to interrogate the connection, if there was one, between replicative senescence (as mediated by telomeres) and epigenetic ageing. In order to interpret these findings correctly, it is necessary to be reminded that epigenetic age, as imputed by the epigenetic clocks is neither a measure of cellular proliferation rate nor a

measure of proliferation or passage number. This is evident from the fact that epigenetic age of isogenic tissues (from the same individual) with high and low turn-over rates (blood and heart for example) are similar [26, 44]. Epigenetic ageing is also not a measure of senescent cells, as is evident from this study where epigenetic age continues to rise inexorably in hTERT-expressing cells, which do not senesce. These characteristics underline the distinctiveness of epigenetic ageing from replicative senescence-mediated ageing, which supports our previous findings [49] and three genome-wide association studies (GWAS) which did not detect a relationship between telomere length and epigenetic ageing [50-53].

Do these two different ageing processes interact? Since hTERT-expressing cells (subsequently referred to as hTERT cells) exhibit greater age, it would appear that hTERT promotes epigenetic ageing. This however is not the case because hTERT cells do not exhibit higher ages than control cells prior to the point of replicative senescence of the latter. This is evident from the similar gradient of age increase between control and hTERT cells. The acquisition of greater age by hTERT cells after senescence of the control cells is a smooth continuum of the ageing gradient. As such, observations from these experiments do not support the proposition that hTERT stimulates epigenetic ageing. Instead, by causing cells to bypass replicative senescence, hTERT allows the inherent process of epigenetic ageing, which occurs regardless of its presence, to continue. Put simply, while hTERT may appear on the surface, to exacerbate the epigenetic ageing of cells, in truth hTERT, by preventing telomere attrition, prolonged the lifespan of the cells, allowing them growing older (as measured by the epigenetic clocks).

Accordingly, telomere synthesis and immortalisation are not necessary for the acquisition of greater age; a point that is clearly made by hTERT IA mutant, which increased epigenetic age in spite of its inability to maintain telomere length or immortalise cells, but is still able to extend lifespan [46]. It is interesting that although both IA and N-DAT116 mutants are reportedly able to increase life-span of human mammary epithelial cells [46, 48], the magnitude of their effect in human neonatal fibroblasts is very different. The hTERT IA mutant, which is far more effective in this regard, is also highly effective in increasing epigenetic age. The hTERT N-DAT116 mutant on the other hand induces only a marginal increase in lifespan and accordingly, no age increase beyond the control cells is evident (measured by the skin and blood clock) and a correspondingly small increase as measured by the pan-tissue clock. These observations are consistent and they point to increased epigenetic ageing in hTERT cells as a result of extension of lifespan.

This conclusion is also consistent with the recently reported genome-wide association study (GWAS) that identified an variant of hTERT that is associated with increased epigenetic ageing [47]. Interestingly, this allele is also associated with longer telomeres. This observation appeared counter-intuitive in the first instance because short telomeres are unequivocally associated with greater age. As such hTERT variants that generate short telomeres would be expected to be associated with increased epigenetic ageing. The apparent paradox disappears when it is realised that while telomere length undoubtedly records the proliferative history of the cell, it also indicates its proliferative or lifespan potential. As such, cells with longer telomeres have longer lifespan, and as empirically demonstrated here, longer lifespan is accompanied by greater epigenetic ageing. In other words, ectopic expression of hTERT (in this study) and expression of a natural hTERT locus variant associated with longer telomeres *in vivo* (suggested by GWAS) would increase cellular lifespan, with the consequence of greater epigenetic ageing.

The distinctiveness and independence of epigenetic ageing from replicative senescence, exerts a serious impact on ageing intervention strategies. It is likely that re-activation of hTERT expression or elimination of senescent cells will go some way to mitigate the effects of ageing. These measures however, are unlikely to be sufficient to halt ageing altogether since they will not prevent epigenetic ageing. Interventions that prevent or eliminate senescent cells hold great promise for extending human healthspan. Our study suggests that these interventions might not arrest epigenetic aging, which is disconcerting considering the over-whelming evidence that point to the association between accelerated epigenetic ageing and a host of disparate diseases and conditions [17, 28-41]. To what extent epigenetic aging of various cells causes the decline in organ function remains an area of active research, but it is arguable that to maximise healthspan there may be a need to develop compounds that target epigenetic ageing as well. In this regard the new skin & blood clock can form the basis of an assay to test for such interventions. This clock out-performs the pan-tissue clock which is already highly accurate for most tissues and cells in the body, but for unknown reasons exhibit a considerable age off-set when used on some cells cultured *in vitro*. Furthermore, the pan tissue clock also differed substantially from the skin & blood clock when applied to adult human coronary artery cells: unlike the skin & blood clock, it led to a substantial offset and did not reveal the increase of epigenetic age in function of cell growth. We have at present, no explanation for this curious observation. Overall, it appears that the skin & blood clock is more suitable for cultured cells, which is particularly important because the ability to accurately measure cellular age *in vitro* will allow the yet unknown mechanism of the epigenetic clock to be elucidated more easily. Gratifyingly, the compatibility of the skin & blood clock with cells *in vitro* does not come with any loss of compatibility with cells *in vivo,* as was recently described [44].

In summary, these experiments greatly advance our understanding of the connection between epigenetic ageing and senescence-mediated ageing and on this, they have successfully provided empirical evidence that

these two mechanisms of ageing are distinct and uncoupled. With the tools that are available (epigenetic clock and primary cells) and the realisation of the difference between these two ageing processes, we are in much improved position to proceed towards understanding the mechanism of epigenetic ageing and its role in human pathology.

MATERIALS AND METHODS

Isolation and culture of primary cells

Primary human neonatal fibroblasts were isolated from circumcised foreskins. Informed consent was obtained prior to collection of human skin samples with approval from the Oxford Research Ethics Committee; reference 10/H0605/1. The tissue was cut into small pieces and digested overnight at 4 °C with 0.5 mg/ml Liberase DH in CnT-07 keratinocyte medium (CellnTech) supplemented with penicillin/streptomycin (Sigma) and gentamycin/amphotericin (Life Tech). Following digestion, the epidermis was peeled off from the tissue pieces. The de-epidermised tissue pieces were placed faced down on plastic cell culture plates and allowed partially dry before addition of DMEM supplemented with 10% FBS and antibiotics. After several days incubation in a 37 °C, 5% CO_2 humidified environment, fibroblasts can be seen to migrate out from the tissue pieces and when their growth reached confluence, they were trypsinised, counted and seeded into fresh plates for experiments. Adult human coronary artery endothelial cells (HCAEC) were purchased from Cell Applications (USA) and cultured in MesoEndo Cell Growth Medium (Sigma) at 37 °C humidified incubator with 5% CO_2.

Neonatal foreskin fibroblasts

100,000 cells were seeded into a 10cm plate and cultured as described above. Upon confluence the cells were harvested with trypsin digestion followed by neutralisation with soybean trypsin inhibitor. The number of cells was ascertained and 100,000 was taken and seeded into a fresh plate. The remaining cells were used for DNA extraction. Population doubling was calculated with the following formula: [log(number of cells harvested) – log(number of cells seeded)] x 3.32. Cumulative population doubling was obtained by addition of population doubling of each passage.

Adult human coronary artery endothelial cells

500,000 cells were seeded into a fibronectin-coated 75cm^2 flask and cultured as described above. The procedure of passing the cells, counting and ascertaining population doubling is similar to those described for neonatal foreskin fibroblasts above.

Retroviral-mediated transduction of cells with hTERT vectors

The procedure of transducing neonatal foreskin fibroblasts and adult human coronary artery endothelial cells are similar with the exception of the media that is used to collect the retroviruses.

The various retroviral vectors bearing wildtype hTERT (Addgene, cat. 1774), IA mutant, N-DAT116 mutant, HA mutant or N-DAT92 mutant (kind gifts from Dr. Christopher Counter, USA) were individually transfected into Phoenix A cells using the calcium chloride method according to the manufacturer's instructions (Profection Cat No: E1200 Promega). They next day, media were removed from the transfectants and replaced with either DMEM supplemented with 10% foetal calf serum (for subsequent use on neonatal fibroblasts) or MesoEndo media (for infection of human coronary artery endothelial cells). The following day, the media containing recombinant retroviruses were collected, filtered through 0.45micron filter and mixed with polybrene (Sigma) up to 9ug/ml and used to feed the cells intended for infection. The next day, fresh media containing puromycin (1ug/ml) was given to the cells. After 3-4 days when all the control cells in the uninfected plates were dead, the surviving infectants were grown and used for experiments as described above.

DNA extraction

DNA was extracted from cells using the Zymo Quick DNA mini-prep plus kit (D4069) according to the manufacturer's instructions and DNA methylation levels were measured on Illumina 850 EPIC arrays according to the manufacturer's instructions.

Cellular senescence assay

Cells were trypsinised, neutralised and counted. After centrifugation at 8,000 revolutions per minute in a micro-centrifuge, cell pellet was resuspended in 200 μl reaction buffer (Cell Signaling, Senescence β-Galactosidase Staining Kit #9860) containing 10 mM FDG and 0.2% of TritonX-100. After an hour of incubation at 37ºC, measurements of fluorescence were made with a plate reader with emission at 488 nm. The fluorescence reading is divided by the cell number to obtain the fluorescence index.

DNA methylation data

The Illumina BeadChips (EPIC or 450K) measures bisulfite-conversion-based, single-CpG resolution DNAm levels at different CpG sites in the human genome. These data were generated by following the standard protocol of Illumina methylation assays, which quantifies methylation levels by the β value using the ratio of intensities between methylated and un-methylated alleles. Specifically, the β value is calculated from the intensity of the methylated (M corresponding to signal A) and un-methylated (U corresponding to signal B) alleles, as the ratio of fluorescent signals $\beta = Max(M,0)/[Max(M,0)+Max(U,0)+100]$. Thus, β values range from 0 (completely un-methylated) to 1 (completely methylated). We used the "noob" normalization method, which is implemented in the "minfi" R package. Both pan-tissue clock and Skin & blood clock algorithms were previously published [26, 44].

Western blot analysis

30 μg of protein lysates were separated on 6 % polyacrylamide gel and transferred onto PVDF membrane (Bio-Rad, cat. 170-4156) using semidry Trans-Blot® Turbo™ Transfer System (Bio-Rad) and high molecular weight standard protocol. Membranes were blocked in 5 % TBS-T milk at room temperature for a minimum of 1 hour with gentle rocking and incubated overnight at room temperature with the following primary antibodies: hTERT (Rockland, cat. 600-401-252, 1:10 000 dilution) and GAPDH (Santa Cruz, cat. sc-25778, 1:30 000 dilution).

Telomerase catalytic activity (TRAP) assay

Telomerase catalytic activity (TRAP) was measured using TRAPEZE® RT Telomerase Detection Kit (Millipore, cat. S7710) according to manufacturer's instructions. Briefly, for each sample 1 million cells was resuspended in CHAPS buffer supplemented with 0.2U/μl of Superaze in inhibitor and incubated on ice for 30 min. Cellular debris were pelleted for 20 min at 12 000 g at 4 °C, supernatant aliquoted into fresh low protein binding tubes and stored at -80°C until further use; 5μl of the lysates was used for protein concentration measurement. Real-time quantitative PCR was performed using RotorGene Q. All reactions were run in triplicate using master mix provided with the kit and AccuStart II Taq DNA polymerase (Quanta Bioscience, cat. 733-2258). Equivalent of 2500 cells was used per reaction. Cycling parameters were 30 min at 30°C, then 2.0 min at 95 °C, followed by 45 cycles of 15 sec at 94 °C, 60 sec at 59 °C and 10 sec at 45 °C where fluorescence readings were taken.

Data was collected and analysed by RotorGene Q analysis software using standard curve prepared from artificial template provided with the kit. The following controls were run with the samples, positive and negative hTERT control, non-template control and heat inactivated control for each sample analysed.

Abbreviations

CpG - CpG island; hTERT - the catalytic sub-unit of telomerase; SASP - senescence-associated secretory phenotype.

AUTHOR CONTRIBUTIONS

SK and KR performed the experiments. SH carried out the statistical analysis. HC provided skin tissue samples. KR, SH and SK conceived the study, KR wrote the manuscript.

ACKNOWLEDGMENTS

CONFLICTS OF INTEREST

UC Regents, the employer of SH, has filed patent applications directed at the epigenetic biomarkers mentioned in the article. The other authors declare no conflict of interest.

FUNDING

REFERENCES

1. Hayflick L. The limited in vitro lifetime of human diploid cell strains. Exp Cell Res. 1965; 37:614–36. https://doi.org/10.1016/0014-4827(65)90211-9

2. Hayflick L, Moorhead PS. The serial cultivation of human diploid cell strains. Exp Cell Res. 1961; 25:585–621. https://doi.org/10.1016/0014-4827(61)90192-6

3. Watson JD. Origin of concatemeric T7 DNA. Nat New Biol. 1972; 239:197–201. https://doi.org/10.1038/newbio239197a0

4. Olovnikov AM. A theory of marginotomy. The incomplete copying of template margin in enzymic synthesis of polynucleotides and biological significance of the phenomenon. J Theor Biol. 1973; 41:181–90. https://doi.org/10.1016/0022-5193(73)90198-7

5. Harley CB, Futcher AB, Greider CW. Telomeres shorten during ageing of human fibroblasts. Nature. 1990; 345:458–60. https://doi.org/10.1038/345458a0

6. Harley CB, Vaziri H, Counter CM, Allsopp RC. The telomere hypothesis of cellular aging. Exp Gerontol. 1992; 27:375–82. https://doi.org/10.1016/0531-5565(92)90068-B

7. Greider CW, Blackburn EH. The telomere terminal transferase of Tetrahymena is a ribonucleoprotein enzyme with two kinds of primer specificity. Cell. 1987; 51:887–98. https://doi.org/10.1016/0092-8674(87)90576-9

8. Blackburn EH, Greider CW, Szostak JW. Telomeres and telomerase: the path from maize, Tetrahymena and yeast to human cancer and aging. Nat Med. 2006; 12:1133–38. https://doi.org/10.1038/nm1006-1133

9. Vaziri H, Benchimol S. Reconstitution of telomerase activity in normal human cells leads to elongation of telomeres and extended replicative life span. Curr Biol. 1998; 8:279–82. https://doi.org/10.1016/S0960-9822(98)70109-5

10. Bodnar AG, Ouellette M, Frolkis M, Holt SE, Chiu CP, Morin GB, Harley CB, Shay JW, Lichtsteiner S, Wright WE. Extension of life-span by introduction of telomerase into normal human cells. Science. 1998; 279:349–52. https://doi.org/10.1126/science.279.5349.349

11. Young AR, Narita M. SASP reflects senescence. EMBO Rep. 2009; 10:228–30. https://doi.org/10.1038/embor.2009.22

12. Campisi J, d'Adda di Fagagna F. Cellular senescence: when bad things happen to good cells. Nat Rev Mol Cell Biol. 2007; 8:729–40. https://doi.org/10.1038/nrm2233

13. Kuilman T, Peeper DS. Senescence-messaging secretome: SMS-ing cellular stress. Nat Rev Cancer. 2009; 9:81–94. https://doi.org/10.1038/nrc2560

14. Baker DJ, Wijshake T, Tchkonia T, LeBrasseur NK, Childs BG, van de Sluis B, Kirkland JL, van Deursen JM. Clearance of p16Ink4a-positive senescent cells delays ageing-associated disorders. Nature. 2011; 479:232–36. https://doi.org/10.1038/nature10600

15. Regulski MJ. Cellular Senescence: What, Why, and How. Wounds. 2017; 29:168–74.

16. Boccardi V, Herbig U. Telomerase gene therapy: a novel approach to combat aging. EMBO Mol Med. 2012; 4:685–87. https://doi.org/10.1002/emmm.201200246

17. Horvath S, Raj K. DNA methylation-based biomarkers and the epigenetic clock theory of ageing. Nat Rev Genet. 2018; 19:371–84. https://doi.org/10.1038/s41576-018-0004-3

18. Teschendorff AE, Menon U, Gentry-Maharaj A, Ramus SJ, Weisenberger DJ, Shen H, Campan M, Noushmehr H, Bell CG, Maxwell AP, Savage DA, Mueller-Holzner E, Marth C, et al. Age-dependent DNA methylation of genes that are suppressed in stem cells is a hallmark of cancer. Genome Res. 2010; 20:440–46. https://doi.org/10.1101/gr.103606.109

19. Hernandez DG, Nalls MA, Gibbs JR, Arepalli S, van der Brug M, Chong S, Moore M, Longo DL, Cookson MR, Traynor BJ, Singleton AB. Distinct DNA methylation changes highly correlated with chronological age in the human brain. Hum Mol Genet. 2011; 20:1164–72. https://doi.org/10.1093/hmg/ddq561

20. Rakyan VK, Down TA, Maslau S, Andrew T, Yang TP, Beyan H, Whittaker P, McCann OT, Finer S, Valdes AM, Leslie RD, Deloukas P, Spector TD. Human aging-associated DNA hypermethylation occurs preferentially at bivalent chromatin domains. Genome Res. 2010; 20:434–39. https://doi.org/10.1101/gr.103101.109

21. Bell JT, Tsai PC, Yang TP, Pidsley R, Nisbet J, Glass D, Mangino M, Zhai G, Zhang F, Valdes A, Shin SY, Dempster EL, Murray RM, et al, and MuTHER Consortium. Epigenome-wide scans identify differentially methylated regions for age and age-related phenotypes in a healthy ageing population. PLoS Genet. 2012; 8:e1002629. https://doi.org/10.1371/journal.pgen.1002629

22. Numata S, Ye T, Hyde TM, Guitart-Navarro X, Tao R, Wininger M, Colantuoni C, Weinberger DR, Kleinman JE, Lipska BK. DNA methylation signatures in development and aging of the human prefrontal cortex. Am J Hum Genet. 2012; 90:260–72. https://doi.org/10.1016/j.ajhg.2011.12.020

23. Bocklandt S, Lin W, Sehl ME, Sánchez FJ, Sinsheimer JS, Horvath S, Vilain E. Epigenetic predictor of age. PLoS One. 2011; 6:e14821. https://doi.org/10.1371/journal.pone.0014821

24. Florath I, Butterbach K, Müller H, Bewerunge-Hudler M, Brenner H. Cross-sectional and longitudinal changes in DNA methylation with age: an epigenome-wide analysis revealing over 60 novel age-associated CpG sites. Hum Mol Genet. 2014; 23:1186–201. https://doi.org/10.1093/hmg/ddt531

25. Hannum G, Guinney J, Zhao L, Zhang L, Hughes G, Sadda S, Klotzle B, Bibikova M, Fan JB, Gao Y, Deconde R, Chen M, Rajapakse I, et al. Genome-wide methylation profiles reveal quantitative views of human aging rates. Mol Cell. 2013; 49:359–67. https://doi.org/10.1016/j.molcel.2012.10.016

26. Horvath S. DNA methylation age of human tissues and cell types. Genome Biol. 2013; 14:R115. https://doi.org/10.1186/gb-2013-14-10-r115

27. Weidner CI, Lin Q, Koch CM, Eisele L, Beier F, Ziegler P, Bauerschlag DO, Jöckel KH, Erbel R, Mühleisen TW, Zenke M, Brümmendorf TH, Wagner W. Aging of blood can be tracked by DNA methylation changes at just three CpG sites. Genome Biol. 2014; 15:R24. https://doi.org/10.1186/gb-2014-15-2-r24

28. Horvath S, Erhart W, Brosch M, Ammerpohl O, von Schönfels W, Ahrens M, Heits N, Bell JT, Tsai PC, Spector TD, Deloukas P, Siebert R, Sipos B, et al. Obesity accelerates epigenetic aging of human liver. Proc Natl Acad Sci USA. 2014; 111:15538–43. https://doi.org/10.1073/pnas.1412759111

29. Horvath S, Garagnani P, Bacalini MG, Pirazzini C, Salvioli S, Gentilini D, Di Blasio AM, Giuliani C, Tung S, Vinters HV, Franceschi C. Accelerated epigenetic aging in Down syndrome. Aging Cell. 2015; 14:491–95. https://doi.org/10.1111/acel.12325

30. Horvath S, Gurven M, Levine ME, Trumble BC, Kaplan H, Allayee H, Ritz BR, Chen B, Lu AT, Rickabaugh TM, Jamieson BD, Sun D, Li S, et al. An epigenetic clock analysis of race/ethnicity, sex, and coronary heart disease. Genome Biol. 2016; 17:171. https://doi.org/10.1186/s13059-016-1030-0

31. Horvath S, Langfelder P, Kwak S, Aaronson J, Rosinski J, Vogt TF, Eszes M, Faull RL, Curtis MA, Waldvogel HJ, Choi OW, Tung S, Vinters HV, et al. Huntington's disease accelerates epigenetic aging of human brain and disrupts DNA methylation levels. Aging (Albany NY). 2016; 8:1485–512. https://doi.org/10.18632/aging.101005

32. Horvath S, Levine AJ. HIV-1 infection accelerates age according to the epigenetic clock. J Infect Dis. 2015; 212:1563–73. https://doi.org/10.1093/infdis/jiv277

33. Horvath S, Ritz BR. Increased epigenetic age and granulocyte counts in the blood of Parkinson's disease patients. Aging (Albany NY). 2015; 7:1130–42. https://doi.org/10.18632/aging.100859

34. Marioni RE, Shah S, McRae AF, Chen BH, Colicino E, Harris SE, Gibson J, Henders AK, Redmond P, Cox SR, Pattie A, Corley J, Murphy L, et al. DNA methylation age of blood predicts all-cause mortality in later life. Genome Biol. 2015; 16:25. https://doi.org/10.1186/s13059-015-0584-6

35. Levine AJ, Quach A, Moore DJ, Achim CL, Soontornniyomkij V, Masliah E, Singer EJ, Gelman B, Nemanim N, Horvath S. Accelerated epigenetic aging in brain is associated with pre-mortem HIV-associated neurocognitive disorders. J Neurovirol. 2016; 22:366–75. https://doi.org/10.1007/s13365-015-0406-3

36. Levine ME, Lu AT, Bennett DA, Horvath S. Epigenetic age of the pre-frontal cortex is associated with neuritic plaques, amyloid load, and Alzheimer's disease related cognitive functioning. Aging (Albany NY). 2015; 7:1198–211. https://doi.org/10.18632/aging.100864

37. Levine ME, Lu AT, Chen BH, Hernandez DG, Singleton AB, Ferrucci L, Bandinelli S, Salfati E, Manson JE, Quach A, Kusters CD, Kuh D, Wong A, et al. Menopause accelerates biological aging. Proc Natl Acad Sci USA. 2016; 113:9327–32. https://doi.org/10.1073/pnas.1604558113

38. Levine ME, Hosgood HD, Chen B, Absher D, Assimes T, Horvath S. DNA methylation age of blood predicts future onset of lung cancer in the women's health initiative. Aging (Albany NY). 2015; 7:690–700. https://doi.org/10.18632/aging.100809

39. Chen BH, Marioni RE, Colicino E, Peters MJ, Ward-Caviness CK, Tsai PC, Roetker NS, Just AC, Demerath EW, Guan W, Bressler J, Fornage M, Studenski S, et al. DNA methylation-based measures of biological age: meta-analysis predicting time to death. Aging (Albany NY). 2016; 8:1844–65. https://doi.org/10.18632/aging.101020

40. Dugué PA, Bassett JK, Joo JE, Jung CH, Ming Wong E, Moreno-Betancur M, Schmidt D, Makalic E, Li S, Severi G, Hodge AM, Buchanan DD, English DR, et al. DNA methylation-based biological aging and cancer risk and survival: pooled analysis of seven prospective studies. Int J Cancer. 2018; 142:1611–19. https://doi.org/10.1002/ijc.31189

41. Maierhofer A, Flunkert J, Oshima J, Martin GM, Haaf T, Horvath S. Accelerated epigenetic aging in Werner syndrome. Aging (Albany NY). 2017; 9:1143–52. https://doi.org/10.18632/aging.101217

42. Quach A, Levine ME, Tanaka T, Lu AT, Chen BH, Ferrucci L, Ritz B, Bandinelli S, Neuhouser ML, Beasley JM, Snetselaar L, Wallace RB, Tsao PS, et al. Epigenetic clock analysis of diet, exercise, education, and lifestyle factors. Aging (Albany NY). 2017; 9:419–46. https://doi.org/10.18632/aging.101168

43. Petkovich DA, Podolskiy DI, Lobanov AV, Lee SG, Miller RA, Gladyshev VN. Using DNA Methylation Profiling to Evaluate Biological Age and Longevity Interventions. Cell Metab. 2017; 25:954–960.e6. https://doi.org/10.1016/j.cmet.2017.03.016

44. Horvath S, Oshima J, Martin GM, Lu AT, Quach A, Cohen H, Felton S, Matsuyama M, Lowe D, Kabacik S, Wilson JG, Reiner AP, Maierhofer A, et al. Epigenetic clock for skin and blood cells applied to Hutchinson Gilford Progeria Syndrome and ex vivo studies. Aging (Albany NY). 2018; 10:1758–75. https://doi.org/10.18632/aging.101508

45. Counter CM, Hahn WC, Wei W, Caddle SD, Beijersbergen RL, Lansdorp PM, Sedivy JM, Weinberg RA. Dissociation among in vitro telomerase activity, telomere maintenance, and cellular immortalization. Proc Natl Acad Sci USA. 1998; 95:14723–28. https://doi.org/10.1073/pnas.95.25.14723

46. Armbruster BN, Banik SS, Guo C, Smith AC, Counter CM. N-terminal domains of the human telomerase catalytic subunit required for enzyme activity in vivo. Mol Cell Biol. 2001; 21:7775–86. https://doi.org/10.1128/MCB.21.22.7775-7786.2001

47. Lu AT, Xue L, Salfati EL, Chen BH, Ferrucci L, Levy D, Joehanes R, Murabito JM, Kiel DP, Tsai PC, Yet I, Bell JT, Mangino M, et al. GWAS of epigenetic aging rates in blood reveals a critical role for TERT. Nat Commun 2018; 9:387. https://doi.org/10.1038/s41467-017-02697-5

48. Mukherjee S, Firpo EJ, Wang Y, Roberts JM. Separation of telomerase functions by reverse genetics. Proc Natl Acad Sci USA. 2011; 108:E1363–71. https://doi.org/10.1073/pnas.1112414108

49. Lowe D, Horvath S, Raj K. Epigenetic clock analyses of cellular senescence and ageing. Oncotarget. 2016; 7:8524–31. https://doi.org/10.18632/oncotarget.7383

50. Breitling LP, Saum KU, Perna L, Schöttker B, Holleczek B, Brenner H. Frailty is associated with the epigenetic clock but not with telomere length in a German cohort. Clin Epigenetics. 2016; 8:21. https://doi.org/10.1186/s13148-016-0186-5

51. Nwanaji-Enwerem JC, Colicino E, Trevisi L, Kloog I, Just AC, Shen J, Brennan K, Dereix A, Hou L, Vokonas P, Schwartz J, Baccarelli AA. Long-term ambient particle exposures and blood DNA methylation age: findings from the VA normative aging study. Environ Epigenet. 2016; 2. https://doi.org/10.1093/eep/dvw006

52. Marioni RE, Harris SE, Shah S, McRae AF, von Zglinicki T, Martin-Ruiz C, Wray NR, Visscher PM, Deary IJ. The epigenetic clock and telomere length are independently associated with chronological age and mortality. Int J Epidemiol. 2016; 45: 424–32. https://doi.org/10.1093/ije/dyw041

53. Belsky DW, Moffitt TE, Cohen AA, Corcoran DL, Levine ME, Prinz JA, Schaefer J, Sugden K, Williams B, Poulton R, Caspi A. Eleven telomere, epigenetic clock, and biomarker-composite quantifications of biological aging: do they measure the same thing? Am J Epidemiol. 2018; 187:1220–30. https://doi.org/10.1093/aje/kwx346

Human Foreskin Fibroblasts (Donor A)

Vector p16 (55 CPD)   **hTERT p20 (82 CPD)**

Supplementary Figure 1. Senescence-associated β-galactosidase assay on Human Foreskin Fibroblasts infected either with hTERT or empty vector at high cumulative population doubling (CPD). Scale bar measures 200μm.

Human Foreskin Fibroblasts (Donor A)

Vector p5 (20 CPD)   **hTERT p5 (20 CPD)**

Vector p16 (54 CPD)   **hTERT p20 (82 CPD)**
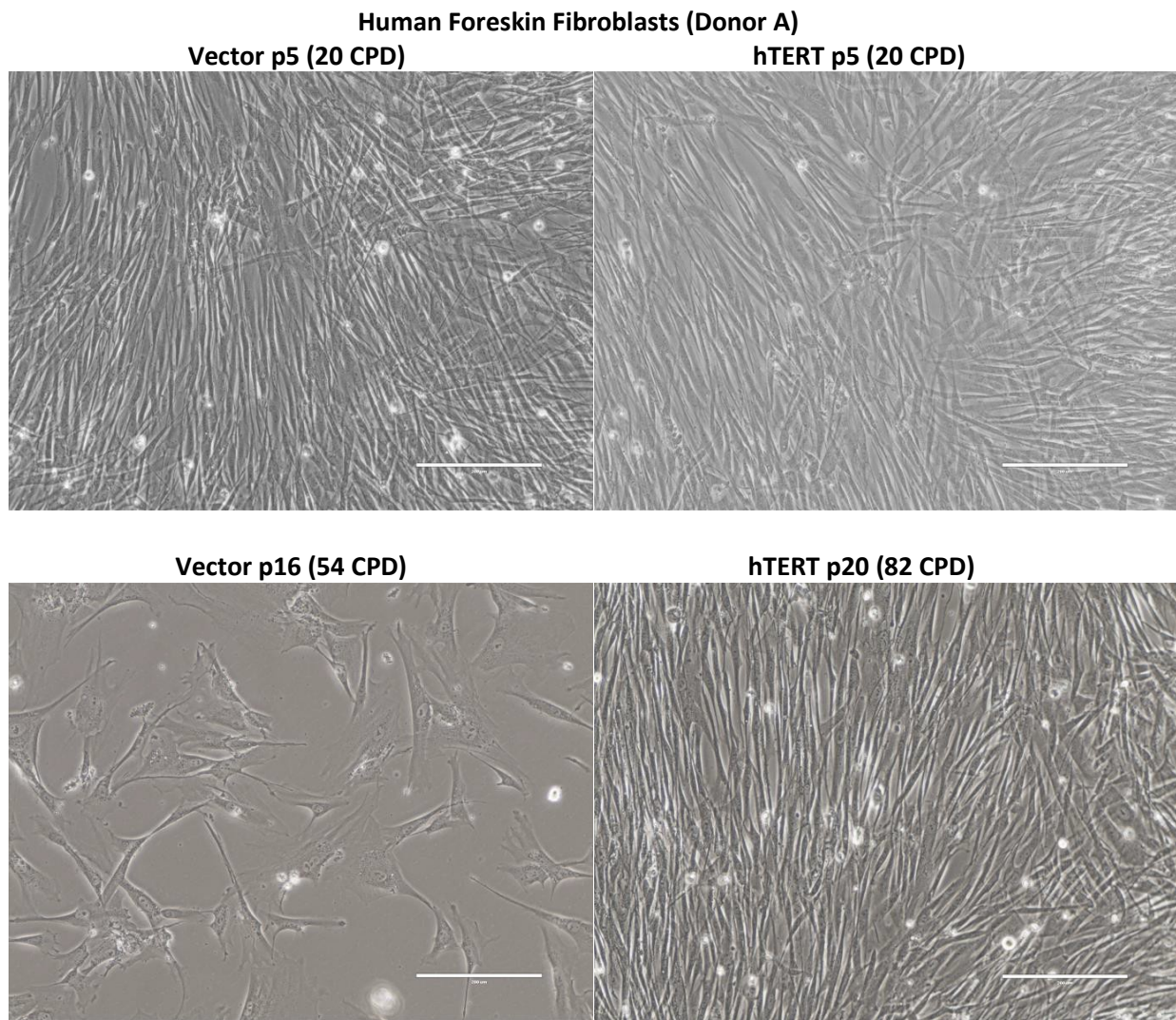
Supplementary Figure 2A. Phase contrast pictures of Human Foreskin Fibroblasts harbouring either hTERT expressing vector or empty vector at low and high cumulative population doubling (CPD). Scale bar measures 200µm.

Human Coronary Artery Endothelial Cells

Vector (8 CPD)

hTERT (16 CPD)
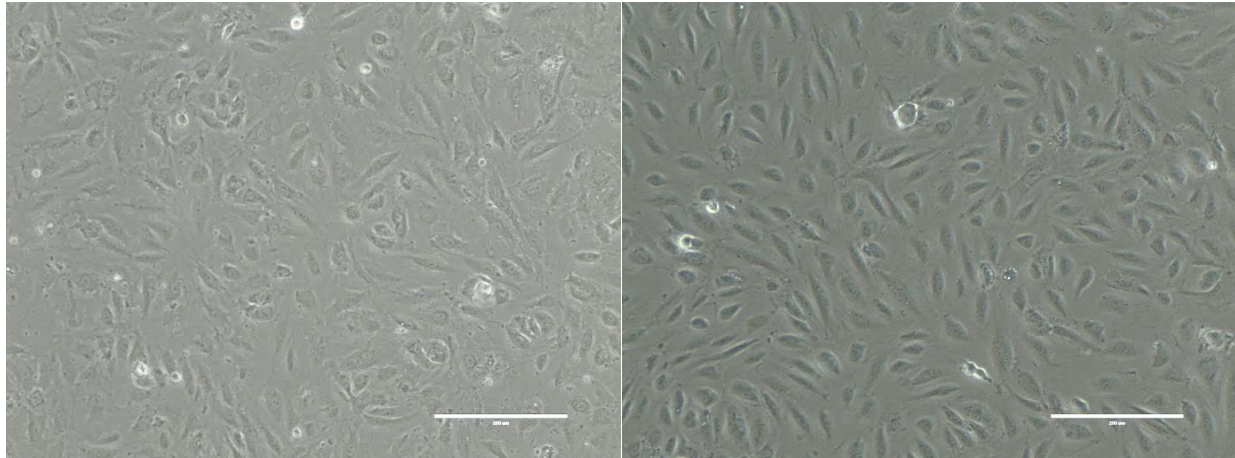
Vector (18 CPD)

hTERT (62 CPD)
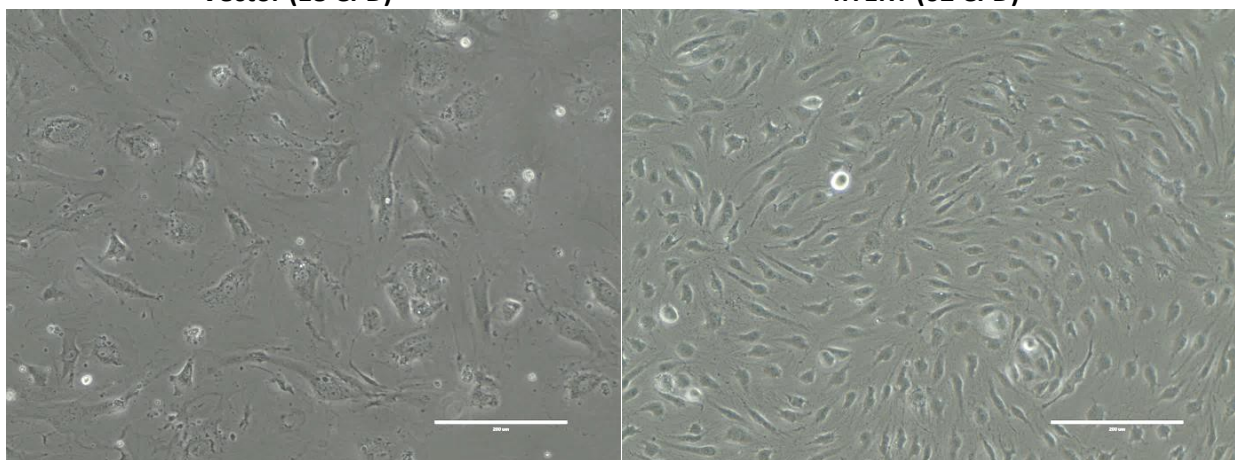
Supplementary Figure 2B. Phase contrast pictures of Human Coronary Artery Endothelial Cells harbouring either hTERT expressing vector or empty vector at low and high cumulative population doubling (CPD). Scale bar measures 200µm.
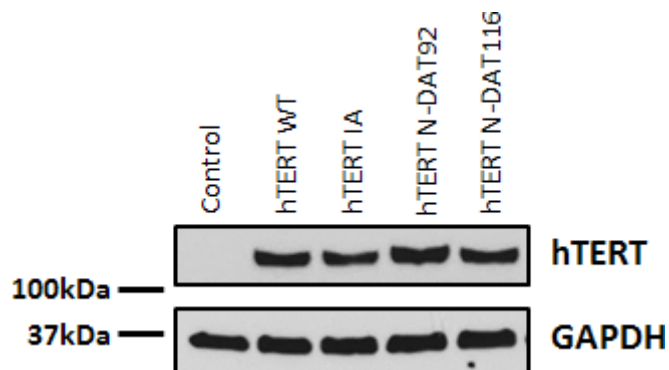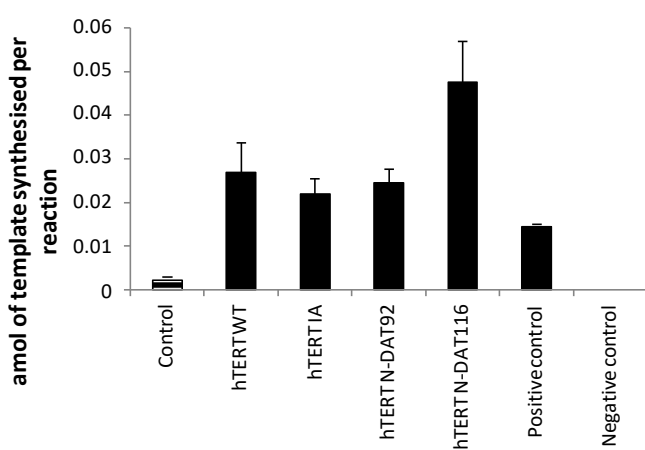
Supplementary Figure 3. (**A**) Western blot analysis of hTERT protein in human foreskin fibroblasts harbouring various hTERT constructs. (**B**) Telomerase catalytic activity (TRAP) assay on the same samples. Bars represent amount of artificial template in atto mole synthesised by telomerase in each sample.

Epigenetic clock for skin and blood cells applied to Hutchinson Gilford Progeria Syndrome and *ex vivo* studies

Steve Horvath[1,2], Junko Oshima[3,4], George M. Martin[3], Ake T. Lu[1], Austin Quach[1], Howard Cohen[5], Sarah Felton[6], Mieko Matsuyama[7], Donna Lowe[8], Sylwia Kabacik[8], James G. Wilson[9], Alex P. Reiner[10], Anna Maierhofer[11], Julia Flunkert[11], Abraham Aviv[12], Lifang Hou[13], Andrea A. Baccarelli[14], Yun Li[15], James D. Stewart[16], Eric A. Whitsel[16,17], Luigi Ferrucci[18], Shigemi Matsuyama[7,19], Kenneth Raj[8]

[1]Department of Human Genetics, David Geffen School of Medicine, University of California Los Angeles, Los Angeles, CA 90095, USA

[2]Department of Biostatistics, Fielding School of Public Health, University of California Los Angeles, Los Angeles, CA 90095, USA

[3]Department of Pathology, University of Washington, Seattle, WA 98195, USA

[4]Department of Clinical Cell Biology and Medicine, Graduate School of Medicine, Chiba University, Chiba, Japan

[5]Elizabeth House, Warlingham, Surrey CR6 9LF, United Kingdom

[6]Department of Dermatology, Oxford University Hospitals NHS Foundation Trust, Oxford OX3 7LJ, United Kingdom

[7]Department of Medicine, Case Western Reserve University, Cleveland, OH 44106, USA

[8]Radiation Effects Department, Centre for Radiation, Chemical and Environmental Hazards, Public Health England, Chilton, Didcot, Oxfordshire, OX11 0RQ, United Kingdom

[9]Department of Physiology and Biophysics, University of Mississippi Medical Center, Jackson, MS 39216, USA

[10]Public Health Sciences Division, Fred Hutchinson Cancer Research Center, Seattle, WA 98109, USA

[11]Institute of Human Genetics, Julius Maximilians University, Würzburg, Germany

[12]Center of Development and Aging, New Jersey Medical School, Rutgers State University of New Jersey, Newark, NJ 07103, USA

[13]Center for Population Epigenetics, Robert H. Lurie Comprehensive Cancer Center and Department of Preventive Medicine, Northwestern University Feinberg School of Medicine, Chicago, IL 60611, USA

[14]Laboratory of Environmental Epigenetics, Departments of Environmental Health Sciences and Epidemiology, Columbia University Mailman School of Public Health, New York, NY 10032, USA

[15]Departments of Genetics, Biostatistics, Computer Science, University of North Carolina, Chapel Hill, NC 27599, USA

[16]Department of Epidemiology, Gillings School of Global Public Health, University of North Carolina, Chapel Hill, NC 27599, USA

[17]Department of Medicine, School of Medicine, University of North Carolina, Chapel Hill, NC 27516, USA

[18]Longitudinal Studies Section, Translational Gerontology Branch, National Institute on Aging, National Institutes of Health, Baltimore, MD 21224, USA

[19]Department of Pathology and Pharmacology, Case Comprehensive Centre, Case Western Reserve University, Cleveland, OH 44106, USA

Correspondence to: Steve Horvath; **email:** shorvath@mednet.ucla.edu

ABSTRACT

DNA methylation (DNAm)-based biomarkers of aging have been developed for many tissues and organs. However, these biomarkers have sub-optimal accuracy in fibroblasts and other cell types used in *ex vivo* studies. To address this challenge, we developed a novel and highly robust DNAm age estimator (based on 391 CpGs) for human fibroblasts, keratinocytes, buccal cells, endothelial cells, lymphoblastoid cells, skin, blood, and saliva samples. High age correlations can also be observed in sorted neurons, glia, brain, liver, and even bone samples. Gestational age correlates with DNAm age in cord blood. When used on fibroblasts from Hutchinson Gilford Progeria Syndrome patients, this age estimator (referred to as the skin & blood clock) uncovered an epigenetic age acceleration with a magnitude that is below the sensitivity levels of other DNAm-based biomarkers. Furthermore, this highly sensitive age estimator accurately tracked the dynamic aging of cells cultured *ex vivo* and revealed that their proliferation is accompanied by a steady increase in epigenetic age. The skin & blood clock predicts lifespan and it relates to many age-related conditions. Overall, this biomarker is expected to become useful for forensic applications (e.g. blood or buccal swabs) and for a quantitative *ex vivo* human cell aging assay.

INTRODUCTION

While our arsenal of potential anti-aging interventions is brimming with highly promising candidates that delay aging in model organisms, it remains to be seen whether these interventions delay aging in humans. The relatively slow pace of this stage is primarily due to the fact that while efficacy of age-related interventions can be reasonably tested in short-lived model organisms, they are not quickly testable in humans, who live much longer. Apart from the impractical measure of human life-span, it is not immediately obvious how the efficacy of an intervention on human aging can be ascertained. To address this challenge, robust biomarkers of aging that are equally effective in *in vivo* as well as *ex vivo* studies are required. These biomarkers must be applicable especially to widely used cell types that are easily derived from accessible human tissues such as blood and skin.

Such a potential biomarker that has gained significant interest in recent years is DNA methylation (DNAm). Chronological time has been shown to elicit predictable hypo- and hyper-methylation changes at many regions across the genome [1-5], and as a result, DNAm based biomarkers of aging were developed to estimate chronological age [6-10]. The blood-based age estimator by Hannum (2013) [9] and the pan-tissue estimator by Horvath (2013) [6] produce age estimates (DNAm age) that are widely used in epidemiological studies [11, 12]. Mathematical adjustment of these age estimates in context of their corresponding chronological ages produces a measure of the rate of epigenetic aging, which is referred to as epigenetic age acceleration that can take a positive or negative value. Positive values of epigenetic age acceleration (indicative of faster epigenetic aging) have been repeatedly observed to be associated with many age-related diseases and conditions [11-24]. This indicates that epigenetic age is more than an alternative measure of chronological age but is instead an indicator of the state of health and as such, of biological age.

As indicated by its name, the pan-tissue age estimator applies to all sources of DNA (except for sperm) [6]. Despite its many successful applications, the pan-tissue DNAm age estimator performs sub-optimally when used to estimate fibroblast age [6]. This is particularly perplexing because fibroblasts are widely used in *ex vivo* studies of various interventions. As a case in point, the Progeria Research Foundation provides fibroblast lines derived from skin biopsies from patients with Hutchinson Gilford Progeria Syndrome (HGPS) for use in research. In spite of clear acceleration of clinical manifestations of aging in HGPS, this is not mirrored in epigenetic age measurements by current DNA methylation-based estimators [6]. While this could be due to a genuinely interesting distinction between epigenetic and phenotypic aging, it is also possible that the current epigenetic age estimators fail to capture aspects of aging that are specific to fibroblasts and epithelial cells. The discernment between the two possibilities requires an age estimator that is well-suited for accurately measuring the epigenetic age of fibroblasts. However, an epigenetic age estimator that is highly accurate and equally compatible with fibroblasts and other readily accessible human cells is currently not available. Such an epigenetic age estimator would be very valuable in performing ex vivo experiments because it would allow testing anti-aging properties of new compounds in human cells and minimize the need to carry out such tests in humans. Ex vivo studies often employ keratinocytes, fibroblasts and microvascular endothelial cells, which can be readily isolated from skin biopsies.

Here, we describe a novel powerful epigenetic age estimator (called the skin & blood clock) that outperforms existing DNAm-based biomarkers when it comes to estimating the chronological ages of human donors of fibroblasts, keratinocytes, microvascular endothelial cells, skin cells, coronary artery endothelial cells, lymphoblastoid cells, blood, and saliva samples.

RESULTS

DNA methylation data sets

We analyzed both novel and existing DNA methylation data sets that were generated on the Illumina Infinium platform (Table 1). DNA was extracted from human fibroblasts, keratinocytes, buccal cells, endothelial cells, blood, and saliva. We analyzed data from two Illumina platforms (Infinium 450K and the EPIC array, also known as the 850K array) to ensure that the resulting estimator would apply to the latest Illumina platform (the EPIC array).

The DNAm age estimator for skin and blood

To ensure an unbiased validation of the test data, we used only the training data to define and construct the DNAm age estimator. As detailed in Methods, a transformed version of chronological age was regressed on methylation states of CpGs using elastic net regression [25], which automatically selected 391 CpGs (Methods). We refer to the 391 CpGs as (epigenetic) clock CpGs since their weighted average (formed by the regression coefficients) amounts to a highly accurate epigenetic aging clock.

The following description will demonstrate that the resulting age estimator (referred to as skin & blood clock) performs remarkably well across a wide spectrum of cells that are most frequently used in *ex vivo* studies. The new skin & blood clock even outperforms the pan-tissue clock (Horvath 2013) [6] in all metrics of accuracy (age correlation, median error) in fibroblasts, microvascular endothelial cells, buccal epi-

Table 1. DNA methylation data. The rows correspond to Illumina DNA methylation data sets.

No.	Data Source	Use	n	Source	Median Age (Range)
1	existing, Portales-Casamar 2016, GSE80261	Train	216	Buccal	11 (5,18)
2	existing, Berko 2014, GSE50759	Train	96	Buccal	7 (1,28)
3	novel, blood methylation	Train	278	whole blood	69 (2,92)
4	existing, Yang 2017, GSE104471	Train	72	Epithelium	30 (24,74)
5	existing, Ivanov 2016, GSE77136	Train	21	Fibroblast	33 (0.1,85)
6	existing, Wagner 2014, GSE52026	Train	10	Fibroblast	37 (23,63)
7	novel fibroblasts	Train	48	Fibroblast	50 (0.42,94)
8	novel, Cell Applications	Train	11	Fibroblast	56 (7,94)
9	existing, Borman 2016, SkinE-MTAB-4385	Train	108	Skin	49.25 (18,78)
10	existing, cord blood, GSE79056	Train	36	cord blood	0 (-0.28,0.04)
11	existing, Jessen 2016, GSE94876	Test	120	Buccal	46 (35,60)
12	Lussier 2018, GSE109042	Test	53	Buccal	10 (3.5,18)
13	existing, Vandiver 2015, GSE51954	Test	78	Dermis+Epidermis	65 (20,92)
14	novel, Kenneth Raj	Test	23	Endothelial	19 (19,19)
15	novel, Kenneth Raj	Test	44	Endothelial	19 (17,26)

		Use	n	Tissue	Median age (range)
16	novel, Kenneth Raj	Test	48	Fibroblast	0 (0,0)
17	novel, Kenneth Raj	Test	48	Fibroblast	0 (0,0)
18	novel, Progeria Research Foundation+ vendors	Test	88	Fibroblast	8 (0,77)
19	novel, Junko Oshima	Test	11	Fibroblast	36 (0,62)
20	novel, Kenneth Raj	Test	43	Keratinocyte	0 (0,0)
21	novel, Blood methylation Inf 450	Test	100	Whole Blood	53 (19,82)
22	novel, Lymphoblastoid cell	Test	100	Lymphoblast	53 (19,82)
23	novel, Saliva methylation	Test	120	Saliva	44 (18, 81)
24	existing, Horvath 2015, GSE111223	Test	229	Saliva	68 (36,88)
25	existing, cord blood, GSE62924	Test	38	cord blood	0 (-.10,0.04)
26	existing, cord blood, GSE80283	Test	183	cord blood	-0.22(-0.3,-0.1)

The table reports the data set number, relevant citation (first author and publication year), public availability (for example, Gene Expression Omnibus identifier), sample size (n), source of the DNA (for example, tissue), median age, age range (minimum and maximum age). The column 'Use' reports whether the data set was used as a training set or test set.

thelial cells, keratinocytes, and dermis/epidermis samples (Figure 1 and Supplementary Figure 1). As indicated by its name, the new skin & blood clock is also a highly accurate age estimator of blood methyltion data, where it provides more accurate age estimates than the widely used estimators by Horvath (2013) [6] and Hannum (2013) [9] (Figure 2A,D,G and Supplementary Figure 2). Further, it outperforms the Horvath and Hannum DNAm age estimators when applied to lymphoblastoid cell lines (Figure 2B,E,H), i.e. B cells that have been immortalized using EBV transformation. Interestingly, the DNAm age of blood is highly correlated with the DNAm age estimate of the lymphoblastoid cell line collected from the same donor at the same time (r=0.83, Figure 2C). The skin & blood clock accurately estimates age in two different saliva DNA methylation data sets (age correlations r=0.9 and r=0.95) and outperforms the pan-tissue DNAm age estimator in these data (Supplementary Figure 3). The skin & blood clock also applies to cord blood samples as can be seen from the fact that it accurately estimates gestational age in three different data (with correlations ranging from r=0.15 to r=0.66, Supplementary Figure 4).

Skin & blood clock applied to brain, liver, bone, and other body parts

The skin & blood clock leads to DNAm age estimates that strongly correlate with chronological age in a host of different cell types and tissues including sorted neurons and glial cells (Supplementary Figure 5), brain samples (Supplementary Figure 6), liver samples (Supplementary Figure 7), and trabecular bone samples (Supplementary Figure 8). In the following, we provide more details on the individual studies.

In sorted neurons, DNAm age correlates strongly (r=0.83) with chronological age but the DNAm age estimator is substantially lower than chronological age (mean DNAm Age=6 years in a group of people whose mean chronological age is 31 years, Supplementary Figure 5A). Interestingly, the DNAm age of glial cells is significantly higher than that of neurons from the same individual (p=0.00024, Supplementary Figure 5B,C). Chronological age is also highly correlated with DNAm age estimates in different brain regions (r between 0.67 and 0.96, Supplementary Figure 6) but the age estimates tend to be systematically lower than chronological age. In particular, the cerebellum ages substantially slower than other brain regions echoing previous results for the pan-tissue clock [17].

DNAm age of liver tissue is highly correlated with chronological age (r=0.86, Supplementary Figure 7) and the corresponding measure of epigenetic age acceleration correlates with body mass index (r=0.27, p=0.027, Supplementary Figure 7B). These results echo earlier results obtained from the pan-tissue DNAm age estimator [13].

An analysis of 30 different body parts from a 112 year old woman reveals a) that most body parts have roughly the same age and b) that the cerebellum is substantially younger (Supplementary Figure 9) which is consistent with previous results [17].

Epigenetic age of fibroblasts from Hutchinson Gilford Progeria fibroblasts

Previously, the use of the pan-tissue clock revealed epigenetic age acceleration in segmental progeroid syn-

dromes such as Down syndrome and Werner syndrome [15, 24], but not in syndrome X, whose patients exhibit dramatically delayed development (seemingly eternal toddler-like state) [26]. The status of the epigenetic aging rate in regards to HGPS and Atypical Werner Syndrome (AWS) is less clear. These two conditions can be caused by different progeroid mutations of the *LMNA* gene (Figure 3). It is not yet known whether HGPS patients, who generally appear normal at birth but exhibit a "failure-to-thrive" syndrome, exhibit any epigenetic age acceleration.
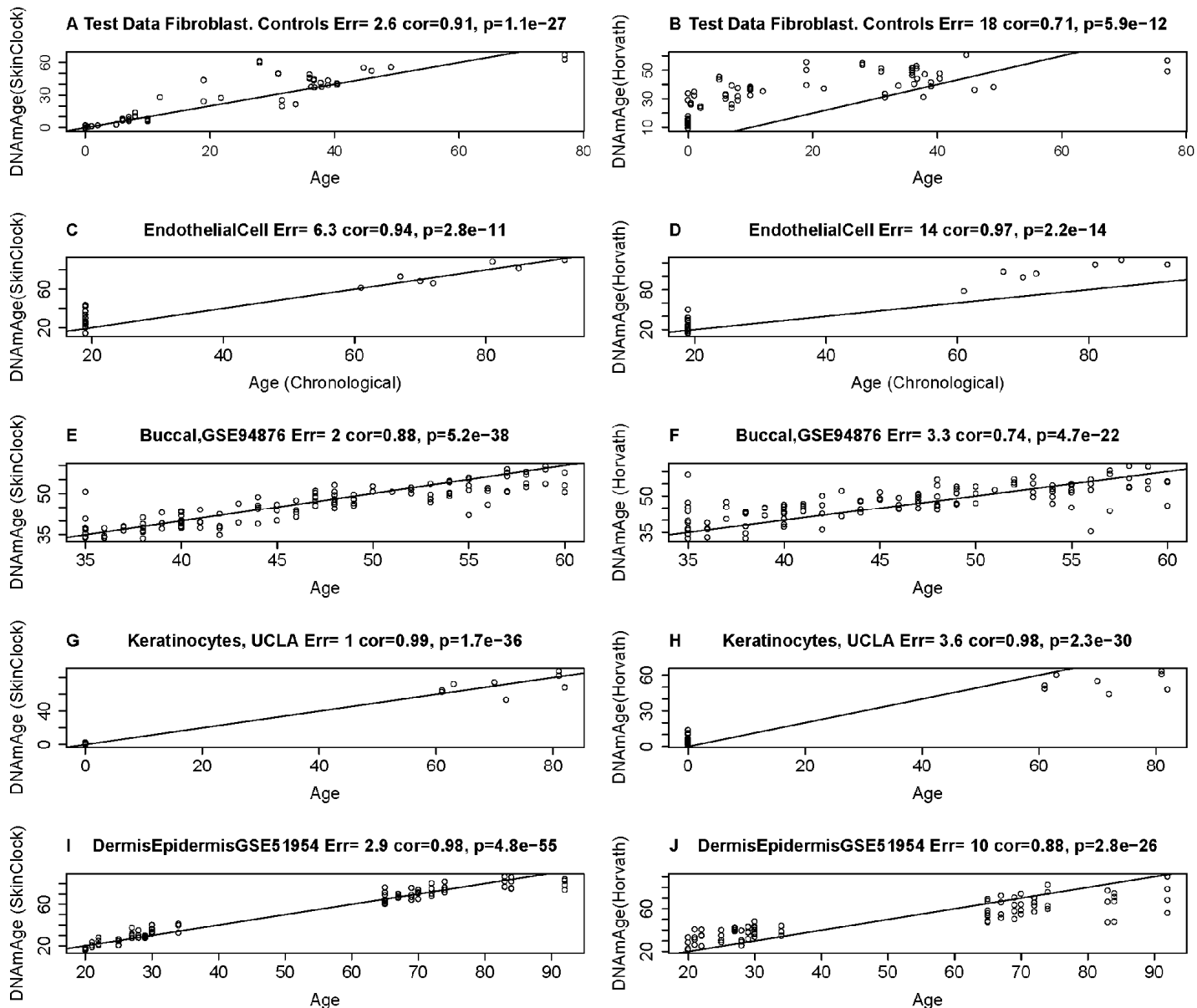
Figure 1. Age estimation accuracy of the skin & blood clock in fibroblasts, keratinocytes, and microvascular endothelial cells. The left and right panels relate chronological age (x-axis) to DNAm Age estimates (y-axis) from the skin & blood clock (**A,C,E,G,I**) and the pan-tissue clock (Horvath 2013) (B,D,F,H,J) [6] respectively. Each row corresponds to a different tissue/cell type. DNA methylation data from fibroblasts (**A,B**), microvascular endothelial cells (**C,D**), buccal epithelial cells (**E,F**), keratinocytes (**G,H**) and whole skin (dermis/epidermis) samples (**I,J**). Each panel reports the Pearson correlation coefficient and the error (defined as median absolute deviation between DNAm age and chronological age).
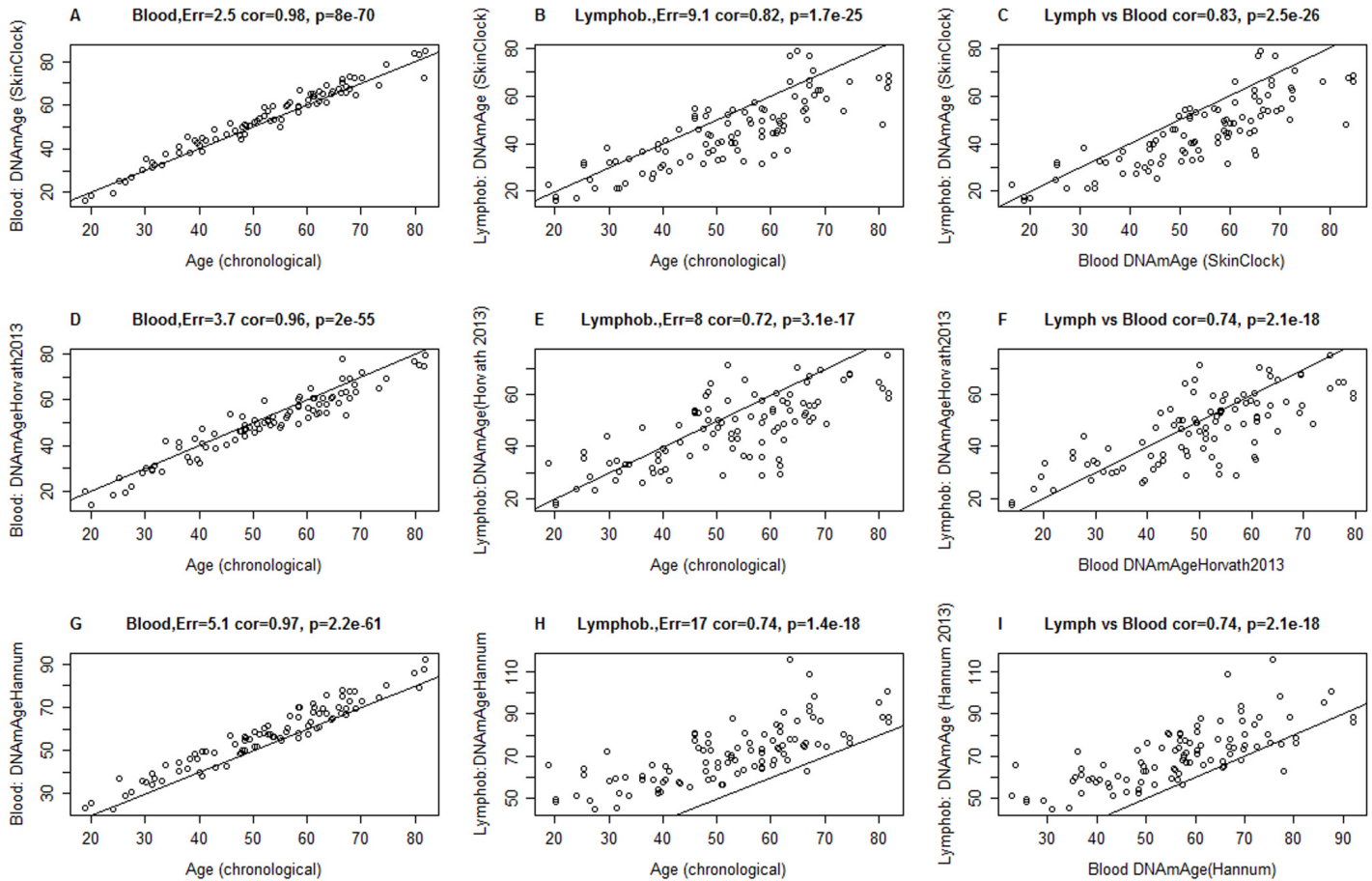
Figure 2. Comparison of DNAm age estimators in whole blood and lymphoblastoid cell line data. The rows correspond to 3 different age estimators: (**A,B,C**) the novel skin & blood clock (**D,E,F**), the pan-tissue clock (Horvath 2013) [6], (**G,H,I**) Hannum clock 9]. Panels in the first and second column report the accuracy in blood (**A,D,C**) and lymphoblastoid cell lines (**B,E,H**), respectively. Panels in the third column (**C,F,I**) report the relationship between DNAm age estimates in blood (x-axis) versus those in lymphoblastoid cell lines (y-axis). Panels report Pearson correlation coefficient and the estimation error, which is defined as median absolute deviation between the DNAm age estimate and chronological age. The lymphoblastoid cell lines were generated from the same individuals for whom whole blood was assessed, which facilitated the comparison in the third column.

HGPS is associated with many clinical manifestations of accelerated aging including loss of subcutaneous fat, joint contractures, and a striking aged appearance during the first to third years of life [27]. Virtually all HGPS patients die of myocardial infarction at a median age of 14.6 years [28]. Classic HGPS is caused by a recurrent heterozygous pathological variant, c.1824C>T in exon 11 of the *LMNA* gene, which activates a cryptic splice site and causes a 50-amino acid in-frame deletion (Δ50) [29]. The resulting abnormal protein, termed progerin, lacks the proteolytic site for an essential but transient post-translational modification by the ZMPSTE24 metalloprotease. This causes retention of the C-terminal farnesylated moiety, resulting in aberrant nuclear structure and function [29]. Non-classical HGPS mutations at the exon 11 and intron 11 boundary,

including c.1968+1G>A [30] and c.1968+2T>C [31], can also activate the cryptic splice site, leading to the accumulation of progerin and an infantile-onset HGPS phenotype. Biallelic ZMPSTE24 mutations also cause accumulations of farnesylated lamin A and a varying degree of progeroid phenotypes, depending on the residual enzymatic activity of ZMPSTE24 [32, 33]. In rare instances, a homozygous amino acid substitution of lamin A can present with a phenotype similar to HGPS or mandibuloacral dysplasia, as described in cases with [p.Met540Thr; p.Met540Thr] [34] and [p.Thr528Met; p.Met540Thr] [35].

A small subset of cases of Atypical Werner syndrome (AWS) (those with some features of Werner syndrome, without mutations in *WRN* or altered expressions of the

WRN protein) may be caused by accumulations of low levels of progerin [36, 37]. Pathological lamin A variants found in some patients with AWS include c.1968G>A and c.1968+5G>A [36]. While there is a general genotype-phenotype correlation between the amount of progerin and the severity of the disease, the amounts and structures of progerin can vary among those who carry the same *LMNA* splice mutation, and the severity of the disease can vary among patients within the same family [36, 37]. The median age of death of classic HGPS is ~14.6 years [38], while the range in AWS patients with low levels of progerin is 37 to 60 years [36].

The original pan-tissue DNAm age estimator did not detect any age acceleration in HGPS individuals (Supplementary Table 1). By contrast, the application of the novel skin & blood clock showed that while DNAm age is highly correlated with chronological age in normal fibroblasts, those from HGPS cases exhibited accelerated epigenetic aging (Figure 4). The correlation between age and DNAm age in HGPS children (<10 years old) is substantially lower (r=0.71) than that of control children (r=0.71, Figure 4B). The epigenetic age acceleration effects become particularly pronounced after adjusting for differences in cell population doubling levels and when the analysis was restricted to children who are younger than 10 years old (p=0.00021, Table 3). There is a non-significant trend of increased DNAm age in Atypical Werner Syndrome cases with low levels of progerin. It is perhaps not unexpected that AWS, which presents with a lower progerin concentration (Figure 3) is not significantly associated with greater magnitude of epigenetic age acceleration.

Although non-classic HGPS patients often present at later ages, they can nevertheless be diagnosed at ages that are slightly younger than patients with classic HGPS [27]. It should indeed be noted that the cases examined in this study (see Methods for mutation details), have exceptionally early manifestations − as early as birth or younger than 5 months of age. Interestingly, their DNA methylation age acceleration is comparable and consistent with that of classic HGPS, which as mentioned, is an early onset progeria condition (Figure 4D).
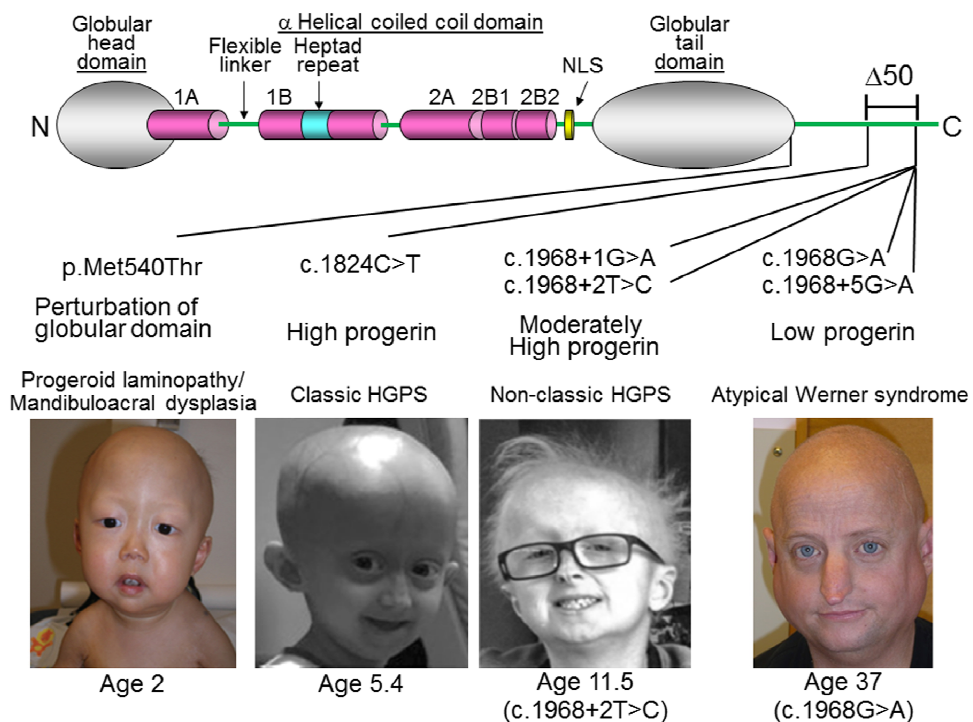
Figure 3. *LMNA* mutations in progeria patients. The diagram shows the structure of lamin A. It consists of globular head domain, linker regions, α-helical coiled coil domain and globular tail domain. Locations of the progeria *LMNA* mutations in this study were shown with molecular mechanism of mutant lamin A protein and clinical phenotype, as previously reported in [34] (p.Met540Thr), [29] (c.1824C>T), [30] (c.1968+1G>A), [31] (c.1968+2T>C), and [36] (c.2968G>A and c.1968+5G>A). Δ50 indicates the region of deletion in progerin, also present in ZMPSTE24 mutant progeria [32]. Photos were reproduced with permission.

Table 2. Epigenetic clock results for fibroblast samples from The Progeria Research Foundation.

Cell-line ID	Progeria	Mutation	Sex	Age	DNAmAge SkinClock	AgeAccelS kinClock
PSADFN086	NonClassic	LM Exon 11 c.1968+1G>A	m	0.58	0.39	-3.49
PSADFN257	NonClassic	LM Exon 10 homozygous c.1619 T>C (p.Met540Thr)	m	1.83	4.44	-0.51
PSADFN257.re plicate	NonClassic	LM Exon 10 homozygous c.1619 T>C (p.Met540Thr)	m	1.8	4.84	-0.08
PSADFN317	NonClassic	ZMPste24 Exon 6 heterozygous c.743C>T(p.Pro248Leu)and Exon 10 heterozygous c.1349G>A (p.Trp450Stop)	m	3.8	8.86	2.23
PSADFN318	NonClassic	ZMPste24 Exon 6 heterozygous c.743 C>T(p.Pro248Leu)and Exon 10 heterozygous c.1349G>A (p.Trp450Stop)	m	0.4	7.48	3.75
PSADFN392	NonClassic	LM Exon 11 c.1968+2T>C	m	7.3	21.61	11.99
HGADFN003	Classic	LM Exon 11 heterozygous c.1824C>T	m	2	3.39	-1.70
HGADFN169	Classic	LM Exon 11 heterozygous c.1824C>T	m	8.5	23.73	13.08
HGADFN143	Classic	LM Exon 11 heterozygous c.1824C>T	m	8.8	15.61	4.71
HGADFN167	Classic	LM Exon 11 heterozygous c.1824C>T	m	8.4	17.88	7.32
HGADFN271	Classic	LM Exon 11 heterozygous c.1824C>T	m	1.3	10.73	6.24
HGADFN164	Classic	LM Exon 11 heterozygous c.1824C>T	f	4.66	10.64	3.28
HGADFN178	Classic	LM Exon 11 heterozygous c.1824C>T	f	6.92	4.36	-4.93
HGADFN122	Classic	LM Exon 11 heterozygous c.1824C>T	f	5	6.96	-0.70
HGADFN127	Classic	LM Exon 11 heterozygous c.1824C>T	f	3.8	2.10	-4.53
HGADFN155	Classic	LM Exon 11 heterozygous c.1824C>T	f	1.1	0.59	-3.73
HGADFN188	Classic	LM Exon 11 heterozygous c.1824C>T	f	2.3	1.23	-4.11
HGADFN367	Classic	LM Exon 11 heterozygous c.1824C>T	f	3	17.10	11.16

The columns report the cell line identifier, the disease status, mutational analysis, sex, age, DNAm age estimate (based on the skin & blood clock), and the measure of age acceleration (defined as residual from a regression line). Classic HGPS cases exhibit the following mutation: LMNA Exon 11, heterozygous c.1824C>T (p.Gly608Gly). By contrast, non-classic HGPS cases exhibit mutations elsewhere in the LMNA gene.
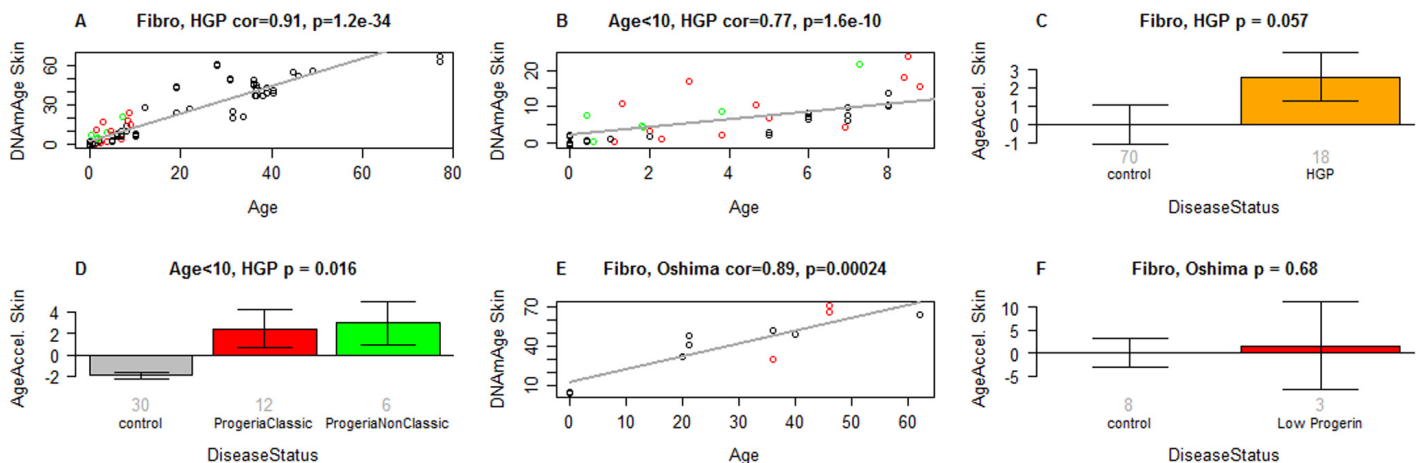
Figure 4. Skin & blood clock analysis of fibroblasts from HGP individuals of the Progeria Research Foundation. (**A,B**) The new skin & blood clock was used to estimate DNAm age (y-axis) in fibroblasts from HGP individuals and controls. (**A**) All individuals. (**B**) Children younger than 10 years old. Dots are colored by disease status: red=classical progeria, green=non-classical progeria, black=controls. The grey line corresponds to a regression line through control individuals. The epigenetic age acceleration effect for each individual (point) corresponds to the vertical distance to the black regression line. The fact that red and green points tend to lie above the grey line indicates that HGP cases exhibit suggestive accelerated epigenetic aging effect. (**C**) Mean epigenetic age acceleration (y-axis) versus HGP status. By definition, the mean age acceleration measure in controls is zero. (**D**) Epigenetic age acceleration (y-axis) versus disease status in individuals younger than 10. (**E**, **F**) report results for fibroblast samples from atypical Werner syndrome cases (low progerin) provided by co-author Junko Oshima. (**E**) DNAm age versus chronological age for atypical Werner syndrome samples (colored in red) and controls (colored in black). (**F**) Epigenetic age acceleration versus disease status. The title of the bar plots also reports a P-value from a nonparametric group comparison test (Kruskal Wallis test). Each bar plot reports the mean value and one standard error.

Table 3. Multivariate regression model analysis of HGPS based on the novel skin & blood clock.

Outcome: DNAmAge (SkinClock)						
	Data: All, n=88			**Data: Age<10, n=44**		
Covariate	**Coef**	**St. Error**	**P-value**	**Estimate**	**SE**	**P-value**
Intercept	-3.55	2.99	2.39E-1	7.34	2.97	1.84E-2
Age	1.64	1.29E-1	3.44E-20	-5.90E-1	8.33E-1	4.84E-1
Age^2	-1.07E-2	2.08E-3	2.14E-6	2.40E-1	9.58E-2	1.70E-2
Fibroblast Population Doubl. Level	4.46E-1	1.65E-1	8.52E-3	-1.20E-1	1.32E-1	3.71E-1
HGP.Disease	4.81	2.27	3.76E-2	5.18	1.25	2.12E-4

DNAm age is regressed on chronological age, the square of age, the population doubling level of the fibroblast cell culture, and HGPS disease status. The table reports estimates of the regression coefficients and corresponding standard errors, Wald test P-values. The left panel and right panel report the results for all n=88 fibroblast samples and for n=44 samples from children (younger than 10 years old), respectively.

Detailed results for the lines of skin fibroblasts provided by The Progeria Research Foundation are presented in Table 2 and Supplementary Table 2. The skin & blood clock provides marginally significant evidence (p=0.062) that fibroblasts from boys with classic HGPS are epigenetically older than those from girls with classic HGPS, but this gender effect is not apparent when classic and non-classic HGPS samples are pooled for analyses (Supplementary Figure 10).

It is to be further noted that the epigenetic age acceleration of HGPS fibroblasts revealed by the skin & blood clock escaped detection when measurements were carried out with the pan-tissue clock; indeed, the opposite

appears to be the case (Supplementary Figure 11C, Supplementary Table 2). Evidently, the ability to detect such epigenetic age changes in fibroblasts is dependent upon the choice of the DNAm age estimator that is used.

Ex vivo studies of anti-aging interventions

While it may appear obvious that the skin & blood clock is superior in terms of compatibility with fibroblasts, it was still necessary to verify and validate this deduction by applying this clock to non-progeria fibroblasts and other cell types. To this end, fibroblasts derived from non-progeria neonatal foreskins are ideal

as they pose minimal to no confounding factors that could alter their age. While the skin & blood clock correctly estimated the neonatal fibroblast cells to be of ages close to zero years, the pan-tissue age estimator leads to age estimates that are greater than 10 years (Figure 5A and B). Analyses of other skin cell types namely, keratinocytes and microvascular endothelial cells derived from neonatal foreskins also demonstrated greater accuracy of the skin & blood clock over the other age estimators. This conclusion continues to hold true even when the analyses were extended to isogenic skin cells derived from adult tissues (Supplementary Figure 1).
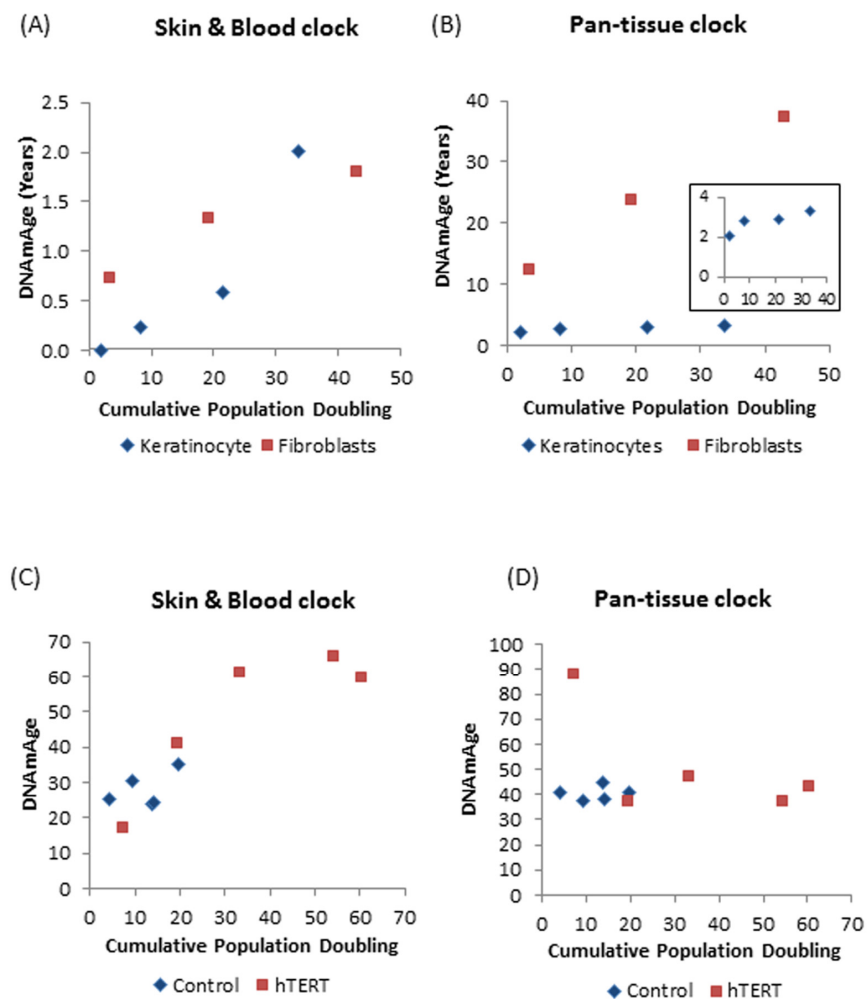
Figure 5. DNAm age versus population doubling levels. Each panel reports a DNAm age estimate (y-axis) versus cumulative population doubling level, respectively. Plots in the left and right panels correspond to the new skin & blood clock (**A,C**) and the pan-tissue clock (**B,D**) respectively. (**A,B**) Tracking of the epigenetic ages of neonatal fibroblasts (Red squares) and keratinocytes (Blue diamonds) in function of population doubling. Inset graph in (**B**) is a plot of ages of only the keratinocyte population. (**C,D**) Epigenetic ages of human coronary artery endothelial cells derived from a 26 year old donor, in function of cumulative population doubling. Ages of uninfected control cells, which senesced after cumulative population doubling of 20, are shown in blue while those bearing hTERT, with extended proliferative capacity are in red. The blue dots with the highest cumulative doubling are at points when the cells reached replicative senescence. Cells with hTERT (represented by red squares) do not senesce and the last dots indicate the termination of the experiment.

Having established the robustness of the skin & blood clock in measuring age of cells isolated from human tissues, we proceeded to test the applicability of the clock on human cells cultured *ex vivo*. As observed previously using the pan-tissue age estimator, the skin & blood clock revealed that human fibroblasts cultured *ex vivo* undergo epigenetic aging. However, unlike the former which over-estimates the DNAm age of fibroblasts (Figure 5B), the skin & blood clock correctly estimated the age of the neonatal cells to within 6 months (Figure 5A). Proliferation of human fibroblasts in culture, measured as population doubling, was observed to correlate with continual increase in DNAm age. Similar correlation was also seen with neonatal foreskin keratinocytes (Figure 5A and B). Although this association was revealed by both clocks, the resolution and accuracy of the skin & blood clock are clearly much greater and better. The new clock also out-performs the pan-tissue clock when applied to non-blood or skin cells; namely, the human coronary artery endothelial cells, whose increase in epigenetic age in function of population doubling was readily detected by the former but not the latter. Cells whose proliferative capacity was extended by hTERT beyond their otherwise natural limits (senescence), continued to age epigenetically, underscoring the correlation between cellular prolifera-tion and DNA methylation aging.

By its ability to quantitatively track aging of human cells *ex vivo,* the skin & blood clock lends itself to be used in the development of an *ex vivo* human cell aging assay that can be used for testing and screening com-pounds with anti-aging or pro-aging effects.

Analysis of blood samples from human cohort studies

Epigenetic clocks are associated with a host of different age-related phenotypes and conditions (reviewed in [11, 12]). In the following, we report the results of several post-hoc analyses that demonstrate that the new skin & blood clock satisfies most of the properties observed for other blood based DNAm age estimators.

Similar to what has been observed with previous age estimators, epigenetic age acceleration in blood (according to the skin & blood clock) is highly predictive of time to all-cause mortality (p=9.6E-7) according to a univariate Cox regression model fixed effects meta-analysis across multiple epidemiological cohort studies (Supplementary Figure 12).

Blood samples from individuals with Down syndrome exhibit positive epigenetic age acceleration compared to controls (p=0.034, Supplementary Figure 13) consistent with previous findings [15].

Similar to the previous epigenetic aging clock analyses of blood [21], cross sectional studies of n=3700 blood samples from postmenopausal women from the Women's Health Initiative revealed relationships to lifestyle factors and dietary variables (Supplementary Table 3). Slow epigenetic age acceleration in blood was associated with higher education (p=6E-5), physical exercise (p=4E-3), fish consumption (p=2E-4), poultry consumption (p=3E-4), high mean carotenoid levels (p=8E-6), beta cryptoxhanthin (p=2E-7), beta carotene levels (p=4E-4), and HDL levels (p=5E-4, Supplemen-tary Table 3). Conversely, faster epigenetic aging in blood is associated with higher C-reactive protein levels (p=1E-3), body mass index (p=0.01), triglyceride levels (p=3E-3), and insulin (p=2E-3). However, it is worth emphasizing that the respective correlation coefficients were weak ($|r|<0.11$, Supplementary Table 3). Physical exercise was associated with a slower epigenetic aging effect in African American women (p=4E-3) and perhaps in Caucasian women (p=0.07) but not in Hispanic women (p=0.74). Current smoking status was only associated with increased age acceleration in Caucasian women (p=0.04).

Epigenetic age acceleration is highly conserved across a 9 year follow up time period (r=0.71, Supplementary Figure 14). In other words, if an individual exhibits positive epigenetic age acceleration at age 40 then he/she will probably continue to exhibit positive epigenetic age acceleration at age 49.

Collectively these characteristics demonstrate that although the new clock is highly and uniquely accurate for skin cells, it has not acquired this at the cost of losing any of the features shared amongst existing age estimators in being also highly accurate with blood DNA methylation data, buccal cells, saliva. As such, this clock could become useful for forensic applications.

Relationship to other DNAm age estimators

The skin & blood clock (based on 391 CpGs) shares 45 CpGs (out of 71 CpGs) with the blood-based clock from Hannum (2013) and 60 CpGs (out of 353 CpGs) with the pan tissue clock from Horvath (2013) as detailed in Supplementary Table 4. Despite this significant overlap, epigenetic age acceleration of the skin & blood clock exhibits only moderate correlations with corresponding epigenetic age acceleration measures by Horvath (2013) and Hannum (2013) (r=0.5 and r=0.59, p<1.E-110) in the blood samples from the Women's Health Initiative (BA23 study).

Leukocyte telomere length and blood cell counts

We find a weak negative correlation between leuko-

cyte telomere length and epigenetic age acceleration of blood (r=-0.087, p=0.0088 in n=905 samples from the Framingham Heart Study, r =-0.081, p=0.0011 in n=1639 samples from the Jackson Heart Study, and r=-0.117, p=0.00079 in the 818 samples from the Women's Health Initiative). This weak negative relationship between telomere length and epigenetic age acceleration is similar to that of the Hannum-based DNAm age estimator and other blood based biomarkers [11, 39, 40].

Epigenetic age acceleration measured by the skin & blood clock is only weakly correlated with, or affected by blood cell type counts, as is evident from the analyses of postmenopausal women from the Women's Health Initiative (Supplementary Figure 15). The strongest correlations are observed with exhausted CD8+ T cells (r=0.22), naive CD8+ T cells (r=-0.21), and naive CD4+T cells (r=-0.19, Supplementary Figure 15B-D). These correlations suggest that individuals with positive epigenetic age accelerations exhibit an adaptive immune system that is older than expected.

DISCUSSION

We present a new DNA methylation-based biomarker (based on 391 CpGs) that was developed to accurately measure the age of human fibroblasts, keratinocytes, buccal cells, endothelial cells, skin and blood samples. Perhaps unexpectedly, we also observe strong age correlations in sorted neurons, glia, brain, liver and bone samples. The need for the new skin & blood clock became apparent when it was observed that the existing DNA methylation-based age estimators that are highly accurate in measuring ages of blood and many cell types of the body, perform poorly when applied to human fibroblasts and other skin cells. The implications of this anomaly extend beyond theoretical curiosity as it impacts the reliability of conclusions drawn from epigenetic age analyses of skin cells. As a case in point, the apparent lack of epigenetic age acceleration of HGPS fibroblasts indicated by measurements using the pan-tissue age estimator revealed an important limitation.

Skin cells are among the most common cell types employed in laboratories. This is owed largely to the ease by which cells such as keratinocytes, fibroblasts, and microvascular endothelial cells can be isolated from skin, allowing cells from many donors to be easily acquired and used; a characteristic that is not afforded by internal organs. The ability to use these cells to investigate epigenetic age *ex vivo* is paramount if we are to identify constituents of the epigenetic clock and elucidate how they function together to drive the ticking of the clock.

The skin & blood that we derived is well-suited to meet all these needs. By applying it to fibroblasts from HGPS cases, we detect a significant epigenetic age acceleration effect after adjusting for fibroblast population doubling levels. For reasons yet to be determined, the pan-tissue DNA methylation age estimator failed to detect this subtle increase in epigenetic age acceleration. In considering the modest increase in age acceleration of HGPS cells, it is worth noting that changes in the methylation state of clock CpGs in the early years of life already occur at a frenetic rate, which is approximately twenty-four times greater than that which takes place after the age of twenty [6]. Hence, it is difficult to envisage that the accelerated rate of epigenetic aging in HGPS cells from young donors could be very much greater in magnitude. This hypothesis can in theory be tested by measuring the epigenetic age of HGPS cells from patients older than twenty years of age, when the basal rate of normal epigenetic aging is significantly reduced, allowing for any age acceleration to become even more apparent. It is however difficult to achieve this as the median age of death of HGPS patients is approximately 14 years old. The ability of the skin & blood clock to nevertheless detect epigenetic age acceleration in young HGPS patients over and above an already very high normal background rate, attests to its sensitivity.

It is also conceivable that there may be specific, as well as overlapping aging mechanisms in patients with different segmental progeroid syndromes (i.e. HGPS versus classical WS) that differentially contribute to their respective rates of DNAm acceleration. Alternatively, these differences might be attributable, at least in part, to the consequences rather than the causes of the patterns of diverse pathologies that characterize these different phenotypes.

In addition to resolving the conundrum of HGPS described above, the skin & blood clock outperforms widely used existing biomarkers when it comes to accurately measuring the age of an individual based on DNA extracted from skin, dermis, epidermis, blood, saliva, buccal swabs, and endothelial cells. Thus, the biomarker can also be used for forensic and biomedical applications involving human specimens. The biomarker applies to the entire age span starting from newborns, e.g. DNAm of cord blood samples correlates with gestational week (Supplementary Figure 4). Furthermore, the skin & blood clock confirms the effect of lifestyle and demographic variables on epigenetic aging. Essentially it highlights a significant trend of accelerated epigenetic aging with sub-clinical indicators of poor health. Conversely, reduced aging rate is correlated with known health-improving features such as physical exercise, fish consumption, high carotenoid

levels (Supplementary Table 3). As with the other age predictors, the skin & blood clock is also able to predict time to death. Collectively, these features show that while the skin & blood clock is clearly superior in its performance on skin cells, it crucially retained all the other features that are common to other existing age estimators.

The skin & blood clock is particularly well suited for forensic applications because it greatly outperforms the considered alternative DNAm based estimators when it comes to measuring chronological age in blood, buccal cells, saliva, and other cell types (Figure 1, Figure 2, Supplementary Figures 2-4).

The performance of the skin & blood clock is equally impressive when applied to *ex vivo* cell culture system. Studies with fibroblasts and endothelial cells revealed that increase in population doublings is significantly associated with increased DNAm age including hTERT immortalized cells, which corroborates the findings in previous studies [41, 42].

We have coupled the skin & blood clock with human primary cell cultures to generate an *ex vivo* human cell aging assay that is highly sensitive. This assay is able to detect epigenetic aging of a few years, within a few months. The benefits of this assay are self-evident. The two most obvious are its use to test and screen for potential pharmaceuticals that can alter the rate of epigenetic aging, and its use to test and detect potential age-inducing hazards in the arena of health protection.

Many of our key observations are critically dependent upon the choice of a DNAm age estimator, i.e., they could only be observed with the new skin & blood clock assay. For example, the original pan-tissue clock could not detect an age acceleration effect in HGPS. Looking ahead, there might be valuable applications of this more robust epigenetic clock for example, in the evaluation of clinical trials of pharmaceutical interventions in segmental progeroid syndromes such as the most recent clinical trial of a farnesyltransferase inhibitor, lonafarnib, to treat HGPS that reportedly lowers mortality rates (6.3% death in the treated group vs 27% death in the matched untreated group after 2.2 years of follow-up) [28]. We are likely to see an increase of such clinical trials. For example, *in vitro* studies of the effects of rapamycin or another mTOR inhibitor, metformin, showed a reduction of progerin accumulation accompanied by the amelioration of cellular HGPS phenotypes [43, 44]. Reactivation of the antioxidant NRF2 was also shown to alleviate cellular defects of HGPS in an animal model [45]. Beyond therapeutic aims, prophylactic interventions would certainly be sought-after, and the ability of the skin & blood clock to

accurately measure the age of cells from highly accessible human tissues will reveal whether the tested treatments are widely targeted across cell and tissue types - an important feature that is not hitherto afforded by other age estimators.

Due to its superior accuracy, we expect that this novel set of epigenetic biomarkers will be useful for both *ex vivo* studies involving cultures of various somatic cell types, including fibroblasts, keratinocytes, and endothelial cells, as well as *in vivo* studies utilizing samples of peripheral blood and biopsies of skin.

METHODS

The R software code underlying the new skin & blood clock can be found in the Supplement.

Definition of DNAm age using a penalized regression model

A penalized regression model (implemented in the R package glmnet [46]) was used to regress a calibrated version of chronological age on the CpG probes in the training set. We restricted the analysis to CpGs that were present both on the Illumina 450K and EPIC platforms and were in one of the following subsets: 1) most significant CpGs with high positive/negative correlation with chronological age in different cell types or 2) 500 CpGs with the least significant correlation with age. The alpha parameter of glmnet was chosen as 0.5 (elastic net regression) and the lambda value was chosen using cross-validation on the training data. DNAm age was defined as predicted age.

Fibroblasts from The Progeria Research Foundation

Human primary dermal fibroblast cell lines were obtained from The Progeria Research Foundation (PRF) Cell and Tissue Bank (www.progeriaresearch.org). The fibroblast cell lines originated from cases with classic mutations, non-classic mutations and parental controls as detailed in Table 2. The following citations provide additional details on cases carrying the specific variants: *LMNA* c.1968+1G>A heterozygote [30], *LMNA* c.1968+2T>C heterozygote [31], *LMNA* p.Met540Thr homozygotes [34] and compound heterozygotes of ZMPSTE24 p.Pro248Leu and p.Trp450* [32]. Additional details can be found in the Supplement.

Isolation and culture of cells for *ex vivo* experiments

Informed consent was obtained prior to collection of human skin samples with approved by the Oxford Research Ethics Committee; reference 10/H0605/1. Human skin samples were acquired under ethical appro-

val. Primary human skin keratinocytes, fibroblasts and microvascular endothelial cells were isolated from neonatal foreskin and adult facial/neck skin. Keratinocytes were cultured in CnT media (CellnTec) on fibronectin/collagen-coated plates, fibroblasts were cultured in DMEM (Sigma) supplemented with 10% foetal calf serum and CD31-selected microvascular endothelial cells were cultured in Endothelial Cell Growth Medium MV (PromoCell, C-22020) on gelatin-coated plates. Human Coronary Artery Endothelial Cells (HCAEC) from a male, aged 26 years, were obtained from Sigma and grown in MesoEndo Cell Growth Medium (Sigma). HCAEC were immortalized with pBABE-neo-hTERT (Addgene, cat. 1774) and after selection, were cultured in parallel with uninfected control until control reached senescence. All cells were maintained in a 37°C, 5% CO2 humidified environment. At each passaging step, cells were counted, population doubling calculated and 10,000 were seeded into a fresh 10cm plate. Remaining cells were used for DNA extraction. Population doubling was calculated with the following formula: [log(number of cells harvested) – log(number of cells seeded)] x 3.32. Cumulative population doubling was obtained by addition of population doubling of each passage. Additional details can be found in the Supplement.

Sample preparation

DNA was extracted from cells using the Zymo Quick DNA mini-prep plus kit (D4069) according to the manufacturer's instructions and DNA methylation levels were measured on Illumina 450 or Illumina 850 EPIC arrays according to the manufacturer's instructions.

Blood methylation data from different epidemiological cohorts

A number of validation studies were used to test associations between DNAm age and various aging-related traits including time to all-cause mortality. Details on these studies can be found in the Supplement and in [20, 40].

Competing interests

The Regents of the University of California is the sole owner of a provisional patent application directed at this invention for which SH is a named inventor.

Ethics approval

This study was reviewed by the UCLA institutional review board (IRB#14-000140, IRB#15-001479). Collection of human skin samples were carried out under the ethical approval issues by the Oxford Research Ethics Committee; reference 10/H0605/1 (United Kingdom)

AUTHOR CONTRIBUTIONS

SH developed the skin & blood clock. SH, SM, KR conceived the study. SH carried out the statistical analysis. The remaining authors contributed data, helped with the write up, and participated in the interpretation of the results.

ACKNOWLEDGEMENTS

CONFLICTS OF INTEREST

The authors have no conflict of interests to declare.

FUNDING

mental Hazards with King's College London) in partnership with Public Health England (PHE).

REFERENCES

1. Fraga MF, Esteller M. Epigenetics and aging: the targets and the marks. Trends Genet. 2007; 23:413–18. https://doi.org/10.1016/j.tig.2007.05.008

2. Rakyan VK, Down TA, Maslau S, Andrew T, Yang TP, Beyan H, Whittaker P, McCann OT, Finer S, Valdes AM, Leslie RD, Deloukas P, Spector TD. Human aging-associated DNA hypermethylation occurs preferentially at bivalent chromatin domains. Genome Res. 2010; 20:434–39. https://doi.org/10.1101/gr.103101.109

3. Teschendorff AE, Menon U, Gentry-Maharaj A, Ramus SJ, Weisenberger DJ, Shen H, Campan M, Noushmehr H, Bell CG, Maxwell AP, Savage DA, Mueller-Holzner E, Marth C, et al. Age-dependent DNA methylation of genes that are suppressed in stem cells is a hallmark of cancer. Genome Res. 2010; 20:440–46. https://doi.org/10.1101/gr.103606.109

4. Jung M, Pfeifer GP. Aging and DNA methylation. BMC Biol. 2015; 13:7. https://doi.org/10.1186/s12915-015-0118-4

5. Zheng SC, Widschwendter M, Teschendorff AE. Epigenetic drift, epigenetic clocks and cancer risk. Epigenomics. 2016; 8:705–19. https://doi.org/10.2217/epi-2015-0017

6. Horvath S. DNA methylation age of human tissues and cell types. Genome Biol. 2013; 14:R115. https://doi.org/10.1186/gb-2013-14-10-r115

7. Bocklandt S, Lin W, Sehl ME, Sánchez FJ, Sinsheimer JS, Horvath S, Vilain E. Epigenetic predictor of age. PLoS One. 2011; 6:e14821. https://doi.org/10.1371/journal.pone.0014821

8. Garagnani P, Bacalini MG, Pirazzini C, Gori D, Giuliani C, Mari D, Di Blasio AM, Gentilini D, Vitale G, Collino S, Rezzi S, Castellani G, Capri M, et al. Methylation of ELOVL2 gene as a new epigenetic marker of age. Aging Cell. 2012; 11:1132–34. https://doi.org/10.1111/acel.12005

9. Hannum G, Guinney J, Zhao L, Zhang L, Hughes G, Sadda S, Klotzle B, Bibikova M, Fan JB, Gao Y, Deconde R, Chen M, Rajapakse I, et al. Genome-wide methylation profiles reveal quantitative views of human aging rates. Mol Cell. 2013; 49:359–67. https://doi.org/10.1016/j.molcel.2012.10.016

10. Lin Q, Weidner CI, Costa IG, Marioni RE, Ferreira MR, Deary IJ, Wagner W. DNA methylation levels at individual age-associated CpG sites can be indicative for life expectancy. Aging (Albany NY). 2016; 8:394–401. https://doi.org/10.18632/aging.100908

11. Horvath S, Raj K. DNA methylation-based biomarkers and the epigenetic clock theory of ageing. Nat Rev Genet. 2018; 19:371–84. https://doi.org/10.1038/s41576-018-0004-3

12. Nwanaji-Enwerem JC, Weisskopf MG, Baccarelli AA. Multi-tissue DNA methylation age: molecular relationships and perspectives for advancing biomarker utility. Ageing Res Rev. 2018; 45:15–23. https://doi.org/10.1016/j.arr.2018.04.005

13. Horvath S, Erhart W, Brosch M, Ammerpohl O, von Schönfels W, Ahrens M, Heits N, Bell JT, Tsai PC, Spector TD, Deloukas P, Siebert R, Sipos B, et al. Obesity accelerates epigenetic aging of human liver. Proc Natl Acad Sci USA. 2014; 111:15538–43. https://doi.org/10.1073/pnas.1412759111

14. Marioni RE, Shah S, McRae AF, Chen BH, Colicino E, Harris SE, Gibson J, Henders AK, Redmond P, Cox SR, Pattie A, Corley J, Murphy L, et al. DNA methylation age of blood predicts all-cause mortality in later life. Genome Biol. 2015; 16:25. https://doi.org/10.1186/s13059-015-0584-6

15. Horvath S, Garagnani P, Bacalini MG, Pirazzini C, Salvioli S, Gentilini D, Di Blasio AM, Giuliani C, Tung S, Vinters HV, Franceschi C. Accelerated epigenetic aging in Down syndrome. Aging Cell. 2015; 14:491–95. https://doi.org/10.1111/acel.12325

16. Horvath S, Levine AJ. HIV-1 Infection Accelerates Age According to the Epigenetic Clock. J Infect Dis. 2015; 212:1563–73. https://doi.org/10.1093/infdis/jiv277

17. Horvath S, Mah V, Lu AT, Woo JS, Choi OW, Jasinska AJ, Riancho JA, Tung S, Coles NS, Braun J, Vinters HV, Coles LS. The cerebellum ages slowly according to the epigenetic clock. Aging (Albany NY). 2015; 7:294–306. https://doi.org/10.18632/aging.100742

18. Levine ME, Hosgood HD, Chen B, Absher D, Assimes T, Horvath S. DNA methylation age of blood predicts future onset of lung cancer in the women's health initiative. Aging (Albany NY). 2015; 7:690–700. https://doi.org/10.18632/aging.100809

19. Levine ME, Lu AT, Chen BH, Hernandez DG, Singleton AB, Ferrucci L, Bandinelli S, Salfati E, Manson JE, Quach A, Kusters CD, Kuh D, Wong A, et al. Menopause accelerates biological aging. Proc Natl Acad Sci USA. 2016; 113:9327–32. https://doi.org/10.1073/pnas.1604558113

20. Chen BH, Marioni RE, Colicino E, Peters MJ, Ward-Caviness CK, Tsai PC, Roetker NS, Just AC, Demerath EW, Guan W, Bressler J, Fornage M, Studenski S, et al. DNA methylation-based measures of biological age: meta-analysis predicting time to death. Aging (Albany NY). 2016; 8:1844–65. https://doi.org/10.18632/aging.101020

21. Quach A, Levine ME, Tanaka T, Lu AT, Chen BH, Ferrucci L, Ritz B, Bandinelli S, Neuhouser ML, Beasley JM, Snetselaar L, Wallace RB, Tsao PS, et al. Epigenetic clock analysis of diet, exercise, education, and lifestyle factors. Aging (Albany NY). 2017; 9:419–46. https://doi.org/10.18632/aging.101168

22. Dugue PA, Bassett JK, Joo JE, Jung CH, Ming Wong E, Moreno-Betancur M, Schmidt D, Makalic E, Li S, Severi G, Hodge AM, Buchanan DD, English DR, et al. DNA methylation-based biological aging and cancer risk and survival: pooled analysis of seven prospective studies. Int J Cancer. 2018; 42:1611-19. https://doi.org/10.1002/ijc.31189

23. Simpkin AJ, Howe LD, Tilling K, Gaunt TR, Lyttleton O, McArdle WL, Ring SM, Horvath S, Smith GD, Relton CL. The epigenetic clock and physical development during childhood and adolescence: longitudinal analysis from a UK birth cohort. Int J Epidemiol. 2017; 46:549–58. https://doi.org/10.1093/ije/dyw307

24. Maierhofer A, Flunkert J, Oshima J, Martin GM, Haaf T, Horvath S. Accelerated epigenetic aging in Werner syndrome. Aging (Albany NY). 2017; 9:1143–52. https://doi.org/10.18632/aging.101217

25. Zou H, Hastie T. Regularization and variable selection via the elastic net. J R Stat Soc Series B Stat Methodol. 2005; 67:301–20. https://doi.org/10.1111/j.1467-9868.2005.00503.x

26. Walker RF, Liu JS, Peters BA, Ritz BR, Wu T, Ophoff RA, Horvath S. Epigenetic age analysis of children who seem to evade aging. Aging (Albany NY). 2015; 7:334–39. https://doi.org/10.18632/aging.100744

27. Merideth MA, Gordon LB, Clauss S, Sachdev V, Smith AC, Perry MB, Brewer CC, Zalewski C, Kim HJ, Solomon B, Brooks BP, Gerber LH, Turner ML, et al. Phenotype and course of Hutchinson-Gilford progeria syndrome. N Engl J Med. 2008; 358:592–604. https://doi.org/10.1056/NEJMoa0706898

28. Gordon LB, Kleinman ME, Massaro J, D'Agostino RB Sr, Shappell H, Gerhard-Herman M, Smoot LB, Gordon CM, Cleveland RH, Nazarian A, Snyder BD, Ullrich NJ, Silvera VM, et al. Clinical Trial of the Protein Farnesylation Inhibitors Lonafarnib, Pravastatin, and Zoledronic Acid in Children With Hutchinson-Gilford Progeria Syndrome. Circulation. 2016; 134:114–25.

https://doi.org/10.1161/CIRCULATIONAHA.116.022188

29. Eriksson M, Brown WT, Gordon LB, Glynn MW, Singer J, Scott L, Erdos MR, Robbins CM, Moses TY, Berglund P, Dutra A, Pak E, Durkin S, et al. Recurrent de novo point mutations in lamin A cause Hutchinson-Gilford progeria syndrome. Nature. 2003; 423:293–98. https://doi.org/10.1038/nature01629

30. Moulson CL, Fong LG, Gardner JM, Farber EA, Go G, Passariello A, Grange DK, Young SG, Miner JH. Increased progerin expression associated with unusual LMNA mutations causes severe progeroid syndromes. Hum Mutat. 2007; 28:882–89. https://doi.org/10.1002/humu.20536

31. Bar DZ, Arlt MF, Brazier JF, Norris WE, Campbell SE, Chines P, Larrieu D, Jackson SP, Collins FS, Glover TW, Gordon LB. A novel somatic mutation achieves partial rescue in a child with Hutchinson-Gilford progeria syndrome. J Med Genet. 2017; 54:212–16. https://doi.org/10.1136/jmedgenet-2016-104295

32. Ahmad Z, Zackai E, Medne L, Garg A. Early onset mandibuloacral dysplasia due to compound heterozygous mutations in ZMPSTE24. Am J Med Genet A. 2010; 152A:2703–10. https://doi.org/10.1002/ajmg.a.33664

33. Barrowman J, Wiley PA, Hudon-Miller SE, Hrycyna CA, Michaelis S. Human ZMPSTE24 disease mutations: residual proteolytic activity correlates with disease severity. Hum Mol Genet. 2012; 21:4084–93. https://doi.org/10.1093/hmg/dds233

34. Bai S, Lozada A, Jones MC, Dietz HC, Dempsey M, Das S. Mandibuloacral Dysplasia Caused by LMNA Mutations and Uniparental Disomy. Case Rep Genet. 2014; 2014:508231. https://doi.org/10.1155/2014/508231

35. Verstraeten VL, Broers JL, van Steensel MA, Zinn-Justin S, Ramaekers FC, Steijlen PM, Kamps M, Kuijpers HJ, Merckx D, Smeets HJ, Hennekam RC, Marcelis CL, van den Wijngaard A. Compound heterozygosity for mutations in LMNA causes a progeria syndrome without prelamin A accumulation. Hum Mol Genet. 2006; 15:2509–22.

https://doi.org/10.1093/hmg/ddl172

36. Hisama FM, Lessel D, Leistritz D, Friedrich K, McBride KL, Pastore MT, Gottesman GS, Saha B, Martin GM, Kubisch C, Oshima J. Coronary artery disease in a Werner syndrome-like form of progeria characterized by low levels of progerin, a splice variant of lamin A. Am J Med Genet A. 2011; 155A:3002–06. https://doi.org/10.1002/ajmg.a.34336

37. Barthélémy F, Navarro C, Fayek R, Da Silva N, Roll P, Sigaudy S, Oshima J, Bonne G, Papadopoulou-

Legbelou K, Evangeliou AE, Spilioti M, Lemerrer M, Wevers RA, et al. Truncated prelamin A expression in HGPS-like patients: a transcriptional study. Eur J Hum Genet. 2015; 23:1051–61.
https://doi.org/10.1038/ejhg.2014.239

38. Gordon LB, Massaro J, D'Agostino RB Sr, Campbell SE, Brazier J, Brown WT, Kleinman ME, Kieran MW, and Progeria Clinical Trials Collaborative. Impact of farnesylation inhibitors on survival in Hutchinson-Gilford progeria syndrome. Circulation. 2014; 130:27–34.
https://doi.org/10.1161/CIRCULATIONAHA.113.008285

39. Chen BH, Carty CL, Kimura M, Kark JD, Chen W, Li S, Zhang T, Kooperberg C, Levy D, Assimes T, Absher D, Horvath S, Reiner AP, Aviv A. Leukocyte telomere length, T cell composition and DNA methylation age. Aging (Albany NY). 2017; 9:1983–95.
https://doi.org/10.18632/aging.101293

40. Levine ME, Lu AT, Quach A, Chen BH, Assimes TL, Bandinelli S, Hou L, Baccarelli AA, Stewart JD, Li Y, Whitsel EA, Wilson JG, Reiner AP, et al. An epigenetic biomarker of aging for lifespan and healthspan. Aging (Albany NY). 2018; 10:573–91.
https://doi.org/10.18632/aging.101414

41. Lu AT, Xue L, Salfati EL, Chen BH, Ferrucci L, Levy D, Joehanes R, Murabito JM, Kiel DP, Tsai PC, Yet I, Bell JT, Mangino M, et al. GWAS of epigenetic aging rates in blood reveals a critical role for TERT. Nat Commun. 2018; 9:387. https://doi.org/10.1038/s41467-017-02697-5

42. Lowe D, Horvath S, Raj K. Epigenetic clock analyses of cellular senescence and ageing. Oncotarget. 2016; 7:8524–31.
https://doi.org/10.18632/oncotarget.7383

43. Cao K, Graziotto JJ, Blair CD, Mazzulli JR, Erdos MR, Krainc D, Collins FS. Rapamycin reverses cellular phenotypes and enhances mutant protein clearance in Hutchinson-Gilford progeria syndrome cells. Sci Transl Med. 2011; 3:89ra58.
https://doi.org/10.1126/scitranslmed.3002346

44. Park SK, Shin OS. Metformin alleviates ageing cellular phenotypes in Hutchinson-Gilford progeria syndrome dermal fibroblasts. Exp Dermatol. 2017; 26:889–95.
https://doi.org/10.1111/exd.13323

45. Kubben N, Zhang W, Wang L, Voss TC, Yang J, Qu J, Liu GH, Misteli T. Repression of the Antioxidant NRF2 Pathway in Premature Aging. Cell. 2016; 165:1361–74. https://doi.org/10.1016/j.cell.2016.05.017

46. Friedman J, Hastie T, Tibshirani R. Regularization Paths for Generalized Linear Models via Coordinate Descent. J Stat Softw. 2010; 33:1–22.
https://doi.org/10.18637/jss.v033.i01

SUPPLEMENTARY MATERIAL

Please browse the Full Text version to check the data related to this manuscript:

Supplementary Results, Methods and References

Supplementary Figures

Supplementary Tables

Supplementary Dataset 1

Supplementary Dataset 2

Research Paper

An epigenetic biomarker of aging for lifespan and healthspan

Morgan E. Levine[1], Ake T. Lu[1], Austin Quach[1], Brian H. Chen[2], Themistocles L. Assimes[3], Stefania Bandinelli[4], Lifang Hou[5], Andrea A. Baccarelli[6], James D. Stewart[7], Yun Li[8], Eric A. Whitsel[7,9], James G Wilson[10], Alex P Reiner[11], Abraham Aviv[12], Kurt Lohman[13], Yongmei Liu[14], Luigi Ferrucci[2,*], Steve Horvath[1,15,*]

[1]Department of Human Genetics, David Geffen School of Medicine, University of California Los Angeles, Los Angeles, CA 90095, USA

[2]Longitudinal Studies Section, Translational Gerontology Branch, National Institute on Aging, National Institutes of Health, USA. Baltimore, MD 21224, USA

[3]Department of Medicine, Stanford University School of Medicine, Stanford, CA 94305, USA

[4]Geriatric Unit, Azienda Toscana Centro, Florence, Italy

[5]Center for Population Epigenetics, Robert H. Lurie Comprehensive Cancer Center and Department of Preventive Medicine, Northwestern University Feinberg School of Medicine, Chicago, IL 60611, USA

[6]Laboratory of Environmental Epigenetics, Departments of Environmental Health Sciences and Epidemiology, Columbia University Mailman School of Public Health, New York, NY 10032, USA

[7]Department of Epidemiology, Gillings School of Global Public Health, University of North Carolina, Chapel Hill, NC 27599, USA

[8]Department of Genetics, Department of Biostatistics, Department of Computer Science, University of North Carolina, Chapel Hill, NC 27599, USA

[9]Department of Medicine, School of Medicine, University of North Carolina, Chapel Hill, NC 27599, USA

[10]Department of Physiology and Biophysics, University of Mississippi Medical Center, Jackson, MS 39216, USA

[11]Public Health Sciences Division, Fred Hutchinson Cancer Research Center, Seattle, WA 98109, USA

[12]Center of Human Development and Aging, New Jersey Medical School, Rutgers State University of New Jersey, Newark, NJ 07103, USA

[13]Department of Biostatistics, Division of Public Health Sciences, Wake Forrest School of Medicine, Winston-Salem, NC 27157, USA

[14]Department of Epidemiology & Prevention, Division of Public Health Sciences, Wake Forrest School of Medicine, Winston-Salem, NC 27157, USA

[15]Department of Biostatistics, Fielding School of Public Health, University of California Los Angeles, Los Angeles, CA 90095, USA

*Co-senior authors

ABSTRACT

Identifying reliable biomarkers of aging is a major goal in geroscience. While the first generation of epigenetic biomarkers of aging were developed using chronological age as a surrogate for biological age, we hypothesized that incorporation of composite clinical measures of phenotypic age that capture differences in lifespan and healthspan may identify novel CpGs and facilitate the development of a more powerful epigenetic biomarker of

aging. Using an innovative two-step process, we develop a new epigenetic biomarker of aging, DNAm PhenoAge that strongly outperforms previous measures in regards to predictions for a variety of aging outcomes, including all-cause mortality, cancers, healthspan, physical functioning, and Alzheimer's disease. While this biomarker was developed using data from whole blood, it correlates strongly with age in every tissue and cell tested. Based on an in-depth transcriptional analysis in sorted cells, we find that increased epigenetic, relative to chronological age, is associated with increased activation of pro-inflammatory and interferon pathways, and decreased activation of transcriptional/translational machinery, DNA damage response, and mitochondrial signatures. Overall, this single epigenetic biomarker of aging is able to capture risks for an array of diverse outcomes across multiple tissues and cells, and provide insight into important pathways in aging.

INTRODUCTION

One of the major goals of geroscience research is to define 'biomarkers of aging'[1, 2], which can be thought of as individual-level measures of aging that capture inter-individual differences in the timing of disease onset, functional decline, and death over the life course. While chronological age is arguably the strongest risk factor for aging-related death and disease, it is important to distinguish chronological time from biological aging. Individuals of the same chronological age may exhibit greatly different susceptibilities to age-related diseases and death, which is likely reflective of differences in their underlying biological aging processes. Such biomarkers of aging will be crucial to enable evaluation of interventions aimed at promoting healthier aging, by providing a measurable outcome, which unlike incidence of death and/or disease, does not require extremely long follow-up observation.

One potential biomarker that has gained significant interest in recent years is DNA methylation (DNAm). Chronological time has been shown to elicit predictable hypo- and hyper-methylation changes at many regions across the genome [3-7], and as a result, the first generation of DNAm based biomarkers of aging were developed to predict chronological chronological age [8-13]. The blood-based algorithm by Hannum [10] and the multi-tissue algorithm by Horvath [11] produce age estimates (DNAm age) that correlate with chronological age well above r=0.90 for full age range samples. Nevertheless, while the current epigenetic age estimators exhibit statistically significant associations with many age-related diseases and conditions [14-27], the effect sizes are typically small to moderate. One explanation is that using chronological age as the reference, by definition, may exclude CpGs whose methylation patterns don't display strong time-dependent changes, but instead signal the departure of biological age from chronological age. Thus, it is important to not only capture CpGs that display changes with chronological time, but also those that account for differences in risk and physiological status among individuals of the same chronological age.

Previous work by us and others have shown that "phenotypic aging measures", derived from clinical biomarkers [28-32], strongly predict differences in the risk of all-cause mortality, cause-specific mortality, physical functioning, cognitive performance measures, and facial aging among same-aged individuals. What's more, in representative population data, some of these measures have been shown to be better indicators of remaining life expectancy than chronological age [28], suggesting that they may be approximating individual-level differences in biological aging rates. As a result, we hypothesize that a more powerful epigenetic biomarker of aging could be developed by replacing prediction of chronological age with prediction of a surrogate measure of "phenotypic age" that, in and of itself, differentiates morbidity and mortality risk among same-age individuals.

RESULTS

Overview of the statistical model and analysis

Our development of the new epigenetic biomarker of aging proceeded along three main steps (Fig. 1). In step 1, a novel measure of 'phenotypic age' was developed using clinical data from the third National Health and Nutrition Examination Survey (NHANES). Details on the phenotypic age estimator can be found in Table 1 and in Supplement 1. In step 2, DNAm from whole blood was used to predict phenotypic age, such that:

$$DNAm\ PhenoAge = intercept + CpG_1 \times \beta_1 + CpG_2 \times \beta_2 + \cdots CpG_{513} \times \beta_{513}$$

The coefficient values of this model can be found in Supplement 2 (Table S6). Predicted estimates from this model represent a person's epigenetic age, which we refer to as 'DNAm PhenoAge'. Using multiple independent datasets, we then tested whether DNAm PhenoAge was associated with a number of aging-related outcomes. We also tested whether it differed as a function of social, behavioral, and demographic characteristics, and whether it was applicable to tissues other than whole blood.

Finally, in step 3, we examine the underlying biology of the 513 CpGs in the DNAm PhenoAge measure by examining differential expression, GO and pathway enrichment, chromosomal locations, and heritability.

Estimating phenotypic age from clinical biomarkers

For step 1, NHANES III was used to generate a measure of phenotypic age. NHANES III is a nationally-representative sample, with over twenty-three years of mortality follow-up, from which our analytical sample included 9,926 adults with complete biomarker data. A Cox penalized regression model—where the hazard of mortality was regressed on forty-two clinical markers and chronological age—was used to select variables for inclusion in our phenotypic age score. The forty-two biomarkers considered represent those that were available in both NHANES III and IV. Based on 10-fold cross-validation, ten variables (including chronological age) were selected for the phenotypic age predictor (Table 1, Table S1). These nine biomarkers and chronological age were then combined in a phenotypic age estimate (in units of years) as detailed in Methods.

Validation data for phenotypic age came from NHANES IV, and included up to 12 years of mortality follow-up for n=6,209 national representative US adults. In this population, phenotypic age is correlated with chronological age at r=0.94. Results from all-cause and cause-specific (competing risk) mortality predictions, adjusting for chronological age (Table 2), show that a one year increase in phenotypic age is associated with a 9% increase in the risk of all-cause
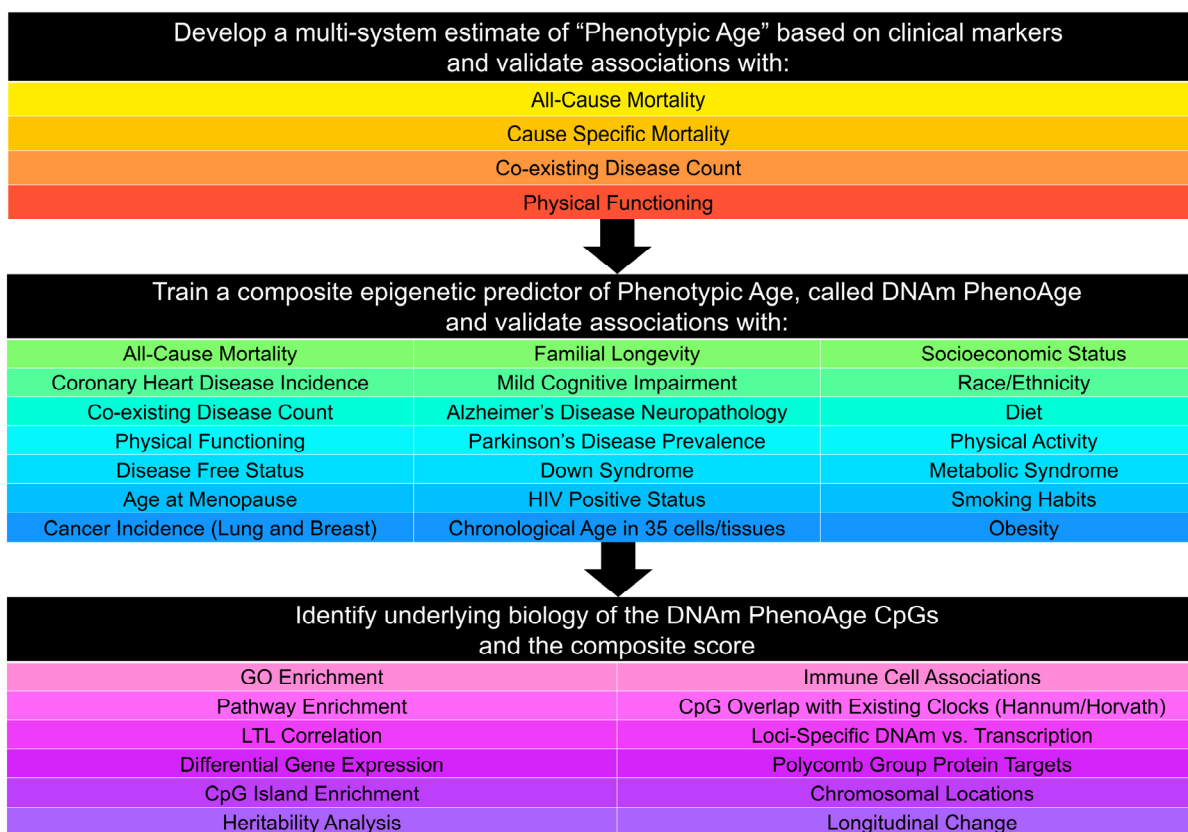
Figure 1. Roadmap for developing DNAm PhenoAge. The roadmap depicts our analytical procedures. In step 1, we developed an estimate of 'Phenotypic Age' based on clinical measure. Phenotypic age was developed using the NHANES III as training data, in which we employed a proportional hazard penalized regression model to narrow 42 biomarkers to 9 biomarkers and chronological age. This measure was then validated in NHANES IV and shown to be a strong predictor of both morbidity and mortality risk. In step 2, we developed an epigenetic biomarker of phenotypic age, which we call DNAm PhenoAge, by regressing phenotypic age (from step 1) on blood DNA methylation data, using the InCHIANTI data. This produced an estimate of DNAm PhenoAge based on 513 CpGs. We then validated our new epigenetic biomarker of aging, DNAm PhenoAge, using multiple cohorts, aging-related outcomes, and tissues/cells. In step 3, we examined the underlying biology of the 513 CpGs and the composite DNAm PhenoAge measure, using a variety of complementary data (gene expression, blood cell counts) and various genome annotation tools including chromatin state analysis and gene ontology enrichment.

mortality (HR=1.09, p=3.8E-49), a 9% increase in the risk of mortality from aging-related diseases (HR=1.09, p=4.5E-34), a 10% increase in the risk of CVD mortality (HR=1.10, p=5.1E-17), a 7% increase in the risk of cancer mortality (HR=1.07, p=7.9E-10), a 20% increase in the risk of diabetes mortality (HR=1.20, p=1.9E-11), and a 9% increase in the risk of chronic lower respiratory disease mortality (HR=1.09, p=6.3E-4). Further, phenotypic age is highly associated with comorbidity count (p=3.9E-21) and physical functioning measures (p=2.1E-10, Supplement 1: Fig. S1).

An epigenetic biomarker of aging (DNAm PhenoAge)

For step 2 (Fig. 1), data from n=456 participants at two time-points in the Invecchiare in Chianti (InCHIANTI) study was used to relate blood DNAm levels to phenotypic age. InCHIANTI was used as training data for the new epigenetic biomarker because the study assessed all clinical measures needed to estimate phenotypic age, contained data on DNAm, and had a large age range population (21-100 years). A total of 20,169 CpGs were considered when generating the new

DNAm measure. They represented those CpGs available on all three chips (27k, 450k, EPIC), so as to facilitate usability across platforms. Elastic net regression, with 10-fold cross-validation, produced a model in which phenotypic age is predicted by DNAm levels at 513 of the 20,169 CpGs. The linear combination of the weighted 513 CpGs yields a DNAm based estimator of phenotypic age that we refer to as 'DNAm PhenoAge' (mean=58.9, s.d.=18.2, range=9.1-106.1), in contrast to the previously published Hannum and Horvath 'DNAm Age' measures.

While our new clock was trained on cross-sectional data in InCHIANTI, we capitalized on the repeated time-points to test whether changes in DNAm PhenoAge are related to changes in phenotypic age. As expected, between 1998 and 2007, mean change in DNAm PhenoAge was 8.51 years, whereas mean change in clinical phenotypic age was 8.88 years. Moreover, participants' clinical phenotypic age (adjusting for chronological age) at the two time-points was correlated at r=0.50, whereas participants' DNAm PhenoAge (adjusting for chronological age) at the two time-points was correlated at r=0.68 (Supplement 1: Fig. S2). We also find that the change in phenotypic age between

Table 1. Phenotypic aging measures and Gompertz coefficients.

Variable		Units	Weight
Albumin	Liver	g/L	-0.0336
Creatinine	Kidney	umol/L	0.0095
Glucose, serum	Metabolic	mmol/L	0.1953
C-reactive protein (log)	Inflammation	mg/dL	0.0954
Lymphocyte percent	Immune	%	-0.0120
Mean (red) cell volume	Immune	fL	0.0268
Red cell distribution width	Immune	%	0.3306
Alkaline phosphatase	Liver	U/L	0.0019
White blood cell count	Immune	1000 cells/uL	0.0554
Age		Years	0.0804

Table 2. Mortality validations for phenotypic age.

Mortality Cause	Cases	HR	P-Value
All-Cause	1052	1.09	3.8E-49
Aging-Related	661	1.09	4.5E-34
CVD	272	1.10	5.1E-17
Cancer	265	1.07	7.9E-10
Alzheimer's	30	1.04	2.6E-1
Diabetes	41	1.20	1.9E-11
Chronic lower respiratory diseases	53	1.09	6.3E-4

1998 and 2007 is highly correlated with the change in DNAm PhenoAge between these two time-points (r=0.74, p=3.2E-80, Supplement 1: Fig. S2).

DNAm PhenoAge strongly relates to all-cause mortality

In step 2 (Fig. 1), the epigenetic biomarker, DNAm PhenoAge, was calculated in five independent large-scale samples—two samples from Women's Health Initiative (WHI) (n=2,016; and n=2,191), the Framingham Heart Study (FHS) (n=2,553), the Normative Aging Study (NAS) (n=657), and the Jackson Heart Study (JHS) (n=1,747). The first four studies used the Illumina 450K array while the JHS employed the latest Illumina EPIC array platform. In these studies, DNAm PhenoAge correlated with chronological age at r=0.66 in WHI (Sample 1), r=0.69 in WHI (Sample 2), r=0.78 in FHS, r=0.62 in the NAS, and r=0.89 in JHS. The five validation samples were then used to assess the effects of DNAm PhenoAge on mortality in comparison to the Horvath and Hannum DNAm Age measures. DNAm PhenoAge was significantly associated with subsequent mortality risk in all studies (independent of chronological age), such that, a one year increase in DNAm PhenoAge is associated with a 4.5% increase in the risk of all-cause mortality (Meta(FE)=1.045, Meta p=7.9E-47, Fig. 2). To better conceptualize what this increase represents, we compared the predicted life expectancy and mortality risk for person's representing the top 5% (fastest agers), the average, and the bottom 5% (slowest agers). Results suggest that those in the top 5% of fastest agers have a mortality hazard of death that is about 1.62 times that of the average person, i.e. the hazard of death is 62% higher than that of an average person. Further, contrasting the 5% fastest agers with the 5% slowest agers, we find that the hazard of death of the fastest agers is 2.58 times higher than that of the bottom 5% slowest agers (HR=$1.045^{11.0}$/$1.045^{-10.5}$). Additionally, both observed and predicted Kaplan-Meier survival estimates showed that faster agers had much lower life expectancy and survival rates compared to average and/or slow agers (Fig. 2).

As shown in Fig. 2, the DNAm age based measures from Hannum and Horvath also related to all-cause mortality, consistent with what has been reported previously [15, 19, 23, 33, 34]. To directly compare the three epigenetic measures, we contrasted their accuracy in predicting 10-year and 20-year mortality risk, using receiver operating characteristics (ROC) curves. DNAm PhenoAge (adjusted for age) predicts both 10-year mortality and 20-year mortality significantly better than the Horvath and Hannum DNAmAge measures (Supplement 1: Table S2). When examining a model that

includes all three measures (Supplement 1: Table S3), we find that only DNAm PhenoAge is positively associated with mortality (HR=1.04, p=1.33E-8), whereas Horvath DNAm Age is now negatively associated (HR=0.98, p=2.72E-2), and Hannum DNAm Age has no association (HR=1.01, p=4.66E-1).

DNAm PhenoAge strongly relates to aging-related morbidity

Given that aging is believed to also influence disease incidence/prevalence, we examined whether DNAm PhenoAge relates to diverse age-related morbidity outcomes. We observe strong associations between DNAm PhenoAge and a variety of other aging outcomes using the same five validation samples (Table 3). For instance, independent of chronological age, higher DNAm PhenoAge is associated with an increase in a person's number of coexisting morbidities (β=0.008 to 0.031; Meta P-value=1.95E-20), a decrease in likelihood of being disease-free (β=-0.002 to -0.039; Meta P-value=2.10E-10), an increase in physical functioning problems (β=-0.016 to -0.473; Meta P-value=2.05E-13), an increase in the risk of coronary heart disease (CHD) risk (β=0.016 to 0.073; Meta P-value=3.35E-11).

DNAm PhenoAge and smoking

Cigarette exposure has been shown to have an epigenetic fingerprint[35-37], which has been reflected in previous DNAm risk predictors[38]. Similarly, we find that DNAm PhenoAge significantly differs between never (n=1,097), current (n=209), and former smokers (n=710) (p=0.0033) (Supplement 1, Fig. S3A); however, conversely, we do not find a robust association between pack-years and DNAm PhenoAge (Supplement 1, Fig. S3B-D). Given the association between DNAm PhenoAge and smoking, we re-evaluated the morbidity and mortality associations (fully-adjusted) in our four samples, stratifying by smoking status (Supplement 1: Fig. S4 and Table S4). We find that DNAm PhenoAge is associated with mortality among both smokers (adjusted for pack-years) (Meta(FE)=1.050, Meta p=7.9E-31), and non-smokers (Meta(FE)=1.033, Meta p=1.2E-10). DNAm PhenoAge relates to the number of coexisting morbidities, physical functioning status, disease free status, and CHD for both smokers and non-smokers (Supplement 1: Table S4). In previous work we showed that Horvath DNAm age of blood predicts lung cancer risk in the first WHI sample [20]. Using the same data, we find that a one year increase in DNAm PhenoAge (adjusting for chronological age, race/ethnicity, pack-years, and smoking status) is associated with a 5% increase in the risk of lung cancer incidence and/or

mortality (HR=1.05, p=0.031). Further, when restricting the model to current smokers only, we find that the effect of DNAm PhenoAge on future lung cancer incidence and/or mortality is even stronger (HR=1.10, p=0.014).

DNAm PhenoAge in other tissues

One advantage of developing biological aging estimates based on molecular markers (like DNAm), rather than clinical risk measures (e.g. those in the phenotypic age variable), is that they may lend themselves to measuring tissue/cell specific aging. Although DNAm PhenoAge was developed using samples from whole blood, our empirical results show that it strongly correlates with chronological age in a host of different tissues and cell types (Fig. 3). For instance, when examining all tissues concurrently, the correlation between DNAm PhenoAge and chronological age was 0.71. Age correlations in brain tissue ranged from 0.54 to 0.92, while correlations were also found in breast (r=0.47), buccal cells (r=0.88), dermal fibroblasts (r=0.87), epidermis (r=0.84), colon (r=0.88), heart (r=0.66), kidney (r=0.64), liver (r=0.80), lung (r=055), and saliva (r=0.81).
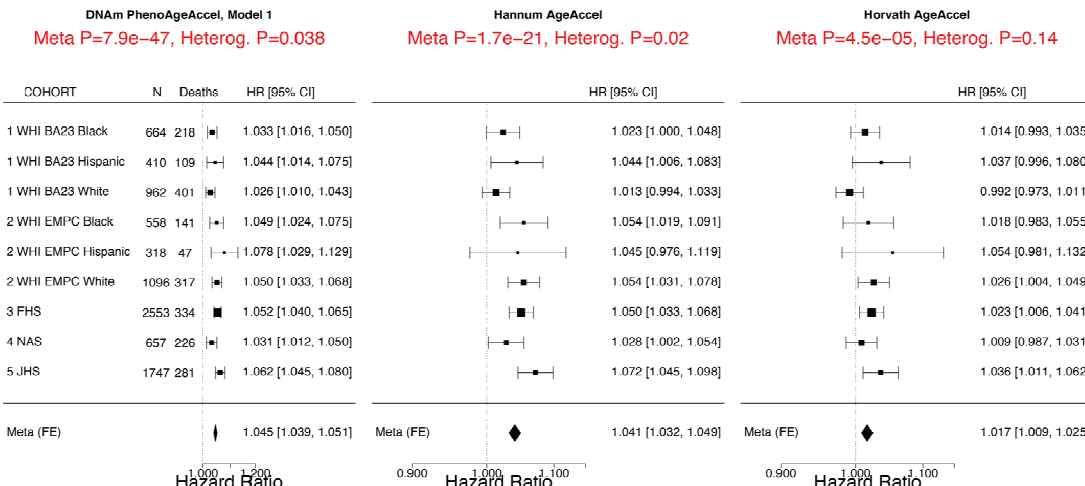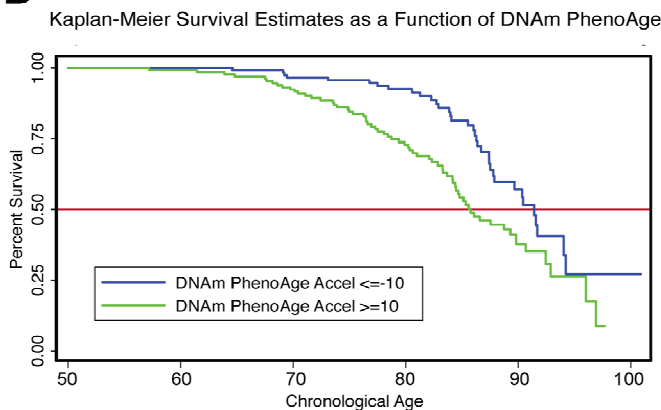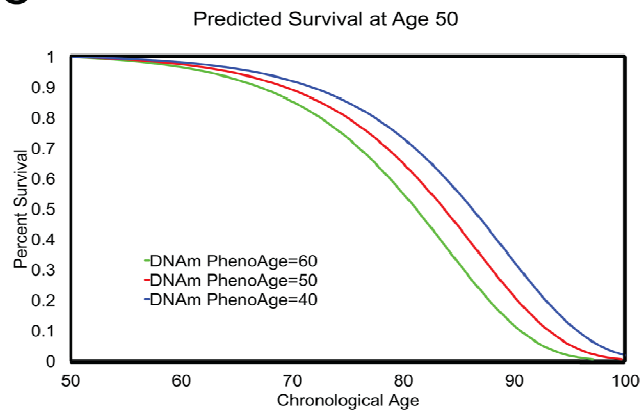
Figure 2. Mortality Prediction by DNAm PhenoAge. (**A**) Using five samples from large epidemiological cohorts—two samples from the Women's health Initiative, the Framingham Heart Study, the Normative Aging Study, and the Jackson Heart Study—we tested whether DNAm PhenoAge was predictive of all-cause mortality. The Fig. displays a forest plot for fixed-effect meta-analysis, based on Cox proportional hazard models, and adjusting for chronological age. Results suggest that DNAm PhenoAge is predictive of mortality in all samples, and that overall, a one year increase in DNAm PhenoAge is associated with a 4.5% increase in the risk of death (p=9.9E-47). This is contrasted against the first generation of epigenetic biomarkers of aging by Hannum and Horvath, which exhibit less significant associations with lifespan (p=1.7E-21 and p=4.5E-5, respectively). (**B** and **C**) Using the WHI sample 1, we plotted Kaplan-Meier survival estimates using actual data from the fastest versus the slowest agers (panel **B**). We also applied the equation from the proportional hazard model to predict remaining life expectancy and plotted predicted survival assuming a chronological age of 50 and a DNAm PhenoAge of either 40 (slow ager), 50 (average ager), or 60 (fast ager) (panel **C**). Median life expectancy at age 50 was predicted to be approximately 81 years for the fastest agers, 83.5 years for average agers, and 86 years for the slowest agers.

Table 3. Morbidity validation for DNAm PhenoAge.

Sample	Comorbidity		Disease Free		CHD Risk		Physical Functioning	
	Coefficient	P-value	Coefficient	P-value	Coefficient	P-value	Coefficient	P-value
DNAm PhenoAge								
WHI BA23 White	0.008	2.38E-01	-0.002	3.82E-01	0.016	5.36E-02	-0.396	1.04E-04
WHI BA23 Black	0.013	6.15E-02	-0.006	2.40E-02	0.021	2.02E-02	-0.423	4.50E-04
WHI BA23 Hispanic	0.024	1.64E-02	-0.004	3.67E-01	0.033	5.07E-02	-0.329	7.37E-02
WHI EMPC White	0.031	2.95E-07	-0.026	1.63E-02	0.023	1.89E-01	-0.361	3.81E-05
WHI EMPC Black	0.014	7.67E-02	-0.023	6.98E-02	0.048	2.27E-02	-0.473	3.75E-04
WHI EMPC Hispanic	0.003	7.83E-01	0.002	9.28E-01	0.073	1.98E-01	-0.377	6.54E-02
FHS	0.022	3.93E-07	-0.034	1.59E-03	0.028	5.47E-06	-0.016	4.60E-01
NAS	0.023	7.59E-06	-0.062	2.00E-04	0.030	2.27E-02	NA	NA
JHS	0.018	1.86E-08	-0.039	5.92E-05	0.033	4.73E-02	NA	NA
Meta P-value (Stouffer)		**1.95E-20**		**2.14E-10**		**3.35E-11**		**2.05E-13**
DNAmAge Hannum								
WHI BA23 White	0.007	3.90E-01	-0.003	3.48E-01	0.013	2.36E-01	-0.399	2.90E-03
WHI BA23 Black	0.022	2.72E-02	-0.007	6.03E-02	0.015	2.67E-01	-0.345	4.29E-02
WHI BA23 Hispanic	0.010	4.33E-01	-0.010	6.24E-02	0.011	6.10E-01	-0.599	1.16E-02
WHI EMPC White	0.025	1.53E-03	-0.020	1.55E-01	0.022	3.30E-01	-0.284	1.43E-02
WHI EMPC Black	0.022	6.34E-02	-0.008	6.62E-01	0.055	6.12E-02	-0.323	9.56E-02
WHI EMPC Hispanic	-0.012	4.17E-01	0.035	2.09E-01	-0.012	8.85E-01	-0.345	2.54E-01
FHS	0.019	5.94E-04	-0.030	2.55E-02	0.022	1.55E-02	0.040	1.32E-01
NAS	0.009	2.19E-01	-0.026	2.26E-01	0.025	1.83E-01	NA	NA
JHS	0.020	2.09E-05	-0.036	9.91E-03	0.086	1.64E-04	NA	NA
Meta P-value (Stouffer)		**1.50E-08**		**1.64E-04**		**1.40E-05**		**2.03E-05**
DNAmAge Horvath								
WHI BA23 White	0.007	3.49E-01	-0.004	1.69E-01	0.001	9.12E-01	-0.440	5.10E-04
WHI BA23 Black	0.018	3.96E-02	-0.006	6.25E-02	0.009	4.07E-01	-0.305	4.52E-02
WHI BA23 Hispanic	0.012	3.65E-01	-0.007	1.86E-01	-0.001	9.78E-01	-0.204	4.12E-01
WHI EMPC White	0.031	1.99E-04	-0.043	5.56E-03	0.000	9.88E-01	-0.288	1.74E-02
WHI EMPC Black	0.016	1.93E-01	-0.003	8.56E-01	0.033	2.87E-01	-0.144	4.68E-01
WHI EMPC Hispanic	-0.025	8.99E-02	-0.016	5.70E-01	-0.064	4.63E-01	-0.012	9.70E-01
FHS	0.011	5.82E-02	-0.021	8.34E-02	0.007	5.19E-01	0.027	3.16E-01
NAS	0.011	7.90E-02	-0.039	4.53E-02	0.006	7.14E-01	NA	NA
JHS	0.014	2.03E-03	-0.040	1.78E-03	0.049	3.93E-02	NA	NA
Meta P-value (Stouffer)		**3.26E-06**		**6.36E-07**		**1.49E-01**		**1.43E-03**

Alzheimer's disease and brain samples

Based on the accuracy of the age prediction in other tissues/cells, we examined whether aging in a given tissue was associated with tissue-associated outcomes. For instance, using data from approximately 700 postmortem samples from the Religious Order Study (ROS) and the Memory and Aging Project (MAP) [39, 40] we tested the association between pathologically diagnosed Alzheimer's disease and DNAm PhenoAge in dorsolateral prefrontal cortex (DLPFX). Results suggest (Fig. 4) that those who are diagnosed with Alzheimer's disease (AD), based on postmortem autopsy, have DLPFX that appear more than one year older than same aged individuals who are not diagnosed with AD postmortem (p=4.6E-4). Further, age adjusted DNAm PhenoAge was found to be positively associated with neuropathological hallmarks of Alzheimer's disease, such as amyloid load (r=0.094, p=0.012), neuritic plaques (r=0.11, p=0.0032), and neurofibrillary tangles (r=0.10, p=0.0073).
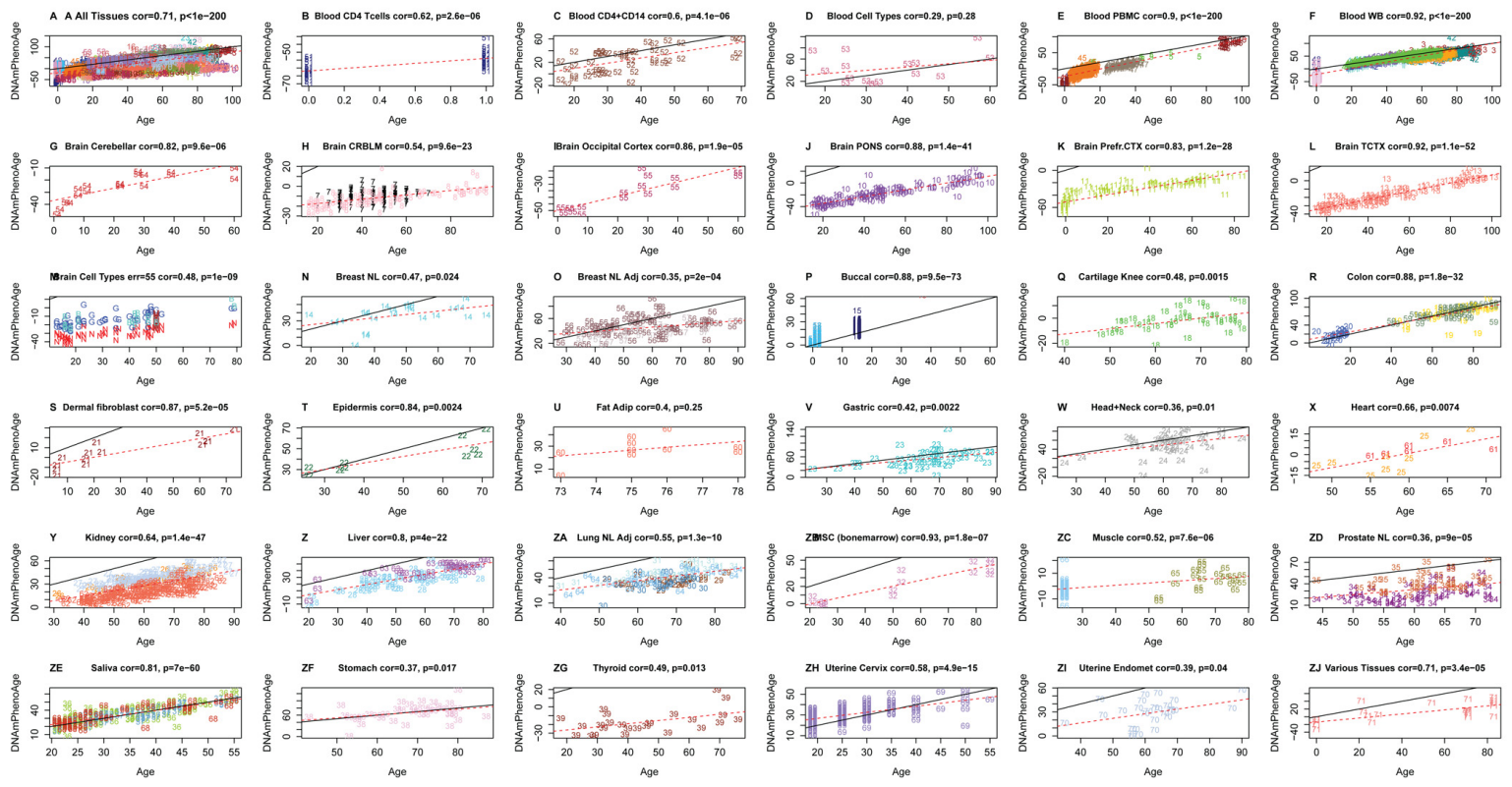
Figure 3. Chronological age versus DNAm PhenoAge in a variety of tissues and cells. Although DNAm PhenoAge was developed using methylation data from whole blood, it also tracks chronological age in a wide variety of tissues and cells. (**A**) The correlation across all tissues/cells we examined is r=0.71. (**B-ZJ**) report results in different sources of DNA as indicated in panel headings. The numbers correspond to the data sets from (Horvath 2013). Overall, correlations range from r=0.35 (breast, panel O) to r=0.92 (temporal cortex in brain, panel L).

Lifestyle and demographic variables

In evaluating the relationship between DNAm PhenoAge in blood and additional characteristics we observe significant differences between racial/ethnic groups (p=5.1E-5), with non-Hispanic blacks having the highest DNAm PhenoAge on average, and non-Hispanic whites having the lowest (Supplement 1: Fig. S5). We also find evidence of social gradients in DNAm PhenoAge, such that those with higher education (p=6E-9) and higher income (p=9E-5) appear younger (Figure 5). DNAm PhenoAge relates to exercise and dietary habits, such that increased exercise (p=7E-5) and markers of fruit/vegetable consumption (such as carotenoids, p=2E-27) are associated with lower DNAm PhenoAge (Figure 5, Supplement 1: Fig. S6). Cross-sectional studies in the WHI also revealed that DNAmPhenoAge acceleration is positively correlated with C-reactive protein (r=0.18, p=5E-22, Figure 5), insulin (r=0.15, p=2E-20), glucose (r=0.10, p=2E-10), triglycerides (r=0.09, p=5E-9), waist to hip ratio (r=0.15, p=5E-22) but it is negatively correlated with HDL cholesterol (r=-0.09, p=7E-9).

DNAm PhenoAge and Immunosenescence

To test the hypothesis that DNAm PhenoAge captures aspects of age-related decline of the immune system, we correlated DNAm PhenoAge with estimated blood cell count (Supplement 1, Fig. S7). After adjusting for age, we find that DNAm PhenoAgeAccel is negatively correlated with naïve CD8+ T cells (r=-0.35, p=9.2E-65), naïve CD4+ T cells (r=-0.29, p=4.2E-42), CD4+ helper T cells (r=-0.34, p=3.6E-58), and B cells (r=-0.18, p=8.4E-17). Further, DNAm PhenoAgeAccel is positively correlated with the proportion of granulocytes (r=0.32, p=2.3E-51), exhausted CD8+ (defined as CD28-CD45RA-) T cells (r=0.20, p=1.9E-20), and plasma blast cells (r=0.26, p=6.7E-34). These results are consistent with age related changes in blood cells [41] and suggest that DNAm PhenoAge may capture aspects of immuno-senescence in blood. However, three lines of evidence suggest that DNAm PhenoAge is not simply a measure of immunosenescence. First, another measure of immunosenescence, leukocyte telomere length, is only weakly correlated with DNAm PhenoAgeAccel (r=-0.13 p=0.00019 in the WHI; r=-

0.087, P=7.6E-3 in Framingham Heart study; JHS p=7.83E-7, Supplement 1, Fig. S8). Second, the strong association between DNAm PhenoAge and mortality does not simply reflect changes in blood cell composition, as can be seen from the fact that in Supplement 1, Fig. S9 the robust association remains even after adjusting for estimates of seven blood cell count measures (Meta(FE)=1.036, Meta p=5.6E-21). Third, DNAmPhenoAge correlates with chronological age in non-blood tissue.

DNA sequence characteristics of the 513 CpGs in DNAm PhenoAge

Of the 513 CpGs in DNAm PhenoAge, we find that, 41 CpGs were also in the Horvath DNAm age measure (Supplement 2: Table S6). This represents a 4.88-fold increase over what would be expected by chance (p=8.97E-15). Of the 41 overlapping CpGs, the average absolute value for their age correlations was r=0.40, and 31 had age correlations with absolute values in the top 20% of what is found among the 513 CpGs in the DNAm PhenoAge score. We also observed 6 CpGs that

overlapped between the Hannum DNAm Age score and the DNAm PhenoAge score—five of which were also found in the Horvath DNAm Age measure. All six CpGs had extremely high age correlations (half positive, half negative), with absolute values between r=0.49 and r=0.76. The five CpGs that are found in all three epigenetic aging measures were: cg05442902 (*P2RXL1*), cg06493994 (*SCGN*), cg09809672 (*EDARADD*), cg19722847 (*IPO8*), and cg22736354 (*NHLRC1*).

Several additional DNAm biomarkers have been described in the literature [12, 13]. A direct comparison of 6 DNAm biomarkers (including DNAm PhenoAge) reveals that DNAm PhenoAge stands out in terms of its predictive accuracy for lifespan, its relationship with smoking status, its relationship with leukocyte telomere length, naïve CD8+ T cells and CD4+ T cells (Supplement 1: Table S5).

Next, we conducted a functional enrichment analysis of the chromosomal locations of the 513 CpGs and found that 149 CpGs whose age correlation exceeded 0.2 tended to be located in CpG islands (p=0.0045, Supple-
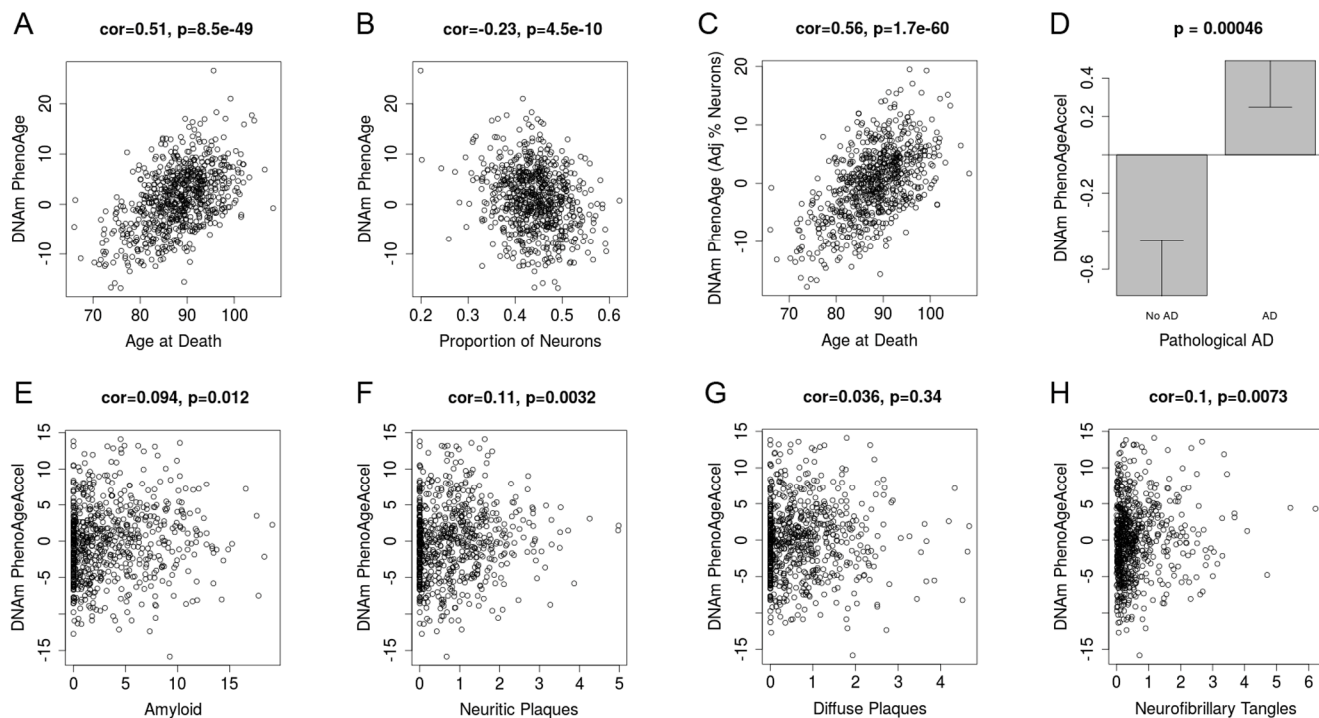
Figure 4. DNAm PhenoAge measured in dorsolateral prefrontal cortex relates to Alzheimer's disease and related neuropathologies. Using postmortem data from the Religious Order Study (ROS) and the Memory and Aging Project (MAP), we find a moderate/high correlation between chronological age and DNAm PhenoAge (panel **A**). We also estimate the Pproportion of neurons via the CETS algorithm and show that it correlates with DNAm PhenoAge (B). Further, the correlation between chronological agen and DNAm PhenoAge is increased after adjusting for the estimated proportion on neurons in each sample (panel **C**). We also find that DNAm PhenoAge is significantly higher (p=0.00046) among those with Alzheimer's disease versus controls (panel **D**), and that it positively correlates with amyloid load (p=0.012, panel **E**), neuritic plaques (p=0.0032, panel **F**), diffuse plaques (p=0.036, panel **G**), and neurofibrillary tangles (p=0.0073, panel **H**).

ment 1: Fig. S10) and were significantly enriched with polycomb group protein targets (p=8.7E-5, Supplement 1: Fig. S10), which in line with results of epigenome wide studies of aging effects [4, 5, 42].

Transcriptional and genetic studies of DNAm PhenoAge

Using the genome-wide data from FHS and WHI, we estimated the heritability of DNAm PhenoAge. The heri-

tability estimated by the SOLAR polygenic model for those of European ancestry in the FHS was $h^2=0.33$, while the heritability estimated for those of European ancestry in WHI, using GCTA-GREML analysis [43] was $h^2=0.51$.

Using the monocyte data mentioned above, as well as PBMC expression data on 2,188 persons from the FHS, we conducted a transcriptional analysis to identify differential expression associated with DNAm PhenoAge-

		Pooled WHI samples			
		Adjusted for ethnicity and dataset			
				PhenoAgeAccel	
		n	μ	bicor	p
Diet	log2(Total energy)	3700	10.58	0.01	0.40
	Carbohydrate	3700	48.64	-0.02	0.23
	Protein	3700	16.39	-0.01	0.45
	Fat	3700	35.05	0.03	0.12
	log2(1+Red meat)	3700	0.69	0.05	2E-3
	log2(1+Poultry)	3700	0.39	-0.02	0.14
	log2(1+Fish)	3700	0.25	-0.03	0.10
	log2(1+Dairy)	3700	1.21	-0.01	0.76
	log2(1+Whole grains)	3700	1.00	-0.02	0.19
	log2(1+Nuts)	3700	0.10	-0.04	0.03
	log2(Fruits)	3700	0.57	-0.02	0.13
	log2(Vegetables)	3700	0.71	-0.03	0.09
Dietary biomarkers	Retinol	2267	0.58	0.03	0.17
	Mean carotenoids	2266	0.06	-0.22	2E-27
	Lycopene	2267	0.36	-0.11	3E-7
	log2(alpha-Carotene)	2267	-4.21	-0.19	5E-20
	log2(beta-Carotene)	2266	-2.15	-0.18	2E-17
	log2(Lutein+Zeaxanthin)	2267	-2.38	-0.17	2E-16
	log2(beta-Cryptoxanthin)	2267	-3.76	-0.17	2E-15
	log2(alpha-Tocopherol)	2267	3.87	-0.03	0.19
	log2(gamma-Tocopherol)	2267	0.88	0.07	6E-4
Measurements	log2(C-reactive protein)	2809	1.57	0.18	5E-22
	log2(Insulin)	4042	5.78	0.15	2E-20
	log2(Glucose)	4144	6.57	0.10	2E-10
	log2(Triglyceride)	4148	7.02	0.09	5E-9
	Total cholesterol	4148	224.00	-0.04	4E-3
	LDL cholesterol	4084	140.00	-0.05	2E-3
	HDL cholesterol	4145	53.00	-0.09	7E-9
	log2(Creatinine)	2748	-0.43	0.01	0.52
	Systolic blood pressure	4177	129.00	0.08	1E-6
	Diastolic blood pressure	4178	76.00	0.02	0.12
	log2(Waist / hip ratio)	4037	-0.28	0.15	5E-22
	BMI	4145	28.88	0.13	5E-16
Socio-behavioral	Education	4143	7.00	-0.09	6E-9
	Income	4054	3.00	-0.06	9E-5
	log2(1+Exercise)	3914	2.75	-0.06	7E-5
	Current smoker	2321	0.00	0.10	3E-6
	log2(1+Alcohol)	3700	0.14	-0.04	0.02

Figure 5. Lifestyle factors versus DNAm PhenoAge acceleration in blood in the WHI. In this cross sectional analysis, the correlation test analysis (bicor, biweight midcorrelation) between select variables and DNAm PhenoAgeAccel reveals that education, income, exercise, proxies of fruit/vegetable consumption, and HDL cholesterol are negatively associated (blue) with DNAm PhenoAge, i.e. younger epigenetic age. Conversely, CRP, insulin, glucose, triglycerides, BMI, waist-to-hip ratio, systolic blood pressure, and smoking have a positive association (red) with DNAm PhenoAge. All results have been adjusted for ethnicity and batch/data set. Similar results based on multivariate regression models can be found in Supplementary Figure 6B.

Accel (Supplement 3: Table S7). Overall, we find that genes show similar associations with chronological age and DNAm PhenoAgeAccel. DNAm PhenoAgeAccel represents aging differences among same-aged individuals and is adjusted so as to exhibit a correlation of r=0.0 with chronological age. Thus, this observation suggests that genes whose transcription increases with age are upregulated among epigenetically older compared to epigenetically younger persons of the same chronological age (Supplement 1: Fig. S11); the same applies for genes that show decreases with chronological age being downregulated in epi-genetically older versus younger persons of the same age.

Using the transcriptional data from monocytes described above (adjusting for array, sex, race/ethnicity, age, and imputed cell counts), we tested for GO enrichment among genes that are positively associated with DNAm PhenoAge and those that are negatively associated with DNAm PhenoAge (Supplement 4: Table S8). Among those with positive aging associations (over-expression among epigenetically older individuals), we observed enrichment for a number of pro-inflammatory signaling pathways. These pathways included, but are not limited to: multiple toll-like receptor signaling pathways (7,9,3,2), regulation of inflammatory response, JAK-STAT cascade, response to lipopoly-saccharide, tumor necrosis factor-mediated signaling pathway, and positive regulation of NF-kappaB transcription factor activity. Additionally, positively associated genes were also enriched for a number anti-viral response pathways—type I interferon signaling, defense response to virus, interferon-gamma-mediated signaling pathway, cellular response to interferon-alpha, etc. Other interesting GO terms enriched among positively associated genes included: response to nutrient, JAK-STAT cascade involved in growth hormone signaling pathway, multicellular organism growth, and regulation of DNA methylation.

When testing for enrichment among genes that were negatively associated with DNAm PhenoAgeAccel (decreased expression among epigenetically older persons) we observed that many were implicated in processes involving transcriptional and translational machinery, as well as damage recognition and repair. These included: translational initiation; regulation of translational initiation; ribosomal large subunit assembly; ribosomal small subunit assembly; translational elongation; transcription initiation from RNA polymerase I promoter; transcription-coupled nucleotide-excision repair; nucleotide-excision repair, DNA incision, 5'-to lesion; nucleotide-excision repair, DNA damage recognition; DNA damage response, detection of DNA damage; and regulation of DNA damage checkpoint.

DISCUSSION

Using a novel two-step method, we were successful in developing a DNAm based biomarker of aging that is highly predictive of nearly every morbidity and mortality outcome we tested. Training an epigenetic predictor of phenotypic age instead of chronological age led to substantial improvement in mortality/healthspan predictions over the first generation of DNAm based biomarkers of chronological age from Hannum[10], Horvath[11] and other published DNAm biomarkers. In doing so, this is the first study to conclusively demonstrate that DNAm biomarkers of aging are highly predictive of cardiovascular disease and coronary heart disease. DNAm PhenoAge also tracks chronological age and relates to disease risk in samples other than whole blood. Finally, we find that an individual's DNAm PhenoAge, relative to his/her chronological age, is moderately heritable and is associated with activation of pro-inflammatory, interferon, DNAm damage repair, transcriptional/ translational signaling, and various markers of immuno-senescence: a decline of naïve T cells and shortened leukocyte telomere length (Supplementary Information).

The ability of our measure to predict multifactorial aging conditions is consistent with the fundamental underpinnings of Geroscience research [1, 44], which posits that aging mechanisms give rise to multiple pathologies and thus, differences in the rate of aging will have implications for a wide array of diseases and conditions. Further, these results answer a fundamental biological question of whether differences in multi-system dysregulation (estimated using clinical phenotypic age measures), healthspan, and lifespan are reflected at the epigenetic level, in the form of differential DNAm at specific CpG sites.

The improvement over previous epigenetic biomarkers, likely comes down to the types of CpGs selected for the various measures. Only 41 of the 513 CpGs in DNAm PhenoAge were shared with the Horvath clock, while only five CpGs were shared between all three clocks (DNAm PhenoAge, Horvath, and Hannum). In general, these CpGs did not tend to be drivers of the DNAm PhenoAge score, and instead represented those with large age correlations. This may explain the improvements of DNAm PhenoAge over previous epigenetic biomarkers of aging. While the previous DNAm age estimators selected CpGs to optimize prediction of chronological age, the CpGs in DNAm PhenoAge were optimized to predict a multi-system proxy of physiological dysregulation (phenotypic age). In doing so, we were able to not only capture CpGs that exhibited strong correlations with age, but also those that captured variations in risk of death and disease

among same aged individuals. In general, the CpGs with the highest weights in the new clock did not correlate with chronological age (Supplement 1: Fig. S12), but instead were related to the difference between phenotypic and chronological age—i.e. divergence in the rate of aging.

While DNAm PhenoAge greatly outperformed all previous DNAm biomarkers of aging (Supplement 1: Table S5), the utility of DNAm PhenoAge for estimating risk does not imply that it should replace clinical biomarkers when it comes to informing medical and health-related decisions. In fact, but perhaps not surprisingly, the phenotypic age measure used to select CpGs is a better predictor of morbidity and mortality outcomes than DNAm PhenoAge. While the addition of error in performing a two-step process, rather than training a DNAm predictor directly on mortality may contribute, we don't believe this accounts for the difference in predictive performance. In fact, a recent DNAm measure by Zhang et al. [38] was trained to directly predict mortality risk, yet it appears to be a weaker predictor than both our DNAm PhenoAge measure and our clinical phenotypic age measure (Supplement 1: Table S9). The first generation of DNAm age estimators only exhibit weak associations with clinical measures of physiological dysregulation [24, 45]. Physiological dysregulation, which is more closely related to our clinical age measure "phenotypic age" than to chronological age, is not only the result of exogenous/endogenous stress factors (such as obesity, infections) but also a result of age related molecular alterations, one example of which are modifications to the epigenome. Over time, dysregulation within organ systems leads to pathogenesis of disease (age-related molecular changes → physiological dysregulation → morbidity → mortality)[46]. However, stochasticity and variability exist at each of these transitions. Therefore, measures of physiological dysregulation, will be better predictors of transition to the next stage in the aging trajectory (i.e. morbidity and mortality) than will measures of age related molecular alterations, like DNAm PhenoAge. Similarly, quantification of disease pathogenesis (cancer stage, Alzheimer's stage) is likely a better predictor of mortality risk than clinical phenotypic aging measures. As a result, clinical phenotypic aging measures may be preferable to epigenetic measures when the goal is risk prediction, and samples come from blood.

That being said, when the aim is to study the mechanisms of the aging process, DNAm measures have advantages over clinical measures. First, they may better capture "pre-clinical aging" and thus may be more suited for differentiating aging in children, young adults, or extremely healthy individuals, for whom

measures like CRP, albumin, creatinine, glucose, etc. are still fairly homogenous. Second, as demonstrated, these molecular measures can capture cell and/or tissue specific aging rates and therefore may also lend themselves to in vitro studies of aging, studies for which blood is not available, studies using postmortem samples, and/or studies comparing aging rates between tissues/cells. While the fundamental drivers of aging are believed to be shared across cells/tissues, that is not to say that all the cells and tissues within an individual will age at the same rate. In fact, it is more likely that individuals will vary in their patterning of aging rates across tissues, and that this will have implications for death and disease risk. Relatedly, it is not known how predictions based on DNAm PhenoAge measures from non-blood samples will compare to phenotypic age predictions. It may be the case that various outcomes will be more tightly related to aging in specific cells/tissues, rather than blood. Finally, examination of DNAm based aging rates facilitates the direct study of the proposed mechanisms of aging, of which "epigenetic alterations" is one of the seven hypothesized "pillars of aging" [1].

While more work needs to be done to model the biology linking DNAm PhenoAge and aging outcomes, we began to explore this using differential expression, functional enrichment, and heritability estimates. Overall, we found that CpGs that had larger increases with aging tended to be located in CpG islands and enriched with polycomb group protein targets, consistent with what has been reported in previous epigenome wide studies of aging effects [4-7, 42]. While typically DNAm of CpG islands and/or polycomb recruitment is linked to transcriptional silencing [47], for the most part, we did not observe associations between DNAm and expression for co-locating CpG-gene pairs—this was also true when only considering CpGs located in islands. These findings may suggest that the genes annotated to the CpGs in our score are not part of the link between changes in DNAm and aging. Nevertheless, we also recognize that these null results could stem from the fact that 1) associations were only tested in monocytes, 2) DNAm and expression represents what is present globally for each sample, rather than on a cell-by-cell basis, and 3) stronger associations between DNAm and gene expression levels may only exist early in life.

Nevertheless, we do identify potentially promising transcriptional pathways when considering DNAm PhenoAge as a whole. For instance, we observe that higher DNAm PhenoAge is associated with increases in the activation of proinflammatory pathways, such as NF-kappaB; increased interferon (IFN) signaling; decreases in ribosomal–related and translational

machinery pathways; and decreases in damage recognition and repair pathways. These findings are consistent with previous work describing aging associated changes, comprising increases in dysregulated inflammatory activation, increased DNA damage, and loss of translational fidelity. For instance, there exists a large body of literature highlighting the importance of an increased low-grade pro-inflammatory status as a driver of the aging process, termed inflamm-aging [41, 48, 49]. IFN signaling pathways have been shown to be markers of DNA damage and mediators of cellular senescence[50]. Additionally, it has been shown that breakdown of the transcriptional and translational machinery may play a central role in the aging process [51, 52]. For instance, the ribosome is believed to be a key regulator of proteostasis, and in turn, aging [51, 53]. Relatedly, loss of integrity in DNA damage repair pathways is considered another hallmark of the aging process [54-56].

In general, many of these pathways will have implications for adaptation to exogenous and endogenous stressors. Factors related to stress resistance and response have repeatedly been shown to be drivers of differences in lifespan and aging [49, 57-61]. This may partially account for our findings related to smoking. In general, it is not surprising that a biomarker of aging and mortality risk relates to smoking, given that life expectancies of smokers are on average ten years shorter than never smokers, and smoking history is associated with a drastic increase in the risk of a number of age-related conditions. However, perhaps more interestingly, we find that the effects of DNAm PhenoAge on mortality appear to be higher for smokers than non-smokers, which could suggest that DNAm PhenoAge represent differences in innate resilience/ vulnerability to pro-aging stressors, such as cigarette smoke.

Interestingly, we observed moderately high heritability estimates for DNAm PhenoAge. For instance, we estimated that genetic differences accounted for one-third to one-half of the variance in DNAm PhenoAge, relative to chronological age. In moving forward, it will be useful to identify the genetic architecture underlying differences in epigenetic aging. Finally, we reported that individuals' DNAm PhenoAges—relative to their chronological ages—remained fairly stable over a nine-year period. However, it is unclear whether it is attributable to genetic influences, or the fact that social and behavioral characteristics tend to also remain stable for most individuals.

If the goal is to utilize accurate quantifiable measures of the rate of aging, such as DNAm PhenoAge, to assess the efficacy of aging interventions, more work will be needed to evaluate the dynamics of DNAmPhenoAge

following various treatments. For instance, it remains to be seen whether interventions can reverse DNAmPhenoAge in the short term. Along these lines, it will be essential to determine causality—does DNAm drive the aging process, or is it simply a surrogate marker of organismal senescence? If the former is true, DNAm PhenoAge could provide insight into promising targets for therapies aimed at lifespan, and more importantly, healthspan extension.

Overall, DNAm PhenoAge is an attractive composite biomarker that captures organismal age and the functional state of many organ systems and tissues, above and beyond what is explained by chronological time. Our validation studies in multiple large and independent cohorts demonstrate that DNAm PhenoAge is a highly robust predictor of both morbidity and mortality outcomes, and represents a promising biomarker of aging, which may prove to be beneficial to both basic science and translational research.

METHODS

Using the NHANES training data, we applied a Cox penalized regression model—where the hazard of aging-related mortality (mortality from diseases of the heart, malignant neoplasms, chronic lower respiratory disease, cerebrovascular disease, Alzheimer's disease, Diabetes mellitus, nephritis, nephrotic syndrome, and nephrosis) was regressed on forty-two clinical markers and chronological age to select variables for inclusion in our phenotypic age score. Ten-fold cross-validation was employed to select the parameter value, lambda, for the penalized regression. In order to develop a sparse parsimonious phenotypic age estimator (fewer biomarker variables preferred to produce robust results) we selected a lambda of 0.0192, which represented a one standard deviation increase over the lambda with minimum mean-squared error during cross-validation (Supplement 1, Fig. S13). Of the forty-two biomarkers included in the penalized Cox regression model, this resulted in ten variables (including chronological age) that were selected for the phenotypic age predictor.

These nine biomarkers and chronological age were then included in a parametric proportional hazards model based on the Gompertz distribution. Based on this model, we estimated the 10-year (120 months) mortality risk of the j-the individual. Next, the mortality score was converted into units of years (Supplement 1). The resulting phenotypic age estimate was regressed on DNA methylation data using an elastic net regression analysis. The penalization parameter was chosen to minimize the cross validated mean square error rate (Supplement 1, Fig. S14), which resulted in 513 CpGs.

Estimation of blood cell counts based on DNAm levels

We estimate blood cell counts using two different software tools. First, Houseman's estimation method [62] was used to estimate the proportions of CD8+ T cells, CD4+ T, natural killer, B cells, and granulocytes (mainly neutrophils). Second, the Horvath method, implemented in the advanced analysis option of the epigenetic clock software [11, 18], was used to estimate the percentage of exhausted CD8+ T cells (defined as CD28-CD45RA-), the number (count) of naïve CD8+ T cells (defined as CD45RA+CCR7+) and plasmablasts. We and others have shown that the estimated blood cell counts have moderately high correlations with corresponding flow cytometric measures [62, 63].

Additional descriptions of methods and materials can be found in Supplement 1.

Ethics approval

This study was reviewed by the UCLA institutional review board (IRB#13-000671, IRB#15-000697, IRB#16-001841, IRB#15-000682).

Availability of data and materials

The WHI data are available at dbGaP under the accession numbers phs000200.v10.p3. The FHS data are available at dbGaP under the accession numbers phs000342 and phs000724. The Normative Aging data are available from dbGAP phs000853.v1.p1. The Jackson Heart Study data are available from https: // www.jacksonheartstudy.org/Research/Study-Data.

CONFLICTS OF INTEREST

FUNDING

REFERENCES

1. Kennedy BK, Berger SL, Brunet A, Campisi J, Cuervo AM, Epel ES, Franceschi C, Lithgow GJ, Morimoto RI, Pessin JE, Rando TA, Richardson A, Schadt EE, et al. Geroscience: linking aging to chronic disease. Cell. 2014; 159:709–13. https://doi.org/10.1016/j.cell.2014.10.039

2. Burch JB, Augustine AD, Frieden LA, Hadley E, Howcroft TK, Johnson R, Khalsa PS, Kohanski RA, Li XL, Macchiarini F, Niederehe G, Oh YS, Pawlyk AC, et al. Advances in geroscience: impact on healthspan and chronic disease. J Gerontol A Biol Sci Med Sci. 2014 (Suppl 1); 69:S1–3. https://doi.org/10.1093/gerona/glu041

3. Fraga MF, Esteller M. Epigenetics and aging: the targets and the marks. Trends Genet. 2007; 23:413–18. https://doi.org/10.1016/j.tig.2007.05.008

4. Rakyan VK, Down TA, Maslau S, Andrew T, Yang TP, Beyan H, Whittaker P, McCann OT, Finer S, Valdes AM, Leslie RD, Deloukas P, Spector TD. Human aging-associated DNA hypermethylation occurs preferentially at bivalent chromatin domains. Genome Res. 2010; 20:434–39. https://doi.org/10.1101/gr.103101.109

5. Teschendorff AE, Menon U, Gentry-Maharaj A, Ramus SJ, Weisenberger DJ, Shen H, Campan M, Noushmehr H, Bell CG, Maxwell AP, Savage DA, Mueller-Holzner E, Marth C, et al. Age-dependent DNA methylation of genes that are suppressed in stem cells is a hallmark of cancer. Genome Res. 2010; 20:440–46. https://doi.org/10.1101/gr.103606.109

6. Jung M, Pfeifer GP. Aging and DNA methylation. BMC Biol. 2015; 13:7. https://doi.org/10.1186/s12915-015-0118-4

7. Zheng SC, Widschwendter M, Teschendorff AE. Epigenetic drift, epigenetic clocks and cancer risk. Epigenomics. 2016; 8:705–19. https://doi.org/10.2217/epi-2015-0017

8. Bocklandt S, Lin W, Sehl ME, Sánchez FJ, Sinsheimer JS, Horvath S, Vilain E. Epigenetic predictor of age. PLoS One. 2011; 6:e14821. https://doi.org/10.1371/journal.pone.0014821

9. Garagnani P, Bacalini MG, Pirazzini C, Gori D, Giuliani C, Mari D, Di Blasio AM, Gentilini D, Vitale G, Collino S, Rezzi S, Castellani G, Capri M, et al. Methylation of ELOVL2 gene as a new epigenetic marker of age. Aging Cell. 2012; 11:1132–34. https://doi.org/10.1111/acel.12005

10. Hannum G, Guinney J, Zhao L, Zhang L, Hughes G, Sadda S, Klotzle B, Bibikova M, Fan JB, Gao Y, Deconde R, Chen M, Rajapakse I, et al. Genome-wide methylation profiles reveal quantitative views of human aging rates. Mol Cell. 2013; 49:359–67. https://doi.org/10.1016/j.molcel.2012.10.016

11. Horvath S. DNA methylation age of human tissues and cell types. Genome Biol. 2013; 14:R115. https://doi.org/10.1186/gb-2013-14-10-r115

12. Weidner CI, Lin Q, Koch CM, Eisele L, Beier F, Ziegler P, Bauerschlag DO, Jöckel KH, Erbel R, Mühleisen TW,

Zenke M, Brümmendorf TH, Wagner W. Aging of blood can be tracked by DNA methylation changes at just three CpG sites. Genome Biol. 2014; 15:R24. https://doi.org/10.1186/gb-2014-15-2-r24

13. Lin Q, Weidner CI, Costa IG, Marioni RE, Ferreira MR, Deary IJ, Wagner W. DNA methylation levels at individual age-associated CpG sites can be indicative for life expectancy. Aging (Albany NY). 2016; 8:394–401. https://doi.org/10.18632/aging.100908

14. Horvath S, Erhart W, Brosch M, Ammerpohl O, von Schönfels W, Ahrens M, Heits N, Bell JT, Tsai PC, Spector TD, Deloukas P, Siebert R, Sipos B, et al. Obesity accelerates epigenetic aging of human liver. Proc Natl Acad Sci USA. 2014; 111:15538–43. https://doi.org/10.1073/pnas.1412759111

15. Marioni RE, Shah S, McRae AF, Chen BH, Colicino E, Harris SE, Gibson J, Henders AK, Redmond P, Cox SR, Pattie A, Corley J, Murphy L, et al. DNA methylation age of blood predicts all-cause mortality in later life. Genome Biol. 2015; 16:25. https://doi.org/10.1186/s13059-015-0584-6

16. Marioni RE, Shah S, McRae AF, Ritchie SJ, Muniz-Terrera G, Harris SE, Gibson J, Redmond P, Cox SR, Pattie A, Corley J, Taylor A, Murphy L, et al. The epigenetic clock is correlated with physical and cognitive fitness in the Lothian Birth Cohort 1936. Int J Epidemiol. 2015; 44:1388–96. https://doi.org/10.1093/ije/dyu277

17. Horvath S, Garagnani P, Bacalini MG, Pirazzini C, Salvioli S, Gentilini D, Di Blasio AM, Giuliani C, Tung S, Vinters HV, Franceschi C. Accelerated epigenetic aging in Down syndrome. Aging Cell. 2015; 14:491–95. https://doi.org/10.1111/acel.12325

18. Horvath S, Levine AJ. HIV-1 Infection Accelerates Age According to the Epigenetic Clock. J Infect Dis. 2015; 212:1563–73. https://doi.org/10.1093/infdis/jiv277

19. Horvath S, Pirazzini C, Bacalini MG, Gentilini D, Di Blasio AM, Delledonne M, Mari D, Arosio B, Monti D, Passarino G, De Rango F, D'Aquila P, Giuliani C, et al. Decreased epigenetic age of PBMCs from Italian semi-supercentenarians and their offspring. Aging (Albany NY). 2015; 7:1159–70. https://doi.org/10.18632/aging.100861

20. Levine ME, Hosgood HD, Chen B, Absher D, Assimes T, Horvath S. DNA methylation age of blood predicts future onset of lung cancer in the women's health initiative. Aging (Albany NY). 2015; 7:690–700. https://doi.org/10.18632/aging.100809

21. Levine ME, Lu AT, Bennett DA, Horvath S. Epigenetic age of the pre-frontal cortex is associated with neuritic plaques, amyloid load, and Alzheimer's disease related cognitive functioning. Aging (Albany NY). 2015:

7:1198–211. https://doi.org/10.18632/aging.100864

22. Levine ME, Lu AT, Chen BH, Hernandez DG, Singleton AB, Ferrucci L, Bandinelli S, Salfati E, Manson JE, Quach A, Kusters CD, Kuh D, Wong A, et al. Menopause accelerates biological aging. Proc Natl Acad Sci USA. 2016; 113:9327–32. https://doi.org/10.1073/pnas.1604558113

23. Chen BH, Marioni RE, Colicino E, Peters MJ, Ward-Caviness CK, Tsai PC, Roetker NS, Just AC, Demerath EW, Guan W, Bressler J, Fornage M, Studenski S, et al. DNA methylation-based measures of biological age: meta-analysis predicting time to death. Aging (Albany NY). 2016; 8:1844–65. https://doi.org/10.18632/aging.101020

24. Quach A, Levine ME, Tanaka T, Lu AT, Chen BH, Ferrucci L, Ritz B, Bandinelli S, Neuhouser ML, Beasley JM, Snetselaar L, Wallace RB, Tsao PS, et al. Epigenetic clock analysis of diet, exercise, education, and lifestyle factors. Aging (Albany NY). 2017; 9:419–46. https://doi.org/10.18632/aging.101168

25. Dugue PA, Bassett JK, Joo JE, Jung CH, Ming Wong E, Moreno-Betancur M, Schmidt D, Makalic E, Li S, Severi G, Hodge AM, Buchanan DD, English DR, et al. DNA methylation-based biological aging and cancer risk and survival: pooled analysis of seven prospective studies. Int J Cancer. 2018; 142:1611-19. https://doi.org/10.1002/ijc.31189

26. Simpkin AJ, Howe LD, Tilling K, Gaunt TR, Lyttleton O, McArdle WL, Ring SM, Horvath S, Smith GD, Relton CL. The epigenetic clock and physical development during childhood and adolescence: longitudinal analysis from a UK birth cohort. Int J Epidemiol. 2017; 46:549–58. https://doi.org/10.1093/ije/dyw307

27. Maierhofer A, Flunkert J, Oshima J, Martin GM, Haaf T, Horvath S. Accelerated epigenetic aging in Werner syndrome. Aging (Albany NY). 2017; 9:1143–52. https://doi.org/10.18632/aging.101217

28. Levine ME. Modeling the rate of senescence: can estimated biological age predict mortality more accurately than chronological age? J Gerontol A Biol Sci Med Sci. 2013; 68:667–74. https://doi.org/10.1093/gerona/gls233

29. Belsky DW, Caspi A, Houts R, Cohen HJ, Corcoran DL, Danese A, Harrington H, Israel S, Levine ME, Schaefer JD, Sugden K, Williams B, Yashin AI, et al. Quantification of biological aging in young adults. Proc Natl Acad Sci USA. 2015; 112:E4104–10. https://doi.org/10.1073/pnas.1506264112

30. Li S, Wong EM, Joo JE, Jung CH, Chung J, Apicella C, Stone J, Dite GS, Giles GG, Southey MC, Hopper JL. Genetic and Environmental Causes of Variation in the Difference Between Biological Age Based on DNA

Methylation and Chronological Age for Middle-Aged Women. Twin Res Hum Genet. 2015; 18:720–26. https://doi.org/10.1017/thg.2015.75

31. Sebastiani P, Thyagarajan B, Sun F, Schupf N, Newman AB, Montano M, Perls TT. Biomarker signatures of aging. Aging Cell. 2017; 16:329–38. https://doi.org/10.1111/acel.12557

32. Ferrucci L, Hesdorffer C, Bandinelli S, Simonsick EM. Frailty as a Nexus Between the Biology of Aging, Environmental Conditions and Clinical Geriatrics. Public Health Rev. 2010; 32:475–88. https://doi.org/10.1007/BF03391612

33. Christiansen L, Lenart A, Tan Q, Vaupel JW, Aviv A, McGue M, Christensen K. DNA methylation age is associated with mortality in a longitudinal Danish twin study. Aging Cell. 2016; 15:149–54. https://doi.org/10.1111/acel.12421

34. Perna L, Zhang Y, Mons U, Holleczek B, Saum KU, Brenner H. Epigenetic age acceleration predicts cancer, cardiovascular, and all-cause mortality in a German case cohort. Clin Epigenetics. 2016; 8:64. https://doi.org/10.1186/s13148-016-0228-z

35. Breitling LP, Yang R, Korn B, Burwinkel B, Brenner H. Tobacco-smoking-related differential DNA methylation: 27K discovery and replication. Am J Hum Genet. 2011; 88:450–57. https://doi.org/10.1016/j.ajhg.2011.03.003

36. Joehanes R, Just AC, Marioni RE, Pilling LC, Reynolds LM, Mandaviya PR, Guan W, Xu T, Elks CE, Aslibekyan S, Moreno-Macias H, Smith JA, Brody JA, et al. Epigenetic Signatures of Cigarette Smoking. Circ Cardiovasc Genet. 2016; 9:436–47. https://doi.org/10.1161/CIRCGENETICS.116.001506

37. Lee KW, Pausova Z. Cigarette smoking and DNA methylation. Front Genet. 2013; 4:132. https://doi.org/10.3389/fgene.2013.00132

38. Zhang Y, Wilson R, Heiss J, Breitling LP, Saum KU, Schöttker B, Holleczek B, Waldenberger M, Peters A, Brenner H. DNA methylation signatures in peripheral blood strongly predict all-cause mortality. Nat Commun. 2017; 8:14617. https://doi.org/10.1038/ncomms14617

39. Bennett DA, Schneider JA, Arvanitakis Z, Wilson RS. Overview and findings from the religious orders study. Curr Alzheimer Res. 2012; 9:628–45. https://doi.org/10.2174/156720512801322573

40. Bennett DA, Schneider JA, Buchman AS, Barnes LL, Boyle PA, Wilson RS. Overview and findings from the rush Memory and Aging Project. Curr Alzheimer Res. 2012; 9:646–63. https://doi.org/10.2174/156720512801322663

41. Franceschi C, Bonafè M, Valensin S, Olivieri F, De Luca M, Ottaviani E, De Benedictis G. Inflamm-aging. An evolutionary perspective on immunosenescence. Ann N Y Acad Sci. 2000; 908:244–54. https://doi.org/10.1111/j.1749-6632.2000.tb06651.x

42. Horvath S, Zhang Y, Langfelder P, Kahn RS, Boks MP, van Eijk K, van den Berg LH, Ophoff RA. Aging effects on DNA methylation modules in human brain and blood tissue. Genome Biol. 2012; 13:R97. https://doi.org/10.1186/gb-2012-13-10-r97

43. Yang J, Lee SH, Goddard ME, Visscher PM. GCTA: a tool for genome-wide complex trait analysis. Am J Hum Genet. 2011; 88:76–82. https://doi.org/10.1016/j.ajhg.2010.11.011

44. Sierra F, Kohanski R. Geroscience and the trans-NIH Geroscience Interest Group, GSIG. Geroscience. 2017; 39:1–5. https://doi.org/10.1007/s11357-016-9954-6

45. Belsky DW, Moffitt TE, Cohen AA, Corcoran DL, Levine ME, Prinz JA, Schaefer J, Sugden K, Williams B, Poulton R, Caspi A. Eleven Telomere, Epigenetic Clock, and Biomarker-Composite Quantifications of Biological Aging: Do They Measure the Same Thing? Am J Epidemiol. 2017. https://doi.org/10.1093/aje/kwx346

46. Kubben N, Misteli T. Shared molecular and cellular mechanisms of premature ageing and ageing-associated diseases. Nat Rev Mol Cell Biol. 2017; 18:595–609. https://doi.org/10.1038/nrm.2017.68

47. Merlo A, Herman JG, Mao L, Lee DJ, Gabrielson E, Burger PC, Baylin SB, Sidransky D. 5′ CpG island methylation is associated with transcriptional silencing of the tumour suppressor p16/CDKN2/MTS1 in human cancers. Nat Med. 1995; 1:686–92. https://doi.org/10.1038/nm0795-686

48. Finch CE. CHAPTER 1 - Inflammation and Oxidation in Aging and Chronic Diseases. The Biology of Human Longevity. (Burlington: Academic Press), 2007. pp. 1-112.

49. Finch CE. Evolution in health and medicine Sackler colloquium: Evolution of the human lifespan and diseases of aging: roles of infection, inflammation, and nutrition. Proc Natl Acad Sci USA. 2010 (Suppl 1); 107:1718–24. https://doi.org/10.1073/pnas.0909606106

50. Moiseeva O, Mallette FA, Mukhopadhyay UK, Moores A, Ferbeyre G. DNA damage signaling and p53-dependent senescence after prolonged beta-interferon stimulation. Mol Biol Cell. 2006; 17:1583–92. https://doi.org/10.1091/mbc.E05-09-0858

51. Gonskikh Y, Polacek N. Alterations of the translation apparatus during aging and stress response. Mech

Ageing Dev. 2017 (Suppl C); 168:30–36. https://doi.org/10.1016/j.mad.2017.04.003

52. Wolters S, Schumacher B. Genome maintenance and transcription integrity in aging and disease. Front Genet. 2013; 4:19. https://doi.org/10.3389/fgene.2013.00019

53. Steffen KK, Dillin A. A Ribosomal Perspective on Proteostasis and Aging. Cell Metab. 2016; 23:1004–12. https://doi.org/10.1016/j.cmet.2016.05.013

54. Garinis GA, Uittenboogaard LM, Stachelscheid H, Fousteri M, van Ijcken W, Breit TM, van Steeg H, Mullenders LH, van der Horst GT, Brüning JC, Niessen CM, Hoeijmakers JH, Schumacher B. Persistent transcription-blocking DNA lesions trigger somatic growth attenuation associated with longevity. Nat Cell Biol. 2009; 11:604–15. https://doi.org/10.1038/ncb1866

55. Schumacher B, Garinis GA, Hoeijmakers JH. Age to survive: DNA damage and aging. Trends Genet. 2008; 24:77–85. https://doi.org/10.1016/j.tig.2007.11.004

56. McMurray CT, Vijg J. Editorial overview: Molecular and genetic bases of disease: the double life of DNA. Curr Opin Genet Dev. 2014; 26:v–vii. https://doi.org/10.1016/j.gde.2014.09.002

57. Levine ME, Crimmins EM. A Genetic Network Associated With Stress Resistance, Longevity, and Cancer in Humans. J Gerontol A Biol Sci Med Sci. 2016; 71:703–12. https://doi.org/10.1093/gerona/glv141

58. Zhou KI, Pincus Z, Slack FJ. Longevity and stress in Caenorhabditis elegans. Aging (Albany NY). 2011; 3:733–53. https://doi.org/10.18632/aging.100367

59. Lin YJ, Seroude L, Benzer S. Extended life-span and stress resistance in the Drosophila mutant methuselah. Science. 1998; 282:943–46. https://doi.org/10.1126/science.282.5390.943

60. Yu BP, Chung HY. Stress resistance by caloric restriction for longevity. Ann N Y Acad Sci. 2001; 928:39–47. https://doi.org/10.1111/j.1749-6632.2001.tb05633.x

61. Martin GM, Austad SN, Johnson TE. Genetic analysis of ageing: role of oxidative damage and environmental stresses. Nat Genet. 1996; 13:25–34. https://doi.org/10.1038/ng0596-25

62. Houseman EA, Accomando WP, Koestler DC, Christensen BC, Marsit CJ, Nelson HH, Wiencke JK, Kelsey KT. DNA methylation arrays as surrogate measures of cell mixture distribution. BMC Bioinformatics. 2012; 13:86. https://doi.org/10.1186/1471-2105-13-86

63. Horvath S, Gurven M, Levine ME, Trumble BC, Kaplan H, Allayee H, Ritz BR, Chen B, Lu AT, Rickabaugh TM, Jamieson BD, Sun D, Li S, et al. An epigenetic clock analysis of race/ethnicity, sex, and coronary heart disease. Genome Biol. 2016; 17:171. https://doi.org/10.1186/s13059-016-1030-0

SUPPLEMENTARY MATERIAL

Please browse the Full Text version of this manuscript to see Supplementary Methods, Tables, and Figures presented in Supplements 1-4.

Leukocyte telomere length, T cell composition and DNA methylation age

Brian H. Chen[1,2,3,*], Cara L. Carty[4,*], Masayuki Kimura[5], Jeremy D. Kark[6], Wei Chen[7], Shengxu Li[7], Tao Zhang[7], Charles Kooperberg[8], Daniel Levy[2,3], Themistocles Assimes[9], Devin Absher[10], Steve Horvath[11,12], Alexander P. Reiner[8,13], Abraham Aviv[5]

[1]Longitudinal Studies Section, Translational Gerontology Branch, Intramural Research Program, National Institute on Aging, National Institutes of Health, Baltimore, MD 21224, USA

[2]Framingham Heart Study, National Heart, Lung, and Blood Institute, Framingham, MA 01702, USA

[3]Population Sciences Branch, Division of Intramural Research, National Heart, Lung and Blood Institute, Bethesda, MD 20892, USA

[4]Division of Biostatistics and Study Methodology, Center for Translational Science, George Washington University and Children's National Medical Center, Washington, DC 20010, USA

[5]Center of Development and Aging, New Jersey Medical School, Rutgers State University of New Jersey, Newark, NJ 07103, USA

[6]Epidemiology Unit, Hebrew University-Hadassah School of Public Health and Community Medicine, Jerusalem, Israel

[7]Department of Epidemiology, School of Public Health and Tropical Medicine, Tulane University, New Orleans, LA 70118, USA

[8]Division of Public Health Sciences, Fred Hutchinson Cancer Research Center, Seattle, WA 98109, USA

[9]Department of Medicine, Stanford University School of Medicine, Stanford, CA 94305, USA

[10]HudsonAlpha Institute for Biotechnology, Huntsville, AL 35806, USA

[11]Human Genetics, David Geffen School of Medicine, University of California Los Angeles, Los Angeles, CA 90095, USA

[12]Biostatistics, School of Public Health, University of California Los Angeles, Los Angeles, CA 90095, USA

[13]Department of Epidemiology, University of Washington, Seattle, WA 98195, USA

* Equal contribution

Correspondence to: Abraham Aviv; **email:** avivab@njms.rutgers.edu

ABSTRACT

Both leukocyte telomere length (LTL) and DNA methylation age are strongly associated with chronological age. One measure of DNA methylation age— the extrinsic epigenetic age acceleration (EEAA)— is highly predictive of all-cause mortality. We examined the relation between LTL and EEAA. LTL was measured by Southern blots and leukocyte DNA methylation was determined using Illumina Infinium HumanMethylation450 BeadChip in participants in the Women's Health Initiative (WHI; n=804), the Framingham Heart Study (FHS; n=909) and the Bogalusa Heart study (BHS; n=826). EEAA was computed using 71 DNA methylation sites, further weighted by proportions of naïve CD8$^+$ T cells, memory CD8$^+$ T cells, and plasmablasts. Shorter LTL was associated with in-

creased EEAA in participants from the WHI (r=-0.16, p=3.1x10^{-6}). This finding was replicated in the FHS (r=-0.09, p=6.5x10^{-3}) and the BHS (r=-0.07, p=3.8x 10^{-2}). LTL was also inversely related to proportions of memory CD8$^+$ T cells (p=4.04x10^{-16}) and positively related to proportions of naive CD8$^+$ T cells (p=3.57x10^{-14}). These findings suggest that for a given age, an individual whose blood contains comparatively more memory CD8$^+$ T cells and less naive CD8$^+$ T cells would display a relatively shorter LTL and an older DNA methylation age, which jointly explain the striking ability of EEAA to predict mortality.

INTRODUCTION

Aging eludes precise definition at the systemic level and denotes a multitude of processes at the cellular level. Two of these processes─ age-dependent telomere shortening [1] and DNA methylation (DNAm) profiles of cytosine phosphate guanines (CpGs) [2-4] have been used as indices of biological age. The age estimates resulting from multivariable regression models of DNAm profiles are referred to as 'DNAm age' or 'epigenetic age'.

The discrepancy between DNAm age and chronological age is an estimate of the 'epigenetic age acceleration', which has been found to increase in Down syndrome [5], obesity [6], HIV [7] and early menopause [8]. Notably, measures of epigenetic age in blood have been reported to be predictive of all-cause mortality after adjusting for chronological age and traditional risk factors such as sex, hypertension, and prior history of disease [9-11]. A recent meta-analysis showed that among several estimates of epigenetic age acceleration, one particular measure, i.e., extrinsic epigenetic age acceleration (EEAA), was superior in predicting all-cause mortality [10], but the reason for this has remained unclear. EEAA is defined as the weighted average of DNAm age and imputed proportions of naïve CD8$^+$ T cells, memory CD8$^+$ T cells and plasmablasts [12]. Here we show a novel correlation between leukocyte telomere length (LTL) and EEAA. We infer that this correlation reflects the aging of the immune system, as expressed in the age-dependent change of the proportions of naive CD8$^+$ T cells and memory CD8$^+$ T cells.

RESULTS

Major characteristics of participants from the WHI (the discovery cohort), the FHS and the BHS are displayed in Table S1 and Figure S1 (available as Supplementary data on line).

In WHI, LTL was negatively correlated with chronological age (r= -0.33, p = 1.9 x 10^{-22}) (Figure 1). LTL, adjusted for age, was also negatively correlated with EEAA (r = -0.22, p = 2.7 x 10^{-10}). This correlation persisted after further adjustment for race/ethnicity, sex,

BMI and current smoking status (r = -0.16, p = 3.1 x 10^{-6}) and was replicated in both FHS (r = -0.09, p = 6.5 x 10^{-3}) and BHS (r = -0.07, p = 3.8 x 10^{-2}) (Figure 1). In sensitivity analyses using the WHI sample, the relationship remained significant (p = 0.005) after additional adjustment for the covariates: systolic and diastolic blood pressure, education level, income, diabetes, high density lipoprotein cholesterol, low density lipoprotein cholesterol, triglycerides, and C-reactive protein. Tests for interaction showed no differences in LTL and EEAA associations by sex (Table S2) or race/ethnicity (Table S3) after adjusting for age, BMI, and current smoking status. Thus, subsequent analyses were conducted on the pooled data from all three cohorts.

As EEAA was built on specific 71 CpG sites described by Hannum et al. [3] and further modified for imputed proportions of naïve CD8$^+$ T cells, memory CD8$^+$ T cells, and plasmablasts [12], its correlation with LTL may be due to an intrinsic property of the CpG sites, the leukocyte proportions, or both.

We therefore examined (first in WHI and then in FHS and BHS) the relationship between LTL and imputed proportions of these three cell populations. In WHI, the proportion of naïve CD8$^+$ T cells was positively correlated with LTL (r = 0.19, p = 2.84 x 10^{-8}) after adjusting for age, sex, BMI, race/ethnicity, and current smoking status (Table 1). This finding was consistent in the two replication cohorts (r = 0.19, p = 3.53 x 10^{-9} in FHS and r = 0.21, p = 2.47 x 10^{-9} in BHS). The proportion of memory CD8$^+$ T cells was negatively correlated with LTL in WHI (r = -0.20, p =1.76 x 10^{-8}) and the replication cohorts (r = -0.16, p =1.06 x 10^{-6} in FHS, and r = -0.18, p =1.50 x 10^{-7} in BHS). Plasmablast proportion was negatively correlated with LTL in WHI (r = -0.09, p = 0.01) but was not significant in the replication cohorts (r = 0.03, p = 0.41 in FHS and r = 0.03, p = 0.35 in BHS). No sex or racial/ethnic differences were detected in any of these correlations (p > 0.05).

Meta-analyses, combining the three cohorts (Table 1), showed that after adjustment for age, sex, race/ethnicity, BMI and current smoking status, LTL was negatively correlated, r = -0.12, with the EEAA at p = 7.32 x 10^{-5},

positively correlated with the proportion of naïve CD8$^+$ T cells, r = 0.20, p = 3.57 x 10^{-14}, and negatively correlated with the proportion of memory CD8$^+$ cells, r = -0.18, p = 4.04 x 10^{-16}. No significant correlations were found between LTL and the proportion of plasmablasts.

Chen et al. introduced a measure of epigenetic age acceleration that was independent of cell proportions, known as IEAA [10]. We examined the relation between LTL and two versions of IEAA—one using the Horvath set of CpGs [13] and one using the Hannum et al. CpGs [3]. The IEAA using the Hannum CpGs was
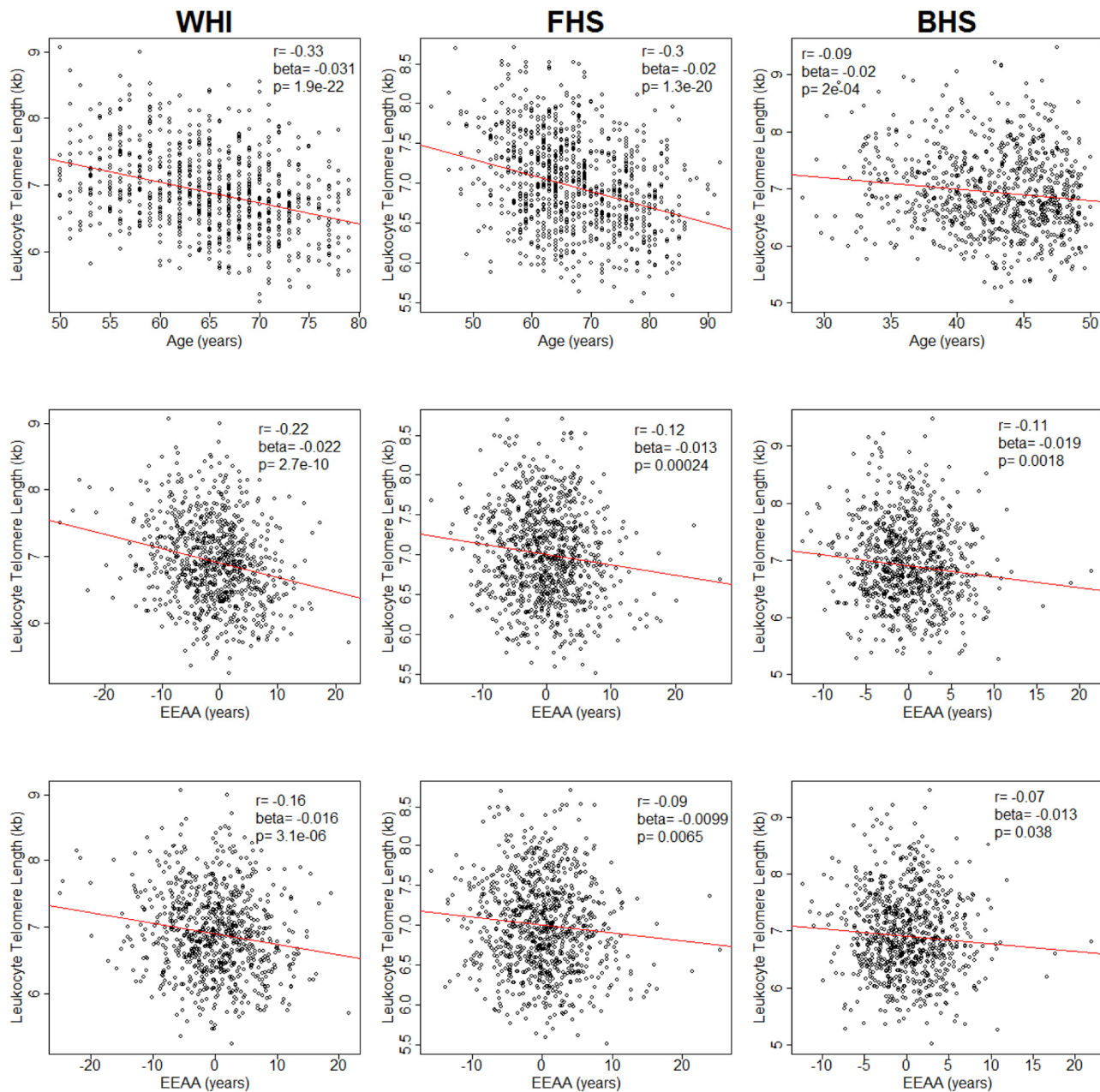
Figure 1. Plots of leukocyte telomere length (LTL) against chronological age (upper row) and extrinsic epigenetic age acceleration (EEAA) (second and third rows). Second row displays unadjusted EEAA. Third row displays EEAA adjusted for BMI, sex, race/ethnicity, and current smoking status. First column displays associations for the Women's Health Initiative (WHI, n=804). Second column displays associations for the Framingham Heart Study (FHS, n=909). Third column displays associations for the Bogalusa Heart Study (BHS, n=826).

not associated with LTL (WHI: r = -0.05, p = 0.16; FHS: r = 0.01, p = 0.88; BHS: r = 0.02, p = 0.66). The IEAA using the Horvath CpGs was not associated with LTL in WHI (r = -0.05, p = 0.12) and FHS (r = 0, p = 0.95) but was significant in BHS (r = 0.08, p = 0.016).

Finally, we performed two additional sets of analyses to ascertain that the correlation between LTL and EAAA arises from correlation between LTL and CD8 $^+$ T cells. First, we adjusted for the proportions naïve CD8$^+$ T cells, memory CD8$^+$ cells and plasmablasts. This led to non-significant correlations between LTL and EEAA in all cohorts (WHI: r = -0.04, p = 0.28; FHS: r = 0, p = 0.99; BHS: r = 0.04, p = 0.31). Second, we also examined EEAA using another set of CpG sites, described by Horvath [14]. This latter measure of EEAA showed similar associations in WHI (r = -0.18, p = 1.9 x 10^{-7}) and FHS (r = -0.11, p = 1.1 x 10^{-3}) but was not significant in BHS (r = -0.03, p = 0.36).

DISCUSSION

The two key observations of this study are: (a) LTL is inversely correlated with EEAA; and (b) the LTL-EEAA

correlation largely reflects the proportions of imputed naïve and memory CD8$^+$ T cell populations in the leukocytes from which DNA was extracted. These correlations were independently replicated in two well-characterized cohorts, providing confidence in their validity. To our knowledge, this is the first study showing association between LTL and a specific formulation of the epigenetic age, but only when it was weighted by the proportions of T naïve cells, T memory cells and plasmoblats (i.e., the EEAA). A previous study, using the Hannum formulation [3], showed no significant association between LTL and epigenetic age [14]. Overall, these findings might explain the ability of EEAA to predict all-cause mortality, given that EEAA captures not only leukocyte DNAm age but also a key aspect of immune senescence (principally naïve and memory T cells), which increases risks of a host of age-related diseases and of death [15].

TL in every leukocyte lineage generally reflects the individual's TL across somatic cells [16,17], which is highly heritable [18,19], but highly variable between individuals. Such variability (SD ~ 0.7 kb) is already displayed across newborns [20-22]. After birth, TL

Table 1. Partial correlation coefficients (Pearson) and linear regression coefficients for associations of leukocyte telomere length with blood cell subpopulations in three cohorts (WHI, FHS, BHS).

		CD8$^+$ naïve	CD8$^+$ memory	Plasmablasts
WHI*	r (Pearson)	0.19	-0.20	-0.09
	beta	0.0023	-0.031	-0.229
	p-value	2.8x10^{-8}	1.8x10^{-8}	0.01
FHS	r (Pearson)	0.19	-0.16	0.03
	beta	0.0026	-0.025	0.076
	p-value	3.5x10^{-9}	1.1x10^{-6}	0.41
BHS	r (Pearson)	0.21	-0.18	0.03
	beta	0.0037	-0.038	0.148
	p-value	2.5x10^{-9}	1.5x10^{-7}	0.35
Meta-analysis†	r (Pearson)	0.20	-0.18	-0.01
	beta	0.0027	-0.030	-0.018
	p-value	3.6x10^{-14}	4.0 x10^{-16}	0.88

* Discovery cohort; †Meta-analysis of correlation coefficients was conducted using the DerSimonian-Laird random-effects meta-analytical approach. Meta-analysis of linear regression beta coefficients was conducted using a random effects model with the DerSimonian-Laird estimator. WHI = Women's Health Initiative; FHS = Framingham Heart Study; BHS = Bogalusa Heart Study. All associations adjusted for age, sex, BMI, race/ethnicity, and current smoking status (regression model: Telomere length in kb = Cell Proportion + age (in FHS and BHS) + sex + BMI + race (in WHI and BHS) + current smoking).

shortening in leukocyte lineages reflects hematopoietic stem cell replication. In a subset of leukocyte lineages, replication continues in sites outside the bone marrow, including the thymus and secondary lymphoid organs, where antigenic stimulation induces their further proliferation and differentiation [23].

The involution of the thymus with aging brings about the progressive, age-dependent decline in the proportion of naïve CD8^{+} T cells with the concomitant increase in the proportion of memory CD8^{+} T cells (Figure S2) [23-26]. Decreasing naïve T-cell number may affect immune function and competence and in part explains the declining cellular immune function observed with aging [27]. For example, both the number and diversity of T cell populations correlate with vaccine response and resistance to opportunistic infections [28,29]. As TL is shorter and (*in vitro*) proliferative potential is compromised in memory compared to naïve cells [21,30], LTL would be comparatively shorter when a high proportion of memory CD8^{+} T cells is present in a sample of leukocytes. In contrast, LTL would be comparatively longer when a high proportion of naive CD8^{+} T cells is present in the sample. From this perspective, for a given age, an individual with comparatively more memory CD8^{+} T cells and less naive CD8^{+} T cells appears to have an older biological profile of the immune system; such an individual also displays a shorter age-adjusted LTL and an older EEAA profile.

This inference has considerable ramifications for the two competing views about the biological meaning of LTL dynamics (LTL at birth and its shortening thereafter).

The first and more popular view considers LTL as a biomarker— a 'telomeric clock'— of human aging. However, given that LTL variation across newborns is as wide as that in adults [20-22], the 'telomeric clock' does not start at the same zero 'biological time' in different individuals [31].

For this reason, the second view suggests that although in itself LTL is an inadequate marker of human aging, it can forecast major aging-related diseases [32]. As LTL is highly heritable [18,19], having constitutively short (or long) telomeres precedes the onset of LTL-associated diseases by decades [33,34]. It is thus likely that TL might play an active role in disease development. This conjecture is supported by findings that not only LTL but also LTL-associated alleles are associated with the incidence of two major disease categories— cardiovascular disease and cancer [32,35]. Such findings largely exclude reverse causality, i.e., the possibility that cardiovascular disease, major cancers or their underlying causes bring about changes in LTL.

These competing interpretations of the biological meaning of LTL are not mutually exclusive for the following reasons: Because of wide LTL variation between newborns, only a fraction of the inter-individual variation in LTL between adults reflects variation in age-dependent LTL shortening after birth. Herein lies the relevance of the correlations of LTL with EEAA and with the relative numbers of naïve and memory CD8^{+} T cells. As TL shortening in T cells of adults reflects their antigen-mediated replicative histories, the associations of LTL with EEAA (and naïve and memory CD8^{+} T cells) suggest that the shortening of LTL with age captures, in part, the aging of the immune system. Thus, age-dependent variation in LTL shortening might partially record different histories of the immune responses in different individuals under different environmental settings.

Notably, in the FHS, LTL and DNAm were measured 10 years apart (Materials and Methods), but we doubt that this 10-year gap had major influence on the findings, given that LTL in adults displays strong tracking, such that individuals maintain their comparative LTL ranking throughout adulthood [33,34]. In fact, the age-dependent trajectories of not only LTL [17,33,34] but also DNAm age [36] are largely determined prior to adulthood. As the immune system is primarily fashioned during early life [37], it is reasonable to propose that to gain further mechanistic insight, the focus of studying both LTL and epigenetic age should be shifted from adults to children.

Finally, our findings are based on imputation using the DNA Methylation Age Calculator (Materials and Methods) rather than direct measurements of the numbers of T cells. There is no reason to believe that direct measurements of T cells would have generated different conclusions, albeit the absolute values of the LTL-EEAA might have been slightly different. In fact, DNAm profiling may provide a valuable tool to follow LTL dynamics under different environmental settings in relation to changing proportions of naïve and memory CD8^{+} T cells without the necessity to resort to direct measurements of the numbers of these cells. Such an approach may enable stored DNA samples to be reexamined for the study of LTL and lymphocyte population dynamics.

MATERIALS AND METHODS

Participants originated from the Women's Health Initiative (WHI), the Framingham Heart Study (FHS) and the Bogalusa Heart Study (BHS); all signed informed consents approved by respective institutional review boards. All participants consented for the use of

their DNA in genetic research. Analytic codes can be obtained from authors (BHC, CLC) upon request.

Women's Health Initiative

Details on the WHI have been published previously [38-40]. The cohort comprised white (of European ancestry) and African American postmenopausal women with both LTL and DNAm age measures in blood samples collected at baseline (1993-98). These women were part of two WHI ancillary studies measuring LTL or DNAm age. Data are available from this page: https://www.whi.org/researchers/Stories/June%202015%20WHI%20Investigators'%20Datasets%20Released.aspx; also see the following link: https://www.whi.org/researchers/data/Documents/WHI%20Data%20Preparation%20and%20Use.pdf

Framingham Heart Study

The FHS Offspring Cohort began enrollment in 1971 and included offspring and spouses of the offspring of the FHS original cohort. LTL was measured in samples from the sixth examination (1995-1998); DNAm analysis was performed on samples from the eighth examination (2005-2008). These populations were described previously [41-43]. The FHS data are available in dbGaP (accession number "phs000724.v2.p9").

Bogalusa Heart Study

The BHS is a study of the natural history of cardiovascular disease beginning in childhood in the biracial community (65% white, 35% African American) of Bogalusa, Louisiana [44]. LTL data were available for participants, who had blood samples collected on 2 occasions, a baseline examination in 1995–1996 and a follow-up examination in 2001–2006. The LTL and DNAm analyses were performed on samples from the latter examination. The longitudinal cardiovascular risk factor phenotype and genotype data of the BHS cohort are available via application through the NHLBI Biologic Specimen and Data Repository Information Coordinating Center website (https: //biolincc.nhlbi.nih.gov/studies/bhs). The longitu-dinal datasets of risk factor variables since childhood, calculated variables, LTL and genome-wide DNA methylation data generated from the proposed study will be made available to outside researchers on this website.

Leukocyte telomere length measurements

LTL was measured by the mean length terminal restriction fragments using the Southern blot method, as previously described [45]. The inter-assay coefficient of variation for blinded pair sets was 2.0% for the WHI, 1.4% for the BHS and 2.4% for the FHS.

Extrinsic Epigenetic Age Acceleration (EEAA) and Intrinsic Epigenetic Age Acceleration (IEAA)

EEAA was defined as the residual variation resulting from a univariate model regressing the epigenetic age described by Hannum et al. on chronological age [3], which was further weighted by the proportions of 3 cell types: naïve ($CD8^+CD45RA^+CCR7^+$) T cells, memory ($CD8^+CD28^-CD45RA^-$) T cells, and plasmablasts; the weights were determined by the correlation between the respective variable and chronological age [46]. The cell proportions were estimated from the DNAm data, as implemented in the online DNA Methylation Age Calculator (https://dnamage.genetics.ucla.edu/).

By construction, EEAA is positively correlated with the memory $CD8^+$ T cells, plasmablast cells, and negatively correlated with naïve $CD8^+$ T cells. Thus, EEAA captures both age-related DNAm changes and age-related changes in the composition of naïve T cells, memory T cells and plasmablasts.

We have also examined the correlation between LTL and IEAA, which was calculated as the residual resulting from multivariate regression of the epigenetic age on chronological age and estimated numbers of naive $CD8^+$ T cells, memory $CD8^+$ T cells, plasma-blasts, $CD4^+$ T cells, natural killer cells, monocytes, and granulocytes. By definition, IEAA is not correlated with chronological age and is, at most, only very weakly correlated with measures of leukocyte counts. IEAA is meant to capture properties of the aging process that exhibit some preservation across various cell and tissue types and organs.

DNA methylation quantification

Bisulfite treated genomic DNA was hybridized to the Illumina Infinium HumanMethylation450 BeadChip (Illumina, Inc, San Diego, CA, USA). Background-corrected DNAm beta values were uploaded to the online DNA Methylation Age Calculator to obtain age acceleration measures.

Statistical analysis

Cohort differences for continuous and categorical variables were tested using one-way ANOVA or Fisher's exact tests, respectively. Sex and race interactions were tested using a Wald test. Beta coefficients were estimated using linear regression with DNAm age as the dependent variable and LTL as the independent variable, adjusted for age, body mass index

(BMI), and current smoking status. Partial correlation coefficients were adjusted for age, BMI, and current smoking status using the pcor command in the ppcor R package [47]. Meta-analysis of correlation coefficients was conducted using the DerSimonian-Laird random-effects meta-analytical approach using the metacor.DSL command in the metacor R package. Meta-analysis of linear regression estimates was conducted using the DerSimonian-Laird random-effects model implemented in the rma command in the metafor R package. Tests for differences between two correlations was conducted using the r. test command in the psych R package [48].

ACKNOWLEDGEMENTS

CONFLICTS OF INTEREST

FUNDING

REFERENCES

1. Blackburn EH, Epel ES, Lin J. Human telomere biology: A contributory and interactive factor in aging, disease risks, and protection. Science. 2015; 350:1193–98. https://doi.org/10.1126/science.aab3389

2. Bocklandt S, Lin W, Sehl ME, Sánchez FJ, Sinsheimer JS, Horvath S, Vilain E. Epigenetic predictor of age. PLoS One. 2011; 6:e14821. https://doi.org/10.1371/journal.pone.0014821

3. Hannum G, Guinney J, Zhao L, Zhang L, Hughes G, Sadda S, Klotzle B, Bibikova M, Fan JB, Gao Y, Deconde R, Chen M, Rajapakse I, et al. Genome-wide methylation profiles reveal quantitative views of human aging rates. Mol Cell. 2013; 49:359–67. https://doi.org/10.1016/j.molcel.2012.10.016

4. Horvath S. DNA methylation age of human tissues and cell types. Genome Biol. 2013; 14:R115. https://doi.org/10.1186/gb-2013-14-10-r115

5. Horvath S, Garagnani P, Bacalini MG, Pirazzini C, Salvioli S, Gentilini D, Di Blasio AM, Giuliani C, Tung S, Vinters HV, Franceschi C. Accelerated epigenetic aging in Down syndrome. Aging Cell. 2015; 14:491–95. https://doi.org/10.1111/acel.12325

6. Horvath S, Erhart W, Brosch M, Ammerpohl O, von Schönfels W, Ahrens M, Heits N, Bell JT, Tsai PC, Spector TD, Deloukas P, Siebert R, Sipos B, et al. Obesity accelerates epigenetic aging of human liver. Proc Natl Acad Sci USA. 2014; 111:15538–43. https://doi.org/10.1073/pnas.1412759111

7. Horvath S, Levine AJ. HIV-1 infection accelerates age according to the epigenetic clock. J Infect Dis. 2015; 212:1563–73. https://doi.org/10.1093/infdis/jiv277

8. Levine ME, Lu AT, Chen BH, Hernandez DG, Singleton AB, Ferrucci L, Bandinelli S, Salfati E, Manson JE, Quach A, Kusters CD, Kuh D, Wong A, et al. Menopause accelerates biological aging. Proc Natl Acad Sci USA. 2016; 113:9327–32. https://doi.org/10.1073/pnas.1604558113

9. Marioni RE, Shah S, McRae AF, Chen BH, Colicino E, Harris SE, Gibson J, Henders AK, Redmond P, Cox SR, Pattie A, Corley J, Murphy L, et al. DNA methylation age of blood predicts all-cause mortality in later life. Genome Biol. 2015; 16:25. https://doi.org/10.1186/s13059-015-0584-6

10. Chen BH, Marioni RE, Colicino E, Peters MJ, Ward-Caviness CK, Tsai PC, Roetker NS, Just AC, Demerath EW, Guan W, Bressler J, Fornage M, Studenski S, et al. DNA methylation-based measures of biological age: meta-analysis predicting time to death. Aging (Albany NY). 2016; 8:1844–65. https://doi.org/10.18632/aging.101020

11. Christiansen L, Lenart A, Tan Q, Vaupel JW, Aviv A, McGue M, Christensen K. DNA methylation age is associated with mortality in a longitudinal Danish twin study. Aging Cell. 2016; 15:149–54. https://doi.org/10.1111/acel.12421

12. Horvath S, Levine AJ. HIV-1 Infection Accelerates Age According to the Epigenetic Clock. J Infect Dis. 2015; 212:1563–73. https://doi.org/10.1093/infdis/jiv277

13. Horvath S. DNA methylation age of human tissues and cell types. Genome Biol. 2013; 14:R115. https://doi.org/10.1186/gb-2013-14-10-r115

14. Marioni RE, Harris SE, Shah S, McRae AF, von Zglinicki T, Martin-Ruiz C, Wray NR, Visscher PM, Deary IJ. The epigenetic clock and telomere length are independently associated with chronological age and mortality. Int J Epidemiol. 2016; Epub ahead of print. https://doi.org/10.1093/ije/dyw041

15. Jagger A, Shimojima Y, Goronzy JJ, Weyand CM. Regulatory T cells and the immune aging process: a mini-review. Gerontology. 2014; 60:130–37. https://doi.org/10.1159/000355303

16. Kimura M, Gazitt Y, Cao X, Zhao X, Lansdorp PM, Aviv A. Synchrony of telomere length among hematopoietic cells. Exp Hematol. 2010; 38:854–59. https://doi.org/10.1016/j.exphem.2010.06.010

17. Daniali L, Benetos A, Susser E, Kark JD, Labat C, Kimura M, Desai K, Granick M, Aviv A. Telomeres shorten at equivalent rates in somatic tissues of adults. Nat Commun. 2013; 4:1597. https://doi.org/10.1038/ncomms2602

18. Hjelmborg JB, Dalgård C, Möller S, Steenstrup T, Kimura M, Christensen K, Kyvik KO, Aviv A. The heritability of leucocyte telomere length dynamics. J Med Genet. 2015; 52:297–302. https://doi.org/10.1136/jmedgenet-2014-102736

19. Slagboom PE, Droog S, Boomsma DI. Genetic determination of telomere size in humans: a twin study of three age groups. Am J Hum Genet. 1994; 55:876–82.

20. Factor-Litvak P, Susser E, Kezios K, McKeague I, Kark JD, Hoffman M, Kimura M, Wapner R, Aviv A. Leukocyte Telomere Length in Newborns: Implications for the Role of Telomeres in Human Disease. Pediatrics. 2016; 137:e20153927. https://doi.org/10.1542/peds.2015-3927

21. Aubert G, Baerlocher GM, Vulto I, Poon SS, Lansdorp PM. Collapse of telomere homeostasis in hemato-poietic cells caused by heterozygous mutations in telomerase genes. PLoS Genet. 2012; 8:e1002696. https://doi.org/10.1371/journal.pgen.1002696

22. Okuda K, Bardeguez A, Gardner JP, Rodriguez P, Ganesh V, Kimura M, Skurnick J, Awad G, Aviv A. Telomere length in the newborn. Pediatr Res. 2002; 52:377–81. https://doi.org/10.1203/00006450-200209000-00012

23. Nikolich-Žugich J. Aging of the T cell compartment in mice and humans: from no naive expectations to foggy memories. J Immunol. 2014; 193:2622–29. https://doi.org/10.4049/jimmunol.1401174

24. Hamann D, Roos MT, van Lier RA. Faces and phases of human CD8 T-cell development. Immunol Today. 1999; 20:177–80. https://doi.org/10.1016/S0167-5699(99)01444-9

25. Chou JP, Effros RB. T cell replicative senescence in human aging. Curr Pharm Des. 2013; 19:1680–98.

26. Weng NP, Akbar AN, Goronzy J. CD28(-) T cells: their role in the age-associated decline of immune function. Trends Immunol. 2009; 30:306–12. https://doi.org/10.1016/j.it.2009.03.013

27. Appay V, Sauce D. Naive T cells: the crux of cellular immune aging? Exp Gerontol. 2014; 54:90–93. https://doi.org/10.1016/j.exger.2014.01.003

28. Lewin SR, Heller G, Zhang L, Rodrigues E, Skulsky E, van den Brink MR, Small TN, Kernan NA, O'Reilly RJ, Ho DD, Young JW. Direct evidence for new T-cell generation by patients after either T-cell-depleted or unmodified allogeneic hematopoietic stem cell transplantations. Blood. 2002; 100:2235–42.

29. Roux E, Dumont-Girard F, Starobinski M, Siegrist CA, Helg C, Chapuis B, Roosnek E. Recovery of immune reactivity after T-cell-depleted bone marrow transplantation depends on thymic activity. Blood. 2000; 96:2299–303.

30. Weng NP, Levine BL, June CH, Hodes RJ. Human naive and memory T lymphocytes differ in telomeric length and replicative potential. Proc Natl Acad Sci USA. 1995; 92:11091–94. https://doi.org/10.1073/pnas.92.24.11091

31. Aviv A, Kark JD, Susser E. Telomeres, atherosclerosis, and human longevity: a causal hypothesis. Epidemiology. 2015; 26:295–99. https://doi.org/10.1097/EDE.0000000000000280

32. Stone RC, Horvath K, Kark JD, Susser E, Tishkoff SA, Aviv A. Telomere Length and the Cancer-Atherosclerosis Trade-Off. PLoS Genet. 2016; 12:e1006144. https://doi.org/10.1371/journal.pgen.1006144

33. Benetos A, Kark JD, Susser E, Kimura M, Sinnreich R, Chen W, Steenstrup T, Christensen K, Herbig U, von Bornemann Hjelmborg J, Srinivasan SR, Berenson GS, Labat C, Aviv A. Tracking and fixed ranking of

leukocyte telomere length across the adult life course. Aging Cell. 2013; 12:615–21. https://doi.org/10.1111/acel.12086

34. Toupance S, Labat C, Temmar M, Rossignol P, Kimura M, Aviv A, Benetos A. Short Telomeres, but Not Telomere Attrition Rates, Are Associated With Carotid Atherosclerosis. Hypertension. 2017; 70:420–25. https://doi.org/10.1161/HYPERTENSIONAHA.117.093 54

35. Haycock PC, Burgess S, Nounu A, Zheng J, Okoli GN, Bowden J, Wade KH, Timpson NJ, Evans DM, Willeit P, Aviv A, Gaunt TR, Hemani G, et al, and Telomeres Mendelian Randomization Collaboration. Association between telomere length and risk of cancer and non-neoplastic diseases: a mendelian randomization study. JAMA Oncol. 2017; 3:636–51; Epub ahead of print. https://doi.org/10.1001/jamaoncol.2016.5945

36. Kananen L, Marttila S, Nevalainen T, Kummola L, Junttila I, Mononen N, Kähönen M, Raitakari OT, Hervonen A, Jylhä M, Lehtimäki T, Hurme M, Jylhävä J. The trajectory of the blood DNA methylome ageing rate is largely set before adulthood: evidence from two longitudinal studies. Age (Dordr). 2016; 38:65. https://doi.org/10.1007/s11357-016-9927-9

37. Gensollen T, Iyer SS, Kasper DL, Blumberg RS. How colonization by microbiota in early life shapes the immune system. Science. 2016; 352:539–44. https://doi.org/10.1126/science.aad9378

38. The Women's Health Initiative Study Group. Design of the Women's Health Initiative clinical trial and observational study. Control Clin Trials. 1998; 19:61–109. https://doi.org/10.1016/S0197-2456(97)00078-0

39. Anderson GL, Manson J, Wallace R, Lund B, Hall D, Davis S, Shumaker S, Wang CY, Stein E, Prentice RL. Implementation of the Women's Health Initiative study design. Ann Epidemiol. 2003 (Suppl); 13:S5–17. https://doi.org/10.1016/S1047-2797(03)00043-7

40. Carty CL, Kooperberg C, Liu J, Herndon M, Assimes T, Hou L, Kroenke CH, LaCroix AZ, Kimura M, Aviv A, Reiner AP. Leukocyte Telomere Length and Risks of Incident Coronary Heart Disease and Mortality in a Racially Diverse Population of Postmenopausal Women. Arterioscler Thromb Vasc Biol. 2015; 35:2225–31. https://doi.org/10.1161/ATVBAHA.115.305838

41. Feinleib M, Kannel WB, Garrison RJ, McNamara PM, Castelli WP. The Framingham Offspring Study. Design and preliminary data. Prev Med. 1975; 4:518–25. https://doi.org/10.1016/0091-7435(75)90037-7

42. Kannel WB, Feinleib M, McNamara PM, Garrison RJ, Castelli WP. An investigation of coronary heart disease in families. The Framingham offspring study. Am J Epidemiol. 1979; 110:281–90. https://doi.org/10.1093/oxfordjournals.aje.a112813

43. Demissie S, Levy D, Benjamin EJ, Cupples LA, Gardner JP, Herbert A, Kimura M, Larson MG, Meigs JB, Keaney JF, Aviv A. Insulin resistance, oxidative stress, hypertension, and leukocyte telomere length in men from the Framingham Heart Study. Aging Cell. 2006; 5:325–30. https://doi.org/10.1111/j.1474-9726.2006.00224.x

44. The Bogalusa Heart Study 20th Anniversary Symposium. Am J Med Sci. 1995; 310:S1–138. https://doi.org/10.1097/00000441-199512000-00001

45. Kimura M, Stone RC, Hunt SC, Skurnick J, Lu X, Cao X, Harley CB, Aviv A. Measurement of telomere length by the Southern blot analysis of terminal restriction fragment lengths. Nat Protoc. 2010; 5:1596–607. https://doi.org/10.1038/nprot.2010.124

46. Klemera P, Doubal S. A new approach to the concept and computation of biological age. Mech Ageing Dev. 2006; 127:240–48. https://doi.org/10.1016/j.mad.2005.10.004

47. Kim S. ppcor: An R Package for a Fast Calculation to Semi-partial Correlation Coefficients. Commun Stat Appl Methods. 2015; 22:665–74. https://doi.org/10.5351/CSAM.2015.22.6.665

48. Steiger JH. Tests for Comparing Elements of a Correlation Matrix. Psychol Bull. 1980; 87:245–51. https://doi.org/10.1037/0033-2909.87.2.245

SUPPLEMENTAL MATERIAL

Table S1. Study population characteristics.

Variable	WHI	FHS	BHS
Sample size, n	804	909	826
Median age in years, (25th and 75th percentiles)	66 (60, 70)	66 (61, 74)[a]	44 (40, 47)
Female sex (n, %)	804 (100%)	469 (52%)	470 (57%)
Median BMI in kg/m^2 (25th and 75th percentiles)	29.31 (25.51, 33.50)	27.58 (24.69, 30.66)	29.34 (25.62, 34.65)
Current smoker (n, %)	95 (12%)	91 (10%)	224 (27%)
Race/ethnicity (n, %)			
White	467 (58%)	917 (100%)	576 (70%)
African American	337 (42%)	0 (0%)	250 (30%)
Median biomarker distributions (25th and 75th percentiles)			
LTL (kb)	6.87 (6.47, 7.31)	6.96 (6.58, 7.39)	6.85 (6.45, 7.39)
EEAA (years)[†]	-0.83 (-4.94, 2.89)	-0.21 (-3.69, 3.14)	-0.27 (-2.81, 2.72)

[†] Extrinsic epigenetic age acceleration (EEAA) [a] Represents age at sample collection for DNA methylation. Age at LTL sample collection was median=57, 25th percentile=52, and 75th percentile=65 years of age.

Table S2. Sex-specific associations for leukocyte telomere length (kb) and extrinsic epigenetic age acceleration (*years*). All models adjusted for age, body mass index, race (BHS only) and smoking status.

Cohort	Sex	Partial correlation coefficient (p-value)	Beta* (p-value)
FHS	Male	-0.08 (0.09)	-0.78 (0.09)
	Female	-0.11 (0.02)	-1.03 (0.02)
BHS	Male	-0.04 (0.47)	-0.24 (0.47)
	Female	-0.11 (0.02)	-0.63 (0.02)

* Regression model (stratified by sex): EEAA = leukocyte telomere length + age + BMI + race (in BHS) + smoking.**Wald test for differences in beta coefficients across sexes were p=0.58 for FHS and p=0.34 for BHS.

Table S3. Race-specific associations for leukocyte telomere length (kb) and extrinsic epigenetic age acceleration (*years*). All models adjusted for age, body mass index, sex (BHS only) and smoking status.

Cohort	Sex	Partial correlation coefficient (p-value)	Beta* (p-value)
WHI	White	-0.17 (0.0003)	-1.72 (0.0003)
	African American	-0.19 (0.0004)	-2.21 (0.0004)
BHS	White	-0.06 (0.15)	-0.35 (0.15)
	African American	-0.10 (0.12)	-0.65 (0.12)

* Regression model (stratified by race/ethnicity): EEAA = leukocyte telomere length + age + BMI + sex (BHS only) smoking. ** Wald test for differences in beta coefficients across racial/ethnic groups were p= 0.33 for WHI and p=0.50 for BHS.
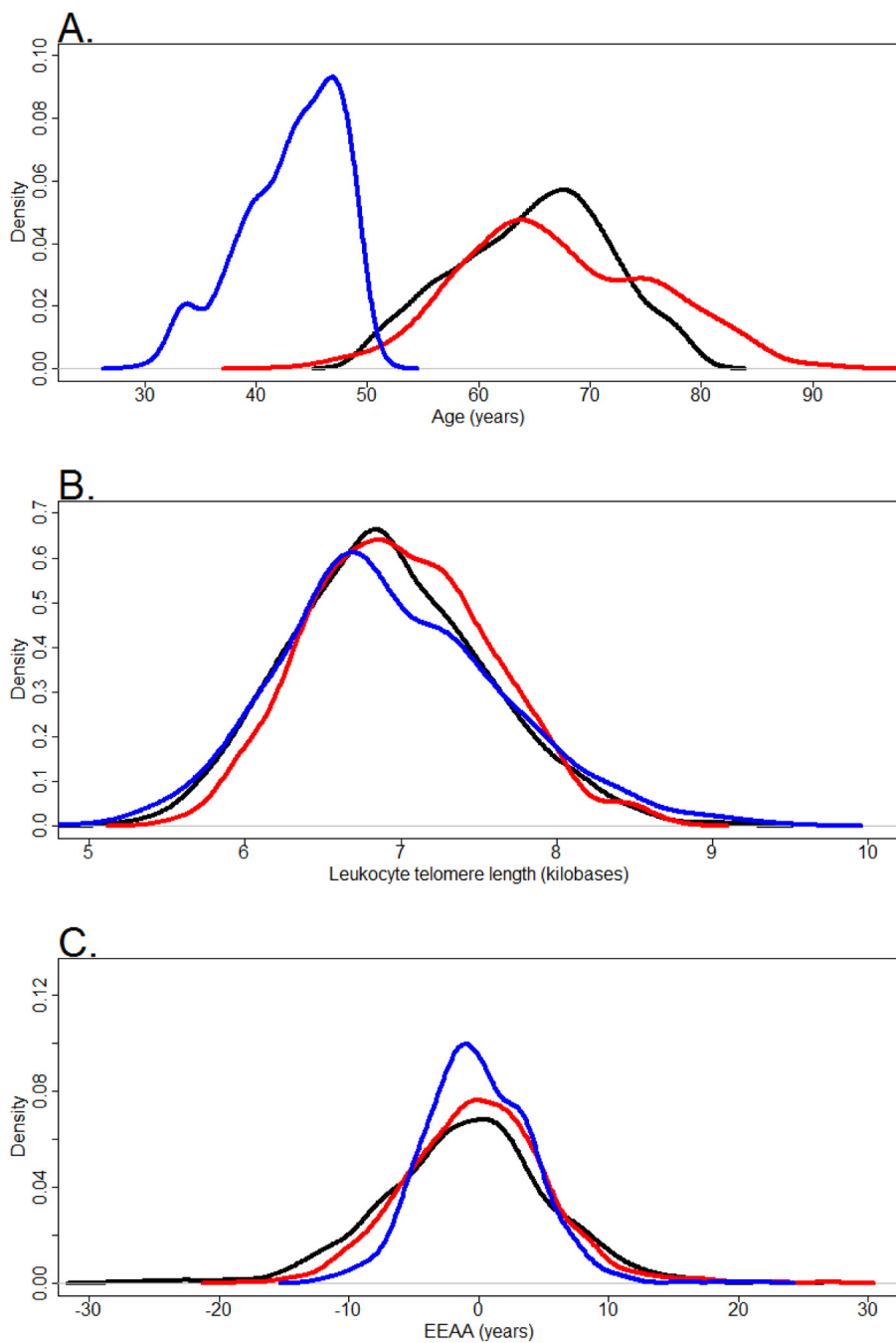
Figure S1. Kernel density distributions across study populations for (A) chronological age, (B) leukocyte telomere length, (C) extrinsic epigenetic age acceleration. Blue=Bogalusa Heart Study. Red=Framingham Heart Study. Black=Women's Health Initiative.
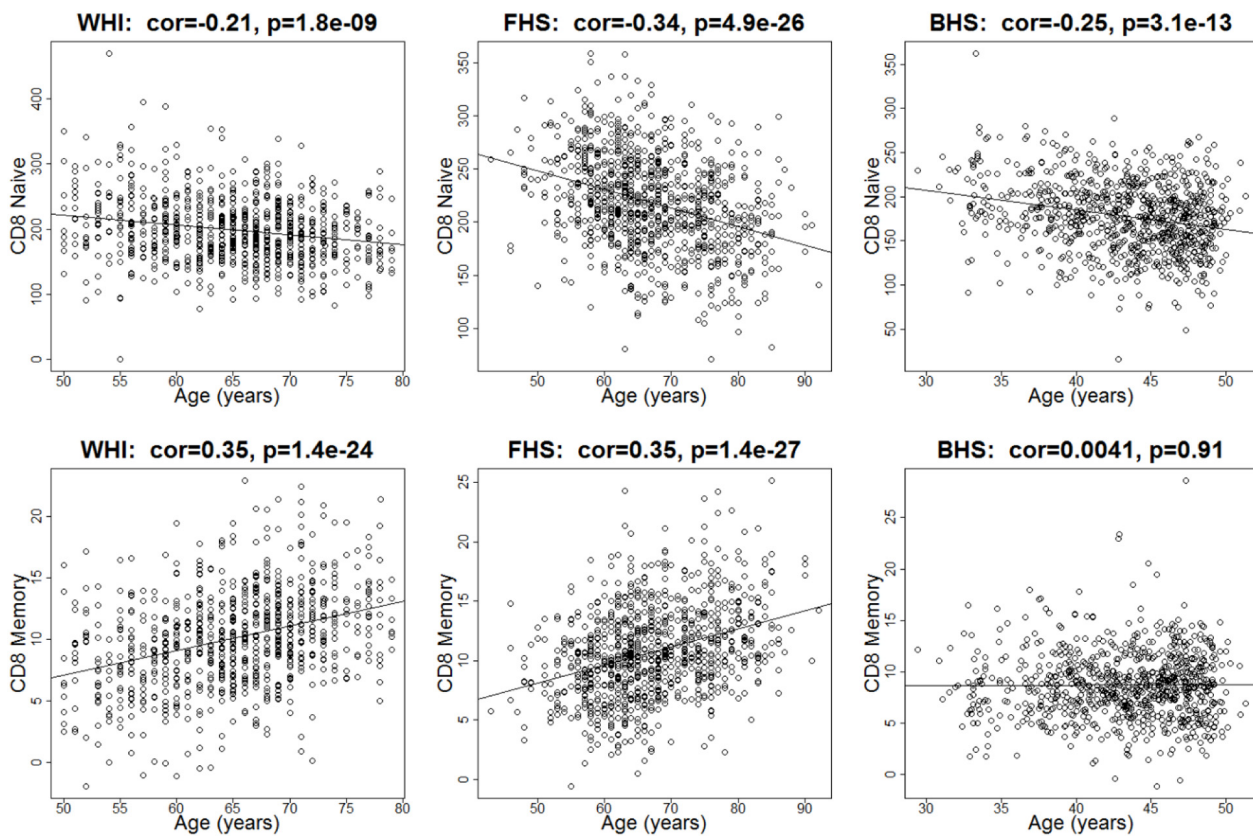
Figure S2. Plots of cell abundances for naïve CD8+ T cells (row 1) and memory CD8+ T cells (row 2) against chronological age by cohort. Women's Health Initiative (WHI) in column 1. Framingham Heart Study (FHS) in column 2. Bogalusa Heart Study (BHS) in column 3. Cell proportions were estimated from DNA methylation data. The lack of significant correlation in the BHS between memory CD8+T cells and age may be attributable to the younger age and narrower age range in BHS compared to WHI and FHS.

Accelerated epigenetic aging in Werner syndrome

Anna Maierhofer[1], Julia Flunkert[1], Junko Oshima[2, 3], George M. Martin[2], Thomas Haaf[1*], Steve Horvath[4, 5*]

[1]Institute of Human Genetics, Julius Maximilians University, Würzburg, Germany

[2]Department of Pathology, University of Washington, Seattle, WA 98105, USA

[3]Department of Clinical Cell Biology and Medicine, Graduate School of Medicine, Chiba University, Chiba, Japan

[4]Department of Human Genetics, David Geffen School of Medicine, University of California Los Angeles, Los Angeles, CA 90095, USA

[5]Department of Biostatistics, Fielding School of Public Health, University of California Los Angeles, Los Angeles, CA 90095, USA

[*]Joint last authors

ABSTRACT

Individuals suffering from Werner syndrome (WS) exhibit many clinical signs of accelerated aging. While the underlying constitutional mutation leads to accelerated rates of DNA damage, it is not yet known whether WS is also associated with an increased epigenetic age according to a DNA methylation based biomarker of aging (the "Epigenetic Clock"). Using whole blood methylation data from 18 WS cases and 18 age matched controls, we find that WS is associated with increased extrinsic epigenetic age acceleration (p=0.0072) and intrinsic epigenetic age acceleration (p=0.04), the latter of which is independent of age-related changes in the composition of peripheral blood cells. A multivariate model analysis reveals that WS is associated with an increase in DNA methylation age (on average 6.4 years, p=0.011) even after adjusting for chronological age, gender, and blood cell counts. Further, WS might be associated with a reduction in naïve CD8+ T cells (p=0.025) according to imputed measures of blood cell counts. Overall, this study shows that WS is associated with an increased epigenetic age of blood cells which is independent of changes in blood cell composition. The extent to which this alteration is a cause or effect of WS disease phenotypes remains unknown.

INTRODUCTION

Werner syndrome (WS, OMIM: 277700) is an autosomal recessive progeroid syndrome characterized by the appearance of multiple features of aging beginning in early adulthood. Approximately 90% of individuals presenting with WS have mutations in the *WRN* gene, which encodes a 1432 amino acid protein with a central domain characteristic of members of the Rec Q family of helicases. The clinical phenotype of WS includes scleroderma-like skin changes, bilateral ocular cataracts, type 2 diabetes mellitus, osteoporosis, hypogonadism, and atherosclerosis. The most common causes of death are cancer and myocardial infarction and the average age at death is 54 years [1, 2].

Little is known about the association of epigenetic alterations with WS. Several recent studies have proposed to measure the physiological age of tissue samples by combining the DNA methylation levels of multiple dinucleotide markers, known as Cytosine phosphate Guanines or CpGs [3-7]. In particular, the "Epigenetic Clock" was developed to measure the age of sorted human cell types (CD4+ T cells or neurons), all tissues, and organs including blood, brain, breast, kidney, liver, and lung [6]. The epigenetic clock is defined as a weighted average across 353 CpG sites. The resulting age estimate (in units of years) is referred to as "DNA methylation age" (DNAm age) or "epigenetic age". Recent studies support the idea that epigenetic age estimates are at least passive biomarkers

of biological age. For instance, the epigenetic age of blood has been found to be predictive of all-cause mortality [8-12], frailty [13], lung cancer [14], and cognitive and physical functioning [15]. Further, the utility of the epigenetic clock method using various tissues and organs has been demonstrated in studies of Alzheimer's disease [16], centenarian status [10, 17], Down syndrome [18], HIV infection [19], Huntington's disease [20], obesity [21], lifetime stress [22], menopause [23], osteoarthritis [24], and Parkinson's disease [25]. Despite many diverse applications of the epigenetic clock, we are not aware of any studies that have analyzed epigenetic aging rates in WS.

Here we show for the first time that measures of epigenetic age acceleration are indeed associated with WS status. Different from typical epigenome-wide asso-

ciation studies (EWAS) that interrogate individual CpGs, the current study posits a single hypothesis: WS is associated with epigenetic age acceleration in blood cells. In a secondary analysis, we also relate WS status to abundance measures of blood cell types that were estimated using DNA methylation data.

RESULTS

Subjects and tissue

We analyzed DNA methylation levels by the Illumina Infinium MethylationEPIC BeadChip in whole blood of 18 patients with confirmed mutations in the *WRN* gene (16 male, 2 female) and 18 controls, which were matched for age and for gender (with one exception: 15 male, 3 female) (Table 1).
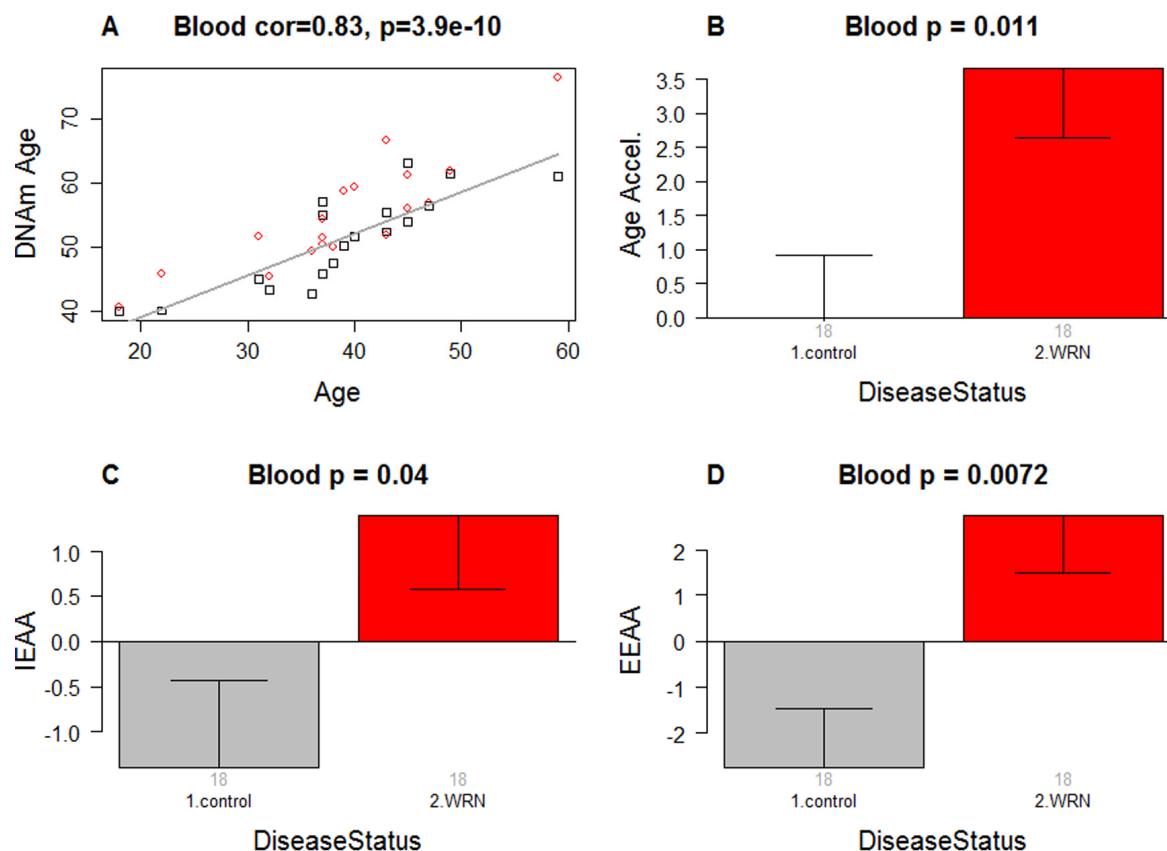
Figure 1. Epigenetic age analysis of Werner syndrome. (**A**) DNA methylation age (y-axis) versus chronological age (x-axis). Dots correspond to subjects and are colored by WS status (red=case, black=control). We define three measures of epigenetic age acceleration. (**B**) presents results for the "universal" measure of epigenetic age acceleration, which is defined as residual to a regression line through the control samples, i.e. the vertical distance of a point from the line. By definition, the mean age acceleration in controls is zero. (**C**) The bar plots relate measures of intrinsic epigenetic age acceleration to WS status. This measure is independent of blood cell counts. (**D**) shows findings for the measure of extrinsic epigenetic age acceleration, which does relate to changes in cell composition. Each bar plot depicts the mean value (y-axis), 1 standard error, and the group size (underneath the bar). The p-value results from the Kruskal Wallis test, which is a non-parametric group comparison test.

Table 1. Sample characteristics of matched WS cases and controls.

Sample ID	Disease status	Registry #	gender	age
PWM18	WS	CHAR1010	male	18
CM18	control		male	18
PWM22	WS	KERA1010	male	22
CM22	control		male	22
PWF31	WS	PA1010	female	31
CF31	control		female	31
PWM32	WS	BOERN1010	male	32
CM32	control		male	32
PWF36	WS	TIT1010	female	36
CF36	control		female	36
PWM37-1	WS	AFRI1010	male	37
CM37-1	control		male	37
PWM37-2	WS	TORON1010	male	37
CM37-2	control		male	37
PWM37-3	WS	VELO1010	male	37
CM37-3	control		male	37
PWM38	WS	ZE1010	male	38
CM38	control		male	38
PWM39	WS	MASS1010	male	39
CM39	control		male	39
PWM40	WS	MARY1010	male	40
CM40	control		male	40
PWM43-1	WS	HAWI1010	male	43
CM43-1	control		male	43
PWM43-2	WS	NY1010	male	43
CM43-2	control		male	43
PWM45-1	WS	BIA1010	male	45
CM45-1	control		male	45
PWM45-2	WS	USC1010	male	45
CM45-2	control		male	45
PWM47	WS	CHAP1010	male	47
CM47	control		male	47
PWM49	WS	CONST1010	male	49
CM49	control		male	49
PWF59	WS	TY1010	female	59
CM59	control		male	59

Accuracy of the epigenetic clock

DNAm age (also referred to as epigenetic age) was calculated as described in [6]. Mathematical details and software tutorials for the epigenetic clock can be found in the Additional files of [6]. An online age calculator can be found at our webpage (https://dnamage.genetics. ucla.edu). All of the described epigenetic measures of aging and age acceleration are implemented in our freely available software.

As expected, DNAm age has a strong linear relationship with chronological age (r=0.83, Figure 1A).

Werner syndrome is associated with intrinsic and extrinsic epigenetic age acceleration

In this article, we consider three measures of epigenetic age acceleration (Methods). The first measure, which will be referred to as a universal measure of age acceleration (denoted AgeAccel) applies to virtually all tissues and cell types (with the exception of sperm). The other two measures (referred to as intrinsic and extrinsic age acceleration, respectively) only apply to peripheral blood cells. The universal measure AgeAccel is defined as the difference between DNAm age value and the value predicted by a linear regression model in controls. The measure of intrinsic epigenetic age acceleration (IEAA) measures "pure" epigenetic aging effects in blood cells that are not confounded by differences in blood cell counts. The measure of extrinsic epigenetic age acceleration (EEAA) aims to measure aging in immune related components and also relates to age-associated changes in blood cell composition such as the decrease of naïve CD8+ T cells and the increase in memory or exhausted CD8+ T cells [26-28]. EEAA is defined on the basis of a weighted average of the epigenetic age measure from [5] and three blood cell types that are known to change with age: naïve (CD45RA+CCR7+) cytotoxic T cells, exhausted (CD28-CD45RA-) cytotoxic T cells, and plasma B cells. By definition, EEAA has a positive correlation with the amount of exhausted CD8+ T cells and plasma blast cells and a negative correlation with the amount of naïve CD8+ T cells. Blood cell counts were estimated based on DNA methylation data as described in Methods. By construction, our three measures of epigenetic age acceleration are uncorrelated (r=0) with chronological age at the time of blood draw.

WS is significantly associated with epigenetic age acceleration according to all three measures of epigenetic age acceleration (Figure 1B,C,D). The strongest association can be observed for EEAA (p=0.0072).

To estimate the actual amount of age acceleration, we regressed DNAm age on disease status, age, gender, and blood cell count estimates. According to this multi-variate regression model, the blood of WS cases is 6.4 years older than that of age matched controls (Table 2).

Conditional logistic regression analysis

Our previous multivariate linear model analysis ignored the fact that cases and controls were grouped into matched pairs. To adjust for this matched pair design, we used a conditional logistic regression analysis that automatically adjusted for chronological age and gender. According to univariate conditional logistic regression models, WS status (dependent variable) is significantly associated with *AgeAccel* (p=0.047, regression coefficient=0.258, standard error=0.130), IEAA (p=0.045, coef=0.271, SE=0.135) and to a lesser extent with EEAA (p=0.071, coef=0.164, SE=0.0907).

Suggestive evidence for a decreased abundance of naïve CD8+ T cells in Werner syndrome

In a secondary analysis, we related disease status to blood cell count estimates based on DNA methylation data (Figure 2). Comparison of age adjusted blood cell counts between WS patients and controls revealed a significant decrease of naïve CD8+ T cells (CD8+CD45RA+CCR7+) in WS cases (p=0.025, Figure 2C). However, the p-value (p=0.025) is not significant after adjusting for multiple comparisons. Further, WS was not associated with naïve CD8+ T counts in a conditional logistic regression model analy-

Table 2. Multivariate model analysis.

Covariate	Coef	Std. Error	T-statistic	P-value
Age	0.66293	0.103509	6.4046	6.2×10^{-7}
Werner Syndrome	4.250449	1.560597	2.7236	0.011
Gender(female)	-1.97987	2.141069	-0.9247	0.36
CD4+T cell	35.42897	27.09406	1.3076	0.20
Granulocyte	34.03732	19.64958	1.7322	0.094
Natural Killer cell	17.97726	24.01823	0.7484	0.46
Naïve CD8+ T cell	-0.00363	0.021163	-0.1716	0.86

DNA methylation age (outcome) is regressed on chronological age, disease status, gender, and blood cell counts. Note that WS is associated with an increased age of 4.250449/0.662930=6.4 years.

Figure 2. Age adjusted blood cell counts versus Werner syndrome status. WS status (x-axis) versus the age adjusted estimate of (**A**) plasma blasts, (**B**) exhausted CD8+ T cells (defined as CD8+CD28-CD45RA-), (**C**) naïve CD8+ T cell count, (**D**) naïve CD4+ T cell count, (**E**) CD8+ T cells, (**F**) CD4+ T cells, (**G**) natural killer cells, (**H**) B cells, (**I**) monocytes, (**J**) granulocytes. The abundance measures of blood cell counts were estimated based on DNA methylation levels using the epigenetic clock software. Each bar plot depicts the mean value (y-axis), one standard error, and the group size (underneath the bar). The p-value results from a non-parametric group comparison test (Kruskal Wallis).

sis (p=0.16) that adjusted for the matched pair design. None of the blood cell counts were related to WS status according to our conditional logistic regression model analysis.

DISCUSSION

Using a novel DNA methylation data set, we demonstrate accelerated epigenetic aging effects in WS. WS has a significant relationship with all three measures of epigenetic age acceleration. The observed accelerated epigenetic aging effects do not reflect confounding due to changes in blood cell composition because a) they can be observed for cell-intrinsic measures of age acceleration (IEAA) and b) they remain significant in multivariate models that adjust for blood cell counts.

Since all of our WS cases had confirmed mutations in the *WRN* gene, the epigenetic aging effects must be a consequence of loss of function mutations in the *WRN* gene. In the following, we discuss several theories that might explain the observed epigenetic age acceleration in blood.

The helicase theory of accelerated epigenetic aging

The *WRN* gene encodes a 1432 amino acid protein with a central domain characteristic of members of the Rec Q family of helicases. Since the WRN probably plays an important role in a DNA helicase it stands to reason that the observed accelerated epigenetic aging effect in WS results from a process in which DNA helicases play an important role. More generally it might result from a process that involves both DNA and RNA helicases. Helicases are enzymes that bind and may even remodel nucleic acid or nucleic acid protein complexes. There are both RNA helicases and DNA helicases (such as WRN). DNA helicases function in cellular processes where double-stranded DNA must be separated, including DNA replication, DNA repair, and transcription. By contrast, RNA helicases are involved in shaping the form of RNA molecules, during all processes involving RNA, such as transcription, splicing, and translation. Interestingly, two recent papers suggest that RNA helicases affect epigenetic aging rates in the cerebellum: a genome-wide association study of epigenetic aging rates in the cerebellum implicated DHX57 (DEAH-Box Helicase 57) which is an RNA helicase [29]. Further, an epigene-

tic clock analysis of tissues from centenarians found that "helicase activity" might explain the finding that the cerebellum ages more slowly than other brain regions [17]. Overall, these results suggest that both RNA and DNA helicases affect epigenetic aging rates. The helicase theory of epigenetic aging has the following shortcomings. First, the relationship between RNA helicase activity and epigenetic age acceleration could only be observed in the cerebellum (and not yet in peripheral blood cells). Second, DNA helicases (such as WRN) may have little in common with RNA helicases. Third, helicase genes are not a smoking gun for any particular molecular process because they are ubiquitous and essential proteins for many processes.

The epigenomic instability theory of accelerated epigenetic aging

The WRN protein has exonuclease and helicase activities and is involved in DNA repair, DNA replication, recombination, transcription, and telomere maintenance [30, 31]. Thus, the discovery that loss of function of *WRN* is the cause of WS supports a major role for genomic instability as a fundamental mechanism of aging [32]. A recent study provides evidence of an important role of WRN in the maintenance of chromatin stability of mesenchymal stem cells [40]. We hypothesized that the epigenetic clock might relate to the actions of an epigenomic maintenance system [6]. Under this hypothesis, our results suggest that loss of function of *WRN* affects the epigenomic maintenance system resulting in increased epigenetic age. The main problem with the epigenomic instability theory of accelerated aging is the paucity of mechanistic details.

The telomere theory of accelerated epigenetic aging

This theory posits that epigenetic age acceleration in WS could result from telomere shortening. It was suggested that genomic instability is caused by telomere loss during DNA replication and that loss of WRN helicase activity promotes telomere loss [33]. Fibroblasts from WS patients grow poorly in culture and display a reduced lifespan. However, ectopic expression of telomerase in WS fibroblast cell lines partially rescues them from accelerated replicative senescence and increases genomic integrity [34, 35]. The average telomere erosion rate in bulk-cultured WS cells was shown to vary from that of normal fibroblasts to four times that of normal. At the single cell level, WS fibroblasts display telomere dynamics not significantly different from those in control fibroblasts, suggesting that the accelerated replicative senescence observed in WS fibroblasts is not caused by accelerated telomere

shortening [36]. In contrast, an *in vivo* study showed that TRF (Telomere Restriction Fragment) lengths in skin samples of WS patients in their thirties were comparable with that of healthy samples, but were shorter in older WS patients compared to controls. Regression analyses is showed that the TRF length in skin and muscle of individuals with WS was significantly shorter than those in controls [37]. A major problem with this telomere theory of epigenetic age acceleration is that intrinsic epigenetic age acceleration is not correlated with telomere length in peripheral blood cells or adipose tissue [13, 21, 38].

The immunosenescence theory of accelerated epigenetic aging

This theory posits that the observed accelerated epigenetic aging effects in blood result from changes in blood cell composition that mirror those observed in immunosenescence. It is well known that a profound age-associated alteration in the T cell compartment is the reduction of naïve CD8+ T cells, which are involved in protection against infectious diseases and play an important role in immune surveillance against malignancies [27]. The theory is supported a) by our suggestive finding regarding the reduction of naïve CD8+ T cells in WS. However, the immunosenescence theory has several severe shortcomings including the following. First, the observed decrease in naïve CD8+ T cells only led to a p-value of 0.025 that is not significant after adjusting for multiple comparisons. This suggestive result requires replication in a larger study preferably involving flow cytometric measures. Second, the theory is inconsistent with our observed lack of an association between exhausted CD8+T cells and WS. Third, the observed epigenetic age acceleration effects are independent of changes in blood cell composition according to our multivariate model analysis.

Limitations

We acknowledge the following limitations. First, our sample size was relatively small (18 cases and 18 controls). Second, we focused only on peripheral blood cells. Future studies should evaluate whether accelerated epigenetic aging effects can also be found in other tissues. Third, there is an interesting quantitative difference between the degree of accelerated epigenetic aging deduced from these peripheral blood cell studies of WS patients (6.4 years) and the premature ages of death of these patients. The most recently available data from both Japan and the US indicate that the mean age of death for WS patients is 54 years; this contrasts typical longevities in Japan of ~ 80 years and in the US of ~74 years [39, 40]. This discrepancy might reflect the fact that the epigenetic age of blood is only an

incomplete measure of organismal age. We believe that organismal age will be better estimated by combining the epigenetic age estimates of multiple tissues and organs.

CONCLUSIONS

We demonstrate that WS is associated with increased epigenetic age acceleration in blood according to several highly robust epigenetic measures of age acceleration. This finding reflects cell-intrinsic epigenetic aging effects that are independent of changes in cell composition. Epigenetic age acceleration of blood is not specific to WS but can also be observed in other conditions such as Down syndrome [18] and to a lesser extent in Parkinson's disease [25]. The degree to which these observed epigenetic age acceleration effects are causes or effects of the many geriatric disorders seen in WS remains unknown. A recent study providing evidence of an important role of WRN in the maintenance of chromatin stability of mesenchymal stem cells, however, is consistent with an important causal role [41].

MATERIALS AND METHODS

Methylation analysis

Whole blood DNA samples of WS patients were sent to us from the International Registry of Werner Syndrome (http://www.wernersyndrome.org/; Seattle, WA). Whole blood samples of controls were collected in the Institute of Human Genetics of the University of Wuerzburg. Sodium bisulfite conversion of genomic DNA was performed using the EZ DNA Methylation™ Kit (Zymo Research, Irvine, CA, USA) according to the provided manual. The Infinium MethylationEPIC BeadChip (Illumina, San Diego, CA, USA) was used according to the manufacturer's protocol to analyze genome-wide DNA methylation. Chips were scanned by iScan (Illumina). Genome Studio (Illumina) was used for background subtraction and normalization to internal controls.

Measures of epigenetic age acceleration

The name of our universal measure of age acceleration (*AgeAccel*) reflects that it applies to virtually all sources of human DNA (with the exception of sperm). Here we defined it as follows. First, we regressed DNAm age on chronological age in controls. Next, we used the resulting model to predict the DNAm age of each subject. Next, the universal measure was defined as the difference between the observed measure of DNAm age and the predicted value. Thus, a high positive value for *AgeAccel* indicates that the observed DNAm age is

higher than that predicted based on controls. *AgeAccel* has a relatively weak correlation with blood cell counts [19] but it still relates to blood cell counts.

To subtract out the effect of blood cell counts, we find it useful to define a measure of intrinsic epigenetic age acceleration (IEAA) which measures "pure" epigenetic aging effects that are not confounded by differences in blood cell counts. It is defined as the residual resulting from a multivariate regression model of DNAm age on chronological age and various blood immune cell counts (naïve CD8+ T cells, exhausted CD8+ T cells, plasma B cells, CD4 T cells, natural killer cells, monocytes, and granulocytes).

The measure of extrinsic epigenetic age acceleration (EEAA) aims to measure epigenetic aging in immune related components. EEAA is defined using the following three steps. First, we calculated the epigenetic age measure from Hannum et al based on 71 CpGs [5]. The resulting age estimate is correlated with certain blood cell types [9]. Second, we increased the contribution of blood cell types to the age estimate by forming a weighted average of the Hannum estimate with 3 cell types that are known to change with age: naïve (CD45RA+CCR7+) cytotoxic T cells, exhausted (CD28-CD45RA-) cytotoxic T cells, and plasma B cells using the approach of [42]. The resulting measure of blood age is referred to as BioAge4 in our epigenetic clock software. Third, we defined a measure of age acceleration (EEAA) as the residual resulting from a univariate model regressing BioAge4 on chronological age. By definition, our measure of EEAA has a positive correlation with the amount of exhausted CD8+ T cells and plasma blast cells and a negative correlation with the amount of naïve CD8+ T cells. EEAA is known as BioAge4HAStaticAdjAge in our software.

Blood cell counts were estimated based on DNA methylation data as described in the section entitled "Estimating blood cell counts based on DNA methylation levels". By construction, EEAA tracks both age-related changes in blood cell composition and intrinsic epigenetic changes. By definition, none of our three measures of epigenetic age acceleration are correlated with the chronological age. IEAA differs across ethnic groups [43] but has a negligible association with behavioral/lifestyle factors [44].

Estimating blood cell counts based on DNA methylation levels

We estimate blood cell proportions using two different software tools. Houseman's estimation method [45], which is based on DNA methylation signatures from purified leukocyte samples, was used to estimate the

proportions of CD8+ T cells, CD4+ T, natural killer, B cells, and granulocytes. Granulocytes are also known as polymorphonuclear leukocytes. The advanced analysis option of the epigenetic clock software [6, 19] was used to estimate the percentage of exhausted CD8+ T cells (defined as CD28-CD45RA-) and the number (count) of naïve CD8+ T cells (defined as (CD45RA+CCR7+). Using another data set, we found that estimated blood cell counts correlate strongly with corresponding flow cytometric measurements $r = 0.63$ for CD8 + T cells, $r = 0.77$ for CD4+ T, $r = 0.67$ B cell, $r = 0.68$ naïve CD8+ T cell, $r = 0.86$ for naïve CD4+ T, and $r = 0.49$ for exhausted CD8+ T cells [43].

ACKNOWLEDGEMENTS

CONFLICTS OF INTEREST

FUNDING

REFERENCES

1. Goto M. Hierarchical deterioration of body systems in Werner's syndrome: implications for normal ageing. Mech Ageing Dev. 1997; 98:239–54. doi: 10.1016/S0047-6374(97)00111-5

2. Oshima J, Hisama FM. Search and insights into novel genetic alterations leading to classical and atypical Werner syndrome. Gerontology. 2014; 60:239–46. doi: 10.1159/000356030

3. Bocklandt S, Lin W, Sehl ME, Sánchez FJ, Sinsheimer JS, Horvath S, Vilain E. Epigenetic predictor of age. PLoS One. 2011; 6:e14821. doi: 10.1371/journal.pone.0014821

4. Garagnani P, Bacalini MG, Pirazzini C, Gori D, Giuliani C, Mari D, Di Blasio AM, Gentilini D, Vitale G, Collino S, Rezzi S, Castellani G, Capri M, et al. Methylation of ELOVL2 gene as a new epigenetic marker of age. Aging Cell. 2012; 11:1132–34. doi: 10.1111/acel.12005

5. Hannum G, Guinney J, Zhao L, Zhang L, Hughes G, Sad-

da S, Klotzle B, Bibikova M, Fan JB, Gao Y, Deconde R, Chen M, Rajapakse I, et al. Genome-wide methylation profiles reveal quantitative views of human aging rates. Mol Cell. 2013; 49:359–67. doi: 10.1016/j.molcel.2012.10.016

6. Horvath S. DNA methylation age of human tissues and cell types. Genome Biol. 2013; 14:R115. doi: 10.1186/gb-2013-14-10-r115

7. Lin Q, Weidner CI, Costa IG, Marioni RE, Ferreira MR, Deary IJ, Wagner W. DNA methylation levels at individual age-associated CpG sites can be indicative for life expectancy. Aging (Albany NY). 2016; 8:394–401. doi: 10.18632/aging.100908

8. Christiansen L, Lenart A, Tan Q, Vaupel JW, Aviv A, McGue M, Christensen K. DNA methylation age is associated with mortality in a longitudinal Danish twin study. Aging Cell. 2016; 15:149–54. doi: 10.1111/acel.12421

9. Marioni RE, Shah S, McRae AF, Chen BH, Colicino E, Harris SE, Gibson J, Henders AK, Redmond P, Cox SR, Pattie A, Corley J, Murphy L, et al. DNA methylation age of blood predicts all-cause mortality in later life. Genome Biol. 2015; 16:25. doi: 10.1186/s13059-015-0584-6

10. Horvath S, Pirazzini C, Bacalini MG, Gentilini D, Di Blasio AM, Delledonne M, Mari D, Arosio B, Monti D, Passarino G, De Rango F, D'Aquila P, Giuliani C, et al. Decreased epigenetic age of PBMCs from Italian semi-supercentenarians and their offspring. Aging (Albany NY). 2015; 7:1159–70. doi: 10.18632/aging.100861

11. Perna L, Zhang Y, Mons U, Holleczek B, Saum KU, Brenner H. Epigenetic age acceleration predicts cancer, cardiovascular, and all-cause mortality in a German case cohort. Clin Epigenetics. 2016; 8:64. doi: 10.1186/s13148-016-0228-z

12. Chen BH, Marioni RE, Colicino E, Peters MJ, Ward-Caviness CK, Tsai PC, Roetker NS, Just AC, Demerath EW, Guan W, Bressler J, Fornage M, Studenski S, et al. DNA methylation-based measures of biological age: meta-analysis predicting time to death. Aging (Albany NY). 2016; 8:1844–65. doi: 10.18632/aging.101020

13. Breitling LP, Saum KU, Perna L, Schöttker B, Holleczek B, Brenner H. Frailty is associated with the epigenetic clock but not with telomere length in a German cohort. Clin Epigenetics. 2016; 8:21. doi: 10.1186/s13148-016-0186-5

14. Levine ME, Hosgood HD, Chen B, Absher D, Assimes T, Horvath S. DNA methylation age of blood predicts future onset of lung cancer in the women's health initiative. Aging (Albany NY). 2015; 7:690–700. doi: 10.18632/aging.100809

15. Marioni RE, Shah S, McRae AF, Ritchie SJ, Muniz-Terrera G, Harris SE, Gibson J, Redmond P, Cox SR, Pattie A, Corley J, Taylor A, Murphy L, et al. The epigenetic clock is correlated with physical and cognitive fitness in the Lothian Birth Cohort 1936. Int J Epidemiol. 2015; 44:1388–96. doi: 10.1093/ije/dyu277

16. Levine ME, Lu AT, Bennett DA, Horvath S. Epigenetic age of the pre-frontal cortex is associated with neuritic plaques, amyloid load, and Alzheimer's disease related cognitive functioning. Aging (Albany NY). 2015; 7:1198–211. doi: 10.18632/aging.100864

17. Horvath S, Mah V, Lu AT, Woo JS, Choi OW, Jasinska AJ, Riancho JA, Tung S, Coles NS, Braun J, Vinters HV, Coles LS. The cerebellum ages slowly according to the epigenetic clock. Aging (Albany NY). 2015; 7:294–306. doi: 10.18632/aging.100742

18. Horvath S, Garagnani P, Bacalini MG, Pirazzini C, Salvioli S, Gentilini D, Di Blasio AM, Giuliani C, Tung S, Vinters HV, Franceschi C. Accelerated epigenetic aging in Down syndrome. Aging Cell. 2015; 14:491–95. doi: 10.1111/acel.12325

19. Horvath S, Levine AJ. HIV-1 infection accelerates age according to the epigenetic clock. J Infect Dis. 2015; 212:1563–73. doi: 10.1093/infdis/jiv277

20. Horvath S, Langfelder P, Kwak S, Aaronson J, Rosinski J, Vogt TF, Eszes M, Faull RL, Curtis MA, Waldvogel HJ, Choi OW, Tung S, Vinters HV, et al. Huntington's disease accelerates epigenetic aging of human brain and disrupts DNA methylation levels. Aging (Albany NY). 2016; 8:1485–512. doi: 10.18632/aging.101005

21. Horvath S, Erhart W, Brosch M, Ammerpohl O, von Schönfels W, Ahrens M, Heits N, Bell JT, Tsai PC, Spector TD, Deloukas P, Siebert R, Sipos B, et al. Obesity accelerates epigenetic aging of human liver. Proc Natl Acad Sci USA. 2014; 111:15538–43. doi: 10.1073/pnas.1412759111

22. Zannas AS, Arloth J, Carrillo-Roa T, Iurato S, Röh S, Ressler KJ, Nemeroff CB, Smith AK, Bradley B, Heim C, Menke A, Lange JF, Brückl T, et al. Lifetime stress accelerates epigenetic aging in an urban, African American cohort: relevance of glucocorticoid signaling. Genome Biol. 2015; 16:266. doi: 10.1186/s13059-015-0828-5

23. Levine ME, Lu AT, Chen BH, Hernandez DG, Singleton AB, Ferrucci L, Bandinelli S, Salfati E, Manson JE, Quach A, Kusters CD, Kuh D, Wong A, et al. Menopause accelerates biological aging. Proc Natl Acad Sci USA. 2016; 113:9327–32. doi: 10.1073/pnas.1604558113

24. Vidal L, Lopez-Golan Y, Rego-Perez I, Horvath S, Blanco FJ, Riancho JA, Gomez-Reino JJ, Gonzalez A. Specific increase of methylation age in osteoarthritis cartilage. Osteoarthritis Cartilage. 2016; 24:S63. doi: 10.1016/j.joca.2016.01.140

25. Horvath S, Ritz BR. Increased epigenetic age and granulocyte counts in the blood of Parkinson's disease patients. Aging (Albany NY). 2015; 7:1130–42. doi: 10.18632/aging.100859

26. Fagnoni FF, Vescovini R, Mazzola M, Bologna G, Nigro E, Lavagetto G, Franceschi C, Passeri M, Sansoni P. Expansion of cytotoxic CD8+ CD28- T cells in healthy ageing people, including centenarians. Immunology. 1996; 88:501–07. doi: 10.1046/j.1365-2567.1996.d01-689.x

27. Fagnoni FF, Vescovini R, Passeri G, Bologna G, Pedrazzoni M, Lavagetto G, Casti A, Franceschi C, Passeri M, Sansoni P. Shortage of circulating naïve CD8(+) T cells provides new insights on immunodeficiency in aging. Blood. 2000; 95:2860–68.

28. Gruver AL, Hudson LL, Sempowski GD. Immuno-senescence of ageing. J Pathol. 2007; 211:144–56. doi: 10.1002/path.2104

29. Lu AT, Hannon E, Levine ME, Hao K, Crimmins EM, Lunnon K, Kozlenkov A, Mill J, Dracheva S, Horvath S. Genetic variants near MLST8 and DHX57 affect the epigenetic age of the cerebellum. Nat Commun. 2016; 7:10561. doi: 10.1038/ncomms10561

30. Yu CE, Oshima J, Fu YH, Wijsman EM, Hisama F, Alisch R, Matthews S, Nakura J, Miki T, Ouais S, Martin GM, Mulligan J, Schellenberg GD. Positional cloning of the Werner's syndrome gene. Science. 1996; 272:258–62. doi: 10.1126/science.272.5259.258

31. Rossi ML, Ghosh AK, Bohr VA. Roles of Werner syndrome protein in protection of genome integrity. DNA Repair (Amst). 2010; 9:331–44. doi: 10.1016/j.dnarep.2009.12.011

32. Hisama FM, Oshima J, Martin GM. How Research on Human Progeroid and Antigeroid Syndromes Can Contribute to the Longevity Dividend Initiative. Cold Spring Harb Perspect Med. 2016; 6:a025882. doi: 10.1101/cshperspect.a025882

33. Crabbe L, Verdun RE, Haggblom CI, Karlseder J. Defective telomere lagging strand synthesis in cells lacking WRN helicase activity. Science. 2004; 306:1951–53. doi: 10.1126/science.1103619

34. Wyllie FS, Jones CJ, Skinner JW, Haughton MF, Wallis C, Wynford-Thomas D, Faragher RG, Kipling D. Telomerase prevents the accelerated cell ageing of Werner syndrome fibroblasts. Nat Genet. 2000; 24:16–17. doi: 10.1038/71630

35. Crabbe L, Jauch A, Naeger CM, Holtgreve-Grez H, Karlseder J. Telomere dysfunction as a cause of

genomic instability in Werner syndrome. Proc Natl Acad Sci USA. 2007; 104:2205–10. doi: 10.1073/pnas.0609410104

36. Baird DM, Davis T, Rowson J, Jones CJ, Kipling D. Normal telomere erosion rates at the single cell level in Werner syndrome fibroblast cells. Hum Mol Genet. 2004; 13:1515–24. doi: 10.1093/hmg/ddh159

37. Ishikawa N, Nakamura K, Izumiyama-Shimomura N, Aida J, Ishii A, Goto M, Ishikawa Y, Asaka R, Matsuura M, Hatamochi A, Kuroiwa M, Takubo K. Accelerated in vivo epidermal telomere loss in Werner syndrome. Aging (Albany NY). 2011; 3:417–29. doi: 10.18632/aging.100315

38. Marioni RE, Harris SE, Shah S, McRae AF, von Zglinicki T, Martin-Ruiz C, Wray NR, Visscher PM, Deary IJ. The epigenetic clock and telomere length are independently associated with chronological age and mortality. Int J Epidemiol. 2016; 45:424–32. doi: 10.1093/ije/dyw041

39. Goto M, Ishikawa Y, Sugimoto M, Furuichi Y. Werner syndrome: a changing pattern of clinical manifestations in Japan (1917~2008). Biosci Trends. 2013; 7:13–22.

40. Huang S, Lee L, Hanson NB, Lenaerts C, Hoehn H, Poot M, Rubin CD, Chen DF, Yang CC, Juch H, Dorn T, Spiegel R, Oral EA, et al. The spectrum of WRN mutations in Werner syndrome patients. Hum Mutat. 2006; 27:558–67. doi: 10.1002/humu.20337

41. Zhang W, Li J, Suzuki K, Qu J, Wang P, Zhou J, Liu X, Ren R, Xu X, Ocampo A, Yuan T, Yang J, Li Y, et al. Aging stem cells. A Werner syndrome stem cell model unveils heterochromatin alterations as a driver of human aging. Science. 2015; 348:1160–63. doi: 10.1126/science.aaa1356

42. Klemera P, Doubal S. A new approach to the concept and computation of biological age. Mech Ageing Dev. 2006; 127:240–48. doi: 10.1016/j.mad.2005.10.004

43. Horvath S, Gurven M, Levine ME, Trumble BC, Kaplan H, Allayee H, Ritz BR, Chen B, Lu AT, Rickabaugh TM, Jamieson BD, Sun D, Li S, et al. An epigenetic clock analysis of race/ethnicity, sex, and coronary heart disease. Genome Biol. 2016; 17:171. doi: 10.1186/s13059-016-1030-0

44. Quach A, Levine ME, Tanaka T, Lu AT, Chen BH, Ferrucci L, Ritz B, Bandinelli S, Neuhouser ML, Beasley JM, Snetselaar L, Wallace RB, Tsao PS, et al. Epigenetic clock analysis of diet, exercise, education, and lifestyle factors. Aging (Albany NY). 2017.

45. Houseman EA, Accomando WP, Koestler DC, Christensen BC, Marsit CJ, Nelson HH, Wiencke JK, Kelsey KT. DNA methylation arrays as surrogate measures of cell mixture distribution. BMC Bioinformatics. 2012; 13:86. doi: 10.1186/1471-2105-13-86

An epigenetic aging clock for dogs and wolves

Michael J. Thompson[1][*], Bridgett vonHoldt[2][*], Steve Horvath[3][*] , Matteo Pellegrini[*]

[1]Molecular, Cell and Developmental Biology, University of California, Los Angeles, Los Angeles, CA 90095, USA
[2]Ecology and Evolutionary Biology, Princeton University, Princeton, NJ 08544, USA
[3]Department of Human Genetics and Biomathematics, David Geffen School of Medicine at UCLA, Los Angeles, CA 90095, USA
*Joint first or last authors

Correspondence to: Steve Horvath; **email:** shorvath@mednet.ucla.edu
Keywords: epigenetic clock, biological age, canine, dog, wolf, DNA methylation
Received: February 6, 2016   **Accepted:** March 18, 2017   **Published:** March 26, 2017

ABSTRACT

Several articles describe highly accurate age estimation methods based on human DNA-methylation data. It is not yet known whether similar epigenetic aging clocks can be developed based on blood methylation data from canids. Using Reduced Representation Bisulfite Sequencing, we assessed blood DNA-methylation data from 46 domesticated dogs (*Canis familiaris*) and 62 wild gray wolves (*C. lupus*). By regressing chronological dog age on the resulting CpGs, we defined highly accurate multivariate age estimators for dogs (based on 41 CpGs), wolves (67 CpGs), and both combined (115 CpGs). Age related DNA methylation changes in canids implicate similar gene ontology categories as those observed in humans suggesting an evolutionarily conserved mechanism underlying age-related DNA methylation in mammals.

INTRODUCTION

Technological breakthroughs surrounding genomic platforms have led to major insights about age related DNA methylation changes in humans [1-9]. In mammals, DNA methylation represents a form of genome modification that regulates gene expression by serving as a maintainable mark whose absence marks promoters and enhancers. During development, germline DNA methylation is erased but is established anew at the time of implantation [10]. Abnormal methylation changes that occur because of aging contribute to the functional decline of adult stem cells [11-13]. Even small changes of the epigenetic landscape can lead to robustly altered expression patterns, either directly by loss of regulatory control or indirectly, via additive effects, ultimately leading to transcriptional changes of the stem cells [14].

Several studies describe highly accurate age estimation methods based on combining the DNA methylation levels of multiple CpG dinucleotide markers [15-18]. We recently developed a multi-tissue epigenetic age estimation method (known as the epigenetic clock) that combines the DNA methylation levels of 353 epigenetic markers known as CpGs [17]. The weighted average of these 353 epigenetic markers gives rise to an estimate of tissue age (in units of years), which is referred to as "DNA methylation age" or as "epigenetic age". DNA methylation age is highly correlated (r=0.96) with chronological age across the entire lifespan [8, 19, 20]. We and others have shown that the human epigenetic clock relates to biological age (as opposed to simply being a correlate of chronological age), e.g. the DNA methylation age of blood is predictive of all-cause mortality even after adjusting for a variety of known risk factors [21-25]. Epigenetic age acceleration (i.e. the difference between epigenetic and chronological age) is associated with lung cancer [26], cognitive and physical functioning [27], Alzheimer's disease [28], centenarian status [25, 29], Down syndrome [30], HIV infection [31], Huntington's disease [32], obesity [33], menopause [34], osteoarthritis [35], and Parkinson's disease [36]. Moreover, we have demonstrated the human epigenetic clock applies without change to chimpanzees [17] but it no longer applies to other animals due to lack of sequence conservation.

Many research questions and preclinical studies of anti-aging interventions will benefit from analogous epigenetic clocks in animals. To this end we sought to develop an accurate epigenetic clock for dogs and wolves. Dogs are increasingly recognized as a valuable model for aging studies [37, 38]. Dogs are an attractive model in aging research because their lifespan (around 12 years) is intermediate between that of mice (2 years) and humans (80 years), thus serving as a more realistic model for human aging than most rodents. Dogs have already been adopted to model multiple human diseases in gene mapping studies (e.g. squamous cell carcinoma [39], bladder cancer [40]) and cancers are often the cause of age-related mortality in domestic dogs [41].

The maximum lifespan of dogs is known to correlate with the size of their breed [42-44]. Based on previous studies in human [17], we expect that the age acceleration (difference between epigenetic age and chronological age) correlates with longevity. We hypothesize that dogs whose epigenetic age is larger than their chronological age are aging more quickly, while those with negative value are aging more slowly. Thus, we would expect to see a correlation between age acceleration and dog breed size.

We also sought to build an epigenetic clock for gray wolves because alternative age estimation methods have limitations. Gray wolf age estimates have traditionally been conducted through tooth wear patterns, cranial suture fusions, closure of the pulp cavity, and cementum annuli [45, 46]. Based on tooth wear patterns, the age structure of a wolf pack is typically skewed towards younger animals (<1-4 years old), with few individuals >5 years of age [46, 47]. Sexually maturity is reached between 10 months and 2 years of age [48, 49]. In a wild social carnivore, group living often results in high mortality rates. Gray wolves live on average 6-8 years in natural populations, but can live up to 13+ years in captivity with increased reproductive success [45, 46].

RESULTS

Data set

We used Reduced Representation Bisulfite Sequencing to generate DNA methylation data of 46 domestic dogs (26 females, 20 males) and 62 gray wolves from Yellowstone National Park (26 females, 36 males). The age distribution of wolves is skewed towards younger animals (Dogs: mean=5 years, median=4, range=0.5-14; Wolves: mean=2.7, median=2, range=0.5-8) due to younger mortality rates in natural populations compared to domestic species, and that estimating the age in wild specimens lacks precision. Additionally, we included

729 humans (388 females, 341 males) with a large age range (mean=47.4, range=14-94).

Based on calculations and criteria described in the Methods section, we constructed a matrix of high confidence methylation levels across 108 canid blood samples. Previous work has shown that there are locus-specific significant methylation differences between dogs and wolves [50]. Here, however, we sought to identify a clock that correlated with age across both canid species; thus, we removed the methylation sites that showed species-specific divergence. This yielded a set of 252,240 CpG sites for our modeling efforts. Of these, 105,521 could be mapped to syntenic CpGs in the human genome (hg19) for functional annotation purposes. Further, a subset of 9,017 sites are measured by the human Illumina 405K array, which allowed us to test for conservation of age correlations between these evolutionarily divergent species (humans, dogs, and wolves).

From these input sets of 10s to 100s of thousands of CpGs, regression models were obtained using an algorithm (see Methods) that selects a much smaller number of CpGs by allowing regression coefficients to go to zero. As the space of possible models is combinatorially vast, there is no guarantee of global optimality of the resulting models, and there are likely a large number of models that would yield comparable results. Thus, we make no assertions of biological significance for the exact identity or number of CpGs in a given model used here.

Conservation of age-correlated methylation between dogs and wolves

To initially gauge whether it might be possible to create a DNAm age clock for a multi-species group (i.e. canids), we looked at the conservation of age-correlated methylation in the two canid species. The global correlation between the age effects across the two species is small in magnitude (r=0.07, Fig. 1A) which could be due to the following reasons: i) it could reflect poor accuracy of the chronological age estimate in wolves, ii) it could reflect the relatively small sample size, iii) it could reflect that wolves tended to be younger than dogs in our study, i.e. the chronological age distributions differed.

Conservation of age-correlated methylation between canid species and human

To test for more distant evolutionary conservation of age effects on DNA methylation between canids and humans, we computed age correlations over a set of 729 human blood methylation array samples [6] and

examined syntenic locations between the canine (canFam3) and human (hg19) genomes as described in Methods. While the subset of measured DNA-methylation sites common to all 3 species is relatively small (~9000 CpGs), we see that the conservation of age-correlation between "canids" (pooled samples of dogs and wolves) and human is statistically significant, though small in magnitude (r=0.20, p=1×10^{-81}, Fig. 1B). This conservation holds for dogs alone (r=0.20, p=6×10^{-85}) but is weaker for wolves alone (r=0.11, p=1×10^{-25}, Fig. 1C, 1D).

The high correlation between dogs and humans is remarkable because the two data sets were generated on different platforms (RRBS versus the Illumina 450K array).

Leave one out estimate of the accuracy of the canid epigenetic clock

DNAm age (also referred to as epigenetic age) was calculated for each sample by regressing an elastic net on the methylation profiles of all other samples and predicting the age of the sample of interest. In the course of our work, we found that pre-selecting subsets of CpGs was helpful and computationally expedient. This was done by computing correlations between methylation and age and taking only those with absolute correlation above 0.3. These pre-selection steps were also performed in a leave-one-out manner for all cross-validated results presented here. These predictions (in years) were obtained by taking the exponential of the output of the epigenetic aging model where ages were
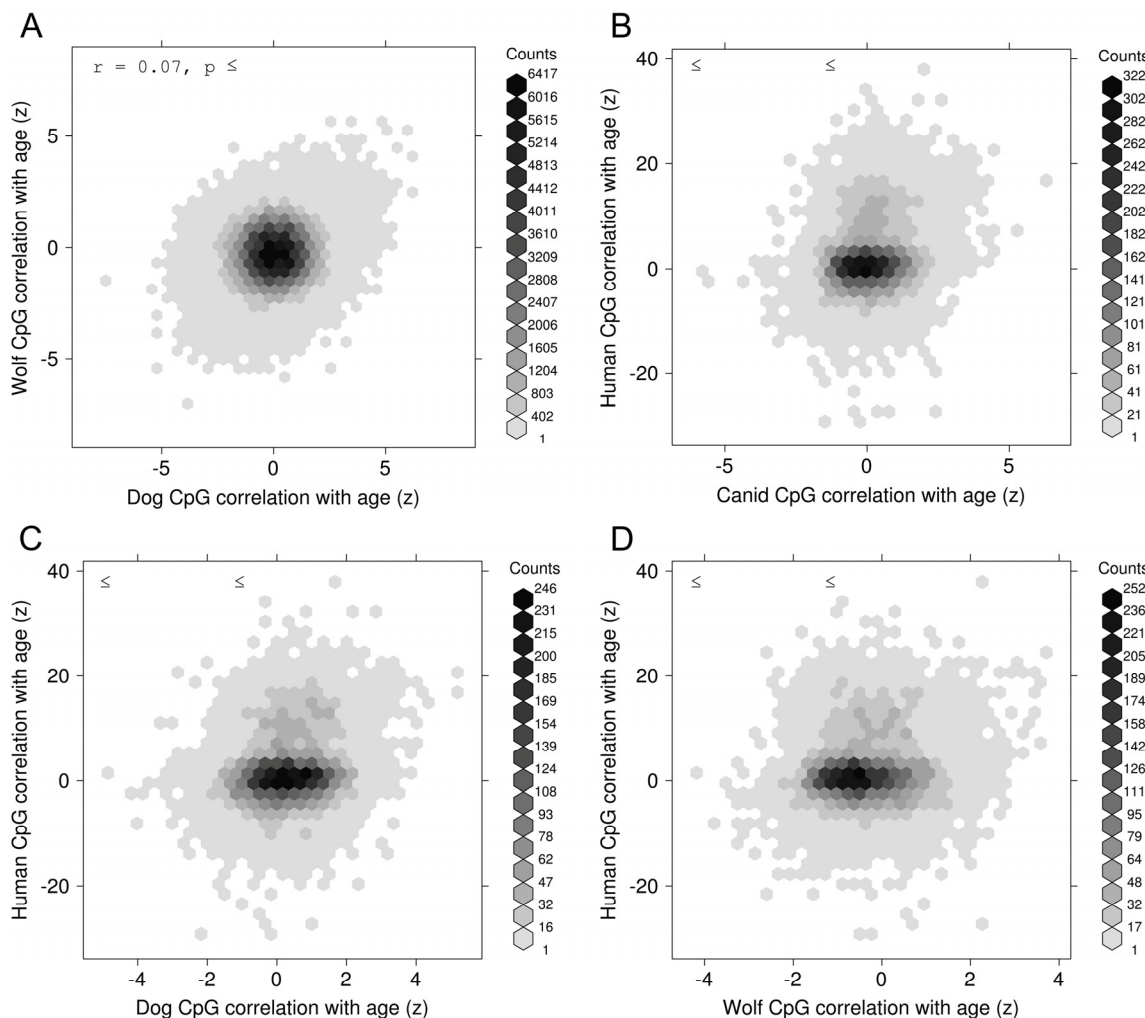
Figure 1. Conservation of epigenetic aging. Normalized correlation (z) between age and DNA methylation for CpG sites in one species versus the same correlation computed at syntenic CpG sites in another species. The species comparisons are shown, as follows: (**A**) Wolves versus Dogs, (**B**) Human versus Canid (pooled dogs and wolves), (**C**) Human versus Dogs, and (**D**) Human versus Wolves.

log-transformed prior to regression. We see a strong linear relationship between DNAm age and true age for our 108 canid samples (Fig. 2A). The correlation between predicted and actual ages using leave-one-out cross-validation was 0.8 and the median absolute error was 0.8 (years). The average number of CpGs in the 108 individual regression models was 122.3.

To examine the effects of pooling two species of canids, we performed the same prediction (DNAm age calcula-

tion) procedure on dogs and wolves, separately. We find that the performance of these models is lower than the canid model, with dogs showing a correlation of r=0.65 and wolves r=0.54 (Fig. 2B). The average number of CpGs in the dog-only and wolf-only models were 58.5 and 62.9, respectively. These models, on average, contain fewer CpGs than the combined canid models as the smaller number of samples in each subset provides less statistical support for the regression algorithm.
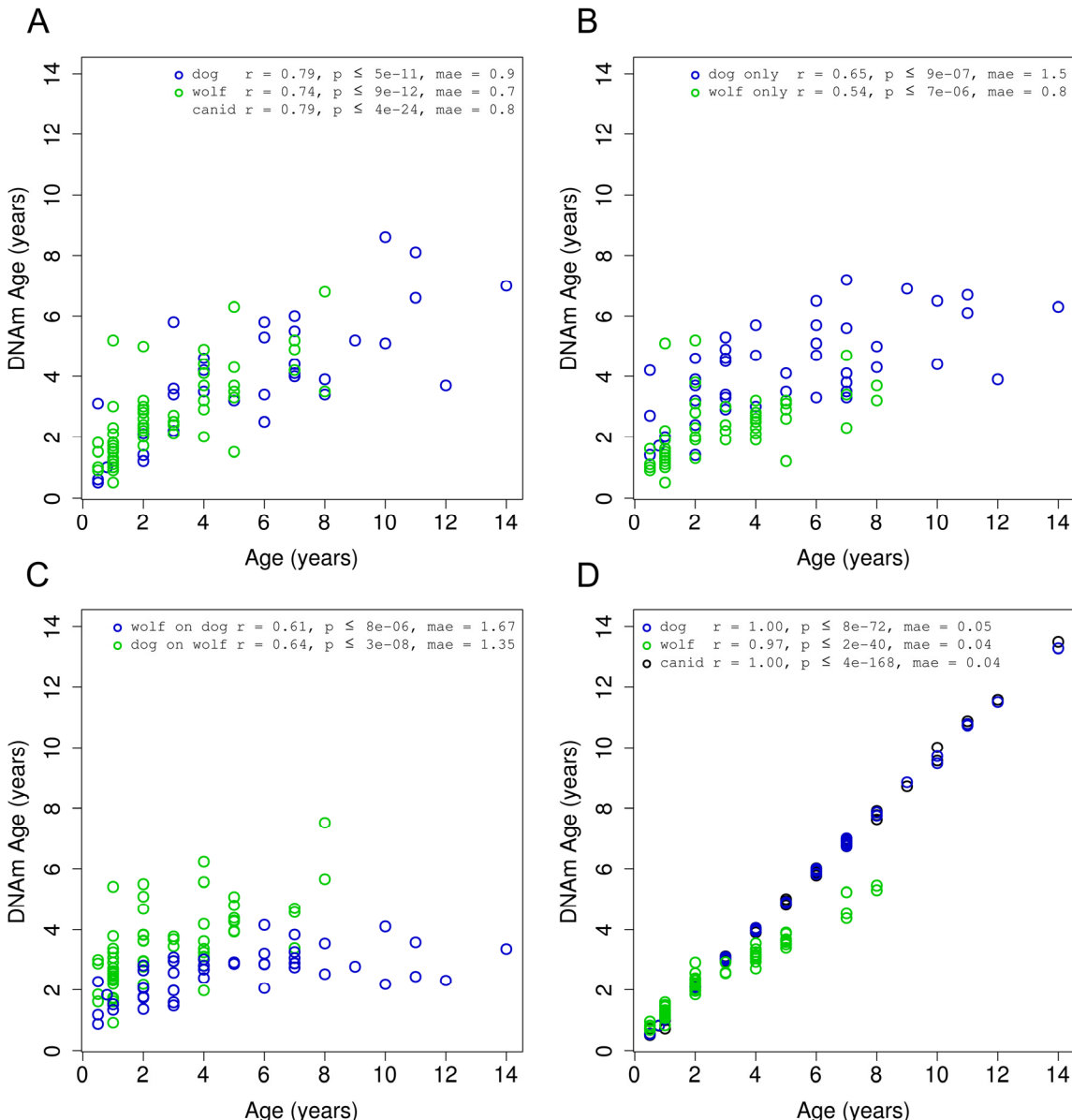
Figure 2. Accuracy of canid age clock. DNA methylation age (y-axis) versus chronological age (x-axis) for all canid samples (green = dog, blue = wolf). (**A**) Results obtained using a leave-one-out cross validation over all 108 samples. (**B**) Results obtained in each species separately using a leave-one-out cross validation. (**C**) Results obtained by regressing on all samples in one species and predicting age on samples from the other species. (**D**) Final models for each grouping of samples.

As another means of assessing the robustness of a multi-species clock, we built one clock for each species using all samples in that species and then applied it to all samples in the other species. These clocks have similar correlation to the dog only or wolf only clocks, close to 0.6, utilizing a single regression model with 67 and 41 CpGs for the dog and wolf model, respectively (Fig. 2C).

Final epigenetic aging clocks based on all animals

To determine the accuracy of our final models, we regressed the penalized elastic net over the set of dogs (41 CpGs), wolves (67 CpGs), and then both combined (115 CpGs) (Fig. 2D). The penalized regression routine ("elastic net") utilizes an internal cross-validation to select the optimal penalty parameter. While the entire set of canids, and the subset of domesticated dogs could be fit exactly (r=1.0), the wolf data alone was slightly less amenable.

Age acceleration as a function of dog size

With the largest variation in size among terrestrial vertebrates, the domestic dog not only spends most of its life in an environment and lifestyle like its human companions, but also displays a high similarity of analogues to human disease [51, 52]. Though dog breeds are diverse in nearly every aspect, smaller breeds are known to live longer than larger breeds [42-44]. Recent genomic surveys have identified nine loci linked to canine size determination, with seven of these loci

supporting growth, cellular proliferation, and metabolism [53]. Of these, the growth hormone IGF1 has not only been of historic interest as a causative locus controlling body size in mice [54-56], but also has the most significant association with body size [57, 58].
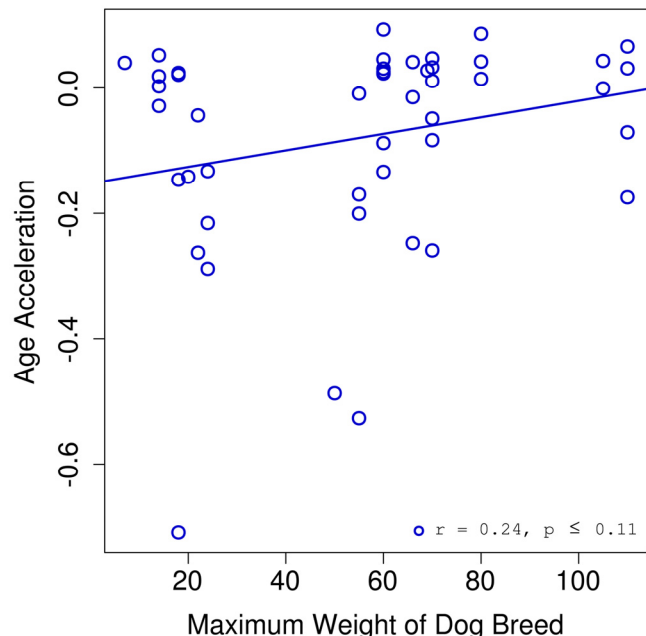
Figure 3. Age acceleration and dog breed. Age acceleration (difference between predicted epigenetic age and actual chronological age) is plotted against the maximum weight for the breed of each dog sample.

Table 1. Functional enrichment studies of age related CpGs in canids.

Functional Annotation	Hypergeometric FDR Q-Value
A. Functional roles of CpGs that lose methylation with age	
compartment pattern specification	2.8×10^{-4}
proximal tubule development	4.3×10^{-4}
carbohydrate derivative transport	8.8×10^{-4}
Notch signaling pathway	1.3×10^{-3}
B. Functional roles of CpGs that gain methylation with age	
regulation of transcription, DNA-dependent	1.6×10^{-11}
regulation of RNA biosynthetic process	8.8×10^{-12}
organ development	1.0×10^{-11}
embryonic organ morphogenesis	1.8×10^{-10}
anatomical structure development	8.3×10^{-10}
Set 'Suz12 targets': genes identified by ChIP on chip as targets of the Polycomb protein SUZ12 in human embryonic stem cells.	2.6×10^{-10}
Genes with high-CpG-density promoters (HCP) bearing the H3K27 tri-methylation (H3K27me3) mark in brain.	6.9×10^{-9}
Genes with high-CpG-density promoters (HCP) bearing histone H3 trimethylation mark at K27 (H3K27me3) in neural progenitor cells (NPC).	1.5×10^{-8}

We found a correlation of 0.25 between age acceleration and breed weight (Fig. 3). Given the limited sample size for dogs (n = 46) we did not reach a significance below the standard threshold of 0.05. However, we expect that a study with a larger cohort might have sufficient power to show that these trends are in fact significant.

Functional significance of DNAm age sites

As described in Methods, mapping of canid CpGs to the human genome yielded 105,521 sites. We utilized this entire set as "background" and selected subsets of CpGs based on the statistical significance of their correlation with age as "foreground". These subsets are not meant to correspond exactly to any of the particular regression models, but to capture the general association of age-related CpGs (from which the regression models are drawn) and biological function inferred via proximity of the CpGs to known genes.

We also partitioned the CpGs into groups with positive (gain of methylation) or negative (loss of methylation) with age, as these two groups have been noted to correspond to separate classes of biomolecular function in previous work [17, 59]. As negatively correlated sites generally partition to distal parts of gene bodies or intergenic regions, they tend to have limited annotation. Conversely, positively correlated sites localize to promoter regions of genes for which there is generally more detailed annotation. To ensure the selection of statistically significant age-related CpGs, we performed a multiple-testing correction [60] on the p-values and selected only those with adjusted values <= 0.05. The annotation tool (GREAT) accesses a large and diverse number of databases and function ontologies. Here, we report those results edited down to non-redundant highlights. We found that a subset of 91 negatively-correlated CpGs (0.1% of total) localized to 125 genes that function in cellular organization and the Notch pathway, an evolutionarily conserved cell-to-cell signaling pathway important for cell proliferation and differentiation (Table 1A). The subset of 90 positively-correlated CpGs (0.1% of total) localized to 71 genes with vital roles in embryonic organismal development and chromatin states (Table 1B). In summary, the canid genes whose DNA-methylation changes are most strongly correlated to age (both negatively and positively) are critical developmental genes; those that determine cell fate and organ development in the embryonic stage of life, as has been noted in previous work with DNA-methylation in humans [17, 59].

DISCUSSION

More broadly, our study demonstrates that DNA-methylation correlates with age in dogs and wolves as it does in human and related species. This age-dependence of DNA-methylation is conserved at syntenic sites in the respective genomes of these canid species as well for more distantly related mammalian genomes such as human. Strikingly, the age associations of syntenic CpGs is well conserved (r=0.20) even though the data were generated on different platforms (RRBS vs Illumina methylation array). Overall, our study demonstrates that dogs age in a similar fashion to humans when it comes to DNA methylation changes.

Race/ethnicity and sex have a significant effect on the epigenetic age of blood in humans [61]. Further, genetic loci have been found that affect epigenetic aging rates in humans [62]. It will be interesting to determine whether sex effects can also be observed in dogs and whether genetic background relates to the ticking rate of the canid clock. Based on our preliminary blood samples of 108 canid specimens, including both dogs and wolves, we accurately measured the methylation status of several hundred thousand CpGs. We demonstrate that these data can produce highly accurate age estimation methods (epigenetic clocks) for dogs and wolves separately. By first removing sites that were variable between dogs and wolves, we could also establish a highly accurate epigenetic clock for all canids (i.e. dogs and wolves combined). This clock allows us to estimate the age of half the canids to within a year.

Our study has several limitations including the following. First, the sample size was relatively low (n=108). There is no doubt that more accurate clocks could be build based on larger sample sizes. Second, we only focused on blood tissue. Future studies could explore other sources of DNA such as buccal swabs. Third, the chronological ages of the wolves are probably not very accurate since they were estimated by the investigators.

In human studies, we have found that lifestyle factors (e.g. diet) have at best a weak effect on cell-intrinsic epigenetic aging rates measured by the 353 CpG based clock [63]. By contrast, extrinsic measures of epigenetic age acceleration, which also capture age related changes in blood cell composition, relate to lifestyle factors that are known to be protective in humans (e.g. consumption of fish, vegetables, moderate alcohol, and to higher levels of education). Biomarkers of metabolic syndrome were associated with increased DNAm age but we could not detect a protective effect of metformin in this observational study [63]. The presented canid aging clocks open up the possibility of assessing dietary and pharmacological intervention on canid aging. The genome coordinates for the CpGs and corresponding regression coefficients of our final canid age estimator and of our dog age estimator can be found in Table 2 and Table 3, respectively.

Table 2. Multivariate model of canid age.

Canine coordinate (canFam3)	Coef	Mean meth	Corr(age,meth)	Human coordinate (hg19)	Proximal genes
Intercept term	4.382				
chr1: 815007	-0.405	0.95	-0.27	chr18: 77637184	KCNG2 (+13517), PQLC1 (+74479)
chr1: 48720985	0.5191	0.95	0.31		
chr1: 49472858	0.2594	0.64	0.28		
chr1: 90590933	-0.0041	0.94	-0.32	chr9: 1872401	Intergenic
chr1: 98573761	-0.0837	0.6	-0.42		
chr1: 98573781	-0.1991	0.2	-0.37		
chr1: 101051499	-0.2786	0.79	-0.4	chr19: 57398441	ZIM2 (-46345)
chr1: 108136920	0.933	0.98	0.22	chr19: 48626542	PLA2G4C (-12469), LIG1 (+47317)
chr1: 117122008	-0.2091	0.82	-0.33	chr19: 36035408	TMEM147 (-1088)
chr1: 117495962	-0.1664	0.86	-0.41	chr19: 35540744	FXYD3 (-66421), HPN (+9335)
chr1: 121791246	-0.3188	0.67	-0.38	chr19: 30153492	PLEKHF1 (-2470)
chr1: 121796139	0.3134	0.96	0.28		
chr1: 121864927	0.3367	0.83	0.3	chr19: 30042558	POP4 (-52365), VSTM2B (+25153)
chr2: 10101121	-0.0266	0.65	-0.29		
chr2: 30853505	-0.0048	0.93	-0.28	chr10: 4714389	Intergenic
chr2: 36347652	0.0248	0.37	0.36	chr5: 140749805	PCDHGA6 (-3845), PCDHGB3 (-25)
chr2: 71080824	0.0288	0.86	0.33	chr1: 30051475	Intergenic
chr2: 82210243	-0.387	0.94	-0.22	chr1: 15602565	Intergenic
chr2: 84377388	-0.4829	0.97	-0.36	chr1: 11951757	NPPB (-32770), KIAA2013 (+34722)
chr2: 84445018	0.0924	0.26	0.33	chr1: 11864680	CLCN6 (-1587), MTHFR (-1379)
chr3: 1128258	-0.0993	0.94	-0.37		
chr3: 51442070	-0.0641	0.8	-0.3	chr15: 88733456	NTRK3[d] (+66204)
chr3: 60468935	-0.2449	0.82	-0.43	chr4: 8834358	HMX1 (+39184)
chr3: 62880832	0.4931	0.88	0.25	chr4: 17638199	MED28 (+21946)
chr3: 84450199	-0.0696	0.89	-0.49	chr4: 25978965	SMIM20 (+63140)
chr4: 28034141	-0.6356	0.14	-0.33	chr10: 79971431	Intergenic
chr4: 28162022	-0.1129	0.89	-0.32	chr10: 80116134	Intergenic
chr4: 28489863	0.0289	0.7	0.24	chr10: 80479452	Intergenic
chr4: 79153238	0.1058	0.09	0.42	chr5: 27038840	CDH9 (-148)
chr5: 4750111	-0.089	0.35	-0.5	chr11: 129969307	ST14 (-60149), APLP2 (+29507)
chr14: 41413362	-0.2829	0.57	-0.33	chr7: 28355716	CREB5 (-96427)
chr14: 59995975	-0.0142	0.73	-0.34	chr7: 121776852	AASS (-2977)
chr15: 17780647	1.3988	0.97	0.29	chr14: 20915434	TEP1 (-33855), OSGEP (+7829)
chr15: 17785631	-0.3897	0.94	-0.43	chr14: 20921454	APEX1 (-1899), OSGEP (+1809)
chr16: 131577	-0.0629	0.73	-0.31		
chr16: 247019	0.8011	0.83	0.34		
chr17: 18033866	0.2802	0.82	0.32	chr2: 23704553	Intergenic
chr18: 1791242	-0.0118	0.94	-0.35	chr7: 50515762	FIGNL1 (+1659)
chr18: 25850449	-0.2607	0.92	-0.34		
chr18: 33813035	-0.1549	0.78	-0.41	chr11: 33962891	LMO2 (-49056)
chr18: 43740411	-0.1646	0.94	-0.34	chr11: 45669463	CHST1 (+17708)
chr18: 48905778	0.0765	0.72	0.41	chr11: 68925723	Intergenic
chr18: 49633631	-0.0336	0.49	-0.22	chr11: 67984189	SUV420H1 (-3308)
chr18: 53920336	-0.0957	0.8	-0.4		
chr20: 44455198	0.3338	0.72	0.46		
chr20: 49366316	-0.0004	0.71	-0.28	chr19: 12895268	HOOK2 (-8932), JUNB (-7041)
chr21: 23088752	-0.4109	0.88	-0.28	chr11: 75219103	GDPD5 (+17844)
chr21: 47917499	-0.0235	0.84	-0.29	chr11: 27349807	Intergenic
chr22: 56299850	-0.2509	0.89	-0.32	chr13: 108022629	Intergenic

chr23: 24782165	-0.1049	0.89	-0.33	chr3: 18277027	Intergenic
chr23: 24782179	-0.658	0.94	-0.31	chr3: 18277013	Intergenic
chr24: 42551119	-0.2892	0.93	-0.35	chr20: 56148739	PCK1 (+12604), ZBP1 (+46789)
chr24: 45589901	0.2135	0.97	0.27	chr20: 59877087	CDH4[b] (+49606)
chr26: 220859	0.0037	0.98	0.27		
chr26: 5991914	-0.2154	0.93	-0.37	chr12: 124138408	TCTN2 (-17251), GTF2H3 (+20033)
chr26: 11457252	-0.3679	0.94	-0.28	chr12: 114784708	TBX5[a,b,c,d] (+61538)
chr26: 37645878	-0.4125	0.93	-0.3		
chr27: 1189935	-0.0497	0.78	-0.39	chr12: 54471815	HOXC4[a,b,c,d] (+24155)
chr27: 2886690	-0.0004	0.86	-0.44	chr12: 52559286	KRT80 (+26497), C12orf44 (+95532)
chr27: 45394279	-0.4689	0.93	-0.45		
chr28: 23823079	-0.2956	0.91	-0.31		
chr28: 40564054	-0.0603	0.96	-0.33	chr10: 134593678	NKX6-2[a,b,c,d] (+5877)
chr30: 15275091	-0.0557	0.89	-0.31		
chr30: 27934524	-0.0484	0.93	-0.26	chr15: 63648005	CA12 (+26354), APH1B (+78253)
chr30: 38620897	0.8567	0.94	0.33	chr15: 78043186	Intergenic
chr31: 27720671	0.0332	0.16	0.46	chr21: 34444104	OLIG1[a,d] (+1655)
chr31: 36955453	-0.5267	0.91	-0.36	chr21: 44079991	PDE9A (+6127)
chr31: 37492782	-0.4942	0.49	-0.56		
chr32: 1431916	-0.2835	0.07	-0.3	chr4: 77752402	Intergenic
chr32: 38110814	-0.076	0.87	-0.35		
chr33: 22992599	-0.0003	0.93	-0.34	chr3: 119042586	ARHGAP31 (+29367)
chr33: 25783582	0.3819	0.98	0.34	chr3: 122422615	PARP14 (+23151), HSPBAP1 (+90055)
chr33: 31142995	-0.8311	0.95	-0.3	chr3: 194291430	ATP13A3 (-72338), TMEM44 (+62719)
chr34: 40858941	-0.1582	0.93	-0.38	chr3: 177096996	Intergenic
chr35: 2307155	-0.1171	0.94	-0.32	chr6: 1886203	Intergenic
chr36: 2545193	0.2403	0.84	0.47	chr2: 157179898	NR4A2 (+9329)
chr36: 19969591	0.0515	0.27	0.38	chr2: 177025691	HOXD1[a,b,c,d] (-27615), HOXD4[a,b,c,d] (+9742)
chr37: 6301	-0.1058	0.69	-0.43		
chr37: 25454687	0.4555	0.32	0.33	chr2: 219736500	WNT10A[a,b,c,d] (-8584), WNT6[a,b,c,d] (+11957)
chr38: 16230281	0.1055	0.92	0.23	chr1: 221912099	DUSP10 (+3418)
chr38: 22365525	-0.1451	0.89	-0.36	chr1: 159724037	CRP (-39659), DUSP23 (-26755)
chr38: 22792877	0.7599	0.72	0.43	chr1: 159145579	DARC (-29621), CADM3[d] (+4181)
chrX: 80013740	-0.133	0.85	-0.29		

Genome coordinates and coefficient values for predicting a log (base e) transformed version of chronological age. These coefficients were found by regressing a log-transformed version of age on the RRBS DNA-methylation measured from 108 canid blood samples. Since chronological age was log-transformed prior to regression, it is important to exponentiate the age estimate from this model to arrive at age estimates in units of years. We provide the mean methylation and Pearson correlation with age for each individual CpG. Where possible, we identify, via synteny to the human genome, genes that are proximal to the CpGs in our models. Numbers in parentheses are the distance in bases to the Transcription Start Site of the gene. Additionally, we note those genes with experimentally inferred relevance to cellular identity (pluripotency).

Genes experimentally identified as targets of pluripotency factors and the Polycomb repressor complex [69, 70]
[a] genes identified by ChIP on chip as targets of the Polycomb protein EED in human embryonic stem cells.
[b] genes possessing the trimethylated H3K27 (H3K27me3) mark in their promoters in human embryonic stem cells, as identified by ChIP on chip
[c] Polycomb Repression Complex 2 (PRC) targets; identified by ChIP on chip on human embryonic stem cells as genes that: possess the trimethylated H3K27 mark in their promoters and are bound by SUZ12 and EED Polycomb proteins
[d] genes identified by ChIP on chip as targets of the Polycomb protein SUZ12 in human embryonic stem cells

Table 3. Multivariate model of domesticated dog age.

Canine coordinate (canFam3)	Coef	Mean Meth	Corr(age,meth)	Human coordinate (hg19)	proximal genes
(Intercept)	-6.9009				
chr1: 98804509	-0.1771	0.92	-0.56	chr9: 95371248	ECM2 (-72912), IPPK (+61298)
chr2: 34467253	-0.1762	0.96	-0.52	chr10: 323319	Intergenic
chr2: 50165769	1.8403	0.97	0.56	chr5: 63460330	RNF180 (-1378)
chr3: 54128482	0.1444	0.77	0.51	chr15: 85429683	PDE8A[a,b] (-93987), SLC28A1 (+1771)
chr4: 28320267	-0.4038	0.94	-0.43	chr10: 80292869	Intergenic
chr5: 19204758	-0.5393	0.31	-0.62	chr11: 114000061	ZBTB16[a,b,c,d] (+69747)
chr5: 32946701	0.1414	0.63	0.67	chr17: 8027247	ALOXE3[b,d] (-4883), HES7[a,b,c,d] (+154)
chr5: 57889544	0.1104	0.88	0.45	chr1: 3202081	Intergenic
chr6: 31347568	-0.0245	0.64	-0.5	chr16: 11536754	ENSG00000188897 (+80689), RMI2 (+97467)
chr6: 77030251	0.5807	0.82	0.6	chr1: 68732333	WLS[a,d] (-34106)
chr7: 54060517	0.3047	0.06	0.48	chr18: 33708261	ELP2 (-1599), SLC39A6 (+1019)
chr8: 50434546	0.0351	0.91	0.42	chr14: 78126349	SPTLC2 (-43234), ALKBH1 (+48013)
chr9: 58841067	0.318	0.15	0.61	chr9: 126779366	LHX2[a,b,c,d] (+5478)
chr10: 21355951	0.3876	0.86	0.52		
chr10: 55453590	-0.4182	0.95	-0.75	chr2: 54776879	SPTBN1 (+93458)
chr10: 56694481	0.4854	0.09	0.46	chr2: 56151248	EFEMP1 (+25)
chr10: 62832468	0.2077	0.77	0.6	chr2: 63279783	OTX1[a,b,c,d] (+1847)
chr10: 62832512	0.2347	0.58	0.67	chr2: 63279827	OTX1[a,b,c,d] (+1891)
chr11: 4422863	0.7296	0.91	0.44	chr5: 113831979	Intergenic
chr11: 56812470	0.0579	0.87	0.47	chr9: 102590004	NR4A3[a,b,c,d] (+996)
chr11: 68812130	1.204	0.95	0.5	chr9: 117441733	C9orf91 (+68248)
chr12: 67228192	1.4284	0.98	0.39	chr6: 110931985	Intergenic
chr12: 67482078	-0.2241	0.19	-0.53	chr6: 111267687	GTF3C6 (-12075), AMD1 (+71715)
chr12: 67482081	-0.0314	0.26	-0.48	chr6: 111267690	GTF3C6 (-12072), AMD1 (+71718)
chr12: 71716109	0.0065	0.82	0.34		
chr14: 8324605	0.3087	0.65	0.59	chr7: 127670876	LRRC4 (+246)
chr14: 34373167	0.2091	0.76	0.64	chr7: 20371740	ITGB8 (+995)
chr18: 36757482	-0.403	0.83	-0.63	chr11: 30565405	MPPED2 (+36637)
chr19: 22964392	-0.0157	0.89	-0.54	chr2: 128408298	GPR17 (+4860), LIMS2 (+13821)
chr20: 43010636	0.4045	0.97	0.5		
chr20: 44455198	0.0664	0.72	0.47		
chr20: 56821233	1.2199	0.98	0.42	chr19: 2210771	SF3A2[a] (-25748), DOT1L (+46624)
chr22: 49950553	0.1423	0.54	0.63	chr13: 100636088	ZIC2[a] (+2063)

chr24: 37978456	-0.0979	0.77	-0.59		
chr28: 39644410	0.0856	0.84	0.37		
chr30: 38620897	1.4441	0.94	0.51	chr15: 78043186	Intergenic
chr31: 37492782	-0.0028	0.47	-0.51		
chr33: 23073877	-0.0296	0.96	-0.52	chr3: 119134135	TMEM39A (+48393)
chr34: 40999085	-0.1395	0.97	-0.46	chr3: 177284378	Intergenic
chr36: 2545142	0.432	0.5	0.62	chr2: 157179848	NR4A2 (+9379)

Genome coordinates and coefficient values for predicting a log (base e) transformed version of chronological age. These coefficients were found by regressing a log-transformed version of age on the RRBS DNA-methylation measured from 46 domesticated dog blood samples. Since chronological age was log-transformed prior to regression, it is important to exponentiate the age estimate from this model to arrive at age estimates in units of years. We provide the mean methylation and Pearson correlation with age for each individual CpG. Where possible we identify, via synteny to the human genome, genes that are proximal to the CpGs in our models. Numbers in parentheses are the distance in bases to the Transcription Start Site of the gene. Additionally, we note those genes with experimentally inferred relevance to cellular identity (pluripotency).

Genes experimentally identified as targets of pluripotency factors and the Polycomb repressor complex [69, 70]
[a] genes identified by ChIP on chip as targets of the Polycomb protein EED in human embryonic stem cells.
[b] genes possessing the trimethylated H3K27 (H3K27me3) mark in their promoters in human embryonic stem cells, as identified by ChIP on chip
[c] Polycomb Repression Complex 2 (PRC) targets; identified by ChIP on chip on human embryonic stem cells as genes that: possess the trimethylated H3K27 mark in their promoters and are bound by SUZ12 and EED Polycomb proteins
[d] genes identified by ChIP on chip as targets of the Polycomb protein SUZ12 in human embryonic stem cells

METHODS

Reduced representation bisulfite sequencing (RRBS)

We obtained previously published canine RRBS methylation data as CGmap files (see Janowitz, Koch, et al. 2016) [50]. Both wolf and dog data were aligned to the canine genome (canFam3).

Data processing

For each CpG site in each sample we estimated the methylation frequency as the number of methylated mapped read counts over the total mapped read counts and computed a corresponding 95% confidence interval from the binomial distribution [64]. For inclusion in our analysis, we required that each CpG site had confident methylation frequencies in at least 95% of samples. Confidence was defined as having a confidence interval smaller than 0.63 (roughly equivalent to requiring a minimum of 15 mapped reads at that site). For the remaining elements in the data matrix, we used the frequencies calculated regardless of confidence or imputed missing values using R package "softImpute" with type option "ALS" [65].

Culling species-specific differential methylation

To exclude species-specific differential methylation as a confounder, we first constructed a methylation matrix with no dog samples with ages greater than the maximum observed wolf age (8 years). For each CpG we then computed a t-test of the dog methylation values versus the wolf methylation values and excluded those with t >= 2 from use in regression modelling.

Computing age correlations for DNA methylation

When comparing age-correlations computed in datasets of different sizes, we use a z-score instead of the Pearson correlation coefficient. A Student t-test statistic for testing whether a Pearson correlation (r_s) is different from zero is given by

$$Z_s = \frac{\sqrt{m_s - 2} \cdot r_s}{\sqrt{1 - r_s^2}}$$

where m_s denotes the number of observations (i.e. samples) in the s-th data set.

Regression

Penalized regression models were built using glmnet [66]. Given that we would like to see a reduction in the number of predictors from potentially hundreds of thousands of CpGs as input, we utilized the "elastic net" version of glmnet corresponding to an alpha parameter of 0.5. For all results reported here, the internally cross-validated (cv.glmnet) was utilized to automatically select the optimal penalty parameter.

Functional annotation and multi-species synteny

Canid methylation sites (using coordinates from the CanFam3 draft genome) were first mapped to the human genome (hg19) where possible so that functional analysis tools with access to the most complete and detailed annotations could be utilized. This mapping was made using the "liftOver" tool and associated human to canine chain files available at the UCSC Genome Browser[67]. The human genome coordinates were then used as input to the Genomic Regions Enrichment of Annotations Tool (GREAT) [68].

CONFLICTS OF INTEREST

The Regents of the University of California is the owner of a provisional patent application directed at this invention for which the authors are named inventors.

FUNDING

REFERENCES

1. Rakyan VK, Down TA, Maslau S, Andrew T, Yang TP, Beyan H, Whittaker P, McCann OT, Finer S, Valdes AM, Leslie RD, Deloukas P, Spector TD. Human aging-associated DNA hypermethylation occurs preferentially at bivalent chromatin domains. Genome Res. 2010; 20:434–39. doi: 10.1101/gr.103101.109

2. Teschendorff AE, Menon U, Gentry-Maharaj A, Ramus SJ, Weisenberger DJ, Shen H, Campan M, Noushmehr H, Bell CG, Maxwell AP, Savage DA, Mueller-Holzner E, Marth C, et al. Age-dependent DNA methylation of genes that are suppressed in stem cells is a hallmark of cancer. Genome Res. 2010; 20:440–46. doi: 10.1101/gr.103606.109

3. Horvath S, Zhang Y, Langfelder P, Kahn RS, Boks MP, van Eijk K, van den Berg LH, Ophoff RA. Aging effects on DNA methylation modules in human brain and blood tissue. Genome Biol. 2012; 13:R97. doi: 10.1186/gb-2012-13-10-r97

4. Numata S, Ye T, Hyde TM, Guitart-Navarro X, Tao R, Wininger M, Colantuoni C, Weinberger DR, Kleinman JE, Lipska BK. DNA methylation signatures in development and aging of the human prefrontal cortex. Am J Hum Genet. 2012; 90:260–72. doi: 10.1016/j.ajhg.2011.12.020

5. Alisch RS, Barwick BG, Chopra P, Myrick LK, Satten GA, Conneely KN, Warren ST. Age-associated DNA methylation in pediatric populations. Genome Res. 2012; 22:623–32. doi: 10.1101/gr.125187.111

6. Johansson A, Enroth S, Gyllensten U. Continuous Aging of the Human DNA Methylome Throughout the Human Lifespan. PLoS One. 2013; 8:e67378. doi: 10.1371/journal.pone.0067378

7. Teschendorff AE, West J, Beck S. Age-associated epigenetic drift: implications, and a case of epigenetic thrift? Hum Mol Genet. 2013; 22:R7–15. doi: 10.1093/hmg/ddt375

8. Jung M, Pfeifer GP. Aging and DNA methylation. BMC Biol. 2015; 13:7. doi: 10.1186/s12915-015-0118-4

9. Zheng SC, Widschwendter M, Teschendorff AE. Epigenetic drift, epigenetic clocks and cancer risk. Epigenomics. 2016; 8:705–19. doi: 10.2217/epi-2015-0017

10. Cedar H, Bergman Y. Programming of DNA methylation patterns. Annu Rev Biochem. 2012; 81:97–117. doi: 10.1146/annurev-biochem-052610-091920

11. Przybilla J, Galle J, Rohlf T. Is adult stem cell aging driven by conflicting modes of chromatin remodeling? BioEssays. 2012; 34:841–48. doi: 10.1002/bies.201100190

12. Przybilla J, Rohlf T, Loeffler M, Galle J. Understanding epigenetic changes in aging stem cells--a computational model approach. Aging Cell. 2014; 13:320–28. doi: 10.1111/acel.12177

13. Beerman I, Bock C, Garrison BS, Smith ZD, Gu H, Meissner A, Rossi DJ. Proliferation-dependent alterations of the DNA methylation landscape underlie hematopoietic stem cell aging. Cell Stem Cell.

2013; 12:413–25. doi: 10.1016/j.stem.2013.01.017

14. Beerman I, Rossi DJ. Epigenetic regulation of hematopoietic stem cell aging. Exp Cell Res. 2014; 329:192–99. doi: 10.1016/j.yexcr.2014.09.013

15. Bocklandt S, Lin W, Sehl ME, Sánchez FJ, Sinsheimer JS, Horvath S, Vilain E. Epigenetic predictor of age. PLoS One. 2011; 6:e14821. doi: 10.1371/journal.pone.0014821

16. Hannum G, Guinney J, Zhao L, Zhang L, Hughes G, Sadda S, Klotzle B, Bibikova M, Fan JB, Gao Y, Deconde R, Chen M, Rajapakse I, et al. Genome-wide methylation profiles reveal quantitative views of human aging rates. Mol Cell. 2013; 49:359–67. doi: 10.1016/j.molcel.2012.10.016

17. Horvath S. DNA methylation age of human tissues and cell types. Genome Biol. 2013; 14:R115. doi: 10.1186/gb-2013-14-10-r115

18. Lin Q, Weidner CI, Costa IG, Marioni RE, Ferreira MR, Deary IJ, Wagner W. DNA methylation levels at individual age-associated CpG sites can be indicative for life expectancy. Aging (Albany NY). 2016; 8:394–401. doi: 10.18632/aging.100908

19. Gibbs WW. Biomarkers and ageing: the clock-watcher. Nature. 2014; 508:168–70. doi: 10.1038/508168a

20. Benayoun BA, Pollina EA, Brunet A. Epigenetic regulation of ageing: linking environmental inputs to genomic stability. Nat Rev Mol Cell Biol. 2015; 16:593–610. doi: 10.1038/nrm4048

21. Marioni RE, Shah S, McRae AF, Chen BH, Colicino E, Harris SE, Gibson J, Henders AK, Redmond P, Cox SR, Pattie A, Corley J, Murphy L, et al. DNA methylation age of blood predicts all-cause mortality in later life. Genome Biol. 2015; 16:25. doi: 10.1186/s13059-015-0584-6

22. Christiansen L, Lenart A, Tan Q, Vaupel JW, Aviv A, McGue M, Christensen K. DNA methylation age is associated with mortality in a longitudinal Danish twin study. Aging Cell. 2016; 15(1):149-54. doi: 10.1111/acel.12421

23. Perna L, Zhang Y, Mons U, Holleczek B, Saum KU, Brenner H. Epigenetic age acceleration predicts cancer, cardiovascular, and all-cause mortality in a German case cohort. Clin Epigenetics. 2016; 8:64. doi: 10.1186/s13148-016-0228-z

24. Chen BH, Marioni RE, Colicino E, Peters MJ, Ward-Caviness CK, Tsai PC, Roetker NS, Just AC, Demerath EW, Guan W, Bressler J, Fornage M, Studenski S, et al. DNA methylation-based measures of biological age: meta-analysis predicting time to death. Aging (Albany NY). 2016; 8:1844–65. doi: 10.18632/aging.101020

25. Horvath S, Pirazzini C, Bacalini MG, Gentilini D, Di Blasio AM, Delledonne M, Mari D, Arosio B, Monti D, Passarino G, De Rango F, D'Aquila P, Giuliani C, et al. Decreased epigenetic age of PBMCs from Italian semi-supercentenarians and their offspring. Aging (Albany NY). 2015; 7:1159–70. doi: 10.18632/aging.100861

26. Levine ME, Hosgood HD, Chen B, Absher D, Assimes T, Horvath S. DNA methylation age of blood predicts future onset of lung cancer in the women's health initiative. Aging (Albany NY). 2015; 7:690–700. doi: 10.18632/aging.100809

27. Marioni RE, Shah S, McRae AF, Ritchie SJ, Muniz-Terrera G, Harris SE, Gibson J, Redmond P, Cox SR, Pattie A, Corley J, Taylor A, Murphy L, et al. The epigenetic clock is correlated with physical and cognitive fitness in the Lothian Birth Cohort 1936. Int J Epidemiol. 2015; 44:1388–96. doi: 10.1093/ije/dyu277

28. Levine ME, Lu AT, Bennett DA, Horvath S. Epigenetic age of the pre-frontal cortex is associated with neuritic plaques, amyloid load, and Alzheimer's disease related cognitive functioning. Aging (Albany NY). 2015; 7:1198–211. doi: 10.18632/aging.100864

29. Horvath S, Mah V, Lu AT, Woo JS, Choi OW, Jasinska AJ, Riancho JA, Tung S, Coles NS, Braun J, Vinters HV, Coles LS. The cerebellum ages slowly according to the epigenetic clock. Aging (Albany NY). 2015; 7:294–306. doi: 10.18632/aging.100742

30. Horvath S, Garagnani P, Bacalini MG, Pirazzini C, Salvioli S, Gentilini D, Di Blasio AM, Giuliani C, Tung S, Vinters HV, Franceschi C. Accelerated epigenetic aging in Down syndrome. Aging Cell. 2015; 14:491–95. doi: 10.1111/acel.12325

31. Horvath S, Levine AJ. HIV-1 infection accelerates age according to the epigenetic clock. J Infect Dis. 2015; 212:1563–73. doi: 10.1093/infdis/jiv277

32. Horvath S, Langfelder P, Kwak S, Aaronson J, Rosinski J, Vogt TF, Eszes M, Faull RL, Curtis MA, Waldvogel HJ, Choi OW, Tung S, Vinters HV, et al. Huntington's disease accelerates epigenetic aging of human brain and disrupts DNA methylation levels. Aging (Albany NY). 2016; 8:1485–512. doi: 10.18632/aging.101005

33. Horvath S, Erhart W, Brosch M, Ammerpohl O, von Schönfels W, Ahrens M, Heits N, Bell JT, Tsai PC, Spector TD, Deloukas P, Siebert R, Sipos B, et al. Obesity accelerates epigenetic aging of human liver. Proc Natl Acad Sci USA. 2014; 111:15538–43. doi: 10.1073/pnas.1412759111

34. Levine ME, Lu AT, Chen BH, Hernandez DG, Singleton AB, Ferrucci L, Bandinelli S, Salfati E, Manson JE, Quach A, Kusters CD, Kuh D, Wong A, et al. Menopause accelerates biological aging. Proc Natl

Acad Sci USA. 2016; 113:9327–32. doi: 10.1073/pnas.1604558113

35. Vidal L, Lopez-Golan Y, Rego-Perez I, Horvath S, Blanco FJ, Riancho JA, Gomez-Reino JJ, Gonzalez A. Specific increase of methylation age in osteoarthritis cartilage. Osteoarthritis Cartilage. 2016; 24:S63. doi: 10.1016/j.joca.2016.01.140

36. Horvath S, Ritz BR. Increased epigenetic age and granulocyte counts in the blood of Parkinson's disease patients. Aging (Albany NY). 2015; 7:1130–42. doi: 10.18632/aging.100859

37. Boyko AR. The domestic dog: man's best friend in the genomic era. Genome Biol. 2011; 12:216. doi: 10.1186/gb-2011-12-2-216

38. Kaeberlein M, Creevy KE, Promislow DE. The dog aging project: translational geroscience in companion animals. Mamm Genome. 2016; 27:279–88. doi: 10.1007/s00335-016-9638-7

39. Karyadi DM, Karlins E, Decker B, vonHoldt BM, Carpintero-Ramirez G, Parker HG, Wayne RK, Ostrander EA. A copy number variant at the KITLG locus likely confers risk for canine squamous cell carcinoma of the digit. PLoS Genet. 2013; 9:e1003409. doi: 10.1371/journal.pgen.1003409

40. Decker B, Parker HG, Dhawan D, Kwon EM, Karlins E, Davis BW, Ramos-Vara JA, Bonney PL, McNiel EA, Knapp DW, Ostrander EA. Homologous Mutation to Human BRAF V600E Is Common in Naturally Occurring Canine Bladder Cancer--Evidence for a Relevant Model System and Urine-Based Diagnostic Test. Mol Cancer Res. 2015; 13:993–1002. doi: 10.1158/1541-7786.MCR-14-0689

41. Bronson RT. Variation in age at death of dogs of different sexes and breeds. Am J Vet Res. 1982; 43:2057–59.

42. O'Neill DG, Church DB, McGreevy PD, Thomson PC, Brodbelt DC. Longevity and mortality of owned dogs in England. Vet J. 2013; 198:638–43. doi: 10.1016/j.tvjl.2013.09.020

43. Speakman JR. Body size, energy metabolism and lifespan. J Exp Biol. 2005; 208:1717–30. doi: 10.1242/jeb.01556

44. Li Y, Deeb B, Pendergrass W, Wolf N. Cellular proliferative capacity and life span in small and large dogs. J Gerontol A Biol Sci Med Sci. 1996; 51:B403–08. doi: 10.1093/gerona/51A.6.B403

45. Landon DB, Peterson RO, Mech LD. Evaluation of age determination techniques for gray wolves. J Wildl Manage. 1998; 62:674–82. doi: 10.2307/3802343

46. Gipson PH, Nowak RM, Mech LD. Accuracy and precision of estimating age of gray wolves by tooth wear. J Wildl Manage. 2002; 64:752–58. doi: 10.2307/3802745

47. LD M. Estimated age structure of wolves in northeastern Minnesota. 2006. USGS Northern Prairie Wildlife Research Center.

48. Medjo DC, Mech LD. Reproductive activity in nine- and ten-month-old wolves. J Mammal. 1976; 57:406–08. doi: 10.2307/1379708

49. Gese EM, Mech LD. Dispersal of wolves (Canis lupus) in northeastern Minnesota. Can J Zool. 1991; 69:2946–55. doi: 10.1139/z91-415

50. Janowitz Koch IC, Thompson MJ, Deere-Machemer KA, Wang J, Duarte L, Gnanadesikan GE, McCoy EL, Rubbi L, Stahler DR. pellegrini M, Ostrander EA, Wayne RK, Sinsheimer JS, vonHoldt BM. The concerted impact of domestication and transposon insertions on methylation patterns between dogs and grew wolves. Mol Ecol. 2016; 25:1838–55. doi: 10.1111/mec.13480

51. Ostrander EA, Wayne RK. The canine genome. Genome Res. 2005; 15:1706–16. doi: 10.1101/gr.3736605

52. Parker HG, Shearin AL, Ostrander EA. Man's best friend becomes biology's best in show: genome analyses in the domestic dog. Annu Rev Genet. 2010; 44:309–36. doi: 10.1146/annurev-genet-102808-115200

53. Schoenebeck JJ, Ostrander EA. Insights into morphology and disease from the dog genome project. Annu Rev Cell Dev Biol. 2014; 30:535–60. doi: 10.1146/annurev-cellbio-100913-012927

54. Mathews LS, Hammer RE, Brinster RL, Palmiter RD. Expression of insulin-like growth factor I in transgenic mice with elevated levels of growth hormone is correlated with growth. Endocrinology. 1988; 123:433–37. doi: 10.1210/endo-123-1-433

55. Bartke A. Minireview: role of the growth hormone/insulin-like growth factor system in mammalian aging. Endocrinology. 2005; 146:3718–23. doi: 10.1210/en.2005-0411

56. Powell-Braxton L, Hollingshead P, Warburton C, Dowd M, Pitts-Meek S, Dalton D, Gillett N, Stewart TA. IGF-I is required for normal embryonic growth in mice. Genes Dev. 1993; 7:2609–17. doi: 10.1101/gad.7.12b.2609

57. Boyko AR, Quignon P, Li L, Schoenebeck JJ, Degenhardt JD, Lohmueller KE, Zhao K, Brisbin A, Parker HG, vonHoldt BM, Cargill M, Auton A, Reynolds A, et al. A simple genetic architecture underlies morphological variation in dogs. PLoS Biol. 2010; 8:e1000451.

doi: 10.1371/journal.pbio.1000451

58. Sutter NB, Bustamante CD, Chase K, Gray MM, Zhao K, Zhu L, Padhukasahasram B, Karlins E, Davis S, Jones PG, Quignon P, Johnson GS, Parker HG, et al. A single IGF1 allele is a major determinant of small size in dogs. Science. 2007; 316:112–15. doi: 10.1126/science.1137045

59. Thompson MJ, Rubbi L, Dawson DW, Donahue TR, Pellegrini M. Pancreatic cancer patient survival correlates with DNA methylation of pancreas development genes. PLoS One. 2015; 10:e0128814. doi: 10.1371/journal.pone.0128814

60. Benjamini Y, and Hochberg, Y. Controlling the false discovery rate: a practical and powerful approach to multiple testing. J R Stat Soc Ser B Methodological. 1995; 57:289-300.

61. Horvath S, Gurven M, Levine ME, Trumble BC, Kaplan H, Allayee H, Ritz BR, Chen B, Lu AT, Rickabaugh TM, Jamieson BD, Sun D, Li S, et al. An epigenetic clock analysis of race/ethnicity, sex, and coronary heart disease. Genome Biol. 2016; 17:171. doi: 10.1186/s13059-016-1030-0

62. Lu AT, Hannon E, Levine ME, Hao K, Crimmins EM, Lunnon K, Kozlenkov A, Mill J, Dracheva S, Horvath S. Genetic variants near MLST8 and DHX57 affect the epigenetic age of the cerebellum. Nat Commun. 2016; 7:10561. doi: 10.1038/ncomms10561

63. Quach A, Levine ME, Tanaka T, Lu AT, Chen BH, Ferrucci L, Ritz B, Bandinelli S, Neuhouser ML, Beasley JM, Snetselaar L, Wallace RB, Tsao PS, et al. Epigenetic clock analysis of diet, exercise, education, and lifestyle factors. Aging (Albany NY). 2017. 14;9(2):419-446

64. Clopper CP, Pearson ES. E.S. The use of confidence or fiducial limits illustrated in the case of the binomial. Biometrika. 1934; 26:404–13. doi: 10.1093/biomet/26.4.404

65. Mazumder R, Hastie T, Tibshirani R. Spectral Regularization Algorithms for Learning Large Incomplete Matrices. J Mach Learn Res. 2010; 11:2287–322.

66. Friedman J, Hastie T, Tibshirani R. Regularization Paths for Generalized Linear Models via Coordinate Descent. J Stat Softw. 2010; 33:1–22. doi: 10.18637/jss.v033.i01

67. Kent WJ, Sugnet CW, Furey TS, Roskin KM, Pringle TH, Zahler AM, Haussler D. The human genome browser at UCSC. Genome Res. 2002; 12:996–1006. doi: 10.1101/gr.229102

68. McLean CY, Bristor D, Hiller M, Clarke SL, Schaar BT, Lowe CB, Wenger AM, Bejerano G. GREAT improves functional interpretation of cis-regulatory regions. Nat Biotechnol. 2010; 28:495–501. doi: 10.1038/nbt.1630

69. Subramanian A, Tamayo P, Mootha VK, Mukherjee S, Ebert BL, Gillette MA, Paulovich A, Pomeroy SL, Golub TR, Lander ES, Mesirov JP. Gene set enrichment analysis: a knowledge-based approach for interpreting genome-wide expression profiles. Proc Natl Acad Sci USA. 2005; 102:15545–50. doi: 10.1073/pnas.0506580102

70. Ben-Porath I, Thomson MW, Carey VJ, Ge R, Bell GW, Regev A, Weinberg RA. An embryonic stem cell-like gene expression signature in poorly differentiated aggressive human tumors. Nat Genet. 2008; 40:499–507. doi: 10.1038/ng.127

Longitudinal study of surrogate aging measures during human immunodeficiency virus seroconversion

Janice M Leung[1,2,3], Nick Fishbane[1], Meaghan Jones[4], Alexander Morin[4], Stella Xu[1], Joseph CY Liu[1], Julie MacIsaac[4], MJ Milloy[3], Kanna Hayashi[3,5], Julio Montaner[3], Steve Horvath[6], Michael Kobor[4], Don D Sin[1,2], P Richard Harrigan[4], SF Paul Man[1,2]

[1]Centre for Heart Lung Innovation, St. Paul's Hospital, University of British Columbia, Vancouver, V6Z 1Y6, Canada
[2]Division of Respiratory Medicine, Department of Medicine, St. Paul's Hospital, University of British Columbia, Vancouver, V6Z 1Y6, Canada
[3]BC Centre for Excellence in HIV/AIDS, St. Paul's Hospital, University of British Columbia, Vancouver, V6Z 1Y6, Canada
[4]Centre for Molecular Medicine and Therapeutics, University of British Columbia, Vancouver, V5Z 4H4, Canada
[5]Department of Medicine, University of British Columbia, Vancouver, V6Z 1Y6, Canada
[6]Departments of Human Genetics and Biostatistics, University of California Los Angeles, Los Angeles, CA 90095, USA

ABSTRACT

Persons living with human immunodeficiency virus (HIV) harbor an increased risk of age-related conditions. We measured changes in telomere length and DNA methylation in the peripheral blood of 31 intravenous drug users, who were followed longitudinally with blood samples pre-HIV (T1), immediately post-HIV (T2; 1.9±1 year from T1), and at a later follow-up time (T3; 2.2±1 year from T2). Absolute telomere length measurements were performed using polymerase chain reaction methods. Methylation profiles were obtained using the Illumina Human Methylation450 platform. Methylation aging was assessed using the Horvath method. Telomere length significantly decreased between T1 and T2 (227±46 at T1 vs. 201±48 kbp/genome at T2, p=0.045), while no differences were observed between T2 and T3 (201±48 at T2 vs. 186±27 kbp/genome at T3, p=0.244). Methylation aging as measured by the age acceleration residual increased over the time course of HIV infection (p=0.035). CpG sites corresponding to *PCBP2* and *CSRNP1* were differentially methylated between T1 and T2 at a q-value <0.05. Telomere shortening and methylation changes can therefore be observed in the short-term period immediately following HIV seroconversion. Further studies to confirm these results in larger sample sizes and to compare these results to non-HIV and non-injection drug users are warranted.

INTRODUCTION

With the benefit of combination antiretroviral therapy (cART), persons living with human immunodeficiency virus (PLWH) have survived to older ages [1, 2] with fewer opportunistic infections and AIDS-defining cancers [3, 4]. Despite these gains, the rise in the number of age-related conditions such as coronary artery disease [5], chronic obstructive pulmonary disease [6, 7], and non-AIDS-defining cancers [8] has sparked interest in how PLWH age. The precise nature

of this heightened aging process, whether in fact accelerated or merely accentuated [9], is still unknown. PLWH appear to have shorter peripheral blood telomere lengths compared with uninfected individuals [10-12], yet whether this represents a gradual attrition over the course of HIV infection or an abrupt shortening during periods of acute illness and profound immuno-suppression has not been established. Recently, it has been shown in a cohort of cART-treated, virally suppressed PLWH that while telomere length, a surrogate marker of cellular aging, is shorter in PLWH

compared with HIV-uninfected individuals, the slope of telomere length vs. age is no different between the two groups [11]. This might suggest that abrupt shortening does indeed occur early on in the course of disease, possibly at the period of intense immunosuppression related to acute HIV infection and prior to the institution of cART.

Identifying the timing of an aging trigger along the course of HIV infection has important scientific and clinical ramifications. At the very least, this allows further investigation into the biology of HIV aging to be situated in the appropriate time frame. Cellular changes observed within this time period provide important clues into the susceptibility of PLWH to age-related conditions. Shortening or preventing the onset of this time period may be one strategy that can improve outcomes in an aging HIV-infected population. Such investigations, however, require longitudinal sampling from subjects before and after HIV seroconversion. In this study, we examined surrogate peripheral blood aging markers in a cohort of injection drug users (IDU) followed longitudinally before and after acquiring HIV, aiming to 1) identify when age acceleration might occur in HIV and 2) describe potential key biologic pathways perturbed during he HIV seroconversion period. Useful biomarkers of aging, according to criteria adopted by the American Federation of Aging Research, are required to fulfill the following objectives: 1) predict the rate of aging; 2) reflect a biologic process associated with aging; 3) be able to be tested repeatedly in an individual without harm; and 4) translate from animals to humans [13]. Our choices of surrogate aging measures, both of which meet these criteria, focus on two distinct mechanisms, the first relating to replicative senescence by measuring peripheral blood telomere length and the second relating to age-associated methylation changes via a DNA methylation clock [14, 15]. Shortened telomere length has been shown in some studies to predict mortality [16], age-related diseases [17], and has been widely used as a biomarker of aging. A recent study also demonstrated that the DNA methylation clock is a useful biomarker for detecting accelerated aging effects due to HIV infection [18], but the behavior over time of this biomarker is not yet known. Here we demonstrate for the first time that changes in surrogate aging biomarkers may be observed shortly after HIV infection.

RESULTS

Study cohort

Demographics for the 31 patients enrolled in the study are provided in Table 1. The cohort had a mean age of 35.8 years and 48% were male. Nearly all patients (90%) had concurrent hepatitis C infection. The samples were collected between 1999 and 2004; by T3, only seven (22%) were on cART. The mean time intervals (± standard deviation [SD]) were 1.9 ± 1 years between T1 and T2 and 2.2 ± 1 years between T2 and T3.

Absolute telomere length measurements

29 paired samples from T1 and T2 and 17 paired samples from T2 and T3 were included in the final analysis after samples from two individuals between T1 and T2 and two individuals between T2 and T3 failed qPCR runs. The correlation between telomere length and age is shown in Figure 1A (p=0.017, Pearson's rho=-0.268). The mean telomere length (± SD) was 227 ± 46 kbp/genome at T1, 201 ± 48 kbp/genome at T2,

Table 1. Demographics of the study cohort.

Characteristic	Result (n=31)
Age (years ± SD)	35.8 ±10.1
Male Sex (%)	15 (48.4%)
Ever Smoker (%)	28 (90.3%)
CD4 Count at T2 (cells/mm^3 ± SD)	386 ± 213
CD4 Count at T3 (cells/mm^3 ± SD)	273 ± 150
Viral Load at T2 (copies/mL ± SD)	96,432 ± 164,340
Viral Load at T3 (copies/mL ± SD)	58,461 ± 55,575
On cART at T3 (%)	7 (22.6%)
Hepatitis C	28 (90%)
Current Homelessness	15 (48.4%)
Injection Drug Use Within Last 6 Months	25 (81%)
Previous Incarceration	25 (88.2%)
History of Physical Abuse	27 (87.0%)
History of Sexual Abuse	15 (48.4%)
Heavy Alcohol Use Within Last 6 Months (>4 drinks/day)	5 (16.1%)

Abbreviations: SD – standard deviation; cART – combination antiretroviral therapy

and 186 ± 27 kbp/genome at T3 (Figure 1B). Paired t-test analysis showed that the telomere length at T2 was significantly shorter than T1 (p=0.045), but that the telomere length at T3 was not significantly different from T2 (p=0.244). There were no significant differences at the T3 time point between the telomere lengths of subjects on cART and those not being treated with cART, nor were there any differences between those with detectable or undetectable viral loads or between those with CD4 counts <200 cells/mm^3 or ≥200 cells/mm^3.
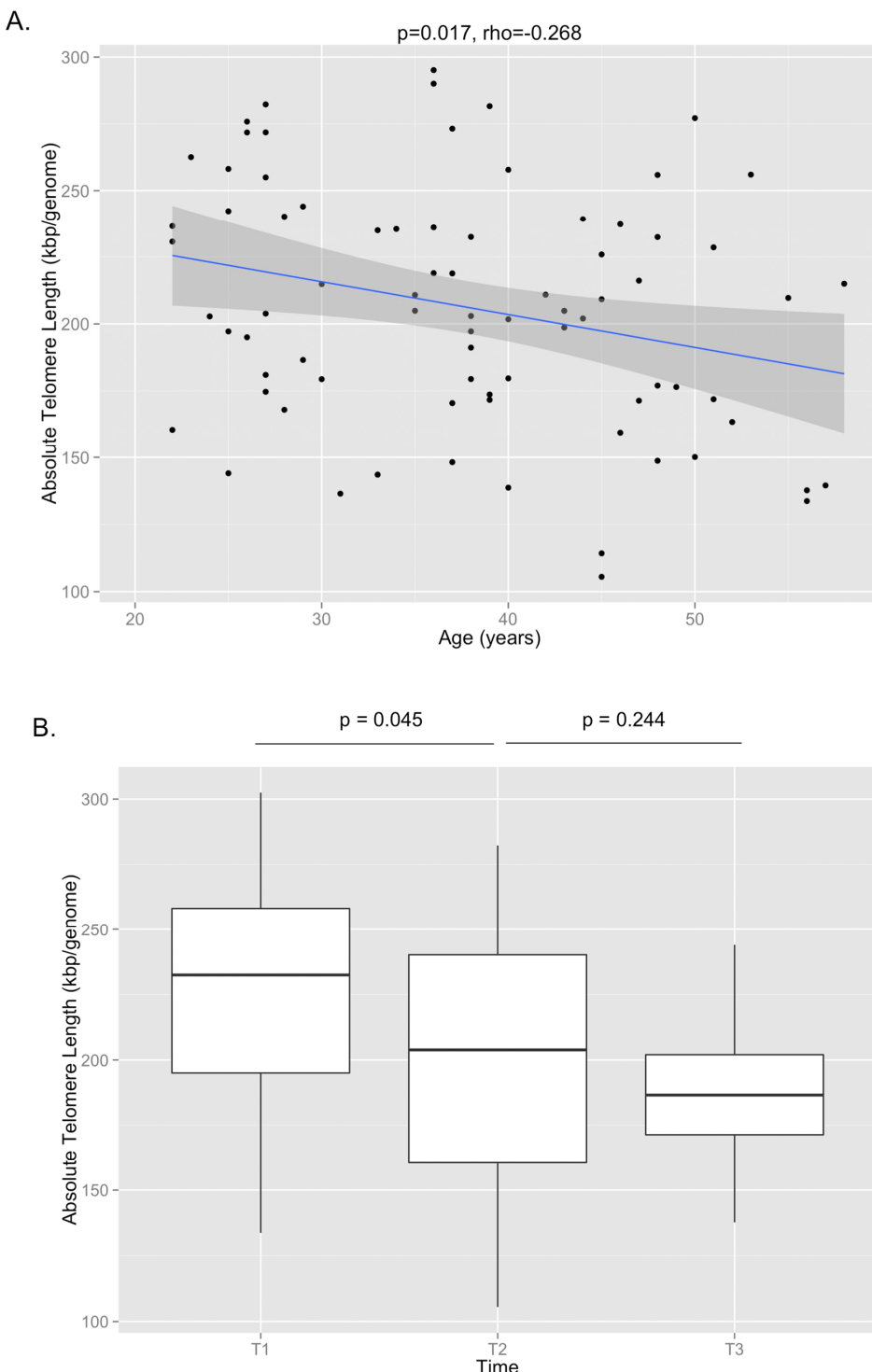
Figure 1. (**A**)The correlation between absolute telomere length and age is shown, demonstrating that shorter telomere lengths are observed with older age (p=0.017, Pearson's rho=-0.268). (**B**) Absolute telomere length measurements are shown for T1, T2, and T3. By paired t-test, there was a significant decrease in telomere length between T1 and T2 (p=0.045), but no significant change between T2 and T3 (p=0.244).

DNA methylation age

The DNA methylation age was calculated for each subject at the various time points. The correlation between DNA methylation age and chronologic age is shown in Figure 2A. To determine the magnitude of age acceleration over the duration of HIV infection, the correlation between the age acceleration residual and time point in days along the course of the study is shown in Figure 2B. Epigenetic age acceleration was positive correlated with days since HIV infection (p=0.035, Pearson's r=0.236) which shows that HIV infection accelerates the biological aging rate of blood.

A.
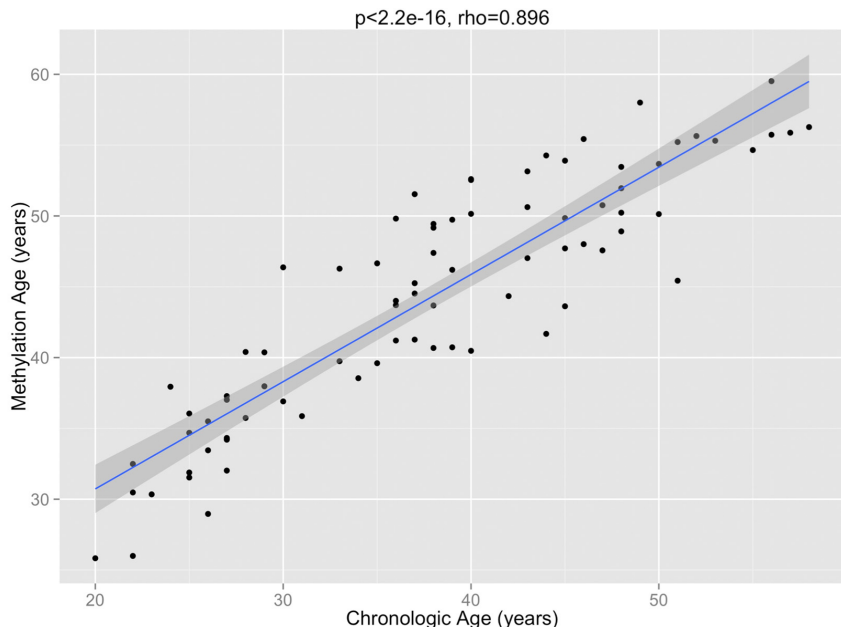
B.
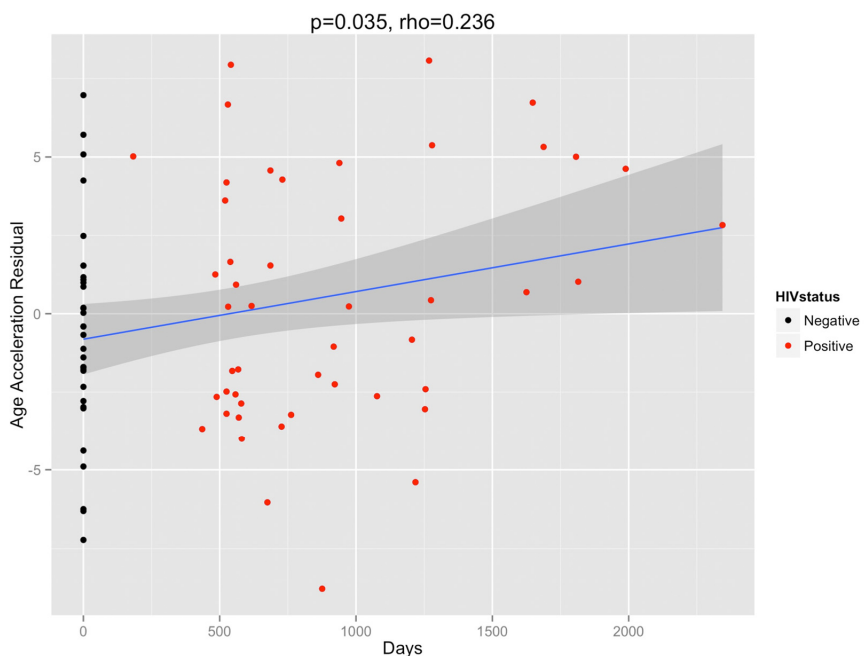
Figure 2. (**A**) The correlation between DNA methylation age and chronologic age from all subjects inclusive of all time points is shown, demonstrating a high correlation between the two measures (p<2.2e-16, Pearson's rho=0.896). (**B**) The age acceleration residual (greater positivity on this scale represents more advanced methylation age in relation to chronologic age) increases over the time course of HIV infection (p=0.035, Pearson's rho=0.236). Black dots represent HIV-negative time points (T1) while red dots represent HIV-positive time points (T2 and T3).

DNA methylation profiling

CD4 and CD8 T cell type proportion percentages at T1, T2, and T3 are provided in Supplementary Figure 1A and 1B. CD4 cell percentages decreased significantly between T1 and T2 ($p<0.001$), whereas CD8 cell percentages increased significantly between T1 and T2 ($p<0.001$). There were no significant changes in either CD4 or CD8 cell percentages between T2 and T3. Cell percentages of monocytes, NK cells, granulocytes, and B cells were not significantly different between the three time points (Supplementary Figure 1C, 1D, 1E, 1F).

The top differentially methylated CpG sites between T1 and T2 are listed in Table 2. After adjustment for cellular composition of blood, there were two CpG sites differentially methylated between T1 and T2 with a q-value <0.05. These were cg07151565, corresponding to *PCBP2* (hypomethylated in T2 vs. T1, q-value=0.012), and cg23654821, corresponding to *CSRNP1* (hyper-methylated in T2 vs. T1, q-value=0.028). There were four additional CpG sites that were differentially methylated with a q-value <0.20. These sites are shown in a volcano plot in Figure 3. One CpG site was found to be differentially methylated between T2 and T3, how-ever only at a q-value of 0.065. This was cg07926733

Table 2. Differentially methylated CpG sites (T2 vs. T1).

CpG Site	Gene	Beta-Value Difference	q-value
cg07151565	*PCBP2*	-0.043	0.012
cg23654821	*CSRNP1*	0.085	0.028
cg10252135	*PDE7a*	0.023	0.180
cg21149466	Unknown	-0.057	0.180
cg02854554	*FAM46C*	0.056	0.180
cg25353281	*PNKD;TMBIM1*	0.083	0.180
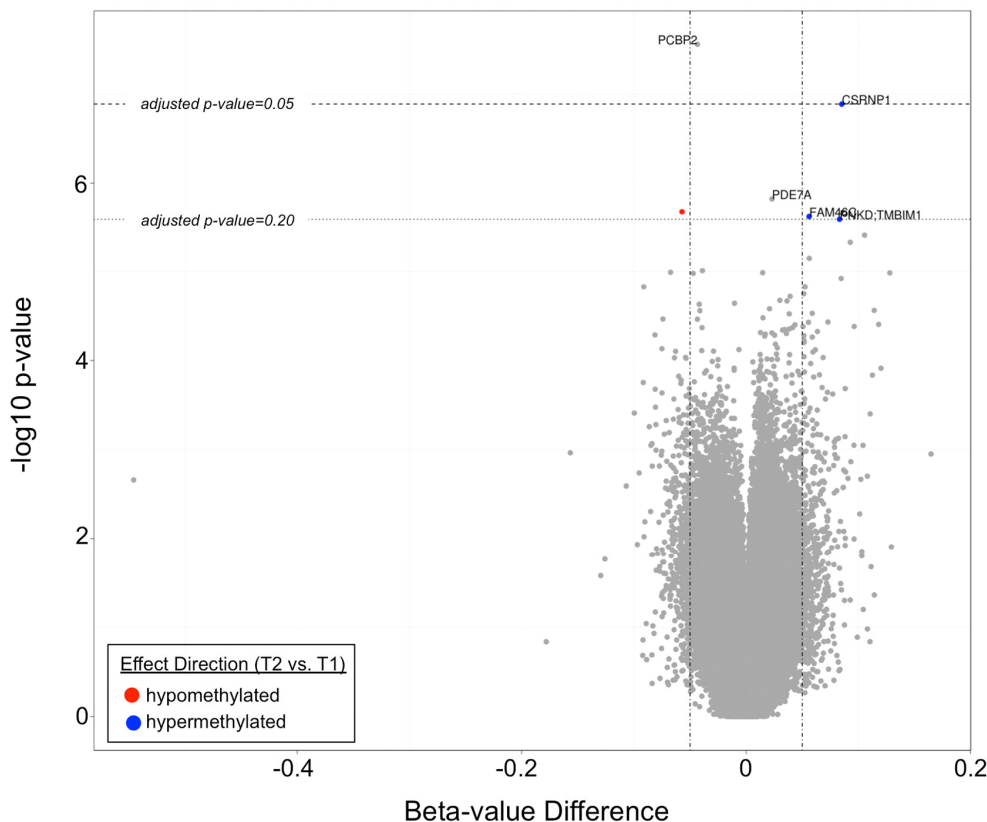
Figure 3. A volcano plot demonstrating differentially methylated CpG sites in T2 vs. T1. Two CpG sites (corresponding to *PCBP2* and *CSRNP1*) had q-values <0.05, while four additional CpG sites (corresponding to *PDE7a*, *FAM46C*, *PNKD:TMBIM1*, and an unknown gene) had q-values <0.20.

(corresponding gene currently unknown). The mean beta-value difference (T3 vs. T2) was 0.064.

Pyrosequencing validation

Pyrosequencing validation was carried out for five of the six differentially methylated CpG sites between T1 and T2 (cg10252135 was not validated due to the small beta-value difference of 0.023 which was within the range of pyrosequencing error) and for the one differentially methylated CpG site between T2 and T3. Spearman correlation plots for the six CpG sites are shown in Supplementary Figure 2. Four CpG sites had Spearman correlation rho values near or above 0.8, indicating agreement between the two methods (cg02854554, cg23654821, cg25353281, and cg07926733).

DISCUSSION

In this study investigating longitudinal blood samples of IDUs who subsequently contracted HIV, we found an acute telomere shortening signal in the immediate post-seroconversion period. Telomere length subsequently stabilized in the post-seroconversion period with no significant changes observed between the T2 and T3 time points. The magnitude of telomere length shortening between T1 and T2, almost 30 kbp/genome in an average time span of two years or less (equivalent to a loss of ~650 base pairs/year), was a striking finding reflecting the severity of replicative senescence in HIV. A previous study that used the same method of telomere length measurement across a large general population sample showed that an equivalent drop in telomere length would have taken roughly 40 years [11]. On average, leukocyte telomere length is expected to decline only by approximately 25 base pairs per year in the general population [19]. No doubt, the VIDUS population, all IDUs, represent a specific high-risk group of individuals, but the additional stress of acute HIV infection may account for the extra telomere length loss. Future prospective studies evaluating the equivalent drop in telomere length for IDUs who did not contract HIV would be key to determining whether these findings are HIV-specific.

Telomere length, however, reflects only one particular aspect of the complex process of aging. Moreover, it is an imperfect reflection, carrying only a correlation of 0.3 with chronologic age [19]. Studies that have evaluated the association between telomere length with mortality have also yielded conflicting results [20]. For these reasons, we chose to measure aging by an additional method. While telomere shortening is a surrogate measure of the limits of cellular replication and of oxidative stress, DNA methylation changes over

time represent the loss of methylation fidelity through cell division, a process known as "epigenetic drift" [21]. Overall patterns of methylation changes suggest that methylation tends to increase in promoter regions and decrease in non-island regions with age [22]. Recently developed methylation clocks, constructed based on these principles, can thus serve as additional evidence of aging in HIV. We observed greater deviations of the DNA methylation age from expected trajectories the further subjects were from their HIV diagnosis date. It is important to note, though, that the DNA methylation aging clock reflects a separate process of senescence from telomere shortening, with at best only a weak correlation between the two different measures [23]. In our data, we do not observe a significant correlation between epigenetic age acceleration and telomere length (p=0.60, rho=-0.06, Supplementary Figure 3) which shows that the epigenetic clock relates to a biological process that is distinct from that of telomere attrition.

By using a genome-wide DNA methylation platform, we performed a preliminary investigation into the unique biology of the HIV peri-seroconversion period. Methylation changes between T1 and T2 were subtle, with an average beta-value difference in CpG sites between the two time points not exceeding 10%, yet still revealed interesting genes that might serve as the target for future mechanistic work. The most significant changes were observed at CpG sites associated with the *PCBP2* and *CSRNP1* genes, which had q-values <0.05. *PCBP2*, found to be hypermethylated following seroconversion, encodes for poly(RC) binding protein 2, which has been demonstrated to be a translational coactivator of a number of viruses including polio [24] [25], norovirus [26], and hepatitis C [27, 28]. Notably, it has also been reported to play a role in HIV-1 gene expression [29]. Depletion of PCBP2 through siRNA results in increased expression of HIV-1 Gag and Env protein, for instance. *CSRNP1*, hypomethylated following seroconversion, encodes for cysteine-serine-rich nuclear protein 1 which through the Wnt signaling pathway has been shown to have a tumor suppressive function [30]. While there are no reported associations with HIV infection to our knowledge in the literature, the increased risk borne by PLWH for both AIDS-related and non-AIDS-related malignancies suggests this may be a relevant gene for investigating oncologic risk in this population. Genes found to be differentially methylated between T1 and T2 at lesser statistical significance included *PDE7a* (involved in cAMP degradation) [31], *FAM46C* (involved in the enhancement of viral replication) [32], *PNKD* (involved in familial paroxysmal nonkinesigenic dyskinesia) [33], and *TMBIM1* (involved in vascular remodeling through matrix metalloproteinase 9) [34]. As far as we are aware, none of these have previously been reported to

have associations with HIV infection. Further validation of these targets, particularly with additional HIV-negative samples, is necessary at this point.

This study has several limitations which should be noted. First, without concurrent RNA or protein samples, DNA methylation alone cannot tell us the direction of gene expression or protein transcription. While genes methylated at their promoter CpG islands have traditionally been thought to be transcriptionally silent, this is no longer considered an exact rule [35]. Therefore, despite significant associations between HIV seroconversion and *PCBP2* and *CSRNP1* we are unable to determine whether these genes are up- or down-regulated, only that it is possible their expression may be altered by their methylation status. Second, the changes we observe in telomere length and DNA methylation with HIV seroconversion are limited here to IDUs, a unique population at a high risk for additional infections and health problems such as bacterial endocarditis and hepatitis C. Whether similar changes occur in non-IDUs contracting HIV are observed is unknown. Such investigations are hampered by the fact that very few cohorts exist that have longitudinally tracked high-risk populations prior to and following HIV infection. It should be noted that in a previous analysis of HIV-infected patients, telomere length was not significantly affected by Hepatitis C status (data not shown). Third, DNA methylation is highly associated with cell type composition. We have used a statistical method to deconvolute the cell composition of our whole blood samples; however, these methods can only partially account for the many cell subtypes that exist in peripheral blood [36]. Currently, statistical deconvolution methods have not included subsets of NK cells or myeloid cells that may also contribute to the overall methylation signature. Finally, the small sample size of our study is a limitation and certainly further work in larger cohorts would be key to strengthening these findings. In particular, expansion of the cohort to include IDUs who remained HIV-negative throughout the study period would be important to determine whether the findings of this study are specific to the HIV or IDU populations. We were also underpowered in this study to determine whether aging is more pronounced in those with more severe HIV, as marked by higher viral loads and lower CD4 cell counts. Subgroup analyses in a larger cohort would be important to pursue to investigate this hypothesis.

The results of this study suggest that the time period shortly after HIV seroconversion may be critical in the aging process of PLWH. Given that this is a time where profound changes occur in the immune system, with rapid destruction of CD4 T cells and proliferation of CD8 T cells, targeting this interval with immediate cART initiation may be one therapeutic intervention that can mitigate downstream aging complications. Such a theory warrants further prospective study and may be imperative in a population whose demographics are quickly aging.

MATERIALS AND METHODS

Study cohort

Subjects were enrolled from the Vancouver Injection Drug Users Study (VIDUS), a prospective cohort study of >1,000 IDUs in the Vancouver area that began in 1996 [37] (University of British Columbia Research Ethics Board Approval Number H01-50086). Enrollment criteria into the study included: 1) injection of illicit drugs at least once during the previous month, 2) residence in the Greater Vancouver area, and 3) ability to provide written informed consent. VIDUS participants were tested every six months for HIV and hepatitis C. Subjects included in this analysis had to have tested positive for HIV during follow-up with available peripheral blood samples prior to and after HIV seroconversion. Peripheral blood cell pellets were frozen at -70 degrees Celsius prior to use. 31 subjects were enrolled with pre- (T1) and post-seroconversion (T2) samples, with 19 of these subjects further providing an additional third blood sample (T3) approximately two years after the immediate post-seroconversion period.

Absolute telomere length measurement

Genomic DNA from peripheral blood cell pellets was harvested using the Qiagen DNeasy Blood & Tissue Kit (Qiagen, Venlo, the Netherlands). Absolute telomere length was measured by quantitative PCR consistent with methods outlined by O'Callaghan and Fenech [38]. Briefly, standard curves were generated from known quantities of synthesized oligomers of telomere (*TEL*) DNA [(TTAGGG)14] and single copy reference gene (*36B4*) DNA [CAGCAAGTGGGAAGGTGTAATCCG TCTCCACAGACAAGGCCAGGACTCGTTTGTACC CGTTGATGATAGAATGGG] (Sigma-Aldrich, St. Louis, MO). Sample telomere DNA length was then assessed based on the ratio of telomere DNA length to *36B4* DNA length as obtained from their respective standard curves. DNA from a short telomere cell line (*HEK293*) and a long telomere cell line (*K562*) (ATCC, Manassas, VA) were used as inter-experimental plate controls [39]. The telomere lengths measured using this method reflect an average length across the population of cells included in the sample. Samples were run in triplicate using the ABI ViiA 7 Real Time PCR System (Applied Biosystems, Foster City, CA). All samples

were concurrently run to avoid significant batch effects. Paired t-tests were performed to compare telomere lengths at T1, T2, and T3 with p-values <0.05 (two-tailed tests) considered significant.

DNA methylation profiling

DNA extracted from the peripheral blood cell pellets was bisulfite-converted using the EZ DNA Methylation™ Kit (Zymo, Irvine, CA). This step converts unmethylated cytosine residues to uracil while leaving methylated cytosine residues intact. DNA methylation profiles were then obtained using the Illumina Infinium Methylation 450K assay, which interrogates 485,512 cytosine-guanine (CpG) sites spanning 99% of RefSeq genes, with an average of 17 CpG sites per gene [40]. In total, 96% of all CpG islands in the genome are assessed. Beta-values (the ratio of the methylated probe intensity to the overall intensity, ranging from 0 indicating all unmethylated to 1 indicating all methylated) are calculated for each CpG site and converted to M-values (the log2 ratio of the intensity of the methylated probe versus unmethylated probe) for statistical analyses [41]. These data were normalized using functional normalization which corrects for technical variation and is recommended for data sets where global methylation changes are expected [42]. CpG sites were filtered for detection quality and probe binding specificity [43].

DNA methylation age

We used the DNA methylation age-based biomarker of aging from Horvath because a) its accurate measurement of age across tissues is unprecedented [14]; b) it has been found to be useful for studying aging effects in HIV infection [18]; c) it is prognostic for all-cause mortality [15, 44]; d) it correlates with measures of cognitive and physical fitness in the elderly [45]; e) it has been used in many applications including Down syndrome [46], obesity [23], lifetime stress [47], and Parkinson's disease [48]; and f) it is applicable to populations of all ages, not just the elderly [49, 50].

Here, we calculated the DNA methylation age for each sample according to the Horvath algorithm (http://labs.genetics.ucla.edu/Horvath/dnamage/) [14]. This method uses the weighted regression of 353 CpG sites on the Illumina 450K platform to calculate a methylation age. The age estimate (referred to as DNAm age or epigenetic age) is calibrated so that it is in units of years. The measure of epigenetic age acceleration was defined as the residual from regressing DNAm age on chronological age. By definition, this measure of age acceleration is not correlated with chronological age. Greater positivity in the age acceleration residual is indicative of faster age acceleration. The correlation between the age acceleration residual and duration of time along the study was calculated using a Pearson's correlation test. P-values <0.05 were considered significant.

Differentially methylated CpG sites

Because methylation profiles can be affected by cell type proportions [51], we used a deconvolution method for calculating the percentage of CD4 T cells, CD8 T cells, natural killer cells, monocytes, B-cells, and granulocytes in whole blood samples based on the methylation signature [52]. Differences in normalized methylation M-values between T1 and T2, T2 and T3, and T1 and T3 were modeled using a linear regression framework, adjusting for the differences in the cellular composition of peripheral blood between time points:

Methylation difference ~ intercept + CD4 T cell-difference + CD8 T cell-difference + natural killer cell-difference + monocyte-difference + B-cell-difference + granulocyte-difference

The coefficient of interest for which a t-statistic p-value is calculated is the intercept, the null hypothesis being that the methylation difference (represented by the intercept) between time points is 0. This inference was implemented using the limma algorithm [53]. CpG sites with false discovery rate (FDR) q-values <0.05 were considered to be differentially methylated with a high degree of confidence; however, given the small sample size, CpG sites with q-values <0.20 (considered differentially methylated with a medium degree of confidence) were also identified and retained for pyrosequencing validation.

Pyrosequencing validation

CpG sites considered to be differentially methylated between time points at a q-value <0.20 were validated using bisulfite pyrosequencing methods. Further details on pyrosequencing methods and primer design are provided in the Supplementary Materials. Reproducibility was assessed between pyrosequencing and the Illumina 450K normalized beta-values using Spearman's rank correlation.

Statistical program

All statistical analyses were performed using R version 3.2.1.

CONFLICTS OF INTEREST

The authors declare no conflicts of interest.

REFERENCES

1. Hogg RS, Heath KV, Yip B, Craib KJ, O'Shaughnessy MV, Schechter MT, Montaner JS. Improved survival among HIV-infected individuals following initiation of antiretroviral therapy. JAMA. 1998; 279:450–54. doi: 10.1001/jama.279.6.450

2. Samji H, Cescon A, Hogg RS, Modur SP, Althoff KN, Buchacz K, Burchell AN, Cohen M, Gebo KA, Gill MJ, Justice A, Kirk G, Klein MB, et al, and North American AIDS Cohort Collaboration on Research and Design (NA-ACCORD) of IeDEA. Closing the gap: increases in life expectancy among treated HIV-positive individuals in the United States and Canada. PLoS One. 2013; 8:e81355.
doi: 10.1371/journal.pone.0081355

3. Palella FJ Jr, Baker RK, Moorman AC, Chmiel JS, Wood KC, Brooks JT, Holmberg SD, and HIV Outpatient Study Investigators. Mortality in the highly active antiretroviral therapy era: changing causes of death and disease in the HIV outpatient study. J Acquir Immune Defic Syndr. 2006; 43:27–34. doi: 10.1097/01.qai.0000233310.90484.16

4. Gebo KA, Fleishman JA, Moore RD. Hospitalizations for metabolic conditions, opportunistic infections, and injection drug use among HIV patients: trends between 1996 and 2000 in 12 states. J Acquir Immune Defic Syndr. 2005; 40:609–16. doi: 10.1097/01.qai.0000171727.55553.78

5. Hsue PY, Lo JC, Franklin A, Bolger AF, Martin JN, Deeks SG, Waters DD. Progression of atherosclerosis as assessed by carotid intima-media thickness in patients with HIV infection. Circulation. 2004; 109:1603–08.
doi: 10.1161/01.CIR.0000124480.32233.8A

6. Crothers K, Butt AA, Gilbert CL, Rodriguez-Barradas MC, Crystal S, Justice AC. Veterans Aging Cohort 5 Project Team. Increased COPD among HIV-positive compared to HIV-negative veterans. Chest. 2006; 130:1326-33. doi: 10.1378/chest.130.5.1326

7. Crothers K, Huang L, Goulet JL, Goetz MB, Brown ST, Rodriguez-Barradas MC, Oursler KK, Rimland D, Gibert CL, Butt AA, Justice AC. HIV infection and risk for incident pulmonary diseases in the combination antiretroviral therapy era. Am J Respir Crit Care Med. 2011; 183:388–95. doi: 10.1164/rccm.201006-0836OC

8. Simard EP, Pfeiffer RM, Engels EA. Cumulative incidence of cancer among individuals with acquired immunodeficiency syndrome in the United States. Cancer. 2011; 117:1089–96. doi: 10.1002/cncr.25547

9. Pathai S, Bajillan H, Landay AL, High KP. Is HIV a model of accelerated or accentuated aging? J Gerontol A Biol Sci Med Sci. 2014; 69:833–42. doi: 10.1093/gerona/glt168

10. Pathai S, Lawn SD, Gilbert CE, McGuinness D, McGlynn L, Weiss HA, Port J, Christ T, Barclay K, Wood R, Bekker LG, Shiels PG. Accelerated biological ageing in HIV-infected individuals in South Africa: a case-control study. AIDS. 2013; 27:2375–84. doi: 10.1097/QAD.0b013e328363bf7f

11. Liu JC, Leung JM, Ngan DA, Nashta NF, Guillemi S, Harris M, Lima VD, Um SJ, Li Y, Tam S, Shaipanich T, Raju R, Hague C, et al. Absolute leukocyte telomere length in HIV-infected and uninfected individuals: evidence of accelerated cell senescence in HIV-associated chronic obstructive pulmonary disease. PLoS One. 2015; 10:e0124426.
doi: 10.1371/journal.pone.0124426

12. Côté HC, Soudeyns H, Thorne A, Alimenti A, Lamarre V, Maan EJ, Sattha B, Singer J, Lapointe N, Money DM, Forbes J, Wong J, Bitnun A, et al, and CIHR Emerging Team in HIV therapy, aging (CARMA). Leukocyte telomere length in HIV-infected and HIV-exposed uninfected children: shorter telomeres with uncontrolled HIV viremia. PLoS One. 2012; 7:e39266. doi: 10.1371/journal.pone.0039266

13. Research AFfA. 2011. Biomarkers of Aging. American Federation for Aging Research).

14. Horvath S. DNA methylation age of human tissues and cell types. Genome Biol. 2013; 14:R115. doi: 10.1186/gb-2013-14-10-r115

15. Marioni RE, Shah S, McRae AF, Chen BH, Colicino E, Harris SE, Gibson J, Henders AK, Redmond P, Cox SR, Pattie A, Corley J, Murphy L, et al. DNA methylation age of blood predicts all-cause mortality in later life. Genome Biol. 2015; 16:25. doi: 10.1186/s13059-015-0584-6

16. Rode L, Nordestgaard BG, Bojesen SE. Peripheral blood leukocyte telomere length and mortality among 64,637 individuals from the general population. J Natl Cancer Inst. 2015; 107:djv074. doi: 10.1093/jnci/djv074

17. Armanios M. Telomeres and age-related disease: how telomere biology informs clinical paradigms. J Clin

Invest. 2013; 123:996–1002. doi: 10.1172/JCI66370

18. Horvath S, Levine AJ. HIV-1 infection accelerates age according to the epigenetic clock. J Infect Dis. 2015; 212:1563–73. doi: 10.1093/infdis/jiv277

19. Müezzinler A, Zaineddin AK, Brenner H. A systematic review of leukocyte telomere length and age in adults. Ageing Res Rev. 2013; 12:509–19. doi: 10.1016/j.arr.2013.01.003

20. Sanders JL, Newman AB. Telomere length in epidemiology: a biomarker of aging, age-related disease, both, or neither? Epidemiol Rev. 2013; 35:112–31. doi: 10.1093/epirev/mxs008

21. Egger G, Liang G, Aparicio A, Jones PA. Epigenetics in human disease and prospects for epigenetic therapy. Nature. 2004; 429:457–63. doi: 10.1038/nature02625

22. Jones MJ, Goodman SJ, Kobor MS. DNA methylation and healthy human aging. Aging Cell. 2015; 14:924–32. doi: 10.1111/acel.12349

23. Horvath S, Erhart W, Brosch M, Ammerpohl O, von Schönfels W, Ahrens M, Heits N, Bell JT, Tsai PC, Spector TD, Deloukas P, Siebert R, Sipos B, et al. Obesity accelerates epigenetic aging of human liver. Proc Natl Acad Sci USA. 2014; 111:15538–43. doi: 10.1073/pnas.1412759111

24. Spear A, Sharma N, Flanegan JB. Protein-RNA tethering: the role of poly(C) binding protein 2 in poliovirus RNA replication. Virology. 2008; 374:280–91. doi: 10.1016/j.virol.2007.12.039

25. Chase AJ, Daijogo S, Semler BL. Inhibition of poliovirus-induced cleavage of cellular protein PCBP2 reduces the levels of viral RNA replication. J Virol. 2014; 88:3192–201. doi: 10.1128/JVI.02503-13

26. Murray CJ, Lopez AD. Alternative projections of mortality and disability by cause 1990-2020: Global Burden of Disease Study. Lancet. 1997; 349:1498–504. doi: 10.1016/S0140-6736(96)07492-2

27. Xin Z, Han W, Zhao Z, Xia Q, Yin B, Yuan J, Peng X. PCBP2 enhances the antiviral activity of IFN-α against HCV by stabilizing the mRNA of STAT1 and STAT2. PLoS One. 2011; 6:e25419.
doi: 10.1371/journal.pone.0025419

28. Wang L, Jeng KS, Lai MM. Poly(C)-binding protein 2 interacts with sequences required for viral replication in the hepatitis C virus (HCV) 5' untranslated region and directs HCV RNA replication through circularizing the viral genome. J Virol. 2011; 85:7954–64. doi: 10.1128/JVI.00339-11

29. Woolaway K, Asai K, Emili A, Cochrane A. hnRNP E1 and E2 have distinct roles in modulating HIV-1 gene expression. Retrovirology. 2007; 4:28.

doi: 10.1186/1742-4690-4-28

30. Ishiguro H, Tsunoda T, Tanaka T, Fujii Y, Nakamura Y, Furukawa Y. Identification of AXUD1, a novel human gene induced by AXIN1 and its reduced expression in human carcinomas of the lung, liver, colon and kidney. Oncogene. 2001; 20:5062–66. doi: 10.1038/sj.onc.1204603

31. Han P, Zhu X, Michaeli T. Alternative splicing of the high affinity cAMP-specific phosphodiesterase (PDE7A) mRNA in human skeletal muscle and heart. J Biol Chem. 1997; 272:16152–57.
doi: 10.1074/jbc.272.26.16152

32. Schoggins JW, Wilson SJ, Panis M, Murphy MY, Jones CT, Bieniasz P, Rice CM. A diverse range of gene products are effectors of the type I interferon antiviral response. Nature. 2011; 472:481–85. doi: 10.1038/nature09907

33. Lee HY, Xu Y, Huang Y, Ahn AH, Auburger GW, Pandolfo M, Kwiecinski H, Grimes DA, Lang AE, Nielsen JE, Averyanov Y, Servidei S, Friedman A, et al. The gene for paroxysmal non-kinesigenic dyskinesia encodes an enzyme in a stress response pathway. Hum Mol Genet. 2004; 13:3161–70.
doi: 10.1093/hmg/ddh330

34. Zhao H, Ito A, Sakai N, Matsuzawa Y, Yamashita S, Nojima H. RECS1 is a negative regulator of matrix metalloproteinase-9 production and aged RECS1 knockout mice are prone to aortic dilation. Circ J. 2006; 70:615–24. doi: 10.1253/circj.70.615

35. van Eijk KR, de Jong S, Boks MP, Langeveld T, Colas F, Veldink JH, de Kovel CG, Janson E, Strengman E, Langfelder P, Kahn RS, van den Berg LH, Horvath S, Ophoff RA. Genetic analysis of DNA methylation and gene expression levels in whole blood of healthy human subjects. BMC Genomics. 2012; 13:636. doi: 10.1186/1471-2164-13-636

36. Houseman EA, Kim S, Kelsey KT, Wiencke JK. DNA Methylation in Whole Blood: uses and Challenges. Curr Environ Health Rep. 2015; 2:145–54. doi: 10.1007/s40572-015-0050-3

37. Strathdee SA, Patrick DM, Currie SL, Cornelisse PG, Rekart ML, Montaner JS, Schechter MT, O'Shaughnessy MV. Needle exchange is not enough: lessons from the Vancouver injecting drug use study. AIDS. 1997; 11:F59–65. doi: 10.1097/00002030-199708000-00001

38. O'Callaghan NJ, Fenech M. A quantitative PCR method for measuring absolute telomere length. Biol Proced Online. 2011; 13:3. doi: 10.1186/1480-9222-13-3

39. Fehrer C, Voglauer R, Wieser M, Pfister G, Brunauer

R, Cioca D, Grubeck-Loebenstein B, Lepperdinger G. Techniques in gerontology: cell lines as standards for telomere length and telomerase activity assessment. Exp Gerontol. 2006; 41:648–51. doi: 10.1016/j.exger.2006.03.016

40. Morris TJ, Beck S. Analysis pipelines and packages for Infinium HumanMethylation450 BeadChip (450k) data. Methods. 2015; 72:3–8. doi: 10.1016/j.ymeth.2014.08.011

41. Du P, Zhang X, Huang CC, Jafari N, Kibbe WA, Hou L, Lin SM. Comparison of Beta-value and M-value methods for quantifying methylation levels by microarray analysis. BMC Bioinformatics. 2010; 11:587. doi: 10.1186/1471-2105-11-587

42. Fortin JP, Labbe A, Lemire M, Zanke BW, Hudson TJ, Fertig EJ, Greenwood CM, Hansen KD. Functional normalization of 450k methylation array data improves replication in large cancer studies. Genome Biol. 2014; 15:503. doi: 10.1186/s13059-014-0503-2

43. Chen YA, Lemire M, Choufani S, Butcher DT, Grafodatskaya D, Zanke BW, Gallinger S, Hudson TJ, Weksberg R. Discovery of cross-reactive probes and polymorphic CpGs in the Illumina Infinium HumanMethylation450 microarray. Epigenetics. 2013; 8:203–09. doi: 10.4161/epi.23470

44. Christiansen L, Lenart A, Tan Q, Vaupel JW, Aviv A, McGue M, Christensen K. DNA methylation age is associated with mortality in a longitudinal Danish twin study. Aging Cell. 2016; 15:149–54. doi: 10.1111/acel.12421

45. Marioni RE, Shah S, McRae AF, Ritchie SJ, Muniz-Terrera G, Harris SE, Gibson J, Redmond P, Cox SR, Pattie A, Corley J, Taylor A, Murphy L, et al. The epigenetic clock is correlated with physical and cognitive fitness in the Lothian Birth Cohort 1936. Int J Epidemiol. 2015; 44:1388–96. doi: 10.1093/ije/dyu277

46. Horvath S, Garagnani P, Bacalini MG, Pirazzini C, Salvioli S, Gentilini D, Di Blasio AM, Giuliani C, Tung S, Vinters HV, Franceschi C. Accelerated epigenetic aging in Down syndrome. Aging Cell. 2015; 14:491–95. doi: 10.1111/acel.12325

47. Zannas AS, Arloth J, Carrillo-Roa T, Iurato S, Röh S, Ressler KJ, Nemeroff CB, Smith AK, Bradley B, Heim C, Menke A, Lange JF, Brückl T, et al. Lifetime stress accelerates epigenetic aging in an urban, African American cohort: relevance of glucocorticoid signaling. Genome Biol. 2015; 16:266. doi: 10.1186/s13059-015-0828-5

48. Horvath S, Ritz BR. Increased epigenetic age and granulocyte counts in the blood of Parkinson's disease patients. Aging (Albany NY). 2015; 7:1130–42. doi: 10.18632/aging.100859

49. Walker RF, Liu JS, Peters BA, Ritz BR, Wu T, Ophoff RA, Horvath S. Epigenetic age analysis of children who seem to evade aging. Aging (Albany NY). 2015; 7:334–39. doi: 10.18632/aging.100744

50. Simpkin AJ, Hemani G, Suderman M, Gaunt TR, Lyttleton O, Mcardle WL, Ring SM, Sharp GC, Tilling K, Horvath S, Kunze S, Peters A, Waldenberger M, et al. Prenatal and early life influences on epigenetic age in children: a study of mother-offspring pairs from two cohort studies. Hum Mol Genet. 2016; 25:191–201. doi: 10.1093/hmg/ddv456

51. Reinius LE, Acevedo N, Joerink M, Pershagen G, Dahlén SE, Greco D, Söderhäll C, Scheynius A, Kere J. Differential DNA methylation in purified human blood cells: implications for cell lineage and studies on disease susceptibility. PLoS One. 2012; 7:e41361. doi: 10.1371/journal.pone.0041361

52. Houseman EA, Accomando WP, Koestler DC, Christensen BC, Marsit CJ, Nelson HH, Wiencke JK, Kelsey KT. DNA methylation arrays as surrogate measures of cell mixture distribution. BMC Bioinformatics. 2012; 13:86. doi: 10.1186/1471-2105-13-86

53. Smyth GK. Linear models and empirical bayes methods for assessing differential expression in microarray experiments. Stat Appl Genet Mol Biol. 2004; 3:e3. doi: 10.2202/1544-6115.1027

SUPPLEMENTARY MATERIAL

Pyrosequencing Methods

PyroMark Assay Design 2.0 (Qiagen, Inc.) software was used to design the bisulfate pyrosequencing assay covering the targets regions. DNA was subjected to bisulfite conversion using the EZ DNA Methylation Kit (Zymo Research). HotstarTaq DNA polymerase kit (Qiagen, Inc.) was used to amplify the target regions using the biotinylated primer set with the following PCR conditions: 15 minutes at 95°C, 45 cycles of 95°C for 30s, 58°C for 30s, and 72°C for 30s, and a 5 minute 72°C extension step. Streptavidin-coated sepharose beads were bound to the biotinylated-strand of the PCR product and then washed and denatured to yield single-stranded DNA. Sequencing primers were introduced to allow for pyrosequencing (Pyromark™ Q96 MD pyrosequencer, Qiagen, Inc.).

Pyrosequencing Primers

The following primers were used for pyrosequencing validation:

ID: 1 (cg07926733)
PCR Forward: F1 AGTTAAGTTAGAGTAGTATTGG ATTATAGT
PCR Reverse: R1 Biot CCTATCTCCCTTAAATTCTT AAAACT
Seq Primer: S1 Fwd TAGAGGGAGAGAGGT

ID: 2 (cg07151565)
PCR Forward: F1 AGTTGTTAGTTTTGGTTAGTTAT TTATAAT
PCR Reverse: R2 Biot AACCAAATTTCTTTACCCTT TTTTC
Seq Primer: S2 Fwd ATAGTGTTGGTGGGG

ID: 3 (cg23654821)
PCR Forward: F4 GGAGGAGGAAGTAGAGTTATT ATAT
PCR Reverse: R3 Biot ATAAACTAACAAACCTCA ACCTAATCTC
Seq Primer: S7 Fwd ATGTAAGTTGTGTGAATTAT TT

ID: 4 (cg21149466)
PCR Forward: F1 GTTATTAAAGGTGGATGTGTA TAGAAAA
PCR Reverse: R1 Biot AAAAACACATTCAAATCC CTAAATCT
Seq Primer: S1 Fwd TGTAAGTTATAGTATTAGAG AAGT

ID: 5 (cg02854554)
PCR Forward: F1 GTGGGTTAGGAGATTGAATTA
GTTT
PCR Reverse: R1 Biot AAACTCATTTCCTTACCAA TTTACTCA
Seq Primer: S17 Fwd GGTTTAGTTGTTTTTTG

ID: 6 (cg25353281)
PCR Forward: F1 GGTGGGAAGGGAGATATTAATG
PCR Reverse: R1 Biot CCCATTCCACACAACTACTAT
Seq Primer: S1 Fwd AGTTTTTATTTTTGTTTGTAAT GAT

A.

B.
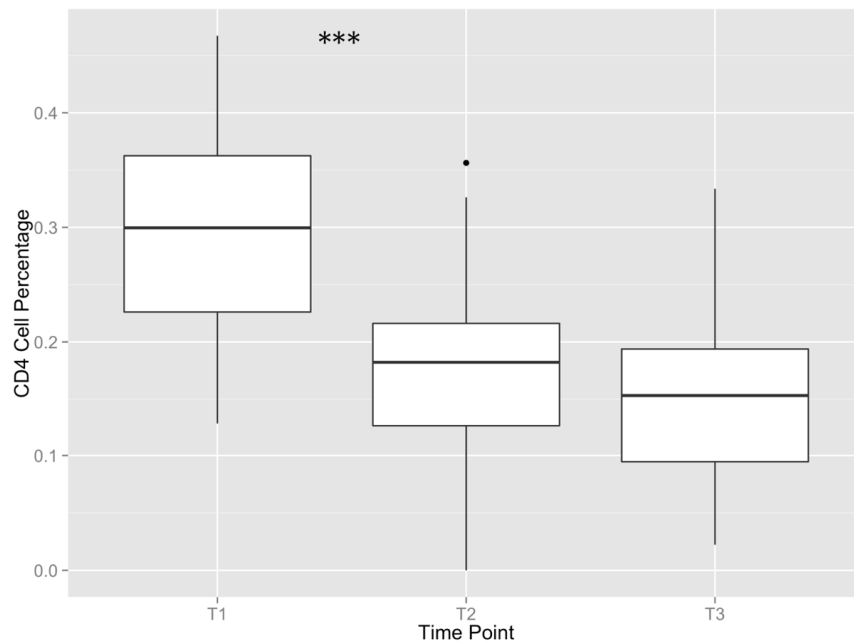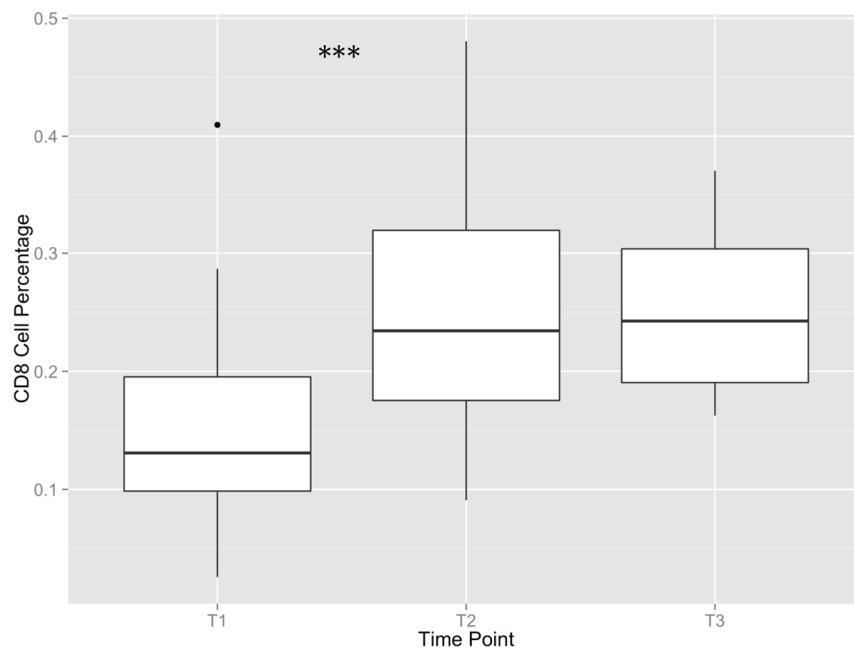
Supplementary Figure 1AB. Deconvolution methods by the Houseman-Jaffe algorithm yielded the cell proportions of (**A**) CD4 cells, (**B**) CD8 cells. Paired t-tests were performed to compare T1 vs. T2 and T2 vs. T3. There were statistically significant differences in the percentage of CD4 and CD8 cells between T1 and T2 (*** signifiying p<0.001). There were no statistically significant differences in the percentage of CD4 and CD8 cells between T2 and T3, nor were there statistically significant differences between any of the time points for monocytes, natural killer cells, granulocytes, and B cells.

C.

D.
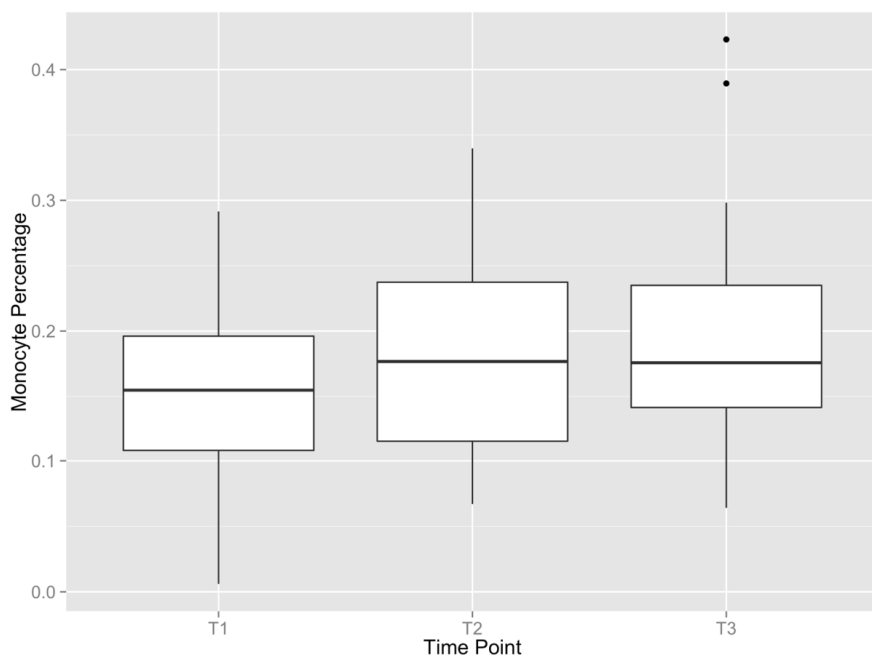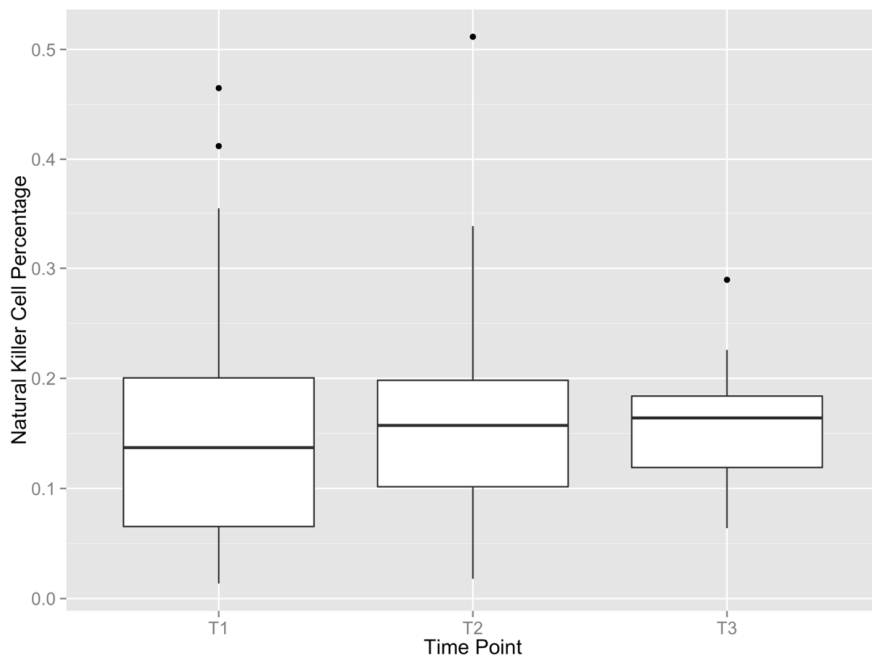
Supplementary Figure 1CD. Deconvolution methods by the Houseman-Jaffe algorithm yielded the cell proportions of (**C**) monocytes, (**D**) natural killer cells. Paired t-tests were performed to compare T1 vs. T2 and T2 vs. T3. There were statistically significant differences in the percentage of CD4 and CD8 cells between T1 and T2 (*** signifiying p<0.001). There were no statistically significant differences in the percentage of CD4 and CD8 cells between T2 and T3, nor were there statistically significant differences between any of the time points for monocytes, natural killer cells, granulocytes, and B cells.

E.

Time Point

F.

Time Point
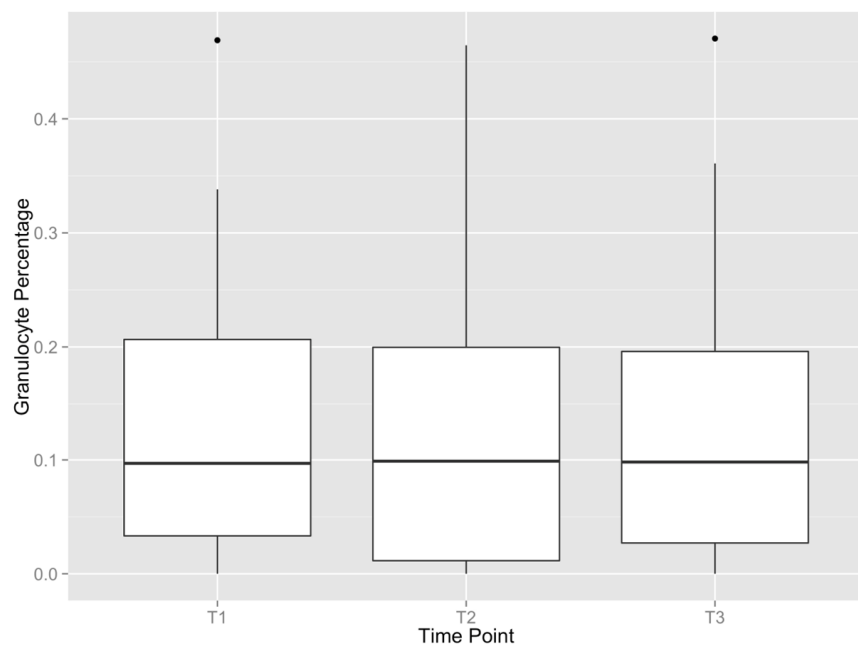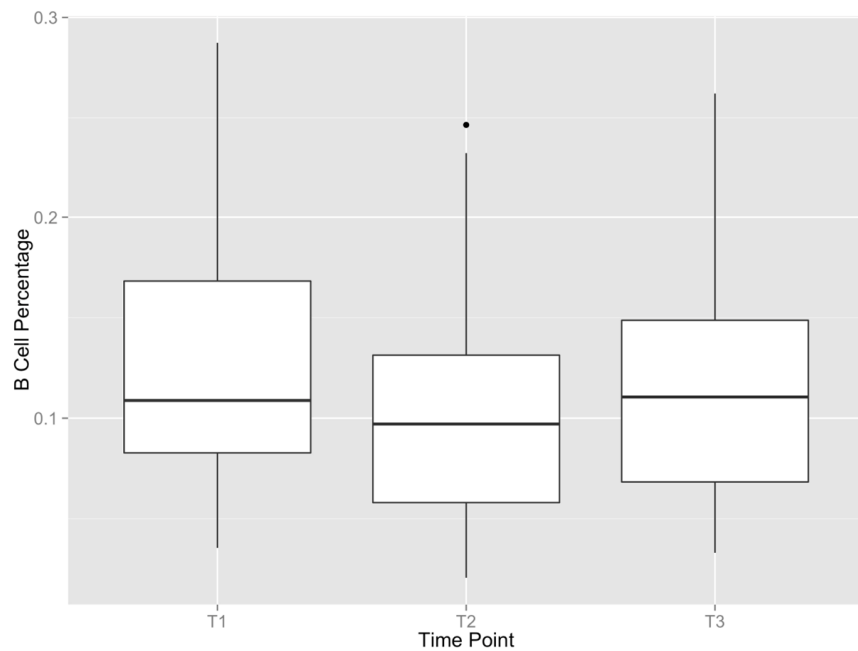
Supplementary Figure 1EF. Deconvolution methods by the Houseman-Jaffe algorithm yielded the cell proportions of (**E**) granulocytes, and **(F)** B-cells. Paired t-tests were performed to compare T1 vs. T2 and T2 vs. T3. There were statistically significant differences in the percentage of CD4 and CD8 cells between T1 and T2 (*** signifiying p<0.001). There were no statistically significant differences in the percentage of CD4 and CD8 cells between T2 and T3, nor were there statistically significant differences between any of the time points for monocytes, natural killer cells, granulocytes, and B cells.

A.

cg07151565, p=0.003, R=0.402

B.

cg02854554, p=5.373e-14, R=0.816
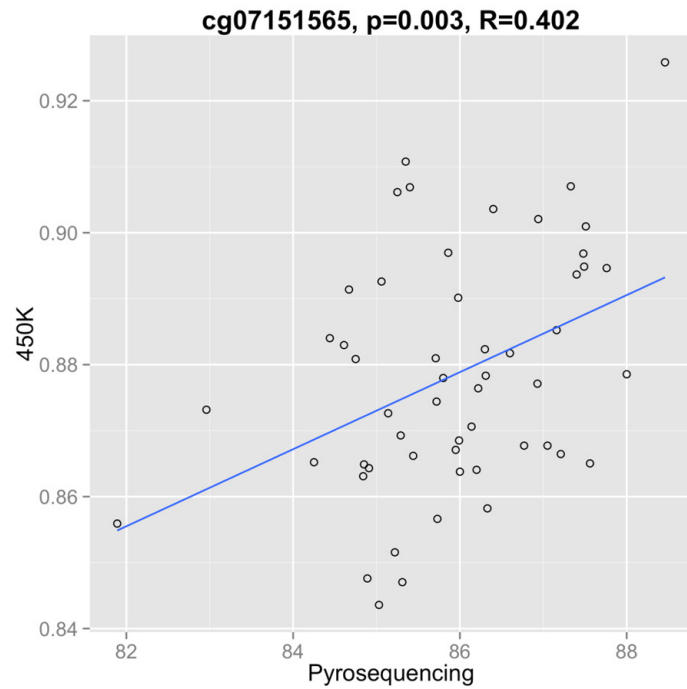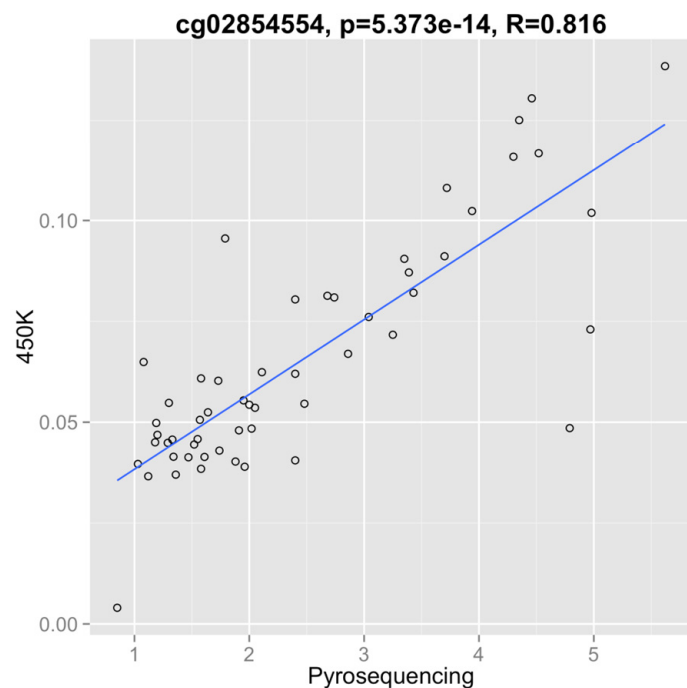
Supplementary Figure 2AB. Spearman correlation plots for 450K methylation beta-values vs.pyrosequencing methylation beta-values. (**A**) cg07151565, (**B**) cg02854554.

C.

cg21149466, p=3.92e-05, R=0.533

D.

cg23654821, p=5.325e-13, R=0.807
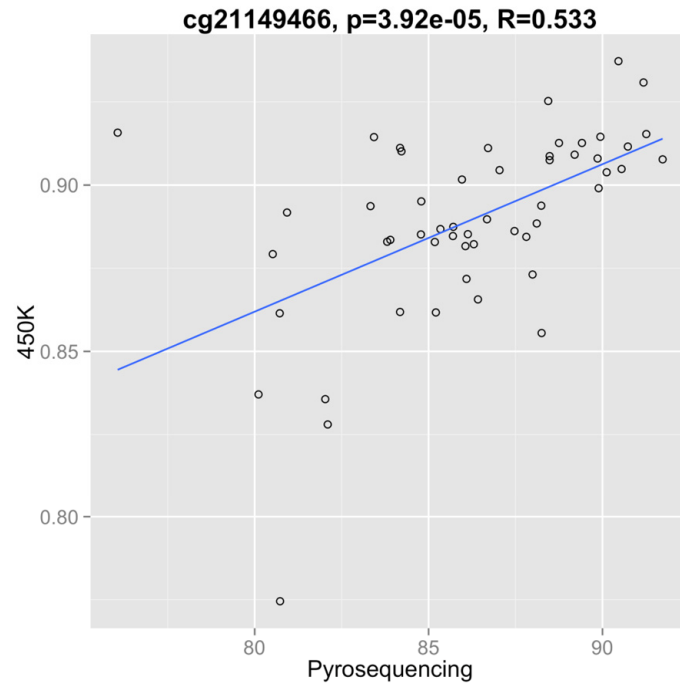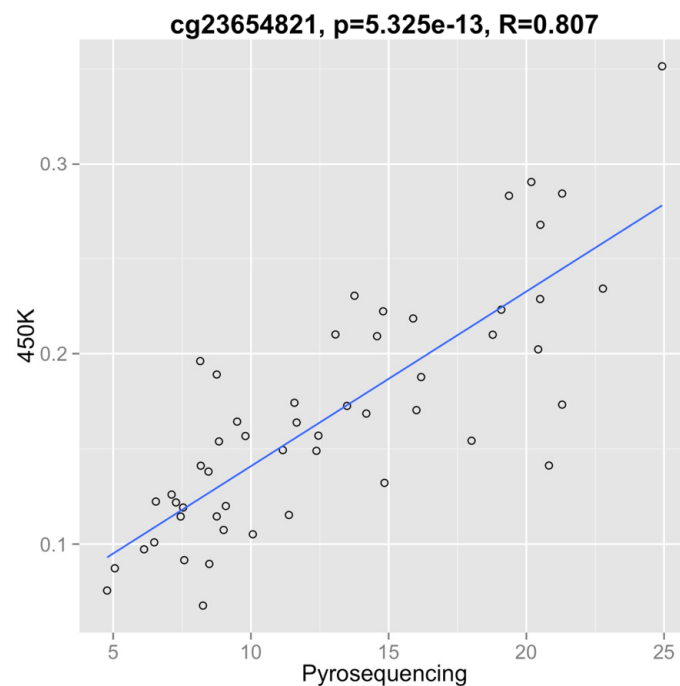
Supplementary Figure 2CD. Spearman correlation plots for 450K methylation beta-values vs.pyrosequencing methylation beta-values. (**C**) cg21149466, (**D**) cg23654821.

E.

F.
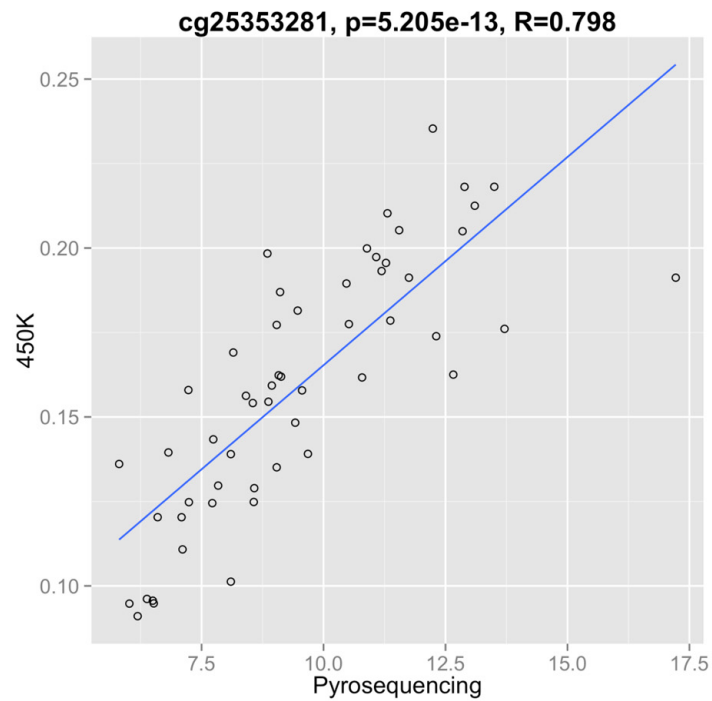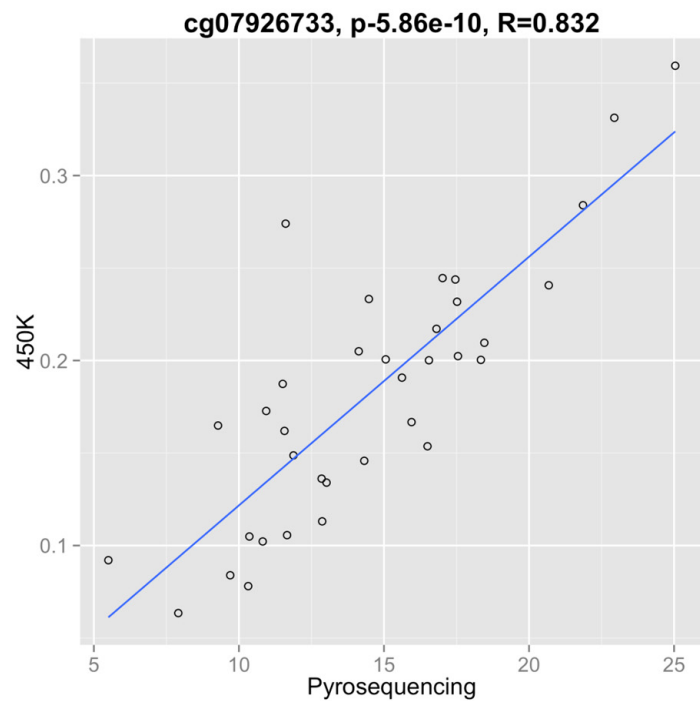
Supplementary Figure 2EF. Spearman correlation plots for 450K methylation beta-values vs.pyrosequencing methylation beta-values. (**E**) cg25353281, (**F**) cg07926733.

A.

B.
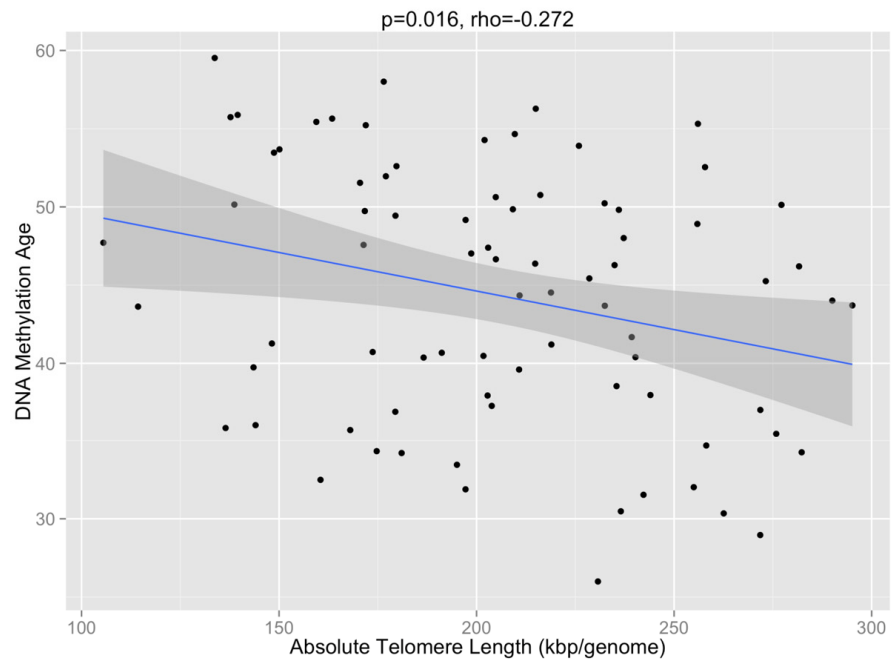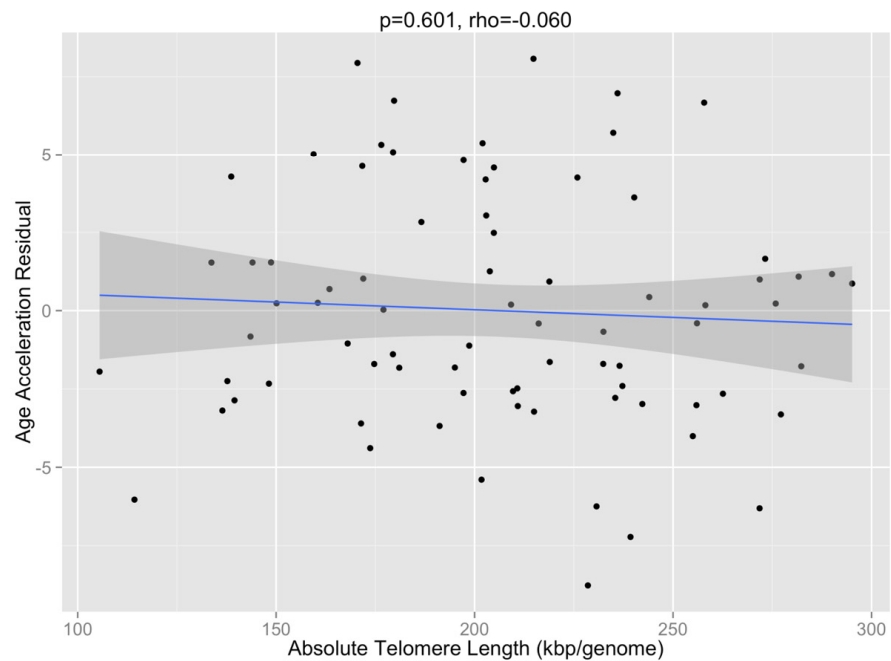
Supplementary Figure 3. Correlation plots between DNA methylation age and telomere length (Figure 3A) and between the age acceleration residual and telomere length (Figure 3B). These demonstrate very weak correlations between methylomic aging changes and telomere length.

Epigenetic clock analysis of diet, exercise, education, and lifestyle factors

Austin Quach[1*], Morgan E. Levine[1*], Toshiko Tanaka[2*], Ake T. Lu[1], Brian H. Chen[2], Luigi Ferrucci[2], Beate Ritz[3,4], Stefania Bandinelli[5], Marian L. Neuhouser[6], Jeannette M. Beasley[7], Linda Snetselaar[8], Robert B. Wallace[8], Philip S. Tsao[9,10], Devin Absher[11], Themistocles L. Assimes[9], James D. Stewart[12], Yun Li[13,14], Lifang Hou[15,16], Andrea A. Baccarelli[17], Eric A. Whitsel[12,18], Steve Horvath[1,19]

[1]Department of Human Genetics, David Geffen School of Medicine, University of California Los Angeles, Los Angeles, CA 90095, USA

[2]Longitudinal Studies Section, Translational Gerontology Branch, National Institute on Aging, National Institutes of Health, USA. Baltimore, MD 21224, USA

[3]Department of Neurology, UCLA School of Medicine, University of California Los Angeles, Los Angeles, CA 90095, USA

[4]Department of Epidemiology, UCLA Fielding School of Public Health, University of California Los Angeles, Los Angeles, CA 90095, USA

[5]Geriatric Unit, Azienda Sanitaria Firenze (ASF), Florence, Italy

[6]Cancer Prevention Program, Division of Public Health Sciences, Fred Hutchinson Cancer Research Center, Seattle, WA 98109, USA

[7]Department of Medicine, New York University, New York, NY 10016, USA

[8]Department of Epidemiology, University of Iowa, 145 N. Riverside Drive, Iowa City, IA 52242, USA

[9]Department of Medicine, Stanford University School of Medicine, Stanford, CA 94305, USA

[10]VA Palo Alto Health Care System, Palo Alto CA 94304, USA

[11]HudsonAlpha Institute for Biotechnology, Huntsville, AL 35806, USA

[12] Department of Epidemiology, Gillings School of Global Public Health, University of North Carolina, Chapel Hill, NC 27599, USA

[13] Department of Genetics, School of Medicine, University of North Carolina, Chapel Hill, NC 27599, USA

[14] Department of Biostatistics, Gillings School of Global Public Health, University of North Carolina, Chapel Hill, NC 27599, USA

[15]Department of Preventive Medicine, Feinberg School of Medicine, Northwestern University Chicago, IL 60611, USA

[16]Robert H. Lurie Comprehensive Cancer Center, Feinberg School of Medicine, Northwestern University Chicago, IL 60611, USA

[17]Laboratory of Environmental Epigenetics, Departments of Environmental Health Sciences Epidemiology, Columbia University Mailman School of Public Health, New York, NY 10032, USA

[18]Department of Medicine, School of Medicine, University of North Carolina, Chapel Hill, NC 27599, USA

[19]Dept. of Biostatistics, Fielding School of Public Health, University of California Los Angeles, Los Angeles, CA 90095, USA

ABSTRACT

Behavioral and lifestyle factors have been shown to relate to a number of health-related outcomes, yet there is a need for studies that examine their relationship to molecular aging rates. Toward this end, we use recent epi-

genetic biomarkers of age that have previously been shown to predict all-cause mortality, chronic conditions and age-related functional decline. We analyze cross-sectional data from 4,173 postmenopausal female participants from the Women's Health Initiative, as well as 402 male and female participants from the Italian cohort study, Invecchiare nel Chianti.

Extrinsic epigenetic age acceleration (EEAA) exhibits significant associations with fish intake (p=0.02), moderate alcohol consumption (p=0.01), education (p=3×10^{-5}), BMI (p=0.01), and blood carotenoid levels (p=1×10^{-5})—an indicator of fruit and vegetable consumption, whereas intrinsic epigenetic age acceleration (IEAA) is associated with poultry intake (p=0.03) and BMI (p=0.05). Both EEAA and IEAA were also found to relate to indicators of metabolic syndrome, which appear to mediate their associations with BMI. Metformin—the first-line medication for the treatment of type 2 diabetes—does not delay epigenetic aging in this observational study. Finally, longitudinal data suggests that an increase in BMI is associated with increase in both EEAA and IEAA.

Overall, the epigenetic age analysis of blood confirms the conventional wisdom regarding the benefits of eating a high plant diet with lean meats, moderate alcohol consumption, physical activity, and education, as well as the health risks of obesity and metabolic syndrome.

INTRODUCTION

A number of behavioral lifestyle factors have been shown to relate to health, including diet, physical activity, moderate alcohol consumption, and educational attainment. For instance, diet is a modifiable behavior with the potential to mitigate chronic disease risk. Various dietary components have been reported to influence intermediate risk factors and the prevalence of age-related disease outcomes; thus there is a growing consensus regarding nutritional recommendations for maintaining optimal health. These dietary factors include whole grain & dietary fiber [1], fish & omega-3 fatty acids [2], and fruits & vegetables [3], all of which may be involved in reducing systemic inflammation [4]. Further, metabolic health has been established as one of the primary mechanisms through which diet affects health and disease [5]. Conditions such as, insulin resistance, hypercholesterolemia, hypertension, hypertryglyceremia, and systemic inflammation can be promoted by poor dietary habits and often coalesce, influencing a person's risk of atherosclerosis, diabetes mellitus, and stroke [6-8].

In addition to diet, other behaviors such as moderate alcohol consumption, increased physical activity, and higher educational attainment have all been linked to reductions in morbidity and mortality risk [9-16]. Yet, despite the strong evidence connecting lifestyle factors to health outcomes, it is still unclear whether these factors directly influence aging on a molecular level. In previous work, leukocyte telomere length (LTL) has been used to investigate the influence of lifestyle factors on replicative aging in blood [17-21]. A cross-sectional study of 2,284 participants from the Nurses' Health Study reported that LTL was associated with BMI, waist circumference, and dietary intake of total fat, polyunsaturated fatty acids, and fiber [22]. LTL was also found to be longer among individuals who were more physically active [23, 24], as well has those with higher levels of education [25].

Another promising measure for investigating the dynamics between lifestyle and aging is the molecular biomarker known as the "epigenetic clock". Chronological age has been shown to have a profound effect on DNA methylation levels [26-34]. As a result, several highly accurate epigenetic biomarkers of chronological age have been proposed [35-39]. These biomarkers use weighted averages of methylation levels at specific CpG sites to produce estimates of age (in units of years), referred to as "DNA methylation age" (DNAm age) or "epigenetic age". Recent studies support the idea that these measures are at least passive biomarkers of biological age. For instance, the epigenetic age of blood has been found to be predictive of all-cause mortality [40-43], frailty [44], lung cancer [45], and cognitive and physical functioning [46], while the blood of the offspring of Italian semi-super-centenarians (i.e. participants aged 105 or older) was shown to have a lower epigenetic age than that of age-matched controls [47]. Further, the utility of the epigenetic clock method using various tissues and organs has been demonstrated in applications surrounding Alzheimer's disease [48], centenarian status [47, 49], development [50], Down syndrome [51], frailty [44], HIV infection [52], Huntington's disease [53], obesity [54], lifetime stress [55], menopause [56], osteoarthritis [57], and Parkinson's disease [58].

However, relatively little is known about the relationship between epigenetic aging rates and lifestyle factors, such as diet, alcohol consumption, physical activity, and educational attainment. Here, we investigate these relationships by leveraging blood DNA methylation data from two large epidemiological cohorts. In our primary analysis, we use data from older women within the Women's Health Initiative (WHI) to

examine the relationships between epigenetic age acceleration in blood and dietary variables, education, alcohol, and exercise. In our secondary analysis, we sought to validate the results in the Invecchiare nel Chianti (InCHIANTI) Study, which is a population-based prospective cohort study of residents ages 21 or older from two areas in the Chianti region of Tuscany, Italy.

Since our study revealed that metabolic syndrome is associated with accelerated epigenetic aging, we also carried out a post-hoc analysis that evaluated the effect of metformin, which is a widely-used medication against type 2 diabetes.

RESULTS

Sample characteristics

The WHI sample consisted of 4,173 postmenopausal women including 2,045 Caucasians, 1,192 African Americans, and 717 Hispanics. Chronological age ranged from 50-82 years (mean=64, s.d.=7.1). The InCHIANTI sample was composed of 402 participants from a European (Italian) population, including 178 men (44%) and 229 women (56%). We used the most current cross-sectional wave for this cohort, and at that time-point participants ranged in age from 30 to 100 years (mean=71, s.d.=16). Additional details on participant characteristics can be found in the Methods and in Table 1.

Dietary and metabolic associations with measures of age acceleration

Here we leverage two distinct measures of epigenetic age acceleration which are based on different sets of CpGs: *intrinsic* epigenetic age acceleration (IEAA), and *extrinsic* epigenetic age acceleration (EEAA) (Methods). Epigenetic age acceleration is broadly defined as the epigenetic age left unexplained by chronological age, where intrinsic and extrinsic denote additional modifications to this concept. In addition to adjusting for chronologic age, IEAA also adjusts the epigenetic clock for blood cell count estimates, arriving at a measure that is unaffected by both variation in chronologic age and blood cell composition. EEAA, on the other hand, integrates known age-related changes in blood cell counts with a blood-based measure of epigenetic age [37] before adjusting for chronologic age, making EEAA dependent on age-related changes in blood cell composition. In essence, IEAA can be interpreted as a measure of cell-intrinsic aging and EEAA as a measure of immune system aging, where for both, a positive value indicates that the epigenetic age of an individual (organ or tissue) is higher than

expected based on their chronological age—or that the individual is exhibiting accelerated epigenetic aging. We find that IEAA is only moderately correlated with EEAA (r=0.37), and that measurements on the same individuals at different time points (mean difference 3.0 years between visit dates) showed moderately strong correlations (IEAA r=0.70, EEAA r=0.66).

We first used a robust correlation test to relate our two measures of epigenetic aging (IEAA and EEAA) to select reported dietary exposures, blood nutrient levels, cardiometabolic plasma biomarkers, and lifestyle factors, designating a Bonferroni-corrected significance threshold of $\alpha=7\times10^{-4}$ (Figure 1). The correlation test results for specific racial/ethnic groups are presented in Supplementary Figure 1 and select marginal associations are shown as bar plots in Supplementary Figure 2. Pairwise correlations between dietary variables, metabolic biomarkers, and lifestyle factors are presented in Supplementary Figure 3.

EEAA exhibits weak but statistically significant correlations with fish intake (r=-0.07, p=2×10^{-5}), alcohol consumption (r=-0.07, p=3×10^{-5}, Supplementary Figure 4), plasma levels of mean carotenoids (r=-0.13, p=2×10^{-9}), alpha-carotene (r=-0.11, p=9×10^{-8}), beta-carotene (r=-0.11, p=3×10^{-7}), lutein+zeaxanthin (r=-0.9, p=1×10^{-5}), beta-cryptoxanthin (r=-0.11, p=3×10^{-7}), gamma-tocopherol (r=0.09, p=9×10^{-6}), triglyceride (r=0.7, p=6×10^{-6}), C-reactive protein (CRP, r=0.12, p=2×10^{-10}), insulin (r=0.11, p=3×10^{-12}), HDL cholesterol (r=-0.09, p=2×10^{-8}), glucose (r=0.06, p=2×10^{-4}), systolic blood pressure (r=0.07, p=4×10^{-6}), waist-to-hip ratio (WHR, r=0.09, p=2×10^{-8}), BMI (r=0.09, p=2×10^{-8}), education (r=-0.10, p=3×10^{-10}), income (r=-0.06, p=1×10^{-4}), and exercise (r=-0.07, p=2×10^{-5}, Figure 1). In contrast, the intrinsic epigenetic aging rate exhibits weaker correlations with dietary variables and lifestyle factors: IEAA is only associated with BMI (r=0.08, p=1×10^{-6}), and plasma levels of gamma-tocopherol (r=0.08, p=2×10^{-4}), CRP (r=0.08, p=6×10^{-5}), insulin (r=0.07, p=2×10^{-5}), glucose (r=0.06, p=8×10^{-5}), and triglyceride levels (r=0.05, p=5×10^{-4}, Figure 1).

Meta-analysis of multivariable linear models link epigenetic age acceleration to diet

Associations with EEAA

We have recently shown that ethnicity relates to epigenetic aging rates: e.g. Hispanics have lower levels of IEAA compared to other ethnic groups [59]. Given the potential for confounding by sociodemographic and lifestyle factors, we used Stouffer's method to meta-analyze multivariate linear models, stratified by racial/ethnic group, in order to re-examine the

suggestive associations from our marginal correlation analysis. After adjusting for sex and dataset (Figure 2A), we find that lower EEAA is significantly associated with greater intake of fish (t_{meta}=-2.92, p_{meta}=0.003), higher education (t_{meta}=-4.14, p_{meta}=3x10^{-5}), lower BMI (t_{meta}=4.86, p_{meta}=1x10^{-6}), and current drinker status (t_{meta}=-3.23, p_{meta}=0.001). However, we find no association for current smoking status, and poultry intake, and only a trend toward association with physical activity (t_{meta}=-1.70, p_{meta}=0.09). In the subset of WHI participants with circulating carotenoid measurements, we also find that mean carotenoid levels are associated with EEAA (t_{meta}=-4.34, p_{meta}=1x10^{-5}, Supplementary Figure 5A).

		n	μ	IEAA bicor	IEAA p	EEAA bicor	EEAA p
Diet	log2(Total energy)	3687	10.53	0.00	0.96	-0.02	0.19
	Carbohydrate	3687	49.01	0.02	0.29	0.00	0.96
	Protein	3687	16.50	-0.02	0.15	-0.03	0.10
	Fat	3687	34.66	0.00	0.97	0.02	0.15
	log2(1+Red meat)	3687	0.75	0.03	0.10	0.02	0.28
	log2(1+Poultry)	3687	0.45	-0.05	4E-3	-0.03	0.05
	log2(1+Fish)	3687	0.31	-0.02	0.30	-0.07	2E-5
	log2(1+Dairy)	3687	1.25	0.00	0.99	-0.02	0.29
	log2(1+Whole grains)	3687	1.03	0.00	0.85	-0.02	0.19
	log2(1+Nuts)	3687	0.19	0.01	0.51	-0.02	0.36
	log2(Fruits)	3687	0.32	0.00	0.81	-0.03	0.04
	log2(Vegetables)	3687	0.62	0.00	0.98	-0.04	0.01
Blood nutrients	Retinol	2268	0.59	0.02	0.46	-0.01	0.69
	Mean carotenoids	2267	0.01	-0.06	4E-3	-0.13	2E-9
	Lycopene	2268	0.40	-0.02	0.44	-0.03	0.17
	log2(alpha-Carotene)	2268	-4.22	-0.04	0.04	-0.11	9E-8
	log2(beta-Carotene)	2267	-2.18	-0.06	0.01	-0.11	3E-7
	log2(Lutein+Zeaxanthin)	2268	-2.38	-0.04	0.09	-0.09	1E-5
	log2(beta-Cryptoxanthin)	2268	-3.74	-0.06	2E-3	-0.11	3E-7
	log2(alpha-Tocopherol)	2268	3.94	-0.04	0.07	-0.06	0.01
	log2(gamma-Tocopherol)	2268	0.68	0.08	2E-4	0.09	9E-6
Measurements	log2(C-reactive protein)	2809	1.54	0.08	6E-5	0.12	2E-10
	log2(Insulin)	4043	5.81	0.07	2E-5	0.11	3E-12
	log2(Glucose)	4145	6.66	0.06	8E-5	0.06	2E-4
	log2(Triglyceride)	4149	7.05	0.05	5E-4	0.07	6E-6
	Total cholesterol	4149	227.31	0.03	0.04	0.01	0.62
	LDL cholesterol	4085	142.85	0.03	0.06	0.01	0.41
	HDL cholesterol	4146	54.86	-0.04	0.01	-0.09	1E-8
	log2(Creatinine)	2748	-0.42	0.01	0.74	0.02	0.26
	Systolic blood pressure	4165	130.17	0.04	5E-3	0.07	4E-6
	Diastolic blood pressure	4165	75.86	0.05	3E-3	0.04	0.01
	log2(Waist / hip ratio)	4165	-0.28	0.05	3E-3	0.09	2E-8
	BMI	4165	29.69	0.08	1E-6	0.09	2E-8
Socio-behavioral	Education	4130	6.80	-0.02	0.14	-0.10	3E-10
	Income	4041	3.73	0.00	0.79	-0.06	1E-4
	log2(1+Exercise)	4142	2.53	-0.04	0.01	-0.07	2E-5
	Current smoker	4142	0.12	0.00	0.78	-0.01	0.66
	log2(1+Alcohol)	3687	1.10	-0.02	0.21	-0.07	3E-5

Table header: Pooled WHI samples — Adjusted for ethnicity and dataset

Figure 1. Marginal correlations with epigenetic age acceleration in the WHI. Correlations (bicor, biweight midcorrelation) between select variables and the two measures of epigenetic age acceleration are colored according to their magnitude with positive correlations in red, negative correlations in blue, and statistical significance (p-values) in green. Blood biomarkers were measured from fasting plasma collected at baseline. Food groups and nutrients are inclusive, including all types and all preparation methods, e.g. folic acid includes synthetic and natural, dairy includes cheese and all types of milk, etc. Variables are adjusted for ethnicity and dataset (BA23 or AS315).

Table 1. Characteristics of the WHI and InCHIANTI samples.

			WHI		InCHIANTI	
			Count	Percent	Count	Percent
Ethnic	American Indian or Alaskan Native		56	1%		
	Asian or Pacific Islander		140	3%		
	Black or African-American		1277	28%		
	Hispanic/Latino		784	17%		
	White (not of Hispanic origin)		2196	49%		
	Other		37	1%		
WHI data set	BA23		2098	47%		
	AS315		2392	53%		
Sex	Male				178	44%
	Female				229	56%
Current smoker	Nonsmoker		4027	90%	367	90%
	Smoker		439	10%	40	10%
Education	< Primary		43	1%	80	20%
	> Primary		154	3%	154	38%
	> Lower secondary		293	7%	91	22%
	> Upper secondary		2588	58%	62	15%
	> Higher		1393	31%	20	5%
Physical activity	Active		894	20%	329	81%
	Inactive		3572	80%	78	19%
			Mean	SD	Mean	SD
Diet	Total energy, kcal	kcal/day	1641	777	2069	573
	Carbohydrate	% kcal	49.0	9.1	52.4	6.9
	Protein	% kcal	16.5	3.3	15.8	2.0
	Fat	% kcal	34.6	8.1	30.9	5.5
	Red meat	serv/day	0.8	0.7	1.1	0.5
	Poultry	serv/day	0.4	0.3	0.2	0.2
	Fish	serv/day	0.3	0.3	0.2	0.2
	Dairy	serv/day	1.6	1.3	2.8	1.8
	Whole grains	serv/day	1.2	0.9		
	Nuts	serv/day	0.2	0.3	0.0	0.1
	Fruits	serv/day	1.7	1.3	1.9	0.9
	Vegetables	serv/day	1.9	1.3	1.6	0.8
	Alcohol	g/day	3.6	9.6	12.7	14.9
Measurements	IEAA	years	0.0	4.7	0.2	4.6
	EEAA	years	0.0	6.0	-0.2	6.5
	C-reactive protein	mg/L	5.2	6.6	3.9	7.4
	Insulin	mg/dL	57.1	115.3		
	Glucose	mg/dL	106.3	38.0	93.0	21.3
	Triglycerides	mg/dL	146.4	85.6	122.7	81.5
	Total cholesterol	mg/dL	228.4	42.7	207.2	36.6
	LDL cholesterol	mg/dL	144.9	39.7	125.5	32.1
	HDL cholesterol	mg/dL	54.0	14.3	57.6	15.7
	Creatinine	mg/dL	0.8	0.2	0.9	0.4
	Systolic blood pressure	mmHg	130.0	18.0	129.3	19.8
	Diastolic blood pressure	mmHg	75.8	9.4	77.2	10.3
	Waist / hip ratio	cm/cm	0.8	0.1	0.9	0.1
	BMI	cm/m2	29.7	6.0	27.0	4.3

The cohort samples are listed for each column and variables of interest are listed for each row. The upper portion of the table correspond to categorical variables and are described using counts and percentages; the lower portion of the table displays continuous variables which are described using means and standard deviations (SD).

A

EEAA	WHI Caucasian		WHI African		WHI Hispanic		WHI Asian		InCHIANTI		Meta-analysis	
n	1807		1058		618		100		402		3985	
	β	p	β	p	β	p	β	p	β	p	meta-t	meta-p
log2(1 + Fish)	-0.83	0.19	-1.05	0.12	-1.13	0.24	-0.55	0.78	-3.61	0.02	-2.92	3E-3
log2(1 + Poultry)	-0.72	0.20	0.41	0.51	-0.15	0.83	2.06	0.29	-1.35	0.35	-0.73	0.46
Current drinker	-0.66	0.02	-0.01	0.99	-1.58	9E-4	-2.13	0.07	-0.11	0.87	-3.23	1E-3
Education	-0.19	0.01	-0.20	0.05	-0.23	0.03	-0.03	0.91	-0.13	0.06	-4.14	3E-5
BMI	0.09	5E-4	0.10	3E-3	0.07	0.10	0.17	0.13	0.02	0.82	4.86	1E-6
Physically active	-0.61	0.09	-0.11	0.82	-0.09	0.87	-2.69	0.08	-0.23	0.78	-1.70	0.09
Current smoker	0.19	0.66	1.09	0.06	-0.80	0.23	-0.25	0.93	-2.34	0.02	0.07	0.94

B

IEAA	WHI Caucasian		WHI African		WHI Hispanic		WHI Asian		InCHIANTI		Meta-analysis	
n	1807		1058		618		100		402		3985	
	β	p	β	p	β	p	β	p	β	p	meta-t	meta-p
log2(1 + Fish)	0.61	0.24	-0.85	0.12	0.38	0.60	1.03	0.53	-2.51	0.03	-0.38	0.71
log2(1 + Poultry)	-1.20	0.01	-0.15	0.76	-0.42	0.43	-2.28	0.17	-2.86	0.01	-3.30	1E-3
Current drinker	-0.09	0.70	-0.11	0.75	-0.43	0.23	1.04	0.29	0.61	0.25	-0.36	0.72
Education	0.01	0.84	-0.10	0.21	0.03	0.73	-0.34	0.16	-0.01	0.78	-0.68	0.49
BMI	0.08	3E-5	0.04	0.17	0.02	0.60	0.35	5E-4	-0.03	0.56	4.14	4E-5
Physically active	0.06	0.84	-0.40	0.28	-0.15	0.71	-2.22	0.09	-0.43	0.48	-1.06	0.29
Current smoker	0.07	0.83	0.23	0.62	0.30	0.56	0.01	1.00	-1.25	0.11	0.12	0.91

Figure 2. Meta-analysis of multivariable linear models of EEAA and IEAA in the WHI and InCHIANTI. EEAA (panel **A**) and IEAA (panel **B**) were regressed on potential confounding factors, fish and poultry intake, and current drinker status for the ethnic strata with sufficient sample sizes (n>100). Individual columns correspond to coefficient estimates (β) colored blue or red for negative and positive values respectively, and p-values (p) colored in green according to magnitude of significance, with the exception of the last two columns which denote Stouffer's method meta-t and meta-p values. Models are adjusted for originating dataset (WHI BA23 or AS315) and for sex (InCHIANTI).

Multivariate linear models were used to examine whether variations in cardiometabolic biomarkers and/or the number of symptoms for metabolic syndrome accounted for any of the associations between EEAA and lifestyle factors. The inclusion of biomarkers in an unstratified model shows that EEAA positively relates to CRP (log2, β=0.31, p=3x10^-4, Figure 3A, model 3) and that this is accompanied by a concomitant diminishing in the effect size of BMI (67% decrease in coefficient magnitude, Figure 3A, model 2 vs. model 5), suggesting that higher CRP may partially explain the positive association between BMI and EEAA. When metabolic syndrome (MetS) was included in the model, results showed that higher EEAA is positively associated with the number of metabolic syndrome symptoms (β=0.29, p=0.002, Figure 3A, model 4). In the subset of participants with both biomarker and caro-

tenoid measurements, EEAA was negatively associated with mean carotenoid levels (β=-1.10, p=1x10^-4) while appearing to diminish associations with biomarkers (Supplementary Figure 6A, model 5).

Additionally, we find that for the small subset of individuals for whom we have EEAA measurements at two time points (n=239, mean time interval = 2.7 years), increase in BMI (β=0.40, p=0.002) but not initial BMI (β=-0.01, p=0.81) is significantly associated with increased EEAA (higher follow-up EEAA after adjusting for the initial EEAA, dataset, and ethnicity).

Associations with IEAA
We conducted an analogous meta-analysis of ethnically-stratified linear models of IEAA and found that lower IEAA was significantly associated with poultry intake

A

EEAA n=2725	Model 1 Minimal		Model 2 Food		Model 3 Biomarkers		Model 4 MetS		Model 5 Full	
	β	p	β	p	β	p	β	p	β	p
log2(1 + Fish)			-1.23	0.01					-1.13	0.02
log2(1 + Poultry)			-0.03	0.94					-0.05	0.90
Current drinker			-0.63	0.01					-0.54	0.03
Education	-0.27	7E-6	-0.22	2E-4	-0.24	5E-5	-0.25	2E-5	-0.20	8E-4
BMI	0.09	1E-5	0.09	2E-5	0.02	0.46	0.06	0.01	0.03	0.26
Physically active	-0.54	0.06	-0.44	0.14	-0.41	0.15	-0.49	0.08	-0.33	0.25
Current smoker	0.30	0.38	0.33	0.32	0.23	0.50	0.26	0.43	0.28	0.41
African American	-2.31	1E-17	-2.32	5E-17	-2.34	6E-16	-2.22	3E-16	-2.36	1E-15
Hispanic	1.07	8E-4	0.98	2E-3	0.93	4E-3	1.11	5E-4	0.83	0.01
log2(C-reactive protein)					0.31	3E-4			0.31	3E-4
log2(Insulin)					0.19	0.25			0.19	0.24
log2(Triglycerides)					0.25	0.24			0.34	0.14
log2(Glucose)					0.34	0.32			0.41	0.27
HDL Cholesterol					-0.01	0.33			-0.01	0.28
Systolic blood pressure					0.01	0.13			0.01	0.08
Diastolic blood pressure					0.00	0.95			0.00	0.75
log2(Waist-to-hip ratio)					0.25	0.80			0.48	0.63
Metabolic syndrome symptoms							0.29	2E-3	-0.16	0.30

B

IEAA n=2725	Model 1 Minimal		Model 2 Food		Model 3 Biomarkers		Model 4 MetS		Model 5 Full	
	β	p	β	p	β	p	β	p	β	p
log2(1 + Fish)			-0.04	0.92					0.01	0.99
log2(1 + Poultry)			-0.70	0.03					-0.71	0.03
Current drinker			-0.07	0.72					0.00	0.99
Education	-0.03	0.58	-0.02	0.72	-0.01	0.82	-0.01	0.75	-0.01	0.90
BMI	0.06	2E-4	0.06	9E-5	0.02	0.19	0.03	0.07	0.03	0.20
Physically active	-0.24	0.30	-0.23	0.31	-0.16	0.49	-0.19	0.39	-0.16	0.48
Current smoker	0.26	0.33	0.26	0.34	0.26	0.33	0.23	0.38	0.25	0.35
African American	-0.56	0.01	-0.50	0.02	-0.51	0.03	-0.48	0.03	-0.45	0.05
Hispanic	-1.51	3E-9	-1.47	1E-8	-1.60	6E-10	-1.47	8E-9	-1.54	3E-9
log2(C-reactive protein)					0.10	0.13			0.11	0.12
log2(Insulin)					0.13	0.31			0.13	0.34
log2(Triglycerides)					0.40	0.02			0.35	0.06
log2(Glucose)					0.35	0.20			0.31	0.30
HDL Cholesterol					0.00	0.89			0.00	0.72
Systolic blood pressure					0.00	0.67			0.00	0.93
Diastolic blood pressure					0.01	0.42			0.01	0.39
log2(Waist-to-hip ratio)					-0.17	0.83			-0.24	0.77
Metabolic syndrome symptoms							0.27	4E-4	0.07	0.58

Figure 3. Multivariate linear models of EEAA and IEAA with and without biomarkers in the WHI. EEAA (panel **A**) and IEAA (panel **B**) were regressed on potential confounding factors, fish and poultry intake and current drinker status, and select biomarkers. Individual columns list the corresponding coefficient estimates (β) and p-values (p) for each fitting. Coefficients are colored according to sign (positive = red, negative = blue) and significance according to magnitude (green). Models 1 through 5 correspond to a minimal model, a model including dietary intake variables, a model including potential explanatory biomarkers, a model including number of metabolic syndrome symptoms and a complete model with all of the variables above, respectively. Models are adjusted for originating dataset (BA23 or AS315).

(t_{meta}=-3.30, p_{meta}=0.001) and lower BMI (t_{meta}=4.14, p_{meta}=4x10^{-5}), after adjusting for potential confounders (Figure 2B). In the subset of participants with measured carotenoids, IEAA was significantly associated with mean carotenoid levels (t_{meta}=-2.47, p_{meta}=0.01, Supplementary Figure 5B). When regressed on clinical biomarkers IEAA was significantly associated with triglycerides (log2, β=0.40, p=0.02, Figure 3B, model 3). Their inclusion diminished the association between IEAA and BMI (60% decrease in coefficient magnitude, Figure 3B, model 2 vs. model 5). Number of metabolic syndrome symptoms was also significantly associated with IEAA (β=0.27, p=4x10^{-4}, Figure 3B, model 4), and diminished the association between IEAA and BMI by 50%. In the subset of WHI participants with circulating carotenoid measurements, we find a trend toward association between IEAA and mean carotenoid levels (β=-0.40, p=0.07, Supplementary Figure 6B, model 5). Finally, in the participants with epigenetic profiling at two time points, increase in BMI (β=0.22, p=0.03) but not initial BMI (β=-0.22, p=0.44) is significantly associated with increased IEAA (higher follow-up IEAA after adjusting for the initial IEAA, dataset, and ethnicity).

Metformin and epigenetic age acceleration

Considering the significant association between our measures of epigenetic aging and markers of diabetes, we investigated the potential of metformin to modulate epigenetic aging. As shown in Supplementary Figure **7**, women in the No Metformin group were the oldest, with mean ages around 65 years, compared to mean ages around 64 years for the Metformin Now group and 62.5 years for the Metformin Future group. Those in the No Metformin group also appeared to have a higher proportion of college graduates compared to the other two groups, whose members tended to have lower educational attainment. The two Metformin groups had much higher proportions of Non-Hispanic blacks, and somewhat higher proportions of Hispanics. As expected, women who were prescribed Metformin had the highest fasting insulin, fasting glucose, and HOMA-IR levels, with current Metformin users being the highest of all. Similarly, among Metformin users, fasting insulin, fasting glucose, and HOMA-IR levels were inversely associated with timing of Metformin initiation. This suggests that 1) women who had been on Metformin the longest at the time of blood draw were
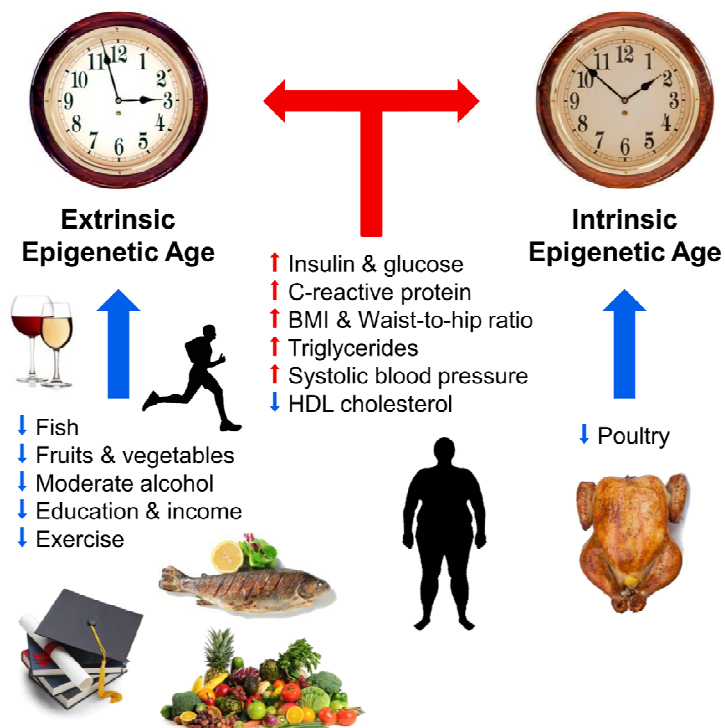
Figure 4. Pictorial summary of our main findings. The blue and red arrows depict anti-aging and pro-aging effects in blood respectively. The two clocks symbolize the extrinsic epigenetic clock (enhanced version of the Hannum estimate) and the intrinsic epigenetic clock (Horvath 2013) which are dependent and independent of blood cell counts, respectively.

the most insulin resistant—arguably because they were long-time diabetics—and 2) among women who would use Metformin in the future, those who would receive prescriptions sooner—who may already have pre-diabetes or diabetes at the time of blood draw—were more insulin resistant than women who were prescribed Metformin later.

As shown in Supplementary Figure 8, when examining the full sample, IEAA and EEAA were highest for women in the Metformin Now group, although differences between Metformin Now and Metformin Future were not significant. Further, the timing of Metformin prescription relative to the timing of blood draw was not associated with either IEAA or EEAA. Overall, these results held for IEAA when restricting the sample to only Non-Hispanic whites, Non-Hispanic blacks, or women at least 65 years of age. Results for EEAA held when restricting the sample to only Hispanics, women less than 65 years of age, or those with fasting glucose levels under 126 mg/dL. Nevertheless, there were no strata in which women in the Metformin Now group had significantly lower IEAA or EEAA than women in either the No Metformin or the Metformin Future group.

Given that Metformin may not be effective for all or that not all women prescribed Metformin may comply with their physician's recommendations, we compared future Metformin users to current Metformin users who had fasting glucose levels under 140 mg/dL (Supplementary Figure 9). Similar to Supplementary Figure 8, no significant differences were found for the two metformin groups, and in most cases those currently on Metformin had somewhat higher IEAA and EEAA than those who would be prescribed Metformin in the future.

Finally, when using women with repeat blood draws to compare the change in IEAA and EEAA for those who started Metformin between the two visits to those who didn't (Supplementary Table 1), we find that, while those who start Metformin appear to have lower IEAA (β=-0.79), the difference is not significant (P=0.46). Results for EEAA show very little difference between those who start Metformin between first and second blood draws, and those who don't (β=-0.003, P=0.99). Given that we only have 11 women who start Metformin, our null results, particularly for IEAA, may be due to a lack a power. Thus, in moving forward, this analysis may be worth revisiting in a randomized control trial or after acquiring larger sample sizes.

DISCUSSION

To our knowledge, this is the first study to examine associations between lifestyle factors and measures of epigenetic age acceleration in blood. Our main findings are summarized graphically in Figure 4. Overall, our dietary results are consistent with some of the current Dietary Guidelines for Americans [60, 61], reflecting potential health benefits associated with higher intake of fish, poultry, and fruits and vegetables. The weak correlations between dietary factors and epigenetic aging rates probably reflect that a relatively large proportion of the variance in aging rates (around 40 percent) is explained by genetic factors [38, 59, 62]. We find that education, physical activity, low body mass index are associated with a slow extrinsic age acceleration both in univariate correlation tests (Figure 1) and in multivariate regression models (Figure 2A, 3A). However, consistent with our previous work, smoking status was not associated with epigenetic age acceleration [45], which highlights that not every poor lifestyle choice is associated with an increased epigenetic aging effect in blood tissue.

EEAA, inflammation, and metabolic functioning

The age-related changes in immune functioning and inflammation are believed to contribute to increased susceptibility of a wide range of diseases later in life, including diabetes, some cancers, cardiovascular, neurodegenerative, auto-immune, and infectious diseases [63, 64]. In our analysis, EEAA, a biomarker which explicitly incorporates aspects of immune system aging such as age-related changes in blood cell counts, was associated with cardiometabolic biomarkers, fish, fruit, vegetable, and alcohol intake.

Our finding that fish intake was negatively associated with EEAA is consistent with prospective studies suggesting that fish consumption is protective against various age-related diseases [65-67]. The benefits of fish intake may be mediated in part through the omega-3 fatty acids, eicosapentaenoic acid (EPA) and docosahexaenoic acid (DHA), which stimulate the synthesis of anti-inflammatory cytokines [68]. This is further supported by our finding that CRP—a well-known marker of inflammation—was the most significant explanatory biomarker of EEAA. This suggests that one reason higher fish consumption may lower EEAA is because it has beneficial anti-inflammatory or metabolic effects. The consensus between these associations also appears to converge on MetS as a potential mediating factor; this was further supported by our results showing that the number of MetS characteristics significantly relates to EEAA. Though CRP is not included in most MetS diagnostic criteria, the association between the two has been previously established [69].

We also find that alcohol consumption was negatively associated with EEAA even after adjusting for potential

confounders such as socioeconomic status; this is consistent with prospective studies which have identified light to moderate alcohol intake as a protective factor against all-cause and CHD-related mortality [70, 71] and is supported by a recent publication that also found an inverse association between epigenetic age and alcohol intake in Caucasian and African American individuals (n=656, n=180, respectively) [72]. In our study, we find that the potential benefits of alcohol consumption are observed using a threshold of more than one serving per month, though the effect size of this variable was also stable when adding weekly and daily intake levels (Supplementary Figure 4A-D). The association appears to be driven by wine consumption though there is also a trend towards association with beer (Supplementary Figures 4E-H). This is consistent with other studies have suggested that wine may have added benefits compared to light alcohol consumption [73]. This finding may also be related to the anti-inflammatory effects of light alcohol consumption, which are associated with decreased circulating levels of inflammatory markers such as IL-6 and CRP [74]. Alternatively, this may be the result of reverse causation, whereby individuals suffering from health issues abstain from alcohol consumption [75], though interventional studies support a causal protective effect of moderated alcohol intake on cardiovascular blood biomarkers [76].

Though EEAA only trended toward association with reported fruit and vegetable intake, we find significant associations with blood carotenoid levels, which are quantitative surrogates of fruit and vegetable intake; this is likely a reflection of the bias and inaccuracy of self-reported diet. This is in agreement with the wide range of literature supporting the protective effects of high fruit and vegetable intake against age-related diseases CHD [77, 78], stroke [79], type-2 diabetes [80], breast cancer[81], and all-cause mortality [82]. The association between fruit and vegetables with aging of the blood immune system may be partially mediated by anti-inflammatory [83, 84] and cardiometabolic effects, however it is interesting to note that the explanatory power of mean carotenoid levels remained even after including the other explanatory factors into the model, suggesting the possibility of independent anti-aging mechanisms (Supplementary Figure 6A, model 5).

Our results for EEAA also share similarities with previously reported findings showing that LTL relates to BMI [22], metabolic factors, vegetable consumption [85], and dietary intake of foods high in omega-3 fatty acids [86]. This agreement is likely a reflection of the shared immunological basis, which is supported by the weak negative correlation between EEAA and age-

adjusted LTL. In contrast, IEAA is not significantly associated with LTL, supporting the idea that these measures represent different aspects of aging.

Intrinsic epigenetic aging and metabolic health

Results showed that BMI has a positive association with IEAA (Figure 3B, model 2). The statistically significant but weak correlations between BMI and epigenetic age acceleration in blood (r<0.10) are much smaller than those we recently reported for human liver (r=0.42) [54], suggesting that associations between aging signatures and risk factors may vary in strength depending on the tissue, and may be stronger in organs/tissues most affected by the risk. Interestingly, IEAA was also associated with number of metabolic syndrome characteristics, suggesting a role in tracking metabolic aging processes (Figure 3B, model 4).

We did find that reported poultry intake was negatively associated with IEAA, even after adjusting for potential confounders and explanatory factors (Figure 3B, model 5). Given the relative inert behavior of IEAA, the mechanism by which poultry may affect aging is unclear.

Lack of an effect of metformin

Metformin, which is a first-line medication for the treatment of type 2 diabetes, has garnered substantial interest by aging researchers [87]. The fact that we did not detect an anti-aging effect of metformin in our study could be due to the following factors: a) it could reflect the limitations/biases of an observational study, b) it could reflect the limited sample size, or c) that metformin does not affect epigenetic aging rates of blood tissue. Future randomized controlled trials should revisit the question whether metformin affects epigenetic aging rates in blood or other tissues.

Generalization to the InCHIANTI

Our results from the InCHIANTI show some validation of our findings from the WHI: fish intake was related to EEAA, and poultry was related to IEAA. Associations with available biomarkers of cardiometabolic health, however, were not found to be validated, and in a few cases were reversed in directions, within the InCHIANTI (data not shown).

The discrepancies between the WHI and InCHIANTI cohorts may be due to numerous differences in the study population (cultural, demographic, genetic, health status, Table 1) and data collection methodology (dietary assessment). Despite being younger, on average, US participants from the WHI had higher body

mass indexes (BMI), and worse metabolic health than their Italian counterparts—as indicated by their greater prevalence of metabolic syndrome (23% in the WHI versus 7.6% in the InCHIANTI).

The InCHIANTI study is also arguably underpowered (n=402) when it comes to detecting the weak associations with epigenetic age acceleration. According to sample size calculations (*PASS* software), we find that n=1820 samples are needed to provide 80% power to detect a correlation of r=0.08 at a two-sided significance level of α=0.01. Similarly, n=1163 samples are needed to detect a correlation of r=0.10.

Limitations

While our study of the WHI benefits from having a relatively large sample size, associations with epigenetic aging may not be detectable in smaller studies given the weak effect sizes observed here. This situation is exacerbated by self-reported lifestyle habits which are notorious for bias and inaccuracy, limiting their ability to represent true lifestyle habits and potentially producing false negative results. Further, as evidenced by our results from the ethnic strata and the InCHIANTI, studies conducted in different ethnic populations may not be entirely consistent due to fundamental differences in age, diet, culture, and demographics. There were several potential limitations to this study, which include the assumption of non-confounding from unmeasured variables such as existing patient co-morbidities and the assumption of accuracy and long-term consistency of reported dietary habits. This is the first longitudinal study to show that an increase in BMI is associated with an increase in epigenetic age acceleration but larger longitudinal studies will be needed to dissect causal relationships between epigenetic aging rates and dietary measures, education, exercise, and lifestyle factors.

Conclusions about epigenetic age acceleration

Our large sample size (n>4500) provides sufficient statistical power for one of our main conclusions: diet has only a weak effect on epigenetic aging rates in blood. These findings will be valuable for researchers who plan to use epigenetic biomarkers in dietary intervention studies. The wide range of associations found with EEAA suggest that immune system aging may be closely linked to conventional notions of metabolic health and may be sensitive to variations in environment and lifestyle. In contrast, IEAA has few associations, which is consistent with the hypothesis that cell-intrinsic aging remains relatively stable, more likely being determined by an intrinsic aging or developmental process under genetic control. Further,

using longitudinal data in the WHI, we found that change in both EEAA and IEAA are significantly associated with change in BMI, suggesting that both modes of epigenetic aging may respond to changes in lifestyle, at least with respect to change in obesity. Overall, our results are consistent with previous literature supporting the protective effects of fish, poultry and alcohol consumption, exercise, education, as well as the risk of obesity and dyslipidemia.

METHODS

Estimation of DNA methylation age

DNAm age (also referred to as epigenetic age) was calculated from human samples profiled with the Illumina Infinium 450K platform, described in detail in [38]. Briefly, the epigenetic clock is defined as a prediction method of age based on the DNAm levels of 353 CpGs. Predicted age, referred to as DNAm age, correlates with chronological age in sorted cell types (CD4+ T cells, monocytes, B cells, glial cells, neurons), tissues, and organs, including: whole blood, brain, breast, kidney, liver, lung, saliva [38].

We also applied the Hannum measure of DNAm age based on 71 CpGs which was developed using DNA methylation data from blood [37].

Despite high correlations, DNAm age estimates can deviate substantially from chronological age at the individual level, and adjusting for age we can arrive at measures of epigenetic age acceleration as described in the following.

Estimation of Intrinsic and Extrinsic Epigenetic Age Acceleration (IEAA, EEAA)

In this article, we consider two measures of epigenetic age acceleration. These measures, referred to as intrinsic and extrinsic age acceleration only apply to blood. IEAA is derived from the Horvath measure of DNAm age based on 353 CpGs [38], and is defined as the residual resulting from regressing Horvath DNAm age on chronological age and estimates of plasmablasts, naive and exhausted CD8+ T cells, CD4+ T cells, natural killer cells, monocytes, and granulocytes. Thus, IEAA is independent of chronological age and most of the variation in blood cell composition. IEAA is meant to capture cell-intrinsic properties of the aging process that exhibits preservation across various cell types and organs.

EEAA can be interpreted as an enhanced version of the Hannum measure of DNAm age based on 71 CpGs [37]. EEAA up-weights the contributions of age related

blood cell counts [43]. Specifically, EEAA is defined using the following three steps. First, we calculated the epigenetic age measure from Hannum et al, which already correlated with certain blood cell types [40]. Second, we increased the contribution of immune blood cell types to the age estimate by forming a weighted average of Hannum's estimate with 3 cell types that are known to change with age: naïve (CD45RA+CCR7+) cytotoxic T cells, exhausted (CD28-CD45RA-) cytotoxic T cells, and plasmablasts using the Klemera Doubal approach [88]. The weights used in the weighted average are determined by the correlation between the respective variable and chronological age. The weights were chosen on the basis of the WHI data and the same (static) weights were used for all data sets. Finally, EEAA was defined as the residual variation resulting from a univariate model regressing the resulting age estimate on chronological age. Thus, EEAA tracks both age related changes in blood cell composition and intrinsic epigenetic changes.

In a recent large scale meta-analysis involving over 13 thousand subjects from 13 cohorts, we have shown that both IEAA and EEAA are predictive of mortality, independent of chronological age, even after adjusting for additional risk factors, and within the racial/ethnic groups that we examined (Caucasians, Hispanics, African Americans) [43].

IEAA and EEAA can be obtained from the online DNAm age calculator (http://labs.genetics.ucla.edu/horvath/dnamage/), where they are denoted as *AAHOAdjCellCounts* and *BioAge4HAStaticAdjAge*, respectively.

Dietary assessment in the Women's Health Initiative (WHI)

Participants were selected from the WHI, a national study that began in 1993 and enrolled postmenopausal women between the ages of 50-79 years into either randomized clinical trials (RCTs) or into an observational study [89] (more details available in Supplementary Information). Participants completed self-administered questionnaires at baseline which provided personal information on a wide range of topics, including sociodemographic information (age, education, race, income), and current health behaviors (recreational physical activity, tobacco and alcohol exposure, and diet). Participants also visited clinics at baseline where certified Clinical Center staff collected blood specimens and performed anthropometric measurements including weight, height, hip and waist circumferences, and systolic and diastolic blood pressures; body mass index and waist to hip ratio were calculated from these measurements (Table 1).

Dietary intake levels were assessed at baseline using the WHI Food Frequency Questionnaire [90]. Briefly, participants were asked to report on dietary habits in the past three months, including intake, frequency, and portion sizes of foods or food groups, along with questions concerning topics such as food preparation practices and types of added fats. Nutrient intake levels were then estimated from these responses. For current drinker, we use the threshold of more than one serving equivalent (14g) within the last 28 days.

Estimation of blood cell counts based on DNA methylation levels

We estimate blood cell counts using two different software tools. First, Houseman's estimation method [91], which is based on DNA methylation signatures from purified leukocyte samples, was used to estimate the proportions of CD8+ T cells, CD4+ T, natural killer, B cells, and granulocytes (also known as polymorpho-nuclear leukocytes). Second, the advanced analysis option of the epigenetic clock software [38, 52] was used to estimate the percentage of exhausted CD8+ T cells (defined as CD28-CD45RA-) and the number (count) of naïve CD8+ T cells (defined as CD45RA+CCR7+). We and others have shown that the estimated blood cell counts have moderately high correlations with corresponding flow cytometric measures [91, 92]. For example, flow cytometric measurements from the MACS study correlate strongly with DNA methylation based estimates: r=0.63 for CD8+T cells, r=0.77 for CD4+ T cells, r=0.67 for B cell, r=0.68 for naïve CD8+ T cell, r=0.86 for naïve CD4+ T, and r=0.49 for exhausted CD8+ T cells [92].

Blood biomarkers and DNA methylation in the WHI

Two separate subsamples were aggregated for our study within the WHI (BA23 and AS315). Both had baseline blood specimens collected after an overnight fast in EDTA tubes and stored at -70C. These samples were processed at the WHI core laboratory and select nutrient and cardiovascular biomarkers were measured including lycopene, alpha- & beta-carotene, alpha- & gamma-tocopherol, C-reactive protein, triglycerides, total, LDL, and HDL cholesterol.

For the first subsample (BA23) consisting of 2098 samples, DNA methylation levels were measured using the Illumina Infinium HumanMethylation450 BeadChip at the HudsonAlpha Institute of Biotechnology. This platform uses bisulfite conversion to quantify methylation levels at 485,577 specific CpG sites genome-wide. Samples were prepared according to the standard Illumina protocol, and β methylation values were calculated from the intensity ratio between

methylated and total (methylated and unmethylated) probe fluorescence intensities. Methylation data was processed as described in [38]. In order to test the quality of these array measurements, we perform correlation measures with duplicates within this dataset and with a "gold" standard which is an average of many samples previously collected. Correlation between duplicates and with the gold standard were high (r>0.9), indicative of high quality measurements.

The second WHI data set is described in the following.

WHI-EMPC description

The Women's Health Initiative – Epigenetic Mechanisms of PM-Mediated CVD (WHI-EMPC, AS315) is an ancillary study of epigenetic mechanisms underlying associations between ambient particulate matter (PM) air pollution and cardiovascular disease (CVD) in the Women's Health Initiative clinical trials (CT) cohort. The WHI-EMPC study population is a stratified, random sample of 2,200 WHI CT participants who were examined between 1993 and 2001; had available buffy coat, core analytes, electrocardiograms, and ambient concentrations of PM; but were not taking anti-arrhythmic medications at the time. As such, WHI-EMPC is representative of the larger, multiethnic WHI CT population from which it was sampled: n = 68,132 participants aged 50-79 years who were randomized to hormone therapy, calcium/vitamin D supplementation, and/or dietary modification in 40 U.S. clinical centers at the baseline exam (1993-1998) and re-examined in the fasting state one, three, six, and nine years later [93].

Illumina Infinium HumanMethylation450 BeadChip data from the Northwestern University Genomics Core Facility for WHI-EMPC participants sampled in stages 1a (800 participants), 1b (1200 participants), and 2 (200 participants x 2 samples each) was quality controlled and batch adjusted. Batch adjustment involved applying empirical Bayes methods of adjusting for stage and plate as implemented in ComBat [94].

Dietary assessment in the Invecchiare nel Chianti (InCHIANTI)

The InCHIANTI Study is a population-based prospective cohort study of residents ages 30 or older from two areas in the Chianti region of Tuscany, Italy. Data on demographic and lifestyle factors such as smoking, years of education, BMI, and physical activity were collected during the baseline interview. Physical activity in the previous year was categorized as sedentary or active. Smoking was categorized into current smoker versus former or non-smokers (Table 1).

In the InCHIANTI study, dietary intake for the past year was assessed using a 236 item food frequency questionnaire (FFQ) for the European Prospective Investigation on Cancer and nutrition (EPIC) study, previously validated in the InCHIANTI population [95]. The FFQ was administered by a trained interviewer and collected information on how frequently (weekly, monthly, yearly) each specific food was generally consumed. Participants were asked to specify the size of the portion usually consumed, in comparison to a range of portion that are shown in colored photographs. Nutrient data for specific foods were obtained from the Food Composition Database for Epidemiological Studies in Italy [96]. Dietary information was judged as unreliable and excluded from further analysis if reported energy intakes were <600 kcal/day or >4,000 kcal/day and >4,200 kcal/day in women and men, respectively.

Blood biomarkers and DNA methylation in the InCHIANTI

Sampling and data collection procedures have been described elsewhere [97]. Briefly, participants were enrolled between 1998 and 2000 and were examined at three-year intervals. Serum samples obtained from blood collected in evacuated tubes without anti-coagulant were centrifuged at 2000g for 10 min, and stored at -80 °C for measurement of glucose, total, LDL, and HDL, cholesterol, triglycerides, CRP, and creatinine. DNA methylation was assayed using the Illumina Infinium HumanMethylation450 platform for n=407 participants with sufficient DNA at both baseline (years 1998-2000) and year 9 follow-up visits (2007-2009).

Assessment of metabolic syndrome

Metabolic syndrome status was assessed using the ATPIII NCEP 2004 criteria defined by the presence of 3 or more of the following characteristics: waist circumference >88cm (if male, >102cm), systolic blood pressure >130mmHg or diastolic blood pressure >85mmHg, fasting plasma glucose >100mg/dL, HDL cholesterol <50mg/dL (if male, <40mg/dL), and triglycerides >150mg/dL. In regression models, we use total number of metabolic syndrome characteristics as an ordinal variable, ranging from 0 to 5.

Statistical analyses

Dietary analysis
Biweight midcorrelation, an outlier-robust correlation measure, was used to assess marginal linear relationships between epigenetic aging measures and dietary, cardiometabolic, and socioeconomic factors. To

adjust for possible socioeconomic and lifestyle confounders, we fit ethnically-stratified multivariable linear models adjusting for education, exercise, BMI, and current drinker and smoker status. We used Stouffer's method to infer the meta-analytic significance of each variable over the different ethnic strata using the square-root of the sample size as the Z-score weighting factor. Specifically for the WHI, the age acceleration measures were adjusted for differences in originating dataset and within the InCHIANTI the measures were adjusted for sex. Models including regression on biomarkers, and number of metabolic syndrome symptoms were not stratified by ethnicity due to lack of coverage for biomarker profiling. Models were designed based on common prior knowledge and in cases where there was co-linearity between confounding variables, choice for adjustment was selected based on variable commonality in order to improve comparability with other studies, e.g. BMI was chosen over WHR because BMI is more commonly measured and reported. Variables with skewness >1 were log transformed (possibly adding +1 to avoid forming the logarithm of zero). Mean carotenoids was computed as the mean across standardized measures of lycopene, log2(alpha-carotene), log2(beta-carotene), log2(lutein + zeaxanthin), and log2(beta-cryptoxanthin). Repeat measurements on the same individuals were omitted from the analysis.

Metformin analysis

Prescription medication use was collected at baseline for women in both the clinical trial and the observational study. Follow-up recording of new medication was done at years 1, 3, 6, and 9 for women enrolled in clinical trial and at year 3 for those enrolled in the observational study. At each of these waves, participants were asked to bring in their prescription medication bottles and interviewers recorded the National Drug Code (NDC), the product name, and generic name for each drug. In our analysis, those who took prescription drugs that fell under the Therapeutic Class Codes (TCCODE), 272500 or 279970 were coded as taking Metformin. TCCODE 272500 covered the following drugs: Metformin HCL, Metformin ER, Fortamet, Glucophage XR, Glucophage, and Riomet; all of which were Metformin HCL tablets. TCCODE 279970 covered the following drugs: Glucovance, Glyburide/Metformin HCL, and Metaglip; the first two of which were Glyburide and Metformin HCL combination tablets, whereas the later is a Glipizide Metformin HCL combination tablet. In our study, approximately 12% (n=489) of women were reported as using Metformin at some time during the study. Women were also asked the age at which they started using prescribed medication. On average, women in our study began metformin use at age 65, with the youngest and

oldest ages of initiation reported as 41 and 85, respectively.

We utilized the reported age of Metformin initiation to estimate whether women were using metformin at the time of blood draw (when DNAm age was measured), and if so, how long they had been on the drug. For those women who started using Metformin after the date of blood draw, we were also able to calculate the time between blood draw and starting on Metformin. Based on this, we classified women in to three categories— "No Metformin" (those who never used Metformin), "Metformin Now" (those on Metformin at the time of blood draw), and "Metformin Future" (those who began Metformin after blood draw). In our sample, 4,073 women were in the No Metformin group, 139 were in the Metformin Now group, and 350 were in the Metformin Future group.

Kruskal Wallis tests were used to compare the ages at blood draw, education levels, race/ethnicity, fasting glucose levels, fasting insulin levels, and degree of insulin resistance (measured using the Homeostatic Model Assessment of Insulin Resistance--HOMA_IR). Biweight midcorrelations were used to examine whether these characteristics differed as a function of the timing of Metformin initiation among those on Metformin at some point during the study. Next Kruskal Wallis tests and biweight midcorrelations were used to examine whether Metformin group classification and/or the timing of Metformin use was associated with IEAA or EEAA. For these models, both IEAA and EEAA were adjusted for age at blood draw, education, and race/ethnicity. These models were run using the full sample, and stratifying by age at blood draw (<65 years vs. 65+ years), race/ethnicity, and fasting glucose levels (<126 mg/dL vs. 126+ mg/dL). Next, a two group comparison was made for the full sample and stratifying by race/ethnicity between a) 47 women in the Metformin Now group for whom Metformin was potentially effective (fasting glucose < 140 mg/dL), and b) the 350 women in the Metformin Future group. Finally, there were 308 women who 1) had IEAA and EEAA measured during at least two separate WHI visits and 2) were not on Metformin at the time of their first blood draw. Of these women, 11 started Metformin in between their two blood draws. Based on this, we used linear models to compare the change in IEAA and EEAA between women who started Metformin between their first and second IEAA and EEAA measure and those who did not. Models were adjusted for age at first blood draw, age at second blood draw, race/ethnicity, education, glucose levels at first blood draw, and either IEAA or EEAA at first blood draw.

AUTHOR CONTRIBUTIONS

Austin Quach, Morgan E. Levine, Toshiko Tanaka, Brian H. Chen, and Steve Horvath carried out the analysis. Devin Absher, Themistocles L. Assimes, Phil Tsao, Steve Horvath, Beate Ritz, Luigi Ferrucci, Stefania Bandinelli, Eric A. Whitsel, Lifang Hou, Andrea Baccerelli, Yun Li, James Stewart contributed data. Marian L. Neuhouser, Jeannette M. Beasley, Linda Snetselaar, Robert B. Wallace, Ake Lu helped with the interpretation of the findings and drafting of the article. Steve Horvath designed the study.

CONFLICTS OF INTEREST

The Regents of the University of California is the sole owner of a provisional patent application directed at the invention of measures of epigenetic age acceleration for which SH is a named inventor. The other authors declare no conflict of interest.

REFERENCES

1. Kaczmarczyk MM, Miller MJ, Freund GG. The health benefits of dietary fiber: beyond the usual suspects of type 2 diabetes mellitus, cardiovascular disease and colon cancer. Metabolism. 2012; 61:1058–66. doi: 10.1016/j.metabol.2012.01.017

2. Kris-Etherton PM, Harris WS, Appel LJ, and American Heart Association. Nutrition Committee. Fish consumption, fish oil, omega-3 fatty acids, and cardiovascular disease. Circulation. 2002; 106:2747–57. doi: 10.1161/01.CIR.0000038493.65177.94

3. van't Veer P, Jansen MC, Klerk M, Kok FJ. Fruits and vegetables in the prevention of cancer and cardiovascular disease. Public Health Nutr. 2000; 3:103–07. doi: 10.1017/S1368980000000136

4. Giugliano D, Ceriello A, Esposito K. The effects of diet on inflammation: emphasis on the metabolic syndrome. J Am Coll Cardiol. 2006; 48:677–85. doi: 10.1016/j.jacc.2006.03.052

5. Mozaffarian D. Dietary and Policy Priorities for Cardio-vascular Disease, Diabetes, and Obesity. 2016; 133:

187–225. doi: 10.1161/CIRCULATIONAHA.115.018585

6. Alberti KG, Eckel RH, Grundy SM, Zimmet PZ, Cleeman JI, Donato KA, Fruchart JC, James WP, Loria CM, Smith SC Jr, and International Diabetes Federation Task Force on Epidemiology and Prevention, and Hational Heart, Lung, and Blood Institute, and American Heart Association, and World Heart Federation, and International Atherosclerosis Society, and International Association for the Study of Obesity. Harmonizing the metabolic syndrome: a joint interim statement of the International Diabetes Federation Task Force on Epidemiology and Prevention; National Heart, Lung, and Blood Institute; American Heart Association; World Heart Federation; International Atherosclerosis Society; and International Association for the Study of Obesity. Circulation. 2009; 120:1640–45. doi: 10.1161/CIRCULATIONAHA.109.192644

7. Grundy SM, Cleeman JI, Daniels SR, Donato KA, Eckel RH, Franklin BA, Gordon DJ, Krauss RM, Savage PJ, Smith SC Jr, Spertus JA, Costa F, and American Heart Association, and National Heart, Lung, and Blood Institute. Diagnosis and management of the metabolic syndrome: an American Heart Association/National Heart, Lung, and Blood Institute Scientific Statement. Circulation. 2005; 112:2735–52. doi: 10.1161/CIRCULATIONAHA.105.169404

8. Wilson PW, D'Agostino RB, Parise H, Sullivan L, Meigs JB. Metabolic syndrome as a precursor of cardiovascular disease and type 2 diabetes mellitus. Circulation. 2005; 112:3066–72. doi: 10.1161/CIRCULATIONAHA.105.539528

9. Thun MJ, Peto R, Lopez AD, Monaco JH, Henley SJ, Heath CW Jr, Doll R. Alcohol consumption and mortality among middle-aged and elderly U.S. adults. N Engl J Med. 1997; 337:1705–14. doi: 10.1056/NEJM199712113372401

10. Rimm EB, Williams P, Fosher K, Criqui M, Stampfer MJ. Moderate alcohol intake and lower risk of coronary heart disease: meta-analysis of effects on lipids and haemostatic factors. BMJ. 1999; 319:1523–28. doi: 10.1136/bmj.319.7224.1523

11. Warburton DE, Nicol CW, Bredin SS. Health benefits of physical activity: the evidence. CMAJ. 2006; 174:801–09. doi: 10.1503/cmaj.051351

12. González MA, Rodríguez Artalejo F, Calero JR. Relationship between socioeconomic status and ischaemic heart disease in cohort and case-control studies: 1960-1993. Int J Epidemiol. 1998; 27:350–58. doi: 10.1093/ije/27.3.350

13. Madsen M, Andersen AM, Christensen K, Andersen PK, Osler M. Does educational status impact adult mortality in Denmark? A twin approach. Am J Epide-miol. 2010; 172:225–34. doi: 10.1093/aje/kwq072

14. Conti G, Heckman J, Urzua S. THE EDUCATION-HEALTH GRADIENT. Am Econ Rev. 2010; 100:234–38. doi: 10.1257/aer.100.2.234

15. Currie J. Healthy, Wealthy, and Wise: Socioeconomic Status, Poor Health in Childhood, and Human Capital Development. National Bureau of Economic Research Working Paper Series. 2008; No. 13987.

16. Cutler DM, Lleras-Muney A. Understanding differences in health behaviors by education. J Health Econ. 2010; 29:1–28. doi: 10.1016/j.jhealeco.2009.10.003

17. Mirabello L, Huang WY, Wong JY, Chatterjee N, Reding D, Crawford ED, De Vivo I, Hayes RB, Savage SA. The association between leukocyte telomere length and cigarette smoking, dietary and physical variables, and risk of prostate cancer. Aging Cell. 2009; 8:405–13. doi: 10.1111/j.1474-9726.2009.00485.x

18. Boccardi V, Esposito A, Rizzo MR, Marfella R, Barbieri M, Paolisso G. Mediterranean diet, telomere maintenance and health status among elderly. PLoS One. 2013; 8:e62781. doi: 10.1371/journal.pone.0062781

19. García-Calzón S, Gea A, Razquin C, Corella D, Lamuela-Raventós RM, Martínez JA, Martínez-González MA, Zalba G, Marti A. Longitudinal association of telomere length and obesity indices in an intervention study with a Mediterranean diet: the PREDIMED-NAVARRA trial. Int J Obes. 2014; 38:177–82. doi: 10.1038/ijo.2013.68

20. Brouilette SW, Moore JS, McMahon AD, Thompson JR, Ford I, Shepherd J, Packard CJ, Samani NJ, and West of Scotland Coronary Prevention Study Group. Telomere length, risk of coronary heart disease, and statin treatment in the West of Scotland Primary Prevention Study: a nested case-control study. Lancet. 2007; 369:107–14. doi: 10.1016/S0140-6736(07)60071-3

21. Kiecolt-Glaser JK, Epel ES, Belury MA, Andridge R, Lin J, Glaser R, Malarkey WB, Hwang BS, Blackburn E. Omega-3 fatty acids, oxidative stress, and leukocyte telomere length: A randomized controlled trial. Brain Behav Immun. 2013; 28:16–24. doi: 10.1016/j.bbi.2012.09.004

22. Cassidy A, De Vivo I, Liu Y, Han J, Prescott J, Hunter DJ, Rimm EB. Associations between diet, lifestyle factors, and telomere length in women. Am J Clin Nutr. 2010; 91:1273–80. doi: 10.3945/ajcn.2009.28947

23. Latifovic L, Peacock SD, Massey TE, King WD. The Influence of Alcohol Consumption, Cigarette Smoking,

and Physical Activity on Leukocyte Telomere Length. Cancer Epidemiol Biomarkers Prev. 2016; 25:374–80. doi: 10.1158/1055-9965.EPI-14-1364

24. Cherkas LF, Hunkin JL, Kato BS, Richards JB, Gardner JP, Surdulescu GL, Kimura M, Lu X, Spector TD, Aviv A. The association between physical activity in leisure time and leukocyte telomere length. Arch Intern Med. 2008; 168:154–58.
doi: 10.1001/archinternmed.2007.39

25. Adler N, Pantell MS, O'Donovan A, Blackburn E, Cawthon R, Koster A, Opresko P, Newman A, Harris TB, Epel E. Educational attainment and late life telomere length in the Health, Aging and Body Composition Study. Brain Behav Immun. 2013; 27:15–21. doi: 10.1016/j.bbi.2012.08.014

26. Christensen BC, Houseman EA, Marsit CJ, Zheng S, Wrensch MR, Wiemels JL, Nelson HH, Karagas MR, Padbury JF, Bueno R, Sugarbaker DJ, Yeh RF, Wiencke JK, Kelsey KT. Aging and environmental exposures alter tissue-specific DNA methylation dependent upon CpG island context. PLoS Genet. 2009; 5:e1000602. doi: 10.1371/journal.pgen.1000602

27. Bollati V, Schwartz J, Wright R, Litonjua A, Tarantini L, Suh H, Sparrow D, Vokonas P, Baccarelli A. Decline in genomic DNA methylation through aging in a cohort of elderly subjects. Mech Ageing Dev. 2009; 130:234–39. doi: 10.1016/j.mad.2008.12.003

28. Rakyan VK, Down TA, Maslau S, Andrew T, Yang TP, Beyan H, Whittaker P, McCann OT, Finer S, Valdes AM, Leslie RD, Deloukas P, Spector TD. Human aging-associated DNA hypermethylation occurs preferentially at bivalent chromatin domains. Genome Res. 2010; 20:434–39.
doi: 10.1101/gr.103101.109

29. Teschendorff AE, Menon U, Gentry-Maharaj A, Ramus SJ, Weisenberger DJ, Shen H, Campan M, Noushmehr H, Bell CG, Maxwell AP, Savage DA, Mueller-Holzner E, Marth C, et al. Age-dependent DNA methylation of genes that are suppressed in stem cells is a hallmark of cancer. Genome Res. 2010; 20:440–46. doi: 10.1101/gr.103606.109

30. Horvath S, Zhang Y, Langfelder P, Kahn RS, Boks MP, van Eijk K, van den Berg LH, Ophoff RA. Aging effects on DNA methylation modules in human brain and blood tissue. Genome Biol. 2012; 13:R97. doi: 10.1186/gb-2012-13-10-r97

31. Numata S, Ye T, Hyde TM, Guitart-Navarro X, Tao R, Wininger M, Colantuoni C, Weinberger DR, Kleinman JE, Lipska BK. DNA methylation signatures in development and aging of the human prefrontal cortex. Am J Hum Genet. 2012; 90:260–72. doi: 10.1016/j.ajhg.2011.12.020

32. Alisch RS, Barwick BG, Chopra P, Myrick LK, Satten GA, Conneely KN, Warren ST. Age-associated DNA methylation in pediatric populations. Genome Res. 2012; 22:623–32. doi: 10.1101/gr.125187.111

33. Johansson A, Enroth S, Gyllensten U. Continuous Aging of the Human DNA Methylome Throughout the Human Lifespan. PLoS One. 2013; 8:e67378. doi: 10.1371/journal.pone.0067378

34. Day K, Waite LL, Thalacker-Mercer A, West A, Bamman MM, Brooks JD, Myers RM, Absher D. Differential DNA methylation with age displays both common and dynamic features across human tissues that are influenced by CpG landscape. Genome Biol. 2013; 14:R102. doi: 10.1186/gb-2013-14-9-r102

35. Bocklandt S, Lin W, Sehl ME, Sánchez FJ, Sinsheimer JS, Horvath S, Vilain E. Epigenetic predictor of age. PLoS One. 2011; 6:e14821.
doi: 10.1371/journal.pone.0014821

36. Garagnani P, Bacalini MG, Pirazzini C, Gori D, Giuliani C, Mari D, Di Blasio AM, Gentilini D, Vitale G, Collino S, Rezzi S, Castellani G, Capri M, et al. Methylation of ELOVL2 gene as a new epigenetic marker of age. Aging Cell. 2012; 11:1132–34. doi: 10.1111/acel.12005

37. Hannum G, Guinney J, Zhao L, Zhang L, Hughes G, Sadda S, Klotzle B, Bibikova M, Fan JB, Gao Y, Deconde R, Chen M, Rajapakse I, et al. Genome-wide methylation profiles reveal quantitative views of human aging rates. Mol Cell. 2013; 49:359–67. doi: 10.1016/j.molcel.2012.10.016

38. Horvath S. DNA methylation age of human tissues and cell types. Genome Biol. 2013; 14:R115. doi: 10.1186/gb-2013-14-10-r115

39. Lin Q, Weidner CI, Costa IG, Marioni RE, Ferreira MR, Deary IJ, Wagner W. DNA methylation levels at individual age-associated CpG sites can be indicative for life expectancy. Aging (Albany NY). 2016; 8:394–401. doi: 10.18632/aging.100908

40. Marioni RE, Shah S, McRae AF, Chen BH, Colicino E, Harris SE, Gibson J, Henders AK, Redmond P, Cox SR, Pattie A, Corley J, Murphy L, et al. DNA methylation age of blood predicts all-cause mortality in later life. Genome Biol. 2015; 16:25. doi: 10.1186/s13059-015-0584-6

41. Christiansen L, Lenart A, Tan Q, Vaupel JW, Aviv A, McGue M, Christensen K. DNA methylation age is associated with mortality in a longitudinal Danish twin study. Aging Cell. 2016; 15:149-54. doi: 10.1111/acel.12421

42. Perna L, Zhang Y, Mons U, Holleczek B, Saum K-U, Brenner H. Epigenetic age acceleration predicts

cancer, cardiovascular, and all-cause mortality in a German case cohort. Clin Epigenetics. 2016; 8:64. doi: 10.1186/s13148-016-0228-z

43. Chen BH, Marioni RE, Colicino E, Peters MJ, Ward-Caviness CK, Tsai PC, Roetker NS, Just AC, Demerath EW, Guan W, Bressler J, Fornage M, Studenski S, et al. DNA methylation-based measures of biological age: meta-analysis predicting time to death. Aging (Albany NY). 2016; 8:1844–65. doi: 10.18632/aging.101020.

44. Breitling LP, Saum KU, Perna L, Schöttker B, Holleczek B, Brenner H. Frailty is associated with the epigenetic clock but not with telomere length in a German cohort. Clin Epigenetics. 2016; 8:21. doi: 10.1186/s13148-016-0186-5

45. Levine ME, Hosgood HD, Chen B, Absher D, Assimes T, Horvath S. DNA methylation age of blood predicts future onset of lung cancer in the women's health initiative. Aging (Albany NY). 2015; 7:690–700. doi: 10.18632/aging.100809

46. Marioni RE, Shah S, McRae AF, Ritchie SJ, Muniz-Terrera G, Harris SE, Gibson J, Redmond P, Cox SR, Pattie A, Corley J, Taylor A, Murphy L, et al. The epigenetic clock is correlated with physical and cognitive fitness in the Lothian Birth Cohort 1936. Int J Epidemiol. 2015; 44:1388–96. doi: 10.1093/ije/dyu277

47. Horvath S, Pirazzini C, Bacalini MG, Gentilini D, Di Blasio AM, Delledonne M, Mari D, Arosio B, Monti D, Passarino G, De Rango F, D'Aquila P, Giuliani C, et al. Decreased epigenetic age of PBMCs from Italian semi-supercentenarians and their offspring. Aging (Albany NY). 2015; 7:1159–70. doi: 10.18632/aging.100861

48. Levine ME, Lu AT, Bennett DA, Horvath S. Epigenetic age of the pre-frontal cortex is associated with neuritic plaques, amyloid load, and Alzheimer's disease related cognitive functioning. Aging (Albany NY). 2015; 7:1198–211. doi: 10.18632/aging.100864

49. Horvath S, Mah V, Lu AT, Woo JS, Choi OW, Jasinska AJ, Riancho JA, Tung S, Coles NS, Braun J, Vinters HV, Coles LS. The cerebellum ages slowly according to the epigenetic clock. Aging (Albany NY). 2015; 7:294–306. doi: 10.18632/aging.100742

50. Walker RF, Liu JS, Peters BA, Ritz BR, Wu T, Ophoff RA, Horvath S. Epigenetic age analysis of children who seem to evade aging. Aging (Albany NY). 2015; 7:334–39. doi: 10.18632/aging.100744

51. Horvath S, Garagnani P, Bacalini MG, Pirazzini C, Salvioli S, Gentilini D, Di Blasio AM, Giuliani C, Tung S, Vinters HV, Franceschi C. Accelerated epigenetic aging in Down syndrome. Aging Cell. 2015; 14:491–95. doi: 10.1111/acel.12325

52. Horvath S, Levine AJ. HIV-1 infection accelerates age according to the epigenetic clock. J Infect Dis. 2015; 212:1563–73. doi: 10.1093/infdis/jiv277

53. Horvath S, Langfelder P, Kwak S, Aaronson J, Rosinski J, Vogt TF, Eszes M, Faull RL, Curtis MA, Waldvogel HJ, Choi OW, Tung S, Vinters HV, et al. Huntington's disease accelerates epigenetic aging of human brain and disrupts DNA methylation levels. Aging (Albany NY). 2016; 8:1485–512. doi: 10.18632/aging.101005

54. Horvath S, Erhart W, Brosch M, Ammerpohl O, von Schönfels W, Ahrens M, Heits N, Bell JT, Tsai PC, Spector TD, Deloukas P, Siebert R, Sipos B, et al. Obesity accelerates epigenetic aging of human liver. Proc Natl Acad Sci USA. 2014; 111:15538–43. doi: 10.1073/pnas.1412759111

55. Zannas AS, Arloth J, Carrillo-Roa T, Iurato S, Röh S, Ressler KJ, Nemeroff CB, Smith AK, Bradley B, Heim C, Menke A, Lange JF, Brückl T, et al. Lifetime stress accelerates epigenetic aging in an urban, African American cohort: relevance of glucocorticoid signaling. Genome Biol. 2015; 16:266. doi: 10.1186/s13059-015-0828-5

56. Levine ME, Lu AT, Chen BH, Hernandez DG, Singleton AB, Ferrucci L, Bandinelli S, Salfati E, Manson JE, Quach A, Kusters CD, Kuh D, Wong A, et al. Menopause accelerates biological aging. Proc Natl Acad Sci USA. 2016; 113:9327–32. doi: 10.1073/pnas.1604558113

57. Vidal L, Lopez-Golan Y, Rego-Perez I, Horvath S, Blanco FJ, Riancho JA, Gomez-Reino JJ, Gonzalez A. Specific increase of methylation age in osteoarthritis cartilage. Osteoarthritis Cartilage. 2016; 24:S63. doi: 10.1016/j.joca.2016.01.140

58. Horvath S, Ritz BR. Increased epigenetic age and granulocyte counts in the blood of Parkinson's disease patients. Aging (Albany NY). 2015; 7:1130–42. doi: 10.18632/aging.100859

59. Horvath S, Gurven M, Levine ME, Trumble BC, Kaplan H, Allayee H, Ritz BR, Chen B, Lu AT, Rickabaugh TM, Jamieson BD, Sun D, Li S, et al. An epigenetic clock analysis of race/ethnicity, sex, and coronary heart disease. Genome Biol. 2016; 17:171. doi: 10.1186/s13059-016-1030-0

60. McGuire S. US Department of Agriculture and US Department of Health and Human Services, Dietary Guidelines for Americans, 2010. Washington, DC: US Government Printing Office, January 2011. Advances in Nutrition: An International Review Journal. 2011; 23:293-294.

61. Committee DGA. Scientific Report of the 2015 Dietary Guidelines Advisory Committee. Washington (DC):

USDA and US Department of Health and Human Services. 2015.

62. Lu AT, Hannon E, Levine ME, Hao K, Crimmins EM, Lunnon K, Kozlenkov A, Mill J, Dracheva S, Horvath S. Genetic variants near MLST8 and DHX57 affect the epigenetic age of the cerebellum. Nat Commun. 2016; 7:10561. doi: 10.1038/ncomms10561

63. Castelo-Branco C, Soveral I. The immune system and aging: a review. Gynecol Endocrinol. 2014; 30:16–22. doi: 10.3109/09513590.2013.852531

64. Finch CE. Evolution in health and medicine Sackler colloquium: Evolution of the human lifespan and diseases of aging: roles of infection, inflammation, and nutrition. Proc Natl Acad Sci USA. 2010 (Suppl 1); 107:1718–24. doi: 10.1073/pnas.0909606106

65. Chowdhury R, Stevens S, Gorman D, Pan A, Warnakula S, Chowdhury S, Ward H, Johnson L, Crowe F, Hu FB, Franco OH. Association between fish consumption, long chain omega 3 fatty acids, and risk of cerebrovascular disease: systematic review and meta-analysis. BMJ. 2012; 345:e6698. doi: 10.1136/bmj.e6698

66. Zheng J-S, Hu X-J, Zhao Y-M, Yang J, Li D. Intake of fish and marine n-3 polyunsaturated fatty acids and risk of breast cancer: meta-analysis of data from 21 independent prospective cohort studies. BMJ. 2013; 346:f3706. doi: 10.1136/bmj.f3706

67. Farina EK, Kiel DP, Roubenoff R, Schaefer EJ, Cupples LA, Tucker KL. Protective effects of fish intake and interactive effects of long-chain polyunsaturated fatty acid intakes on hip bone mineral density in older adults: the Framingham Osteoporosis Study. Am J Clin Nutr. 2011; 93:1142–51. doi: 10.3945/ajcn.110.005926

68. Bannenberg GL, Chiang N, Ariel A, Arita M, Tjonahen E, Gotlinger KH, Hong S, Serhan CN. Molecular circuits of resolution: formation and actions of resolvins and protectins. J Immunol. 2005; 174:4345–55. doi: 10.4049/jimmunol.174.7.4345

69. Ridker PM, Buring JE, Cook NR, Rifai N. C-reactive protein, the metabolic syndrome, and risk of incident cardiovascular events: an 8-year follow-up of 14 719 initially healthy American women. Circulation. 2003; 107:391–97. doi: 10.1161/01.CIR.0000055014.62083.05

70. de Labry LO, Glynn RJ, Levenson MR, Hermos JA, LoCastro JS, Vokonas PS. Alcohol consumption and mortality in an American male population: recovering the U-shaped curve--findings from the normative Aging Study. J Stud Alcohol. 1992; 53:25–32. doi: 10.15288/jsa.1992.53.25

71. Knott CS, Coombs N, Stamatakis E, Biddulph JP. All cause mortality and the case for age specific alcohol consumption guidelines: pooled analyses of up to 10 population based cohorts. BMJ. 2015; 350:h384. doi: 10.1136/bmj.h384

72. Beach SR, Dogan MV, Lei MK, Cutrona CE, Gerrard M, Gibbons FX, Simons RL, Brody GH, Philibert RA. Methylomic Aging as a Window onto the Influence of Lifestyle: Tobacco and Alcohol Use Alter the Rate of Biological Aging. J Am Geriatr Soc. 2015; 63:2519–25. doi: 10.1111/jgs.13830

73. Grønbaek M, Becker U, Johansen D, Gottschau A, Schnohr P, Hein HO, Jensen G, Sørensen TI. Type of alcohol consumed and mortality from all causes, coronary heart disease, and cancer. Ann Intern Med. 2000; 133:411–19. doi: 10.7326/0003-4819-133-6-200009190-00008

74. Volpato S, Pahor M, Ferrucci L, Simonsick EM, Guralnik JM, Kritchevsky SB, Fellin R, Harris TB. Relationship of alcohol intake with inflammatory markers and plasminogen activator inhibitor-1 in well-functioning older adults: the Health, Aging, and Body Composition study. Circulation. 2004; 109:607–12. doi: 10.1161/01.CIR.0000109503.13955.00

75. Fillmore KM, Kerr WC, Stockwell T, Chikritzhs T, Bostrom A. Moderate alcohol use and reduced mortality risk: systematic error in prospective studies. Addict Res Theory. 2006; 14:101–32. doi: 10.1080/16066350500497983

76. Brien SE, Ronksley PE, Turner BJ, Mukamal KJ, Ghali WA. Effect of alcohol consumption on biological markers associated with risk of coronary heart disease: systematic review and meta-analysis of interventional studies. BMJ. 2011; 342:d636. doi: 10.1136/bmj.d636

77. Dauchet L, Amouyel P, Hercberg S, Dallongeville J. Fruit and vegetable consumption and risk of coronary heart disease: a meta-analysis of cohort studies. J Nutr. 2006; 136:2588–93.

78. He FJ, Nowson CA, Lucas M, MacGregor GA. Increased consumption of fruit and vegetables is related to a reduced risk of coronary heart disease: meta-analysis of cohort studies. J Hum Hypertens. 2007; 21:717–28. doi: 10.1038/sj.jhh.1002212

79. He FJ, Nowson CA, MacGregor GA. Fruit and vegetable consumption and stroke: meta-analysis of cohort studies. Lancet. 2006; 367:320–26. doi: 10.1016/S0140-6736(06)68069-0

80. Carter P, Gray LJ, Troughton J, Khunti K, Davies MJ. Fruit and vegetable intake and incidence of type 2 diabetes mellitus: systematic review and meta-

analysis. BMJ. 2010; 341:c4229. doi: 10.1136/bmj.c4229

81. Gandini S, Merzenich H, Robertson C, Boyle P. Meta-analysis of studies on breast cancer risk and diet: the role of fruit and vegetable consumption and the intake of associated micronutrients. Eur J Cancer. 2000; 36:636–46.
doi: 10.1016/S0959-8049(00)00022-8

82. Wang X, Ouyang Y, Liu J, Zhu M, Zhao G, Bao W, Hu FB. Fruit and vegetable consumption and mortality from all causes, cardiovascular disease, and cancer: systematic review and dose-response meta-analysis of prospective cohort studies. BMJ. 2014; 349:g4490. doi: 10.1136/bmj.g4490

83. Holt EM, Steffen LM, Moran A, Basu S, Steinberger J, Ross JA, Hong C-P, Sinaiko AR. Fruit and vegetable consumption and its relation to markers of inflammation and oxidative stress in adolescents. J Am Diet Assoc. 2009; 109:414–21. doi: 10.1016/j.jada.2008.11.036

84. Esmaillzadeh A, Kimiagar M, Mehrabi Y, Azadbakht L, Hu FB, Willett WC. Fruit and vegetable intakes, C-reactive protein, and the metabolic syndrome. Am J Clin Nutr. 2006; 84:1489–97.

85. Ornish D, Lin J, Chan JM, Epel E, Kemp C, Weidner G, Marlin R, Frenda SJ, Magbanua MJ, Daubenmier J, Estay I, Hills NK, Chainani-Wu N, et al. Effect of comprehensive lifestyle changes on telomerase activity and telomere length in men with biopsy-proven low-risk prostate cancer: 5-year follow-up of a descriptive pilot study. Lancet Oncol. 2013; 14:1112–20. doi: 10.1016/S1470-2045(13)70366-8

86. Farzaneh-Far R, Lin J, Epel ES, Harris WS, Blackburn EH, Whooley MA. Association of marine omega-3 fatty acid levels with telomeric aging in patients with coronary heart disease. JAMA. 2010; 303:250–57. doi: 10.1001/jama.2009.2008

87. Barzilai N, Crandall JP, Kritchevsky SB, Espeland MA. Metformin as a Tool to Target Aging. Cell Metab. 2016; 23:1060–65. doi: 10.1016/j.cmet.2016.05.011

88. Klemera P, Doubal S. A new approach to the concept and computation of biological age. Mech Ageing Dev. 2006; 127:240–48. doi: 10.1016/j.mad.2005.10.004

89. The Women's Health Initiative Study Group. Design of the Women's Health Initiative clinical trial and observational study. Control Clin Trials. 1998; 19:61–109. doi: 10.1016/S0197-2456(97)00078-0

90. Patterson RE, Kristal AR, Tinker LF, Carter RA, Bolton MP, Agurs-Collins T. Measurement characteristics of the Women's Health Initiative food frequency questionnaire. Ann Epidemiol. 1999; 9:178–87. doi: 10.1016/S1047-2797(98)00055-6

91. Houseman EA, Accomando WP, Koestler DC, Christensen BC, Marsit CJ, Nelson HH, Wiencke JK, Kelsey KT. DNA methylation arrays as surrogate measures of cell mixture distribution. BMC Bioinformatics. 2012; 13:86. doi: 10.1186/1471-2105-13-86

92. Horvath S, Gurven M, Levine ME, Trumble BC, Kaplan H, Allayee H, Ritz BR, Chen B, Lu AT, Rickabaugh TM, Jamieson BD, Sun D, Li S, et al. An epigenetic clock analysis of race/ethnicity, sex, and coronary heart disease. Genome Biol. 2016; 17:171. doi: 10.1186/s13059-016-1030-0

93. Whitsel EA, Baccarelli A, Hou L. Epigenetic Mechanisms of PM-Mediated CVD. Research Portfo-lio Online Reporting Tools. National Institutes of Health: U.S. Department of Health and Human Services: https://projectreporter.nih.gov/project_info_description.cfm?aid=8369149&icde=27485446).

94. Johnson WE, Li C, Rabinovic A. Adjusting batch effects in microarray expression data using empirical Bayes methods. Biostatistics. 2007; 8:118–27. doi: 10.1093/biostatistics/kxj037

95. Pisani P, Faggiano F, Krogh V, Palli D, Vineis P, Berrino F. Relative validity and reproducibility of a food frequency dietary questionnaire for use in the Italian EPIC centres. Int J Epidemiol. 1997 (Suppl 1); 26:S152–60. doi: 10.1093/ije/26.suppl_1.S152

96. Bartali B, Frongillo EA, Bandinelli S, Lauretani F, Semba RD, Fried LP, Ferrucci L. Low nutrient intake is an essential component of frailty in older persons. J Gerontol A Biol Sci Med Sci. 2006; 61:589–93. doi: 10.1093/gerona/61.6.589

97. Ferrucci L, Bandinelli S, Benvenuti E, Di Iorio A, Macchi C, Harris TB, Guralnik JM. Subsystems contributing to the decline in ability to walk: bridging the gap between epidemiology and geriatric practice in the InCHIANTI study. J Am Geriatr Soc. 2000; 48:1618–25.
doi: 10.1111/j.1532-5415.2000.tb03873.x

SUPPLEMENTARY INFORMATION

Selection of participants from the Women's Health Initiative BA23 dataset

Participants included individuals from the Women's Health Initiative (WHI), a national study that began in 1993 and enrolled postmenopausal women between the ages of 50-79 years into either randomized clinical trials (RCTs) or into an observational study; in our sample, 1,657 of these individuals were enrolled in at least one of the RCTs and the remaining 441 were enrolled in the observational study. For this analysis, women were selected from one of two large WHI sub-cohorts that had previously undergone genotyping as well as profiling for cardiovascular disease related blood biomarkers through two core WHI ancillary studies (Supplementary Figure 10).

The first cohort is known as the WHI SNP Health Association Resource (SHARe) cohort of minorities that includes >8000 African American women and >3500 Hispanic women. These women were genotyped through the WHI core study M5-SHARe (www.whi.org/researchers/data/WHIStudies/StudySites/M5) and underwent baseline blood biomarker profiling through WHI Core study W54-SHARe (www.whi.org/researchers/data/WHIStudies/StudySites/M5). The second cohort consists of a combination of European Americans from the two Hormonal Therapy (HT) trials selected for GWAS and biomarkers in core studies W58 (www.whi.org/researchers/data/WHIStudies/StudySites/W58) and W63 (www.whi.org/researchers/data/ HIStudies/StudySites/ W63).

While none of the participants of our study suffered from coronary heart disease at baseline, roughly half of the samples developed CHD at a later point. From the M5-SHARe and W54-SHARe cohorts, two sample sets were formed. The first (sample set 1) is a sample set of 637 CHD cases and 631 non-CHD cases as of Sept 30, 2010. The second sample set (sample set 2) is a non-overlapping sample of 432 cases of coronary heart disease and 472 non-cases as of September 17, 2012. We acknowledge a potential for selection bias using the above-described sampling scheme in WHI but suspect if such bias is present it is minimal. First, some selection bias is introduced by restricting our methylation profiling at baseline to women with GWAS & biomarker data from baseline as well, given the requirement that these participants must have signed the WHI supplemental consent for broad sharing of genetic data in 2005. However, we believe that selection bias at this stage is minimized by the inclusion of participants who died between the time of the start of the WHI study

and the time of supplemental consent in 2005, which resulted in the exclusion of only ~6-8% of all WHI participants. Nevertheless, participants unable or unwilling to sign consent in 2005 may not represent a random subset of all participants who survived to 2005. Second, some selection bias may also occur if similar gross differences exist in the characteristics of participants who consented to be followed in the two WHI extension studies beginning in 2005 and 2010 compared to non-participants at each stage. We believe these selection biases, if present, have minimal influence on our effect estimates.

A

WHI BA23 dataset

		Adjusted for ethnicity						Caucasian						African American						Hispanic					
				EEAA		IEAA				EEAA		IEAA				EEAA		IEAA				EEAA		IEAA	
		n	μ	bicor	p	bicor	p	n	μ	bicor	p	bicor	p	n	μ	bicor	p	bicor	p	n	μ	bicor	p	bicor	p
Diet	log2(Total energy)	2086	10.51	-0.02	0.33	0.00	0.87	992	10.58	-0.04	0.17	0.00	0.90	666	10.46	0.03	0.40	-0.01	0.85	428	10.45	-0.06	0.20	0.01	0.90
	Carbohydrate	2086	49.40	-0.01	0.59	0.04	0.05	992	49.45	0.01	0.81	0.05	0.11	666	49.03	-0.03	0.47	0.02	0.55	428	49.89	-0.02	0.61	0.06	0.19
	Protein	2086	16.54	-0.02	0.31	-0.03	0.24	992	16.89	-0.02	0.48	0.01	0.71	666	16.10	-0.02	0.70	-0.08	0.03	428	16.40	-0.02	0.65	-0.01	0.87
	Fat	2086	34.20	0.03	0.20	-0.02	0.45	992	33.23	0.01	0.71	-0.02	0.52	666	35.65	0.02	0.66	0.00	0.96	428	34.18	0.09	0.07	-0.05	0.35
	log2(1+Red meat)	2086	0.74	0.02	0.41	0.00	0.95	992	0.75	-0.02	0.51	-0.01	0.70	666	0.73	0.07	0.06	0.00	0.94	428	0.72	0.01	0.87	0.02	0.67
	log2(1+Poultry)	2086	0.46	-0.04	0.06	-0.05	0.02	992	0.41	-0.05	0.15	-0.05	0.09	666	0.52	-0.02	0.69	-0.08	0.04	428	0.47	-0.07	0.17	0.01	0.89
	log2(1+Fish)	2086	0.31	-0.08	6E-4	-0.02	0.34	992	0.29	-0.07	0.04	-0.02	0.52	666	0.37	-0.06	0.11	-0.09	0.03	428	0.25	-0.11	0.02	0.00	0.94
	log2(1+Dairy)	2086	1.25	-0.02	0.26	-0.02	0.43	992	1.42	-0.03	0.30	-0.01	0.72	666	1.02	0.01	0.84	-0.02	0.53	428	1.23	-0.06	0.24	-0.02	0.63
	log2(1+Whole grains)	2086	1.03	-0.01	0.58	0.01	0.76	992	1.00	-0.04	0.16	0.00	0.97	666	1.03	0.04	0.36	0.00	0.97	428	1.07	-0.02	0.63	0.03	0.52
	log2(1+Nuts)	2086	0.18	0.01	0.58	0.03	0.13	992	0.20	0.03	0.31	0.05	0.09	666	0.20	0.01	0.88	0.02	0.58	428	0.11	0.02	0.71	0.05	0.27
	log2(Fruits)	2086	0.33	-0.03	0.20	0.02	0.40	992	0.47	-0.04	0.19	0.02	0.63	666	0.28	0.02	0.57	0.02	0.64	428	0.11	-0.07	0.12	0.02	0.65
	log2(Vegetables)	2086	0.60	-0.05	0.03	0.02	0.34	992	0.93	-0.06	0.08	0.02	0.59	666	0.44	0.01	0.85	0.01	0.89	428	0.10	-0.12	0.02	0.04	0.37
Blood nutrients	Retinol	224	0.59	-0.09	0.18	0.00	0.99	74	0.65	0.05	0.07	0.21	0.07	85	0.57	-0.13	0.24	-0.10	0.38	65	0.56	-0.18	0.15	-0.15	0.24
	Mean carotenoids	224	0.03	-0.19	4E-3	-0.03	0.63	74	0.08	-0.21	0.07	-0.07	0.55	85	-0.02	-0.13	0.22	-0.04	0.75	65	0.03	-0.25	0.04	-0.01	0.95
	Lycopene	224	0.42	-0.12	0.07	-0.03	0.66	74	0.45	-0.11	0.36	0.07	0.56	85	0.37	-0.15	0.18	-0.09	0.40	65	0.44	-0.17	0.17	-0.09	0.49
	log2(alpha-Carotene)	224	-4.28	-0.16	0.02	0.01	0.88	74	-4.07	-0.14	0.24	-0.04	0.74	85	-4.60	-0.11	0.31	0.02	0.85	65	-4.11	-0.22	0.07	0.05	0.70
	log2(beta-Carotene)	224	-2.09	-0.19	4E-3	-0.08	0.26	74	-1.94	-0.13	0.28	-0.03	0.77	85	-2.02	-0.16	0.14	-0.08	0.45	65	-2.35	-0.27	0.03	-0.11	0.38
	log2(Lutein+Zeaxanthin)	224	-2.36	-0.13	0.06	-0.06	0.38	74	-2.44	-0.08	0.52	-0.05	0.70	85	-2.22	-0.13	0.23	-0.16	0.15	65	-2.45	-0.17	0.17	0.08	0.54
	log2(beta-Cryptoxanthin)	224	-3.82	-0.04	0.52	0.03	0.67	74	-3.94	-0.15	0.19	-0.01	0.96	85	-3.82	0.09	0.43	0.08	0.48	65	-3.66	-0.06	0.66	0.02	0.88
	log2(alpha-Tocopherol)	224	3.90	-0.04	0.54	0.00	1.00	74	4.03	-0.10	0.40	0.03	0.78	85	3.81	0.04	0.75	-0.12	0.27	65	3.86	-0.05	0.69	0.13	0.30
	log2(gamma-Tocopherol)	224	0.87	0.05	0.48	0.12	0.07	74	0.87	0.00	0.98	0.07	0.54	85	0.96	0.15	0.17	0.19	0.08	65	0.74	-0.01	0.93	0.08	0.55
Measurements	log2(C-reactive protein)	2073	1.58	0.11	3E-7	0.07	2E-3	991	1.26	0.12	3E-4	0.07	0.04	661	1.90	0.07	0.06	0.08	0.03	421	1.81	0.19	1E-4	0.05	0.33
	log2(Insulin)	2051	5.82	0.09	3E-5	0.06	3E-3	970	5.65	0.12	2E-4	0.06	0.05	656	6.05	0.06	0.13	0.09	0.02	425	5.86	0.09	0.06	0.02	0.65
	log2(Glucose)	2091	6.70	0.04	0.08	0.06	0.01	995	6.67	0.07	0.02	0.05	0.15	666	6.74	0.02	0.62	0.07	0.07	430	6.70	0.00	0.93	0.07	0.17
	log2(Triglyceride)	2091	7.02	0.09	2E-5	0.08	2E-4	995	7.12	0.10	3E-3	0.08	0.02	666	6.76	0.08	0.04	0.09	0.02	430	7.21	0.11	0.02	0.08	0.09
	Total cholesterol	2091	233.03	0.04	0.06	0.03	0.16	995	236.31	0.08	0.01	0.04	0.24	666	231.75	0.02	0.66	0.01	0.79	430	227.37	0.00	0.98	0.04	0.37
	LDL cholesterol	2057	151.23	0.03	0.18	0.01	0.58	976	153.81	0.07	0.02	0.02	0.54	659	152.79	0.01	0.82	0.00	0.92	422	142.83	-0.03	0.50	0.02	0.74
	HDL cholesterol	2091	52.17	-0.06	4E-3	-0.01	0.58	995	51.01	-0.06	0.05	-0.06	0.06	666	54.71	-0.06	0.14	-0.02	0.62	430	50.91	-0.07	0.14	-0.02	0.64
	log2(Creatinine)	2041	-0.42	0.01	0.59	-0.01	0.67	973	-0.45	0.03	0.43	-0.02	0.62	657	-0.33	0.05	0.19	0.03	0.40	411	-0.50	-0.07	0.14	-0.07	0.19
	Systolic blood pressure	2093	132.02	0.05	0.01	0.02	0.26	995	131.92	0.10	2E-3	0.01	0.86	668	134.05	0.03	0.37	0.07	0.08	430	129.06	-0.02	0.63	-0.01	0.88
	Diastolic blood pressure	2093	76.41	0.03	0.24	0.03	0.13	995	75.21	0.06	0.05	0.02	0.49	668	78.71	0.00	0.98	0.08	0.05	430	75.58	-0.03	0.59	-0.01	0.78
	log2(Waist / hip ratio)	2093	-0.27	0.09	8E-5	0.04	0.10	995	-0.28	0.09	0.01	0.06	0.06	668	-0.27	0.06	0.13	-0.01	0.77	430	-0.28	0.13	0.01	0.06	0.23
	BMI	2093	29.85	0.08	6E-4	0.07	2E-3	995	28.83	0.10	1E-3	0.10	2E-3	668	31.71	0.05	0.20	0.06	0.13	430	29.32	0.06	0.20	0.01	0.81
Socio-behavioral	Education	2071	6.66	-0.10	2E-6	0.00	0.83	989	6.86	-0.12	2E-4	0.02	0.43	660	6.85	-0.11	0.01	-0.03	0.40	422	5.90	-0.06	0.20	0.02	0.61
	Income	2019	3.54	-0.08	3E-4	-0.01	0.51	964	3.67	-0.06	0.06	0.02	0.64	642	3.47	-0.08	0.04	-0.06	0.11	413	3.32	-0.11	0.02	0.01	0.80
	log2(1+Exercise)	2090	2.49	-0.08	5E-4	-0.03	0.20	994	2.67	-0.08	0.01	0.01	0.70	667	2.30	-0.04	0.26	-0.11	4E-3	429	2.37	-0.12	0.01	0.02	0.67
	Current smoker	2090	0.14	0.00	0.93	0.00	0.88	994	0.13	-0.03	0.37	0.01	0.80	667	0.16	0.07	0.07	0.02	0.60	429	0.14	-0.01	0.77	0.05	0.27
	log2(1+Alcohol)	2086	1.09	-0.05	0.02	-0.01	0.52	992	1.44	-0.06	0.07	-0.02	0.48	666	0.73	-0.01	0.72	0.01	0.79	428	0.86	0.00	0.92	0.01	0.82

B

WHI AS315 dataset

		Adjusted for ethnicity						Caucasian						African American						Hispanic					
				EEAA		IEAA				EEAA		IEAA				EEAA		IEAA				EEAA		IEAA	
		n	μ	bicor	p	bicor	p	n	μ	bicor	p	bicor	p	n	μ	bicor	p	bicor	p	n	μ	bicor	p	bicor	p
Diet	log2(Total energy)	1601	10.56	-0.02	0.49	0.01	0.77	828	10.62	-0.03	0.37	0.05	0.13	405	10.49	0.04	0.45	0.03	0.52	205	10.58	-0.03	0.71	-0.14	0.05
	Carbohydrate	1601	48.50	0.02	0.47	-0.03	0.30	828	48.09	0.03	0.34	-0.04	0.24	405	48.67	0.03	0.49	0.01	0.88	205	48.34	-0.03	0.68	0.06	0.37
	Protein	1601	16.45	-0.03	0.27	-0.02	0.36	828	16.73	-0.06	0.07	-0.04	0.21	405	15.87	-0.05	0.29	-0.01	0.82	205	16.43	0.08	0.25	-0.01	0.87
	Fat	1601	35.28	0.01	0.58	0.03	0.23	828	34.98	0.03	0.37	0.06	0.11	405	36.32	-0.04	0.47	-0.03	0.57	205	35.65	0.05	0.44	-0.04	0.57
	log2(1+Red meat)	1601	0.77	0.02	0.42	0.07	0.01	828	0.79	0.02	0.59	0.10	3E-3	405	0.76	0.03	0.54	0.09	0.06	205	0.82	0.05	0.46	-0.09	0.20
	log2(1+Poultry)	1601	0.45	-0.02	0.43	-0.04	0.10	828	0.43	-0.05	0.19	-0.02	0.59	405	0.50	0.03	0.54	0.00	0.94	205	0.49	0.01	0.90	-0.16	0.02
	log2(1+Fish)	1601	0.32	-0.06	0.01	-0.01	0.59	828	0.31	-0.09	0.01	0.03	0.46	405	0.36	-0.05	0.27	-0.09	0.09	205	0.26	-0.03	0.72	-0.08	0.24
	log2(1+Dairy)	1601	1.26	-0.01	0.82	0.02	0.37	828	1.42	-0.04	0.27	0.04	0.27	405	1.00	0.05	0.27	0.08	0.11	205	1.30	0.06	0.37	-0.04	0.59
	log2(1+Whole grains)	1601	-0.17	0.04	0.13	0.02	0.45	828	-0.13	-0.04	0.27	0.01	0.79	405	-0.21	-0.06	0.26	-0.02	0.65	205	0.02	0.06	0.40	-0.11	0.13
	log2(1+Nuts)	1601	0.21	-0.05	0.06	-0.01	0.57	828	0.23	-0.03	0.36	0.00	0.93	405	0.21	-0.10	0.05	0.00	0.99	205	0.13	0.07	0.35	0.02	0.75
	log2(Fruits)	1601	0.31	-0.04	0.10	-0.03	0.17	828	0.37	-0.08	0.02	-0.03	0.36	405	0.34	0.01	0.84	0.03	0.53	205	0.10	0.00	0.96	-0.09	0.21
	log2(Vegetables)	1601	0.64	-0.03	0.22	-0.03	0.28	828	0.81	0.00	0.98	0.00	0.95	405	0.54	-0.02	0.63	-0.01	0.81	205	0.15	-0.09	0.18	-0.12	0.08
Blood nutrients	Retinol	2044	0.59	0.00	0.98	0.02	0.43	1040	0.62	0.04	0.20	0.03	0.31	511	0.56	-0.02	0.60	0.03	0.49	281	0.54	-0.06	0.28	-0.01	0.85
	Mean carotenoids	2043	0.01	-0.12	7E-8	-0.06	4E-3	1040	-0.01	-0.14	5E-6	-0.09	4E-3	511	-0.02	-0.12	5E-3	-0.06	0.21	281	0.05	-0.02	0.76	-0.04	0.54
	Lycopene	2044	0.39	-0.02	0.37	-0.01	0.52	1040	0.40	0.01	0.97	-0.02	0.55	511	0.39	-0.03	0.44	-0.05	0.31	281	0.40	-0.02	0.80	0.00	0.94
	log2(alpha-Carotene)	2044	-4.22	-0.11	1E-6	-0.05	0.03	1040	-4.13	-0.11	2E-4	-0.06	0.07	511	-4.53	-0.13	4E-3	-0.05	0.23	281	-4.10	-0.06	0.35	-0.06	0.30
	log2(beta-Carotene)	2043	-2.19	-0.11	8E-6	-0.05	0.01	1040	-2.22	-0.11	6E-4	-0.04	0.19	511	-2.17	-0.12	0.01	-0.06	0.21	281	-2.36	0.01	0.90	0.00	0.95
	log2(Lutein+Zeaxanthin)	2044	-2.39	-0.09	8E-5	-0.03	0.15	1040	-2.47	-0.10	8E-4	-0.05	0.09	511	-2.27	-0.08	0.06	0.00	0.97	281	-2.46	0.06	0.32	-0.09	0.13
	log2(beta-Cryptoxanthin)	2044	-3.74	-0.11	2E-7	-0.07	9E-4	1040	-3.91	-0.17	5E-8	-0.11	4E-4	511	-3.78	-0.11	0.01	-0.05	0.30	281	-3.41	0.05	0.38	0.02	0.75
	log2(alpha-Tocopherol)	2044	3.94	-0.06	0.01	-0.04	0.06	1040	4.01	-0.10	2E-3	-0.10	2E-3	511	3.74	-0.02	0.64	0.10	0.03	281	3.90	-0.05	0.38	-0.07	0.23
	log2(gamma-Tocopherol)	2044	0.66	0.10	1E-5	0.07	8E-4	1040	0.58	0.13	5E-5	0.11	3E-4	511	0.99	0.08	0.08	0.00	0.99	281	0.67	0.06	0.30	-0.01	0.83
Measurements	log2(C-reactive protein)	736	1.44	0.16	9E-6	0.09	0.01	342	1.14	0.18	1E-3	0.18	8E-4	251	1.88	0.16	0.01	-0.01	0.88	113	1.27	0.10	0.30	0.08	0.38
	log2(Insulin)	1992	5.79	0.14	9E-10	0.07	3E-3	1009	5.64	0.11	7E-4	0.06	0.08	513	6.01	0.18	6E-5	0.06	0.16	277	5.96	0.15	0.01	0.02	0.69
	log2(Glucose)	2054	6.63	0.08	4E-4	0.05	0.02	1040	6.60	0.03	0.28	0.06	0.05	513	6.68	0.11	0.01	0.02	0.72	285	6.63	0.18	2E-3	0.12	0.04
	log2(Triglyceride)	2058	7.07	0.05	0.02	0.02	0.36	1046	7.15	0.01	0.77	0.01	0.70	513	6.75	0.09	0.05	0.06	0.16	285	7.20	0.04	0.47	-0.06	0.33
	Total cholesterol	2058	221.49	-0.02	0.27	0.03	0.15	1046	224.23	-0.01	0.87	0.00	0.96	513	220.40	-0.05	0.29	0.07	0.10	285	215.90	0.00	0.99	0.06	0.31
	LDL cholesterol	2028	134.34	0.00	0.87	0.05	0.04	1027	134.76	0.00	0.87	0.03	0.40	512	139.70	0.00	0.97	0.07	0.10	280	129.53	0.01	0.84	0.13	0.03
	HDL cholesterol	2055	57.60	-0.12	2E-8	-0.03	0.13	1043	58.39	-0.09	2E-3	-0.03	0.29	513	57.38	-0.20	5E-6	0.01	0.89	285	54.48	-0.10	0.09	-0.09	0.11
	log2(Creatinine)	707	-0.43	0.06	0.12	0.06	0.11	326	-0.47	0.05	0.10	0.06	0.30	243	-0.32	0.05	0.48	0.06	0.35	109	-0.52	0.05	0.58	0.04	0.69
	Systolic blood pressure	2072	128.27	0.10	8E-6	0.06	0.01	1051	127.42	0.07	0.02	0.04	0.22	517	131.31	0.16	3E-4	0.14	1E-3	286	126.99	0.09	0.13	0.03	0.61
	Diastolic blood pressure	2072	75.29	0.06	0.01	0.06	0.01	1051	74.52	0.05	0.10	0.06	0.04	517	77.30	0.11	0.01	0.08	0.08	286	74.75	0.08	0.20	0.04	0.47
	log2(Waist / hip ratio)	2072	-0.29	0.12	2E-5	0.05	0.02	1051	-0.30	0.08	0.01	0.04	0.18	517	-0.28	0.12	0.01	0.08	0.07	286	-0.28	0.07	0.23	0.03	0.63
	BMI	2072	29.51	0.10	2E-6	0.08	2E-4	1051	28.88	0.07	0.02	0.06	0.05	517	31.55	0.15	4E-4	0.09	0.04	286	29.70	0.10	0.10	0.02	0.71
Socio-behavioral	Education	2059	6.95	-0.09	2E-5	-0.05	0.02	1047	7.08	-0.09	3E-3	-0.05	0.10	512	7.02	-0.07	0.09	-0.12	0.01	283	6.03	-0.17	4E-3	-0.03	0.67
	Income	2022	3.92	-0.05	0.03	0.01	0.75	1025	4.08	-0.05	0.09	0.01	0.75	504	3.68	0.03	0.53	0.01	0.84	277	3.42	-0.10	0.11	-0.07	0.26
	log2(1+Exercise)	2052	2.57	-0.06	0.01	-0.05	0.02	1046	2.74	-0.08	0.01	-0.07	0.03	509	2.21	-0.06	0.17	-0.01	0.74	283	2.28	0.06	0.33	0.02	0.76
	Current smoker	2052	0.10	0.00	0.99	-0.01	0.69	1046	0.10	0.08	0.01	0.01	0.64	509	0.12	0.00	0.97	-0.04	0.41	283	0.10	0.00	0.95	0.02	0.77
	log2(1+Alcohol)	1601	1.11	-0.10	1E-4	-0.03	0.28	828	1.43	-0.12	4E-4	-0.04	0.27	405	0.69	0.00	0.96	-0.05	0.32	205	0.91	-0.11	0.13	-0.06	0.43

Supplementary Figure 1. Related to Figure 1. Stratified correlation analysis for IEAA and EEAA in the WHI. There are two main tables: the top original WHI sample, and the bottom validation sample. The correlations (bicor, biweight midcorrelation) for the two measures of epigenetic age acceleration are colored according to their magnitude, with positive correlations in red, negative correlations in blue, and statistical significance (p-values) in green. Smaller test sample sizes (n) are highlighted in orange, and sample means (μ) are listed. Stratified ethnic groups are displayed as separate groups of columns with the first column showing them in an adjusted aggregate. Blood biomarkers were measured from fasting plasma collected at baseline. Food groups and nutrients are inclusive, including all types and all preparation methods, e.g. folic acid includes synthetic and natural, dairy includes cheese and all types of milk, etc. Minor ethnic strata (Asians, American Indians, and other) in the validation sample are excluded because of small sample are excluded for for clarity.

Supplementary Table 1. Linear models of IEAA and EEAA in WHI metformin users with repeat measurements.

	IEAA		EEAA	
	β Coefficient	P-Value	β Coefficient	P-Value
Started Metformin	-0.79	0.456	-0.003	0.998
IEAA/EEAA (First Blood Draw)	-0.33	2.88e-13	-0.35	8.92e-15
Age (First Blood Draw)	-0.55	1.73e-08	-0.96	4.67e-15
Age (Second Blood Draw)	0.50	6.02e-07	0.98	1.21e-14
Glucose (First Blood Draw)	0.02	0.132	0.03	0.048
Glucose (First Blood Draw)	0.01	0.657	-0.03	0.056
Education	0.27	0.004	-0.02	0.89
Race/Ethnicity (Reference=Non-Hispanic White)				
American Indian	-1.03	0.577	-1.31	0.555
Asian	-1.10	0.450	-3.54	0.044
Non-Hispanic Black	-2.04	0.166	-2.45	0.165
Hispanic	-0.63	0.658	-2.88	0.093
Other	1.32	0.614	-3.60	0.254

Table shows the beta-coefficients and corresponding p-values for linear models of IEAA and EEAA in the middle and right columns, respectively. The left column denotes the regressors in the models.
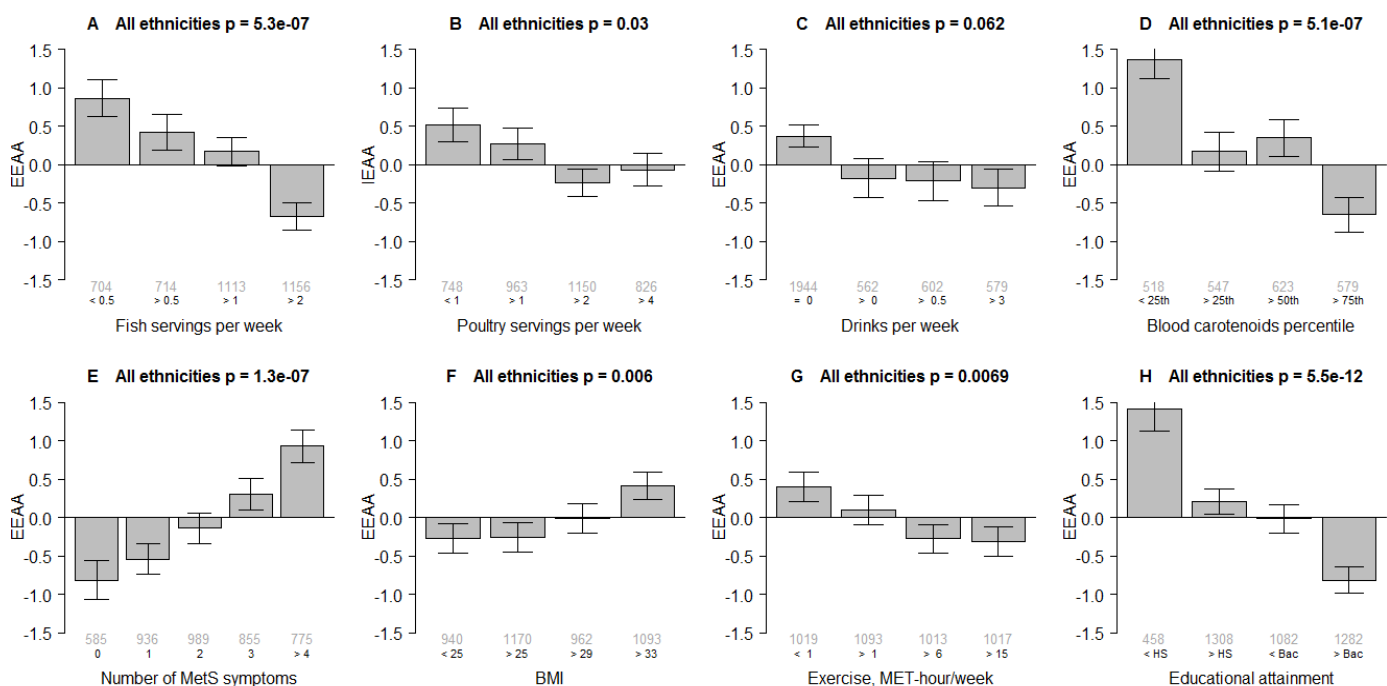
Supplementary Figure 2. EEAA among different levels of select dietary & lifestyle habits and measurements in the WHI. Panels **A-H** show bar plots visualizing the EEAA among stratified levels of fish, poultry (IEAA in this case), alcohol intake, blood carotenoid levels, number of metabolic syndrome symptoms, BMI, exercise, and education. Cut points roughly correspond roughly to quartiles except with number of MetS symptoms and alcohol intake which were selected for evenly-sized strata as much as possible. The sample sizes for each stratum are shown in grey beneath each bar. P-values for differences between strata are listed above each bar plot. Exercise is measured in units of metabolic equivalent hours per week and education uses high school diploma, some college, and bachelor's degree as cut points.

Supplementary Figure 3. Related to Figure 1. Correlations between diet, biomarkers, and sociodemographic factors in the WHI.

Pairwise correlations Adjusted for ethnicity and dataset	Diet												Blood nutrients									Measurements												Socio-behavioral					AA	
	log2(Total energy)	Carbohydrate	Protein	Fat	log2(1+Red meat)	log2(1+Poultry)	log2(1+Fish)	log2(1+Dairy)	log2(1+Whole grains)	log2(1+Nuts)	log2(Fruits)	log2(Vegetables)	Retinol	Mean carotenoids	Lycopene	log2(alpha-Carotene)	log2(beta-Carotene)	log2(Lutein+Zeaxanthin)	log2(beta-Cryptoxanthin)	log2(alpha-Tocopherol)	log2(gamma-Tocopherol)	log2(C-reactive protein)	log2(Insulin)	log2(Glucose)	log2(Triglyceride)	Total cholesterol	LDL cholesterol	HDL cholesterol	log2(Creatinine)	Systolic blood pressure	Diastolic blood pressure	log2(Waist / hip ratio)	BMI	Education	Income	log2(1+Exercise)	Current smoker	log2(1+Alcohol)	EEAA	IEAA
log2(Total energy)		-22	-2	24	62	48	35	63	52	25	25	32	-3	0	2	0	-3	-2	-2	-3	1	6	7	3	2	-6	-6	-3	-1	1	5	6	11	7	4	-1	0	7	-2	0
Carbohydrate	-22		-21	-83	-52	-23	-12	-4	15	-7	42	14	3	16	-3	19	17	8	19	10	-14	-14	-13	-9	2	1	-2	-4	5	1	-4	-8	-15	6	-1	13	-1	-14	0	2
Protein	-2	-21		-11	24	40	26	22	5	-3	-1	17	7	6	2	6	6	7	-1	7	-6	4	3	5	1	-2	-2	-1	-2	-2	-1	1	9	5	3	9	1	-2	-3	-2
Fat	24	-83	-11		45	9	-1	1	-11	12	-39	-20	-9	-21	0	-22	-20	-15	-20	-12	17	15	16	8	2	-3	-3	-2	-3	1	4	9	18	-11	-5	-21	1	-7	2	0
log2(1+Red meat)	62	-52	24	45		38	18	29	19	13	-6	8	-1	16	8	-19	-18	-15	-13	-8	13	13	17	9	7	-5	-5	0	-1	2	3	12	19	-7	1	-12	2	5	2	3
log2(1+Poultry)	48	-23	40	9	38		32	27	27	10	11	24	0	3	3	4	2	4	2	1	-3	6	7	4	1	-2	-3	5	-2	-1	3	3	11	7	9	1	1	9	-3	-5
log2(1+Fish)	35	-12	26	-1	18	32		23	19	11	16	28	4	8	4	7	6	10	3	8	-11	0	-1	1	-3	2	1	0	-2	-2	5	-1	6	10	3	6	1	19	-7	-2
log2(1+Dairy)	63	-4	22	1	29	27	23		37	21	21	20	2	2	-1	7	2	-2	3	1	-6	1	2	1	-1	-5	-5	-1	0	0	1	2	6	10	3	6	1	5	-2	0
log2(1+Whole grains)	52	15	5	-11	19	27	19	37		20	21	28	2	12	1	13	10	7	13	5	-9	-5	-2	-2	3	-4	-4	5	-1	-3	-1	-1	1	8	2	9	0	1	-2	0
log2(1+Nuts)	25	-7	-3	12	13	10	11	21	20		8	9	3	4	2	7	4	7	6	10	-11	3	5	-1	-2	-2	-3	4	-1	0	-2	-2	-2	7	6	2	0	9	-2	1
log2(Fruits)	25	42	-1	-39	-6	11	16	21	21	8		45	4	27	4	23	20	15	36	13	-17	-8	-7	-2	-2	-3	-3	5	2	3	-2	-6	-7	12	4	20	0	1	-3	0
log2(Vegetables)	32	14	17	-20	8	24	28	20	28	9	45		6	20	4	19	13	20	12	7	-10	-6	-6	-2	-7	-3	-4	4	0	1	0	-3	-2	15	12	18	-2	7	-4	0
Retinol	-3	3	7	-9	-1	0	4	2	2	3	4	6		10	9	5	6	11	9	37	-11	-12	4	3	40	23	9	1	21	8	3	9	-5	0	1	3	3	8	-1	2
Mean carotenoids	0	16	6	-21	-16	3	8	2	12	4	27	20	10		56	79	79	71	75	29	-23	-31	-31	-20	-15	25	22	25	6	-9	-7	-26	-34	17	11	18	0	8	-13	-6
Lycopene	2	-3	2	0	8	3	4	-1	1	2	4	4	9	56		28	29	30	25	11	4	-11	-12	-6	-3	24	22	12	1	-5	0	-9	-10	5	8	1	3	12	-3	-2
log2(alpha-Carotene)	0	19	6	-22	-19	4	7	7	13	7	23	19	5	79	28		67	45	49	17	-25	-28	-29	-18	-17	11	11	19	6	-9	-5	-25	-31	19	7	17	-1	6	-11	-4
log2(beta-Carotene)	-3	17	6	-20	-18	2	6	2	10	4	20	13	6	79	29	67		41	53	29	-32	-28	-28	-18	-20	14	15	18	7	-8	-9	-22	-31	13	2	16	0	3	-11	-6
log2(Lutein+Zeaxanthin)	-2	8	7	-15	-15	4	10	-2	7	2	15	20	11	71	30	45	41		46	25	-10	-23	-24	-15	-7	28	21	25	5	-4	-5	-16	-28	13	13	14	0	13	-9	-4
log2(beta-Cryptoxanthin)	2	19	-1	-20	-13	2	3	3	13	5	36	12	9	75	25	49	53	46		26	-22	-23	-20	-14	-8	18	15	17	2	-5	-5	-22	-24	13	6	15	3	6	-11	-6
log2(alpha-Tocopherol)	-3	10	7	-12	-8	1	8	1	5	4	13	7	37	29	11	17	29	25	26		-54	-7	-2	-6	37	36	22	3	2	-6	-4	2	-9	5	3	8	4	5	-6	-4
log2(gamma-Tocopherol)	1	-14	-6	17	13	-3	-11	-6	-9	-7	-17	-10	-11	-23	4	-25	-32	-10	-22	-54		23	19	17	13	14	18	-20	1	8	9	16	22	-10	-7	-11	-6	-13	9	8
log2(C-reactive protein)	6	-14	4	15	13	6	0	1	-5	3	-8	-6	-12	-31	-11	-28	-28	-23	-23	-7	23		35	23	21	2	2	-19	-2	7	4	24	45	-4	-4	-15	1	-7	12	8
log2(Insulin)	7	-13	3	16	17	7	-1	2	-2	5	-7	-6	4	-31	-12	-29	-28	-24	-20	-2	19	35		42	37	-1	0	-39	4	16	10	40	51	-11	-7	-18	0	-14	11	7
log2(Glucose)	3	-9	5	8	9	4	1	1	-2	-1	-2	-2	3	-20	-6	-18	-18	-15	-14	-6	17	23	42		21	1	1	-22	-4	16	7	26	29	-5	-6	-8	13	-6	6	6
log2(Triglyceride)	2	2	1	2	7	1	-3	-1	3	-2	-2	-7	40	-15	-3	-17	-20	-7	-8	37	13	21	37	21		31	17	-49	5	14	7	32	21	-7	-6	-10	1	-9	7	5
Total cholesterol	-6	1	-2	-3	-5	-2	2	-5	-4	-2	-3	-3	23	25	24	11	14	28	18	36	14	2	-1	1	31		93	8	10	7	2	5	-2	-3	-4	3	1	6	1	3
LDL cholesterol	-6	-2	-2	-3	-5	-3	1	-5	-4	-3	-3	-4	9	22	22	11	15	21	15	22	18	2	0	1	17	93		-9	10	4	2	5	1	-4	-5	1	1	4	1	3
HDL cholesterol	-3	-4	-1	-2	0	5	0	-1	5	4	5	4	1	25	12	19	18	25	17	3	-20	-19	-39	-22	-49	8	-9		-4	-4	-5	-31	-25	9	9	11	-1	20	-9	-4
log2(Creatinine)	-1	5	-2	-3	-1	-2	-2	0	-1	-1	2	0	21	6	1	6	7	5	2	2	1	-2	4	-4	5	10	10	-4		4	3	0	-1	2	1	2	-1	1	2	1
Systolic blood pressure	1	1	-2	1	2	-1	-2	0	-3	0	3	1	8	-9	-5	-9	-8	-4	-5	-6	8	7	16	16	14	7	4	-4	4		54	15	13	-9	-6	-6	1	-1	7	4
Diastolic blood pressure	5	-4	-1	4	3	3	5	1	-1	-2	-2	0	3	-7	0	-5	-9	-5	-5	-4	9	4	10	7	7	2	2	-5	3	54		4	14	-2	2	-3	0	2	4	5
log2(Waist / hip ratio)	6	-8	1	9	12	3	-1	2	-1	-2	-6	-3	9	-26	-9	-25	-22	-16	-22	2	16	24	40	26	32	5	5	-31	0	15	4		33	-10	-13	-9	0	-8	9	5
BMI	11	-15	9	18	19	11	6	6	1	-2	-7	-2	-5	-34	-10	-31	-31	-28	-24	-9	22	45	51	29	21	-2	1	-25	-1	13	14	33		-8	-9	-18	1	-13	9	8
Education	7	6	5	-11	-7	7	14	10	8	7	12	15	0	17	5	19	13	13	13	5	-10	-4	-11	-5	-7	-3	-4	9	2	-9	-2	-10	-8		37	11	1	17	-10	-2
Income	4	-1	3	-5	1	9	14	3	2	6	4	12	1	11	8	7	2	13	6	3	-7	-4	-7	-6	-6	-4	-5	9	1	-6	2	-13	-9	37		5	2	23	-6	0
log2(1+Exercise)	-1	13	9	-21	-14	1	9	6	9	2	20	18	3	18	1	17	16	14	15	8	-11	-15	-18	-8	-10	3	1	11	2	-6	-3	-9	-18	11	5		0	10	-7	-4
Current smoker	0	-1	1	1	2	1	1	0	0	0	0	-2	3	0	3	-1	0	0	3	4	-6	1	0	13	1	1	1	-1	-1	1	0	0	1	1	2	0		-3	-1	0
log2(1+Alcohol)	7	-14	-2	-7	5	9	19	5	1	9	1	7	8	8	12	6	3	13	6	5	-13	-7	-14	-6	-9	6	4	20	1	-1	2	-8	-13	17	23	10	-3		-7	-2
EEAA	-2	0	-3	2	2	-3	-7	-2	-2	-2	-3	-4	-1	-13	-3	-11	-11	-9	-11	-6	9	12	11	6	7	1	1	-9	2	7	4	9	9	-10	-6	-7	-1	-7		37
IEAA	0	2	-2	0	3	-5	-2	0	0	1	0	0	2	-6	-2	-4	-6	-4	-6	-4	8	8	7	6	5	3	3	-4	1	4	5	5	8	-2	0	-4	0	-2	37	

Supplementary Figure 3. Related to Figure 1. Correlations between diet, biomarkers, and sociodemographic factors in the WHI. The percent correlations (biweight midcorrelation, -100 < %r < 100) between adjusted dietary and biomarker factors are colored according to their magnitude, with positive correlations in red, negative correlations in blue. Blood biomarkers were measured from fasting plasma collected at baseline. At 903 ≤ n ≤ 4200 samples, the Bonferroni corrected significance threshold corresponds approximately to a percent correlation of | %r | ≥ 10 (shown in bold). Food groups and nutrients are inclusive, including all types and all preparation methods, e.g. folic acid includes synthetic and natural, and dairy includes cheese and all types of milk. Variables have been adjusted for ethnicity and originating dataset (WHI BA23 or WHI AS315).

Supplementary Figure 4. EEAA among different strata of ethnic groups, levels and types of alcohol intake in the WHI. Panels **A**-**D** show bar plots visualizing the EEAA among stratified levels of alcohol intake (medium servings per week) for select ethnic groupings. Panels **E**-**H** show bar plots visualizing the EEAA among non- and current drinkers (at least one drink per month) of different types of alcoholic drinks: all types, beer, wine, and liquor. The sample sizes for each stratum are shown in grey beneath each bar. P-values for differences between strata are listed above each bar plot.

A

EEAA n=922	Model 1 Minimal β	p	Model 2 Food β	p	Model 3 Biomarkers β	p	Model 4 MetS β	p	Model 5 Full β	p
log2(1 + Fish)			-1.45	0.05					-1.41	0.06
log2(1 + Poultry)			0.55	0.39					0.54	0.39
Mean carotenoids			-1.25	**5E-6**					-1.10	**1E-4**
Current drinker			-0.60	0.12					-0.52	0.18
Education	-0.33	**3E-4**	-0.24	**0.01**	-0.30	**1E-3**	-0.32	**5E-4**	-0.23	**0.02**
BMI	0.12	**9E-5**	0.03	**0.03**	0.03	0.36	0.09	**0.01**	0.02	0.55
Physically active	-0.17	0.71	0.14	0.76	-0.04	0.93	-0.17	0.71	0.21	0.64
Current smoker	0.65	0.23	0.26	0.63	0.50	0.36	0.61	0.26	0.25	0.65
African American	-3.22	**3E-14**	-3.13	**3E-13**	-3.43	**2E-14**	-3.19	**5E-14**	-3.29	**6E-13**
Hispanic	0.24	0.64	0.34	0.51	-0.05	0.92	0.26	0.62	0.09	0.86
log2(C-reactive protein)					0.32	**0.02**			0.24	0.06
log2(Insulin)					0.54	**0.03**			0.45	0.08
log2(Triglycerides)					-0.18	0.58			-0.01	0.97
log2(Glucose)					-0.75	0.22			-0.50	0.44
HDL Cholesterol					-0.03	0.06			-0.02	0.17
Systolic blood pressure					0.02	0.09			0.02	0.06
Diastolic blood pressure					-0.01	0.58			-0.01	0.55
log2(Waist-to-hip ratio)					-0.77	0.61			-1.22	0.43
Metabolic syndrome symptoms							0.27	0.07	-0.13	0.62

B

IEAA n=922	Model 1 Minimal β	p	Model 2 Food β	p	Model 3 Biomarkers β	p	Model 4 MetS β	p	Model 5 Full β	p
log2(1 + Fish)			-0.34	0.57					-0.22	0.71
log2(1 + Poultry)			-0.59	0.25					-0.60	0.23
Mean carotenoids			-0.41	0.06					-0.40	0.07
Current drinker			0.17	0.58					0.16	0.59
Education	-0.15	**0.04**	-0.13	0.07	-0.13	0.08	-0.14	**0.05**	-0.12	0.12
BMI	0.08	**1E-3**	0.07	**0.01**	0.05	0.10	0.06	**0.02**	0.06	0.05
Physically active	-0.16	0.65	-0.06	0.87	-0.13	0.71	-0.16	0.65	-0.04	0.91
Current smoker	-0.16	0.72	-0.32	0.46	-0.13	0.77	-0.18	0.68	-0.23	0.61
African American	-0.80	**0.02**	-0.64	0.06	-0.69	**0.05**	-0.78	**0.02**	-0.52	0.15
Hispanic	-1.48	**4E-4**	-1.32	**2E-3**	-1.54	**3E-4**	-1.47	**4E-4**	-1.42	**1E-3**
log2(C-reactive protein)					0.08	0.46			0.04	0.70
log2(Insulin)					0.25	0.22			0.26	0.21
log2(Triglycerides)					0.54	**0.04**			0.76	**0.01**
log2(Glucose)					-0.39	0.42			-0.08	0.88
HDL Cholesterol					0.01	0.53			0.00	0.83
Systolic blood pressure					0.01	0.15			0.02	**0.05**
Diastolic blood pressure					-0.02	0.42			-0.01	0.46
log2(Waist-to-hip ratio)					0.19	0.88			0.38	0.76
Metabolic syndrome symptoms							0.15	0.21	-0.30	0.14

A

EEAA n	Caucasian 886 β	p	African 481 β	p	Hispanic 259 β	p	Asian 100 β	p	Meta-analysis 886 meta-t	meta-p
log2(1 + Fish)	-1.18	0.18	-0.99	0.28	-0.91	0.50	-0.67	0.73	-1.88	0.06
log2(1 + Poultry)	0.03	0.97	-0.03	0.98	0.47	0.65	1.82	0.35	0.41	0.68
Mean carotenoids	-0.98	**2E-3**	-0.93	**0.02**	-0.68	0.17	-1.25	0.16	-4.34	**1E-5**
Current drinker	-0.80	**0.04**	0.17	0.77	-0.95	0.18	-2.36	**0.04**	-2.31	**0.02**
Education	-0.05	0.62	-0.17	0.22	-0.47	**2E-3**	0.04	0.89	-2.20	**0.03**
BMI	0.03	0.43	0.14	**2E-3**	0.07	0.28	0.11	0.37	2.85	**4E-3**
Physically active	-0.54	0.28	0.47	0.44	1.06	0.19	-2.49	0.11	-0.24	0.81
Current smoker	1.15	0.06	0.75	0.35	-2.29	**0.02**	-0.82	0.76	0.87	0.38

B

IEAA n	Caucasian 886 β	p	African 481 β	p	Hispanic 259 β	p	Asian 100 β	p	Meta-analysis 886 meta-t	meta-p
log2(1 + Fish)	0.20	0.78	-0.90	0.24	-0.21	0.85	1.05	0.52	-0.35	0.73
log2(1 + Poultry)	-0.50	0.43	0.13	0.85	-0.84	0.30	-2.23	0.18	-1.20	0.23
Mean carotenoids	-0.62	**0.02**	-0.43	0.20	-0.14	0.71	0.24	0.75	-2.47	**0.01**
Current drinker	-0.27	0.40	0.42	0.38	-0.42	0.46	1.09	0.27	-0.16	0.87
Education	-0.02	0.80	-0.22	0.06	-0.06	0.63	-0.35	0.15	-1.72	0.09
BMI	0.04	0.22	0.05	0.19	0.04	0.41	0.36	**8E-4**	2.72	**0.01**
Physically active	-0.10	0.82	0.05	0.92	0.91	0.16	-2.26	0.09	0.02	0.99
Current smoker	-0.17	0.74	-0.70	0.30	-0.55	0.48	0.13	0.96	-1.05	0.29

Supplementary Figure 5. Related to Figure 2. Meta-analysis of multivariable linear models of EEAA and IEAA including carotenoid levels in the WHI. Analogous to Figure 2 except including mean carotenoid levels: EEAA (panel **A**) and IEAA (panel **B**) were regressed on potential confounding factors, fish and poultry intake, mean across standardized measures of carotenoids, and current drinker status for the ethnic strata with sufficient sample sizes (n>100). Individual columns correspond to coefficient estimates (β) colored blue or red for negative and positive values respectively, and p-values (p) colored in green according to magnitude of significance, with the exception of the last two columns which denote Stouffers's method meta-t and meta-p values. Models are adjusted for originating dataset (WHI BA23 or WHI AS315).

A

EEAA n=922	Model 1 Minimal β	p	Model 2 Food β	p	Model 3 Biomarkers β	p	Model 4 MetS β	p	Model 5 Full β	p
log2(1 + Fish)			-1.45	0.05					-1.41	0.06
log2(1 + Poultry)			0.55	0.39					0.54	0.39
Mean carotenoids			-1.25	**5E-6**					-1.10	**1E-4**
Current drinker			-0.60	0.12					-0.52	0.18
Education	-0.33	**3E-4**	-0.24	**0.01**	-0.30	**1E-3**	-0.32	**5E-4**	-0.23	**0.02**
BMI	0.12	**9E-5**	0.07	**0.03**	0.03	0.36	0.09	**0.01**	0.02	0.55
Physically active	-0.17	0.71	0.14	0.76	-0.04	0.93	-0.17	0.71	0.21	0.64
Current smoker	0.65	0.23	0.26	0.63	0.50	0.36	0.61	0.26	0.25	0.65
African American	-3.22	**3E-14**	-3.13	**3E-13**	-3.43	**2E-14**	-3.19	**5E-14**	-3.29	**6E-13**
Hispanic	0.24	0.64	0.34	0.51	-0.05	0.92	0.26	0.62	0.09	0.86
log2(C-reactive protein)					0.32	**0.02**			0.24	0.08
log2(Insulin)					0.54	**0.03**			0.45	0.08
log2(Triglycerides)					-0.18	0.58			-0.01	0.97
log2(Glucose)					-0.75	0.22			-0.50	0.44
HDL Cholesterol					-0.03	0.06			-0.02	0.17
Systolic blood pressure					0.02	0.09			0.02	0.06
Diastolic blood pressure					-0.01	0.58			-0.01	0.55
log2(Waist-to-hip ratio)					-0.77	0.61			-1.22	0.43
Metabolic syndrome symptoms							0.27	0.07	-0.13	0.62

B

| IEAA n=922	Model 1 Minimal β	p	Model 2 Food β	p	Model 3 Biomarkers β	p	Model 4 MetS β	p	Model 5 Full β	p
log2(1 + Fish)			-0.34	0.57					-0.22	0.71
log2(1 + Poultry)			-0.59	0.25					-0.60	0.23
Mean carotenoids			-0.41	0.06					-0.40	0.07
Current drinker			0.17	0.58					0.16	0.59
Education	-0.15	**0.04**	-0.13	0.07	-0.13	0.08	-0.14	**0.05**	-0.12	0.12
BMI	0.08	**1E-3**	0.07	**0.01**	0.05	0.10	0.06	**0.02**	0.05	0.05
Physically active	-0.16	0.65	-0.06	0.87	-0.13	0.71	-0.16	0.65	-0.04	0.91
Current smoker	-0.16	0.72	-0.32	0.46	-0.13	0.77	-0.18	0.68	-0.23	0.61
African American	-0.80	**0.02**	-0.64	0.06	-0.69	**0.05**	-0.78	**0.02**	-0.52	0.15
Hispanic	-1.48	**4E-4**	-1.32	**2E-3**	-1.54	**3E-4**	-1.47	**4E-4**	-1.42	**1E-3**
log2(C-reactive protein)					0.08	0.46			0.04	0.70
log2(Insulin)					0.25	0.22			0.26	0.21
log2(Triglycerides)					0.54	**0.04**			0.76	**0.01**
log2(Glucose)					-0.39	0.42			-0.08	0.88
HDL Cholesterol					0.01	0.53			0.00	0.83
Systolic blood pressure					0.01	0.15			0.02	**0.05**
Diastolic blood pressure					-0.02	0.42			-0.01	0.46
log2(Waist-to-hip ratio)					0.19	0.88			0.38	0.76
Metabolic syndrome symptoms							0.15	0.21	-0.30	0.14

Supplementary Figure 6. Related to Figure 3. Multivariate linear models of EEAA and IEAA including carotenoid levels and with and without biomarkers in the WHI. Analogous to Figure 3 except including mean carotenoid levels: EEAA (panel **A**) and IEAA (panel **B**) were regressed on potential confounding factors, fish and poultry intake and current drinker status, and select biomarkers. Individual columns list the corresponding coefficient estimates (β) and p-values (p) for each fitting. Coefficients are colored according to sign (positive = red, negative = blue) and significance according to magnitude (green). Models 1 through 5 correspond to a minimal model, a model including dietary intake variables, a model including potential explanatory biomarkers, a model including number of metabolic syndrome symptoms and a complete model with all of the variables above, respectively. Models are adjusted for originating dataset (BA23 or AS315).

Supplementary Figure 7. Characteristics of non-, current, and future metformin users in the WHI. Panels **A-F** show barplots comparing the age at blood draw, educational attainment, ethnicity, fasting glucose, insulin, and insulin resistance of non-, current, and future metformin users (colored in green, red, and blue). Panels G-I show plotting fasting glucose, insulin, and insulin resistance as a function of years after blood draw until metformin with current and future users colored in red and blue respectively.
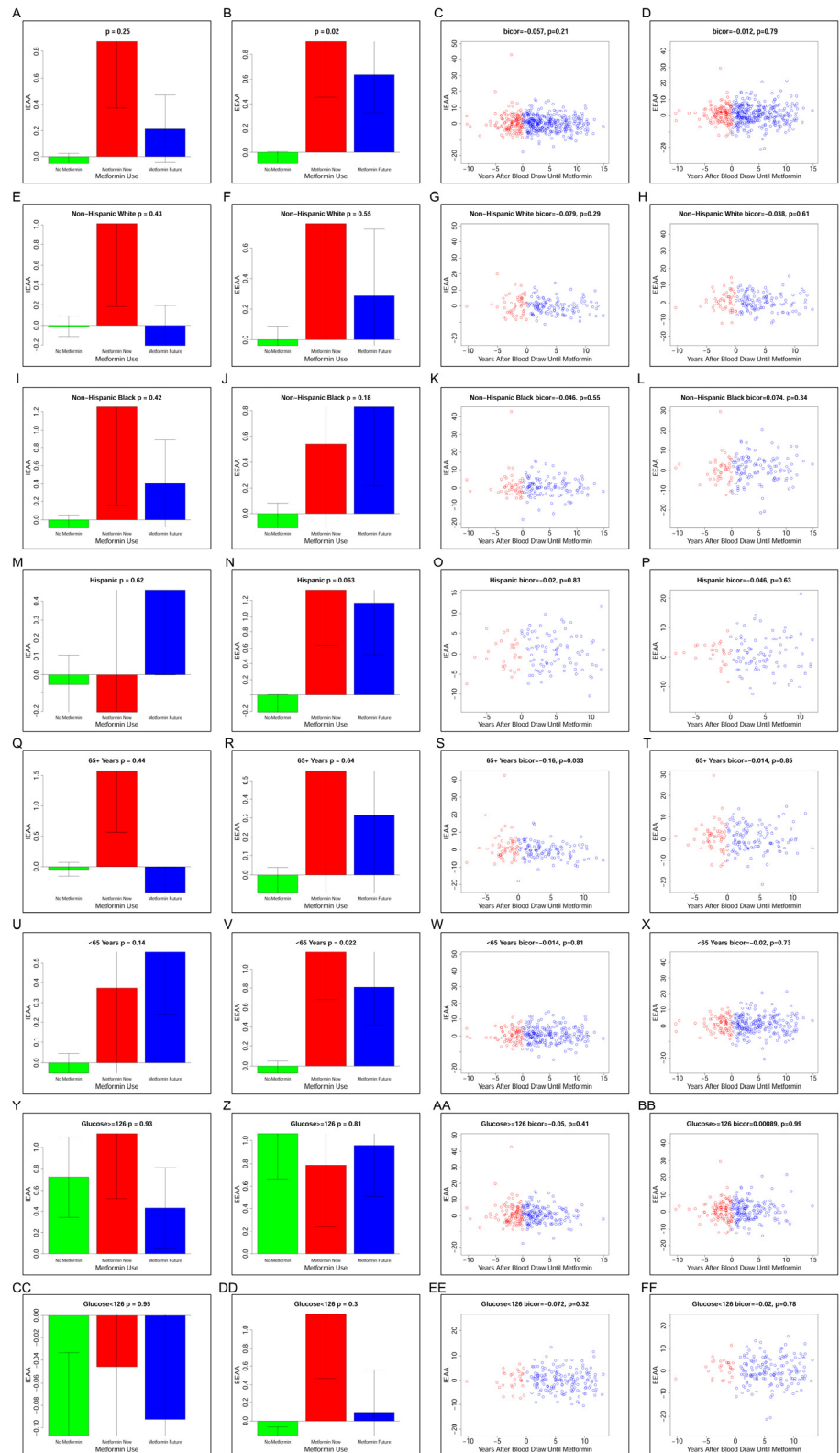
Supplementary Figure 8. IEAA and EEAA among non-, current, and future users of metformin in the WHI. Columns 1 and 2 show barplots with IEAA and EEAA on the y-axis and no metformin, current metformin, and later metformin usage strata (green, red, and blue respectively). Columns 3 and 4 show scatterplots with IEAA and EEAA plotted as a function of years after blood draw until metformin usage with current and future metformin users colored in red and blue respectively. Rows show the same plots for different sociodemographic strata: all available WHI participants, non-hispanic white, non-hispanic black, hispanic, > 65 years old, < 65 years old, hyperglycemic, and non-hyperglycemic groups. P-values (and correlation coefficients) are shown and the top of each plot.
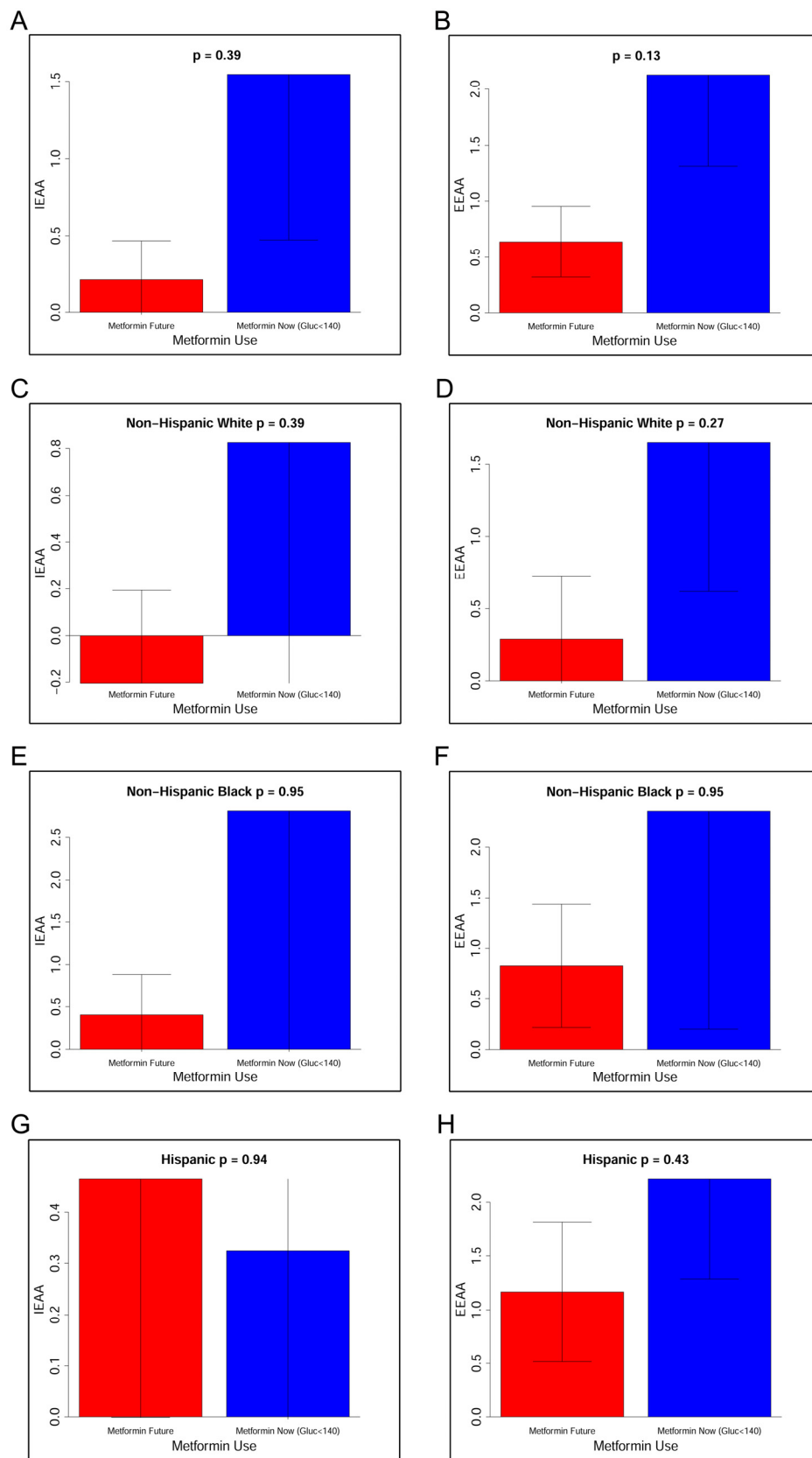
Supplementary Figure 9. IEAA and EEAA of future and non-hyperglycemic current metformin users in the WHI.
Columns 1 and 2 show the IEAA and EEAA of future metformin users and current metformin users with fasting glucose levels of < 140mg/dL colored in red and blue respectively. Rows correspond to different ethnic strata: all ethnic groups, non-hispanic white, non-hispanic black, and hispanic. P-values for each comparison are shown at the top of each plot.
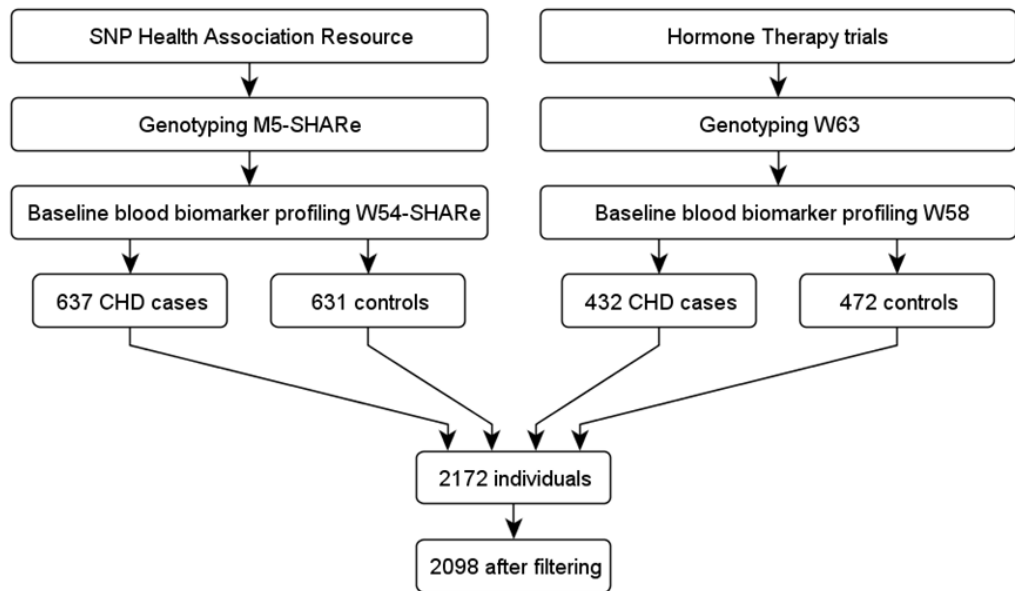
Supplementary Figure 10. Schematic denoting the selection of the WHI BA23 study sample. The study participants were originally selected for a case-control GWAS on coronary heart disease (CHD). Participants were selected from either the SNP Health Association Resource or the Hormone Therapy trials, and underwent genotyped and core blood biomarkers profiling. The data from these individuals were agglomerated and filtered for missing data.

Specific premature epigenetic aging of cartilage in osteoarthritis

Laura Vidal-Bralo[1], Yolanda Lopez-Golan[1], Antonio Mera-Varela[1], Ignacio Rego-Perez[2], Steve Horvath[3], Yuhua Zhang[4], Álvaro del Real[5], Guangju Zhai[4], Francisco J Blanco[2], Jose A. Riancho[5], Juan J Gomez-Reino[1], Antonio Gonzalez[1]

[1]Laboratorio Investigacion 10 and Rheumatology Unit, Instituto Investigacion Sanitaria, Hospital Clinico Universitario de Santiago, Travesia Choupana, sn. 15706- Santiago de Compostela, Spain

[2]Grupo de Reumatología, Instituto de Investigación Biomédica de A Coruña, Complexo Hospitalario Universitario de A Coruña, Universidade da Coruña. As Xubias, sn. 15006- A Coruña, Spain

[3]Department of Human Genetics, David Geffen School of Medicine, University of California Los Angeles, Los Angeles, CA 90095, USA

[4]Discipline of Genetics, Faculty of Medicine, Memorial University of Newfoundland, A1B- St. John's, NL, Canada

[5]Department of Internal Medicine, Hospital U. M. Valdecilla-IDIVAL, University of Cantabria, Cardenal Herrera Oria, 39011, Santander, Spain

Correspondence to: Antonio Gonzalez; **email:** agmartinezp@ser.es

ABSTRACT

Osteoarthritis (OA) is a disease affecting multiple tissues of the joints in the elderly, but most notably articular cartilage. Premature biological aging has been described in this tissue and in blood cells, suggesting a systemic component of premature aging in the pathogenesis of OA. Here, we have explored epigenetic aging in OA at the local (cartilage and bone) and systemic (blood) levels. Two DNA methylation age-measures (DmAM) were used: the multi-tissue age estimator for cartilage and bone; and a blood-specific biomarker for blood. Differences in DmAM between OA patients and controls showed an accelerated aging of 3.7 years in articular cartilage (95 % CI = 1.1 to 6.3, *P* = 0.008) of OA patients. By contrast, no difference in epigenetic aging was observed in bone (0.04 years; 95 % CI = -1.8 to 1.9, *P* = 0.3) and in blood (-0.6 years; 95 % CI = -1.5 to 0.3, *P* = 0.2) between OA patients and controls. Therefore, premature epigenetic aging according to DNA methylation changes was specific of OA cartilage, adding further evidence and insight on premature aging of cartilage as a component of OA pathogenesis that reflects damage and vulnerability.

INTRODUCTION

OA is the most common chronic disease affecting the joints with about a 45 % lifetime risk of developing OA of the knee [1, 2]. It can affect any joint, but it occurs most often in knees, hips, spine, or hands. Symptoms include pain and stiffness, bony enlargement, crepitus with movement and decreased function of the joint. OA pathogenesis is complex and includes multiple risk factors that are still incompletely known, but old age is a critical contributor [3, 4]. The relationship between old age and OA is not fully understood. Classically, it

was suspected that the association was related to the "wear and tear" of articular cartilage by continuous mechanical stress. Today, we know that this model of OA is insufficient because OA involves an active response to injury comprising remodeling of articular cartilage and neighboring bone, in addition of synovial inflammation and damage to ligaments and menisci [2]. In addition, the other component of the association with old age, biological aging, has shown unsuspected complexity, including its multidimensionality, variable progression, possibility of modulation and the pivotal role played by senescent cells [5].

The many facets of biological aging have been typified in nine cellular and molecular hallmarks: genomic instability, telomere attrition, epigenetic alterations, loss of proteostasis, deregulated nutrient sensing, mitochondrial dysfunction, cellular senescence, stem cell exhaustion, and altered intercellular communication [6]. Variable progression of biological aging with dissociation between biological and chronological age is observed in progeroid syndromes. Less dramatically, it is also observed as a reflection of lifestyle with smoking, heavy drinking, obesity, stress and depression as accelerators, and exercise and caloric restriction as rejuvenators. The pivotal role of cellular senescence and of the senescence-associated secretory phenotype has been established in multiple studies, but most strikingly with the reversal of age-associated changes obtained with their removal [7]. This rejuvenation has been obtained either through genetic manipulation or with senolytic drugs in mice in spite of the eliminated senescent cells were only a minor fraction in mouse tissues [5]. All these aspects could be of relevance for OA as exemplified by the secretory phenotype that includes secretion of metalloproteases and pro-inflammatory mediators, which could be involved in OA cartilage damage [2-4]. There is already persuasive evidence of accelerated biological aging at the affected cartilage [3, 4]. Many of the aging hallmarks have been described as exacerbated in OA chondrocytes and articular cartilage, including telomere length shortening, mitochondrial dysfunction, cellular senescence and genome instability [3, 4]. In contrast, biological age has not been studied in any other joint tissue although a systemic component of premature aging has been suggested by accelerated telomere length shortening in blood cells of 160 hand OA subjects compared with 926 controls [8]. Telomere shortening correlated with radiographic severity of OA in the hands in this study. These findings have not yet been independently confirmed, with a small subsequent study showing no telomere attrition in blood of knee OA patients [9], and a second small study reporting telomere shortening only in knee OA patients experiencing high stress and chronic pain [10]. A systemic premature aging component in OA is an attractive hypothesis because it is congruent with some epidemiological studies that have found increased prevalence of old-age comorbidities [11-14], frailty [15], and mortality in OA patients [16-18]. The two aspects, local and systemic, of premature aging could contribute to OA by further impairing cartilage and joint function, decreasing mobility and increasing joint vulnerability.

An opportunity to explore a different aging hallmark in OA cartilage, bone and blood has become possible thanks to the recent development of biomarkers of epigenetic aging [19-24]. The available biomarkers, called DNA methylation age-measures (DmAM), combine methylation levels at CpG sites that experience methylation changes with aging. The mechanism seems to include slowly accumulating failures of methylation maintenance (epigenetic drift) that could be accelerated by somatic mutations, cell divisions and environmental stress [19, 21, 25, 26]. Some of the changes are tissue-specific; others are shared by several tissues. This motivates a distinction between DmAM that are tissue-specific and include as few as 3 CpG sites showing strong correlation with age in blood, [20, 24] or in saliva [23], and biomarkers applicable to many tissues that require investigating more CpG sites [19, 21]. The most comprehensive is the "epigenetic clock" method by Horvath, which includes 353 CpG and is valid for multiple tissues including bone and cartilage [19, 27, 28]. The DmAM are useful biomarkers of biological age that show accelerated aging in several diseases of old age [19-21, 29, 30] and in subjects under elevated lifetime stress [26], and that correlate with cognitive and physical fitness in the elderly and with all-cause and cause-specific mortality [30-35].

RESULTS

The cartilage samples from OA patients showed premature aging in comparison with cartilage from controls (Figure 1A). The difference in the estimated mean age obtained with Horwath's DmAM was of 3.7 years (Table 1). This result was obtained with the whole set of samples that included cartilage from the tibial plateau and from the femoral head. A significant premature aging was also observed with the subgroup of tibial plateau samples, with a mean difference of 5.3 years (95 % CI = 2.4 to 8.2). Cartilages from the femoral heads were too few for meaningful analysis. All the comparisons were adjusted for age and sex as covariates.

In contrast with the cartilage results, there were no differences in epigenetic aging of bone (Figure 1B). The mean estimated age obtained from DNA methylation data was very similar in patients with hip OA and in controls (Table 1). The lack of difference was validated in a sub-analysis including only the fracture controls (ΔDmAM = 0.5 years, 95 % CI = -1.50 to 2.54, P = 0.6). Bone samples from cadaver controls were too few for meaningful analysis. All the comparisons were adjusted for age and sex as covariates.

The study of epigenetic aging in blood required de novo analyzes of methylation levels at the 8 CpG sites. The MS-SNuPE assays showed a 93.0 % call rate, and between-plate CV of 3.2 %. Age of the 182 controls without OA was accurately predicted with the 8CpG DmAM (Figure 2), as shown by the good fit of the mean age estimate (mean difference age – DmAM = -

0.1 years, SD = 8.7 years). Comparison of the epigenetic ages obtained in this way did not show differences between OA patients and controls (Figure 2). The epigenetic ages for each of the joint-specific OA subgroups were very similar to the epigenetic age for the control subjects, as shown for the hand OA patients (Figure 2A), knee OA patients (Figure 2B) and hip OA patients (Figure 2C). This similarity in blood cells was clearly shown by the near zero year ΔDmAM (Table 1). The largest difference in blood was observed between patients with hip OA and controls, but it was not significant and with direction opposed to premature aging in the OA subjects. All the comparisons were adjusted for age and sex as covariates.
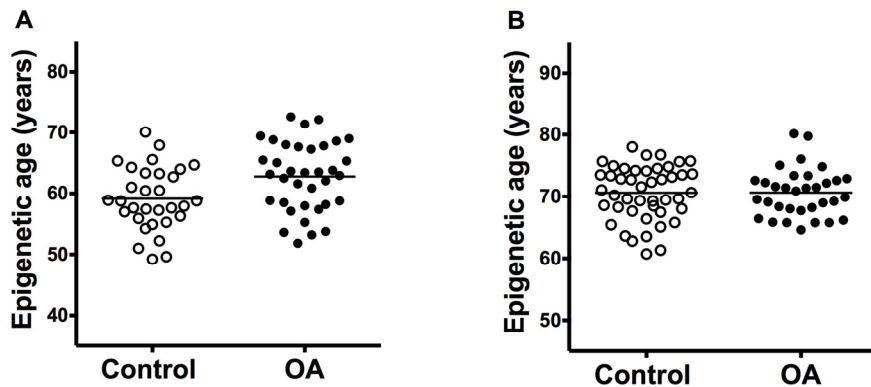
Figure 1. Comparison of epigenetic age in joint tissues from controls and patients with OA. (**A**) Accelerated aging in OA cartilage samples (n = 31) in comparison with control cartilage (n = 36) with ΔDmAM = 3.7 years (P = 0.008); and (**B**) no difference (ΔDmAM = 0.04 years, P = 0.3) in bone samples between OA patients (n = 33) and controls (n = 45). Epigenetic ages are represented as age- and sex-adjusted values with horizontal lines for the mean of each group.

Table 1. Specific premature epigenetic aging in OA cartilage compared with control cartilage. ΔDmAM = (age- and sex-adjusted mean DmAM in OA patients) − (age- and sex-adjusted mean DmAM in controls); CI = confidence interval.

| Tissue	OA set	ΔDmAM[a] (95% CI)	*P*-value
Cartilage	Knee/hip	3.7 (1.1 to 6.3)	0.008
Bone	Hip	0.04 (-1.8 to 1.9)	0.3
Blood	Hand	0.01 (-1.1 to 1.1)	0.98
	Knee	0.04 (-0.9 to 1.0)	0.9
	Hip	-0.7 (-1.7 to 0.3)	0.11

DISCUSSION

Our results showed for the first time premature epigenetic aging as detected with DmAM in cartilage of the OA affected joint, but not in bone nearby the OA affected joint, or in blood cells of OA patients irrespective of the joint affected. These results add epigenetic aging to the list of hallmarks of aging showing accelerated changes in OA cartilage. Each of these hallmarks provide complementary and non-redundant evidence of the different facets of the premature biological aging taking place in chondrocytes and the extracellular matrix of the OA affected cartilage. In addition, our results could be interpreted as questioning systemic premature aging in OA, or even a local component of premature aging in nearby bone, but exploration of other aging hallmarks would be required to exclude them.

Previously, several hallmarks of biological aging have been found exacerbated in chondrocytes and cartilage from OA patients [3, 4]. Our work adds epigenetic aging to the list of hallmarks that show premature biological aging in this tissue. This is a significant addition because the different aging hallmarks, although extensively interconnected, show tissue and disease specificity and the involvement of each of them cannot be assumed from the presence of other hallmarks [5, 6, 35]. They need to be tested in the specific tissue or situation under study. This necessity is exemplified by the lack of correlation between epigenetic age and telomere length observed in the elderly population [35]. In addition, diseases of abnormal telomere attrition are different from diseases in which the dominant mechanism is genomic instability and both are different from normal aging. The first group includes pulmonary fibrosis, dyskeratosis congenita and aplastic anemia, whereas genome instability is the dominant aging hallmark in progeroid syndromes such as Hutchinson-Gilford progeria syndrome and Werner's syndrome [5, 6]. In addition, the DNA methylation changes that are included in the Horvath DmAM have been shown to be independent from cellular senescence and mitotic age [19]. Similar lack of redundancy is observed between the other aging hallmarks, making it necessary to study each of them to know their involvement in OA.

Epigenetic changes with age are not restricted to DNA methylation. They encompass also histone modifications regulated by sirtuins and chromatin remodeling [6]. None of the other age-associated epigenetic changes has yet been analyzed in the context of OA, but they are of interest given their potential reversibility as with histone deacetylase inhibitors or inhibitors of histone acetyltransferases as anti-aging drugs [6]. The meaning of these epigenetic changes is still poorly understood.

They likely contribute to the loss of transcriptional regulation and increase of transcriptional noise observed with aging [5, 6]. Changes in DNA methylation are concentrated in genes with some functional categories including cell growth and survival, organismal development and cancer [19], and in sites within gluco-
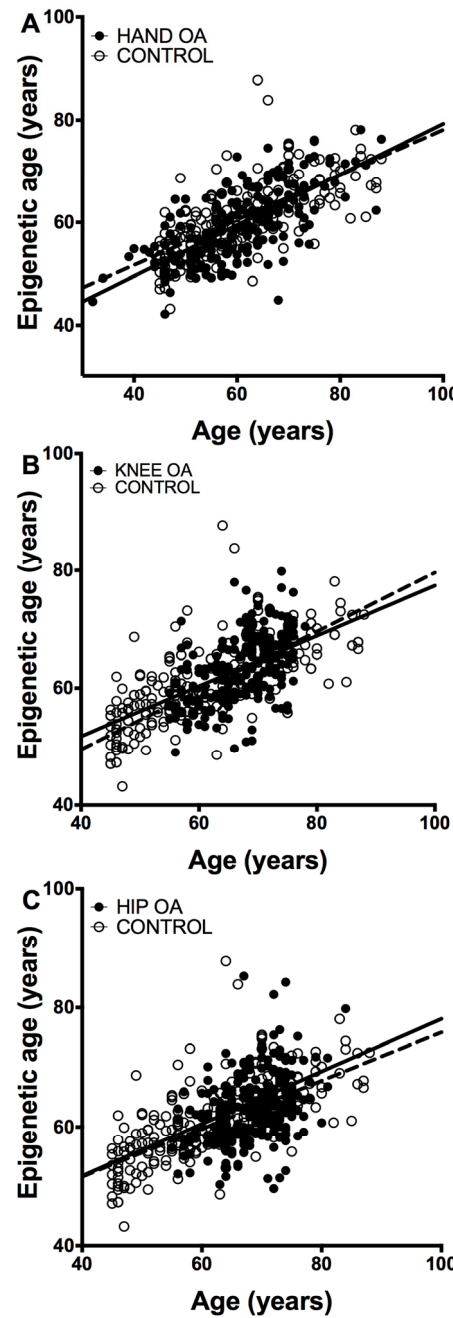
Figure 2. Lack of accelerated epigenetic aging in blood cells of OA patients. The scatterplots represent age in the horizontal axis against epigenetic age in the vertical axis from the controls without OA (empty circles, n =182) together with (**A**) the hand OA (n = 206), (**B**) the knee OA (n = 229), and (**C**) the hip OA (n = 273) patients (filled circles). Straight lines represent least squares regression fit to the data.

corticoid response elements [26], but the pattern of hypermethylation and hypomethylation has not yet being linked to specific molecular or cellular processes [19, 20]. Interpretation of the changes should also include the magnitude of the change: the increase in 3.7 years in ΔDmAM observed in the OA cartilage samples of our study is a modest acceleration compared with changes observed in tumoral tissue, but similar to the reported in a recent abstract in hip OA cartilage, which provides independent confirmation of our findings [36], and in blood of HIV infected patients [37], or in blood of Down syndrome patients [29], but larger than the observed in blood from patients with Parkinson disease [38], or in blood of women after menopause [39].

Some of the previously described aging hallmarks are strongest in the damaged cartilage and less clear in cartilage of preserved areas. Hallmarks showing this pattern are mean telomere length shortening [40-42] senescence-associated heterochromatin foci [41, 42], and senescence-associated β-galactosidase (SA-β-gal). These results have been interpreted as representing, at least in part, consequences of cellular stress and the senescence status of the chondrocytes in OA. However, it is possible that epigenetic aging is a biomarker of cellular vulnerability more than of damage and, therefore, a potential target for treatment. Experiments aimed to differentiate between the two mechanisms are necessary but there are already preliminary results showing similar epigenetic aging in damaged and in preserved cartilage from the same OA patient [36]. Potential treatments could include specific senolytic drugs [5] that have not yet been assayed in chondrocytes, and other approaches with capacity to delay aging in OA chondrocytes as already shown for statins [38] and sirtuin activation [37, 39].

Our results are contrary to widespread premature epigenetic aging given the lack of increased ΔDmAM at the blood and bone levels. However, the only previous direct evidence of a systemic component of accelerate aging in OA was obtained with telomere length in blood cells of OA patients [8, 10], and it is likely that telomere length and DmAM capture different aspects of biological aging [6, 19, 21, 25, 27]. Telomere attrition results from cell divisions, in the absence of the enzyme telomerase, and from DNA damage induced by extrinsic stress, as oxidative or inflammatory stress. The authors that found accelerated telomere length attrition in blood of OA patient interpreted it as reflecting oxidative stress and low-level chronic inflammation [8], or associated with chronic pain and high stress [10]. In contrast, epigenetic aging as measured with DmAM seems to be due to perturbations of the DNA methylation maintenance system [19, 21, 25]. Therefore, our results do not question systemic accelerated aging as detected with telomere shortening, but exclude the epigenetic aspect of aging.

The lack of accelerated aging in blood and in bone was not attributable to insufficient power. In effect, blood samples were enough to exclude ΔDmAM half as fast as the observed in cartilage (1-β > 0.95 to exclude a difference of 1.83 years for each of the three joints). Bone samples, in turn, were enough to detect ΔDmAM as large as the observed in cartilage (1-β = 0.90). In addition, the use of different DmAM for cartilage and bone, in one side, and for blood, in the other, does not interfere with our results because no analysis compared results across different DmAM. We also avoided biases due to differences in age or sex between the OA patients and the controls by adjusting for these two variables, as recommended [19-21]. However, limitations of our study are that the different tissues were not from the same subjects, the lack of other joint tissues, and the absence of a larger number of cartilage samples from femoral heads allowing specific analysis of epigenetic aging at this site. The meaning of these limitations seems modest because bone and cartilage are arguably the most relevant tissues in OA [2], and because epigenetic aging in hip cartilage from OA patients has been independently found [36], as already mentioned. In any case, we cannot completely exclude that other tissues or joints show a different behavior than the reporter here, or that additional insight could be gained from analyzing several tissues from the same subjects, as epigenetic age correlation between tissues.

In summary, we have found specific accelerated aging as measured with DNA methylation in cartilage from OA affected joints. Knowledge of the mechanisms of this type of premature aging will help to understand OA pathology, but already it is apparent that these particular mechanisms are not widespread. This was indicated by the results obtained with the same DNA methylation methodology in bone near the affected joint and in blood cells. They showed absence of a systemic component of premature aging. These results cannot exclude that other hallmarks of aging could be more widespread than the DNA methylation changes analyzed here.

METHODS

Cartilage and bone epigenetic age

Epigenetic age was estimated with the 353 age-related CpG probes according with Horvath [19]. Methylation information of these sites has been obtained in previous studies addressing cartilage and bone samples (Table 2 and Supplementary Table 1) [43-46]. Cartilage samples were from 31 controls and 36 OA patients (Table 2).

Table 2. Main characteristics of the sample collections used in this study. N = number of samples, SD = standard deviation.

Tissue	Set	N	Age Mean ± SD (Range)	Woman %
Cartilage	Control knee/hip[a]	31	64.8 ± 15.0 (40-95)	48.4
	Knee/hip OA	36	67.1 ± 9.3 (41-80)	75.0
Bone	Control hip[a]	45	78.0 ± 11.0 (40-104)	93.3
	Hip OA	33	75.4 ± 6.7 (58-89)	100.0
Blood	Control	182	60.7 ± 11.5 (45-88)	46.7
	Hand OA	206	60.6 ± 10.1 (32-88)	88.4
	Knee OA	229	67.7 ± 5.6 (55-78)	82.1
	Hip OA	273	68.4 ± 5.5 (55-84)	59.7

[a] 3 cartilage and 4 bone control samples were from undefined localization

The controls were from tibial plateau of 18 cadavers with no macroscopic signs of OA [43], and the femoral head of 10 subjects with hip fracture and without macroscopic or microscopic evidence of OA [46]. In addition, 3 cartilage samples from cadavers without information of status and location were included [45]. The OA samples included 29 from the tibial plateau of severe knee OA patients [43, 46], and 7 from the femoral head of severe hip OA patients [46], obtained at the time of joint replacement. Bone samples were from 45 controls and 33 hip OA patients (Table 2). The controls included femoral heads of 34 subjects with osteoporotic hip fracture (OP) and 7 cadavers [44]. They lacked OA lesions on macroscopic examination of the hip joints and the bone pieces excluded subchondral and fractured regions. Patients with fractures due to high-energy trauma or with disorders causing secondary OP or OA were not included. In addition, 4 control bone samples from cadavers that lacked detailed information of status and place of retrieval were included.[45] The bone samples of the 33 hip OA patients were obtained from femoral heads at the time of total joint replacement for primary hip OA [44]. Methylation data were obtained either with the Human Methylation 27 BeadChip (Illumina), [43, 44] or with the HumanMethylation 450 Bead-Chip microarray (Illumina, San Diego, California, USA) [45, 46]. These samples were obtained with informed consent of the donors and approval of the relevant ethics committees as reported in the primary publications [43-46].

Analysis of epigenetic aging in blood

Epigenetic aging in blood was assessed with a 8 CpG DmAM specific for whole blood and amenable to assay in large number of samples [24]. Methylation data were obtained for this study with methylation-sensitive single-nucleotide primer extension (MS-SNuPE) following the reported procedure [47]. Genomic DNA from 890 subjects of Spanish ancestry was assayed (Table 2 and Supplementary Table 1). This collection of samples included 182 controls recruited at the time of intravenous urography. They had not OA signs at exploration including both hands or in the radiographs either at the hip or column joints, and they did not complain of OA symptoms in a systematic question-naire. The remaining 708 subjects were suffering from primary OA as assessed by a rheumatologist. The subjects affected by knee OA, 229, or hip OA, 273, were selected from consecutive patients aged 55–75 years at the time of surgery that were undergoing total joint replacement. The patients with hand OA, 206, were selected among those attending the Rheumatology Unit fulfilling the American College of Rheumatology classification criteria for hand OA [48]. Exclusion criteria were inflammatory, infectious, traumatic or congenic joint pathology, as well as, lesions due to crystal deposition or osteonecrosis. Morbid obesity and occupational strain were not exclusion causes. All donors provided blood DNA samples for genetic studies with written informed consent according to the

Declaration of Helsinki (most recently at the General Assembly on October 2008) and the approval of the Ethics Committee for Clinical Research of Galicia, as described [49].

Statistical analysis

We estimated the epigenetic age of the cartilage and bone samples with Horvath's DmAM [19], and of the blood samples with the 8 CpG DmAM [24]. Comparisons between samples from OA patients and controls were done with analysis of variance (ANOVA) including age and sex as covariates. Mean differences in DmAM estimates (ΔDmAM) were calculated as:

ΔDmAM = (age- and sex-adjusted mean DmAM in OA patients) – (age- and sex-adjusted mean DmAM in controls)

Age- and sex-adjustment was done with the residuals from multiple linear regression of estimated age *versus* age and sex. All these analyses were done with Statistica 7.0 (Stat Soft, Inc.). Post-hoc power analysis was done with G*Power 3 for α = 0.05 [50].

CONFLICTS OF INTEREST

The authors declare they have no conflict of interest.

REFERENCES

1. Murphy L, Schwartz TA, Helmick CG, Renner JB, Tudor G, Koch G, Dragomir A, Kalsbeek WD, Luta G, Jordan JM. Lifetime risk of symptomatic knee osteoarthritis. Arthritis Rheum. 2008; 59:1207–13.
   doi: 10.1002/art.24021

2. Loeser RF, Goldring SR, Scanzello CR, Goldring MB. Osteoarthritis: a disease of the joint as an organ. Arthritis Rheum. 2012; 64:1697–707.
   doi: 10.1002/art.34453

3. Loeser RF. Aging and osteoarthritis. Curr Opin Rheumatol. 2011; 23:492–96.
   doi: 10.1097/BOR.0b013e3283494005

4. Lotz M, Loeser RF. Effects of aging on articular cartilage homeostasis. Bone. 2012; 51:241–48.
   doi: 10.1016/j.bone.2012.03.023

5. Bhatia-Dey N, Kanherkar RR, Stair SE, Makarev EO, Csoka AB. Cellular Senescence as the Causal Nexus of Aging. Front Genet. 2016; 7:13.
   doi: 10.3389/fgene.2016.00013

6. López-Otín C, Blasco MA, Partridge L, Serrano M, Kroemer G. The hallmarks of aging. Cell. 2013; 153:1194–217. doi: 10.1016/j.cell.2013.05.039

7. Zhu Y, Tchkonia T, Pirtskhalava T, Gower AC, Ding H, Giorgadze N, Palmer AK, Ikeno Y, Hubbard GB, Lenburg M, O'Hara SP, LaRusso NF, Miller JD, et al. The Achilles' heel of senescent cells: from transcriptome to senolytic drugs. Aging Cell. 2015; 14:644–58. doi: 10.1111/acel.12344

8. Zhai G, Aviv A, Hunter DJ, Hart DJ, Gardner JP, Kimura M, Lu X, Valdes AM, Spector TD. Reduction of leucocyte telomere length in radiographic hand osteoarthritis: a population-based study. Ann Rheum Dis. 2006; 65:1444–48. doi: 10.1136/ard.2006.056903

9. Tamayo M, Mosquera A, Rego JI, Fernández-Sueiro JL, Blanco FJ, Fernández JL. Differing patterns of peripheral blood leukocyte telomere length in rheumatologic diseases. Mutat Res. 2010; 683:68–73. doi: 10.1016/j.mrfmmm.2009.10.010

10. Sibille KT, Langaee T, Burkley B, Gong Y, Glover TL, King C, Riley JL 3rd, Leeuwenburgh C, Staud R, Bradley LA, Fillingim RB. Chronic pain, perceived stress, and cellular aging: an exploratory study. Mol Pain. 2012; 8:12. doi: 10.1186/1744-8069-8-12

11. Rahman MM, Kopec JA, Anis AH, Cibere J, Goldsmith CH. Risk of cardiovascular disease in patients with osteoarthritis: a prospective longitudinal study. Arthritis Care Res (Hoboken). 2013; 65:1951–58. doi: 10.1002/acr.22092

12. Haugen IK, Ramachandran VS, Misra D, Neogi T, Niu J, Yang T, Zhang Y, Felson DT. Hand osteoarthritis in relation to mortality and incidence of cardiovascular disease: data from the Framingham heart study. Ann Rheum Dis. 2015; 74:74–81.
    doi: 10.1136/annrheumdis-2013-203789

13. Louati K, Vidal C, Berenbaum F, Sellam J. Association between diabetes mellitus and osteoarthritis: systematic literature review and meta-analysis. RMD Open. 2015; 1:e000077. doi: 10.1136/rmdopen-2015-000077

14. Huang SW, Wang WT, Chou LC, Liao CD, Liou TH, Lin HW. Osteoarthritis increases the risk of dementia: a nationwide cohort study in Taiwan. Sci Rep. 2015; 5:10145. doi: 10.1038/srep10145

15. Castell MV, van der Pas S, Otero A, Siviero P, Dennison E, Denkinger M, Pedersen N, Sanchez-Martinez M, Queipo R, van Schoor N, Zambon S, Edwards M, Peter R, et al. Osteoarthritis and frailty in elderly individuals across six European countries: results from the European Project on OSteoArthritis (EPOSA). BMC Musculoskelet Disord. 2015; 16:359. doi: 10.1186/s12891-015-0807-8

16. Barbour KE, Lui LY, Nevitt MC, Murphy LB, Helmick CG, Theis KA, Hochberg MC, Lane NE, Hootman JM, Cauley JA, and Study of Osteoporotic Fractures Research Group. Hip Osteoarthritis and the Risk of All-Cause and Disease-Specific Mortality in Older Women: A Population-Based Cohort Study. Arthritis Rheumatol. 2015; 67:1798–805. doi: 10.1002/art.39113

17. Nüesch E, Dieppe P, Reichenbach S, Williams S, Iff S, Jüni P. All cause and disease specific mortality in patients with knee or hip osteoarthritis: population based cohort study. BMJ. 2011; 342:d1165. doi: 10.1136/bmj.d1165

18. Kluzek S, Sanchez-Santos MT, Leyland KM, Judge A, Spector TD, Hart D, Cooper C, Newton J, Arden NK. Painful knee but not hand osteoarthritis is an independent predictor of mortality over 23 years follow-up of a population-based cohort of middle-aged women. Ann Rheum Dis. 2015.

19. Horvath S. DNA methylation age of human tissues and cell types. Genome Biol. 2013; 14:R115. doi: 10.1186/gb-2013-14-10-r115

20. Weidner CI, Lin Q, Koch CM, Eisele L, Beier F, Ziegler P, Bauerschlag DO, Jöckel KH, Erbel R, Mühleisen TW, Zenke M, Brümmendorf TH, Wagner W. Aging of blood can be tracked by DNA methylation changes at just three CpG sites. Genome Biol. 2014; 15:R24. doi: 10.1186/gb-2014-15-2-r24

21. Hannum G, Guinney J, Zhao L, Zhang L, Hughes G, Sadda S, Klotzle B, Bibikova M, Fan JB, Gao Y, Deconde R, Chen M, Rajapakse I, et al. Genome-wide methylation profiles reveal quantitative views of human aging rates. Mol Cell. 2013; 49:359–67. doi: 10.1016/j.molcel.2012.10.016

22. Florath I, Butterbach K, Müller H, Bewerunge-Hudler M, Brenner H. Cross-sectional and longitudinal changes in DNA methylation with age: an epigenome-wide analysis revealing over 60 novel age-associated CpG sites. Hum Mol Genet. 2014; 23:1186–201. doi: 10.1093/hmg/ddt531

23. Bocklandt S, Lin W, Sehl ME, Sánchez FJ, Sinsheimer JS, Horvath S, Vilain E. Epigenetic predictor of age. PLoS One. 2011; 6:e14821. doi: 10.1371/journal.pone.0014821

24. Vidal-Bralo L, Lopez-Golan Y, Gonzalez A. Simplified Assay for Epigenetic Age Estimation in Whole Blood of Adults. Front Genet. 2016; 7:126. doi: 10.3389/fgene.2016.00126

25. Teschendorff AE, West J, Beck S. Age-associated epigenetic drift: implications, and a case of epigenetic thrift? Hum Mol Genet. 2013; 22:R7–15. doi: 10.1093/hmg/ddt375

26. Zannas AS, Arloth J, Carrillo-Roa T, Iurato S, Röh S, Ressler KJ, Nemeroff CB, Smith AK, Bradley B, Heim C, Menke A, Lange JF, Brückl T, et al. Lifetime stress accelerates epigenetic aging in an urban, African American cohort: relevance of glucocorticoid signaling. Genome Biol. 2015; 16:266. doi: 10.1186/s13059-015-0828-5

27. Horvath S, Erhart W, Brosch M, Ammerpohl O, von Schönfels W, Ahrens M, Heits N, Bell JT, Tsai PC, Spector TD, Deloukas P, Siebert R, Sipos B, et al. Obesity accelerates epigenetic aging of human liver. Proc Natl Acad Sci USA. 2014; 111:15538–43. doi: 10.1073/pnas.1412759111

28. Horvath S, Mah V, Lu AT, Woo JS, Choi OW, Jasinska AJ, Riancho JA, Tung S, Coles NS, Braun J, Vinters HV, Coles LS. The cerebellum ages slowly according to the epigenetic clock. Aging (Albany NY). 2015; 7:294–306. doi: 10.18632/aging.100742

29. Horvath S, Garagnani P, Bacalini MG, Pirazzini C, Salvioli S, Gentilini D, Di Blasio AM, Giuliani C, Tung S, Vinters HV, Franceschi C. Accelerated epigenetic aging in Down syndrome. Aging Cell. 2015; 14:491–95. doi: 10.1111/acel.12325

30. Perna L, Zhang Y, Mons U, Holleczek B, Saum KU, Brenner H. Epigenetic age acceleration predicts cancer, cardiovascular, and all-cause mortality in a German case cohort. Clin Epigenetics. 2016; 8:64. doi: 10.1186/s13148-016-0228-z

31. Marioni RE, Shah S, McRae AF, Ritchie SJ, Muniz-Terrera G, Harris SE, Gibson J, Redmond P, Cox SR, Pattie A, Corley J, Taylor A, Murphy L, et al. The epigenetic clock is correlated with physical and cognitive fitness in the Lothian Birth Cohort 1936. Int J Epidemiol. 2015; 44:1388–96. doi: 10.1093/ije/dyu277

32. Christiansen L, Lenart A, Tan Q, Vaupel JW, Aviv A, McGue M, Christensen K. DNA methylation age is associated with mortality in a longitudinal Danish twin study. Aging Cell. 2016; 15:149–54. doi: 10.1111/acel.12421

33. Horvath S, Pirazzini C, Bacalini MG, Gentilini D, Di Blasio AM, Delledonne M, Mari D, Arosio B, Monti D, Passarino G, De Rango F, D'Aquila P, Giuliani C, et al. Decreased epigenetic age of PBMCs from Italian semi-supercentenarians and their offspring. Aging (Albany NY). 2015; 7:1159–70. doi: 10.18632/aging.100861

34. Marioni RE, Shah S, McRae AF, Chen BH, Colicino E, Harris SE, Gibson J, Henders AK, Redmond P, Cox SR, Pattie A, Corley J, Murphy L, et al. DNA methylation age of blood predicts all-cause mortality in later life. Genome Biol. 2015; 16:25. doi: 10.1186/s13059-015-0584-6

35. Breitling LP, Saum KU, Perna L, Schöttker B, Holleczek B, Brenner H. Frailty is associated with the epigenetic clock but not with telomere length in a German cohort. Clin Epigenetics. 2016; 8:21. doi: 10.1186/s13148-016-0186-5

36. Reynard L. The aging process and epigenetics: relationship with OA. Osteoarthritis Cartilage. 2015 (Suppl 2); 23:A18–18. doi: 10.1016/j.joca.2015.02.034

37. Wu Y, Chen L, Wang Y, Li W, Lin Y, Yu D, Zhang L, Li F, Pan Z. Overexpression of Sirtuin 6 suppresses cellular senescence and NF-κB mediated inflammatory responses in osteoarthritis development. Sci Rep. 2015; 5:17602. doi: 10.1038/srep17602

38. Yudoh K, Karasawa R. Statin prevents chondrocyte aging and degeneration of articular cartilage in osteoarthritis (OA). Aging (Albany NY). 2010; 2:990–98. doi: 10.18632/aging.100213

39. Platas J, Guillén MI, Pérez Del Caz MD, Gomar F, Castejón MA, Mirabet V, Alcaraz MJ. Paracrine effects of human adipose-derived mesenchymal stem cells in inflammatory stress-induced senescence features of osteoarthritic chondrocytes. Aging (Albany NY). 2016; 8:1703–17. doi: 10.18632/aging.101007

40. Price JS, Waters JG, Darrah C, Pennington C, Edwards DR, Donell ST, Clark IM. The role of chondrocyte senescence in osteoarthritis. Aging Cell. 2002; 1:57–65. doi: 10.1046/j.1474-9728.2002.00008.x

41. Harbo M, Bendix L, Bay-Jensen AC, Graakjaer J, Søe K, Andersen TL, Kjaersgaard-Andersen P, Koelvraa S, Delaisse JM. The distribution pattern of critically short telomeres in human osteoarthritic knees. Arthritis Res Ther. 2012; 14:R12. doi: 10.1186/ar3687

42. Harbo M, Delaisse JM, Kjaersgaard-Andersen P, Soerensen FB, Koelvraa S, Bendix L. The relationship between ultra-short telomeres, aging of articular cartilage and the development of human hip osteoarthritis. Mech Ageing Dev. 2013; 134:367–72. doi: 10.1016/j.mad.2013.07.002

43. Fernández-Tajes J, Soto-Hermida A, Vázquez-Mosquera ME, Cortés-Pereira E, Mosquera A, Fernández-Moreno M, Oreiro N, Fernández-López C, Fernández JL, Rego-Pérez I, Blanco FJ. Genome-wide DNA methylation analysis of articular chondrocytes reveals a cluster of osteoarthritic patients. Ann Rheum Dis. 2014; 73:668–77. doi: 10.1136/annrheumdis-2012-202783

44. Delgado-Calle J, Fernández AF, Sainz J, Zarrabeitia MT, Sañudo C, García-Renedo R, Pérez-Núñez MI, García-Ibarbia C, Fraga MF, Riancho JA. Genome-wide profiling of bone reveals differentially methylated regions in osteoporosis and osteoarthritis. Arthritis Rheum. 2013; 65:197–205. doi: 10.1002/art.37753

45. Lokk K, Modhukur V, Rajashekar B, Märtens K, Mägi R, Kolde R, Koltšina M, Nilsson TK, Vilo J, Salumets A, Tõnisson N. DNA methylome profiling of human tissues identifies global and tissue-specific methylation patterns. Genome Biol. 2014; 15:r54. doi: 10.1186/gb-2014-15-4-r54

46. Aref-Eshghi E, Zhang Y, Liu M, Harper PE, Martin G, Furey A, Green R, Sun G, Rahman P, Zhai G. Genome-wide DNA methylation study of hip and knee cartilage reveals embryonic organ and skeletal system morphogenesis as major pathways involved in osteoarthritis. BMC Musculoskelet Disord. 2015; 16:287. doi: 10.1186/s12891-015-0745-5

47. Kaminsky ZA, Assadzadeh A, Flanagan J, Petronis A. Single nucleotide extension technology for quantitative site-specific evaluation of metC/C in GC-rich regions. Nucleic Acids Res. 2005; 33:e95. doi: 10.1093/nar/gni094

48. Altman R, Alarcón G, Appelrouth D, Bloch D, Borenstein D, Brandt K, Brown C, Cooke TD, Daniel W, Gray R, Greenwald R, Hochberg M, Howell D, et al. The American College of Rheumatology criteria for the classification and reporting of osteoarthritis of the hand. Arthritis Rheum. 1990; 33:1601–10. doi: 10.1002/art.1780331101

49. Rodriguez-Lopez J, Pombo-Suarez M, Liz M, Gomez-Reino JJ, Gonzalez A. Lack of association of a variable number of aspartic acid residues in the asporin gene with osteoarthritis susceptibility: case-control studies in Spanish Caucasians. Arthritis Res Ther. 2006; 8:R55. doi: 10.1186/ar1920

50. Faul F, Erdfelder E, Lang AG, Buchner A. G*Power 3: a flexible statistical power analysis program for the social, behavioral, and biomedical sciences. Behav Res Methods. 2007; 39:175–91. doi: 10.3758/BF03193146

SUPPLEMENTARY MATERIAL

Table S1. Detailed description of the sample collections used in this study. N= Sample size; Std Dev = Standard deviation

Tissue	Study	Set	N	Age Mean	Age Range	Std.Dev.	Woman %
Blood	Current study	Controls	182	60.70	45 to 88	11.51	46.70
		Hand OA	206	60.58	32 to 88	10.06	88.35
		Knee OA	229	67.66	55 to 78	5.63	82.09
		Hip OA	273	68.38	55 to 84	5.50	59.70
Cartilage	Fernández-Tajes J et al, Ann Rheum Dis 2014; 73:668	Knee Controls	18	59.28	40 to 79	10.83	33.33
		Knee OA	29	68.52	54 to 79	7.25	69.00
	Aref-Eshghi E et al, BMC Musculoskelet Disord 2015; 16:287	Knee OA	6	65.35	54 to 78	10.63	100.00
		Hip Controls	10	79.37	63 to 95	11.38	90.00
		Hip OA	7	60.93	41 to 80	14.29	100.00
	Lokk K et al, Genome Biol 2014; 15:R54	Controls	3	49.00	40 to 54	7.81	0.00
Bone		Controls	4	51.75	40 to 60	8.42	25.00
	Delgado-Calle J et al, Arthritis Rheum 2013; 65:197	Hip Cadaver	7	80.29	69 to 92	8.08	100.00
		Hip Fracture	34	80.68	65 to 104	7.11	100.00
		Hip OA	33	75.42	58 to 89	6.74	100.00

DNA methylation-based measures of biological age: meta-analysis predicting time to death

Brian H. Chen[1,2,3*], Riccardo E. Marioni[4,5,6*], Elena Colicino[7*], Marjolein J. Peters[8], Cavin K. Ward-Caviness[9], Pei-Chien Tsai[10], Nicholas S. Roetker[11], Allan C. Just[7], Ellen W. Demerath[11], Weihua Guan[12], Jan Bressler[13], Myriam Fornage[13,14], Stephanie Studenski[1], Amy R. Vandiver[15], Ann Zenobia Moore[1], Toshiko Tanaka[1], Douglas P. Kiel[16,17], Liming Liang[18,19], Pantel Vokonas[18], Joel Schwartz[18], Kathryn L. Lunetta[20,2], Joanne M. Murabito[2,21], Stefania Bandinelli[22], Dena G. Hernandez[23], David Melzer[24], Michael Nalls[23], Luke C. Pilling[24], Timothy R. Price[23], Andrew B. Singleton[23], Christian Gieger[9,25], Rolf Holle[26], Anja Kretschmer[9,25], Florian Kronenberg[27], Sonja Kunze[9,25], Jakob Linseisen[9], Christine Meisinger[9], Wolfgang Rathmann[28], Melanie Waldenberger[9,25], Peter M. Visscher[4,6,29], Sonia Shah[6,29], Naomi R. Wray[6], Allan F. McRae[6,29], Oscar H. Franco[30], Albert Hofman[18,30], André G. Uitterlinden[8,30], Devin Absher[31], Themistocles Assimes[32], Morgan E. Levine[33], Ake T. Lu[33], Philip S. Tsao[32,34], Lifang Hou[35,36], JoAnn E. Manson[37], Cara L. Carty[38], Andrea Z. LaCroix[39], Alexander P. Reiner[40,41], Tim D. Spector[10], Andrew P. Feinberg[15,42], Daniel Levy [2,43*], Andrea Baccarelli [7,44*], Joyce van Meurs[8*], Jordana T. Bell[10*], Annette Peters[9*], Ian J. Deary[4,45*], James S. Pankow[11*], Luigi Ferrucci[1*], Steve Horvath[33,46*]

[1]Longitudinal Studies Section, Translational Gerontology Branch, Intramural Research Program, National Institute on Aging, National Institutes of Health, Baltimore, MD 21224, USA
[2]The NHLBI's Framingham Heart Study, Framingham, MA 01702, USA
[3]Population Sciences Branch, Division of Intramural Research, National Heart, Lung, and Blood Institute, National Institutes of Health, Bethesda, MD 01702, USA
[4]Centre for Cognitive Ageing and Cognitive Epidemiology, University of Edinburgh, 7 George Square, Edinburgh, EH8 9JZ, UK
[5]Medical Genetics Section, Centre for Genomic and Experimental Medicine, Institute of Genetics and Molecular Medicine, University of Edinburgh, Edinburgh, EH4 2XU, UK
[6]Queensland Brain Institute, University of Queensland, Brisbane, QLD, Australia
[7]Laboratory of Environmental Epigenetics, Departments of Environmental Health Sciences and Epidemiology, Columbia University Mailman School of Public Health, New York, NY 10032, USA
[8]Department of Internal Medicine, Erasmus University Medical Centre, Rotterdam, 3000 CA, The Netherlands
[9]Institute of Epidemiology II, Helmholtz Zentrum München, 85764 Neuherberg, Germany
[10]Department of Twin Research and Genetic Epidemiology, Kings College London, London SE1 7EH, UK
[11]Division of Epidemiology and Community Health, University of Minnesota, Minneapolis, MN 55455, USA
[12]Division of Biostatistics, University of Minnesota School of Public Health, Minneapolis, MN, 55455, USA
[13]Human Genetics Center, School of Public Health, University of Texas Health Sciences Center at Houston, Houston, TX, USA
[14]Human Genome Sequencing Center, Baylor College of Medicine, Houston, TX, USA
[15]Center for Epigenetics, Johns Hopkins University, Baltimore, MD 21205, USA
[16]Department of Medicine, Beth Israel Deaconess Medical Center and Harvard Medical School, Boston, MA, USA
[17]Institute for Aging Research, Hebrew Senior Life, Boston, MA 02215, USA

[18]Department of Epidemiology, Harvard School of Public Health, Boston, MA 02115, USA

[19]Department of Biostatistics, Harvard School of Public Health, Boston, MA 02115, USA

[20]Department of Biostatistics, Boston University School of Public Health, Boston, MA 02118, USA

[21]Section of General Internal Medicine, Department of Medicine, Boston University School of Medicine, Boston, MA 02118, USA

[22]Geriatric Unit, Usl Centro Toscana, Florence, Italy

[23]Laboratory of Neurogenetics, Intramural Research Program, National Institute on Aging, National Institutes of Health, Bethesda, MD 20814, USA

[24]Epidemiology and Public Health, Medical School, University of Exeter, RILD, Exeter EX2 5DW, UK

[25]Research Unit of Molecular Epidemiology, Helmholtz Zentrum München, 85764 Neuherberg, Germany

[26]Institute of Health Economics and Health Care Management, Helmholtz Zentrum München, 85764 Neuherberg, Germany

[27]Division of Genetic Epidemiology, Department of Medical Genetics, Molecular and Clinical Pharmacology, Innsbruck Medical University, Innsbruck 6020, Austria

[28]Institute for Biometrics and Epidemiology, German Diabetes Center, Leibniz Center for Diabetes Research at Heinrich Heine University, 40225 Düsseldorf, Germany

[29]University of Queensland Diamantina Institute, University of Queensland, Brisbane, Queensland, Australia

[30]Department of Epidemiology, Erasmus University Medical Centre, Rotterdam, 3015 CN, The Netherlands

[31]HudsonAlpha Institute for Biotechnology, Huntsville, AL 35806, USA

[32]Department of Medicine, Stanford University School of Medicine, Stanford, CA 94305, USA;

[33]Human Genetics, David Geffen School of Medicine, University of California Los Angeles, Los Angeles, CA 90095, USA

[34]VA Palo Alto Health Care System, Palo Alto CA 94304, USA

[35]Department of Preventive Medicine, Feinberg School of Medicine, Northwestern University Chicago, IL 60611, USA

[36]Robert H. Lurie Comprehensive Cancer Center, Feinberg School of Medicine, Northwestern University Chicago, IL 60611, USA

[37]Department of Medicine, Brigham and Women's Hospital, Harvard Medical School, and the Department of Epidemiology, Harvard T.H. Chan School of Public Health, Boston, MA 02215, USA

[38]Center for Translational Science Children's National Medical Center, George Washington University Washington, DC 20010, USA

[39]Department of Family Medicine and Public Health, University of California-San Diego, La Jolla, CA 92093-0725, USA

[40]Department of Epidemiology, University of Washington School of Public Health, Seattle, WA 98195, USA

[41]Public Health Sciences Division, Fred Hutchinson Cancer Research Center, Seattle, WA 98109, USA

[42]Departments of Medicine, Molecular Biology/Genetics, Oncology, and Biostatistics, Johns Hopkins University School of Medicine, Baltimore, MD 21205, USA

[43]Population Sciences Branch, Division of Intramural Research, National Heart, Lung, and Blood Institute, National Institutes of Health, Bethesda, MD 01702, USA

[44]Department of Environmental Health, Harvard T.H. Chan School of Public Health, Boston, MA 02115, USA

[45]Department of Psychology, University of Edinburgh, 7 George Square, Edinburgh, EH8 9JZ, UK

[46]Department of Biostatistics, School of Public Health, University of California Los Angeles, Los Angeles, CA 90095, USA

*Joint first or senior authors

Correspondence to: Steve Horvath; email: shorvath@mednet.ucla.edu

ABSTRACT

Estimates of biological age based on DNA methylation patterns, often referred to as "epigenetic age", "DNAm age", have been shown to be robust biomarkers of age in humans. We previously demonstrated that independent of chronological age, epigenetic age assessed in blood predicted all-cause mortality in four human cohorts. Here, we expanded our original observation to 13 different cohorts for a total sample size of 13,089 individuals, including three racial/ethnic groups. In addition, we examined whether incorporating information on blood cell composition into the epigenetic age metrics improves their predictive power for mortality. All considered measures of epigenetic age acceleration were predictive of mortality ($p \leq 8.2 \times 10^{-9}$), independent of chronological age, even after adjusting for additional risk factors ($p < 5.4 \times 10^{-4}$), and within the racial/ethnic groups that we examined (non-Hispanic whites, Hispanics, African Americans). Epigenetic age estimates that incorporated information on blood cell composition led to the smallest p-values for time to death ($p = 7.5 \times 10^{-43}$). Overall, this study a) strengthens the evidence that epigenetic age predicts all-cause mortality above and beyond chronological age and traditional risk factors, and b) demonstrates that epigenetic age estimates that incorporate information on blood cell counts lead to highly significant associations with all-cause mortality.

INTRODUCTION

DNA methylation-based biomarkers, often referred to as "epigenetic age" or "epigenetic clock", are robust estimators of chronological age of an individual [1–4]. For example, a measure of epigenetic age based on levels of methylation in 353 CpG dinucleotide markers (cytosine linked to guanine by a phosphate group) allow the estimation of the age of an individual. This estimate is consistent across most types of biological specimens, including whole blood, brain, breast, kidney, liver, lung, and saliva and cell types, including CD4+ T cells, monocytes, B cells, glial cells, and neurons [3].

Recent studies suggested that epigenetic age is associated with age-related health outcomes above and beyond chronological age. For example, we and others have shown that individuals whose epigenetic age was greater than their chronological age (i.e., individuals exhibiting epigenetic "age acceleration") were at an increased risk for death from all causes, even after accounting for known risk factors [5–7]. Further, we recently showed that the offspring of semi-supercentenarians (subjects who reached an age of 105-109 years) have a lower epigenetic age than age-matched controls [8]. Based on these findings, it has been hypothesized that epigenetic age captures some aspect of biological age and the resulting susceptibility to disease and multiple health outcomes. A first step in testing this hypothesis is to test whether epigenetic age predicts longevity in multiple populations and across ethnic groups.

In many studies epigenetic age is estimated from DNA derived from blood samples. It is well known that blood cell composition changes with age and some of these changes might be independent predictors of mortality [9–12]. Thus, it is of interest to understand whether considering information on blood cell composition in measures of epigenetic age improves their predictive power for mortality.

Here, we evaluated the ability to predict time to death for blood-based epigenetic age measures, both published and novel measures that incorporate information on blood cell composition. Due to the well documented age-related changes in blood cell composition, we distinguished epigenetic measures of age that were independent of changes in blood cell composition (cell-intrinsic measures), and measures that incorporated age-related changes in blood cell composition ("extrinsic" measures). By increasing the number of independent cohort studies, we more than doubled the number of mortality events available for analysis, which allowed for detailed subgroup analyses including those based on race/ethnicity.

RESULTS

Cohort studies

Our meta-analysis included 13 population-based cohorts. An overview of the cohorts is provided in Table 1. Our study involved 3 racial/ethnic groups: non-Hispanic whites (n=9,215), Hispanics (n=431), and Blacks (n=3,443). Detailed descriptions of each cohort can be found in the Supplemental Materials.

Epigenetic age estimation

We used two methods for estimating the epigenetic age of each blood sample (Table 2). First, we used the approach by Horvath (2013) based on 353 CpGs, as described in [3] and Methods. Second, we used the approach by Hannum et al. (2013) based on 71 CpGs [2]. Both epigenetic age estimates were correlated with chronological age at the time of blood draw (Table 1) with biweight midcorrelation coefficients ranging from 0.65 to 0.89. But birth cohorts were excluded from this correlation analysis because it is not meaningful to calculate correlations with chronological age in this situation. The Horvath and Hannum estimates were also highly correlated with each other (r=0.76) even though the underlying sets of CpGs share only 6 CpGs in common. (Supplementary Table 1).

Estimated blood cell counts that relate to chronological age

We estimated the abundance of ten blood cell types based on observed DNA methylation patterns (Methods) – exhausted/senescent CD8+ T cells (CD8+CD28-CD45RA-), CD8+ naïve, CD8+ total, CD4+ naïve, CD4+ total, natural killer cells, B cells, monocytes, granulocytes, and plasmablasts. To study age-related changes in blood cell composition, we correlated these estimated blood cell counts with chronological age in all of the cohort studies (Supplementary Table 2). Our results are congruent with findings from flow cytometric studies that demonstrate that the abundance of naïve CD8+ T cells decreases with age (reflecting thymic involution), whereas exhausted/senescent CD8+ T cells increase with age [9–12].

Table 1. Baseline characteristics of participating cohorts.

Cohort	N	N$_{deaths}$ (%)	Follow-up duration (years)*	Age (years)*	r$_{Horvath}$†	r$_{Hannum}$‡
1. WHI (White)	995	309 (31%)	15.4 (14.0-16.4)	68 (65-72)	0.67 (p=5.1x10^{-131})	0.73 (p=8.0x10^{-167})
2. WHI (Black)	675	176 (26%)	15.4 (13.7-16.5)	62 (57-67)	0.70 (p=1.2x10^{-100})	0.76 (p=3.0x10^{-128})
3. WHI (Hispanic)	431	78 (18%)	15.2 (14.1-16.3)	61 (56-67)	0.78 (p=8.9x10^{-90})	0.79 (p=1.3x10^{-93})
4. LBC 1921	445	312 (70%)	10.2 (6.2-12.9)	79 (78-79)	0.15 (p=1.5x10^{-3})	0.13 (p=6.0x10^{-3})
5. LBC 1936	919	106 (12%)	7.5 (6.9-8.4)	69 (68-70)	0.15 (p=4.9x10^{-6})	0.16 (p=1.1x10^{-6})
6. NAS	647	221 (34%)	11.6 (8.6-12.9)	72 (68-77)	0.69 (p=1.3x10^{-92})	0.76 (p=8.2x10^{-123})
7. ARIC (Black)	2,768	1,075 (39%)	20.3 (14.3-21.4)	57 (52-62)	0.65 (p<1x10^{-200})	0.71 (p<1x10^{-200})
8. FHS	2,614	236 (9%)	6.2 (5.6-6.9)	66 (60-73)	0.84 (p<1x10^{-200})	0.86 (p<1x10^{-200})
9. KORA	1,257	42 (3%)	4.4 (4.0-4.8)	61 (54-68)	0.84 (p<1x10^{-200})	0.88 (p<1x10^{-200})
10. InCHIANTI	506	91 (18%)	15.0 (14.6-15.5)	67 (57-73)	0.82 (p=3.2x10^{-124})	0.85 (p=2.1x10^{-142})
11. Rotterdam	710	32 (5%)	5.6 (5.3-5.8)	58 (54-62)	0.72 (p=1.9x10^{-114})	0.76 (p=1.3x10^{-134})
12. Twins UK	805	30 (4%)	8.5 (7.5-8.5)	58 (51-65)	0.87 (p<1x10^{-200})	0.89 (p<1x10^{-200})
13. BLSA (white)	317	26 (8%)	5.3 (4.0-6.6)	66 (58-73)	0.85 (p=1.1x10^{-89})	0.88 (p=7.2x10^{-104})
Total	**13,089**	**2734 (21%)**				

The last 3 columns report robust correlation coefficients (biweight midcorrelation) between chronological age and two epigenetic age estimates (Horvath and Hannum).
* Median (25th percentile - 75th percentile)
† Biweight midcorrelation coefficient of chronological age with epigenetic age using the Horvath method.
‡ Biweight midcorrelation coefficient of chronological age with epigenetic age using the Hannum method.

Measures of epigenetic age acceleration

Despite high correlations, epigenetic age can deviate substantially from chronological age at the individual level. The difference between epigenetic age and chronological age can be used to define "delta age" but the resulting measure exhibits a negative correlation with chronological age. By contrast, all of our measures of epigenetic age acceleration are defined such that they are uncorrelated with chronological age.

Table 2. Overview of various measures of epigenetic age acceleration.

Measure of age acceleration	Short name of measure	Epigenetic age estimate	Uses blood counts	Correlation with blood counts	Conserved in breast tissue
(Universal) epigenetic age acceleration	$AgeAccel_{Horvath}$ (AgeAccel)	Horvath: 353 CpGs	no	weak	yes
Intrinsic epigenetic age acceleration (Horvath)	IEAA.Horvath (IEAA)	Horvath: 353 CpGs	yes	very weak	yes
Age acceleration based on Hannum	$AgeAccel_{Hannum}$	Hannum: 71 CpGs	no	moderate	no
Intrinsic epigenetic age acceleration (Hannum)	IEAA.Hannum	Hannum: 71 CpGs	yes	very weak	no
Extrinsic epigenetic age acceleration	EEAA	Enhanced Hannum	yes	strong	no

Description of the differences between epigenetic age and age acceleration measures. Column "Correlation with blood counts" relates to Supplementary Table 4. Column "Conserved in breast tissue" relates to Figure 1.
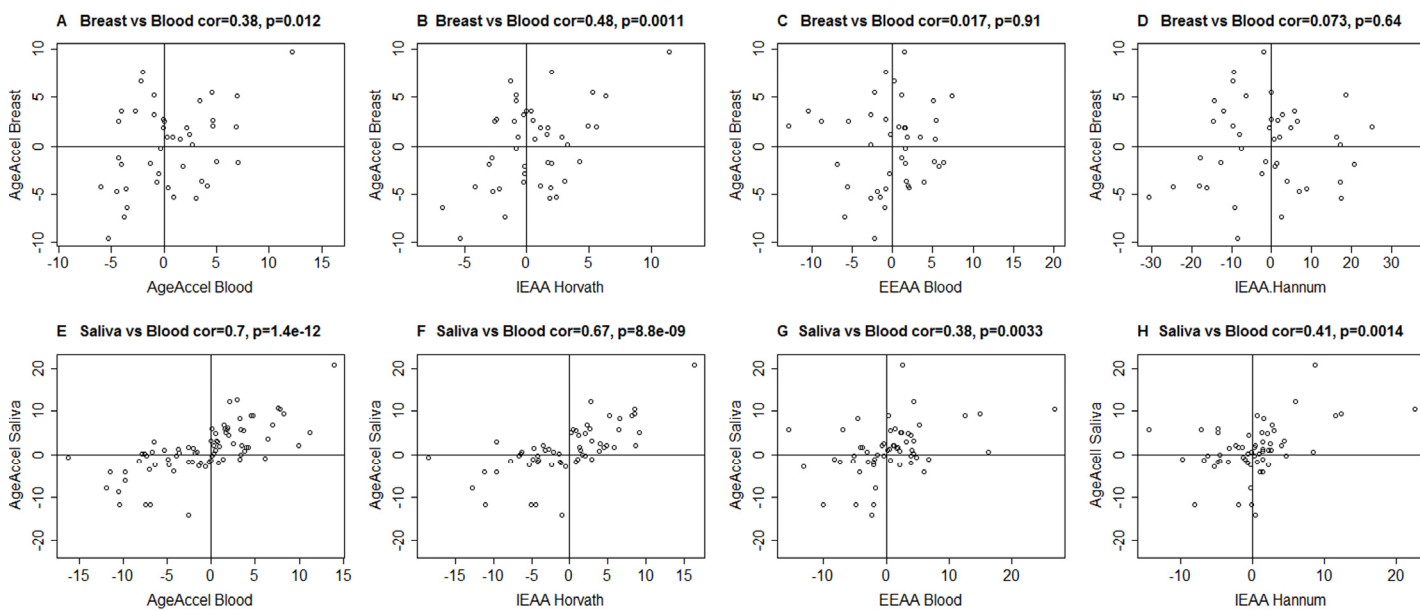
Figure 1. Epigenetic age acceleration in blood versus that in breast or saliva. (**A**-**D**) Epigenetic age acceleration in healthy female breast tissue (y-axis) versus various measures of epigenetic age acceleration in blood: (**A**) universal measure of age acceleration in blood, (**B**) intrinsic epigenetic age acceleration based on the Horvath estimate of epigenetic age, (**C**) extrinsic epigenetic age acceleration, (**D**) intrinsic epigenetic age acceleration based on the Hannum estimate of epigenetic age. (**E**-**H**) analogous plots for epigenetic age acceleration in saliva (y-axis) and (**E**) AgeAccel, (**F**) IEAA based on Horvath, (**G**) EEAA, (**H**) IEAA based on the Hannum estimate. The y-axis of each plot represents the universal measure of age acceleration defined as the raw residual resulting from regressing epigenetic age (based on Horvath) on chronological age.

An overview of several measures of epigenetic age acceleration is presented in Table 2. One such measure (denoted as *AgeAccel*) is defined as the residual that results from regressing epigenetic age on chronological age. Thus, a positive value of *AgeAccel* indicates that the epigenetic age is higher than expected, based on chronological age. These Horvath and Hannum based measures of age acceleration are denoted by *AgeAccel$_{Horvath}$* and *AgeAccel$_{Hannum}$*, respectively. For the sake of brevity and consistency with other publications from our group, we abbreviate *AgeAccel$_{Horvath}$* as *AgeAccel*.

AgeAccel$_{Hannum}$ and to a lesser extent *AgeAccel* were previously shown to correlate with blood cell counts [5]. Thus, we distinguished two broad categories of measures of epigenetic age acceleration when dealing with DNA methylation from blood or peripheral blood mononuclear cells (PBMCs): intrinsic and extrinsic epigenetic measures, which are independent of, or enhanced by blood cell count information, respectively. We define *intrinsic* epigenetic age acceleration (*IEAA*) as the residual resulting from regressing epigenetic age on chronological age and measures of blood cell counts (Methods). By definition, *IEAA* is not correlated with chronological age and is weakly correlated with estimated measures of blood cell counts (Supplementary Table 4). *IEAA* is meant to capture cell-intrinsic properties of the aging process that exhibit some pre-

servation across various cell types and organs. Compared to our other measures of age acceleration, *IEAA*, adapted from the Horvath measure of epigenetic age, exhibited significant correlations with epigenetic age acceleration in breast tissue (r=0.48, p=0.0011, Figure 1B) and saliva (r=0.67, p=8.8x10^{-9}, Figure 1F). By contrast, an analogous measure of *IEAA* based on the Hannum measure showed much weaker correlations (r=0.073 in breast and r=0.41 in saliva Figure 1D, 1H). For this reason, we focused on the Horvath measure of *IEAA*.

The age-related changes to blood cell composition (Supplementary Table 4) can be leveraged to capture aspects of immunosenescence. Using these measures, we derived a novel extrinsic epigenetic age acceleration (*EEAA*) measure by up-weighting the blood cell count contributions of *AgeAccel$_{Hannum}$* (Methods and Supplementary Table 4).

Descriptive statistics (minimum, maximum, median) of the measures of epigenetic age acceleration can be found in Supplementary Table 3.

Cox regression models of all-cause mortality

We used Cox regression models to assess the predictive value of our measures of epigenetic age acceleration for all-cause mortality. All of our Cox models were adjusted
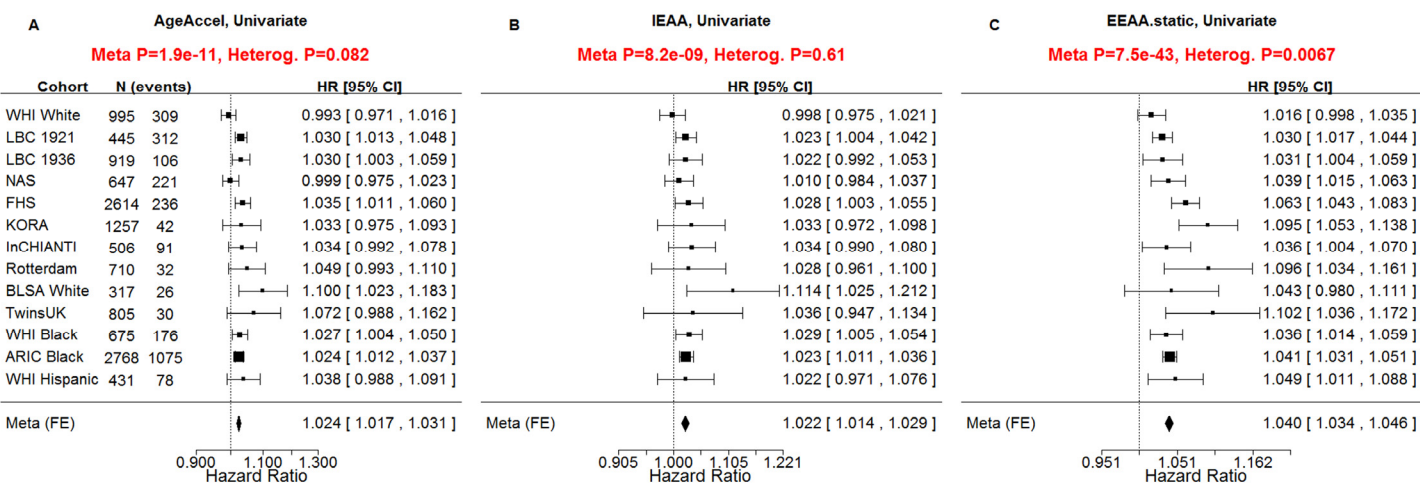
Figure 2. Univariate Cox regression meta-analysis of all-cause mortality. A univariate Cox regression model was used to relate the censored survival time (time to all-cause mortality) to (**A**) the universal measure of age acceleration (*AgeAccel*), (**B**) intrinsic epigenetic age acceleration (*IEAA*), (**C**) extrinsic epigenetic age acceleration (*EEAA*). The rows correspond to the different cohorts. Each row depicts the hazard ratio and a 95% confidence interval. The coefficient estimates from the respective studies were meta-analyzed using a fixed-effect model weighted by inverse variance (implemented in the *metafor* R package [34]). It is not appropriate to compare the hazard ratios and confidence intervals of the different measures directly because the measures have different scales/distributions. However, it is appropriate to compare the meta analysis p values (red sub-title of each plot). The p-value of the heterogeneity test (Cochran's *Q*-test) is significant if the cohort-specific estimates differed substantially.

for the age at baseline (blood draw). Additional multivariate models further adjusted for covariates assessed at baseline (chronological age, body mass index, educational level, alcohol intake, smoking pack-years, prior history of diabetes, prior history of cancer, hypertension status, self-reported recreational physical activity).
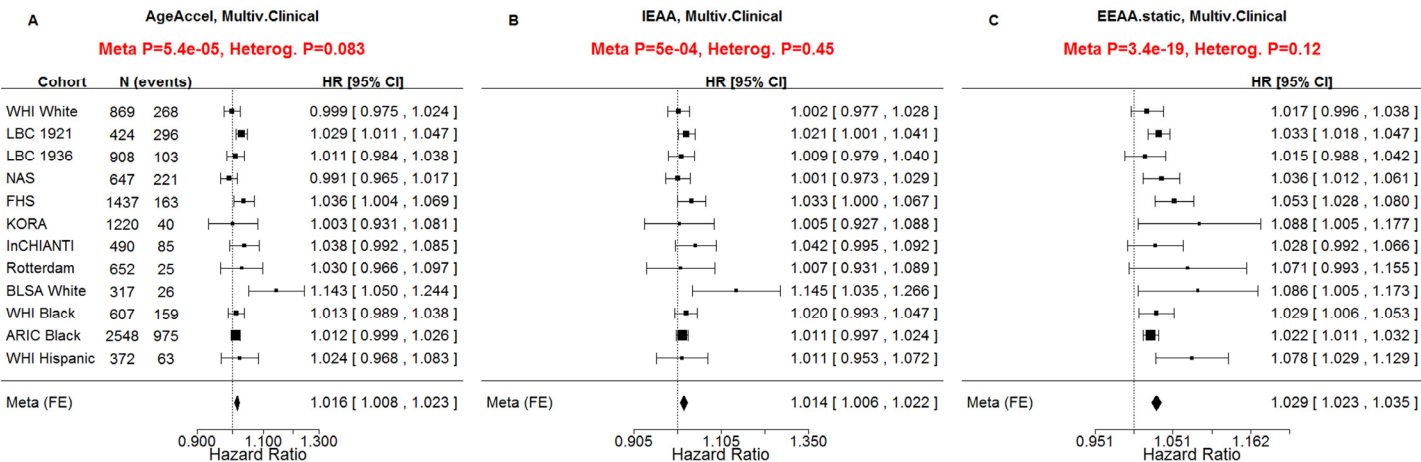

Figure 3. Multivariate Cox regression meta-analysis adjusted for clinical covariates. A multivariate Cox regression model was used to relate the censored survival time (time to all-cause mortality) to (**A**) the universal measure of age acceleration (*AgeAccel*), (**B**) intrinsic epigenetic age acceleration (*IEAA*), (**C**) extrinsic epigenetic age acceleration (*EEAA*). The multivariate Cox regression model included the following additional covariates: chronological age, body mass index (category), educational level (category), alcohol intake, smoking pack years, prior history of diabetes, prior history of cancer, hypertension status, recreational physical activity (category). The rows correspond to the different cohorts. Each row depicts the hazard ratio and a 95% confidence interval. The coefficient estimates from the respective studies were meta-analyzed using a fixed-effect model weighted by inverse variance (implemented in the *metafor* R package [34]). The sub-title of each plot reports the meta-analysis p-value and a heterogeneity test p-value (Cochran's Q-test).
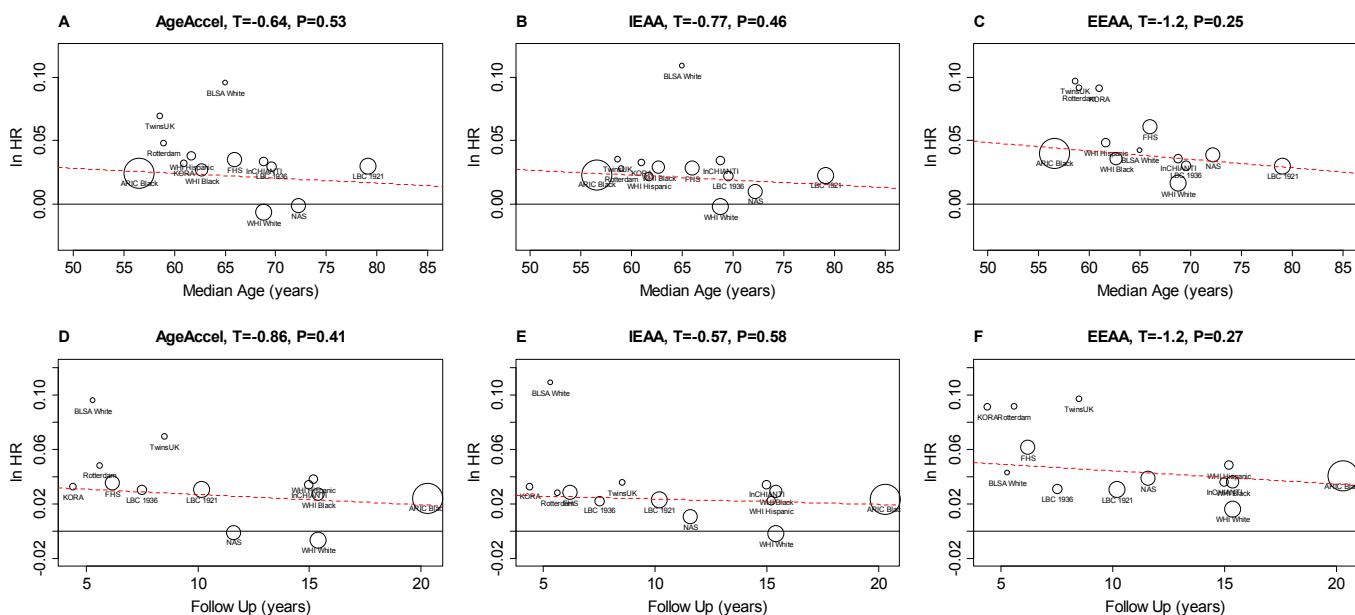
Figure 4. Hazard ratio of death versus cohort characteristics. Each circle corresponds to a cohort (data set). Circle sizes correspond to the square root of the number of observed deaths, because the statistical power of a Cox model is determined by the number of observed deaths. (**A-C**) The y-axis of each panel corresponds to the natural log of the hazard ratio (ln HR) of a univariate Cox regression model for all-cause mortality. Each panel corresponds to a different measure of epigenetic age acceleration (**A**) universal age acceleration, (**B**) intrinsic age acceleration, (**C**) extrinsic age acceleration. Panels (**D-F**) are analogous to those in A-C but the x-axis corresponds to the median age of the subjects at baseline (Table 1). The title of each panel reports the Wald test statistic (*T*) and corresponding p-value resulting from a weighted linear regression model (y regressed on x) where each point (data set) is weighted by the square root of the number of observed deaths. The dotted red line represents the regression line. The black solid line represents the line of identify (i.e., no association).

Table 3. Subgroup analysis by demographic factors.

Subgroup	Age-adjusted		Full model	
	HR	*p*-value	HR	*p*-value
Race				
White	1.05	3.0×10^{-26}	1.03	1.3×10^{-5}
Black	1.04	7.8×10^{-20}	1.02	7.6×10^{-3}
Hispanic	1.05	1.1×10^{-2}	1.06	5.3×10^{-2}
$p_{interaction}$		0.62		0.14
Sex				
Men	1.04	7.1×10^{-15}	1.03	1.9×10^{-2}
Women	1.04	3.7×10^{-10}	1.03	1.9×10^{-5}
$p_{interaction}$		0.63		0.95
Follow-up duration				
<5 years	1.02	0.20	0.98	0.79
5-10 years	1.02	1.8×10^{-3}	1.02	0.17
>10 years	1.03	4.5×10^{-9}	1.02	4.1×10^{-2}
$p_{interaction}$		0.67		0.84
BMI categories				
Underweight	1.11	9.4×10^{-3}	1.04	8.9×10^{-3}
Normal	1.06	6.1×10^{-19}	1.04	2.3×10^{-2}
Overweight	1.04	1.46×10^{-8}	1.03	5.0×10^{-2}
Obese	1.04	2.2×10^{-11}	1.02	7.1×10^{-2}
$p_{interaction}$		0.05		0.75
Smoking status				
Never	1.03	6.9×10^{-6}	1.04	4.8×10^{-3}
Former	1.05	4.2×10^{-22}	1.03	6.3×10^{-4}
Current	1.06	2.1×10^{-4}	1.01	0.47
$p_{interaction}$		0.05		0.20
Physical activity status				
Yes	1.05	3.8×10^{-6}	1.02	1.9×10^{-3}
No	1.03	2.5×10^{-2}	1.03	2.2×10^{-2}
$p_{interaction}$		0.23		0.65

Age-adjusted and fully adjusted associations for *EEAA* to all-cause mortality by subgroup (rows). The fully adjusted model includes the following covariates: body mass index, educational level, alcohol intake, smoking pack-years, prior history of diabetes, prior history of cancer, hypertension status, self-reported recreational physical activity.

Our novel measure of extrinsic age acceleration *EEAA* led to smaller p-values for the associations with all-cause mortality than the original measure *AgeAccel_Hannum* in univariate Cox models (p_{EEAA}=7.5x10^{-43}, $p_{AgeAccelHannum}$=1.4x10^{-34}, Supplementary Figure 1) and in multivariate Cox models (p_{EEAA}=3.4x10^{-19}, $p_{AgeAccelHannum}$=6x10^{-15}, Supplementary Figure 2). Further, when both *EEAA* and *AgeAccel_Hannum* were included in the same Cox model, only *EEAA* remained significant in the WHI data and FHS univariate models. Since these results indicate that *EEAA* outperforms the closely related measure *AgeAccel_Hannum* when it comes to mortality prediction, we removed the latter from subsequent analyses.

All considered measures of epigenetic age acceleration were predictive of time to death in univariate Cox models ($p_{AgeAccel}$=1.9x10^{-11}, p_{IEAA}=8.2x10^{-9}, p_{EEAA}=7.5x10^{-43}, Figure 2) and multivariate Cox models adjusting for risk factors and pre-existing disease status ($p_{AgeAccel}$=5.4x10^{-5}, p_{IEAA}=5.0x10^{-4}, p_{EEAA}=3.4x10^{-19}, Figure 3).

Interpreting effect sizes and variance of epigenetic age acceleration

Subjects differed substantially in terms of their measures of epigenetic age acceleration, e.g. *EEAA* ranged from -28 to 28 years in the WHI (standard deviation =6.4 years, Supplementary Table 3).

About five percent of the participants of the WHI exhibited an *EEAA* value larger than 10, which is associated with a 48% increased hazard of death as can be seen from the following calculation. The HR of *EEAA* is 1.040 if EEAA=1 (Figure 2c) but it is HR=1.48=(1.040)^{10} if EEAA=10. Negative values of age acceleration were associated with a lower hazard of mortality. For example, 20% of subjects had an *EEAA* value less than -5, which is associated with an 18% decrease in the hazard of death (HR=0.82=1.04^{-5}).

Subgroup analysis

With few exceptions, we found that the associations between *EEAA* and time to death remained highly signi-

Table 4. Subgroup analysis by prevalent disease status.

Subgroup	Age-adjusted		Full model	
	HR	*p*-value	HR	*p*-value
Cancer status				
Yes	1.05	2.5x10^{-10}	1.02	0.18
No	1.05	2.3x10^{-13}	1.03	1.7x10^{-4}
$p_{interaction}$		0.92		0.73
Coronary artery disease status				
Yes	1.04	2.4x10^{-5}	1.01	0.60
No	1.04	1.5x10^{-12}	1.02	1.5x10^{-4}
$p_{interaction}$		0.43		0.99
Hypertension status				
Yes	1.04	7.4x10^{-17}	1.03	2.9x10^{-3}
No	1.05	7.1x10^{-6}	1.02	8.6x10^{-3}
$p_{interaction}$		0.41		0.45
Type 2 diabetes status				
Yes	1.04	8.6x10^{-13}	1.03	1.7x10^{-3}
No	1.04	1.2x10^{-10}	1.02	9.3x10^{-3}
$p_{interaction}$		0.70		0.25

Age-adjusted and fully adjusted associations for *EEAA* to all-cause mortality in different subgroups (rows). The fully adjusted model includes the following covariates: body mass index, educational level, alcohol intake, smoking pack-years, prior history of diabetes, prior history of cancer, hypertension status, self-reported recreational physical activity.

ficant in subgroups stratified by race, sex, follow-up duration, body mass index, smoking status, physical activity (Table 3) and in subgroups stratified by prevalent disease at baseline such as cancer, coronary artery disease, hypertension and type 2 diabetes (Table 4). Only one subgroup led to an insignificant finding (p>0.05) in our univariate model analysis: namely subjects with less than 5 years of follow up (Table 3). For multivariate models, we failed to observe significant associations for the following subgroups: i) less than 5 years of follow up, ii) between 5 and 10 years of follow up, iii) current smokers, iv) obese individuals, v) Hispanics, vi) individuals with cancer, and vii) subjects with coronary artery disease. The insignificant results in multivariate models in cancer patients or CAD patients might reflect the relatively low sample sizes or that epigenetic age acceleration is dwarfed by other predictors of mortality in subjects with severe diseases. Hazard ratio estimates remained highly consistent across all subgroups examined.

We did not observe significant differences in the estimated hazard ratios across any subgroup (Tables 3 and 4). Specifically, racial/ethnic differences in HR were not observed (interaction p=0.62 in age-adjustment models and p=0.14 in full models). Overall, these subgroup analysis results confirm that epigenetic age acceleration is an independent predictor of earlier mortality even after adjusting for possible confounders and within major subgroups of the population.

Hazard ratio of death versus follow up time and median age

The large number of cohorts allowed us to relate cohort characteristics (such as median age or median follow up removing time) to strength of association with mortality. We did not find a statistically significant relationship between the hazard ratio of death for the median age of the cohort or the follow up time (Figure 4).

Robustness analysis

To assess the robustness of our findings, we also carried out a leave-one-out analysis by re-running the metaanalysis after removing data from individual cohorts. The resulting p-values are highly robust with respect to a single data set from the analysis (Supplementary Table 5). In our study, we used a fixed effects meta-analysis method for the sake of consistency with previous analyses [5]. However, our results remain qualitatively the same after using a random effects meta-analysis method (Supplementary Figure 4).

DISCUSSION

The current study corroborates previous findings regarding the predictive power of DNA methylation-based biomarkers of age for mortality [5,6,8]. We further examined novel variants of these measures that are either independent of blood cell counts or are enhanced by changes in blood cell sub-populations. We showed that the extrinsic measure *EEAA* out-performs previous measures of age acceleration when it comes to predicting all-cause mortality. Furthermore, the associations between epigenetic age acceleration and mortality did not differ significantly across subgroups of race/ethnicity, sex, BMI, smoking status, physical activity status, or major chronic diseases. The consistency of the associations across multiple subgroups lends support to the notion that epigenetic age acceleration captures some aspect of biological aging over and above chronological age and other risk factors.

The development of suitable measures of biological age has been a key goal in the field of aging research [13]. Many biomarkers of age have been posited including epigenetic alterations of the DNA (e.g., DNA methylation), transcriptomic changes in blood [14], telomere length [15], whole-body function such as gait speed (reviewed in [16]). The current study does not aim to replace existing blood based biomarkers, but rather, we aimed to demonstrate that it complements existing markers. Above all, this study shows that epigenetic age captures an aspect of biological age, as assessed through lifespan, above and beyond chronological age, blood cell composition, and a host of traditional risk factors of mortality.

The measures of epigenetic age acceleration are attractive because they are highly robust and because their measurement only involve DNA methylation data. While actual flow cytometry data will always be preferable to imputed blood cell count data (based on DNA methylation data), the measures of age acceleration do not require the measurement of flow data. Rather, measures of intrinsic and extrinsic epigenetic age used blood cell count estimates resulting from DNA methylation data. The measure of extrinsic age acceleration EEAA reflects aspects of immuno-senescence because, by construction, it correlates with age-related changes in blood cell composition, such as T lymphocyte populations, which underlie much of the age-related decline in the protective immune response [9–12]. Thus, the high predictive significance of *EEAA* for all-cause mortality probably reflects the fact that it assesses multiple aspects of the biological age of the immune system including both changes in blood cell

composition and cell-intrinsic epigenetic changes. It has been known for decades that poor T cell functioning is predictive of mortality [17].

The findings surrounding the predictive utility of intrinsic epigenetic age acceleration are biologically compelling and point to a new frontier in aging research. Our study strongly suggests *IEAA* is reflective of an intrinsic epigenetic clock that is associated with mortality independent of chronological age, changes in blood cell composition, and traditional risk factors of mortality. *IEAA* probably captures a cell-type independent component of the aging process for the following reasons. First, *IEAA* is moderately preserved across different tissues and cell types collected from the same subject (Figure 1). Second, *IEAA* but not *EEAA* is predictive of lung cancer [18]. Third, only *IEAA* and *AgeAccel* relate to centenarian status [8].

Overall, our results inform the ongoing debate about whether epigenetic biomarkers of age capture an aspect of biological age. While epigenetic processes are unlikely to be the only mediators of chronological age on mortality—in fact, multiple risk factors have stronger effects on mortality—our results suggest that at least one of the mediating processes relates to the epigenetic age of blood tissue and that this process is independent of age-dependent changes in blood cell composition. Future studies will be useful for gaining a mechanistic understanding of this intrinsic epigenetic aging process.

MATERIALS AND METHODS

Measures of epigenetic age

We used an epigenetic biomarker of age based on 353 CpG markers as one measure of epigenetic age because: a) it is an accurate measurement of age across multiple tissues [3]; b) we previously showed that it is predictive of all-cause mortality [5]; c) it correlated with measures of cognitive/physical fitness and neuro-pathology in the elderly [19,20]; and d) it was associated with conditions that are of interest in aging research including Down's syndrome [21], Huntington's disease [22], Parkinson's disease [23], obesity [24], HIV infection [25], menopause [26], centenarian status [27], ethnicity and sex [28], and cellular senescence [3,29]. This epigenetic age estimator not only lends itself to measuring aging effects in elderly subjects; but also applies to prenatal brain samples [30] and blood samples from minors [31]. Epigenetic age is defined as the predicted value of age based on the DNA methylation levels of 353 CpGs. Mathematical details and software tutorials for estimating epigenetic age can be found in the additional

files of [3]. All of the described epigenetic measures of aging and age acceleration are implemented in our freely available software (https://dnamage.genetics.ucla.edu) [3].

DNA methylation age estimate by Hannum et al (2013)

We also used an alternative measure of epigenetic age developed by Hannum et al (2013) [2]. The resulting age estimate is based on the 71 CpGs and coefficient values from the third supplementary table [2]. The authors developed this age prediction method by using an elastic net regression model for predicting chronological age based on DNA methylation levels from whole blood.

Measures of epigenetic age acceleration

Table 2 provides an overview of our measures of epigenetic age acceleration. The universal measure of age acceleration (*AgeAccel*), which is valid for a wide range of tissue types, is defined as the residual resulting from a linear regression model that regresses the Horvath estimate of epigenetic age on chronological age. Thus, a positive value for *AgeAccel* indicates that the observed epigenetic age is higher than that predicted, based on chronological age. *AgeAccel* has a relatively weak correlation with blood cell counts [25], but it still relates to estimated blood cell counts, as seen in Supplementary Table 4.

To estimate "pure" epigenetic aging effects that are not influenced by differences in blood cell counts ("intrinsic" epigenetic age acceleration, *IEAA*), we obtained the residual resulting from a multivariate regression model of epigenetic age on chronological age and various blood immune cell counts (naive CD8+ T cells, exhausted CD8+ T cells, plasmablasts, CD4+ T cells, natural killer cells, monocytes, and granulocytes) imputed from methylation data.

Extrinsic epigenetic age acceleration measures capture both cell intrinsic methylation changes and extracellular changes in blood cell composition. Our measure of *EEAA* is defined using the following three steps. First, we calculated the epigenetic age measure from Hannum et al [2], which already correlated with certain blood cell types [5]. Second, we increased the contribution of immune blood cell types to the age estimate by forming a weighted average of Hannum's estimate with 3 cell types that are known to change with age: naïve (CD45RA+CCR7+) cytotoxic T cells, exhausted (CD28-CD45RA-) cytotoxic T cells, and plasmablasts using the Klemera-Doubal approach [32]. The weights

used in the weighted average are determined by the correlation between the respective variable and chronological age [32]. The weights were chosen on the basis of the WHI data. Thus, the same (static) weights were used for all data sets. *EEAA* was defined as the residual variation resulting from a univariate model regressing the resulting age estimate on chronological age. By construction, *EEAA* is positively correlated with the estimated abundance of exhausted CD8+ T cells, plasmablast cells, and a negative correlated with naive CD8+ T cells. Blood cell counts were estimated based on DNA methylation data as described in the next section. By construction, the measures of *EEAA* track both age related changes in blood cell composition and intrinsic epigenetic changes. None of our four measures of epigenetic age acceleration are correlated with chronological age.

Estimating blood cell counts based on DNA methylation levels

We estimate blood cell proportions using two different software tools. Houseman's estimation method [33], which is based on DNA methylation signatures from purified leukocyte samples, was used to estimate the proportions of cytotoxic (CD8+) T cells, helper (CD4+) T, natural killer, B cells, and granulocytes. The software does not allow us to identify the type of granulocytes in blood (neutrophil, eosinophil, or basophil) but we note that neutrophils tend to be the most abundant granulocyte (~60% of all blood cells compared with 0.5-2.5% for eosinophils and basophils). To estimate the percentage of exhausted CD8+ T cells (defined as CD28-CD45RA-), plasmablasts, and the number (count) of naïve CD8+ T cells (defined as CD45RA+CCR7+), we used the "Horvath method" [25], which is implemented in the advanced analysis option of the epigenetic age calculator software [3]. We and others have shown that imputed blood cell counts have moderately high correlations with corresponding flow cytometric data, e.g. r=0.86 for naïve CD4+ T cells, r=0.68 for naïve CD8+T, and r=0.49 for exhausted CD8+ T cells [28].

Cox regression models and meta-analysis

Here, we used Cox models for analyzing the censored survival time data (from the age at blood draw until age at death or last follow-up). We regressed the censored survival times on covariates using Cox regression models implemented in the R function *coxph* in the *survival* package. The resulting coefficient values (interpreted as log hazard ratios) and standard errors were combined using the R software package *metafor* [34]. The meta-analysis was carried out with the R command *rma* (with arguments *method="FE"* to get fixed effects estimates). The forest plots were created using the R function *forest* (with argument *atransf=exp* to exponentiate the estimate of the log hazard ratios).

Sample exclusions

In addition to cohort-specific quality checks, we further excluded individuals who had ever been diagnosed with leukemia (ICD-9: 203-208), reported receiving chemotherapy, and whose methylation beta value distributions deviated substantially from a gold standard (according to the quality statistic *corSampleVSgold standard*<0.80 from the online age calculator [35–37]).

AUTHOR CONTRIBUTIONS

All co-authors contributed data or analyzed the data or helped interpret the findings or helped write the article. BHC coordinated the analysis of the cohort studies and created the software code. SH, D. Levy, A. Baccarelli, J van Meurs, J. Bell, A. Peters, I. Deary, J. Pankow, L. Ferrucci, led cohort studies of this effort. SH developed and implemented the novel measures of epigenetic age acceleration and wrote the first draft of the article.

FUNDING

CONFLICTS OF INTEREST

The Regents of the University of California is the sole owner of a provisional patent application directed at the invention of measures of epigenetic age acceleration for which SH is a named inventor. The other authors declare no conflicts of interest.

REFERENCES

1. Bocklandt S, Lin W, Sehl ME, Sánchez FJ, Sinsheimer JS, Horvath S, Vilain E. Epigenetic predictor of age. PLoS One. 2011; 6:e14821. doi.org/10.1371/journal.pone.0014821

2. Hannum G, Guinney J, Zhao L, Zhang L, Hughes G, Sadda S, Klotzle B, Bibikova M, Fan JB, Gao Y, Deconde R, Chen M, Rajapakse I, et al. Genome-wide methylation profiles reveal quantitative views of human aging rates. Mol Cell. 2013; 49:359–67. doi.org/10.1016/j.molcel.2012.10.016

3. Horvath S. DNA methylation age of human tissues and cell types. Genome Biol. 2013; 14:R115. doi.org/10.1186/gb-2013-14-10-r115

4. Lin Q, Weidner CI, Costa IG, Marioni RE, Ferreira MR, Deary IJ, Wagner W. DNA methylation levels at individual age-associated CpG sites can be indicative for life expectancy. Aging (Albany NY). 2016; 8:394–401.doi.org/10.18632/aging.100908

5. Marioni RE, Shah S, McRae AF, Chen BH, Colicino E, Harris SE, Gibson J, Henders AK, Redmond P, Cox SR, Pattie A, Corley J, Murphy L, et al. DNA methylation age of blood predicts all-cause mortality in later life. Genome Biol. 2015; 16:25. doi.org/10.1186/s13059-015-0584-6

6. Christiansen L, Lenart A, Tan Q, Vaupel JW, Aviv A, McGue M, Christensen K. DNA methylation age is associated with mortality in a longitudinal Danish twin study. Aging Cell. 2016; 15:149–54. doi.org/10.1111/acel.12421

7. Perna L, Zhang Y, Mons U, Holleczek B, Saum K-U, Brenner H. Epigenetic age acceleration predicts cancer, cardiovascular, and all-cause mortality in a German case cohort. Clin Epigenetics. 2016; 8:64. doi.org/10.1186/s13148-016-0228-z

8. Horvath S, Pirazzini C, Bacalini MG, Gentilini D, Di Blasio AM, Delledonne M, Mari D, Arosio B, Monti D, Passarino G, De Rango F, D'Aquila P, Giuliani C, et al. Decreased epigenetic age of PBMCs from Italian semi-supercentenarians and their offspring. Aging (Albany NY). 2015; 7:1159–70. doi.org/10.18632/aging.100861

9. Fagnoni FF, Vescovini R, Passeri G, Bologna G, Pedrazzoni M, Lavagetto G, Casti A, Franceschi C, Passeri M, Sansoni P. Shortage of circulating naive CD8(+) T cells provides new insights on immuno-deficiency in aging. Blood. 2000; 95:2860–68.

10. Franceschi C. Inflammaging as a major characteristic of old people: can it be prevented or cured? Nutr Rev. 2007; 65:S173–76. doi.org/10.1301/nr.2007.dec.S173-S176

11. Franceschi C, Bonafè M, Valensin S, Olivieri F, De Luca M, Ottaviani E, De Benedictis G. Inflamm-aging. An evolutionary perspective on immunosenescence. Ann N Y Acad Sci. 2000; 908:244–54. doi.org/10.1111/j.1749-6632.2000.tb06651.x

12. Miller RA. The aging immune system: primer and prospectus. Science. 1996; 273:70–74. doi.org/10.1126/science.273.5271.70

13. Baker GT 3rd, Sprott RL. Biomarkers of aging. Exp Gerontol. 1988; 23:223–39. doi.org/10.1016/0531-5565(88)90025-3

14. Peters MJ, Joehanes R, Pilling LC, Schurmann C, Conneely KN, Powell J, Reinmaa E, Sutphin GL, Zhernakova A, Schramm K, Wilson YA, Kobes S, Tukiainen T, et al, and NABEC/UKBEC Consortium. The transcriptional landscape of age in human peripheral blood. Nat Commun. 2015; 6:8570. doi.org/10.1038/ncomms9570

15. Sanders JL, Newman AB. Telomere length in epidemiology: a biomarker of aging, age-related disease, both, or neither? Epidemiol Rev. 2013; 35:112–31. doi.org/10.1093/epirev/mxs008

16. Sanders J, Boudreau R, Newman A. 2012. Understanding the Aging Process Using Epidemiologic Approaches. (Dordrecht Heidelberg New York: Springer).

17. Roberts-Thomson IC, Whittingham S, Youngchaiyud U, Mackay IR. Ageing, immune response, and mortality. Lancet. 1974; 2:368–70. doi.org/10.1016/S0140-6736(74)91755-3

18. Levine ME, Hosgood HD, Chen B, Absher D, Assimes T, Horvath S. DNA methylation age of blood predicts future onset of lung cancer in the women's health initiative. Aging (Albany NY). 2015; 7:690–700. doi.org/10.18632/aging.100809

19. Marioni RE, Shah S, McRae AF, Ritchie SJ, Muniz-Terrera G, Harris SE, Gibson J, Redmond P, Cox SR, Pattie A, Corley J, Taylor A, Murphy L, et al. The epigenetic clock is correlated with physical and cognitive fitness in the Lothian Birth Cohort 1936. Int J Epidemiol. 2015; 44:1388–96. doi.org/10.1093/ije/dyu277

20. Levine ME, Lu AT, Bennett DA, Horvath S. Epigenetic age of the pre-frontal cortex is associated with neuritic plaques, amyloid load, and Alzheimer's disease related cognitive functioning. Aging (Albany NY). 2015; 7:1198–211. doi.org/10.18632/aging.100864

21. Horvath S, Garagnani P, Bacalini MG, Pirazzini C, Salvioli S, Gentilini D, Di Blasio AM, Giuliani C, Tung S, Vinters HV, Franceschi C. Accelerated epigenetic aging in Down syndrome. Aging Cell. 2015; 14:491–95. doi.org/10.1111/acel.12325

22. Horvath S, Langfelder P, Kwak S, Aaronson J, Rosinski J, Vogt TF, Eszes M, Faull RL, Curtis MA, Waldvogel HJ, Choi OW, Tung S, Vinters HV, et al. Huntington's disease accelerates epigenetic aging of human brain and disrupts DNA methylation levels. Aging (Albany NY). 2016; 8:1485–512.

doi.org/10.18632/aging.101005

23. Horvath S, Ritz BR. Increased epigenetic age and granulocyte counts in the blood of Parkinson's disease patients. Aging (Albany NY). 2015; 7:1130–42. doi.org/10.18632/aging.100859

24. Horvath S, Erhart W, Brosch M, Ammerpohl O, von Schönfels W, Ahrens M, Heits N, Bell JT, Tsai P-C, Spector TD, Deloukas P, Siebert R, Sipos B, et al. Obesity accelerates epigenetic aging of human liver. Proc Natl Acad Sci USA. 2014; 111:15538–43. doi.org/10.1073/pnas.1412759111

25. Horvath S, Levine AJ. HIV-1 infection accelerates age according to the epigenetic clock. J Infect Dis. 2015; 212:1563–73. doi.org/10.1093/infdis/jiv277

26. Levine ME, Lu AT, Chen BH, Hernandez DG, Singleton AB, Ferrucci L, Bandinelli S, Salfati E, Manson JE, Quach A, Kusters CD, Kuh D, Wong A, et al. Menopause accelerates biological aging. Proc Natl Acad Sci USA. 2016; 113:9327–32. doi.org/10.1073/pnas.1604558113

27. Horvath S, Mah V, Lu AT, Woo JS, Choi OW, Jasinska AJ, Riancho JA, Tung S, Coles NS, Braun J, Vinters HV, Coles LS. The cerebellum ages slowly according to the epigenetic clock. Aging (Albany NY). 2015; 7:294–306. doi.org/10.18632/aging.100742

28. Horvath S, Gurven M, Levine ME, Trumble BC, Kaplan H, Allayee H, Ritz BR, Chen B, Lu AT, Rickabaugh TM, Jamieson BD, Sun D, Li S, et al. An epigenetic clock analysis of race/ethnicity, sex, and coronary heart disease. Genome Biol. 2016; 17:171. doi.org/10.1186/s13059-016-1030-0

29. Lowe D, Horvath S, Raj K. Epigenetic clock analyses of cellular senescence and ageing. Oncotarget. 2016; 7:8524–31. doi:10.18632/oncotarget.7383.

30. Spiers H, Hannon E, Schalkwyk LC, Smith R, Wong CC, O'Donovan MC, Bray NJ, Mill J. Methylomic trajectories across human fetal brain development. Genome Res. 2015; 25:338–52. doi.org/10.1101/gr.180273.114

31. Walker RF, Liu JS, Peters BA, Ritz BR, Wu T, Ophoff RA, Horvath S. Epigenetic age analysis of children who seem to evade aging. Aging (Albany NY). 2015; 7:334–39. doi.org/10.18632/aging.100744

32. Klemera P, Doubal S. A new approach to the concept and computation of biological age. Mech Ageing Dev. 2006; 127:240–48. doi.org/10.1016/j.mad.2005.10.004

33. Houseman EA, Accomando WP, Koestler DC, Christensen BC, Marsit CJ, Nelson HH, Wiencke JK, Kelsey KT. DNA methylation arrays as surrogate

measures of cell mixture distribution. BMC Bioinformatics. 2012; 13:86. doi.org/10.1186/1471-2105-13-86

34. Viechtbauer W. Conducting Meta-Analyses in R with the metafor Package. J Stat Softw. 2010; 36:1–48. doi.org/10.18637/jss.v036.i03.

35. Curb JD, McTiernan A, Heckbert SR, Kooperberg C, Stanford J, Nevitt M, Johnson KC, Proulx-Burns L, Pastore L, Criqui M, Daugherty S, and WHI Morbidity and Mortality Committee. Outcomes ascertainment and adjudication methods in the Women's Health Initiative. Ann Epidemiol. 2003 (Suppl); 13:S122–28. doi.org/10.1016/S1047-2797(03)00048-6

36. Deary IJ, Gow AJ, Pattie A, Starr JM. Cohort profile: the Lothian Birth Cohorts of 1921 and 1936. Int J Epidemiol. 2012; 41:1576–84. doi.org/10.1093/ije/dyr197

37. Ferrucci L, Bandinelli S, Benvenuti E, Di Iorio A, Macchi C, Harris TB, Guralnik JM. Subsystems contributing to the decline in ability to walk: bridging the gap between epidemiology and geriatric practice in the InCHIANTI study. J Am Geriatr Soc. 2000; 48:1618–25. doi.org/10.1111/j.1532-5415.2000.tb 03873.x

Supplementary Table 1. Average pairwise correlations between chronological age, *epigenetic age* based on the Horvath method, and *epigenetic age* based on Hannum.

	Age	*Epigenetic age* (Horvath)	*Epigenetic age* (Hannum)
Age	-	0.74	0.81
Epigenetic age (Horvath)	0.74	-	0.76
Epigenetic age (Hannum)	0.81	0.76	-

Supplementary Table 2. Correlations between estimated blood cell abundances and chronological age.

Cohort	Plasmablasts	CD8+CD28- CD45RA-	CD8+ naive	CD4+ naive	CD8+ total	CD4+ total	NK cells	B cells	Monocytes	Granulocytes
ARIC	0.03	0.16	-0.22	-0.13	-0.06	-0.08	0.13	-0.08	0.09	0.04
FHS	0.23	0.36	-0.38	-0.22	-0.19	-0.23	0.20	-0.27	0.17	0.16
InCHIANTI	0.06	0.32	-0.43	-0.34	-0.19	-0.20	0.23	-0.20	0.08	0.11
KORA	0.20	0.48	-0.53	-0.37	-0.07	-0.37	0.12	-0.22	0.20	0.16
LBC1921	0.03	0.03	-0.14	-0.09	0.10	0.01	0.05	-0.07	0.10	-0.07
LBC1936	0.11	0.04	-0.05	-0.09	-0.03	0.00	-0.05	-0.13	-0.09	0.05
NAS	0.04	0.28	-0.21	-0.07	0.01	-0.16	0.12	-0.10	-0.01	0.08
RSIII	0.11	0.20	-0.26	-0.16	-0.10	-0.14	0.06	-0.16	0.14	0.11
TwinsUK	-0.02	0.21	-0.35	-0.08	-0.14	0.07	0.27	-0.02	0.10	-0.14
WHI White	0.09	0.21	-0.17	-0.13	-0.13	-0.10	0.17	-0.12	0.10	0.04
WHI Black	0.12	0.24	-0.21	-0.13	-0.07	-0.17	0.16	-0.18	0.11	0.07
WHI Hispanic	0.08	0.26	-0.21	-0.15	-0.11	-0.13	0.17	-0.10	0.03	0.08
MEAN	**0.09**	**0.23**	**-0.26**	**-0.16**	**-0.08**	**-0.12**	**0.14**	**-0.14**	**0.09**	**0.06**

The values shown are robust correlation coefficients (biweight midcorrelation, which is based on medians). Colors reflect the direction and magnitude of the correlation coefficients (blue=negative correlation, red=positive correlation).

Supplementary Table 3. Descriptive statistics of measures of epigenetic age acceleration by cohort.

Epigenetic age acceleration measure	Cohort	SD	Min	25th percentile	Median (50th percentile)	75th percentile	Max
AgeAccel	ARIC	5.081	-34.380	-3.191	-0.100	3.220	25.620
AgeAccel	FHS	4.621	-16.490	-3.110	-0.367	2.460	35.160
AgeAccel	InCHIANTI	4.999	-33.600	-3.084	-0.338	2.223	29.770
AgeAccel	KORA	4.937	-24.810	-3.423	-0.117	2.905	20.660
AgeAccel	LBC1921	6.971	-24.240	-3.884	-0.170	3.943	39.730
AgeAccel	LBC1936	6.485	-30.160	-3.879	0.116	3.801	42.100
AgeAccel	NAS	5.365	-16.930	-3.706	-0.498	2.909	32.830
AgeAccel	RSIII	6.003	-18.570	-4.325	-0.046	4.276	20.050
AgeAccel	TwinsUK	4.108	-13.760	-2.514	0.274	2.899	13.560
AgeAccel	WHI (white)	5.153	-22.560	-2.843	-0.103	3.443	22.790
AgeAccel	WHI (Black)	6.091	-21.900	-5.424	-1.977	1.824	39.930
AgeAccel	WHI (Hispanic)	4.494	-14.080	-3.831	-0.535	2.458	14.790
AgeAccel	BLSA	4.828	-11.620	-2.966	0.290	3.197	25.180
AgeAccel	ARIC	5.914	-38.770	-3.766	0.105	3.648	39.350
AgeAccelHannum	FHS	5.279	-23.480	-3.303	-0.174	3.001	36.680
AgeAccelHannum	InCHIANTI	6.028	-43.640	-3.152	0.431	3.573	31.490
AgeAccelHannum	KORA	4.996	-30.280	-3.266	-0.314	2.711	37.410
AgeAccelHannum	LBC1921	7.203	-25.140	-4.574	-0.821	3.722	51.840
AgeAccelHannum	LBC1936	6.670	-27.520	-4.172	0.131	4.183	31.650
AgeAccelHannum	NAS	5.161	-12.250	-3.310	-0.787	2.511	22.750
AgeAccelHannum	RSIII	6.090	-18.600	-3.825	0.115	4.152	17.970
AgeAccelHannum	TwinsUK	5.246	-17.040	-2.949	0.320	3.821	20.260
AgeAccelHannum	WHI (white)	5.557	-23.460	-3.644	-0.086	3.441	21.760
AgeAccelHannum	WHI (Black)	6.317	-23.490	-4.773	-0.891	3.045	31.480
AgeAccelHannum	WHI (Hispanic)	5.357	-12.740	-2.139	1.133	4.469	20.880
AgeAccelHannum	BLSA	5.709	-15.720	-2.942	0.429	3.801	31.730
AgeAccelHannum	ARIC	4.928	-34.020	-3.010	-0.057	3.068	23.810
IEAA	FHS	4.491	-16.010	-2.901	-0.199	2.547	32.160
IEAA	InCHIANTI	4.783	-30.930	-2.898	-0.374	2.364	29.470
IEAA	KORA	4.647	-29.350	-3.276	-0.114	2.761	18.740
IEAA	LBC1921	6.228	-22.890	-3.664	0.135	3.554	24.600
IEAA	LBC1936	6.162	-26.310	-3.596	0.035	3.718	34.090
IEAA	NAS	4.929	-24.190	-3.019	-0.458	2.694	22.500
IEAA	RSIII	5.130	-16.610	-3.330	-0.026	3.387	15.190
IEAA	TwinsUK	4.016	-14.590	-2.257	0.234	2.718	13.100
IEAA	WHI (white)	4.797	-21.460	-2.608	0.183	3.287	21.440

IEAA	WHI (Black)	5.588	-20.320	-3.202	0.067	3.197	42.660
IEAA	WHI (Hispanic)	4.333	-13.520	-3.971	-1.397	1.864	12.480
IEAA	BLSA	4.488	-10.370	-2.658	0.017	3.330	23.120
EEAA	ARIC	6.673	-32.940	-4.096	0.135	4.149	38.560
EEAA	FHS	5.800	-26.100	-3.607	0.113	3.315	38.250
EEAA	InCHIANTI	6.710	-44.360	-3.327	0.576	4.236	33.630
EEAA	KORA	5.405	-26.610	-3.526	-0.339	3.189	37.600
EEAA	LBC1921	7.745	-21.180	-5.262	-0.973	4.306	52.120
EEAA	LBC1936	7.116	-30.590	-4.439	0.168	4.589	31.530
EEAA	NAS	5.596	-13.730	-3.443	-0.579	2.987	23.540
EEAA	RSIII	6.861	-22.380	-4.392	0.267	4.794	21.080
EEAA	TwinsUK	5.840	-22.790	-3.409	0.401	4.023	23.020
EEAA	WHI (white)	6.089	-22.710	-3.888	0.015	4.008	22.320
EEAA	WHI (Black)	6.906	-27.600	-5.735	-1.382	2.827	27.900
EEAA	WHI (Hispanic)	5.779	-14.310	-1.679	2.371	5.651	23.450
EEAA	BLSA	6.256	-18.040	-3.435	0.921	4.724	29.230

Supplementary Table 4. Pairwise correlations (mean and standard error (SE) across cohorts) between blood cell counts estimated from DNA methylation profiles (rows) and several measures of epigenetic age acceleration (columns).

BloodCell	*AgeAccel* average *r* (SE)	*IEAA* average *r* (SE)	*EEAA* average *r* (SE)	*AgeAccel$_{Hannum}$* average *r* (SE)	*IEAA.Hannum* average *r* (SE)
Plasma Blast	0.02 (0.031)	0 (0.002)	0.28 (0.034)	0.20 (0.033)	0 (0.018)
Exhausted CD8+	0.18 (0.039)	0 (0.009)	0.50 (0.033)	0.29 (0.044)	0 (0.046)
CD8.naive	-0.18 (0.043)	0 (0.011)	-0.52 (0.04)	-0.35 (0.048)	0 (0.05)
CD4.naive	-0.09 (0.033)	0.07 (0.017)	-0.36 (0.038)	-0.28 (0.041)	0.06 (0.046)
CD8T	0.19 (0.026)	0 (0.023)	0 (0.046)	0 (0.041)	-0.01 (0.024)
CD4T	-0.20 (0.032)	0 (0.004)	-0.46 (0.034)	-0.34 (0.036)	0 (0.026)
NK	0.13 (0.026)	0 (0.002)	0.17 (0.042)	0.10 (0.042)	0 (0.03)
Bcell	-0.08 (0.051)	-0.11 (0.028)	-0.05 (0.068)	-0.01 (0.061)	-0.02 (0.035)
Monocyte	0.05 (0.026)	0 (0.006)	0.12 (0.042)	0.07 (0.04)	0 (0.019)
Granulocyte	-0.03 (0.033)	0 (0.005)	0.16 (0.049)	0.14 (0.042)	0 (0.018)

AgeAccel=univeral measure of age acceleration based on Horvath estimate. *IEAA*=intrinsic epigenetic age acceleration based on the Horvath estimate. *EEAA* = extrinsic epigenetic age acceleration which is an enhanced version of the Hannum estimate. *AgeAccel$_{Hannum}$*=univeral measure of age acceleration based on the Hannum estimate. *IEAA.Hannum*=intrinsic epigenetic age acceleration based on Hannum estimate. By design, the intrinsic measures have only weak correlations with blood cell counts. By contrast, *AgeAccel$_{Hannum}$* and *EEAA* have moderately strong correlations with blood cell counts.

Supplementary Table 5. Leave-one-out analysis by cohort for relating *EEAA* to time to death.

Cohort removed	Age-adjusted model	Fully adjusted model
(None)	1.04 (p=1.81×10^{-42})	1.02 (p=1.94×10^{-7})
ARIC	1.04 (p=1.00×10^{-26})	1.03 (p=1.09×10^{-6})
FHS	1.04 (p=1.23×10^{-34})	1.02 (p=5.09×10^{-6})
LBC 1921	1.04 (p=1.17×10^{-38})	1.02 (p=3.21×10^{-6})
LBC 1936	1.04 (p=1.94×10^{-41})	1.02 (p=1.39×10^{-7})
WHI (Whites)	1.04 (p=2.61×10^{-43})	1.02 (p=2.77×10^{-7})
WHI (Blacks)	1.04 (p=3.46×10^{-40})	1.02 (p=7.42×10^{-7})
WHI (Hispanics)	1.04 (p=4.29×10^{-41})	1.02 (p=6.17×10^{-7})
NAS	1.04 (p=3.91×10^{-40})	1.02 (p=2.42×10^{-7})
InCHIANTI	1.04 (p=1.98×10^{-41})	1.02 (p=7.38×10^{-7})
Rotterdam	1.04 (p=4.35×10^{-41})	1.02 (p=2.16×10^{-7})
KORA	1.04 (p=1.93×10^{-39})	1.02 (p=3.76×10^{-7})
TwinsUK	1.04 (p=3.76×10^{-41})	1.02 (p=4.66×10^{-7})

The table reports hazards ratios and corresponding p-values based on a Cox regression. The fully adjusted model includes the following covariates: body mass index, educational level, alcohol intake, smoking pack-years, prior history of diabetes, prior history of cancer, hypertension status, self-reported recreational physical activity.
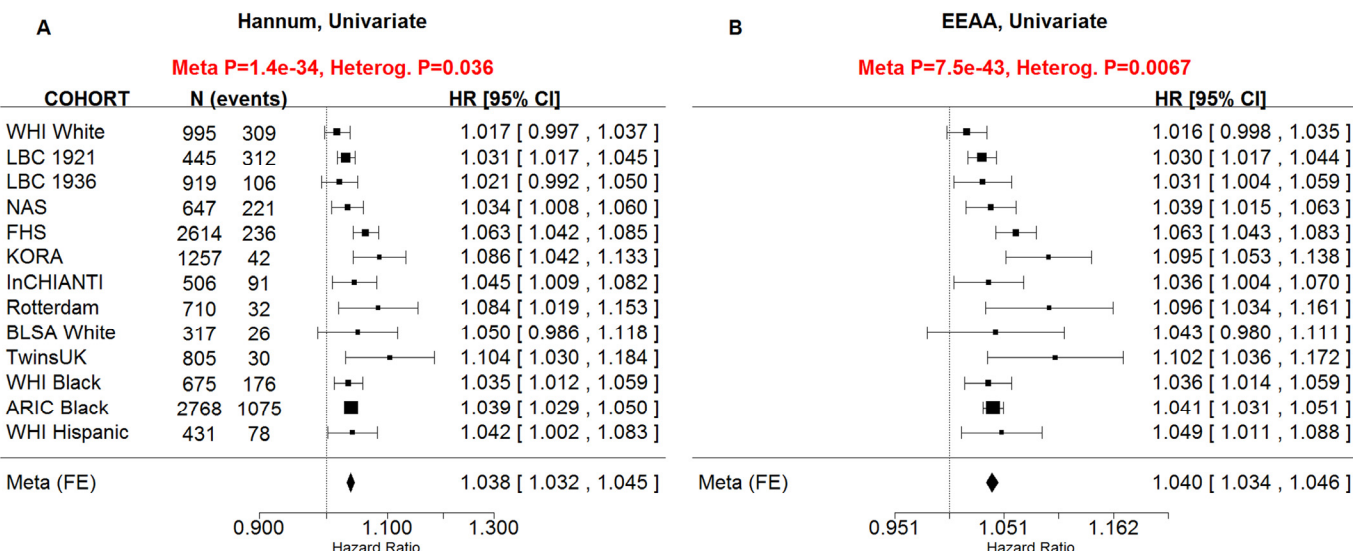
Supplementary Figure 1. Univariate Cox regression model analysis of all-cause mortality, contrasting existing and novel measures of age acceleration. The rows correspond to the different cohorts. Each row depicts the hazard ratio and a 95% confidence interval. To combine the coefficient estimates from the respective studies into a single estimate, we applied a fixed-effect model weighted by inverse variance (implemented in the metafor R package [30]). (**A**) This measure of age acceleration is based on Hannum et al [1]. Specifically, we estimated the age using the 71 CpGs and coefficient values from Hannum. Next, the measure of age acceleration was defined as residuals resulting from regressing the epigenetic age estimate on chronological age. (**B**) Extrinsic epigenetic age acceleration (EEAA). The sub-title of each plot reports the meta-analysis p-value and a heterogeneity test p-value (Cochran's Q-test). It is not appropriate to compare the hazard ratios and confidence intervals of the different measures directly because the measures have different scales/distributions. However, it is appropriate to compare the meta-analysis p-values (colored in red).
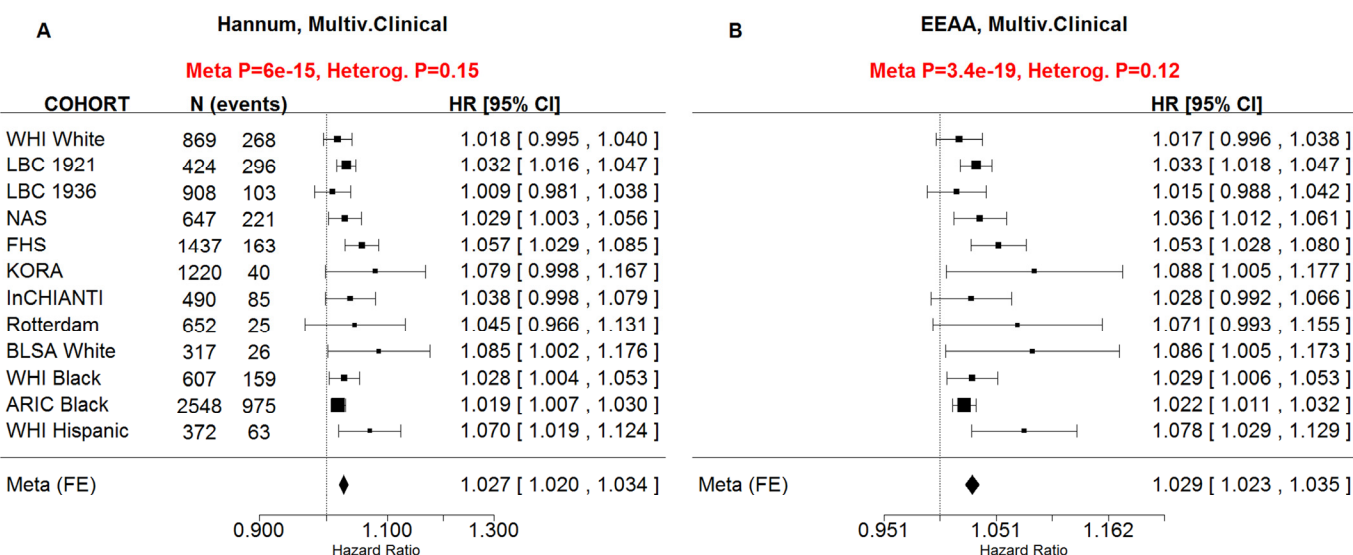
Supplementary Figure 2. Multivariate Cox regression model analysis of all-cause mortality, contrasting existing and novel measures of age acceleration. The multivariate Cox regression model included the following additional covariates: chronological age, body mass index (category), educational level (category), alcohol intake, smoking pack years, prior history of diabetes, prior history of cancer, hypertension status, recreational physical activity (category). The rows correspond to separate cohorts. Each row depicts the hazard ratio (HR) and a 95% confidence interval. (**A**) Age acceleration based on Hannum et al [6], (**B**) Extrinsic epigenetic age acceleration (EEAA). The sub-title of each plot reports the meta-analysis p-value and a heterogeneity test p-value (Cochran's Q-test).

Supplementary Figure 3 — Panel A: AgeAccel, Multiv.Clin.+Cell

Meta P=2e-04, Heterog. P=0.45

Cohort	N	(events)	HR [95% CI]
WHI White	869	268	1.002 [0.977 , 1.028]
LBC 1921	424	296	1.022 [1.003 , 1.042]
LBC 1936	908	103	1.007 [0.978 , 1.037]
NAS	647	221	1.004 [0.978 , 1.030]
FHS	1437	163	1.039 [1.006 , 1.074]
KORA	1220	40	1.014 [0.935 , 1.100]
InCHIANTI	490	85	1.047 [0.999 , 1.098]
Rotterdam	652	25	0.991 [0.915 , 1.074]
BLSA White	317	26	1.135 [1.016 , 1.268]
WHI Black	607	159	1.018 [0.992 , 1.046]
ARIC Black	2548	975	1.011 [0.998 , 1.025]
WHI Hispanic	372	63	1.027 [0.966 , 1.091]
Meta (FE)			**1.015 [1.007 , 1.023]**

Hazard Ratio: 0.900 1.100 1.300

Panel B: IEAA, Multiv.Clin.+Cell

Meta P=0.00021, Heterog. P=0.44

HR [95% CI]
1.001 [0.976 , 1.027]
1.022 [1.003 , 1.042]
1.007 [0.978 , 1.037]
1.004 [0.978 , 1.030]
1.039 [1.006 , 1.074]
1.014 [0.935 , 1.100]
1.047 [0.999 , 1.098]
0.991 [0.915 , 1.074]
1.135 [1.016 , 1.268]
1.019 [0.993 , 1.046]
1.011 [0.998 , 1.025]
1.026 [0.965 , 1.090]
Meta (FE) 1.015 [1.007 , 1.023]

Hazard Ratio: 0.905 1.105 1.350

Panel C: EEAA.static, Multiv.Clin.+Cell

Meta P=4.1e-07, Heterog. P=0.5

HR [95% CI]
1.014 [0.987 , 1.042]
1.023 [1.004 , 1.042]
1.007 [0.973 , 1.042]
1.013 [0.984 , 1.044]
1.053 [1.019 , 1.087]
1.098 [0.990 , 1.218]
1.055 [1.001 , 1.112]
1.023 [0.930 , 1.125]
1.029 [0.921 , 1.149]
1.024 [0.995 , 1.055]
1.015 [1.002 , 1.029]
1.061 [0.999 , 1.126]
Meta (FE) 1.021 [1.013 , 1.030]

Hazard Ratio: 0.905 1.051 1.221

Supplementary Figure 3. Multivariate Cox regression analysis of all-cause mortality adjusted for blood cell counts and clinical covariates. A multivariate Cox regression model was used to relate the censored survival time (time to all-cause mortality) to (**A**) the universal measure of age acceleration (AgeAccel), (**B**) intrinsic epigenetic age acceleration (IEAA), (**C**) extrinsic epigenetic age acceleration (EEAA). The multivariate Cox regression model included blood cell counts (exhausted CD8+ T cells, naïve CD8+, CD4+ T cells, natural killer, monocytes, granulocytes, and plasmablasts) and clinical covariates (chronological age, body mass index, educational level, alcohol intake, smoking pack years, prior history of diabetes, prior history of cancer, hypertension status, recreational physical activity). The rows correspond to the different cohorts. Each row depicts the hazard ratio (HR) and a 95% confidence interval. Estimates were meta-analyzed using a fixed-effect model weighted by inverse variance. The sub-title of each plot reports the meta-analysis p-value and a heterogeneity test p-value (Cochran's Q-test).

Supplementary Figure 4 — Panel A: AgeAccel, Univariate

Meta P=1.5e-06, Heterog. P=0.082

| Cohort	N	(events)	HR [95% CI]
WHI White	995	309	0.993 [0.971 , 1.016]
LBC 1921	445	312	1.030 [1.013 , 1.048]
LBC 1936	919	106	1.030 [1.003 , 1.059]
NAS	647	221	0.999 [0.975 , 1.023]
FHS	2614	236	1.035 [1.011 , 1.060]
KORA	1257	42	1.033 [0.975 , 1.093]
InCHIANTI	506	91	1.034 [0.992 , 1.078]
Rotterdam	710	32	1.049 [0.993 , 1.110]
BLSA White	317	26	1.100 [1.023 , 1.183]
TwinsUK	805	30	1.072 [0.988 , 1.162]
WHI Black	675	176	1.027 [1.004 , 1.050]
ARIC Black	2768	1075	1.024 [1.012 , 1.037]
WHI Hispanic	431	78	1.038 [0.988 , 1.091]
Meta (DL)			**1.025 [1.015 , 1.035]**

Hazard Ratio: 0.900 1.100 1.300

Panel B: IEAA, Univariate

Meta P=8.2e-09, Heterog. P=0.61

HR [95% CI]
0.998 [0.975 , 1.021]
1.023 [1.004 , 1.042]
1.022 [0.992 , 1.053]
1.010 [0.984 , 1.037]
1.028 [1.003 , 1.055]
1.033 [0.972 , 1.098]
1.034 [0.990 , 1.080]
1.028 [0.961 , 1.100]
1.114 [1.025 , 1.212]
1.036 [0.947 , 1.134]
1.029 [1.005 , 1.054]
1.023 [1.011 , 1.036]
1.022 [0.971 , 1.076]
Meta (DL) 1.022 [1.014 , 1.029]

Hazard Ratio: 0.905 1.000 1.105 1.221

Panel C: EEAA.static, Univariate

Meta P=2.3e-16, Heterog. P=0.0067

HR [95% CI]
1.016 [0.998 , 1.035]
1.030 [1.017 , 1.044]
1.031 [1.004 , 1.059]
1.039 [1.015 , 1.063]
1.063 [1.043 , 1.083]
1.095 [1.053 , 1.138]
1.036 [1.004 , 1.070]
1.096 [1.034 , 1.161]
1.043 [0.980 , 1.111]
1.102 [1.036 , 1.172]
1.036 [1.014 , 1.059]
1.041 [1.031 , 1.051]
1.049 [1.011 , 1.088]
Meta (DL) 1.043 [1.033 , 1.054]

Hazard Ratio: 0.951 1.051 1.162

Supplementary Figure 4. Random effects meta-analysis for univariate Cox models. The figure is analogous to Figure 2 in our article except that it uses a random-effects meta-analysis (DerSimonian-Laird) instead of a fixed-effects model. A univariate Cox regression model was used to relate the censored survival time (time to all-cause mortality) to (**A**) the universal measure of age acceleration (AgeAccel), (**B**) intrinsic epigenetic age acceleration (IEAA), (**C**) extrinsic epigenetic age acceleration (EEAA). To combine the coefficient estimates from the respective studies into a single estimate, we applied the DerSimonian-Laird random effects model. The sub-title of each plot reports the meta-analysis p-value and a heterogeneity test p-value (Cochran's Q-test).

Huntington's disease accelerates epigenetic aging of human brain and disrupts DNA methylation levels

Steve Horvath[1,2], Peter Langfelder[1], Seung Kwak[3], Jeff Aaronson[3], Jim Rosinski[3], Thomas F. Vogt[3], Marika Eszes[4,5], Richard L.M. Faull[4,5], Maurice A. Curtis[4,5], Henry J. Waldvogel[4,5], Oi-Wa Choi[6], Spencer Tung[7], Harry V. Vinters[7], Giovanni Coppola[6,8,9], and X. William Yang[6,8,9]

[1]Human Genetics, David Geffen School of Medicine, University of California Los Angeles, Los Angeles, CA 90095, USA
[2]Biostatistics, Fielding School of Public Health, University of California Los Angeles, Los Angeles, CA 90095, USA
[3]CHDI Management/CHDI Foundation, Princeton, NJ 08540, USA
[4]Department of Anatomy and Medical Imaging, Faculty of Medical and Health Science (FMHS), University of Auckland, Auckland, New Zealand
[5]Centre for Brain Research, Faculty of Medical and Health Science (FMHS), University of Auckland, Auckland, New Zealand
[6]Center for Neurobehavioral Genetics, Semel Institute for Neuroscience & Human Behavior, University of California, Los Angeles (UCLA), Los Angeles, CA 90095, USA
[7]Pathology and Laboratory Medicine, and Neurology, UCLA David Geffen School of Medicine, Los Angeles, CA 90095, USA
[8]Department of Psychiatry and Biobehavioral Sciences, David Geffen School of Medicine at UCLA, Los Angeles, CA 90095, USA
[9]UCLA Brain Research Institute, Los Angeles, CA 90095, USA

Abstract: Age of Huntington's disease (HD) motoric onset is strongly related to the number of CAG trinucleotide repeats in the *huntingtin* gene, suggesting that biological tissue age plays an important role in disease etiology. Recently, a DNA methylation based biomarker of tissue age has been advanced as an epigenetic aging clock. We sought to inquire if HD is associated with an accelerated epigenetic age. DNA methylation data was generated for 475 brain samples from various brain regions of 26 HD cases and 39 controls. Overall, brain regions from HD cases exhibit a significant epigenetic age acceleration effect (p=0.0012). A multivariate model analysis suggests that HD status increases biological age by 3.2 years. Accelerated epigenetic age can be observed in specific brain regions (frontal lobe, parietal lobe, and cingulate gyrus). After excluding controls, we observe a negative correlation (r=-0.41, p=5.5x10^{-8}) between HD gene CAG repeat length and the epigenetic age of HD brain samples. Using correlation network analysis, we identify 11 co-methylation modules with a significant association with HD status across 3 broad cortical regions. In conclusion, HD is associated with an accelerated epigenetic age of specific brain regions and more broadly with substantial changes in brain methylation levels.

INTRODUCTION

Huntington's disease (HD) is a dominantly inherited neurodegenerative disorder clinically characterized by progressive movement disorder, cognitive dysfunction, and psychiatric impairment [1]. HD is caused by a CAG trinucleotide repeat expansion resulting in an elongated polyglutamine stretch near the N-terminus of the huntingtin (HTT) protein [2]. HD patients have CAG repeat lengths greater than 36 on one of the *HTT* alleles. Although HD affects a number of brain regions such as the cortex, thalamus, and subthalamic nucleus, the

striatum is the most severely affected region [3]. Large postmortem pathological series and neuroimaging studies suggest that CAG repeat length is highly correlated with caudate but not cortical atrophy [4-6]. The hallmark of HD neuropathology is massive degeneration of the striatal medium-sized spiny neurons (MSNs) and, to a lesser extent, the deep layer cortical pyramidal neurons [7]. HD neurodegeneration mainly affects the MSNs of the neostriatal nuclei, caudate nucleus and putamen, explaining the grave motor symptoms. Despite the specificity of neurodegeneration in HD, HTT is broadly present in cells throughout the brain [8].

HD is one of several polyglutamine disorders (including inherited ataxias, muscular dystrophy, and several forms of mental retardation [3]) that are caused by the expansion of unstable CAG trinucleotide repeats. The differential pathogenesis of polyglutamine disorders may be due to differences in polyglutamine protein context or functions because these disorders exhibit distinct patterns of neuronal loss and clinical manifestation despite nearly ubiquitous expression of these proteins, at least in the brain, and in the case of HTT the ubiquitous expression throughout the body and during development.

The age of onset of HD motor symptoms strongly correlates with the number of CAG trinucleotide repeats in *HTT* [9-11]. HD patients are usually clinically diagnosed in their 40s, but the age of onset can range from earlier than 10 for individuals with high repeat lengths to over 80 years for those with repeat lengths below 40. Overall, three non-mutually exclusive hypotheses could explain adult onset in HD: First, normal aging renders MSNs more vulnerable to mutant HTT toxicity [12]. Second, mutant HTT progressively produces cumulative defects over time. Third, mutant HTT toxicity accelerates the biological age of affected cells and tissues, which makes them vulnerable to dysfunction and cell death. We are not aware of any data or results that would support this third hypothesis. Irrespective of the validity of this "accelerated biological age hypothesis in HD", there is little doubt that biological age plays an important role in HD. For example, the product of CAG repeat length and chronological age ("CAP score") relates to clinical outcomes in HD according to recent longitudinal studies of HD patient cohorts [10]. Here, we address the challenge of directly testing whether HD is associated with accelerated aging in brain tissue by exploiting our DNA methylation based biomarker of tissue age, which is referred to as the epigenetic clock.

DNA methylation levels lend themselves to defining a biomarker of tissue age because chronological age has a profound effect on DNA methylation levels [13-17]. We recently developed an epigenetic measure of tissue age by combining the DNA methylation levels of 353 dinucleotide markers known as cytosine phosphate guanines or CpGs [18]. The weighted average of these 353 epigenetic markers gives rise to an estimate of tissue age (in units of years), which is referred to as "DNA methylation age" or as "epigenetic age". This epigenetic clock method to estimate age appears to apply to any tissue or cell type that contains DNA (with the exception of sperm) including individual cell types (helper T cells, neurons, glial cells), complex tissues and organs (blood, brain, bone, breast, kidney, liver, lung [18-20]) and extending to prenatal brain samples [21]. The epigenetic clock method for estimating age is particularly attractive in the context of neuro-degenerative diseases for the following reasons. First, it applies to all brain regions, sorted brain cells [18-20], beginning with prenatal brain samples [21]. Second, recent findings suggest that the epigenetic clock captures aspects of the biological age of brain tissue, e.g. the epigenetic age of the frontal lobe relates to neuropathological variables and to Alzheimer's disease (AD) related cognitive functioning [22].

To explore changes in the brain methylome in HD individuals, we also carried out a systems biological analysis of DNA methylation levels. We constructed co-methylation modules and identified those that are associated with HD status in several brain regions.

RESULTS

Accuracy of the epigenetic clock in brain samples from HD patients and controls

We collected 475 brain samples from multiple brain regions of 65 individuals (26 HD, 18 Alzheimer's disease, and 21 controls) and profiled the samples using the Illumina 450k platform. An overview of our data set is presented in Table 1. Individual level data such as postmortem interval can be found in Supplementary Table 1. Epigenetic age (referred to as DNAm age) was calculated as described in [18]. As expected, DNAm age has a strong linear relationship with chronological age in brain tissue samples (r=0.94, Supplementary Figure 1A). However, 4 samples deviate strongly from the linear trend. To err on the side of caution, we "winsorized" the DNAm age estimates of these 4 putative outliers by replacing them with the second most extreme age estimate from the same individual (based on the remaining non-cerebellar brain regions). Winsorisation effectively limits the adverse effects of severe outliers in the DNAm age estimate. We did not use DNAm age estimates from the cerebellum in this

winsorization approach because the cerebellum ages more slowly than other brain regions [20]. After the winsorization, the correlation between DNAm age and chronological age increased slightly (from r=0.94 to r=0.95, Figure 1A).
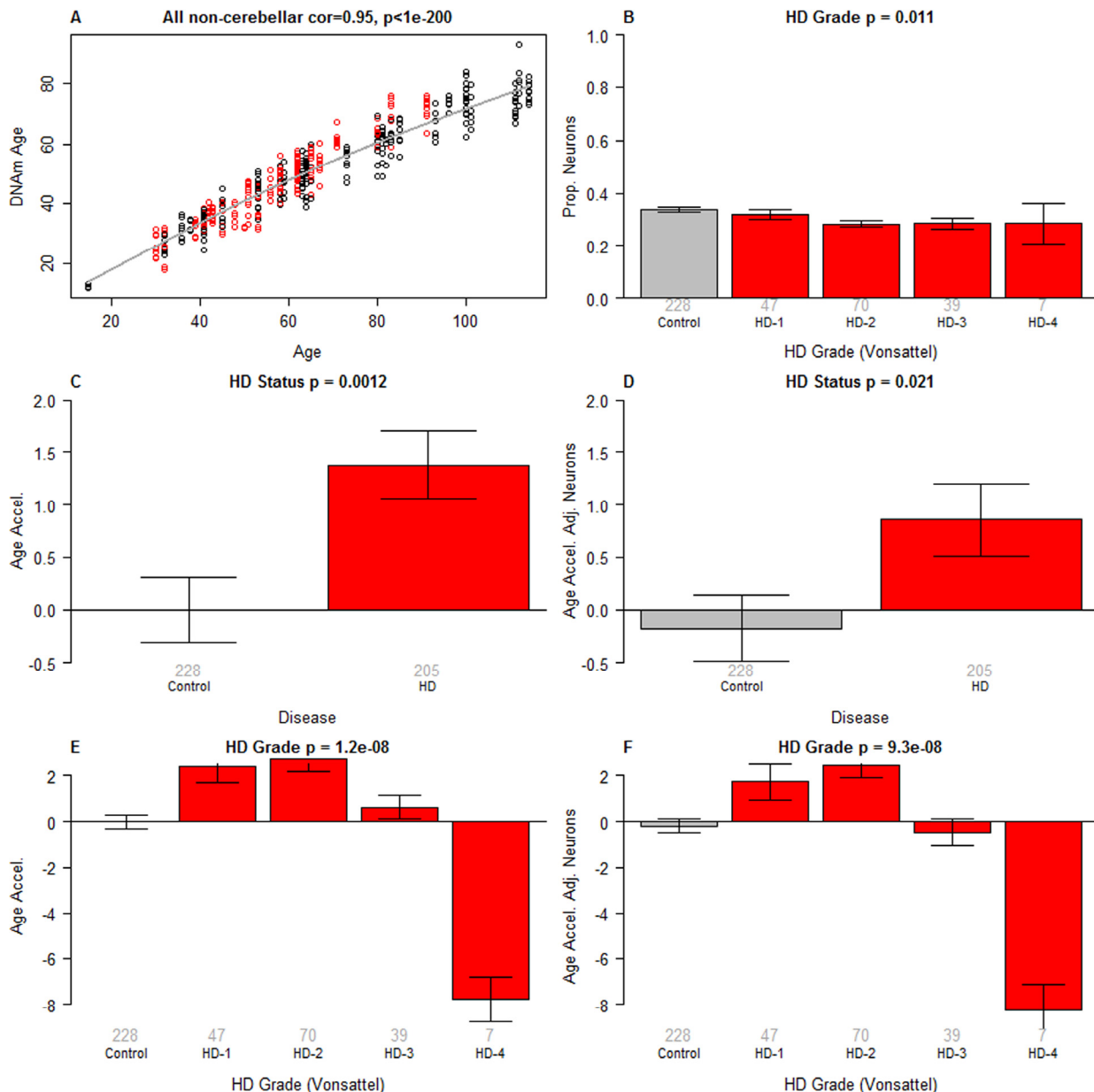
To formally measure epigenetic age acceleration effects, we constructed a regression model of DNAm age on chronological age in non-HD samples (grey line in Figure 1A). We then defined age acceleration for each sample (HD or non-HD) as the corresponding residual

Figure 1. Epigenetic clock analysis of non-cerebellar brain regions. (**A**) Scatter plot of (winsorized) DNAm age versus chronological age (x-axis). Red dots correspond to HD cases, black dots to non-HD samples. The curve corresponds to a spline regression line (2 degrees of freedom) through the non-HD samples. Epigenetic age acceleration was defined as the vertical distance of each sample from the spline regression line. (**B**) HD Vonsattel grade vs the proportion of neurons (y-axis). The proportion of neurons was estimated based on DNA methylation data using the CETS method [23]. (**C,D**) HD status versus (**C**) epigenetic age acceleration, D) an intrinsic measure of epigenetic age acceleration that adjusts for the proportion of neurons. (**E,F**) HD Vonsattel grade versus (**E**) age acceleration and (**F**) an intrinsic measure of epigenetic age acceleration that adjusts for the proportion of neurons. All bar plots show the mean value (y-axis) and one standard error and report the results from a non-parametric group comparison test (Kruskal Wallis). The "winsorized" the DNAm age estimates changed the values of four putative outliers as described in Supplementary Figure 1.

resulting from the regression model. Thus, positive age acceleration means the (methylation state of the) sample appears to be older than would be expected from non-HD samples. We find that HD is significantly associated with epigenetic age acceleration (Figure 1C), and that this finding holds even when one uses the un-winsorized version of DNAm age (Supplementary Figure 1B). We also defined an "intrinsic" measure of age acceleration as the residual that results by regressing DNAm age on both chronological age and the proportion of neurons which was estimated using the CETS method [23]. The resulting cell-intrinsic measure of age acceleration, which is not confounded by the abundance of neurons, is again associated with HD status (Figure 1D). We find that epigenetic age acceleration relates significantly to Vonsattel grade (VS grade), a semi-quantitative (0-4) measure of neuro-pathologic abnormalities of post-mortem HD brains based on macroscopic and microscopic criteria [24]. VS grade 1 and 2 samples exhibit the highest positive age acceleration whereas VS grade 4 samples exhibit *negative* epigenetic age acceleration (Figure 1E) which persists even after controlling for the proportion of neurons/glia (Figure 1F). This unexpected negative age acceleration in VS grade 4 samples, which can also be observed in specific brain regions (Supplementary Figure 2), may be due to one of the following explanations. First, it could be a false positive that reflects the low sample size (n=7) of grade 4 samples.

However, we think this explanation is unlikely since one already observes a diminished epigenetic age acceleration in grade 3 samples and because we find a similar negative relationship of epigenetic age acceleration with CAG repeat length (as described below). Second, it might reflect the severe loss of neurons even though moderate changes in cell composition do not seem to affect the estimate of DNAm age [18, 20]. However, we observe the same effect when using our cell intrinsic measure of age acceleration that adjusts for the proportion of neurons (Figure 1F). Further, only a marginally significant association between the proportion of neurons and VS grade can be observed in the brain regions of our study (p=0.011, Figure 1B). We next studied epigenetic age acceleration in individual brain regions. After removing grade 4 samples, we find that HD has a suggestive association with epigenetic age acceleration in the parietal lobe (p=0.072, Figure 2B), frontal lobe (p=0.077, Figure 2F), and cingulate gyrus (p=0.047, Figure 2K). No significant associations could be observed in the occipital lobe (Figure 2H,I). Comparisons in other brain regions, including the caudate nucleus (Figure 2Q,R), were inconclusive, possibly due to HD disease stage (the striatum is more affected than the cortex and may thus be equivalent to HD stage 3 or 4) or due to the low group sizes (group sizes are shown under each bar in the bar plot panels in Figure 2).

Table 1. Overview of the brain methylation data set.

	Disease Status		
	Huntington's	Alzheimer's	Control
Brain samples (n)	215	125	135
Frontal lobe (n)	50	21	32
Occipital lobe (n)	31	24	20
Parietal lobe (n)	62	0	35
Temporal lobe (n)	8	23	6
Caudate nucleus (n)	17	0	12
Cerebellum (n)	10	23	9
Cingulate gyrus (n)	21	0	12
Hippocampus (n)	8	18	7
Midbrain (n)	8	16	1
No. of individuals	26	18	21
No. of women	10	13	6
Mean Age (range)	56.1 (30, 91)	84.6 (58, 114)	59.1 (15, 93)
Mean Postmortem interval	14.8 (3.5, 46)	20.5 (21, 52)	16.4 (6.0, 36)
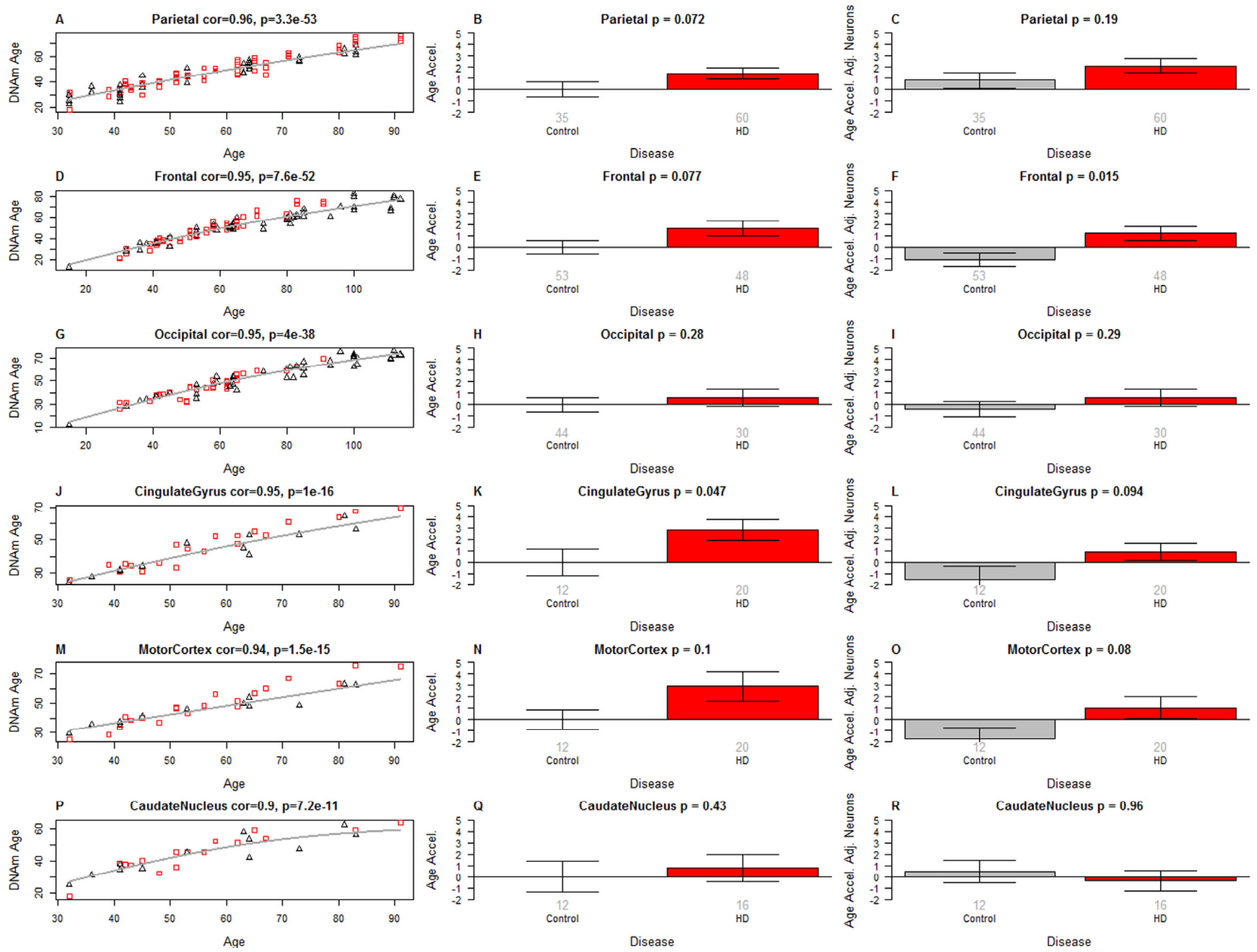
Figure 2. **Epigenetic age acceleration in specific brain regions.** Rows correspond to different brain regions. The first column (**A,D,G,J,M,P**) depicts DNAm age (y-axis) versus chronological age (x-axis) in different brain regions. The grey line corresponds to a spline regression model (based on 2 degrees of freedom) through non-HD samples. Epigenetic age acceleration was defined as the vertical distance of each sample from the spline regression line. The bar plots in the second column (**B,E,H,K,N,Q**) show the relationship between epigenetic age acceleration (y-axis) and HD status. The bar plots in the third column (**C,F,I,L,O,R**) involve the intrinsic measure of age acceleration that adjusts for the proportion of neurons. The rows correspond to samples from the parietal lobe, frontal lobe, occipital lobe, cingulate gyrus, motor cortex, and caudate nucleus. Each bar plot depicts the mean value and one standard error and reports a non-parametric group comparison test p-value (Kruskal Wallis Test). HD grade 4 samples were removed from this analysis.

Regression analysis that adjusts for possible confounders

We next asked whether the observed epigenetic age acceleration could be due to confounding by known or unknown confounders. To answer this question, we studied age acceleration using three different multivariate linear regression models that include known and inferred confounders (Table 2). The first model regressed DNAm age on HD status, chronological age, sex, brain bank, and brain region. We find that HD status remains highly significantly associated with DNAm age ($p=6.7 \times 10^{-5}$) even after adjusting for these known confounders. In the second linear model, which contains the estimated proportion of neurons as covariate, HD status remains highly significantly associated with

DNAm age (p=0.00070). The third model is similar to the first but also adjusts for the first five principal components (PCs) estimated from the DNA methylation data. These PCs are likely to reflect unobserved confounders (technical variation, changes in cell composition) and so can be viewed as inferred confounders. Although including 5 PCs in a multivariate model may be overly conservative, HD status remains marginally significantly associated with DNAm age (p=0.065). Overall, the multivariate model analysis strongly suggests that the epigenetic age acceleration effects observed in HD are not due to confounding effects. The multivariate models allow us to estimate the increase in biological age due to HD status. HD status increases the biological age by 3.2 years according to model 1 or by 2.7 years according to model 2 (caption of Table 2).

Table 2. Linear model that regresses DNAm age on HD status and other covariates.

Covariate	Contrast	Model 1		Model 2		Model 3	
		Coef (SE)	P-value	Coef (SE)	P-value	Coef (SE)	P-value
Huntington		2.06 (0.517)	6.7×10^{-5}	1.704 (0.503)	0.00070	0.9 (0.486)	0.065
Age		0.646 (0.012)	$<2 \times 10^{-16}$	0.64 (0.011)	$<2 \times 10^{-16}$	0.632 (0.011)	$<2 \times 10^{-16}$
Sex	Female vs Male	-0.981 (0.49)	0.046	-0.84 (0.474)	0.077	0.611 (2.637)	0.817
Brain Bank	UCLA vs NewZealand	-0.093 (1.224)	0.94	1.049 (1.198)	0.382	1.32 (1.139)	0.247
Tissue	Caudate Nucleus vs Frontal	-1.237 (1.266)	0.33	-3.412 (1.278)	0.008	-3.239 (1.201)	0.007
	Cingulate Gyrus vs Frontal	-1.631 (1.224)	0.18	-1.961 (1.183)	0.098	-0.729 (1.119)	0.52
	CRBM vs Frontal	-5.353 (1.121)	1.8×10^{-6}	-3.854 (1.113)	0.001	16.194 (10.299)	0.12
	Hippocampus vs Frontal	1.327 (1.191)	0.27	-0.077 (1.175)	0.95	1.08 (1.131)	0.34
	Midbrain vs Frontal	-1.115 (1.274)	0.38	-4.12 (1.334)	0.002	-1.327 (1.331)	0.32
	Motor Cortex vs Frontal	1.539 (1.224)	0.21	1.699 (1.182)	0.151	1.64 (1.112)	0.14
	Occipital vs Frontal	-2.886 (1.115)	0.01	-1.704 (1.096)	0.121	-2.218 (1.037)	0.033
	Parietal vs Frontal	0.835 (1.065)	0.43	1.781 (1.042)	0.088	1.382 (0.982)	0.16
	Sensory Cortex vs Frontal	-0.173 (1.224)	0.89	0.079 (1.183)	0.95	0.179 (1.116)	0.87
	Temporal vs Frontal	0.191 (1.156)	0.87	0.228 (1.116)	0.84	0.621 (1.053)	0.56
	Visual Cortex vs Frontal	0.4 (1.233)	0.75	2.178 (1.23)	0.077	0.408 (1.192)	0.73
Prop. Neurons				-13.966 (2.395)	5.5×10^{-9}		

PC1			862.505 (313.408)	0.006
PC2			147.452 (64.232)	0.022
PC3			-36.821 (13.872)	0.008
PC4			59.519 (11.864)	5.3×10^{-7}
PC5			8.251 (26.496)	0.76

Coefficients, standard error, and corresponding p-values for three multivariate models.

According to model 1, the age acceleration due to HD status amounts to 3.3 years (=2.159/0.646).

Model 2 is similar to model 1 but includes the (estimated) proportion of neurons as covariate. Model 3 is similar to model 1 but includes principal components. Since the analysis ignores the dependency of observations (due to multiple brain regions coming from the same individual), the p-values should only be interested as descriptive measures (as opposed to inferential measures). The multivariate models allow us to estimate the increase in biological age due to HD status. HD status is associated with an increase of 3.2 years (=2.06/0.646) according to model 1, an increase of 2.7 years (=1.704/0.64) according to model 2, and am increase of 1.4 years according to model 3.
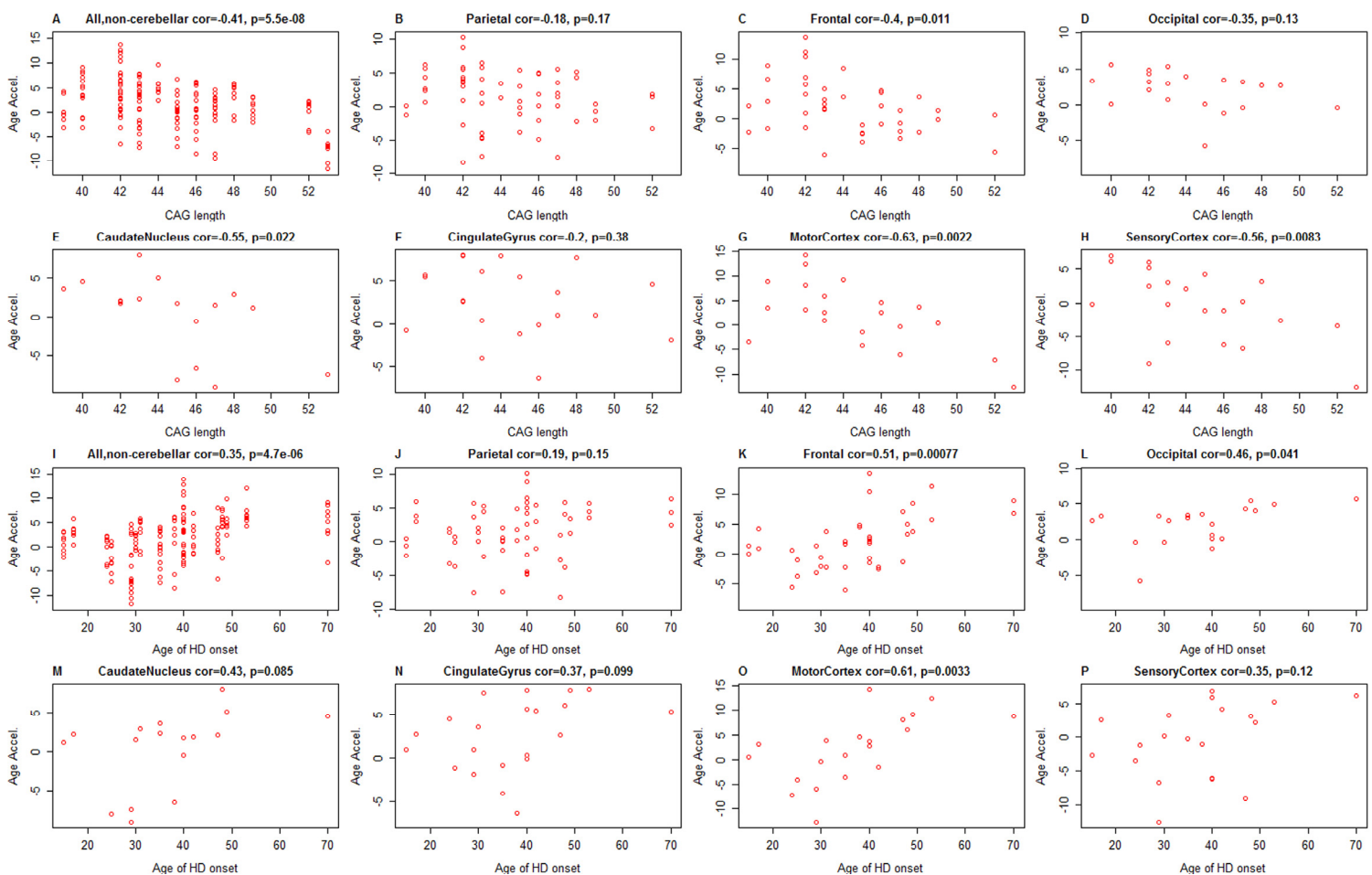
Figure 3. CAG length and age of HD onset versus epigenetic age acceleration in HD patients. Results for CAG length and for age of onset can be found in the first two rows and the last two rows, respectively. (**A**-**H**) CAG length (x-axis) versus epigenetic age acceleration in (**A**) all non-cerebellar samples, (**B**) parietal lobe, (**C**) frontal lobe, (**D**) occipital lobe, (**E**) caudate nucleus, (**F**) cingulate gyrus, (**G**) motor cortex, (**H**) sensory cortex. (**I**-**P**) Age of HD motoric onset (x-axis) versus epigenetic age acceleration in (**I**) all non-cerebellar samples, (**J**) parietal lobe, (**K**) frontal lobe, (**L**) occipital lobe, (**M**) caudate nucleus, (N) cingulate gyrus, (**O**) motor cortex, (**P**) sensory cortex.

CAG-repeat length versus epigenetic age acceleration

The graded impact of CAG length on HD age of onset and disease manifestation leads to the "polyglutamine trigger" hypothesis, which suggests that polyglutamine expansion in the context of endogenous HTT protein leads to subtle but repeat-length-dependent graded molecular changes in affected cells that act in a dominant fashion to trigger the disease [25]. The search of CAG-repeat-length dependent, continuous molecular changes have implicated altered energetics [26], gene expression, and epigenetic changes [27-30]. After removing controls, we find a significant negative correlation between CAG length and epigenetic age acceleration of HD brain samples (r=-0.41, p=5.5x10^{-8}, Figure 3A) and in specific brain regions from HD cases (Figure 3B-H). This negative correlation probably relates to the finding that VS grade 4 samples exhibit negative age acceleration because a) the seven grade 4 samples also exhibited the highest CAG length (of 53 trinucleotide replicates), and b) VS grade is strongly correlated with CAG length in our HD cases (r=0.75, p=9.0x10^{-5}, Supplementary Figure 3A).

For a subset of 21 HD subjects, we also had information on the age of HD motoric onset. We found a significant positive correlation between the age of HD motoric onset and epigenetic age acceleration (Figure 3I-P). The marginal associations between age acceleration and the clinical parameters (age of onset, CAG length, and HD grade) are congruent with the pairwise correlations between the clinical parameters in the 21 HD subjects (Supplementary Figure 3): CAG length has a strong positive correlation with HD grade (r=0.75) and a strong negative correlation with age of onset (r=-0.55, p=0.0098, Supplementary Figure 3B). Age of onset was highly correlated with chronological age at death in our data set (r=0.78, p=3.5x10^{-5}). No significant correlation could be observed between HD grade and age of onset (Supplementary Figure 3C).

In contrast to our findings of epigenetic age acceleration in brains of HD cases, we find no difference in epigenetic age acceleration between Alzheimer's disease brains and controls (Supplementary Figure 4), which might reflect the low sample size as discussed below. We could not find a significant age acceleration effect due to HD in several brain regions (Supplementary Figure 5), which might reflect the low sample sizes.

Table 3. The most significant CpGs from our EWAS of HD status across three brain regions.

CpG name	Gene	Chrom.	Z statistic meta	p meta analysis	p Frontal	p Occipital	p Parietal
cg01524723		3	7.87	3.6E-15	7.2E-07	5.3E-06	3.5E-05
cg10112599	TMEM8A	16	7.74	9.9E-15	1.1E-06	4.8E-06	6.9E-05
cg11540707	IDE	10	7.61	2.8E-14	2.8E-05	1.7E-03	9.5E-09
cg22897634	GRIK2	6	7.45	9.2E-14	1.8E-06	5.7E-05	4.4E-05
cg05482066		8	7.43	1.1E-13	1.3E-06	6.2E-04	6.6E-06
cg27250180		21	7.36	1.8E-13	8.0E-06	4.2E-05	2.8E-05
cg14593290	DDC	7	7.33	2.4E-13	1.9E-07	3.7E-04	1.2E-04
cg00249621	TSPYL5	8	7.27	3.7E-13	1.3E-04	1.0E-02	1.6E-09
cg00160777	CHP2	16	7.16	8.1E-13	5.0E-06	8.4E-03	4.8E-07
cg14937409	KRI1	19	7.11	1.2E-12	8.3E-07	2.8E-04	2.2E-04
cg04195855	LRRK1	15	7.09	1.3E-12	7.0E-07	1.9E-03	4.1E-05
cg08291433		11	7.08	1.5E-12	4.4E-06	9.9E-04	1.8E-05
cg21535199	LCE1F	1	-7.14	9.4E-13	4.5E-05	2.3E-02	5.8E-09
cg08718119	LOC642846	12	-7.27	3.7E-13	8.4E-07	9.8E-03	1.0E-06
cg14227325	RGPD8	2	-7.4	1.3E-13	3.0E-05	1.9E-03	5.6E-08
cg17863923	RGPD1	2	-7.45	9.7E-14	1.7E-04	3.7E-04	3.2E-08

The second column reports the gene symbol of a neighboring gene. The CpGs were selected according to the meta analysis p-value (5th column) across the 3 regions (frontal, occipital, and parietal lobe). The meta analysis Z statistic (4rd column) is positive/negative for CpGs that are hyper/hypo methylated in HD compared to non-HD samples. "p Frontal" denotes the Kruskal Wallis p value for disease status in the frontal lobe samples. Bar plots can be found in Supplementary Figure 9.
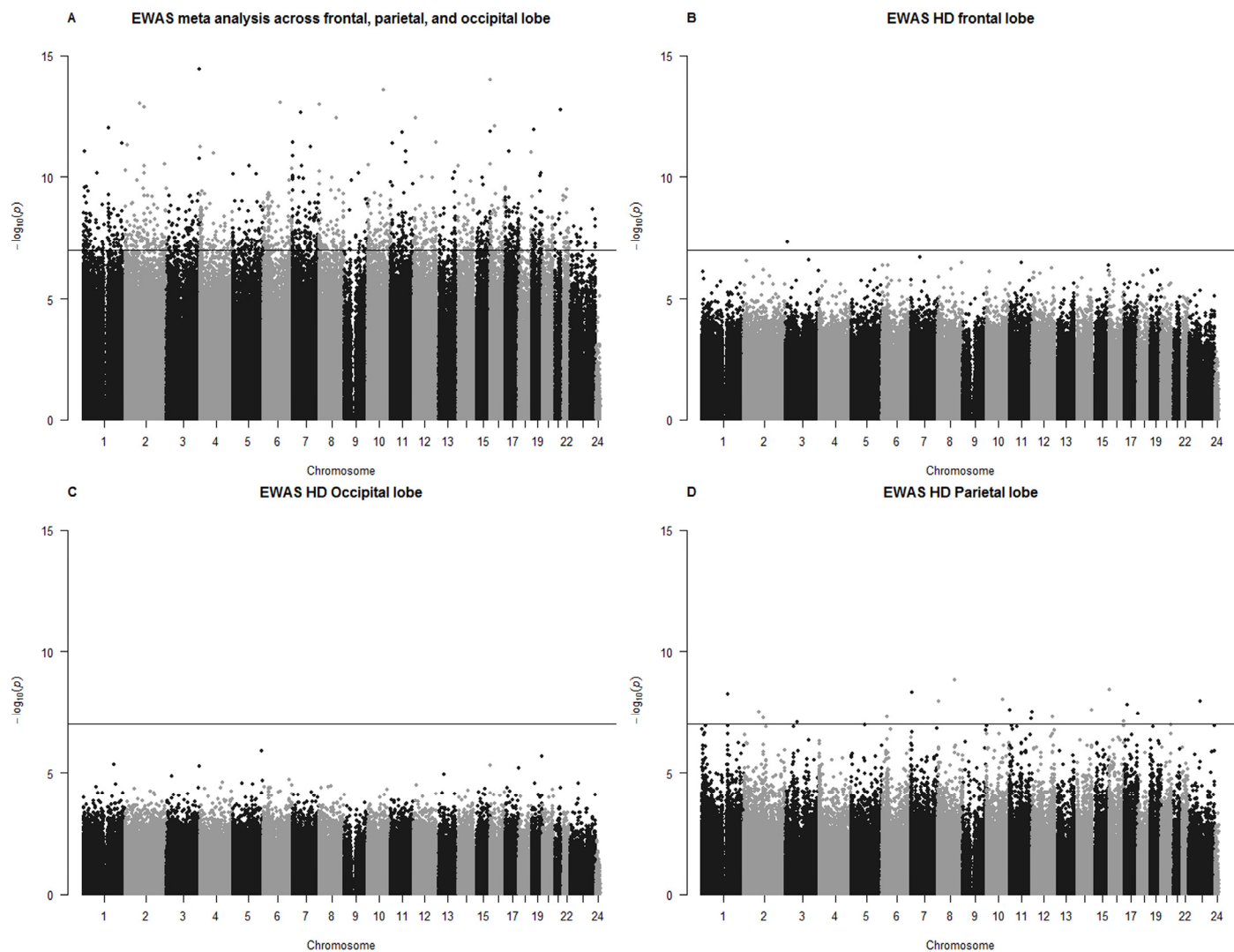
Figure 4. Manhattan plots for EWAS results. (**A**) The y-axis shows log (base 10) transformed p-values resulting from a meta analysis across 3 lobes (frontal, parietal, and occipital lobe). Meta analysis p-value resulted from the *limma* R function that also included the batch as covariate. EWAS results (Kruskal Wallis test) for individual lobes can be found in (**B**) frontal lobe, (**C**) occipital lobe, (**D**) parietal lobe. The horizontal line corresponds to a Bonferroni corrected significance level of p=0.05/500000. The statistical analysis ignored the dependence between observations arising from the fact that multiple samples were collected from the same individual. Therefore, the p-values should be considered as descriptive (rather than inferential) measures.

Epigenome-wide association study (EWAS)

In a secondary analysis, we related HD status to individual epigenetic markers (CpGs). Here we focused on 327k CpGs (out of over 485k) with highest variance across the samples (Methods).

Since sex and age has profound effects on DNA methylation levels (which are largely preserved across brain regions Supplementary Figure 6), we adjusted the DNA methylation levels for age and sex by forming residuals. Further, we restricted the analysis to samples from post mortem lobes for which we had sufficient sample sizes (Table 1) namely the frontal lobe (Figure 4B), occipital lobe (Figure 4C), and parietal lobe (Figure 4D). The association between HD and age-adjusted methylation levels is strongly preserved across the lobes (Supplementary Figure 7). After combining the EWAS results from each of the 3 lobes using meta analysis, we found that 1467 CpGs are significantly associated with HD at a Bonferroni corrected significance level of $1 \times 10^{-7} = 0.05/500000$ (Figure 4A).

The 16 most significant (p <1.2x10^{-12}) HD related CpGs are presented in Table 3 and in Supplementary Figure 8. The meta-analysis p-values need be interpreted as descriptive (hypothesis promoting) rather than inferential measure for the following reasons. First, the meta analysis did not adjust for the fact that multiple samples were collected from each individual. Second, the distribution of EWAS p-values exhibit high inflation factors (lambda=7.3 for the meta analysis, 3.5 for the frontal lobe, 3.0 parietal lobe, 2.2 for the occipital lobe, Supplementary Figure 9). Detailed results for all CpGs can be found in Supplementary File 11.

WGCNA reveals HD-dependent co-methylation modules

In light of the low sample size we conducted weighted correlation network analysis (WGCNA) [31-34], which

is a systems biological analysis method that has been successfully applied to DNA methylation data, e.g. to study aging effects [35]. WGCNA constructs modules of co-methylated CpGs and identifies modules (as opposed to individual CpGs) that correlate with HD status. Among other advantages, this circumvents the problem of multiple comparisons (485k CpGs on the Illumina Infinium 450K array). We applied WGCNA to the same sex and age adjusted methylation data that were used in our EWAS. We again focused on samples from three lobes (frontal, occipital, parietal) for which we had sufficient sample sizes. To prevent between-lobe differences in methylation from confounding the module analysis, we employed a consensus network [36] analysis across the three lobes that essentially conditions out between-lobe differences. The analysis identified 54 co-methylation modules; by construction, these modules contain CpGs co-methylated in each of
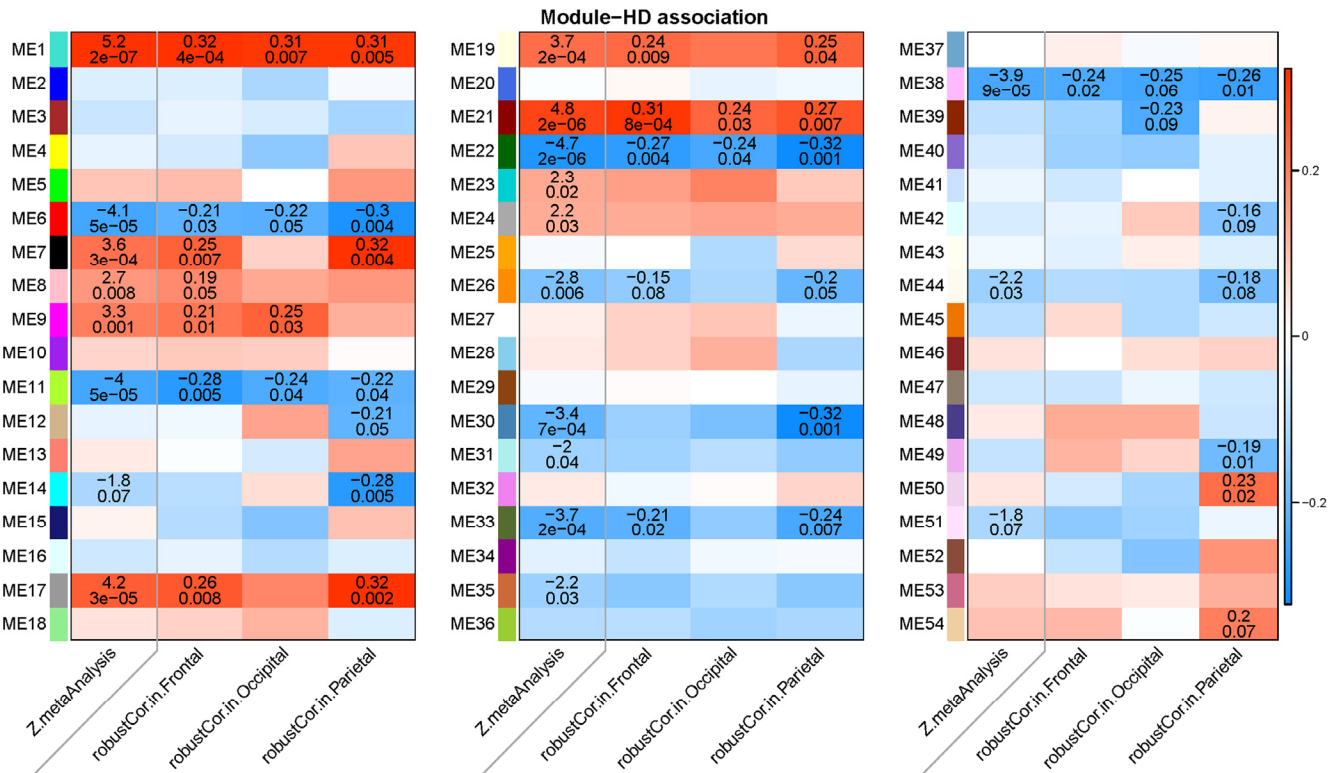
Figure 5. Heat map of correlations between modules and HD status in different lobes. The rows correspond to modules found in a consensus module analysis across three lobes (frontal lobe, occipital lobe, parietal lobe). Each module (eigenvector) was correlated to HD status and to the proportion of neurons in the respective brain regions using a robust correlation test (biweight midcorrelation). Columns 2-4 in each panel report the robust correlation coefficients and the corresponding p-value (underneath the correlation coefficient) in the frontal, occipital, and parietal lobe, respectively. Each cell is color-coded according to the sign and strength of the correlation coefficient as shows in the color legend at the right hand side. Stouffer's meta analysis method was used to combine the three robust correlation test statistics across the three lobes. The first column of each panel presents a meta analysis Z statistic for HD status (Stouffer's method applied to the results from the 3 lobes) and corresponding p-value. The remaining columns present analogous results for the estimated proportion of neurons.

the three lobes. In this manner, network analysis reduced hundreds of thousands of variables across the 3 lobes to a relatively small number (n=54) of modules. Since the methylation profiles of probes in each module are strongly correlated in each of the 3 lobes, it is useful to summarize each module using a single representative profile. Toward this end, we defined the module representative as the first singular vector resulting from the singular value decomposition of the scaled methylation levels. We refer to this representative methylation profile, which can be interpreted as the weighted average of the CpGs inside a module, as the eigenvector (also known as eigengene or eigenprofile).

To identify modules related to HD status, we correlated the 54 module eigenvectors with HD status in the 3 lobes (Figure 5). We then used a meta-analysis of the eigenvector-HD correlations to quantify the overall relationship between a consensus module and HD status across all 3 lobes. Eleven modules passed a Bonferroni corrected meta-analysis significance threshold of $p=0.05/54= 9.3\times10^{-4}$ that adjusts for the number of modules (n=54). Five of these modules are hyper-methylated in HD: module 1 (meta-analysis $p=2\times10^{-7}$), module 21 ($p=2\times10^{-6}$), module 17 ($p=3\times10^{-5}$), module 19 ($p=2\times10^{-4}$), and module 7 ($p=3\times10^{-4}$). Six modules are hypo-methylated in HD (module 22 $p=2\times10^{-6}$, module 6 $p=5\times10^{-5}$, module 11 $p=5\times10^{-5}$, module 38 $p=9\times10^{-5}$, module 33 $p=2\times10^{-4}$, module 30 $p=7\times10^{-4}$). The network analyses provide several layers of information. First, the strength and significance of associations between modules and HD status are strongest in the parietal lobe, followed by the frontal lobe and then the occipital lobe. Second, the meta-analysis significance Z statistics allow us to rank modules by their overall association with HD status. Module 1 exhibits the strongest positive association whereas module 22 the strongest negative association with HD status (first column in the 3 heat maps of Figure 5). We also related the module eigengenes to the age of motor onset but found only suggestive associations that were not significant after adjusting for multiple comparisons (Supplementary Figure 10).

WGCNA provides a continuous ("fuzzy") measure of module membership (MM) for all CpGs with respect to each of the modules. The module membership measures how similar the methylation profile of a CpG is to the eigenvector of the co-methylation module. CpGs whose profiles are highly similar to the eigenvector can be identified as intramodular hub nodes[33]; such hubs are often useful for implicating relevant biological pathways and prioritizing genes for functional studies[37]. The module membership measures of all CpGs can be found on our webpage HDinHD[38] (www.HDinHD.org). The module membership values

of intramodular hubs can be found in Supplementary File 12.

Enrichment analysis using the software tool HDinHD

We used a functional enrichment tool known as HDinHD[38] (www.HDinHD.org) to relate co-methylation modules to existing gene sets, either published or generated by other HDinHD users. We adapted the gene enrichment analysis to the special case of DNA methylation data as described in Methods. The most significant results from a hypergeometric test can be found in Table 4. Methylation module M1, which has the strongest positive association with HD status, is highly enriched with genes involved in sensory perception of chemical stimulus ($p=6.2\times10^{-17}$) and olfactory receptor activity ($p=9.5\times10^{-16}$). Interestingly, our methylation module 1 overlaps with a transcriptional module (also labelled module 1 in HDinHD) that has been found in several *co-expression* network analyses of transcriptomic data sets. In particular, it overlaps significantly ($p=1.1\times10^{-45}$) with a co-expression module (labelled M.1) that was found in striatal brain expression data from a mouse model of HD [39]. To be clear, our module 1 is distinct from the co-expression module M.1 but the two modules share a significant number of genes in common. Further, co-methylation module 1 overlaps with a striatal coexpression module also labelled M.1 ($p=9.4\times10^{-24}$) that was found in a consensus WGCNA across 3 mouse data sets. Further, it overlaps significantly with a cortical co-expression module labelled M.1 ($p=1.9\times10^{-11}$) which was found in a consensus network analysis across three developmental time points from an allelic series of HD mouse models [38]. Genes inside the striatal co-expression module (M.1) have a positive correlation with CAG length in the allelic series [38]. Further, it overlaps significantly with a human co-expression module found in the prefrontal cortex (also labelled M.1=1.1×10^{-17}) and the visual cortex ($p=2.4\times10^{-11}$). Co-methylation module 1 is also enriched with genes that play a role in olfactory receptor activity and the detection of a chemical stimulus.

Two HD related co-methylation modules (modules 6 and 11) are highly enriched in genes that are bound by RNA polymerase II (using a gene list from [40]).

Relationship to prior work

Several articles point to an epigenetic modulation of HD pathophysiology [30], in the form of HDAC reduction [41] and/or epigenetic signatures [42, 43]. Our experimental analysis is focused on DNA methylation

levels. Recent publications looked at methylation levels of *selected* genes in HD patients [44] and analyzed cortical samples from 7 HD patients and 6 controls [45]. Previous work has demonstrated that post-translational modifications of histone proteins are significantly altered in HD cellular and animal models as well as HD patients (reviewed in [46]). For example, H3K4me3, a marker of active gene expression [47], is reduced at promoters of selective downregulated genes in cortical

and striatal regions in both R6/2 Htt model mice and HD patients [42]. Furthermore, studies have shown a potential therapeutic role for histone deacetylase (HDAC) inhibitors in numerous HD rodent and cell models (reviewed in [46]). DNA (de)methylation in HD has been investigated in transgenic models [48].

Modified bisulfite sequencing with single base pair resolution was employed to measure DNA methylation

Table 4. Co-methylation modules that are enriched with gene lists from HDinHD.

Module	Gene Set Identifier	Description	Source	p-value
1	WGCNA.HD.013.01	MODULE1 (co-expression)	WGCNA of mouse HD data from Giles 2012, Q150 striatum, adjusted for age	1.1×10^{-45}
1	WGCNA.HD.010.01	MODULE1	WGCNA of mouse HD data|Consensus WGCNA across mouse R6/2, Q150, Allelic Series striatum	9.4×10^{-24}
1	WGCNA.HD.019.01	MODULE1	WGCNA of mouse HD| Consensus WGCNA of 2-, 6-, 10-month Allelic Series cortex	1.9×10^{-11}
1	WGCNA.HD.004.01	MODULE1	WGCNA of human HD data: Harvard Brain Tissue Resource - Prefrontal Cortex	1.1×10^{-17}
1	WGCNA.HD.005.01	MODULE1	WGCNA of human HD data: Harvard Brain Tissue Resource - Visual Cortex	2.4×10^{-11}
1	GO:0050907	Detection of chemical stimulus involved in sensory perception	GO.BP	6.2×10^{-17}
1	GO:0004984	olfactory receptor activity	GO.MF	9.5×10^{-16}
6	JAM:002734	Annotated genes bound by RNA polymerase II	Table_S2 from Lee 2006	4.6×10^{-56}
6	GO:0031981	nuclear lumen	GO.CC	1.4×10^{-40}
6	GO:0090304	nucleic acid metabolic process	GO.BP	5.1×10^{-37}
6	GO:0016070	RNA metabolic process	GO.BP	3.1×10^{-33}
11	JAM:002734	Annotated genes bound by RNA polymerase II	Table_S2 from Lee 2006	7.8×10^{-13}

in the STHdh cellular model of HD [65]. The results from this study demonstrated that there was a bias towards hypomethylation associated with CpG-poor regions in the mHtt expressing STHdh111/111 compared to control STHdh7/7 cells.

Other DNA modifications may be relevant to HD pathology: global levels of 5hmC were reduced in the striatum and cortex of presymptomatic YAC128 mice [49] and 7-methylguanine was found to be reduced in the motor cortex from HD cases [50].

DISCUSSION

To our knowledge this is the first study to demonstrate that HD is associated with epigenetic age acceleration in specific brain regions, namely frontal lobe, cingulate gyrus and the parietal lobe. Although the positive age acceleration effects that we observed could be the result of cell type abundance differences between HD and control samples, there are several reasons that make this unlikely. First, our intrinsic measure of age acceleration that adjusts for the abundance of neurons also reveals an accelerated aging effect. Second, epigenetic age acceleration can be observed in brain regions that are relatively unaffected by the disease (e.g. the parietal lobe Figure 2B). Third, our multivariate analysis suggests that the age acceleration effect is independent of the proportion of neurons and unobserved confounders. Finally, the epigenetic age *acceleration* in Vonsattel (VS) grades 1 and 2 and to a lesser extent in grade 3 cannot reflect the loss of neurons because grade 4 samples, which are associated with the most severe loss of medium spiny neurons, appear to exhibit *negative* epigenetic age acceleration (Figure 1E,F, Supplementary Figure 2). The negative age acceleration in VS grade 4 is unexpected and could be a false positive reflecting the very small sample size.

Our study contributes to an increasing body of evidence suggesting that epigenetic age acceleration is associated with neurodegenerative disorders [22, 51, 52]. Future research will be needed to evaluate to what extent increased epigenetic age acceleration is specific to HD. Using our own relatively small data set (Table 1), we find no difference between Alzheimer's disease brains and controls when it comes to epigenetic age acceleration (Supplementary Figure 4). However, we recently analyzed a large (n=700) number of prefrontal cortex samples from AD cases and controls to show that epigenetic age acceleration has significant correlations with neuropathologic variables and measures of cognitive functioning [22]. We also found evidence that epigenetic age is increased in brain samples from Down syndrome [51] and HIV+ individuals [53].

A question our study left unanswered is whether the aging acceleration in HD is specific to the methylation-based biomarker of age or whether it could be observed using other biomarkers of aging. Until recently few suitable biomarkers of tissue age have been available, making it challenging to directly test whether HD is associated with accelerated aging in brain tissue. Leukocyte telomere length could be a promising biomarker since telomere shortening is related to premature senescence and could be a marker of early cell death in neurodegenerative disorders. Indeed, recent evidence suggests that leukocyte telomeres are shortened in HD and several neurodegenerative disorders [54]. However, it remains to be seen to what extent leukocytes lend themselves as "surrogate" tissue for brain when it comes to assessing aging. Telomere length is probably not a suitable marker to directly measure the age of brain tissue because a) terminally differentiated neurons do not replicate and b) telomere measurements of brain tissue are inherently variable due to the cellular complexity within the sample [55].

A key advance of our study in the polyglutamine disease field is to apply epigenome-wide DNA methylation data from multiple brain regions of HD individuals and controls to identify HD related co-methylation networks. Our systems biological analysis identified 11 co-methylation modules that are strongly associated with HD status in several lobes. Interestingly, the most significant co-methylation module overlaps with a co-expression module found in transcriptomic data from HD mouse models (Table 4). Our study has several limitations. While our epigenetic age analysis is not likely to be confounded by changes in cell composition, we cannot make the same claim about our WGCNA analysis, although our consensus analysis across three lobes mitigates this problem. Second, we studied only a relatively small number of individuals because it is very difficult to secure brain samples from human post mortem HD cases. Third, we focused on CpG methylation as opposed to hydroxy methylation (5hmC). It is noteworthy that the brain has the highest 5hmC levels in the body [56-58] and non-CpG methylation is prominent in neuronal tissue [56, 59, 60].

We can only speculate on why striatal samples do not seem to exhibit accelerated epigenetic aging. It might reflect low statistical power (due to small sample sizes), it might reflect severe neuronal loss, or it might suggest that epigenetic age acceleration can only be detected at the early stages of the disease. Future epigenetic clock analyses of the striatum and of striatal neurons should focus on the early stage of striatal degeneration (Vonsattel stage 0-1) or employ HD mouse models in

which MSN cell loss is not a major feature. Studies in the rat striatum suggest that normal aging modulates the neurotoxicity of mutant huntingtin [12]. Future studies could explore whether the onset of HD can be delayed by slowing down the epigenetic aging rate. The positive youth-promoting side effects of such a treatment (delayed aging) would probably be attractive to most patients.

Overall, our study strongly suggests that HD pathogenesis is associated with large scale DNA methylation changes and with an accelerated epigenetic age in brain tissue. It remains to be seen whether epigenetic age acceleration is prognostic of age of onset or the rate of disease progression.

METHODS

Sample collection. Postmortem brain samples from HD and AD cases and neurologically normal controls were collected at UCLA (n=218 samples from 32 individuals) and University of Auckland (n=257 samples from 33 individuals). The UCLA samples were provided by the Brain tissue and CSF resource/bank of the Mary Easton Alzheimer Disease Research Centre at UCLA (by H. Vinters).

Cubes 3x3x3mm with approximate mass of ~30 mg were cut from histological specimens collected during necropsies. Tissue samples were frozen and stored at -80C. In order to avoid batch effects, all tissue samples were shipped to the same UCLA core facility for DNA extraction and DNA methylation profiling. The Auckland samples were obtained from the Neurological Foundation of New Zealand Human Brain Bank (University of Auckland, NZ). The tissue used for this study had been processed according to a detailed protocol, which has been previously published [61, 62], dissected into blocks, snap frozen on dry ice, and stored at -80°C.

Age of HD motoric onset was available for 21 subjects from the NZ tissue bank (median age=38, ranging from 15 to 70). A total of 475 Illumina arrays were generated from 65 individuals (26 HD, 18 Alzheimer's disease, and 21 controls). After adjusting for chronological age, we could not detect an age acceleration effect due to AD status (Supplementary Figure 4). We profiled the following brain regions: caudate nucleus (n = 29 arrays), cingulate gyrus (n=33), cerebellum (n=42), hippocampus (n=33), parietal cortex (n=64), frontal lobe (n=70), occipital cortex (n=43), temporal cortex (n=37), midbrain (n=26), motor cortex (n=33), sensory cortex (n=33), and visual cortex (n=32). We also grouped the samples into broader categories: parietal lobe (parietal lobe and sensory cortex), frontal lobe (right frontal lobe, left frontal lobe, frontal gyrus, motor cortex), occipital lobe (occipital lobe and visual cortex). In our WGCNA analysis, we focused on 3 lobes for which sufficient sample sizes (n>=75) were available: parietal (n=97), frontal (n=103), and occipital (n=75). We omitted temporal samples from the WGCNA analysis due to the relatively low sample size (n=37).

Ethics review and IRB. All individuals whose brains reside in the UCLA tissue bank (or their legal next-of-kin) signed the "Consent for Autopsy" form by the Department of Pathology at UCLA, and research procurement was performed under IRB Research Protocol Number 11-002504. Further, the epigenetic analysis is covered by IRB Research Protocol Number: 19119.

The studies using tissue from the Neurological Foundation Human Brain Bank was approved by the University of Auckland Human Participants Ethics Committee Ref #011654. All tissue was obtained with full informed consent of the families.

DNA extraction. AllPrep DNA/RNA/miRNA Universal Kit (Qiagen, cat # 80224) was used for the DNA extractions for frozen tissue samples. 30mg of frozen tissue was lysed with 600uL guanidine-isothiocyanate–containing Buffer RLT Plus in a 2.0mL micro centrifuge tube, and homogenized by using TissueLyser II (Qiagen) with 5mm stainless steel beads. Tissue lysate was continued with the AllPrep protocol for simultaneous extraction of genomic DNA and total RNA using RNeasy Mini spin column technology.

DNA methylation data pre-processing. Our novel DNA methylation data have been posted on Gene Expression Omnibus (GSE72778).

Bisulfite conversion using the Zymo EZ DNA Methylation Kit (ZymoResearch, Orange, CA, USA) as well as subsequent hybridization of the HumanMethy-lation450k Bead Chip (Illumina, SanDiego, CA), and scanning (iScan, Illumina) were performed according to the manufacturers protocols by applying standard settings. DNA methylation levels (β values) were determined by calculating the ratio of intensities between methylated (signal A) and un-methylated (signal B) sites. Specifically, the β value was calculated from the intensity of the methylated (M corresponding to signal A) and un-methylated (U corresponding to signal B) sites, as the ratio of fluorescent signals $\beta = Max(M,0)/[Max(M,0)+Max(U,0)+100]$. Thus, β values range from 0 (completely un-methylated) to 1 (completely methylated) [63].

DNA methylation age and epigenetic clock. DNA methylation levels give rise to particularly promising biomarkers of aging since chronological age (i.e. the calendar years that have passed since birth) has a profound effect on DNA methylation levels in most human tissues and cell types [13-17, 35, 64-67]. Several recent studies propose to measure accelerated aging effects using DNA methylation levels [18, 68, 69]. Here we use the epigenetic clock method (based on the DNAm levels of 353 CpGs) because a) it is largely unaffected by differences in cell composition and b) it applies to all brain regions. The method applies to two commercially standardized methylation platforms: the Illumina 450K and 27K arrays. The epigenetic clock method is an attractive biomarker of aging because (1) it applies to most human tissues; (2) its accurate measurement of chronological age is unprecedented [18]. The following results suggest that the epigenetic clock captures aspects of biological age. The epigenetic age of blood has been found to be predictive of all-cause mortality even after adjusting for a variety of known risk factors [70, 71]. Further, the blood of the offspring of Italian semi-supercentenarians (i.e. individuals who reached an age of at least 105) has a lower epigenetic age than that of age-matched controls [72]. The epigenetic age of blood relates to cognitive and physical fitness in the elderly [73] and to Parkinson's disease status [52]. The utility of the epigenetic clock method has been demonstrated in applications surrounding obesity [19], Down syndrome [51], and HIV infection [53].

Predicted age, referred to as DNAm age, correlates with chronological age in sorted cell types (CD4 T cells, monocytes, B cells, glial cells, neurons) and tissues and organs including whole blood, brain, breast, kidney, liver, lung, saliva [18].

Mathematical details and software tutorials for the epigenetic clock can be found in the Additional files of [18]. An online age calculator can be found at our webpage (https://dnamage.genetics.ucla.edu).

Epigenome-wide association study. For the epigenome-wide association study and the subsequent network analysis we focused on those CpGs whose variance was at least 5×10^{-4} in at least one of the 3 lobes. This restriction resulted in 326777 CpGs retained for further analysis. DNA methylation data were adjusted for chronological age and sex by regressing methylation levels on age and sex and retaining the residuals. For association testing, we used the Kruskal-Wallis test because it is relatively insensitive to the distribution of the methylation levels and potential outliers. We used

the "estlambda" function in the GenABEL R package to calculate the inflation factors [74].

Meta-analysis. Our analysis methods make extensive use of meta-analysis. A simple yet powerful meta-analysis method, known as Stouffer's method, relies on combining the Z statistics from individual data sets (the 3 brain lobes). Specifically, for each CpG i and data set (brain lobe) a, one obtains a Z statistic Z_{ia}, for example, by the inverse normal transformation of the p-value. Next, a meta-analysis Z_i statistic for each CpG is calculated as

$$Z_i = \frac{1}{\sqrt{N_{sets}}} \sum_{a=1}^{N_{sets}} Z_{ia} \ .$$

The meta-analysis statistic Z_i is approximately normally distributed with mean 0 and variance 1; the corresponding p-value is then calculated using the normal distribution.

Weighted Correlation Network Analysis. Weighted Correlation Network Analysis (WGCNA)[31, 32] uses as input a matrix of pairwise correlations between all pairs of CpGs across the measured samples in a data set. To minimize effects of possible outliers, we use the biweight midcorrelation[75] with argument maxPOutliers = 0.05. One then forms a "signed hybrid" pairwise co-methylation similarity that equals the correlation if the correlation is positive, and equals zero otherwise. Next the co-methylation similarity is raised to the power β=6 (WGCNA default) to arrive at the network adjacency. This procedure has the effect of suppressing low correlations that may be due to noise. The result is a network adjacency that is zero for negatively correlated CpGs and is positive for positively correlated CpGs. Adjacency of weakly correlated CpGs is nearly zero due to the power transformation.

Consensus module analysis. Consensus modules are defined as sets of nodes that are highly connected in multiple networks; loosely speaking, one could identify the consensus module in individual network analyses across multiple sets, so the module can be said to arise from a consensus of multiple data sets [36].

Within WGCNA, consensus modules are identified using a consensus dissimilarity that is used as input to a clustering procedure. To describe our definition of the consensus dissimilarity, we introduce the following component-wise quantile function for a set of k matrices $A^{(1)}, A^{(2)}, \ldots, A^{(k)}$:

$$Quantile_{q;i,j} = Quantile_q\left(A_{i,j}^{(1)}, A_{i,j}^{(2)}, ..., A_{i,j}^{(k)}\right).$$

Thus, each component of the quantile matrix is the given quantile ($0 \leq q \leq 1$) of the corresponding components in the individual input matrices. Using this notation, we define the consensus network corresponding to input networks $A^{(1)}$, $A^{(2)}$, . . . , $A^{(k)}$ and quantile q as

$$Consensus_q\left(A^{(1)}, A^{(2)}, ..., A^{(k)}\right)$$
$$= Quantile_q\left(cTOM^{(1)}, cTOM^{(2)}, ..., cTOM^{(k)}\right),$$

where $cTOM$ stands for calibrated Topological Overlap Measure (TOM). The calculation of $cTOM$ starts with calculating the standard TOM [31] in each input data set (network). The calibration aims to make TOM values comparable between different networks. In this work we use as calibration the quantile normalization implemented in the R package *preprocessCore* [76]. We treat the independent components (say the lower triangle) of TOM for each input network as a vector of measurements corresponding to one "sample;" thus, quantiles of the calibrated TOM matrices in each network equal each other and equal the average of the corresponding quantiles in the original, uncalibrated TOM matrices.

Given the consensus network defined above, one defines the consensus dissimilarity $ConsDiss_{ij}$ as

$$ConsDiss_{ij} = 1 - Consensus_q\left(A^{(1)}, A^{(2)}, ..., A^{(k)}\right).$$

The consensus dissimilarity is used as input to average-linkage hierarchical clustering. Branches of the resulting dendrogram are then identified using the Dynamic Tree Cut algorithm [77]. Modules are labeled by (in principle arbitrary) numeric labels and, for easier visualization, also by colors. Not all CpGs will be assigned to modules; the label 0 and color grey are reserved for CpGs not assigned to any module.

Consensus module eigenvectors. The module identification procedure results in modules containing CpGs with highly correlated methylation profiles. It is useful to summarize such modules using a single methylation profile per input data set. We use the module eigenvector E, defined as the left-singular vector of the standardized methylation matrix with the largest singular value[31]. Since consensus modules are defined across k independent data sets, one can form their summary profiles in each lobe. Thus, a consensus module gives rise to k eigenvectors, one in each input data set, that provide a summary "methylation value" for each sample in the data set. This allows one to relate consensus module eigenvectors to other information, for example to disease status or other traits, in each data set, and study similarities and differences between the input data sets in terms of the module-trait associations.

Continuous measure of module membership. Module eigenvectors lead to a natural measure of similarity (membership) of all individual CpGs to all modules. We define a fuzzy measure of module membership of CpG i in module I as

$$MM_i^I = \text{cor}(x_i, E^I),$$

where x_i is the methylation profile of CpG i and E^I is the eigenvector of module I. This definition is applicable to every individual network (data set). The value of module membership lies between -1 and 1. Higher MM_i^I indicate that the methylation profile of CpG i is similar to the summary profile of module I. Since we use signed networks here, we consider module membership near -1 low. The advantage of using correlation to quantify module membership is that the corresponding statistical significance (p-values) can be easily computed. Genes with highest module membership are called hub CpGs. Hub CpGs are centrally located inside the module and represent the methylation profiles of the entire module.

Module membership in consensus modules. In a consensus module analysis, we calculate the fuzzy module membership MM for each CpG in each data set. Thus, for each consensus analysis of 3 data sets there are 3 values for the module membership of each CpG in each module. We then use meta-analysis to summarize the 3 module memberships into a single meta-analysis Z statistic[37]. Genes with the highest module membership meta-analysis Z statistics are called consensus hub CpGs. It has been shown that consensus hub CpGs can be useful in studying functional categories associated with clinical traits[37].

Enrichment analysis of co-methylation modules. We used Illumina-supplied probe annotation to map CpG probes to genes. Since each gene is represented by multiple CpGs (up to a thousand per gene), we applied the following stepwise procedure to represent each gene by a single CpGs.

Step 1: Apply consensus WGCNA to assign each CpG to a consensus co-methylation module. Call the consensus quantile used for this consensus analysis q. This analysis reduces the original hundreds of thousands of CpGs to typically less than 100 modules (in the brain data case, about 320k CpGs were reduced to 54 modules).

Step 2: Define an artificial module assignment where the "module" label equals the gene identifier. Thus, there is one module for each gene to which at least 1 CpG maps. Discard all CpGs that do not map to a gene.

Step 3a: For each of the artificial modules that contain at least 3 CpGs, calculate intramodular connectivity in each of the input sets. At present we don't use kME but kIM which is defined as the sum of intramodular adjacencies. This results in a vector of kIM in each input data set. Use quantile normalization to calibrate the kIM vectors across the input data sets. Then calculate the consensus of the kIM vectors using the same consensus quantile q that was used for the consensus WGCNA.

Step 3b: For each of the artificial modules that contain 2 CpGs, calculate the standard deviation of each of the CpGs in each of the input sets. This results in a vector of standard deviations for CpGs in each data set. Use quantile normalization to calibrate the std. deviation vectors across the data sets. Then calculate the consensus of the calibrated standard deviation vectors using the same consensus quantile q that was used for the consensus WGCNA.

Step 4: Represent each gene with at least 3 CpGs by the consensus hub CpG, i.e. the CpG with the highest consensus kIM. Represent each gene with 2 CpGs by the CpG with the highest consensus standard deviation. Represent each gene with 1 CpG by the single CpG. Thus, we move from 300k CpGs to about 20k representative CpGs (which are mapped in a one to one fashion to the gene identifiers).

Step 5: Assign each gene to a co-methylation module (from WGCNA) using the color label (from step 1) of the representative CpG.

Step 6: Next apply the *enrichmentAnalysis* function (from R package *anRichment*) to the genes and corresponding color labels from step 5.

We then used standard hypergeometric test (Fisher's exact test) to evaluate the significance of the overlaps of the gene-mapped methylation modules with reference gene sets including Gene Ontology, KEGG, Reactome, gene lists from [78] in the WGCNA R package, and modules from several WGCNA analyses on various HD-related gene expression data. All gene sets used in our analysis can be accessed at (https://labs.genetics.ucla.edu/horvath/htdocs/CoexpressionNetwork/GeneAnnotation/). These HD related genes as are part of the HDinHD software tool [38] (www.HDinHD.org).

Steps 3-5 are implemented in the R function "*consensusRepresentatives*" included in the package WGCNA since version 1.50. Additionally, the *anRichment* R package (https://labs.genetics.ucla.edu/horvath/htdocs/CoexpressionNetwork/GeneAnnotation/) contains the function "*representativeCpG*" that further tailors the consensus representative selection to methylation data assayed on the Illumina Infinium 450k microarray.

Funding

Conflict of Interests Statement

The authors declare no conflict of interest..

REFERENCES

1. Walker FO. Huntington's disease. Lancet. 2007; 369:218-28.
2. NoAuthorListed A. A novel gene containing a trinucleotide repeat that is expanded and unstable on Huntington's disease chromosomes. The Huntington's Disease Collaborative Research Group. Cell. 1993; 72:971-83.
3. Orr HT and Zoghbi HY. Trinucleotide repeat disorders. Annu Rev Neurosci. 2007; 30:575-621.
4. Aylward EH, Harrington DL, Mills JA, Nopoulos PC, Ross CA, Long JD, Liu D, Westervelt HK and Paulsen JS. Regional atrophy associated with cognitive and motor function in prodromal Huntington disease. J Huntingtons Dis. 2013; 2:477-89.
5. Hadzi TC, Hendricks AE, Latourelle JC, Lunetta KL, Cupples LA, Gillis T, Mysore JS, Gusella JF, MacDonald ME, Myers RH and Vonsattel JP. Assessment of cortical and striatal involvement in 523 Huntington disease brains. Neurology. 2012; 79:1708-15.
6. Tabrizi SJ, Scahill RI, Owen G, Durr A, Leavitt BR, Roos RA, Borowsky B, Landwehrmeyer B, Frost C, Johnson H, Craufurd D, Reilmann R, Stout JC, et al. Predictors of phenotypic progression and disease onset in premanifest and early-stage Huntington's disease in the TRACK-HD study: analysis of 36-month observational data. Lancet Neurol. 2013; 12:637-49.
7. Vonsattel JP and DiFiglia M. Huntington disease. J Neuropathol Exp Neurol. 1998; 57:369-84.
8. Ross CA. Intranuclear neuronal inclusions: a common pathogenic mechanism for glutamine-repeat neurodegenerative diseases? Neuron. 1997; 19:1147-50.
9. Djousse L, Knowlton B, Hayden M, Almqvist EW, Brinkman R, Ross C, Margolis R, Rosenblatt A, Durr A, Dode C, Morrison PJ, Novelletto A, Frontali M, et al. Interaction of normal and expanded CAG repeat sizes influences age at onset of Huntington disease. Am J Med Genet A. 2003; 119A:279-82.
10. Ross CA, Aylward EH, Wild EJ, Langbehn DR, Long JD, Warner JH, Scahill RI, Leavitt BR, Stout JC, Paulsen JS, Reilmann R, Unschuld PG, Wexler A, et al. Huntington disease: natural

history, biomarkers and prospects for therapeutics. Nat Rev Neurol. 2014; 10:204-16.

11. Gusella JF and Macdonald M. Genetic criteria for Huntington's disease pathogenesis. Brain Res Bull. 2007; 72:78-82.

12. Diguet E, Petit F, Escartin C, Cambon K, Bizat N, Dufour N, Hantraye P, Déglon N and Brouillet E. Normal Aging Modulates the Neurotoxicity of Mutant Huntingtin. PLoS ONE. 2009; 4:e4637.

13. Rakyan VK, Down TA, Maslau S, Andrew T, Yang TP, Beyan H, Whittaker P, McCann OT, Finer S, Valdes AM, Leslie RD, Deloukas P and Spector TD. Human aging-associated DNA hypermethylation occurs preferentially at bivalent chromatin domains. Genome research. 2010; 20:434-39.

14. Teschendorff AE, Menon U, Gentry-Maharaj A, Ramus SJ, Weisenberger DJ, Shen H, Campan M, Noushmehr H, Bell CG, Maxwell AP, Savage DA, Mueller-Holzner E, Marth C, et al. Age-dependent DNA methylation of genes that are suppressed in stem cells is a hallmark of cancer. Genome research. 2010; 20:440-446.

15. Numata S, Ye T, Hyde Thomas M, Guitart-Navarro X, Tao R, Wininger M, Colantuoni C, Weinberger Daniel R, Kleinman Joel E and Lipska Barbara K. DNA Methylation Signatures in Development and Aging of the Human Prefrontal Cortex. Am J Hum Genet. 2012; 90:260-72.

16. Alisch RS, Barwick BG, Chopra P, Myrick LK, Satten GA, Conneely KN and Warren ST. Age-associated DNA methylation in pediatric populations. Genome Res. 2012; 22:623-32.

17. Johansson A, Enroth S and Gyllensten U. Continuous Aging of the Human DNA Methylome Throughout the Human Lifespan. PLoS One. 2013; 8:e67378.

18. Horvath S. DNA methylation age of human tissues and cell types. Genome Biol. 2013; 14:115.

19. Horvath S, Erhart W, Brosch M, Ammerpohl O, von Schönfels W, Ahrens M, Heits N, Bell JT, Tsai P-C, Spector TD, Deloukas P, Siebert R, Sipos B, et al. Obesity accelerates epigenetic aging of human liver. Proc Natl Acad Sci U S A 2014; 111:15538-43.

20. Horvath S, Mah V, Lu AT, Woo JS, Choi OW, Jasinska AJ, Riancho JA, Tung S, Coles NS, Braun J, Vinters HV and Coles LS. The cerebellum ages slowly according to the epigenetic clock. Aging (Albany NY). 2015; 7:294-306. doi: 10.18632/aging.100742.

21. Spiers H, Hannon E, Schalkwyk LC, Smith R, Wong CC, O'Donovan MC, Bray NJ and Mill J. Methylomic trajectories across human fetal brain development. Genome research. 2015; 25:338-52.

22. Levine M, Lu A, Bennett D and Horvath S. Epigenetic age of the pre-frontal cortex is associated with neuritic plaques, amyloid load, and Alzheimer's disease related cognitive functioning. Aging (Albany NY). 2015; 7:1198-211. doi: 10.18632/aging.100864.

23. Guintivano J, Aryee MJ and Kaminsky ZA. A cell epigenotype specific model for the correction of brain cellular heterogeneity bias and its application to age, brain region and major depression. Epigenetics. 2013; 8:290-302.

24. Vonsattel JP, Myers RH, Stevens TJ, Ferrante RJ, Bird ED and Richardson EP, Jr. Neuropathological classification of Huntington's disease. J Neuropathol Exp Neurol. 1985; 44:559-77.

25. Gusella JF and MacDonald ME. Molecular genetics: unmasking polyglutamine triggers in neurodegenerative disease. Nat Rev Neurosci. 2000; 1:109-15.

26. Seong IS, Ivanova E, Lee JM, Choo YS, Fossale E, Anderson M, Gusella JF, Laramie JM, Myers RH, Lesort M and MacDonald ME. HD CAG repeat implicates a dominant property of huntingtin in mitochondrial energy metabolism. Hum Mol Genet. 2005; 14:2871-80.

27. Biagioli M, Ferrari F, Mendenhall EM, Zhang Y, Erdin S, Vijayvargia R, Vallabh SM, Solomos N, Manavalan P, Ragavendran A, Ozsolak F, Lee JM, Talkowski ME, et al. Htt CAG repeat expansion confers pleiotropic gains of mutant huntingtin function in chromatin regulation. Hum Mol Genet. 2015; 24:2442-57.

28. Lee J, Hwang YJ, Ryu H, Kowall NW and Ryu H. Nucleolar dysfunction in Huntington's disease. Biochim Biophys Acta. 2014; 1842:785-90.

29. Wang F, Fischhaber PL, Guo C and Tang TS. Epigenetic modifications as novel therapeutic targets for Huntington's disease. Epigenomics. 2014; 6:287-97.

30. Valor LM and Guiretti D. What's wrong with epigenetics in Huntington's disease? Neuropharmacology. 2014; 80:103-14.

31. Zhang B and Horvath S. A general framework for weighted gene co-expression network analysis. Statistical Applications in Genetics and Molecular Biology. 2005; 4:17.

32. Langfelder P and Horvath S. WGCNA: an R package for weighted correlation network analysis. BMC Bioinformatics. 2008; 9:559.

33. Horvath S and Dong J. Geometric Interpretation of Gene Coexpression Network Analysis. PLoS Comput Biol. 2008; 4:1000117.

34. Horvath S. Weighted Network Analysis. Applications in Genomics and Systems Biology: Springer. 2011.

35. Horvath S, Zhang Y, Langfelder P, Kahn R, Boks M, van Eijk K, van den Berg L and Ophoff RA. Aging effects on DNA methylation modules in human brain and blood tissue. Genome Biol. 2012; 13:97.

36. Langfelder P and Horvath S. Eigengene networks for studying the relationships between co-expression modules. BMC systems biology. 2007; 1:54.

37. Langfelder P, Mischel PS and Horvath S. When is hub gene selection better than standard meta-analysis? PLoS ONE. 2013; 8:61505.

38. Langfelder P, Cantle J, Chatzopoulou D, Wang N, Gao F, Al-Ramahi I, Lu X, Ramos E, El-Zein K, Zhao Y, Deverasetty S, Tebbe A, Schaab C, et al. Integrated genomics and proteomics to define huntingtin CAG length-dependent molecular networks in HD mouse brains. Nature neuroscience. 2016; 19:623-33.

39. Giles P, Elliston L, Higgs GV, Brooks SP, Dunnett SB and Jones L. Longitudinal analysis of gene expression and behaviour in the HdhQ150 mouse model of Huntington's disease. Brain Res Bull. 2012; 88:199-209.

40. Lee TI, Jenner RG, Boyer LA, Guenther MG, Levine SS, Kumar RM, Chevalier B, Johnstone SE, Cole MF, Isono K-i, Koseki H, Fuchikami T, Abe K, et al. Control of Developmental Regulators by Polycomb in Human Embryonic Stem Cells. Cell. 2006; 125:301-13.

41. Mielcarek M, Landles C, Weiss A, Bradaia A, Seredenina T, Inuabasi L, Osborne GF, Wadel K, Touller C, Butler R, Robertson J, Franklin SA, Smith DL, et al. HDAC4 reduction: a novel therapeutic strategy to target cytoplasmic huntingtin and ameliorate neurodegeneration. PLoS Biol. 2013; 11:1001717.

42. Vashishtha M, Ng CW, Yildirim F, Gipson TA, Kratter IH, Bodai L, Song W, Lau A, Labadorf A, Vogel-Ciernia A, Troncoso J, Ross

CA, Bates GP, et al. Targeting H3K4 trimethylation in Huntington disease. Proc Natl Acad Sci U S A. 2013; 110:3027-36.

43. Seong IS, Woda JM, Song JJ, Lloret A, Abeyrathne PD, Woo CJ, Gregory G, Lee JM, Wheeler VC, Walz T, Kingston RE, Gusella JF, Conlon RA, et al. Huntingtin facilitates polycomb repressive complex 2. Hum Mol Genet. 2010; 19:573-83.

44. Villar-Menendez I, Blanch M, Tyebji S, Pereira-Veiga T, Albasanz JL, Martin M, Ferrer I, Perez-Navarro E and Barrachina M. Increased 5-methylcytosine and decreased 5-hydroxymethylcytosine levels are associated with reduced striatal A2AR levels in Huntington's disease. Neuromolecular Med. 2013; 15:295-309.

45. De Souza RA, Islam SA, McEwen LM, Mathelier A, Hill A, Mah SM, Wasserman WW, Kobor MS and Leavitt BR. DNA Methylation Profiling in Human Huntington's Disease Brain. Hum Mol Genet. 2016. Epub ahead of print.

46. Glajch KE and Sadri-Vakili G. Epigenetic Mechanisms Involved in Huntington's Disease Pathogenesis. J Huntingtons Dis. 2015; 4:1-15.

47. Santos-Rosa H, Schneider R, Bannister AJ, Sherriff J, Bernstein BE, Emre NC, Schreiber SL, Mellor J and Kouzarides T. Active genes are tri-methylated at K4 of histone H3. Nature. 2002; 419:407-11.

48. Ng CW, Yildirim F, Yap YS, Dalin S, Matthews BJ, Velez PJ, Labadorf A, Housman DE and Fraenkel E. Extensive changes in DNA methylation are associated with expression of mutant huntingtin. Proc Natl Acad Sci U S A. 2013; 110:2354-59.

49. Wang F, Yang Y, Lin X, Wang JQ, Wu YS, Xie W, Wang D, Zhu S, Liao YQ, Sun Q, Yang YG, Luo HR, Guo C, et al. Genome-wide loss of 5-hmC is a novel epigenetic feature of Huntington's disease. Hum Mol Genet. 2013; 22:3641-53.

50. Thomas B, Matson S, Chopra V, Sun L, Sharma S, Hersch S, Rosas HD, Scherzer C, Ferrante R and Matson W. A novel method for detecting 7-methyl guanine reveals aberrant methylation levels in Huntington disease. Anal Biochem. 2013; 436:112-20.

51. Horvath S, Garagnani P, Bacalini M, Pirazzini C, Salvioli S, Gentilini D, DiBlasio A, Giuliani C, Tung S, Vinters H and Franceschi C. Accelerated Epigenetic Aging in Down Syndrome. Aging Cell. 2015; 14:491-95.

52. Horvath S and Ritz BR. Increased epigenetic age and granulocyte counts in the blood of Parkinson's disease patients. Aging (Albany NY). 2015; 7:1130-42. doi: 10.18632/aging.100859.

53. Horvath S and Levine AJ. HIV-1 infection accelerates age according to the epigenetic clock. J Infect Dis. 2015; 212:1563-73.

54. Kota LN, Bharath S, Purushottam M, Moily NS, Sivakumar PT, Varghese M, Pal PK and Jain S. Reduced Telomere Length in Neurodegenerative Disorders May Suggest Shared Biology. The Journal of Neuropsychiatry and Clinical Neurosciences. 2014; 27:92-96.

55. Aubert G, Hills M and Lansdorp PM. Telomere Length Measurement - caveats and a critical assessment of the available technologies and tools. Mutation research. 2012; 730:59-67.

56. Xie W, Barr CL, Kim A, Yue F, Lee AY, Eubanks J, Dempster EL and Ren B. Base-resolution analyses of sequence and parent-of-origin dependent DNA methylation in the mouse genome. Cell. 2012; 148:816-31.

57. Li W and Liu M. Distribution of 5-hydroxymethylcytosine in different human tissues. J Nucleic Acids. 2011; 2011:870726.

58. Song CX and He C. The hunt for 5-hydroxymethylcytosine: the sixth base. Epigenomics. 2011; 3:521-23.

59. Lister R, Mukamel EA, Nery JR, Urich M, Puddifoot CA, Johnson ND, Lucero J, Huang Y, Dwork AJ, Schultz MD, Yu M, Tonti-Filippini J, Heyn H, et al. Global epigenomic reconfiguration during mammalian brain development. Science. 2013; 341:1237905.

60. Varley KE, Gertz J, Bowling KM, Parker SL, Reddy TE, Pauli-Behn F, Cross MK, Williams BA, Stamatoyannopoulos JA, Crawford GE, Absher DM, Wold BJ and Myers RM. Dynamic DNA methylation across diverse human cell lines and tissues. Genome research. 2013; 23:555-67.

61. Waldvogel HJ, Bullock JY, Synek BJ, Curtis MA, van Roon-Mom WMC and Faull RLM. The collection and processing of human brain tissue for research. Cell and Tissue Banking. 2008; 9:169-79.

62. Waldvogel HJ, Curtis MA, Baer K, Rees MI and Faull RL. Immunohistochemical staining of post-mortem adult human brain sections. Nat Protoc. 2006; 1:2719-32.

63. Dunning M, Barbosa-Morais N, Lynch A, Tavare S and Ritchie M. Statistical issues in the analysis of Illumina data. BMC Bioinformatics. 2008; 9:85.

64. Christensen B, Houseman E, Marsit C, Zheng S, Wrensch M, Wiemels J, Nelson H, Karagas M, Padbury J, Bueno R, Sugarbaker D, Yeh R, Wiencke J, et al. Aging and Environmental Exposures Alter Tissue-Specific DNA Methylation Dependent upon CpG Island Context. PLoS Genet. 2009; 5:1000602.

65. Bollati V, Schwartz J, Wright R, Litonjua A, Tarantini L, Suh H, Sparrow D, Vokonas P and Baccarelli A. Decline in genomic DNA methylation through aging in a cohort of elderly subjects. Mech Ageing Dev. 2009; 130:234-39.

66. Vivithanaporn P, Heo G, Gamble J, Krentz H, Hoke A, Gill M and Leistung C. Neurologic disease burden in treated HIV/AIDS predicts survival. Neurology. 2010; 75:1150-58.

67. Day K, Waite L, Thalacker-Mercer A, West A, Bamman M, Brooks J, Myers R and Absher D. Differential DNA methylation with age displays both common and dynamic features across human tissues that are influenced by CpG landscape. Genome Biol. 2013; 14:102.

68. Bocklandt S, Lin W, Sehl ME, Sanchez FJ, Sinsheimer JS, Horvath S and Vilain E. Epigenetic predictor of age. PLoS ONE. 2011; 6:14821.

69. Garagnani P, Bacalini MG, Pirazzini C, Gori D, Giuliani C, Mari D, Di Blasio AM, Gentilini D, Vitale G, Collino S, Rezzi S, Castellani G, Capri M, et al. Methylation of ELOVL2 gene as a new epigenetic marker of age. Aging Cell. 2012; 11:1132-34.

70. Marioni R, Shah S, McRae A, Chen B, Colicino E, Harris S, Gibson J, Henders A, Redmond P, Cox S, Pattie A, Corley J, Murphy L, et al. DNA methylation age of blood predicts all-cause mortality in later life. Genome Biol. 2015; 16:25.

71. Christiansen L, Lenart A, Tan Q, Vaupel JW, Aviv A, McGue M and Christensen K. DNA methylation age is associated with mortality in a longitudinal Danish twin study. Aging Cell. 2016; 15:149-54.

72. Horvath S, Pirazzini C, Bacalini MG, Gentilini D, Di Blasio AM, Delledonne M, Mari D, Arosio B, Monti D, Passarino G, De Rango F, D'Aquila P, Giuliani C, et al. Decreased epigenetic age of PBMCs from Italian semi-supercentenarians and their offspring. Aging (Albany NY). 2015; 7:1159-70. doi: 10.18632/aging.100861.

73. Marioni RE, Shah S, McRae AF, Ritchie SJ, Muniz-Terrera G, Harris SE, Gibson J, Redmond P, Cox SR and Pattie A. The epigenetic clock is correlated with physical and cognitive fitness in the Lothian Birth Cohort 1936. International journal of epidemiology. 2015:77.

74. Aulchenko YS, Ripke S, Isaacs A and van Duijn CM. GenABEL: an R library for genome-wide association analysis. Bioinformatics. 2007; 23:1294-96.

75. Langfelder P and Horvath S. Fast R Functions For Robust Correlations And Hierarchical Clustering. J Stat Software. 2012; 46.

76. Bolstad BM, Irizarry RA, Åstrand M and Speed TP. A comparison of normalization methods for high density oligonucleotide array data based on variance and bias. Bioinformatics. 2003; 19:185-93.

77. Langfelder P, Zhang B and Horvath S. Defining clusters from a hierarchical cluster tree: the Dynamic Tree Cut library for R. Bioinformatics. 2008; 24:719-20.

78. Miller JA, Cai C, Langfelder P, Geschwind DH, Kurian SM, Salomon DR and Horvath S. Strategies for aggregating gene expression data: The collapseRows R function. BMC Bioinformatics. 2011; 12:322.

SUPPLEMENTARY DATA

Supplementary Table 1. Individual level data on the subjects.

|	PersonID	BrainBank	Age	Disease	PostMortemInterval	CAGlength
1	1	UCLA	65	AD	9.0	NA
2	2	UCLA	15	Control	6.0	NA
3	3	UCLA	59	AD	10.0	NA
4	4	UCLA	85	AD	22.0	NA
5	5	UCLA	100	AD	52.0	NA
6	6	UCLA	80	AD	10.0	NA
7	7	UCLA	80	AD	22.0	NA
8	8	UCLA	101	AD	28.0	NA
9	9	UCLA	64	AD	34.0	NA
10	10	UCLA	59	AD	20.0	NA
11	11	UCLA	50	HD	46.0	NA
12	12	UCLA	93	Control	22.0	NA
13	13	UCLA	85	Control	36.0	NA
14	14	UCLA	96	AD	NA	NA
15	15	UCLA	63	Control	28.0	NA
16	16	UCLA	58	HD	16.0	NA
17	17	UCLA	100	AD	26.0	NA
18	18	UCLA	81	Control	23.0	NA
19	19	UCLA	85	Control	12.0	NA
20	20	UCLA	53	Control	12.0	NA
21	21	UCLA	38	Control	24.0	NA
22	22	UCLA	62	HD	23.0	NA
23	23	UCLA	82	AD	17.0	NA
24	24	UCLA	111	AD	16.0	NA
25	25	UCLA	53	Control	23.0	NA
26	26	UCLA	64	AD	29.0	NA
27	27	UCLA	58	AD	16.0	NA
28	28	UCLA	30	HD	8.0	NA
29	29	UCLA	93	AD	4.0	NA
30	30	UCLA	65	HD	23.0	NA
31	31	UCLA	114	AD	13.0	NA

| 32	32	UCLA	112	AD	NA	NA
33	33	NewZealand	45	Control	12.0	NA
34	34	NewZealand	81	Control	7.0	18
35	35	NewZealand	64	Control	17.0	NA
36	36	NewZealand	36	Control	11.0	22
37	37	NewZealand	32	Control	13.0	NA
38	38	NewZealand	41	Control	16.0	NA
39	39	NewZealand	64	Control	7.0	18
40	40	NewZealand	53	Control	16.5	NA
41	41	NewZealand	73	Control	13.0	23
42	42	NewZealand	41	Control	16.0	22
43	43	NewZealand	83	Control	14.0	24
44	44	NewZealand	63	Control	16.0	NA
45	45	NewZealand	39	HD	15.0	52
46	46	NewZealand	42	HD	12.0	42
47	47	NewZealand	71	HD	16.0	42
48	48	NewZealand	53	HD	9.0	53
49	49	NewZealand	48	HD	18.0	45
50	50	NewZealand	45	HD	15.0	43
51	51	NewZealand	80	HD	9.0	40
52	52	NewZealand	43	HD	3.5	49
53	53	NewZealand	41	HD	11.0	39
54	54	NewZealand	67	HD	9.0	42
55	55	NewZealand	91	HD	18.0	40
56	56	NewZealand	62	HD	11.0	45
57	57	NewZealand	58	HD	14.0	44
58	58	NewZealand	53	HD	12.0	47
59	59	NewZealand	56	HD	16.0	46
60	60	NewZealand	51	HD	15.5	48
61	61	NewZealand	51	HD	15.0	46
62	62	NewZealand	32	HD	14.0	47
63	63	NewZealand	65	HD	14.0	43
64	64	NewZealand	62	HD	9.0	43
65	65	NewZealand	83	HD	13.0	42
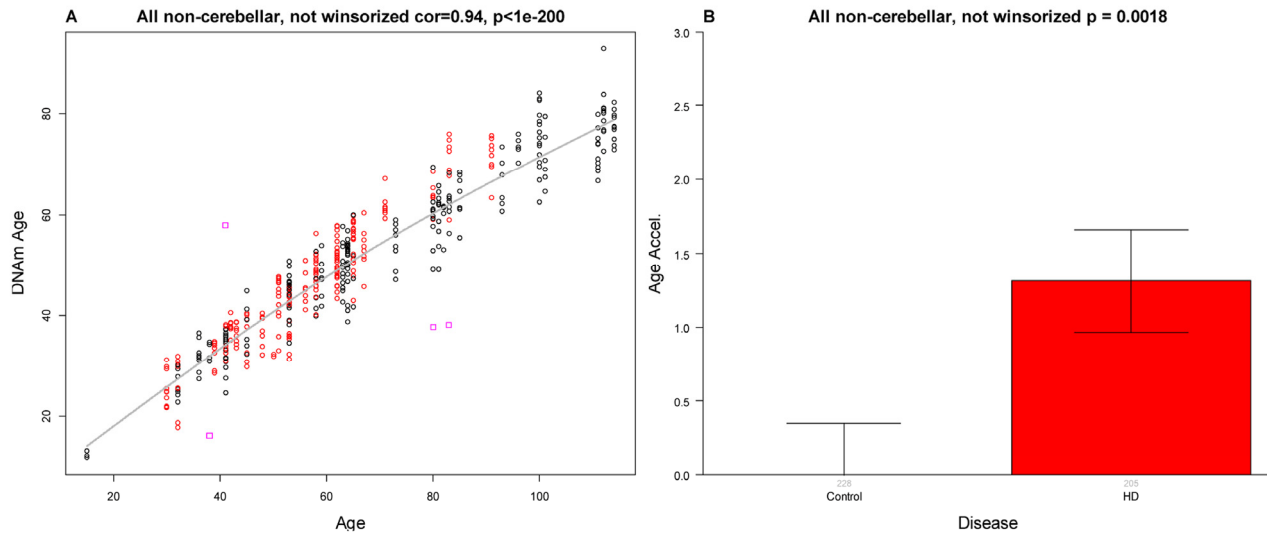
Supplementary Figure 1. Epigenetic age analysis across all non-cerebellar brain regions. (**A**) DNAm age (y-axis) versus chronological age sample collection (i.e. death). Red dots correspond to HD cases, black dots to controls, magenta dots correspond to putative outliers. The curve corresponds to a spline regression line (2 degrees of freedom) through the control samples. The scatter plot reports a Pearson correlation coefficient and corresponding p-value. Epigenetic age acceleration was defined as the vertical distance of each sample from the spline regression line. (**B**) The bar plot presents mean epigenetic age acceleration (and one standard error) versus disease status. By definition, the mean epigenetic age acceleration in controls is zero. The p-value results from a non-parametric group comparison test (Kruskal Wallis).
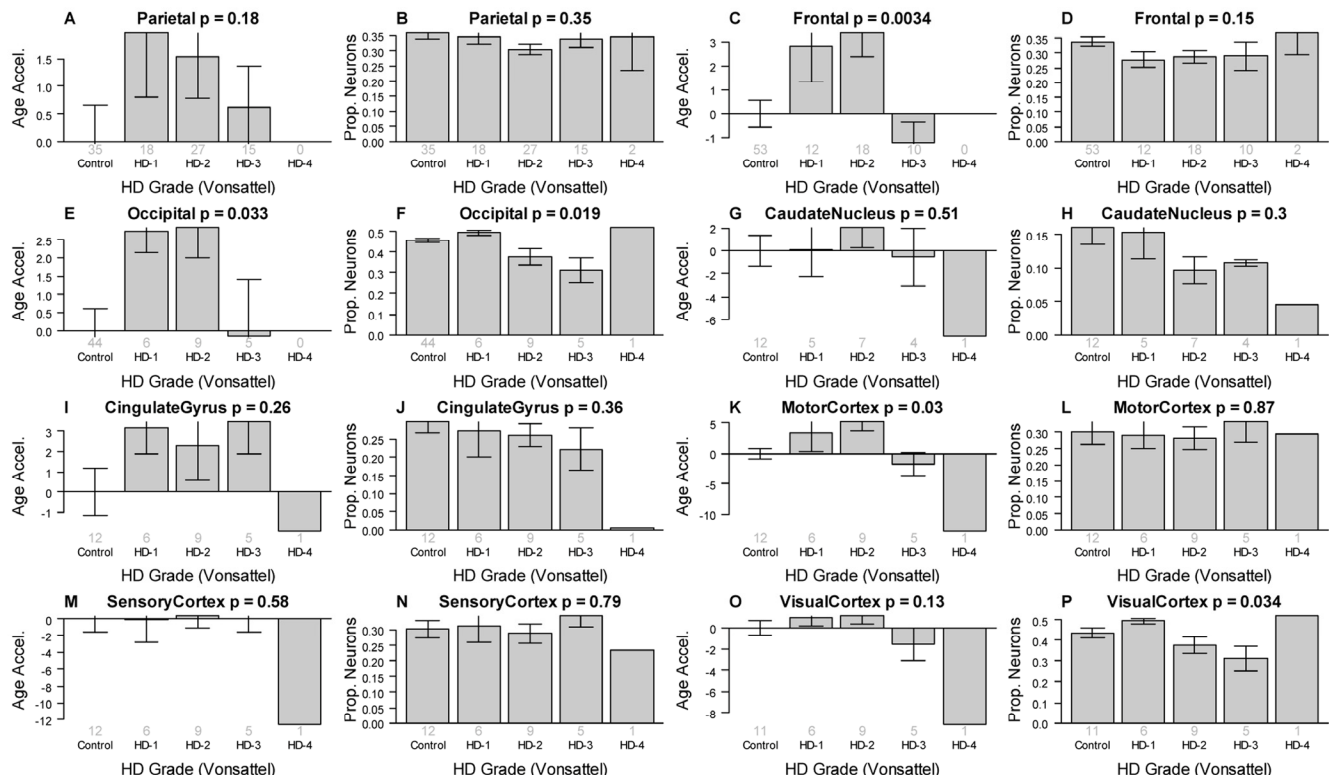
Supplementary Figure 2. HD Vonsattel grade (x-axis) versus epigenetic age acceleration and proportion of neurons. The panels correspond to different brain regions. **A,C,E,G,I,K,M,O**) Mean age acceleration (with 1 standard error) versus HD Vonsattel grade (x-axis). For the sake of comparison, the first bar reports the mean age acceleration in control samples. By definition, the mean age acceleration in control samples is zero. **B,D,F,H,J,L,N,P**) Estimated proportion of neurons versus VS grade.
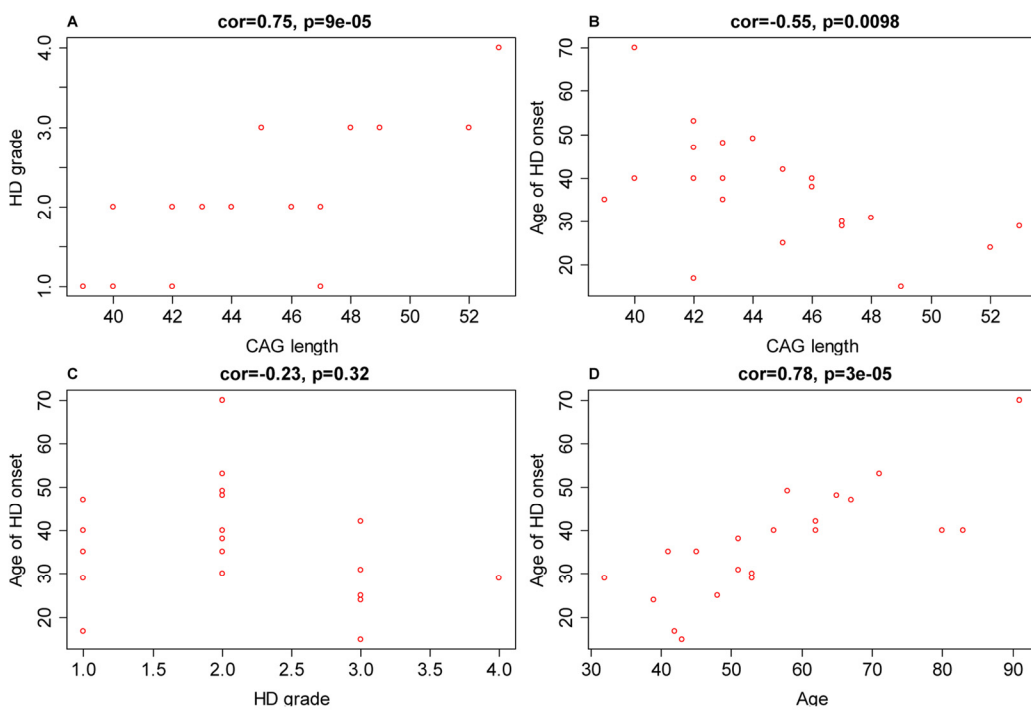
Supplementary Figure 3. Correlations between CAG length, HD grade, and age of HD onset in HD subjects. (**A-C**) Pairwise scatter plots based on 21 HD subjects from the New Zealand tissue bank. (**D**) Chronological age (at death) versus age of onset.
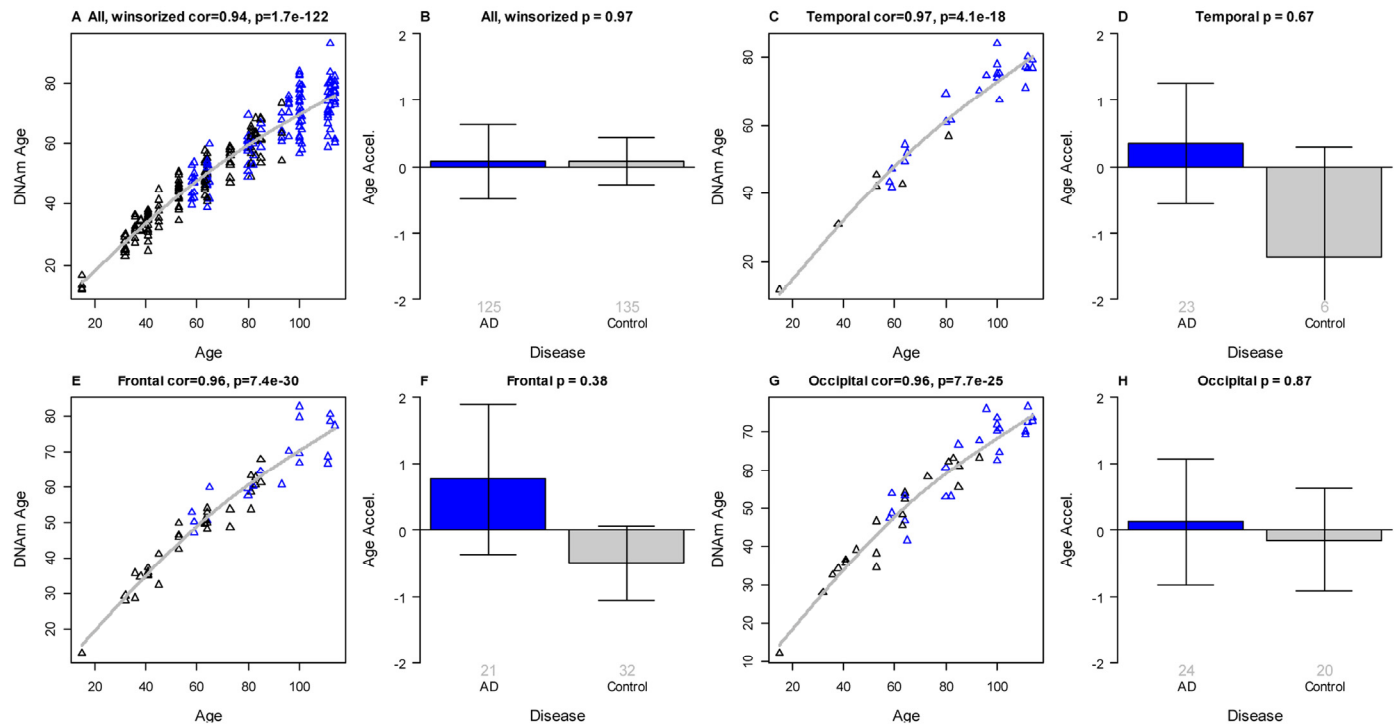

Supplementary Figure 4. Epigenetic age analysis of Alzheimer's disease. Here we removed all HD samples. Blue and red dots correspond to Alzheimer's disease and control samples respectively. The bar plots report Kruskal Wallis test p-values. Results for (**A,B**) all brain regions, (**C,D**) temporal lobe, (**E,F**) frontal lobe, (**G,H**) occipital lobe.
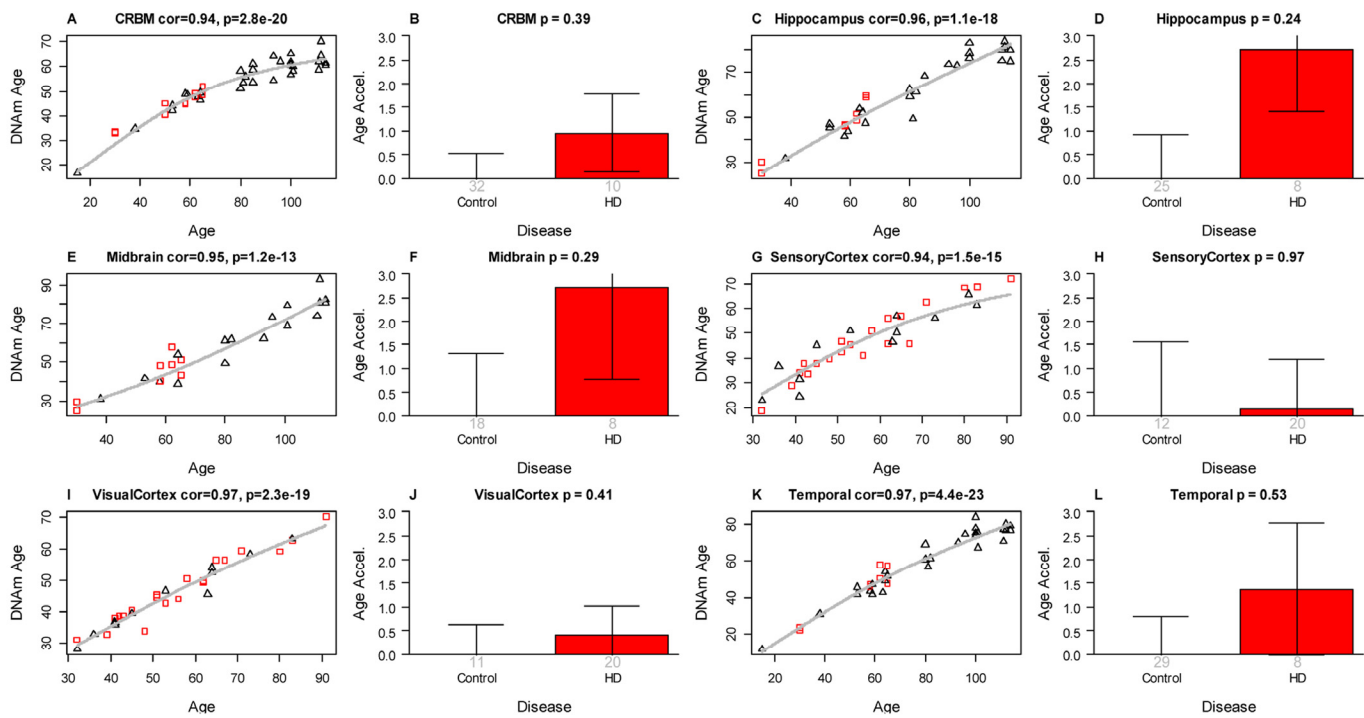
Supplementary Figure 5. Epigenetic age analysis in brain regions that lead to insignificant results. Here we used winsorized DNAm age estimates. We use ANOVA instead of the Kruskal Wallis test in the bar plots because of the low group sizes. Samples with HD grade 4 were removed from the analysis.
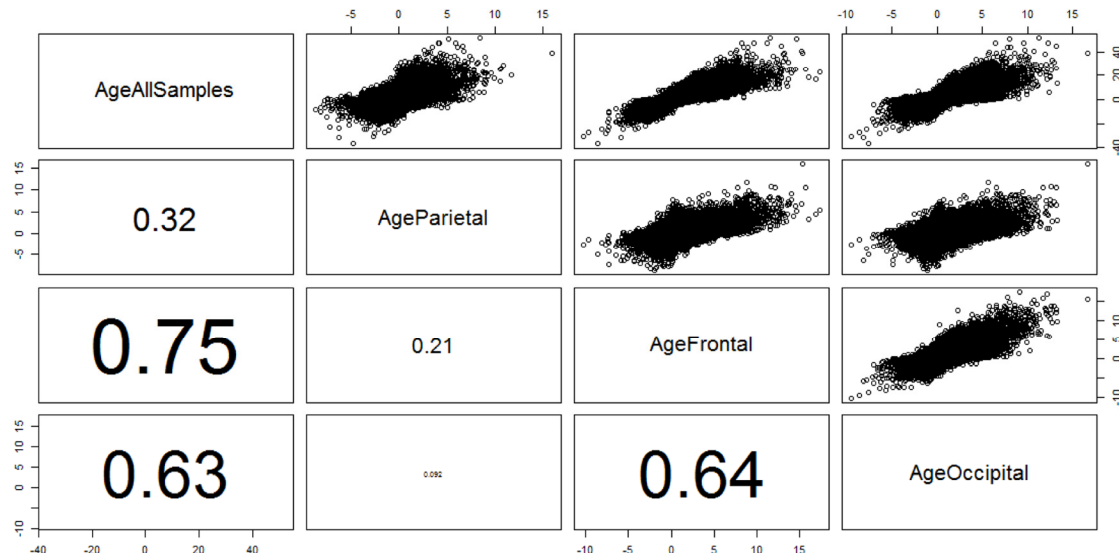

Supplementary Figure 6. The effect of chronological age on DNA methylation levels are preserved across lobes. The axis of each plot shows the signed log (base 10) transformed p-value of a correlation test. The panels above the diagonal show scatter plots. The numbers in the lower diagonal show the corresponding correlation coefficients.
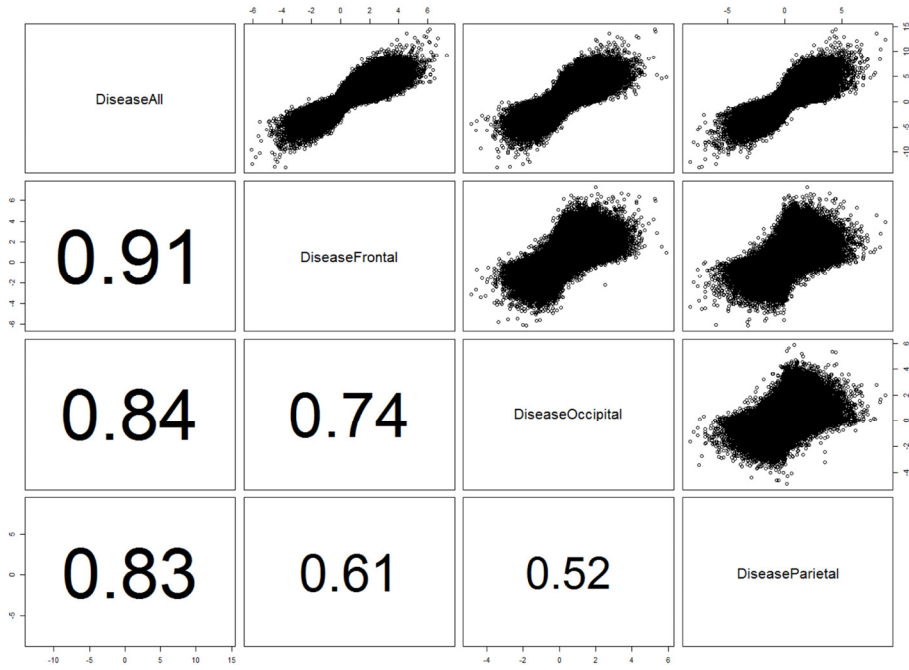
Supplementary Figure 7. The effect of HD status on DNA methylation levels are preserved across lobes. The axis of each plot shows the signed log (base 10) transformed p-value of a group comparison test. The panels above the diagonal show scatter plots. The numbers in the lower diagonal show the corresponding correlation coefficients.
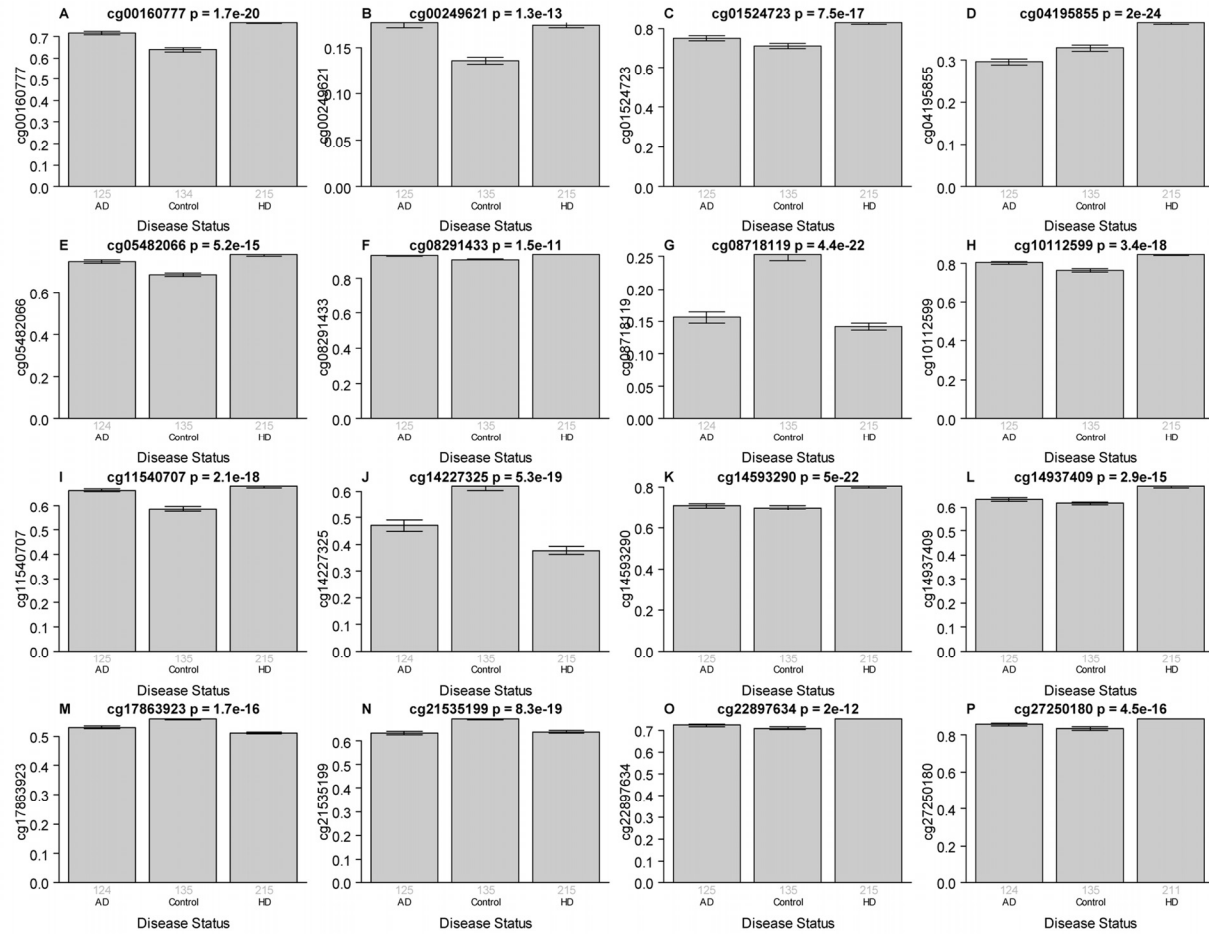
Supplementary Figure 8. The most significant CpGs resulting from our EWAS meta analysis versus disease status. The panels correspond to the CpGs in Table 3. Each bar plot relates the DNA methylation levels (beta values) to disease status. This statistical analysis (and p-values) differs from those presented in Table 3 for the following reasons. First, the y-axis shows beta values that were not adjusted for chronological age. Second, the grouping variable (x-axis) takes on 3 levels (HD, Alzheimer's disease, and controls) whereas a binary grouping variable (HD vs non-HD) was used to select the CpGs of Table 3. Brain regions are ignored (i.e. lumpted together).
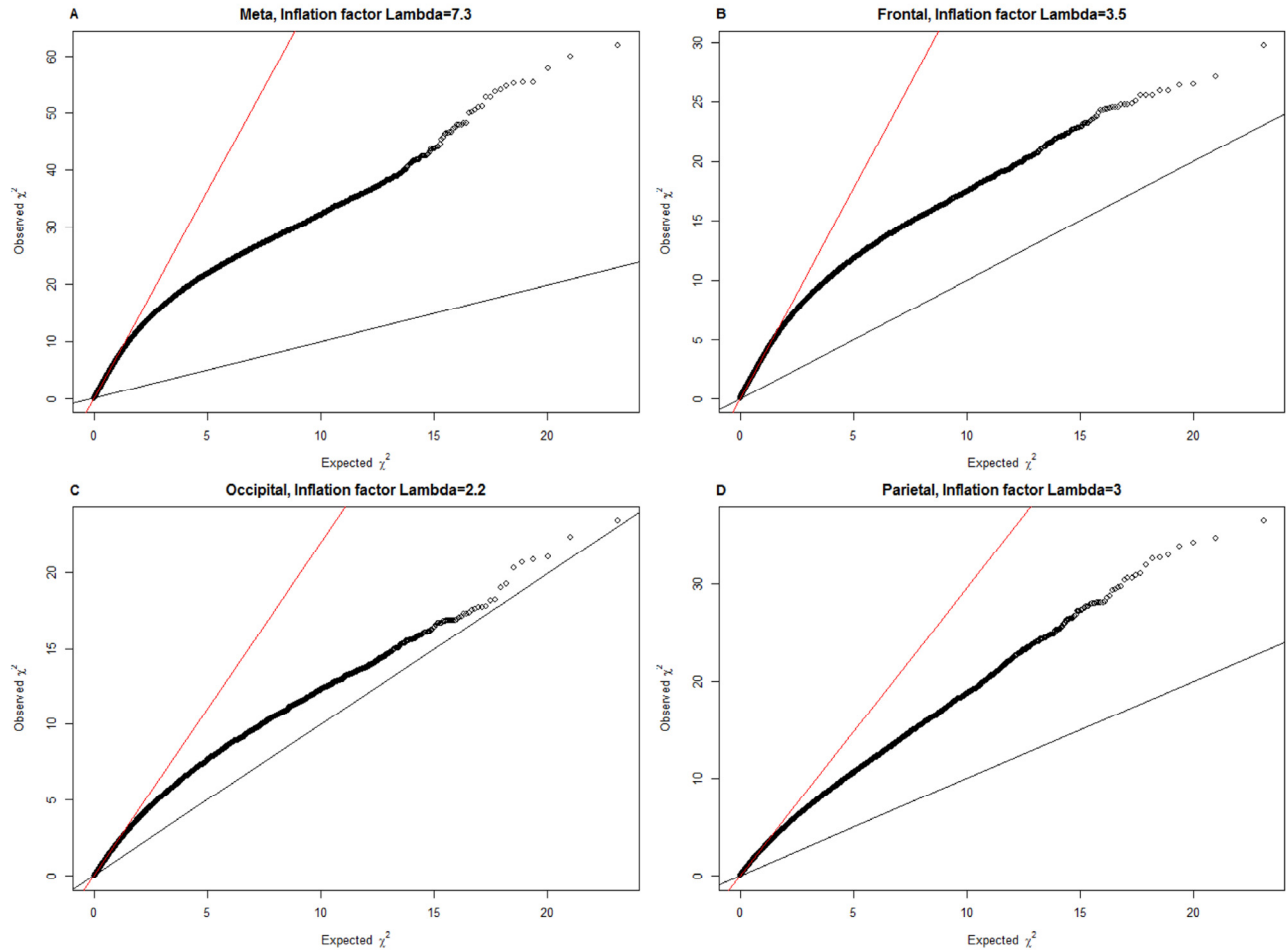
Supplementary Figure 9. Estimation of inflation factors (lambda values) for the EWAS of HD. The panels correspond to the respective studies in Figure 3. Each panel shows the estimated lambda inflation factor and plot resulting from the estlambda R function. Lambda factors for (**A**) p-values resulting from a meta analysis across 3 lobes (frontal, parietal, and occipital lobe), (**B**) frontal lobe, (**C**) occipital lobe, (**D**) parietal lobe.
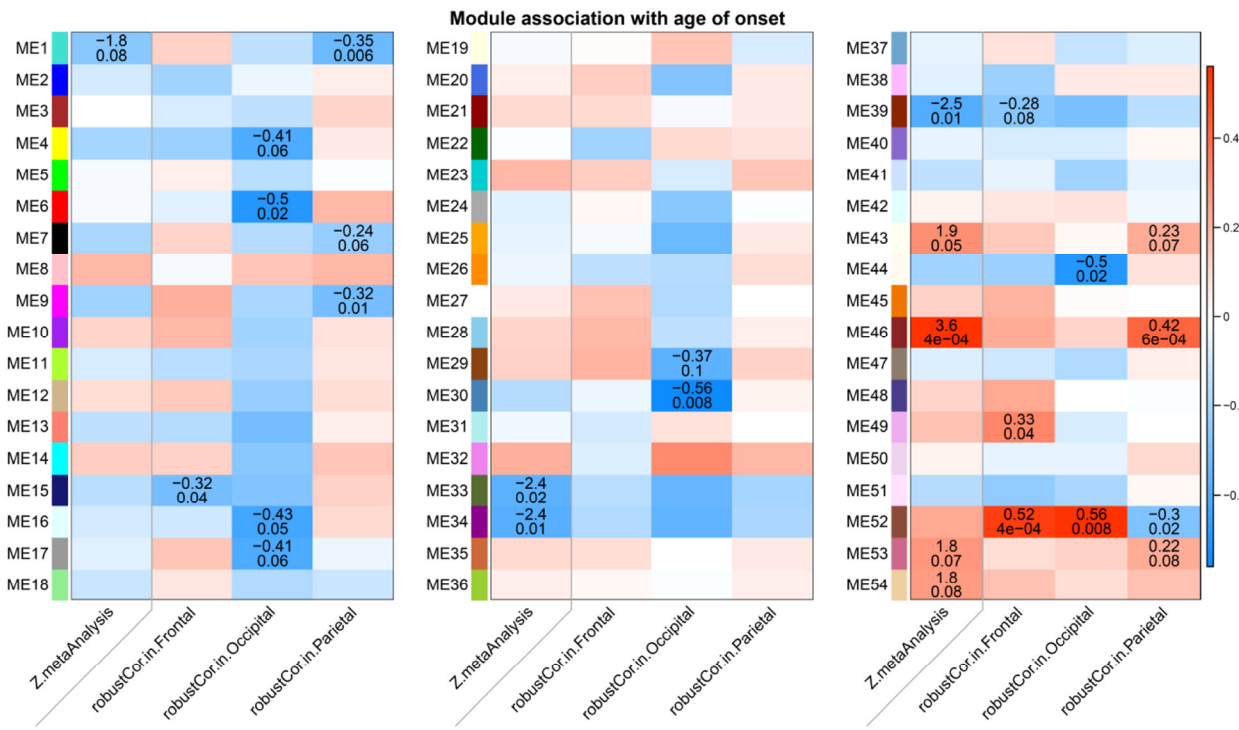
Supplementary Figure 10. Correlations between module eigengenes and age at HD motor onset. The Figure is analogous to Figure 5 but the correlation values and Z statistics refer to age of onset. The first column in each panel reports a Z statistic. The remaining columns report robust correlation coefficients in different brain regions.

Supplementary Data Sets

Please browse the full text version of this manuscript to see links to Supplementary Files:

Supplementary File 11. EWAS results for HD status in multiple brain regions. The file reports Kruskal Wallis test p-values and corresponding Z statistics for samples from the frontal lobe, occipital lobe, and parietal lobe. Further, it reports the meta analysis results across the three brain region. The meta-analysis p-valuea should be interpreted as a descriptive (hypothesis promoting) rather than inferential measure since the analysis did not adjust for the fact that multiple samples were collected from each individual. Results are reported for 326777 CpG from the Illumina Inf450k array, which satisfied our filtering criteria (high variance, few missing values).

Supplementary File 12. Module membership information for intramodular hubs in the consensus modules. The column correspond to the consensus

modules presented in Figure 5. The Z statistics result from the application of the "consensusKME" R function. High positive Z statistics indicate that the CpG is an intramodular hub in the respective module. A CpG can be a hub in multiple modules. The module membership measure should be interpreted as a fuzzy measure of module membership. Due to space constraints, we only report those CpGs for which the absolute value of the Z statistic exceeds 17 for at least one of the modules.

Epigenetic age of the pre-frontal cortex is associated with neuritic plaques, amyloid load, and Alzheimer's disease related cognitive functioning

Morgan E. Levine[1,2], Ake T. Lu[1], David A. Bennett[3,4], and Steve Horvath[1,5]

[1]Human Genetics, David Geffen School of Medicine, University of California Los Angeles, Los Angeles, CA 90095, USA;
[2]Center for Neurobehavioral Genetics, University of California Los Angeles, Los Angeles, CA 90095, USA;
[3]Rush Alzheimer's Disease Center, Rush University Medical Center, Chicago, IL 60612, USA;
[4]Department of Neurological Sciences, Rush University Medical Center, Chicago, IL 60612, USA;
[5]Biostatistics, School of Public Health, University of California Los Angeles, Los Angeles, CA 90095, USA.

Abstract: There is an urgent need to develop molecular biomarkers of brain age in order to advance our understanding of age related neurodegeneration. Recently, we developed a highly accurate epigenetic biomarker of tissue age (known as epigenetic clock) which is based on DNA methylation levels. Here we use n=700 dorsolateral prefrontal cortex (DLPFC) samples from Caucasian subjects of the Religious Order Study and the Rush Memory and Aging Project to examine the association between epigenetic age and Alzheimer's disease (AD) related cognitive decline, and AD related neuropathological markers.

Epigenetic age acceleration of DLPFC is correlated with several neuropathological measurements including diffuse plaques (r=0.12, p=0.0015), neuritic plaques (r=0.11, p=0.0036), and amyloid load (r=0.091, p=0.016). Further, it is associated with a decline in global cognitive functioning (β=-0.500, p=0.009), episodic memory (β=-0.411, p=0.009) and working memory (β=-0.405, p=0.011) among individuals with AD. The neuropathological markers may mediate the association between epigenetic age and cognitive decline. Genetic complex trait analysis (GCTA) revealed that epigenetic age acceleration is heritable (h^2=0.41) and has significant genetic correlations with diffuse plaques (r=0.24, p=0.010) and possibly working memory (r=-0.35, p=0.065). Overall, these results suggest that the epigenetic clock may lend itself as a molecular biomarker of brain age.

INTRODUCTION

Cognitive aging is on a continuum from normality, to mild cognitive impairment (MCI), to dementia [1-3]. Aging is also tied to an increasing susceptibility for a number of neurodegenerative diseases. After the age of 65 the risk of developing a neurodegenerative form of dementia, such as Alzheimer's Disease (AD), has been shown to double every five years, and by age 85, the prevalence of dementia is estimated to be as high as 31% [4].

AD dementia is an irreversible progressive neurodegenerative disease affecting the central nervous system. It is typically characterized by the presence of amyloid-beta plaques and hyperphosphorylated paired

helical filament tau protein–rich neurofibrillary tangles (NFT) [5]. Both types of lesions have been linked to AD dementia, MCI, and cognitive decline. There is also evidence that NFT mediates the association between amyloid plaques and clinical manifestations of AD [6]. While the exact physiology through which NFT and amyloid-beta plaques influence AD pathogenesis remains somewhat unclear, the presence of such deposits among those afflicted with AD is typically associated with much steeper trajectories of cognitive deficit accumulation with age [7, 8]. Cognition is not a unitary process but is composed of several dissociable cognitive systems, such as episodic memory the clinical hallmark of AD dementia.

Epigenetic alterations, such as DNA methylation (DNAm), have been linked to the both AD pathology [9] and cognitive aging in the absence of AD dementia [10]. DNAm refers to the addition of a methyl group to a cytosine nucleotide at cytosine-phosphate-guanine (CpG) sites. Hyper- or hypo methylation of sites can change over time, as a function of genes and environment, and have implications for gene expression via alterations in chromatin structure. We recently developed a highly accurate molecular biomarker of aging based on DNA methylation (DNAm) levels [11], known as "epigenetic clock", which can be used to measure the age of human cells, tissues, and organs. Given that aging is associated with a normal loss in cognitive ability as well as the rapidly increasing susceptibility to AD, an aging biomarker based on DNAm could account for between-person differences in either the rate of cognitive aging among non-demented individuals or the rate of disease progression among those with AD. As a result, the goals of our study were to 1) examine the association between DNAm age and AD neuropathology, 2) test whether DNAm age relates to AD dementia status and measures of cognitive functioning, 3) determine if differences in DNAm age reflect cognitive decline in persons with or with AD-dementia, 4) examine whether neuropathology underlies the association between higher DNAm age and worse cognitive functioning. We hypothesize that participants who have higher levels of neuropathology, lower cognitive functioning, and/or who are diagnosed with AD will have higher DNAm age in PFC samples at death—signifying that their brains are biologically older. We also hypothesize that neuropathology will mediate the association between DNAm age and cognition.

RESULTS

Study Sample

Our analytic sample included Caucasian subjects from the Religious Order Study (ROS) and the Rush Memory and Aging Project (MAP) [12, 13]. Both are longitudinal community based cohort studies of aging and dementia. The majority of participants in both studies are 75-80 years old at baseline with no known dementia. All participants agree to organ donation at death. Participants sign and informed consent, repository consent, and Anatomical Gift Act. The studies were approved by the Institutional Review Board of Rush University Medical Center. Inclusion in the studies requires participants to consent to undergoing annual clinical evaluations as well as postmortem organ donation. The ROS sample includes Catholic priests, nuns, and brothers from across the United States, whereas the MAP sample includes a more general community based population from northeastern Illinois. For our analysis, we excluded subjects with missing DNAm age, or who were diagnosed with dementias other than AD leaving us with 700 Caucasian subjects. Participants were administered annual structured interviews and a battery of cognitive tests such as episodic memory (EM), working memory (WM), and semantic memory (SM), perceptual orientation (PO), and perceptual speed (PS). Tests were averaged to yield a measure of global cognitive functioning (GCF). Neuropathological assessments were carried out postmortem as described in Methods.

Sample characteristics

As shown in Table 1, upon enrollment into the two studies, subjects were 63-102 years of age (mean= 81.36, standard deviation=6.59). Cognitive follow-up time after baseline ranged from 0 to 16 years, with a mean of 4.07 years (s.d.=3.42). Of 700 participants, 615 had at least three measures of cognitive functioning (baseline plus two follow-up), while half of our participants had seven or more cognitive measures. Average lifespan was approximately 89 years (s.d.=6.44). Overall, subjects from ROS (n=375) were 5 years younger at baseline and lived 1.5 years longer compared to those from MAP (n=325). Nearly two-thirds of participants (63.6%) were female.

Just over 300 of our 700 participants were diagnosed with AD dementia. Mean GCF, EM, WM, SM, PO, and PS were -0.33 (s.d.=0.90), -0.28 (s.d.=1.08),-0.23 (s.d.=0.90), -0.31 (s.d.=0.99), -0.34 (s.d.=0.92), and -0.53 (s.d.=1.06), respectively. Additionally, between- and within-person standard deviations were 0.82 and 0.47 for GCF, respectively; 1.00 and 0.55 for EM, respectively; 0.77 and 0.53 for WM, respectively; 0.91 and 0.53 for SM, respectively; 0.83 and 0.52 for PO, respectively; and 0.95 and 0.59 for PS, respectively. Finally, mean overall amyloid level was 3.47

(s.d.=3.68), mean neuritic plaque average 0.80 (s.d.=0.84), mean diffuse plaque average 0.71 (s.d.=0.80), mean NFT (silverstain) average 0.60 (s.d.=0.77), and mean overall paired helical filament (PHF) tangle score 6.52 (s.d.=8.16).

Epigenetic age relates to neuropathological variables

We estimated the epigenetic age (also known as DNAm age) of each brain samples by averaging the DNAm levels of 353 CpGs as described in Methods and [11].
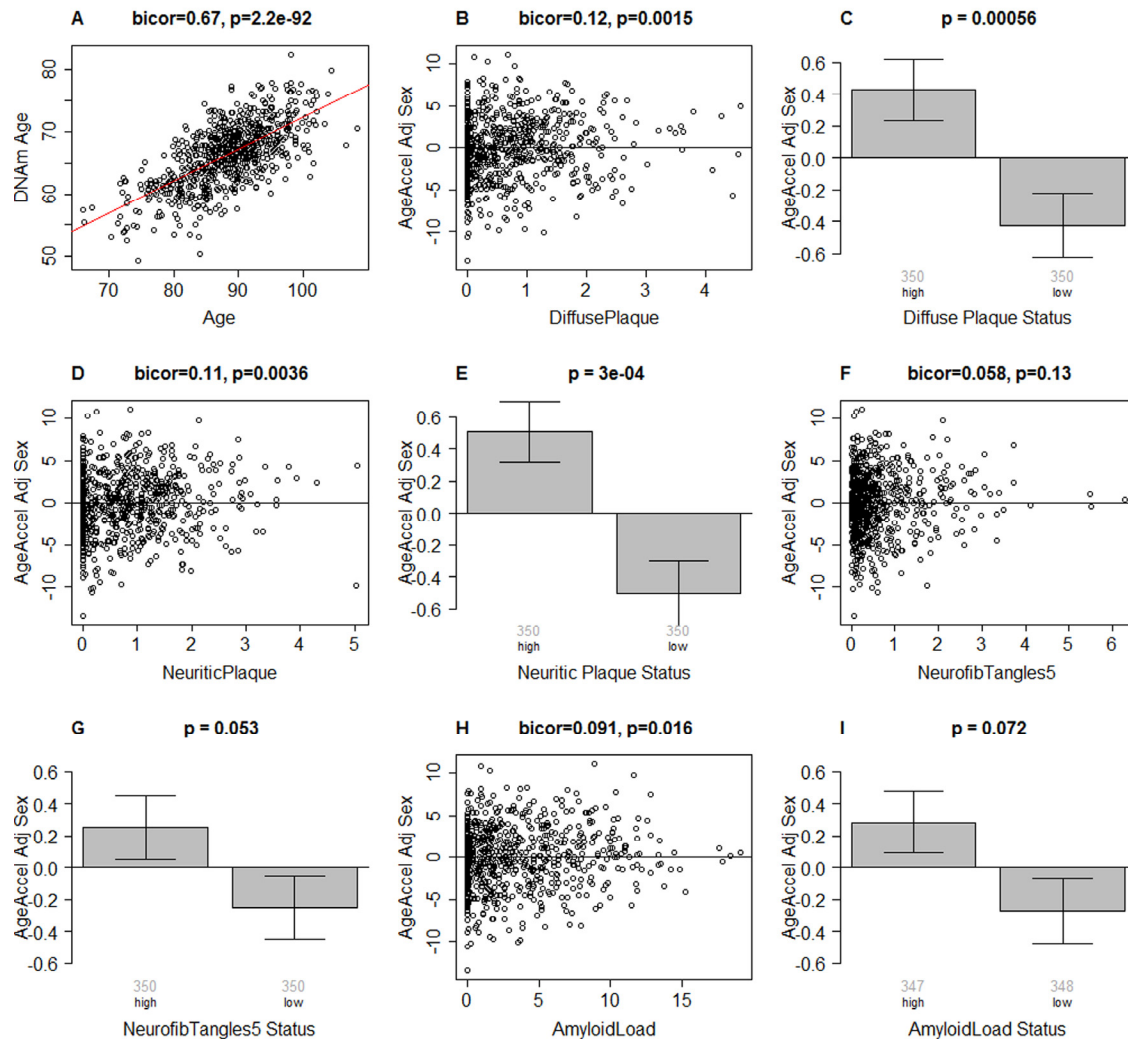
Figure 1. Epigenetic age of DLPFC samples versus neuropathological measures. (**A**) Scatter plot relating the DNAm age of each PFC sample (y-axis) versus chronological age at time of death (x-axis). The red line depicts a linear regression line. The y-axis of the remaining panels (**B-I**) involves the measure of epigenetic age acceleration which has been adjusted for sex. The scatter plots relate epigenetic age acceleration (y-axis) to (**B**) diffuse plaques, (**D**) neuritic plaques, (**F**) NFTs, and (**H**) amyloid load. The title of each scatter plot reports a robust correlation coefficient (biweight midcorrelation) and a corresponding p-value. (**C,E,G,I**) The x-axis of the bar plots involve a binary grouping variable that results from using the median value for dichotomizing (**C**) diffuse plaques, (**E**) neuritic plaques, (**G**) NFT, and (**I**) beta-amyloid load, respectively. Each bar plot depicts the mean value, one standard error, and reports the p-value results from a non-parametric group comparison test (Kruskal Wallis test). The title of each scatter plot reports a robust correlation coefficient (biweight midcorrelation) and a corresponding p-value.

Table 1. Sample characteristics

Variable	Statistic
Age at Enrollment, Mean (Std. Dev.)	81.4 (6.95)
Age at Death, Mean (Std. Dev.)	88.1 (6.60)
DNAm Age, Mean (Std. Dev.)	66.2 (5.04)
GCF, Mean (Std. Dev.)	-0.33 (0.90)
EM, Mean (Std. Dev.)	-0.28 (1.08)
WM, Mean (Std. Dev.)	-0.23 (0.90)
SM, Mean (Std. Dev.)	-0.31 (0.99)
PO, Mean (Std. Dev.)	-0.34 (0.92)
PS, Mean (Std. Dev.)	-0.53 (1.06)
Amyloid Load, Mean (Std. Dev.)	3.47 (3.68)
NP, Mean (Std. Dev.)	0.80 (0.84)
DP, Mean (Std. Dev.)	0.71 (0.80)
NFT, Mean (Std. Dev.)	0.60 (0.77)
Tangle Score, Mean (Std. Dev.)	6.52 (8.16)
Sex (Female=1), Frequency	0.636
Study (ROS=1), Frequency	0.536
AD Status, Frequency	0.433

DNAm age (in units of years) estimates the number of years that passed since birth. DNAm age was highly correlated with chronological age at time of death across all samples (correlation r=0.67, Figure 1A). We defined a measure of epigenetic age acceleration as residual resulting from regressing DNAm age on chronological age and sex. Thus, a positive value of age acceleration indicates that the epigenetic age is higher than expected based on chronological age and sex. Our study addresses the hypothesis that epigenetic age acceleration (that measures deviations between DNAm age and chronological age) captures aspects of the biological age of brain tissue. We test this hypothesis by relating epigenetic age acceleration to various measures of neuropathology and cognitive functioning.

Results from biweight midcorrelation showed that epigenetic age acceleration is associated with several postmortem neuropathological indices. Epigenetic age acceleration had a correlation of 0.12 with diffuse plaques (p=0.0015, Figure 1B,C), 0.11 with neuritic plaques (p=0.0036, Figure 1D,E), and 0.019 with amyloid load (p=0.016, Figure 1H,I). Further, it showed a marginally significant association with neurofibrillary tangle status (p=0.053 in Figure 1G) when the latter was defined by dichotomizing the NFT variable by its median value. These associations were also examined using multivariate models (Table 2), adjusting for age at death, sex, and study (ROS vs MAP), and again, we found positive associations between DNAm age and neuritic plaques (β=0.45, p=0.004), diffuse plaques

(β=0.47, p=0.004), amyloid load (β=0.10, p=0.006), NFT (β=0.38, p=0.021), and Tangle Score (β=0.03, p=0.041).

DNAm age, cognitive functioning and AD status

As shown in Table 3, we used linear models, adjusting standard errors to account for multiple observations, to examine whether postmortem estimates of DNAm age were associated with GCF, EM, WM, SM, PO, PS, and/or AD status. We found associations between DNAm age and both GCF and EM, the clinical hallmark of AD. For instance, results showed that a one unit decrease in GCF was associated with about a one third of a year increase in DNAm age (β = -0.34, P = 0.019), while a one unit decrease in EM was also associated with about a one third of a year increase in DNAm age (β = -0.30, P = 0.009). By contrast, we did not find a relationship between DNAm age and WM (β = -0.16, P = 0.172), SM (β = -0.21, P = 0.072), PO (β = -0.10, P = 0.270), or PS (β = -0.13, P = 0.191). We also examined whether AD dementia status was associated with higher DNAm age. Results showed a moderate, but non-significant association (β = 0.38, P = 0.103).

Table 2. Multivariate associations between DNAm age and neuropathological measures

	Beta Coefficient (One-Tailed P-Value)
Amyloid Load	0.100 (0.006)
NP	0.451 (0.004)
DP	0.468 (0.004)
NFT	0.377 (0.021)
Tangle Score	0.030 (0.041)
Results are from independent multivariate models that adjust for age at death, study, and sex	

Table 3. Associations between DNAm age and cognitive functioning, and mediation by AD status

	β (SE)	P-value
GCF	-0.340 (0.163)	0.019
EM	-0.297 (0.126)	0.009
WM	-0.160 (0.170)	0.172
SM	-0.205 (0.140)	0.072
PO	-0.102 (0.166)	0.270
PS	-0.134 (0.153)	0.191
AD Status	0.377 (0.298)	0.103

DNAm age was used as the dependent variable for all models. All models were run adjusting for study (ROS or MAP), age at death, age a clinical evaluation (accept for the model for AD), and sex. GCF=Global Cognitive Functioning, EM=Episodic Memory, WM=Working Memory, SM=Semantic Memory, PO=Perceptual Orientation, PS=Processing Speed. P-values represent significance assuming a one-tailed hypothesis test. Standard errors were adjusted via clustering by Sample ID, in order to account for multiple observations (except for the model for AD).

Table 4. Associations between DNAm age and cognitive functioning, by AD status

	Non-Demented Participants (n=397)		AD Participants (n=303)	
	β (SE)	P-value	β (SE)	P-value
GCF	-0.059 (0.503)	0.454	-0.500 (0.210)	0.009
EM	-0.209 (0.322)	0.258	-0.411 (0.173)	0.009
WM	0.340 (0.328)	0.836	-0.405 (0.177)	0.011
SM	-0.047 (0.429)	0.456	-0.262 (0.160)	0.051
PO	-0.049 (0.312)	0.437	-0.102 (0.210)	0.313
PS	-0.058 (0.304)	0.425	-0.178 (0.205)	0.193

DNAm age was used as the dependent variable for all models. All models were run adjusting for study (ROS or MAP), age at death, age a clinical evaluation, and sex. GCF=Global Cognitive Functioning, EM=Episodic Memory, WM=Working Memory. P-values represent significance assuming a one-tailed hypothesis test. Standard errors were adjusted via clustering by Sample ID, in order to account for multiple observations.

Using linear models, we then examined the association between DNAm age and cognitive functioning by AD dementia status (Table 4). Overall, we found no association between DNAm age and any of the cognitive functioning measures among participants without AD dementia which might reflect the relatively low variance of cognitive measures among controls. However, among participants with AD dementia, GCF, EM, and WM were all associated with DNAm age. Results showed that for persons who developed AD dementia, every one unit decrease in GCF was associated with a half a year increase in DNAm (β = -0.50, P = 0.009). Similarly, for persons who developed AD dementia, every one unit decrease in EM or WM was associated with about a 0.4 year increase in DNAm (EM: β = -0.41, P = 0.009; WM: β = -0.40, P = 0.011).

Mediation analysis involving neuropathological variables and cognitive scores

Using multivariate linear models, with DNAm age as the dependent variable and adjusting for study (ROS vs MAP), age at clinical assessment, age at death, and sex, we examined whether neuropathological measures accounted for the association between worse cognitive functioning (GCF, EM) and higher DNAm age (Table 5 and Table 6). All models were run on n=695 participants who had complete neuropathology data. Standard errors were adjusted to account for repeat cognitive measures. For each cognitive measure, seven models were run. The first model shows the association between the cognitive measure and DNAm age, after adjusting for covariates. We find that (as reported previously), GCF and EM were inversely associated with DNAm age (GCF: β=-0.336, P=0.020; EM: β=-0.286, P=0.012). Model 2, is similar to model 1, but includes the addition of amyloid load, to examine whether it alters the association between cognitive functioning and DNAm age. We find that amyloid load is significantly associated with DNAm age. Furthermore, it accounts for 31.8% and 30.8% of the association between DNAm age and GCF and EM, respectively. Model 3, is similar to model 1, but with the addition of neuritic plaques. We find that NP is significantly associated with DNAm age and accounts for 66.1% of the association between DNAm age and GCF, as well as 65.0% of the association between DNAm age and EM. Model 4, includes the addition of diffuse plaques, which is significantly associated with DNAm age. However, diffuse plaques only account for 15.5% of the association between DNAm age and GCF, and 17.8% of the association between DNAm age and EM. Model 5, includes the addition of neurofibrillary tangles, which is not significantly associated with DNAm age, yet NFT

accounts for 25.9% of the association between DNAm age and GCF, and 23.4% of the association between DNAm age and EM. Model 6, includes the addition of overall tangle score, which, like NFT, is not significantly associated with DNAm age, yet it account for a significant proportion of the association between DNAm age and GCF (24.4%), as well as DNAm age and EM (19.9%). Finally, Model 7 is similar to model 1, but with the addition of all five neuropathology variables. We find that the inclusion of all these measures accounts for 52.4% of the association between DNAm age and GCF, and 51.4% of the association between DNAm age and EM.

Heritability and genetic correlation analysis

We estimated the heritability of epigenetic age accelera-tion using the GCTA software [14, 15] from SNP markers measured on the same subjects. We find that epigenetic age acceleration in DLPFC is highly heritable (h^2=0.41, Table 7), which is similar to heritability estimate reported for blood [11, 16].

We find that diffuse plaques are highly heritable (h^2=0.38, Table 7) and have a significant genetic correlation with epigenetic age acceleration (r=0.24, p=0.010, Table 7). Neuritic plaques also exhibit a significant genetic correlation with epigenetic age acceleration (r=0.78, p=0.014) but the result needs to be interpreted with caution since neuritic plaques are at best weakly heritable (h^2=0.05). We also find a suggestive genetic correlation with working memory at the last assessment (r=-0.35, p=0.065) but working memory is only weakly heritable (h^2=0.07).

Table 5. Neuropathological mediation of the association between GCF and DNAm age

	Beta Coefficient (One-Tailed P-Value)						
	Model1	Model2	Model3	Model4	Model5	Model6	Model7
GCF	-0.336 (0.020)	-0.229 (0.087)	-0.114 (0.256)	-0.284 (0.044)	-0.249 (0.088)	-0.254 (0.084)	-0.160 (0.193)
Amyloid		0.094 (0.015)					0.026 (0.305)
Neuritic Plaques			0.553 (0.004)				0.514 (0.025)
Diffuse Plaques				0.360 (0.044)			0.144 (0.268)
NFT					0.231 (0.139)		-0.028 (0.537)
Tangles						0.019 (0.165)	-0.016 (0.720)

Table 6. Neuropathological aediation of the association between EM and DNAm age

	Beta Coefficient (One-Tailed P-Value)						
	Model 1	Model 2	Model 3	Model 4	Model 5	Model 6	Model 7
EM	-0.286 (0.012)	-0.198 (0.064)	-0.100 (0.229)	-0.235 (0.032)	-0.219 (0.057)	-0.229 (0.048)	-0.139 (0.161)
Amyloid		0.094 (0.015)					0.028 (0.287)
Neuritic Plaques			0.538 (0.005)				0.487 (0.033)
Diffuse Plaques				0.368 (0.044)			0.165 (0.243)
NFT					0.210 (0.164)		-0.032 (0.540)
Tangles						0.016 (0.202)	-0.017 (0.725)

DISCUSSION

Overall, we found that postmortem DNAm age in DLPFC was associated with neuropathological variables (Figure 1 and Table 2) and with pre-mortem measures of cognitive decline, after adjusting for chronological age, sex, and other possible confounders (Tables 3 and 4). Our mediation analysis (Tables 5-6) suggests that a proportion (up to 66%) of the association between DNAm age and measures of cognitive function is mediated by neuropathological measures. Our genetic analysis (Table 7) indicates that pleiotropic genetic loci affect epigenetic age acceleration, neuropathological variables, and cognitive traits.

The association between cognitive function and DNAm age is consistent with previous work showing that general cognitive ability—defined as a composite score for six cognitive function tests comprising working memory, non-verbal reasoning, constructional ability,

and processing speed—was associated with DNAm age in pre-mortem blood samples [17]. However, previous work has not examined the role of neuropathology or AD dementia in the association between DNAm age and cognitive decline. Our study showed that about half of the association between DNAm age and cognition was accounted for by variations in neuropathological variables. For instance, we found that worse GCF and EM was associated with higher DNAm age; however, this association was significantly reduced or eliminated after adjusting for amyloid load or neuritic plaques.

Previous studies have shown that there is little or no age effect on many cognitive domains after accounting for common neuropathologies [18]. The extended preclinical phase of dementia is typically characterized by an accumulation of neuropathology underlying cognitive decline, and as such, pathologies have been shown to relate to decline across the entire continuum, from normal, to MCI, to dementia [19, 20].

Table 7. Heritability analysis and genetic correlations

Trait (residuals)	Heritability		Genetic correlation with epigenetic age acceleration	
	Estimate	P	Estimate	P
DNAm age	0.41	0.19	--	--
Mean GCF	<0.01	0.50	--	--
Mean WM	0.17	0.32	-0.19	0.12
Mean EM	< 0.01	0.50	--	--
Last GCF	< 0.01	0.50	--	--
Last WM	0.07	0.43	-0.35	0.065
Last EM	< 0.01	0.50	--	--
Amyloid	0.03	0.46	--	--
Neuritic plaque	0.05	0.43	0.78	0.014
Diffuse plaque	0.38	0.080	0.24	0.010
NFT	< 0.01	0.50	--	--
Tangles	< 0.01	0.50	--	--

The GCTA software was used to estimate the heritability (first two columns) and the genetic correlations with epigenetic age acceleration (last two columns).

Nevertheless, declines in cognitive functioning have been shown to be significantly steeper among those with AD [21-24]. In contrast to those with non-pathological cognitive aging, the more drastic cognitive decline associated with AD is thought to reflect AD-mediated neuronal injury, larger decreases in brain volume, functional disconnection between PFC and the hippocampus, and dramatic increases in ventricle size [3, 25].

While our results showed that DNAm age was associated with cognitive decline among persons with a clinical diagnosis of AD, we did not find an association between AD dementia status and DNAm age. One poten-tial explanation for the lack of association between AD dementia status and DNAm age is that the clinical diagnosis AD is only an incomplete measure of the underlying neuropathology such as the accumulation of amyloid-beta plaques and NFT. For this reason, AD reflects a heterogeneous group, which is why the severity of AD (as estimated by cognitive decline or neuropathology) may be more strongly associated with DNAm age than AD dementia status alone. Among our participants, we found that both the between-person and within-person variance in GCF and EM change was much higher for those with AD versus those without AD dementia (Table 8), suggesting that 1) the AD group may be far more heterogeneous in regards to

neurocognitive decline, and 2) experience far more cognitive aging changes. Additionally, this interpretation is supported by our analysis of neuropathological variables, for which we found strong associations between DNAm age and all five measures (amyloid load, neuritic plaques, diffuse plaques, NFT, and overall tangle score). Additionally, results from step-wise models showed that neuropathological variables, especially amyloid load and neuritic plaques, may explain the association between DNAm age and cognitive functioning. This suggests that increased DNAm age may influence changes in the regulation of amyloid proteins, contributing to AD neuropathology, and thus manifesting as steeper cognitive declines [26].

Finally, our genetic analysis showed that DNAm age, neuropathology, and cognitive decline may be pleiotropic, which could reflect mediation among these factors. For instance, alleles could be associated with faster cognitive decline via acceleration of the biological aging process, which in turn leads to a faster accumulation of neuropathology (Figure 2A). Another alternative is that physiological consequences associated with neuropathological accumulation could influence both biological brain aging and cognitive decline, simultaneously (Figure 2B). Finally, loci could pleiotropically influence both neuropathology and biological aging, independently, with no causal pathway between them (Figure 2C). In moving forward, examina-

Table 8. Between- and within-person statistics for cognitive function, by AD

		No AD			AD		
		Mean	Std. Dev.	N	Mean	Std. Dev.	N
GCF	Overall	0.126	0.496	2554	-0.894	0.954	2105
	Between		0.448	397		0.786	300
	Within		0.235			0.649	
EM	Overall	0.252	0.649	2482	-0.928	1.139	2029
	Between		0.607	397		0.951	300
	Within		0.323			0.731	
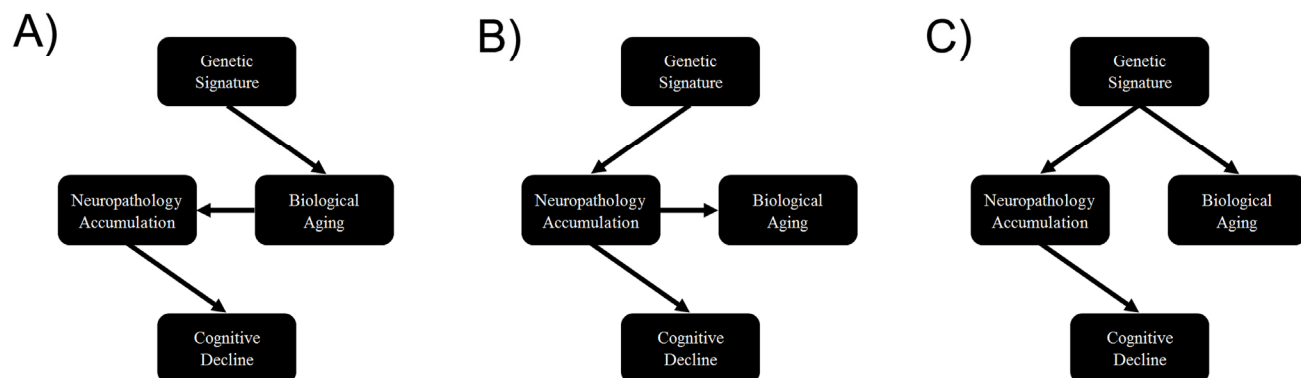
Figure 2. Causal scenarios that might explain the significant genetic correlations between epigenetic age, neuropathology and cognitive decline. Genetic variants form a causal anchor that affect biological age (and associated measures such as epigenetic age) and various measures of neuropathology and cognitive decline.

tion of these pathways will be important for facilitating our understanding of brain aging and neurodegenerative disease.

There are limitations to this study. First, DNAm age was only measured postmortem, which prevented us from determining if it was predictive of AD status or cognitive decline. Furthermore, DNAm age changes with time, yet in our sample it was only measured at a single time-point. For that reason we were unable to examine if larger changes in DLPFC DNAm age were associated with steeper cognitive decline or AD. Nevertheless, our study was strengthened by the inclusion of neuropathological variables, longitudinal measurements of multiple cognitive functioning domains, measurement of DNAm age in DLPFC rather than whole blood, and availability of postmortem data for neuropathologic indices.

Overall, our study shows that epigenetic aging in DLPFC is associated with the severity of cognitive decline as well as neuropathological hallmarks of AD. These results strongly suggests that the epigenetic clock lend itself as a molecular biomarker of brain age.

METHODS

Study sample. Our analytic sample included 700 non-Latino white subjects from the Religious Order Study (ROS) and the Rush Memory and Aging Project (MAP) [12, 13]. Both are longitudinal community based cohort studies of aging and dementia. The majority of participants in both studies are 75-80 years old at baseline with no known dementia. Inclusion in the studies requires participants to consent to undergoing annual clinical evaluations as well as postmortem organ donation. The ROS sample includes Catholic priests, nuns, and brothers from across the United States, whereas the MAP sample includes a more general community based population from northeastern Illinois. For our analysis, excluded subjects included those with missing DNAm age, or who were diagnosed with dementias other than AD.

Clinical evaluations. Participants were administered annual structured interviews to assess cognitive functioning. These included tests for EM (immediate recall (word list), delayed recall (word list), word recognition (word list), immediate recall (East Boston story), delayed recall (East Boston story), logical memory immediate recall, logical memory delayed recall), WM (digits forward, digits backward, digit ordering), SM (Boston naming, category fluency, reading test), PO (line orientation, progressive matrices), and PS (symbol digits modality-oral, number

comparison, stroop color naming, stroop color reading). For each domain, composite measures were calculated as the average across tests. Before taking the average, each cognitive test was converted to a z-score (with mean of zero and standard deviation of 1). Finally, GCF is meant to represent overall cognitive functioning. At each wave it was estimated as the average across z-scores from the 19 cognitive tests for EM, WM, SM, PO, and PS.

Neuropathological examination. Upon participants' death, brains were extracted, weighed, sectioned into 1 cm-thick coronal slabs, and stored. Neuropathological indices were examined in order to diagnose cognitive pathologies such as AD, Lewy Body diseases, and cerebrovascular disease [27]. Modified Bielschowsky silver stain was used to identify AD pathology based on NIA-Reagan and modified CERAD criteria. Global AD pathologic burden was estimated by averaging standardized numbers of neuritic plaques, diffuse plaques, and NFT across five brain regions as described in [28]. Moreover, amyloid load was quantified as abundance of amyloid-β, labeled with a N-terminal directed monoclonal antibody, while PHFtau tangles, was quantified as the density of paired helical filament tau tangles.

We focused on the following aggregated neuropathological variables (Figure 1 and elsewhere):
a) "neuritic plaques" and "diffuse plaques" were defined as average of 5 scaled scores (namely scaled mid-frontal, temporal cortex, inferior parietal cortex, entorhinal cortex, and hippocampus plaques) [29, 30].
b) "NFT" measures the tangle average across 5 regions (mid-frontal cortex, mid-temporal cortex, inferior parietal cortex, entorhinal cortex, and hippocampus CA1) [29].
c) "Amyloid load" measures the overall amyloid load, which was defined as the mean amyloid scores across 8 regions (namely hippocampus entorhinal cortex, mid-frontal, inferior parietal cortex, anterior gyrus, calcarine cortex, cingulate regions, superior frontal gyrus) [29, 31, 32].
d) Overall tangle score which reports the PHFtau tangle score across 8 regions (hippocampus, entorhinal cortex, midfrontal gyrus, inferior temporal, anterior gyrus, calcarine cortex. cingulate region, superior frontal gyrus).

DNA methylation data. DNAm was measured using the Illumina Infinium HumanMethylation450 BeadChip. The Illumina BeadChips measures bisulfite-conversion-based, single-CpG resolution DNA methylation levels at 485577 different CpG sites in the human genome. These data were generated by following the standard

protocol of Illumina methylation assays, which quantifies methylation levels by the β value using the ratio of intensities between methylated and un-methylated alleles. Specifically, the β value is calculated from the intensity of the methylated (M corresponding to signal A) and un-methylated (U corresponding to signal B) alleles, as the ratio of fluorescent signals β = Max(M,0) / [Max(M,0) + Max(U,0) + 100]. Thus, β values range from 0 (completely un-methylated) to 1 (completely methylated) (Dunning, 2008). The DNA methylation data are available at the following webpage https://www.synapse.org/#!Synapse:syn3168763. We focused on brain samples of Caucasian subjects from ROS and MAP that include brain donation at the time of death (n=700) [12, 13]. Additional details on the DNA methylation data can be found in [9].

Epigenetic clock analysis and DNAm age. Several recent studies have proposed to measure the age of tissue samples by combining the DNA methylation levels of multiple dinucleotide markers, known as Cytosine phosphate Guanines or CpGs [11, 33, 34]. In particular, the epigenetic clock based on 353 Cytosine phosphate Guanine (CpG) markers was developed to measure the age (known as "DNA methylation age" or "epigenetic age") of human tissues, organs and cell types—including brain, breast, kidney, liver, lung, blood [11], and even applies to prenatal brain samples [35]. The epigenetic clock method - applied to two commercially standardized methylation platforms: the Illumina 450K array and the 27K arrays - is an attractive biomarker of aging because (1) it applies to most human tissues; (2) its accurate measurement of chronological age is unprecedented [11]; (3) it is predictive of all-cause mortality even after adjusting for a variety of known risk factors [16]; (4) it correlates with measures of cognitive and physical fitness in the elderly [17]; (5) it has already been useful in detecting accelerated aging due to obesity [36], Down syndrome [37], Parkinson's disease [38], and HIV infection [39]; and . Further, the epigenetic clock was used to show that age acceleration of blood may predict the future onset of lung cancer [40], that the cerebellum ages slowly [41], that the blood of subjects with a severe developmental disorder ages normally [42], and that semi-supercentenarians and their offspring age more slowly [47].

Weighted DNAm measures across the 353 CpGs from the epigenetic clock were used to measure the DNAm age of DLPFC samples. These CpGs and their weights (coefficient values) were chosen in independent data sets by regressing chronological age on CpGs. DNAm age is then defined as predicted age, in years [43].

Statistical analysis. Biweight midcorrelations and ordinary least squares regression models were used to examine whether postmortem neuropathology was associated with postmortem DNAm age in DLPFC, after controlling for age at death, study (ROS vs. MAP), and sex. For the bar plots in Figure 1, we defined a grouping variable (high versus low) by dichotomizing the respective neuropathological variable according to the median value. The median was chosen in order to arrive at equal group sizes (high versus low) and to avoid overfitting due to the selection of an optimal threshold. Multivariate linear regression models were fit in the whole sample and in strata defined by AD dementia status (according to the clinical diagnosis). Here we did not use a linear mixed effects model since our dependent variable (DNAm age) is a time-invariant variable based on postmortem brain tissue. The linear models were used to determine whether GCF, WM, EM, SM, PO, and PS over all waves leading up to death were related to postmortem DNAm age in DLPFC. Standard errors for cognitive decline models were adjusted to account for multiple observations. These models also included potential confounders, such as age of clinical evaluation, age at death, study (ROS vs. MAP), and sex. Finally, step-wise linear models were run with DNAm age as the dependent variable and cognitive measures as the independent models. For these models we examined how the association between DNAm age and cognition was altered with the inclusion of either one or all of the neuropathology measure.

We report one-sided (one-tailed) p-values for the cognitive scores and neuropathology variables in our multivariate model analyses because our hypotheses involving cognitive scores are one-sided (e.g. that *higher* DNAm age is associated with *worse* cognitive functioning and *higher* levels of neuropathology).

Genetic analysis. Of the study samples, a total of 1102 individuals (632 normal/ 470 AD) were available with both genotypes and cognitive functioning or neuropathological measure. The GCTA software was used to estimate the heritability and genetic correlations based on both genotyped and imputed SNP markers. We used IMPUTE2 [44, 45] with haplotypes phased using SHAPEIT[46] to impute SNP and INDEL markers, with a reference panel based on the 1000 Genome haplotypes from 2,504 individuals (released in October 2014). As study individuals were genotyped on either Affymetrix SNP Array 6.0 or Illumina HumanOmniExpress, we performed imputation on each subset of individuals stratified by platform. We merged the imputation outputs across platforms and pruned in the markers with info measure > 0.4 in both sets. The other quality control was based on minor allele

frequency (MAF) ≥ 0.02. We converted the IMPUTE2 output format to MaCH dosage format in order to use it as input for the GCTA software.

Conflict of interest statement

The authors declare no conflict of interest.

REFERENCES

1. Deary IJ, Corley J, Gow AJ, Harris SE, Houlihan LM, Marioni RE, Penke L, Rafnsson SB and Starr JM. Age-associated cognitive decline. Br Med Bull. 2009; 92:135-152.

2. Singh-Manoux A, Kivimaki M, Glymour MM, Elbaz A, Berr C, Ebmeier KP, Ferrie JE and Dugravot A. Timing of onset of cognitive decline: results from Whitehall II prospective cohort study. BMJ. 2012; 344:d7622.

3. Sperling RA, Aisen PS, Beckett LA, Bennett DA, Craft S, Fagan AM, Iwatsubo T, Jack CR, Jr., Kaye J, Montine TJ, Park DC, Reiman EM, Rowe CC, et al. Toward defining the preclinical stages of Alzheimer's disease: recommendations from the National Institute on Aging-Alzheimer's Association workgroups on diagnostic guidelines for Alzheimer's disease. Alzheimers Dement. 2011; 7:280-292.

4. von Strauss E, Viitanen M, De Ronchi D, Winblad B and Fratiglioni L. Aging and the occurrence of dementia: findings from a population-based cohort with a large sample of nonagenarians. Archives of neurology. 1999; 56:587-592.

5. Rosenberg RN. The molecular and genetic basis of AD: the end of the beginning: the 2000 Wartenberg lecture. Neurology. 2000; 54:2045-2054.

6. Bennett DA, Schneider JA, Wilson RS, Bienias JL and Arnold SE. Neurofibrillary tangles mediate the association of amyloid load with clinical Alzheimer disease and level of cognitive function. Archives of neurology. 2004; 61:378-384.

7. Petersen RC. Mild Cognitive Impairment. The New England Journal of Medicine. 2011:2227-2234.

8. Bennett DA, Wilson RS, Arvanitakis Z, Boyle PA, de Toledo-Morrell L and Schneider JA. Selected Findings from the Religious Orders Study and Rush Memory and Aging Project. Journal of Alzheimer's disease : JAD. 2013; 33:S397-S403.

9. De Jager PL, Srivastava G, Lunnon K, Burgess J, Schalkwyk LC, Yu L, Eaton ML, Keenan BT, Ernst J, McCabe C, Tang A, Raj T, Replogle J, et al. Alzheimer's disease: early alterations in brain DNA methylation at ANK1, BIN1, RHBDF2 and other loci. Nat Neurosci. 2014; 17:1156-1163.

10. Marioni RE, Shah S, McRae AF, Ritchie SJ, Muniz-Terrera G, Harris SE, Gibson J, Redmond P, Cox SR and Pattie A. The epigenetic clock is correlated with physical and cognitive fitness in the Lothian Birth Cohort 1936. International journal of epidemiology. 2015:dyu277.

11. Horvath S. DNA methylation age of human tissues and cell types. Genome Biol. 2013; 14(R115).

12. Bennett DA, Schneider JA, Arvanitakis Z and Wilson RS. Overview and findings from the religious orders study. Curr Alzheimer Res. 2012; 9:628-645.

13. Bennett DA, Schneider JA, Buchman AS, Barnes LL, Boyle PA and Wilson RS. Overview and findings from the rush Memory and Aging Project. Curr Alzheimer Res. 2012; 9:646-663.

14. Lee SH, Wray NR, Goddard ME and Visscher PM. Estimating missing heritability for disease from genome-wide association studies. Am J Hum Genet. 2011; 88:294-305.

15. Visscher PM, Hemani G, Vinkhuyzen AA, Chen GB, Lee SH, Wray NR, Goddard ME and Yang J. Statistical power to detect genetic (co)variance of complex traits using SNP data in unrelated samples. PLoS Genet. 2014; 10:e1004269.

16. Marioni R, Shah S, McRae A, Chen B, Colicino E, Harris S, Gibson J, Henders A, Redmond P, Cox S, Pattie A, Corley J, Murphy L, et al. DNA methylation age of blood predicts all-cause mortality in later life. Genome Biol. 2015; 16:25.

17. Marioni RE, Shah S, McRae AF, Ritchie SJ, Muniz-Terrera G, Harris SE, Gibson J, Redmond P, Cox SR, Pattie A, Corley J, Taylor A, Murphy L, et al. The epigenetic clock is correlated with physical and cognitive fitness in the Lothian Birth Cohort 1936. Int J Epidemiol. 2015; 44:1388-1396.

18. Yu L, Boyle PA, Leurgans S, Schneider JA and Bennett DA. Disentangling the effects of age and APOE on neuropathology and late life cognitive decline. Neurobiol Aging. 2014; 35:819-826.

19. Boyle PA, Wilson RS, Yu L, Barr AM, Honer WG, Schneider JA and Bennett DA. Much of late life cognitive decline is not due to common neurodegenerative pathologies. Ann Neurol. 2013; 74:478-489.

20. Boyle PA, Yu L, Wilson RS, Schneider JA and Bennett DA. Relation of neuropathology with cognitive decline among older persons without dementia. Frontiers in Aging Neuroscience. 2013; 5:50.

21. Hatanpaa K, Isaacs KR, Shirao T, Brady DR and Rapoport SI. Loss of proteins regulating synaptic plasticity in normal aging of the human brain and in Alzheimer disease. J Neuropathol Exp Neurol. 1999; 58:637-643.

22. Ohnishi T, Matsuda H, Tabira T, Asada T and Uno M. Changes in brain morphology in Alzheimer disease and normal aging: is Alzheimer disease an exaggerated aging process? AJNR American journal of neuroradiology. 2001; 22(9):1680-1685.

23. Grundman M, Petersen RC, Ferris SH, Thomas RG, Aisen PS, Bennett DA, Foster NL, Jack Jr CR, Galasko DR and Doody R. Mild cognitive impairment can be distinguished from Alzheimer disease and normal aging for clinical trials. Archives of neurology. 2004; 61:59-66.

24. Kensinger EA, Brierley B, Medford N, Growdon JH and Corkin S. Effects of normal aging and Alzheimer's disease on emotional memory. Emotion (Washington, DC). 2002; 2:118-134.

25. Grady CL, Furey ML, Pietrini P, Horwitz B and Rapoport SI. Altered brain functional connectivity and impaired short-term memory in Alzheimer's disease. Brain. 2001; 124:739-756.

26. Levine ZA, Larini L, LaPointe NE, Feinstein SC and Shea J-E. Regulation and aggregation of intrinsically disordered peptides. Proceedings of the National Academy of Sciences of the United States of America. 2015; 112:2758-2763.

27. Schneider JA, Arvanitakis Z, Leurgans SE and Bennett DA. The neuropathology of probable Alzheimer disease and mild cognitive impairment. Ann Neurol. 2009; 66:200-208.

28. Bennett DA, Wilson RS, Schneider JA, Evans DA, Aggarwal NT, Arnold SE, Cochran EJ, Berry-Kravis E and Bienias JL. Apolipoprotein E epsilon4 allele, AD pathology, and the clinical expression of Alzheimer's disease. Neurology. 2003; 60:246-252.

29. Barnes LL, Schneider JA, Boyle PA, Bienias JL and Bennett DA. Memory complaints are related to Alzheimer disease pathology in older persons. Neurology. 2006; 67:1581-1585.

30. Hensley K, Barnes LL, Christov A, Tangney C, Honer WG, Schneider JA, Bennett DA and Morris MC. Analysis of postmortem ventricular cerebrospinal fluid from patients with and without dementia indicates association of vitamin E with neuritic plaques and specific measures of cognitive performance. J Alzheimers Dis. 2011; 24:767-774.

31. Bell KF, Ducatenzeiler A, Ribeiro-da-Silva A, Duff K, Bennett DA and Cuello AC. The amyloid pathology progresses in a neurotransmitter-specific manner. Neurobiol Aging. 2006; 27:1644-1657.

32. Bennett DA, Schneider JA, Wilson RS, Bienias JL and Arnold SE. Education modifies the association of amyloid but not tangles with cognitive function. Neurology. 2005; 65:953-955.

33. Hannum G, Guinney J, Zhao L, Zhang L, Hughes G, Sadda S, Klotzle B, Bibikova M, Fan J-B, Gao Y, Deconde R, Chen M, Rajapakse I, et al. Genome-wide Methylation Profiles Reveal Quantitative Views of Human Aging Rates. Mol Cell. 2013; 49:359-367.

34. Weidner CI, Lin Q, Koch CM, Eisele L, Beier F, Ziegler P, Bauerschlag DO, Jockel KH, Erbel R, Muhleisen TW, Zenke M, Brummendorf TH and Wagner W. Aging of blood can be tracked by DNA methylation changes at just three CpG sites. Genome Biol. 2014; 15:R24.

35. Spiers H, Hannon E, Schalkwyk LC, Smith R, Wong CC, O'Donovan MC, Bray NJ and Mill J. Methylomic trajectories across human fetal brain development. Genome research. 2015; 25:338-352.

36. Horvath S, Erhart W, Brosch M, Ammerpohl O, von Schönfels W, Ahrens M, Heits N, Bell JT, Tsai P-C, Spector TD, Deloukas P, Siebert R, Sipos B, et al. Obesity accelerates epigenetic aging of human liver. Proc Natl Acad Sci U S A 2014; 111:15538-15543.

37. Horvath S, Garagnani P, Bacalini M, Pirazzini C, Salvioli S, Gentilini D, DiBlasio A, Giuliani C, Tung S, Vinters H and Franceschi C. Accelerated Epigenetic Aging in Down Syndrome. Aging Cell. 2015; 14:491-495.

38. Horvath S and Ritz BR. Increased epigenetic age and granulocyte counts in the blood of Parkinson's disease patients. Aging (Albany NY). 2015; this issue.

39. Horvath S and Levine AJ. HIV-1 infection accelerates age according to the epigenetic clock. J Infect Dis. 2015; 212:1563-1573.

40. Levine ME, Hosgood HD, Chen B, Absher D, Assimes T and Horvath S. DNA methylation age of blood predicts future onset of lung cancer in the women's health initiative. Aging (Albany NY). 2015; 7:690-700.

41. Horvath S, Mah V, Lu AT, Woo JS, Choi OW, Jasinska AJ, Riancho JA, Tung S, Coles NS, Braun J, Vinters HV and Coles LS. The cerebellum ages slowly according to the epigenetic clock. Aging (Albany NY). 2015; 7:294-306.

42. Walker RF, Liu JS, Peters BA, Ritz BR, Wu T, Ophoff RA and Horvath S. Epigenetic age analysis of children who seem to evade aging. Aging (Albany NY). 2015; 7:334-339.

43. Horvath S, Zhang Y, Langfelder P, Kahn R, Boks M, van Eijk K, van den Berg L and Ophoff RA. Aging effects on DNA methylation modules in human brain and blood tissue. Genome Biol. 2012; 13:R97.

44. Howie B, Fuchsberger C, Stephens M, Marchini J and Abecasis GR. Fast and accurate genotype imputation in genome-wide association studies through pre-phasing. Nat Genet. 2012; 44:955-959.

45. Howie BN, Donnelly P and Marchini J. A Flexible and Accurate Genotype Imputation Method for the Next Generation of Genome-Wide Association Studies. PLoS Genet. 2009; 5:e1000529.

46. O'Connell J, Gurdasani D, Delaneau O, Pirastu N, Ulivi S, Cocca M, Traglia M, Huang J, Huffman JE, Rudan I, McQuillan R, Fraser RM, Campbell H, et al. A General Approach for Haplotype Phasing across the Full Spectrum of Relatedness. PLoS Genet. 2014; 10:e1004234.

47. Horvath S, Pirazzini C, Bacalini MG, Gentilini D, DiBlasio AM, Delledonne M, Mari D, Arosio B, Passarino DMG, DeRango F, D'Aquila P, Giuliani C, Marasco E, Collino S, Descombes P, Garagnani P, Franceschi C. Decreased epigenetic age of PBMCs from Italian semi-supercentenarians and their offspring. Aging (US Albany); 2015; this issue

Increased epigenetic age and granulocyte counts in the blood of Parkinson's disease patients

Steve Horvath[1,2] and Beate R. Ritz[3,4,5]

[1]Department of Human Genetics, David Geffen School of Medicine, University of California Los Angeles, Los Angeles, CA 90095, USA;

[2]Department of Biostatistics, UCLA Fielding School of Public Health, University of California Los Angeles, Los Angeles, CA 90095, USA;

[3]Department of Neurology, UCLA School of Medicine, University of California Los Angeles, Los Angeles, CA 90095, USA;

[4]Department of Epidemiology, UCLA Fielding School of Public Health, University of California Los Angeles, Los Angeles, CA 90095, USA;

[5]Department of Environmental Health, UCLA Fielding School of Public Health, University of California Los Angeles, Los Angeles, CA 90095, USA.

Abstract: It has been a long standing hypothesis that blood tissue of PD Parkinson's disease (PD) patients may exhibit signs of accelerated aging. Here we use DNA methylation based biomarkers of aging ("epigenetic clock") to assess the aging rate of blood in two ethnically distinct case-control data sets. Using n=508 Caucasian and n=84 Hispanic blood samples, we assess a) the intrinsic epigenetic age acceleration of blood (IEAA), which is independent of blood cell counts, and b) the extrinsic epigenetic age acceleration rate of blood (EEAA) which is associated with age dependent changes in blood cell counts. Blood of PD subjects exhibits increased age acceleration according to both IEAA (p=0.019) and EEAA (p=6.1x10^{-3}). We find striking differences in imputed blood cell counts between PD cases and controls. Compared to control subjects, PD subjects contains more granulocytes (p=1.0x10^{-9} in Caucasians, p=0.00066 in Hispanics) but fewer T helper cells (p=1.4x10^{-6} in Caucasians, p=0.0024 in Hispanics) and fewer B cells (p=1.6x10^{-5} in Caucasians, p=4.5x10^{-5} in Hispanics). Overall, this study shows that the epigenetic age of the immune system is significantly increased in PD patients and that granulocytes play a significant role.

INTRODUCTION

The progressive motor and non-motor decline in Parkinson's disease (PD) leads to disability and loss of quality of life. Onset is insidious with some non-motor symptoms occurring years before diagnosis [1]. The extensive loss of dopamine neurons prior to diagnosis makes early interventions the ultimate treatment goal. For this to become reality, development of biomarkers with the potential of early detection and treatment of PD

during a period coined the 'molecular prodrome' is critical [2]. While blood provides an easily accessible tissue, biomarker development based on it has remained an elusive goal. Even though substantial evidence exists that inflammation contributes to the pathogenesis of PD [3], the question remains whether blood tissue also reflects earliest changes in PD such that blood cell counts or immune markers can help predict onset or even become a treatment target. This idea inspired research as early as 1985, when Marttila et al. observed

that PD patients exhibit signs of immune suppression partially resembling those seen in normal aging but being quantitatively exaggerated with a decrease in helper (CD4+) T cells [4].

Until recently relatively few molecular biomarkers of aging have lent themselves for rigorously testing whether PD is associated with accelerated aging in the immune system and blood. Telomere length can be used as a molecular aging marker but its association with PD status remains ambiguous despite considerable research effort. A keyword search for ["telomere" AND "Parkinson's disease"] in Pubmed led to the identification of 10 articles. After eliminating a commentary and a study of mice, we reviewed references [5-12]. Two of these studies did not find an association between telomere length and PD status [5, 8]. Three studies, including the largest study to date [12], found borderline significant (P=0.02) associations in the opposite direction from what would be expected, i.e. counter to the aging hypothesis PD cases had longer telomeres [6, 9, 12]. Here, we answer the challenge to explore these counterintuitive results observed in a methodologically strong study by exploiting an entirely new class of molecular biomarker of aging based on epigenetic data. Several recent studies have proposed to measure the physiological age of tissue samples by combining the DNA methylation levels of multiple dinucleotide markers, known as Cytosine phosphate Guanines or CpGs [13-15]. In particular, the epigenetic clock (based on 353 CpG markers) was developed to measure the age (known as "DNA methylation age" or "epigenetic age") of sorted human cell types (CD4+T cells or neurons), tissues, and organs—including blood, brain, breast, kidney, liver, lung [14], and even prenatal brain samples [16].

The epigenetic clock method - applied to two commercially standardized methylation platforms: the Illumina 450K array and the 27K arrays - is an attractive biomarker of aging because (1) it applies to most human tissues; (2) its accurate measurement of chronological age is unprecedented [14]; (3) it is predictive of all-cause mortality even after adjusting for a variety of known risk factors [17]; (4) it correlates with measures of cognitive and physical fitness in the elderly [18]; and (5) it has already been useful in detecting accelerated aging due to obesity [19], Down syndrome [20], and HIV infection [21]. Further, the epigenetic clock was used to show that age acceleration of blood may predict the future onset of lung cancer [22], the cerebellum ages slowly [23], and 3) that the blood of subjects with a severe developmental disorder ages normally [24]. Despite many diverse applications of the epigenetic clock [16, 25-27], we are not aware of

any study that related epigenetic age acceleration to PD status.

In this large epigenetic study of PD, we show for the first time that measures of epigenetic age acceleration are associated with PD status. Different from typical epigenome wide association studies (EWAS) that interrogate individual CpGs, the current study posits two broad hypotheses: First, that a measure of epigenetic age acceleration is associated with PD status. Second, that (imputed) measures of blood cell types (based on DNA methylation levels) are associated with PD status. To address these hypotheses, we leverage a large and unique community-based case control study described in the following.

RESULTS

Study design and study population

The Parkinson's disease, Environment, and Genes (PEG) case-control study aims to identify environmental risk factors (e.g. neurotoxic pesticide exposures) for Parkinson's disease. The PEG study is a large population-based study of Parkinson's disease of mostly rural and township residents of California's central valley [28]. Cases were identified with the help of local neurologists, clinics, and community outreach and controls were randomly sampled from Medicare lists and residential tax assessor's records. All covariates were ascertained in interviews with subjects.

Every PD patient was evaluated by a UCLA movement disorder specialist. Most subjects were seen multiple times. Blood was drawn early in the disease, on average 1.5 years after PD diagnosis. We only used DNA samples from wave 1 (PEG1).

In our analysis we started out with analyzing all subjects (irrespective of race/ethnicity). Next we focused on specific ethnic strata (Caucasians only or Hispanics only).

DNA methylation data sets

The first blood DNA methylation data set was comprised of 508 Caucasians (non-Hispanic whites) and the second of 84 Hispanics enrolled in the PEG study, respectively. Descriptive information for the data sets we used can be found in Table 1. When we related various demographic and known risk factors to PD status in a marginal analysis, education was associated positively (p=0.0085 in Caucasians, p=0.27 in Hispanics, Table 1) and smoking negatively with PD in this subsample. The first association reflects a

well-known ascertainment bias in epidemiological case-control studies: healthy controls with little incentive to participate in research tend to be more highly educated. For smoking, our finding is consistent with the literature which is reviewed and discussed in [29].

Our marginal analysis also shows that exposure to pesticides (total organophosphate count in residential or occupational settings) is strongly associated with an increased PD risk (p=4x10^{-6} Table 1) consistent with our previous publications [30].

Table 1. Overview of the two DNA methylation data sets

|	Caucasian (Data Set 1)			Hispanic (Data Set 2)		
	P-value	PD	control	P-value	PD	control
Sample size		289	219		46	38
No. Female	0.47	125	102	0.05	14	20
Smoking Status	0.013			0.21		
Smoking: current		15	13		3	4
Smoking: former		120	118		21	6
Smoking: never		154	88		22	8
	P-value	**mean (SE), min, max**	**mean (SE), min, max**	**P-value**	**mean (SE), min, max**	**mean (SE), min, max**
Smoking: total pack years	0.0051	11.4 (1.3),0,175	14.8 (1.6),0,125	0.65	5.7 (2),0,73	7 (2.9),0,39
Age	0.053	71 (0.6),37,91	68 (0.8),35,92	0.60	67.3 (1.6),37,83	65 (2.1),36,86
Year Born	0.14	1932 (0.6),1915,1966	1935 (0.8),1912,1969	0.27	1938 (2),1920,1964	1944 (4),1918,1969
Education: no. of years in school	0.0085	14.1 (0.2),6,30	14.8 (0.2),5,27	0.16	9.6 (0.72),0,20	11.2 (1),1,19
PD Family History	0.16	0.15 (0.021),0,1	0.11 (0.021),0,1	0.30	0.15 (0.05),0,1	0.6 (0.056),0,1
Caffeinated Coffee: lifetime weighted ave. (cup/day)	0.21	1.8 (0.12),0,14	2.2 (0.18),0,19	0.54	1.6 (0.48),0,20	1.3 (0.29),0,4
Organophospate count (residential+occuputation)	2.8x10-8	9 (0.59),0,46	4.9 (0.47),0,41	1.7x10-3	13.3 (1.63),0,37	5.9 (2.4),0,30
Year diagnosed with PD		2001 (0.3),1998,2007			2002 (0.3),1998,2006	
Levodopa Medication status		0.7 (0.03)			0.67 (0.07)	
Levodopa mg/day		350 (16),0,2300			369 (41),0,1020	

Data sets 1 and 2 are comprised of Caucasians (non-Hispanic whites) and Hispanics, respectively. The p-value resulted from relating the respective variables to PD status using a non-parametric group comparison test (Kruskal Wallis test) or Fisher's exact test (for categorical variables).

Accuracy of the epigenetic clock

DNAm age (also referred to as epigenetic age) was calculated as described in [14] from human samples profiled with the Illumina Infinium 450K platform. The epigenetic clock is defined as a prediction method of age based on the DNAm levels of 353 CpGs. Predicted age, referred to as DNAm age, correlates with chronological age in sorted cell types (CD4 T cells, monocytes, B cells, glial cells, neurons), tissues and organs, including: whole blood, brain, breast, kidney, liver, lung, saliva [14]. Mathematical details and software tutorials for the

epigenetic clock can be found in the Additional files of [14]. An online age calculator can be found at our webpage (https://dnamage.genetics.ucla.edu). All of the described epigenetic measures of aging and age acceleration are implemented in our freely available software.

As expected, DNAm age has a strong linear relationship with chronological age (Figure 1). The high accuracy of the epigenetic clock is validated in both data sets in which DNAm age is highly correlated with chronological age (r=0.82 in Caucasians; r=0.81 in Hispanics, Figure 1A-C).
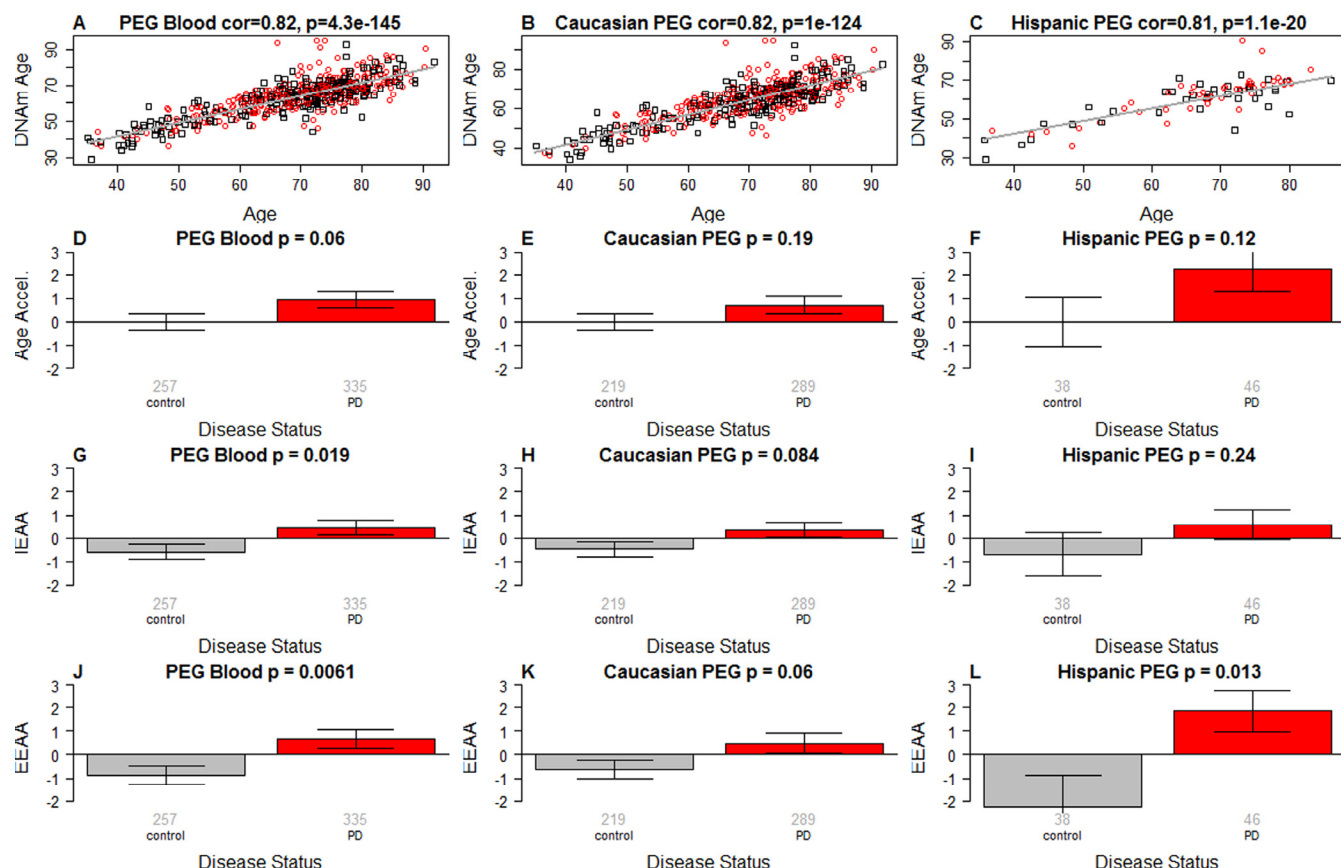

Figure 1. Epigenetic age analysis of PD. (**A-C**) DNA methylation age (y-axis) versus chronological age (x-axis) in (A) all subjects, (**B**) Caucasians only, and (**C**) Hispanics only. Dots corresponds to subjects and are colored by PD disease status (red=PD, black=control). We define three measures of epigenetic age acceleration. (**D-F**) presents results for the "universal" measure of epigenetic age acceleration, which is defined as residual to a regression line through the control samples, i.e. the vertical distance of a point from the line. By definition, the mean age acceleration in controls is zero. (**G-I**) The bar plots relate measures of intrinsic epigenetic age acceleration to PD status. This measure is independent of blood cell counts. The fourth row (panels **J**-L) reports findings for the measure of extrinsic epigenetic age acceleration, which does relate to changes in cell composition. Each bar plot depicts the mean value (y-axis), 1 standard error, and the group size (underneath the bar). The p-value results from a Student T-test.

### Three measures of epigenetic age acceleration

In this article, we consider three measures of epigenetic age acceleration (as detailed in Methods). The first measure, which will be referred to as universal measure of age acceleration (denoted *AgeAccel*) applies to virtually all tissues and cell types (with the exception of sperm) [25]. The other two measures (referred to as intrinsic and extrinsic age acceleration, respectively) only apply to blood. The universal measure *AgeAccel* is defined as the difference between DNAm age value and the value predicted by a spline regression model in controls.

The measure of intrinsic epigenetic age acceleration (IEAA) measures "pure" epigenetic ageing effects in blood that are not confounded by differences in blood cell counts.

The measure of *extrinsic* epigenetic age acceleration (EEAA) aims to measure ageing in immune related components also relates to age related changes in blood cell composition such as the decrease of naive CD8+ T cells and the increase in memory or exhausted CD8+ T cells [31-33]. EEAA is defined on the basis of a weighted average of the epigenetic age measure from Hannum et al (2013) [13] and three blood cell types that are known to change with age: naive (CD45RA+CCR7+) cytotoxic T cells, exhausted (CD28-CD45RA-) cytotoxic T cells, and plasma B cells. By definition, EEAA has a positive correlation with the amount of exhausted CD8 T cells and plasma blast cells and a negative correlation with the amount of naive CD8+ T cells. Blood cell counts were estimated based on DNA methylation data as described in the section entitled "Estimating blood cell counts based on DNA methylation levels".
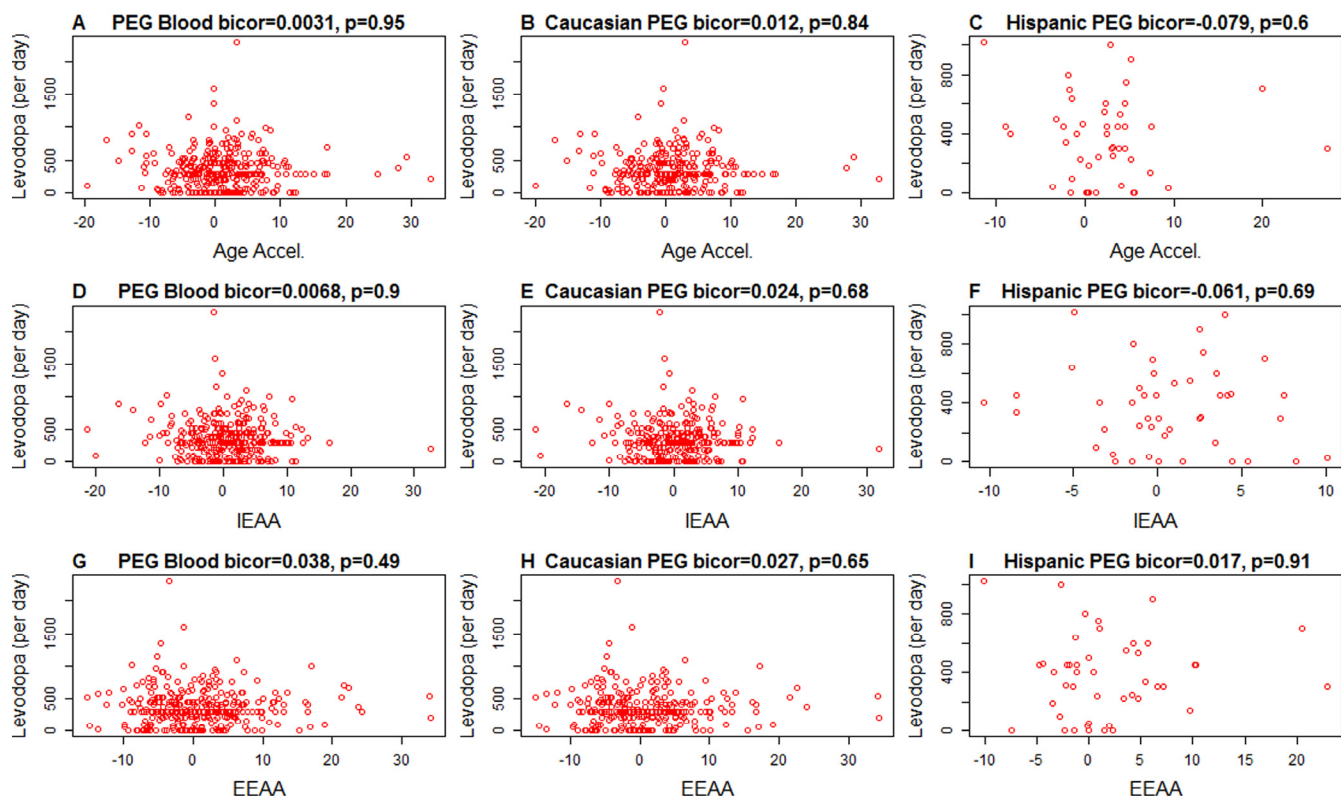
Figure 2. Levodopa medication (x-axis) versus epigenetic age acceleration in PD subjects. Each scatter plot depicts the amount of levodopa medication (milligram per day) versus (**A,B,C**) universal epigenetic age acceleration, (**D,E,F**) intrinsic epigenetic age acceleration (**G,H,I**), extrinsic epigenetic age acceleration. The first, second, and third column correspond to all subjects, Caucasians only, and Hispanics only, respectively. Each dot (PD patient) is colored in red for the sake of consistency with Figure 1. The heading of each plot reports a robust correlation coefficient (biweight midcorrelation and a corresponding p-value).
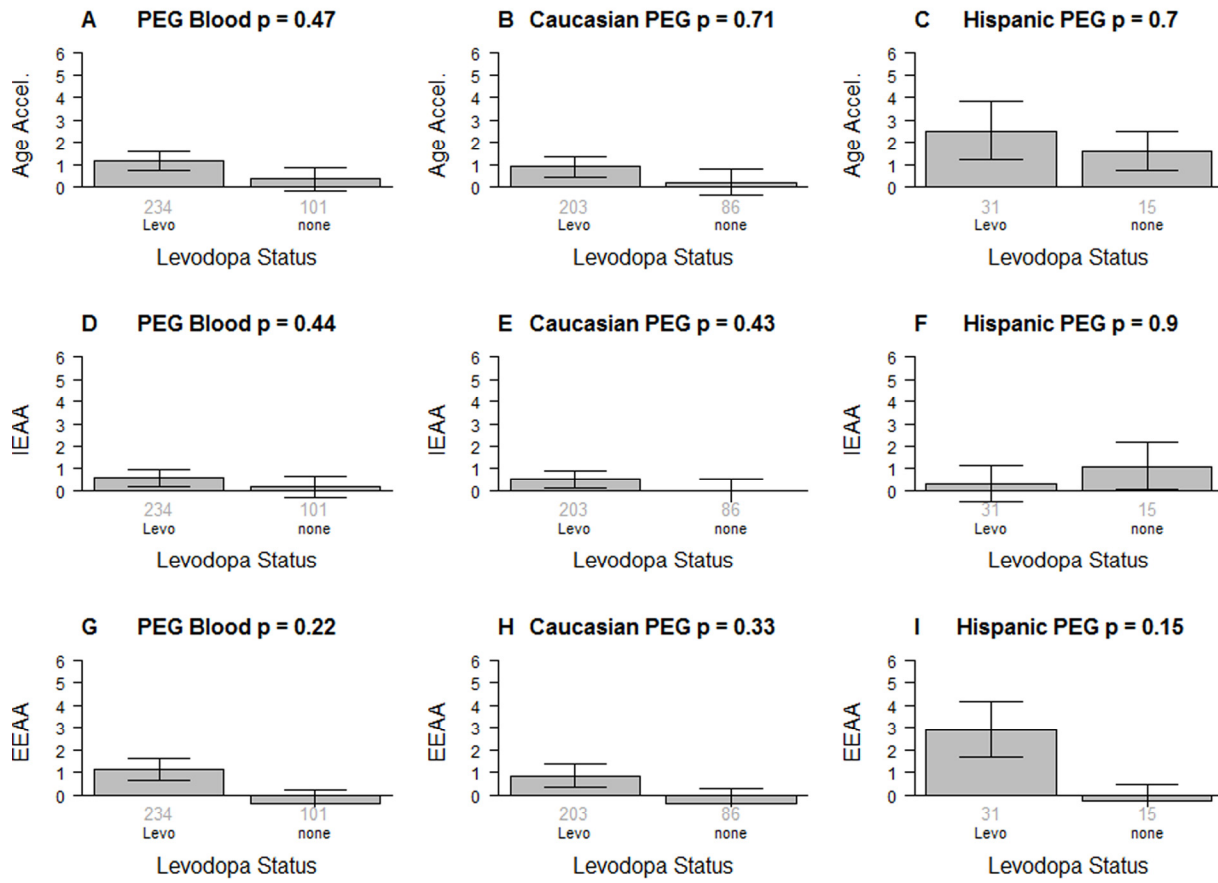
Figure 3. Levodopa medication status versus epigenetic age acceleration in PD patients. The first, second, and third column correspond to all subjects, Caucasians only, and Hispanics only, respectively. Levodopa medication status versus (**A,B,C**) universal epigenetic age acceleration, (**D,E,F**) intrinsic epigenetic age acceleration (**G,H,I**), extrinsic epigenetic age acceleration. Each bar plot depicts the mean value (y-axis), 1 standard error, and the group size (underneath the bar). The p-value results from a non-parametric group comparison test (Kruskal Wallis).

The three different measures of epigenetic age acceleration are not independent of each other. The universal measure AgeAccel is correlated with IEAA (r=0.90 in Caucasians and r=0.77 in Hispanics) and with EEAA (r=0.55 in Caucasians and r=0.74 in Hispanics). IEAA is also correlated with EEAA (r=0.41 in Caucasians and again r=0.41 in Hispanics). By construction, our three measures of epigenetic age acceleration are uncorrelated (r=0) with chronological age at the time of blood draw.

PD is associated with intrinsic and extrinsic epigenetic age acceleration

PD status has a (marginally) significant relationship with all 3 measures of age acceleration: p=0.06 for the universal measure of age acceleration (Figure 1A-C),

p=0.019 for IEAA (Figure 1G-I), and p=0.0061 for EEAA (Figure 1J-L).

It is unlikely that Levodopa medication explains the increased epigenetic age acceleration since we find no significant association between the amount of Levodopa medication and any of the measures of age acceleration in PD patients (Figure 2). These results were corroborated in a second analysis in which we related medication status (binary grouping variable) to the measures of epigenetic age acceleration in PD patients (Figure 3) and found no associations.

None of the measures of epigenetic age acceleration were significantly associated with smoking status, pesticide exposure, or family history of PD; however, sex had a significant association: compared to men,

women have a low EEAA (p-value=2.9×10^{-6} in Caucasians and p=0.016 in Hispanics) and a low IEAA (p=0.0050 in Caucasians, p=0.35 in Hispanics). By study design, sex was not associated with PD status in Caucasians (p=0.45) but there was a marginally significant association in Hispanics (p=0.04). Family history of PD was not predictive of PD status.

In a multivariate logistic regression analysis with PD status as the outcome we find that AgeAccel (p=0.037) remains a significant covariate even after adjusting for chronological age (at the time of blood draw), blood cell counts, pesticide exposure (organophosphate), smoking (cumulative pack years), education (number of years in school), coffee consumption (life time measured as a weighted average cup per day), and ethnicity. In an analogous model, IEAA is only marginally significant (p=0.084, Table 2). EEAA is significantly associated with PD status (p=0.031, Table 2) after adjusting for chronological age, pesticide exposure (organophosphate), smoking (cumulative pack years), education (number of years in school), coffee consumption (life time measured as a weighted average cup per day), and ethnicity.

To estimate the actual amount of age acceleration, we regressed DNAm age on disease status, age, granulocytes, smoking, ethnicity, and sex. According to this multivariate regression model, the blood of PD patients is 1.5 years older than that of age matched controls.

PD patients have more granulocytes but fewer helper T cells and B cells than controls

We find striking differences in blood cell composition between PD cases and controls (Figure 4). Compared to control samples, PD patients have more granulocytes (p=1.0×10^{-9} in Caucasians, p=0.00066 in Hispanics Figure 4O,P) and plasma cells (activated B cells) (p=0.00065 in Caucasians Figure 4S) but fewer helper (CD4+) T cells (p=1.4×10^{-6} in Caucasians, p=0.0024 in Hispanics, Figure 4G,H), fewer naïve CD4+ T cells (p=0.0074 in Caucasians, p=0.13 in Hispanics Figure 4I,J), fewer B cells (p=1.6×10^{-5} in Caucasians, p=4.5×10^{-5} in Hispanics Figure 4Q,R), and fewer cytotoxic (CD8+) T cells (p=0.0017 in Caucasians, p=0.072 in Hispanics Figure 4A,B).

Table 2. Logistic model that regresses PD status on covariates.

Logistic model. Outcome= PD	Measure= AgeAccel			Measure= IEAA			Measure =EEAA		
Covariates	Coef	SE	P-value	Coef	SE	P-value	Coef	SE	P-value
Age	0.016	0.0085	0.061	0.015	0.0085	0.071	0.023	0.008	0.004
Measure of Age Acceleration	0.036	0.017	0.037	0.031	0.018	0.084	0.031	0.014	0.031
Granulocyte	3.5	1.6	0.027	2.7	1.5	0.07			
CD4+T cell	-3.8	2.3	0.11	-4.9	2.3	0.029			
CD8+T cell	-1.6	3	0.59	-1.3	3	0.67			
Organo phosphate exposure	0.054	0.012	4E-6	0.055	0.012	3.7E-6	0.059	0.012	4E-7
Smoking (total pack years)	-0.0081	0.0043	0.063	-0.0082	0.0043	0.06	-0.0077	0.004	0.067
Number of years in school	-0.058	0.028	0.036	-0.058	0.028	0.035	-0.049	0.027	0.064
LifetimeCoffee (ave cup/day)	-0.035	0.041	0.4	-0.034	0.041	0.41	-0.037	0.04	0.36
Ethnicity(Hispanic)	0.32	0.35	0.36	0.31	0.35	0.37	0.3	0.34	0.37
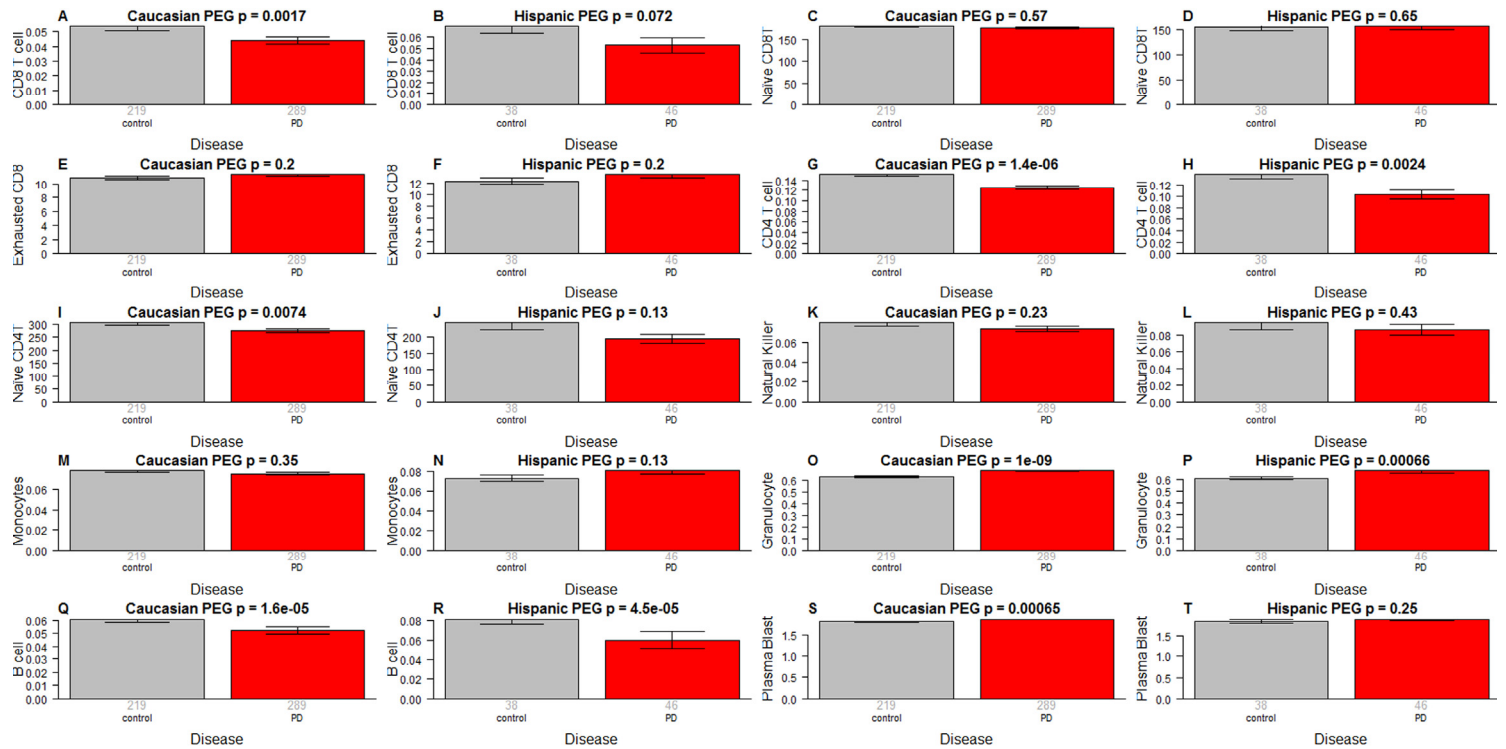
Figure 4. Blood cell counts versus PD status. As indicated in the heading of each panel, the panels alternate between the two data sets. PD status (x-axis) versus (**A,B**) proportion of cytotoxic CD8+ T cells, (**C,D**) naïve CD8+ T cell count, (**E,F**) percentage of exhausted CD8+ T cells (defined as CD8+CD28-CD45RA-), (**G,H**) proportion of helper CD4+ T cells, (**I,J**) naïve CD4+ T cell count, (**K,L**) proportion of natural killer cells, (**M,N**) proportion of monocytes, (**O,P**) granulocytes, (**Q,R**) B cells, (**S,T**) plasma blasts (activated B cells). The abundance measures of blood cell counts were estimated based on DNA methylation levels using the epigenetic clock software. The y-axis of (**E,F**) reports a percentage, that of (**C,D,I,J**) a cell counts but it is best to interpret these measures as ordinal abundance measures. The y-axis of the other panels reports estimated proportions based on the Houseman method [45]. Each bar plot depicts the mean value (y-axis), 1 standard error, and the group size (underneath the bar). The p-value results from a non-parametric group comparison test (Kruskal Wallis).

A multivariate logistic regression analysis shows that granulocyte count remains a significant predictor of PD status (p=0.027, Table 2) even after adjusting for other covariates. We did not observe significant association between PD status and the amount of naïve CD8+ T cells (Figure 4C,D), exhausted CD8+ T cells (Figure 4E,F), natural killer cells (Figure 4K,L) or monocytes (Figure 4M,N).

It is unlikely that medications explain the difference in blood cell counts because both medication status and amount of medication have no more than a weak association with blood cell counts in PD subjects (Figure 5): when relating the amount of Levodopa (mg per day) to blood cell counts in PD subjects, we only found a weak marginally significant correlation with CD4+ T cells (r=-0.14, p=0.017 in Caucasians, Figure 5G).

We only observed relatively weak associations between Levodopa medication status (binary) and blood cell counts (Figure 6). In Caucasian PD patients, we found that medicated patients have fewer CD4+ T cells (p=0.0018 Figure 6G), granulocytes (p=0.025 Figure 6O), and B cells (p=0.012 Figure 6Q) but more exhausted CD8+ T cells (p=0.019 Figure 6E). In Hispanic PD patients, we could not detect a significant association between medication status and blood cell counts, which might reflect the small number (n=15) of un-medicated PD patients in this group.

DISCUSSION

We and others have shown that epigenetic biomarkers of aging based on genome-wide DNA methylation levels are highly robust and reproducible (see also Figure 1A,B) [13-15, 17, 19]. We use these biomarkers
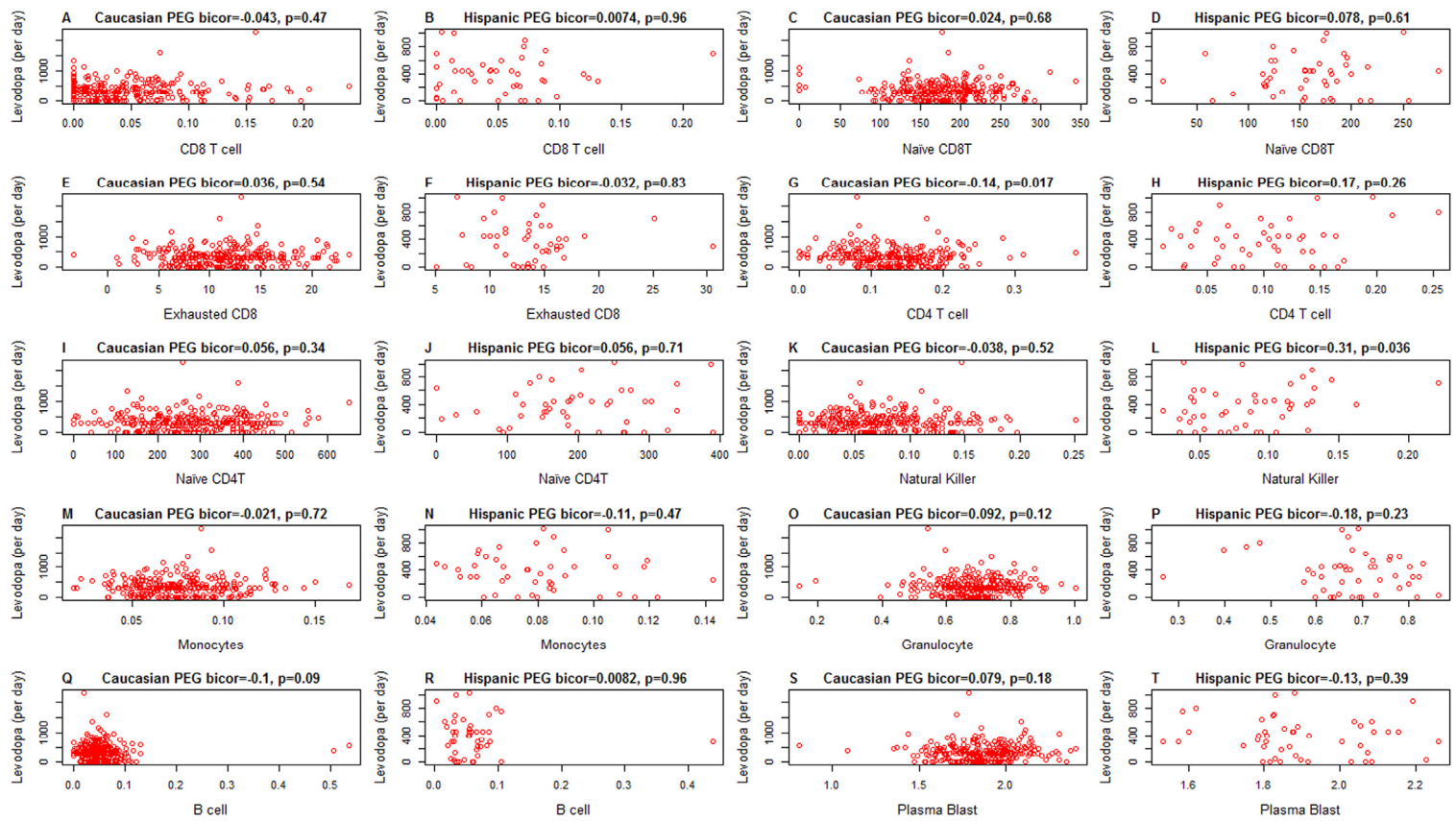
Figure 5. Amount of medication (x-axis) versus epigenetic age acceleration in PD subjects. As indicated in the heading of each panel, the panels alternate between the two data sets. PD status (x-axis) versus (**A,B**) proportion of CD8+ T cells, (**C,D**) naïve CD8+ T cell count, (**E,F**) exhausted CD4+T cell counts (defined as CD8+CD28-CD45RA-), (**G,H**) proportion of CD4+ T cells, (**I,J**) naïve CD4 T cell count, (**K,L**) proportion of natural killer cells, (**M,N**) proportion of monocytes, (**O,P**) granulocytes, (**Q,R**) B cells, (**S,T**) plasma blasts (activated B cells). All cell types were estimated based on DNA methylation levels as described in Methods. The heading of each plot reports a robust correlation coefficient (biweight midcorrelation and a corresponding p-value).

of aging to explore the contributions of aging in a large community-based study of PD. Ours is the first data substantiating the longstanding hypothesis regarding accelerated aging effects in PD using epigenetic biomarkers of aging. PD status has a significant relationship with all 3 measures of age acceleration but the strongest associations can be observed for the extrinsic measure EEAA, which also keeps track of age related changes in blood cell composition.

However, the observed accelerated aging effects do not simply reflect changes in blood cell composition as can be seen from the fact that PD subjects also exhibit increased intrinsic epigenetic aging rates.

Our study demonstrates an unexpectedly strong association between granulocytes and PD status. Several previous studies evaluated blood cell counts in

PD subjects using flow cytometric method [34-38]. The most recent study including the largest number of patients yet (88 PD cases and 77 age-gender matched controls)[38] reported reduced numbers of T helper and B lymphocytes in Parkinson's disease. Our study corroborates these findings for T helper ($p=1.4\times10^{-6}$) and B cells ($p=1.6\times10^{-5}$ Figure 4Q) however, granulocytes exhibited a far more significant association with PD status ($p=1.0\times10^{-9}$ Figure 4O) in our population. Our study does not allow us to identify the type of granulocytes (neutrophil, eosinophil, or basophil) with the strongest effect. Yet, given the abundance of neutrophils (~60% of all blood cells compared with 0.5-2.5% for eosinophils and basophils) we suspect that they are responsible for the signal we saw in blood. An increased neutrophil/lymphocyte ratio has been observed in PD subjects [39] and differential neutrophil infiltration has been shown to contribute to

regional differences with brain inflammation favoring the substantia nigra pars compacta over the cortex [40]. We acknowledge the following limitations. First, the one-time only blood sampling protocol early in disease does not allow us to establish temporality of cause and effect. We hypothesize that accelerated aging of the immune system and/or altered blood cell counts (including neutrophils) precede the onset of motor and cognitive symptoms in PD but future studies are needed to determine whether these blood based biomarkers are prognostic of incident PD.

Second, we necessarily focused only on blood tissue. Future studies should evaluate whether accelerated epigenetic aging effects can also be found in other tissues (notably brain tissue).

Finally, we did not relate individual CpGs to PD status since this is beyond the scope of this article which

focuses on epigenetic aging effects and blood cell counts. We refer the reader to future publications from our group and other DNA methylation studies of Parkinson disease (PD) and related disorders [41-43]. Our study also has strengths including a novel data set for two distinct ethnic populations, a large sample size (total n=592), powerful epigenetic biomarkers of aging, an unprecedented breadth of blood cell counts, a community (population)-based design, and extensive clinical evaluations by movement disorder specialists to establish PD diagnoses.

Increased levels of epigenetic age acceleration or blood cell counts are not specific to PD but our results may inform the future development of DNA methylation based biomarkers of PD. Overall, our results support the notion that neuroinflammation, which leads to brain cell death and PD disease progression, is fueled by activated glial cells communicating with peripheral immune cells.
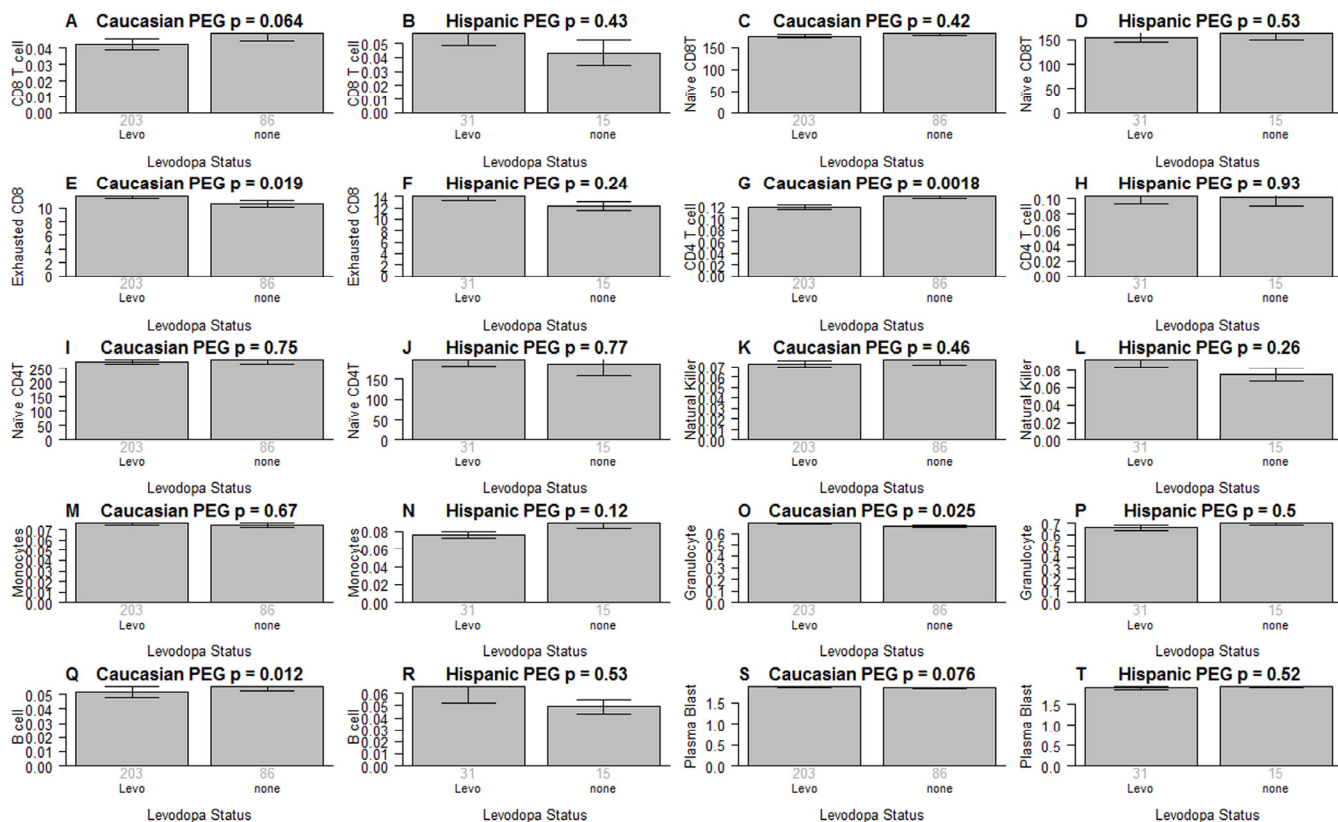
Figure 6. Medication status versus blood cell counts in PD patients. As indicated in the heading of each panel, the panels alternate between the two data sets. Levodopa medication status (x-axis) versus (**A,B**) proportion of CD8+ T cells, (**C,D**) naïve CD8+ T cell count, (**E,F**) exhausted CD+T cell counts (defined as CD8+CD28-CD45RA-), (**G,H**) proportion of CD4+ T cells, (**I,J**) naïve CD4+ T cell count, (**K,L**) proportion of natural killer cells, (**M,N**) proportion of monocytes, (**O,P**) granulocytes, (**Q,R**) B cells, (**S,T**) plasma blasts (activated B cells). All cell types were estimated based on DNA methylation levels as described in Methods. Each bar plot depicts the mean value (y-axis), 1 standard error, and the group size (underneath the bar). The p-value results from a non-parametric group comparison test (Kruskal Wallis).

METHODS

Ethics review and IRB. Informed consent was obtained from all subjects. This study was reviewed by the UCLA institutional review board (IRB#13-000671 and IRB#14-000061).

Preprocessing of Illumina Infinium 450K arrays. In brief, bisulfite conversion using the Zymo EZ DNA Methylation Kit (ZymoResearch, Orange, CA, USA) as well as subsequent hybridization of the HumanMethylation450k Bead Chip (Illumina, SanDiego, CA), and scanning (iScan, Illumina) were performed according to the manufacturers protocols by applying standard settings. DNA methylation levels (β values) were determined by calculating the ratio of intensities between methylated (signal A) and un-methylated (signal B) sites. Thus, β values range from 0 (completely un-methylated) to 1 (completely methylated).

Measures of epigenetic age acceleration. The name of our universal measure of age acceleration (*AgeAccel*) reflects that it applies to virtually all sources of human DNA (with the exception of sperm). Here we defined it as follows. First, we regressed DNAm age on chronological age in controls. Next, we used the resulting model to predict the DNAm age of each subject. Next the universal measure was defined as the difference between the observed measure of DNAm age and the predicted value. Thus, a high positive value for *AgeAccel* indicates that the observed DNAm age is higher than that predicted based on controls. *AgeAccel* has a relatively weak correlation with blood cell counts [21] but it still relates to blood cell counts. To subtract out the effect of blood cell counts, we find it useful to define a measure of intrinsic epigenetic age acceleration (IEAA) which measures "pure" epigenetic ageing effects that are not confounded by differences in blood cell counts. It is defined as the residual resulting from a multivariate regression model of DNAm age on chronological age and various blood immune cell counts (naive CD8+ T cells, exhausted CD8+ T cells, plasma B cells, CD4+ T cells, natural killer cells, monocytes, and granulocytes).

The measure of *extrinsic* epigenetic age acceleration (EEAA) aims to measure epigenetic ageing in immune related components. EEAA is defined using the following three steps. First, we calculated the epigenetic age measure from Hannum et al (2013) [13] based on 71 CpGs. The resulting age estimate is correlated with certain blood cell types [17]. Second, we increased the contribution of blood cell types to the age estimate by forming a weighted average of the Hannum estimate with 3 cell types that are known to change with age: naive (CD45RA+CCR7+) cytotoxic T cells, exhausted (CD28-CD45RA-) cytotoxic T cells, and plasma B cells using the approach of [44]. The resulting measure of blood age is referred to as BioAge4 in our epigenetic clock software. Third, we defined a measure of age acceleration (EEAA) as the residual resulting from a univariate model regressing BioAge4 on chronological age. By definition, our measure of EEAA has a positive correlation with the amount of exhausted CD8+ T cells and plasma blast cells and a negative correlation with the amount of naive CD8+ T cells. Blood cell counts were estimated based on DNA methylation data as described in the section entitled "Estimating blood cell counts based on DNA methylation levels". By construction, EEAA tracks both age related changes in blood cell composition and intrinsic epigenetic changes. By definition, none of our three measures of epigenetic age acceleration are correlated with the chronological age.

Estimating blood cell counts based on DNA methylation levels. We estimate blood cell proportions using two different software tools. Houseman's estimation method [45], which is based on DNA methylation signatures from purified leukocyte samples, was used to estimate the proportions of CD8+ T cells, CD4+ T, natural killer, B cells, and granulocytes. Granulocytes are also known as polymorphonuclear leukocytes. The advanced analysis option of the epigenetic clock software [14, 21] was used to estimate the percentage of exhausted CD8+ T cells (defined as CD28-CD45RA-) and the number (count) of naïve CD8+ T cells (defined as (CD45RA+CCR7+).

Funding

Conflict of interest statement

The authors declare no conflict of interest.

REFERENCES

1. Schrag A, Horsfall L, Walters K, Noyce A and Petersen I. Prediagnostic presentations of Parkinson's disease in primary care: a case-control study. The Lancet Neurology. 14:57-64.
2. Schapira AH, Olanow CW, Greenamyre JT and Bezard E. Slowing of neurodegeneration in Parkinson's disease and Huntington's disease: future therapeutic perspectives. Lancet. 2014; 384:545-555.
3. Hirsch EC and Hunot S. Neuroinflammation in Parkinson's disease: a target for neuroprotection? Lancet Neurol. 2009; 8:382-397.

4. Marttila RJ, Eskola J, Soppi E and Rinne UK. Immune functions in Parkinson's disease lymphocyte subsets, concanavalin A-induced suppressor cell activity and in vitro immunoglobulin production. J Neurol Sci. 1985; 69:121-131.

5. Guan JZ, Maeda T, Sugano M, Oyama J, Higuchi Y, Suzuki T and Makino N. A percentage analysis of the telomere length in Parkinson's disease patients. J Gerontol A Biol Sci Med Sci. 2008; 63:467-473.

6. Wang H, Chen H, Gao X, McGrath M, Deer D, De Vivo I, Schwarzschild MA and Ascherio A. Telomere length and risk of Parkinson's disease. Mov Disord. 2008; 23:302-305.

7. Maeda T, Guan JZ, Oyama J, Higuchi Y and Makino N. Aging-associated alteration of subtelomeric methylation in Parkinson's disease. J Gerontol A Biol Sci Med Sci. 2009; 64:949-955.

8. Eerola J, Kananen L, Manninen K, Hellstrom O, Tienari PJ and Hovatta I. No evidence for shorter leukocyte telomere length in Parkinson's disease patients. J Gerontol A Biol Sci Med Sci. 2010; 65:1181-1184.

9. Hudson G, Faini D, Stutt A, Eccles M, Robinson L, Burn DJ and Chinnery PF. No evidence of substantia nigra telomere shortening in Parkinson's disease. Neurobiol Aging. 2011; 32:2107.e2103-2105.

10. Watfa G, Dragonas C, Brosche T, Dittrich R, Sieber CC, Alecu C, Benetos A and Nzietchueng R. Study of telomere length and different markers of oxidative stress in patients with Parkinson's disease. J Nutr Health Aging. 2011; 15:277-281.

11. Maeda T, Guan JZ, Koyanagi M, Higuchi Y and Makino N. Aging-associated alteration of telomere length and subtelomeric status in female patients with Parkinson's disease. J Neurogenet. 2012; 26:245-251.

12. Schurks M, Buring J, Dushkes R, Gaziano JM, Zee RY and Kurth T. Telomere length and Parkinson's disease in men: a nested case-control study. Eur J Neurol. 2014; 21:93-99.

13. Hannum G, Guinney J, Zhao L, Zhang L, Hughes G, Sadda S, Klotzle B, Bibikova M, Fan J-B and Gao Y. Genome-wide methylation profiles reveal quantitative views of human aging rates. Molecular cell. 2013; 49:359-367.

14. Horvath S. DNA methylation age of human tissues and cell types. Genome Biol. 2013; 14(R115).

15. Weidner CI, Lin Q, Koch CM, Eisele L, Beier F, Ziegler P, Bauerschlag DO, Jockel KH, Erbel R, Muhleisen TW, Zenke M, Brummendorf TH and Wagner W. Aging of blood can be tracked by DNA methylation changes at just three CpG sites. Genome Biol. 2014; 15:R24.

16. Spiers H, Hannon E, Schalkwyk LC, Smith R, Wong CC, O'Donovan MC, Bray NJ and Mill J. Methylomic trajectories across human fetal brain development. Genome research. 2015; 25:338-352.

17. Marioni R, Shah S, McRae A, Chen B, Colicino E, Harris S, Gibson J, Henders A, Redmond P, Cox S, Pattie A, Corley J, Murphy L, et al. DNA methylation age of blood predicts all-cause mortality in later life. Genome Biol. 2015; 16:25.

18. Marioni RE, Shah S, McRae AF, Ritchie SJ, Muniz-Terrera G, Harris SE, Gibson J, Redmond P, Cox SR and Pattie A. The epigenetic clock is correlated with physical and cognitive fitness in the Lothian Birth Cohort 1936. International journal of epidemiology. 2015:dyu277.

19. Horvath S, Erhart W, Brosch M, Ammerpohl O, von Schönfels W, Ahrens M, Heits N, Bell JT, Tsai P-C, Spector TD, Deloukas P, Siebert R, Sipos B, et al. Obesity accelerates epigenetic aging of human liver. Proc Natl Acad Sci U S A 2014; 111:15538-15543.

20. Horvath S, Garagnani P, Bacalini M, Pirazzini C, Salvioli S, Gentilini D, DiBlasio A, Giuliani C, Tung S, Vinters H and Franceschi C. Accelerated Epigenetic Aging in Down Syndrome. Aging Cell. 2015; 14:491-495.

21. Horvath S and Levine AJ. HIV-1 infection accelerates age according to the epigenetic clock. J Infect Dis. 2015; 212:1563-1573.

22. Levine ME, Hosgood HD, Chen B, Absher D, Assimes T and Horvath S. DNA methylation age of blood predicts future onset of lung cancer in the women's health initiative. Aging (Albany NY). 2015; 7:690-700.

23. Horvath S, Mah V, Lu AT, Woo JS, Choi OW, Jasinska AJ, Riancho JA, Tung S, Coles NS, Braun J, Vinters HV and Coles LS. The cerebellum ages slowly according to the epigenetic clock. Aging (Albany NY). 2015; 7:294-306.

24. Walker RF, Liu JS, Peters BA, Ritz BR, Wu T, Ophoff RA and Horvath S. Epigenetic age analysis of children who seem to evade aging. Aging (Albany NY). 2015; 7:334-339.

25. Lin Q and Wagner W. Epigenetic Aging Signatures Are Coherently Modified in Cancer. PLoS Genet. 2015; 11:e1005334.

26. Kananen L, Nevalainen T, Jylhävä J, Marttila S, Hervonen A, Jylhä M and Hurme M. Cytomegalovirus infection accelerates epigenetic aging. Experimental Gerontology. 2015; 72:227-229.

27. Miller GE, Yu T, Chen E and Brody GH. Self-control forecasts better psychosocial outcomes but faster epigenetic aging in low-SES youth. Proceedings of the National Academy of Sciences. 2015; 112:10325-10330.

28. Costello S, Cockburn M, Bronstein J, Zhang X and Ritz B. Parkinson's Disease and Residential Exposure to Maneb and Paraquat From Agricultural Applications in the Central Valley of California. American Journal of Epidemiology. 2009; 169:919-926.

29. Ritz B, Lee PC, Lassen CF and Arah OA. Parkinson disease and smoking revisited: ease of quitting is an early sign of the disease. Neurology. 2014; 83:1396-1402.

30. Wang A, Cockburn M, Ly TT, Bronstein JM and Ritz B. The association between ambient exposure to organophosphates and Parkinson's disease risk. Occup Environ Med. 2014; 71:275-281.

31. Fagnoni FF, Vescovini R, Mazzola M, Bologna G, Nigro E, Lavagetto G, Franceschi C, Passeri M and Sansoni P. Expansion of cytotoxic CD8+ CD28- T cells in healthy ageing people, including centenarians. Immunology. 1996; 88:501-507.

32. Fagnoni FF, Vescovini R, Passeri G, Bologna G, Pedrazzoni M, Lavagetto G, Casti A, Franceschi C, Passeri M and Sansoni P. Shortage of circulating naive CD8+ T cells provides new insights on immunodeficiency in aging. Blood. 2000; 95:2860-2868.

33. Gruver AL, Hudson LL and Sempowski GD. Immunosenescence of ageing. The Journal of Pathology. 2007; 211:144-156.

34. Bas J, Calopa M, Mestre M, Mollevi DG, Cutillas B, Ambrosio S and Buendia E. Lymphocyte populations in Parkinson's disease and in rat models of parkinsonism. J Neuroimmunol. 2001; 113:146-152.

35. Calopa M, Bas J, Callen A and Mestre M. Apoptosis of peripheral blood lymphocytes in Parkinson patients. Neurobiol Dis. 2010; 38:1-7.

36. Niwa F, Kuriyama N, Nakagawa M and Imanishi J. Effects of peripheral lymphocyte subpopulations and the clinical correlation with Parkinson's disease. Geriatr Gerontol Int. 2012; 12:102-107.

37. Saunders JA, Estes KA, Kosloski LM, Allen HE, Dempsey KM, Torres-Russotto DR, Meza JL, Santamaria PM, Bertoni JM, Murman DL, Ali HH, Standaert DG, Mosley RL, et al. CD4+ regulatory and effector/memory T cell subsets profile motor dysfunction in Parkinson's disease. Journal of neuroimmune pharmacology : the official journal of the Society on NeuroImmune Pharmacology. 2012; 7:927-938.

38. Stevens CH, Rowe D, Morel-Kopp MC, Orr C, Russell T, Ranola M, Ward C and Halliday GM. Reduced T helper and B lymphocytes in Parkinson's disease. J Neuroimmunol. 2012; 252:95-99.

39. Akil E, Bulut A, Kaplan I, Ozdemir HH, Arslan D and Aluclu MU. The increase of carcinoembryonic antigen (CEA), high-sensitivity C-reactive protein, and neutrophil/lymphocyte ratio in Parkinson's disease. Neurol Sci. 2015; 36:423-428.

40. Ji KA, Eu MY, Kang SH, Gwag BJ, Jou I and Joe EH. Differential neutrophil infiltration contributes to regional differences in brain inflammation in the substantia nigra pars compacta and cortex. Glia. 2008; 56:1039-1047.

41. Jowaed A, Schmitt I, Kaut O and Wüllner U. Methylation Regulates Alpha-Synuclein Expression and Is Decreased in Parkinson's Disease Patients' Brains. The Journal of Neuroscience. 2010; 30:6355-6359.

42. Matsumoto L, Takuma H, Tamaoka A, Kurisaki H, Date H, Tsuji S and Iwata A. CpG Demethylation Enhances Alpha-Synuclein Expression and Affects the Pathogenesis of Parkinson's Disease. PLoS ONE. 2010; 5:e15522.

43. Desplats P, Spencer B, Coffee E, Patel P, Michael S, Patrick C, Adame A, Rockenstein E and Masliah E. α-Synuclein Sequesters Dnmt1 from the Nucleus. Journal of Biological Chemistry. 2011; 286:9031-9037.

44. Klemera P and Doubal S. A new approach to the concept and computation of biological age. Mech Ageing Dev. 2006; 127:240-248.

45. Houseman E, Accomando W, Koestler D, Christensen B, Marsit C, Nelson H, Wiencke J and Kelsey K. DNA methylation arrays as surrogate measures of cell mixture distribution. BMC Bioinformatics. 2012; 13:86.

Decreased epigenetic age of PBMCs from Italian semi-supercentenarians and their offspring

Steve Horvath[1,2*], Chiara Pirazzini[3,4*], Maria Giulia Bacalini[3,4,5], Davide Gentilini[6], Anna Maria Di Blasio[6], Massimo Delledonne[5,7], Daniela Mari[8,9], Beatrice Arosio[8,9], Daniela Monti[10], Giuseppe Passarino[11], Francesco De Rango[11], Patrizia D'Aquila[11], Cristina Giuliani[12], Elena Marasco[3,4], Sebastiano Collino[13], Patrick Descombes[14], Paolo Garagnani[3,4,15,§], and Claudio Franceschi[3,4,16,17,§]

[1]Human Genetics, David Geffen School of Medicine, University of California Los Angeles, Los Angeles, CA 90095, USA;

[2]Biostatistics, School of Public Health, University of California Los Angeles, Los Angeles, CA 90095, USA;

[3]Department of Experimental, Diagnostic and Specialty Medicine, University of Bologna, 40126 Bologna, Italy;

[4]Interdepartmental Center "L. Galvani", University of Bologna, 40126 Bologna, Italy;

[5]Personal Genomics S.r.l., 37134 Verona, Italy;

[6]Istituto Auxologico Italiano IRCCS, Cusano Milanino, 20095 Milan, Italy;

[7]Functional Genomics Center, Department of Biotechnology, University of Verona, 37134 Verona, Italy;

[8]Geriatric Unit, Department of Medical Sciences and Community Health, University of Milan, 20122 Milan, Italy;

[9]Geriatric Unit, Fondazione IRCCS Ca' Granda, Ospedale Maggiore Policlinico, 20122 Milan, Italy;

[10]Department of Experimental and Clinical Biomedical Sciences, University of Florence, 50139 Florence, Italy;

[11]Department of Cell Biology, University of Calabria, 87036 Rende, Italy;

[12]Department of Biological, Geological and Environmental Sciences, Laboratory of Molecular Anthropology and Centre for Genome Biology, University of Bologna, 40126 Bologna, Italy;

[13]Molecular Biomarkers, Nestlé Institute of Health Sciences SA, EPFL Innovation Park, 1015, Lausanne, Switzerland;

[14]Functional Genomics, Nestlé Institute of Health Sciences SA, EPFL Innovation Park, 1015, Lausanne, Switzerland;

[15] CRBA, Center for Applied Biomedical Research, St. Orsola-Malpighi University Hospital, 40138 Bologna, Italy;

[16]CNR, Institute of Organic Synthesis and Photoreactivity (ISOF), 40129 Bologna, Italy;

[17]IRCCS, Institute of Neurological Sciences of Bologna, 40139 Bologna, Italy.

*Joint first authors
§Denotes co-senior authorship

Abstract: Given the dramatic increase in ageing populations, it is of great importance to understand the genetic and molecular determinants of healthy ageing and longevity. Semi-supercentenarians (subjects who reached an age of 105-109 years) arguably represent the gold standard of successful human ageing because they managed to avoid or postpone the onset of major age-related diseases. Relatively few studies have looked at epigenetic determinants of extreme longevity in humans. Here we test whether families with extreme longevity are epigenetically distinct from controls according to an epigenetic biomarker of ageing which is known as "epigenetic clock". We analyze the DNA methylation levels of peripheral blood mononuclear cells (PBMCs) from Italian families constituted of 82 semi-supercentenarians (mean age: 105.6 ± 1.6 years), 63 semi-supercentenarians' offspring (mean age: 71.8 ± 7.8 years), and 47 age-matched controls (mean age: 69.8 ± 7.2 years). We demonstrate that the offspring of semi-supercentenarians have a lower epigenetic age than age-matched controls (age difference=5.1 years, p=0.00043) and that centenarians are younger (8.6 years) than expected based on their chronological age. By contrast, no significant difference could be observed for estimated blood cell counts (such as naïve or exhausted cytotoxic T cells or helper T cells). Future studies will be needed to replicate these findings in different populations and to extend them to other tissues. Overall, our results suggest that epigenetic processes might play a role in extreme longevity and healthy human ageing.

INTRODUCTION

Ageing researchers and the general public have long been intrigued by centenarians because these subjects managed to avoid, postpone or overcome the major age-related diseases such as cancer [1], cardiovascular diseases [2], diabetes [3], osteoporotic fractures [4] and dementia [5, 6].

We find it useful to further distinguish centenarians from semi-supercentenarians (*i.e.* subjects that reach the age of 105 years, 105+) and supercentenarians (subjects that reach the age of 110 years, 110+) because subjects in these latter categories are extremely rare. As of January 1, 2015, in Italy 100+ are 19,095 out 60,795,612 living individuals, 105+, which constitute a subgroup of 100+, are 872 (1:69,720 living individuals) and 110+, which constitute an even smaller subgroup, are 27 (1:2,251,689 living individuals), according to the data base from the Italian National Institute of Statistics [7]. On the whole, 105+ and 110+ subjects have to be considered very rare cohorts of particular interest for the study of both the ageing phenotype and the healthy ageing determinants. This means that 105+ and 110+ are most informative for ageing research, even if it is not yet known whether 105+ reach the last decades of their life according to a molecular trajectory which progresses at a normal rate of change or whether the attainment of this remarkable age results from a slower molecular ageing rate.

A rich literature describes the relationship between blood-based markers and age [8-12] and many genetic studies were devoted to clarify whether exceptional longevity is a highly heritable trait [13-17]. More recently, a variety of "omics" studies have looked at gene expression [18-21], metagenomic [22] or lipidomic [23, 24] data. Different from genetic studies, functional genomic studies of centenarians face the challenge of identifying a proper control group, as shorter-lived controls from their birth cohort are no

longer available. To address this challenge, we decided to compare the centenarians' offspring (CO) with the offspring of shorter-lived controls. CO are useful for finding suitable molecular markers and for estimating the trajectories of healthy ageing [25] because: i) longevity runs in families, which probably reflects shared genetic, epigenetic and environmental factors; ii) CO are on average 20-30 years younger than their centenarian parent, *i.e.* they are in their seventies or eighties, which is a critical age when the physiological decline and the onset of the major age-related diseases may occur; iii) it is feasible to recruit controls for CO that are age-matched and born from non-centenarian parents [25]. The comparison of CO to age matched controls has already been successfully applied to identify biochemical and metabolomics parameters related to exceptional longevity [24, 26-31] and to define survival scores [32, 33].

Many biomarkers of different origin have been used to disentangle the complexity underlying the ageing phenotype, *e.g.* inflammatory biomarkers [28-31], N-glycans [34-37] and telomere length. Telomere length is an attractive biomarker of ageing because a) telomere length shortening plays an essential role in the *in vitro* ageing of somatic cells and b) telomeres of different organs/cells are known to shorten with age [38-42]. While telomere erosion is clearly linked to ageing, a rich body of literature suggests that it is not the sole reason for *in vivo* ageing. For example, no significant association could be observed between telomere length and survival among the elderly and oldest old in Danish [43] and Japanese [28] populations.

Several recent studies propose biomarkers of ageing based DNA methylation levels [44-49]. DNA methylation levels give rise to powerful epigenetic bio-markers of ageing since chronological age (*i.e.* the calendar years that have passed since birth) has a profound effect on DNA methylation levels in most

human tissues and cell types [50-59]. While previous epigenetic biomarkers of ageing apply to a single tissue, the recently developed "epigenetic clock" (based on 353 dinucleotide markers known as Cytosine phosphate Guanines or CpGs) applies to most human cell types, tissues, and organs [48]. Predicted age, referred to as "DNA methylation age" (DNAm age), correlates with chronological age in sorted cell types (CD4 T cells, monocytes, B cells, glial cells, neurons), tissues and organs including whole blood, brain, breast, kidney, liver, lung, saliva [48] and even prenatal brain samples [60]. The epigenetic clock is an attractive biomarker of ageing because a) it applies to most human tissues, b) its accurate measurement of chronological age is unprecedented [61], c) it possesses independent predictive value for all-cause mortality [62], d) it correlates with measures of cognitive and physical fitness in the elderly [63] and e) it has been found useful for detecting accelerated ageing effects due to obesity [64], Down syndrome [65] and HIV infection [66]. Furthermore, it demonstrates that the cerebellum ages more slowly than other brain regions [67].

Here, we analyze a novel peripheral blood mononuclear cells (PBMCs) methylation data set in an unprecedented Italian population of 105+, in their relative CO and in a cohort of healthy controls age- and sex-matched in respect of the CO group in order to test the hypothesis that these families age slowly according to the epigenetic clock.

RESULTS

Data set

We used the Illumina Infinium 450K array to generate DNA methylation data from PBMCs of 192 Italian subjects. We removed 8 samples (7 semi-supercentenarians and 1 control) from the analysis because they were potential outliers according to an unsupervised hierarchical clustering analysis based on the inter-array correlation. Our subsequent epigenetic clock analysis involved 3 distinct groups. The first group involved 75 subjects (mean age: 106 years, age range from 99 to 113 years) will be referred to as semi-supercentenarians (105+) although it included one subject aged 99. The second group, CO, involved 63 offspring from centenarians (mean age: 72 years, age range from 50 to 89 years). The third group involved 46 control subjects (mean age: 70 years, age range from 52 to 85 years), *i.e.* subjects who did not have a centenarian parent. The first group (semi-supercentenarians), the second (CO) and the third group (controls) contained 59, 25 and 37 females, respectively. By design, CO did not

differ from controls in terms of gender (p=0.8) or chronological age (p=0.31).

Accuracy of the epigenetic clock

DNAm age (also referred to as "epigenetic age") was calculated using the DNA methylation levels of PBMCs applying a previously described method [48].

DNAm age was highly correlated with chronological age across all samples (correlation r=0.89, Figure 1A).

Three measures of epigenetic age acceleration

In this article, we consider three measures of epigenetic age acceleration (as detailed in Methods). The first one, which will be referred to as universal measure of age acceleration (denoted Age Accel), applies to virtually all tissues and cell types (with the exception of sperm) [48]. The other two measures (referred to as intrinsic and extrinsic age acceleration, respectively) only apply to blood. The universal measure is defined as the difference between DNAm age value and the value predicted by the linear regression model in groups 1 and 2 (*i.e.* in semi-supercentenarians or their offspring). The term "universal" refers to the fact that this measure can be defined in a vast majority of tissues and cell types [48]. A positive value of the universal age acceleration measure indicates that DNA methylation age is higher than that predicted from the regression model for COs or semi-supercentenarians of the same age.

The measure of intrinsic epigenetic age acceleration (IEAA) measures "pure" epigenetic ageing effects in blood that are not confounded by differences in blood cell counts.

The measure of extrinsic epigenetic age acceleration (EEAA) aims to measure ageing in immune related components also relates to age-related changes in blood cell composition such as the decrease of naive CD8+ T cells and the increase in memory or exhausted CD8+ T cells [29, 68-70]. EEAA is defined on the basis of a weighted average of the epigenetic age measure from Hannum et al (2013) [47] and three blood cell types that are known to change with age: naive (CD45RA+CCR7+) cytotoxic T cells, exhausted (CD28-CD45RA-) cytotoxic T cells and plasma B cells. By definition, EEAA has a positive correlation with the amount of exhausted CD8 T cells and plasma blast cells and a negative correlation with the amount of naive CD8+ T cells. Blood cell counts were estimated based on DNA methylation data as described in Methods (section "Estimating blood cell counts based on DNA methylation levels").
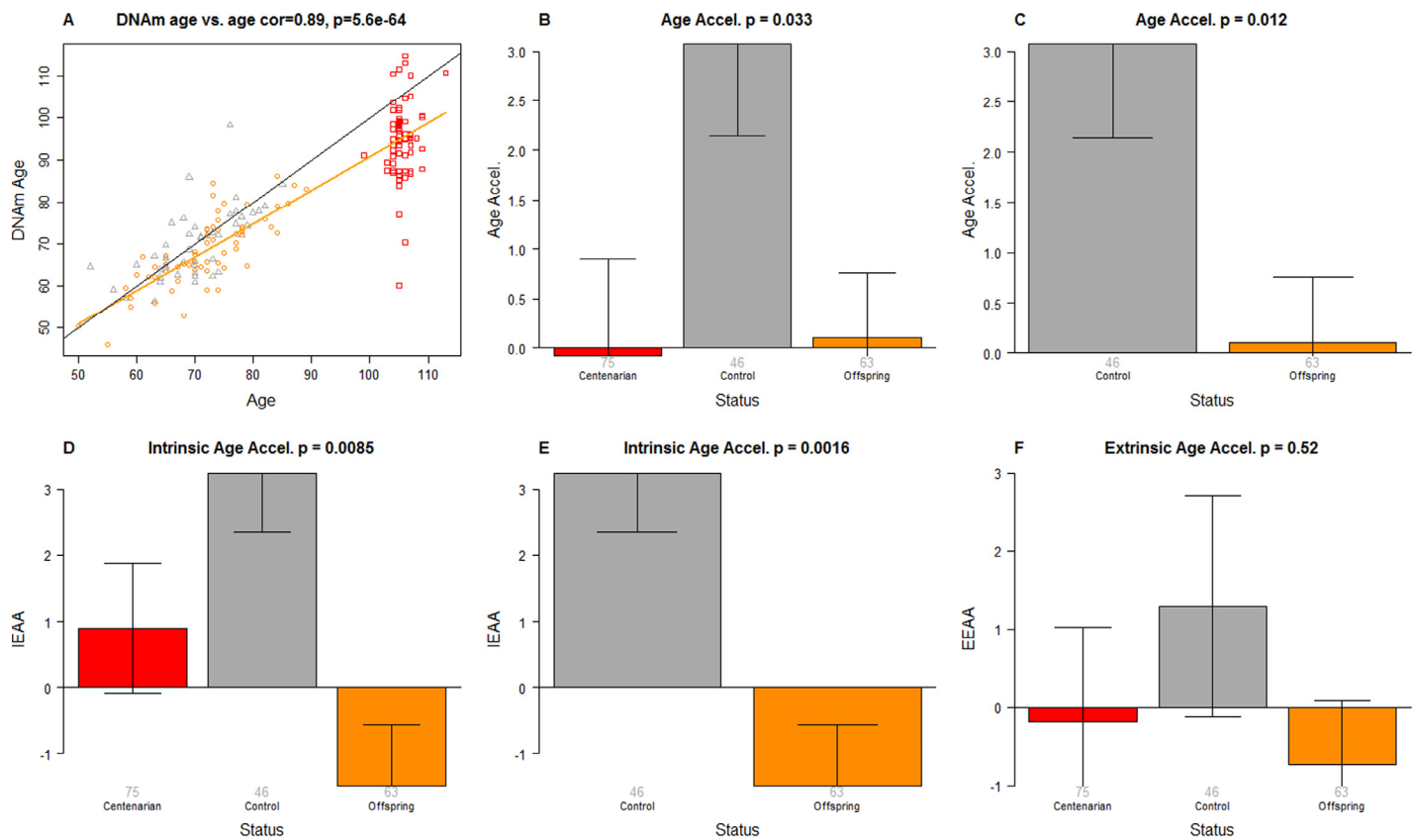
Figure 1. **Epigenetic age analysis of PBMCs from centenarians and controls**. (**A**) Scatter plot relating the DNAm age of each PBMC sample (y-axis) versus chronological age (x-axis). Points are colored by status. The color of each dot corresponds to the status of each PBMC sample: red for centenarians, orange for offspring of centenarians, grey for controls. The black line corresponds to y=x. The orange line depicts the regression line based on the offspring of centenarians and centenarians (orange and red dots). The vertical distance to the orange line corresponds to the universal measure of age acceleration Age Accel. The bar plots depict group status (x-axis) versus (**B**, **C**) universal age acceleration, (**D**, **E**) intrinsic age acceleration, (**F**) extrinsic age acceleration. Each bar plot depicts the mean value, one standard error, and reports the p-value results from a non-parametric group comparison test (Kruskal Wallis test).

Table 1. Multivariate model of DNAm age in non-centenarians

Covariate	Coefficient	Std. Error	T statistic	P-value
Offspring	-3.804	1.043	-3.647	0.00043
Age	0.743	0.071	10.442	$< 2 \times 10^{-16}$
Sex (female)	0.174	1.065	0.163	0.87
Naïve CD8+T cell	-0.007	0.011	-0.617	0.54
Exhausted CD8+ T cell	-0.044	0.159	-0.274	0.79
Plasma Blast cell	-7.62	3.706	-2.055	0.042
Helper T cell (CD4)	-28.3	8.728	-3.247	0.0016
Natural Killer cell	12.5	7.962	1.572	0.13
Monocyte	-9.2	9.313	-0.988	0.33

Coefficients and p-values from regressing DNAm age on offspring status, age, sex, and various blood cell counts in non-centenarian subjects (subjects younger than 90). The model explained 67% of the variance. The offspring of centenarians are 5.1 years (=3.804/0.743) younger than age matched controls.

The three different measures of epigenetic age acceleration are not independent of each other. The universal measure Age Accel has a moderately high correlation with IEAA (r=0.65, p=1.8x10^{-23}) and with EEAA (r=0.71, p=1.6x10^{-29}). But IEAA has only a weak correlation with EEAA (r=0.19, p=0.01). By construction, our three measures of epigenetic age acceleration are uncorrelated (r=0) with chronological age at the time of blood draw.

Offspring of semi-supercentenarians have a slow intrinsic ageing rate

We find that PBMCs of the offspring of 105+ age more slowly than that of age matched controls according to a) the Age Accel measure (Kruskal Wallis test p=0.012, Figure 1C) and b) the intrinsic measure of age acceleration (p=0.0016 Figure 1E). According to a multivariate model analysis in non-centenarians (Table

1), CO are 5.1 years younger (p=0.00051) than age matched controls even after adjusting for sex and estimated blood cell counts.

Semi-supercentenarians appear to age more slowly than expected

Interestingly, the DNAm age of 105+ is systematically lower than their chronological age as can be seen from the fact that the red dots lie beneath the black line in Figure 1A. The DNAm age of 105+ differs significantly from that of controls (p=0.028) but not from that of the CO (p=0.29) according to a multivariate model analysis (Table 2) that adjusted for chronological age, sex, and estimated blood cell counts. According to this model, 105+ are on average 8.6 years younger than expected based on chronological age. The systematic underestimate of age in centenarians has also been observed in most other tissues from centenarians [67].
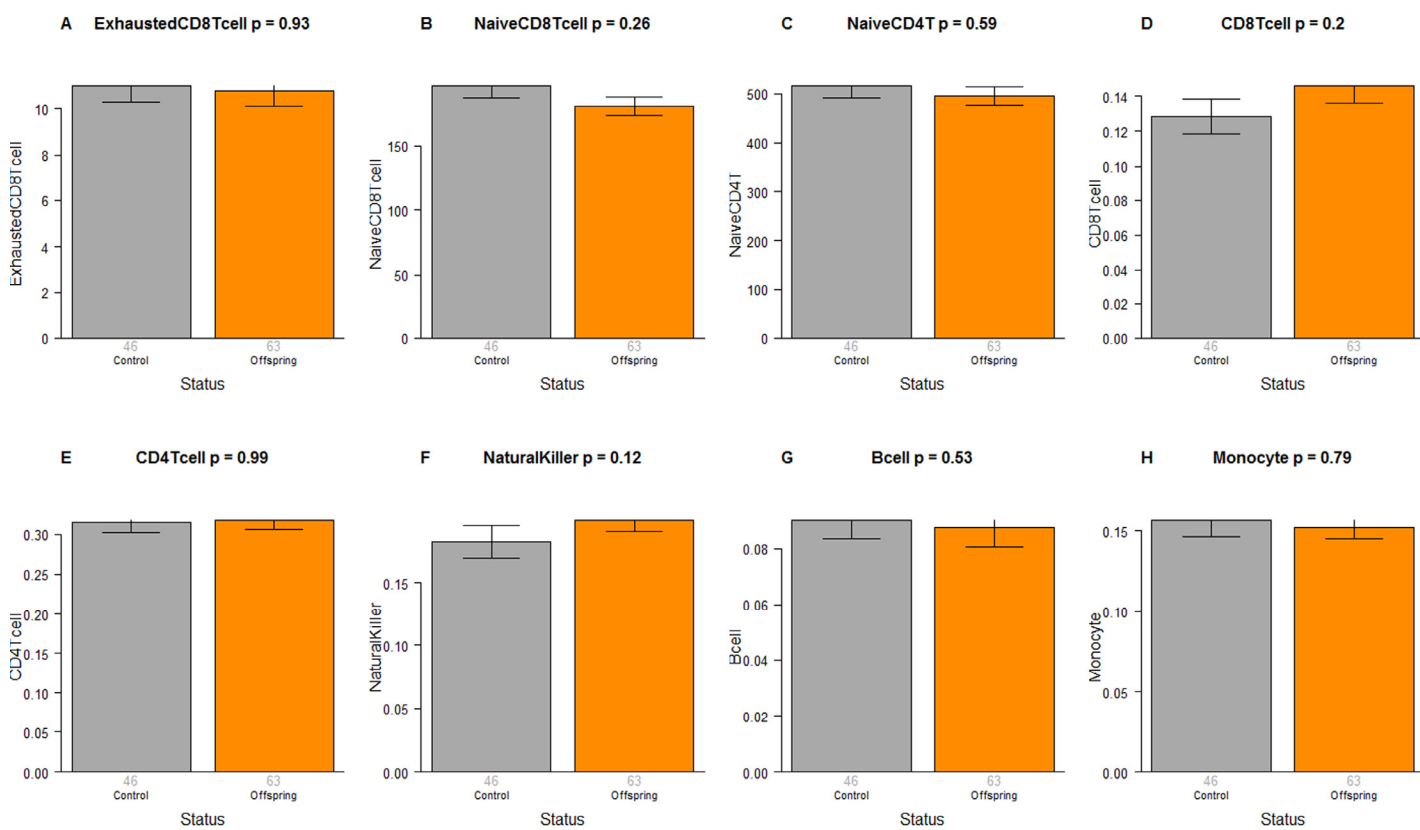

Figure 2. **Blood cell counts in offspring of semi-supercentenarians versus age matched controls**. Group status (offspring of semi-supercentenarian or control) versus estimated abundance of (**A**) exhausted cytotoxic T cells, (**B**) naïve cytotoxic T cells, (**C**) naïve helper T cells, (**D**) cytotoxic T cells, (**E**) helper T cells, (**F**) natural killer cells, (**G**) B cells, (**H**) monocytes. Each bar plot reports the mean value and one standard error. The p-value results from a non-parametric group comparison test (Kruskal Wallis). The abundance measures of blood cell counts were estimated based on DNA methylation levels using the epigenetic clock software. Roughly speaking, the y-axis of (**A**) reports a percentage while that for (**B**, **C**) corresponds to counts but it is best to interpret the y-axis in (**A-C**) as ordinal abundance measure. The y-axis in (**D-H**) reports estimated proportions based on the Houseman method [78].

Table 2. Multivariate model of DNA methylation age in all subjects.

Covariate	Coefficient	Std. Error	T statistic	P-value
StatusControlvsCentenarian	6.583	2.98	2.208	0.029
StatusOffspringvsCentenarian	3.03	2.84	1.069	0.29
Age	0.765	0.080	9.578	$< 2 \times 10^{-16}$
Sex (female)	-1.025	1.02	-1.005	0.32
Naïve CD8+T cell	-0.014	0.010	-1.444	0.15
Exhausted CD8+ T cell	-0.118	0.142	-0.832	0.41
Plasma Blast cell	-6.046	2.83	-2.135	0.034
Helper T cell (CD4)	-38.069	7.53	-5.054	1.1×10^{-6}
Natural Killer cell	-1.926	7.25	-0.265	0.79
Monocyte	-14.782	8.00	-1.848	0.066

Coefficients and p-values from regressing DNAm age on offspring status, age, sex, and various blood cell counts in non-centenarian subjects (subjects younger than 90). The model explained 85% of the variance. Centenarians are 8.6 years (=6.583/0.765) younger than expected based on chronological age.
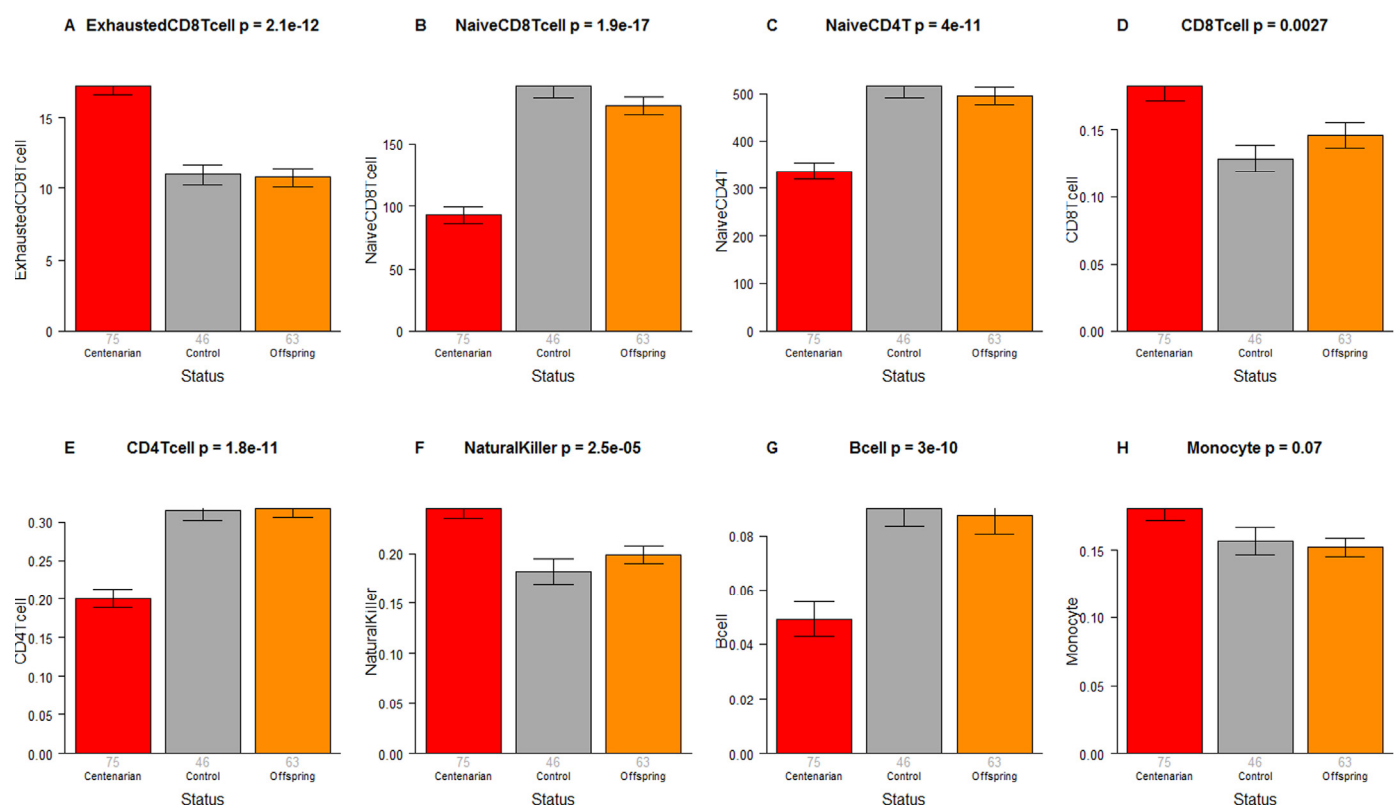
Figure 3. **Blood cell counts across three groups**. Group status (semi-supercentenarian, offspring of semi-supercentenarian, or control) versus estimated abundance of (**A**) exhausted cytotoxic T cells, (**B**) naïve cytotoxic T cells, (**C**) naïve helper T cells, (**D**) cytotoxic T cells, (**E**) helper T cells, (**F**) natural killer cells, (**G**) B cells, (**H**) monocytes. Each bar plot reports the mean value and one standard error. The p-value results from a non-parametric group comparison test (Kruskal Wallis). Roughly speaking, the y-axis of (**A**) reports a percentage while that for (**B**, **C**) corresponds to counts but it is best to interpret the y-axis in (**A-C**) as ordinal abundance measure. The y-axis in (**D-H**) reports estimated proportions based on the Houseman method [78].

While our results in the CO suggests that the age difference of 8.6 years reflects a lower epigenetic ageing rate in 105+, we cannot rule out that confounders play a role as well (due to the lack of suitable controls for centenarians).

Extrinsic age acceleration and blood cell counts are not significant

The CO do not differ from age matched controls in terms of the extrinsic measure of age acceleration (Figure 1F) or in terms of estimated blood cell counts (Figure 2) but future studies with large samples should revisit these analyses. When comparing 105+ to younger subjects (CO and controls), we find that 105+ contain more exhausted cytotoxic T cells (Figure 3A), fewer naïve cytotoxic T cells (Figure 3B), fewer naïve helper T cells (Figure 3C), more cytotoxic T cells (Figure 3D), fewer helper T cells (Figure 3E), more natural killer cells (Figure 3F), and fewer B cells (Figure 3G). These findings are congruent with those from many previous studies of age related changes in blood cell composition (e.g. [10, 29, 68-72]).

DISCUSSION

This article leverages three epigenetic biomarkers of ageing to characterize semi-supercentenarians and their offspring.

To the best of our knowledge, this is the first study that demonstrates that the offspring of semi-supercentenarians have a lower intrinsic epigenetic ageing rate in PBMCs. A similar trend was reported by Gentilini [73] that, by analyzing whole-genome methylation data from PBMCs in a smaller cohort (including 21 female centenarians, their 21 female offspring, 21 offspring of both non-long-lived parents and 21 young women), observed an age-related decrease in global DNA methylation and a delay of this process in centenarians' offspring. In the present study, the reported p-values (p=0.00051 in Table 1, p=0.012 in Figure 1C) remain significant even after adjusting for multiple comparisons since our study only involved three major hypothesis tests corresponding to the three related measures of epigenetic age acceleration (*i.e.* Age Accel, IEAA, EEAA). This remarkable finding is mirrored by the result that semi-supercentenarians appear to be younger (8.6 years, Table 2) than expected based on chronological age. Future studies will be needed to investigate how an epigenetic trajectory of healthy ageing relates to that of clinical measures of physiological or pathological ageing.

Strengths of this study include a) access to PBMCs from a unique collection of semi-supercentenarians and

their offspring; b) careful matching between the offspring of semi-supercentenarians and unrelated control offspring from non-centenarians; c) state of the art epigenetic biomarkers of ageing. The following limitations need also to be acknowledged. First, our results should be replicated in other populations (ideally involving semi-supercentenarians and their offspring) who differ from our Italian cohort in terms of genetic background, lifestyle and cultural habits. Further, it will be of great interest to extend this kind of epigenetic clock analysis to other accessible fluids and tissues such as buccal epithelium, saliva, skin, adipose, muscle. It is beyond the scope of this article to carry out an epigenome wide association studies (EWAS) based on 486k individual CpGs on the Illumina array. The number of semi-supercentenarians included in this study is relatively small but these subjects are very rare, *i.e.* about one in 69,720 Italian living individuals and 6 out of the top 50 oldest living people are Italian (https://en.wikipedia.org/wiki/List_of_oldest_living_people).

The epigenetic clock and related methylation-based biomarkers of ageing are arguably the most accurate measures of the wider process of epigenetic remodeling that occurs in different cell types, tissues and organs during human ageing [46, 48, 74, 75]. Previous studies have shown that epigenetic age relates to cognitive status, physical fitness, and all-cause of mortality in aged populations [62, 63, 79-81]. The current study adds to an increasing body of evidence that suggests that the epigenetic age of PBMCs relates to biological age or physiological age but other complementary biomarkers of ageing undoubtedly play a crucial role. It is highly unlikely that a single blood-based biomarker of ageing (such as epigenetic age) captures all aspects of physiological age.

Overall, our results suggest that the offspring of semi-supercentenarians are informative when it comes to detecting epigenetic determinants of healthy ageing. By understanding why the offspring of centenarians are protected against epigenetic ageing, we might be able to learn how to extend the benefits of successful ageing to the general population.

MATERIALS AND METHODS

Description of the dataset. The subjects were recruited in three Italian centers (Bologna , Milan and University of Calabria at Rende). The study was approved by the local Ethical Committee (S. Orsola Hospital - University of Bologna; Prot. n. 2006061707, amendment 08/11/2011; Fondazione IRCCS Cà Granda Ospedale Maggiore Policlinico, Prot. n. 2035, amendment 30/11/2011; University of Calabria

9/9/2004 amendment on 24/11/2011). A written informed consent form was obtained from all participants.

This novel dataset (measured on the Illumina 450K array) includes 192 subjects: 82 semi-supercentenarians (33 from Bologna, 29 from Milan and 20 from Calabria), 63 offspring of semi-supercentenarians (22 from Bologna, 28 from Milan and 13 from Calabria) and 47 control subjects whose parents were not centenarians (16 from Bologna, 17 from Milan and 14 from Calabria).

DNA extraction and bisulphite treatment of DNA. Extraction of genomic DNA from PBMCs was performed using the AllPrep DNA/RNA/protein kit (QIAGEN, Hilden, Germany). Sodium bisulphite conversion for Infinium HumanMethylation450 BeadChip was performed using the EZ-DNA Methylation-Gold Kit and the EZ-96 DNA Methylation Kit respectively Genome-wide DNA methylation was analyzed using the Infinium HumanMethylation450 BeadChip (Illumina, San Diego, CA) following manufacturer's instructions. Arrays were scanned by HiScan (Illumina). GenomeStudio (Illumina) was used to perform background subtraction.

DNA methylation age and epigenetic clock. The epigenetic clock software implements a data normalization step that repurposes the BMIQ normalization method from Teschendorff [76] so that it automatically references each sample to a gold standard based on type II probes as detailed in Additional file 2 from [48]. All of the described epigenetic measures of ageing and age acceleration are implemented in our freely available software [48]. The epigenetic clock is defined as a prediction method of age based on the DNA methylation levels of 353 CpGs. Predicted age, referred to as DNAm age, correlates with chronological age in sorted cell types (CD4 T cells, monocytes, B cells, glial cells, neurons), tissues and organs, including: whole blood, brain, breast, kidney, liver, lung, saliva [48]. Mathematical details and software tutorials for the epigenetic clock can be found in the Additional files of [48]. An online age calculator can be found at our webpage (https://dnamage.genetics.ucla.edu).

Measures of epigenetic age acceleration. The name of our universal measure of age acceleration (Age Accel) reflects that it applies to virtually all sources of human DNA (with the exception of sperm). Here we defined it as follows. First, we regressed DNAm age on chronological age in semi-supercentenarians and their offspring. Next, we used the resulting model to predict the age subject. Next the universal measure was defined

as the difference between the observed measure of DNAm age and the predicted value. Thus, a high positive value for Age Accel indicates that the observed DNAm age is higher than that predicted based on semi-supercentenarians and their offspring. Age Accel has a relatively weak correlation with blood cell counts [66] but it still relates to estimated blood cell counts as can be seen from Table 1. To subtract out the effect of blood cell counts, we find it useful to define a measure of intrinsic epigenetic age acceleration (IEAA) that measures "pure" epigenetic ageing effects that are not confounded by differences in blood cell counts. It is defined as the residual resulting from a multivariate regression model of DNAm age on chronological age and various blood immune cell counts (naive CD8 T cells, exhausted CD8 T cells, plasma B cells, CD4 T cells, natural killer cells and monocytes).

The measure of extrinsic epigenetic age acceleration (EEAA) aims to measure epigenetic ageing in immune related components. EEAA is defined using the following three steps. First, we calculated the epigenetic age measure from Hannum et al (2013) [47], which is weakly correlated with certain blood cell types [62]. Second, we increased the contribution of blood cell types to the age estimate by forming a weighted average of the Hannum's estimate with 3 cell types that are known to change with age: naive (CD45RA+CCR7+) cytotoxic T cells, exhausted (CD28-CD45RA-) cytotoxic T cells, and plasma B cells using the approach of [77]. The resulting measure of blood age is referred to as BioAge4 in our epigenetic clock software. Third, we defined a measure of age acceleration (EEAA) as the residual resulting from a univariate model regressing BioAge4 on chronological age. By definition, our measure of EEAA has a positive correlation with the amount of exhausted CD8 T cells and plasma blast cells and a negative correlation with the amount of naive CD8+ T cells. Blood cell counts were estimated based on DNA methylation data as described in the section entitled "Estimating blood cell counts based on DNA methylation levels". By construction, EEAA tracks both age related changes in blood cell composition and intrinsic epigenetic changes. By definition, none of our three measures of epigenetic age acceleration are correlated with the chronological age.

Estimating blood cell counts based on DNA methylation levels. We estimate blood cell proportions using two different software tools. Houseman's estimation method [78], which is based on DNA methylation signatures from purified leukocyte samples, was used to estimate the proportions of cytotoxic (CD8+) T cells, helper (CD4+) T, natural killer B cells. The advanced analysis option of the epigenetic clock

software [48] was used to estimate the percentage of exhausted CD8+ T cells (defined as CD28-CD45RA-) and the number (count) of naïve CD8+ T cells (defined as (CD45RA+CCR7+).

Authors' contributions

CF and PG conceived of the study and directed this study. SH carried out the epigenetic age analysis. CF, PG, SH and CP wrote the paper. DG, DM, DM, BA, GP, PDA, FDR, EM and CG collected the samples and generated the DNA methylation data. CF, PG, SH, CP MGB, SC, PD, MD, DM, DM, BA, GP, PDA, FDR, EM, DG, AMDB and CG helped interpret the data, provided critical observations and edited the manuscript.

Conflict of interest statement

All authors declare no conflict of interest.

REFERENCES

1. Salvioli S, Capri M, Bucci L, Lanni C, Racchi M, Uberti D, Memo M, Mari D, Govoni S and Franceschi C. Why do centenarians escape or postpone cancer? The role of IGF-1, inflammation and p53. Cancer Immunol Immunother. 2009; 58:1909-1917.

2. Olivieri F, Spazzafumo L, Antonicelli R, Marchegiani F, Cardelli M, Sirolla C, Galeazzi R, Giovagnetti S, Mocchegiani E and Franceschi C. Combination of biomarkers to predict mortality in elderly patients with myocardial infarction. Mech Ageing Dev. 2008; 129:231-237.

3. Ferrannini E, Vichi S, Beck-Nielsen H, Laakso M, Paolisso G and Smith U. Insulin action and age. European Group for the Study of Insulin Resistance (EGIR). Diabetes. 1996; 45:947-953.

4. Passeri G, Pini G, Troiano L, Vescovini R, Sansoni P, Passeri M, Gueresi P, Delsignore R, Pedrazzoni M and Franceschi C. Low vitamin D status, high bone turnover, and bone fractures in centenarians. J Clin Endocrinol Metab. 2003; 88:5109-5115.

5. Evert J, Lawler E, Bogan H and Perls T. Morbidity profiles of centenarians: survivors, delayers, and escapers. J Gerontol A Biol Sci Med Sci. 2003; 58:232-237.

6. Atzmon G, Schechter C, Greiner W, Davidson D, Rennert G and Barzilai N. Clinical phenotype of families with longevity. Journal of the American Geriatrics Society. 2004; 52:274-277.

7. Statistics INIo. 2015. ISTAT. www.istat.it/en/products/data-bases.

8. Hausman DB, Fischer JG and Johnson MA. Protein, lipid, and hematological biomarkers in centenarians: Definitions, interpretation and relationships with health. Maturitas. 2012; 71:205-212.

9. Franceschi C, Valensin S, Fagnoni F, Barbi C and Bonafè M. Biomarkers of immunosenescence within an evolutionary perspective: the challenge of heterogeneity and the role of antigenic load. Experimental Gerontology. 1999; 34:911-921.

10. Colonna-Romano G, Buffa S, Bulati M, Candore G, Lio D, Pellicano M, Vasto S and Caruso C. B Cells Compartment in Centenarian Offspring and Old People. Current Pharmaceutical Design. 2010; 16:604-608.

11. Trougakos IP, Petropoulou C, Franceschi C and Gonos ES. Reduced Expression Levels of the Senescence Biomarker Clusterin/Apolipoprotein J in Lymphocytes from Healthy Centenarians. Annals of the New York Academy of Sciences. 2006; 1067:294-300.

12. Atzmon G, Barzilai N, Hollowell JG, Surks MI and Gabriely I. Extreme Longevity Is Associated with Increased Serum Thyrotropin. The Journal of Clinical Endocrinology & Metabolism. 2009; 94:1251-1254.

13. Sebastiani P, Bae H, Sun FX, Andersen SL, Daw EW, Malovini A, Kojima T, Hirose N, Schupf N, Puca A and Perls TT. Meta-analysis of genetic variants associated with human exceptional longevity. Aging (Albany NY). 2013; 5:653-661.

14. Deelen J, Beekman M, Uh HW, Helmer Q, Kuningas M, Christiansen L, Kremer D, van der Breggen R, Suchiman HE, Lakenberg N, van den Akker EB, Passtoors WM, Tiemeier H, et al. Genome-wide association study identifies a single major locus contributing to survival into old age; the APOE locus revisited. Aging Cell. 2011; 10:686-698.

15. Deelen J, Beekman M, Uh HW, Broer L, Ayers KL, Tan Q, Kamatani Y, Bennet AM, Tamm R, Trompet S, Guethbjartsson DF, Flachsbart F, Rose G, et al. Genome-wide association meta-analysis of human longevity identifies a novel locus conferring survival beyond 90 years of age. Hum Mol Genet. 2014; 23:4420-4432.

16. Freudenberg-Hua Y, Freudenberg J, Vacic V, Abhyankar A, Emde AK, Ben-Avraham D, Barzilai N, Oschwald D, Christen E, Koppel J, Greenwald B, Darnell RB, Germer S, et al. Disease variants in genomes of 44 centenarians. Mol Genet Genomic Med. 2014; 2:438-450.

17. Garagnani P, Giuliani C, Pirazzini C, Olivieri F, Bacalini MG, Ostan R, Mari D, Passarino G, Monti D, Bonfigli AR, Boemi M, Ceriello A, Genovese S, et al. Centenarians as super-controls to assess the biological relevance of genetic risk factors for common age-related diseases: a proof of principle on type 2 diabetes. Aging (Albany NY). 2013; 5:373-385.

18. de Magalhães JP, Curado J and Church GM. Meta-analysis of age-related gene expression profiles identifies common signatures of aging. Bioinformatics. 2009; 25:875-881.

19. Rodwell GE, Sonu R, Zahn JM, Lund J, Wilhelmy J, Wang L, Xiao W, Mindrinos M, Crane E, Segal E, Myers BD, Brooks JD, Davis RW, et al. A transcriptional profile of aging in the human kidney. PLoS Biol. 2004; 2:e427.

20. Zahn J, Poosala S, Owen A, Ingram DK, Lustig A, Carter A, Weeraratna AT, Taub DD, Gorospe M, Mazan-Mamczarz K, Lakatta EG, Boheler KR, Xu X, et al. AGEMAP: a gene expression database for aging in mice. PLoS Genet. 2007; 3:e201.

21. Zahn J, Sonu R, Vogel H, Crane E, Mazan-Mamczarz K, Rabkin R, Davis R, Becker K, Owen A and Kim S. Transcriptional profiling of aging in human muscle reveals a common aging signature. PLoS Genet. 2006; 2:e115.

22. Rampelli S, Candela M, Turroni S, Biagi E, Collino S, Franceschi C, O'Toole PW and Brigidi P. Functional metagenomic profiling of intestinal microbiome in extreme ageing. Aging (Albany NY). 2013; 5:902-912.

23. Gonzalez-Covarrubias V, Beekman M, Uh HW, Dane A, Troost J, Paliukhovich I, van der Kloet FM, Houwing-Duistermaat J, Vreeken RJ, Hankemeier T and Slagboom EP. Lipidomics of familial longevity. Aging Cell. 2013; 12:426-434.

24. Collino S, Montoliu I, Martin FP, Scherer M, Mari D, Salvioli S, Bucci L, Ostan R, Monti D, Biagi E, Brigidi P, Franceschi C and Rezzi S. Metabolic signatures of extreme longevity in northern Italian centenarians reveal a complex remodeling of lipids, amino acids, and gut microbiota metabolism. PLoS One. 2013; 8:e56564.

25. Gueresi P, Miglio R, Monti D, Mari D, Sansoni P, Caruso C, Bonafede E, Bucci L, Cevenini E, Ostan R, Palmas MG, Pini E, Scurti M, et al. Does the longevity of one or both parents influence the health status of their offspring? Exp Gerontol. 2013; 48:395-400.

26. Ostan R, Bucci L, Cevenini E, Palmas MG, Pini E, Scurti M, Vescovini R, Caruso C, Mari D, Vitale G, Franceschi C and Monti D. Metabolic syndrome in the offspring of centenarians: focus on prevalence, components, and adipokines. Age (Dordrecht, Netherlands). 2013; 35:1995-2007.

27. Vitale G, Brugts MP, Ogliari G, Castaldi D, Fatti LM, Varewijck AJ, Lamberts SW, Monti D, Bucci L, Cevenini E, Cavagnini F, Franceschi C, Hofland LJ, et al. Low circulating IGF-I bioactivity is associated with human longevity: findings in centenarians' offspring. Aging (Albany NY). 2012; 4:580-589.

28. Arai Y, Martin-Ruiz CM, Takayama M, Abe Y, Takebayashi T, Koyasu S, Suematsu M, Hirose N and von Zglinicki T. Inflammation, But Not Telomere Length, Predicts Successful Ageing at Extreme Old Age: A Longitudinal Study of Semi-supercentenarians. EBioMedicine. 2015; 2:1549-1558.

29. Fagnoni FF, Vescovini R, Passeri G, Bologna G, Pedrazzoni M, Lavagetto G, Casti A, Franceschi C, Passeri M and Sansoni P. Shortage of circulating naive CD8+ T cells provides new insights on immunodeficiency in aging. Blood. 2000; 95:2860-2868.

30. Franceschi C, Bonafè M, Valensin S, Olivieri F, De Luca M, Ottaviani E and De Benedictis G. Inflamm-aging. An evolutionary perspective on immunosenescence. Ann N Y Acad Sci. 2000; 908:244-254.

31. Larbi A, Franceschi C, Mazzatti D, Solana R, Wikby A and Pawelec G. Aging of the immune system as a prognostic factor for human longevity. Physiology (Bethesda). 2008; 23:64-74.

32. De Benedictis G and Franceschi C. The unusual genetics of human longevity. Sci Aging Knowledge Environ. 2006; 2006:pe20.

33. Franceschi C. Inflammaging as a major characteristic of old people: can it be prevented or cured? Nutr Rev. 2007; 65:S173-176.

34. Borelli V, Vanhooren V, Lonardi E, Reiding KR, Capri M, Libert C, Garagnani P, Salvioli S, Franceschi C and Wuhrer M. Plasma N-Glycome Signature of Down Syndrome. J Proteome Res. 2015; 14:4232-4245.

35. Dall'Olio F, Vanhooren V, Chen CC, Slagboom PE, Wuhrer M and Franceschi C. N-glycomic biomarkers of biological aging and longevity: a link with inflammaging. Ageing Res Rev. 2013; 12:685-698.

36. Vanhooren V, Desmyter L, Liu XE, Cardelli M, Franceschi C, Federico A, Libert C, Laroy W, Dewaele S, Contreras R and Chen C. N-glycomic changes in serum proteins during human aging. Rejuvenation Res. 2007; 10:521-531a.

37. Vanhooren V, Dewaele S, Libert C, Engelborghs S, De Deyn PP, Toussaint O, Debacq-Chainiaux F, Poulain M, Glupczynski Y, Franceschi C, Jaspers K, van der Pluijm I, Hoeijmakers J, et al. Serum N-glycan profile shift during human ageing. Exp Gerontol. 2010; 45:738-743.

38. Blackburn EH and Gall JG. A tandemly repeated sequence at the termini of the extrachromosomal ribosomal RNA genes in Tetrahymena. J Mol Biol. 1978; 120:33-53.

39. Lin J, Epel E, Cheon J, Kroenke C, Sinclair E, Bigos M, Wolkowitz O, Mellon S and Blackburn E. Analyses and comparisons of telomerase activity and telomere length in human T and B cells: insights for epidemiology of telomere maintenance. J Immunol Methods. 2010; 352:71-80.

40. Mondello C, Petropoulou C, Monti D, Gonos ES, Franceschi C and Nuzzo F. Telomere Length in Fibroblasts and Blood Cells from Healthy Centenarians. Experimental Cell Research. 1999; 248:234-242.

41. Cherif H, Tarry JL, Ozanne SE and Hales CN. Ageing and telomeres: a study into organ- and gender-specific telomere shortening. Nucleic Acids Res. 2003; 31:1576-1583.

42. Daniali L, Benetos A, Susser E, Kark JD, Labat C, Kimura M, Desai KK, Granick M and Aviv A. Telomeres shorten at equivalent rates in somatic tissues of adults. Nat Commun. 2013; 4:1597.

43. Bischoff C, Petersen HC, Graakjaer J, Andersen-Ranberg K, Vaupel JW, Bohr VA, Kølvraa S and Christensen K. No Association Between Telomere Length and Survival Among the Elderly and Oldest Old. Epidemiology. 2006; 17:190-194.

44. Bocklandt S, Lin W, Sehl ME, Sanchez FJ, Sinsheimer JS, Horvath S and Vilain E. Epigenetic predictor of age. PLoS ONE. 2011; 6:e14821.

45. Koch C and Wagner W. Epigenetic-aging-signature to determine age in different tissues. Aging (Albany, NY). 2011; 3:1018–1027.

46. Garagnani P, Bacalini MG, Pirazzini C, Gori D, Giuliani C, Mari D, Di Blasio AM, Gentilini D, Vitale G, Collino S, Rezzi S, Castellani G, Capri M, et al. Methylation of ELOVL2 gene as a new epigenetic marker of age. Aging Cell. 2012; 11:1132-1134.

47. Hannum G, Guinney J, Zhao L, Zhang L, Hughes G, Sadda S, Klotzle B, Bibikova M, Fan J-B, Gao Y, Deconde R, Chen M, Rajapakse I, et al. Genome-wide Methylation Profiles Reveal Quantitative Views of Human Aging Rates. Mol Cell. 2013; 49:359-367.

48. Horvath S. DNA methylation age of human tissues and cell types. Genome Biol. 2013; 14:R11.

49. Weidner CI, Lin Q, Koch CM, Eisele L, Beier F, Ziegler P, Bauerschlag DO, Jockel KH, Erbel R, Muhleisen TW, Zenke M, Brummendorf TH and Wagner W. Aging of blood can be tracked by DNA methylation changes at just three CpG sites. Genome Biol. 2014; 15:R24.

50. Christensen B, Houseman E, Marsit C, Zheng S, Wrensch M, Wiemels J, Nelson H, Karagas M, Padbury J, Bueno R, Sugarbaker D, Yeh R, Wiencke J, et al. Aging and Environmental Exposures Alter Tissue-Specific DNA Methylation Dependent upon CpG Island Context. PLoS Genet. 2009; 5:e1000602.

51. Bollati V, Schwartz J, Wright R, Litonjua A, Tarantini L, Suh H, Sparrow D, Vokonas P and Baccarelli A. Decline in genomic DNA

methylation through aging in a cohort of elderly subjects. Mech Ageing Dev. 2009; 130:234-239.

52. Rakyan VK, Down TA, Maslau S, Andrew T, Yang TP, Beyan H, Whittaker P, McCann OT, Finer S, Valdes AM, Leslie RD, Deloukas P and Spector TD. Human aging-associated DNA hypermethylation occurs preferentially at bivalent chromatin domains. Genome research. 2010; 20:434-439.

53. Teschendorff AE, Menon U, Gentry-Maharaj A, Ramus SJ, Weisenberger DJ, Shen H, Campan M, Noushmehr H, Bell CG, Maxwell AP, Savage DA, Mueller-Holzner E, Marth C, et al. Age-dependent DNA methylation of genes that are suppressed in stem cells is a hallmark of cancer. Genome research. 2010; 20:440-446.

54. Vivithanaporn P, Heo G, Gamble J, Krentz H, Hoke A, Gill M and Leistung C. Neurologic disease burden in treated HIV/AIDS predicts survival. Neurology. 2010; 75:1150-1158.

55. Horvath S, Zhang Y, Langfelder P, Kahn R, Boks M, van Eijk K, van den Berg L and Ophoff RA. Aging effects on DNA methylation modules in human brain and blood tissue. Genome Biol. 2012; 13:R97.

56. Numata S, Ye T, Hyde Thomas M, Guitart-Navarro X, Tao R, Wininger M, Colantuoni C, Weinberger Daniel R, Kleinman Joel E and Lipska Barbara K. DNA Methylation Signatures in Development and Aging of the Human Prefrontal Cortex. Am J Hum Genet. 2012; 90:260-272.

57. Alisch RS, Barwick BG, Chopra P, Myrick LK, Satten GA, Conneely KN and Warren ST. Age-associated DNA methylation in pediatric populations. Genome Res. 2012; 22:623-632.

58. Johansson A, Enroth S and Gyllensten U. Continuous Aging of the Human DNA Methylome Throughout the Human Lifespan. PLoS One. 2013; 8:e67378.

59. Day K, Waite L, Thalacker-Mercer A, West A, Bamman M, Brooks J, Myers R and Absher D. Differential DNA methylation with age displays both common and dynamic features across human tissues that are influenced by CpG landscape. Genome Biol. 2013; 14:R102.

60. Spiers H, Hannon E, Schalkwyk LC, Smith R, Wong CC, O'Donovan MC, Bray NJ and Mill J. Methylomic trajectories across human fetal brain development. Genome research. 2015; 25:338-352.

61. Gibbs W. Biomarkers and ageing: The clock-watcher. Nature. 2014; 508:168–170.

62. Marioni R, Shah S, McRae A, Chen B, Colicino E, Harris S, Gibson J, Henders A, Redmond P, Cox S, Pattie A, Corley J, Murphy L, et al. DNA methylation age of blood predicts all-cause mortality in later life. Genome Biol. 2015; 16:25.

63. Marioni RE, Shah S, McRae AF, Ritchie SJ, Muniz-Terrera G, Harris SE, Gibson J, Redmond P, Cox SR, Pattie A, Corley J, Taylor A, Murphy L, et al. The epigenetic clock is correlated with physical and cognitive fitness in the Lothian Birth Cohort 1936. Int J Epidemiol. 2015; 44:1388-1396.

64. Horvath S, Erhart W, Brosch M, Ammerpohl O, von Schönfels W, Ahrens M, Heits N, Bell JT, Tsai P-C, Spector TD, Deloukas P, Siebert R, Sipos B, et al. Obesity accelerates epigenetic aging of human liver. Proc Natl Acad Sci U S A 2014; 111:15538-15543.

65. Horvath S, Garagnani P, Bacalini M, Pirazzini C, Salvioli S, Gentilini D, DiBlasio A, Giuliani C, Tung S, Vinters H and Franceschi C. Accelerated Epigenetic Aging in Down Syndrome. Aging Cell. 2015; 14:491-495.

66. Horvath S and Levine AJ. HIV-1 infection accelerates age according to the epigenetic clock. J Infect Dis. 2015; 212:1563-1573.

67. Horvath S, Mah V, Lu AT, Woo JS, Choi OW, Jasinska AJ, Riancho JA, Tung S, Coles NS, Braun J, Vinters HV and Coles LS. The cerebellum ages slowly according to the epigenetic clock. Aging (Albany NY). 2015; 7:294-306.

68. Fagnoni FF, Vescovini R, Mazzola M, Bologna G, Nigro E, Lavagetto G, Franceschi C, Passeri M and Sansoni P. Expansion of cytotoxic CD8+ CD28- T cells in healthy ageing people, including centenarians. Immunology. 1996; 88:501-507.

69. Gruver AL, Hudson LL and Sempowski GD. Immunosenescence of ageing. The Journal of Pathology. 2007; 211:144-156.

70. Effros RB, Boucher N, Porter V, Zhu X, Spaulding C, Walford RL, Kronenberg M, Cohen D and Schächter F. Decline in CD28+ T cells in centenarians and in long-term T cell cultures: a possible cause for both in vivo and in vitro immunosenescence. Exp Gerontol. 1994; 29:601-609.

71. Potestio M, Pawelec G, Di Lorenzo G, Candore G, D'Anna C, Gervasi F, Lio D, Tranchida G, Caruso C and Romano GC. Age-related changes in the expression of CD95 (APO1/FAS) on blood lymphocytes. Exp Gerontol. 1999; 34:659-673.

72. Prelog M. Aging of the immune system: A risk factor for autoimmunity? Autoimmunity Reviews. 2006; 5:136-139.

73. Gentilini D, Mari D, Castaldi D, Remondini D, Ogliari G, Ostan R, Bucci L, Sirchia SM, Tabano S, Cavagnini F, Monti D, Franceschi C, Di Blasio AM, et al. Role of epigenetics in human aging and longevity: genome-wide DNA methylation profile in centenarians and centenarians' offspring. Age (Dordrecht, Netherlands). 2013; 35:1961-1973.

74. Bacalini MG, Gentilini D, Boattini A, Giampieri E, Pirazzini C, Giuliani C, Fontanesi E, Scurti M, Remondini D, Capri M, Cocchi G, Ghezzo A, Del Rio A, et al. Identification of a DNA methylation signature in blood cells from persons with Down Syndrome. Aging (Albany, NY). 2015; 7:82-96.

75. Gentilini D, Garagnani P, Pisoni S, Bacalini MG, Calzari L, Mari D, Vitale G, Franceschi C and Di Blasio AM. Stochastic epigenetic mutations (DNA methylation) increase exponentially in human aging and correlate with X chromosome inactivation skewing in females. Aging (Albany NY). 2015; 7:568-578.

76. Teschendorff AE, Marabita F, Lechner M, Bartlett T, Tegner J, Gomez-Cabrero D and Beck S. A beta-mixture quantile normalization method for correcting probe design bias in Illumina Infinium 450 k DNA methylation data. Bioinformatics. 2013; 29:189-196.

77. Klemera P and Doubal S. A new approach to the concept and computation of biological age. Mech Ageing Dev. 2006; 127:240-248.

78. Houseman E, Accomando W, Koestler D, Christensen B, Marsit C, Nelson H, Wiencke J and Kelsey K. DNA methylation arrays as surrogate measures of cell mixture distribution. BMC Bioinformatics. 2012; 13:86.

79. Christiansen L, Lenart A, Tan Q, Vaupel JW, Aviv A, McGue M, Christensen K. DNA methylation age is associated with mortality in a longitudinal Danish twin study. Aging Cell 2015, Nov 17. doi: 10.1111/acel.12421. Epub ahead of print.

80. Levine ME, Lu AT, Bennett DA, Horvath S. Epigenetic age of the pre-frontal cortex is associated with neuritic plaques, amyloid load, and Alzheimer's disease related cognitive functioning. Aging (Albany, NY) 2015; this issue.

81. Horvath S, Ritz BR (2015) Increased epigenetic age and granulocyte counts in the blood of Parkinson's disease patients. Aging (Albany, NY) 2015; this issue.

DNA methylation age of blood predicts future onset of lung cancer in the women's health initiative

Morgan E. Levine[1,2], H. Dean Hosgood[3], Brian Chen[4], Devin Absher[5,*], Themistocles Assimes[6,*], and Steve Horvath[1,7,*]

[1] Human Genetics, David Geffen School of Medicine, University of California LA, Los Angeles, CA 90095, USA;

[2] Center for Neurobehavioral Genetics, University of California Los Angeles, Los Angeles, California 90095, USA;

[3] Department of Epidemiology and Population Health, Albert Einstein College of Medicine, Bronx, NY 10461, USA;

[4] Longitudinal Study Section, Translational Gerontology Branch, Intramural Research Program, National Institute on Aging, National Institutes of Health, Bethesda, MD 20892, USA;

[5] HudsonAlpha Institute for Biotechnology, Huntsville, AL 35806, USA;

[6] Department of Medicine, Stanford University School of Medicine, Stanford, CA Stanford University School of Medicine, Stanford, CA 94305, USA;

[7] Biostatistics, School of Public Health, University of California Los Angeles, Los Angeles, CA 90095, USA.

[*] Joint senior authors

Abstract: Lung cancer is considered an age-associated disease, whose progression is in part due to accumulation of genomic instability as well as age-related decline in system integrity and function. Thus even among individuals exposed to high levels of genotoxic carcinogens, such as those found in cigarette smoke, lung cancer susceptibility may vary as a function of individual differences in the rate of biological aging. We recently developed a highly accurate candidate biomarker of aging based on DNA methylation (DNAm) levels, which may prove useful in assessing risk of aging-related diseases, such as lung cancer. Using data on 2,029 females from the Women's Health Initiative, we examined whether baseline measures of "intrinsic epigenetic age acceleration" (IEAA) predicted subsequent lung cancer incidence. We observed 43 lung cancer cases over the nearly twenty years of follow-up. Results showed that standardized measures of IEAA were significantly associated with lung cancer incidence (HR: 1.50, P=3.4×10^{-3}). Furthermore, stratified Cox proportional hazard models suggested that the association may be even stronger among older individuals (70 years or above) or those who are current smokers. Overall, our results suggest that IEAA may be a useful biomarker for evaluating lung cancer susceptibility from a biological aging perspective.

INTRODUCTION

Lung cancer is one of the most deadly of all cancers. While lung cancer accounts for only 14% of cancer incidence, it has an overall 5-year survival rate below 20% [1] and contributes to over a quarter of all cancer deaths [2]. In 2012 alone, an estimated 1.6 million people worldwide died from lung cancer. Lung cancer

also carries a high financial burden, costing the United States about $12 billion, annually [3] and as a result, prevention of lung cancer has become a key area of focus in medical research. Decades of research has identified smoking as the leading preventable cause of lung cancer, for which it is estimated to contribute to nearly 90% of all cases [4]. Lung cancer was an exceedingly rare disease at the end of the 19th century.

However, the growing popularity of smoking during the 20th century—particularly among males—gave way to rapidly increasing lung cancer rates. Tobacco smoke contains an array of chemicals, including a large number of genotoxic carcinogens, with the potential to cause mutations in essential genes, including those responsible for regulating cellular growth [5]. Not surprisingly, smoking history is the primary criterion used to decide who should undergo lung cancer screening with low-dose computed tomography (LDCT) [6].

In addition to smoking, chronological age is also a strong predictor of lung cancer risk. Like many other forms of cancer, lung cancer is considered an age-associated disease whose incidence rises steeply over the lifecourse, peaking around the seventh to eighth decade of life [1]. The link between lung cancer and age is hypothesized to arise in-part as a result of increasing accumulation of unrepaired damage [7] brought on by exposure to carcinogens, such as those found in cigarette smoke, as well as the age-related decline in immune system functioning [8] and increased cellular senescence [9]. Nevertheless, the rate of these changes significantly varies across individuals, and as a result, chronological age may not be the best proxy of the biological aging process underlying susceptibility to lung cancer incidence. DNA methylation levels at CpG dinucleotides may serve as a useful biomarker for assessing aging-related lung cancer susceptibility. Recently, we have developed a highly accurate candidate biomarker of aging based on DNA methylation (DNAm) levels [10], known as the "epigenetic clock", which can be used to measure the age of human cells, tissues, and organs. Given that both smoking is seen as a pro-aging factor, and that lung cancer is an age-associated disease, a measure of epigenetic age acceleration could provide information about which individuals are at the highest risk of developing lung cancer.

Our previous work has shown that age acceleration effects are highly heritable [11], which suggests they could be capturing innate differences in the degree of energy allocation for maintenance and repair, which in turn influences the rate of physiological decline with age. Thus individuals with naturally decelerated aging rates may be less susceptible to exogenous toxins such as cigarette exposure. In this context, we examined whether intrinsic epigenetic age acceleration (IEAA)—which refers to epigenetic age acceleration adjusted for abundance measures of blood cell counts—predicts development of lung cancer. Different from typical epigenome wide association studies (EWAS), the current study involves a single hypothesis based on DNA methylation data: that a measure of epigenetic age acceleration predicts incidence of lung cancer. We hypothesize that variations in IEAA will account for differential risk of lung cancer, especially among current smokers and/or older adults (ages 70+), for whom lung cancer susceptibility is the greatest.

RESULTS

Sample characteristics

As shown in Table 1, the mean age of our samples at baseline was 65.3 years (s.d.=7.1). Standardized IEAA ranged from -4.3 to 8.5. Overall, approximately half of our sample was non-Hispanic white (47.7%), just under one-third (31.9%) were African American, and about 20% were Hispanic. The majority of our sample reported never smoking (54.4%), whereas 35.2% were former smokers, and 10.4% were current smokers. The mean number of pack-years for the full sample was 9.5 (s.d.=18.6), while the number of pack-years was 19.4 among former smokers and 25.9 among current smokers. Over the approximately 20 years of follow-up, we observed 28,688 total person-years and a total of 43 lung cancer incidences among the 2,029 participants in our sample.

Table 1. Sample Characteristics (N=2,029)

Variable	Statistic
Standardized IEAA, Mean (S.D.)	0 (1)
Chronological Age, Mean (S.D.)	65.34 (7.10)
Non-Hispanic Black, Frequency (N)	0.32 (647)
Hispanic, Frequency (N)	0.20 (414)
Former Smoker, Frequency (N)	0.35 (714)
Current Smoker, Frequency (N)	0.10 (211)
Pack-Years Smoking, Mean (S.D.)	9.53 (18.55)
CHD Incidence, Frequency (N)	0.31 (646)
Lung Cancer Incidence, Frequency (N)	0.021 (43)
Person-Years, Total	28,688
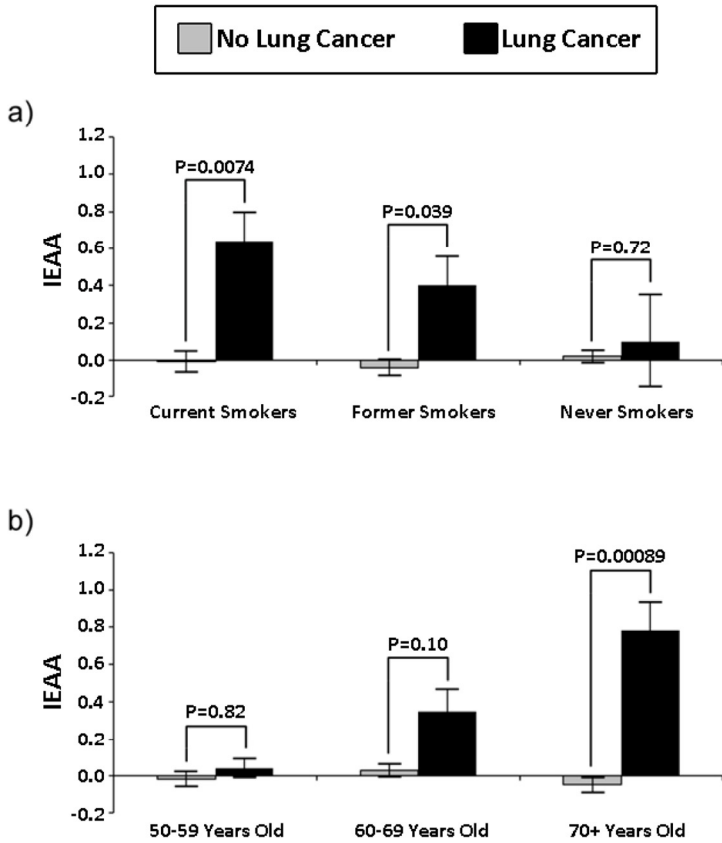
Figure 1. Smoking and age stratified barplots of standardized IEAA in cung cancer cases and controls.

IEAA predicts lung cancer incidence

The association between lung cancer and baseline IEAA was first examined using Kruskal Wallis tests. Results suggest that IEAA was significantly associated with subsequent lung cancer incidence for the full sample (P=9.7x10^{-4}). Additionally, in smoking and age stratified models (Figure 1), we found that IEAA was significantly associated with lung cancer incidence among current smokers (P=7.4x10^{-3}), former smokers (P=.039), and women in the oldest age group (70+) (P=8.9x10^{-4}). Results for current smokers and older women remain significant even after adjusting for multiple comparisons (Bonferroni P<8.3x10^{-3}).

Next we examined the associations using Cox proportional hazard models, adjusting for age, race/ethnicity, pack years, and smoking status. We found that IEAA at baseline significantly predicted lung cancer incidence (Table 2). The results using the full sample showed that a one unit increase in IEAA was associated with a 50% increase in the risk of developing

lung cancer (HR: 1.50; P=3.4x10^{-3}). Results for age-stratified models also showed that IEAA was more predictive of lung cancer incidence in older compared to younger age groups. For instance, among participants who were ages 50-59 at baseline, there was no association between IEAA and lung cancer incidence (HR: 0.94; P=0.91). However among those 60-69 years of age at baseline there was a marginal association (HR: 1.35; P=0.11) found, and among those 70-79 years old at baseline there was a statistically significant association between baseline IEAA and subsequent lung cancer incidence (HR: 2.51; P=7.7x10^{-4}), such that a one unit increase in IEAA was associated with an over two and a half fold increase in the risk of developing lung cancer.

We used the results from our Cox models to calculate Kaplan-Meier curves (lung cancer incidence) for women ages 70-79. These curves were calculated assuming 1) a chronological age of 75, 2) Non-Hispanic white race/ethnicity, 3) current smoking status, and 4) having 30 pack-years of smoking history. Three curves were calculated, varying the level of baseline IEAA

(standardized) so that it equaled -1, 0, and 1, respectively. As shown in Figure 2, having a standardized IEAA level equal to one greatly increased the likelihood of developing lung cancer over twenty years of follow-up. For instance, after ten years, only about 5% of individuals in the negative age acceleration group (IEAA=-1) were predicted to develop lung cancer, and after twenty-years the number was only predicted to rise to about 10%. In the average age acceleration group (IEAA=0), about 12%, and 25% of individuals were predicted to develop lung cancer after ten and twenty years, respectively. However, for women with positive age acceleration (IEAA=1), it was predicted that after ten years almost 25% would develop lung cancer, and after twenty years,

over half would have developed lung cancer. When examining these trends in younger groups as well, not only was lung cancer risk lower overall, but IEAA did not have as strong an effect on lung cancer incidence (Figure 3). For instance, estimates suggest that among those with negative age acceleration, the 10-year lung cancer incidence would only be 0.5% for smokers age 55, and 2% for smokers age 65. If they had average age acceleration, the 10-year lung cancer incidence was predicted to be only 1% for smokers age 55, and 4% for smokers age 65. Finally, for those with positive age acceleration, the 10-year lung cancer incidence was estimated to be 2% for smokers age 55 and 8% for smokers age 65.
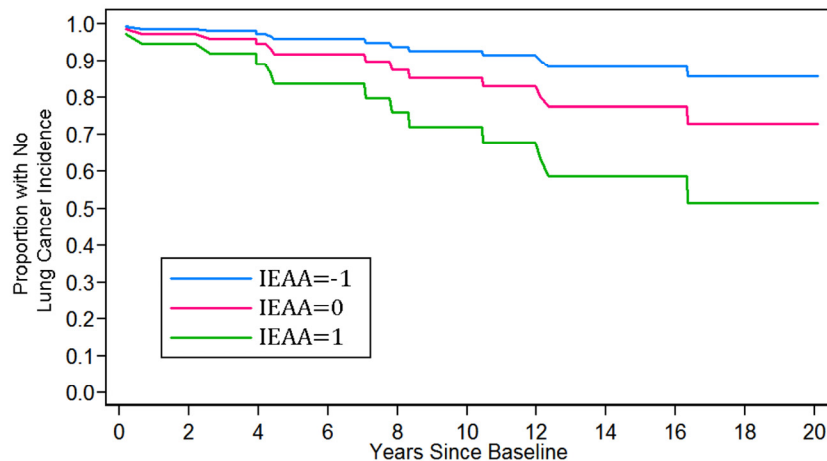

Figure 2. Kaplan -Meier curves for 20-year lung cancer incidence.

Table 2. Cox proportional hazard model of lung cancer, by age

	Hazard Ratio (P-Value)			
	All Ages	50-59	60-69	70+
IEAA	$1.50 \ (3.4 \times 10^{-3})$	0.94 (0.91)	1.35 (0.11)	$2.51 \ (7.7 \times 10^{-4})$
Age	$1.09 \ (2.0 \times 10^{-3})$	1.45 (0.17)	1.11 (0.19)	1.26 (0.05)
Black	0.87 (0.73)	1.12 (0.94)	0.64 (0.37)	1.88 (0.46)
Hispanic	1.25 (0.67)	0.90 (0.95)	0.72 (0.68)	6.53 (0.04)
CHD	0.64 (0.22)	0.00 (0.99)	0.61 (0.27)	0.90 (0.87)
Former Smoker	2.22 (0.09)	2.39 (0.53)	2.35 (0.18)	2.02 (0.41)
Current Smoker	$6.17 \ (3.8 \times 10^{-4})$	3.22 (0.44)	5.38 (0.02)	$14.78 \ (3.2 \times 10^{-3})$
Pack Years	$1.03 \ (1.7 \times 10^{-7})$	1.01 (0.56)	$1.03 \ (1.1 \times 10^{-4})$	$1.04 \ (2.1 \times 10^{-3})$
N	2,029	505	947	577
Events	43	4	27	12
Total Person-Years	28,688	7,595	13,540	7,554
R^2	0.036	0.012	0.045	0.054

Next we examined the association between IEAA and lung cancer incidence, stratified by smoking status, and adjusting for chronological age, race/ethnicity, CHD, and pack-years (except in the model for never smokers). We found that overall, IEAA was most predictive in current smokers, which also (as expected) was the group with the highest incidence rate of lung cancer (5.9%). Our results showed that for current smokers, a one unit increase in standardized IEAA was associated with an over two-fold increase in the risk of developing lung cancer (HR: 2.06; P=6.1x10^{-3}). For former smokers, who had a lung cancer incidence rate of about 3%, epigenetic age only marginally predicted lung incidence (HR: 1.40; P=0.11), and finally for never smokers, who had an incidence rate of only 0.7%, there was no association found (HR: 1.21; P=0.60) between IEAA and lung cancer risk.
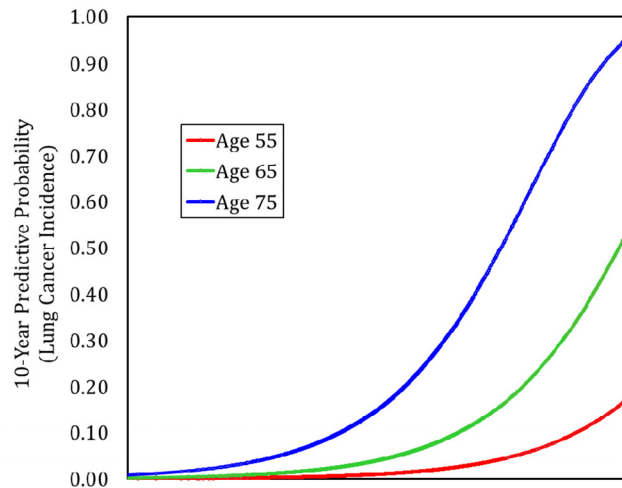
Figure 3. Predicted 10-Year lung cancer incidence by age and IEAA

Table 3. Cox proportional hazard model of lung cancer, by smoking status

	Hazard Ratio (P-Value)		
	Current Smokers	Former Smokers	Never Smokers
IEAA	2.06 (6.1x10^{-3})	1.41 (0.11)	1.21 (0.60)
Age	1.15 (0.02)	1.04 (0.31)	1.14 (0.03)
Black	0.69 (0.65)	0.86 (0.77)	1.17 (0.90)
Hispanic	2.06 (0.65)	0.00 (0.99)	6.79 (0.02)
CHD	0.53 (0.33)	0.38 (0.12)	1.52 (0.57)
Pack Years	1.04 (2.3x10^{-3})	1.02 (2.4x10^{-4})	
N	211	714	1,104
Events	13	22	8
Total Person-Years	2,799	10,015	15,875
R2	0.122	0.037	0.008
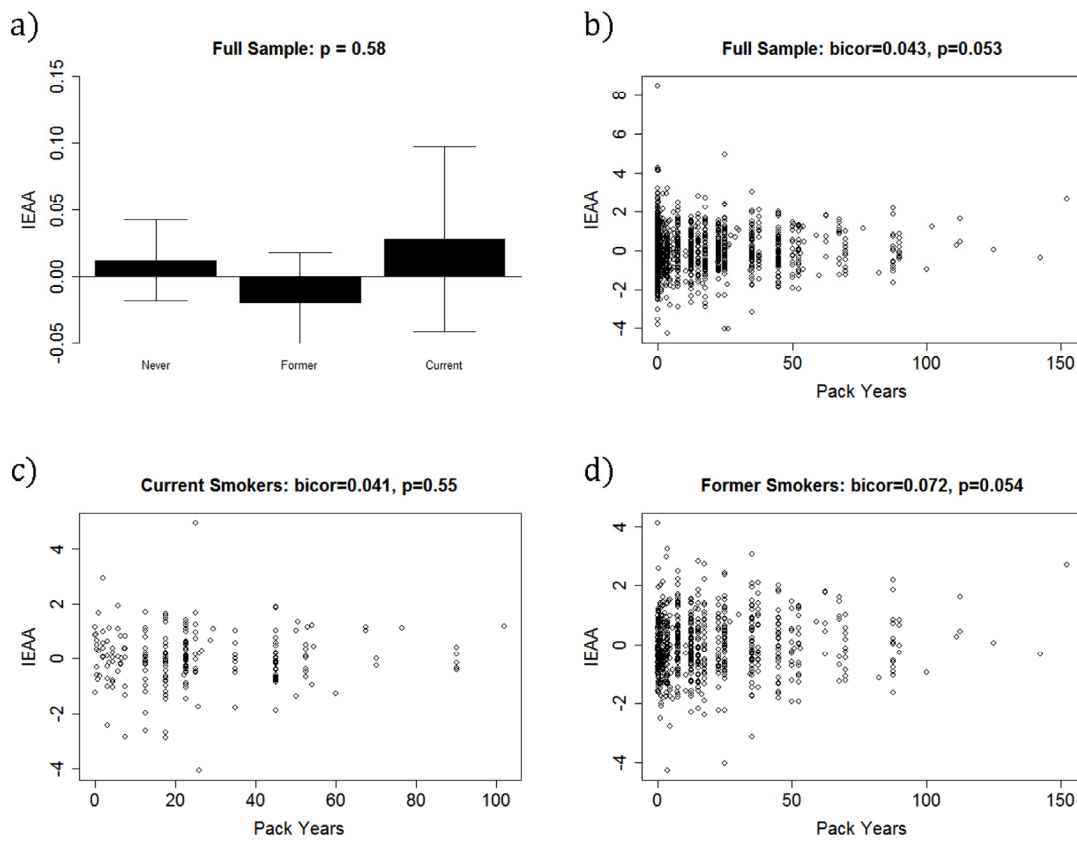
Figure 4. Baseline IEAA by smoking status and pack-years.

IEAA & smoking history

Finally, to assess whether cigarette use increased IEAA, we used the Kruskal Wallis test and biweight midcorrelation to examine the association between IEAA and both smoking status and pack-years. Barplots (Figure 4) showed no association between IEAA and smoking status (p=0.58). Using biweight midcorrelation we also examined whether higher pack-years of smoking was associated with an increase in IEAA. Overall, we found a positive but weak association when considering all participants (bicor=0.043, p=0.053) and former smokers (bicor=0.072, p=0.054) but no association among current smokers (bicor=0.041, p=0.55).

DISCUSSION

We have shown that a blood based measure of accelerated aging (IEAA) is a significant prognosticator of lung cancer incidence in a multi-ethnic sample of women. This suggests that IEAA may serve as a useful marker of the aging-related decline that influences lung cancer susceptibility, particularly among individuals exposed to high levels of cigarette smoke. Our results indicated that having an aging acceleration rate that is one standard deviation above the mean (standardized IEAA=1) is associated with as a high as a 2.5-fold increase in the risk of developing lung cancer. Given the lethality of lung cancer, identifying susceptible individuals early is essential.

Biomarkers which capture biological signals representing susceptibility could aid both primary and secondary prevention strategies for lung cancer by 1) raising awareness and influencing positive behavioral change among high-risk individuals, and 2) facilitating targeted screening and prevention strategies [12]. LDCT imaging aimed at early detection of lung cancer is a promising prevention strategy; however, screening criteria remains solely based on demographic and behavioral characteristics, particularly smoking history and age [6]. The use of high-dimensional omics markers has the potential to inform eligibility criteria and facilitate prevention. For instance, while we know that

smoking status is the largest predictor of lung cancer, and that the likelihood of incidence rises steeply with age, significant variation after accounting for age and smoking still exist. These differences may stem from individual-level variations in the rate of physiological alterations and system dysregulation that precede cancer pathogenesis, and ultimately could reflect differences in the rate of biological aging.

Aging is thought of as a time-dependent decline in system functioning, putting the organism at increased risk of death and disease [13]. Thus, under specific environmental circumstances, aging could enable the development of diseases such as lung cancer. There is evidence suggesting aging and cancer are inherently linked [14]. Cancer incidence is strongly age-dependent—the majority of lung cancer incidences occur among individuals who are 65 years or older [15]. There is speculation that both cancer and aging may occur as a result of damage accumulation and genomic instability, which if unresolved, can cause physiological degradation and contribute to cancer cell formation [7]. Additionally, interventions such as caloric restriction, which have been shown to retard aging in model organisms, also appear to have strong effects on cancer incidence, progression, and metastasis [16]. Together this could be taken to suggest individuals who age at an accelerated rate, have increased risk of cancer, including lung cancer, compared to their slower aging peers.

The link between aging and cancer is consistent with our results showing that participants who are epigenetically older have a higher incidence of lung cancer. Our model predicted that only 5% of older smokers with negative age acceleration (standardized IEAA equal to -1) would develop lung cancer over the following ten years, compared to 12% of older smokers with average age acceleration (IEAA=0), and 25% of older smokers with positive age acceleration (standardized IEAA equal to 1). We also showed that the ability for IEAA to predict lung cancer was strongest among individuals ages 70 and older. A one unit difference in IEAA was associated with a 2.5-fold increase in lung cancer among individuals ages 70+, compared to an only 50% increase when considering the entire 50+ year old sample. The ability of IEAA to predict lung cancer among the oldest age group is most likely due to the fact that this is the age group for whom lung cancer risk is the greatest. In the U.S., incidence of lung cancer has been shown to peak around ages 75 to 79—with 80% of lung cancer mortality occurring in individuals ages 65 and older, and 20% occurring in those who are 80 years or older [15]. Our results also show that lung cancer is most common in the oldest age groups and that this is particularly true among those

with accelerated aging. For instance, among individuals who were epigenetically younger than expected (IEAA=-1) it was predicted that 0.5% of smokers age 55, 2% of smokers age 65, and 7.5% of smokers age 75 would develop lung cancer over the next ten years. However, among individuals who were epigenetically older than expected (IEAA=1) it was predicted that 2% of smokers age 55, 8% of smokers age 65, and 29% of smokers age 75 would develop lung cancer over the next ten years. This likely ties back to the aging-dependent nature of lung cancer. Middle-aged individuals with accelerated aging phenotypes, may not have reached the point where they are biologically old enough to increase their risk of lung cancer incidence. On the other hand, older individuals with accelerated epigenetic aging, may have crossed the threshold that, under particular environmental circumstances such as smoking, puts them at risk of developing lung cancer. *In vivo* studies in mice showed that there was no effect of Bin1 ablation on cancer incidence in mice who were less than or equal to 12 months of age; however lung adenocarcinomas were present in half of the mosaic mice who were 18 to 20 months of age [17]. Additionally, an in vivo study using rats showed that intravenously administered rhabdomyosarcoma cells had increased colony forming capacity in lung if administered to old (15-month) rather than middle-aged (12-month) animals [18]. Together, these findings suggest that lung cancer incidence may results from exposure to endogenous carcinogens in the presence of aging-associated epigenetic alterations. This potential assumption is further supported by our findings from smoking-stratified models where we found a strong significant association between IEAA and lung cancer among smokers, compared to an only moderate association for former smokers and no association for never smokers. Furthermore, smoking status and pack-years was not associated with IEAA. This suggests that IEAA does not mediate the association between smoking and lung cancer, but rather that IEAA may only influence lung cancer if a person is a smoker. This could also mean that smoking is a bigger risk-factor for people who have accelerated aging phenotypes. If validated, this could be a useful marker for targeting smoking cessation interventions. Given that epigenetic age acceleration has been shown to be highly heritable [11], these findings could signify innate differences in susceptibility to endogenous stressors. Large-scale multinational genome-wide association studies (GWAS) of the genetic variation associated with lung cancer initially found that the 5p15 and 15q25 regions were associated with risk of lung cancer among smokers [19-24]. In moving forward, it may be useful to determine if genetic loci which influence lung cancer risk and longevity in smokers are associated with differences in IEAA.

Our study has several limitations which need to be acknowledged. First, our small number of lung cancer cases (n=43) prevented us from further stratifying our models (e.g. looking at the effect of IEAA in 70+ year old current smokers). Thus, validation of our findings in independent samples remains an important next step for understanding the relationship between IEAA and lung cancer. Second, our study was restricted to females who have lower rates of smoking and lung cancer compared to males in the U.S. Nevertheless, exposure to second-hand smoke could contribute to higher rates of lung cancer among non-smokers in our female-only sample, compared to a male-only sample. Third, we did not have data on histological subtype, or stage of lung cancer at diagnosis. Fourth, due to the sampling procedures, our-time to event analysis could be biased given that inclusion in the sample is dependent upon survival to 2010. Nevertheless, we also conducted analysis using logistic regression models and ran Cox models excluding cases diagnosed within 1, 3, and 5 years of baseline. Both procedures produced analogous results to what was reported.

The epigenetic clock has been shown to predict other aging-related outcomes, such as all-cause mortality [25], and cognitive and physical functions [26]. Further, it was used to show that 1) Down syndrome is associated with accelerated aging effects [27], 2) the cerebellum ages slowly [28], and 3) that the blood of subjects with a severe developmental disorder ages normally [29]. However, to the best of our knowledge, our study is the first to show its ability to predict future onset of lung cancer. Given that lung cancer has the highest cancer mortality rate, identifying susceptibility markers has the potential to extend life expectancy and improve quality of life through early detection and diagnosis. Our study demonstrates that a surrogate tissue (blood) lends itself for detecting accelerated aging effects that predispose the malignant transformation of other tissues (such as lung). Currently, we don't have any evidence that epigenetic aging effects in blood tissue lend themselves for prognostication of other kinds of cancers. If IEAA is found to be causal, rather than a byproduct of another causal pathway in lung cancer, alteration in CpG methylation could prove to be an effective method for preventing lung cancer among at-risk populations. Further, investigating this association in other populations (especially males) to establish whether lung cancer susceptibility loci operate through IEAA, and to determine whether interventions that modify methylation can decrease lung cancer risk, represent important next steps.

METHODS

Sample description. Participants included a subsample of 2,029 participants of the Women's Health Initiative (WHI) study, a national study that began in 1993, which enrolled postmenopausal women between the ages of 50-79 years [30]. Women who were ineligible to participate in the trials or who chose not to be randomized were invited to participate in the observation arm of the study. Participants selected for this study were part of an integrative genomics study with a primary aim of identifying novel genomic determinants of CHD. Thus, a case-control sampling design was adopted. All cases and controls were required to have already undergone genome wide genotyping at baseline as well as profiling of seven cardiovascular biomarkers as dictated by the aims of other ancillary WHI studies. The study design also resulted in oversampling of African American and Hispanics.

Smoking status. Smoking history was assessed at baseline from self-reports. Participants were first asked whether or not they had smoked at least 100 cigarettes in their lifetime. Those reporting 'no' to this question were classified as never smokers. Women reporting that they had smoked at least 100 cigarettes in their lifetime were then asked whether they smoked cigarettes now. Those who answered 'yes' were classified as current smokers and those who answered 'no' were classified as former smokers. Additionally, our study also utilized a variable for pack-years of smoking, which was based on current and former smokers' self-reports of the number of years they actively smoked, as well as the average number of cigarettes smoked per day.

Lung cancer incidence. Incident lung cancer cases were defined as either the first occurrence of lung cancer or a death due to lung cancer. Incidences were self-reported during annual health updates. Additionally, medical records were used to verify lung cancer incidence after being reviewed by physician adjudicators [31]. Characteristics of lung cancer were coded in accordance with the International Classification of Diseases for Oncology (ICD-O_2) from the Surveillance Epidemiology and End Result (SEER) [32]. National Death Index searches were performed to improve mortality ascertainment and lung cancer mortality was also verified via review of death certificates. Person-days for lung cancer incidence—which we converted to person-years, using precision to four decimal places—was also recorded by the WHI. Finally, participants with no reported lung cancer incidence or death were censored and the number of days (converted to years)

between baseline and their last day of observation in the WHI was set as their observation time.

DNA methylation data from blood. Methylation analysis was performed at HudsonAlpha Institute of Biotechnology using the Illumina Infinium Human-Methylation450 BeadChip. The Illumina BeadChips measures bisulfite-conversion-based, single-CpG resolution DNA methylation levels at 485577 different CpG sites in the human genome. These data were generated by following the standard protocol of Illumina methylation assays, which quantifies methylation levels by the β value using the ratio of intensities between methylated and un-methylated alleles. Specifically, the β value is calculated from the intensity of the methylated (M corresponding to signal A) and un-methylated (U corresponding to signal B) alleles, as the ratio of fluorescent signals β = Max(M,0) / [Max(M,0) + Max(U,0) + 100]. Thus, β values range from 0 (completely un-methylated) to 1 (completely methylated) (Dunning, 2008).

Intrinsic Epigenetic Age Acceleration (IEAA) in blood. We used the 353 CpGs and coefficient values reported in [11] to define DNAm age. These CpGs and coefficient values were chosen in independent data sets by regressing age on CpGs using the elastic net penalized regression model (implemented in the R package glmnet) [33]. DNAm age is defined as predicted age, in years.

Based on DNAm age, one can define several epigenetic measures of age acceleration, e.g. one can regress DNAm age on chronological age and form residuals. However, the resulting measure may still show some relationship to blood cell counts. Instead, we focus here on a measure of intrinsic epigenetic age acceleration (IEAA) where the term "intrinsic" implies that it is unconfounded by differences in blood cell types. Measures of IEAA are attractive for this study since they measure pure, unconfounded epigenetic aging effects, rather than measuring the age-related functional decline of the immune system—in blood cell composition such as the decrease of naive CD8+ T cells and the increase in memory or exhausted CD8+ T cells [34-37]. This measure, which is also known as "age acceleration adjusted for blood cell counts" and denoted by AAHOAdjCellCounts in our software, is defined as residual resulting from regressing DNAm age on chronological age and seven measures of blood cells counts including: naive CD8 T cells, exhausted CD8 T cells, plasma B cells (effector B cells), CD4 T cells, natural killer cells, monocytes, and granulocytes. The abundance measures of blood cells were imputed based on DNA methylation data as described in [38].

For IEAA, a positive value indicates that DNA methylation age is higher than expected given the individual's chronological age (accelerated aging), whereas a negative value indicates that DNA methylation age is lower than expected given the individual's chronological age (decelerated aging).

Statistical analysis. Kruskal Wallis tests were used to initially examine the association between IEAA at baseline and subsequent lung cancer incidence. Next, Cox proportional hazard models were used to test whether differences in IEAA predicted incidence of lung cancer. These models were run on the full sample of participants—adjusting for age, race/ethnicity, CHD status, pack-years and smoking status (never, former, current)—and stratifying by 1) 10-year age groups (50-59, 60-69, 70-79) and 2) smoking status. Based on these models, we calculated predictive probabilities for 10-year incidence of lung cancer based on IEAA. We adjusted for CHD status, given that it was an important inclusion criteria when the pilot sample was selected.

Funding

Conflict of interest statement

The authors declare there are no potential conflicts of interest.

REFERENCES

1. Howlader N, Noone A, Krapcho M, Garshell J, Neyman N, Altekruse S, Kosary C, Yu M, Ruhl J and Tatalovich Z. SEER Cancer Statistics Review, 1975-2010.[Based on the November 2012 SEER data submission, posted to the SEER web site, April 2013.]. Bethesda, MD: National Cancer Institute. 2013.
2. Group UCSW. United States Cancer Statistics: 1999–2011 incidence and mortality web-based report. Atlanta (GA): Department of Health and Human Services, Centers for Disease Control and Prevention, and National Cancer Institute. 2014.
3. Bender E. Epidemiology: The dominant malignancy. Nature. 2014; 513:S2-3.
4. Warren GW, Alberg AJ, Kraft AS and Cummings KM. The 2014 Surgeon General's report: "The health consequences of smoking--50 years of progress": a paradigm shift in cancer care. Cancer. 2014; 120:1914-1916.

5. Hecht SS. Lung carcinogenesis by tobacco smoke. Int J Cancer. 2012; 131:2724-2732.

6. National Lung Screening Trial Research T, Aberle DR, Adams AM, Berg CD, Black WC, Clapp JD, Fagerstrom RM, Gareen IF, Gatsonis C, Marcus PM and Sicks JD. Reduced lung-cancer mortality with low-dose computed tomographic screening. The New England journal of medicine. 2011; 365:395-409.

7. Lopez-Otin C, Blasco MA, Partridge L, Serrano M and Kroemer G. The hallmarks of aging. Cell. 2013; 153:1194-1217.

8. Derhovanessian E, Solana R, Larbi A and Pawelec G. Immunity, ageing and cancer. Immun Ageing. 2008; 5:11.

9. Rodier F and Campisi J. Four faces of cellular senescence. J Cell Biol. 2011; 192:547-556.

10. Horvath S, Zhang Y, Langfelder P, Kahn RS, Boks MP, van Eijk K, van den Berg LH and Ophoff RA. Aging effects on DNA methylation modules in human brain and blood tissue. Genome Biol. 2012; 13:R97.

11. Horvath S. DNA methylation age of human tissues and cell types. Genome Biol. 2013; 14:R115.

12. Cassidy A, Duffy SW, Myles JP, Liloglou T and Field JK. Lung cancer risk prediction: a tool for early detection. Int J Cancer. 2007; 120:1-6.

13. Yin D and Chen K. The essential mechanisms of aging: Irreparable damage accumulation of biochemical side-reactions. Experimental gerontology. 2005; 40:455-465.

14. Campisi J. Aging, cellular senescence, and cancer. Annu Rev Physiol. 2013; 75:685-705.

15. Akgun KM, Crothers K and Pisani M. Epidemiology and management of common pulmonary diseases in older persons. The journals of gerontology Series A, Biological sciences and medical sciences. 2012; 67:276-291.

16. Longo VD and Fontana L. Calorie restriction and cancer prevention: metabolic and molecular mechanisms. Trends Pharmacol Sci. 2010; 31:89-98.

17. Chang MY, Boulden J, Katz JB, Wang L, Meyer TJ, Soler AP, Muller AJ and Prendergast GC. Bin1 ablation increases susceptibility to cancer during aging, particularly lung cancer. Cancer research. 2007; 67:7605-7612.

18. Anisimov VN, Zhukovskaya NV, Loktionov AS, Vasilyeva IA, Kaminskaya EV and Vakhtin YB. Influence of host age on lung colony forming capacity of injected rat rhabdomyosarcoma cells. Cancer Lett. 1988; 40:77-82.

19. Landi MT, Chatterjee N, Yu K, Goldin LR, Goldstein AM, Rotunno M, Mirabello L, Jacobs K, Wheeler W, Yeager M, Bergen AW, Li Q, Consonni D, et al. A genome-wide association study of lung cancer identifies a region of chromosome 5p15 associated with risk for adenocarcinoma. Am J Hum Genet. 2009; 85:679-691.

20. Amos CI, Wu X, Broderick P, Gorlov IP, Gu J, Eisen T, Dong Q, Zhang Q, Gu X, Vijayakrishnan J, Sullivan K, Matakidou A, Wang Y, et al. Genome-wide association scan of tag SNPs identifies a susceptibility locus for lung cancer at 15q25.1. Nature genetics. 2008; 40:616-622.

21. Hung RJ, McKay JD, Gaborieau V, Boffetta P, Hashibe M, Zaridze D, Mukeria A, Szeszenia-Dabrowska N, Lissowska J, Rudnai P, Fabianova E, Mates D, Bencko V, et al. A susceptibility locus for lung cancer maps to nicotinic acetylcholine receptor subunit genes on 15q25. Nature. 2008; 452:633-637.

22. Wang Y, Broderick P, Webb E, Wu X, Vijayakrishnan J, Matakidou A, Qureshi M, Dong Q, Gu X, Chen WV, Spitz MR, Eisen T, Amos CI, et al. Common 5p15.33 and 6p21.33 variants influence lung cancer risk. Nature genetics. 2008; 40:1407-1409.

23. Wu C, Hu Z, Yu D, Huang L, Jin G, Liang J, Guo H, Tan W, Zhang M, Qian J, Lu D, Wu T, Lin D, et al. Genetic variants on chromosome 15q25 associated with lung cancer risk in Chinese populations. Cancer research. 2009; 69:5065-5072.

24. Truong T, Hung RJ, Amos CI, Wu X, Bickeboller H, Rosenberger A, Sauter W, Illig T, Wichmann HE, Risch A, Dienemann H, Kaaks R, Yang P, et al. Replication of lung cancer susceptibility loci at chromosomes 15q25, 5p15, and 6p21: a pooled analysis from the International Lung Cancer Consortium. J Natl Cancer Inst. 2010; 102:959-971.

25. Marioni RE, Shah S, McRae AF, Chen BH, Colicino E, Harris SE, Gibson J, Henders AK, Redmond P, Cox SR, Pattie A, Corley J, Murphy L, et al. DNA methylation age of blood predicts all-cause mortality in later life. Genome Biol. 2015; 16:25.

26. Marioni RE, Shah S, McRae AF, Ritchie SJ, Muniz-Terrera G, Harris SE, Gibson J, Redmond P, Cox SR and Pattie A. The epigenetic clock is correlated with physical and cognitive fitness in the Lothian Birth Cohort 1936. Int J Epidemiol. 2015:dyu277.

27. Horvath S, Garagnani P, Bacalini MG, Pirazzini C, Salvioli S, Gentilini D, Di Blasio AM, Giuliani C, Tung S, Vinters HV and Franceschi C. Accelerated epigenetic aging in Down syndrome. Aging cell. 2015; 14:491-495.

28. Horvath S, Mah V, Lu AT, Woo JS, Choi OW, Jasinska AJ, Riancho JA, Tung S, Coles NS, Braun J, Vinters HV and Coles LS. The cerebellum ages slowly according to the epigenetic clock. Aging (Albany NY). 2015; 7:294-306.

29. Walker RF, Liu JS, Peters BA, Ritz BR, Wu T, Ophoff RA and Horvath S. Epigenetic age analysis of children who seem to evade aging. Aging (Albany NY). 2015; 7:334-339.

30. Design of the Women's Health Initiative clinical trial and observational study. The Women's Health Initiative Study Group. Control Clin Trials. 1998; 19:61-109.

31. Curb JD, McTiernan A, Heckbert SR, Kooperberg C, Stanford J, Nevitt M, Johnson KC, Proulx-Burns L, Pastore L, Criqui M, Daugherty S, Morbidity WHI and Mortality C. Outcomes ascertainment and adjudication methods in the Women's Health Initiative. Annals of epidemiology. 2003; 13:S122-128.

32. Cunningham J. The SEER program code manual: Cancer Statistics Branch, National Cancer Institute, National Institutes of Health. 1994.

33. Friedman J, Hastie T and Tibshirani R. Regularization paths for generalized linear models via coordinate descent. Journal of statistical software. 2010; 33:1.

34. Fagnoni F, Vescovini R, Mazzola M, Bologna G, Nigro E, Lavagetto G, Franceschi C, Passeri M and Sansoni P. Expansion of cytotoxic CD8+ CD28-T cells in healthy ageing people, including centenarians. Immunology. 1996; 88:501.

35. Fagnoni FF, Vescovini R, Passeri G, Bologna G, Pedrazzoni M, Lavagetto G, Casti A, Franceschi C, Passeri M and Sansoni P. Shortage of circulating naive CD8+ T cells provides new insights on immunodeficiency in aging. Blood. 2000; 95:2860-2868.

36. Gruver A, Hudson L and Sempowski G. Immunosenescence of ageing. The Journal of pathology. 2007; 211:144-156.

37. Effros RB, Boucher N, Porter V, Zhu X, Spaulding C, Walford RL, Kronenberg M, Cohen D and Schächter F. Decline in CD28+ T cells in centenarians and in long-term T cell cultures: a possible cause for both in vivo and in vitro immunosenescence. Experimental gerontology. 1994; 29: 601-609.

38. Horvath S and Levine AJ. HIV-1 Infection Accelerates Age According to the Epigenetic Clock. J Infect Dis. 2015.

Epigenetic age analysis of children who seem to evade aging

Richard F. Walker[1], Jia Sophie Liu[2], Brock A. Peters[2], Beate R. Ritz[3], Timothy Wu[4,5], Roel A. Ophoff[4,5], and Steve Horvath[4,6]

[1]Physician's Scientific and Regulatory Services, Inc., Indian Rocks Beach, FL 33785, USA;

[2] Department of Research, Complete Genomics Inc. Mountain View CA94043 USA，BGI-Shenzhen，Shenzhen 518083, China

[3]Epidemiology, School of Public Health, University of California Los Angeles, Los Angeles, CA 90095, USA;

[4]Human Genetics, David Geffen School of Medicine, University of California Los Angeles, Los Angeles, CA 90095, USA;

[5]UCLA Center for Neurobehavioral Genetics, Semel Institute for Neuroscience and Human Behavior, University of California Los Angeles, Los Angeles, CA 90095, USA;

[6]Biostatistics, School of Public Health, University of California Los Angeles, Los Angeles, CA 90095, USA.

Abstract: We previously reported the unusual case of a teenage girl stricken with multifocal developmental dysfunctions whose physical development was dramatically delayed resulting in her appearing to be a toddler or at best a preschooler, even unto the occasion of her death at the age of 20 years. Her life-long physician felt that the disorder was unique in the world and that future treatments for age-related diseases might emerge from its study. The objectives of our research were to determine if other such cases exist, and if so, whether aging is actually slowed. Of seven children characterized by dramatically slow developmental rates, five also had associated disorders displayed by the first case. All of the identified subjects were female. To objectively measure the age of blood tissue from these subjects, we used a highly accurate biomarker of aging known as "epigenetic clock" based on DNA methylation levels. No statistically significant differences in chronological and epigenetic ages were detected in any of the newly discovered cases.
Our study shows that a) there are multiple children who maintain the façade of persistent toddler-like features while aging from birth to young adulthood and b) blood tissue from these cases is not younger than expected.

INTRODUCTION

We previously reported the unusual case of a teenage girl stricken with multifocal developmental dysfunctions including bilateral hip dislocations, abnormal brain development, tracheomalacia, gastro-intestinal disorders and dysmorphic features [1, 2]. In addition to these problems, her physical and functional development was dramatically delayed resulting in her appearing to be a toddler or at best a preschooler, even unto the occasion of her death at the age of 20 years (Figure 1). Her developmental rate, albeit significantly delayed, continued nonetheless. But the extremely slow rate of change gave the impression that she was not aging at all.

As the result of her persistent "toddler-like" appearance, she received extensive notoriety from the media, and was featured as the "girl who doesn't age" in press articles and television broadcasts [3-6]. Dr. Lawrence Pakula, the pediatrician who cared for her from birth described his patient's strange affliction, that did not fit any disease category, as an "unknown syndrome" later to be called "syndrome X" [5]. While the word syndrome accurately describes a group of symptoms that collectively indicate or characterize a disease, Pakula was also quoted as saying that "there's no one else like her in the world". While most of the individual defects she experienced are not uncommon in many children, it was her retaining toddler-like features while aging from birth to young adulthood that made the case

particularly unusual. Even children with growth retardation or failure to thrive exhibit maturation of facial and other physical/functional features with passage of time, indicating that their developmental program is still functional. In contrast, the peculiar trait of the first case suggested that her rate of aging was dramatically delayed or even arrested. If so, then perhaps an etiological understanding of her pathology might lead to novel treatments for age related diseases [2, 6].

The objectives of this study were two-fold. The first was to determine if other such cases of syndrome X actually exist and thus might represent a novel syndrome. Then, because the case's appearance remained that of a toddler despite the passage of time, our second objective was to determine if there was any evidence that the arrested development in such children is linked to a slowing down of aging at the molecular level.

Objectively measuring the age of tissue such as blood poses a significant methodological and conceptual challenge since it is debatable whether known causes of cellular senescence such as telomere length represent tissue, much less organismal aging [7-10]. We recently developed a biomarker of aging called epigenetic clock that is based upon DNA methylation (DNAm) levels [11]. The epigenetic clock is currently the preferred biomarker of organismal aging because a) it is more strongly correlated with chronological age than previous biomarkers including telomere length [12, 13], b) it is prognostic of all-cause mortality in later life [14], and c) it correlates with measures of physical and mental fitness in older age [15]. The utility of the method has been demonstrated in recent case studies, e.g. a) obesity accelerates epigenetic aging in liver tissue [13], b) trisomy 21 (Down syndrome) accelerates epigenetic aging [16], c) HIV infection accelerates epigenetic age [22], and d) the cerebellum ages slowly [23].

RESULTS

Here we applied the epigenetic clock method to assess the epigenetic age of blood tissue from 7 syndrome X cases and n=106 controls (total n=113) as described in the following.

Selection of cases and controls

The first case who passed away at the age of 20 due to respiratory complications [17], was not part of this epigenetic study. To achieve our study objectives, we first needed to determine whether the clinical condition of the first case was indeed unique in the world. Many families with children suffering from developmental

delay and related complications responded to the broadcasts covering the first case seeking help from Dr. Walker. The parents of subjects described in this study volunteered to participate because one of their children was diagnosed with clinical symptoms comparable to those of our first case. Ethical review of this study was conducted and approved by the UCLA IRB on April 30, 2014 (IRB#14-000140, "Genetic and epigenetic study of children with severely delayed development or aging").
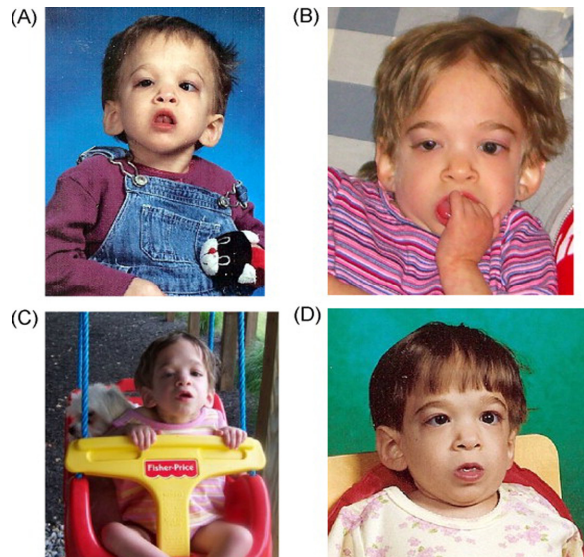
Figure 1. **Photographs of the first case at various ages**. (**A**) 5 years old, (**B**) 10 years old, (**C**) 11 years old, (**D**) 15 years old. Note that only minimal changes in physical appearance can be observed during the transition from childhood to adolescence. The case was not part of this study. Credits: Reproduced with kind permission from the publisher of [1].

Each family provided detailed information to allow verification that their child's condition was in fact, similar to those reported for the first case. As expected, the majority of respondents had children with developmental delay easily attributable to known factors. These families were excluded from the study. On the other hand, several subjects were identified as potential candidates for further study after careful review of their medical and family records (such as written descriptions, diaries, and pictures). Like the first case, all failed to grow even when provided with hormone replacement or hypercaloric diets and appeared to be significantly younger than their chronological ages. They were also afflicted with similar neurological, gastrointestinal, cardiac, and orthopedic problems suggesting that their clinical conditions might actually represent a novel syndrome.

(A)   (B)   Age 2.5   (C)   Age 6   9 year old sister

Figure 2. **Photographs of one of the cases in the current study at various ages**. (**A**) 2.5 years old, (**B**) 4 years old, (**C**) 6 years old next to her 9 year old sister. Note that only minimal changes in physical appearance can be observed.

The following criteria were used for inclusion in the study. Except for the first two which were required, all subjects met a majority of the remaining criteria although differing to some degree in severity.

1.   Physical appearance and developmental characteristics of an infant/toddler despite chronological ages normally associated with more mature features.
2.   Retarded growth rate of height standard deviation score (SDS) more than 3 SDS below the mean for chronological age and sex; failure of hormonal and/or dietary interventions intended to overcome the deficit.
3.   Dysmorphic features,
4.   Club feet and hip dislocations,
5.   Brain abnormalities including but not limited to agenesis of corpus callosum, pachygyria, lissencephaly and polymicrogyria,
6.   Minimal cognitive development, lack of speech, visual and/or hearing defects,
7.   Laryngotracheomalacia and reactive airway disease,
8.   Gastrointestinal developmental disorders and swallowing dysfunction often requiring G-tube for feeding.

Apart from seven families with potentially affected children, we also included five "control" families with children whose ages were comparable to those of the study subjects. We also included 62 unrelated healthy control subjects aged between 35 and 61.

Thirteen of twenty suspected syndrome X children did not meet the stringent inclusion criteria because they exhibited growth problems of known etiology or did not present as toddlers or pre-schoolers at an inappropriate age. However, five suspected cases met the stringent inclusion criteria and presented no evidence of chromosomal abnormalities according to a karyotype and microarray-based comparative genomic hybridization (CGH) analysis. We consider these five female subjects aged 2.3, 2.5, 5.8, 9.6, and 11.3 years as representing "pure" cases of syndrome X. Apparent lack of physical maturation in one of these children is shown in Figure 2. While two of the 20 suspected cases did not meet all of the syndrome X criteria, we studied them as well because they displayed strikingly delayed aging, atypical of their diagnosed syndromes. These included a 5.5 year old girl with Turner syndrome (Ring-X) and a 25.3 year old woman with trisomy 21 (Down syndrome). The fact that the Down syndrome (DS) case failed to develop/age in a typical fashion is interesting since DS subjects arguably exhibit several clinical manifestations of accelerated aging including early onset Alzheimer's disease [18-20].

Epigenetic age analysis

Epigenetic age was calculated using the epigenetic clock method/software described in Methods and in [11]. DNAm age of blood was highly correlated with chronological age in all subjects (r=0.98; Figure 3A) and in subjects younger than 12 years (r=0.92; Figure 3B), which validates the high accuracy of this biomarker of aging. Surprisingly, we did not find any evidence that blood tissue from the five pure syndrome X subjects was younger than expected based on their chronological age (Figure 3C, D). The mean DNAm age of the five pure syndrome X subjects was 6.7 years (standard error=1.0) which is not significantly different

from the mean chronological age of 6.3 years (standard error=1.8). Notably, the oldest pure syndrome X case had a DNAm age of 14.5 years which was 3.2 years older than her true chronological age. The DNAm age of the case with Turner syndrome was 1.5 years older than her chronological age (5.5) which was well within the margin of error. The case with Down syndrome and syndrome X-like developmental characteristics exhibited a DNAm age of 31.2 years which was 6 years older than her chronological age. The results for this DS subject are congruent with those from a recent study [16] that demonstrated that DS subjects exhibit accelerated epigenetic aging effects.

The small sample size did not provide sufficient statistical power for detecting any obvious abnormalities in the DNA methylation profiles. No statistically significant epigenetic markers (CpGs) were found after correcting for multiple comparisons. None of the CpGs were significant at a false discovery rate threshold of 0.05.
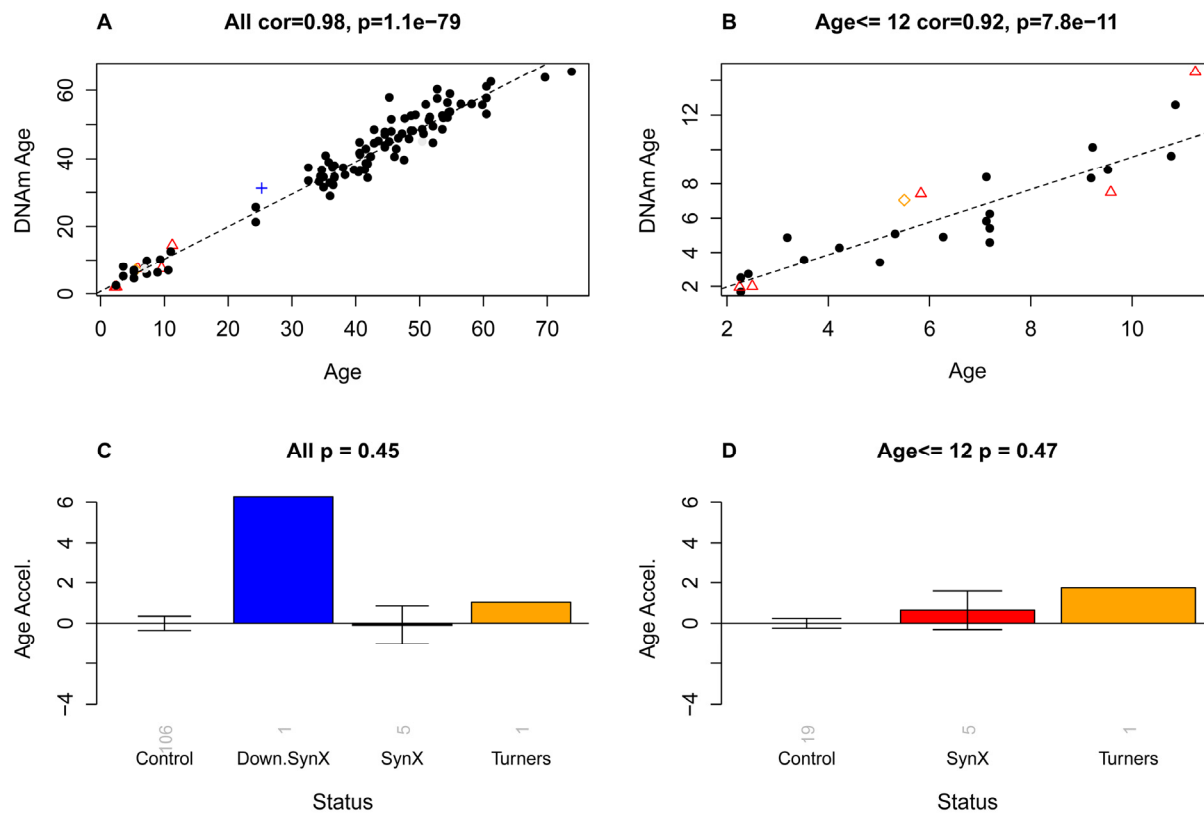
Figure 3. Epigenetic age versus chronological age and disease status. The first row (A,B) shows scatter plots between chronological age (x-axis) and DNAm age (y-axis) in (A) all subjects and (B) in subjects younger than or equal to 12. Red triangles indicate the pure syndrome X subjects. The blue cross and the orange diamond correspond to the Down syndrome and Turner syndrome case, respectively. The dashed black line corresponds to a regression line through control subjects. Note that the red triangles do not lie below the regression line, i.e. there is no evidence that these subjects are younger than expected. For each subject, a measure of epigenetic age acceleration was defined as vertical distance between the corresponding point and the regression line in the scatter plot. (C,D) Mean epigenetic age acceleration (y-axis) versus disease status in (C) all subjects and (D) younger subjects, respectively. By definition, the mean age acceleration measure in controls is zero. The title of the bar plots also reports a p-value from a non-parametric group comparison test (Kruskal Wallis test). Each bar plot depicts the mean value and 1 standard error.

DISCUSSION

We identified five new cases whose clinical presentations were similar to the first case. Prior screening eliminated any of the recognized causes of developmental delay and selected subjects also retained youthful facial and structural/functional features atypical of children suffering growth retardation of known etiology. As with the first case, the newly discovered cases lacked any obvious genetic problems according to karyotype and a microarray comparative genome hybridization analysis. Thus, while extremely rare, the first case described was not unique in the world. Furthermore, since such children require extensive medical care to survive, especially during the first years after birth, it may be that most succumb before ever being diagnosed. While the protocol did not mandate gender selection/preference, all subjects were female. It is not known whether this occurrence was due to chance alone or is a sex linked aspect of the putative syndrome. According to the epigenetic clock method, blood tissue from these cases is age appropriate. These findings are consistent with leukocyte telomere measurements in our first case [1]. Incidentally, leukocyte telomere length captures another dimension of aging and is at best weakly correlated with DNAm age after correcting for chronological age [12, 13].

Our results demonstrate that despite the clinical appearance of delayed maturation in children afflicted with syndrome X, the epigenetic clock indicates that the rate of development in blood and perhaps other tissues is normal. Thus, while we cannot exclude tissue-specific ageing as causal in syndrome X, the current findings suggest that the observed delay in whole body development results from other, yet undiscovered factors.

Overall, our analysis of blood tissue shows that aging in our study subjects is not arrested in all tissues. Future studies should assess whether other tissue types from these subjects (or their bodies as a whole) evade epigenetic aging.

METHODS

DNA methylation data. The DNA methylation data set has been deposited in Gene Expression Omnibus (GSE64495).

Blood samples were drawn sequentially on a given day from all members of the same family into anticoagulant (EDTA) containing tubes, immediately frozen on dry ice and shipped overnight to the processing center. Tubes were coded to prevent bias in subsequent analysis. Genomic DNA was extracted and purified using the RecoverEase DNA Isolation Kit (Agilent Technologies, La Jolla, CA, USA). Bisulfite conversion using the Zymo EZ DNA Methylation Kit (ZymoResearch, Orange, CA, USA) as well as subsequent hybridization of the Human Methylation450K Bead Chip (Illumina, SanDiego, CA), and scanning (iScan, Illumina) were performed according to the manufacturers protocols by applying standard settings. DNA methylation levels (β values) were determined by calculating the ratio of intensities between methylated (signal A) and un-methylated (signal B) alleles. Specifically, the β value was calculated from the intensity of the methylated (M corresponding to signal A) and un-methylated (U corresponding to signal B) alleles, as the ratio of fluorescent signals $\beta = \text{Max}(M,0)/[\text{Max}(M,0)+\text{Max}(U,0)+100]$. Thus, β values ranged from 0 (completely un-methylated) to 1 (completely methylated). We used background corrected beta values that result from the BeadStudio software (version 3.2).

Estimation of DNAm age using the epigenetic clock method. Statistically speaking, the epigenetic clock is a prediction method of age based on the DNAm levels of 353 CpGs dinucleotides. Predicted age, referred to as DNAm age, correlates with chronological age in sorted cell types (CD4 T cells, monocytes, B cells, glial cells, neurons) as well as in tissues and organs including whole blood, brain, breast, kidney, liver, lung, saliva [11]. Mathematical details and software tutorials for the epigenetic clock can be found in the Additional files of reference [11]. An online age calculator is provided at our webpage [21].

Legal statements

Figure 1 is reproduced from Walker et al 2009 (PMID: 19428454). We have obtained an official license from the publisher (Elsevier) to reproduce this Figure in our article. Further, we have obtained the signed permission from the parents of the subjects depicted in Figure 2 regarding the use of these photographs.

Conflict of interest statement

The authors declare no conflict of interest.

REFERENCES

1. Walker RF, Pakula LC, Sutcliffe MJ, Kruk PA, Graakjaer J and Shay JW. A case study of "disorganized development" and its possible relevance to genetic determinants of aging. Mechanisms of Ageing and Development. 2009; 130:350-356.

2. Walker RF. Developmental Theory of Aging Revisited: Focus on Causal and Mechanistic Links Between Development and Senescence. Rejuvenation Research. 2011; 14:429-436.

3. Schindehette S. Frozen in Time. People Magazine 2001; 56.

4. James S. 2005. A child frozen in time. Dateline NBC News.

5. Brown B. 2009. Doctors Baffled, Intrigued by Girl Who Doesn't Age. ABC News 20/20, June 23, 2009.

6. Gates S. 2013. Brooke Greenberg's 'Syndrome X' condition defies age baffles doctors (Video). Huffington Post, April 5, 2013.

7. Campisi J. Senescent cells, tumor suppression, and organismal aging: good citizens, bad neighbors. Cell. 2005; 120: 513-522.

8. Collado M, Blasco MA and Serrano M. Cellular Senescence in Cancer and Aging. Cell. 2007; 130:223-233.

9. Chen J-H, Hales CN and Ozanne SE. DNA damage, cellular senescence and organismal ageing: causal or correlative? Nucleic Acids Research. 2007; 35:7417-7428.

10. Sanders J, Boudreau R and Newman A. 2012. Understanding the Aging Process Using Epidemiologic Approaches. (Dordrecht Heidelberg New York: Springer).

11. Horvath S. DNA methylation age of human tissues and cell types. Genome Biol. 2013; 14(R115).

12. Boks MP, Derks EM, Weisenberger DJ, Strengman E, Janson E, Sommer IE, Kahn RS and Ophoff RA. The Relationship of DNA Methylation with Age, Gender and Genotype in Twins and Healthy Controls. PLoS ONE. 2009; 4:e6767.

13. Horvath S, Erhart W, Brosch M, Ammerpohl O, von Schönfels W, Ahrens M, Heits N, Bell JT, Tsai P-C, Spector TD, Deloukas P, Siebert R, Sipos B, et al. Obesity accelerates epigenetic aging of human liver. Proc Natl Acad Sci U S A 2014; 111:15538-15543.

14. Marioni R, Shah S, McRae A, Chen B, Colicino E, Harris S, Gibson J, Henders A, Redmond P, Cox S, Pattie A, Corley J, Murphy L, et al. DNA methylation age of blood predicts all-cause mortality in later life. Genome Biol. 2015; 16:25.

15. Marioni RE, Shah S, McRae AF, Ritchie SJ, Muniz-Terrera G, Harris SE, Gibson J, Redmond P, Cox SR, Pattie A, Corley J, Taylor A, Murphy L, et al. The epigenetic clock is correlated with physical and cognitive fitness in the Lothian Birth Cohort 1936. Int J Epidemiol. 2015; Epub ahead of print.

16. Horvath S, Garagnani P, Bacalini M, Pirazzini C, Salvioli S, Gentilini D, DiBlasio A, Giuliani C, Tung S, Vinters H and Franceschi C. Accelerated Epigenetic Aging in Down Syndrome. Aging Cell. 2015; 14:491-495.

17. James S. 2013. Maryland 20-Year-Old Dies Never Having Aged. Digital Reporter via Good Morning America. (http://abcnews.go.com/Health/maryland-20-year-dies-aged/story?id=20712718: ABC News), pp. Story ID=20712718.

18. Devenny DA, Wegiel J, Schupf N, Jenkins E, Zigman W, Krinsky-McHale SJ and Silverman WP. Dementia of the Alzheimer's type and accelerated aging in Down syndrome. Sci Aging Knowledge Environ. 2005; 6.

19. Patterson D and Cabelof DC. Down syndrome as a model of DNA polymerase beta haploinsufficiency and accelerated aging. Mechanisms of Ageing and Development. 2012; 133:133-137.

20. Moran J. 2013. Aging and Down Syndrome. A Health & Well-Being Guidebook.

21. Horvath S. 2013. Webpage: http://labs.genetics.ucla.edu/horvath/dnamage.

22. Horvath S, Levine AJ. 20150 HIV-1 infection accelerates age according to the epigenetic clock. J Infect Dis. 2015; PMID: 25969563.

23. Horvath S, Mah V, Lu AT, Woo JS, Choi O, Jasinska AJ, Riancho JA, Tung S, Coles NS, Braun J, Vinters HV, and Coles LS The cerebellum ages slowly according to the epigenetic clock. Aging (Albany NY) 2015; 5: Ahead of print.

The cerebellum ages slowly according to the epigenetic clock

Steve Horvath[1,2,] Vei Mah[3], Ake T. Lu[1], Jennifer S. Woo[3], Oi-Wa Choi[4], Anna J. Jasinska[4], José A. Riancho[5], Spencer Tung[3], Natalie S. Coles[6], Jonathan Braun[3], Harry V. Vinters[3], and L. Stephen Coles[6,*]

[1]Human Genetics, David Geffen School of Medicine, University of California Los Angeles, Los Angeles, CA 90095, USA;
[2]Biostatistics, School of Public Health, University of California Los Angeles, Los Angeles, CA 90095, USA;
[3]Pathology and Laboratory Medicine, UCLA David Geffen School of Medicine, Los Angeles, CA 90095, USA;
[4]Center for Neurobehavioral Genetics, University of California, Los Angeles, CA 90095, USA;
[5]Department of Internal Medicine, H.U. Marqués de Valdecilla-IFIMAV-University of Cantabria, Santander 39008, Spain;
[6]UCLA Molecular Biology Institute; Department of Chemistry and Biochemistry; Los Angeles, CA 90095, USA.
*Passed away during the study

Abstract: Studies that elucidate why some human tissues age faster than others may shed light on how we age, and ultimately suggest what interventions may be possible. Here we utilize a recent biomarker of aging (referred to as epigenetic clock) to assess the epigenetic ages of up to 30 anatomic sites from supercentenarians (subjects who reached an age of 110 or older) and younger subjects. Using three novel and three published human DNA methylation data sets, we demonstrate that the cerebellum ages more slowly than other parts of the human body. We used both transcriptional data and genetic data to elucidate molecular mechanisms which may explain this finding. The two largest superfamilies of helicases (SF1 and SF2) are significantly over-represented (p=9.2x10^{-9}) among gene transcripts that are over-expressed in the cerebellum compared to other brain regions from the same subject. Furthermore, SNPs that are associated with epigenetic age acceleration in the cerebellum tend to be located near genes from helicase superfamilies SF1 and SF2 (enrichment p=5.8x10^{-3}). Our genetic and transcriptional studies of epigenetic age acceleration support the hypothesis that the slow aging rate of the cerebellum is due to processes that involve RNA helicases.

INTRODUCTION

Since it is difficult to study what one cannot measure, the development of suitable measures of biological age has been a major goal of gerontology [1, 2]. Many biomarkers of aging have been studied ranging from telomere length [3, 4] to whole-body function such as gait speed. DNA methylation (DNAm) levels are particularly promising biomarkers of aging since chronological age (i.e. the calendar years that have passed since birth) has a profound effect on DNA methylation levels in most human tissues and cell types

[5-14]. Several recent studies propose to measure accelerated aging effects using DNA methylation levels [15-20]. While previous epigenetic age predictors apply to a single tissue, our recently developed "epigenetic clock" (based on 353 dinucleotide markers known as Cytosine phosphate Guanines or CpGs) applies to most human cell types, tissues, and organs [19]. Predicted age, referred to as DNA methylation age, correlates with chronological age in sorted cell types (CD4 T cells, monocytes, B cells, glial cells, neurons), tissues and organs including whole blood, brain, breast, kidney, liver,

lung, saliva [19], and even prenatal brain samples [21]. The epigenetic clock is an attractive biomarker of aging for the following reasons: a) it is more highly correlated with chronological age than previous biomarkers [22, 23], b) it applies to most tissues, cell types, and fluids that contain human DNA (with the exception of sperm), c) it relates, to some extent, to biological age since DNAm age of blood is predictive of all-cause mortality even after adjusting for chronological age and a variety of known risk factors [24]. Similarly, markers of physical and mental fitness are also found to be associated with the epigenetic age of blood (lower abilities associated with age acceleration) [25]. Perhaps the most exciting feature of the epigenetic clock is the prospect of using it for comparing the ages of different tissues and cell types from the same individual [19]. While the mathematical algorithm lends itself for contrasting the ages of different tissues, it remains an open research question whether the results are biologically meaningful. To provide empirical data for addressing this question, we proceed with all due caution in this study.

RESULTS

We had previously shown that tissues from the same middle aged individuals exhibit similar DNAm ages [19] and additional data from the public domain confirm this result (Figure 1). But it is not yet known whether some tissues collected from centenarians - and particularly supercentenarians appear to be younger than the rest of the body, which would indicate that they are better protected against aging. Here we assess the epigenetic ages of an unprecedented number of tissues (up to 30 tissues) from supercentenarians and younger controls. An overview of our data sets is presented in Table 1. Apart from three novel DNA methylation data sets, we also analyzed three publicly available data sets.

DNA methylation age vs. actual age in different tissues
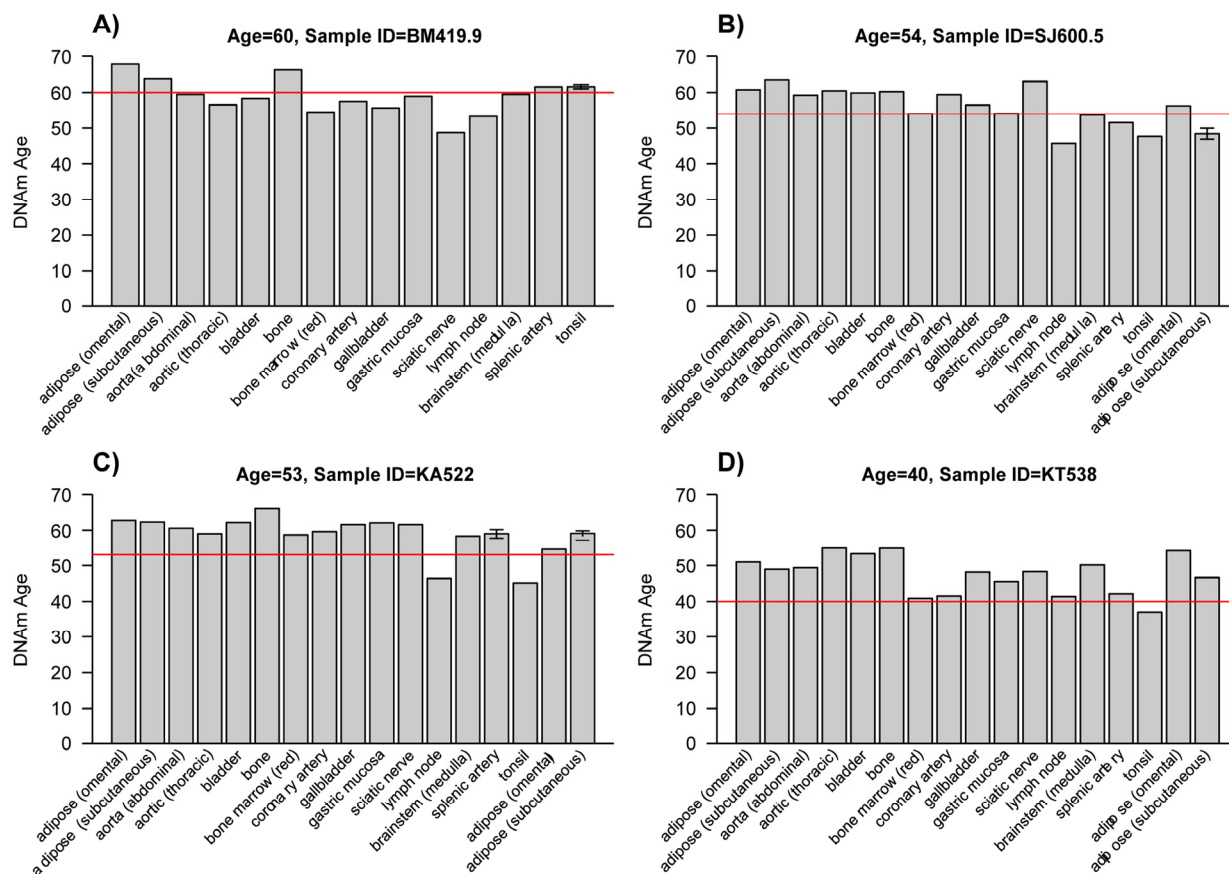
Figure 1. DNA methylation ages of various tissues from four middle-aged individuals. Here we use data set 4 (Lokk, et al; 2014) to assess the tissue ages of 4 subjects (each of which corresponds to a different panel and person identifier such as BM419.9). Bars report the DNAm age in the corresponding tissue. The red horizontal line reports the chronological age. These plots confirm that tissues from the same middle aged individuals exhibit similar DNAm ages.
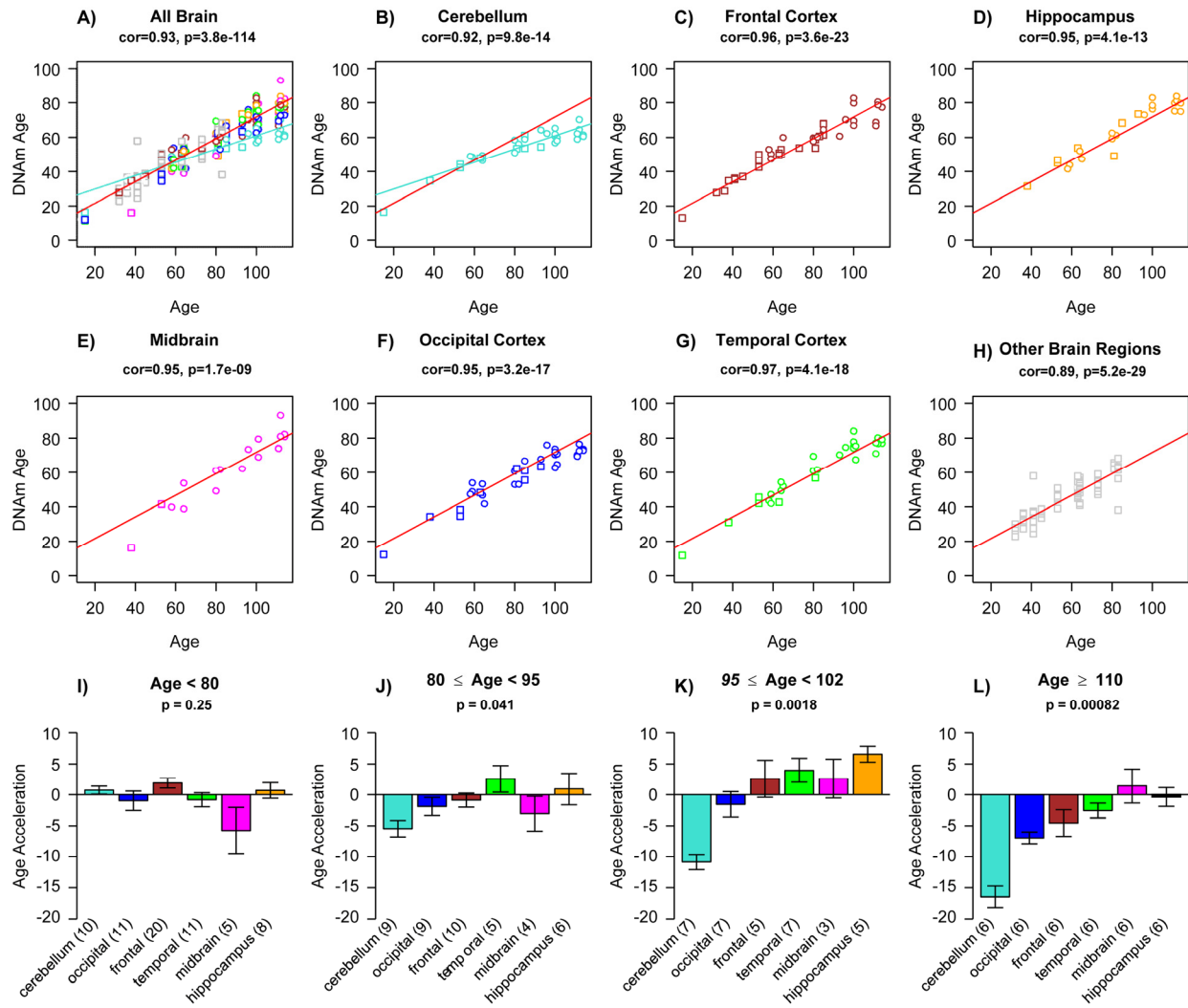
Figure 2. **Epigenetic age acceleration in various brain regions**. (**a**) Scatter plot relating the DNAm age of each brain sample (y-axis) versus the corresponding chronological age (x-axis). Points are colored by brain regions (e.g. turquoise for cerebellum) as indicated in (**b-h**). Linear regression lines through cerebellar samples and non-cerebellar samples are colored in turquoise and red, respectively. Note that cerebellar samples (turquoise points) exhibit a lower rate of change (i.e. slope of the turquoise line) than non-cerebellar samples. In the scatter plots, circles and squares correspond to brain regions from Alzheimer's disease subjects and controls, respectively. Scatter plots show (**b**) cerebellar samples only, (**c**) frontal lobe, (**d**) hippocampus, (**e**) midbrain, (**f**) occipital cortex, (**g**) temporal cortex, and (**h**) remaining brain regions, which include caudate nucleus, cingulate gyrus, motor cortex, sensory cortex and parietal cortex. The subtitle of each scatter plot reports a Pearson correlation coefficient and corresponding p-value. Epigenetic age acceleration was defined as the vertical distance of each sample from the red regression line in (**a**). (**i-l**) Age acceleration versus brain region in different age groups as indicated in the respective titles. Cerebellar samples tend have the lowest (negative) age acceleration (turquoise bars) followed by occipital cortex (blue bars). Each bar plot depicts the mean value and one standard error and reports a non-parametric group comparison test p-value (Kruskal Wallis Test).

Epigenetic age (referred to as DNAm age) was calculated as described in [19] from human samples profiled with the Illumina Infinium 450K platform. As expected, DNAm age has a strong linear relationship with chronological age in brain tissue samples (Figure 2a-h). We did not find a relationship between Alzhei-mer's disease (AD) and age acceleration in these samples from older subjects, which is why we ignored disease status in the analysis. Strikingly, the DNAm age of cerebellar samples exhibits a lower rate of change with age than non-cerebellar samples (as can be seen by comparing the turquoise line with the red line in Figure

2a,b). To formally measure age acceleration effects, we defined age acceleration as the residual resulting from a linear model that regressed DNAm age against chronological age in non-cerebellar brain sample. Thus, a tissue sample that exhibits negative age acceleration appears to be younger than expected based simply on chronological age.

All brain regions have similar DNAm ages in subjects younger than 80 (Figure 2i), but brain region becomes an increasingly significant determinant of age acceleration in older subjects (as can be seen from the Kruskal Wallis test p-values in Figure 2i-l).

Note that the cerebellum and to a lesser extent the occipital cortex exhibit negative epigenetic age acceleration in the oldest old (Figure 2k), i.e. these brain regions are younger than expected. These results can also be observed by focusing on six individual centenarians (Figure 3) and when evaluating two

independent validation data sets (Figure 5).

Comprehensive tissue analysis of a supercentenarian

To study age acceleration effects in non-brain tissues as well, we profiled a total of 30 tissues of a 112 year old woman (Figure 3a) who is described in Methods. We generated at least 2 replicate measurements per tissue and found that replicate age estimates are highly reproducible (r=0.71, Figure 4). Interestingly, the cerebellum exhibited the lowest (negative) age acceleration effect compared to the remaining 29 other regions. In contrast, bone, bone marrow, and blood exhibit relatively older DNAm ages. Given that bone appears to be older than other parts of the body, it is worth mentioning that our novel data demonstrate that the epigenetic clock applies to bone samples (largely comprised of osteocytes/osteoblasts) as well (Figure 6). To understand why the cerebellum evades epigenetic aging, we turned to transcriptional and genetic data.
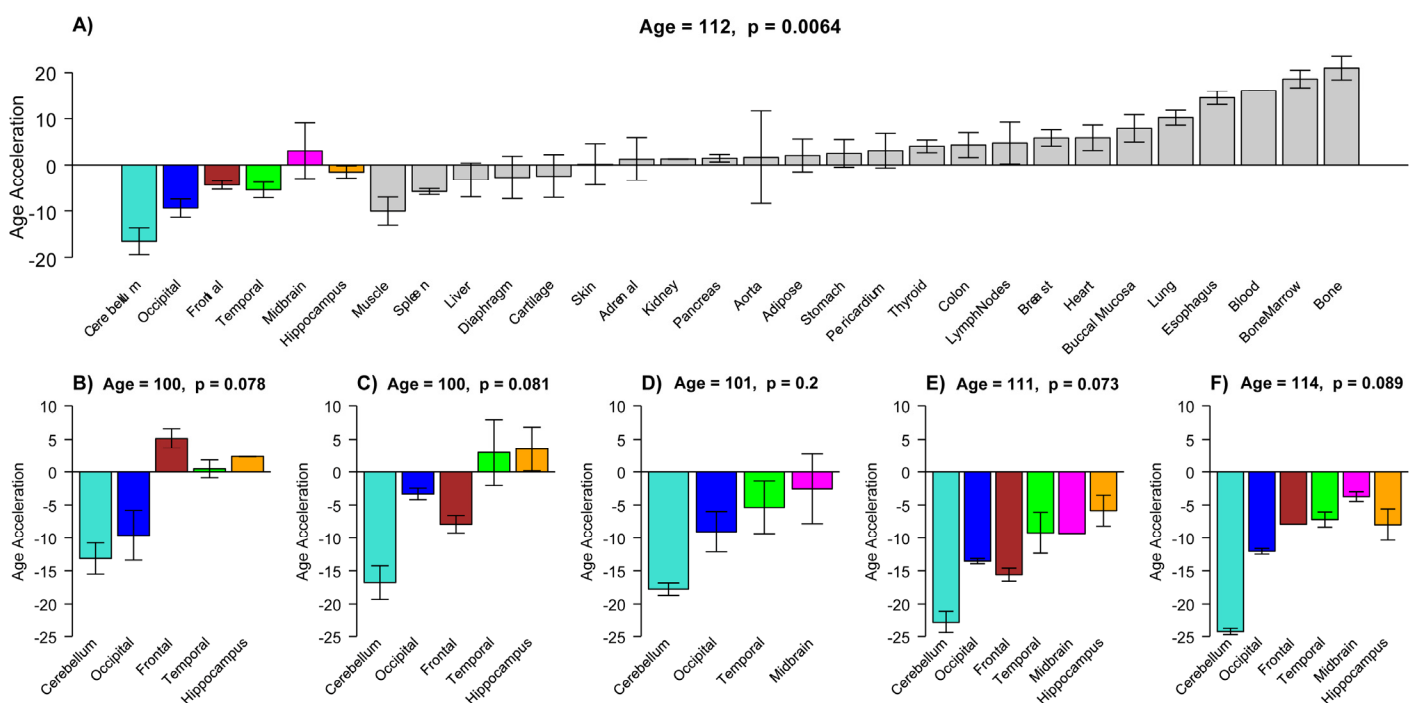
Figure 3. Epigenetic age acceleration in tissues from individual centenarians. (a) Mean DNAm age acceleration per tissue (y-axis) for the 30 tissues and organs collected from a 112 year old woman. (b-f) Age acceleration in brain regions of 5 additional centenarians (whose age is in the title). Age acceleration here is defined relative to age of non-cerebellar brain samples as indicated by the red regression line in Figure 2a. Bars corresponding to different brain regions are colored as in Figure 2. For each of the six centenarians, cerebellar samples (turquoise bars) take on the lowest (negative values). Each bar plot reports the mean value and one standard error. Number of replicate measurements for each tissue was two except for bone and bone marrow, which were four.

Table 1. Overview of the DNA methylation datasets. The rows correspond to the datasets used in this article. Columns report the tissue source, DNA methylation platform, number of subjects, access information and citation and a reference to the use in this text.

| Tissue source	Platform	No. arrays	No. subjects	No. females	Mean Age (range)	GEO/ArrayExpress ID	Citation	Figure
1. Brain	Illumina 450K	260	39	19	73 (15, 114)	GSE64509	Current article	2
2. Multiple tissues	Illumina 450K	64	1	1	112	GSE64491	Current article	3,4
3. Bone	Illumina 450k	48	48	46	78 (49-104)	GSE64490	Current article	6
4. Multiple tissues	Illumina 450K	70	4	1	52 (40, 6)	GSE50192	Lokk 2014	1
5. Brain+ blood	Illumina 450K	531	122	72	85 (40,105)	GSE59685	Lunnon 2014	5
6. Brain	Illumina 450K	87	46	16	62 (25,96)	GSE61431	Pidsley 2014	5

Table 2. Functional enrichment of differentially expressed genes in the cerebellum compared to pons, frontal cortex and temporal cortex.

| Category	Term	DAVID			GWAS MAGENTA CRBM
1239 transcripts over-expressed in cerebellum		**n**	**FE**	**P Bonf.**	**P-value**
Cellular Compartment	nuclear lumen (GO:0031981)	202	2.5	6.0×10^{-35}	1.6×10^{-3}
	nucleoplasm (GO:0005654)	125	2.5	2.4×10^{-20}	0.018
	nucleolus (GO:0005730)	101	2.6	1.7×10^{-16}	0.014
	spliceosome (GO:0005681)	32	4.4	2.2×10^{-9}	0.29
Biol. Process	transcription (GO:0006350)	265	1.9	9.5×10^{-26}	0.15
	mRNA processing (GO_0006397)	55	3.4	1.4×10^{-12}	0.38
	chromatin modification (GO:0016568)	55	3.1	4.5×10^{-10}	0.026
Molecular F.	RNA binding (GO:0003723)	93	1.9	7.1×10^{-7}	0.040
	helicase activity (GO:0004386)	31	3.3	8.5×10^{-6}	3.0×10^{-3}
INTERPRO	DEAD-like helicase, N-terminal (IPR014001)	31	4.4	9.2×10^{-9}	5.8×10^{-3}
808 under-expressed in cerebellum					
Biol. Process	synaptic transmission (GO:0007268)	39	3.1	2.2×10^{-6}	0.50
	neuron differentiation (GO:0030182)	49	2.7	2.4×10^{-6}	0.030
	neuron projection development (GO:0010975)	19	6.5	9.6×10^{-7}	0.54

Characterizing gene transcripts that are over/under expressed in cerebellum

Using gene expression data from multiple brain regions of the Gibbs [26] data set (GSE15745), we identified 1239 gene transcripts that were significantly over expressed in cerebellum compared to the pons, temporal cortex and frontal cortex from the same subjects at a false discovery rate (FDR) of 0.05. The results of a functional enrichment analysis with the "Database for Annotation, Visualization and Integrated Discovery" (DAVID, v6.7) [27] can be found in Table 1. The 1239 over-expressed genes are highly enriched with genes that are located in the nucleus and are known to play a significant role in gene transcription, mRNA processing, RNA splicing and chromatin modifications.
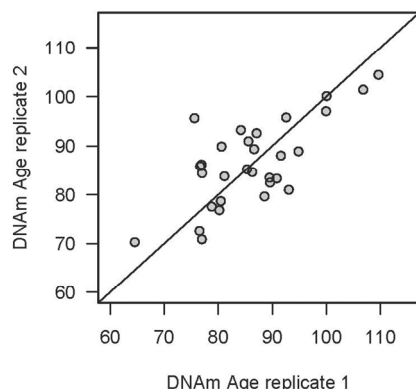

Figure 4. Reproducibility of DNAm age in the 112 year old supercentenarian. For each of the 30 tissues of the supercentenarian, we assessed at least two replicates (two independent DNA extractions for distant regions of the same tissue).
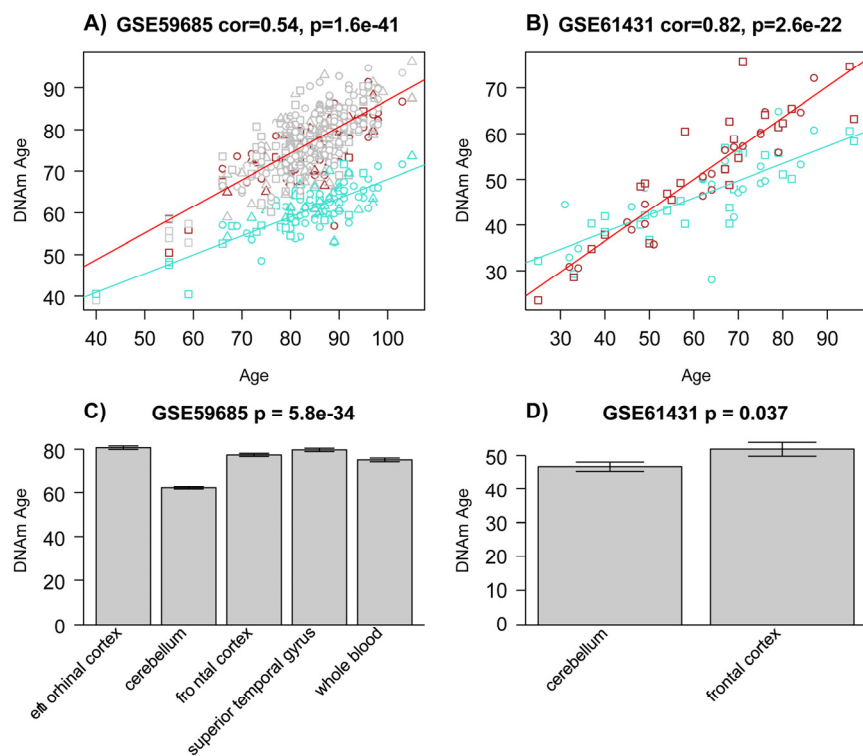
Figure 5. **Epigenetic age acceleration in two multi-tissue data sets**. The first column **(a, c)** report results for samples from data set 5 [42]. The last column **(b, d)** reports findings for data set 6 [43]. **(a-b)** Scatter plots relating the DNAm age of each sample (y-axis) versus the corresponding chronological age (x-axis). Linear regression lines through cerebellar samples and non-cerebellar samples are colored in turquoise and red, respectively. Note that cerebellar samples (turquoise points) tend to lie below non-cerebellar samples. (**a**) Squares, circles, and triangles correspond to samples from controls, AD, and mixed dementia subjects, respectively. (**b**) Squares and circles corresponds to controls and schizophrenia subjects, respectively. (**c**) The barplots depict the mean DNAmAge (y-axis) versus tissue type for all subjects from panel A for whom all 5 tissue types (including whole blood) were available. (**d**) Analogous plot for all subjects from data set 6 for whom both brain regions were available.

Thirty one of these over-expressed genes are involved in helicase activity (Bonferroni corrected p-value=8.5x10^{-6}). RNA and DNA helicases are considered to be enzymes that catalyze the separation of double-stranded nucleic acids in an energy-dependent manner often coupled to ATP hydrolysis. However RNA helicases can function in other roles such as RNA folding, ribosome biogenesis, anchoring of substrates to form ribonucleoprotein complexes as well as disruption of RNA-protein complexes [28]. Helicases have been classified into six superfamilies (SF1-SF6)[29, 30]. We find that the two largest superfamilies (SF1 and SF2) are over-represented among the 1239 gene transcripts (p=9.2x10^{-9}) with enrichment of genes with helicase or ATP binding domains including DEAD/DEAH box domains (IPR014001). Specifically when we considered genes listed on rnahelicase.org that are involved in pre-mRNA splicing (AQR, SNRNP200, DHX8, DHX15, DHX16, DHX38, EIF4A3, DDX39B, DDX3X, DDX3Y, DDX5, DDX23, DDX42 and DDX46), seven of these 14 (AQR, SNRNP200, DHX16, DHX38, DDX5, DDX42 and DDX46) are significantly overexpressed in cerebellum compared to cerebral cortex (p = 1.28x10^{-5}).
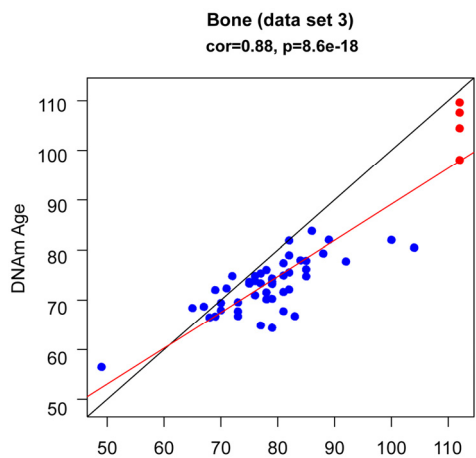
Figure 6. DNAm age (y-axis) versus age (x-axis) in bone (osteocytes/osteoblasts). The blue dots corresponds to the samples in data set 3 (bone). The red dots corresponds to the replicate bone samples from the 112 year old super centenarian.

Similarly, we identified 808 gene transcripts that were under-expressed in cerebellum at an FDR threshold of 0.05. The top gene ontology categories among these under-expressed are specifically related to neuronal function and include neuron projection development, neuron differentiation, and synaptic transmission.

Genetic enrichment analysis

To determine which of the cerebellum associated transcriptional differences might play a causal role in keeping the cerebellum young, we tested whether the gene categories from Table 2 show enrichment for SNPs that relate to epigenetic age acceleration in cerebellum. The MAGENTA approach [31] was used to test whether the sets of functionally related genes in Table 2 are enriched for SNP associations with epigenetic age acceleration in cerebellar samples. Toward this end, we applied MAGENTA to results from our GWAS meta-analysis of epigenetic acceleration in cerebellum (Methods). The meta analysis was based on four independent data sets for which both SNP data and cerebellar DNA methylation data were measured on the same subjects (n = 354, see Methods). The MAGENTA results can be found in the last column of Table 2. Even after adjusting for multiple comparisons, significant enrichment results can be observed for the GO category "nuclear lumen" (p=0.0016), and the molecular function "helicase activity" (p=0.0030). Helicase superfamilies SF1 and SF2 (particularly SF2) are highly enriched (p = 5.8x10^{-3}) based on SNPs associated with the following genes DHX57, CHD8, DHX15, DDX19A, DDX19B, DDX2, BLM, SMARCA5, SNORA67, EIF4A1, HLTF, C9orf102. Interestingly, another DEAD box related gene, DHX16, was the most significantly (q-value=1.5x10^{-5}) over-expressed gene in cerebellum compared to other brain regions but it was not implicated in our GWAS analysis.

DISCUSSION

While our study of a supercentenarian suggests that the epigenetic age of cerebellar tissue is younger than other part of the body we need to highlight several caveats. Although the epigenetic clock lends itself for comparing the epigenetic ages of multiple tissues, it remains to be seen whether the difference between nervous and non-nervous tissue reflects differences in biological aging rates. We are on safer ground when it comes to comparing the ages of different brain regions. We are confident in the finding that the cerebellum has a lower epigenetic age than other brain regions in older subjects since this effect could be observed in three independent data sets and 6 individual centenarians. This finding raises several questions. The most pressing question is whether this implies that the cerebellum is biologically younger than other brain regions? While the epigenetic age of blood has been shown to relate to biological age [24, 25], the same cannot yet been said about brain tissue. As a matter of fact, our study provides the first admittedly indirect and circumstantial evidence that the epigenetic age of brain tissue relates to biological age because the cerebellum exhibits fewer neuro-pathological hallmarks of age related dementias compared to other brain regions. But prospective studies

in model organisms will be needed to show that the epigenetic age of brain tissue predicts the future onset of age related diseases even after correcting for chronological age and known risk factors. Another open question is why does the cerebellum have a slower aging rate? In an attempt to address this question, we used both transcriptional and genetic data. We found several gene ontology categories that are enriched in genes that are over-expressed in the cerebellum (including helicases). But the results from our differential expression analysis must be interpreted with caution for two reasons. First, cellular heterogeneity may confound these results since the cerebellum involves distinct cell types. Second, this cross-sectional analysis does not lend itself for dissecting cause and effect relationships. To partially address these concerns, we used genetic data. It is striking that SNPs that relate to the epigenetic age acceleration of the cerebellum also tend to be located near RNA helicase genes as observed in our transcriptional data. These results suggest that RNA helicase genes might play a role in slowing down the epigenetic age of the cerebellum. Unfortunately, RNA helicase genes are not a "smoking gun" for any particular molecular process. RNA helicases are ubiquitous and essential proteins for most processes of RNA metabolism (e.g. ribosome biogenesis, pre-mRNA splicing, translation initiation) and also function as regulators of gene expression by non-coding RNAs, detection of specific RNA molecules, sensing of small compounds or transduction of metabolic signals [32]. Although we could not find any prior literature on the role of RNA helicases in tissue aging, the same cannot be said for DNA helicases: e.g. WRN, which is a member of the RecQ helicase family, is implicated in Werner's syndrome, which is a recessively inherited progeria.

The interpretation of our main finding (regarding the epigenetic age of the cerebellum) is also complicated by the fact that we still don't know what is being measured by epigenetic age. While many articles suggest that age-related changes in DNAm levels represent random noise others suggest that there might be a purposeful biological mechanism [33-35]. DNAm age might measure the cumulative work of an Epigenomic Maintenance System (EMS) [19]. Under the EMS hypothesis, our findings suggest that cerebellar DNA is epigenetically more stable and requires less "maintenance work". But many other explanations could explain our findings including the following: a) the cerebellum has a lower metabolic rate than cortex [36-38], b) it has far fewer mitochondrial DNA (mtDNA) deletions than cortex especially in older subjects [39], and it accumulates less oxidative damage to both mtDNA and nuclear DNA than does cortex [40].

In conclusion, this is probably the first study to show that the cerebellum ages more slowly than other brain regions and possibly many other parts of the body. By understanding why the cerebellum is protected against aging, it might be possible to understand the cause of tissue aging, which remains a central mystery of biology.

METHODS

Description of datasets listed in Table 1. All data presented in this article have been made publicly available in public repositories. Gene Expression Omnibus accession numbers are presented in Table 1.

Data set 1: Bisulphite converted DNA from these samples were hybridized to the Illumina Infinium 450K Human Methylation Beadchip. 260 arrays were generated from 39 subjects (19 females). Twenty-one subjects presented with Alzheimer's Disease (AD) whereas 18 subjects did not have any neurodegenerative disease. None of the subjects had brain malignancies. After adjusting for chronological age, we could not detect an age acceleration effect due to AD status, which is why we ignored AD status in the analysis. We profiled the following brain regions: caudate nucleus (n = 12 arrays), cingulate gyrus (n=12 arrays), cerebellum (32), hippocampus (25), inferior parietal cortex (11), left frontal lobe (9), left occipital cortex (12), left temporal cortex (18), midbrain (18), middle frontal gyrus (12), motor cortex (12), right frontal lobe (20), right occipital cortex (21), right temporal cortex (11), sensory cortex (12), superior parietal cortex (12), and visual cortex (11).

Data set 2: Multiple tissues from a 112 year old, female supercentenarian. 64 arrays were generated from 30 tissues/regions (listed in Figure 3).

Data set 3: Novel bone data set. The trabecular bone pieces were obtained from the central part of the femoral head of Spanish (Caucasian) patients with hip fractures (due to osteoporosis) or subjects with osteoarthritis. Since osteoarthritis status was not related to DNA methylation age, we ignored it in the analysis.

Data set 4: Multiple tissues (listed in Figure 1) from GEO: GSE50192 [41].

Data set 5: Various brain regions and whole blood from (GEO data GSE59685) [42].

Specifically, the following tissues were available: entorhinal cortex, cerebellum, frontal cortex, superior temporal gyrus, and whole blood.

Data set 6: Pre-frontal cortex and cerebellum samples from schizophrenics and controls (GEO data GSE61431) [43].

Disease status could be ignored in data sets 5 and 6 because our tissue comparisons involved samples from the same subjects. Our results were qualitatively the same after using a multivariate regression model that accounted for disease status.

DNA extraction. AllPrep DNA/RNA/miRNA Universal Kit (Qiagen, cat # 80224) was used for the DNA extractions for frozen tissue samples. Cubes 3x3x3mm with approximate mass of ~30 mg were cut from histological specimens collected during necropsies. Bone was dissected into bone and bone marrow (3x3x3mm each specimen) and separated into 2 different microcentrifuge tubes for DNA extractions. The procedure was conducted on dry ice without thawing the samples down to preserve RNA quality for prospective studies. 30mg of frozen tissue was lysed with 600uL guanidine-isothiocyanate–containing Buffer RLT Plus in a 2.0mL microcentrifuge tube, and homogenized by using TissueLyser II (Qiagen) with 5mm stainless steel beads. Tissue lysate was continued with the AllPrep protocol for simultaneous extraction of genomic DNA and total RNA using RNeasy Mini spin column technology. DNA yields were on average 16ug, with the highest yield from Spleen tissue (46 ug) and the lowest yield from Adipose tissue (2.2 ug).

We did not use bone specimens where we could macroscopically see both solid bone and bone marrow, so we did not use any additional washing steps to remove bone marrow.

Preprocessing of Illumina Infinium 450K arrays. In brief, bisulfite conversion using the Zymo EZ DNA Methylation Kit (ZymoResearch, Orange, CA, USA) as well as subsequent hybridization of the HumanMethylation450k Bead Chip (Illumina, SanDiego, CA), and scanning (iScan, Illumina) were performed according to the manufacturers protocols by applying standard settings. DNA methylation levels (β values) were determined by calculating the ratio of intensities between methylated (signal A) and un-methylated (signal B) sites. Specifically, the β value was calculated from the intensity of the methylated (M corresponding to signal A) and un-methylated (U corresponding to signal B) sites, as the ratio of fluorescent signals $\beta = Max(M,0)/[Max(M,0)+Max(U,0)+100]$. Thus, β values range from 0 (completely un-methylated) to 1 (completely methylated) [44].

Many authors have described methods for dealing with the two types of probes found on the Illumina 450k array [45-47]. This is not a concern for the epigenetic clock since it mainly involves type II probes. But our software implements a data normalization step that repurposes the BMIQ normalization method from Teschendorff [46] so that it automatically references each sample to a gold standard based on type II probes (details can be found in Additional file 2 from [19]).

DNA methylation age and epigenetic clock. Many articles describe sets of CpGs that correlate with age in multiple tissues [5, 7, 8, 14, 48-50]. Although these reports firmly establish the strong effect of age on epigenetic modifications, individual CpG sites are unsuitable for global contrasting of the epigenetic ages of different tissues derived from the same individual. Epigenetic age was calculated as reported previously. The epigenetic clock is defined as a prediction method of age based on the DNAm levels of 353 CpGs. Predicted age, referred to as DNAm age, correlates with chronological age in sorted cell types (CD4 T cells, monocytes, B cells, glial cells, neurons) and tissues and organs including whole blood, brain, breast, kidney, liver, lung, saliva [19]. Mathematical details and software tutorials for the epigenetic clock can be found in the Additional files of [19]. An online age calculator can be found at our webpage (https://dnamage.genetics.ucla.edu).

Finding gene transcripts that were differentially expressed in cerebellum compared to three other brain regions. The data set from Gibbs et al [26] also contained gene expression data from the brain regions of the same subjects for whom DNA methylation data were available. We used these data to find genes that were over-expressed in cerebellum compared to the pons, temporal cortex, and frontal cortex.

Since multiple brain regions were available for each subject, we used a paired T test to find genes that were differentially expressed between a) cerebellum and pons, b) cerebellum and temporal cortex, and c) cerebellum and frontal cortex. The matched design (3 brain regions from the same subjects) allowed us to condition out chronological age, ethnicity, gender, and other subject level confounders. For each of the three matched pairwise comparisons, we obtained a T-statistic based on the differences in expression values. Next we combined the resulting three T statistics using a conservative meta analysis approach: the scaled Stouffer method implemented in the "rankPvalue" R function [51, 52]. The resulting meta analysis p-values were transformed to local false discovery rates (q-values) using the *qvalue* R package [53]. At a 1-sided false discovery rate (FDR) threshold (qValueHighScale) of 0.05 we found 1239 Illumina probes that were over-expressed in cerebellum. Details on these and all other probes on the Illumina array can be found in Supplementary Table S1 (MarginalAnalysisGibbsMeta).

Similarly we identified 808 gene transcripts that were significantly under-expressed in cerebellum at a FDR threshold of 0.05.

The results of a functional enrichment analysis with the "Database for Annotation, Visualization and Integrated Discovery" (DAVID, v6.7) [27] applied to the 1239 overexpressed and the 808 underexpressed genes can be found in Supplementary Table S2 (DavidEASEQ05over. xlsx) and Supplementary table S3 (DavidEASEQ05 under.xlsx), respectively.

Also our functional enrichment analysis results using DAVID are qualitatively unchanged when other FDR thresholds (e.g. 0.01) are used.

MAGENTA analysis for GWAS enrichment. MAGENTA is a computational tool that tests for enrichment of genetic associations in predefined biological processes or sets of functionally related genes, using genome-wide association results as input [31]. MAGENTA is designed to analyze datasets for which genotype data are not readily available, such as large genome-wide association study (GWAS) meta-analyses. As input of MAGENTA, we used the results of a genome-wide meta-analysis for epigenetic age acceleration in human cerebellum. In total, this analysis involved cerebellar DNA methylation data and SNP data from 354 Caucasian subjects from the following independent studies: 59 Caucasian individuals from a study for Alzheimer's disease [42], 112 neurologically normal samples from [26], 147 samples from a case control of psychiatric disorders [54], and 36 Caucasian samples from a case control study of schizophrenia [43]. We ignored disease status in our GWAS analysis since it had a negligible effect on age acceleration in cerebellum (t-test $P > 0.1$). Caucasian ethnicity was verified in PLINK or EIGENSTRAT[55].

Age acceleration outcome measure was defined in the same way that we utilized the residuals from regression of DNAm age on chronological age. Quantitative trait association analysis was performed on each study, adjusted for principal components when necessary. Fixed-effects models weighted by inverse variance [56] were applied to combine the association results across studies, yielding a total of 4,586,301 association P values as the input for the MAGENTA analysis. We extended the gene boundary with +/- 50 kilobases to assign SNPs to their nearby genes and selected the GSEA (Genome Set Enrichment Analysis) method with cutoff set at 95th percentile to estimate enrichment P values starting with 10,000 permutations then increased to 100,000 for $P < 1.0 \times 10^{-4}$.

Brief Information of the 112 year old. The likely cause of death was bilateral organizing pneumonia. Neuropathologic findings were those of Alzheimer's disease, Braak stage IV-V, NIA-AA stage A2B2C2 [57]. Neuritic plaques were abundant in hippocampus, frontal cortex and temporal cortex and less prominant in basal ganglia and occipital cortex. Neurofibrillary tangles were abundant in hippocampus and sparse in frontal and temporal cortices.

Ethics review and IRB. All subjects from the UCLA tissue bank signed the "Consent for Autopsy" form by the Department of Pathology at UCLA, and research procurement was performed under IRB Research Protocol Number 11-002504. Further, the epigenetic analysis is covered by IRB Research Protocol Number: 19119.

Conflict of interest statement

The authors declare no conflicts of interest.

REFERENCES

1. Baker G and Sprott R. Biomarkers of aging. Exp Gerontol. 1988; 23:223-239.

2. Sanders J, Boudreau R and Newman A. 2012. Understanding the Aging Process Using Epidemiologic Approaches. (Dordrecht Heidelberg New York: Springer).

3. Blackburn EH and Gall JG. A tandemly repeated sequence at the termini of the extrachromosomal ribosomal RNA genes in Tetrahymena. J Mol Biol. 1978; 120:33-53.

4. Lin J, Epel E, Cheon J, Kroenke C, Sinclair E, Bigos M, Wolkowitz O, Mellon S and Blackburn E. Analyses and comparisons of telomerase activity and telomere length in human T and B cells: insights for epidemiology of telomere maintenance. J Immunol Methods. 2010; 352:71-80.

5. Christensen B, Houseman E, Marsit C, Zheng S, Wrensch M, Wiemels J, Nelson H, Karagas M, Padbury J, Bueno R, Sugarbaker D, Yeh R, Wiencke J, et al. Aging and Environmental Exposures Alter Tissue-Specific DNA Methylation Dependent upon CpG Island Context. PLoS Genet. 2009; 5:e1000602.

6. Bollati V, Schwartz J, Wright R, Litonjua A, Tarantini L, Suh H, Sparrow D, Vokonas P and Baccarelli A. Decline in genomic DNA methylation through aging in a cohort of elderly subjects. Mech Ageing Dev. 2009; 130:234-239.

7. Rakyan VK, Down TA, Maslau S, Andrew T, Yang TP, Beyan H, Whittaker P, McCann OT, Finer S, Valdes AM, Leslie RD, Deloukas P and Spector TD. Human aging-associated DNA hypermethylation occurs preferentially at bivalent chromatin domains. Genome research. 2010; 20:434-439.

8. Teschendorff AE, Menon U, Gentry-Maharaj A, Ramus SJ, Weisenberger DJ, Shen H, Campan M, Noushmehr H, Bell CG, Maxwell AP, Savage DA, Mueller-Holzner E, Marth C, et al. Age-dependent DNA methylation of genes that are suppressed in stem cells is a hallmark of cancer. Genome research. 2010; 20:440-446.

9. Vivithanaporn P, Heo G, Gamble J, Krentz H, Hoke A, Gill M and Leistung C. Neurologic disease burden in treated HIV/AIDS predicts survival. Neurology. 2010; 75:1150-1158.

10. Horvath S, Zhang Y, Langfelder P, Kahn R, Boks M, van Eijk K, van den Berg L and Ophoff RA. Aging effects on DNA methylation modules in human brain and blood tissue. Genome Biol. 2012; 13:R97.

11. Numata S, Ye T, Hyde Thomas M, Guitart-Navarro X, Tao R, Wininger M, Colantuoni C, Weinberger Daniel R, Kleinman Joel E and Lipska Barbara K. DNA Methylation Signatures in Development and Aging of the Human Prefrontal Cortex. Am J Hum Genet. 2012; 90:260-272.

12. Alisch RS, Barwick BG, Chopra P, Myrick LK, Satten GA, Conneely KN and Warren ST. Age-associated DNA methylation in pediatric populations. Genome Res. 2012; 22:623-632.

13. Johansson A, Enroth S and Gyllensten U. Continuous Aging of the Human DNA Methylome Throughout the Human Lifespan. PLoS One. 2013; 8:e67378.

14. Day K, Waite L, Thalacker-Mercer A, West A, Bamman M, Brooks J, Myers R and Absher D. Differential DNA methylation with age displays both common and dynamic features across human tissues that are influenced by CpG landscape. Genome Biol. 2013; 14:R102.

15. Bocklandt S, Lin W, Sehl ME, Sanchez FJ, Sinsheimer JS, Horvath S and Vilain E. Epigenetic predictor of age. PLoS ONE. 2011; 6:e14821.

16. Koch C and Wagner W. Epigenetic-aging-signature to determine age in different tissues. Aging. 2011; 3:1018–1027.

17. Garagnani P, Bacalini MG, Pirazzini C, Gori D, Giuliani C, Mari D, Di Blasio AM, Gentilini D, Vitale G, Collino S, Rezzi S, Castellani G, Capri M, et al. Methylation of ELOVL2 gene as a new epigenetic marker of age. Aging Cell. 2012; 11:1132-1134.

18. Hannum G, Guinney J, Zhao L, Zhang L, Hughes G, Sadda S, Klotzle B, Bibikova M, Fan J-B, Gao Y, Deconde R, Chen M, Rajapakse I, et al. Genome-wide Methylation Profiles Reveal Quantitative Views of Human Aging Rates. Mol Cell. 2013; 49:359-367.

19. Horvath S. DNA methylation age of human tissues and cell types. Genome Biol. 2013; 1:(R115.

20. Weidner CI, Lin Q, Koch CM, Eisele L, Beier F, Ziegler P, Bauerschlag DO, Jockel KH, Erbel R, Muhleisen TW, Zenke M, Brummendorf TH and Wagner W. Aging of blood can be tracked by DNA methylation changes at just three CpG sites. Genome Biol. 2014; 15:R24.

21. Spiers H, Hannon E, Schalkwyk LC, Smith R, Wong CC, O'Donovan MC, Bray NJ and Mill J. Methylomic trajectories across human fetal brain development. Genome research. 2015; 25:338-352.

22. Boks MP, Derks EM, Weisenberger DJ, Strengman E, Janson E, Sommer IE, Kahn RS and Ophoff RA. The Relationship of DNA Methylation with Age, Gender and Genotype in Twins and Healthy Controls. PLoS ONE. 2009; 4:e6767.

23. Horvath S, Erhart W, Brosch M, Ammerpohl O, von Schönfels W, Ahrens M, Heits N, Bell JT, Tsai P-C, Spector TD, Deloukas P, Siebert R, Sipos B, et al. Obesity accelerates epigenetic aging of human liver. Proc Natl Acad Sci U S A 2014; 111:15538-15543.

24. Marioni R, Shah S, McRae A, Chen B, Colicino E, Harris S, Gibson J, Henders A, Redmond P, Cox S, Pattie A, Corley J, Murphy L, et al. DNA methylation age of blood predicts all-cause mortality in later life. Genome Biol. 2015; 16:25.

25. Marioni RE, Shah S, McRae AF, Ritchie SJ, Muniz-Terrera G, Harris SE, Gibson J, Redmond P, Cox SR, Pattie A, Corley J, Taylor A, Murphy L, et al. The epigenetic clock is correlated with physical and cognitive fitness in the Lothian Birth Cohort 1936. Int J Epidemiol. 2015; Epub ahead of prin

26. Gibbs JR, van der Brug MP, Hernandez DG, Traynor BJ, Nalls MA, Lai S-L, Arepalli S, Dillman A, Rafferty IP, Troncoso J, Johnson R, Zielke HR, Ferrucci L, et al. Abundant Quantitative Trait Loci Exist for DNA Methylation and Gene Expression in Human Brain. PLoS Genet. 2010; 6:e1000952.

27. Huang DW, Sherman BT and Lempicki RA. Systematic and integrative analysis of large gene lists using DAVID bioinformatics resources. Nat Protocols. 2008; 4:44-57.

28. Leitão A, Costa M and Enguita F. Unzippers, Resolvers and Sensors: A Structural and Functional Biochemistry Tale of RNA Helicases. International Journal of Molecular Sciences. 2015; 16:2269-2293.

29. Gorbalenya AE, Koonin EV, Donchenko AP and Blinov VM. Two related superfamilies of putative helicases involved in replication, recombination, repair and expression of DNA and RNA genomes. Nucleic acids research. 1989; 17:4713-4730.

30. Singleton MR, Dillingham MS and Wigley DB. Structure and mechanism of helicases and nucleic acid translocases. Annual review of biochemistry. 2007; 76:23-50.

31. Segre AV, Groop L, Mootha VK, Daly MJ and Altshuler D. Common inherited variation in mitochondrial genes is not enriched for associations with type 2 diabetes or related glycemic traits. PLoS Genet. 2010; 6:8

32. Enguita FJ and Leitao AL. The art of unwinding: RNA helicases at the crossroads of cell biology and human disease. J Biochem Pharmacol Res. 2014; 2:144-158.

33. Rando Thomas A and Chang Howard Y. Aging, Rejuvenation, and Epigenetic Reprogramming: Resetting the Aging Clock. Cell. 2012; 148:46-57.

34. Teschendorff AE, West J and Beck S. Age-associated epigenetic drift: implications, and a case of epigenetic thrift? Human Molecular Genetics. 2013; 22:R7-R15.

35. Issa J-P. Aging and epigenetic drift: a vicious cycle. J Clin Invest. 2014; 124:24-29.

36. Sakamoto S and Ishii K. Low cerebral glucose extraction rates in the human medial temporal cortex and cerebellum. J Neurol Sci 1999; 172:41-48.

37. Bentourkia M, Bol A, Ivanoiu A, Labar D and Sibomana M. Comparison of regional cerebral blood flow and glucose metabolism in the normal brain: Effect of aging. J Neurol Sci. 2000; 181:19-28.

38. Noda A, Ohba H, Kakiuchi T, Futatsubashi M and Tsukada H. Age-related changes in cerebral blood flow and glucose metabolism in conscious rhesus monkeys. Brain Res. 2002; 936:76–81.

39. Corral-Debrinski M, Horton T, Lott M, Shoffner J and Beal M. Mitochondrial DNA deletions in human brain: Regional variability and increase with advanced age. . Nat Genet 1992; 2:324-329.

40. Mecocci P, MacGarvey U, Kaufman A, Koontz D and Shoffner J. Oxidative damage to mitochondrial DNA shows marked age-dependent increases in human brain. . Ann Neurol 1993; 34:609-616.

41. Lokk K, Modhukur V, Rajashekar B, Martens K, Magi R, Kolde R, Koltsina M, Nilsson T, Vilo J, Salumets A and Tonisson N. DNA methylome profiling of human tissues identifies global and tissue-specific methylation patterns. Genome Biology. 2014; 15:r54.

42. Lunnon K, Smith R, Hannon E, De Jager PL, Srivastava G, Volta M, Troakes C, Al-Sarraj S, Burrage J, Macdonald R, Condliffe D, Harries LW, Katsel P, et al. Methylomic profiling implicates cortical deregulation of ANK1 in Alzheimer's disease. Nat Neurosci. 2014; 17:1164-1170.

43. Pidsley R, Viana J, Hannon E, Spiers H, Troakes C, Al-Saraj S, Mechawar N, Turecki G, Schalkwyk L, Bray N and Mill J. Methylomic profiling of human brain tissue supports a neurodevelopmental origin for schizophrenia. Genome Biology. 2014; 15:483.

44. Dunning M, Barbosa-Morais N, Lynch A, Tavare S and Ritchie M. Statistical issues in the analysis of Illumina data. BMC Bioinformatics. 2008; 9:85.

45. Maksimovic J, Gordon L and Oshlack A. SWAN: Subset-quantile Within Array Normalization for Illumina Infinium HumanMethylation450 BeadChips. Genome Biology. 2012; 13:R44.

46. Teschendorff AE, Marabita F, Lechner M, Bartlett T, Tegner J, Gomez-Cabrero D and Beck S. A beta-mixture quantile normalization method for correcting probe design bias in Illumina Infinium 450 k DNA methylation data. Bioinformatics. 2013; 29:189-196.

47. Yousefi P, Huen K, Schall RA, Decker A, Elboudwarej E, Quach H, Barcellos L and Holland N. Considerations for normalization of DNA methylation data by Illumina 450K BeadChip assay in population studies. Epigenetics. 2013; 8:1141-1152.

48. Hernandez D, Nalls M, Gibbs J and et al. Distinct DNA methylation changes highly correlated with chronological age in the human brain. Hum Mol Genet. 2011; 20:1164–1172.

49. Maegawa S, Hinkal G, Kim HS, Shen L, Zhang L, Zhang J, Zhang N, Liang S, Donehower LA and Issa J-PJ. Widespread and tissue specific age-related DNA methylation changes in mice. Genome research. 2010; 20:332-340.

50. Grönniger E, Weber B, Heil O, Peters N, Stäb F, Wenck H, Korn B, Winnefeld M and Lyko F. Aging and Chronic Sun Exposure Cause Distinct Epigenetic Changes in Human Skin. PLoS Genet. 2010; 6:e1000971.

51. Langfelder P, Mischel PS and Horvath S. When is hub gene selection better than standard meta-analysis? PLoS ONE. 2013; 8:e61505.

52. Langfelder P and Horvath S. WGCNA: an R package for weighted correlation network analysis. BMC Bioinformatics. 2008; 9:559.

53. Storey JD and Tibshirani R. Statistical significance for genomewide studies. Proceedings of the National Academy of Sciences of the United States of America. 2003; 100:9440-9445.

54. Zhang D, Cheng L, Badner JA, Chen C, Chen Q, Luo W, Craig DW, Redman M, Gershon ES and Liu C. Genetic Control of Individual Differences in Gene-Specific Methylation in Human Brain. The American Journal of Human Genetics. 2010; 86:411-419.

55. Price AL, Patterson NJ, Plenge RM, Weinblatt ME, Shadick NA and Reich D. Principal components analysis corrects for stratification in genome-wide association studies. Nat Genet. 2006; 38:904-909.

56. Begum F, Ghosh D, Tseng GC and Feingold E. Comprehensive literature review and statistical considerations for GWAS meta-analysis. Nucleic Acids Research. 2012; 40:3777-3784.

57. Montine T, Phelps C, Beach T, Bigio E, Cairns N, Dickson D, Duyckaerts C, Frosch M, Masliah E, Mirra S, Nelson P, Schneider J, Thal D, et al. National Institute on Aging–Alzheimer's Association guidelines for the neuropathologic assessment of Alzheimer's disease: a practical approach. Acta Neuropathol. 2012; 123:1-11.